

Dissertation zur Erlangung des Doktorgrades
der Fakultät für Chemie und Pharmazie
der Ludwig-Maximilians-Universität München

Modular Approaches to Photopharmacology

Martin Reynders
aus
Wiesbaden, Deutschland
2021

Erklärung

Diese Dissertation wurde im Sinne von § 7 der Promotionsordnung vom 28. November 2011 von Herrn Prof. Dr. Dirk Trauner betreut.

Eidesstattliche Versicherung

Diese Dissertation wurde eigenständig und ohne unerlaubte Hilfe erarbeitet.

München, den 27. Mai 2021

Martin Reynders

Dissertation eingereicht am:	31.05.2021
1. Gutachter:	Prof. Dr. Dirk Trauner
2. Gutachter:	Dr. Oliver Thorn-Seshold
Mündliche Prüfung am:	14.06.2021

Acknowledgement

First, I want to express my deep gratitude to Prof. Dr. Dirk Trauner for the possibility to carry out research in his group. The great working environment and the provided resources greatly facilitated research. The freedom to pursue bold ideas and his support helped me to grow as a scientist and person.

Many days of my PhD were spent in the laboratory of Prof. Dr. Michele Pagano and I would like to thank him for his support and for accommodating me in the ideal research environment he provides.

I want to acknowledge my thesis committee Dr. Oliver Thorn-Seshold, Prof. Dr. Konstantin Karaghiosoff, Prof. Dr. Oliver Trapp, and Prof. Dr. Susanne Koch for their commitment.

I would also like to thank my collaborators at other institutions: Prof. Dr. Stefan Laufer, Prof. Dr. Stefan Knapp, Dr. Apirat Chaikuad, Dr. Benedict-Tilman Berger, Katharina Bauer and Prof. Dr. Pierre Koch.

Special thanks go out the current and past members of the Trauner and Pagano groups, especially Chris, Nynke, Bryan, Tom, Belinda, Christian, Antonio, Daniele, Luca, Greg, Martin, Alex, Peter, Johannes, Giulio, Anna, Joseph, Oliver, Philipp, James, Schatzi and everyone else who provided a great atmosphere in the lab and outside.

I am grateful for all the help by Lukas Jaschik, Philipp Peslalz, Marleen Bérouti, Kilian Rossmann, Qiao Lin, Farhan Chowdhury and Hanee Kim whom I had the pleasure to supervise during my PhD.

In addition, I would like to thank technical staff members Heike Traub, Aleksandra Grilc, Luis de la Osa de la Rosa, Dr. Martin Sumser, Carrie Louis, Mariia Palchyk, Michael Gayer, Heidi Buchholz, Philip Morton, Rogelio Fuertez, Dr. Werner Spahl, Sonja Kosak, Dr. David Stephenson, Ronald McLurkin, Dr. Chin Lin, Jeffrey Estrada, for keeping things up and running.

Lastly, I want to thank my friends, my family, and my girlfriend for the unconditional support throughout the past years of this adventure.

Summary

Physiological function is the result of a complex but well-regulated set of interactions between biological molecules. Our understanding of physiology goes hand in hand with the precision of the tools that are available to study biological systems. The development of optogenetics represents an advancement of the available tools, by employing light as an orthogonal stimulus to control biological function with spatiotemporal precision. In addition to genetic methods, pharmacological probes can be used to perturb native systems. Photopharmacology covers the creation and application of light-responsive small molecules pharmaceuticals. These so-called photoswitches can be turned on and off with light. Photopharmaceuticals can be used to precisely perturb and study biological systems. Additionally, photopharmacology holds a therapeutic promise by targeting drugs to specific tissues and cells with light and thus, mitigating side effects in healthy cells.

However, the generation of photopharmaceuticals remains challenging. Photoswitches need to achieve high activity as one isomer and at the same time the other isomer of the very same compound should be inactive. This thesis provides modular approaches to photopharmacology to facilitate the development of light-controlled probes for new targets. Based on proteolysis targeting chimeras (PROTACs) we have developed photochemically targeting chimeras (PHOTACs). PHOTACs catalyze the ubiquitylation and degradation of target proteins with light. PHOTACs are modular, bifunctional molecules combining an E3 ligase ligand fused to a photoswitch and a ligand targeting a protein of interest. As proof-of-concept we developed PHOTACs targeting the epigenetic reader proteins BRD2-4 for light-controlled degradation. This work also illustrates how to tune the photophysical properties of PHOTACs for specific applications and demonstrates that PHOTACs can be controlled using bioluminescence. The generality of this approach is then validated through variation of the targeting ligand, creating PHOTACs for the controlled degradation of FKBP12, MDM2 and cell cycle kinases with light.

The second part of this work features a strategy to generate light-controlled, covalent kinase inhibitors based on diazocines and the synthesis of these photoswitches. Both methods have in common that photoisomerization leads to a gain of function, induced protein degradation for PHOTACs and covalent reactivity with a native cysteine for the kinase inhibitors. These approaches allow the rapid generation of new light-controlled tools and potential therapeutics in photomedicine.

Publications

Sections of this work have been published in peer-reviewed journals:

- (1) **Reynders, M.**; Matsuura, B. S.; Bérouti, M.; Simoneschi, D.; Marzio, A.; Pagano, M.; Trauner, D. PHOTACs Enable Optical Control of Protein Degradation. *Sci. Adv.* 2020, 6 (8), eaay5064. <https://doi.org/10.1126/sciadv.aay5064>.
- (2) Maier, M. S.; Hüll, K.; **Reynders, M.**; Matsuura, B. S.; Leippe, P.; Ko, T.; Schäffer, L.; Trauner, D. Oxidative Approach Enables Efficient Access to Cyclic Azobenzenes. *J. Am. Chem. Soc.* 2019, 141 (43), 17295–17304. <https://doi.org/10.1021/jacs.9b08794>.
- (3) **Reynders, M.**; Trauner, D. Optical Control of Targeted Protein Degradation. *Cell. Chem. Biol.* 2021, 28 (7), 969–986. <https://doi.org/10.1016/j.chembiol.2021.05.010>
- (4) **Reynders, M.**; Chaikuad, A.; Berger, B.-T.; Bauer, K.; Koch, P.; Laufer, S.; Knapp, S.; Trauner, D. Controlling the Covalent Reactivity of a Kinase Inhibitor with Light, *Angew. Chem. Int. Ed.* 2021, 133 (37), 20340–20345. <https://doi.org/10.1002/ange.202103767>.

Manuscripts in Preparation:

- (5) **Reynders, M.**; Rossmann, K.; Bérouti, M.; Pagano, M.; Trauner, D. Tuning the Photophysical Properties of PHOTACs, *in preparation*.
- (6) **Reynders, M.**; Pagano, M.; Trauner, D. PHOTACs Controlling the MDM2-p53 Axis, *in preparation*.

Other Publications and patents:

- (7) Trauner, D.; **Reynders, M.**; Matsuura, B.; Berouti, M.; Pagano, M. Photoswitchable Protacs and Synthesis and Uses Thereof, WO2020172655, 2020.
- (8) **Reynders, M.**; Trauner, D. PHOTACs Enable Optical Control of Protein Degradation. In *Targeted Protein Degradation: Methods and Protocols*; Cacace, A. M., Hickey, C. M., Békés, M., Eds.; Methods in Molecular Biology; Springer US: New York, NY, 2021; pp 315–329. https://doi.org/10.1007/978-1-0716-1665-9_17.

Project Affiliation Disclosure

In this statement, I proclaim that the findings in this dissertation are the result of a collaborative effort. I will discuss the findings of a group of individuals who have significantly contributed to the various projects. Alongside the supervision of Prof. Dr. Dirk Trauner, the following individuals were involved in the scientific work presented in this thesis:

Chapter 2: PHOTACs Enable Optical Control of Protein Degradation

Bryan S. Matsuura (synthesis and characterization, immunoblotting), Marleen Bérouti (synthesis and characterization, immunoblotting), Daniele Simoneschi (immunoblotting), Antonio Marzio (immunoblotting), Michele Pagano (supervision).

Chapter 3: Tuning the Photophysical Properties of PHOTACs

Kilian Rossmann (synthesis and characterization), Marleen Bérouti (synthesis and characterization), Michele Pagano (supervision).

Chapter 4: Bioluminescence-Controlled Photopharmacology

Zi Yao (experimental design, reagent generation), Anna C. Love (experimental design, reagent generation), Michele Pagano (supervision), Jennifer A. Prescher (supervision).

Chapter 5: PHOTACs Controlling the MDM2-p53 Axis

Michele Pagano (supervision).

Chapter 6: PHOTACs Targeting Cell Cycle Kinases

Christopher J. Arp (immunoblotting), Daniele Simoneschi (immunoblotting), Michele Pagano (supervision).

Chapter 7: Towards Photoswitchable Molecular Glue Degraders

Michele Pagano (supervision).

Chapter 8: Tag-based PHOTACs Towards Controlling Fusion Proteins with Light

Michele Pagano (supervision).

Chapter 9: Controlling the Covalent Reactivity of a Kinase Inhibitor with Light

Apirat Chaikuad (crystallography and mass spectrometry), Benedict-Tilman Berger (*in cellulo* experiments), Katharina Bauer (*in vitro* experiments), Pierre Koch (supervision), Stefan Laufer (supervision), Stefan Knapp (supervision).

Chapter 11: An Oxidative Approach Enables Efficient Access to Cyclic Azobenzenes

Martin S. Maier (synthesis and characterization), Katharina Hüll (characterization), Bryan S. Matsuura (method development), Philipp Leippe (synthesis), Tongil A. Ko (synthesis), Lukas Schäffer (Synthesis)

Table of Contents

1 – OPTICAL CONTROL OF TARGETED PROTEIN DEGRADATION.....	1
2 – PHOTACS ENABLE OPTICAL CONTROL OF PROTEIN DEGRADATION	31
3 – TUNING THE PHOTOPHYSICAL PROPERTIES OF PHOTACS	153
4 – BIOLUMINESCENCE-CONTROLLED PHOTOPHARMACOLOGY	259
5 – PHOTACS CONTROLLING THE MDM2-P53 AXIS.....	275
6 – PHOTACS TARGETING CELL CYCLE KINASES	305
7 – TOWARDS PHOTOSWITCHABLE MOLECULAR GLUE DEGRADERS	369
8 – TAG-BASED PHOTACS TOWARDS CONTROLLING FUSION PROTEINS WITH LIGHT	401
9 – CONTROLLING THE COVALENT REACTIVITY OF A KINASE INHIBITOR WITH LIGHT	433
10 – EXPANDING PHOTOSWITCHABLE COVALENT INHIBITORS.....	475
11 – AN OXIDATIVE APPROACH ENABLES EFFICIENT ACCESS TO CYCLIC AZOBENZENES	499
APPENDIX.....	533

1 – Optical Control of Targeted Protein Degradation

Martin Reynders^{1,2} and Dirk Trauner^{*,1,3,4}

¹ Department of Chemistry, New York University, New York, NY 10003, USA.

² Department of Chemistry, Ludwig Maximilians University of Munich
81377 Munich, Germany.

³ Perlmutter Cancer Center, New York University School of Medicine, New York, NY
10016, USA.

⁴ NYU Neuroscience Institute, New York University School of Medicine, New York,
NY 10016, USA.

Summary

Molecular glues and proteolysis targeting chimeras (PROTACs) have emerged as small-molecule tools that selectively induce the degradation of a chosen protein and have shown therapeutic promise. Recently, several approaches employing light as an additional stimulus to control induced protein degradation have been reported. Here, we analyze the principles guiding the design of such systems, provide a survey of the literature published to date, and discuss opportunities for further development. Light-responsive degraders enable the precise temporal and spatial control of protein levels, making them useful research tools but also potential candidates for human precision medicine.

Introduction

Proteostasis is the tightly regulated maintenance of protein abundance originating from the interplay of protein synthesis and degradation. The periodic or intermittent fluctuation of protein levels is central to the regulation of many biological processes and the dysregulation of protein abundance is a common disease characteristic. Pharmacological perturbation of protein homeostasis can be achieved at many stages in the life cycle of a protein, which involves translation, folding, trafficking, post-translational modification, and degradation. A variety of proteostasis-altering molecules have emerged that can be used as powerful tool compounds in biology, such as puromycin, and as approved chemotherapeutics, such as Bortezomib.^[1] Puromycin inhibits RNA translation at the ribosome and thereby blocks protein synthesis, while Bortezomib blocks the proteasomal degradation of proteins through inhibition of the 20S proteasome. Whereas these molecules interfere with protein translation and degradation, respectively, in a non-selective way, so-called "molecular glues" recruit a small subset of cellular neosubstrates to E3 ligases to promote their ubiquitylation and proteasomal degradation.^[2] Despite the clinical success of these molecules, such as lenalidomide or pomalidomide, and their well understood mode of action, the systematic development of molecular glues for new substrates has proven to be challenging.^[3]

A more general and rational approach involves proteolysis targeting chimeras (PROTACs) and related bifunctional small molecules.^[4] These combine a ligand for an E3 ubiquitin ligase with a well-defined ligand for a protein of interest (POI). This chimera induces the formation of a ternary complex that leads to the ubiquitylation of the POI, followed by dissociation and proteasomal degradation. In contrast to the "occupancy driven" mode of action of inhibitors, PROTACs are "event driven", i.e. they function catalytically, resulting in increased efficacy compared to inhibitors.^[5] The catalytic mechanism of molecular glues and PROTACs, however, can complicate attempts to control their activity through dosing. Therefore, it would be desirable to provide an external stimulus that could activate (and deactivate) the PROTAC at a chosen time and location, avoiding potentially harmful systemic side effects.

Light can be used as such a stimulus. Indeed, light has been applied extensively to control biological processes with spatiotemporal precision, as exemplified by the

success of optogenetics and photopharmacology. Whereas optogenetics is based on engineered photoreceptors that use naturally abundant chromophores,^[6] photopharmacology does not necessarily require genetic manipulation and uses synthetic chromophores that are externally added.^[7] Two main strategies have emerged to render small molecules responsive to light: a) masking of the pharmacophore with a photocleavable protecting group (PPG), also referred to as caging or photocaging,^[8] and b) incorporation of a reversible photoswitch into the molecule.^[9] Here, we review the application of these principles to the development of light-activated PROTACs (Table 1) and discuss the usefulness of light for controlling targeted protein degradation in general.

Design Challenges and Considerations

The basic requirement for the optical control of targeted protein degradation is simple: The formation of a productive ternary complex must be controlled with light. This can be achieved either with a PPG, or by a photoswitch that renders the compound pharmacologically inactive in one form and active in the other (Fig. 1).

Photocaged compounds are comparatively easy to design because the structure of the active form is usually known beforehand, i.e. as a validated PROTAC, and structure-activity relationships of either ligand (for the E3 ubiquitin ligase and protein of interest (POI), respectively) are usually available (Fig. 1D). Photocaging of the ligand for the ubiquitin ligase, as shown in Fig. 1A, abrogates degradation of the POI and potential off-target proteins, but retains POI inhibitory activity. As a modular approach, it is easily adapted to other PROTACs that engage the same ubiquitin ligase.

Caging the POI ligand would abolish both degradation and the inhibitory effect on the target protein. However, it must be kept in mind that PROTACs caged in this way can still function as molecular glues and recruit neo-substrates to the E3 ligase, as observed for several cereblon binding PROTACs.^[10–13] Further, proteins binding to the PPG could be unintentionally recruited for degradation.

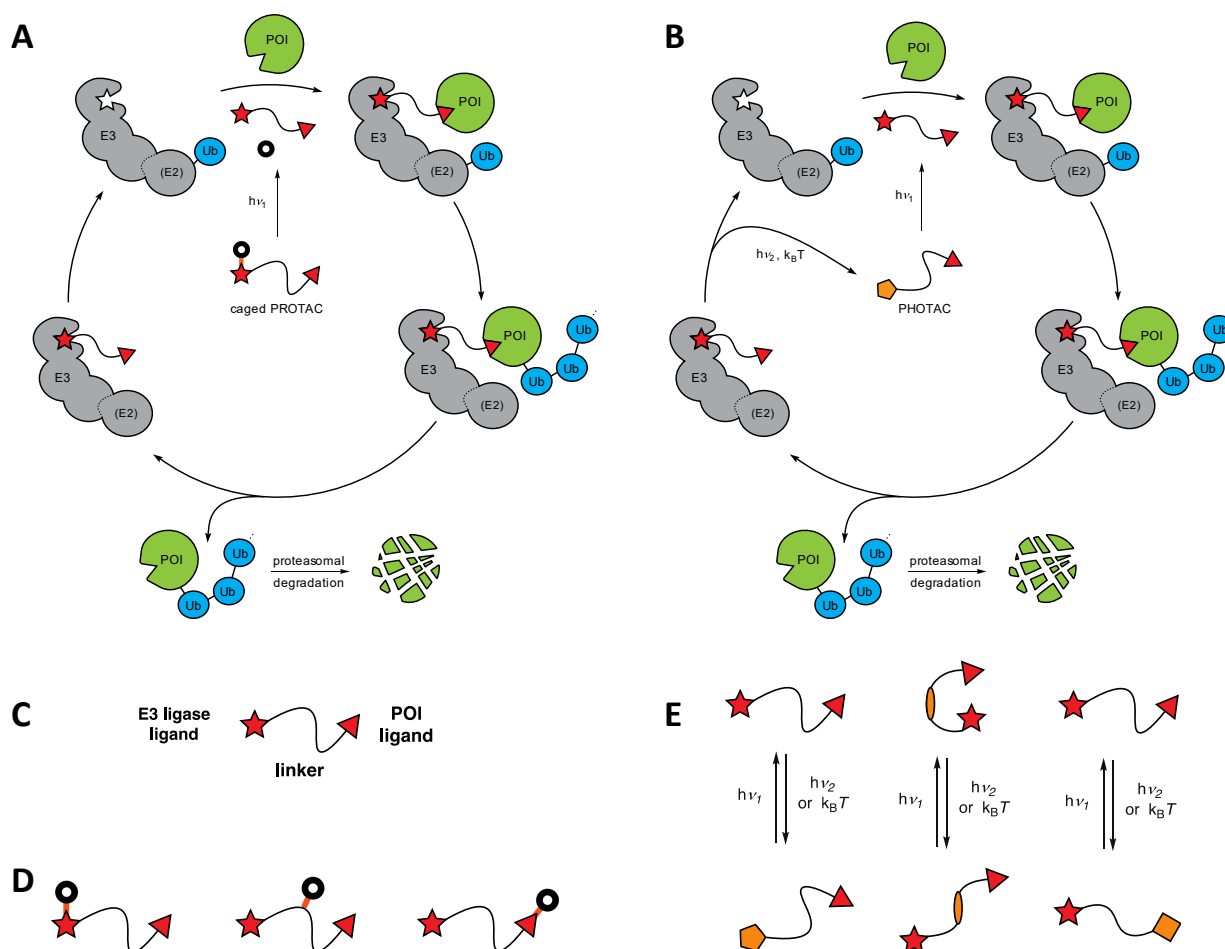


Figure 1. Photocaged and photoswitchable PROTACs. Schematic mechanism of A) a photocaged degrader, and B) a photoswitchable PROTAC (PHOTAC). C) Schematic representation of a PROTAC. D) Different modes of PPG attachment on a PROTAC. E) Strategies to incorporate a photoswitch into PROTACs.

Installing a PPG on the linker connecting both ligands of the bifunctional molecule could also be effective, since the linker is often involved in the formation a productive ternary complex.^[14] A molecule caged in this way, however, may still possess inhibitory activity on both ends and recruit unwanted targets for degradation. Finally, it is conceivable to install more than one PPG, but this approach necessitates efficient cleavage of the PPGs and would further increase the molecular weight, which potentially impairs cellular uptake.^[15]

In any case, efficient and clean photochemical release of the active PROTAC is crucial. Remaining caged compound resulting from incomplete deprotection or photochemical side products that still carry the ligands, could compete with the released PROTAC for ligase or POI binding and prevent formation of the ternary complex.

Photoswitches provide an alternative to PPGs and have been explored for PROTACs as well (Fig. 1B). A photoswitchable PROTAC should form a productive ternary complex in one state of the switch and induce target degradation but be inactive in the other state. Again, the photoswitch can be part of the ligand for the ubiquitin ligase, the linker, or the ligand targeting the POI. Of course, these boundaries are sometimes not clearly defined. Since the photoswitch is embedded in the molecule and not lost after photoactivation, this mode is more difficult to implement in existing PROTACs. On the other hand, no potentially toxic byproducts are formed, and the activation is made reversible, providing a "safety switch" for a powerful degrader and adding an extra level of control.

A photoswitchable ligand for the E3 ubiquitin ligase provides the most modular and general approach. Ideally, in most cases, the corresponding compound should be inactive in the dark and become active upon irradiation, as shown in Fig 1B. However, variants that are active in their dark-adapted form can be used as well, provided they are bistable and can be fully turned off through irradiation. There may also be scenarios where constitutive activity that can be turned off with light has advantages. Since the POI ligand is not directly affected, photoactivatable PROTACs with the switch on the ligase side are likely to retain inhibitory activity on the POI. Given the well documented importance of the linker in PROTACS ("linkerology"),^[16] the photoswitch could also be placed in this position. Again, inhibition of the POI (and of the ubiquitin ligase) in both forms of the photoswitch and the recruitment of neo-substrates or off-targets binding the photoswitch must be considered. The third mode, which has not yet been realized, involves the use of a photoswitchable ligand for the target protein. This design is less general but could circumvent POI inhibition provided the compound is inactive in the dark-adapted form. It benefits from the growing literature on photoswitchable ligands, which can have comparatively low affinity and still function as effective degraders in their active form.

For all three strategies (Fig. 1E), high isomer ratios of the photoswitch upon irradiation with an activating wavelength are desirable to prevent competitive inhibition of the ternary complex formation by the inactive isomer. Such high ratios can be often achieved with azobenzene photoswitches, where photostationary states (PSS)

exceeding $(Z):(E) = 9:1$ are not uncommon. In the opposite direction, PSS of $(Z):(E) = 2:8$ can usually be installed through irradiation with a longer wavelength.

Since the PSS is a function of the wavelength, the concentration of the active species can be reversibly tuned through the color with which the system is irradiated ("color-dosing"). In addition, azobenzene photoswitches thermally relax to their thermodynamically more stable isomer in the dark. The half-life of this process can be tailored by chemical substitution. Depending on the desired pharmacological properties, azobenzene photoswitches can be modified to isomerize within seconds or remain stable for days.

Photocaged Inducers of Targeted Protein Degradation

The first example of a photocaged small molecule that induces targeted protein degradation was reported by Gautier and colleagues.^[17] They installed a bulky version of the 4,5-dimethoxy-2-nitrobenzyl PPG on the plant hormone auxin, a natural molecular glue that promotes ternary complex formation between the SCF^{TIR1} ligase complex and members of the AUX/IAA family of transcription repressors.^[18] The authors further optimized the auxin inducible degron (AID) system, which allowed them to rapidly deplete AID-fusion proteins upon 365 nm or 405 nm irradiation after treatment with **PA-IAA** (Table 1, Entry 8). A potential limitation of this approach is the need for heterologous expression of TIR1 and AID-fusion proteins.

Recently, several groups have reported the successful generation of caged PROTACs to induce the degradation of native target proteins upon light irradiation.^[19–22] Deiters and colleagues developed photocaged molecules that engage the cereblon (CRBN) E3 ubiquitin ligases complex.^[20] Protection of a pomalidomide-derived PROTAC of the former category was achieved through installation of a 6-nitropiperonyloxymethyl group on the nitrogen atom of the glutarimide. Substitution of the glutarimide had previously been shown to abolish PROTAC function.^[23] The authors used JQ1 to target the epigenetic reader proteins BRD2-4 and the resulting photocaged PROTAC (**compound 4**, Table 1, Entry 2) could be activated by 365 nm irradiation to obtain the free PROTAC (Fig. 2H). While inactive in the dark, **compound 4** was shown to degrade BRD4 and a GFP-BRD4 fusion protein in HEK293T cells after a 180 s of UV-irradiation (Fig. 2I). Further, a change of 22Rv1 cell viability was demonstrated after treatment for 72 h. Without UV-activation, the caged PROTAC only slightly reduced growth, but a 39% decrease in viability was observed after 365 nm irradiation for 180 s. In comparison, the unprotected parent PROTAC led to a 51% reduction in viability. The activity difference might be a result of incomplete photoactivation.

In parallel, Pan, Zhong and colleagues^[22] developed photoactivatable PROTACs derived from the known BRD2-4 degrader dBET1.^[24] They explored two different attachment points for the PPG, either on the glutarimide nitrogen to block CRBN binding or on the amide connecting JQ1 to the linker. Installation of a 4,5-dimethoxy-2-nitrobenzyl group on the amide bond to JQ1 gave **pc-PROTAC1** (Table 1, Entry 5), which could be converted to dBET1 upon 365 nm irradiation (Fig. 2A). Introduction of

the PPG reduced binding affinity to the first bromodomain of BRD4 more than 100-fold. While inactive in the dark, the compound was shown to efficiently degrade BRD4 in Ramos cells after 3 min of 365 nm irradiation. The potency was slightly reduced compared to dBET1, as expected from an incomplete photolysis. The antiproliferative effect of activated **pc-PROTAC1** ($GI_{50} = 0.4 \mu\text{M}$) was very similar to dBET1 ($GI_{50} = 0.31 \mu\text{M}$) in Namalwa cells, whereas the unprotected form was significantly less potent ($GI_{50} = 3.1 \mu\text{M}$) (Fig. 2B). Residual activity in the absence of irradiation could be a result of inhibition or recruitment and degradation of off-targets, with the 4,5-dimethoxy-2-nitrobenzyl group as ligand.

Pan, Zhong and colleagues further applied **pc-PROTAC1** to zebrafish to study induced BRD4 degradation during embryogenesis. Strikingly, embryos treated with **pc-PROTAC1** plus 10 min of UV irradiation recapitulated the phenotypic reduction in yolk extension seen with dBET1, whereas the non-irradiated **pc-PROTAC1** mimicked the DMSO control (Fig. 2C). The *in vivo* efficacy of irradiated compound was further demonstrated by Western blotting (Fig. 2D) and degradation of EGFP tagged BRD4. In a second approach to render the glutarimide photoactivatable, they installed a 4,5-dimethoxy-2-nitrobenzyl carbamate to create **pc-PROTAC2** (Table 1, Entry 4). However, photolysis upon 365 nm irradiation did not yield a useful product and this compound was not pursued further. Next, Pan, Zhong and colleagues successfully installed the 4,5-dimethoxy-2-nitrobenzyl carbamate on the glutarimide of the BTK degrader MT-802 developed by the Crews group.^[25] Upon 365 nm irradiation, the resulting **pc-PROTAC3** (Table 1, Entry 6) photolyzed into MT-802 and degraded BTK in Ramos cells, while remaining inactive without irradiation.

In similar work, Wei, Jin, and colleagues prepared light-activatable PROTACs by installing a PPG onto the glutarimide nitrogen of pomalidomide-based degraders that engage CRBN.^[19] Initially, they prepared a photocaged version of the molecular glue pomalidomide itself. **Opto-pomalidomide** (Table 1, Entry 7) was synthesized in one step from pomalidomide and 4,5-Dimethoxy-2-nitrobenzyl chloroformate and was photolyzed with 365 nm irradiation (Fig. 2E).

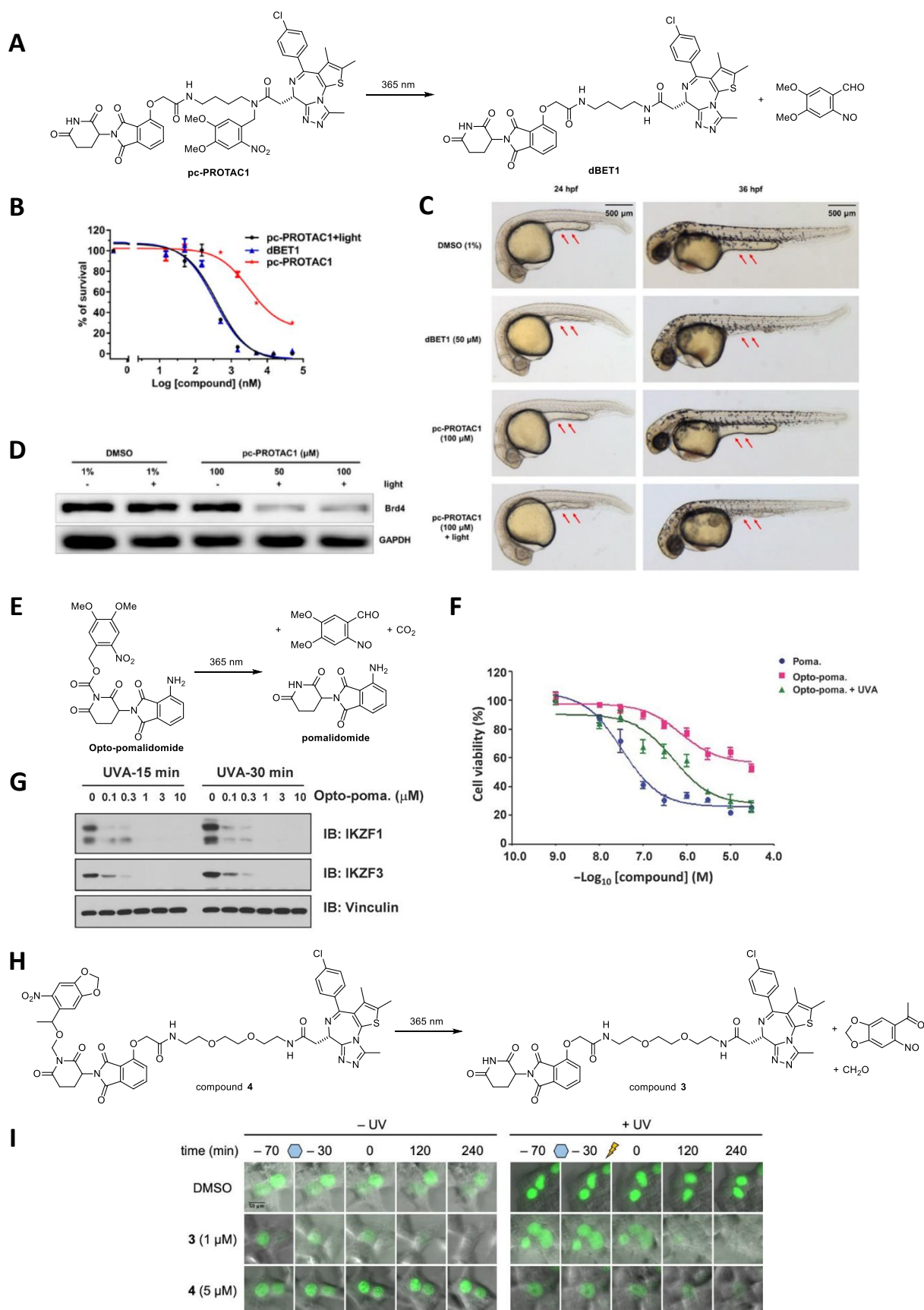


Figure 2. Photocaged degraders recruiting proteins to the E3 ubiquitin ligase CRBN. A) UV-induced activation of **pcPROTAC-1**. B) Viability of Namalwa cells treated with **pcPROTAC-1** for 73 h. Figure adapted with permission from [22] Copyright 2019 American Chemical Society. C) Reduced yolk extension of zebrafish embryos treated

with dBET1 or **pc-PROTAC-1** and UV irradiation. Figure adapted with permission from [22] Copyright 2019 American Chemical Society. D) Immunoblot of BRD4 levels in zebrafish embryos after **pc-PROTAC-1** treatment. Figure adapted with permission from [22] Copyright 2019 American Chemical Society. E) Photolysis of **Opto-pomalidomide**. F) MM.1S cell viability after pomalidomide or **Opto-pomalidomide** treatment. G). Immunoblot analysis of MM.1S cells treated with **Opto-pomalidomide** and UV-A irradiation. Figures 2F and 2G adapted from [19] Copyright 2020 The Authors, some rights reserved; exclusive licensee AAAS. Distributed under a Creative Commons Attribution NonCommercial License 4.0 (CC BY-NC) <http://creativecommons.org/licenses/by-nc/4.0/>. H) Photolysis of **compound 4** to yield the active PROTAC. I) Fluorescence imaging of GFP-BRD4 degradation in HEK293T cells. Figure adapted with permission from [20] Copyright 2020 American Chemical Society.

Opto-pomalidomide showed enhanced degradation of IKZF1 and IKZF3 with increased irradiation time (Fig. 2G). Interestingly, MM.1S cell viability was slightly reduced in the dark, even though on target activity and ternary complex formation should be blocked entirely. However, cytotoxicity of **Opto-pomalidomide** in multiple myeloma cells was strongly increased after UV-A irradiation, recreating the effect of pomalidomide at high concentrations (Fig. 2F).

Based on the results for the photocaged CRBN ligand, they subsequently prepared **Opto-dBET1** (Table 1, Entry 3) by protecting the imide of dBET1 as a 4,5-dimethoxy-2-nitrobenzyl carbamate. Photolysis using 365 nm irradiation yielded dBET1, albeit conversion proceeded at a moderate rate with a half-life of 58 minutes. Nevertheless, inactive **Opto-dBET1** was sufficiently photoactivated to degrade BRD3 and BRD4 in HEK293FT cells in a CRBN-dependent manner. **Opto-dBET1** led to a small reduction of HEK293FT cell viability in the dark which can be explained by BRD2-4 inhibition. When activated by UV-A irradiation, its toxicity significantly increased but failed to match the viability effect of pure dBET1.

Note that **opto-dBET1**, which incorporates the same hydroxy phthalimide as dBET1, and **pc-PROTAC3**, which features a 4-amino phthalimide moiety, were successful, whereas **pc-PROTAC2**, which features a 3-amino phthalimide moiety, was not. This underscores that small differences in the substitution pattern of a caged compound can have a pronounced effect on the photochemistry.

Expanding beyond BRD2-4 as target proteins, Wei, Jin, and co-workers were also able to demonstrate the generality of this approach by degrading ALK-fusion proteins in a light-dependent fashion using **Opto-dALK** (Table 1, Entry 1). Interestingly, this compound again features a 3-amino phthalimide moiety, albeit with a very different POI ligand.

In addition to their CRBN-based degrader, Deiters and coworkers developed a diethylamino coumarin protected PROTAC that engages E3 ubiquitin ligases featuring the von Hippel-Lindau disease tumor suppressor (VHL).^[20] On the POI side, this molecule, termed **compound 2** (Table 1, Entry 9), was designed to recruit estrogen-related receptor α (ERR α). Based on the importance of the hydroxyproline for VHL binding, installment of a PGG on the hydroxy group should render the PROTAC inactive. Photolysis to release the active degrader could be achieved with 365 or 405 nm irradiation. ERR α degradation in MCF-7 cells was not observed in the dark, but was observed after UV-irradiation. However, the photocaged **compound 2** was applied at higher concentrations than the parent PROTAC, indicating incomplete photoactivation or reduced cellular uptake.

Tate and colleagues achieved light-controlled activation of a VHL-based PROTAC targeting BRD4 and EGFP-BRD4 fusion proteins.^[21] They also identified the hydroxyproline as crucial and installed a 4,5-dimethoxy-2-nitrobenzyl PPG yielding **PROTAC 3** (Table 1, Entry 10). Irradiation with 365 nm light gave the uncaged PROTAC in high yields (Fig 3A), which was shown to degrade BRD4 in HeLa cells. While BRD4 degradation was not observed for the photocaged compound, it strongly affected viability at 1 μ M due to inhibition (Fig. 3B), which was confirmed by a cellular thermal shift assay. Activity was retained after a repeated change of the medium, confirming that **PROTAC 3** is efficiently taken up by cells and not easily washed out, and that the remaining catalytic activity is sufficient to induce degradation. The authors further demonstrated degradation of GFP-BRD4 using **PROTAC 3** in HEK293 cells (Fig. 3C).

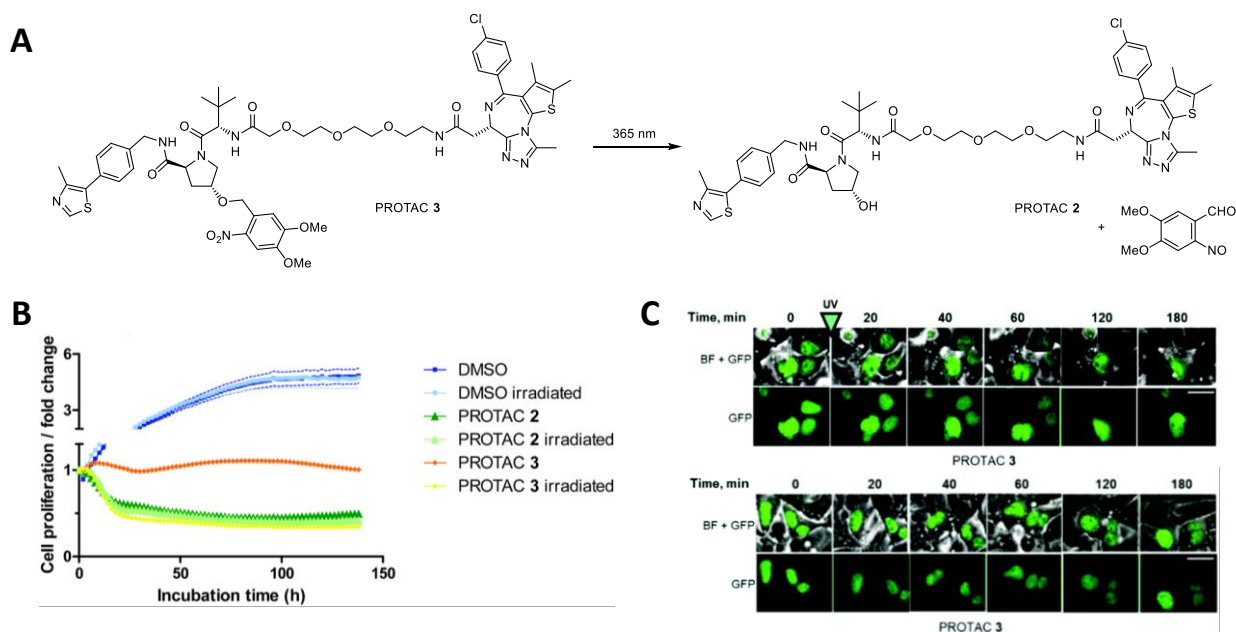


Figure 3. Light-activatable PROTAC binding the von Hippel-Lindau disease tumor suppressor protein (VHL). A) UV-induced activation of **PROTAC 3**. B) Proliferation of HeLa cells treated with DMSO or PROTACs (1 μ M). C) Fluorescence imaging of GFP-BRD4 in **PROTAC 3** (1 μ M) treated HEK2993 cells with or without UV-induced activation. Figures adapted from [21] Reproduced by permission of The Royal Society of Chemistry, Copyright The Authors, some rights reserved. Distributed under a Creative Commons Attribution License 3.0 (CC BY-NC 3.0) <https://creativecommons.org/licenses/by-nc/3.0/>.

Photoswitchable PROTACs

Photocaged PROTACS have proven to be highly effective, but the irreversible activation of a catalytically active molecule is a potential limitation of the PPG approaches. Their inactivation depends on dilution (washout) or metabolism. To impart reversibility, photoswitchable PROTACs based on the azobenzene (*E*)/(*Z*)-isomerization have been explored.[26–28] These photoswitches are either more active as the thermodynamically more stable (*E*)-isomer (Azo-PROTAC4C, photoPROTAC-1) or as the metastable (*Z*)-isomer (PHOTACs).

Jiang, You, and colleagues set out to develop Azo-PROTACs by attaching an azobenzene directly to the phthalimide nitrogen as an amide.[26] They prepared a small series of PROTACs with different linker length connecting the azobenzene derivative to a dasatinib-derived ligand for Abl and BCR-Abl fusions. Out of this series, **Azo-PROTAC 4C** (Table 2, Entry 1) was selected as lead compound due to its ability to degrade Abl and BCR-Abl in the dark. Notably, UV-C irradiation was chosen to convert

Azo-PROTAC 4C into its metastable (*Z*)-isomer (Fig. 4A). Target protein degradation was determined by immunoblotting and (*E*)-**Azo-PROTAC 4C** used at 250 nM was shown to robustly degrade Abl and BCR-Abl over a time course of 48 h in K562 cells, whereas no degradation was observed for (*Z*)-**Azo-PROTAC 4C** for up to 32 h. This is surprising given the reported half-life of 620 min at 25 °C. Substantial amounts of the (*E*)-isomer should be present at earlier timepoints. Further, no concentrations higher than 500 nM were tested for **Azo-PROTAC 4C** which would help to clarify if a “hook effect” due to saturation of both binding partners or remaining activity of (*Z*)-**Azo-PROTAC 4C** could be observed. To demonstrate a light-induced recovery of BCR-Abl levels, K562 cells were treated with *E*-**Azo-PROTAC 4C** for 24 h to degrade BCR-Abl and then subjected to UV irradiation every 4 h. BCR-Abl and Abl levels recovered when subjected to UV irradiation, whereas white light treatment kept protein levels low (Fig. 4B). Unfortunately, viability was not assessed with the (*Z*)-isomer of **Azo-PROTAC 4C**.

Carreira, Crews, and colleagues designed **photoPROTAC-1** (Table 2, Entry 11) using an *ortho*-tetrafluoroazobenzene to connect a VHL binder with a ligand for BET proteins.^[27] The thermal relaxation of this type of azobenzene is very slow, making them essentially bistable. The (*E*)-to-(*Z*) isomerization could be achieved with 530 nm irradiation, generating 68% (*Z*)-**photoPROTAC-1** (Fig. 4C). The reverse (*Z*)-to-(*E*) isomerization can be induced with 415 nm irradiation generating 95% (*E*)-**photoPROTAC-1**. The mixture containing 95% (*E*)-**photoPROTAC-1** induced the degradation of BRD2, but not BRD4, in Ramos cells after 18 h, whereas the mixture containing 68% (*Z*)-**photoPROTAC-1** did not show any strong degradation up to a concentration of 1 μM (Fig. 4D). Interestingly, a sample left under daylight, which contains 65% (*E*)-**photoPROTAC-1**, did not induce efficient degradation of BRD2. Since the hook effect was not observed for **photoPROTAC-1**, the authors hypothesized that the inactive (*Z*)-isomer has such a high affinity to either BRD2 or VHL that it outcompetes binding of the active (*E*)-isomer.

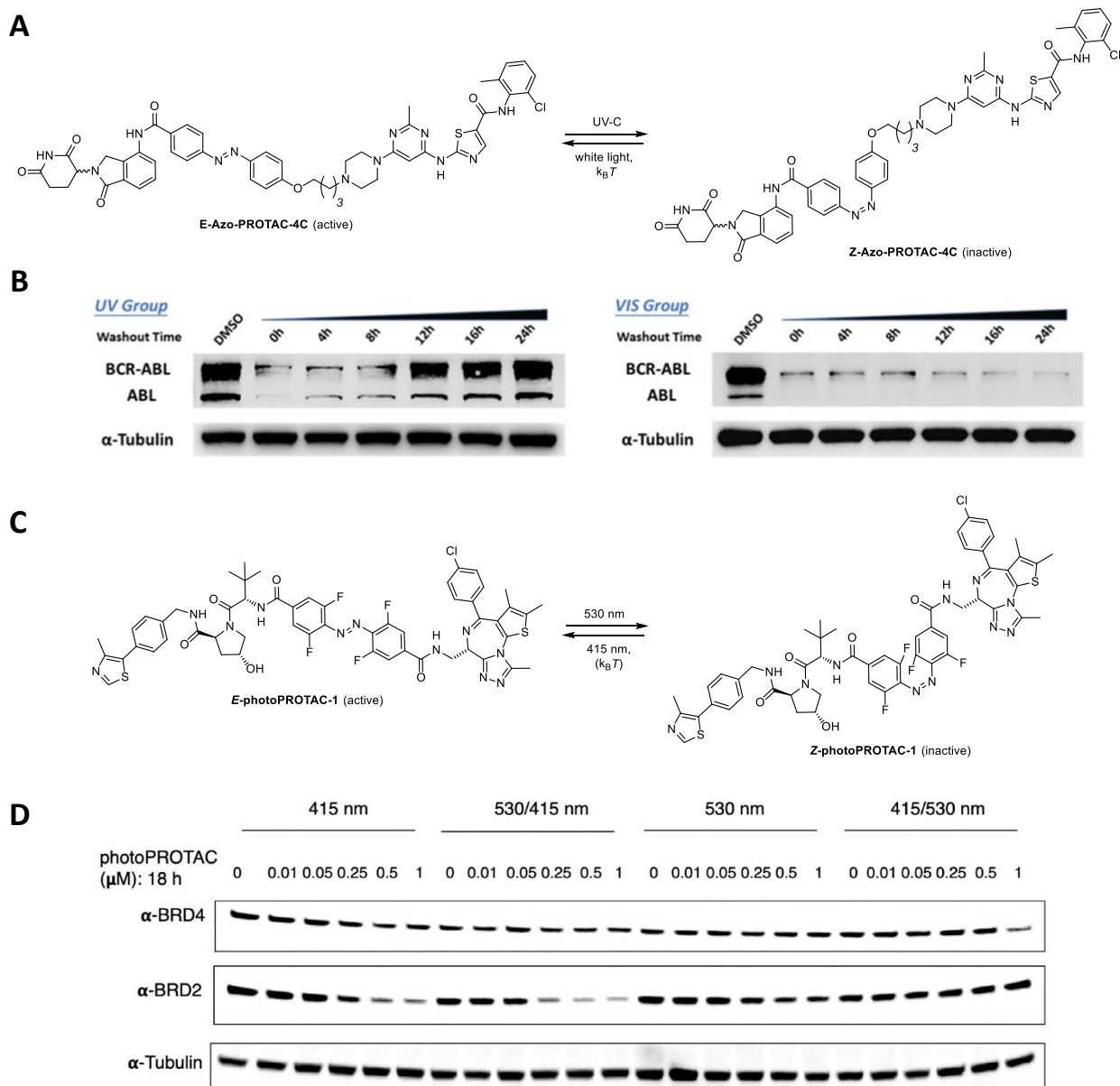


Figure 4. Photoswitchable PROTACs active as the (*E*)-isomer. A) (*E*)/(*Z*)-isomerization of **Azo-PROTAC-4C**. B) Western Blot of K562 cells treated with **Azo-PROTAC-4C** for 24 h and either exposed to UV irradiation every 4 h or exposed to white light. Figure adapted with permission from [26] Copyright 2020 American Chemical Society. C) (*E*)/(*Z*)-isomerization of **photoPROTAC-1**. D) Western blot of Ramos cells treated with **PhotoPROTAC-1** that was either preirradiated once with 415 or 530 nm light or twice (530 then 415 nm and 415 then 530 nm). Figure adapted with permission from [27] (<https://pubs.acs.org/doi/10.1021/acscentsci.9b00713>), Copyright 2019 American Chemical Society.

Trauner, Pagano, and colleagues introduced photoswitchable degraders that rely on CRBN and are inactive in the dark.^[28] These molecules, termed **PHOTACs**, become active degraders only after irradiation to form their (*Z*)-isomer and slowly relax to their

inactive (*E*)-form. The azobenzene was incorporated as an extension of lenalidomide to control the engagement of the CRBN E3 ubiquitin ligase complex and ternary complex formation. This molecular architecture kept the molecular weight low and made **PHOTACs** highly modular. The placement of the switch was also motivated by the efficiency of the synthesis, which started from lenalidomide and involved diazotization of the aniline, followed by azo coupling.

PHOTAC-I-3 (Table 2, Entry 3) emerged as lead compound targeting BRD2-4 from a small series of molecules featuring a variety of linkers and aryl substitutions (**PHOTAC-I-1–8**). **PHOTAC-I-3** undergoes efficient (*E*)-to-(*Z*) isomerization between 370 and 450 nm and thermally relaxes back to the (*E*)-isomer with a half-life of 8.8 h in DMSO. Alternatively, the equilibrium can be shifted to favor the (*E*)-isomer by irradiation with wavelengths larger than 500 nm (Fig. 5A). Quantitative (*Z*)-to-(*E*) isomerization is not possible with irradiation alone at longer wavelengths and can only be achieved through thermal relaxation.

The highest amount of the (*Z*)-isomer was generated through 390 nm irradiation and this wavelength was used for the characterization in RS4;11 cells. Irradiation in the absence of the compounds showed no observable effects at the intensity used. After 4 h of treatment, strong degradation of BRD2, BRD3 and BRD4 was observed in the low micromolar to high nanomolar range when irradiated with 390 nm light, but no visible degradation was seen in the dark. A hook effect was observed in the form of reduced degradation at 10 μ M indicating a mechanism dependent on ternary complex formation (Fig. 5B). Further, cotreatment with the neddylation inhibitor MLN4924 rescued protein levels in cell treated with 1 μ M **PHOTAC-I-3** and 390 nm pulse irradiation, demonstrating a dependence on Cullin-RING ubiquitin ligases. Other controls, such as co-treatment with JQ1 or lenalidomide to rescue BRD4 levels and siRNA-mediated CRBN knockdown, further confirmed that **PHOTAC-I-3** acts as a PROTAC.

RS4;11 cells treated with 1 μ M **PHOTAC-I-3** were monitored over 24 h to ensure that no degradation could be observed in the dark (Fig. 5C). Importantly, (*Z*)-**PHOTAC-I-3** led to downregulation of c-MYC levels and a slow cleavage of PARP1 after 12 h indicating the induction of apoptosis. However partial downregulation of c-MYC levels were also observed in the dark control. This is most likely a consequence of BET

protein inhibition, since the PROTAC was not designed to have a strong effect on BET protein binding upon photoisomerization. This effect was also confirmed when assessing the viability of RS4;11 cells after 72 h of PHOTAC treatment (Fig. 5D). While the strongest effect was observed with pulsed irradiation generating the highest amount of (*Z*)-isomer, **PHOTAC-I-3** still led to a decrease in viability in the dark, albeit with less potency than JQ1.

Trauner, Pagano, and colleagues additionally explored other designs for the incorporation of the azobenzene (**PHOTAC-I-9–13**) of which **PHOTAC-I-10** (Table 2, Entry 6) showed a strongly increased degradation of BRD4 upon 390 nm irradiation. The same strong effect was also observed for RS4;11 viability. Interestingly, all designs that were investigated demonstrated either similar levels of BRD4 degradation as (*E*)- and (*Z*)-isomers or were more potent as the (*Z*)-isomer, but none showed a much stronger effect as the dark-adapted (*E*)-isomer.

To demonstrate the generality of their CRBN-based approach, Trauner, Pagano, and colleagues combined their photoswitches with ligands for FKBP12. A stronger dependence on linker length was observed for the series of **PHOTAC-II-1–5**. **PHOTAC-II-5** (Table 2, Entry 9) only induced the degradation of FKBP12 after 390 nm irradiation but not in the absence of light (Fig. 5F+G). **PHOTAC-II-6** (Table 2, Entry 10) was also able to recapitulate the strong increase in target degradation upon isomerization to the (*Z*)-isomer, albeit a small activity of the (*E*)-isomer remained.

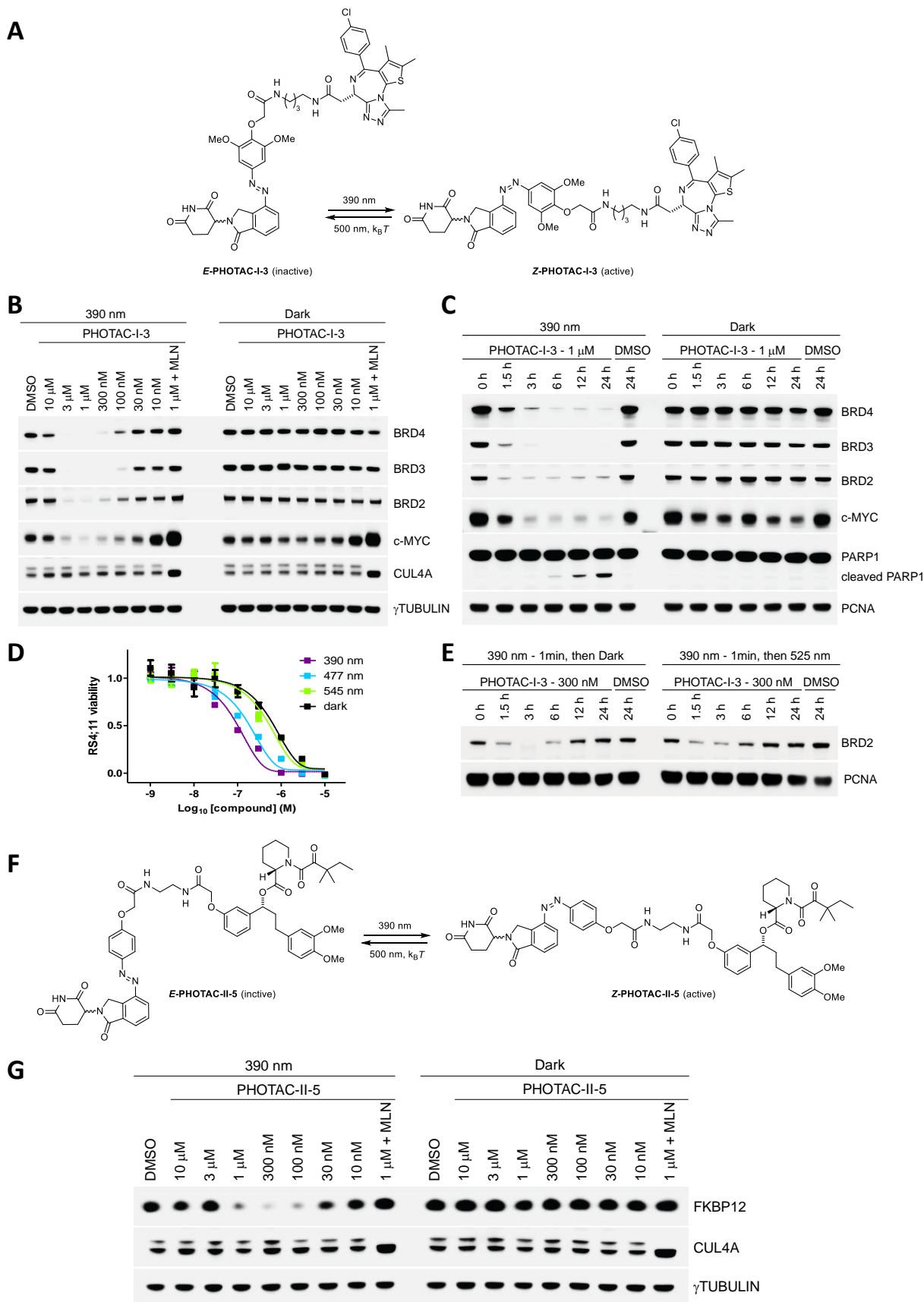


Figure 5. Photoswitchable PROTACs active as the (*Z*)-isomer. A) (*E*)/(*Z*)-isomerization of **PHOTAC-I-3**. B) Immunoblot analysis of RS4;11 cells treated with **PHOTAC-I-3** for 4 h and either irradiated with 390 nm pulses (left) or kept in the dark (right). MLN (MLN4924) was added as an additional control. C) Target protein degradation by

PHOTAC-I-3 (1 μ M) treatment in RS4;11 cells collected at the indicated time points. D) RS4;11 cell viability after 72 h **PHOTAC-I-3** treatment in the dark or under pulsed 390, 477, or 545 nm irradiation. E) RS4;11 immunoblot demonstrating the reversibility of BRD2-degradation by **PHOTAC-I-3** through thermal relaxation (left) or optical inactivation using pulsed 525 nm irradiation. F) (*E*)/(*Z*)-isomerization of **PHOTAC-II-5**. G) Immunoblot analysis of FKBP12 levels in RS4;11 cells treated with **PHOTAC-II-5** for 4 h and either irradiated with of 390 nm pulses (left) or kept in the dark (right). Figures adapted with permission from [28] Copyright 2020 The Authors, some rights reserved; exclusive licensee AAAS. Distributed under a Creative Commons Attribution License 4.0 (CC BY).

An advantage of photoswitches over photocages is their reversibility. To demonstrate this, **PHOTAC-I-3** was irradiated with 390 nm light for 60 seconds in RS4;11 cells to be converted into the active (*Z*)-isomer. Following this, cells were either left in the dark or subjected to 525 nm irradiation and protein levels were monitored over time (Fig. 5E). BRD2 levels initially decreased as a result of degradation by the active isomer, but subsequently returned to base level. Notably, the recovery was faster when (*Z*)-to-(*E*) isomerization was induced by 525 nm irradiation compared to thermal relaxation in the dark. This demonstrates that **PHOTACs** can be “wound-up” to exert their activity for a controlled period of time. The degree of degradation can further be tuned by the color of incident light, as it determines the ratio between active and inactive isomer in the PSS (“colordosing”).

Conclusion and Future Directions

Photocaged and photoswitched PROTACs represent an exciting addition to the chemical toolbox for manipulating cellular function and a new direction in photopharmacology. They combine the ability of PROTACs to remove a target protein with all its functions with the exquisite spatiotemporal precision control that light affords. As such, they have the potential to be used to temporarily knock out proteins in specific cells, complementing methods that operate at the transcriptional level. They could be used, for instance, in neuroscience to answer questions regarding the formation and consolidation of memories. Whereas the impact of protein synthesis inhibitors on memory is well documented,^[29,30] the effect of degraders that can be activated in a particular location and at a given time has not yet been explored. Photoswitchable PROTACs could also be useful for shaping the oscillation of protein levels that underlie important biological processes, such as the circadian rhythm.

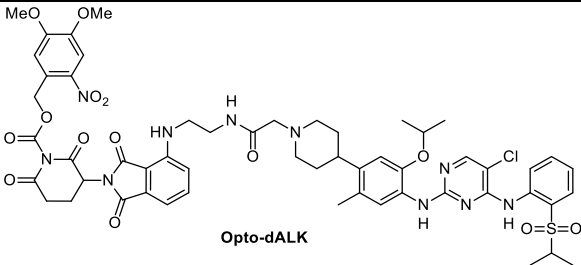
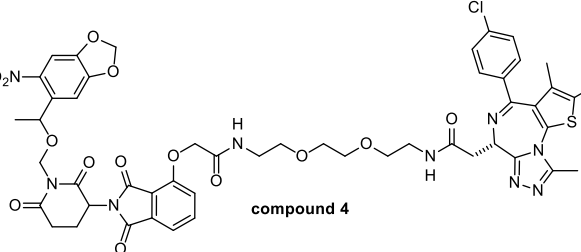
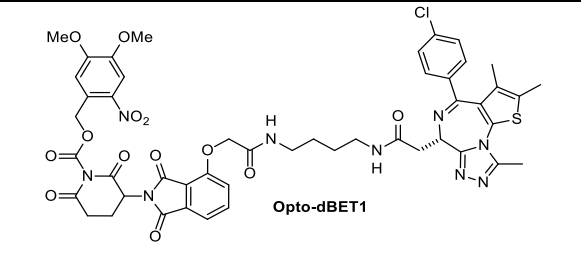
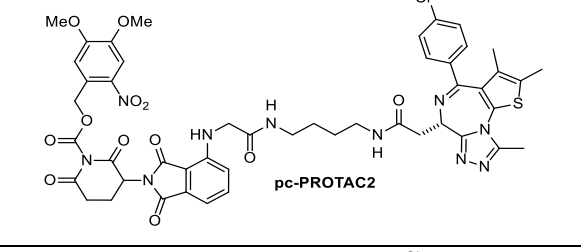
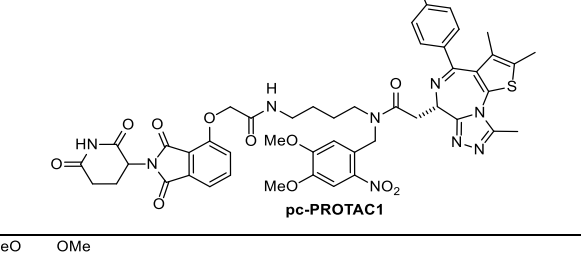
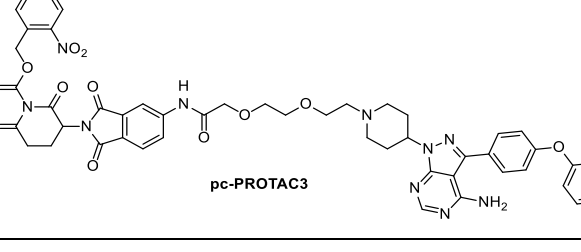
Apart from their value as research tools, light-controlled PROTACs could find a role in precision medicine. Activation in a specific tissue or lesion avoids the side-effects associated with systemic administration. PROTACs operate with a catalytic mechanism of action and potential toxicities are a concern.^[31–33] Locally activated PHOTACs could exert their activity in proximity to the light source, but would lose activity by the combined effects of diffusion and thermal relaxation. This strategy could make new targets amendable to PROTACs where only local activation can mitigate adverse events. Building on the success of photodynamic therapy, light-controlled PROTACs have the potential to expand the options in photomedicine. They would certainly benefit from the recent development of implantable LEDs for localized irradiation and optofluidic systems that combine drug delivery and irradiation.^[34–37]

While the initial results with light-activated degraders are promising, there is still much room for improvement. For instance, the use of UV or violet light to activate the degraders is incompatible with applications that require deep tissue penetration. At the current stage, these wavelengths limit clinical application to surface exposed diseases such as skin cancer or blood cancers that can be subjected to photopheresis.^[38] An important goal therefore, is the development of PPG and photoswitches with red-shifted absorption spectra that operate in the biooptical window.^[39,40] Several new PPGs have been recently developed that undergo photolysis using visible light with wavelength >500 nm.^[8,41–45] Similarly, photoswitches operating with short wavelengths could be replaced with red-shifted versions. For azobenzenes, the most common modification is the introduction of substituents on *ortho* position to the diazene. The resultant switches can undergo (*E*)-to-(*Z*)-isomerization with wavelengths >500 nm.^[46–52] In addition to red-shifting the absorption spectra, efforts have been made to render both azobenzenes and PPGs sensitive to two-photon irradiation in the near-infrared region (NIR).^[53–55] Another promising strategy relying on NIR irradiation is the use of upconverting nanoparticles or hydrogels. These absorb NIR photons and convert them into blue light that could be used to photolyze PPGs and isomerize photoswitches.^[56–58] Other external stimuli such as temperature, magnetic fields or ultrasonic sound could also be used to control the activity of PROTACs in theory, if responsive chemical moieties can be incorporated into the degraders.

Many additional modes can be considered in addition to those discussed above. For instance, photoswitchable molecular glues could be explored as a counterpart to the caged versions (**opto-pomalidomide** or **PA-IAA**). Light-cleavable linkers that promote protein dimerization could be adapted to create PROTACs that are irreversibly destroyed with light.^[59–62] The optical control of protein degradation could be extended to E3 ubiquitin ligases beyond those containing CRBN and VHL, such as DCAF15^[63], DCAF16 (Zhang et al., 2019), RNF4^[65] and RNF114^[66]. Ligands have been identified for these enzymes that could be caged or equipped with photoswitches. In addition, IAP-dependent protein erasers (SNIPERs)^[67] could be adapted for the optical control of protein degradation.

Photocaged and photoswitchable PROTACs must also be seen in the context of optogenetic approaches towards protein degradation. These involve fusion with a photoreceptor protein, such as the light-oxygen-voltage (LOV) domain, that masks a degron in a light-dependent fashion.^[68–72] However, such photosensitive domains are relatively large and background activity in the dark is a concern. Genetic tagging could be merged with photoactivatable PROTACs through adaptation of the dTAG and HaloPROTAC technologies.^[73–75] These involve the genetic fusion of target proteins with an FKBP12^{F36V} domain or HaloTag, respectively, which can then function as a handle for PROTAC engagement, ternary complex formation, ubiquitylation, and eventual degradation of the entire fusion protein. The optical degradation of proteins tagged in such a way and expressed in specific cells or tissues could provide a new dimension to optogenetics.

Table 1: Photocaged molecules that induce target protein degradation.

Entry	E3 Ligase	Target Protein	Structure	Activation wave-length	Ref
1	CRBN	ALK-fusion proteins (EML4-ALK, NMP-ALK)	 <p style="text-align: center;">Opto-dALK</p>	365 nm	[19]
2	CRBN	BRD4, GFP-BRD4	 <p style="text-align: center;">compound 4</p>	365 nm	[20]
3	CRBN	BRD3, BRD4, GFP-BRD2, GFP-BRD3	 <p style="text-align: center;">Opto-dBET1</p>	365 nm	[19]
4	CRBN	-	 <p style="text-align: center;">pc-PROTAC2</p>	365 nm	[22]
5	CRBN	BRD4, EGFP-BRD4	 <p style="text-align: center;">pc-PROTAC1</p>	365 nm	[22]
6	CRBN	BTK	 <p style="text-align: center;">pc-PROTAC3</p>	365 nm	[22]

1 – Optical Control of Targeted Protein Degradation

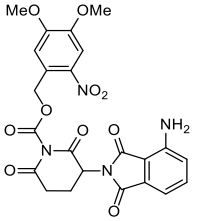
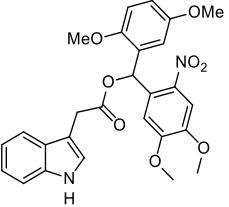
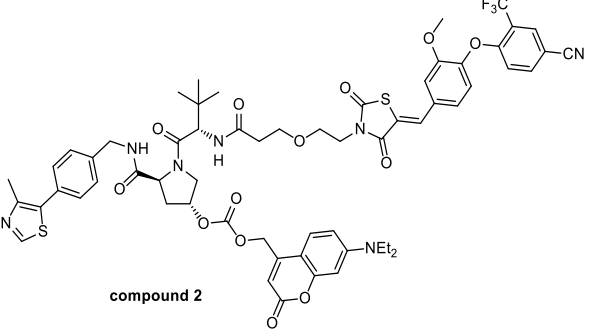
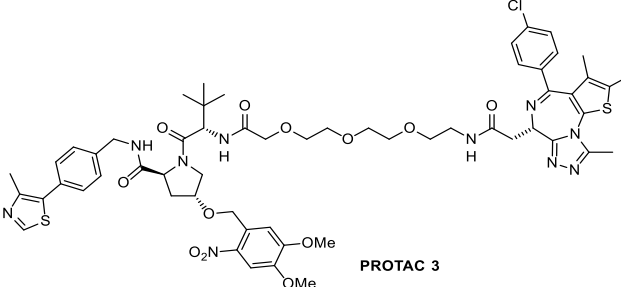
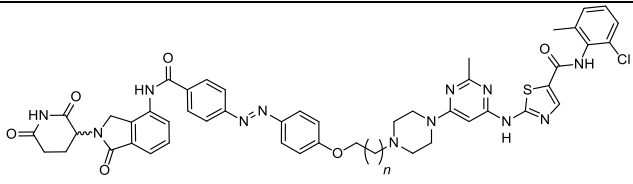
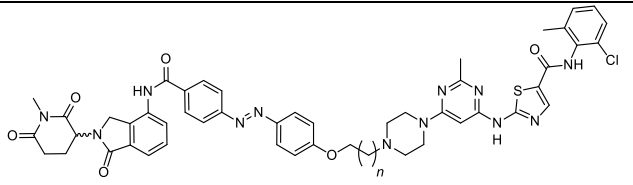
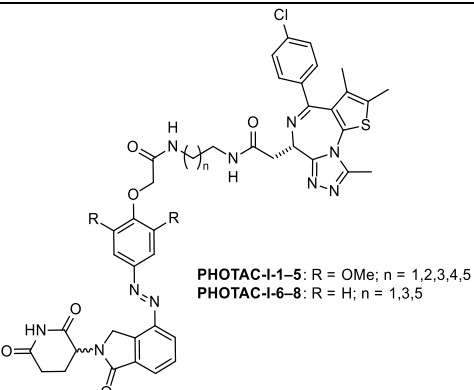
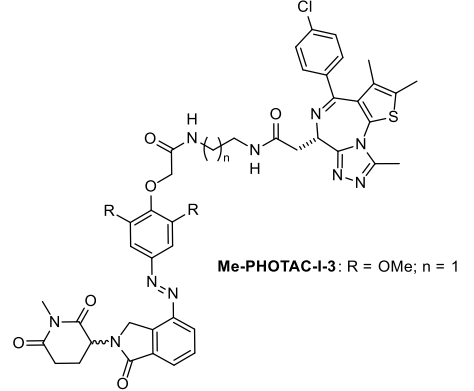
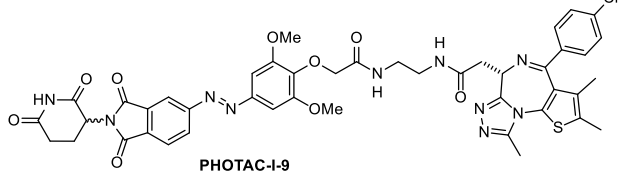
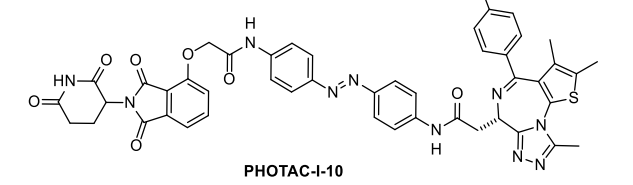
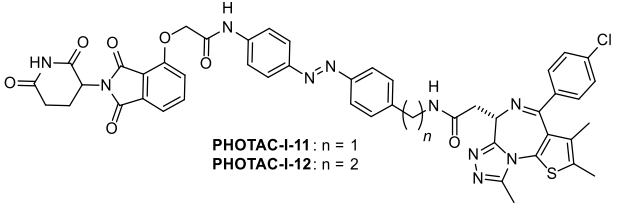
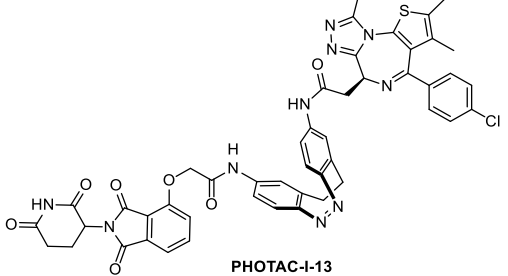
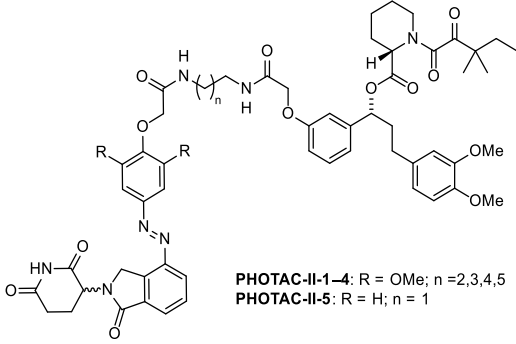
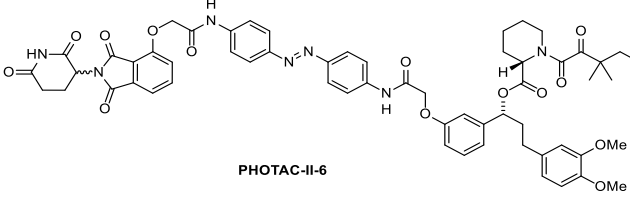
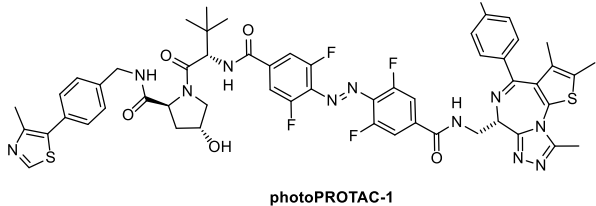
7	CRBN	IKZF1, IKZF3	 <p>Opto-pomalidomide</p>	365 nm	[19]
8	TIR1	AID-fusion proteins (EGFP-AID- NLS, CyclinB1- AID-YFP)	 <p>PA-IAA</p>	365 nm, 405 nm	[17]
9	VHL	ERR α	 <p>compound 2</p>	365 nm, 405 nm	[20]
10	VHL	BRD4, EGFP- BRD4	 <p>PROTAC 3</p>	365 nm	[21]

Table 2: Targets, structures, and properties of photoswitchable PROTACs.

Entry	E3 Ligase	Target Protein	Structure	Activation wave-length	Deactivation wave-length
1	CRBN	ABL, BCR-ABL	 <p>Azo-PROTAC-2C-6C n=1-5</p>	white light, k _B T	UV-C
2	CRBN	-	 <p>Azo-PROTAC-4C (-)</p>	N/A	N/A
3	CRBN	BRD2, BRD3, BRD4	 <p>PHOTAC-I-1-5: R = OMe; n = 1,2,3,4,5 PHOTAC-I-6-8: R = H; n = 1,3,5</p>	370 - 420 nm R=H, 370 - 450 nm R=OMe	>500 nm, k _B T
4	CRBN	-	 <p>Me-PHOTAC-I-3: R = OMe; n = 1</p>	N/A	N/A
5	CRBN	BRD2, BRD3, BRD4	 <p>PHOTAC-I-9</p>	390 nm	>500 nm, k _B T
6	CRBN	BRD2, BRD3, BRD4	 <p>PHOTAC-I-10</p>	390 nm	>500 nm, k _B T

1 – Optical Control of Targeted Protein Degradation

7	CRBN	BRD2, BRD3, BRD4	 <p>PHOTAC-I-11: n = 1 PHOTAC-I-12: n = 2</p>	390 nm	>500 nm, k _B T
8	CRBN	BRD2, BRD3, BRD4	 <p>PHOTAC-I-13</p>	390 nm	>500 nm, k _B T
9	CRBN	FKBP12	 <p>PHOTAC-II-4: R = OMe; n = 2,3,4,5 PHOTAC-II-5: R = H; n = 1</p>	370 - 420 nm R=H, 370 - 450 nm R=OMe	>500 nm, k _B T
10	CRBN	FKBP12	 <p>PHOTAC-II-6</p>	380-450 nm	>500 nm, k _B T
11	VHL	BRD2	 <p>photoPROTAC-1</p>	415 nm, k _B T	530 nm

Significance

The development of light-controlled degraders based on proteolysis targeting chimeras is an exciting direction in chemical optogenetics and photomedicine. Controlling targeted protein degradation with photoresponsive bifunctional molecules allows the precise spatiotemporal modulation of protein abundance in native systems. This can be used to induce oscillations of proteins levels and study the functional consequences. In photomedicine, light-activated PROTACs could provide a safety advantage over conventional PROTACs and could be applied to treat localized diseases. Further development of light-controlled PROTACs based on the design principles summarized herein is a promising direction in photopharmacology.

Acknowledgements

We thank New York University for financial support.

We acknowledge Christopher J. Arp and Tongil A. Ko for critically reading this manuscript. Permissions related to Figure 4D should be directed to the American Chemical Society.

Author Contributions

M.R. and D.T. wrote the manuscript.

Declaration of Interests

M.R. and D.T. are inventors on a patent application on PHOTACs.

References

- [1] D. J. Sherman, J. Li, *Molecules* 2020, 25, 671.
- [2] T. Asatsuma-Okumura, T. Ito, H. Handa, *Pharmacology & Therapeutics* 2019, 202, 132–139.
- [3] C. Mayor-Ruiz, S. Bauer, M. Brand, Z. Kozicka, M. Siklos, H. Imrichova, I. H. Kaltheuner, E. Hahn, K. Seiler, A. Koren, G. Petzold, M. Fellner, C. Bock, A. C. Müller, J. Zuber, M. Geyer, N. H. Thomä, S. Kubicek, G. E. Winter, *Nature Chemical Biology* 2020, 1–9.
- [4] R. Verma, D. Mohl, R. J. Deshaies, *Molecular Cell* 2020, 77, 446–460.
- [5] G. M. Burslem, C. M. Crews, *Cell* 2020, 181, 102–114.
- [6] C. P. O'Banion, D. S. Lawrence, *ChemBioChem* 2018, 19, 1201–1216.
- [7] I. M. Welleman, M. W. H. Hoorens, B. L. Feringa, H. H. Boersma, W. Szymański, *Chem. Sci.* 2020, 11, 11672–11691.
- [8] R. Weinstain, T. Slanina, D. Kand, P. Klán, *Chem. Rev.* 2020, 120, 13135–13272.
- [9] J. Broichhagen, J. A. Frank, D. Trauner, *Acc. Chem. Res.* 2015, 48, 1947–1960.
- [10] M. Hanafi, X. Chen, N. Neamati, *J. Med. Chem.* 2021, 64, 1626–1648.
- [11] M. Ishoey, S. Chorn, N. Singh, M. G. Jaeger, M. Brand, J. Paulk, S. Bauer, M. A. Erb, K. Parapatics, A. C. Müller, K. L. Bennett, G. F. Ecker, J. E. Bradner, G. E. Winter, *ACS Chem. Biol.* 2018, 13, 553–560.
- [12] B. Jiang, E. S. Wang, K. A. Donovan, Y. Liang, E. S. Fischer, T. Zhang, N. S. Gray, *Angewandte Chemie International Edition* 2019, 58, 6321–6326.
- [13] J. Yang, Y. Li, A. Aguilar, Z. Liu, C.-Y. Yang, S. Wang, *J. Med. Chem.* 2019, DOI 10.1021/acs.jmedchem.9b00846.
- [14] M. S. Gadd, A. Testa, X. Lucas, K.-H. Chan, W. Chen, D. J. Lamont, M. Zengerle, A. Ciulli, *Nature Chemical Biology* 2017, 13, 514–521.
- [15] S. D. Edmondson, B. Yang, C. Fallan, *Bioorganic & Medicinal Chemistry Letters* 2019, 29, 1555–1564.
- [16] R. I. Troup, C. Fallan, M. G. J. Baud, *Explor Target Antitumor Ther.* 2020, 1, 273–312.
- [17] Q. Delacour, C. Li, M.-A. Plamont, E. Billon-Denis, I. Aujard, T. Le Saux, L. Jullien, A. Gautier, *ACS Chemical Biology* 2015, 10, 1643–1647.
- [18] S. Kepinski, O. Leyser, *Nature* 2005, 435, 446–451.
- [19] J. Liu, H. Chen, L. Ma, Z. He, D. Wang, Y. Liu, Q. Lin, T. Zhang, N. Gray, H. Ü. Kaniskan, J. Jin, W. Wei, *Science Advances* 2020, 6, eaay5154.
- [20] Y. Naro, K. Darrah, A. Deiters, *J. Am. Chem. Soc.* 2020, DOI 10.1021/jacs.9b12718.

- [21] E. W. Tate, C. S. Kounde, M. M. Shchepinova, C. Saunders, M. X. Muelbaier, M. Rackham, J. D. Harling, *Chem. Commun.* 2020, DOI 10.1039/D0CC00523A.
- [22] G. Xue, K. Wang, D. Zhou, H. Zhong, Z. Pan, *J. Am. Chem. Soc.* 2019, DOI 10.1021/jacs.9b06422.
- [23] D. P. Bondeson, B. E. Smith, G. M. Burslem, A. D. Buhimschi, J. Hines, S. Jaime-Figueroa, J. Wang, B. D. Hamman, A. Ishchenko, C. M. Crews, *Cell Chemical Biology* 2018, 25, 78-87.e5.
- [24] G. E. Winter, D. L. Buckley, J. Paulk, J. M. Roberts, A. Souza, S. Dhe-Paganon, J. E. Bradner, *Science* 2015, 348, 1376–1381.
- [25] A. D. Buhimschi, H. A. Armstrong, M. Toure, S. Jaime-Figueroa, T. L. Chen, A. M. Lehman, J. A. Woyach, A. J. Johnson, J. C. Byrd, C. M. Crews, *Biochemistry* 2018, 57, 3564–3575.
- [26] Y. Jin, M. Lu, Y. Wang, W. Shan, X. Wang, Q.-D. You, Z. Jiang, *Journal of Medicinal Chemistry* 2020, DOI 10.1021/acs.jmedchem.9b02058.
- [27] P. Pfaff, K. T. G. Samarasinghe, C. M. Crews, E. M. Carreira, *ACS Cent. Sci.* 2019, DOI 10.1021/acscentsci.9b00713.
- [28] M. Reynders, B. S. Matsuura, M. Bérouti, D. Simoneschi, A. Marzio, M. Pagano, D. Trauner, *Science Advances* 2020, 6, eaay5064.
- [29] T. Rosenberg, S. Gal-Ben-Ari, D. C. Dieterich, M. R. Kreutz, N. E. Ziv, E. D. Gundelfinger, K. Rosenblum, *Front. Mol. Neurosci.* 2014, 7, DOI 10.3389/fnmol.2014.00086.
- [30] M. A. Sutton, E. M. Schuman, *Cell* 2006, 127, 49–58.
- [31] K. Moreau, M. Coen, A. X. Zhang, F. Pachi, M. P. Castaldi, G. Dahl, H. Boyd, C. Scott, P. Newham, *British Journal of Pharmacology* 2020, 177, 1709–1718.
- [32] K. Raina, J. Lu, Y. Qian, M. Altieri, D. Gordon, A. M. K. Rossi, J. Wang, X. Chen, H. Dong, K. Siu, J. D. Winkler, A. P. Crew, C. M. Crews, K. G. Coleman, *Proceedings of the National Academy of Sciences* 2016, 113, 7124–7129.
- [33] X. Sun, J. Wang, X. Yao, W. Zheng, Y. Mao, T. Lan, L. Wang, Y. Sun, X. Zhang, Q. Zhao, J. Zhao, R.-P. Xiao, X. Zhang, G. Ji, Y. Rao, *Cell Discovery* 2019, 5, 10.
- [34] A. Bansal, F. Yang, T. Xi, Y. Zhang, J. S. Ho, *PNAS* 2018, 115, 1469–1474.
- [35] J. A. Frank, M.-J. Antonini, P.-H. Chiang, A. Canales, D. B. Konrad, I. C. Garwood, G. Rajic, F. Koehler, Y. Fink, P. Anikeeva, *ACS Chem. Neurosci.* 2020, 11, 3802–3813.
- [36] J.-W. Jeong, J. G. McCall, G. Shin, Y. Zhang, R. Al-Hasani, M. Kim, S. Li, J. Y. Sim, K.-I. Jang, Y. Shi, D. Y. Hong, Y. Liu, G. P. Schmitz, L. Xia, Z. He, P. Gamble, W. Z. Ray, Y. Huang, M. R. Bruchas, J. A. Rogers, *Cell* 2015, 162, 662–674.

- [37] Y. Zhang, A. D. Mickle, P. Gutruf, L. A. McIlvried, H. Guo, Y. Wu, J. P. Golden, Y. Xue, J. G. Grajales-Reyes, X. Wang, S. Krishnan, Y. Xie, D. Peng, C.-J. Su, F. Zhang, J. T. Reeder, S. K. Vogt, Y. Huang, J. A. Rogers, R. W. Gereau, *Science Advances* 2019, 5, eaaw5296.
- [38] R. Knobler, M. L. Barr, D. R. Couriel, J. L. M. Ferrara, L. E. French, P. Jaksch, W. Reinisch, A. H. Rook, T. Schwarz, H. Greinix, *Journal of the American Academy of Dermatology* 2009, 61, 652–665.
- [39] R. Weissleder, *Nature Biotechnology* 2001, 19, 316–317.
- [40] J. Yao, L. V. Wang, *Photoacoustics* 2014, 2, 87–101.
- [41] A. P. Gorka, R. R. Nani, M. J. Schnermann, *Acc. Chem. Res.* 2018, 51, 3226–3235.
- [42] R. R. Nani, A. P. Gorka, T. Nagaya, T. Yamamoto, J. Ivanic, H. Kobayashi, M. J. Schnermann, *ACS Cent. Sci.* 2017, 3, 329–337.
- [43] K. Sitkowska, M. F. Hoes, M. M. Lerch, L. N. Lameijer, P. van der Meer, W. Szymański, B. L. Feringa, *Chem. Commun.* 2020, 56, 5480–5483.
- [44] K. Sitkowska, Ben. L. Feringa, W. Szymański, *J. Org. Chem.* 2018, 83, 1819–1827.
- [45] A. Yu. Vorobev, A. E. Moskalensky, *Computational and Structural Biotechnology Journal* 2020, 18, 27–34.
- [46] D. Bléger, J. Schwarz, A. M. Brouwer, S. Hecht, *J. Am. Chem. Soc.* 2012, 134, 20597–20600.
- [47] M. Dong, A. Babalhavaeji, C. V. Collins, K. Jarrah, O. Sadovski, Q. Dai, G. A. Woolley, *Journal of the American Chemical Society* 2017, 139, 13483–13486.
- [48] M. Dong, A. Babalhavaeji, S. Samanta, A. A. Beharry, G. A. Woolley, *Acc. Chem. Res.* 2015, 48, 2662–2670.
- [49] M. J. Hansen, M. M. Lerch, W. Szymanski, B. L. Feringa, *Angewandte Chemie International Edition* 2016, 55, 13514–13518.
- [50] D. B. Konrad, G. Savasci, L. Allmendinger, D. Trauner, C. Ochsenfeld, A. M. Ali, *J. Am. Chem. Soc.* 2020, 142, 6538–6547.
- [51] D. B. Konrad, J. A. Frank, D. Trauner, *Chemistry – A European Journal* 2016, 22, 4364–4368.
- [52] S. Samanta, A. A. Beharry, O. Sadovski, T. M. McCormick, A. Babalhavaeji, V. Tropepe, G. A. Woolley, *J. Am. Chem. Soc.* 2013, 135, 9777–9784.
- [53] Y. Becker, E. Unger, M. A. H. Fichte, D. A. Gacek, A. Dreuw, J. Wachtveitl, P. J. Walla, A. Heckel, *Chem. Sci.* 2018, 9, 2797–2802.

- [54] G. Cabré, A. Garrido-Charles, M. Moreno, M. Bosch, M. Porta-de-la-Riva, M. Krieg, M. Gascón-Moya, N. Camarero, R. Gelabert, J. M. Lluch, F. Busqué, J. Hernando, P. Gorostiza, R. Alibés, *Nature Communications* 2019, 10, 907.
- [55] A.-L. K. Hennig, D. Deodato, N. Asad, C. Herbivo, T. M. Dore, *J. Org. Chem.* 2020, 85, 726–744.
- [56] S. Chen, A. Z. Weitemier, X. Zeng, L. He, X. Wang, Y. Tao, A. J. Y. Huang, Y. Hashimoto-dani, M. Kano, H. Iwasaki, L. K. Parajuli, S. Okabe, D. B. L. Teh, A. H. All, I. Tsutsui-Kimura, K. F. Tanaka, X. Liu, T. J. McHugh, *Science* 2018, 359, 679–684.
- [57] Y. Sasaki, M. Oshikawa, P. Bharmoria, H. Kouno, A. Hayashi-Takagi, M. Sato, I. Ajioka, N. Yanai, N. Kimizuka, *Angewandte Chemie International Edition* 2019, 58, 17827–17833.
- [58] Y. Zhang, Y. Zhang, G. Song, Y. He, X. Zhang, Y. Liu, H. Ju, *Angewandte Chemie International Edition* 2019, 58, 18207–18211.
- [59] K. A. Brown, Y. Zou, D. Shirvanyants, J. Zhang, S. Samanta, P. K. Mantravadi, N. V. Dokholyan, A. Deiters, *Chem. Commun.* 2015, 51, 5702–5705.
- [60] A. Gutnick, M. R. Banghart, E. R. West, T. L. Schwarz, *Nature Cell Biology* 2019, 21, 768–777.
- [61] N. Umeda, T. Ueno, C. Pohlmeier, T. Nagano, T. Inoue, *J. Am. Chem. Soc.* 2011, 133, 12–14.
- [62] M. Zimmermann, R. Cal, E. Janett, V. Hoffmann, C. G. Bochet, E. Constable, F. Beaufils, M. P. Wymann, *Angewandte Chemie International Edition* 2014, 53, 4717–4720.
- [63] L. Li, D. Mi, H. Pei, Q. Duan, X. Wang, W. Zhou, J. Jin, D. Li, M. Liu, Y. Chen, *Signal Transduction and Targeted Therapy* 2020, 5, 1–3.
- [64] X. Zhang, V. M. Crowley, T. G. Wucherpfennig, M. M. Dix, B. F. Cravatt, *Nature Chemical Biology* 2019, 15, 737–746.
- [65] C. C. Ward, J. I. Kleinman, S. M. Brittain, P. S. Lee, C. Y. S. Chung, K. Kim, Y. Petri, J. R. Thomas, J. A. Tallarico, J. M. McKenna, M. Schirle, D. K. Nomura, *ACS Chem. Biol.* 2019, 14, 2430–2440.
- [66] J. N. Spradlin, X. Hu, C. C. Ward, S. M. Brittain, M. D. Jones, L. Ou, M. To, A. Proudfoot, E. Ornelas, M. Woldegiorgis, J. A. Olzmann, D. E. Bussiere, J. R. Thomas, J. A. Tallarico, J. M. McKenna, M. Schirle, T. J. Maimone, D. K. Nomura, *Nature Chemical Biology* 2019, 1.
- [67] M. Naito, N. Ohoka, N. Shibata, *Drug Discovery Today: Technologies* 2019, 31, 35–42.
- [68] J. Baaske, P. Gonschorek, R. Engesser, A. Dominguez-Monedero, K. Raute, P. Fischbach, K. Müller, E. Cachat, W. W. A. Schamel, S. Minguet, J. A. Davies, J. Timmer, W. Weber, M. D. Zurbruggen, *Scientific Reports* 2018, 8, 15024.

- [69] K. M. Bongler, R. Rakhit, A. Y. Payumo, J. K. Chen, T. J. Wandless, *ACS Chemical Biology* 2014, *9*, 111–115.
- [70] A. Hermann, J. F. Liewald, A. Gottschalk, *Current Biology* 2015, *25*, R749–R750.
- [71] C. Renicke, D. Schuster, S. Usherenko, L.-O. Essen, C. Taxis, *Chemistry & Biology* 2013, *20*, 619–626.
- [72] S. Usherenko, H. Stibbe, M. Musc , L.-O. Essen, E. A. Kostina, C. Taxis, *BMC Systems Biology* 2014, *8*, DOI 10.1186/s12918-014-0128-9.
- [73] D. L. Buckley, K. Raina, N. Darricarrere, J. Hines, J. L. Gustafson, I. E. Smith, A. H. Miah, J. D. Harling, C. M. Crews, *ACS Chem. Biol.* 2015, *10*, 1831–1837.
- [74] B. Nabet, J. M. Roberts, D. L. Buckley, J. Paulk, S. Dastjerdi, A. Yang, A. L. Leggett, M. A. Erb, M. A. Lawlor, A. Souza, T. G. Scott, S. Vittori, J. A. Perry, J. Qi, G. E. Winter, K.-K. Wong, N. S. Gray, J. E. Bradner, *Nature Chemical Biology* 2018, *14*, 431.
- [75] H. Tovell, A. Testa, C. Maniaci, H. Zhou, A. R. Prescott, T. Macartney, A. Ciulli, D. R. Alessi, *ACS Chem. Biol.* 2019, *14*, 882–892.

2 – PHOTACs Enable Optical Control of Protein Degradation

Martin Reynders^{1,2}, Bryan S. Matsuura¹, Marleen Bérouti^{1,2},
Daniele Simoneschi^{3,4}, Antonio Marzio^{3,4},
Michele Pagano^{3,4,5}, and Dirk Trauner^{1,4,6}

¹ Department of Chemistry, New York University, New York, NY 10003, USA.

² Department of Chemistry, Ludwig Maximilians University of Munich
81377 Munich, Germany.

³ Department of Biochemistry and Molecular Pharmacology, New York University
School of Medicine, New York, NY 10016, USA.

⁴ Perlmutter Cancer Center, New York University School of Medicine, New York, NY
10016, USA.

⁵ Howard Hughes Medical Institute, New York University School of Medicine, New
York, NY 10016, USA.

⁶ NYU Neuroscience Institute, New York University School of Medicine, New York,
NY 10016, USA.

Abstract

PROTACs (PROteolysis TARgeting Chimeras) are bifunctional molecules that target proteins for ubiquitylation by an E3 ligase complex and subsequent degradation by the proteasome. They have emerged as powerful tools to control the levels of specific cellular proteins. We now introduce photoswitchable PROTACs that can be activated with the spatiotemporal precision that light provides. These trifunctional molecules, which we named PHOTACs (PHOtochemically TARgeting Chimeras), consist of a ligand for an E3 ligase, a photoswitch, and a ligand for a protein of interest. We demonstrate this concept by using PHOTACs that target either BET family proteins (BRD2,3,4) or FKBP12. Our lead compounds display little or no activity in the dark but can be reversibly activated with different wavelengths of light. Our modular approach

provides a method for the optical control of protein levels with photopharmacology and could lead to new types of precision therapeutics that avoid undesired systemic toxicity.

Introduction

Protein levels in cells result from a tightly controlled balance between synthesis and degradation. A wide range of small molecules have been identified that interfere with these processes. Most of them do not address specific proteins as they broadly inhibit the machinery necessary for transcription, translation, trafficking, or degradation. In recent years, proteolysis targeting chimeras (PROTACs) have emerged as a new principle of pharmacology.^[1–3] These bifunctional molecules combine a ligand for an E3 ubiquitin ligase with a second one that targets a protein of interest (POI), thereby promoting the physical interaction of the proteins, the polyubiquitylation of the POI, and its consequent proteasomal degradation. Both ends of the PROTAC are connected via a linker, the exact nature of which needs to be carefully chosen to ensure efficacy, cell permeability, and biodistribution.

First generation PROTACs used peptides to recruit POIs to E3 ligases,^[4] but subsequent ones have relied on smaller and more cell-permeable synthetic ligands. These include hydroxyproline derivatives and molecules derived from thalidomide, which bind the von Hippel–Lindau protein (VHL)^[5,6] and cereblon (CRBN)^[7,8], respectively. VHL and CRBN are the substrate receptors of two cullin-RING ubiquitin ligase (CRL) complexes, namely CRL2^{VHL} and CRL4^{CRBN}. Proteins that have been successfully targeted for degradation through these ubiquitin ligases include the androgen and estrogen receptors,^[9–12] the BET family epigenetic readers BRD2-4^[7,8,13], and FKPB12 and its fusion proteins.^[7,14,15] Soluble kinases, such as CDK9^[16] and BCR-ABL,^[17] as well as receptor tyrosine kinases, such as EGFR^[18] and BTK,^[19,20] have also been amenable to this approach. Covering a broad spectrum from membrane proteins to nuclear hormone receptors, PROTACs have proven to be a highly versatile approach.

PROTACs do not merely inhibit the activity of their targets, like conventional drugs; rather, they decrease the levels of the targets by promoting their proteolysis. The transition from inhibition of proteins to their catalytic degradation enables the targeting

of previously undruggable proteins. However, this mechanistic difference with conventional drugs also poses certain risks when applied systemically, since the POI is degraded and disappears with all of its functions in both cancer and normal cells. For instance, inhibition of BET bromodomains is tolerated, but a complete loss of BRD2 and BRD4 is lethal.^[21,22] Therefore, it would be advantageous to locally activate PROTACs in tissues and cells where their effects (*e.g.*, cytotoxicity) are desirable, while avoiding deleterious effects elsewhere.

One method to localize the effect of drugs and achieve higher selectivity is to control their activity with light. In recent years, the usefulness of light to precisely regulate biological pathways has become increasingly apparent. Optical control can be achieved in a variety of ways: with caged compounds,^[23] genetically engineered photoreceptors (Optogenetics),^[24] or with synthetic photoswitches whose activity can be changed through a combination of photochemical isomerization and thermal relaxation (Photopharmacology).^[25,26]

Herein we report the application of photopharmacology to targeted protein degradation. By incorporating azobenzene photoswitches into PROTACs, we have designed photoswitchable versions that we named PHOTACs (PHOtochemically TArgeting Chimeras). These molecules show little or no proteolytic activity in the dark, but can be activated with blue-violet light (380-440 nm). They can be used to degrade a variety of targets, including BRD2-4 and FKBP12, by binding to the CRL4^{CRBN} complex and promoting proteolysis in a light-dependent fashion. This translates to the optical control of protein levels and, in the case of BRD2-4, of cell proliferation, survival, and viability.

Results

Design, synthesis, and photophysical characterization

The design of our PHOTACs was guided by a desire to render our molecules as diversifiable and modular as possible, whilst ensuring efficient synthetic access. To test the concept, we chose to target CRBN which, together with VHL, accounts for the majority of PROTAC platforms utilized to date. Accordingly, we focused on thalidomide derivatives, such as pomalidomide and lenalidomide, as CRBN ligands. As for the photoswitch, we decided to use azobenzenes, which are known for their fatigue

resistance, large and predictable geometrical changes, and easily tunable photothermal properties. Azobenzenes are also among the smallest photoswitches and do not significantly increase the molecular weight of pharmaceuticals upon substitution. Ideal PHOTACs would be inactive in the dark and lead to efficient degradation of the POI upon irradiation. However, the impact of linker conformation on PROTAC activity is not fully understood. We therefore explored both regular azobenzenes (more stable in their *trans* form) and diazocines (more stable in *cis*).^[27,28]

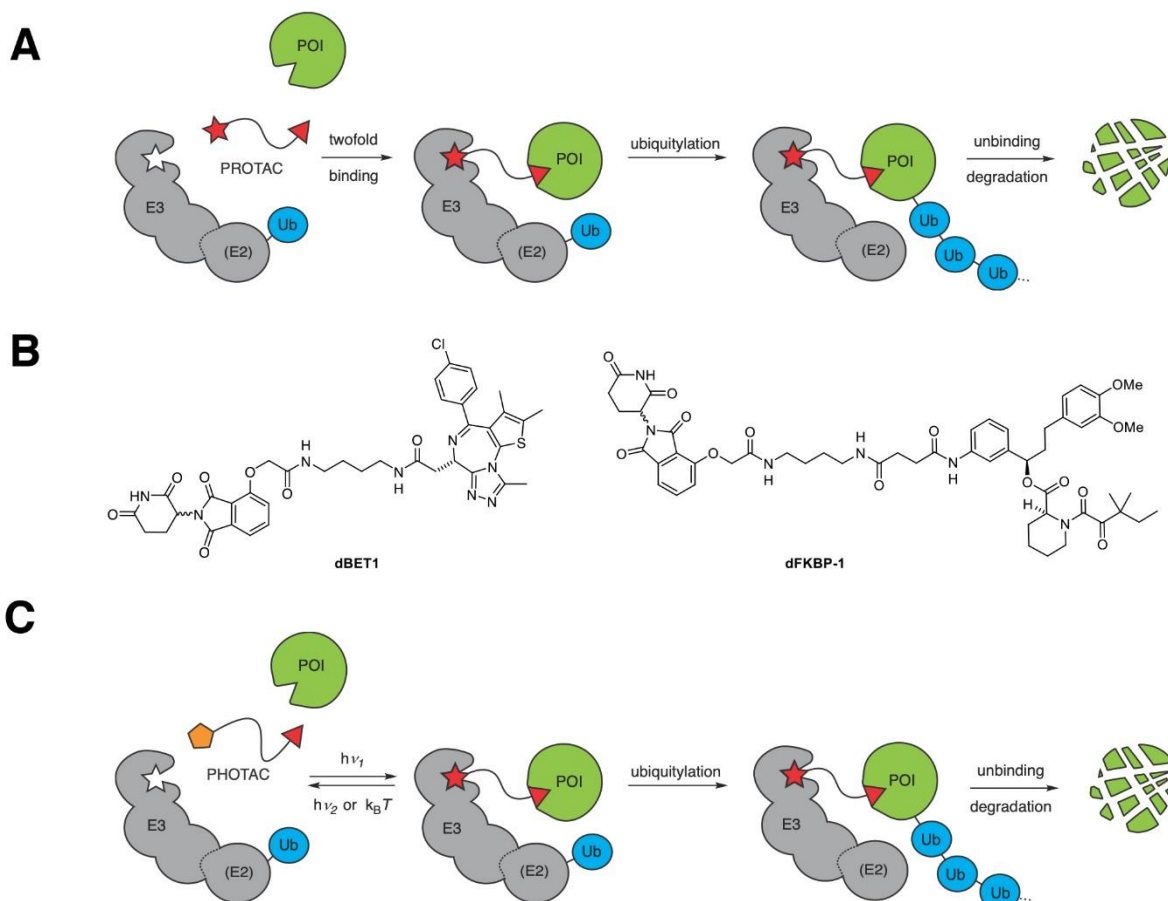


Figure 2.1. PROTACs and PHOTACs. A) Schematic depiction of a PROTAC. Formation of a ternary complex between an E3-ligase, a PROTAC and a protein of interest (POI) leads to degradation of the POI. B) Chemical structures of PROTACs dBET1 and dFKBP-1. C) Schematic depiction of a PHOTAC. The molecules toggles between an inactive form (yellow pentagon) and an active form (red star) upon irradiation.

Several approaches are conceivable for the incorporation of these photoswitches into PHOTACs: (A) they could be part of the ligand for the E3 ligase and change the affinity at this end of the chimera; (B) the photoswitches could mostly reside in the tether, changing the length and orientation of this segment; (C) the azobenzenes could be

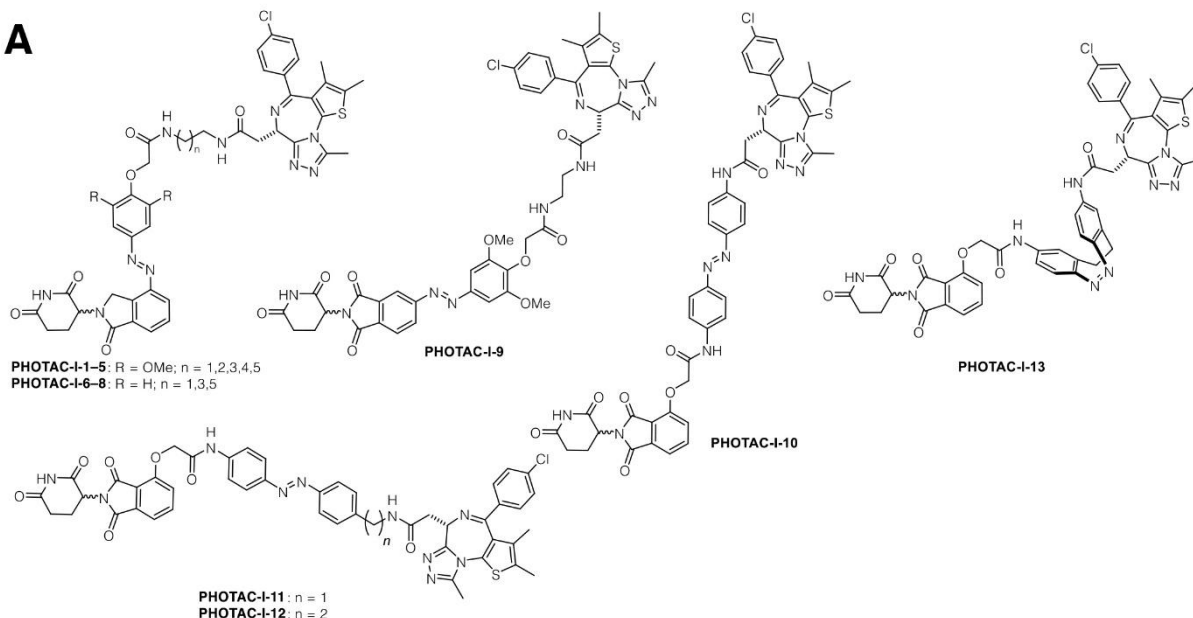
part of a POI ligand, controlling the affinity of the PHOTAC to the POI. It would be difficult, if not impossible, however, to define a strict boundary between ligands and linker, and combinations of all three modes are possible. As for our first POI ligand, we chose (+)-JQ1, a high-affinity inhibitor of BET proteins BRD2-4 and BRDT. PROTACs featuring this ligand, such as dBET1 (Figure 2.1B), have proven to be particularly effective and have been developed for a variety of E3 ligases.

The small library of PHOTACs that resulted from these considerations is depicted in Fig. 2.2A. Amongst these, **PHOTAC-I-3**, emerged as one of the most effective. Its synthesis started with the diazotization of lenalidomide and coupling of the resulting diazonium ion **1** to 2,6-dimethoxyphenol, which yielded azobenzene **2** (Figure 2.2B). Alkylation with *tert*-butyl bromoacetate and subsequent deprotection then afforded the key intermediate **3**. Amide coupling of this carboxylic acid with *N*-Boc-butane-1,4-diamine and deprotection then yielded **4**, which underwent another deprotection followed by peptide coupling with the free acid of (+)-JQ1 (**5**) to afford **PHOTAC-I-3**. HATU coupling of **3** to diaminoalkanes of different length provided easy access to library of PHOTACs with varying linker length (i.e. **PHOTAC-I-1,2,4,5**). **PHOTACs-I-6–8**, which lack two methoxy groups on the azobenzene core, and were synthesized analogously. **PHOTAC-I-9** bears a different substitution pattern and was prepared *via* Baeyer-Mills coupling (see Supporting Information). **PHOTACs-I-10–13**, which have the photoswitch more in the center of the molecule, were synthesized from 4-hydroxy thalidomide and azobenzene building blocks via alkylation and amide couplings (see Supporting Information).

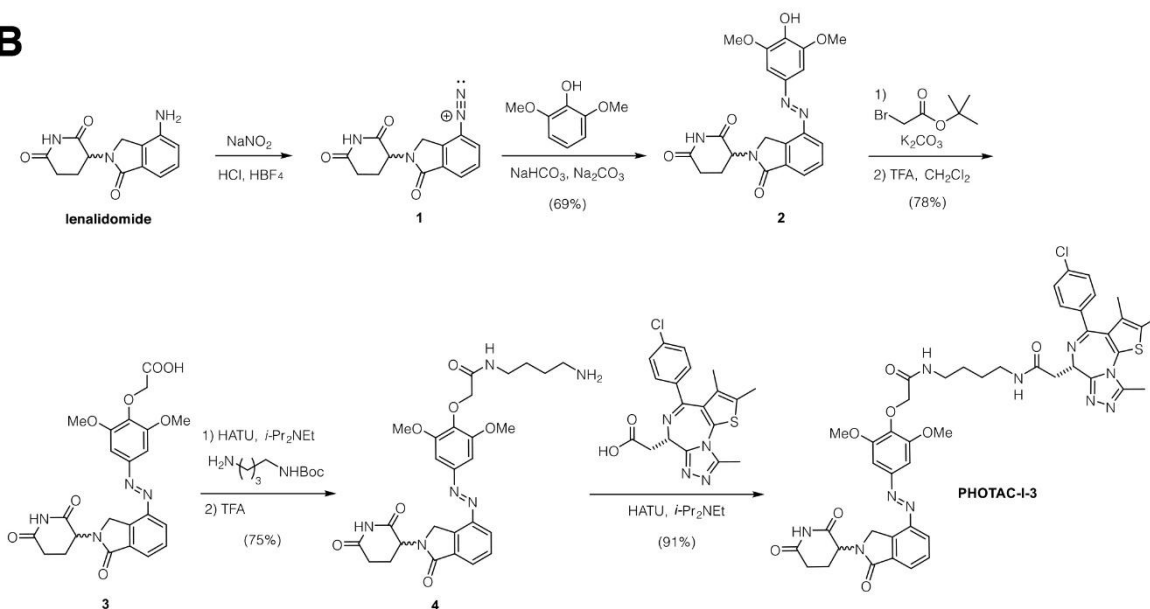
The photoswitching and thermal relaxation properties of one of our lead compounds, **PHOTAC-I-3**, is shown in Fig. 2.3A-E. The optimal wavelength to switch to the *cis* isomer is 390 nm but similar photostationary states (PSS) can be obtained between 380 and 400 nm (Figure 2.3C). At 390 nm a PSS of >90% *cis* could be obtained. Rapid *cis* to *trans* isomerization could be achieved by irradiation with wavelengths >450 nm, achieving PSS of ca >70% *trans* (Figure 2.3C). In the absence of light, *cis* **PHOTAC-I-3** slowly isomerized back to its *trans* form with a half-life of 8.8 h at 37 °C in DMSO (Figure 2.3D). Multiple cycles of photochemical isomerization are possible, in keeping with the fatigue-resistance of azobenzene photoswitches (Figure 2.3E). Structurally

related PHOTACs showed similar photophysical and thermal properties (see Supporting Information).

A



B



C

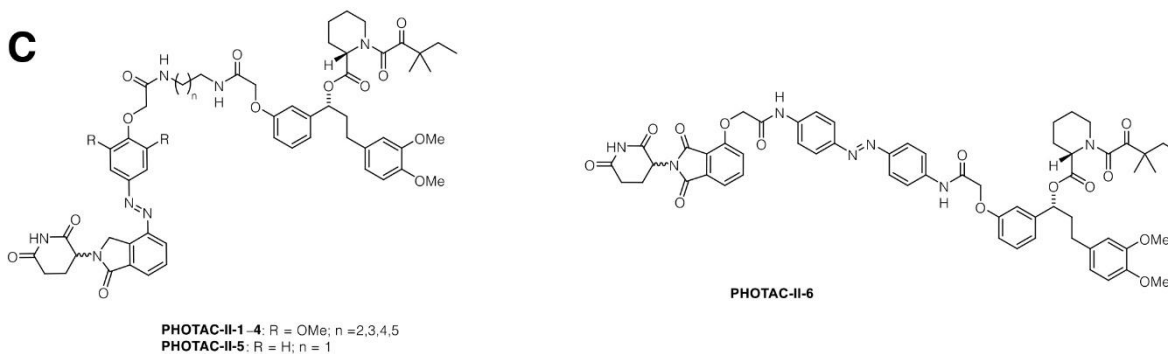


Figure 2.2. Structure and synthesis of PHOTACs. A) Members of the **PHOTAC-I** series targeting BRDs. B) Synthesis of **PHOTAC-I-3** starting from lenalidomide. C) Members of the **PHOTAC-II** series targeting FKBP12.

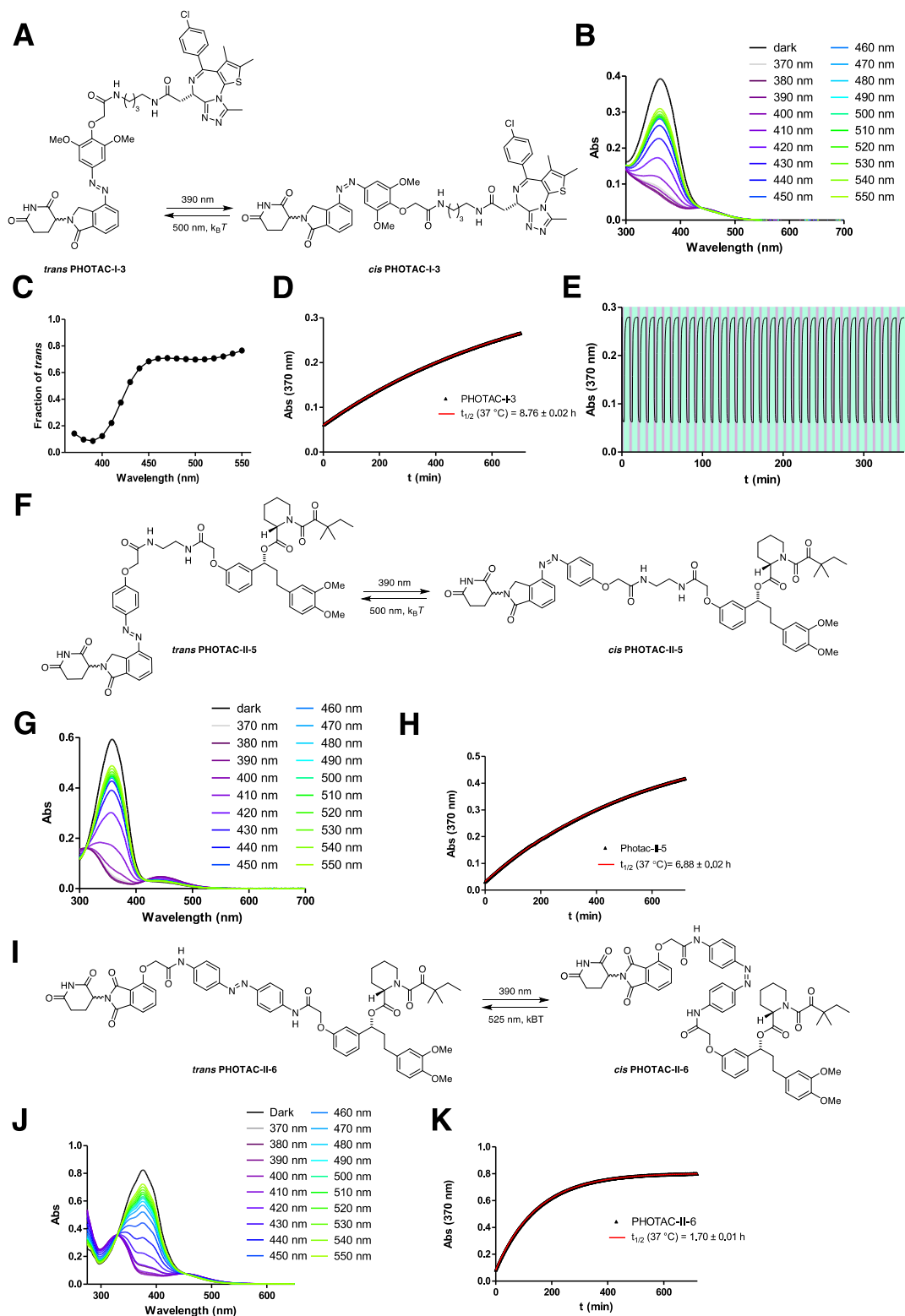


Figure 2.3. Photophysical properties, switching, and bistability of PHOTACs. A) Switching of **PHOTAC-I-3** between the *trans* isomer (left) and *cis* isomer (right). B) UV-VIS spectra **PHOTAC-I-3** following irradiation with different wavelengths for 5 min. C)

Fraction of *trans* **PHOTAC-I-3** in the PSS. D) Thermal relaxation of *cis* **PHOTAC-I-3** at 37 °C in DMSO . E) Reversible switching and photochemical stability of **PHOTAC-I-3**. F) Switching of **PHOTAC-II-5** between the *trans* isomer (left) and *cis* isomer (right). G) UV-VIS spectra **PHOTAC-II-5** following irradiation with different wavelengths for 5 min. H) Thermal relaxation of *cis* **PHOTAC-II-5** at 37 °C in DMSO. I) Switching of **PHOTAC-II-6** between the *trans* isomer (left) and *cis* isomer (right). J) UV-VIS spectra **PHOTAC-II-6** following irradiation with different wavelengths for 5 min. K) Thermal relaxation of *cis* **PHOTAC-II-6** at 37 °C in DMSO.

Optical control of BRD2-4 with PHOTACs.

To assess the biological activity of our PHOTACs, we tested their effect on the viability of RS4;11 lymphoblast cells. Cells were treated in a 96-well plate with increasing concentrations of PHOTACs and were either irradiated with 390 nm light pulses (100 ms every 10s) for 72 h or incubated with the compound in the dark. Subsequently, we performed cell viability assays (Promega MTS), as previously described. **PHOTAC-I-3** showed a promising activity difference upon irradiation (Figure 2.4A). The EC₅₀ was determined to be 88.5 nM when irradiated with 390 nm light and 631 nM in the dark, resulting in a 7.1-fold EC₅₀ difference. This indicates that cytotoxicity increases upon irradiation and that **PHOTAC-I-3** is less toxic in the dark. Similar trends were observed for **PHOTAC-I-1,2,4–8,10**, all of which were more active in viability assays following pulse irradiation (SI Figure S2.3). By contrast, **PHOTACs-I-9,11–13** showed no light-dependent differences in activity (SI Figure S2.3). In a control experiment, the BET inhibitor (+)-JQ1 alone showed no light-dependent toxicity either (Figure 2.4B).

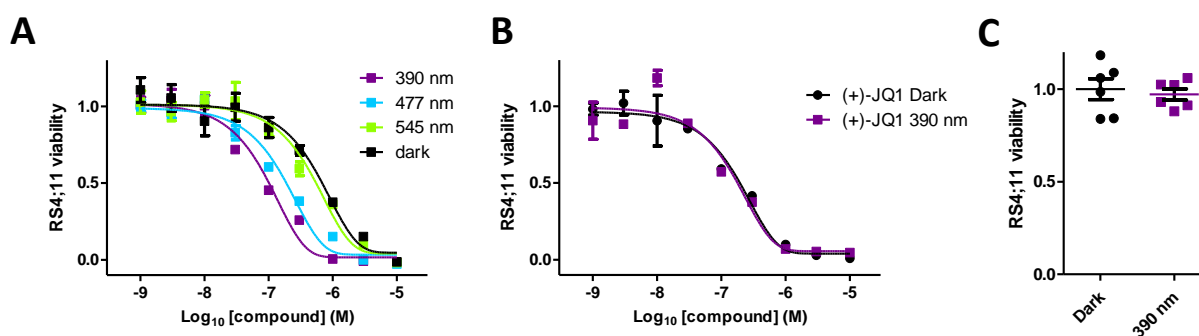


Figure 4. Light-dependent viability of RS4;11 cells. A) Viability of RS4;11 acute lymphoblastic leukemia cells after treatment with **PHOTAC-I-3** for 72 h in the dark or under pulsed (100 ms every 10 s) 390 nm, 477 nm or 545 nm irradiation. B) RS4;11 Viability after (+)-JQ1 treatment for 72 h in the dark or under pulsed (100 ms every 10 s) 390 nm irradiation. C) Viability of RS4;11 cells after 72 h in the dark or under pulsed (100 ms every 10 s) 390 nm irradiation.

Next, we analyzed the light dependence of targeted protein degradation in RS4;11 cells by western blot analysis of the BET proteins BRD2-4 (Figure 2.5). To this end, we treated cells with increasing concentrations of our lead compound, **PHOTAC-I-3**, for 4 h and pulse-irradiated with 390 nm light (100 ms every 10 s). We observed a pronounced decrease of BRD4 levels in the presence of **PHOTAC-I-3** (particularly between 100 nM to 3 μ M) when irradiated with 390 nm light, but not in the dark (Figure 2.5A). At 10 μ M, we observed less degradation, which is consistent with the “hook effect” commonly observed with PROTACs.^[5,19,29] BRD3 levels were also significantly reduced upon exposure to concentrations in the range of 100 nM to 3 μ M of **PHOTAC-I-3** when irradiated with violet light, but not in the dark. In comparison, BRD2 was degraded to a lesser extent and within a narrower concentration range. Application of **PHOTAC-I-3** (1 μ M) together with the CRL inhibitor MLN4924 (2.5 μ M), which inhibits neddylation and, consequently, the activity of all cellular CRLs (including CRL4^{CRBN}), rescued BRD2-4 levels upon irradiation. The cereblon-dependent degradation was confirmed by a competition experiment (Figure 2.5E), and further validated by siRNA knockdown of cereblon (Figure S2.7). Methylation of the glutarimide prevented the degradation of BRD4 as previously demonstrated (Figure S2.8).^[30]

As expected from photoactivatable degraders and inhibitors of BRD4, c-MYC levels were also affected.^[13,31,32] Downregulation of this transcription factor, which is a notoriously difficult target for pharmacological intervention,^[33] was more pronounced when cells were pulse-irradiated in the presence of low concentrations of **PHOTAC-I-3** than in the dark. The light-dependent degradation of BRD4 by **PHOTAC-I-3** was also confirmed in two breast cancer cell lines (MB-MDA-231 and MB-MDA-468) (SI Fig. S2.4A,B). Immunoblot analyses of additional PHOTACs are presented in SI Fig. S2.5.

The time dependence of BRD degradation is shown in Fig. 2.5C. BRD2 and BRD3 are largely absent after 1.5 h exposure and irradiation, whereas BRD4 is degraded more slowly. We also observed sustained degradation and c-MYC downregulation over 24 hours. In the dark, **PHOTAC-I-3** had no effect on BRD levels and relatively little effect on c-MYC levels. The slight effect on c-MYC can be explained by inhibition of BRD4 with the (+)-JQ1 derivative **PHOTAC-I-3** in the absence of targeted degradation. Following sustained pulse irradiation, we also observed increasing cleavage of PARP-1 (Fig. 2.5C). This indicator of apoptosis^[34] correlates to the cell viability assay shown

in Fig. 2.4A. Persistent degradation of BRD4 in the dark could be achieved following a brief activation of **PHOTAC-I-3** for 1 min (SI Fig. S2.4C).

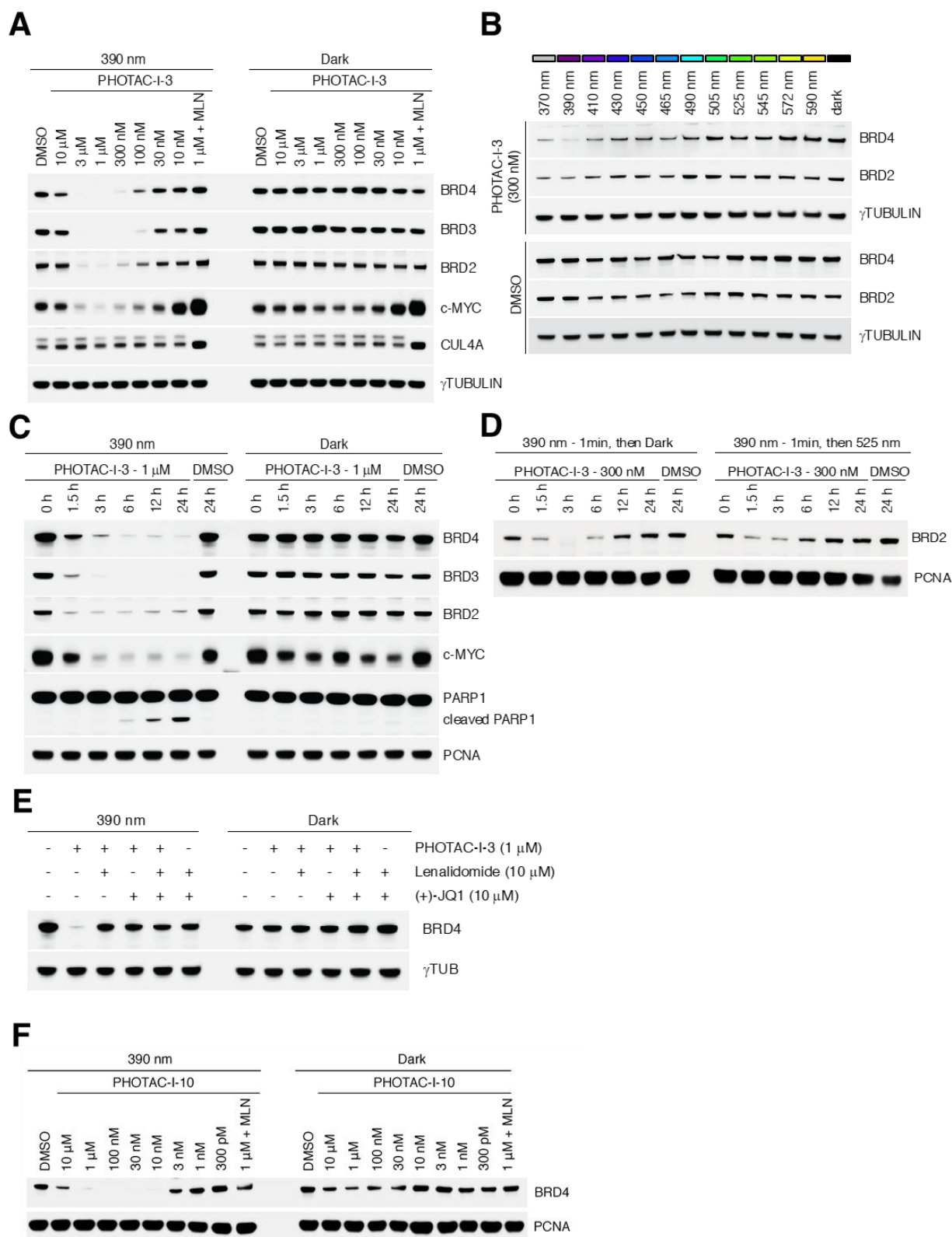


Figure 2.5. Optical control of BRD2-4 levels. A) Immunoblot analysis after treatment of RS4;11 cells with **PHOTAC-I-3** for 4 h at different concentrations. Cells were either irradiated with 100 ms pulses of 390 nm light every 10 s (left) or kept in the dark (right).

B) Color-dosing: Wavelength dependence of BRD2/4 degradation promoted by 300 nM **PHOTAC-I-3**. C) Time course of BRD2-4 degradation, c-MYC levels and PARP1 cleavage assayed by immunoblotting. RS4;11 cells were treated with **PHOTAC-I-3** (1 μ M) and collected at the indicated time points. **PHOTAC-I-3** has no effect on BRD2-4 levels in the dark over several hours. D) Immunoblot of a rescue experiment demonstrating the reversibility of degradation promoted by **PHOTAC-I-3** through thermal relaxation (left) or optical inactivation by 525 nm pulsed irradiation (right, 100 ms every 10 s). E) Immunoblot analysis after treatment of RS4;11 cells with **PHOTAC-I-3** and combinations with lenalidomide or (+)-JQ1 for 4 h to confirm a cereblon-based mechanism. Cells were either irradiated with 100 ms pulses of 390 nm light every 10 s (left) or kept in the dark (right). F) Optical degradation of BRD4 with the thalidomide derivative **PHOTAC-I-10**. Immunoblot analysis of RS4;11 cells after treatment with **PHOTAC-I-10** for 4 h at different concentrations which were either irradiated with 100 ms pulses of 390 nm light every 10 s (left) or kept in the dark (right).

One of the principal advantages of photoswitches over caged compounds is their reversibility. Azobenzene photoswitches can thermally relax to an inactive form or be isomerized back photochemically. We demonstrated the photochemical reversibility with a rescue experiment wherein PHOTAC-I-3 was continuously irradiated for 1 min with the activating wavelength (390 nm) and then pulse irradiated with the deactivating wavelength (525 nm). Under these conditions, cellular BRD2 levels initially decreased but, subsequently, recovered faster than when left in the dark (Figure 2.5D).

Another characteristic feature of photopharmacology is “color-dosing” (*i.e.*, the ability to control the concentration of the active species with the color of the incident light).^[26,35,36] The photostationary state (*i.e.*, the ratio between the two isomers) is a function of the wavelength. Figures 2.3A and 2.5B show that this principle can also be applied to PHOTACs. Cell viability assays gave left-shifted curves as the color gradually approached 390 nm (Fig. 2.4A). Western blots showed maximum degradation at 390 nm and gradually increasing BRD4 levels as the wavelength of the incident light increased (Figure 2.5B). At 370 nm we observed slightly increased protein levels, in agreement with the photostationary states measured at different wavelengths, which are maximized toward the active *cis* isomer at the slightly longer wavelength of 390 nm (Fig. 2.3C).

The effect of **PHOTAC-I-10**, which is derived from thalidomide and has the photoswitch positioned deeper in the linker, on BRD4 levels, is shown in Fig. 2.5F. We found robust photodegradation even with 10 nM **PHOTAC-I-10**. A clear hook-effect was observed.

Once again, the thermally less stable *cis* azobenzene promoted ubiquitylation and degradation.

Optical control of FKBP12 with PHOTACs.

To test whether the PHOTAC approach is generalizable, we turned to the prolyl *cis-trans* isomerase FKBP12. The structures of the corresponding PHOTACs are shown in Fig. 2.2C. PHOTACs of this series consist of a CRBN-targeting glutarimide, an azobenzene photoswitch in different positions, a linker, and the ligand SLF that binds to native FKBP12.^[7,14,37,38] The synthesis of **PHOTACs-II-1–6** is detailed in Supporting Information. The photophysical and thermal characterization of **PHOTACs-II-5** and **PHOTACs-II-6** is shown in Fig. 2.3 F–H and in Fig. 2.3 I–K, respectively.

Amongst the molecules tested, **PHOTAC-II-5** and **PHOTAC-II-6** turned out to be the most useful, and our biological investigations have been focused on these molecules (for **PHOTACs-II-1–4**, see Fig. S2.10). **PHOTAC-II-5**, which has the azobenzene switch in the same position as **PHOTACs-I-1–8**, had a pronounced effect on FKBP12 levels upon pulse irradiation (Fig. 2.6A). The degradation was slower than in the case of BET proteins, but between 6 and 12 hours the protein was largely absent from our cell lysates (Fig. 2.6B). Again, no degradation could be observed in the dark. **PHOTAC-II-6**, wherein the photoswitch was moved further into the linker region, also elicited light-dependent degradation (Fig. 2.6C). The time course of FKBP12 degradation by **PHOTAC-II-6** was similar to the one observed with **PHOTAC-II-5** (Fig. 2.6D). In this case, however, we also observed slight dark activity at the 24-hour time point. Both PHOTACs showed a pronounced “hook effect” and were inactive in the presence of MLN4924.

Discussion

By incorporating photoswitches into PROTACs, we have delineated a general strategy to control targeted protein degradation with the temporal and spatial precision that light affords. As such, we have applied the concept of photopharmacology to an important new target class, *i.e.*, E3 ubiquitin ligases, and have added a highly useful functional feature to existing PROTACs.

As a proof of principle, we developed PHOTACs that combine CRBN ligands with azobenzene photoswitches and ligands for either BET proteins (BRD2,3,4) or FKBP12.

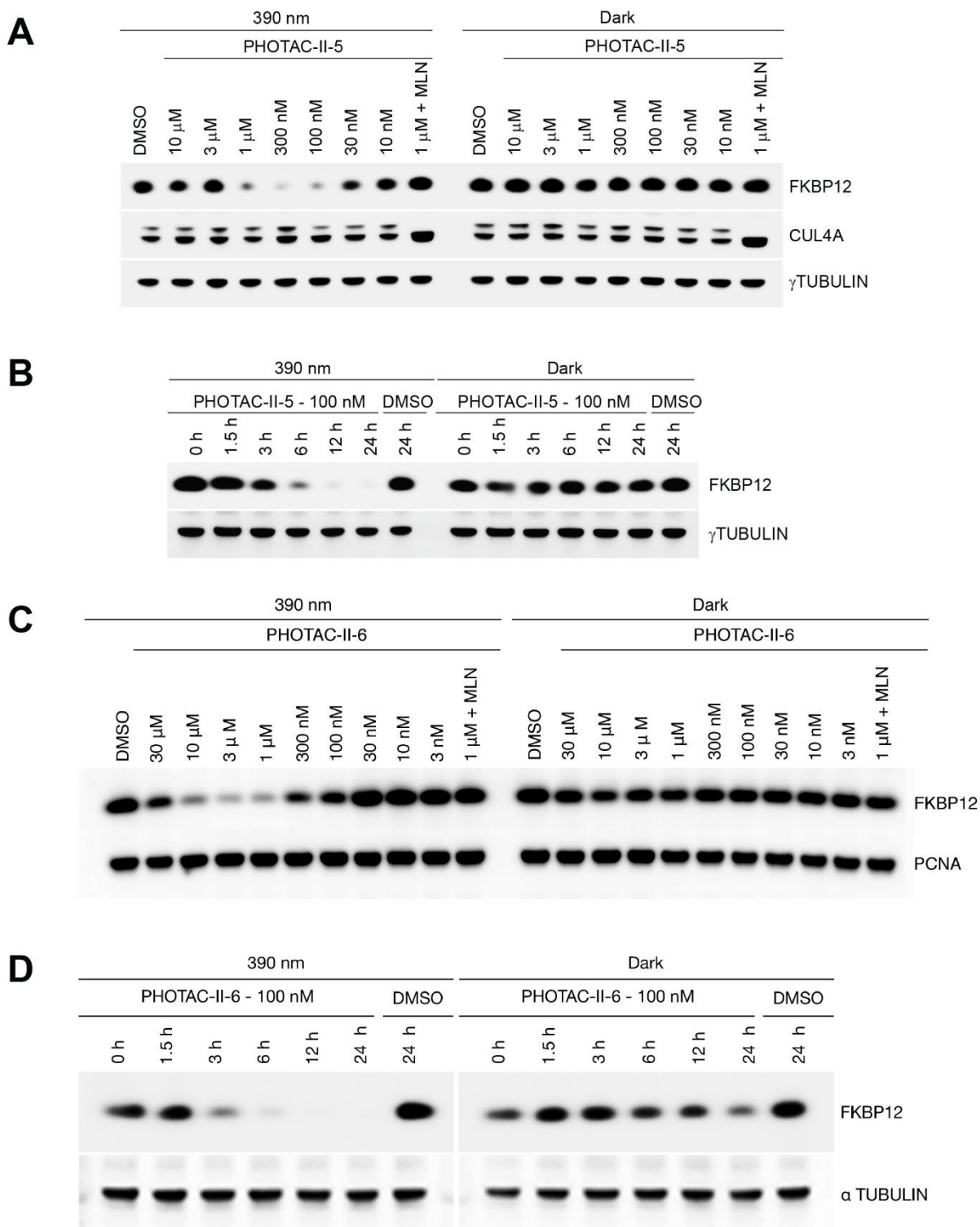


Figure 2.6. Optical control FKBP12 degradation. A) Immunoblot analysis of FKBP12 after treatment of RS4;11 cells with **PHOTAC-II-5** for 4 h at different concentrations. Cells were either irradiated with pulses of 390 nm light (left, 100 ms every 10 s) or kept in the dark (right). B) Time course of FKBP12 degradation visualized by

immunoblotting. RS4;11 cells were treated with **PHOTAC-II-5** (100 nM) and collected at the indicated time points. C) Immunoblot analysis of FKBP12 after treatment of RS4;11 cells with **PHOTAC-II-6** for 4 h at different concentrations. Cells were either irradiated with pulses of 390 nm light (left, 100 ms every 10 s) or kept in the dark (right). D) Time course of FKBP12 degradation visualized by immunoblotting. RS4;11 cells were treated with **PHOTAC-II-6** (100 nM) and collected at the indicated time points.

The modularity of our approach should enable the straightforward development of PHOTACs that target many other classes of proteins. For instance, existing PROTACs that target CDK4/6,^[30] CDK9,^[16] BTK,^[19,20] ABL,^[17,39] ALK,^[40] MET,^[18] MDM2,^[41] and Tau^[42] could be adapted to become light activatable. Our PHOTACs for BRD2,3,4 may enable new insights into epigenetic pathways and potentially serve as precision tools in medicine. Color-dosing and reversibility could be particularly useful in this regard.

Our PHOTACs for FKBP12 could not only enable the optical degradation of wild type prolyl *cis-trans* isomerases, but also of proteins that are tagged with this domain. This would significantly increase the utility of dTAGs, which have emerged as a broadly applicable technology to influence the homeostasis of fusion proteins.^[14,15] In addition, PROTACs that link thalidomide derivatives to an alkyl halide could be modified to optically degrade HALO-tagged proteins.^[43] It should also be noted that some of our photoswitchable thalidomide derivatives, such as synthetic intermediates **2-4**, and derivatives thereof, could function as dimerizers that recruit Ikaros (IKZF1) and Aiolos (IKZF3) to CRBN in a light-dependent fashion.^[44]

The PHOTACs introduced herein have several features that make them useful for biological studies: they are inactive as degraders in the dark and become active upon irradiation. Following activation, they gradually lose their activity through thermal relaxation. Alternatively, they can be quickly inactivated photochemically. In any scenario, their inactivation is much less dependent on dilution, clearance, or metabolism. In the case of compounds of the **PHOTAC-I** series, they still function as inhibitors of BET proteins, which explains the cytotoxicity observed in the dark. The concentrations needed for maximum photoeffect are low (nanomolar range), substantially reducing possible off-target effects. The light needed for photoactivation is not cytotoxic, given the low intensities needed for photoisomerization and the pulse protocol used.^[26,36,45]

In principle, light activation of PROTACs could also be achieved with a caging strategy. Indeed, caged PROTACs have very recently emerged, complementing PHOTACs.^[46,47] The advantage of the latter lies in their reversibility, the low intensities of light needed to trigger the photochemistry, the ease with which the active concentration can be tuned, and the avoidance of potentially toxic byproducts. Fast relaxing PHOTACs may also provide advantages in terms of localization and temporal control.

Genetically encoded degrons fused to a photosensitive LOV2 domain have been reported as an optogenetic approach to protein degradation.^[48,49] Although this approach works well *in vivo* and provides a powerful method to study biological pathways, it requires transfection with a gene of interest, which limits its therapeutic applicability and can potentially create unphysiological protein levels and distributions within a cell. PHOTACs, by contrast, operate like drugs in native tissues.

An important question to address is how exactly the (*E*)- and (*Z*)-isomers of PHOTACs influence ternary complex formation and target degradation. Although an effect of photoswitching on pharmacokinetics cannot be ruled out entirely, the increased activity as a degrader seems to be primarily driven by pharmacodynamics. We consistently observed a “hook effect” and found no activity when we downregulated CRBN or in the presence of the neddylation inhibitor MLN4924, indicating that PHOTACs function as true PROTACs. Whether the photoswitch primarily affects binding to CRBN or the relative positioning of the E3 ligase and the POI remains to be determined. Molecular modeling suggests that the (*E*)-configuration of the photoswitch cannot be accommodated as well by cereblon as the (*Z*)-configuration (see SI Fig. S2.6). The importance of the exact nature, length, and orientation of the linker in PROTACs has been noted (“linkerology”).^[19,50,51] In keeping with this, we also observed a pronounced effect of the diamine spacers on our systems. In the series targeting BET proteins, **PHOTAC-I-3**, which bears a 1,4-diamino butane spacer, showed the largest difference between light and dark activity in MTS assays. Related compounds that feature shorter or longer spacers, showed smaller or no differences (see SI Fig. S2.3). **PHOTAC-I-10**, wherein the photoswitch is positioned more centrally, also showed a light-dependent behavior, whereas analogs with different linker lengths did not. Amongst compounds targeting FKBP12, the lenalidomide derivative **PHOTAC-II-5** and the thalidomide

derivative **PHOTAC-II-6**, which feature different photoswitch incorporation modes, showed the largest light activation. In the case of derivative **PHOTAC-II-5**, longer linkers were detrimental to optical control (Fig. S2.9, S2.10). A satisfying explanation of these observations will require detailed biophysical and structural investigations.

The future development of PHOTACs can be taken into many different directions. The incorporation of red-shifted and faster relaxing photoswitches could further improve the temporal and spatial precision of dark-inactive compounds.^[52] Our synthetic approaches are well suited to increase photoswitch diversity. Different ligands for E3 ligases should be explored, for instance compounds that bind to VHL or the RING ligase MDM2. The optimal position of the photoswitches will depend on the exact nature of the system. Here, we have explored two different modes of photoswitch incorporation but the third variety (photoswitch in the POI ligand), and combinations thereof, should also be considered. The POI ligand should ideally bind to its target without interfering with its function to cleanly distinguish between degradation and inhibition and to avoid unwanted toxicity.

We anticipate that PHOTACs will be useful tools in cell biology, but we believe that their clinical potential is also worthy of consideration. Since PROTACs operate in a catalytic fashion and enable systemic protein knockdown, their toxicity is a major concern.^[53,54] PHOTACs of the type described herein could be activated with light within a tissue or before administration. They would then lose their activity with a given rate, which can be determined through engineering of the switch, or they could be actively turned off with a second wavelength. Moreover, PHOTACs locally activated by light would also lose efficacy by dilution diffusing away from the point of irradiation. The usefulness of light in medicine is well established and the combination of light and molecules has been studied for decades, e.g. in Photodynamic Therapy (PDT).^[55] PDT has been applied with encouraging results to treat non-small cell lung cancer, dermatological cancers, and premalignant lesions of the upper digestive tract, and is currently in clinical trials for the treatment of a large variety of other malignancies, including prostate, brain, and breast cancers.^[55] In the past, we have used PDT both in cultured cells and in mouse models to induce death of prostate cancer cells in a calcium-dependent manner.^[56] However, from a molecular point of view, conventional PDT, while effective, is unspecific. PHOTACs, by contrast, can be reversibly activated

with the temporal and spatial precision that light affords and target specific proteins whose elimination would promote cell death. Therefore, we and others ^[57] believe that PHOTACs may provide a promising new direction in photomedicine.

Materials and Methods

Synthesis

The reagents and solvents used in this study were bought from the following chemical suppliers: ABCR, Acros Organics, Alfa Aesar, Ark Pharm, Combi-Blocks, Oakwood, OxChem, Sigma-Aldrich, Strem, Toronto Research Chemicals and were used as purchased. Dry solvents used in reactions performed under inert atmosphere were obtained by passing the degassed solvents through activated alumina columns.

Column chromatography was carried out on silica gel (60 Å pore size, 40–63 µm, Merck KGaA) using a Teledyne Isco Combiflash EZprep flash purification system.

Determination of Photophysical properties

For UV-VIS studies on the Varian Cary 60 UV-Visible Spectrophotometer, samples were stored and prepared under red light to avoid formation of the (*Z*)-isomers. 10 mM stock solutions were prepared in the dark and diluted to a final concentration of 25 µM for measurement. UV-VIS spectra of **PHOTACs** following irradiation with different wavelengths for 5 min using a monochromator. Measurement was started from the dark-adapted state followed by 370 nm and further increasing the wavelength. By increasing the wavelength from low to high we can observe how much we can switch from (*Z*)- to (*E*)-isomers, whereas going from high to low wavelength, the PSS might not be reached due to low absorptivity above 500 nm. **PHOTAC-I-1–8** were measured in PBS with 10% DMSO, whereas **PHOTAC-II-1–6** were measured in DMSO.

Thermal relaxation was measured by preirradiating **PHOTACs** with 390 nm irradiation and observing the absorption at 370 nm over 12 h at 37 °C in DMSO in tightly sealed cuvettes.

Reversible switching and photochemical stability of **PHOTAC-I-3** was demonstrated in DMSO, cycling the irradiation of the monochromator between 390 nm (3 min) and 500 nm (7 min).

Separated spectra of the (*Z*)- and (*E*)-isomers could be obtained from the internal UV-VIS detector of the LCMS, by irradiating the sample before injection, and were

normalized at the isosbestic point. In the case of non-solvochromic photoswitches, photostationary states were calculated in the region of largest absorption difference between 330 and 390 nm, from the separated spectra obtained by LCMS and the spectra obtained following irradiation with different wavelengths for 5 min, all normalized to the isosbestic point.

LED illumination

For illumination of the cells we used the cell disco system as previously described in the literature.^[36] 5 mm LEDs 370 nm (XSL-370-5E), 390 nm (VL390-5-15), 410 nm (VL410-5-15), 430 nm (VL430-5-15), 450 nm (ELD-450-525), 465 nm (RLS-B465), 477 nm (RLS-5B475-5), 490 nm (LED490-03), 505 nm (B5-433-B505), 525 nm (B5-433-B525), 545 nm (LED545-04), 572 nm (B5-433-20) and 590 nm (CY5111A-WY) were purchased from Roithner Lasertechnik. For experiments using 390 nm, cells were preirradiated for 1 min at 390 nm to quickly switch the photoswitches in the active state. Pulsed irradiation was performed using 100 ms pulses every 10 s in 96- or 6-well plates, controlled by an Arduino system.

Cell culture

The human acute lymphoblastic leukemia RS4;11 (ATCC[®] CRL1873[™]) cell line was purchased from the American Type Culture Collection and cultured in RPMI1640 medium (Gibco) with 10% fetal bovine serum (FBS) and 1% penicillin/ streptomycin (PS) in a humidified incubator at 37 °C with 5% CO₂ in air. For the experiments compounds were serially diluted in RPMI1640 without the dye phenol red (Gibco) to reduce the influence of the dye by absorption. Azobenzene stocks and dilutions were strictly kept in the dark and prepared under red light conditions.

For immunoblotting analysis, cells (2×10^6 for RS4:11) were incubated for the indicated times with PHOTACs, placed in a light-proof box, and preirradiated for 1 min at 390 nm followed by 100 ms pulses every 10 s or were kept in the dark for 4 h. After incubation, cells were collected in the dark by centrifugation (150 g, 5 min) at 4 °C and the pellets were washed twice with ice cold PBS (1 mL).

Colorimetric MTS Assays

The activity of dehydrogenase enzymes in metabolically active cells, as a quantitative measurement for cytotoxicity and proliferation, was determined by colorimetric

measurement of the reduction of [3-(4,5-dimethylthiazol-2-yl)-5-(3-carboxymethoxyphenyl)-2-(4-sulfophenyl)-2H-tetrazolium (MTS) to the formazan derivative. The absorbance of formazan at 490 nm was measured on a FLUOstar Omega microplate reader (BMG Labtech). Cells were treated with different concentrations, ranging of our compounds (from 10 μ M to 1 nM/1 pM) in triplicates or sextuplicates, using 1% DMSO as cosolvent, and incubated on a 96-well plate for 72 h. They were placed in light-proof boxes and exposed to the lighting conditions specified in the experiment for 72 h. Next, 10 μ L of Promega CellTiter 96[®] AQueous One Solution Reagent was added to each well and incubated for further 4-7 hours at 37 °C. The absorbance at 490 nm was then recorded with a 96-well plate reader. Data was analyzed using GraphPad Prism Version 5.01 (GraphPad Software Inc) and fitted using the Sigmoidal dose-response (variable slope) fit. Results represent the mean viability \pm SEM relative to the 1% DMSO treated control.

Immunoblotting Analysis

Cells were lysed in RIPA buffer containing protease and phosphatase inhibitor and protein concentration was determined using BCA (Thermo Fisher). Immunoblotting was performed as previously described (Marzio et al., 2019).^[58] Briefly, samples were resolved under denaturing and reducing conditions using 4%–12% Bis-Tris gels (NuPAGE) and transferred to a PDVF membrane (Immobilon-P, Millipore). Membranes were blocked with 5% nonfat dried milk, incubated with primary antibodies overnight at 4°C. After washing the membranes, secondary antibodies coupled with horseradish peroxidase were applied (Amersham-GE). Immunoreactive bands were visualized by enhanced chemiluminescence reagent (Thermo Fisher Scientific), and signal was acquired using ImageQuant LAS 400 (GE).

Table 2.1. Antibodies used in this study.

Antibodies	Source	Identifier
β -Actin	Cell Signaling Technology	#4970
BRD2	Bethyl	A302-583A
BRD3	Bethyl	A302-368A-1
BRD4	Cell Signaling Technology	#13440
c-MYC	Cell Signaling Technology	#5605

PARP1	Cell Signaling Technology	cat. No. 9542S
PCNA	dako	cat. No. M0879
α TUBULIN	Sigma Aldrich	T6557
γ TUBULIN	Sigma Aldrich	T6074
FKBP12	Santa Cruz Biotechnology	cat. No. sc-133067
CUL4A	Bethyl	A300-739A
MCM2	Santa Cruz Biotechnology	cat. No. sc-9839
anti-Rabbit IgG, peroxidase-linked antibody	Thermo Fisher	NA934
anti-Mouse IgG, peroxidase-linked antibody	Thermo Fisher	NA931
anti-goat IgG-HRP	Santa Cruz Biotechnology	cat. No. sc-2354

siRNA Knockdown of CRBN

Real-time PCR was performed as previously described ^[56]. For knockdown of CRBN, MB-MDA-231 cells were seeded 18 h before transfection. The following ON-TARGET^{plus} siRNA oligos from Dharmacon were transfected with Lipofectamine for 8 hours, according to the manufacturer's instructions (RNAiMAX, ThermoFischer): ON-TARGET^{plus} human CRBN SMARTpool (L-021086-00-0005), ON-TARGET^{plus} non-targeting control siRNA (D-001810-01-05). The medium was replaced and cells were incubated for 40 hours, upon which they were resubjected to another cycle of siRNA transfection. Medium was replaced and after 1 hour, the cells were treated with PHOTAC-I-3 or vehicle for 18 hours under pulsed irradiation at 390 nm or in the dark, upon which the cells were collected and subjected to immunoblotting analysis as described above. Gene silencing was validated by RT-PCR, isolating total RNA using Qiagen's RNeasy kit (cat. no. 74104). Reverse transcription of the mRNA was carried out using 3 μ g of total RNA using random hexamers and oligo(dT)₁₈ primers with SMART MMLV Reverse Transcriptase (RNA to cDNA EcoDry Premix, Takara, cat. no. 639549) according to manufacturer's instruction. The RT-PCR reaction was carried out using PowerUp SYBR Green (ThermoFischer, cat. no. A25742) with the ThermoFischer QuantStudio 3 Real-Time PCR system in a 96-well format. Bar graphs represent the relative ratio of CRBN to GAPDH values. The following primers were used for RT-PCR: human CRBN (primer set 1) ^[59], forward: 5'-CCAGTCTGCCGACATCACAT-3', reverse: 5'-GTCATCGTGCAAAGTCCTGC-3'; human CRBN (primer set 2) ^[60], forward: 5'-CAGTCTGCCGACATCACATAC-3',

reverse: 5'-GCACCATACTGACTT CTTGAGGG-3'; human GAPDH, forward: 5'-TGCACCACCAACTGCTTAGC-3', reverse: 5'-GGCATGGACTGTGGTCATGAG-3'.

Acknowledgements

The authors are indebted to Thomas J. Wandless for a generous gift of SLF ligand. M.P. is grateful to T.M. Thor for continuous support. All data needed to evaluate the conclusions in the paper are present in the paper and/or the Supplementary Materials. Additional data related to this paper may be requested from the authors.

Funding

We thank New York University for financial support. NMR spectra were acquired using the TCI cryoprobe supported by the NIH (OD016343). This work was partially funded by grant R01-CA76584 from the National Institutes of Health to M.P. and a fellowship from the T32-CA009161 (Levy) grant to A.M. M.P. is an investigator with the Howard Hughes Medical Institute.

Conflict of interest

M.R., B.M., M.B., D.T. are inventors on a patent application on PHOTACs. M.P. is a member of the scientific advisory boards of CullGen Inc. and Kymera Therapeutics and a consultant for BeyondSpring Pharmaceutical. All other authors declare that they have no competing interests.

Author contributions

D.T., M.R., and B. M. conceived the study. M.R., B.M., M.B., D.S, and A.M. designed experiments and analyzed the data. D.T. and M.P. supervised the experiments. D.T., M.R. and B.M. wrote the paper with input from all authors.

Supplementary Information

Supplementary Figures

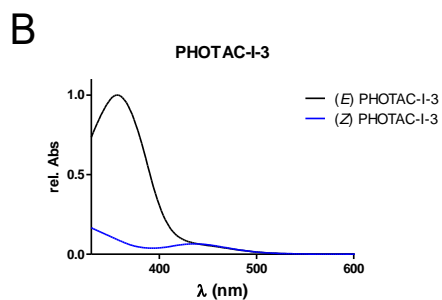
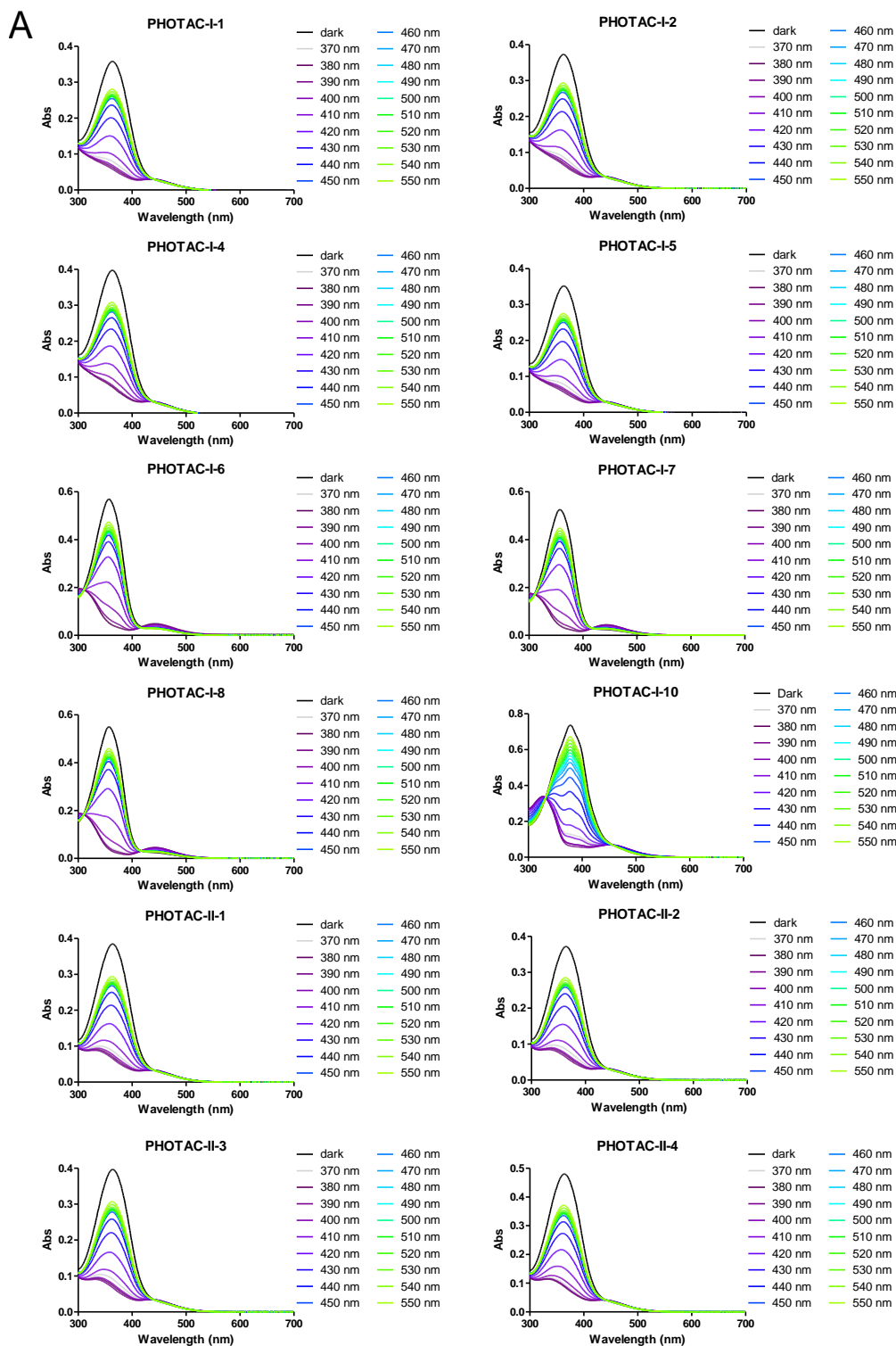


Fig. S2.1. UV-Vis characterization. A) UV-VIS spectra of **PHOTACs-I** and **PHOTACs-II** following irradiation with the indicated wavelengths for 5 min. B) Separated UV-VIS spectra of **(E)-** and **(Z)-PHOTAC-I-3** as obtained from the LCMS and normalized at the isosbestic point.

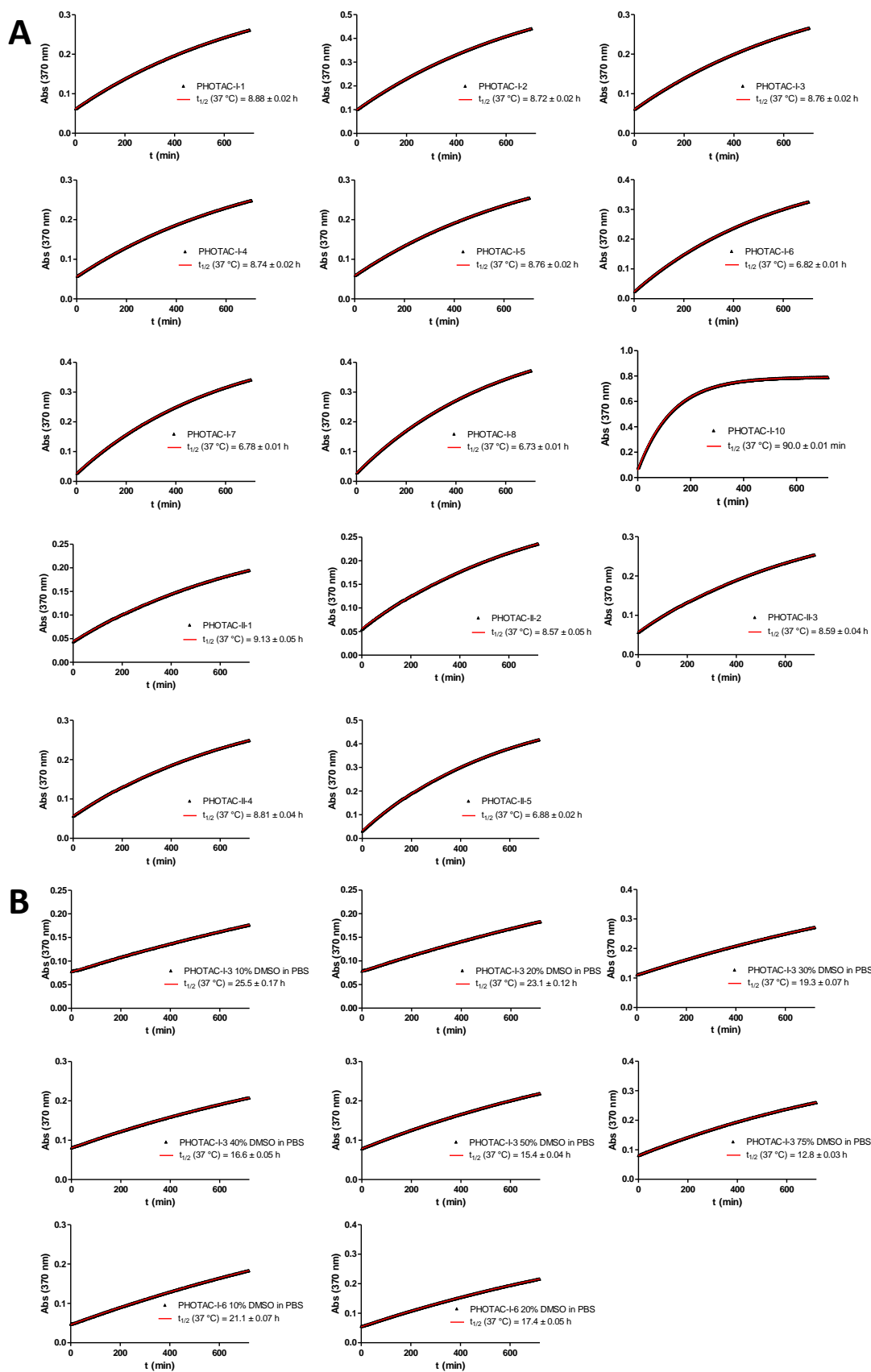
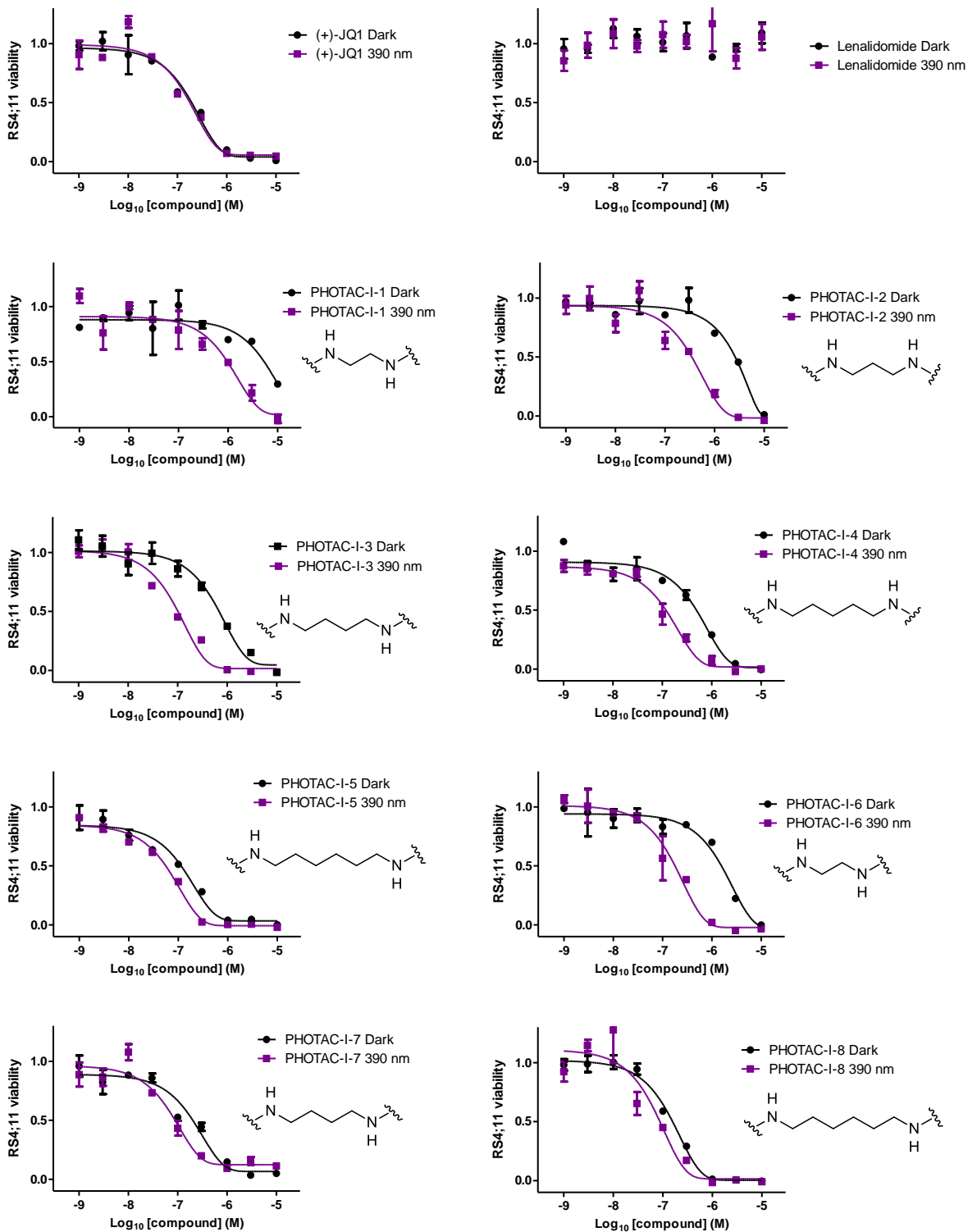


Fig. S2.2. Thermal relaxation. A) Thermal relaxation of (Z)-PHOTACs in DMSO. B) Thermal relaxation of (Z)-PHOTACs in DMSO-PBS mixtures.

2 – PHOTACs Enable Optical Control of Protein Degradation



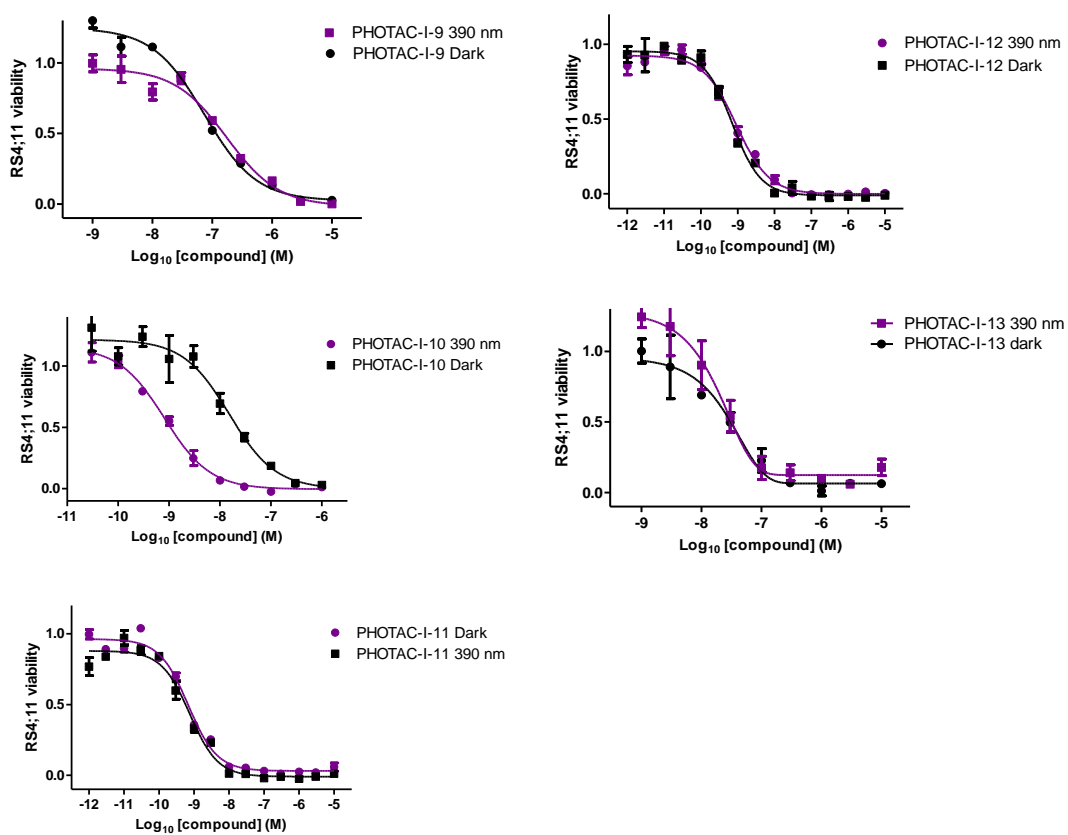


Fig. S2.3. Viability of RS4;11 acute lymphoblastic leukemia cells after treatment with PHOTACs-I for 72 h in the dark or under pulsed (100 ms every 10 s) 390 nm irradiation.

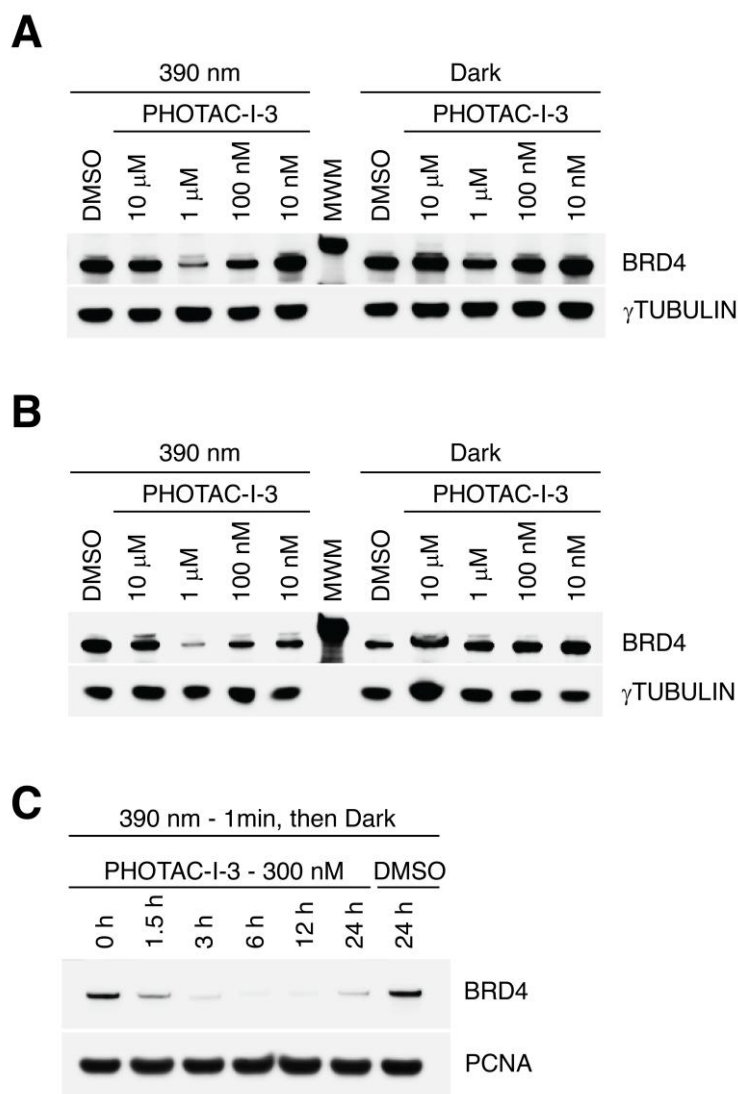


Fig. S2.4. Immunoblot analysis of **PHOTAC-I-3** A) Immunoblot analysis after treatment of MB-MDA-231 cells with **PHOTAC-I-3** for 18 h at different concentrations. Cells were either irradiated with 100 ms pulses of 390 nm light every 10 s (left) or kept the dark (right). B) Immunoblot analysis after treatment of MB-MDA-468 cells with **PHOTAC-I-3** for 18 h at different concentrations. Cells were either irradiated with 100 ms pulses of 390 nm light every 10 s (left) or kept the dark (right). (MWM, molecular weight marker). C) Immunoblot of BRD4 degradation in RS4;11 cells, promoted by **PHOTAC-I-3** (300 nM) after 1 minute of irradiation (100 ms every 10 s), highlighting sustained degradation at the applied dosage.

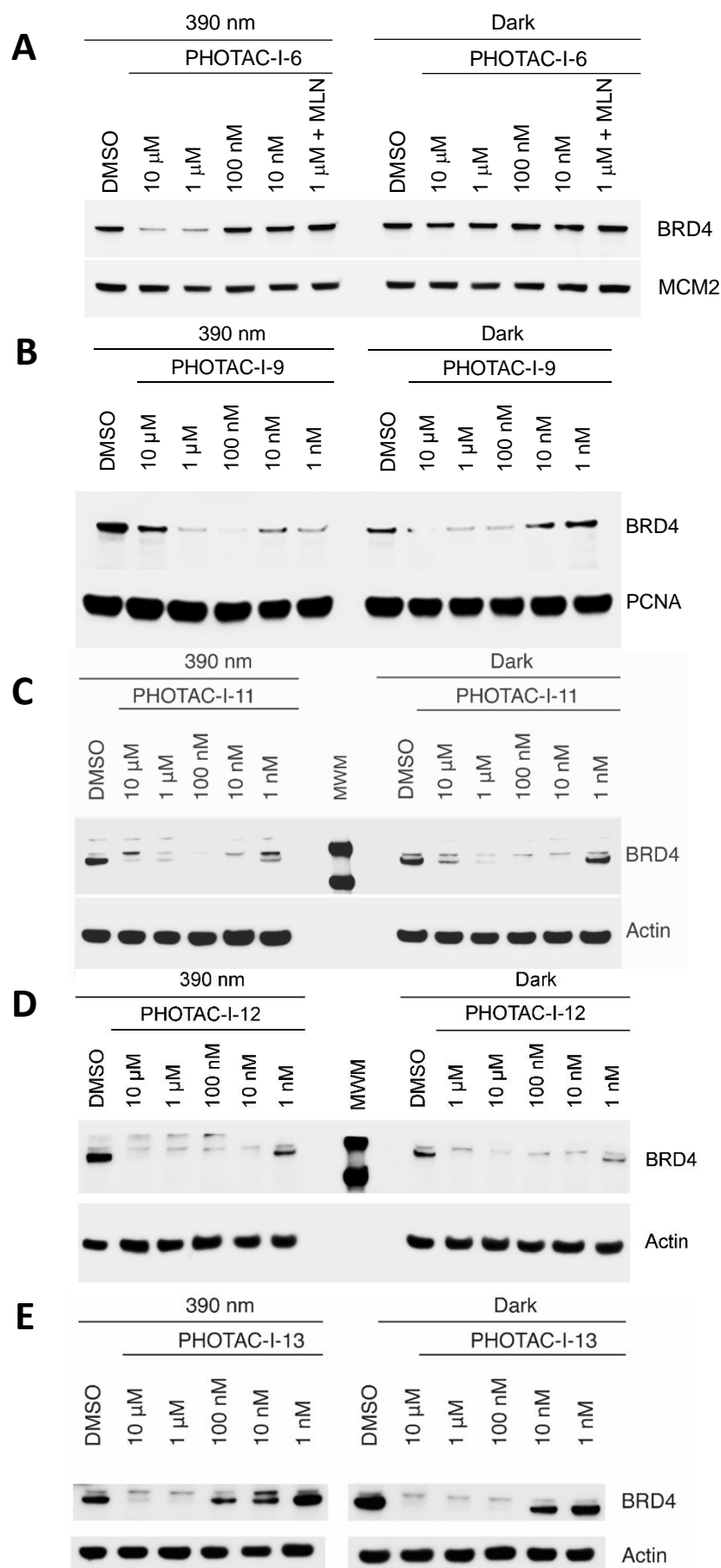


Fig. S2.5. Immunoblot analysis of BRD4 after treatment of RS4;11 cells with PHOTACs. A) **PHOTAC-I-6**, B) **PHOTAC-I-9**, C) **PHOTAC-I-11**, D) **PHOTAC-I-12** or E) **PHOTAC-I-13** for 4 h at different concentrations. Cells were either irradiated with 100 ms pulses of 390 nm light every 10 s (left) or kept the dark (right). (MWM, molecular weight marker).

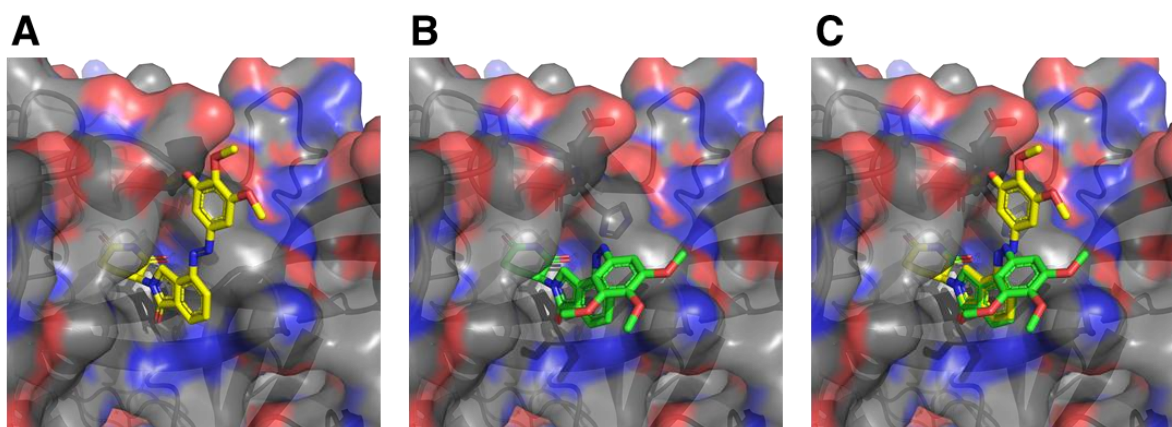


Fig. S2.6. Model of the photoswitch-cereblon interaction. Structure model of an (*E*)- (A) or (*Z*)- (B) azobenzene bound to cereblon. Model derived from the crystal structure of lenalidomide bound to cereblon (PDB: 4CI2)^[61], showing the clash between the (*E*)-azobenzene and cereblon, whereas the (*Z*)-isomer is accommodated by the binding pocket. Models were created using Schrödinger Maestro 11.9. (C) Overlay of both structures.

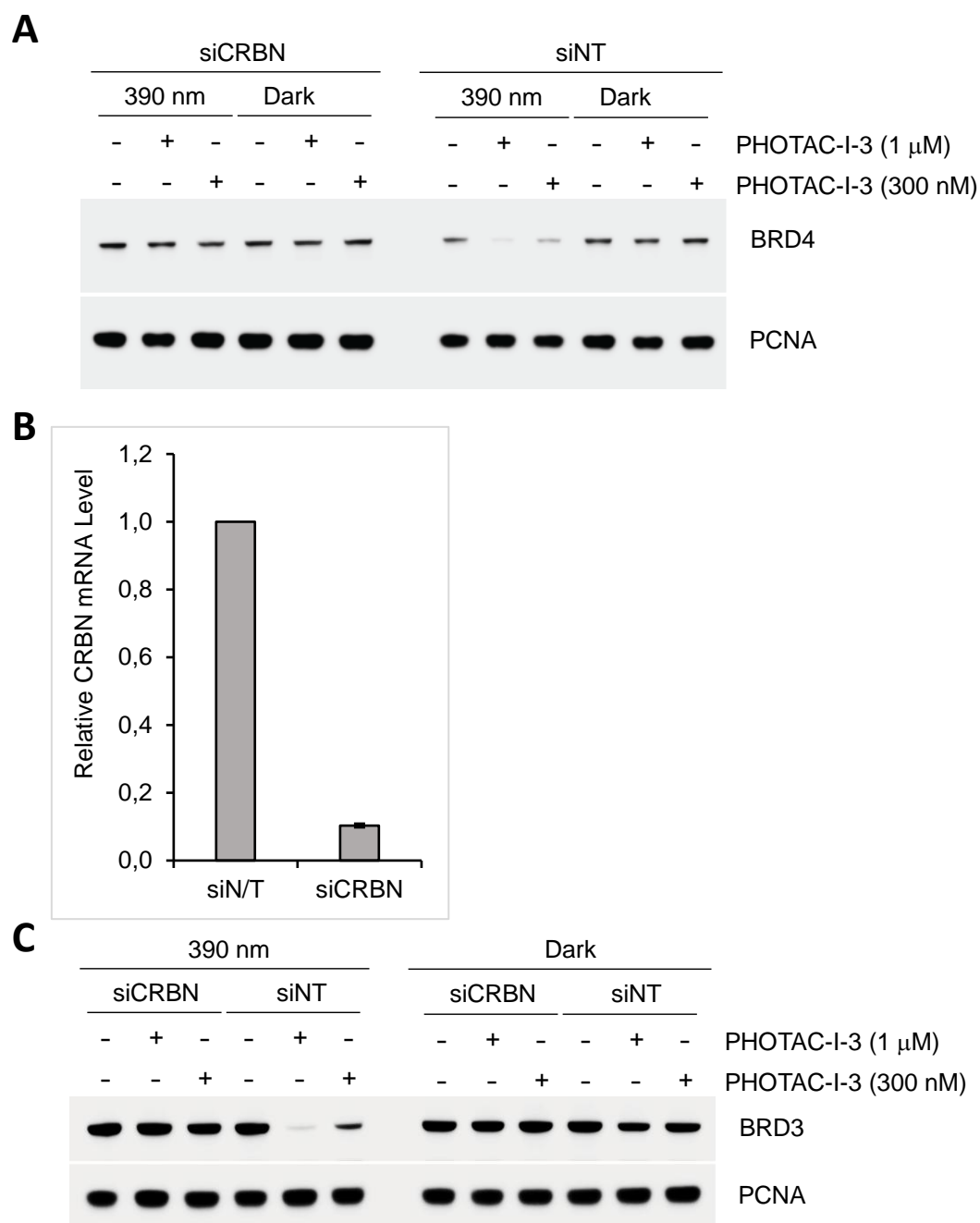


Fig. S2.7. CRBN knockdown control. A) Immunoblot of BRD4 degradation after 18 h of **PHOTAC-I-3** treatment in the dark or with 390 nm pulsed irradiation (100 ms every 10 s) in MB-MDA-231 cells, pre-treated with CRBN siRNA or non-targeting (NT) siRNA. B) mRNA expression levels of CRBN in MB-MDA-231 cells, treated with CRBN siRNA or non-targeting (NT) siRNA. C) Immunoblot of BRD3 degradation after 18h of **PHOTAC-I-3** treatment in the dark or with 390 nm pulsed irradiation (100 ms every 10 s) in MB-MDA-231 cells, pre-treated with CRBN siRNA or non-targeting (NT) siRNA.

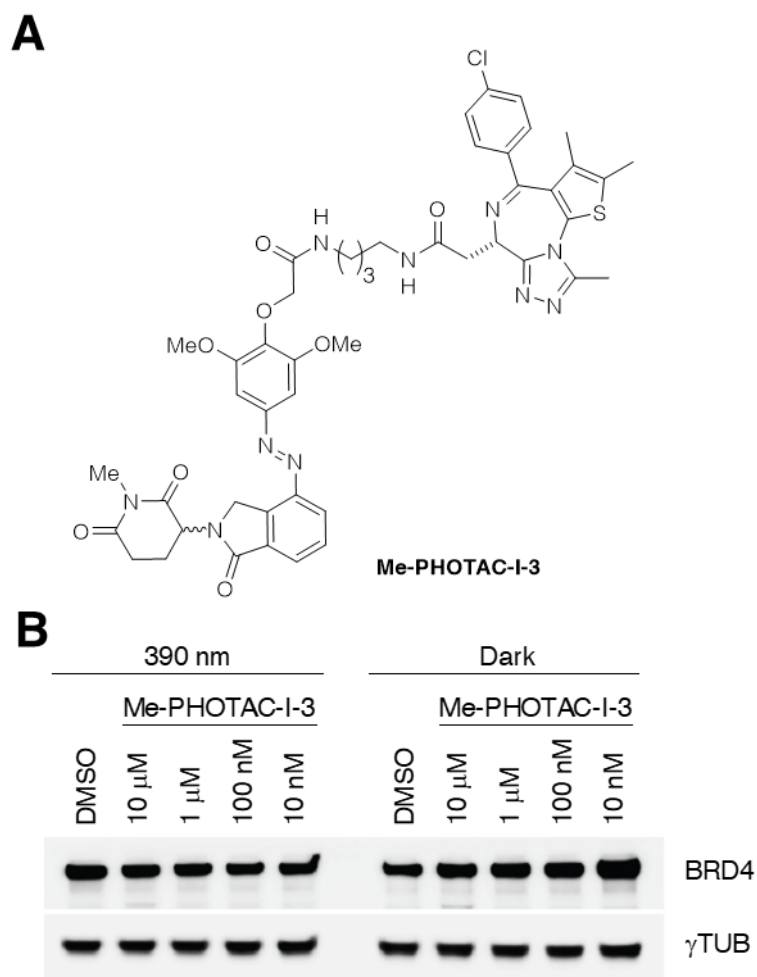


Fig. S2.8. Me-PHOTAC-I-3 control. A) Structure of inactive control **Me-PHOTAC-I-3**
 B) Immunoblot of BRD4 levels after 4 h of **Me-PHOTAC-I-3** treatment in RS4;11 cells in the dark or with 390 nm pulsed irradiation (100 ms every 10 s).

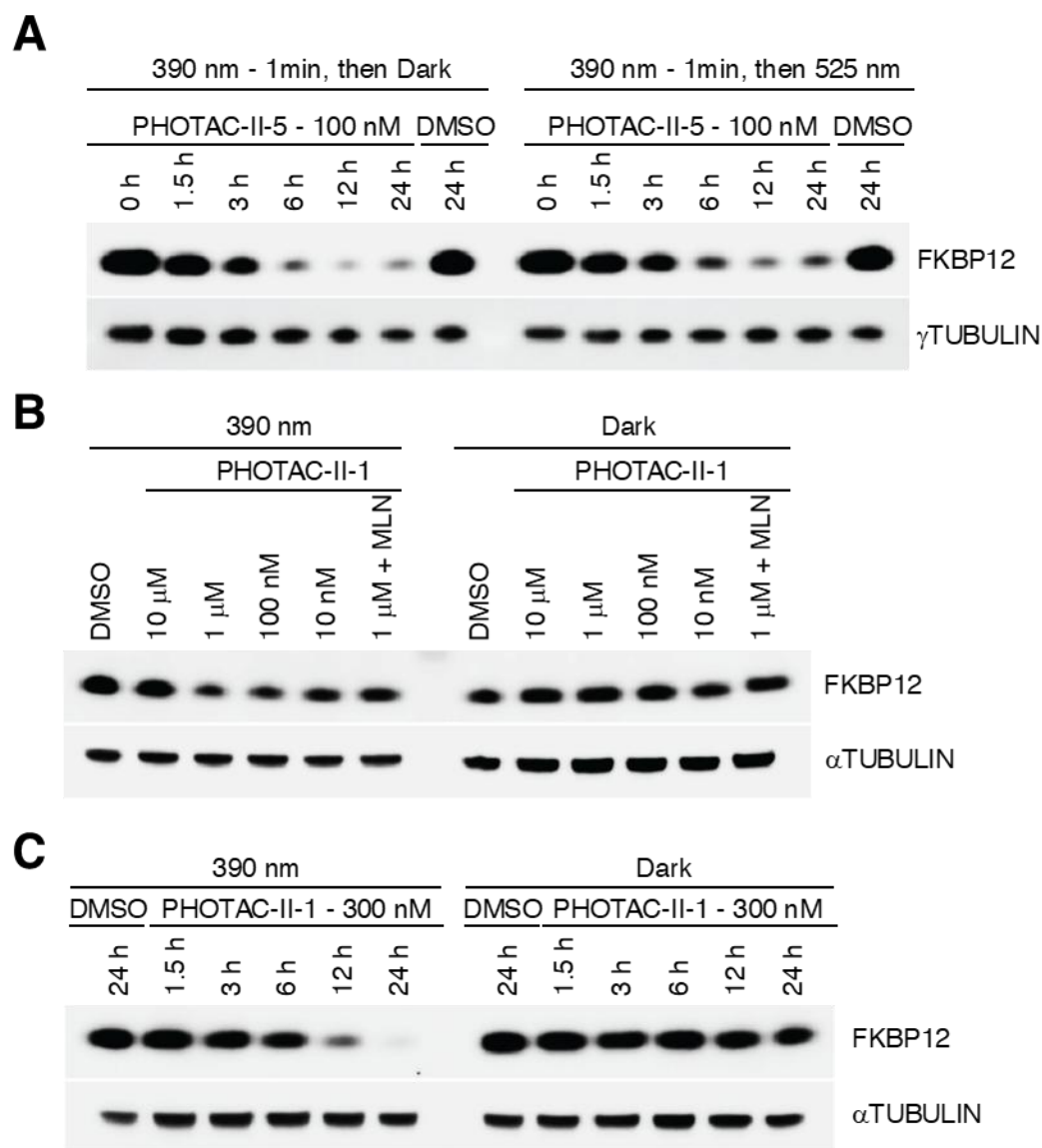


Fig. S2.9. FKBP12 Immunoblots in RS4;11 cells. A) Immunoblot of a rescue experiment demonstrating the reversibility of FKBP12 degradation promoted by **PHOTAC-II-5** through thermal relaxation (left) or optical inactivation by 525 nm pulsed irradiation (right, 100 ms every 10 s). B) Degradation of FKBP12. Immunoblot analysis of FKBP12 after treatment of RS4;11 cells with **PHOTAC-II-1** for 4 h at different concentrations. Cells were either irradiated with 100 ms pulses of 390 nm light every 10 s (left) or kept the dark (right). C) Time course of FKBP12 degradation visualized by immunoblotting. RS4;11 cells were treated with **PHOTAC-II-1** (300 nM) and collected at the indicated time points, showing slow, but sustained FKBP12 degradation over time when irradiated with 390 nm light (left, 100 ms every 10 s), but not when kept in the dark (right).

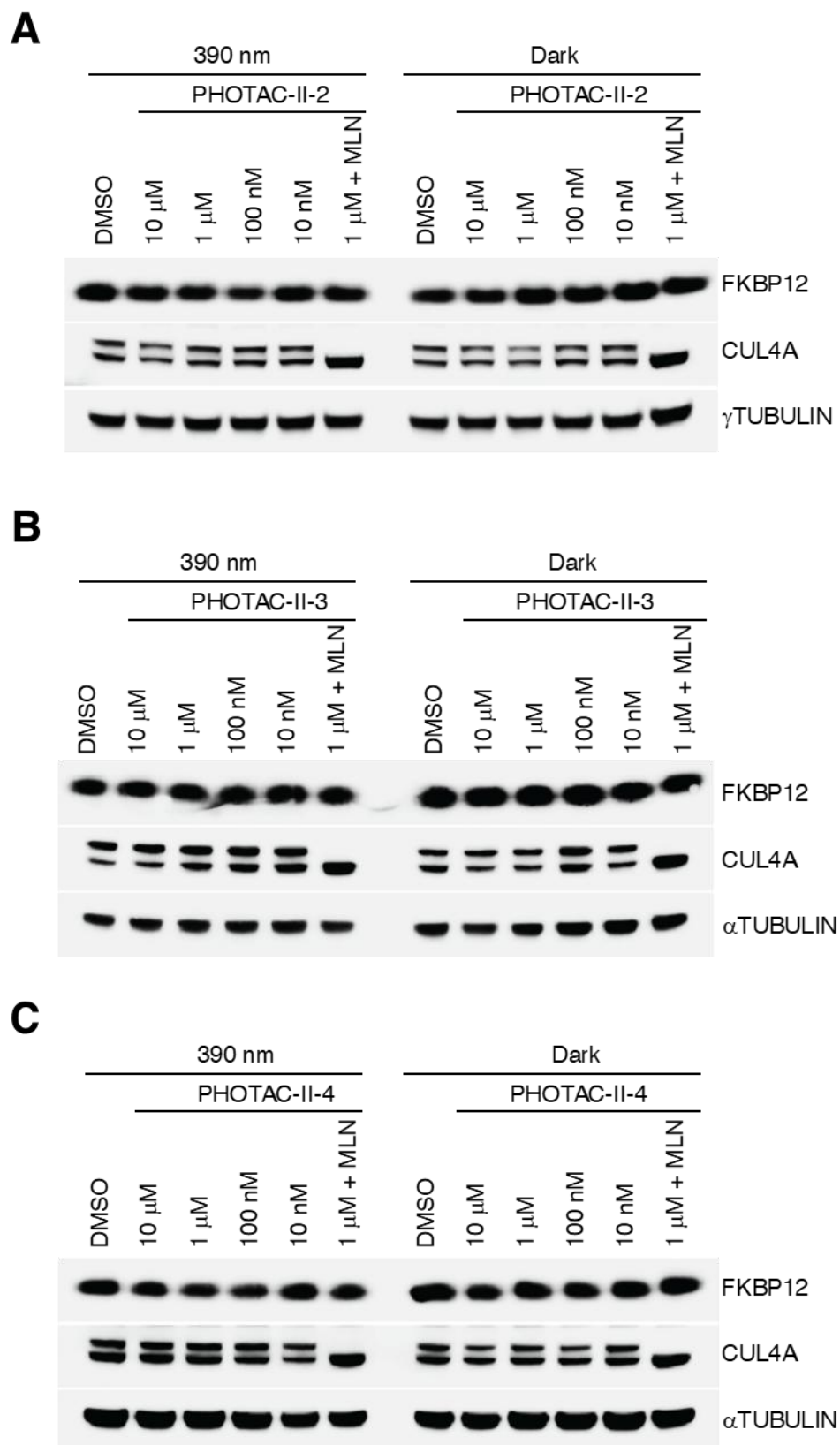


Fig. S2.10. Immunoblot analysis of FKBP12 after treatment of RS4;11 cells. A) **PHOTAC-II-2**, B) **PHOTAC-II-3** or C) **PHOTAC-II-4** for 4 h at different concentrations. Cells were either irradiated with pulses of 390 nm light (right, 100 ms every 10 s) or kept the dark (left).

General information

The reagents and solvents used in this study were bought from the following chemical suppliers: ABCR, Acros Organics, Alfa Aesar, Ark Pharm, Combi-Blocks, Oakwood, OxChem, Sigma-Aldrich, Strem, Toronto Research Chemicals and were used as purchased.

Dry solvents used in reactions performed under inert atmosphere were obtained by passing the degassed solvents through activated alumina columns.

Column chromatography was carried out on silica gel (60 Å pore size, 40–63 µm, Merck KGaA) using a Teledyne Isco Combiflash EZprep flash purification system.

Thin-layer chromatography (TLC) was performed on glass plates precoated with silica gel (0.25 mm, 60-Å pore size, Merck). TLC plates were visualized by exposure to UV light (254 and 366 nm).

NMR spectra were obtained on a Bruker Avance III HD 400 MHz spectrometer equipped with a CryoProbe™ operating at 400 MHz for ¹H and 100 MHz for ¹³C spectra or on a Bruker AVIII-600 High Performance Digital NMR Spectrometer (600 MHz for ¹H and 150 MHz for ¹³C spectra) with CPTCI-cryoprobehead.

Integration results and multiplets are reported as observed and denoted as follows: s (singlet), d (doublet), t (triplet), q (quartet), p (pentet), h (hextet), and m (multiplet) and as combinations thereof.

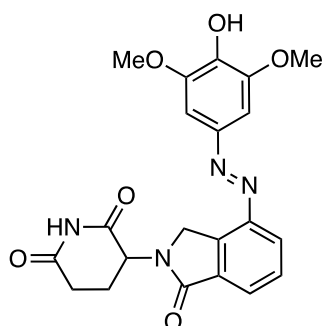
High-resolution mass spectra (HRMS) were recorded on an Agilent Technologies 6224 Accurate-Mass time-of-flight spectrometer with either atmospheric pressure chemical ionization (APCI) or electrospray ionization (ESI) ionization sources.

LCMS were measured on an Agilent Technologies 1260 II Infinity connected to an Agilent Technologies 6120 Quadrupole mass spectrometer with ESI ionization source. Elution was performed using a gradient from 5:95% to 100:0% MeCN:H₂O with 0.1% formic acid over 5 min, if not indicated otherwise. Separated isomer spectra of azobenzenes were obtained by irradiation of the LCMS sample prior to injection.

UVVis spectrometry was performed on a Varian Cary 60 UV-Visible Spectrophotometer using disposable BRAND UV-Cuvette Disposable Spectrophotometer/Photometer Ultra-Micro Cuvettes, BrandTech (10 mm light path), an Agilent Technologies PCB 1500 Water Peltier system for temperature control and samples were irradiated with a Cairn Research Optoscan Monochromator with Optosource High Intensity Arc Lamp equipped with a 75 W UXL-S50A lamp from USHIO Inc. Japan and set to 15 nm full width at half maximum.

Synthetic Procedures and Characterization

(*E*)-3-(4-((4-hydroxy-3,5-dimethoxyphenyl)diazenyl)-1-oxoisindolin-2-yl)piperidine-2,6-dione (**2**)



Lenalidomide (500 mg, 1.93 mmol, 1.0 eq.) was dissolved in 1 M HCl (50 mL). Concentrated aqueous HBF₄ (2 mL, 48 wt.%) was added to the mixture. After completely dissolving of the starting material, 2 M NaNO₂ (1.06 mL) was added to the solution at 0 °C. After stirring for 1 h the solution was added dropwise into a mixture of 2,6-Dimethoxyphenol (357 mg, 2.32 mmol, 1.2 eq.) in H₂O (50 mL), MeOH (20 mL), NaHCO₃ (4.000 g, 47.62 mmol, 24.7 eq.) and Na₂CO₃ (5.000 g, 47.18 mmol, 24.5 eq.). Upon addition the solution turned from violet to strong red and was stirred for 1 additional hour at 0 °C. The reaction was extracted with EtOAc (7x 100 mL) and washed once with brine (1x 100 mL). The organic phase was dried over Na₂SO₄ and concentrated under reduced pressure. Purification of the resulting crude product by flash column chromatography (CH₂Cl₂/MeOH gradient, 0 → 10% MeOH) gave **2** (562.0 mg, 1.324 mmol, 69%) as a yellow solid.

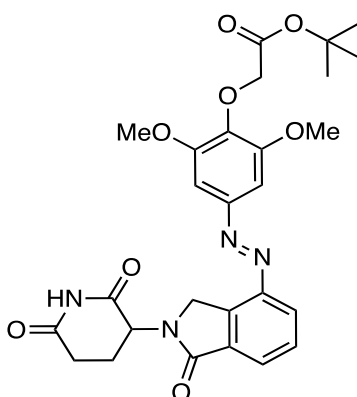
R_f = 0.33 (CH₂Cl₂:MeOH, 19:1).

¹H NMR (400 MHz, DMSO-*d*₆) δ = 11.03 (s, 1H), 9.48 (s, 1H), 8.16 (d, *J* = 7.7 Hz, 1H), 7.87 (d, *J* = 7.4 Hz, 1H), 7.77 (t, *J* = 7.6 Hz, 1H), 7.34 (s, 2H), 5.16 (dd, *J* = 13.1, 5.0 Hz, 1H), 4.82 (d, *J* = 19.0 Hz, 1H), 4.69 (d, *J* = 19.0 Hz, 1H), 3.90 (s, 6H), 2.95 (ddd, *J* = 17.5, 13.4, 5.2 Hz, 1H), 2.63 (d, *J* = 18.8 Hz, 1H), 2.55 (dd, *J* = 13.1, 4.5 Hz, 1H), 2.11 – 2.03 (m, 1H) ppm.

¹³C NMR (100 MHz, DMSO-*d*₆) δ = 173.39, 171.52, 167.76, 148.68, 147.05, 144.80, 140.86, 134.77, 134.21, 129.98, 128.37, 125.04, 101.69, 56.68, 52.30, 48.76, 31.76, 22.7 ppm.

HRMS (ESI): calcd. for $C_{21}H_{21}N_4O_6^+$: 425.1456 m/z $[M+H]^+$
 found: 425.1458 m/z $[M+H]^+$.
LCMS (ESI): t_{ret} = 2.90 min. 425 m/z $[M+H]^+$.

Tert-butyl (E)-2-(4-((2-(2,6-dioxopiperidin-3-yl)-1-oxoisoindolin-4-yl)diazenyl)-2,6-dimethoxyphenoxy)acetate (S1)



To tert-butyl bromoacetate (234 mg, 1.20 mmol, 1 eq.) was added dry DMF (10 mL), **2** (509 mg, 1.20 mmol, 1 eq.) and K_2CO_3 (215 mg, 1.56 mmol, 1.3 eq.) at room temperature. After stirring for 2.5 hours, the mixture was diluted with EtOAc (100 mL), separated against $NaHCO_3$ (50 mL), extracted with EtOAc (3x 50 mL), and washed with 10% LiCl (3x 50 mL) and brine (2x 50 mL). The reaction was concentrated under reduced pressure. Purification of the resulting crude product by flash column chromatography (Hx/Ea gradient, 20 → 100% Ea, the product was eluted at 75%.) gave **S1** (501 mg, 0.93 mmol, 78%) as a yellow solid.

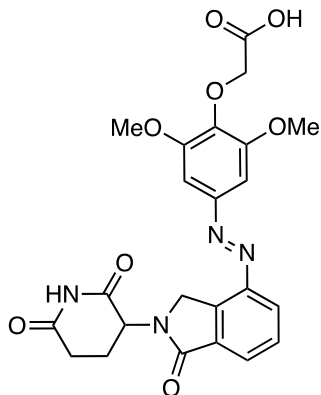
R_f = 0.64 [EtOAc].

1H NMR (400 MHz, $DMSO-d_6$) δ = 11.03 (s, 1H), 8.22 (d, J = 7.7 Hz, 1H), 7.92 (d, J = 7.4 Hz, 1H), 7.80 (t, J = 7.7 Hz, 1H), 7.34 (s, 2H), 5.16 (dd, J = 13.2, 5.0 Hz, 1H), 4.83 (d, J = 19.1 Hz, 1H), 4.70 (d, J = 19.1 Hz, 1H), 4.60 (s, 2H), 3.90 (s, 6H), 2.93 (d, J = 12.7 Hz, 1H), 2.63 (d, J = 19.6 Hz, 1H), 2.58 – 2.52 (m, 1H), 2.11 – 2.03 (m, 1H), 1.43 (s, 9H) ppm.

^{13}C NMR (100 MHz, $\text{DMSO}-d_6$) δ = 173.38, 171.48, 168.16, 167.64, 152.82, 148.14, 146.86, 139.71, 134.96, 134.28, 130.08, 128.97, 125.78, 101.26, 81.47, 69.69, 56.77, 52.31, 48.78 31.75, 28.20, 22.77 ppm.

HRMS (ESI): calcd. for $\text{C}_{27}\text{H}_{31}\text{N}_4\text{O}_8^+$: 539.2137 m/z $[\text{M}+\text{H}]^+$
 found: 539.2172 m/z $[\text{M}+\text{H}]^+$.

LCMS (ESI): $t_{\text{ret}} = 3.42$ (*Z*). 539 m/z $[\text{M}+\text{H}]^+$.
 $t_{\text{ret}} = 3.93$ (*E*) min. 539 m/z $[\text{M}+\text{H}]^+$.

(E)-2-(4-((2-(2,6-dioxopiperidin-3-yl)-1-oxoisoindolin-4-yl)diazenyl)-2,6-dimethoxyphenoxy)acetic acid (3)

S2 (475 mg, 0.88 mmol, 1 eq.) was dissolved in CH₂Cl₂:TFA (1:1; 5 mL each). Upon TFA addition (5 mL) the solution turned from yellow to dark red. After 2 hours the reaction was concentrated under reduced pressure, turning from red to an orange solid. The reaction was dried under high vacuum for 48 h. **3** (557 mg, 0.878 mmol, 99%) was obtained as trifluoroacetate in form of a yellow solid with traces of residual TFA.

$R_f = 0.5$ [CH₂Cl₂:MeOH, 9:1].

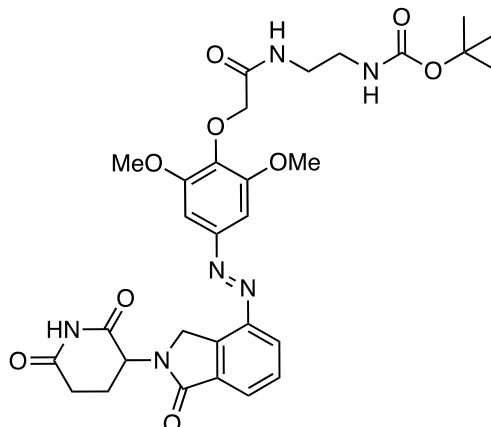
¹H NMR (400 MHz, DMSO-*d*₆) $\delta = 11.03$ (s, 1H), 8.22 (d, $J = 7.8$ Hz, 1H), 7.92 (d, $J = 7.5$ Hz, 1H), 7.80 (t, $J = 7.7$ Hz, 1H), 7.34 (s, 2H), 5.16 (dd, $J = 13.2, 5.0$ Hz, 1H), 4.83 (d, $J = 19.1$ Hz, 1H), 4.70 (d, $J = 19.1$ Hz, 2H), 4.60 (s, 2H), 3.90 (s, 6H), 2.95 (ddd, $J = 17.7, 13.6, 5.3$ Hz, 1H), 2.68 – 2.53 (m, 2H), 2.11 – 2.03 (m, 1H). ppm.

¹³C NMR (100 MHz, DMSO) $\delta = 172.91, 171.01, 169.95, 167.17, 152.58, 147.80, 146.41, 139.24, 134.50, 133.82, 129.63, 128.52, 125.35, 100.87, 68.67, 56.33, 51.85, 48.30, 31.28, 22.30$ ppm.

HRMS (ESI): calcd. for C₂₃H₂₃N₄O₈⁺: 483.1510 m/z [M+H]⁺
found: 483.1549 m/z [M+H]⁺.

LCMS (ESI): $t_{ret} = 2.93$ min. 483.1 m/z [M+H]⁺.

***tert*-butyl (*E*)-(2-(2-(4-((2-(2,6-dioxopiperidin-3-yl)-1-oxoisindolin-4-yl)diazenyl)-2,6-dimethoxyphenoxy)acetamido)ethyl)carbamate (**S4**)**



3 (19.0 mg, 0.039 mmol, 1.0 eq.) and HATU (26.9 mg, 0.083 mmol, 2.1 eq.) were dissolved in dry DMF (1 mL) at room temperature. After 5 minutes of stirring *N*-Boc-1,2-ethyldiamine (33.2 mg, 0.207 mmol, 5.3 eq.) and *i*-Pr₂NEt (26.8 mg, 0.207 mmol, 5.3 eq., 36 μ L) were added to the mixture and stirred for additional 12 h at room temperature. The reaction was diluted with EtOAc (20 mL), separated against H₂O (20 mL), extracted with EtOAc (3x 20 mL), and washed with 10% LiCl (2x 20 mL) and brine (3x 30 mL). The combined organic phase was dried over Na₂SO₄ and concentrated under reduced pressure. Purification of the resulting crude product by flash column chromatography (CH₂Cl₂/MeOH gradient, 0-20% MeOH) gave **S4** (15.3 mg, 0.024 mmol, 62%) as a yellow solid.

$R_f = 0.32$ [Hx:EA, 2:1].

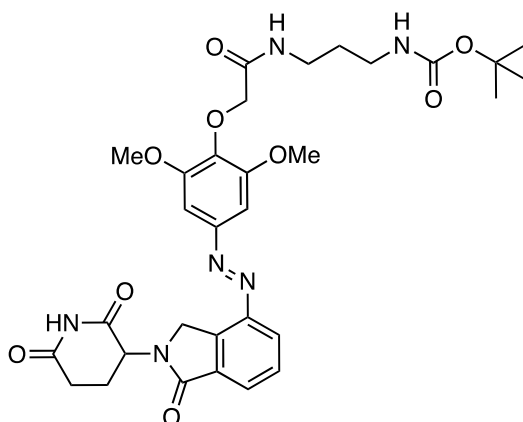
¹H NMR (400 MHz, Chloroform-*d*) δ = 8.21 (d, $J = 7.8$ Hz, 1H), 8.02 (d, $J = 7.5$ Hz, 1H), 7.99 (s, 1H), 7.89 (t, $J = 5.6$ Hz, 1H, br), 7.72 (t, $J = 7.7$ Hz, 1H), 7.22 (s, 2H), 5.27 (dd, $J = 13.3, 5.1$ Hz, 1H), 4.86 (d, $J = 17.9$ Hz, 1H), 4.75 (s, 1H), 4.62 (s, 2H), 4.01 (s, 6H), 3.49 (q, $J = 6.0$ Hz, 2H), 3.32 (d, $J = 5.7$ Hz, 2H), 3.00 – 2.81 (m, 2H), 2.47 (dd, $J = 13.1, 5.0$ Hz, 1H), 2.27 (ddd, $J = 10.3, 5.1, 2.6$ Hz, 1H), 1.44 (d, $J = 4.7$ Hz, 9H) ppm.

¹³C NMR (100 MHz, CDCl₃) δ = 170.98, 170.37, 169.51, 168.57, 156.18, 152.79, 149.09, 146.93, 139.86, 134.12, 133.45, 130.05, 129.66, 126.44, 100.65, 79.66, 72.84, 56.60, 52.15, 48.29, 39.17, 31.76, 28.54, 23.62, 19.18 ppm.

HRMS (ESI): calcd. for C₃₀H₃₇N₆O₉⁺: 265.2617 m/z [M+H]⁺
 found: 265.2629 m/z [M+H]⁺.

LCMS (ESI): $t_{\text{ret}} = 3.11$ (*Z*) min. 623 m/z [M–H][–].
 $t_{\text{ret}} = 3.44$ (*E*) min. 623 m/z [M–H][–].

***tert*-butyl (*E*)-(3-(2-(4-((2-(2,6-dioxopiperidin-3-yl)-1-oxoisindolin-4-yl)diazenyl)-2,6-dimethoxyphenoxy)acetamido)propyl)carbamate (**S5**)**



3 (60.0 mg, 0.095 mmol, 1.0 eq.) and HATU (46.0 mg, 0.142 mmol, 1.5 eq.) were dissolved in dry DMF (5 mL) at room temperature. After 5 minutes of stirring *N*-Boc-1,3-diaminopropane (65.9 mg, 0.378 mmol, 4.0 eq. 70 μL) and *i*-Pr₂NEt (48.9 mg, 0.378 mmol, 4.0 eq., 66 μL) were added to the mixture and stirred for additional 12 h at room temperature. The reaction was diluted with EtOAc (20 mL), separated against H₂O/10% LiCl (1:1, 10 mL:10 mL), extracted with EtOAc (2x 20 mL) and washed with 10% LiCl (2x 20 mL) and brine (2x 20 mL). The combined organic phase was dried over Na₂SO₄ and concentrated under reduced pressure. Purification of the resulting crude product by flash column chromatography (CH₂Cl₂/MeOH gradient, 0-20% MeOH) gave **S5** (51.5 mg, 0.081 mmol, 86%) as a yellow solid.

$R_f = 0.19$ [CH₂Cl₂:MeOH, 9:1].

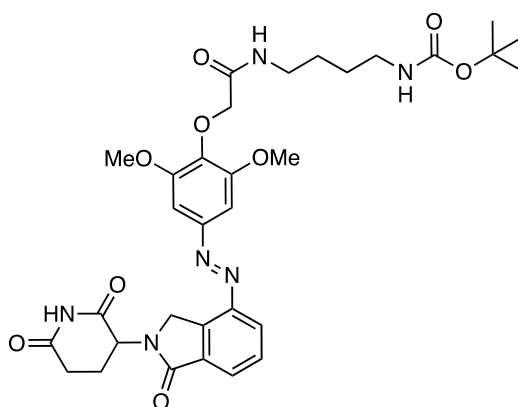
¹H NMR (400 MHz, Chloroform-*d*) $\delta = 8.21$ (d, $J = 7.8$ Hz, 1H), 8.02 (d, $J = 7.5$ Hz, 1H), 7.99 (s, 1H), 7.73 (d, $J = 7.7$ Hz, 1H), 7.70 (s, 1H), 7.22 (s, 2H), 5.27 (dd, $J = 13.3, 5.1$ Hz, 1H), 5.01 (s, 1H), 4.86 (d, $J = 17.9$ Hz, 1H), 4.72 (d, $J = 17.9$ Hz, 1H), 4.60 (s, 2H), 4.00 (s, 6H), 3.43 (q, $J = 6.5$ Hz, 2H), 3.18 (d, $J = 6.3$ Hz, 2H), 2.99 – 2.81 (m, 2H), 2.47 (dd, $J = 13.1, 5.0$ Hz, 1H), 2.27 (dtd, $J = 12.8, 5.1, 2.5$ Hz, 1H), 1.74 (p, $J = 6.6$ Hz, 1H), 1.43 (s, 9H) ppm.

¹³C NMR (100 MHz, CDCl₃) δ = 170.99, 170.05, 169.51, 168.57, 156.22, 152.82, 149.07, 146.93, 139.88, 134.11, 133.45, 130.06, 129.66, 126.42, 100.61, 79.22, 72.83, 56.54, 52.15, 48.29, 37.68, 36.24, 31.76, 30.30, 28.57, 23.63 ppm.

HRMS (ESI): calcd. for C₃₁H₃₉N₆O₉⁺: 639.2773 m/z [M+H]⁺
found: 639.2785 m/z [M+H]⁺.

LCMS (ESI): t_{ret} = 3.23 min (Z). 639.2 m/z [M+H]⁺.

***tert*-butyl (*E*)-(4-(2-(4-((2-(2,6-dioxopiperidin-3-yl)-1-oxoisindolin-4-yl)diazenyl)-2,6-dimethoxyphenoxy)acetamido)butyl)carbamate (**S3**)**



3 (70.0 mg, 0.11 mmol, 1.0 eq.) and HATU (62.9 mg, 0.165 mmol, 1.5 eq.) were dissolved in dry DMF (1 mL) at room temperature. After 5 minutes of stirring *N*-Boc-1,4-diaminobutane (83.1 mg, 0.441 mmol, 4 eq.) and *i*-Pr₂NEt (57 mg, 0.44 mmol, 4 eq., 74 μ L) were added to the mixture and stirred for additional 14 h at room temperature. The reaction was diluted with EtOAc (20 mL), separated against 5% LiCl (20 mL), extracted with EtOAc (3x 20 mL) and washed with 10% LiCl (2x 20 mL) and brine (2x 20 mL). The combined organic phase was dried over Na₂SO₄ and concentrated under reduced pressure. Purification of the resulting crude product by flash column chromatography (CH₂Cl₂/MeOH gradient, 0-20% MeOH) gave **S3** (53.7 mg, 0.082 mmol, 75%) as a yellow solid.

R_f = 0.42 [CH₂Cl₂:MeOH, 19:1].

¹H NMR (400 MHz, Chloroform-*d*) δ = 8.21 (d, J = 7.7 Hz, 1H), 8.10 (s, 1H), 8.01 (d, J = 7.4 Hz, 1H), 7.72 (t, J = 7.7 Hz, 1H), 7.69 (s, 1H), 7.22 (s, 2H), 5.26 (dd, J = 13.3, 5.1 Hz, 1H), 4.86 (d, J = 17.9 Hz, 1H), 4.72 (d, J = 17.9 Hz, 1H), 4.60 (s, 2H), 3.99 (s,

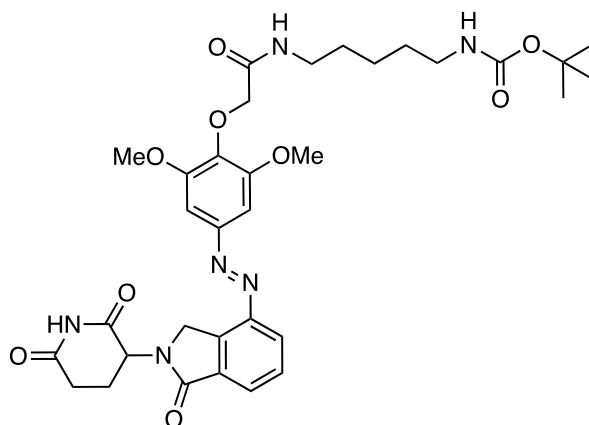
6H), 3.37 (q, $J = 6.5$ Hz, 2H), 3.17 (d, $J = 5.9$ Hz, 2H), 2.99 – 2.81 (m, 2H), 2.47 (dd, $J = 13.1, 5.1$ Hz, 1H), 2.27 (dtd, $J = 12.8, 7.6, 6.3, 3.7$ Hz, 1H), 1.66-1.53 (m, 4H), 1.43 (s, 9H) ppm.

^{13}C NMR (100 MHz, CDCl_3) $\delta = 171.04, 169.58, 169.55, 168.57, 156.14, 152.76, 149.02, 146.92, 139.91, 134.12, 133.45, 130.03, 129.64, 126.41, 100.60, 79.36, 72.89, 56.52, 52.15, 48.30, 40.39, 38.80, 31.76, 28.56, 27.73, 27.13, 23.62$ ppm.

HRMS (APCI): calcd. for $\text{C}_{31}\text{H}_{41}\text{N}_6\text{O}_9^+$: 653.2929 m/z $[\text{M}+\text{H}]^+$
 found: 653.2928 m/z $[\text{M}+\text{H}]^+$.

LCMS (ESI): $t_{\text{ret}} = 3.31$ min (*Z*) 675 m/z $[\text{M}+\text{Na}]^+$.
 $t_{\text{ret}} = 3.63$ min (*E*) 675 m/z $[\text{M}+\text{Na}]^+$.

***Tert*-butyl (*E*)-(5-(2-(4-((2-(2,6-dioxopiperidin-3-yl)-1-oxoisindolin-4-yl)diazenyl)-2,6-dimethoxyphenoxy)acetamido)pentyl)carbamate (**S6**)**



3 (60.0 mg, 0.095 mmol, 1.0 eq.) and HATU (46.0 mg, 0.142 mmol, 1.5 eq.) were dissolved in dry DMF (5 mL) at room temperature. After 5 minutes of stirring *N*-Boc-1,4-diaminopentane (76.9 mg, 0.380 mmol, 4 eq.) and *i*-Pr₂NEt (49.1 mg, 0.380 mmol, 4 eq., 66 μ L) were added to the mixture and stirred for additional 12 h at room temperature. The reaction was diluted with EtOAc (20 mL), separated against 5% LiCl (20 mL), extracted with EtOAc (3x 20 mL) and washed with 10% LiCl (2x 20 mL) and brine (2x 20 mL). The combined organic phase was dried over Na₂SO₄ and concentrated under reduced pressure. Purification of the resulting crude product by flash column chromatography (CH₂Cl₂/MeOH gradient, 0-20% MeOH) yielded **S6** (54.2 mg, 0.081 mmol, 85%) as a yellow solid.

$R_f = 0.42$ [CH₂Cl₂:MeOH, 19:1].

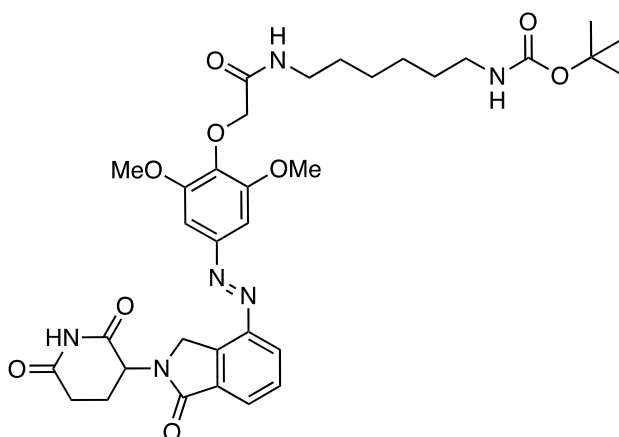
¹H NMR (400 MHz, Chloroform-*d*) $\delta = 8.21$ (d, $J = 7.8$ Hz, 1H), 8.14 (d, $J = 13.9$ Hz, 1H), 8.01 (d, $J = 7.5$ Hz, 1H), 7.72 (t, $J = 7.7$ Hz, 1H), 7.66 (s, 1H), 7.22 (s, 2H), 5.26 (dd, $J = 13.3, 5.1$ Hz, 1H), 4.86 (d, $J = 17.9$ Hz, 1H), 4.73 (d, $J = 17.9$ Hz, 1H), 4.61 (s, 2H), 3.99 (s, 6H), 3.35 (q, $J = 6.8$ Hz, 2H), 3.12 (d, $J = 5.7$ Hz, 3H), 3.00 – 2.81 (m, 2H), 2.47 (qd, $J = 13.1, 5.0$ Hz, 1H), 2.30 – 2.21 (m, 1H), 1.67-1.48 (m, 6H), 1.43 (s, 9H) ppm.

¹³C NMR (100 MHz, CDCl₃) δ = 171.11, 171.04, 169.54, 168.57, 156.14, 152.77, 149.02, 146.93, 139.93, 134.10, 133.44, 130.07, 129.64, 126.39, 100.60, 79.29, 72.90, 56.51, 52.15, 48.31, 40.52, 38.96, 31.76, 29.92, 29.45, 28.56, 24.23, 23.62 ppm.

HRMS (ESI): calcd. for C₃₃H₄₂N₆NaO₉⁺: 689.2905 m/z [M+Na]⁺
found: 689.2935 m/z [M+Na]⁺

LCMS (ESI): t_{ret} = 3.43 min (Z) 665 m/z [M-H]⁻.

***tert*-butyl (*E*)-(6-(2-(4-((2-(2,6-dioxopiperidin-3-yl)-1-oxoisoindolin-4-yl)diazenyl)-2,6-dimethoxyphenoxy)acetamido)hexyl)carbamate (S7)**



3 (60.0 mg, 0.095 mmol, 1.0 eq.) and HATU (46.0 mg, 0.142 mmol, 1.5 eq.) were dissolved in dry DMF (5 mL) at room temperature. After 5 minutes of stirring *N*-Boc-1,4-diaminohexane (81.8 mg, 0.378 mmol, 4 eq., 0.09 mL) and *i*-Pr₂NEt (48.9 mg, 0.378 mmol, 4 eq., 66 μL) were added to the mixture and stirred for additional 13 h at room temperature. The reaction was diluted with EtOAc (20 mL), separated against 5 % LiCl (20 mL), extracted with EtOAc (3x 20 mL) and washed twice with 10% LiCl (2x 20 mL) and brine (2x 20 mL). The combined organic phase was dried over Na₂SO₄ and concentrated under reduced pressure. Purification of the resulting crude product by flash column chromatography (CH₂Cl₂/MeOH gradient, 0-20% MeOH) gave **S7** (56.7 mg, 0.083 mmol, 88%) as a yellow solid.

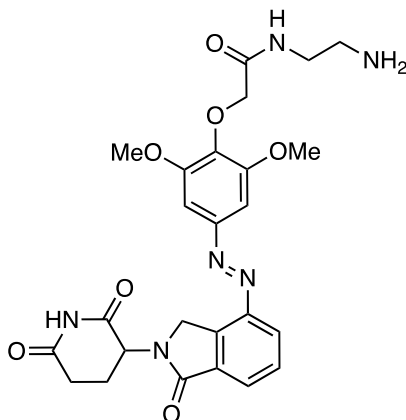
R_f = 0.25 [CH₂Cl₂: MeOH, 19:1].

¹H NMR (400 MHz, Chloroform-*d*) δ = 8.20 (d, J = 7.8 Hz, 2H), 8.01 (d, J = 7.5 Hz, 1H), 7.71 (t, J = 7.7 Hz, 1H), 7.64 (t, J = 5.3 Hz, 1H), 7.21 (s, 2H), 5.26 (dd, J = 13.3, 5.1 Hz, 1H), 4.86 (d, J = 17.9 Hz, 1H), 4.72 (d, J = 17.9 Hz, 1H), 4.61 (s, 2H), 3.99 (s, 6H), 3.34 (q, J = 6.6 Hz, 2H), 3.10 (d, J = 6.1 Hz, 2H), 2.99 – 2.80 (m, 2H), 2.46 (qd, J = 13.1, 5.0 Hz, 1H), 2.26 (dtd, J = 12.8, 5.1, 2.6 Hz, 1H), 1.58 (p, J = 7.1 Hz, 2H), 1.52 – 1.46 (m, 2H), 1.43 (s, 9H), 1.40 – 1.34 (m, 4H) ppm.

¹³C NMR (100 MHz, CDCl₃) δ = 171.16, 169.64, 169.48, 168.56, 156.14, 152.76, 148.99, 146.92, 139.93, 134.08, 133.44, 130.08, 129.63, 126.38, 100.59, 79.25, 72.89, 56.50, 52.13, 48.29, 40.64, 39.02, 31.76, 30.17, 29.67, 28.57, 26.74, 26.63, 23.63 ppm.

HRMS (APCI): calcd. for C₃₄H₄₅N₆O₉⁺: 681.3243 m/z [M+H]⁺
 found: 681.3236 m/z [M+H]⁺.

(*E*)-(2-(2-(4-((2-(2,6-dioxopiperidin-3-yl)-1-oxoisindolin-4-yl)diazenyl)-2,6-dimethoxyphenoxy)acetamido)ethyl)carbamic acid (S8)



S4 (15.3 mg, 0.024 mmol, 1 eq.) was dissolved in TFA:CH₂Cl₂ (1 mL:0.5 mL) and stirred at room temperature. After 2 h, the mixture was diluted with CH₂Cl₂, concentrated under reduced pressure and dried on high vacuum overnight. **S8** (15.6 mg, 0.024 mmol, >99%.) was obtained as trifluoroacetate in form of a yellow solid with traces of residual TFA.

$R_f = 0.18$ [CH_2Cl_2 :MeOH, 7:1].

^1H NMR (400 MHz, $\text{DMSO-}d_6$) $\delta = 11.04$ (s, 1H), 8.23 (dd, $J = 9.3, 7.1$ Hz, 2H), 7.93 (d, $J = 7.5$ Hz, 1H), 7.81 (t, $J = 7.7$ Hz, 3H), 7.37 (s, 2H), 5.17 (dd, $J = 13.3, 5.0$ Hz, 1H), 4.82 (d, $J = 19.1$ Hz, 1H), 4.69 (d, $J = 19.1$ Hz, 1H), 4.44 (s, 2H), 3.94 (s, 6H), 3.45 (q, $J = 6.3$ Hz, 2H), 3.02 – 2.88 (m, 4H), 2.69 – 2.54 (m, 2H) ppm.

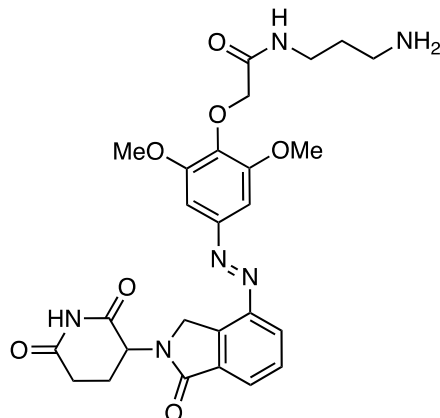
^{13}C NMR (100 MHz, $\text{DMSO-}d_6$) $\delta = 172.92, 171.02, 169.13, 167.14, 152.77, 148.38, 146.35, 139.08, 134.49, 133.84, 129.68, 128.67, 125.54, 100.57, 71.67, 56.36, 51.83, 48.26, 38.80, 36.23, 31.28, 30.70$ ppm.

HRMS (ESI): calcd. for $\text{C}_{25}\text{H}_{29}\text{N}_6\text{O}_7^+$: 525.2092 m/z $[\text{M}+\text{H}]^+$

 found: 525.2096 m/z $[\text{M}+\text{H}]^+$

LCMS (ESI): $t_{\text{ret}} = 2.39$ min. 525 m/z $[\text{M}+\text{H}]^+$.

(*E*)-*N*-(3-aminopropyl)-2-(4-((2-(2,6-dioxopiperidin-3-yl)-1-oxoisindolin-4-yl)diazenyl)-2,6-dimethoxyphenoxy)acetamide (S9**)**



S5 (41.5 mg, 0.061 mmol, 1 eq.) was dissolved in TFA/CH₂Cl₂ (1:1, 1 mL:1 mL) and stirred for 2 h at room temperature. The reaction was diluted with MeOH and concentrated under reduced pressure. The mixture was triturated with CH₂Cl₂ and dried on high vacuum overnight. **S9** (40 mg, 0.061 mmol, >99%) was obtained as a yellow solid with traces of residual TFA.

$R_f = 0.19$ [CH₂Cl₂:MeOH, 9:1].

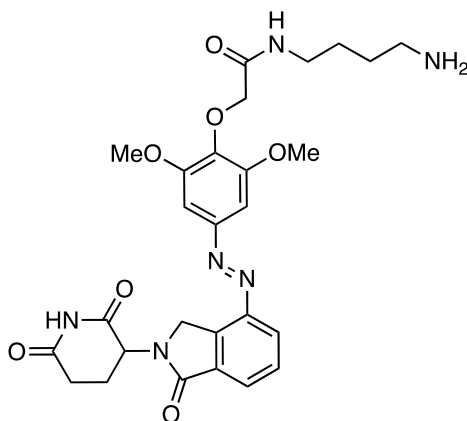
¹H NMR (400 MHz, DMSO-*d*₆) $\delta = 11.04$ (s, 1H), 8.22 (d, *J* = 7.8 Hz, 1H), 8.16 (t, *J* = 5.9 Hz, 1H), 7.93 (d, *J* = 7.5 Hz, 1H), 7.81 (t, *J* = 7.7 Hz, 1H), 7.73 (s, 2H), 7.36 (s, 2H), 5.17 (dd, *J* = 13.2, 5.0 Hz, 1H), 4.82 (d, *J* = 19.1 Hz, 1H), 4.69 (d, *J* = 19.1 Hz, 1H), 4.43 (s, 2H), 3.94 (s, 6H), 3.27 (q, *J* = 6.5 Hz, 2H), 2.95 (ddd, *J* = 17.9, 13.8, 5.2 Hz, 1H), 2.82 (dt, *J* = 12.9, 6.2 Hz, 2H), 2.69 – 2.53 (m, 2H), 2.11 – 2.03 (m, 1H), 1.77 (p, *J* = 6.9 Hz, 2H) ppm.

¹³C NMR (100 MHz, DMSO) $\delta = 172.92, 171.02, 168.55, 167.15, 152.72, 148.34, 146.35, 139.15, 134.48, 133.84, 129.68, 128.70, 125.54, 100.60, 71.72, 56.39, 51.83, 48.27, 36.75, 35.36, 31.28, 27.39, 22.34$ ppm.

HRMS (ESI): calcd. for C₂₆H₃₁N₆O₇⁺: 539.2249 m/z [M+H]⁺
 found: 539.2312 m/z [M+H]⁺.

LCMS (ESI): $t_{ret} = 2.34$ min (*Z*) 539 m/z [M+H]⁺.
 $t_{ret} = 2.45$ min (*E*) 539 m/z [M+H]⁺.

(E)-N-(4-aminobutyl)-2-(4-((2-(2,6-dioxopiperidin-3-yl)-1-oxoisindolin-4-yl)diazenyl)-2,6-dimethoxyphenoxy)acetamide (4**)**



S3 (39.5 mg, 0.057 mmol, 1 eq.) was dissolved in TFA/CH₂Cl₂ (1:1; 1mL:1mL) and stirred for 2 h at room temperature. The reaction was diluted with CH₂Cl₂ and concentrated under reduced pressure. The reaction was triturated with Et₂O and dried on high vacuum overnight. **4** (38 mg, 0.057 mmol, >99%) was obtained as trifluoroacetate in form of a yellow solid with traces of residual TFA.

$R_f = 0.4$ [CH₂Cl₂:MeOH, 8:2].

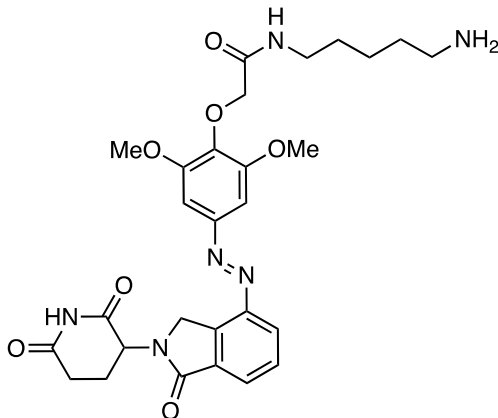
¹H NMR (400 MHz, DMSO-*d*₆) δ = 11.04 (s, 1H), 8.22 (d, J = 7.8 Hz, 1H), 8.02 (t, J = 5.8 Hz, 1H), 7.93 (d, J = 7.5 Hz, 1H), 7.81 (t, J = 7.7 Hz, 1H), 7.70 (s, 2H), 7.37 (s, 2H), 5.17 (dd, J = 13.2, 5.0 Hz, 1H), 4.82 (d, J = 19.1 Hz, 1H), 4.69 (d, J = 19.1 Hz, 1H), 4.42 (s, 2H), 3.95 (s, 6H), 3.25 – 3.19 (m, 2H), 2.95 (ddd, J = 17.9, 13.7, 5.3 Hz, 1H), 2.86 – 2.79 (m, 2H), 2.67 – 2.53 (m, 2H), 2.11 – 2.03 (m, 1H), 1.58 – 1.51 (m, 4H) ppm.

¹³C NMR (100 MHz, DMSO) δ = 172.92, 171.02, 168.11, 167.15, 152.66, 148.34, 146.35, 139.20, 134.48, 133.84, 129.68, 128.70, 125.54, 100.59, 71.83, 56.39, 51.83, 48.28, 38.58, 37.58, 31.28, 26.13, 24.46, 22.33 ppm.

HRMS (APCI): calcd. for C₂₇H₃₃N₆O₉⁺: 553.2405 m/z [M+H]⁺
 found: 553.2384 m/z [M+H]⁺.

LCMS (ESI): $t_{ret} = 2.23$ min (*Z*). 553 m/z [M+H]⁺.
 $t_{ret} = 2.49$ min (*E*). 553 m/z [M+H]⁺.

(E)-N-(5-aminopentyl)-2-(4-((2-(2,6-dioxopiperidin-3-yl)-1-oxoisindolin-4-yl)diazenyl)-2,6-dimethoxyphenoxy)acetamide (S10)



S6 (40.5 mg, 0.057 mmol, 1 eq.) was dissolved in TFA/CH₂Cl₂ (1:1; 1mL:1mL) and stirred for 2 h at room temperature. The reaction was diluted with CH₂Cl₂ and concentrated under reduced pressure. The reaction was triturated with Et₂O and dried on high vacuum overnight. **S10** (38.8 mg, 0.057 mmol, >99%) was obtained as trifluoroacetate in form of a yellow solid with traces of residual TFA.

$R_f = 0.03$ [CH₂Cl₂:MeOH, 8:2].

¹H NMR (400 MHz, DMSO-*d*₆) δ = 11.03 (s, 1H), 8.22 (d, *J* = 7.8 Hz, 1H), 7.97 (d, *J* = 5.7 Hz, 1H), 7.93 (d, *J* = 7.5 Hz, 1H), 7.81 (t, *J* = 7.7 Hz, 1H), 7.68 (s, 2H), 7.36 (s, 2H), 5.17 (dd, *J* = 13.2, 5.0 Hz, 1H), 4.82 (d, *J* = 19.1 Hz, 1H), 4.69 (d, *J* = 19.1 Hz, 1H), 4.42 (s, 2H), 3.95 (s, 6H), 3.19 (q, *J* = 6.7 Hz, 2H), 2.95 (ddd, *J* = 17.9, 13.7, 5.3 Hz, 1H), 2.79 (h, *J* = 5.8 Hz, 2H), 2.68 – 2.53 (m, 2H), 2.11 – 2.03 (m, 1H), 1.53 (dp, *J* = 22.1, 7.5 Hz, 4H), 1.33 (p, *J* = 7.5, 6.9 Hz, 2H) ppm.

¹³C NMR (100 MHz, DMSO) δ = 172.92, 171.02, 168.00, 167.15, 152.64, 148.31, 146.35, 139.24, 134.49, 133.84, 129.67, 128.68, 125.53, 100.61, 71.85, 56.38, 51.83, 48.28, 38.76, 37.92, 31.29, 28.59, 26.67, 23.12, 22.33 ppm.

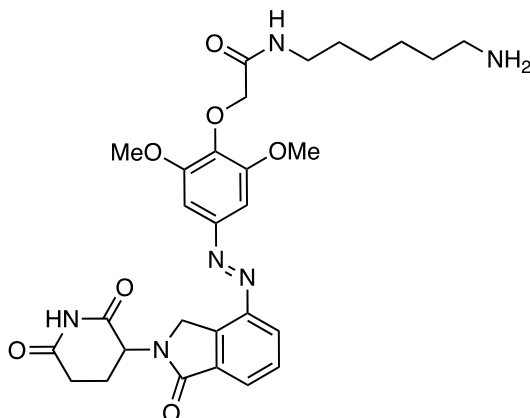
HRMS (ESI): calcd. for C₂₈H₃₅N₆O₇⁺: 567.2562 m/z [M+H]⁺

found: 567.2656 m/z [M+H]⁺.

LCMS (ESI): $t_{ret} = 2.27$ min (*Z*) 567 m/z [M+H]⁺.

$t_{ret} = 2.53$ min (*E*) 567 m/z [M+H]⁺.

(E)-N-(6-aminohexyl)-2-(4-((2-(2,6-dioxopiperidin-3-yl)-1-oxoisindolin-4-yl)diazenyl)-2,6-dimethoxyphenoxy)acetamide (S11)



S7 (51.3 mg, 0.071 mmol, 1 eq.) was dissolved in TFA/CH₂Cl₂ (1:1; 1mL:1mL) and stirred for 2 h at room temperature. The reaction was diluted with CH₂Cl₂ and concentrated under reduced pressure. The reaction was triturated with Et₂O and dried on high vacuum overnight. **S11** (49.3 mg, 0.071 mmol, >99%) was obtained as trifluoroacetate in form of a yellow solid with traces of residual TFA.

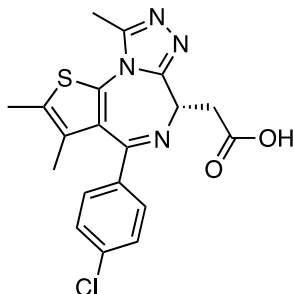
$R_f = 0.19$ [CH₂Cl₂: MeOH, 9:1].

¹H NMR (400 MHz, DMSO-*d*₆) $\delta = 11.03$ (s, 1H), 8.22 (d, $J = 7.8$ Hz, 1H), 7.94 (dd, $J = 11.5, 6.5$ Hz, 2H), 7.81 (t, $J = 7.7$ Hz, 1H), 7.66 (s, 2H), 7.36 (s, 2H), 5.16 (dd, $J = 13.2, 5.0$ Hz, 1H), 4.82 (d, $J = 19.1$ Hz, 1H), 4.69 (d, $J = 19.1$ Hz, 1H), 4.42 (s, 2H), 3.94 (s, 6H), 3.19 (q, $J = 6.6$ Hz, 2H), 2.95 (ddd, $J = 17.9, 13.8, 5.3$ Hz, 1H), 2.78 (h, $J = 5.8$ Hz, 2H), 2.63 (d, $J = 18.1$ Hz, 1H), 2.56 (dd, $J = 13.1, 4.4$ Hz, 1H), 2.06 (d, $J = 5.4$ Hz, 1H), 1.51 (dp, $J = 13.7, 6.9$ Hz, 4H), 1.37 – 1.25 (m, 4H) ppm.

¹³C NMR (100 MHz, DMSO) $\delta = 172.95, 171.04, 167.99, 167.18, 152.64, 148.32, 146.37, 139.28, 134.51, 133.85, 129.70, 128.71, 125.56, 100.63, 71.89, 56.40, 51.86, 48.31, 38.82, 38.09, 31.30, 28.95, 26.98, 25.84, 25.48, 22.35$ ppm.

HRMS (APCI):	calcd. for C ₂₉ H ₃₇ N ₆ O ₇ ⁺ :	581.2718 m/z [M+H] ⁺
	found:	581.2717 m/z [M+H] ⁺ .
LCMS (ESI):	t _{ret} = 2.66 min.	581 m/z [M+H] ⁺ .

(S)-2-(4-(4-chlorophenyl)-2,3,9-trimethyl-6H-thieno[3,2-f][1,2,4]triazolo[4,3-a][1,4]diazepin-6-yl)acetic acid ((+)-JQ1 free acid, 5)

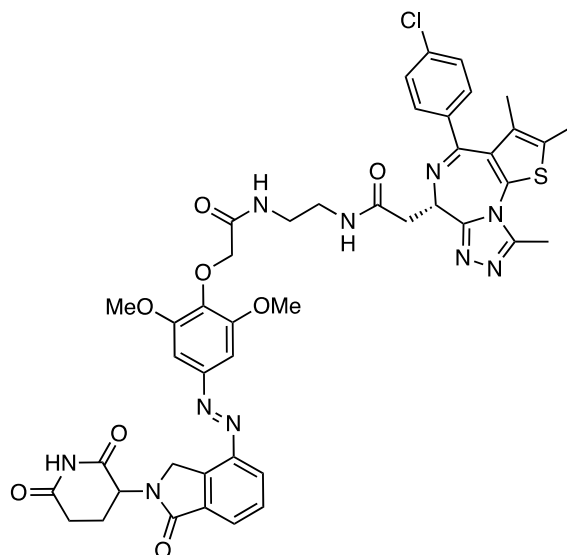


As previously described,^[7] (+)-JQ1 (9 mg, 0.02 mmol, 1 eq.) was dissolved in formic acid (0.5 mL) and stirred for 3 days at room temperature. The reaction was concentrated under reduced pressure and was dried on high vacuum overnight. **(+)-JQ1 free acid, 5** (8.0 mg, 0.02 mmol, >99%) was obtained as yellow solid and used without further purification.

LCMS (ESI): $t_{\text{ret}} = 3.35$ min.

401, 402 m/z [M+H]⁺.

2-((S)-4-(4-chlorophenyl)-2,3,9-trimethyl-6H-thieno[3,2-f][1,2,4]triazolo[4,3-a][1,4]diazepin-6-yl)-N-(2-(2-(4-((E)-2-(2,6-dioxopiperidin-3-yl)-1-oxoisoindolin-4-yl)diazenyl)-2,6-dimethoxyphenoxy)acetamido)ethyl)acetamide (PHOTAC-I-1)



S8 (15.3 mg, 0.024 mmol, 1 eq.) and HATU (11.7 mg, 0.036 mmol, 1.5 eq.) were added to a round bottom flask under nitrogen. **(+)-JQ1 free acid** was taken up in dry DMF (1 mL) and added to the mixture. After addition of *i*-Pr₂NEt (0.025 mL, 0.144 mmol, 6 eq.) the reaction was stirred for 15 h at room temperature. Then the mixture was diluted with EtOAc (20 mL), separated against H₂O (20 mL), extracted with EtOAc (2x 20 mL), and washed twice with 10% LiCl (2x 20 mL) and brine (2x 20 mL). The combined organic phases were dried over Na₂SO₄ and concentrated under reduced pressure. Purification of the resulting crude product by flash column chromatography (CH₂Cl₂/MeOH gradient, 0→20% MeOH) gave **PHOTAC-I-1** (8.6 mg, 0.009 mmol, 38%) as a yellow solid.

$R_f = 0.19$ [CH₂Cl₂:MeOH, 19:1].

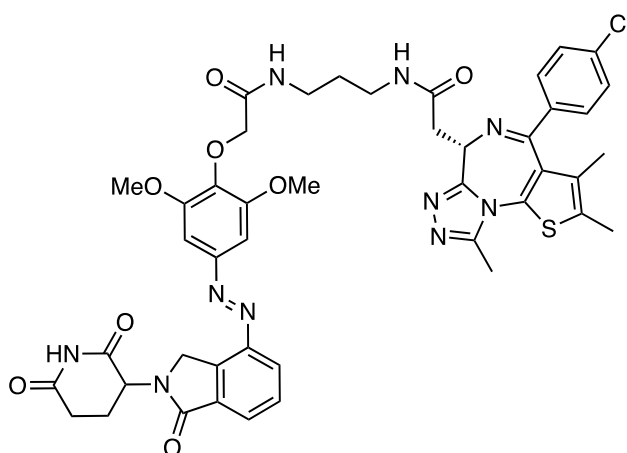
¹H NMR (400 MHz, Methanol-*d*₄) δ = 8.20 (d, *J* = 7.8 Hz, 1H), 7.90 (dd, *J* = 7.5, 4.1 Hz, 1H), 7.74 (td, *J* = 7.7, 2.8 Hz, 1H), 7.40 (dd, *J* = 8.7, 3.0 Hz, 2H), 7.36 – 7.28 (m, 4H), 5.23 – 5.09 (m, 1H), 4.83 (s, 2H), 4.60 – 4.47 (m, 3H), 3.96 (d, *J* = 2.8 Hz, 6H), 3.58 – 3.33 (m, 5H), 3.30 – 3.19 (m, 1H), 2.92 (ddt, *J* = 17.9, 13.4, 4.8 Hz, 1H), 2.79 (ddt, *J* =

17.8, 5.1, 2.8 Hz, 1H), 2.70 – 2.61 (m, 1H), 2.58 (d, $J = 19.6$ Hz, 3H), 2.40 (d, $J = 2.2$ Hz, 3H), 2.25 – 2.14 (m, 1H), 1.66 (s, 3H).

^{13}C NMR (100 MHz, MeOD) $\delta = 174.68, 173.16, 172.58, 172.18, 170.35, 166.19, 156.89, 154.11, 152.07, 150.18, 148.12, 141.02, 138.01, 137.92, 135.56, 134.82, 133.42, 133.14, 132.07, 131.92, 131.57, 131.30, 130.69, 129.74, 126.55, 101.71, 73.23, 56.97, 54.99, 53.91, 50.68, 40.04, 39.91, 38.72, 32.42, 24.03, 14.39, 12.93, 11.58$ ppm.

HRMS (ESI):	calcd. for $\text{C}_{44}\text{H}_{44}\text{ClN}_{10}\text{O}_8\text{S}^+$:	907.2747 m/z $[\text{M}+\text{H}]^+$
	found:	907.2790 m/z $[\text{M}+\text{H}]^+$.
LCMS (ESI):	$t_{\text{ret}} = 3.51$ min (<i>Z</i>).	907 m/z $[\text{M}+\text{H}]^+$.
	$t_{\text{ret}} = 3.67$ min (<i>E</i>).	907 m/z $[\text{M}+\text{H}]^+$.

2-((S)-4-(4-chlorophenyl)-2,3,9-trimethyl-6H-thieno[3,2-f][1,2,4]triazolo[4,3-a][1,4]diazepin-6-yl)-N-(3-(2-(4-((E)-(2-(2,6-dioxopiperidin-3-yl)-1-oxoisoindolin-4-yl)diazenyl)-2,6-dimethoxyphenoxy)acetamido)propyl)acetamide (PHOTAC-I-2)



Into a round bottom flask with dry **(+)-JQ1 free acid** (7.2 mg, 0.018 mmol, 1 eq.) were added **S9** (23.5 mg, 0.036 mmol, 2 eq.) and HATU (11.7 mg, 0.036 mmol, 1.5 eq.) under nitrogen. The reaction was dissolved in dry DMF (1 mL). After addition of *i*-Pr₂NEt (17 mg, 0.13 mmol, 7.2 eq., 0.023 mL) the reaction was stirred for 14 h at room temperature. The mixture was then diluted with EtOAc (20 mL), separated against 5% LiCl (20 mL), extracted with EtOAc (2x 20 mL) and washed twice with 10% LiCl (2x 20 mL) and brine (2x 20 mL). The combined organic phases were dried over Na₂SO₄ and concentrated under reduced pressure. Purification of the resulting crude product by flash column chromatography (CH₂Cl₂/MeOH gradient, 0→20% MeOH) gave **PHOTAC-I-2** (15.1 mg, 0.016 mmol, 91%) as a yellow solid.

$R_f = 0.31$ [CH₂Cl₂:MeOH, 19:1].

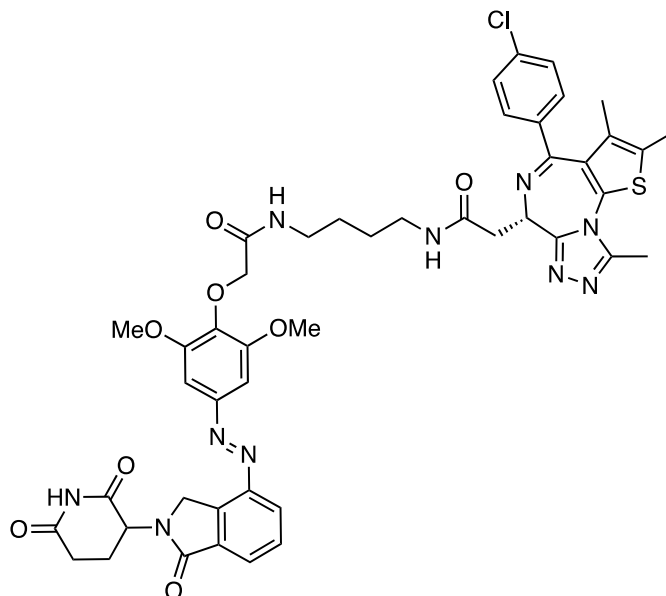
¹H NMR (400 MHz, Chloroform-*d*) δ = 8.52 (s, 1H), 8.18 (d, J = 7.8 Hz, 1H), 7.99 (d, J = 7.5 Hz, 1H), 7.80 (t, J = 5.8 Hz, 1H), 7.69 (t, J = 7.7 Hz, 1H), 7.39 (d, J = 8.4 Hz, 2H), 7.31 (d, J = 8.3 Hz, 2H), 7.21 (d, J = 2.9 Hz, 2H), 7.07 (s, 1H), 5.28 – 5.19 (m, 1H), 4.85 (d, J = 18.0 Hz, 1H), 4.71 (dd, J = 18.1, 3.2 Hz, 1H), 4.63 (d, J = 6.8 Hz, 1H), 4.60 (s, 2H), 3.97 (s, 6H), 3.55 (dd, J = 14.4, 7.6 Hz, 1H), 3.42 (q, J = 6.4 Hz, 2H), 3.35 (q, J = 7.6, 6.9 Hz, 3H), 2.95 – 2.77 (m, 2H), 2.64 (s, 3H), 2.46 (dt, J = 12.9, 4.5 Hz, 1H), 2.38 (s, 3H), 2.28 – 2.18 (m, 1H), 1.79 (p, J = 6.4 Hz, 2H), 1.66 (s, 3H) ppm.

¹³C NMR (100 MHz, CDCl₃) δ = 171.37, 170.84, 169.95, 169.72, 168.57, 164.10, 155.77, 152.78, 150.07, 148.99, 146.90, 139.86, 136.92, 136.69, 134.15, 133.46, 132.26, 131.02, 130.98, 130.58, 130.02, 129.96, 129.57, 128.83, 126.29, 100.64, 72.79, 56.55, 54.55, 52.12, 48.37, 39.39, 36.91, 36.45, 31.73, 29.76, 23.56, 14.52, 13.22, 11.94 ppm.

HRMS (ESI): calcd. for C₄₅H₄₅ClN₁₀NaO₈S⁺: 943.2723 m/z [M+Na]⁺
 found: 943.2738 m/z [M+Na]⁺.

LCMS (ESI): t_{ret} = 3.71 min. 920 m/z [M-H]⁻.

2-((S)-4-(4-chlorophenyl)-2,3,9-trimethyl-6H-thieno[3,2-f][1,2,4]triazolo[4,3-a][1,4]diazepin-6-yl)-N-(4-(2-(4-((E)-(2-(2,6-dioxopiperidin-3-yl)-1-oxoisoindolin-4-yl)diazenyl)-2,6-dimethoxyphenoxy)acetamido)butyl)acetamide (PHOTAC-I-3)



Into a round bottom flask with dry **(+)-JQ1 free acid** (7.2 mg, 0.018 mmol, 1 eq.) were added **4** (26.6 mg, 0.04 mmol, 2 eq.) and HATU (11.7 mg, 0.036 mmol, 1.8 eq.) under nitrogen atmosphere. The solids were dissolved in dry DMF (1 mL). After addition of *i*-Pr₂NEt (18.6 mg, 0.144 mmol, 7.2 eq., 0.025 mL) the reaction was stirred for 16 h at room temperature. The mixture was then diluted with EtOAc (20 mL), separated against 5% LiCl (20 mL), extracted with EtOAc (2x 20 mL), washed twice with 10% LiCl (2x 20 mL) and brine (2x 20 mL). The combined organic phases were dried over Na₂SO₄ and concentrated under reduced pressure. Purification of the resulting crude product by flash column chromatography (CH₂Cl₂/MeOH gradient, 0→20% MeOH) gave **PHOTAC-I-3** (15.6 mg, 0.017 mmol, 85%) as a yellow solid.

$R_f = 0.30$ [CH₂Cl₂:MeOH, 19:1].

¹H NMR (400 MHz, Chloroform-*d*) δ = 8.80 (d, J = 67.2 Hz, 1H), 8.15 (t, J = 8.7 Hz, 1H), 8.00 – 7.92 (m, 1H), 7.75 (d, J = 4.9 Hz, 1H), 7.67 (q, J = 7.2 Hz, 1H), 7.38 (d, J = 8.2 Hz, 2H), 7.31 (d, J = 8.2 Hz, 2H), 7.21 (d, J = 8.8 Hz, 2H), 6.85 (dt, J = 10.4, 5.2 Hz, 1H), 5.21 (dd, J = 9.2, 3.9 Hz, 1H), 4.84 (d, J = 18.0 Hz, 1H), 4.69 (d, J = 18.0 Hz, 1H), 4.62 (d, J = 6.8 Hz, 3H), 3.97 (d, J = 2.5 Hz, 6H), 3.53 (dd, J = 12.5, 7.5 Hz, 1H),

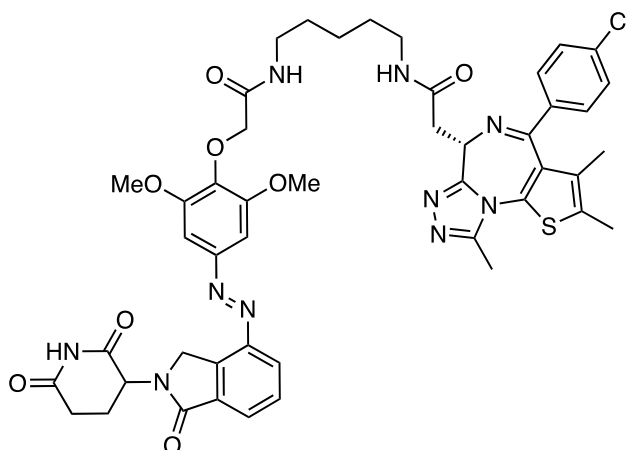
3.42 – 3.23 (m, 5H), 2.90 – 2.72 (m, 2H), 2.64 (d, $J = 5.4$ Hz, 3H), 2.50 – 2.41 (m, 1H), 2.38 (s, 3H), 2.24 – 2.13 (m, 1H), 1.65 (s, 4H), 1.61 (s, 3H) ppm.

^{13}C NMR (100 MHz, CDCl_3) $\delta = 171.44, 170.62, 169.90, 169.64, 168.53, 164.21, 155.74, 152.69, 150.12, 148.91, 146.83, 139.88, 136.96, 136.68, 134.18, 133.45, 132.24, 131.04, 131.01, 130.58, 130.01, 129.94, 129.52, 128.85, 126.20, 100.64, 72.85, 56.54, 54.59, 52.10, 48.35, 39.46, 39.37, 38.78, 31.71, 27.17, 27.04, 23.54, 14.51, 13.21, 11.91$ ppm.

HRMS (ESI): calcd. for $\text{C}_{46}\text{H}_{48}\text{ClN}_{10}\text{O}_8\text{S}^+$: 935.3060 m/z $[\text{M}+\text{H}]^+$
 found: 973.2597 m/z $[\text{M}+\text{H}]^+$.

LCMS (ESI): $t_{\text{ret}} = 3.55$ min (*Z*). 935 m/z $[\text{M}+\text{H}]^+$.
 $t_{\text{ret}} = 3.74$ min (*E*). 935 m/z $[\text{M}+\text{H}]^+$.

2-((*S*)-4-(4-chlorophenyl)-2,3,9-trimethyl-6*H*-thieno[3,2-*f*][1,2,4]triazolo[4,3-*a*][1,4]diazepin-6-yl)-*N*-(5-(2-(4-((*E*)-(2-(2,6-dioxopiperidin-3-yl)-1-oxoisindolin-4-yl)diazenyl)-2,6-dimethoxyphenoxy)acetamido)pentyl)acetamide (PHOTAC-I-4)



Into a round bottom flask with dry **(+)-JQ1 free acid** (7.2 mg, 0.018 mmol, 1 eq.) were added **S10** (24.4 mg, 0.036 mmol, 2 eq.) and HATU (10.5 mg, 0.032 mmol, 1.8 eq.) under nitrogen atmosphere. The solids were dissolved in dry DMF (1 mL). After addition of *i*-Pr₂NEt (16.7 mg, 0.129 mmol, 7.2 eq., 0.023 mL) the reaction was stirred for 15 h at room temperature. The mixture was then diluted with EtOAc (20 mL), separated against 5% LiCl (20 mL), extracted with EtOAc (2x 20 mL), washed twice

with 10% LiCl (2x 20 mL) and brine (2x 20 mL). The combined organic phases were dried over Na₂SO₄ and concentrated under reduced pressure. Purification of the resulting crude product by flash column chromatography (CH₂Cl₂/MeOH gradient, 0→20% MeOH) gave **PHOTAC-I-4** (15.4 mg, 0.016 mmol, 89%) as a yellow solid.

$R_f = 0.31$ [CH₂Cl₂:MeOH, 19:1].

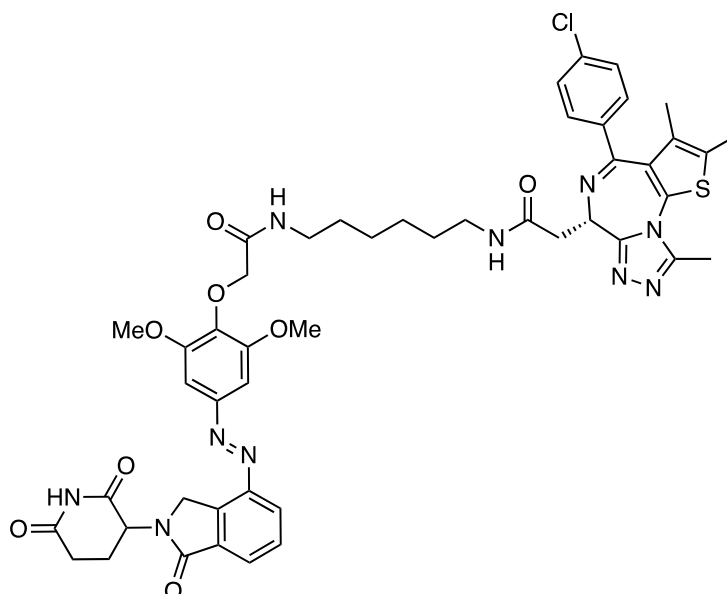
¹H NMR (400 MHz, Chloroform-*d*) $\delta = 8.66$ (d, $J = 14.5$ Hz, 1H), 8.18 (dd, $J = 7.6, 3.5$ Hz, 1H), 7.99 (d, $J = 7.5$ Hz, 1H), 7.69 (t, $J = 7.2$ Hz, 2H), 7.39 (d, $J = 8.1$ Hz, 2H), 7.32 (d, $J = 7.7$ Hz, 2H), 7.22 (d, $J = 5.8$ Hz, 2H), 6.79 – 6.68 (m, 1H), 5.23 (dt, $J = 12.2, 5.2$ Hz, 1H), 4.87 (s, 1H), 4.74 (s, 1H), 4.60 (d, $J = 11.6$ Hz, 3H), 3.98 (s, 6H), 3.55 (dt, $J = 10.9, 5.4$ Hz, 1H), 3.31 (dt, $J = 14.7, 5.9$ Hz, 5H), 2.95 – 2.77 (m, 2H), 2.65 (s, 3H), 2.46 (d, $J = 12.7$ Hz, 1H), 2.39 (s, 3H), 2.31 – 2.14 (m, 1H), 1.66 (s, 3H), 1.57 (q, $J = 6.9$ Hz, 4H), 1.48 – 1.34 (m, 2H) ppm.

¹³C NMR (100 MHz, CDCl₃) $\delta = 171.39, 170.62, 169.82, 169.59, 168.57, 164.15, 155.73, 152.71, 150.09, 148.96, 146.90, 139.89, 136.97, 136.67, 134.17, 133.45, 132.23, 131.05, 131.04, 130.59, 130.09, 129.94, 129.56, 128.86, 126.29, 100.65, 72.86, 56.53, 54.65, 52.11, 48.35, 39.58, 39.51, 38.92, 31.73, 29.37, 29.26, 24.30, 23.57, 14.51, 13.23, 11.92$ ppm.

HRMS (ESI): calcd. for C₄₇H₄₉ClKN₁₀O₈S⁺: 987.2776 m/z [M+K]⁺
found: 987.2755 m/z [M+K]⁺.

LCMS (ESI): $t_{ret} = 3.83$ min 949 m/z [M+H]⁺.

2-((S)-4-(4-chlorophenyl)-2,3,9-trimethyl-6H-thieno[3,2-f][1,2,4]triazolo[4,3-a][1,4]diazepin-6-yl)-N-(6-(2-(4-((E)-2-(2,6-dioxopiperidin-3-yl)-1-oxoisoindolin-4-yl)diazenyl)-2,6-dimethoxyphenoxy)acetamido)hexyl)acetamide (PHOTAC-I-5)



Into a round bottom flask with dry **(+)-JQ1 free acid** (7.6 mg, 0.019 mmol, 1 eq.) were added **S11** (26.3 mg, 0.038 mmol, 2 eq.) and HATU (11.1 mg, 0.034 mmol, 1.8 eq.) under nitrogen atmosphere. The solids were dissolved in dry DMF (1 mL). After addition of *i*-Pr₂NEt (17.6 mg, 0.137 mmol, 7.2 eq., 0.024 mL) the reaction was stirred for 16 h at room temperature. The mixture was then diluted with EtOAc (20 mL), separated against 5% LiCl (20 mL), extracted with EtOAc (2x 20 mL), washed twice with 10% LiCl (2x 20 mL) and brine (2x 20 mL). The combined organic phases were dried over Na₂SO₄ and concentrated under reduced pressure. Purification of the resulting crude product by flash column chromatography (CH₂Cl₂/MeOH gradient, 0→20% MeOH) gave **PHOTAC-I-5** (16.4 mg, 0.017 mmol, 90%) as a yellow solid.

$R_f = 0.31$ [CH₂Cl₂:MeOH, 19:1].

¹H NMR (400 MHz, Chloroform-*d*) δ = 8.78 (d, J = 29.2 Hz, 1H), 8.18 (d, J = 7.6 Hz, 1H), 7.99 (d, J = 7.2 Hz, 1H), 7.69 (t, J = 7.5 Hz, 2H), 7.39 (d, J = 8.3 Hz, 2H), 7.31 (d, J = 8.3 Hz, 2H), 7.26 (s, 1H), 7.22 (s, 1H), 6.72 – 6.60 (m, 1H), 5.22 (td, J = 13.8, 4.9 Hz, 1H), 4.93 – 4.79 (m, 1H), 4.70 (dd, J = 18.0, 5.8 Hz, 1H), 4.62 (s, 3H), 3.98 (d, J = 3.6 Hz, 6H), 3.54 (td, J = 7.7, 3.8 Hz, 1H), 3.38 – 3.21 (m, 5H), 2.96 – 2.74 (m, 2H),

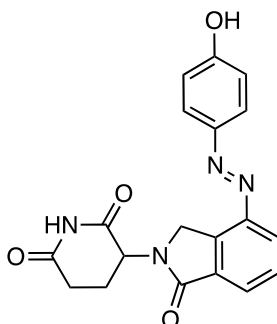
2.64 (d, $J = 10.7$ Hz, 3H), 2.52 – 2.42 (m, 1H), 2.38 (s, 3H), 2.22 (s, 1H), 1.65 (s, 3H), 1.60 – 1.48 (m, 4H), 1.44 – 1.31 (m, 4H) ppm.

^{13}C NMR (100 MHz, CDCl_3) $\delta = 171.42, 170.53, 169.87, 169.53, 168.56, 164.29, 155.70, 152.71, 150.10, 148.94, 146.88, 139.91, 136.98, 136.67, 134.29, 133.46, 132.27, 131.04, 131.02, 130.58, 129.96, 129.75, 129.56, 128.85, 126.29, 100.68, 72.91, 56.51, 54.65, 52.03, 48.24, 39.64, 39.51, 38.98, 31.74, 29.57, 29.55, 26.74, 26.70, 23.58, 14.50, 13.22, 11.88$ ppm.

HRMS (ESI): calcd. for $\text{C}_{48}\text{H}_{51}\text{ClN}_{10}\text{NaO}_8\text{S}^+$: 985.3193 m/z $[\text{M}+\text{Na}]^+$
found: 985.3234 m/z $[\text{M}+\text{Na}]^+$.

LCMS (ESI): $t_{\text{ret}} = 3.93$ min. 963 m/z $[\text{M}+\text{H}]^+$.

(E)-3-(4-((4-hydroxyphenyl)diazenyl)-1-oxoisindolin-2-yl)piperidine-2,6-dione (S12)



Lenalidomide (500 mg, 1.93 mmol, 1.0 eq.) was dissolved in 1 M HCl (50 mL). Concentrated aqueous HBF_4 (1 mL) was added to the mixture. After complete dissolving of the starting material, 2 M NaNO_2 (1.06 mL) was added to the solution at 0 °C. After stirring for 1 h the solution was added dropwise into a mixture of Phenol (217.9 mg, 2.315 mmol, 1.2 eq., 0.204 mL) in H_2O (50 mL), MeOH (20 mL), NaHCO_3 (4.000 g, 47.62 mmol, 24.7 eq.) and Na_2CO_3 (5.000 g, 47.18 mmol, 24.5 eq.) at 0 °C. Upon addition the solution turned from white to orange and stirred for additional 1 h at 0 °C. The reaction was extracted with EtOAc (7x 100 mL) and washed once with brine (1x 100 mL). The organic phase was dried over Na_2SO_4 and then concentrated under reduced pressure. **S12** (605.2 mg, 1.661 mmol, 86%) was obtained as a yellow solid.

$R_f = 0.26$ [CH_2Cl_2 :MeOH, 19:1].

$^1\text{H NMR}$ (400 MHz, $\text{DMSO-}d_6$) $\delta = 11.01$ (s, 1H), 10.42 (s, 1H), 8.13 (d, $J = 7.5$ Hz, 1H), 7.97 – 7.68 (m, 4H), 6.96 (d, $J = 8.1$ Hz, 2H), 5.23 – 5.07 (m, 1H), 4.84 – 4.57 (m, 2H), 2.94 (t, $J = 12.9$ Hz, 1H), 2.67 – 2.54 (m, 2H), 2.10 – 1.95 (m, 1H) ppm.

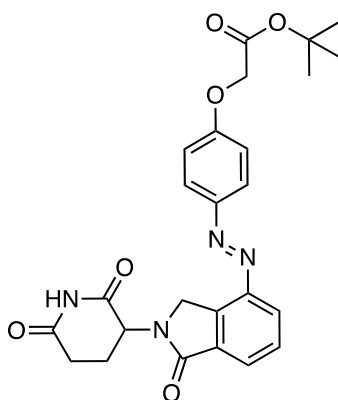
$^{13}\text{C NMR}$ (100 MHz, DMSO) $\delta = 172.92, 171.02, 167.28, 161.61, 146.70, 145.40, 134.16, 133.69, 129.50, 128.11, 125.16, 124.52, 115.97, 51.65, 48.21, 31.25, 22.34$ ppm.

HRMS (ESI): calcd. for $\text{C}_{19}\text{H}_{17}\text{N}_4\text{O}_4^+$: 365.1244 m/z $[\text{M}+\text{H}]^+$

found: 365.1257 m/z $[\text{M}+\text{H}]^+$.

LCMS (ESI): $t_{\text{ret}} = 2.94$ min. 365 m/z $[\text{M}+\text{H}]^+$.

(*E*)-3-(4-((4-(2-(*tert*-butoxy)-2-oxoethoxy)phenyl)diazenyl)-1-oxoisindolin-2-yl)-2,6-dioxopiperidin-1-ium (S13**)**



To a solution of *tert*-butyl bromoacetate (267.6 mg, 1.372 mmol, 1 eq., 0.20 mL) was added **S12** (500 mg, 1.372 mmol, 1 eq.) dissolved in dry DMF (13 mL). After addition of K_2CO_3 (246.6 mg, 1.784 mmol, 1.3 eq.) the reaction was stirred for 6.5 h at room temperature. Upon addition the solution turned from orange to dark red. After 6.5 hours of stirring, the mixture was diluted with EtOAc (100 mL), separated against NaHCO_3 (50 mL), extracted with EtOAc (3x 50 mL), and washed with brine (4x 50 mL). The reaction was concentrated under reduced pressure. Purification of the resulting crude product by flash column chromatography (Hx/Ea gradient, 20 → 100% Ea) gave **S13** (397.7 mg, 0.831 mmol, 61%) as a yellow solid.

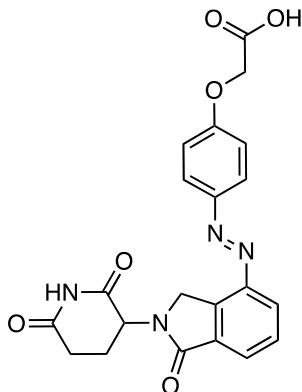
$R_f = 0.44$ [Hx:EA, 1:4].

$^1\text{H NMR}$ (400 MHz, DMSO- d_6) $\delta = 11.01$ (s, 1H), 8.18 (d, $J = 7.7$ Hz, 1H), 8.03 – 7.94 (m, 2H), 7.89 (d, $J = 7.4$ Hz, 1H), 7.78 (t, $J = 7.7$ Hz, 1H), 7.17 – 7.08 (m, 2H), 5.17 (dd, $J = 13.5, 5.0$ Hz, 1H), 4.79 (m, 3H), 4.67 (d, $J = 18.9$ Hz, 1H), 2.92 (d, $J = 12.7$ Hz, 1H), 2.58 (dd, $J = 23.6, 14.7$ Hz, 2H), 2.02 (dd, $J = 16.0, 9.6$ Hz, 1H), 1.44 (s, 9H) ppm.

$^{13}\text{C NMR}$ (100 MHz, DMSO) $\delta = 172.92, 171.01, 167.42, 167.22, 160.89, 146.64, 146.60, 134.26, 133.75, 129.58, 128.58, 124.99, 124.73, 115.18, 81.70, 65.20, 51.66, 48.26, 31.25, 27.70, 22.32$ ppm.

HRMS (APCI): calcd. for $\text{C}_{25}\text{H}_{27}\text{N}_4\text{O}_6^+$: 479.1925 m/z $[\text{M}+\text{H}]^+$
 found: 479.1928 m/z $[\text{M}+\text{H}]^+$.

LCMS (ESI): $t_{\text{ret}} = 4.45$ min. 479 m/z $[\text{M}+\text{H}]^+$.

(E)-3-(4-((4-(carboxymethoxy)phenyl)diazenyl)-1-oxoisindolin-2-yl)-2,6-dioxopiperidin-1-ium (S14)

S13 (331.1 mg, 0.692 mmol, 1 eq.) was dissolved in CH_2Cl_2 :TFA (1:1; 4 mL each). Upon TFA addition (4 mL) the solution turned from yellow to dark red. After 4 hours the reaction was concentrated under reduced pressure, turning from red to an orange solid. The reaction was triturated with Et_2O and dried under high vacuum for 24 h. **S14** (340.5 mg, 0.635 mmol, 92%) was obtained in form of a yellow solid.

$R_f = 0.10$ [CH_2Cl_2 :MeOH, 9:1].

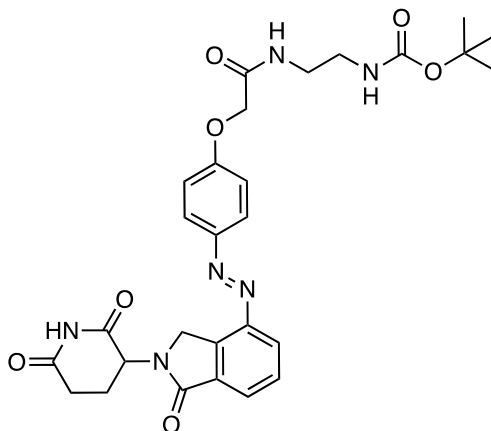
$^1\text{H NMR}$ (400 MHz, $\text{DMSO}-d_6$) $\delta = 11.01$ (s, 1H), 8.22 – 8.13 (m, 1H), 8.02 – 7.94 (m, 2H), 7.88 (d, $J = 7.5$ Hz, 1H), 7.78 (t, $J = 7.8$ Hz, 1H), 7.20 – 7.09 (m, 2H), 5.16 (dd, $J = 13.4, 5.0$ Hz, 1H), 4.80 (m, 3H), 4.67 (d, $J = 19.2$ Hz, 1H), 2.94 (ddd, $J = 18.4, 13.9, 5.3$ Hz, 1H), 2.69 – 2.54 (m, 2H), 2.08 – 1.98 (m, 1H) ppm.

$^{13}\text{C NMR}$ (100 MHz, DMSO) $\delta = 172.93, 171.01, 169.76, 167.23, 161.01, 146.62, 146.62, 134.32, 133.75, 129.58, 128.43, 124.97, 124.74, 115.19, 64.76, 51.68, 48.24, 31.25, 22.32$ ppm.

HRMS (APCI): calcd. for $\text{C}_{21}\text{H}_{19}\text{N}_4\text{O}_6^+$: 423.1299 m/z $[\text{M}+\text{H}]^+$
 found: 423.1284 m/z $[\text{M}+\text{H}]^+$.

LCMS (ESI): $t_{\text{ret}} = 3.01$ min. 423 m/z $[\text{M}+\text{H}]^+$.

***tert*-butyl (*E*)-(2-(2-(4-((2-(2,6-dioxopiperidin-3-yl)-1-oxoisindolin-4-yl)diazenyl)phenoxy)acetamido)ethyl)carbamate (**S15**)**



S14 (50.0 mg, 0.093 mmol, 1.0 eq.) and HATU (45.3 mg, 0.140 mmol, 1.5 eq.) were dissolved in dry DMF (4.5 mL) at room temperature under nitrogen atmosphere. After 5 minutes of stirring *N*-Boc-1,4-diaminoethane (80.7 mg, 0.373 mmol, 4 eq.) and *i*-Pr₂NEt (48.2 mg, 0.373 mmol, 4 eq., 66 μL) were added to the mixture and stirred for further 12 hours. The reaction was diluted with EtOAc (20 mL), separated against H₂O: sat. NaCl (20 mL), extracted with EtOAc (3x 20 mL) and washed with brine (4x 20 mL). The combined organic phase was dried over Na₂SO₄ and concentrated under reduced pressure. **S15** (57.2 mg, 0.092 mmol, 99%) was obtained as an orange solid.

$R_f = 0.38$ [CH₂Cl₂:MeOH, 19:1].

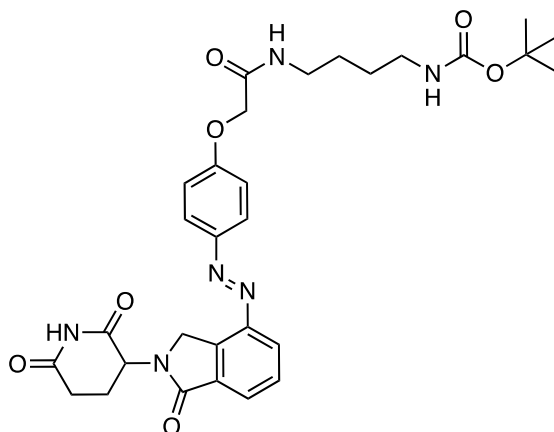
¹H NMR (400 MHz, DMSO-*d*₆) δ = 10.99 (s, 1H), 8.20 (dd, *J* = 16.2, 6.6 Hz, 2H), 7.99 (d, *J* = 8.4 Hz, 2H), 7.89 (d, *J* = 7.4 Hz, 1H), 7.78 (t, *J* = 7.6 Hz, 1H), 7.18 (d, *J* = 8.6 Hz, 2H), 6.87 (q, *J* = 5.7, 4.7 Hz, 1H), 5.17 (dd, *J* = 13.2, 5.1 Hz, 1H), 4.80 (d, *J* = 19.1 Hz, 1H), 4.67 (d, *J* = 19.3 Hz, 1H), 4.61 (s, 2H), 3.18 (q, *J* = 6.3 Hz, 2H), 3.04 (q, *J* = 6.3 Hz, 2H), 2.96 – 2.88 (m, 1H), 2.60 (dd, *J* = 16.2, 12.6 Hz, 2H), 2.09 – 1.98 (m, 1H), 1.37 (s, 9H) ppm.

¹³C NMR (100 MHz, DMSO) δ = 172.91, 171.00, 167.26, 167.21, 160.88, 155.74, 146.68, 146.59, 134.27, 133.74, 129.59, 128.52, 124.99, 124.75, 115.40, 77.73, 67.11, 51.66, 48.24, 38.72, 31.25, 28.22, 22.34, 22.30 ppm.

HRMS (APCI): calcd. for C₂₈H₃₃N₆O₇⁺: 565.2405 m/z [M+H]⁺
 found: 565.2381 m/z [M+H]⁺.

LCMS (ESI): $t_{\text{ret}} = 2.96 \text{ min (Z)}$. 563 m/z [M-H]⁻.
 $t_{\text{ret}} = 3.38 \text{ min (E)}$. 563 m/z [M-H]⁻.

tert-butyl (E)-(4-(2-(4-((2-(2,6-dioxopiperidin-3-yl)-1-oxoisindolin-4-yl)diazenyl)phenoxy)acetamido)butyl)carbamate (S16)



S14 (50.0 mg, 0.093 mmol, 1.0 eq.) and HATU (46.0 mg, 0.142 mmol, 1.5 eq.) were dissolved in dry DMF (4.5 mL) at room temperature. After 5 minutes of stirring *N*-Boc-1,4-diaminobutane (70.2 mg, 0.373 mmol, 4 eq.) and *i*-Pr₂NEt (48.2 mg, 0.373 mmol, 4 eq., 66 μ L) were added to the mixture and stirred for additional 12 h at room temperature. The reaction was diluted with EtOAc (20 mL), separated against 5% LiCl (20 mL), extracted with EtOAc (3x 20 mL) and washed with 10% LiCl (2x 20 mL) and brine (2x 20 mL). The combined organic phase was dried over Na₂SO₄ and concentrated under reduced pressure. Purification of the resulting crude product by flash column chromatography (CH₂Cl₂/MeOH gradient, 0-20% MeOH) gave **S16** (50.9 mg, 0.086 mmol, 92%) as an orange solid.

$R_f = 0.38$ [CH₂Cl₂:MeOH, 19:1].

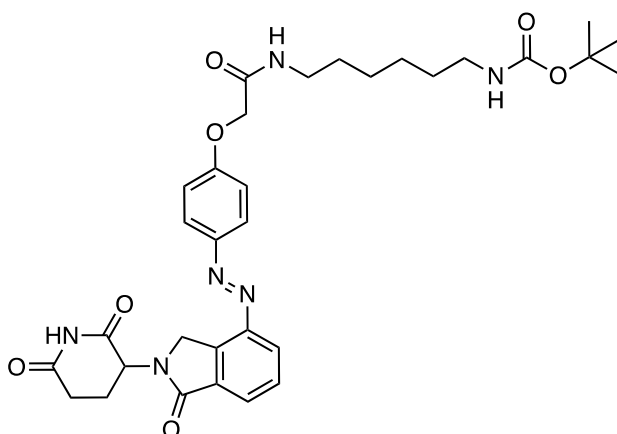
¹H NMR (400 MHz, Chloroform-*d*) $\delta = 8.18$ (d, $J = 7.9$ Hz, 1H), 8.12 (s, 1H), 7.99 (d, $J = 7.5$ Hz, 1H), 7.95 – 7.90 (m, 2H), 7.70 (t, $J = 7.7$ Hz, 1H), 7.05 (d, $J = 8.9$ Hz, 2H), 6.66 (s, 1H), 5.26 (dd, $J = 13.3, 5.1$ Hz, 1H), 4.85 (d, $J = 17.9$ Hz, 1H), 4.74 (d, $J = 18.0$ Hz, 1H), 4.57 (s, 2H), 3.39 (q, $J = 6.6$ Hz, 2H), 3.14 (q, $J = 6.5$ Hz, 2H), 3.01 – 2.79 (m, 2H), 2.46 (qd, $J = 13.1, 5.0$ Hz, 1H), 2.26 (dtd, $J = 12.9, 5.0, 2.5$ Hz, 1H), 1.62 – 1.48 (m, 4H), 1.43 (s, 9H) ppm.

¹³C NMR (100 MHz, CDCl₃) δ = 171.08, 169.55, 168.67, 167.59, 160.02, 156.19, 147.95, 147.09, 134.17, 133.37, 129.70, 129.57, 126.02, 125.12, 115.24, 79.43, 67.62, 52.11, 48.35, 40.26, 38.94, 31.74, 28.56, 27.69, 26.93, 23.61 ppm.

HRMS (APCI): calcd. for C₃₀H₃₇N₆O₇⁺: 593.2718 m/z [M+H]⁺
found: 593.2700 m/z [M+H]⁺.

LCMS (ESI): t_{ret} = 3.17 min (*Z*). 591 m/z [M-H]⁻.
t_{ret} = 3.53 min (*E*). 591 m/z [M-H]⁻.

tert-butyl (E)-(6-(2-(4-((2-(2,6-dioxopiperidin-3-yl)-1-oxoisindolin-4-yl)diazenyl)phenoxy)acetamido)hexyl)carbamate (S17)



S14 (50.0 mg, 0.093 mmol, 1.0 eq.) and HATU (45.3 mg, 0.140 mmol, 1.5 eq.) were dissolved in dry DMF (4.5 mL) at room temperature. After 5 minutes of stirring *N*-Boc-1,4-diaminohexane (80.7 mg, 0.373 mmol, 4 eq.) and *i*-Pr₂NEt (48.2 mg, 0.373 mmol, 4 eq., 66 μ L) were added to the mixture and stirred for additional 12 h at room temperature. The reaction was diluted with EtOAc (20 mL), separated against 5% LiCl (20 mL), extracted with EtOAc (3x 20 mL) and washed with 10% LiCl (2x 20 mL) and brine (2x 20 mL). The combined organic phase was dried over Na₂SO₄ and concentrated under reduced pressure. Purification of the resulting crude product by flash column chromatography (CH₂Cl₂/MeOH gradient, 0-20% MeOH) gave **S17** (57.2 mg, 0.092 mmol, 99%) as an orange solid.

$R_f = 0.34$ [CH₂Cl₂:MeOH, 19:1].

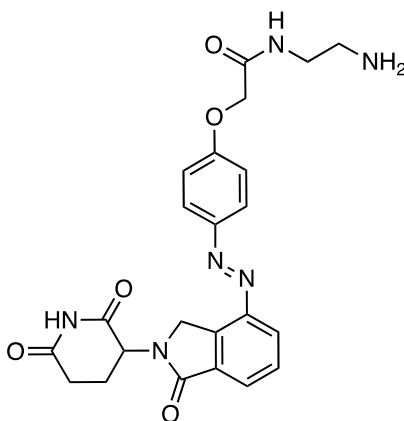
¹H NMR (400 MHz, Chloroform-*d*) δ = 8.19 (d, J = 7.8 Hz, 1H), 8.04 (s, 1H), 7.99 (d, J = 7.5 Hz, 1H), 7.94 (d, J = 8.9 Hz, 2H), 7.70 (t, J = 7.6 Hz, 1H), 7.06 (d, J = 8.9 Hz, 2H), 6.59 (s, 1H), 5.26 (dd, J = 13.3, 5.1 Hz, 1H), 4.86 (d, J = 17.9 Hz, 1H), 4.74 (d, J = 18.0 Hz, 1H), 4.59 (s, 2H), 3.36 (q, J = 6.8 Hz, 2H), 3.09 (s, 2H), 3.00 – 2.79 (m, 2H), 2.46 (dd, J = 13.1, 5.0 Hz, 1H), 2.27 (ddd, J = 13.9, 7.0, 3.6 Hz, 1H), 1.55 (d, J = 7.0 Hz, 2H), 1.50 – 1.43 (m, 2H), 1.44 (s, 9H), 1.34 (d, J = 6.0 Hz, 4H) ppm.

¹³C NMR (100 MHz, CDCl₃) δ = 170.90, 169.91, 169.40, 168.53, 167.38, 159.95, 147.82, 146.98, 134.03, 133.25, 129.63, 129.45, 125.90, 125.00, 115.11, 79.16, 67.54, 51.96, 48.19, 40.29, 38.93, 31.61, 30.00, 29.47, 28.44, 26.34, 26.23, 23.50 ppm.

HRMS (ESI):	calcd. for C ₃₂ H ₄₁ N ₆ O ₇ ⁺ :	621.3031 m/z [M+H] ⁺
	found:	621.3017 m/z [M+H] ⁺ .

LCMS (APCI):	t_{ret} = 3.44 min. (<i>Z</i>)	619 m/z [M-H] ⁻ .
	t_{ret} = 3.80 min. (<i>E</i>)	619 m/z [M-H] ⁻ .

(E)-N-(2-aminoethyl)-2-(4-((2-(2,6-dioxopiperidin-3-yl)-1-oxoisindolin-4-yl)diazenyl)phenoxy)acetamide (S18**)**



S15 (35.0 mg, 0.062 mmol, 1 eq.) was dissolved in TFA/CH₂Cl₂ (1:1; 1mL:1mL) and stirred for 2 h at room temperature. The reaction was diluted with CH₂Cl₂ and concentrated under reduced pressure. The reaction was triturated with Et₂O and dried on high vacuum overnight. **S18** (34.5 mg, 0.06 mmol, 96%) was obtained as trifluoroacetate in form of a yellow solid with traces of residual TFA.

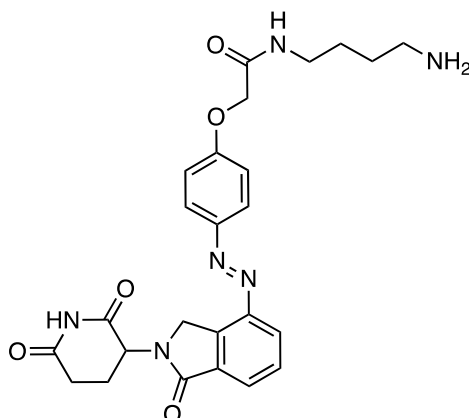
$R_f = 0.13$ [CH₂Cl₂+1%TEA:MeOH, 5:1].

¹H NMR (400 MHz, DMSO-*d*₆) $\delta = 11.02$ (s, 1H), 8.36 (t, $J = 6.0$ Hz, 1H), 8.18 (d, $J = 7.8$ Hz, 1H), 8.01 (d, $J = 8.4$ Hz, 2H), 7.90 (d, $J = 7.4$ Hz, 1H), 7.83 – 7.71 (m, 4H), 7.21 (d, $J = 8.4$ Hz, 2H), 5.19 (d, $J = 13.4$ Hz, 1H), 4.80 (d, $J = 19.1$ Hz, 1H), 4.67 (d, $J = 16.9$ Hz, 3H), 2.99 – 2.87 (m, 3H), 2.69 – 2.51 (m, 1H), 2.11 – 1.98 (m, 1H) ppm.

¹³C NMR (100 MHz, DMSO) $\delta = 172.93, 171.02, 168.11, 167.21, 160.73, 146.76, 146.58, 134.27, 133.76, 129.62, 128.57, 125.07, 124.80, 115.44, 67.14, 51.65, 48.22, 38.72, 36.20, 31.25, 22.35$ ppm.

HRMS (APCI): calcd. for C₂₃H₂₅N₆O₅⁺: 465.1881 m/z [M+H]⁺
 found: 465.1887 m/z [M+H]⁺.

LCMS (ESI): $t_{ret} = 2.00$ min (*Z*). 465 m/z [M+H]⁺.
 $t_{ret} = 2.32$ min (*E*). 465 m/z [M+H]⁺.

***N*-(4-aminobutyl)-2-(4-((2-(2,6-dioxopiperidin-3-yl)-1-oxoisindolin-4-yl)diazenyl)phenoxy)acetamide (**S19**)**

S16 (40.0 mg, 0.067 mmol, 1 eq.) was dissolved in TFA/CH₂Cl₂ (1:1; 1mL:1mL) and stirred for 2 h at room temperature. The reaction was diluted with CH₂Cl₂ and concentrated under reduced pressure. The reaction was triturated with Et₂O and dried on high vacuum overnight. **S19** (40.5 mg, 0.067 mmol, 99%) was obtained as trifluoroacetate in form of a yellow solid with traces of residual TFA.

$R_f = 0.13$ [CH₂Cl₂+1%TEA:MeOH, 5:1].

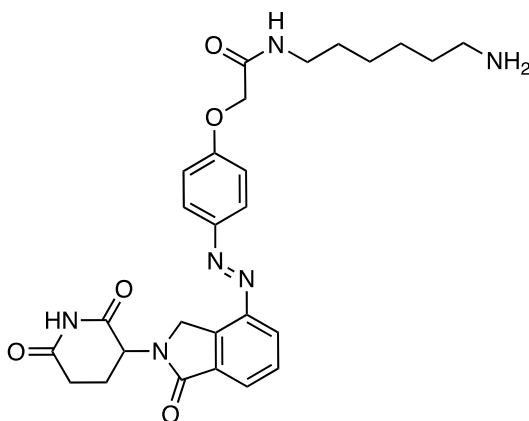
¹H NMR (400 MHz, DMSO-*d*₆) δ = 11.02 (s, 1H), 8.26 (t, J = 5.9 Hz, 1H), 8.18 (d, J = 7.8 Hz, 1H), 8.03 – 7.97 (m, 2H), 7.89 (d, J = 7.5 Hz, 1H), 7.78 (t, J = 7.7 Hz, 1H), 7.67 (s, 2H), 7.22 – 7.14 (m, 2H), 5.18 (dd, J = 13.1, 5.0 Hz, 1H), 4.80 (d, J = 19.1 Hz, 1H), 4.67 (d, J = 19.3 Hz, 1H), 4.62 (s, 2H), 3.17 (q, J = 6.2 Hz, 2H), 2.94 (dd, J = 10.9, 6.4 Hz, 1H), 2.80 (q, J = 6.4 Hz, 2H), 2.65 – 2.54 (m, 2H), 2.05 (d, J = 6.1 Hz, 1H), 1.51 (hept, J = 6.0, 5.4 Hz, 4H) ppm.

¹³C NMR (100 MHz, DMSO) δ = 172.94, 171.03, 167.22, 167.09, 160.89, 146.71, 146.59, 134.28, 133.76, 129.62, 128.53, 125.04, 124.78, 115.41, 67.18, 51.65, 48.22, 38.60, 37.67, 31.25, 26.18, 24.48, 22.34 ppm.

HRMS (APCI): calcd. for C₂₅H₂₉N₆O₅⁺: 493.2194 m/z [M+H]⁺
 found: 493.2177 m/z [M+H]⁺.

LCMS (ESI): $t_{ret} = 2.21$ min (*Z*) 493 m/z [M+H]⁺.
 $t_{ret} = 2.44$ min (*E*) 493 m/z [M+H]⁺.

Tert-butyl-(6-(2-(4-((2-(2,6-dioxopiperidin-3-yl)-1-oxoisindolin-4-yl)diazenyl)phenoxy)-acetamido)hexyl)carbamate (S20)



S17 (44.5 mg, 0.072 mmol, 1 eq.) was dissolved in TFA/CH₂Cl₂ (1:1; 2mL:2mL) and stirred for 2 h at room temperature. The reaction was diluted with CH₂Cl₂ and concentrated under reduced pressure. The reaction was triturated with Et₂O and dried on high vacuum overnight. **S20** (45.6 mg, 0.072 mmol, >99%) was obtained as trifluoroacetate in form of a yellow solid with traces of residual TFA.

$R_f = 0.16$ [CH₂Cl₂+1%TEA:MeOH, 5:1].

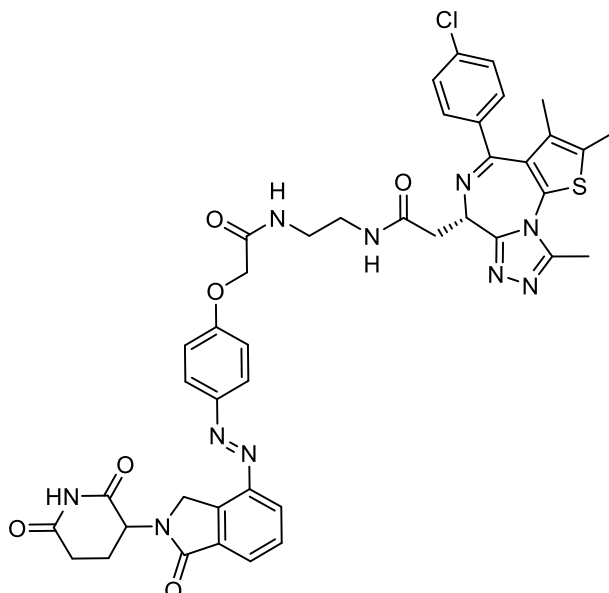
¹H NMR (400 MHz, DMSO-*d*₆) δ = 11.02 (s, 1H), 8.24 – 8.14 (m, 2H), 7.99 (d, *J* = 7.2 Hz, 2H), 7.89 (d, *J* = 7.4 Hz, 1H), 7.78 (t, *J* = 7.7 Hz, 1H), 7.66 (s, 2H), 7.17 (d, *J* = 7.6 Hz, 2H), 5.18 (dd, *J* = 13.2, 5.0 Hz, 1H), 4.80 (d, *J* = 19.1 Hz, 1H), 4.67 (d, *J* = 19.4 Hz, 1H), 4.61 (s, 2H), 3.14 (q, *J* = 6.7 Hz, 2H), 2.94 (ddd, *J* = 21.8, 11.5, 4.6 Hz, 1H), 2.76 (h, *J* = 6.2 Hz, 2H), 2.67 – 2.53 (m, 2H), 2.04 (dt, *J* = 11.8, 4.5 Hz, 1H), 1.57 – 1.39 (m, 4H), 1.29 (tq, *J* = 11.9, 7.0 Hz, 4H) ppm.

¹³C NMR (100 MHz, DMSO) δ = 172.94, 171.03, 167.22, 166.92, 160.95, 146.69, 146.59, 134.29, 133.76, 129.61, 128.51, 125.03, 124.75, 115.40, 67.19, 51.66, 48.23, 38.78, 38.19, 31.25, 28.93, 26.95, 25.84, 25.46, 22.34 ppm.

HRMS (APCI): calcd. for C₂₇H₃₃N₆O₅⁺: 521.2507 m/z [M+H]⁺
found: 521.2498 m/z [M+H]⁺.

LCMS (ESI): $t_{ret} = 2.37$ min (cis) 521 m/z [M+H]⁺.
 $t_{ret} = 2.80$ min (trans) 521 m/z [M+H]⁺.

2-((*R*)-4-(4-chlorophenyl)-2,3,9-trimethyl-6*H*-thieno[3,2-*f*][1,2,4]triazolo[4,3-*a*][1,4]diazepin-6-yl)-*N*-(2-(2-(4-((*E*)-(2-(2,6-dioxopiperidin-3-yl)-1-oxoisoindolin-4-yl)diazenyl)phenoxy)acetamido)ethyl)acetamide (PHOTAC-I-6)



Into a round bottom flask with dry (+)-JQ1 free acid (6.0 mg, 0.015 mmol, 1 eq.) were added **S18** (17.3 mg, 0.030 mmol, 2 eq.) and HATU (8.7 mg, 0.027 mmol, 1.8 eq.) under nitrogen atmosphere. The solids were dissolved in dry DMF (1 mL). After addition of *i*-Pr₂NEt (17.6 mg, 0.137 mmol, 7.2 eq., 0.024 mL) the reaction was stirred for 15 h at room temperature. The mixture was then diluted with EtOAc (20 mL), separated against 5%LiCl (30 mL), extracted with EtOAc (2x 20 mL), washed twice with 10% LiCl (2x 20 mL) and brine (2x 20 mL). The combined organic phases were dried over Na₂SO₄ and concentrated under reduced pressure. Purification of the resulting crude product by flash column chromatography (CH₂Cl₂/MeOH gradient, 0→20% MeOH) gave **PHOTAC-I-6** (12.4 mg, 0.015 mmol, 98%) as a yellow solid.

$R_f = 0.10$ [CH₂Cl₂:MeOH, 19:1].

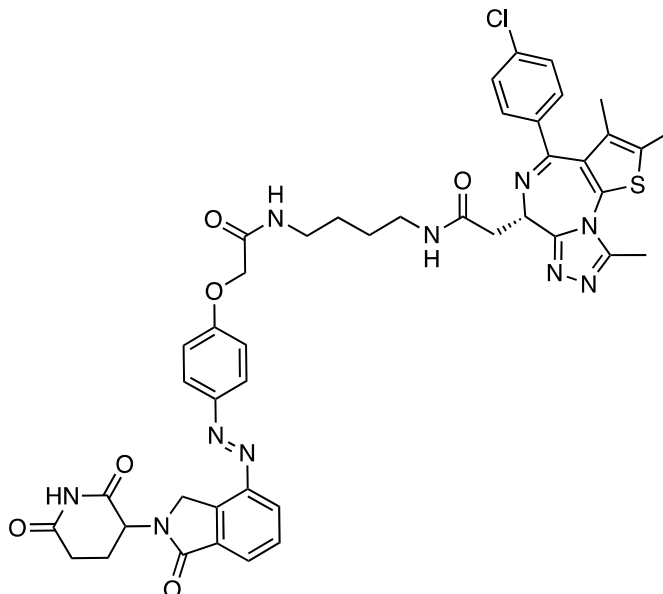
¹H NMR (400 MHz, Chloroform-*d*) δ = 8.71 (s, 1H), 8.09 (d, *J* = 7.8 Hz, 1H), 7.92 (d, *J* = 7.5 Hz, 1H), 7.78 (d, *J* = 8.4 Hz, 2H), 7.65 (t, *J* = 7.7 Hz, 1H), 7.55 (s, 1H), 7.37 (d, *J* = 8.2 Hz, 3H), 7.29 (d, *J* = 8.3 Hz, 2H), 6.93 (d, *J* = 8.6 Hz, 2H), 5.19 (dt, *J* = 13.5, 4.6 Hz, 1H), 4.74 (d, *J* = 18.9 Hz, 1H), 4.64 (dt, *J* = 11.4, 5.9 Hz, 2H), 4.43 (s, 2H), 3.48 (dddd, *J* = 51.8, 22.1, 11.6, 5.5 Hz, 6H), 2.93 – 2.74 (m, 2H), 2.61 (s, 3H), 2.45 (s, 1H), 2.35 (s, 3H), 2.24 – 2.14 (m, 1H), 1.62 (s, 3H) ppm.

^{13}C NMR (100 MHz, CDCl_3) δ = 171.67, 171.50, 169.95, 168.67, 168.28, 164.30, 160.24, 155.76, 150.14, 147.54, 147.01, 137.04, 136.62, 134.10, 133.41, 132.22, 131.10, 130.50, 130.00, 129.73, 129.69, 129.47, 128.88, 125.67, 124.97, 115.18, 67.39, 54.46, 52.25, 48.67, 39.80, 39.33, 39.11, 31.65, 23.44, 14.49, 13.22, 11.91 ppm.

HRMS (ESI): calcd. for $\text{C}_{42}\text{H}_{39}\text{ClN}_{10}\text{NaO}_6\text{S}^+$: 869.2355 m/z $[\text{M}+\text{Na}]^+$
 found: 869.2362 m/z $[\text{M}+\text{Na}]^+$.

LCMS (ESI): $t_{\text{ret}} = 3.44$ min (*Z*). 847 m/z $[\text{M}+\text{H}]^+$.
 $t_{\text{ret}} = 3.74$ min (*E*). 847 m/z $[\text{M}+\text{H}]^+$.

2-((S)-4-(4-chlorophenyl)-2,3,9-trimethyl-6H-thieno[3,2-f][1,2,4]triazolo[4,3-a][1,4]diazepin-6-yl)-N-(4-(2-(4-((E)-(2-(2,6-dioxopiperidin-3-yl)-1-oxoisoindolin-4-yl)diazenyl)phenoxy)acetamido)butyl)acetamide (PHOTAC-I-7)



Into a round bottom flask with dry (+)-JQ1 free acid (6.0 mg, 0.015 mmol, 1 eq.) were added **S19** (18.2 mg, 0.030 mmol, 2 eq.) and HATU (8.7 mg, 0.027 mmol, 1.8 eq.) under nitrogen atmosphere. The solids were dissolved in dry DMF (1 mL). After addition of *i*-Pr₂NEt (13.9 mg, 0.108 mmol, 7.2 eq., 0.020 mL) the reaction was stirred for 16 h at room temperature. The mixture was then diluted with EtOAc (20 mL), separated against 5% LiCl (30 mL), extracted with EtOAc (2x 20 mL), washed twice with 10% LiCl (2x 20 mL) and brine (2x 20 mL). The combined organic phases were dried over Na₂SO₄ and concentrated under reduced pressure. Purification of the resulting crude product by flash column chromatography (CH₂Cl₂/MeOH gradient, 0→20% MeOH) gave **PHOTAC-I-7** (12.7 mg, 0.015 mmol, 97%) as a yellow solid.

$R_f = 0.09$ [CH₂Cl₂:MeOH, 19:1].

¹H NMR (400 MHz, Chloroform-*d*) δ = 8.57 (s, 1H), 8.15 (d, *J* = 7.8 Hz, 1H), 7.95 (d, *J* = 7.5 Hz, 1H), 7.87 (d, *J* = 8.4 Hz, 2H), 7.67 (t, *J* = 7.6 Hz, 1H), 7.39 (d, *J* = 8.2 Hz, 2H), 7.32 (d, *J* = 8.1 Hz, 2H), 7.01 (d, *J* = 8.5 Hz, 2H), 6.92 (t, *J* = 7.1 Hz, 1H), 6.82 (s, 1H), 5.23 (dt, *J* = 13.4, 4.3 Hz, 1H), 4.80 (dd, *J* = 18.1, 3.2 Hz, 1H), 4.71 (dd, *J* = 18.1, 4.5 Hz, 1H), 4.62 (t, *J* = 7.1 Hz, 1H), 4.51 (s, 2H), 3.56 (dd, *J* = 14.3, 8.2 Hz, 1H), 3.34

(qd, $J = 17.8, 15.6, 6.3$ Hz, 5H), 2.94 – 2.75 (m, 2H), 2.64 (s, 3H), 2.51 – 2.43 (m, 1H), 2.37 (s, 3H), 2.27 – 2.18 (m, 1H), 1.65 (s, 3H), 1.57 (s, 4H) ppm.

^{13}C NMR (100 MHz, CDCl_3) $\delta = 171.33, 170.67, 169.81, 168.65, 167.67, 164.26, 160.15, 155.72, 150.14, 147.78, 147.05, 137.03, 136.63, 134.15, 133.40, 132.22, 131.11, 130.58, 129.99, 129.75, 129.69, 129.52, 128.88, 125.86, 125.09, 115.25, 67.60, 54.63, 52.09, 48.45, 39.52, 39.12, 38.85, 31.70, 26.89, 26.79, 23.53, 14.51, 13.22, 11.93$ ppm.

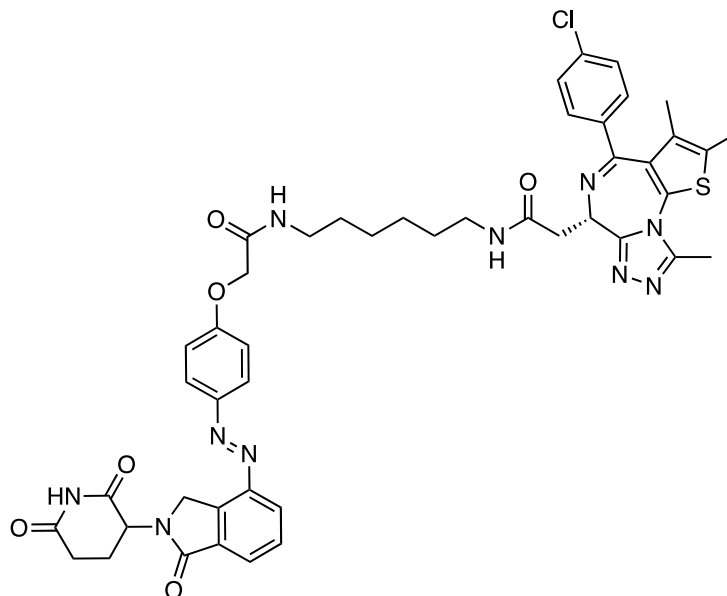
HRMS (ESI): calcd. for $\text{C}_{44}\text{H}_{43}\text{ClKN}_{10}\text{O}_6\text{S}^+$: 913.2408 m/z $[\text{M}+\text{K}]^+$

found: 913.2419 m/z $[\text{M}+\text{K}]^+$.

LCMS (ESI): $t_{\text{ret}} = 3.48$ min (*Z*). 875 m/z $[\text{M}+\text{H}]^+$.

$t_{\text{ret}} = 3.71$ min (*E*). 875 m/z $[\text{M}+\text{H}]^+$.

2-((*S*)-4-(4-chlorophenyl)-2,3,9-trimethyl-6*H*-thieno[3,2-*f*][1,2,4]triazolo[4,3-*a*][1,4]diazepin-6-yl)-*N*-(6-(2-(4-((*E*)-(2-(2,6-dioxopiperidin-3-yl)-1-oxoisindolin-4-yl)diazenyl)phenoxy)acetamido)hexyl)acetamide (PHOTAC-I-8)



Into a round bottom flask with dry (+)-JQ1 free acid (6.0 mg, 0.015 mmol, 1 eq.) were added **S20** (19.0 mg, 0.030 mmol, 2 eq.) and HATU (8.7 mg, 0.027 mmol, 1.8 eq.) under nitrogen atmosphere. The solids were dissolved in dry DMF (1 mL). After addition of *i*-Pr₂NEt (13.9 mg, 0.108 mmol, 7.2 eq., 0.020 mL) the reaction was stirred for 18 h at room temperature. The mixture was then diluted with EtOAc (20 mL),

separated against 5% LiCl (30 mL), extracted with EtOAc (2x 20 mL), washed twice with 10% LiCl (2x 20 mL) and brine (2x 20 mL). The combined organic phases were dried over Na₂SO₄ and concentrated under reduced pressure. Purification of the resulting crude product by flash column chromatography (CH₂Cl₂/MeOH gradient, 0→20% MeOH) gave **PHOTAC-I-8** (12.8 mg, 0.014 mmol, 95%) as a yellow solid.

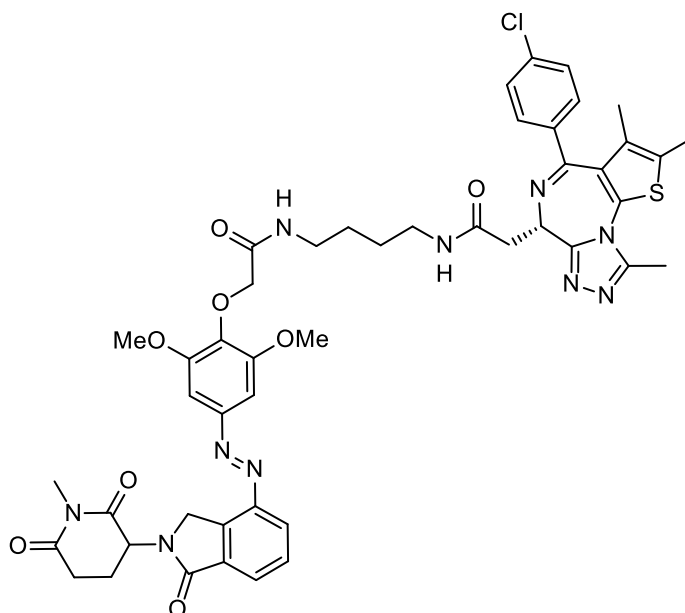
R_f = 0.16 [CH₂Cl₂:MeOH, 19:1].

¹H NMR (400 MHz, Chloroform-*d*) δ = 8.51 (d, *J* = 28.6 Hz, 1H), 8.17 (d, *J* = 7.8 Hz, 1H), 7.97 (d, *J* = 7.4 Hz, 1H), 7.91 (d, *J* = 8.0 Hz, 2H), 7.68 (t, *J* = 7.6 Hz, 1H), 7.39 (d, *J* = 7.9 Hz, 2H), 7.31 (d, *J* = 8.1 Hz, 2H), 7.03 (d, *J* = 8.2 Hz, 2H), 6.76 – 6.66 (m, 1H), 6.61 (d, *J* = 4.7 Hz, 1H), 5.24 (d, *J* = 13.1 Hz, 1H), 4.84 (d, *J* = 18.0 Hz, 1H), 4.73 (d, *J* = 18.1 Hz, 1H), 4.59 (d, *J* = 11.4 Hz, 3H), 3.55 (dd, *J* = 14.0, 8.0 Hz, 1H), 3.29 (dd, *J* = 28.3, 5.6 Hz, 5H), 2.96 – 2.77 (m, 2H), 2.64 (s, 3H), 2.46 (dt, *J* = 13.0, 6.7 Hz, 1H), 2.38 (s, 3H), 2.30 – 2.18 (m, 1H), 1.65 (s, 3H), 1.51 (s, 4H), 1.31 (s, 4H) ppm.

¹³C NMR (100 MHz, CDCl₃) δ = 171.27, 170.59, 169.77, 168.65, 167.62, 164.16, 160.14, 155.76, 150.07, 147.88, 147.09, 136.98, 136.69, 134.19, 133.41, 132.26, 131.05, 130.57, 129.97, 129.73, 129.67, 129.53, 128.86, 125.94, 125.11, 115.25, 67.69, 54.66, 52.07, 48.36, 39.58, 39.43, 38.92, 31.74, 29.47, 29.45, 26.34, 26.27, 23.58, 14.51, 13.23, 11.93 ppm.

HRMS (ESI):	calcd. for C ₄₆ H ₄₇ ClN ₁₀ NaO ₆ S ⁺ :	925.2981 m/z [M+Na] ⁺
	found:	925.2975 m/z [M+Na] ⁺ .
LCMS (ESI):	<i>t</i> _{ret} = 3.57 min (<i>Z</i>)	903 m/z [M+H] ⁺ .
	<i>t</i> _{ret} = 3.85 min (<i>E</i>)	903 m/z [M+H] ⁺ .

2-((S)-4-(4-chlorophenyl)-2,3,9-trimethyl-6H-thieno[3,2-f][1,2,4]triazolo[4,3-a][1,4]diazepin-6-yl)-N-(4-(2-(2,6-dimethoxy-4-((E)-2-(1-methyl-2,6-dioxopiperidin-3-yl)-1-oxoisindolin-4-yl)diazenyl)phenoxy)acetamido)butyl)acetamide (Me-PHOTAC-I-3)



Into a round bottom flask with dry **PHOTAC-I-3** (10.0 mg, 0.011 mmol, 1 eq.) was added K_2CO_3 (3.0 mg, 0.021 mmol, 2 eq.) under nitrogen atmosphere. The solids were dissolved in dry DMF (1 mL) and methyl iodide (1.8 mg, 0.013 mmol, 1.2 eq.) was added. The reaction was stirred for 16 h at room temperature. The mixture was then diluted with EtOAc (20 mL) and separated against 5% LiCl (20 mL). The aqueous phase was extracted with EtOAc (2x 10 mL), and the combined organic phases were washed with 10% LiCl (2x 20 mL) and brine (2x 20 mL). The organic phase was dried over Na_2SO_4 and concentrated under reduced pressure. Purification of the resulting crude product by flash column chromatography ($CH_2Cl_2/MeOH$ gradient, 0→20% MeOH) gave **Me-PHOTAC-I-3** (5.2 mg, 0.005 mmol, 51%) as a yellow solid.

$R_f = 0.37$ [$CH_2Cl_2:MeOH$, 19:1].

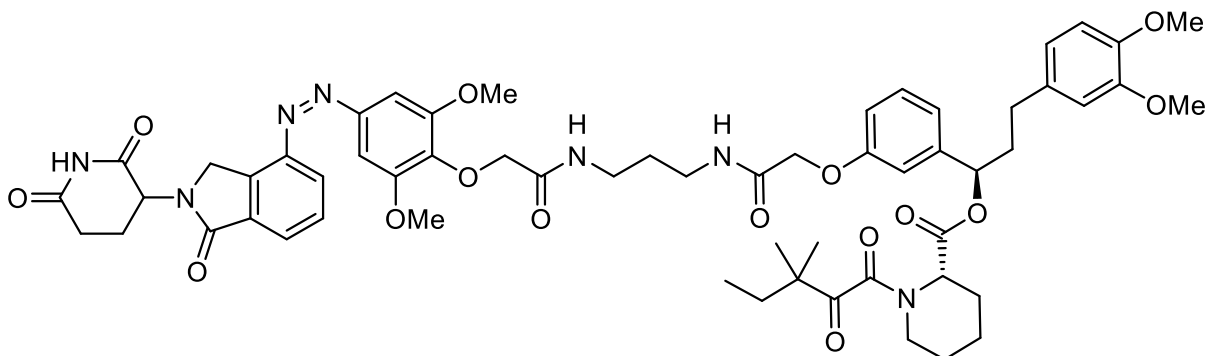
1H NMR (400 MHz, $DMSO-d_6$) $\delta = \delta$ 8.26 – 8.18 (m, 2H), 7.98 – 7.91 (m, 2H), 7.80 (t, $J = 7.7$ Hz, 1H), 7.48 (d, $J = 8.4$ Hz, 2H), 7.41 (d, $J = 8.5$ Hz, 2H), 7.35 (s, 2H), 5.23 (dd, $J = 13.5, 5.0$ Hz, 1H), 4.83 (d, $J = 19.1$ Hz, 1H), 4.69 (d, $J = 19.0$ Hz, 1H), 4.51 (ddd, $J = 7.9, 6.1, 1.3$ Hz, 1H), 4.44 (s, 2H), 3.94 (s, 6H), 3.29 – 3.10 (m, 6H), 3.02 (s,

3H), 3.08 – 2.98 (m, 1H), 2.79 (ddd, $J = 17.3, 4.5, 2.4$ Hz, 1H), 2.59 (s, 3H), 2.63 – 2.55 (m, 1H), 2.40 (s, 3H), 2.12 – 2.04 (m, 1H), 1.61 (s, 3H), 1.58 – 1.44 (m, 4H) ppm. ^{13}C NMR (100 MHz, DMSO- d_6) $\delta = 171.92, 170.64, 169.33, 167.98, 167.19, 163.05, 155.06, 152.58, 149.85, 148.28, 146.38, 139.31, 136.68, 135.23, 134.66, 133.81, 132.22, 130.74, 130.10, 129.83, 129.65, 129.56, 128.45, 128.41, 125.52, 100.61, 71.92, 56.37, 53.84, 52.36, 48.24, 38.20, 37.96, 37.60, 31.42, 26.69, 26.63, 26.62, 21.59, 14.04, 12.67, 11.28$ ppm.

HRMS (ESI): calcd. for $\text{C}_{47}\text{H}_{50}\text{ClN}_{10}\text{O}_8\text{S}^+$: 949.3217 m/z $[\text{M}+\text{H}]^+$
 found: 949.3235 m/z $[\text{M}+\text{H}]^+$.

LCMS (ESI): $t_{\text{ret}} = 3.94$ min (*Z*). 949 m/z $[\text{M}+\text{H}]^+$.
 $t_{\text{ret}} = 4.19$ min (*E*). 949 m/z $[\text{M}+\text{H}]^+$.

(1R)-3-(3,4-dimethoxyphenyl)-1-(3-(2-((3-(2-(4-((2-(2,6-dioxopiperidin-3-yl)-1-oxoisindolin-4-yl)diazenyl)-2,6-dimethoxyphenoxy)acetamido)propyl)-amino)-2-oxoethoxy)phenyl)propyl-(2S)-1-(3,3-dimethyl-2-oxopentanoyl)-piperidine-2-carboxylate (PHOTAC-II-1)



Into a round bottom flask with dry **2-(3-((R)-3-(3,4-dimethoxyphenyl)-1-(((S)-1-(3,3-dimethyl-2-oxopentanoyl)piperidine-2-carbonyl)oxy)propyl)phenoxy)acetic acid** (10.2 mg, 0.017 mmol, 1 eq.) were added **S9** (22.8 mg, 0.035 mmol, 2 eq.) and HATU (12 mg, 0.031 mmol, 1.8 eq.) under nitrogen. The reaction was dissolved in dry DMF (1 mL). After addition of *i*-Pr $_2$ NEt (17 mg, 0.13 mmol, 7.5 eq., 0.023 mL) the reaction was stirred for 14 h at room temperature. The mixture was then diluted with EtOAc (20 mL), separated against 5% LiCl (20 mL), extracted with EtOAc (2x 20 mL) and washed twice with 10% LiCl (2x 20 mL) and brine (2x 20 mL). The combined organic

phases were dried over Na_2SO_4 and concentrated under reduced pressure. Purification of the resulting crude product by flash column chromatography ($\text{CH}_2\text{Cl}_2/\text{MeOH}$ gradient, 0→20% MeOH) gave **PHOTAC-II-1** (17.8 mg, 0.016 mmol, 92%) as a yellow solid.

$R_f = 0.59$ [$\text{CH}_2\text{Cl}_2:\text{MeOH}$, 9:1].

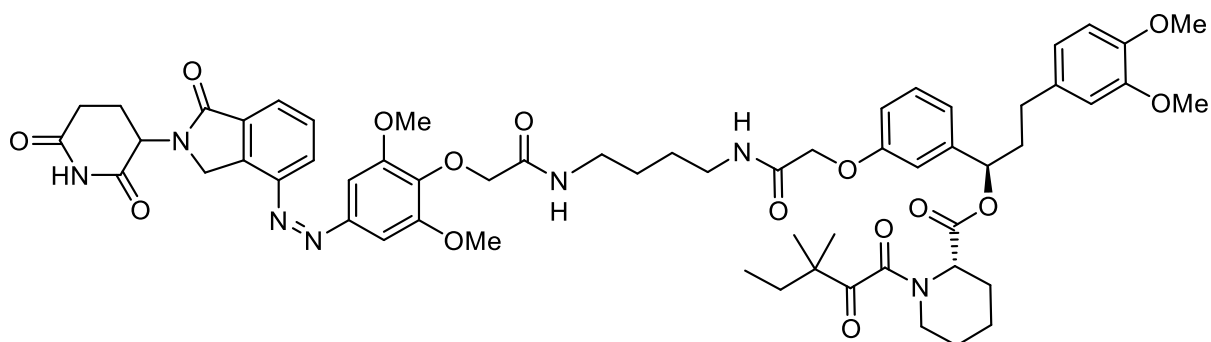
$^1\text{H NMR}$ (600 MHz, Chloroform-*d*) $\delta = 8.33$ (s, 1H), 8.20 (d, $J = 7.7$ Hz, 1H), 8.00 (d, $J = 7.9$ Hz, 1H), 7.84 (t, $J = 6.3$ Hz, 1H), 7.71 (t, $J = 7.7$ Hz, 1H), 7.37 (t, $J = 6.3$ Hz, 1H), 7.28 (t, $J = 7.9$ Hz, 1H), 7.21 (s, 2H), 7.00 – 6.92 (m, 2H), 6.87 (dd, $J = 8.2, 2.8$ Hz, 1H), 6.80 – 6.73 (m, 1H), 6.69 – 6.65 (m, 2H), 5.77 (dd, $J = 8.0, 5.6$ Hz, 1H), 5.30 (d, $J = 4.9$ Hz, 1H), 5.25 (dd, $J = 13.4, 5.1$ Hz, 1H), 4.85 (d, $J = 17.8$ Hz, 1H), 4.72 (d, $J = 17.8$ Hz, 1H), 4.60 (d, 2H), 4.46 (s, 2H), 3.96 (s, 6H), 3.86 – 3.81 (m, 6H), 3.47 – 3.33 (m, 5H), 3.16 (td, $J = 13.2, 3.2$ Hz, 1H), 2.95 – 2.81 (m, 2H), 2.64 – 2.42 (m, 3H), 2.36 (d, $J = 13.9$ Hz, 1H), 2.28 – 2.18 (m, 2H), 2.04 (dtd, $J = 11.6, 9.7, 4.8$ Hz, 1H), 1.83 – 1.57 (m, 7H), 1.47 (qt, $J = 13.0, 4.0$ Hz, 1H), 1.35 (tt, $J = 13.6, 3.6$ Hz, 1H), 1.20 (d, $J = 11.9$ Hz, 6H), 0.87 (t, $J = 7.4$ Hz, 3H) ppm.

$^{13}\text{C NMR}$ (150 MHz, CDCl_3) $\delta = 208.01, 171.22, 170.36, 169.77, 169.65, 168.55, 168.42, 167.38, 157.54, 152.75, 149.04, 148.99, 147.46, 146.88, 141.90, 139.76, 134.09, 133.49, 133.44, 130.08, 130.07, 129.61, 126.37, 120.25, 120.17, 114.23, 113.49, 111.81, 111.41, 100.56, 76.64, 72.73, 67.36, 56.50, 56.04, 55.96, 52.12, 51.39, 48.33, 46.82, 44.28, 38.28, 36.21, 36.08, 32.59, 31.73, 31.35, 29.84, 26.53, 25.06, 23.59, 23.57, 23.25, 21.32, 8.88$ ppm.

HRMS (ESI): calcd. for $\text{C}_{58}\text{H}_{73}\text{N}_8\text{O}_{15}^+$: 1121.5189 m/z $[\text{M}+\text{NH}_4]^+$
 found: 1121.5246 m/z $[\text{M}+\text{NH}_4]^+$.

LCMS (ESI): $t_{\text{ret}} = 4.56$ min. 1104 m/z $[\text{M}+\text{H}]^+$.

(1R)-3-(3,4-dimethoxyphenyl)-1-(3-(2-((4-(2-(4-((2-(2,6-dioxopiperidin-3-yl)-1-oxoisindolin-4-yl)diazenyl)-2,6-dimethoxyphenoxy)acetamido)butyl)-amino)-2-oxoethoxy)phenyl)propyl(2S)-1-(3,3-dimethyl-2-oxopentanoyl)-piperidine-2-carboxylate (PHOTAC-II-2)



Into a round bottom flask with dry **2-(3-((R)-3-(3,4-dimethoxyphenyl)-1-(((S)-1-(3,3-dimethyl-2-oxopentanoyl)piperidine-2-carbonyl)oxy)propyl)phenoxy)acetic acid** (10.2 mg, 0.018 mmol, 1 eq.) were added **3** (23.3 mg, 0.035 mmol, 2 eq.) and HATU (12 mg, 0.031 mmol, 1.8 eq.) under nitrogen. The reaction was dissolved in dry DMF (1 mL). After addition of *i*-Pr₂NEt (17 mg, 0.13 mmol, 7.5 eq., 0.023 mL) the reaction was stirred for 14 h at room temperature. The mixture was then diluted with EtOAc (20 mL), separated against 5% LiCl (20 mL), extracted with EtOAc (2x 20 mL) and washed twice with 10% LiCl (2x 20 mL) and brine (2x 20 mL). The combined organic phases were dried over Na₂SO₄ and concentrated under reduced pressure. Purification of the resulting crude product by flash column chromatography (CH₂Cl₂/MeOH gradient, 0→20% MeOH) gave **PHOTAC-II-2** (17.7 mg, 0.016 mmol, 91%) as a yellow solid.

$R_f = 0.59$ [CH₂Cl₂:MeOH, 9:1].

¹H NMR (600 MHz, Chloroform-*d*) δ = 8.35 (s, 1H), 8.19 (dd, *J* = 7.8, 1.0 Hz, 1H), 7.99 (dd, *J* = 7.5, 1.0 Hz, 1H), 7.74 – 7.67 (m, 2H), 7.28 (t, *J* = 7.9 Hz, 1H), 7.22 (s, 2H), 6.99 – 6.93 (m, 2H), 6.84 – 6.75 (m, 3H), 6.70 – 6.64 (m, 2H), 5.79 – 5.73 (m, 1H), 5.33 – 5.27 (m, 1H), 5.24 (dd, *J* = 13.4, 5.1 Hz, 1H), 4.85 (d, *J* = 17.9 Hz, 1H), 4.72 (d, *J* = 17.8 Hz, 1H), 4.60 (s, 2H), 4.48 (s, 2H), 3.98 (s, 6H), 3.86 – 3.82 (m, 6H), 3.44 – 3.32 (m, 5H), 3.16 (td, *J* = 13.2, 3.2 Hz, 1H), 2.92 – 2.80 (m, 2H), 2.65 – 2.43 (m, 3H), 2.36 (d, *J* = 14.0 Hz, 1H), 2.28 – 2.18 (m, 2H), 2.04 (ddt, *J* = 13.9, 10.1, 5.9 Hz, 1H),

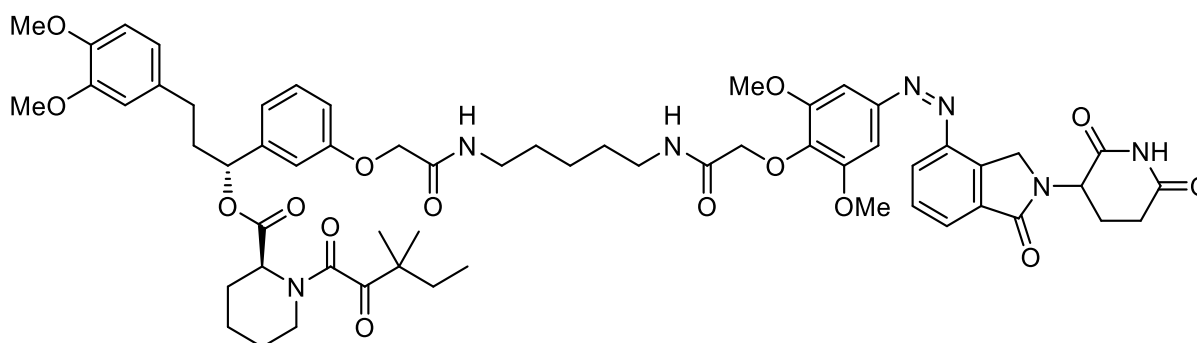
1.78 – 1.59 (m, 9H), 1.48 (qt, $J = 13.2, 4.4$ Hz, 1H), 1.35 (tt, $J = 13.3, 3.4$ Hz, 1H), 1.20 (d, $J = 8.2$ Hz, 6H), 0.87 (t, $J = 7.5$ Hz, 3H) ppm.

^{13}C NMR (150 MHz, CDCl_3) $\delta = 208.03, 171.25, 169.78, 169.69, 169.68, 168.55, 168.20, 167.37, 157.43, 152.73, 149.00, 148.99, 147.47, 146.87, 142.04, 139.81, 134.13, 133.46, 133.44, 130.13, 130.01, 129.59, 126.33, 120.26, 120.24, 113.88, 113.63, 111.82, 111.41, 100.58, 76.54, 72.82, 67.37, 56.50, 56.04, 55.96, 52.15, 51.37, 48.38, 46.82, 44.27, 38.82, 38.69, 38.29, 32.59, 31.72, 31.34, 27.22, 27.20, 26.52, 25.06, 23.56, 23.53, 23.31, 21.29, 8.89$ ppm.

HRMS (ESI): calcd. for $\text{C}_{59}\text{H}_{72}\text{N}_7\text{O}_{15}^+$: 1118.5081 m/z $[\text{M}+\text{H}]^+$
found: 1118.5081 m/z $[\text{M}+\text{H}]^+$.

LCMS (ESI): $t_{\text{ret}} = 4.56$ min. 1118 m/z $[\text{M}+\text{H}]^+$.

(1R)-3-(3,4-dimethoxyphenyl)-1-(3-(2-((5-(2-(4-((Z)-(2-(2,6-dioxopiperidin-3-yl)-1-oxoisoindolin-4-yl)diazenyl)-2,6-dimethoxyphenoxy)acetamido)pentyl)amino)-2-oxoethoxy)phenyl)propyl (2S)-1-(3,3-dimethyl-2-oxopentanoyl)piperidine-2-carboxylate (PHOTAC-II-3)



Into a round bottom flask with dry **2-(3-((R)-3-(3,4-dimethoxyphenyl)-1-(((S)-1-(3,3-dimethyl-2-oxopentanoyl)piperidine-2-carbonyl)oxy)propyl)phenoxy)acetic acid** (10.0 mg, 0.018 mmol, 1 eq.) were added **S10** (25.1 mg, 0.034 mmol, 2 eq.) and HATU (11.7 mg, 0.031 mmol, 1.8 eq.) under nitrogen. The reaction was dissolved in dry DMF (1 mL). After addition of *i*-Pr₂NEt (15.5 mg, 0.12 mmol, 7 eq., 0.021 mL) the reaction was stirred for 14 h at room temperature. The mixture was then diluted with EtOAc (20 mL), separated against 5% LiCl (20 mL), extracted with EtOAc (2x 20 mL) and washed twice with 10% LiCl (2x 20 mL) and brine (2x 20 mL). The combined organic phases were dried over Na₂SO₄ and concentrated under reduced pressure. Purification of the resulting crude product by flash column chromatography (CH₂Cl₂/MeOH gradient, 0→20% MeOH) gave **PHOTAC-II-3** (14.4 mg, 0.013 mmol, 74%) as a yellow solid.

$R_f = 0.28$ [CH₂Cl₂:MeOH, 19:1].

¹H NMR (600 MHz, Chloroform-*d*) δ = 8.36 (d, J = 3.6 Hz, 1H), 8.20 (dd, J = 7.8, 1.0 Hz, 1H), 8.00 (dd, J = 7.5, 1.0 Hz, 1H), 7.71 (t, J = 7.5 Hz, 2H), 7.29 (t, J = 7.9 Hz, 1H), 7.22 (s, 2H), 7.00 – 6.92 (m, 2H), 6.82 (dd, J = 8.2, 2.6 Hz, 1H), 6.80 – 6.72 (m, 2H), 6.71 – 6.63 (m, 2H), 5.77 (dd, J = 8.2, 5.5 Hz, 1H), 5.31 (d, J = 6.1 Hz, 1H), 5.25 (dd, J = 13.4, 5.1 Hz, 1H), 4.86 (d, J = 17.8 Hz, 1H), 4.72 (d, J = 17.8 Hz, 1H), 4.61 (s, 2H),

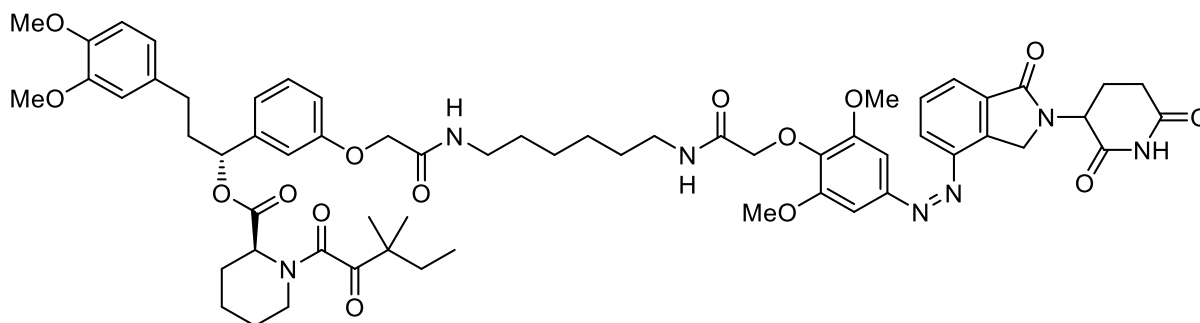
4.47 (s, 2H), 3.98 (s, 6H), 3.87 – 3.81 (m, 6H), 3.35 (q, $J = 6.7$ Hz, 5H), 3.21 – 3.12 (m, 1H), 3.04 – 2.90 (m, 1H), 2.85 (ddd, $J = 18.1, 13.3, 5.2$ Hz, 1H), 2.59 – 2.41 (m, 3H), 2.36 (d, $J = 14.0$ Hz, 1H), 2.24 (m, 2H), 2.04 (m, 1H), 1.81 – 1.57 (m, 9H), 1.48 (m, 1H), 1.44 – 1.30 (m, 3H), 1.20 (d, $J = 8.0$ Hz, 6H), 0.87 (t, $J = 7.4$ Hz, 3H) ppm.

^{13}C NMR (150 MHz, CDCl_3) $\delta = 208.03, 171.19, 169.79, 169.68, 169.64, 168.55, 168.17, 167.38, 157.45, 152.72, 149.03, 149.00, 147.49, 146.89, 142.04, 139.85, 134.11, 133.45, 133.42, 130.14, 130.06, 129.60, 126.36, 120.27, 120.24, 113.85, 113.70, 111.83, 111.42, 100.59, 76.54, 72.81, 67.38, 56.51, 56.05, 55.97, 52.13, 51.37, 48.33, 46.83, 44.28, 39.04, 38.91, 38.30, 32.60, 31.75, 31.35, 29.44, 29.35, 26.53, 25.07, 24.24, 23.59, 23.57, 23.32, 21.30, 8.90$ ppm.

HRMS (APCI): calcd. for $\text{C}_{60}\text{H}_{74}\text{N}_7\text{O}_{15}^+$: 1132.5273 m/z $[\text{M}+\text{H}]^+$
 found: 1132.5217 m/z $[\text{M}+\text{H}]^+$.

LCMS (ESI): $t_{\text{ret}} = 4.67$ (Z) min. 566.7 m/z $[\text{M}+2\text{H}]^{2+}$.
 $t_{\text{ret}} = 4.83$ (E) min. 566.7 m/z $[\text{M}+2\text{H}]^{2+}$.

(1R)-3-(3,4-dimethoxyphenyl)-1-(3-(2-((6-(2-(4-((Z)-(2-(2,6-dioxopiperidin-3-yl)-1-oxoisindolin-4-yl)diazenyl)-2,6-dimethoxyphenoxy)acetamido)hexyl)amino)-2-oxoethoxy)phenyl)propyl (2S)-1-(3,3-dimethyl-2-oxopentanoyl)piperidine-2-carboxylate (PHOTAC-II-4)



Into a round bottom flask with dry **2-(3-((R)-3-(3,4-dimethoxyphenyl)-1-((S)-1-(3,3-dimethyl-2-oxopentanoyl)piperidine-2-carbonyl)oxy)propyl)phenoxy)acetic acid** (10.0 mg, 0.018 mmol, 1 eq.) were added **S11** (23.8 mg, 0.034 mmol, 2 eq.) and HATU (11.7 mg, 0.031 mmol, 1.8 eq.) under nitrogen. The reaction was dissolved in dry DMF (1 mL). After addition of *i*-Pr₂NEt (15.5 mg, 0.12 mmol, 7 eq., 0.021 mL) the reaction was stirred for 14 h at room temperature. The mixture was then diluted with EtOAc (20 mL), separated against 5% LiCl (20 mL), extracted with EtOAc (2x 20 mL) and washed twice with 10% LiCl (2x 20 mL) and brine (2x 20 mL). The combined organic phases were dried over Na₂SO₄ and concentrated under reduced pressure. Purification of the resulting crude product by flash column chromatography (CH₂Cl₂/MeOH gradient, 0→20% MeOH) gave **PHOTAC-II-4** (16.9 mg, 0.015 mmol, 86%) as a yellow solid.

$R_f = 0.33$ [CH₂Cl₂:MeOH, 19:1].

¹H NMR (600 MHz, Chloroform-*d*) δ = 8.30 (s, 1H), 8.20 (dd, J = 7.9, 1.0 Hz, 1H), 8.00 (dd, J = 7.5, 1.0 Hz, 1H), 7.71 (t, J = 7.7 Hz, 1H), 7.65 (t, J = 5.9 Hz, 1H), 7.29 (td, J = 7.9, 3.6 Hz, 1H), 7.22 (s, 2H), 7.00 – 6.88 (m, 2H), 6.85 – 6.75 (m, 2H), 6.72 (t, J = 6.0 Hz, 1H), 6.70 – 6.64 (m, 2H), 5.82 – 5.69 (m, 1H), 5.31 (d, J = 5.9 Hz, 1H), 5.26 (dd, J

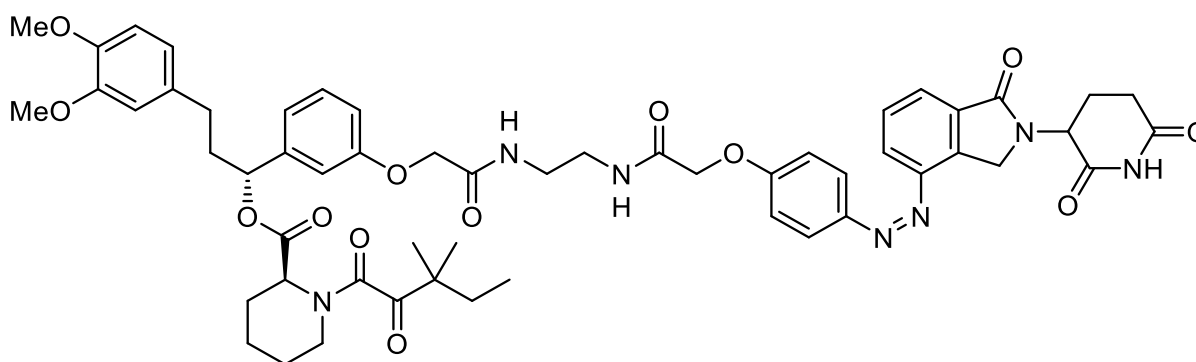
= 13.4, 5.1 Hz, 1H), 4.85 (d, $J = 17.8$ Hz, 1H), 4.72 (d, $J = 17.8$ Hz, 1H), 4.60 (s, 2H), 4.48 (d, $J = 2.5$ Hz, 2H), 3.98 (s, 6H), 3.85 (dd, $J = 4.8, 2.5$ Hz, 6H), 3.40 – 3.30 (m, 5H), 3.16 (td, $J = 13.2, 3.1$ Hz, 1H), 3.01 – 2.78 (m, 2H), 2.61 – 2.42 (m, 3H), 2.36 (d, $J = 14.0$ Hz, 1H), 2.24 (dddd, $J = 17.8, 15.2, 7.8, 5.4$ Hz, 2H), 2.10 – 1.99 (m, 1H), 1.80 – 1.52 (m, 9H), 1.48 (dt, $J = 13.1, 4.0$ Hz, 1H), 1.38 (tt, $J = 10.4, 4.7$ Hz, 5H), 1.21 (d, $J = 8.3$ Hz, 6H), 0.87 (t, $J = 7.4$ Hz, 3H) ppm.

^{13}C NMR (150 MHz, CDCl_3) $\delta = 208.01, 171.17, 169.79, 169.63, 169.50, 168.54, 168.08, 167.37, 157.49, 152.74, 149.01, 148.99, 147.50, 146.91, 142.03, 139.91, 134.10, 133.45, 133.45, 130.14, 130.04, 129.61, 126.36, 120.27, 120.23, 113.89, 113.70, 111.84, 111.43, 100.59, 76.54, 72.88, 67.44, 56.50, 56.06, 55.97, 52.12, 51.37, 48.29, 46.83, 44.28, 39.12, 38.98, 38.30, 32.61, 31.74, 31.35, 29.74, 29.64, 26.69, 26.67, 26.52, 25.08, 23.61, 23.58, 23.32, 21.30, 8.90$ ppm.

HRMS (APCI): calcd. for $\text{C}_{61}\text{H}_{76}\text{N}_7\text{O}_{15}^+$: 1146.5394 m/z $[\text{M}+\text{H}]^+$
 found: 1146.5392 m/z $[\text{M}+\text{H}]^+$.

LCMS (ESI): $t_{\text{ret}} = 4.89$ min. 573 m/z $[\text{M}+2\text{H}]^{2+}$.

(1R)-3-(3,4-dimethoxyphenyl)-1-(3-(2-((2-(2-(4-((Z)-(2-(2,6-dioxopiperidin-3-yl)-1-oxoisindolin-4-yl)diazenyl)phenoxy)acetamido)ethyl)amino)-2-oxoethoxy)phenyl)propyl (2S)-1-(3,3-dimethyl-2-oxopentanoyl)piperidine-2-carboxylate (PHOTAC-II-5)



Into a round bottom flask with dry **2-(3-((R)-3-(3,4-dimethoxyphenyl)-1-((S)-1-(3,3-dimethyl-2-oxopentanoyl)piperidine-2-carbonyl)oxy)propyl)phenoxy)acetic acid** (8.0 mg, 0.014 mmol, 1 eq.) were added **S18** (15.9 mg, 0.027 mmol, 2 eq.) and HATU (9.4 mg, 0.025 mmol, 1.8 eq.) under nitrogen. The reaction was dissolved in dry DMF (1 mL). After addition of *i*-Pr₂NEt (12.4 mg, 0.096 mmol, 7 eq., 0.02 mL) the reaction was stirred for 15 h at room temperature. The mixture was then diluted with EtOAc (20 mL), separated against 5% LiCl (20 mL), extracted with EtOAc (2x 20 mL) and washed twice with 10% LiCl (2x 20 mL) and brine (2x 20 mL). The combined organic phases were dried over Na₂SO₄ and concentrated under reduced pressure. Purification of the resulting crude product by flash column chromatography (CH₂Cl₂/MeOH gradient, 0→20% MeOH) gave **PHOTAC-II-5** (9.1 mg, 0.009 mmol, 65%) as a yellow solid.

$R_f = 0.17$ [CH₂Cl₂:MeOH, 19:1].

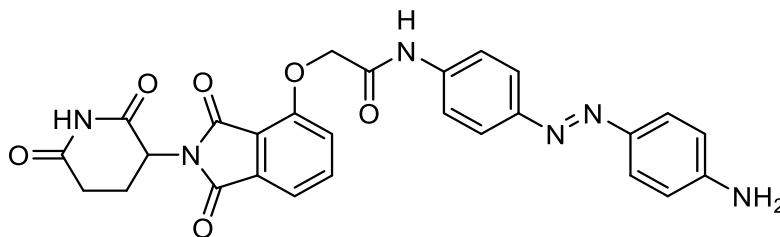
¹H NMR (600 MHz, DMSO-*d*₆) $\delta = 11.02$ (s, 1H), 8.30 (d, *J* = 5.0 Hz, 1H), 8.21 (d, *J* = 5.3 Hz, 1H), 8.17 (d, *J* = 7.8 Hz, 1H), 7.97 (d, *J* = 8.5 Hz, 2H), 7.89 (d, *J* = 7.4 Hz, 1H), 7.78 (t, *J* = 7.6 Hz, 1H), 7.29 (q, *J* = 7.9 Hz, 1H), 7.19 – 7.15 (m, 2H), 6.96 (dd, *J* = 4.3, 2.2 Hz, 2H), 6.92 – 6.88 (m, 1H), 6.82 (d, *J* = 8.1 Hz, 1H), 6.76 – 6.73 (m, 1H), 6.65 (d, *J* = 8.2 Hz, 1H), 5.71 – 5.65 (m, 1H), 5.16 (m, 2H), 4.78 (d, *J* = 19.0 Hz, 1H), 4.67 (d,

$J = 18.9$ Hz, 1H), 4.60 (s, 2H), 4.47 (s, 2H), 3.71 (s, 3H), 3.69 (s, 3H), 3.29 – 3.19 (m, 5H), 3.10 (t, $J = 12.3$ Hz, 1H), 2.94 (ddd, $J = 17.9, 13.4, 5.4$ Hz, 1H), 2.61 (d, $J = 18.2$ Hz, 1H), 2.57 – 2.45 (m, 4H), 2.23 (d, $J = 13.3$ Hz, 1H), 2.20 – 2.08 (m, 1H), 2.06 – 1.98 (m, 2H), 1.74 – 1.50 (m, 4H), 1.40 – 1.29 (m, 1H), 1.14 (s, 3H), 1.12 (s, 3H), 1.04 (d, $J = 6.4$ Hz, 1H), 0.78 (t, $J = 7.4$ Hz, 3H) ppm.

^{13}C NMR (150 MHz, DMSO) $\delta = 207.64, 172.91, 171.00, 169.32, 167.92, 167.46, 167.22, 166.82, 160.86, 157.72, 148.63, 147.06, 146.68, 146.58, 141.63, 134.28, 133.74, 133.13, 129.72, 129.57, 128.49, 124.99, 124.74, 119.91, 119.00, 115.41, 114.13, 112.98, 112.10, 111.87, 75.99, 67.10, 66.97, 55.47, 55.32, 51.66, 50.89, 48.24, 46.17, 43.84, 38.23, 38.16, 37.59, 31.93, 31.25, 30.62, 26.06, 24.36, 22.88, 22.60, 22.33, 20.77, 8.58$ ppm.

HRMS (APCI): calcd. for $\text{C}_{55}\text{H}_{64}\text{N}_7\text{O}_{13}^+$: 1030.4557 m/z $[\text{M}+\text{H}]^+$
 found: 1030.4565 m/z $[\text{M}+\text{H}]^+$.

LCMS (ESI): $t_{\text{ret}} = 4.70$ min. 1030 m/z $[\text{M}+\text{H}]^+$.

(E)-N-(4-((4-aminophenyl)diazenyl)phenyl)-2-((2-(2,6-dioxopiperidin-3-yl)-1,3-dioxoisindolin-4-yl)oxy)acetamide (S21)

To a solution of thalidomide-4-hydroxyacetate^[62] (16.7 mg, 50 μmol , 1.0 eq.) and 4,4'-diaminoazobenzene (32 mg, 150 μmol , 3.0 eq.) in THF (1.9 mL) was added HOBt (6.8 mg, 50 μmol , 1.0 eq.), PyBOP (52 mg, 100 μmol , 2.0 eq.) and triethylamine (35 μL , 26 mg, 250 μmol , 5.0 eq.) at room temperature. The reaction was stirred overnight, upon which the reaction solution was diluted with EtOAc, washed with water, sodium bicarbonate, and brine. The organic layer was dried over sodium sulfate and concentrated in vacuo. The crude product was purified by column chromatography over SiO_2 using 0% \rightarrow 10% MeOH in CH_2Cl_2 as the eluent to afford the desired product **S21** (21 mg, 40 μmol , 79%) as a highly insoluble brown solid.

R_f = 0.51 [CH_2Cl_2 :MeOH, 19:1].

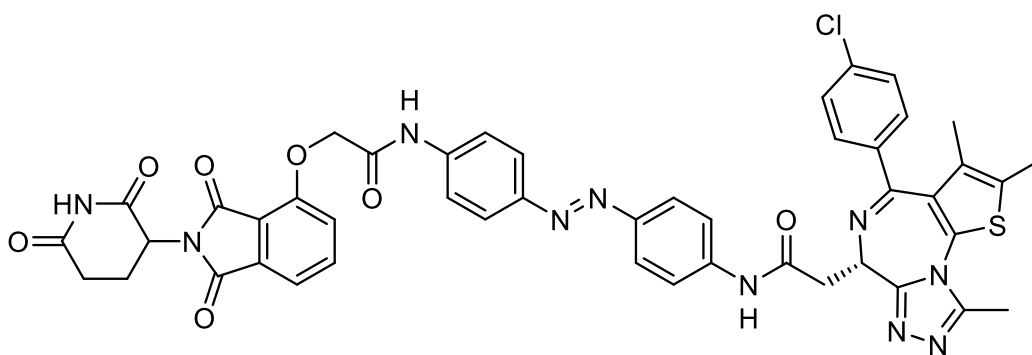
^1H NMR (400 MHz, $\text{DMSO-}d_6$) δ = 11.13 (s, 1H), 10.35 (s, 1H), 7.83 (t, J = 7.9 Hz, 1H), 7.76 (s, 4H), 7.63 (d, J = 8.4 Hz, 2H), 7.51 (t, J = 7.5 Hz, 2H), 6.66 (d, J = 8.5 Hz, 2H), 6.05 (s, 2H), 5.15 (dd, J = 12.9, 5.4 Hz, 1H), 5.05 (s, 2H), 2.99 – 2.80 (m, 1H), 2.59 (t, 2H), 2.07 (d, J = 13.0 Hz, 2H) ppm.

^{13}C NMR (100 MHz, DMSO) δ = 172.8, 169.9, 166.7, 165.9, 165.5, 155.2, 152.5, 148.5, 142.8, 139.4, 137.0, 133.1, 124.9, 122.6, 120.5, 119.6, 116.7, 116.1, 113.4, 67.6, 48.8, 31.0, 22.0 ppm.

HRMS (ESI): calcd. for $\text{C}_{27}\text{H}_{22}\text{N}_6\text{NaO}_6^+$: 549.1493 m/z [$\text{M}+\text{Na}$]⁺
 found: 549.1478 m/z [$\text{M}+\text{Na}$]⁺.

LCMS T_R = 3.521 min

2-((S)-4-(4-chlorophenyl)-2,3,9-trimethyl-6H-thieno[3,2-f][1,2,4]triazolo[4,3-a][1,4]diazepin-6-yl)-N-(4-((E)-4-(2-((2-(2,6-dioxopiperidin-3-yl)-1,3-dioxoisindolin-4-yl)oxy)acetamido)phenyl)diazenyl)phenyl)acetamide (PHOTAC-I-10)



To a solution of **S37** (5.0 mg, 9.5 μmol , 1.0 eq.) and (+)-JQ1 free acid (4.2 mg, 10.4 μmol , 1.1 eq.) DCE (1.0 mL) was added TBTU (4.0 mg, 12.3 μmol , 1.3 eq.) and DIPEA (2 μL , 14.2 μmol , 1.5 eq.) at room temperature. The reaction was allowed to stir at room temperature overnight. Upon completion, the reaction was diluted with EtOAc and washed with water, NaHCO_3 and brine. The organics were dried over sodium sulfate and concentrated in vacuo. The residue was purified by column chromatography over SiO_2 using 0% \rightarrow 10% MeOH in CH_2Cl_2 as the eluent to afford the desired product **PHOTAC-I-10** (3.0 mg, 3.3 μmol , 35%) as an orange amorphous solid.

$R_F = 0.32$ [CH_2Cl_2 :MeOH, 95:5].

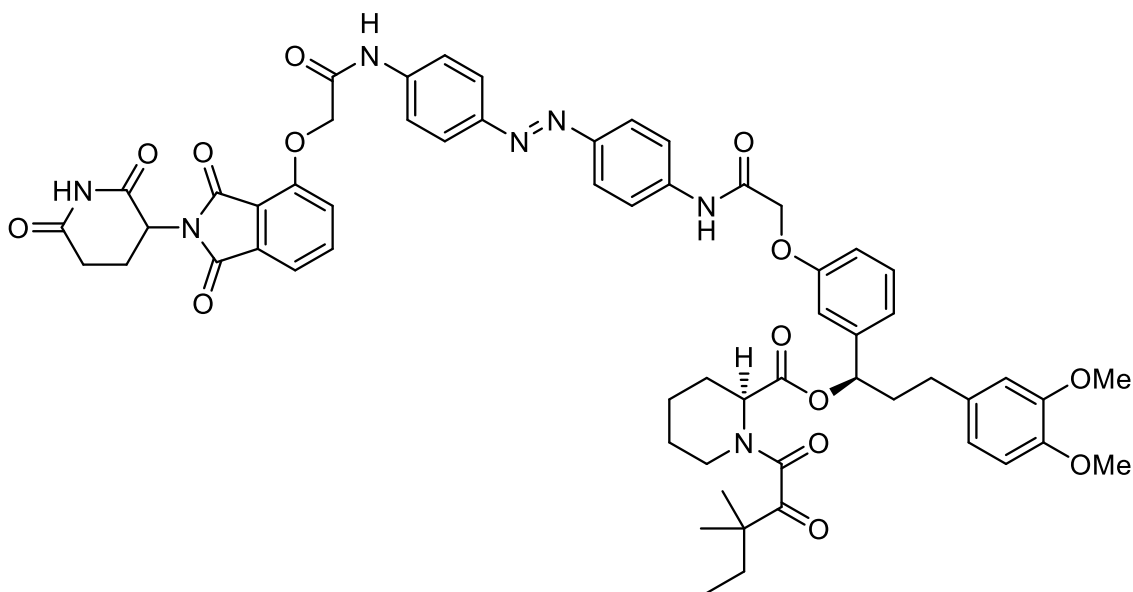
$^1\text{H NMR}$ (400 MHz, Chloroform-*d*) $\delta = 9.46$ (s, 1H), 9.36 (d, $J = 6.0$ Hz, 1H), 8.21 (d, $J = 10.7$ Hz, 1H), 7.82 (d, $J = 1.9$ Hz, 4H), 7.75 (dd, $J = 8.9, 2.3$ Hz, 2H), 7.69 (ddd, $J = 8.5, 7.5, 2.0$ Hz, 1H), 7.66 – 7.60 (m, 2H), 7.51 (dd, $J = 7.4, 3.5$ Hz, 1H), 7.35 (d, $J = 8.4$ Hz, 2H), 7.26 (d, $J = 8.3$ Hz, 2H), 7.17 (d, $J = 1.3$ Hz, 1H), 4.97 (ddd, $J = 12.3, 5.4, 2.0$ Hz, 1H), 4.71 (s, 2H), 4.63 (dd, $J = 8.7, 5.4$ Hz, 1H), 3.87 – 3.76 (m, 1H), 3.49 (dd, $J = 14.3, 5.3$ Hz, 1H), 2.92 – 2.85 (m, 1H), 2.85 – 2.78 (m, 1H), 2.78 – 2.71 (m, 1H), 2.63 (s, 3H), 2.35 (s, 3H), 2.17 – 2.08 (m, 1H), 1.63 (s, 3H) ppm.

¹³C NMR (100 MHz, CDCl₃) δ = 170.9, 170.9, 169.1, 168.1, 166.7, 166.5, 165.0, 164.4, 155.8, 154.4, 150.3, 149.6, 149.0, 140.9, 139.6, 137.4, 137.2, 136.5, 133.6, 132.2, 131.3, 131.1, 130.6, 130.1, 128.9, 124.0, 123.9, 120.1, 120.0, 119.9, 118.0, 68.5, 54.7, 49.6, 40.8, 31.6, 22.7, 14.6, 13.3, 12.0 ppm.

HRMS (ESI): calcd. for C₄₆H₃₇ClN₁₀O₇SNa⁺: 931.2148 *m/z* [M+Na]⁺
found: 931.2167 *m/z* [M+Na]⁺.

LCMS T_R = 4.642 min

(1R)-3-(3,4-dimethoxyphenyl)-1-(3-(2-((4-((E)-4-(2-((2-(2,6-dioxopiperidin-3-yl)-1,3-dioxoisindolin-4-yl)oxy)acetamido)phenyl)diazenyl)phenyl)amino)-2-oxoethoxy)phenyl)propyl (2S)-1-(3,3-dimethyl-2-oxopentanoyl)piperidine-2-carboxylate (PHOTAC-II-6)



To a solution of **S37** (6.0 mg, 11.4 μ mol, 1.0 eq.) and SLF free acid (7.3 mg, 12.5 μ mol, 1.1 eq.) in DMF (1.2 mL) was added HATU (5.6 mg, 14.8 μ mol, 1.3 eq.) and DIPEA (3 μ L, 17.1 μ mol, 1.5 eq.) at room temperature. The reaction was allowed to stir at room temperature overnight. Upon completion, the reaction was diluted with EtOAc and washed with water, NaHCO₃ and brine. The organics were dried over sodium sulfate

and concentrated to afford an orange amorphous solid. The residue was purified by column chromatography using 0% →50% acetone in CH₂Cl₂ to afford the desired product **PHOTAC-II-6** (8.1 mg, 7.4 μmol, 65%) as an orange amorphous solid.

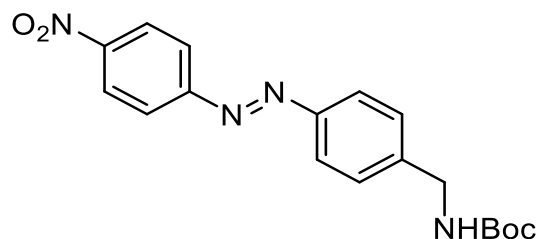
$R_f = 0.15$ [CH₂Cl₂:Acetone, 9:1].

¹H NMR (400 MHz, Chloroform-*d*) δ = 9.55 (s, 1H), 8.55 (d, $J = 22.1$ Hz, 1H), 8.24 (d, $J = 3.7$ Hz, 1H), 7.98 – 7.90 (m, 6H), 7.82 – 7.72 (m, 3H), 7.58 (d, $J = 7.3$ Hz, 1H), 7.34 (t, $J = 7.9$ Hz, 1H), 7.24 (s, 1H), 7.11 – 7.03 (m, 1H), 7.03 – 6.99 (m, 1H), 6.93 (dd, $J = 8.3, 2.4$ Hz, 1H), 6.82 – 6.73 (m, 1H), 6.67 (d, $J = 6.2$ Hz, 2H), 5.81 (dd, $J = 8.0, 5.3$ Hz, 1H), 5.34 (d, $J = 5.6$ Hz, 1H), 5.04 (dd, $J = 12.2, 5.3$ Hz, 1H), 4.79 (s, 2H), 4.65 (s, 2H), 3.85 (d, $J = 5.9$ Hz, 6H), 3.35 (s, 2H), 3.22 – 3.11 (m, 1H), 3.01 – 2.74 (m, 4H), 2.67 – 2.51 (m, 2H), 2.39 – 2.20 (m, 2H), 2.17 (d, $J = 2.1$ Hz, 4H), 2.07 (td, $J = 9.0, 7.2, 3.9$ Hz, 1H), 1.84 – 1.56 (m, 5H), 1.52 – 1.28 (m, 0H), 1.25 (s, 7H), 1.21 (d, $J = 1.8$ Hz, 5H), 0.87 (t, $J = 7.4$ Hz, 4H) ppm.

¹³C NMR (100 MHz, CDCl₃) δ = 208.1, 170.9, 169.9, 168.0, 167.4, 166.6, 166.5, 166.3, 165.0, 157.3, 154.4, 149.5, 149.5, 149.0, 147.5, 142.2, 139.9, 139.3, 137.4, 133.6, 133.4, 130.3, 124.1, 124.0, 120.7, 120.3, 120.3, 120.1, 120.1, 118.6, 118.0, 114.1, 113.8, 111.9, 111.9, 111.4, 76.5, 68.5, 67.7, 56.1, 56.0, 53.9, 53.6, 51.4, 49.6, 46.9, 44.3, 38.3, 32.6, 31.6, 31.3, 31.1, 29.4, 26.5, 25.1, 23.5, 23.4, 22.7, 21.2, 14.3, 8.9 ppm.

HRMS (ESI): calcd. for C₅₉H₆₂N₇O₁₄⁺: 1092.4355 m/z [M+H]⁺
 found: 1092.4334 m/z [M+H]⁺.

LCMS $T_R = 5.265$ min

***tert*-butyl (*E*)-(4-((4-nitrophenyl)diazenyl)benzyl)carbamate (**S22**)**

The following procedure was carried out in two steps:

Oxone Oxidation:

To a solution of 4-nitroaniline (566 mg, 4.1 mmol, 1.0 eq) in CH₂Cl₂ (14.6 mL) was added a solution of oxone (2.5 g, 4.1 mmol, 1.0 eq) in water (14.6 mL). The biphasic mixture was stirred vigorously under N₂ atmosphere. After 3 hours, phases were separated, and the aqueous phase was extracted with CH₂Cl₂. The organic phases were combined and then washed with 1 M HCl, sat. NaCl, dried over Na₂SO₄ and concentrated under reduced pressure to approximately 5 mL. The resulting yellow-black solution of nitrosobenzene in CH₂Cl₂ was carried on to the next step immediately.

Mills Reaction:

To the nitrosobenzene solution in CH₂Cl₂, prepared as described above, was added sequentially *tert*-butyl (4-aminobenzyl)carbamate^[63] (910 mg, 4.1 mmol, 1.0 eq) and glacial AcOH (1.2 mL, 20 mmol, 5.000 eq). The reaction mixture was allowed to stir for 15 hours under N₂ atmosphere, after which time the reaction mixture was found to be an orange-black suspension. EtOAc was added and the organic phase was washed with 1 M NaOH, sat. NaHCO₃, sat. NaCl. The organic phase was then dried over Na₂SO₄ and concentrated under reduced pressure. Crude material was purified by flash column chromatography over SiO₂ using a gradient from 1% → 5% → 10% EtOAc in Hexanes as the eluent, affording **S22** (900 mg, 2.5 mmol, 62%) as a crystalline red solid.

$R_f = 0.24$ [Hexanes:EtOAc, 85:15].

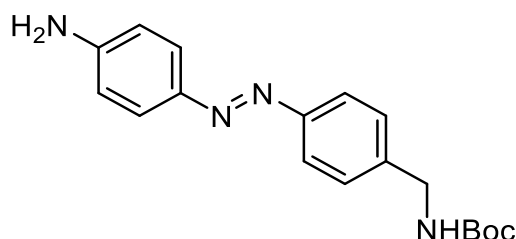
¹H NMR (400 MHz, Chloroform-*d*) δ = 8.37 (d, *J* = 8.8 Hz, 2H), 8.02 (d, *J* = 8.9 Hz, 2H), 7.94 (d, *J* = 8.2 Hz, 2H), 7.46 (d, *J* = 8.2 Hz, 2H), 4.98 (s, 1H), 4.42 (d, *J* = 5.3 Hz, 2H), 1.48 (s, 2H) ppm.

¹³C NMR (101 MHz, CDCl₃) δ = 156.0, 155.8, 151.8, 148.8, 144.0, 128.2, 124.9, 123.9, 123.6, 80.0, 44.5, 28.5 ppm.

HRMS (APCI): calcd. for C₁₃H₁₃N₄O₂⁺: 257.1033 *m/z* [M-Boc+H]⁺
found: 257.1041 *m/z* [M-Boc+H]⁺.

LCMS *T_R* = 4.736 min

***tert*-butyl (*E*)-(4-((4-aminophenyl)diazenyl)benzyl)carbamate (**S23**)**



To a solution of **S22** (100.0 mg, 270 μmol, 1.0 eq.) in dioxane (4.0 mL) and water (0.4 mL) in a pressure tube was added Na₂S·9H₂O (202 mg, 842 μmol, 3.0 eq.). The reaction was sealed and heated to 85 °C. After 1 hour, the reaction was diluted with water and the aqueous layer was extracted 3 times with EtOAc. The organics were combined, washed with brine, dried over sodium sulfate, and concentrated in vacuo to afford an orange-red solid. The reaction was loaded onto isolute and purified by column chromatography over SiO₂ using a stepped gradient from 9:1 →1:1 Hexanes/EtOAc as the eluent to afford **S23** (70.0 mg, 215 μmol, 76%) as a pale orange solid.

R_f = 0.14 [Hexanes:EtOAc, 8:2].

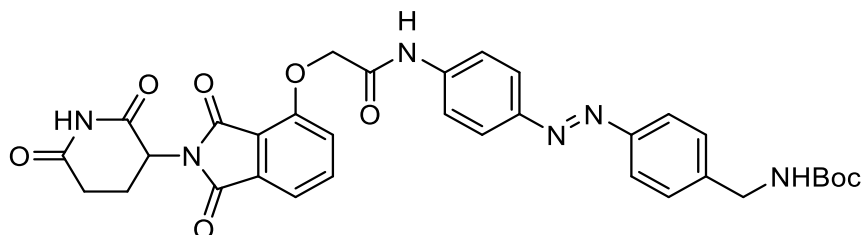
¹H NMR (400 MHz, Chloroform-*d*) δ = 7.80 (dd, *J* = 8.6, 3.0 Hz, 4H), 7.37 (d, *J* = 8.1 Hz, 2H), 6.72 (d, *J* = 8.7 Hz, 2H), 4.96 (s, 1H), 4.36 (d, *J* = 6.0 Hz, 2H), 4.21 – 3.92 (m, 2H), 1.47 (s, 10H).

¹³C NMR (101 MHz, CDCl₃) δ = 156.0, 152.3, 149.8, 145.6, 140.8, 128.1, 125.2, 122.7, 114.7, 79.7, 44.5, 28.5.

HRMS (APCI): calcd. for C₁₈H₂₃N₄O₄⁺: 327.1816 *m/z* [M+H]⁺
found: 327.1804 *m/z* [M+H]⁺.

LCMS $T_R = 4.032$ min

tert-butyl (E)-(4-((4-(2-((2-(2,6-dioxopiperidin-3-yl)-1,3-dioxoisindolin-4-yl)oxy)acetamido)phenyl)diazenyl)benzyl)carbamate (**S24**)



Thalidomide-4-hydroxyacetate^[62] (20.0 mg, 60.2 μ mol, 1.0 eq) and **S23** (29.5 mg, 90.3 μ mol, 1.5 eq) were dissolved in DMF (600 μ L) followed by the addition of HATU (25.2 mg, 66.2 μ mol, 1.1 eq) and DIPEA (21 μ L, 120 μ mol, 2.0 eq) at rt. The reaction was allowed to stir at rt overnight. The reaction was diluted with water, extracted 3 times with EtOAc, organics were combined, washed with bicarb and brine and dried over sodium sulfate. Concentration of organics and purification by column chromatography over SiO₂ using 8:1.5:0.5 DCM/EtOAc/MeOH as the mobile phase afforded **S24** (37 mg, 57.8 μ mol, 96%) as an orange amorphous solid.

$R_f = 0.06$ [Hexanes:EtOAc, 1:1].

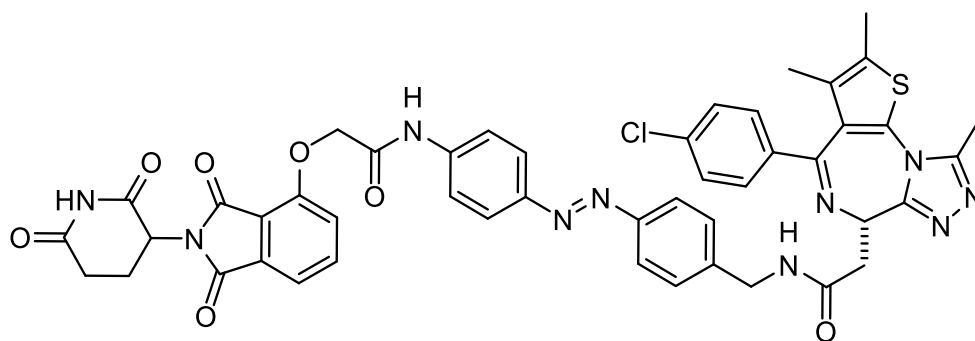
¹H NMR (400 MHz, Acetone-*d*₆) $\delta = 10.03$ (s, 1H), 9.84 (s, 1H), 8.05 – 7.93 (m, 4H), 7.93 – 7.82 (m, 3H), 7.62 (d, $J = 8.4$ Hz, 1H), 7.58 (d, $J = 7.3$ Hz, 1H), 7.51 (d, $J = 8.1$ Hz, 2H), 5.25 (dd, $J = 12.5, 5.4$ Hz, 1H), 5.00 (s, 2H), 4.39 (d, $J = 6.3$ Hz, 2H), 3.09 – 2.91 (m, 1H), 2.92 – 2.78 (m, 3H), 2.39 – 2.20 (m, 1H), 1.46 (s, 9H) ppm.

¹³C NMR (101 MHz, Acetone) $\delta = 172.7, 170.1, 167.7, 167.6, 166.8, 157.0, 155.8, 152.6, 149.8, 144.7, 142.0, 138.1, 134.4, 128.9, 124.7, 123.6, 122.1, 120.5, 119.3, 117.9, 79.1, 69.7, 50.5, 44.6, 32.1, 28.7, 23.4$ ppm.

HRMS (ESI): calcd. for C₃₃H₃₂N₆NaO₈⁺: 663.2174 m/z [M+Na]⁺
found: 663.2178 m/z [M+Na]⁺.

LCMS $T_R = 4.505$ min

2-((S)-4-(4-chlorophenyl)-2,3,9-trimethyl-6H-thieno[3,2-f][1,2,4]triazolo[4,3-a][1,4]diazepin-6-yl)-N-(4-((E)-4-(2-((2-(2,6-dioxopiperidin-3-yl)-1,3-dioxoisindolin-4-yl)oxy)acetamido)phenyl)diazenyl)benzyl)acetamide (PHOTAC-I-11)



S24 (10.0 mg, 15.6 μmol , 1.0 eq) was dissolved in formic acid (1.6 mL), immediately turning the solution to a deep red color, and allowed to stir overnight at rt. After this period, the solvent was evaporated in vacuo to afford an orange amorphous solid. To this was added (+)-JQ1 free acid (6.6 mg, 16.4 μmol , 1.05 eq) in DMF (0.66 mL), HATU (8.9 mg, 23.4 μmol , 1.5 eq), followed by DIPEA (5 μL , 31.2 μmol , 2.0 eq) and the reaction was allowed to stir overnight at room temperature. The reaction was diluted with water, extracted 3 times with EtOAc, organics were combined, washed with bicarb and brine and dried over sodium sulfate. The organic layer was concentrated in vacuo and the residue was purified by semi-preparative reverse phase HPLC (50% \rightarrow 70% MeCN gradient + 0.01% formic acid) affording **PHOTAC-I-11** (6.0 mg, 6.5 μmol , 42%) as a yellow orange amorphous solid.

$R_f = 0.29$ [CH_2Cl_2 :MeOH, 9:1].

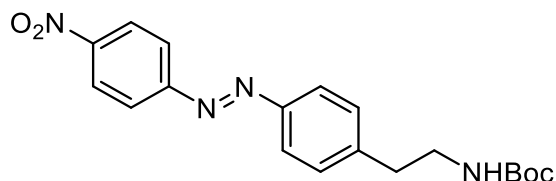
$^1\text{H NMR}$ (400 MHz, Chloroform-*d*) $\delta = 9.58$ (d, $J = 8.8$ Hz, 1H), 8.29 (d, $J = 18.0$ Hz, 1H), 7.96 (qd, $J = 9.0, 2.8$ Hz, 4H), 7.89 – 7.76 (m, 3H), 7.61 (dd, $J = 7.3, 1.4$ Hz, 1H), 7.48 (d, $J = 8.2$ Hz, 2H), 7.36 – 7.29 (m, 3H), 7.26 (d, $J = 8.8$ Hz, 1H), 5.06 (dd, $J = 12.2, 5.2$ Hz, 1H), 4.82 (d, $J = 4.0$ Hz, 2H), 4.79 – 4.65 (m, 2H), 4.46 (dd, $J = 15.3, 5.3$ Hz, 1H), 3.67 – 3.49 (m, 2H), 3.03 – 2.76 (m, 3H), 2.70 (s, 3H), 2.42 (s, 3H), 2.30 – 2.16 (m, 1H), 1.68 (s, 3H) ppm.

¹³C NMR (101 MHz, CDCl₃) δ = 170.9, 170.9, 170.7, 168.0, 166.6, 166.5, 165.1, 164.3, 155.7, 154.4, 152.1, 150.1, 149.5, 141.5, 140.0, 137.4, 137.1, 136.5, 133.6, 132.3, 131.1, 130.6, 130.0, 128.9, 128.5, 124.2, 123.2, 120.0, 120.0, 118.0, 68.5, 54.6, 49.6, 43.4, 41.2, 39.4, 31.6, 22.8, 14.6, 13.3, 12.0 ppm.

HRMS (APCI): calcd. for C₄₇H₄₃ClN₁₁O₇S⁺: 940.2751 *m/z* [M+NH₄]⁺

found: 940.2736 *m/z* [M+NH₄]⁺.

LCMS T_R = 4.422 min

***tert*-butyl (*E*)-(4-((4-nitrophenyl)diazenyl)phenethyl)carbamate (**S25**)**

The following procedure was carried out in two steps:

Oxone Oxidation:

To a solution of 4-nitroaniline (462 mg, 3.3 mmol, 1.0 eq.) in CH₂Cl₂ (12.0 mL) was added a solution of oxone (2.1 g, 3.3 mmol, 1.0 eq.) in water (12.0 mL). The biphasic mixture was stirred vigorously under N₂ atmosphere. After 3 hours, phases were separated, and the aqueous phase was extracted with CH₂Cl₂. The organic phases were combined and then washed with 1 M HCl, sat. NaCl, dried over Na₂SO₄ and concentrated under reduced pressure to approximately 5 mL. The resulting yellow-black solution of nitrosobenzene in CH₂Cl₂ was carried on to the next step immediately.

Mills Reaction:

To the nitrosobenzene solution in DCM, prepared as described above, was added sequentially *tert*-butyl (4-aminophenethyl)carbamate^[64] (791.0 mg, 3.3 mmol, 1.0 eq.) and glacial AcOH (0.96 mL, 17 mmol, 5.0 eq.). The reaction mixture was allowed to stir for 15 hours under N₂ atmosphere, after which time the reaction mixture was found to be an orange-black suspension. EtOAc was added and the organic phase was washed with 3x 1-M-NaOH, 2x sat. NaHCO₃, 2x sat. NaCl. The organic phase was then dried over Na₂SO₄ and concentrated under reduced pressure. Crude material was purified by flash column chromatography over SiO₂ using a gradient from 1% → 5% → 10% EtOAc in Hexanes as the eluent, affording **S25** (724.0 mg, 1.955 mmol, 58%) as a crystalline red solid.

R_f = 0.23 [Hexanes:EtOAc, 9:1].

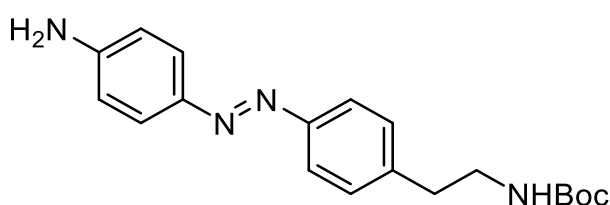
¹H NMR (400 MHz, Chloroform-*d*) δ = 8.36 (dd, *J* = 8.8, 1.6 Hz, 2H), 8.00 (dd, *J* = 8.7, 1.4 Hz, 2H), 7.91 (d, *J* = 8.1 Hz, 2H), 7.37 (d, *J* = 8.2 Hz, 2H), 4.62 (s, 1H), 3.43 (d, *J* = 5.1 Hz, 2H), 2.90 (t, *J* = 7.0 Hz, 2H), 1.44 (s, 9H) ppm.

¹³C NMR (101 MHz, CDCl₃) δ = 155.9, 155.9, 151.3, 148.7, 144.3, 129.9, 124.8, 123.8, 123.5, 79.6, 41.7, 36.4, 28.5 ppm.

HRMS (APCI): calcd. for C₁₄H₁₅N₄O₂⁺: 271.1195 *m/z* [M-Boc+H]⁺
found: 271.1190 *m/z* [M-Boc+H]⁺.

LCMS T_R = 4.858 min

***tert*-butyl (*E*)-(4-((4-aminophenyl)diazenyl)phenethyl)carbamate (**S26**)**



To a solution of **S25** (100.0 mg, 270 μ mol, 1.0 eq.) in dioxane (4.0 mL) and water (0.4 mL) in a pressure tube was added Na₂S·9H₂O (195 mg, 810 μ mol, 3.0 eq.). The reaction was sealed and heated to 85 °C. After 1 hour, the reaction was diluted with water and the aqueous layer was extracted 3 times with EtOAc. The organics were combined, washed with brine, dried over sodium sulfate, and concentrated in vacuo to afford an orange-red solid. The reaction was loaded onto isolute and purified by column chromatography over SiO₂ using a stepped gradient from 9:1 → 1:1 Hexanes/EtOAc as the eluent to afford **S26** (77.0 mg, 226 μ mol, 84%) as a pale orange solid.

R_f = 0.64 [Hexanes:EtOAc, 6:4].

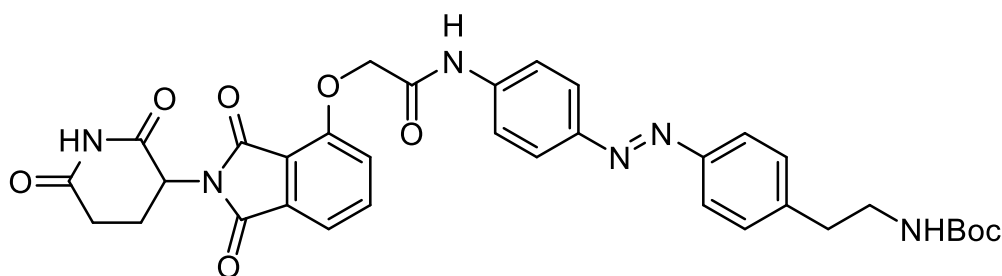
¹H NMR (400 MHz, Chloroform-*d*) δ = 7.80 (d, J = 4.5 Hz, 2H), 7.78 (d, J = 3.9 Hz, 2H), 7.29 (d, J = 8.1 Hz, 2H), 6.73 (d, J = 8.8 Hz, 2H), 4.58 (s, 1H), 4.06 (s, 2H), 3.41 (d, J = 6.7 Hz, 1H), 2.86 (t, J = 7.0 Hz, 2H), 1.44 (s, 9H) ppm.

¹³C NMR (101 MHz, CDCl₃) δ = 156.0, 151.8, 149.7, 145.7, 141.1, 129.5, 125.2, 122.7, 114.7, 79.4, 41.8, 36.1, 28.5 ppm.

HRMS (APCI): calcd. for C₁₉H₂₅N₄O₂⁺: 341.1972 *m/z* [M+H]⁺
found: 341.1973 *m/z* [M+H]⁺.

LCMS T_R = 4.141 min

tert-butyl (E)-4-((4-(2-((2-(2,6-dioxopiperidin-3-yl)-1,3-dioxoisindolin-4-yl)oxy)acetamido)phenyl)diazenyl)phenethyl)carbamate (S27)



Thalidomide-4-hydroxyacetate^[62] (20.0 mg, 60.2 μmol , 1.0 eq.) and **S26** (20.0 mg, 60.2 μmol , 1.0 eq.) were dissolved in DMF (600 μL) followed by the addition of TBTU (25 mg, 66.2 μmol , 1.10 eq.) and DIPEA (21 μL , 120.4 μmol , 2.0 eq.) at rt. The reaction was allowed to stir at room temperature overnight upon which the reaction was diluted with EtOAc, the organics were washed three times with equal portions of water, saturated sodium bicarbonate, and brine. The organic layer was dried over sodium sulfate and concentrated. The crude product was purified by column chromatography over SiO_2 using a gradient of 9:1 hexanes/EtOAc to 100% EtOAc as the eluent to afford product **S27** (38.0 mg, 58.0 μmol , 96%) as an orange amorphous solid.

$R_f = 0.29$ [Hexanes:EtOAc, 6:4].

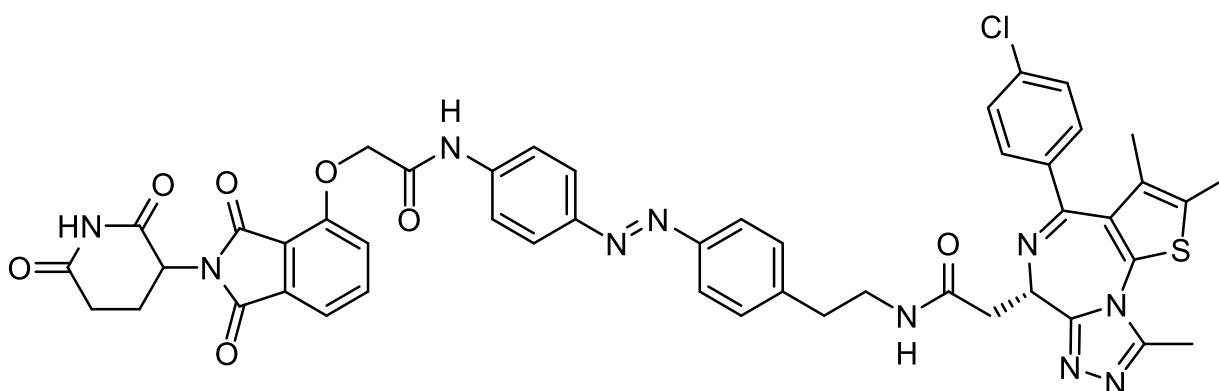
$^1\text{H NMR}$ (400 MHz, Chloroform-*d*) $\delta = 9.54$ (s, 1H), 8.41 (d, $J = 13.7$ Hz, 1H), 7.92 (t, $J = 2.8$ Hz, 4H), 7.83 (dd, $J = 8.3, 1.7$ Hz, 2H), 7.80 – 7.70 (m, 1H), 7.63 – 7.51 (m, 1H), 7.32 (d, $J = 8.0$ Hz, 2H), 7.23 (d, $J = 8.4$ Hz, 1H), 5.04 (dd, $J = 12.3, 5.3$ Hz, 1H), 4.78 (d, $J = 1.9$ Hz, 2H), 4.60 (s, 1H), 3.41 (t, $J = 6.7$ Hz, 2H), 2.97 – 2.78 (m, 6H), 2.25 – 2.15 (m, 1H), 1.44 (s, 9H) ppm.

$^{13}\text{C NMR}$ (101 MHz, CDCl_3) $\delta = 171.0, 168.1, 166.6, 166.5, 165.1, 156.0, 154.4, 151.5, 149.5, 142.4, 139.9, 137.4, 133.6, 129.7, 124.1, 123.1, 120.0$ (overlap of two signals), 118.6, 118.0, 79.5, 68.5, 49.6, 41.8, 36.2, 31.6, 28.5, 22.7 ppm.

HRMS (ESI): calcd. for $\text{C}_{34}\text{H}_{35}\text{N}_6\text{O}_8^+$: 655.2511 m/z $[\text{M}+\text{H}]^+$
found: 655.2530 m/z $[\text{M}+\text{H}]^+$.

LCMS $T_R = 4.599$ min

2-((S)-4-(4-chlorophenyl)-2,3,9-trimethyl-6H-thieno[3,2-f][1,2,4]triazolo[4,3-a][1,4]diazepin-6-yl)-N-(4-((E)-4-(2-((2-(2,6-dioxopiperidin-3-yl)-1,3-dioxoisindolin-4-yl)oxy)acetamido)phenyl)diazenyl)phenethyl)acetamide (PHOTAC-I-12)



S27 (5.0 mg, 9.0 μmol , 1.0 eq) was dissolved in formic acid (1.5 mL) and allowed to stir overnight. After this period the reaction was concentrated and azeotroped to afford an orange residue. This crude material and (+)-JQ1-free acid (4.0 mg, 9.9 μmol , 1.1 eq) were dissolved in DMF (400 μL) followed by the addition of HATU (4.5 mg, 11.7 μmol , 1.3 eq) and DIPEA (2.0 μL , 13.5 μmol , 1.5 eq) at rt. The reaction was allowed to stir at rt overnight. The reaction was diluted with water and extracted 3 times with EtOAc. The organic layers were combined, washed with saturated sodium bicarbonate and brine and dried over sodium sulfate. Concentration of organics and purification by column chromatography over SiO_2 using 8:1.5:0.5 DCM/EtOAc/MeOH as the mobile phase afforded **PHOTAC-I-12** (7.9 mg, 8.4 μmol , 94%) as an orange amorphous solid. $R_f = 0.17$ [CH_2Cl_2 :EtOAc:MeOH, 8:1.5:0.5].

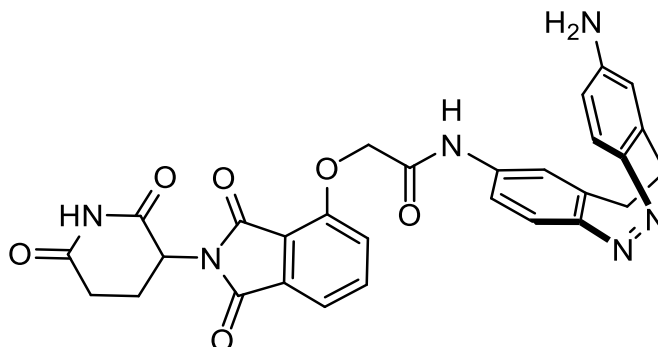
$^1\text{H NMR}$ (400 MHz, Chloroform-*d*) $\delta = 9.57$ (d, $J = 2.4$ Hz, 1H), 8.13 (d, $J = 2.8$ Hz, 1H), 8.03 – 7.89 (m, 4H), 7.78 (dd, $J = 8.0, 4.0$ Hz, 3H), 7.61 (d, $J = 2.0$ Hz, 1H), 7.40 – 7.26 (m, 7H), 6.77 (s, 1H), 5.05 (dd, $J = 11.9, 5.0$ Hz, 1H), 4.81 (s, 2H), 4.56 (t, $J = 6.9$ Hz, 1H), 3.76 – 3.45 (m, 3H), 3.31 (dd, $J = 14.2, 5.8$ Hz, 1H), 3.02 – 2.76 (m, 5H), 2.66 (s, 3H), 2.37 (s, 3H), 2.27 – 2.18 (m, 1H), 1.66 (s, 3H) ppm.

$^{13}\text{C NMR}$ (101 MHz, Chloroform-*d*) $\delta = 170.8, 170.5, 167.9, 166.6, 166.5, 165.1, 164.2, 155.6, 154.4, 151.4, 150.0, 149.5, 142.3, 139.9, 137.4, 137.1, 136.4, 133.6, 132.1,$

131.2, 131.1, 130.6, 130.0, 129.6, 128.9, 124.1, 123.0, 120.1 (overlap 2 peaks), 118.7, 118.1, 68.5, 54.6, 49.6, 40.5, 39.6, 35.6, 31.6, 22.8, 14.5, 13.2, 12.0 ppm.

HRMS (ESI): calcd. $C_{48}H_{42}ClN_{10}O_7S^+$: 937.2642 m/z $[M+H]^+$
found: 937.2675 m/z $[M+H]^+$.

LCMS $T_R = 4.599$ min

(Z)-N-(9-amino-11,12-dihydrodibenzo[c,g][1,2]diazocin-2-yl)-2-((2-(2,6-dioxopiperidin-3-yl)-1,3-dioxoisindolin-4-yl)oxy)acetamide (S28)

Thalidomide-4-hydroxyacetate (20.0 mg, 60 μmol , 1.0 eq.) and (Z)-11,12-dihydrodibenzo[c,g][1,2]diazocine-2,9-diamine^[65] (21.5 mg, 90 μmol , 1.5 eq.) were dissolved in DMF (0.6 mL) followed by the addition of TBTU (21.3 mg, 66 μmol , 1.1 eq.) and DIPEA (21 μL , 120 μmol , 2.0 eq.) at rt. The reaction was allowed to stir at rt overnight. The reaction was diluted with CH_2Cl_2 and successively washed with water, saturated sodium bicarbonate, and brine. The organic layer was dried over sodium sulfate and concentrated. The residue was purified by column chromatography over silica using a 1% to 3% MeOH in CH_2Cl_2 as the eluent to afford **S28** (17.0 mg, 31 μmol , 51%) as an amorphous yellow solid. This product was contaminated with an unknown impurity and used in the next step.

$R_f = 0.08$ [CH_2Cl_2 :MeOH, 95:5].

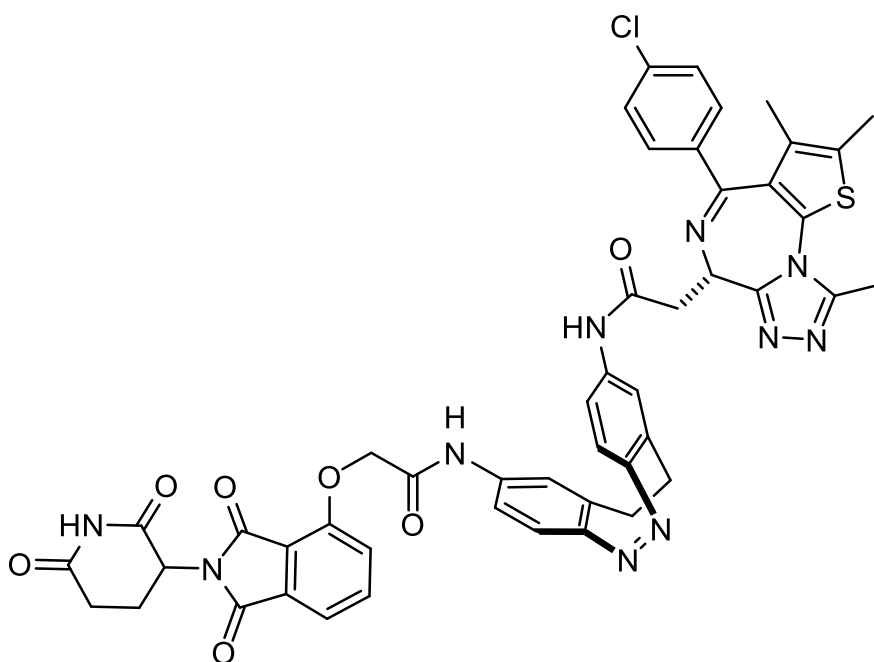
$^1\text{H NMR}$ (400 MHz, $\text{DMSO}-d_6$) δ 11.12 (s, 1H), 10.10 (s, 1H), 7.80 (ddd, $J = 8.5, 7.3, 4.2$ Hz, 1H), 7.50 (d, $J = 7.2$ Hz, 1H), 7.47 – 7.38 (m, 2H), 7.38 – 7.30 (m, 1H), 6.81 (dd, $J = 30.2, 8.4$ Hz, 1H), 6.63 – 6.51 (m, 1H), 6.36 (dd, $J = 8.4, 2.3$ Hz, 1H), 6.20 (d, $J = 2.3$ Hz, 1H), 5.13 (q, $J = 6.5, 5.5$ Hz, 2H), 4.96 (d, $J = 3.2$ Hz, 2H), 2.90 (s, 2H), 2.76 – 2.55 (m, 6H), 2.08 – 1.92 (m, 1H) ppm.

$^{13}\text{C NMR}$ (101 MHz, DMSO) $\delta = 172.8, 169.9, 166.7, 165.6, 165.5, 162.3, 155.2, 151.4, 147.9, 145.4, 136.9, 136.7, 133.0, 129.5, 128.5, 121.0, 120.5, 119.5, 117.4, 116.7, 116.0, 113.6, 111.9, 67.4, 48.8, 31.6, 31.2, 30.9, 22.0$ ppm.

HRMS (APCI): calcd. $\text{C}_{29}\text{H}_{25}\text{N}_6\text{O}_6^+$: 553.1836 m/z $[\text{M}+\text{H}]^+$
found: 553.1828 m/z $[\text{M}+\text{H}]^+$.

LCMS $T_R = 2.931$ min

2-((S)-4-(4-chlorophenyl)-2,3,9-trimethyl-6H-thieno[3,2-f][1,2,4]triazolo[4,3-a][1,4]diazepin-6-yl)-N-((Z)-9-(2-((2-(2,6-dioxopiperidin-3-yl)-1,3-dioxoisindolin-4-yl)oxy)acetamido)-11,12-dihydrodibenzo[c,g][1,2]diazocin-2-yl)acetamide (PHOTAC-I-13)



To a solution of **S28** (5.0 mg, 9.0 μmol , 1.0 eq.) and (+)-JQ1 free acid (4.0 mg, 10 μmol , 1.1 eq.) in DCE (1.8 mL) was added TBTU (3.8 mg, 11.8 μmol , 1.3 eq.) followed by DIPEA (1.8 mg, 2.0 μL , 13.6 μmol , 1.5 eq.) at room temperature. The reaction was allowed to stir overnight upon which the reaction was diluted with EtOAc, washed with equal portions of water, saturated sodium bicarbonate, and brine. The organic layer was dried over sodium sulfate and concentrated under reduced pressure. The residue was purified by column chromatography over SiO_2 using a gradient of 0% \rightarrow 10% MeOH in CH_2Cl_2 as the eluent to afford **PHOTAC-I-13** (5.9 mg, 5.9 μmol , 65%) as an amorphous yellow solid.

$R_f = 0.39$ [CH_2Cl_2 : MeOH, 95:5].

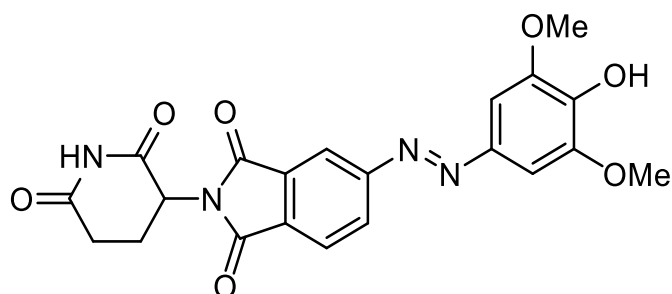
$^1\text{H NMR}$ (400 MHz, Chloroform-*d*) $\delta = 9.23$ (d, $J = 122.5$ Hz, 2H), 7.84 – 7.74 (m, 1H), 7.75 – 7.63 (m, 1H), 7.60 (dd, $J = 7.4, 3.4$ Hz, 1H), 7.42 (dd, $J = 8.6, 2.6$ Hz, 2H), 7.38 – 7.32 (m, 2H), 7.25 (dd, $J = 8.5, 6.2$ Hz, 1H), 6.87 (d, $J = 8.6$ Hz, 1H), 6.81 (d, $J = 8.5$ Hz, 1H), 5.12 – 4.93 (m, 1H), 4.73 (d, $J = 8.6$ Hz, 2H), 4.61 (dd, $J = 9.2, 4.7$ Hz, 1H),

3.79 (ddd, $J = 22.4, 14.1, 9.1$ Hz, 1H), 3.44 (ddd, $J = 19.4, 14.0, 4.8$ Hz, 1H), 3.04 – 2.75 (m, 7H), 2.68 (d, $J = 4.3$ Hz, 3H), 2.64 (d, $J = 0.8$ Hz, 5H), 2.42 (d, $J = 2.4$ Hz, 3H), 2.31 – 2.15 (m, 1H), 1.72 – 1.60 (m, 3H) ppm.

^{13}C NMR (101 MHz, Chloroform- d) $\delta = 168.5, 168.3, 166.5, 164.8, 164.7, 155.4, 154.4, 152.1, 150.1, 137.2, 136.2, 133.5, 131.3, 131.0, 130.5, 129.9, 129.9, 129.2, 128.8, 120.5, 120.2, 118.7, 118.0, 117.8, 68.8, 68.5, 54.6, 54.4, 49.4, 41.0, 31.5, 31.5, 22.6, 14.4, 14.4, 13.1, 11.7$ ppm.

HRMS (APCI): calcd. $\text{C}_{48}\text{H}_{40}\text{ClN}_{10}\text{O}_7\text{S}^+$: 935.2491 m/z [$\text{M}+\text{H}$] $^+$

found: 935.2478 m/z [$\text{M}+\text{H}$] $^+$.

(E)-2-(2,6-dioxopiperidin-3-yl)-5-((4-hydroxy-3,5-dimethoxyphenyl)diazenyl)isoindoline-1,3-dione (S29)

To a solution of 5-aminothalidomide (200 mg, 0.73 μmol , 1.0 eq) and NaNO_2 (424 μl , 848 μmol , 1.16 equiv) in acetone/water (4:1, 8 mL) was added 4 equiv. of HCl (4.0 M in 1,4-dioxane, 732 μL , 2.9 mmol, 4.0 equiv) at 0 °C. After stirring for 1 h, the solution was added in a dropwise fashion to a mixture of 2,6-dimethoxyphenol, (135 mg, 0.88 mmol, 1.2 equiv), NaHCO_3 (1.5 g, 18.1 mmol, 24.7 equiv), Na_2CO_3 (3.7 g, 34.5 mmol, 47.2 equiv) in water/MeOH (5:2, 28 mL) at 0 °C and allowed to stir for an additional hour. After this time period, the reaction was quenched with sat. NH_4Cl and extracted with EtOAc. The organic layers were combined and washed with brine and concentrated under reduced pressure. The residue was purified by column chromatography over SiO_2 using 4:6 Hexanes/EtOAc as the eluent to afford **S29** (49.0 mg, 112 μmol , 15%) as a red solid.

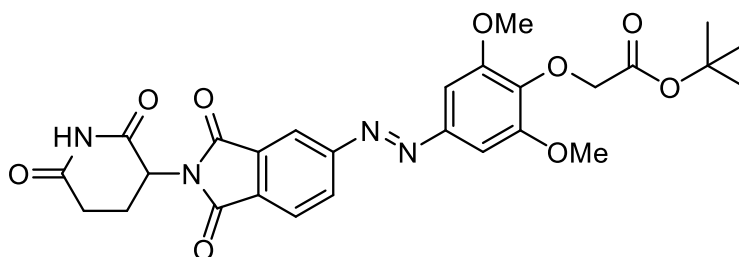
$R_f = 0.23$ [Hexanes:EtOAc, 4:6].

$^1\text{H NMR}$ (400 MHz, Acetone- d_6) $\delta = 9.96$ (s, 1H), 8.31 (dd, $J = 5.3, 2.6$ Hz, 1H), 8.21 (s, 1H), 8.07 (d, $J = 7.9$ Hz, 1H), 7.43 (s, 2H), 5.21 (dd, $J = 12.6, 5.5$ Hz, 1H), 3.98 (s, 6H), 2.99 (m, 1H), 2.88 – 2.77 (m, 2H), 2.32 – 2.25 (m, 1H).

$^{13}\text{C NMR}$ (101 MHz, Acetone) $\delta = 172.6, 169.9, 167.5, 167.5, 157.6, 149.1, 145.8, 142.0, 134.2, 133.0, 130.6, 125.4, 116.0, 102.6, 56.7, 50.5, 32.0, 23.2$.

HRMS (APCI): calcd. for $\text{C}_{21}\text{H}_{19}\text{N}_4\text{O}_7^+$: 439.1248 m/z $[\text{M}+\text{H}]^+$
found: 439.1251 m/z $[\text{M}+\text{H}]^+$.

LCMS $T_R = 3.180$ min

tert-butyl (E)-2-(4-((2-(2,6-dioxopiperidin-3-yl)-1,3-dioxisoindolin-5-yl)diazenyl)-2,6-dimethoxyphenoxy)acetate (S30**)**

S29 (35.0 mg, 78.8 μmol , 1.0 eq) was dissolved in DMF (0.8 mL) at room temperature. To this was added K_2CO_3 (16.6 mg, 0.12 mmol, 1.5 equiv), immediately turning the solution a blue-black color, followed by the addition of *tert*-butyl bromoacetate (16.4 mg, 83.8 μmol , 1.05 eq). The reaction was allowed to stir at room temperature for 2 hours upon which the reaction was quenched with saturated aqueous NH_4Cl . The aqueous layer was extracted three times with EtOAc, the organics were combined, washed with brine, dried over sodium sulfate, and concentrated. The residue was purified by column chromatography over SiO_2 using a gradient of 0 \rightarrow 30% EtOAc in DCM to afford **S30** (17.0 mg, 30.8 μmol , 39%) as an orange film.

$R_f = 0.47$ [CH_2Cl_2 :EtOAc, 7:3].

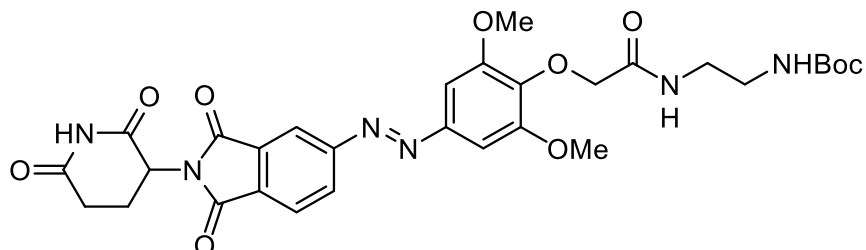
$^1\text{H NMR}$ (400 MHz, Chloroform-*d*) $\delta = 8.37$ (d, $J = 1.6$ Hz, 1H), 8.29 (dd, $J = 7.9, 1.7$ Hz, 1H), 8.06 (d, $J = 8.0$ Hz, 1H), 8.00 (s, 1H), 7.34 (s, 2H), 5.05 (dd, $J = 12.4, 5.4$ Hz, 1H), 4.74 (s, 2H), 3.99 (s, 6H), 3.02 – 2.70 (m, 4H), 2.31 – 2.14 (m, 1H), 1.51 (s, 9H) ppm.

$^{13}\text{C NMR}$ (101 MHz, CDCl_3) $\delta = 170.7, 168.3, 167.8, 166.8, 166.7, 156.9, 152.8, 147.9, 140.6, 133.2, 132.3, 130.1, 129.8, 125.2, 125.0, 119.4, 117.0, 101.5, 81.9, 70.0, 56.5, 49.7, 31.6, 29.9, 28.3, 22.8$ ppm.

HRMS (APCI): calcd. for $\text{C}_{23}\text{H}_{21}\text{N}_4\text{O}_9^+$: 497.1303 m/z [M-tBu+H] $^+$
found: 497.1292 m/z [M-tBu+H] $^+$.

LCMS $T_R = 3.383$ min

tert-butyl (E)-2-(2-(4-((2-(2,6-dioxopiperidin-3-yl)-1,3-dioxoisindolin-5-yl)diazenyl)-2,6-dimethoxyphenoxy)acetamido)ethyl)carbamate (**S31**)



S30 (8.0 mg, 14.5 μmol , 1.0 eq.) was dissolved in formic acid (1.4 mL), immediately turning the solution to a deep red color, and allowed to stir overnight at rt. After this period, the solvent was evaporated in vacuo to afford an orange-red amorphous solid. To this was added *N*-Boc-ethylene diamine (2.8 mg, 17.4 μmol , 1.2 eq.) in DMF (1.4 mL), HATU (8.3 mg, 21.7 μmol , 1.5 eq.), followed by DIPEA (5 μL , 3.7 mg, 28.7 μmol , 2.0 eq.) and the reaction was allowed to stir overnight at room temperature. The reaction was diluted with water, extracted 3 times with EtOAc, organics were combined, washed with bicarb and brine and dried over sodium sulfate. The organic layer was concentrated in vacuo and the residue was purified column chromatography over SiO_2 using 0% \rightarrow 3% MeOH in CH_2Cl_2 as the eluent to afford **S31** (5.7 mg, 8.9 μmol , 62%) as an orange film.

$R_f = 0.09$ [CH_2Cl_2 :MeOH, 97:3].

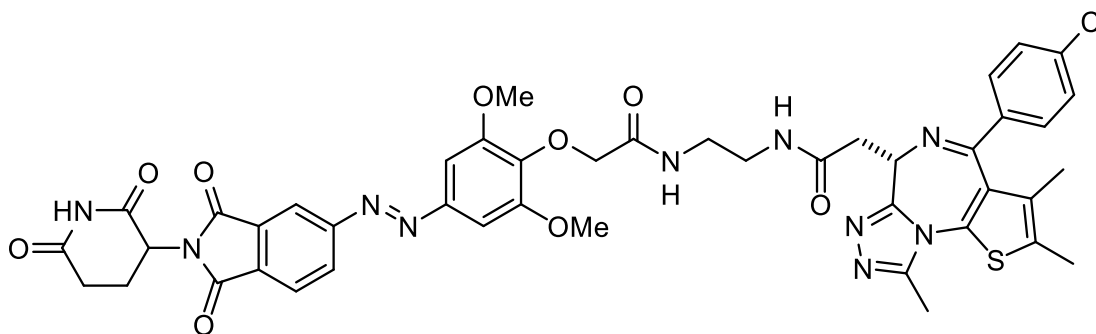
$^1\text{H NMR}$ (400 MHz, Chloroform-*d*) $\delta = 8.35$ (d, $J = 1.5$ Hz, 1H), 8.28 (dd, $J = 7.9, 1.7$ Hz, 1H), 8.17 (s, 1H), 8.04 (d, $J = 7.9$ Hz, 1H), 7.91 – 7.83 (m, 1H), 7.33 f(s, 2H), 5.03 (dd, $J = 12.2, 5.5$ Hz, 1H), 4.90 (s, 1H), 4.63 (s, 2H), 4.01 (s, 6H), 3.49 (d, $J = 6.0$ Hz, 2H), 3.38 – 3.24 (m, 2H), 3.02 – 2.63 (m, 3H), 2.28 – 2.09 (m, 1H), 1.43 (s, 9H) ppm.

$^{13}\text{C NMR}$ (101 MHz, CDCl_3) $\delta = 170.8, 170.3, 167.9, 166.7, 166.7, 156.7, 156.2, 152.8, 148.6, 140.4, 133.2, 132.6, 130.2, 125.0, 116.9, 101.3, 79.7, 72.8, 56.5, 49.7, 40.9, 39.2, 31.6, 28.5, 22.8$ ppm.

HRMS (APCI): calcd. for $\text{C}_{25}\text{H}_{27}\text{N}_6\text{O}_8^+$: 539.1885 m/z [M-Boc+H] $^+$
found: 539.1873 m/z [M-Boc+H] $^+$.

LCMS $T_R = 3.953$ min

2-((S)-4-(4-chlorophenyl)-2,3,9-trimethyl-6H-thieno[3,2-f][1,2,4]triazolo[4,3-a][1,4]diazepin-6-yl)-N-(2-(2-(4-((E)-(2-(2,6-dioxopiperidin-3-yl)-1,3-dioxoisindolin-5-yl)diazenyl)-2,6-dimethoxyphenoxy)acetamido)ethyl)acetamide (PHOTAC-I-9)



S31 (5.7 mg, 8.9 μmol , 1.0 equiv) was dissolved in formic acid and allowed to stir at room temperature for 30 min. After this period, the reaction was concentrated *in vacuo* and azeotroped. The crude residue was used immediately without further purification. This crude material and (+)-JQ1-free acid (3.9 mg, 9.8 μmol , 1.1 eq) were dissolved in DMF (400 μL) followed by the addition HATU (3.7 mg, 9.8 μmol , 1.1 eq) and DIPEA (2.3 μL , 17.9 μmol , 2.0 eq) at rt. The reaction was allowed to stir at rt overnight. The reaction was diluted with water and extracted 3 times with EtOAc. The organic layers were combined, washed with saturated sodium bicarbonate and brine and dried over sodium sulfate. Concentration of organics and purification by column chromatography over SiO_2 using 0% \rightarrow 10% MeOH in DCM as the mobile phase afforded **PHOTAC-I-9** (4.1 mg, 4.4 μmol , 50%) as an orange amorphous solid.

$R_f = 0.23$ [CH_2Cl_2 :MeOH, 9:1].

$^1\text{H NMR}$ (400 MHz, Chloroform-*d*) $\delta = 8.32$ (d, $J = 1.5$ Hz, 1H), 8.26 (dd, $J = 7.9, 1.6$ Hz, 1H), 8.16 (s, 1H), 8.02 (d, $J = 7.9$ Hz, 1H), 7.90 (d, $J = 6.4$ Hz, 1H), 7.42 (d, $J = 8.2$ Hz, 2H), 7.33 (d, $J = 8.6$ Hz, 3H), 7.31 (s, 2H), 5.03 (dd, $J = 12.3, 5.4$ Hz, 1H), 4.69 (t, $J = 6.8$ Hz, 1H), 4.62 (s, 2H), 3.99 (s, 6H), 3.65 – 3.35 (m, 6H), 3.02 – 2.71 (m, 3H), 2.69 (s, 3H), 2.40 (s, 3H), 2.34 (t, $J = 7.5$ Hz, 2H), 1.67 (s, 3H), 1.67 – 1.55 (m, 1H) ppm.

$^{13}\text{C NMR}$ (101 MHz, CDCl_3) $\delta = 176.9, 171.0, 170.8, 170.5, 167.9, 166.8, 166.7, 164.7, 156.7, 155.4, 152.8, 150.3, 148.6, 140.5, 137.5, 136.0, 135.9, 133.1, 132.5, 131.3,$

130.2, 130.2, 129.0, 129.0, 125.0, 117.0, 101.4, 72.8, 56.6, 53.6, 49.7, 40.0, 38.8, 33.7,
32.1, 31.6, 24.9, 22.8, 22.8, 14.6, 13.3, 11.9 ppm.

HRMS (APCI): calcd. for $C_{44}H_{42}ClN_{10}O_9S^+$: 921.2545 m/z $[M + H]^+$
found: 921.2519 m/z $[M + H]^+$.

LCMS $T_R = 4.089$ min

Detailed Methods and Recommendations for the use of PHOTACs

Cell culture

A widely used cell line for PROTACs and PHOTACs is the human acute lymphoblastic leukemia RS4;11 cell line (ATCC® CRL-1873TM). Cells are maintained in phenol red free RPMI1640 medium (Gibco 11835030) with 10% fetal bovine serum (FBS, Gibco) and 1% penicillin/ streptomycin (PS) in a humidified incubator at 37 °C with 5% CO₂ in air. Cell count is maintained between 10⁵ and 10⁶ cells per milliliter.

Reagents

PHOTACs are stored in the dark and prepared as previously described from unpurified commercial reagents. DMSO, MeOH, PBS (pH 7.4) are used as purchased.

Light source

Pulsed irradiation of cells over long periods of time can be performed with a cell disco^[66], a plate of 5 mm LEDs controlled by an Arduino UNO or similar cheap computer. (Fig. S2.11)

For the experiments described here, an Arduino UNO is connected to a 5 V power source and used to control a 5 V relay module. The relay connects the 24 V (2 A) power supply with the LEDs to switch them on and off (Fig. S2.11A). A previously created program^[66] can be used to control the Arduino and a pulsed irradiation of 100 ms every 10 s is chosen (1% duty cycle) to provide constant irradiation, while keeping overall light exposure low and to avoiding excessive heating.

5 mm LED boards with 24 LEDs were used for the pulsed irradiation of 6 well plates (Fig. S2.11B).^[66] These consist of 4 parallel rows each made with slots for 6 LEDs each and a resistor (47 Ω, 1 W). The LEDs are aligned to a 24-well plate to evenly distribute them across the plate. Rubber feet ensure proper spacing between the LEDs and the well plate. LED plates are connected to the Arduino UNO using standard copper wires and can be placed in a humidified incubator.

5 mm LEDs were obtained from Roithner Lasertechnik (370 nm (XSL-370-5E), 390 nm (VL390-5-15), 410 nm (VL410-5-15), 430 nm (VL430-5-15), 450 nm (ELD-450-525), 465 nm (RLS-B465), 477 nm (RLS-5B475-5), 490 nm (LED490-03), 505 nm (B5-433-B505), 525 nm (B5-433-B525), 545 nm (LED545-04), 572 nm (B5-433-20) and 590 nm (CY5111A-WY)). Generally, LEDs with a small bandwidth are recommended to obtain the best isomer ratios and a wide cone angle will ensure equal light distribution across the well plate. Recommended power output for the LEDs is 10-20 mW.

Other light sources can be used to irradiate PHOTACs such as lasers, monochromators or high-power LEDs. For the use of broad, polychromatic light sources a narrow band-pass filter set is recommended for best results.

Further a strong red LED light source with $\lambda > 650$ nm is recommended to prepare samples under “Dark”/red light conditions. Black, non-airtight plastic boxes (20x15x15 cm) are used to shield the controls from light.

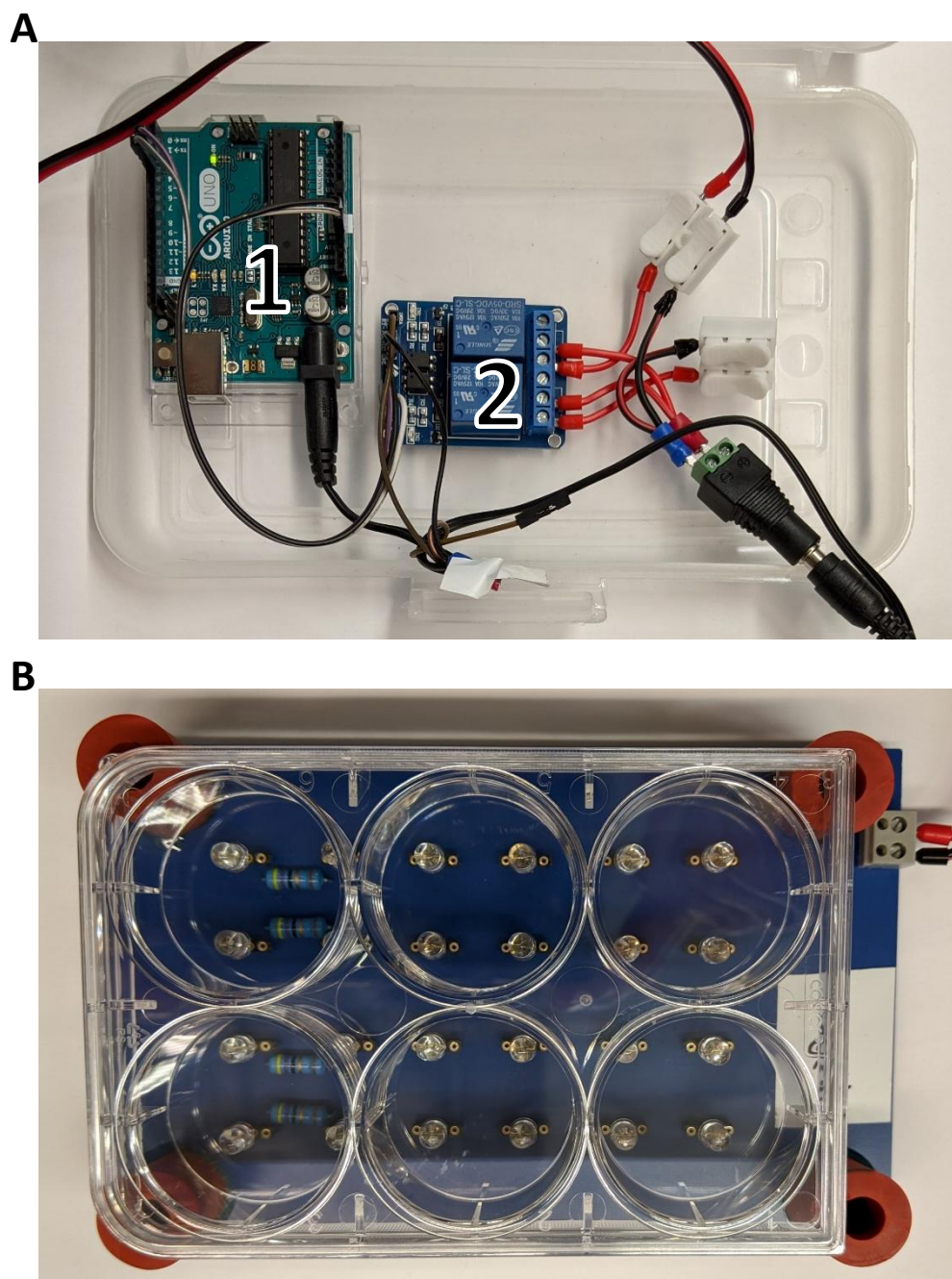


Figure S2.11. Cell disco. A) Programmable Arduino Uno -1- and relay switch -2- setup to control the light source. B) 24-LED plate with 6-well plate used for cell-culture irradiation.

Immunoblotting

1. Lysis buffer is prepared fresh by mixing 1.948 mL of RIPA lysis buffer (stored at 4°C) with 40 µL of a 50x protease inhibitor cocktail stock (cOmplete™ Protease Inhibitor Cocktail, Roche, 1 tablet dissolved in 1 mL RIPA, stored at -20°C) and 12 µL phosphatase inhibitor cocktail (Millipore Sigma).
2. 4x Laemmli sample buffer can be prepared by adding 100 µL of 2-mercaptoethanol per 900 µL 4x Laemmli sample buffer (BIO-RAD) and is stored at -20°C.
3. SDS Page running buffer is prepared by mixing 50 mL Invitrogen™ Novex™ NuPAGE™ MES SDS Running Buffer (20x) and 950 mL purified water.
4. Membrane transfer buffer (TAE buffer containing 20%v/v MeOH) is prepared by adding 1.4 L purified water to 200 mL of a 10x TAE buffer stock, followed by 400 mL MeOH.
5. Washing buffer (TBST) is prepared by dissolving tris base (24 g) and NaCl (175 g) in 20 L purified water, adjusting the pH to 7.4 using HCl and adding 20 mL of Tween 20. After stirring for 30 min the buffer can be used.
6. Blocking buffer is prepared by suspending 25 g of blotting grade milk powder in 500 mL washing buffer (TBST) and can be stored at 4°C.
7. Protein concentration determination assay kit such as Pierce™ BCA Protein Assay Kit.
8. HRP substrate such as SuperSignal™ West Pico PLUS Chemiluminescent Substrate.
9. PVDF membrane.
10. Precast SDS page gels (such as NuPAGE™ 4-12% Bis-Tris Midi Protein Gels, 26-well).

Preparation of PHOTAC stock solutions

PHOTACs should be stored in the dark and are dissolved in DMSO under red LED light ($\lambda > 650$ nm) conditions to create 10 mM stock solutions. The stock solutions should always be stored in the dark to avoid isomerization by ambient light. Storage in the dark will also promote the thermal relaxation of the active cis- to the inactive trans-PHOTACs.

PHOTAC treatment

1. Prior to treatment, place the black plastic boxes and LED plates in the incubator. Add $2 \cdot 10^6$ RS4;11 cells in 2 mL of phenol red free RPMI1640 medium to each of the 6-well plates and allow to equilibrate in the incubator.

2. Dilute PHOTACs to prepare 2x stocks. Perform these steps 2 and 3 under red or low light conditions for best results. For example, dissolve 10 μ L PHOTAC-I-3-stock (10 mM) in 90 μ L DMSO, add 4.9 mL warm phenol red free RPMI1640 medium and mix thoroughly. Tenfold serial dilutions are prepared by mixing 500 μ L of the previous dilution with 4.5 mL phenol red free RPMI1640 medium containing 2% DMSO. For most PHOTACs we recommend an ideal working concentration between 100 nM and 1 μ M, whereas the hook-effect can be observed at concentrations $\geq 10 \mu$ M. (See Note 1, 3)

3. Add 2 mL of the diluted PHOTACs to the wells containing RS4;11 cells and place in the previously prepared boxes. Optionally, cells can be irradiated with the chosen wavelength, i.e. 390 nm, for 1 min to ensure a rapid isomerization right at the start. Cells are then irradiated using the cell disco to ensure a constant isomer ratio throughout the experiment (100 ms pulses every 10 s). For short experiments, a single strong irradiation event can be sufficient to activate most PHOTACs, given their thermal stability. Strong degradation of target proteins BRD2-4 for PHOTAC-I-3 or FKBP12 for PHOTAC-II-5 is observed within 4 hours. (See Notes 2-4)

4. After incubation, collect cells under red light. Carefully take up the medium using serological pipettes and wash the wells two times to resuspend all cells and centrifuge (200 g, 5 min) at 4 °C. Aspirate the supernatant, wash the pellets with ice cold PBS (1 mL) and spin down (400 g, 5 min) at 4 °C. Optionally, cells pellets can be frozen for storage at -80 °C at this point.

5. Lyse cells on ice for 20 min by addition of 37 μ L RIPA lysis buffer containing protease and phosphatase inhibitor cocktails and suspend the cell pellet by repeated pipetting.

6. Spin down lysates at 15000 g for 10 min at 4 °C.

7. Carefully collect the supernatant using thin pipet tips for gel loading to avoid taking up the precipitate.
8. Determine the protein concentration in a 96 well plate, in triplicates (2 μ L supernatant each), using the BCA method, i.e. using a commercial kit such as the Pierce™ BCA Protein Assay Kit.
9. Add 10 μ L 4x Laemmli buffer containing DTT and heat the samples at 95 °C for 10 min. Optionally, samples can be sonicated at this point to avoid DNA contamination.
10. Put a precast gel into the gel cassette, add MES-SDS running buffer and wash all pockets with running buffer.
11. Load 25 μ g protein on a precast gel (Tris-glycine, Invitrogen), and run for 10 min at 100 V, followed by 70-120 min at 130 V (longer runtimes allow for better separation of high molecular weight bands, but low molecular weight proteins will be lost).
12. Prepare transfer buffer and fill the transfer chamber, activate a PVDF membrane in methanol for 5 minutes and assemble the transfer stack.
13. Perform membrane transfer at 30 V for 120 min. Optionally, membrane transfer can be performed in a cold room
14. Wash membranes once briefly in purified water, stain using Ponceau S while shaking for 1 minute, wash two to three times with purified water to remove excess Ponceau S and place the membrane between 2 layers of plastic wrap. Cut membranes into small strip and block in blocking buffer for 30 min.
15. Wash membranes three times with washing buffer and incubate with primary antibodies over night at 4 °C on a shaker, diluted as per the supplier's instructions in TBST with 3%BSA and 0.05% NaN₃.
16. Subsequently, wash membranes twice quickly with washing buffer, followed by washing twice for 10 min to remove primary antibodies.

17. Add secondary HRP-conjugated antibodies, diluted in blocking buffer (1:5000), and incubate for 30 min at RT.

18. Wash membranes twice quickly with washing buffer, followed by washing twice for 10 min then transfer to PBS until imaged.

19. Remove membrane strips from PBS, carefully remove excess PBS on a piece of paper towel, place on a flat surface and add the premixed HRP substrate solution.

20. Image chemiluminescence in incremental steps, using a GE ImageQuant LAS 4000 series or equivalent imaging system.

Notes and Recommendations

1. Working with photochromic compounds: It is important to always consider their photophysical behavior. Azobenzenes effectively absorb light in the visible region of the electromagnetic spectrum and hence isomerize upon exposure to ambient light conditions. The isomer ratio is strongly dependent on the light source as well as the particular spectral overlap and quantum efficiencies of isomerization of the *E*- and *Z*-isomers. For the PHOTACs presented here, irradiation with wavelengths above 600 nm is possible without influencing the isomer ratio. Hence, working under red light/ or orthogonal imaging using red fluorophores (excitation above 600 nm) is recommended for best results. Keep in mind that some light-sources allow for second order diffraction and thus do not emit monochromatic light. Furthermore, we recommend recording emission spectra or obtaining detailed technical information on the light-sources from the supplier to ensure reproducibility.

PHOTACs thermally relax back to their inactive isomer and accidental exposure could be reverted by storage in the dark. Note that this works best at elevated temperatures (i.e. 37 °C).

Activation of PHOTACs under saturating irradiation conditions will establish an equilibrium state between the isomers depending on the spectrum of the used light source. While 390 nm is the ideal wavelength for *E*-to-*Z* isomerization for the PHOTACs discussed herein, wavelength between 370 and 430 nm can activate them well and commercial “black lights” or common 405 nm excitation on microscopes can be used to activate PHOTACs.

For most experiments saturating irradiation conditions (100 ms pulses every 10 s) have been used. Less irradiation can be sufficient to activate PHOTACs and the irradiation protocol can be adjusted freely. It is possible to work without a cell disco and just manually irradiate PHOTACs, for example for approx. 30 s every hour, and still achieve good results, thanks to their thermal bistability.

While the LED boards usually work without defects over many experiments, it is recommended to check the LEDs for proper function before and after the experiments, as one malfunctioning LED will disrupt the whole row.

Given that phenol red is an azobenzene itself, it strongly absorbs in the visible spectrum and can even act as a photosensitizer. We recommend always using phenol red free media.

2. Choice of cell line: Cereblon expression is crucial for the function of the PHOTACs discussed here and knockdown/knockout of CRBN can be used as a negative control. However, the efficacy of PROTACs and PHOTAC can vary across different cell lines. While RS4;11 cells show fast degradation using PHOTACs, adherent cell lines such as MDA-MB-231, MDA-MB-468 or HEK293T show slower response to PHOTACs and require prolonged incubation times. If prolonged irradiation is not desirable, pre-incubation with PHOTACs is possible to reduce irradiation times.

3. Dosing and inactivation of PHOTACs: The commonly observed saturation of POI and the E3 ligase by PROTACs, termed hook-effect, is also observed for PHOTACs. Therefore, high concentration of PHOTACs will inhibit protein degradation and we recommend using working concentrations below 3 μM . We recommend using 2 μM to 100 nM PHOTAC, although ideal concentrations can differ due to target protein expression, resynthesis rates and cell permeability. Further it must be considered that PHOTACs in their inactive form can still act as inhibitors of their target proteins, while being unable to form a productive ternary complex that leads to protein ubiquitylation. This means that the inactive PHOTAC can act as a competitive binder, displacing the active PHOTAC.

After activating PHOTACs with light, such as 390 nm irradiation, inactivation can either occur thermally, which is a slow process on the scale of hours for the current generation of PHOTACs or by irradiation with a second wavelength in the range of 500 to 560 nm (green light). Irradiation with green light induces the *Z*-to-*E* isomerization and shifts the equilibrium towards the inactive form. This *Z*-to-*E* isomerization is not complete and a small fraction of active PHOTAC remains.

The wavelength dependent *E/Z* ratio of azobenzenes at saturating irradiation conditions, known as the photostationary state (PSS), can also be used to dose the amount of active PHOTAC, and thus the amount of target protein, by using different colors of light. Starting with green light (e. g. 550 nm) only small amounts of PHOTAC are activated, but by moving towards blue to violet light (460 to 390 nm) larger fractions of PHOTAC are activated and, consequently, more protein is degraded.

4. Time course and other experiments: Such experiments are useful to observe changes in protein levels over time. To observe the light-induced protein degradation by PHOTACs over time, we recommend preparing an excess of 2x stock of PHOTAC

in phenol red free medium for all timepoints at the start of the assay. Keep the stock in the dark and add it to the cell containing well plate at your chosen timepoints with a joint endpoint of the assay. Thereby cells are irradiated for the same duration and samples are worked up under the same conditions.

The cell disco can further be used to create more complex irradiation patterns and consequently protein level patterns. One can also place a second LED-plate on top of the well plate and connect it to a second program^[66] to modulate PHOTAC activity with different wavelengths. When irradiating from the top, refrain from labelling the well plate as a layer of black marker can absorb a significant amount of light.

For color dosing we recommend starting at long wavelength (600 nm) and slowly moving towards shorter wavelengths.

References

- [1] J. R. Skaar, J. K. Pagan, M. Pagano, *Nat. Rev. Drug Discov.* **2014**, *13*, 889–903.
- [2] A. C. Lai, C. M. Crews, *Nat. Rev. Drug Discov.* **2017**, *16*, 101–114.
- [3] G. M. Burslem, C. M. Crews, *Chem. Rev.* **2017**, *117*, 11269–11301.
- [4] K. M. Sakamoto, K. B. Kim, A. Kumagai, F. Mercurio, C. M. Crews, R. J. Deshaies, *Proc. Natl. Acad. Sci.* **2001**, *98*, 8554–8559.
- [5] D. P. Bondeson, A. Mares, I. E. D. Smith, E. Ko, S. Campos, A. H. Miah, K. E. Mulholland, N. Routly, D. L. Buckley, J. L. Gustafson, N. Zinn, P. Grandi, S. Shimamura, G. Bergamini, M. Faelth-Savitski, M. Bantscheff, C. Cox, D. A. Gordon, R. R. Willard, J. J. Flanagan, L. N. Casillas, B. J. Votta, W. den Besten, K. Famm, L. Kruidenier, P. S. Carter, J. D. Harling, I. Churcher, C. M. Crews, *Nat. Chem. Biol.* **2015**, *11*, 611–617.
- [6] M. Zengerle, K.-H. Chan, A. Ciulli, *ACS Chem. Biol.* **2015**, *10*, 1770–1777.
- [7] G. E. Winter, D. L. Buckley, J. Paulk, J. M. Roberts, A. Souza, S. Dhe-Paganon, J. E. Bradner, *Science* **2015**, *348*, 1376–1381.
- [8] J. Lu, Y. Qian, M. Altieri, H. Dong, J. Wang, K. Raina, J. Hines, J. D. Winkler, A. P. Crew, K. Coleman, C. M. Crews, *Chem. Biol.* **2015**, *22*, 755–763.
- [9] K. M. Sakamoto, K. B. Kim, R. Verma, A. Ransick, B. Stein, C. M. Crews, R. J. Deshaies, *Mol. Cell. Proteomics* **2003**, *2*, 1350–1358.
- [10] A. R. Schneekloth, M. Pucheault, H. S. Tae, C. M. Crews, *Bioorg. Med. Chem. Lett.* **2008**, *18*, 5904–5908.
- [11] X. Han, C. Wang, C. Qin, W. Xiang, E. Fernandez-Salas, C.-Y. Yang, M. Wang, L. Zhao, T. Xu, K. Chinnaswamy, J. Delproposito, J. Stuckey, S. Wang, *J. Med. Chem.* **2019**, *62*, 941–964.
- [12] J. Hu, B. Hu, M. Wang, F. Xu, B. Miao, C.-Y. Yang, M. Wang, Z. Liu, D. F. Hayes, K. Chinnaswamy, J. Delproposito, J. Stuckey, S. Wang, *J. Med. Chem.* **2019**, *62*, 1420–1442.
- [13] C.-Y. Yang, C. Qin, L. Bai, S. Wang, *Drug Discov. Today Technol.* **2019**, *31*, 43–51.
- [14] B. Nabet, J. M. Roberts, D. L. Buckley, J. Paulk, S. Dastjerdi, A. Yang, A. L. Leggett, M. A. Erb, M. A. Lawlor, A. Souza, T. G. Scott, S. Vittori, J. A. Perry, J. Qi, G. E. Winter, K.-K. Wong, N. S. Gray, J. E. Bradner, *Nat. Chem. Biol.* **2018**, *14*, 431.
- [15] A. Bojja, I. A. Klein, B. R. Sabari, A. Dall'Agnese, E. L. Coffey, A. V. Zamudio, C. H. Li, K. Shrinivas, J. C. Manteiga, N. M. Hannett, B. J. Abraham, L. K. Afeyan, Y. E. Guo, J. K. Rimel, C. B. Fant, J. Schuijers, T. I. Lee, D. J. Taatjes, R. A. Young, *Cell* **2018**, *175*, 1842–1855.e16.
- [16] C. M. Olson, B. Jiang, M. A. Erb, Y. Liang, Z. M. Doctor, Z. Zhang, T. Zhang, N. Kwiatkowski, M. Boukhali, J. L. Green, W. Haas, T. Nomanbhoy, E. S. Fischer, R. A. Young, J. E. Bradner, G. E. Winter, N. S. Gray, *Nat. Chem. Biol.* **2018**, *14*, 163–170.
- [17] A. C. Lai, M. Toure, D. Hellerschmied, J. Salami, S. Jaime-Figueroa, E. Ko, J. Hines, C. M. Crews, *Angew. Chem. Int. Ed.* **2016**, *55*, 807–810.
- [18] G. M. Burslem, B. E. Smith, A. C. Lai, S. Jaime-Figueroa, D. C. McQuaid, D. P. Bondeson, M. Toure, H. Dong, Y. Qian, J. Wang, A. P. Crew, J. Hines, C. M. Crews, *Cell Chem. Biol.* **2018**, *25*, 67–77.e3.

- [19] A. Zorba, C. Nguyen, Y. Xu, J. Starr, K. Borzilleri, J. Smith, H. Zhu, K. A. Farley, W. Ding, J. Schiemer, X. Feng, J. S. Chang, D. P. Uccello, J. A. Young, C. N. Garcia-Irrizary, L. Czabaniuk, B. Schuff, R. Oliver, J. Montgomery, M. M. Hayward, J. Coe, J. Chen, M. Niosi, S. Luthra, J. C. Shah, A. El-Kattan, X. Qiu, G. M. West, M. C. Noe, V. Shanmugasundaram, A. M. Gilbert, M. F. Brown, M. F. Calabrese, *Proc. Natl. Acad. Sci.* **2018**, *115*, E7285–E7292.
- [20] A. D. Buhimschi, H. A. Armstrong, M. Toure, S. Jaime-Figueroa, T. L. Chen, A. M. Lehman, J. A. Woyach, A. J. Johnson, J. C. Byrd, C. M. Crews, *Biochemistry* **2018**, *57*, 3564–3575.
- [21] D. Houzelstein, S. L. Bullock, D. E. Lynch, E. F. Grigorieva, V. A. Wilson, R. S. P. Beddington, *Mol. Cell. Biol.* **2002**, *22*, 3794–3802.
- [22] E. Shang, X. Wang, D. Wen, D. A. Greenberg, D. J. Wolgemuth, *Dev. Dyn.* **2009**, *238*, 908–917.
- [23] J. M. Silva, E. Silva, R. L. Reis, *J. Controlled Release* **2019**, *298*, 154–176.
- [24] L. Fenno, O. Yizhar, K. Deisseroth, *Annu. Rev. Neurosci.* **2011**, *34*, 389–412.
- [25] M. M. Lerch, M. J. Hansen, G. M. van Dam, W. Szymanski, B. L. Feringa, *Angew. Chem. Int. Ed.* **2016**, *55*, 10978–10999.
- [26] K. Hüll, J. Morstein, D. Trauner, *Chem. Rev.* **2018**, *118*, 10710–10747.
- [27] R. Siewertsen, H. Neumann, B. Buchheim-Stehn, R. Herges, C. Näther, F. Renth, F. Temps, *J. Am. Chem. Soc.* **2009**, *131*, 15594–15595.
- [28] J. B. Trads, K. Hüll, B. S. Matsuura, L. Laprell, T. Fehrentz, N. Görldt, K. A. Kozek, C. D. Weaver, N. Klöcker, D. M. Barber, D. Trauner, *Angew. Chem. Int. Ed. n.d.*, *0*, DOI 10.1002/anie.201905790.
- [29] E. F. Douglass, C. J. Miller, G. Sparer, H. Shapiro, D. A. Spiegel, *J. Am. Chem. Soc.* **2013**, *135*, 6092–6099.
- [30] M. Brand, B. Jiang, S. Bauer, K. A. Donovan, Y. Liang, E. S. Wang, R. P. Nowak, J. C. Yuan, T. Zhang, N. Kwiatkowski, A. C. Müller, E. S. Fischer, N. S. Gray, G. E. Winter, *Cell Chem. Biol.* **2018**, DOI 10.1016/j.chembiol.2018.11.006.
- [31] J. E. Delmore, G. C. Issa, M. E. Lemieux, P. B. Rahl, J. Shi, H. M. Jacobs, E. Kastritis, T. Gilpatrick, R. M. Paranal, J. Qi, M. Chesi, A. C. Schinzel, M. R. McKeown, T. P. Heffernan, C. R. Vakoc, P. L. Bergsagel, I. M. Ghobrial, P. G. Richardson, R. A. Young, W. C. Hahn, K. C. Anderson, A. L. Kung, J. E. Bradner, C. S. Mitsiades, *Cell* **2011**, *146*, 904–917.
- [32] A. Stathis, F. Bertoni, *Cancer Discov.* **2018**, *8*, 24–36.
- [33] H. Chen, H. Liu, G. Qing, *Signal Transduct. Target. Ther.* **2018**, *3*, 5.
- [34] G. V. Chaitanya, J. S. Alexander, P. P. Babu, *Cell Commun. Signal.* **2010**, *8*, 31.
- [35] A. Rullo, A. Reiner, A. Reiter, D. Trauner, E. Y. Isacoff, G. A. Woolley, *Chem. Commun.* **2014**, *50*, 14613–14615.
- [36] M. Borowiak, W. Nahaboo, M. Reynders, K. Nekolla, P. Jalinot, J. Hasserodt, M. Rehberg, M. Delattre, S. Zahler, A. Vollmar, D. Trauner, O. Thorn-Seshold, *Cell* **2015**, *162*, 403–411.
- [37] J. F. Amara, T. Clackson, V. M. Rivera, T. Guo, T. Keenan, S. Natesan, R. Pollock, W. Yang, N. L. Courage, D. A. Holt, M. Gilman, *Proc. Natl. Acad. Sci.* **1997**, *94*, 10618–10623.

- [38] L. A. Banaszynski, L. Chen, L. A. Maynard-Smith, A. G. Lisa Ooi, T. J. Wandless, *Cell* **2006**, *126*, 995–1004.
- [39] N. Shibata, N. Miyamoto, K. Nagai, K. Shimokawa, T. Sameshima, N. Ohoka, T. Hattori, Y. Imaeda, H. Nara, N. Cho, M. Naito, *Cancer Sci.* **2017**, *108*, 1657–1666.
- [40] C. E. Powell, Y. Gao, L. Tan, K. A. Donovan, R. P. Nowak, A. Loehr, M. Bahcall, E. S. Fischer, P. A. Jänne, R. E. George, N. S. Gray, *J. Med. Chem.* **2018**, *61*, 4249–4255.
- [41] Y. Li, J. Yang, A. Aguilar, D. McEachern, S. Przybranowski, L. Liu, C.-Y. Yang, M. Wang, X. Han, S. Wang, *J. Med. Chem.* **2019**, *62*, 448–466.
- [42] M. C. Silva, F. M. Ferguson, Q. Cai, K. A. Donovan, G. Nandi, D. Patnaik, T. Zhang, H.-T. Huang, D. E. Lucente, B. C. Dickerson, T. J. Mitchison, E. S. Fischer, N. S. Gray, S. J. Haggarty, *eLife* **2019**, *8*, e45457.
- [43] D. L. Buckley, K. Raina, N. Darricarrere, J. Hines, J. L. Gustafson, I. E. Smith, A. H. Miah, J. D. Harling, C. M. Crews, *ACS Chem. Biol.* **2015**, *10*, 1831–1837.
- [44] P. P. Chamberlain, L. G. Hamann, *Nat. Chem. Biol.* **2019**, 1–8.
- [45] “CRC Handbook of Organic Photochemistry and Photobiology, Third Edition - Two Volume Set,” can be found under <https://www.crcpress.com/CRC-Handbook-of-Organic-Photochemistry-and-Photobiology-Third-Edition/Griesbeck-Oelgemoller-Ghetti/p/book/9781439899335>, **n.d.**
- [46] Y. Naro, K. Darrah, A. Deiters, **2019**, DOI 10.26434/chemrxiv.8216714.v1.
- [47] J. Liu, H. Chen, L. Ma, Z. He, D. Wang, Y. Liu, Q. Lin, T. Zhang, N. S. Gray, H. Ü. Kaniskan, J. Jin, W. Wei, *Submitted* **2019**.
- [48] C. Renicke, D. Schuster, S. Usherenko, L.-O. Essen, C. Taxis, *Chem. Biol.* **2013**, *20*, 619–626.
- [49] K. M. Bonger, R. Rakhit, A. Y. Payumo, J. K. Chen, T. J. Wandless, *ACS Chem. Biol.* **2014**, *9*, 111–115.
- [50] K. Cyrus, M. Wehenkel, E.-Y. Choi, H.-J. Han, H. Lee, H. Swanson, K.-B. Kim, *Mol. Biosyst.* **2011**, *7*, 359–364.
- [51] R. P. Nowak, S. L. DeAngelo, D. Buckley, Z. He, K. A. Donovan, J. An, N. Safaee, M. P. Jedrychowski, C. M. Ponthier, M. Ishoey, T. Zhang, J. D. Mancias, N. S. Gray, J. E. Bradner, E. S. Fischer, *Nat. Chem. Biol.* **2018**, *14*, 706–714.
- [52] M. Dong, A. Babalhavaeji, S. Samanta, A. A. Beharry, G. A. Woolley, *Acc. Chem. Res.* **2015**, *48*, 2662–2670.
- [53] K. Raina, J. Lu, Y. Qian, M. Altieri, D. Gordon, A. M. K. Rossi, J. Wang, X. Chen, H. Dong, K. Siu, J. D. Winkler, A. P. Crew, C. M. Crews, K. G. Coleman, *Proc. Natl. Acad. Sci.* **2016**, *113*, 7124–7129.
- [54] X. Sun, J. Wang, X. Yao, W. Zheng, Y. Mao, T. Lan, L. Wang, Y. Sun, X. Zhang, Q. Zhao, J. Zhao, R.-P. Xiao, X. Zhang, G. Ji, Y. Rao, *Cell Discov.* **2019**, *5*, 10.
- [55] D. Van Straten, V. Mashayekhi, H. S. De Bruijn, S. Oliveira, D. J. Robinson, *Cancers* **2017**, *9*, 19.
- [56] S. Kuchay, C. Giorgi, D. Simoneschi, J. Pagan, S. Missiroli, A. Saraf, L. Florens, M. P. Washburn, A. Collazo-Lorduy, M. Castillo-Martin, C. Cordon-Cardo, S. M. Sebt, P. Pinton, M. Pagano, *Nature* **2017**, *546*, 554–558.

- [57] P. Pfaff, K. T. G. Samarasinghe, C. M. Crews, E. M. Carreira, *ACS Cent. Sci.* **2019**, DOI 10.1021/acscentsci.9b00713.
- [58] A. Marzio, J. Puccini, Y. Kwon, N. K. Maverakis, A. Arbini, P. Sung, D. Bar-Sagi, M. Pagano, *Mol. Cell* **2019**, *73*, 224-237.e6.
- [59] K. Dimopoulos, A. S. Helbo, H. F. Munch-Petersen, L. Sjö, J. Christensen, L. S. Kristensen, F. Asmar, N. E. U. Hermansen, C. O'Connel, P. Gimsing, G. Liang, K. Grønbæk, *Mol. Oncol.* **2018**, *12*, 180–195.
- [60] Q. Xu, Y. Hou, P. Langlais, P. Erickson, J. Zhu, C.-X. Shi, M. Luo, Y. Zhu, Y. Xu, L. J. Mandarino, K. Stewart, X. Chang, *BMC Cancer* **2016**, *16*, 297.
- [61] E. S. Fischer, K. Böhm, J. R. Lydeard, H. Yang, M. B. Stadler, S. Cavadini, J. Nagel, F. Serluca, V. Acker, G. M. Lingaraju, R. B. Tichkule, M. Schebesta, W. C. Forrester, M. Schirle, U. Hassiepen, J. Ottl, M. Hild, R. E. J. Beckwith, J. W. Harper, J. L. Jenkins, N. H. Thomä, *Nature* **2014**, *512*, 49–53.
- [62] J. Bradner, D. Buckley, G. Winter, *Methods to Induce Targeted Protein Degradation Through Bifunctional Molecules*, **2016**, US2016176916 (A1).
- [63] M. Jörg, A. Glukhova, A. Abdul-Ridha, E. A. Vecchio, A. T. N. Nguyen, P. M. Sexton, P. J. White, L. T. May, A. Christopoulos, P. J. Scammells, *J. Med. Chem.* **2016**, *59*, 11182–11194.
- [64] M. Stein, A. Breit, T. Fehrentz, T. Gudermann, D. Trauner, *Angew. Chem. Int. Ed.* **2013**, *52*, 9845–9848.
- [65] S. Samanta, C. Qin, A. J. Lough, G. A. Woolley, *Angew. Chem. Int. Ed.* **2012**, *51*, 6452–6455.
- [66] M. Borowiak, W. Nahaboo, M. Reynders, K. Nekolla, P. Jalinot, J. Hasserodt, M. Rehberg, M. Delattre, S. Zahler, A. Vollmar, D. Trauner, O. Thorn-Seshold, *Cell* **2015**, *162*, 403–411.

3 – Tuning the Photophysical Properties of PHOTACs

Martin Reynders^{1,2}, Kilian Rossmann¹, Marleen Bérouti¹, Michele Pagano^{3,4,5}, and Dirk Trauner^{1,4,6}

¹Department of Chemistry, New York University, New York, NY 10003, USA.

²Department of Chemistry, Ludwig Maximilians University of Munich
81377 Munich, Germany.

³Department of Biochemistry and Molecular Pharmacology, New York University School of Medicine, New York, NY 10016, USA.

⁴Perlmutter Cancer Center, New York University School of Medicine, New York, NY 10016, USA.

⁵Howard Hughes Medical Institute, New York University School of Medicine, New York, NY 10016, USA.

⁶NYU Neuroscience Institute, New York University School of Medicine, New York, NY 10016, USA.

Introduction

The targeted degradation of proteins through mono- or bifunctional molecules represents a promising therapeutic approach and a rapidly expanding area of research. Several strategies have emerged to remove a protein of interest, one of them being Proteolysis Targeting Chimeras (PROTACs). PROTACs are bifunctional molecules that induce ternary complex formation between an E3 ubiquitin ligase, and a protein bound by the targeting ligand. This leads to ubiquitylation and subsequent proteasomal degradation of the target. Contrary to the occupancy-based mode of action seen with classical inhibitors binding a specific site of the target, PROTACs can operate catalytically at substoichiometric concentrations and remove the whole protein. This mechanistic advance creates new opportunities for small-molecule degraders, but also brings additional risks.

Recently, Photoswitchable Targeted Chimeras (**PHOTACs**) (**Figure 3.1**) and photocaged PROTACs have emerged to address some of the risks associated with PROTACs. **PHOTACs**, and PROTACs modified with a photolabile protecting group, can be activated through irradiation with light and their activity can thus be controlled in time and space. While photocaged PROTACs irreversibly release the active PROTAC, **PHOTACs** can toggle between an active and inactive isomer.

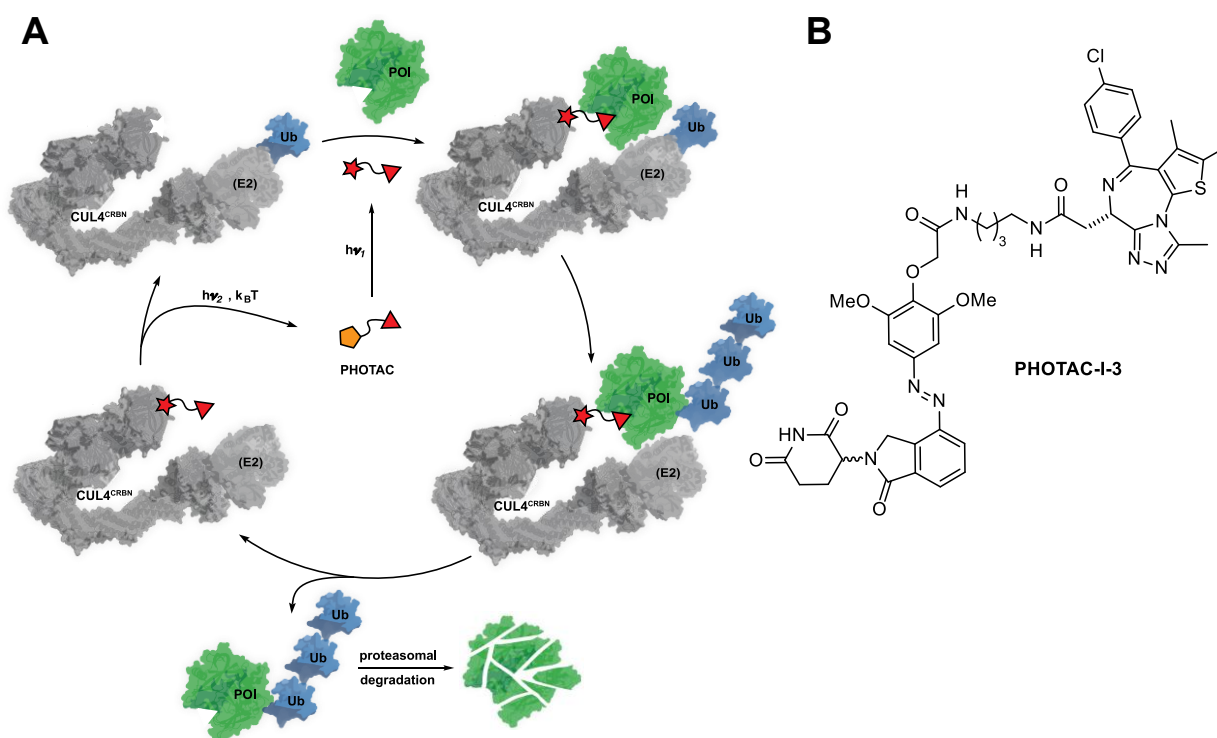


Figure 3.1: A) Schematic mode of action of **PHOTACs**. B) Structure of **PHOTAC-I-3**.

The caged and photoswitchable PROTACs reported so far require ultraviolet, violet, or blue light to control their activity. This is sufficient for 2D cell culture and simple biological experiments, but incompatible with deep tissue applications. Biological chromophores such as flavin or hemoglobin strongly absorb violet and blue light which restricts tissue penetration to several millimeters. Wavelength in the yellow, red, and infrared region of the electromagnetic spectrum constitute the biooptical window, a wavelength range compatible with efficient deep tissue penetration.^[1] Azobenzene photoswitches, as used in **PHOTACs**, have been successfully developed to undergo *E*-to-*Z* isomerization at wavelength greater than 500 nm.^[2–7] Creating light-activated PROTACs that respond to wavelengths in the biooptical is a requirement for future clinical applications.

The precise spatial control of existing caged and photoswitchable PROTACs is partially limited by diffusion. Once activated, caged PROTACs as well as **PHOTACs** can diffuse to non-irradiated areas. An uncaged PROTAC remains active, **PHOTACs** however, can relax to their thermodynamically inactive forms with half-lives of hours to days. Alternatively, **PHOTACs** can be deactivated with a second wavelength, however this isomerization is not quantitative.

Small amounts of an inhibitor are diluted by diffusion and thereby lose their ability to efficiently occupy its target's binding site at all times. In contrast, PROTAC's catalytic mode of action only requires intermittent ternary complex formation. Therefore, activated PHOTACs could remain potent degraders after diffusion from the site of activation. Modifications of the photoswitch to shorten the thermal isomerization half-life or improve bidirectional isomerization yields would be beneficial to precisely localize the drugs effect and counteract diffusion. Furthermore, this would enable precise control over protein levels, which could otherwise only be attempted through color-dosing.

In this work we aim to enhance the photophysical properties of **PHOTACs** and generate structure activity relationship of the photoswitchable glutarimide scaffold to guide future PHOTAC development.

Results

We set out to optimize the photophysical properties and thereby improve upon the first generation of **PHOTACs** with a focus on substituents on the azobenzene photoswitch. PROTACs targeting the BET proteins BRD2-4 have been studied in detail and provide ideal benchmark system to improve upon existing **PHOTACs**.^[8–12] **PHOTAC-I-3** emerged as the lead compound which only degraded BRD2-4 after 390 nm irradiation but appeared unable to form a productive ternary complex in the dark.^[13] However, when the linker was extended by two methylene units in **PHOTAC-I-5**, degradation of BRD3 and BRD4 in the dark could be observed (**Figure S3.1**). We designed **PHOTAC-I-14** by replacing the methoxy groups in **PHOTAC-I-3** with isopropyl groups to enhance steric clash between the *E*-isomer of the azobenzene and cereblon. Synthesis of **PHOTAC-I-14** followed the synthetic route of **PHOTAC-I-3**,^[13] starting with diazonium formation of lenalidomide and coupling to propofol, followed by alkylation. Subsequent deprotections and HATU couplings with the linker and (+)-JQ1 gave **PHOTAC-I-14** in 6 steps.

The photophysical properties of **PHOTAC-I-14** changed slightly compared to **PHOTAC-I-3**, showing a slight blue-shift of the absorption resulting in slightly lower amounts of *Z*-isomer at 390 nm compared to the highest *Z*-isomer amount at 370 nm (**Figure 3.2B**). **Z-PHOTAC-I-14** thermally isomerizes slowly to its *E*-isomer with a half-life of 36.6 h (**Figure 3.2C**). Next, we looked at the effects on RS4;11 viability after 3 days. We did not observe a significant difference on viability between cells kept either in the dark or pulse irradiated with 390 nm light (**Figure 3.2D**). BRD3 and BRD4 levels analyzed by Western blot also remained unchanged after 4 h of **PHOTAC-I-14** treatment in the dark or in combination with 390 nm pulse irradiation (**Figure 3.2E**). The observed effect on viability likely results from BET proteins inhibition, which both isomers should be capable of. Introduction of the isopropyl groups appears to block ternary complex formation and target degradation in both the *E*- and *Z*-isomers.

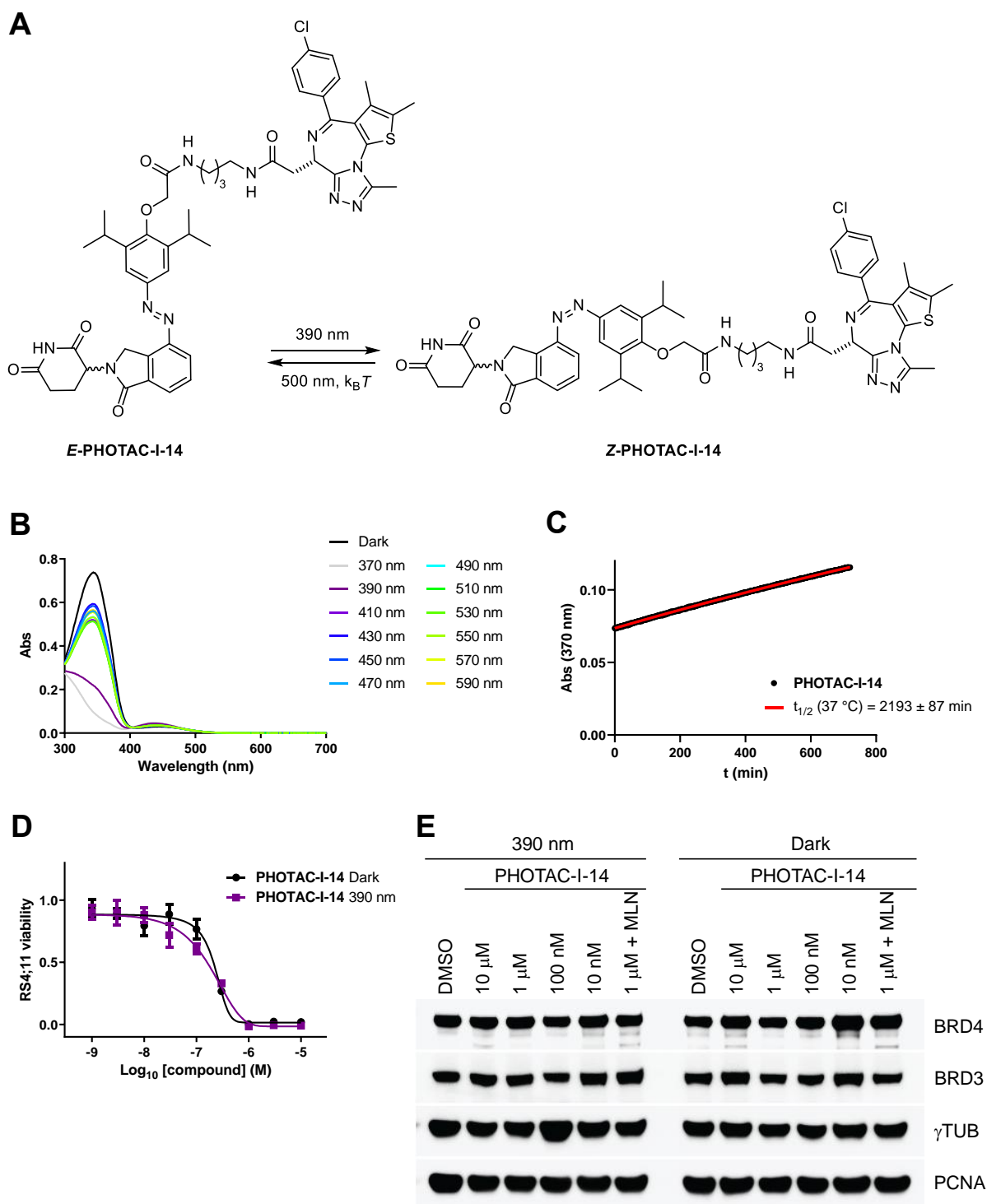


Figure 3.2: Characterization of **PHOTAC-I-14**. A) Structure and isomerization of **PHOTAC-I-14**. B) Absorption spectra of **PHOTAC-I-14** after 5 min of irradiation with the indicated wavelength. C) Thermal *Z*-to-*E* isomerization of **PHOTAC-I-14** at 37 °C in DMSO. D) Viability of RS4;11 cells after treatment with **PHOTAC-I-14** for 72 h in the dark or under pulsed (100 ms every 10 s) 390 nm irradiation.

Next, we sought to employ bridged azobenzenes known as diazocines to improve clash between the azobenzene and cereblon in the inactive state. Diazocines operate under inverse logic, viz. they are thermodynamically stable as the bent *Z*-isomer and undergo reversible isomerization to the elongated *E*-isomer that can adapt either a chair or twist conformation. Another advantage of diazocines over regular azobenzenes is their quantitative *E*-to-*Z* isomerization using green light.^[14,15] Our design was based on incorporating the phthalimide present in thalidomide to form the diazocine as close to cereblon as possible. Molecular modeling suggested that the bent *Z*-isomer may interfere with cereblon binding, whereas the *E*-isomer should be accommodated (**Figure S3.2**).

The synthesis of the diazocine started with the iodination of 4-aminophthalimide,^[16] followed by formation of the ethyl carbamate. Next, we employed consecutive Sonogashira couplings to form the diaryl alkyne, which was reduced and subjected to the key oxidative Baeyer-Mills coupling to give the diazocine.^[17] Installation of the glutarimide under mild conditions,^[18] followed by deprotection and coupling to the (+)JQ-1 derived BET protein ligand yielded **PHOTAC-I-15** (**Figure 3.3**).

The photophysical properties of **PHOTAC-I-15** matched those of a typical diazocine, showing an increased absorption of the *E*-isomer around 500 nm upon irradiation with violet light. The half-life in a 1:1 DMSO:PBS (pH 7.4) mixture was determined as 27 min. No strong difference in RS4;11 viability was observed after 72 h of **PHOTAC-I-15** treatment under pulsed 400 nm irradiation or in the dark. The analysis of BRD3 and BRD4 levels by Western blot after incubation with **PHOTAC-I-15** for 4 h showed degradation of both proteins in the dark and under 400 nm irradiation. This is in accordance with the result of the viability assay and confirmed that the different isomers show no strong difference in their biological activity. Given the limited success of the diazocine scaffold, we focused on azobenzene substitutions to improve our BET **PHOTACs**.

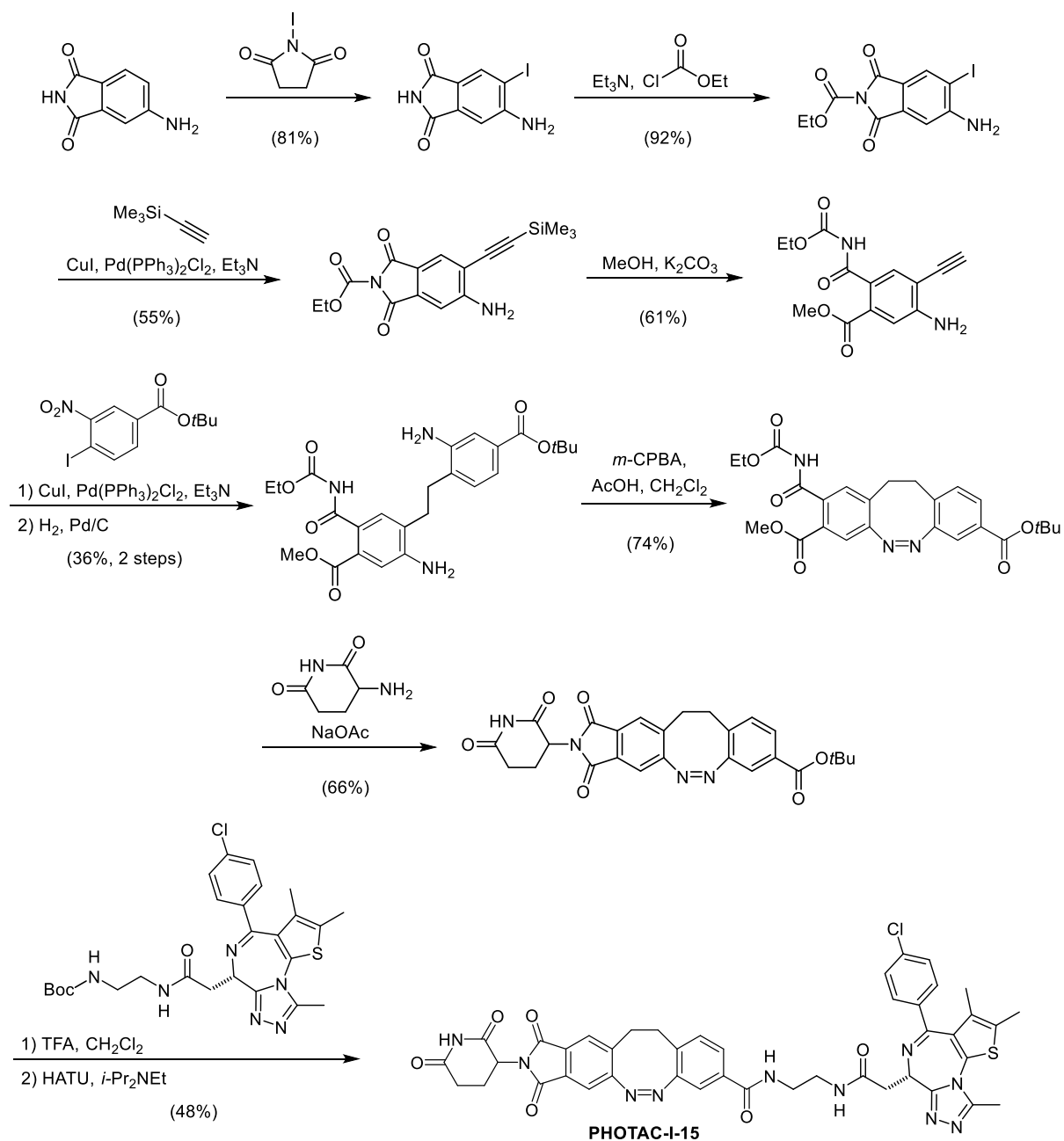


Figure 3.3: Synthesis of PHOTAC-I-15.

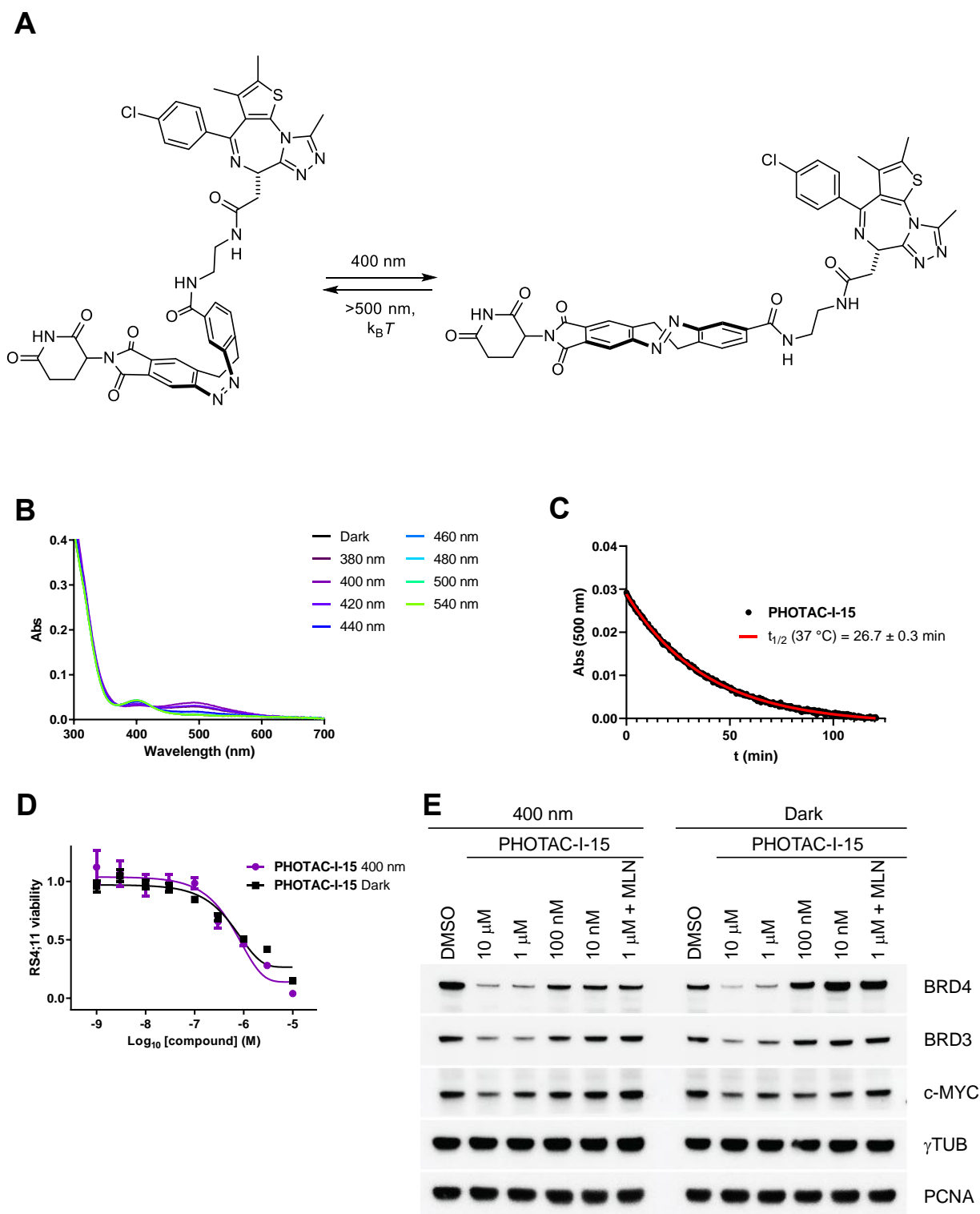


Figure 3.4: Characterization of **PHOTAC-I-15**. A) Structure and isomerization of **PHOTAC-I-15**. B) Absorption spectra of **PHOTAC-I-15** after 5 min of irradiation with the indicated wavelength (Dark covered by 540 nm). C) Thermal *Z*-to-*E* isomerization of **PHOTAC-I-15** at 37 °C in DMSO. D) Viability of RS4;11 cells after treatment with **PHOTAC-I-15** for 72 h in the dark or under pulsed 390 nm irradiation (100 ms every 10 s). E) Immunoblot analysis of RS4;11 cells treated with **PHOTAC-I-15** for 4 h. Cells were either irradiated with pulses of 390 nm light (left, 100 ms every 10 s) or kept in the dark (right). MLN = 1.25 μ M MLN4924.

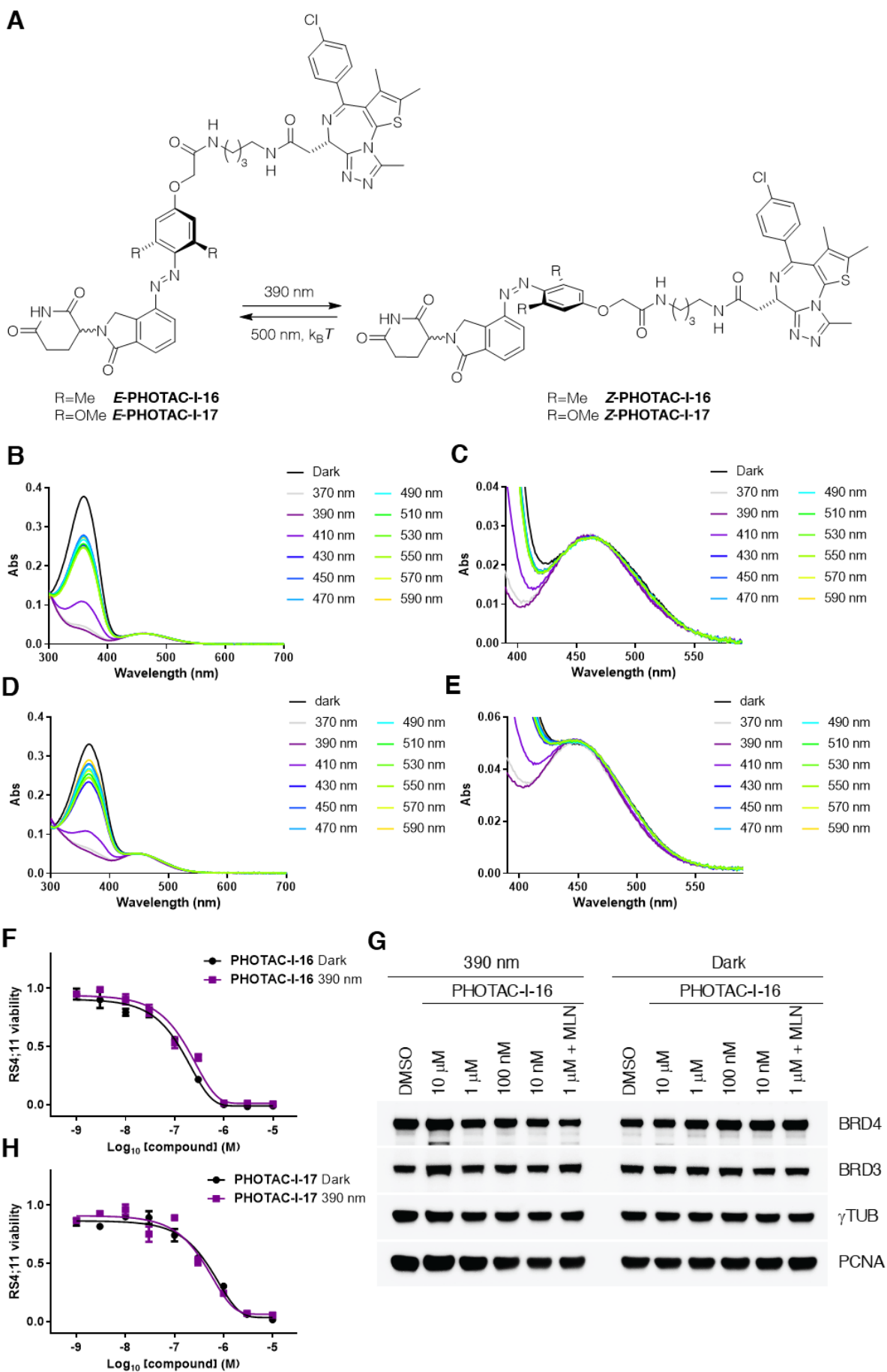


Figure 3.5: Characterization of **PHOTAC-I-16+17**. A) Structure and isomerization of **PHOTAC-I-16+17**. B), C) Absorption spectra of **PHOTAC-I-16** after 5 min of irradiation with the indicated wavelength. D), E) Absorption spectra of **PHOTAC-I-17** after 5 min of irradiation with the indicated wavelength. F), H) Viability of RS4;11 cells after treatment with **PHOTACs-I-16/PHOTAC-I-17** for 72 h in the dark or under pulsed 390 nm irradiation (100 ms every 10 s). G) Western blot analysis of **PHOTAC-I-16**-treated RS4;11 cells after 4 h in the dark or under pulsed 390 nm irradiation (100 ms every 10 s).

The introduction of several substituents in ortho position to the diazene distorts the planar geometry of the *E*-azobenzene, leading to a bathochromic shift of the $n\text{-}\pi^*$ transition. This makes the absorption band of the *E*-azobenzene accessible to induce *E*-to-*Z* isomerization at wavelengths greater than 500 nm. [2,3,6,7,19–21]

With one position ortho to the diazine already occupied, we chose to explore trisubstituted azobenzenes due to their simple access from lenalidomide and the corresponding phenols via diazonium coupling. We first explored the effect of two methyl groups in ortho position on photoswitching and biological effects. **PHOTAC-I-16** did not show any strong change in absorption spectra with 390 nm irradiation generating the largest amount of *Z*-isomer (**Figure 3.5B**). The absorption bands of the $n\text{-}\pi^*$ transitions were not well separated and irradiation between 430 and 590 nm generated similar isomer ratio (**Figure 3.5C**). RS4;11 viability did not show a strong difference between the dark and irradiated states in accordance with the absence of BET protein degradation by either isomer (**Figure 3.5F, G**). Similar results were obtained for **PHOTAC-I-17** where the strong overlap of $n\text{-}\pi^*$ bands persisted (**Figure 3.5D, E**). Both **PHOTAC-I-16** and **PHOTAC-I-17** feature slow thermal relaxation with half-lives larger than 24 h (**Figure S3.3A+B**). The effect of **PHOTAC-I-17** on RS4;11 viability showed reduced potency compared to **PHOTAC-I-16**, but photoisomerization did not influence the cytotoxic effect (**Figure 3.5H**). The observed cytotoxicity for both compounds likely stems from the inhibitory activity of the ligand.

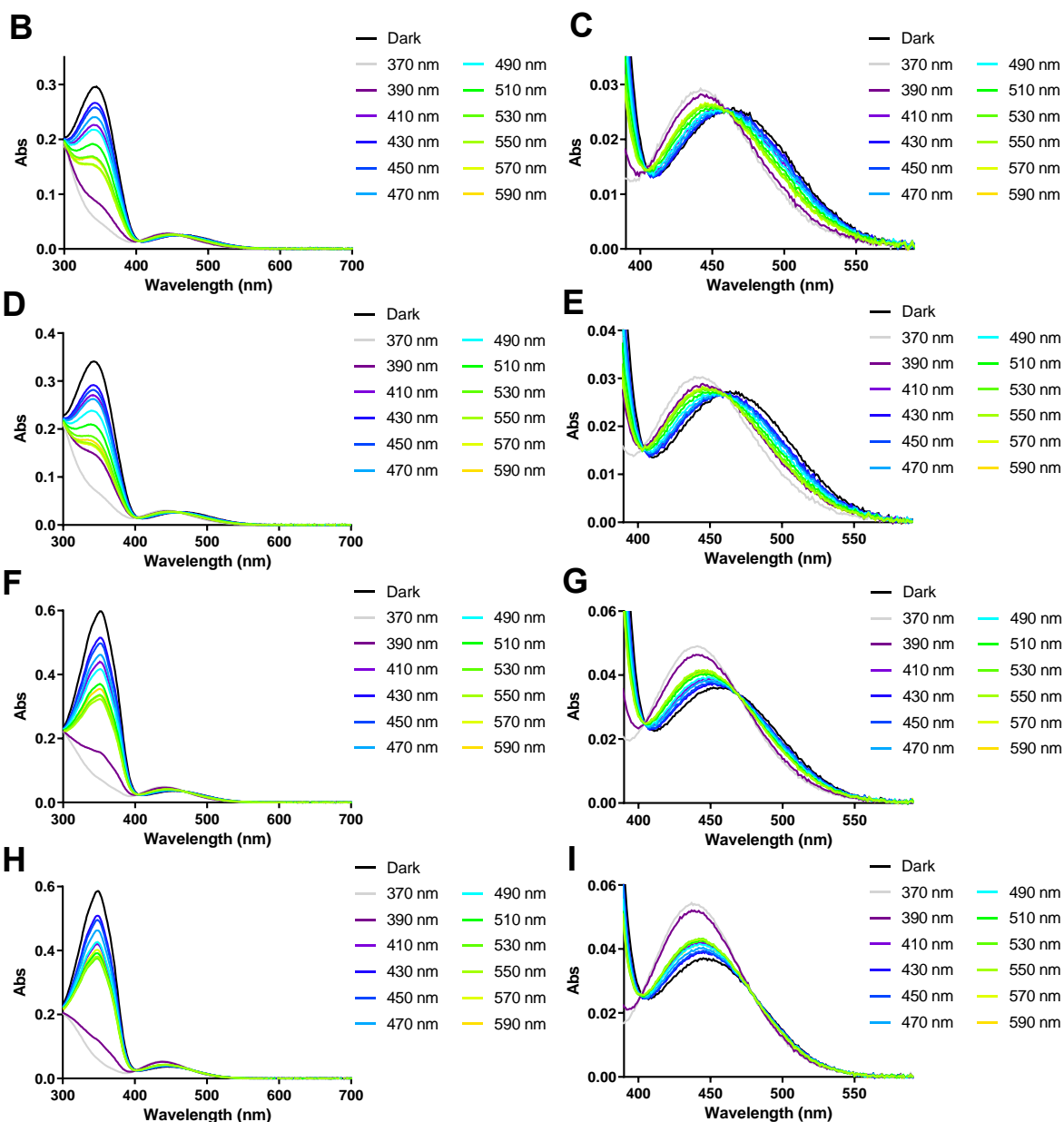
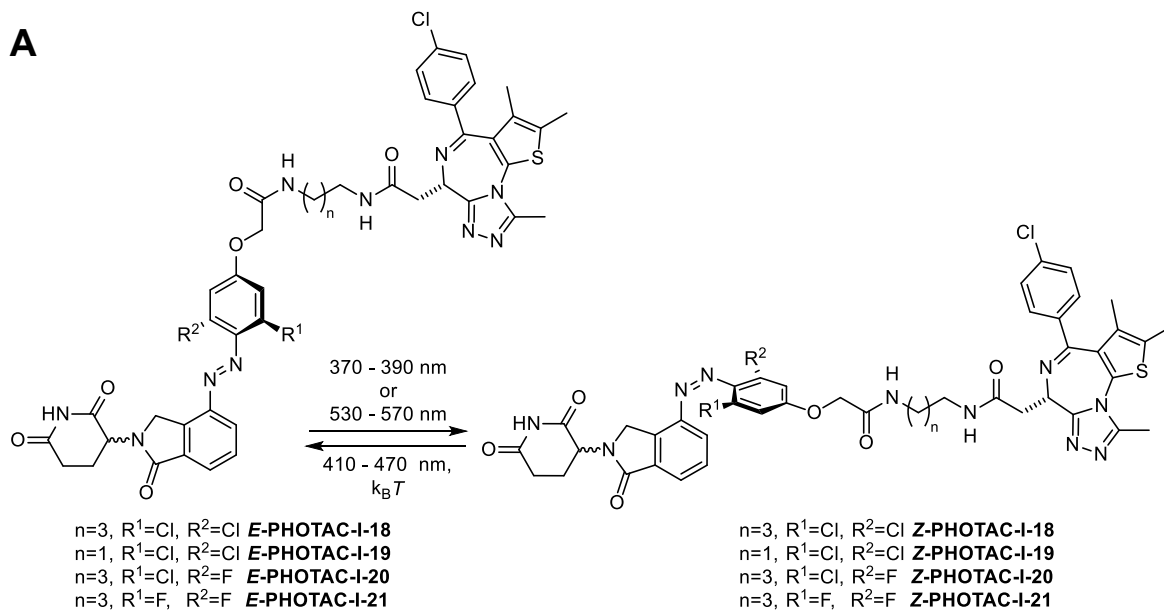


Figure 3.6: Photophysical characterization of **PHOTACs-I-18–21**. A) Structure and isomerization of **PHOTAC-I-18–21**. B)–I) Absorption spectra of **PHOTAC-I-18** (B, C), **PHOTAC-I-19** (D, E), **PHOTAC-I-20** (F, G) and **PHOTAC-I-21** (H, I) after 5 min irradiation with the indicated wavelength.

Next, we explored chlorine and fluorine substitutions, which are commonly used to red-shift the absorption spectra of azobenzene based photopharmaceuticals.^[2,5,21–23] **PHOTACs-I-18–21** (**Figure 3.6A**) were synthesized from the corresponding 3,5-halogen substituted phenols following the general synthetic route.^[13] The dichloro-substituted azobenzenes **PHOTACs-I-18+19** featured the best $n-\pi^*$ transition band separation and correspondingly underwent *E*-to-*Z* isomerization upon green light irradiation (**Figure 3.6B–D**). Mixed chloro-, fluoro-substituted azobenzenes were reported to have improved $n-\pi^*$ band separation.^[7] Yet **PHOTAC-I-20** showed smaller band separation compared to the dichloro switch and the use of two fluorine atoms in other position led to a further decrease in $n-\pi^*$ band separation for **PHOTAC-I-21** (**Figure 3.6F–I**).

All halogen substituted PHOTACs were responsive to green light to induce *E*-to-*Z* isomerization, but the highest ratios of *Z*-isomer could be obtained with 370 nm to 390 nm irradiation (**Figure S3.4**). Thermal relaxation of **PHOTAC-I-18–21** proceeded slow with half-lives exceeding 12 h (**PHOTAC-I-19**), 24 h (**PHOTAC-I-21**) and 36 h (**PHOTAC-I-18+20**) (**Figure S3.3C–F**).

The viability in RS4;11 cells was investigated with 390 nm irradiation to compare the highest possible amount of *Z*-isomer with the dark-adapted *E*-isomer. **PHOTACs-I-18** showed a strong increase in potency with an IC_{50} around 30 nM, however no difference between the dark and irradiated state (**Figure 3.7A**). Employing a shorter linker in **PHOTAC-I-19** led to a decrease in potency but failed to generate a viability difference between the dark and irradiated forms (**Figure 3.7B**). Some degradation of BRD4 after 4 h of **PHOTAC-I-18** treatment at a concentration of 1 μ M could be detected in both 390 nm pulse irradiated and non-irradiated cells (**Figure 3.7E**). These results indicate that the out-of-plane conformation of **Z-PHOTAC-18** can form a productive ternary complex that induces target degradation. No light-dependent effect on RS4;11 viability could be observed for **PHOTAC-I-20** (**Figure 3.7C**).

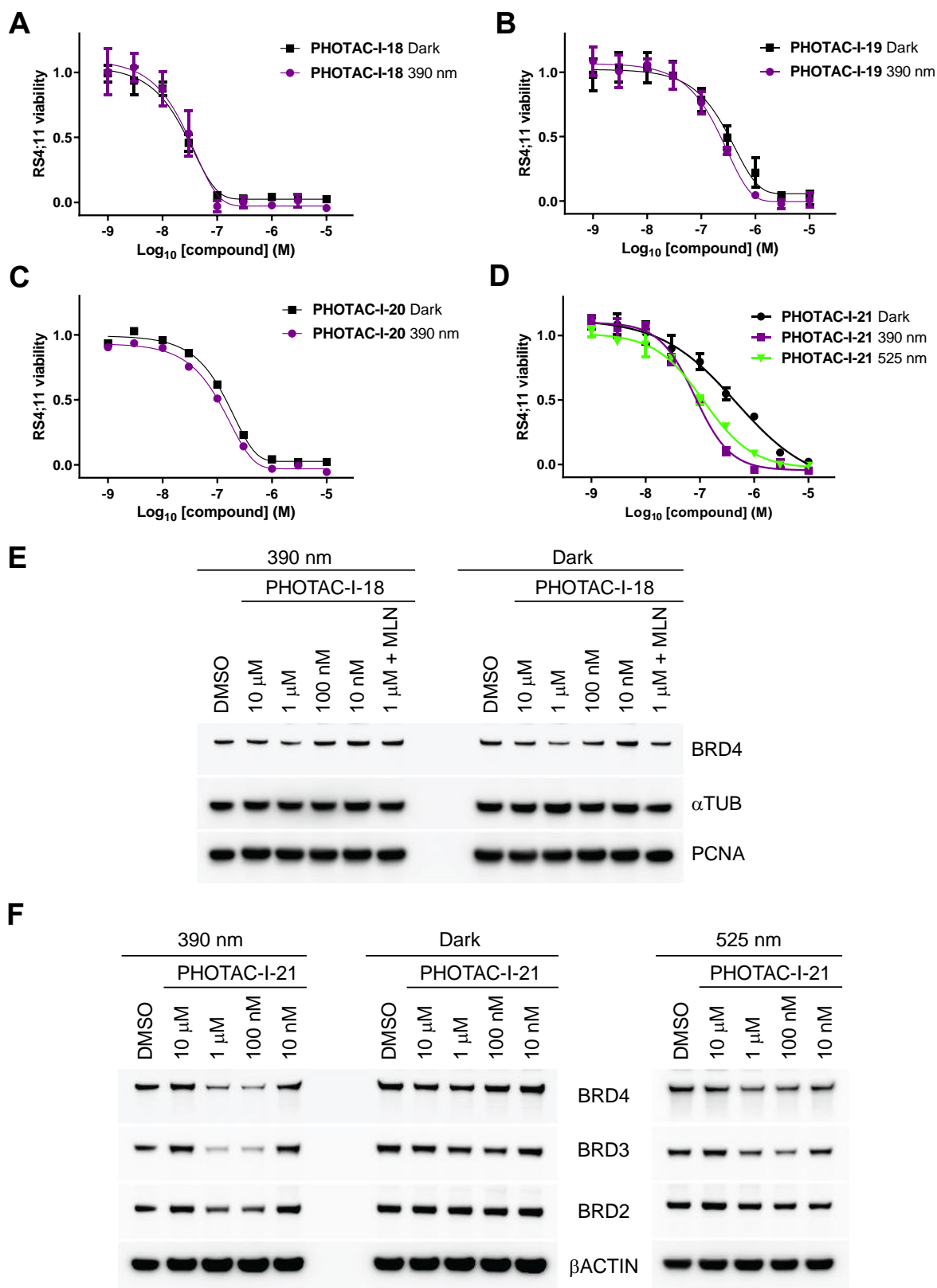


Figure 3.7: *In cellulo* characterization of redshifted PHOTACs. A)–C) Viability of RS4;11 cells after treatment with **PHOTAC-I-18** (A), **PHOTAC-I-19** (B) or **PHOTAC-I-20** (C) for 72 h in the dark or under pulsed 390 nm irradiation (100 ms every 10 s). D) Viability of RS4;11 cells after treatment with **PHOTAC-I-21** for 72 h in the dark or under pulsed 390 nm irradiation (100 ms every 10 s). E) Immunoblot analysis after treatment of RS4;11 cells with **PHOTAC-I-18** for 4 h at the indicated concentrations. Cells were

either irradiated with 100 ms pulses of 390 nm light every 10 s (left) or kept the dark (right). MLN = 1.25 μ M MLN4924. F) Immunoblot analysis after treatment of RS4;11 cells with **PHOTAC-I-21** for 4 h at the indicated concentrations. Cells were either irradiated with 100 ms pulses of 390 nm light every 10 s (left), kept the dark (center) or irradiated with 100 ms pulses of 525 nm light every 10 s (right).

In contrast to other ortho substituents investigated so far, **PHOTAC-I-21** bearing two fluorine substituents on the azobenzene did show an increased cytotoxicity upon irradiation. (**Figure 3.7D**) Notably, the effect on RS4;11 viability in the dark (IC_{50} = 4.64 μ M) is lower compared to other substituents. Pulsed 390 nm irradiation led to an increase in cytotoxicity (IC_{50} = 0.808 μ M) which was recapitulated by pulsed 525 nm irradiation, showing slightly lower potency (IC_{50} = 1.17 μ M). Western blot analysis showed strong degradation of BRD4, BRD3 and some degradation of BRD2 upon treatment with 390 nm irradiation and 1 μ M or 100 nM **PHOTAC-I-21** (**Figure 3.7F**). Potent BET protein degradation was not observed in the dark. Pulsed irradiation with green light (525 nm) was able to reduce BRD4 and BRD3 levels after 4 h of **PHOTAC-I-21** treatment, albeit to a lesser extent than 390 nm irradiation. This observation could be explained by the different amounts of the active *Z*-isomer formed: 85% upon 390 nm irradiation compared to 38% when activated with 525 nm light (**Figure S3.4F**).

In an attempt to increase the steric demand around the diazene and further distort the planar geometry of the *E*-azobenzene, we synthesized the phthalimide based degrader **PHOTAC-I-22** (**Figure 3.8A**) to improve the bathochromic shift of the $n-\pi^*$ transition. The preparation started with diazonium formation of pomalidomide and coupling to 3,5-dichlorophenol, followed by alkylation with *tert*-butyl bromoacetate to yield **3.26**. The *E*-isomer of this intermediate already shows an extension of the absorption beyond 600 nm which can be used to induce *E*-to-*Z* isomerization with yellow light (**Figure S3.5**). Continuation of the synthesis and coupling to (+)-JQ1 as targeting ligand gave **PHOTAC-I-22** (**Figure 3.8A**) which retained the good photophysical properties.

The highest amount of *Z*-isomer could be generated through irradiation with wavelengths *E*-to-*Z* isomerization with green greater than 550 nm due to the well separated absorption bands (**Figure 3.8B, C**). Even though RS4;11 viability was

strongly reduced in a dose-dependent manner by **PHOTAC-I-22**, we could not observe a light dependence (**Figure 3.8D**). This was confirmed by immunoblot analysis of RS4;11 cells where BRD4, BRD2 and most strongly BRD3 degradation was induced by **PHOTAC-I-22** both upon pulsed 565 nm irradiation and in the dark (**Figure 3.8E**).

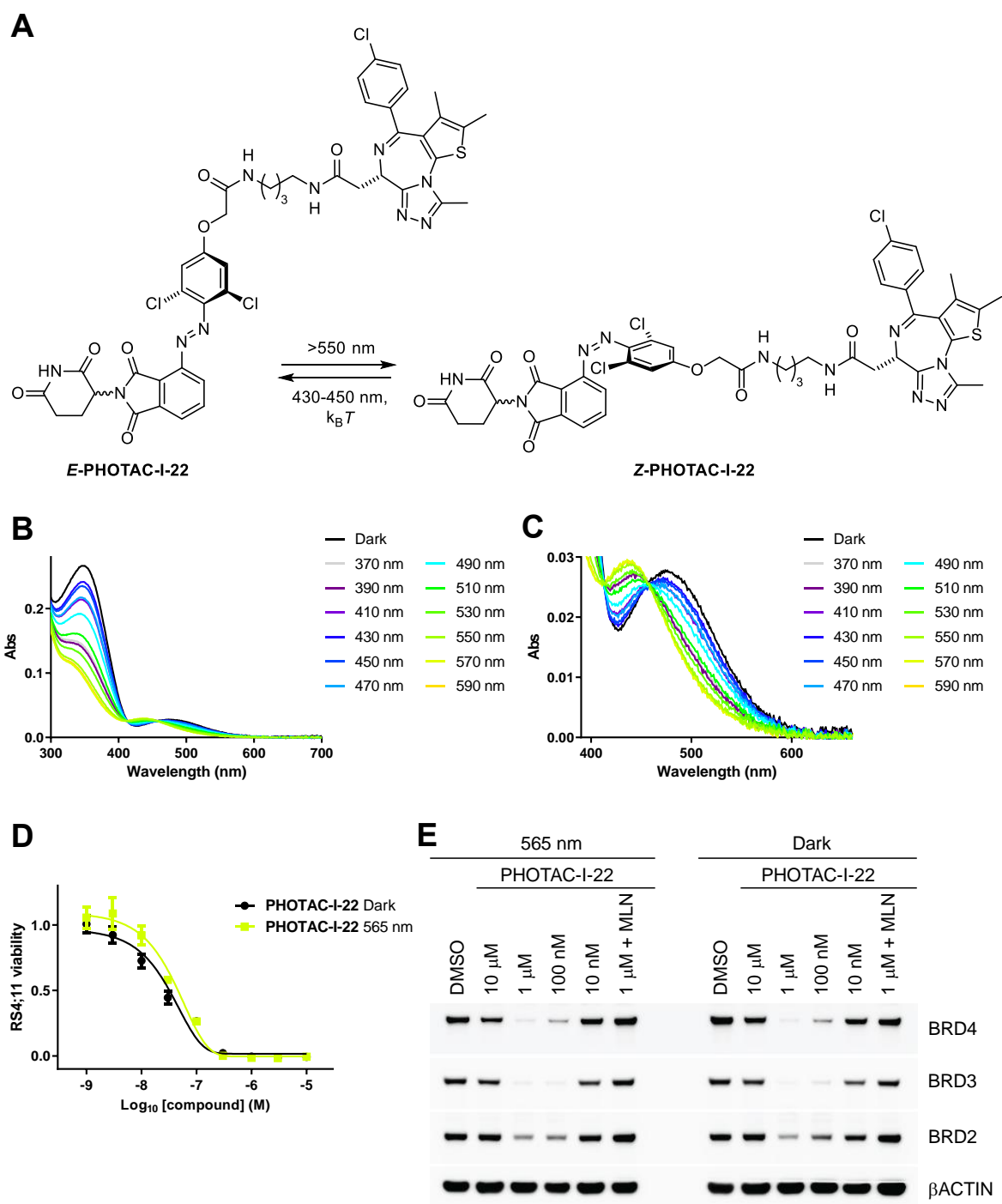


Figure 3.8: Characterization of **PHOTAC-I-22**. A) Structure and isomerization of **PHOTAC-I-22**. B)+C) Absorption spectra of **PHOTAC-I-22** after 5 min of irradiation with the indicated wavelength. D) Viability of RS4;11 cells after treatment with **PHOTAC-I-22** for 72 h in the dark or under pulsed 565 nm irradiation (100 ms every 10 s). E) Immunoblot analysis of RS4;11 cells treated with **PHOTAC-I-22** for 4 h. Cells

were either irradiated with pulses of 565 nm light (left, 100 ms every 10 s) or kept in the dark (right). MLN = 1.25 μ M MLN4924.

All photoswitchable PROTACs described so far thermally isomerize with half-lives of several hours to days. This is beneficial to reduce the intensity or frequency of irradiation required to keep the photoswitch in the active form, but it also limits the spatial precision by allowing for diffusion from the site of irradiation. Classical occupancy driven photopharmacology is less susceptible to off-location activity through diffusion since high occupancy of the target can only be obtained at the site of irradiation. In contrast, PHOTACs function through a catalytic and event driven mechanism that does not necessitate high target occupancy.^[24] Generally, in photopharmacology, the required irradiation schedule and the desired spatial localization can be balanced through modulation of the thermal half-life.

Although very short thermal half-lives are detrimental to achieving high target occupancy, they could be tolerated by the event driven mechanism of PROTACs.^[25] A common strategy to drastically decrease the half-life of an azobenzene is introduction of a dialkylamino group in para position to the diazene.^[26] We chose to replace the phenolic oxygen on the azobenzene with a methylamino group to keep the overall structural change as small as possible. **PHOTAC-I-23+24 (Figure 3.9A, S3.6A)** could be prepared via azo coupling of lenalidomide with the corresponding substituted anilines.

PHOTAC-I-23 features a bathochromic absorption shift and can undergo efficient *E*-to-*Z* isomerization when irradiated with blue light (430 to 450 nm) (**Figure 3.9B**). The *Z*-isomer is short-lived in PBS (pH 7.4) with a half-life of 0.45 s when used with 2% DMSO as cosolvent and 0.65 s when used with 10% DMSO (**Figure 3.9D, E**). However, in a 1:1 mixture of DMSO and PBS the half-life of the thermal *Z*-to-*E* isomerization increases to 117 s, highlighting the strong environmental dependence of this process (**Figure 3.9F**).

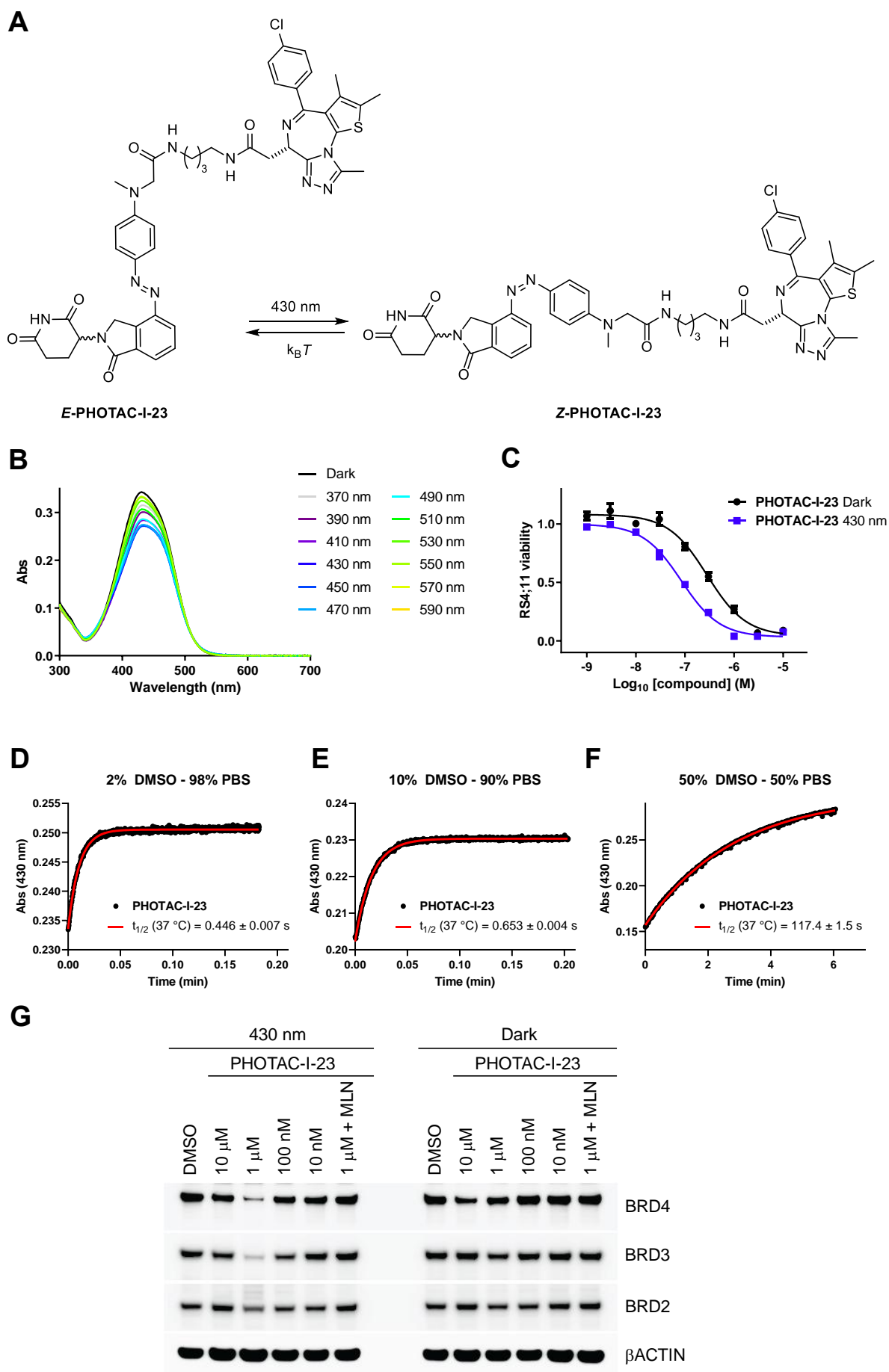


Figure 3.9: Characterization of PHOTAC-I-23. A) Structure and isomerization of

PHOTAC-I-23. B) Absorption spectra of **PHOTAC-I-23** in DMSO after 5 min of irradiation with the indicated wavelength. C) Viability of RS4;11 cells after treatment with **PHOTAC-I-23** for 72 h in the dark or under pulsed 430 nm irradiation (100 ms every 10 s). D)–F) Thermal *Z*-to-*E* isomerization of **PHOTAC-I-23** in PBS with increasing amounts of DMSO as cosolvent. G) Immunoblot analysis of RS4;11 cells treated with **PHOTAC-I-23** for 4 h. Cells were either irradiated with pulses of 565 nm light (left, 100 ms every 10 s) or kept in the dark (right). MLN = 1.25 μ M MLN4924.

When pulsed with 430 nm irradiation (100 ms per 10s) **PHOTAC-I-23** treatment reduced RS4;11 viability with an IC_{50} of 0.840 μ M compared to an IC_{50} of 2.83 μ M in the dark (**Figure 3.9C**). The light-dependence and overall antiproliferative effect is largely lost when employing a shorter linker in **PHOTAC-I-24** (**Figure S3.6D**). Western blot analysis showed that **PHOTAC-I-23** could induce strong degradation of BRD3, BRD4 and partial degradation of BRD2 when irradiated with 430 nm pulses, but not in the dark (**Figure 3.9G**). This means that the *Z*-isomer is sufficiently long-lived in the cellular environment to induce ternary complex formation and ubiquitylation of the BET proteins. It is possible that **Z-PHOTAC-I-23** is temporarily stabilized by the less polar environment when bound to either cereblon or a BET protein. The rapid thermal relaxation in aqueous environments should enable excellent spatiotemporal control of these amino substituted **PHOTACs**.

Conclusion

Here we explored the effect of different photoswitch substituents and their ability to modulate the corresponding **PHOTACs**' effect on targeted protein degradation. Subtle changes in the structure of PROTACs and **PHOTACs** can have a strong influence on their ability to degrade target proteins. The design of **PHOTACs** is a delicate balancing act between ensuring efficient protein degradation by one isomer while keeping the other isomer inactive. This is exemplified by several substituents that resulted in both the *E*- and *Z*-isomer being unable to efficiently degrade BET proteins as seen for **PHOTAC-I-14** and **PHOTAC-I-16** or compounds where both isomers were potent PROTACs, such as **PHOTAC-I-15** and **PHOTAC-I-22**.

Nevertheless, we were able to identify **PHOTACs** with improved photophysical properties so that **PHOTACs** could be adjusted for the desired application. **PHOTAC-I-21** features a bathochromic shift of absorption bands that makes it possible to activate

target protein degradation using green light. This allows for deeper tissue penetration of the activating light and could enable the application of **PHOTACs** in photomedicine beyond surface exposed diseases. It should be noted that some permutation of linker and the photoswitches described herein may be necessary to expand the red-shifted **PHOTACs** to new protein targets. Further, red-shifted azobenzenes characterized in this study, such as **PHOTAC-I-22** which absorbs beyond 600 nm, could provide useful building blocks for other applications of photoswitches and serve as starting point to further redshift this type of azobenzene.

To apply **PHOTACs** as tools to study biological function, a high level of precision control can be more important than irradiation wavelength and light penetration. **PHOTAC-I-23** offers precise spatial and temporal control of BET protein degradation due to its fast intrinsic inactivation. This showcases that a short-lived species such as **Z-PHOTAC-I-23** can be sufficient to intermittently form a productive ternary complex, highlighting the event-based mechanism of PROTACs.

Funding

We thank New York University for financial support. NMR spectra were acquired using the TCI cryoprobe supported by the NIH (OD016343). This work was partially funded by grant R01-CA76584 from the National Institutes of Health to M.P.. M.P. is an investigator with the Howard Hughes Medical Institute.

Conflict of interests

M.R., M.B., M.P. and D.T. are listed as inventors on a patent application on photoswitchable PROTACs. M.P. is a member of the scientific advisory boards of CullGen Inc. and Kymera Therapeutics and a consultant for BeyondSpring Pharmaceutical. All other authors declare that they have no competing interests.

Author contributions

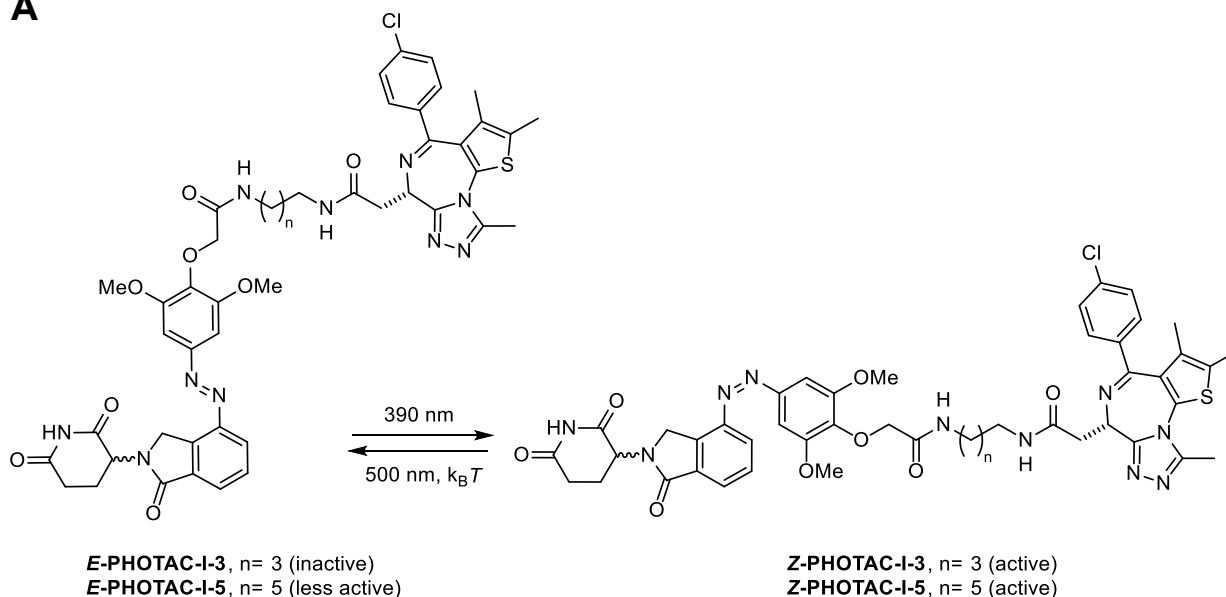
M.R., conceived the study. M.R., K.R., M.B., performed chemical synthesis and characterized compounds. M.R. and K.R. performed biological evaluation. D.T. and M.P. supervised the experiments. M.R. and D.T. wrote the manuscript with input from all authors.

Acknowledgements

We acknowledge Tongil Ko for critically reading this manuscript.

Supporting Figures

A



B

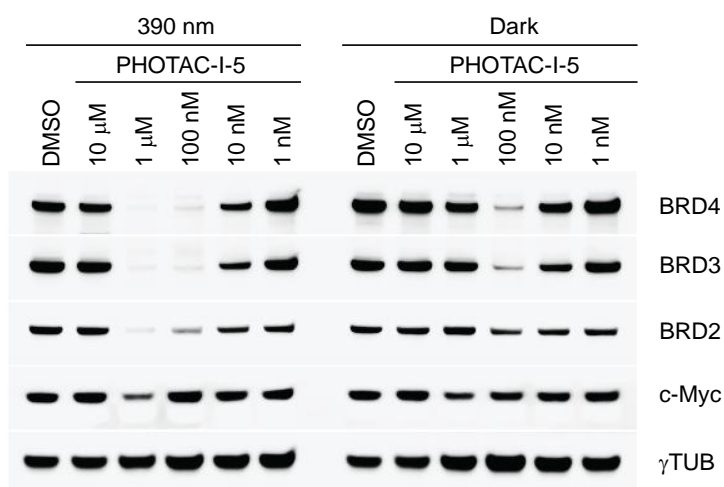


Figure S3.1: A) Structure of **PHOTAC-I-3+5**. B) Immunoblot of BRD4, BRD3, BRD2 and c-Myc levels in RS4;11 cells after 4 h of **PHOTAC-I-5** treatment with pulsed 390 nm irradiation (100 ms every 10 s) or in the dark.

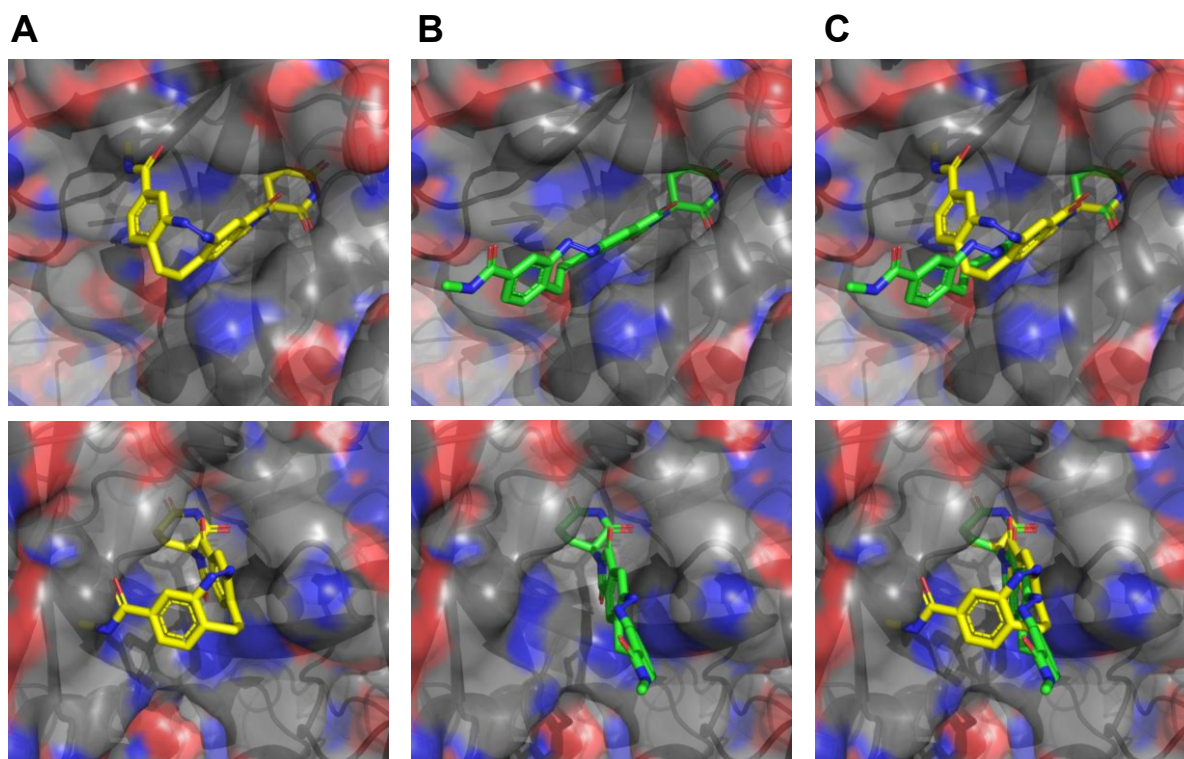


Figure S3.2: Structure model of a (*Z*)-diazocine (**A**) or (*E*)-diazocine (twist conformation) (**B**) bound to cereblon (PDB: 4C13)^[27]. The (*Z*)-isomer clashed with cereblon, but the (*E*)-isomer fits into the binding pocket of thalidomide. (**C**) Overlay of both structures. Models were created using Schrödinger Maestro 11.9.

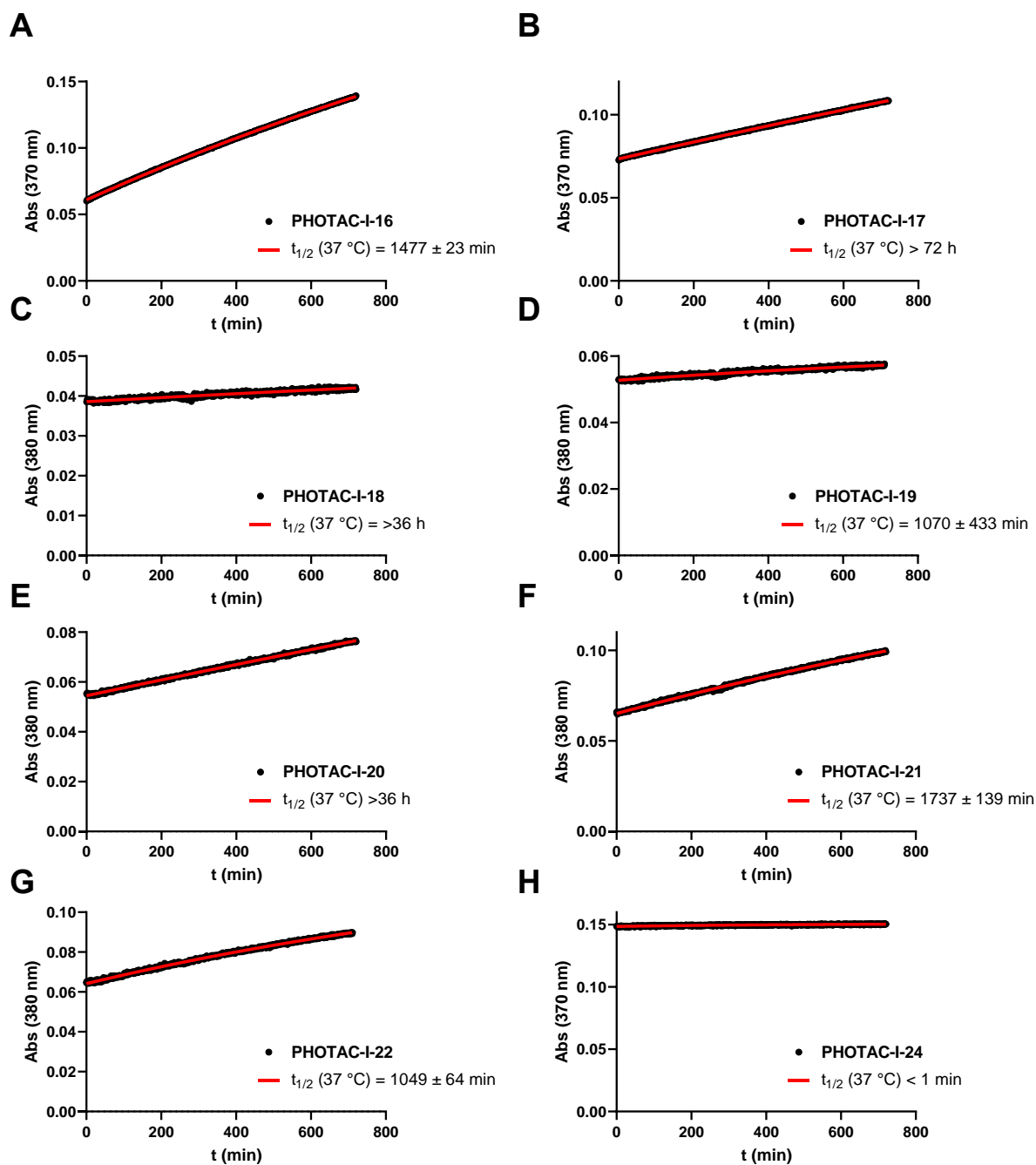


Figure S3.3: Thermal relaxation of **Z-PHOTACs**. Thermal *E*-to-*Z* isomerization of A) **Z-PHOTAC-I-16**, B) **Z-PHOTAC-I-17**, C) **Z-PHOTAC-I-18**, D) **Z-PHOTAC-I-19**, E) **Z-PHOTAC-I-20**, F) **Z-PHOTAC-I-21**, G) **Z-PHOTAC-I-22** or H) **Z-PHOTAC-I-24** in DMSO at 37 °C.

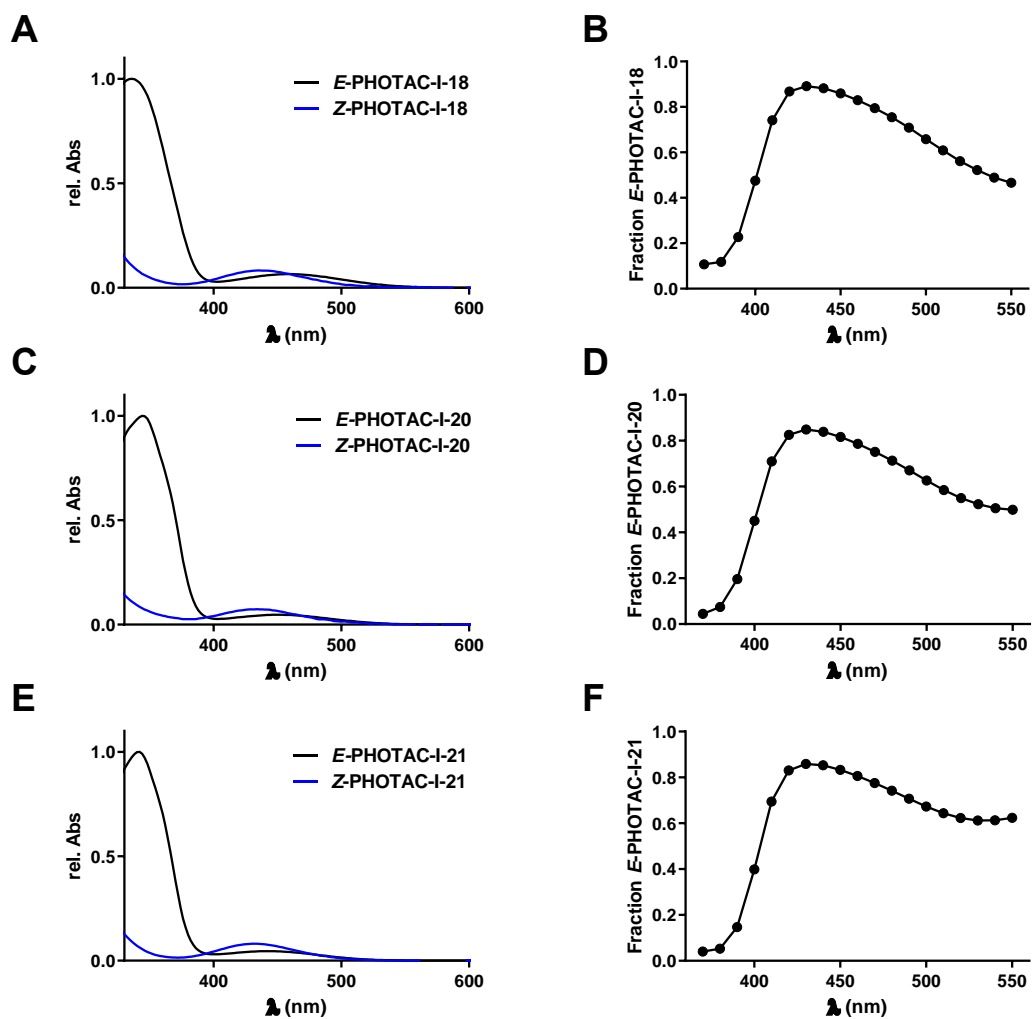


Figure S3.4: A) Isolated absorption spectra of **PHOTAC-I-18** isomers as obtained by LCMS. B) Calculated fraction of ***E*-PHOTAC-I-18** after 5 min irradiation with the indicated wavelength. C) Isolated absorption spectra of **PHOTAC-I-20** isomers as obtained by LCMS. D) Calculated fraction of ***E*-PHOTAC-I-20** after 5 min irradiation with the indicated wavelength. E) Isolated absorption spectra of **PHOTAC-I-21** isomers as obtained by LCMS. F) Calculated fraction of ***E*-PHOTAC-I-21** after 5 min irradiation with the indicated wavelength.

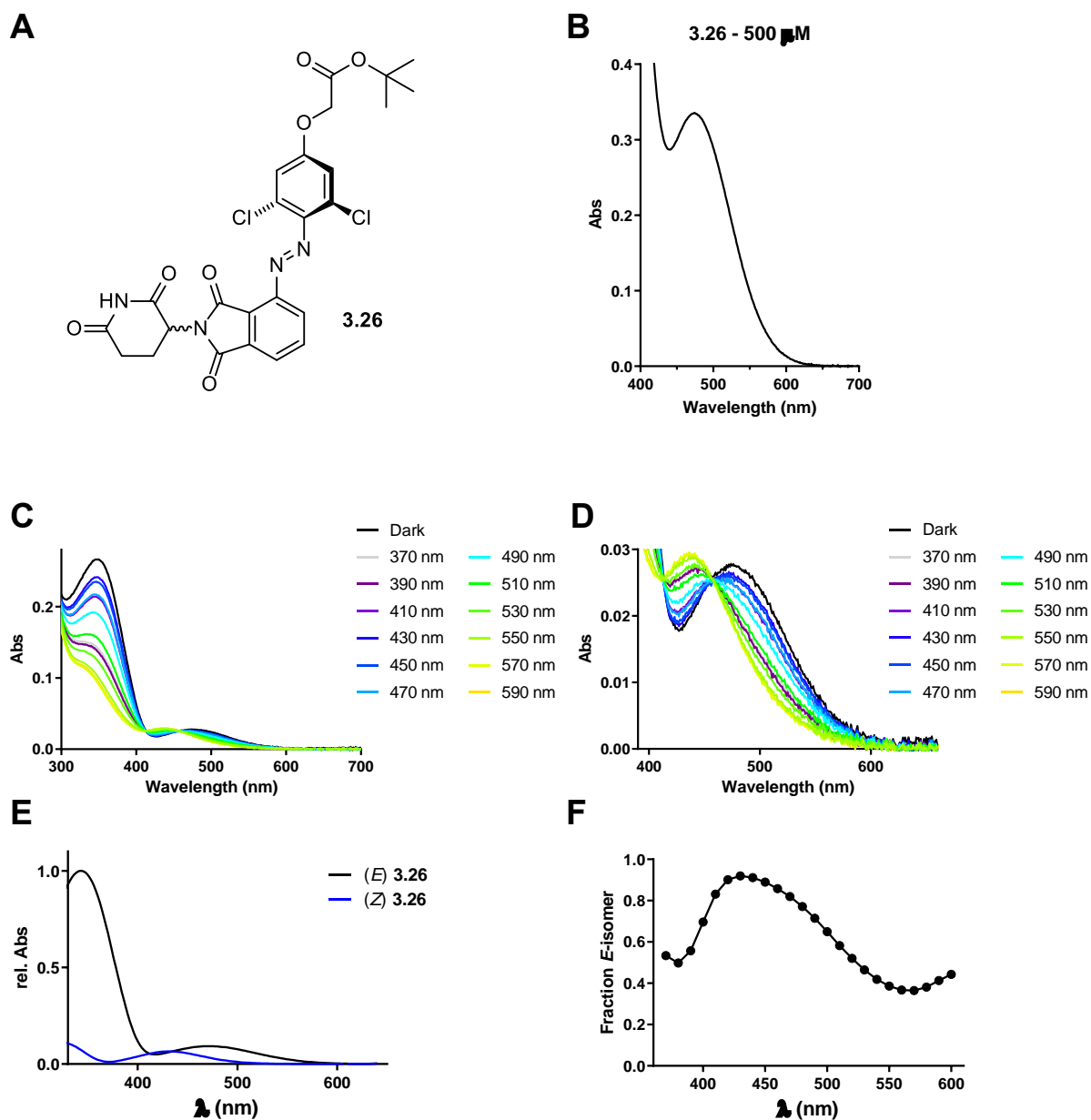


Figure S3.5: Characterization of **3.26**. A) Structure and isomerization of **3.26**. B) Absorption spectrum of a 500 μM **3.26** DMSO solution. C), D) Absorption spectra of **3.26** after 5 min of irradiation with the indicated wavelength. E) Isolated absorption spectra of **3.26** isomers as obtained by LCMS. F) Calculated fraction of **E-3.26** after 5 min irradiation with the indicated wavelength.

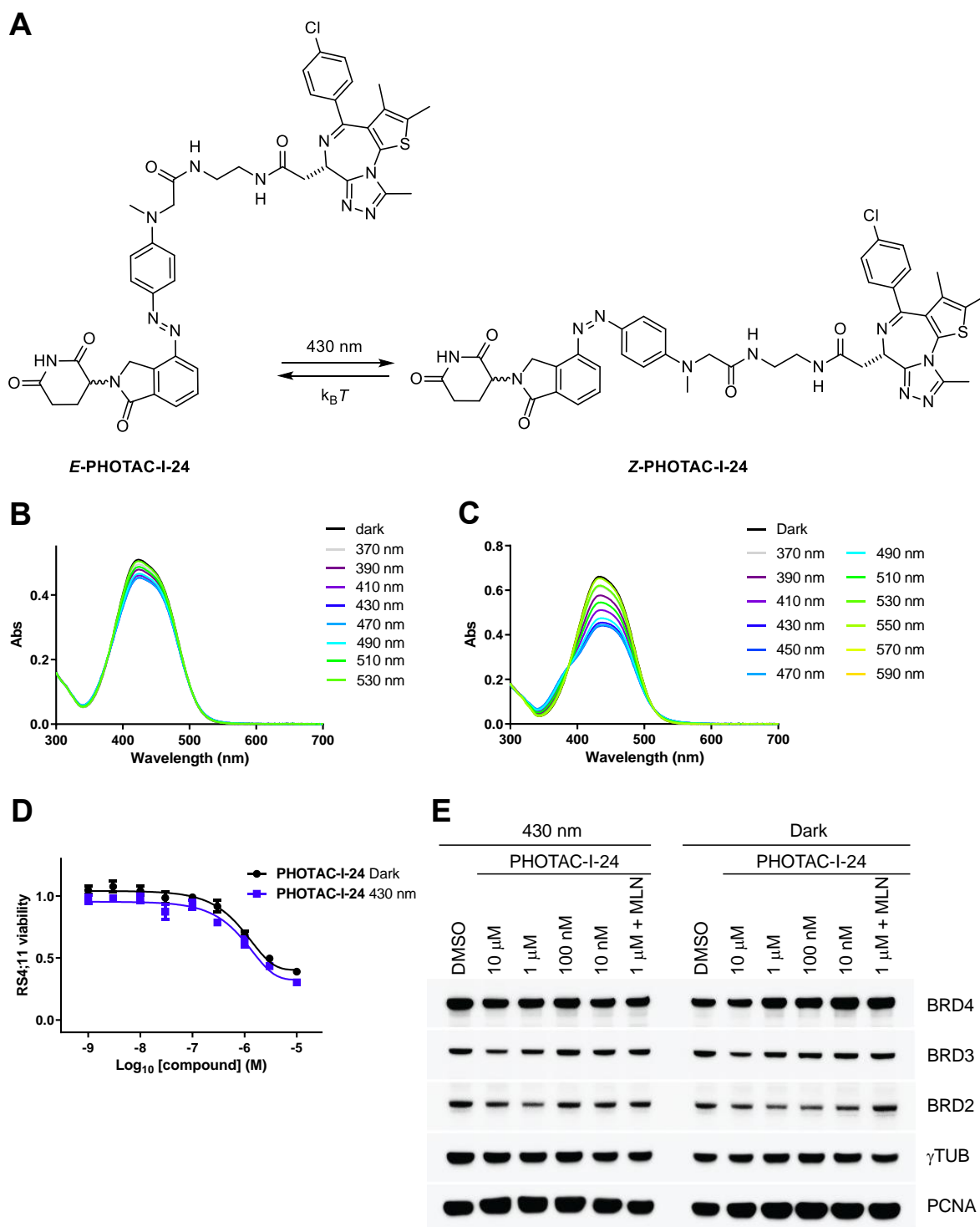


Figure S3.6: Characterization of **PHOTAC-I-24**. A) Structure and isomerization of **PHOTAC-I-24**. B) Absorption spectra of **PHOTAC-I-24** in a 9:1 PBS (pH 7.4):DMSO mixture after 5 min of irradiation with the indicated wavelength. C) Absorption spectra of **PHOTAC-I-24** after 5 min of irradiation with the indicated wavelength in DMSO. D) Viability of RS4;11 cells after treatment with **PHOTAC-I-24** for 72 h in the dark or under pulsed 430 nm irradiation (100 ms every 10 s). E) Immunoblot analysis of RS4;11 cells treated with **PHOTAC-I-24** for 4 h. Cells were either irradiated with pulses of 430 nm light (left, 100 ms every 10 s) or kept in the dark (right). MLN = 1.25 μ M MLN4924.

Methods

Determination of Photophysical properties

UV-Vis spectrometry was performed on a Varian Cary 60 UV-Visible Spectrophotometer using BRAND UV-Cuvette Disposable Spectrophotometer/Photometer Ultra-Micro Cuvettes, BrandTech (10 mm light path). Temperature was controlled using an Agilent Technologies PCB 1500 Water Peltier system and samples were irradiated with a Cairn Research Optoscan Monochromator with Optosource High Intensity Arc Lamp equipped with a 75 W UXL-S50A lamp from USHIO Inc. Japan and set to 15 nm full width at half maximum. Samples were stored and prepared under red light to avoid formation of the *Z*-isomers. 10 mM stock solutions were prepared in the dark and diluted to a final concentration of 25 μ M to measure the UV-VIS spectra of **PHOTACs** following irradiation with different wavelengths for 5 min using the monochromator. Measurement was started from the dark-adapted state, followed by 370 nm and further stepwise wavelength increase up to 600 nm. By increasing the wavelength from low to high *Z*- to *E*-isomerization can be observed, whereas going the reverse direction from high to low wavelength, the PSS might not be reached due to low absorptivity above 500 nm. Generally, due to the limited intensity and spectral width of the monochromator, slightly different PSSs could be generated with a true monochromatic, high-intensity light source. Spectra were recorded in DMSO to avoid any artifacts of aggregation or precipitation.

Thermal relaxation was measured by preirradiating **PHOTACs** with 390 nm light and observing the absorption at a suitable wavelength (370 nm, 380 nm, 430 nm or 500 nm) over up to 12 h at 37 °C in DMSO or solvent mixtures in tightly sealed cuvettes. Half-lives were determined by nonlinear regression using GraphPad Prism Version 9.02.

Separated spectra of the *Z*- and *E*-isomers were obtained from the internal UV-VIS detector of the LCMS by irradiating the sample before injection and were normalized at the isosbestic point. Isomer ratios were calculated in the region of largest absorption difference between 330 and 390 nm from the separated spectra obtained by LCMS and the spectra obtained following irradiation with different wavelengths for 5 min, normalized at the isosbestic point.

LED illumination

For illumination of the cells we used the cell disco system as previously described in the literature.^[28] 5 mm LEDs 390 nm (VL390-5-15), 400 nm (RLS-UV400), 430 nm (VL430-5-15), 525 nm (B5-433-B525) and 565 nm (LED565-03U) were purchased from Roithner Lasertechnik. For viability experiments using 390 nm, cells were preirradiated for 30 s at 390 nm to quickly switch the photoswitches in the active state. Pulsed irradiation was performed using 100 ms pulses every 10 s (unless indicated otherwise) in 96- or 6-well plates, controlled by an Arduino system.

Cell culture

The human acute lymphoblastic leukemia RS4;11 (ATCC[®] CRL1873[™]) cell line was purchased from the American Type Culture Collection and cultured in phenol red-free RPMI1640 medium (Gibco) with 10% fetal bovine serum (FBS) and 1% penicillin/streptomycin (PS) in a humidified incubator at 37 °C with 5% CO₂ in air. For the experiments compounds were serially diluted in phenol red-free RPMI1640 (Gibco) as 2x stock solutions resulting in a final concentration of 1% DMSO during the assay. Azobenzene stocks and dilutions were strictly kept in the dark and prepared under red light conditions.

For immunoblotting analysis, cells (2×10^6 cells for RS4:11) were incubated for the indicated times with PHOTACs, placed in a light-proof box, and preirradiated for 10 s at 390 nm followed by 100 ms pulses every 10 s or were kept in the dark for the indicated duration (commonly 4 h). After incubation, cells were collected in the dark by centrifugation (200 g, 5 min) at 4 °C and the pellets were washed twice with ice cold PBS (1 mL).

Colorimetric MTS Assays

The activity of dehydrogenase enzymes in metabolically active cells, as a quantitative measurement for cytotoxicity and proliferation, was determined by colorimetric measurement of the reduction of [3-(4,5-dimethylthiazol-2-yl)-5-(3-carboxymethoxyphenyl)-2-(4-sulfophenyl)-2H-tetrazolium (MTS) to the formazan product. The absorbance of formazan was measured at 500 nm on a FLUOstar Omega microplate reader (BMG Labtech). Cells were treated with different concentrations of

PHOTACs prepared by serial dilution (usually 10 μM to 1 nM) in triplicates using 1% DMSO as cosolvent, and incubated in a 96-well plate for 72 h. The cells were placed in light-proof boxes and exposed to the lighting conditions specified in the experiment for 72 h. Next, 10 μL of Promega CellTiter 96[®] AQueous One Solution Reagent was added to each well and incubated for further 4-7 hours at 37 °C. The absorbance at 500 nm was measured on a FLUOstar Omega 96-well plate reader (BMG Labtech).

Data was analyzed using GraphPad Prism Version 9.02 (GraphPad Software Inc) and fitted using the [Inhibitor] vs. response -- Variable slope (four parameters) fit. Results represent the mean viability \pm SEM relative to the 1% DMSO treated control.

Immunoblotting Analysis

Cells were lysed in RIPA buffer containing protease and phosphatase inhibitors (cOmplete[™], Mini Protease Inhibitor Cocktail, SigmaAldrich, 4693124001 and Phosphatase Inhibitor Cocktail 3, SigmaAldrich, P0044-1ML) and protein concentration was determined using the BCA method (Thermo Fisher, 23225). Immunoblotting was performed as previously described.^[13,29] Briefly, samples were resolved under denaturing and reducing conditions using 4%–12% Bis-Tris gels (NuPAGE) and transferred to a PDVF membrane (Immobilon-P, Millipore). Membranes were blocked with 5% nonfat dried milk, incubated with primary antibodies overnight at 4°C. After washing the membranes, secondary antibodies coupled with horseradish peroxidase were applied. Immunoreactive bands were visualized using SuperSignal[™] Western Blot Enhancer or SuperSignal[™] West Femto Maximum Sensitivity Substrate (Thermo Fisher Scientific) and the signal was acquired using an ImageQuant LAS 400 (GE). The following antibodies were used:

Antibodies	Source	Identifier
BRD2	Bethyl	A302-583A
BRD3	Bethyl	A302-368A-1
BRD4	Cell Signaling Technology	#13440
c-Myc	Cell Signaling Technology	#5605
PCNA	dako	M0879
γ TUBULIN	Sigma Aldrich	T6557

α TUBULIN	Sigma Aldrich	T6074
β Actin	Cell Signaling Technology	#4970
anti-Rabbit IgG, peroxidase-linked antibody	Thermo Fisher	NA934
anti-Mouse IgG, peroxidase-linked antibody	Thermo Fisher	NA931
anti-goat IgG-HRP	Santa Cruz Biotechnology	sc-2354

Synthetic Procedures and Characterization

General information

The reagents and solvents used in this study were bought from the following chemical suppliers: ABCR, Acros Organics, Alfa Aesar, Ark Pharm, Combi-Blocks, Oakwood, OxChem, Sigma-Aldrich, Strem, Toronto Research Chemicals and were used as purchased.

Dry solvents used in reactions performed under inert atmosphere were obtained by passing the degassed solvents through activated alumina columns.

Column chromatography was carried out on silica gel (60 Å pore size, 40–63 µm, Merck KGaA) using a Teledyne Isco Combiflash EZprep flash purification system.

Thin-layer chromatography (TLC) was performed on glass plates precoated with silica gel (0.25 mm, 60-Å pore size, Merck). TLC plates were visualized by exposure to UV light (254 and 366 nm).

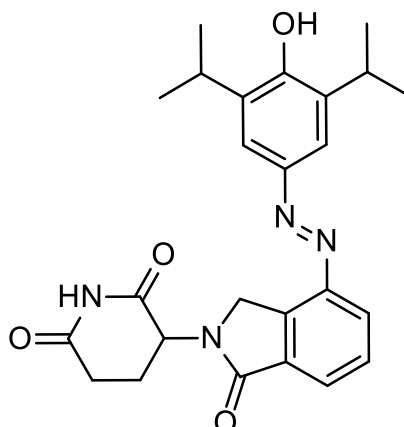
NMR spectra were obtained on a Bruker Avance III HD 400 MHz spectrometer equipped with a CryoProbe™ operating at 400 MHz for ¹H and 100 MHz for ¹³C spectra or on a Bruker AVIII-600 High Performance Digital NMR Spectrometer (600 MHz for ¹H and 150 MHz for ¹³C spectra) with CPTCI-cryoprobehead.

Integration results and multiplets are reported as observed and denoted as follows: s (singlet), d (doublet), t (triplet), q (quartet), p (pentet), h (hextet), sept (septet) and m (multiplet) and as combinations thereof.

High-resolution mass spectra (HRMS) were recorded on an Agilent Technologies 6224 Accurate-Mass time-of-flight spectrometer with either atmospheric pressure chemical ionization (APCI) or electrospray ionization (ESI) ionization sources.

LCMS were measured on an Agilent Technologies 1260 II Infinity connected to an Agilent Technologies 6120 Quadrupole mass spectrometer with APCI ionization source. Elution was performed using a gradient from 5:95% to 100:0% MeCN:H₂O with 0.1% formic acid over 5 min, if not indicated otherwise. Separated isomer spectra of azobenzenes were obtained by irradiation of the LCMS sample prior to injection.

3-(4-((4-Hydroxy-3,5-diisopropylphenyl)diazenyl)-1-oxoisindolin-2-yl)piperidine-2,6-dione (3.1)



Lenalidomide (519 mg, 2.00 mmol, 1.0 eq.) was dissolved in 1 M HCl (20 mL) and concentrated aq. HBF₄ (2 mL) was added to the mixture. After completely dissolving the starting material, 2 M NaNO₂ (1.1 mL) was added to the solution at 0 °C. After stirring for 1 h the solution was added dropwise into a mixture of propofol (357 mg, 2.00 mmol, 1.0 eq.) in H₂O (50 mL), MeOH (20 mL), NaHCO₃ (4.15 g, 49.37 mmol, 24.7 eq.) and Na₂CO₃ (5.18 g, 49.37 mmol, 24.7 eq.) and stirred for an additional 1 h at 0 °C. The reaction was extracted with EtOAc (7x 50 mL) and washed once with brine (1x 50 mL). The organic phase was dried over Na₂SO₄ and concentrated under reduced pressure. Purification of the resulting crude product by flash column chromatography (CH₂Cl₂/MeOH gradient, 0 → 10% MeOH) gave **3.1** (519 mg, 1.16 mmol, 58%) as a yellow solid.

R_f = 0.30 [CH₂Cl₂: MeOH, 19:1].

¹H NMR (400 MHz, DMSO-d₆) δ = 11.01 (s, 1H), 9.12 (s, 1H), 8.13 (d, J = 7.8 Hz, 1H), 7.85 (d, J = 7.5 Hz, 1H), 7.74 (t, J = 6.8 Hz, 1H), 7.67 (s, 2H), 5.13 (dd, J = 13.0, 4.7 Hz, 1H), 4.81 (d, J = 18.9 Hz, 1H), 4.70 (d, J = 18.9 Hz, 1H), 3.44 – 3.32 (m, 2H), 2.92 (ddd, J = 17.9, 13.3, 5.4 Hz, 1H), 2.67 – 2.52 (m, 2H), 2.11 – 2.00 (m, 1H), 1.24 (d, J = 6.8 Hz, 12H) ppm.

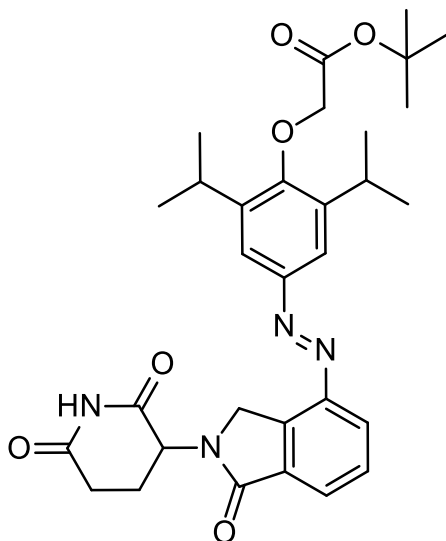
¹³C NMR (100 MHz, DMSO-d₆) δ = 172.93, 171.05, 167.32, 155.35, 146.75, 145.96, 135.92, 134.48, 129.44, 127.97, 127.39, 124.39, 118.71, 51.98, 48.30, 31.31, 26.40, 22.77, 22.29 ppm.

HRMS (ESI): calcd. For C₂₅H₂₇N₄O₄⁺: 449.2183 m/z [M+H]⁺.

Found: 449.2188 m/z [M+H]⁺.

LCMS (ESI): t_{ret} = 4.05 min. 449 m/z [M+H]⁺.

***tert*-Butyl-2-(4-((2-(2,6-dioxopiperidin-3-yl)-1-oxoindolin-4-yl)diazenyl)-2,6-diisopropylphenoxy)acetate (**3.2**)**



To *tert*-Butyl bromoacetate (52.4 mg, 269 μmol , 1.2 eq., 40 μL) was added dry DMF (10 mL), **3.1** (101 mg, 224 μmol , 1.0 eq.) and *i*Pr₂NEt (43.8 mg, 336 μmol , 1.5 eq., 59 μL) at room temperature. After stirring for 3 h, the mixture was diluted with EtOAc (20 mL), separated against NaHCO₃ (30 mL), extracted with EtOAc (3x 30 mL), and washed with 10% aq. LiCl (3x 30 mL) and brine (2x 30 mL). The reaction was concentrated under reduced pressure. Purification of the resulting crude product by flash column chromatography (Hexane/EtOAc gradient, 20 \rightarrow 100% EtOAc) gave **3.2** (83.0 mg, 0.147 mmol, 66%) as a yellow solid.

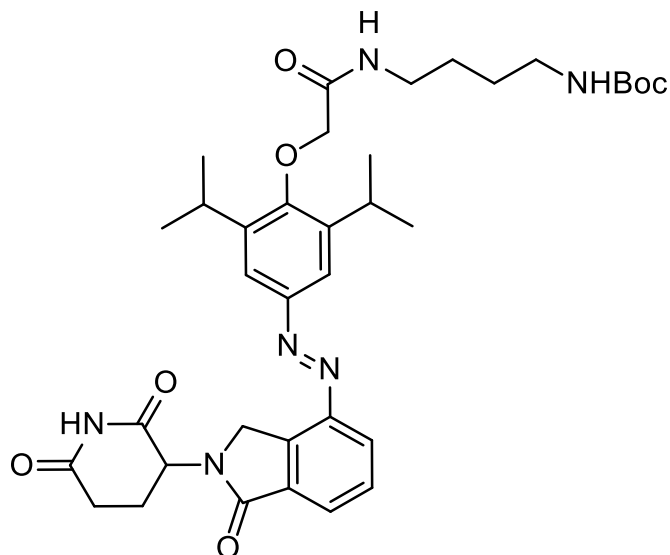
R_f = 0.29 [EtOAc:Hexane, 1:1].

¹H NMR (400 MHz, DMSO-d₆) δ = 11.01 (d, J = 2.8 Hz, 1H), 8.21 (d, J = 7.7 Hz, 1H), 7.91 (d, J = 7.5 Hz, 1H), 7.79 (t, J = 7.7 Hz, 1H), 7.72 (s, 2H), 5.13 (dd, J = 13.1, 5.1 Hz, 1H), 4.82 (d, J = 19.0 Hz, 1H), 4.72 (d, J = 19.0 Hz, 1H), 4.41 (s, 2H), 3.47 – 3.32 (m, 2H), 2.92 (ddd, J = 17.6, 13.3, 5.3 Hz, 1H), 2.69 – 2.50 (m, 2H), 2.11 – 2.02 (m, 1H), 1.49 (s, 9H), 1.25 (d, J = 6.6 Hz, 12H) ppm.

¹³C NMR (100 MHz, DMSO-d₆) δ = 172.92, 171.00, 167.41, 167.17, 156.24, 149.45, 146.55, 142.82, 134.64, 133.80, 129.57, 128.22, 125.30, 118.80, 81.51, 71.73, 51.99, 48.30, 31.29, 27.73, 26.31, 23.66, 22.28 ppm.

HRMS (ESI): calcd. For C₃₂H₄₂N₄O₇Na⁺: 617.2951 m/z [M+MeOH+Na]⁺.
 Found: 617.2942 m/z [M+MeOH+Na]⁺.

LCMS (ESI): t_{ret} = 4.32 min. 563 m/z [M+H]⁺.

***tert*-Butyl-2-(4-((2-(2,6-dioxopiperidin-3-yl)-1-oxoisindolin-4-yl)diazenyl)-2,5-dimethoxyphenoxy)acetate (3.3)**

3.2 (84.2 mg, 150 μmol , 1.0 eq.) was dissolved in a CH_2Cl_2 :TFA mixture (1:1; 4 mL). After 6 h the reaction was concentrated under reduced pressure. The mixture was triturated with MeOH, concentrated, and dried under high vacuum for 24 h. The crude solid was dissolved in dry DMF (5 mL) at room temperature and HATU (86.1 mg, 227 μmol , 2.0 eq) was added to the mixture. After 5 min of stirring *N*-Boc-1,4-diaminobutane (56.3 mg, 299 μmol , 2.0 eq., 57 μL) and *i*Pr₂NEt (599 μmol , 4.0 eq., 104 μL) were added to the mixture and stirred for additional 12 h at room temperature. The reaction was diluted with EtOAc (20 mL), separated against a 5% aq. LiCl solution (20 mL), extracted with EtOAc (2x 20 mL), and washed with 10% LiCl (2x 20 mL) and brine (2x 20 mL). The combined organic phase was dried over Na_2SO_4 and concentrated under reduced pressure. Purification of the resulting crude product by flash column chromatography (CH_2Cl_2 /MeOH gradient, 0-20% MeOH) gave **3.3** (60 mg, 88.7 μmol , 59%) as a yellow solid.

$R_f = 0.33$ [CH_2Cl_2 :MeOH, 19:1].

¹H NMR (400 MHz, DMSO) $\delta = 11.02$ (s, 1H), 8.28 – 8.18 (m, 2H), 7.92 (d, $J = 7.5$ Hz, 1H), 7.80 (t, $J = 7.7$ Hz, 1H), 7.74 (s, 2H), 6.82 (t, $J = 5.7$ Hz, 1H), 5.14 (dd, $J = 13.1, 5.1$ Hz, 1H), 4.83 (d, $J = 19.0$ Hz, 1H), 4.72 (d, $J = 19.0$ Hz, 1H), 4.25 (s, 2H), 3.38 – 3.36 (m, 2H), 3.19 (q, $J = 6.4$ Hz, 2H), 2.95 (m, 3H), 2.69 – 2.54 (m, 2H), 2.11 – 2.03 (m, 1H), 1.46 (m, 4H), 1.38 (s, 9H), 1.27 (d, $J = 6.8$ Hz, 12H) ppm.

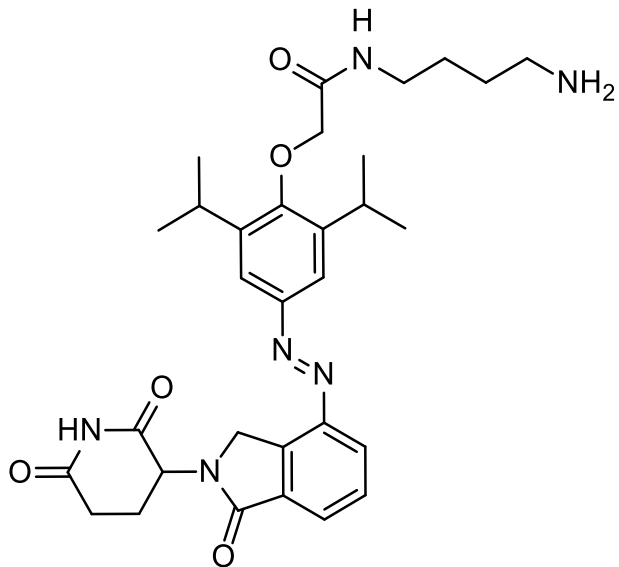
^{13}C NMR (100 MHz, DMSO) δ = 172.95, 171.02, 167.20, 167.00, 164.33, 155.64, 149.53, 146.58, 142.88, 134.62, 133.82, 129.60, 128.34, 125.34, 118.89, 77.37, 73.26, 52.02, 48.38, 40.43, 38.09, 31.30, 28.30, 27.02, 26.55, 26.34, 23.78, 22.29 ppm.

HRMS (ESI): calcd. For $\text{C}_{36}\text{H}_{48}\text{N}_6\text{O}_7^+$: 677.3663 m/z $[\text{M}+\text{H}]^+$.

Found: 677.3644 m/z $[\text{M}+\text{H}]^+$.

LCMS (ESI): $t_{\text{ret}} = 4.31$ min. 621 m/z $[\text{M}+\text{H}-t\text{-Butyl}]^+$.

***N*-(4-Aminobutyl)-2-(4-((2-(2,6-dioxopiperidin-3-yl)-1-oxoisindolin-4-yl)diazenyl)-2,6-diisopropylphenoxy)acetamide (3.4)**



3.3 (67.2 mg, 99.3 μmol) was dissolved in a CH_2Cl_2 :TFA mixture (1:1; 4 mL). After 6 h the reaction was concentrated under reduced pressure. The mixture was triturated with MeOH, concentrated, and then dried under high vacuum for 48 h. **3.4** (56.0 mg, 97.1 μmol , 98%) was obtained as orange solid with traces of residual TFA.

$R_f = 0.13$ [CH_2Cl_2 +1% NEt_3 :MeOH, 5:1].

^1H NMR (400 MHz, DMSO) $\delta = 11.02$ (s, 1H), 8.32 (t, $J = 5.9$ Hz, 1H), 8.21 (d, $J = 7.4$ Hz, 1H), 7.92 (d, $J = 7.4$ Hz, 1H), 7.79 (t, $J = 7.7$ Hz, 1H), 7.74 (s, 2H), 7.74 – 7.66 (m, 2H), 5.14 (dd, $J = 13.2, 5.1$ Hz, 1H), 4.82 (d, $J = 19.0$ Hz, 1H), 4.71 (d, $J = 19.0$ Hz, 1H), 4.26 (s, 2H), 3.42 – 3.27 (m, 2H), 3.22 (q, $J = 6.2$ Hz, 2H), 2.93 (ddd, $J = 17.6, 13.4, 5.4$ Hz, 1H), 2.84 (q, $J = 6.2$ Hz, 2H), 2.68 – 2.52 (m, 2H), 2.06 (ddd, $J = 14.2, 6.6, 4.1$ Hz, 1H), 1.61 – 1.51 (m, $J = 4.8, 3.9$ Hz, 4H), 1.27 (d, $J = 6.8$ Hz, 12H) ppm.

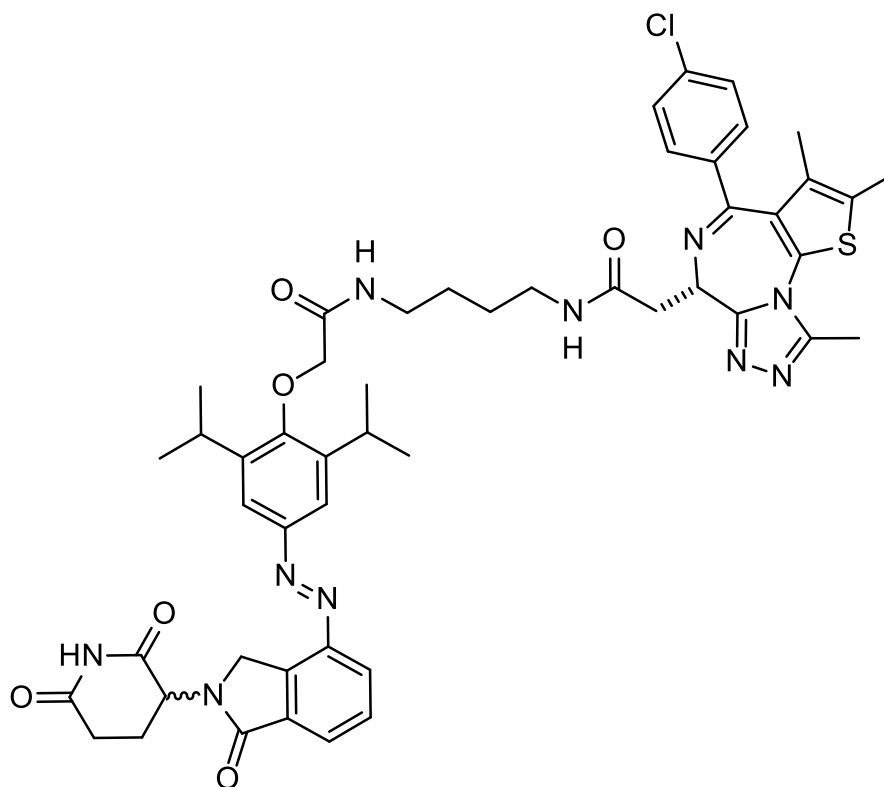
^{13}C NMR (100 MHz, DMSO) $\delta = 172.92, 171.01, 167.16, 167.14, 155.48, 149.55, 146.55, 142.84, 134.60, 133.81, 129.59, 128.30, 125.35, 118.89, 73.20, 51.98, 48.30, 38.58, 37.69, 31.29, 26.31, 26.15, 24.46, 23.77, 22.28$ ppm.

HRMS (ESI): calcd. For $\text{C}_{31}\text{H}_{40}\text{N}_6\text{O}_5^+$: 577.3133 m/z $[\text{M}+\text{H}]^+$.

Found: 577.3132 m/z $[\text{M}+\text{H}]^+$.

LCMS (ESI): $t_{\text{ret}} = 2.46$ min. 577 m/z $[\text{M}+\text{H}]^+$.

2-((S)-4-(4-chlorophenyl)-2,3,9-trimethyl-6H-thieno[3,2-f][1,2,4]triazolo[4,3-a][1,4]diazepin-6-yl)-N-(4-(2-(4-((2-(2,6-dioxopiperidin-3-yl)-1-oxoisindolin-4-yl)diazenyl)-2,6-diisopropylphenoxy)acetamido)butyl)acetamide (PHOTC-I-14)



Into a round bottom flask with dry (+)-JQ acid (9.5 mg, 23.7 μmol , 1 eq.) were added **3.4** (27.3 mg, 47.4 μmol , 2 eq.) and HATU (13.5 mg, 35.5 μmol , 1.5 eq.) under nitrogen atmosphere. The solids were dissolved in dry DMF (1 mL). After addition of *i*-Pr₂NEt (166 μmol , 7.0 eq., 29 μL) the reaction was stirred for 24 h at room temperature. The mixture was then diluted with EtOAc (20 mL), separated against 10% LiCl (30 mL), extracted with EtOAc (2x 20 mL), washed twice with 10% LiCl (2x 20 mL) and brine (2x 20 mL). The reaction was dried over Na₂SO₄ and concentrated under reduced pressure. Purification of the resulting crude product by flash column chromatography (CH₂Cl₂/MeOH gradient, 0→20% MeOH) gave **PHOTAC-I-14** (14.0 mg, 14.6 μmol , 62%) as an orange solid.

$R_f = 0.09$ [CH₂Cl₂:MeOH, 19:1].

¹H NMR (400 MHz, CDCl₃) δ = 8.37 (d, *J* = 4.1 Hz, 1H), 8.20 (d, *J* = 7.8 Hz, 1H), 7.99 (d, *J* = 7.5 Hz, 1H), 7.70 (t, *J* = 7.7 Hz, 1H), 7.66 (s, 2H), 7.42 (d, *J* = 8.3 Hz, 2H), 7.34 (d, *J* = 8.2 Hz, 2H), 7.03 (t, *J* = 6.0 Hz, 1H), 6.98 (t, *J* = 5.8 Hz, 1H), 5.23 (dd, *J* = 13.4, 5.0 Hz, 1H), 4.85 (d, *J* = 17.9 Hz, 1H), 4.73 (d, *J* = 18.0 Hz, 1H), 4.67 (t, *J* = 7.0 Hz,

1H), 4.32 (s, 2H), 3.61 (dd, J = 14.4, 8.0 Hz, 1H), 3.49 – 3.32 (m, 5H), 3.24 (hept, J = 7.0 Hz, 2H), 2.98 – 2.79 (m, 2H), 2.68 (s, 3H), 2.55 – 2.45 (m, 1H), 2.40 (s, 3H), 2.29 – 2.20 (m, 1H), 1.72 – 1.61 (m, 7H), 1.31 (dd, J = 6.9, 1.7 Hz, 12H) ppm.

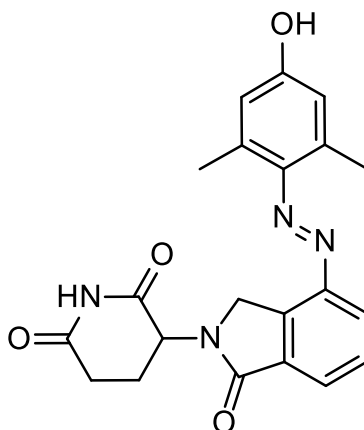
¹³C NMR (100 MHz, CDCl₃) δ = 171.28, 170.43, 169.66, 168.67, 168.29, 164.66, 155.41, 154.88, 150.43, 150.23, 147.14, 142.94, 137.45, 136.02, 134.20, 133.38, 132.16, 131.64, 131.27, 130.59, 130.18, 129.66, 129.54, 128.96, 126.09, 119.41, 73.10, 54.45, 52.18, 48.34, 39.31, 39.09, 38.90, 31.76, 27.20, 26.96, 24.08, 23.54, 14.54, 13.28, 11.89 ppm.

HRMS (APCI): calcd. For C₅₀H₅₆ClN₁₀O₆S⁺: 959.3788 m/z [M+H]⁺.

Found: 959.3780 m/z [M+H]⁺.

LCMS (ESI): t_{ret} = 4.44 min. 959 m/z [M+H]⁺.

3-(4-((4-Hydroxy-2,6-dimethylphenyl)diazenyl)-1-oxoisindolin-2-yl)piperidine-2,6-dione (3.5)



Lenalidomide (519 mg, 2.00 mmol, 1.0 eq.) was dissolved in 1 M HCl (30 mL). Concentrated aqueous HBF₄ (2 mL) was added to the mixture. After completely dissolving of the starting material, 2 M NaNO₂ solution (1.1 mL) was added to the mixture at 0 °C. After stirring for 1 h the solution was added dropwise into a mixture of 3,5-Dimethylphenol (244 mg, 2.00 mmol, 1.0 eq.) in H₂O (50 mL), MeOH (20 mL), NaHCO₃ (4.15 g, 49.4 mmol, 24.7 eq.) and Na₂CO₃ (5.18 g, 49.4 mmol, 24.7 eq.) and stirred for an additional 1 h at 0 °C. The reaction was extracted with EtOAc (7x 50 mL) and washed once with brine (1x 50 mL). The organic phase was dried over Na₂SO₄ and concentrated under reduced pressure. Purification of the resulting crude product by flash column chromatography (CH₂Cl₂/MeOH gradient, 0 → 10% MeOH) gave **3.5** (706 mg, 1.80 mmol, 90%) as a red solid.

R_f = 0.30 [CH₂Cl₂:MeOH, 19:1].

¹H NMR (400 MHz, DMSO) δ = 11.00 (s, 1H), 10.11 (d, J = 1.2 Hz, 1H), 8.08 (d, J = 7.8 Hz, 1H), 7.85 (d, J = 7.4 Hz, 1H), 7.75 (t, J = 7.6 Hz, 1H), 6.63 (s, 2H), 5.15 (dd, J = 13.3, 5.1 Hz, 1H), 4.74 (d, J = 18.5 Hz, 1H), 4.61 (d, J = 18.5 Hz, 1H), 2.92 (ddd, J = 18.2, 13.6, 5.4 Hz, 1H), 2.69 – 2.41 (m, 2H), 2.46 (s, 6H), 2.11 – 2.00 (m, 1H) ppm.

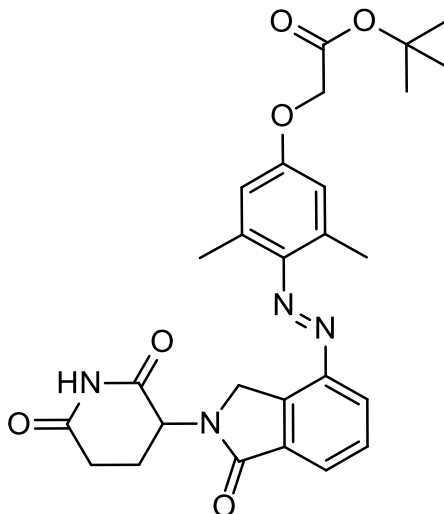
¹³C NMR (100 MHz, DMSO) δ = 172.88, 171.00, 167.37, 159.21, 147.20, 142.71, 136.12, 134.24, 133.59, 129.48, 126.45, 124.27, 116.31, 51.80, 48.19, 31.24, 22.42, 20.94 ppm.

HRMS (APCI): calcd. for C₂₁H₂₁N₄O₅⁺: 393.1557 m/z [M+H]⁺.

Found: 393.1560 m/z [M+H]⁺.

LCMS (ESI): t_{ret} = 3.30 min. 393 m/z [M+H]⁺.

***tert*-Butyl-2-(4-((2-(2,6-dioxopiperidin-3-yl)-1-oxoisindolin-4-yl)diazenyl)-3,5-dimethylphenoxy)acetate (3.6)**



To *tert*-Butyl bromoacetate (150 mg, 769 μmol , 1.2 eq., 114 μL) was added dry DMF (6 mL), **3.5** (250 mg, 637 μmol , 1.0 eq.) and *i*Pr₂NEt (1.27 mmol, 2.0 eq., 222 μL) at room temperature. After stirring for 2.5 h, the mixture was diluted with EtOAc (100 mL), separated against NaHCO₃ (50 mL), extracted with EtOAc (3x 50 mL), and washed with 10% LiCl (3x 50 mL) and brine (2x 50 mL). The mixture was concentrated under reduced pressure. Purification of the resulting crude product by flash column chromatography (Hexane/EtOAc gradient, 20 \rightarrow 100% EtOAc) gave **3.6** (184 mg, 363 μmol , 57%) as an orange solid.

R_f = 0.40 [EtOAc:Hexane 4:1].

¹H NMR (400 MHz, DMSO) δ = 11.00 (s, 1H), 8.13 (d, *J* = 7.8 Hz, 1H), 7.89 (d, *J* = 7.4 Hz, 1H), 7.78 (t, *J* = 7.6 Hz, 1H), 6.80 (s, 2H), 5.16 (dd, *J* = 13.3, 5.2 Hz, 1H), 4.79 – 4.72 (m, 3H), 4.63 (d, *J* = 18.7 Hz, 1H), 2.92 (ddd, *J* = 18.2, 13.6, 5.4 Hz, 1H), 2.67 – 2.42 (m, 2H), 2.48 (s, 6H), 2.10 – 2.01 (m, 1H), 1.45 (s, 9H) ppm.

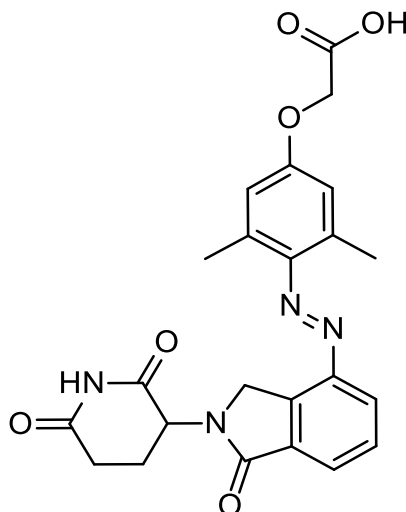
¹³C NMR (100 MHz, DMSO) δ = 172.88, 170.97, 167.54, 167.28, 158.35, 147.02, 144.20, 135.23, 134.30, 133.66, 129.55, 127.02, 124.80, 115.27, 81.56, 64.98, 51.81, 48.21, 31.24, 27.71, 22.38, 20.59 ppm.

HRMS (ESI): calcd. for C₂₇H₃₀N₄O₆Na⁺: 529.2058 m/z [M+Na]⁺;

Found: 529.2050 m/z [M+Na]⁺.

LCMS (ESI): t_{ret} = 4.36 min. 507 m/z [M+H]⁺.

2-(4-((2-(2,6-Dioxopiperidin-3-yl)-1-oxoisindolin-4-yl)diazenyl)-3,5-dimethylphenoxy)acetic acid (3.7)



3.6 (110.0 mg, 217.0 μmol , 1 eq.) was dissolved in a CH_2Cl_2 :TFA mixture (1:1; 4 mL). After 4 h the reaction was concentrated under reduced pressure. The mixture was triturated with MeOH, concentrated, and then dried under high vacuum for 48 h. **3.7** (96.00 mg, 213.0 μmol , 98%) was obtained as red solid with traces of residual TFA.

$R_f = 0.15$ [CH_2Cl_2 :MeOH, 9:1].

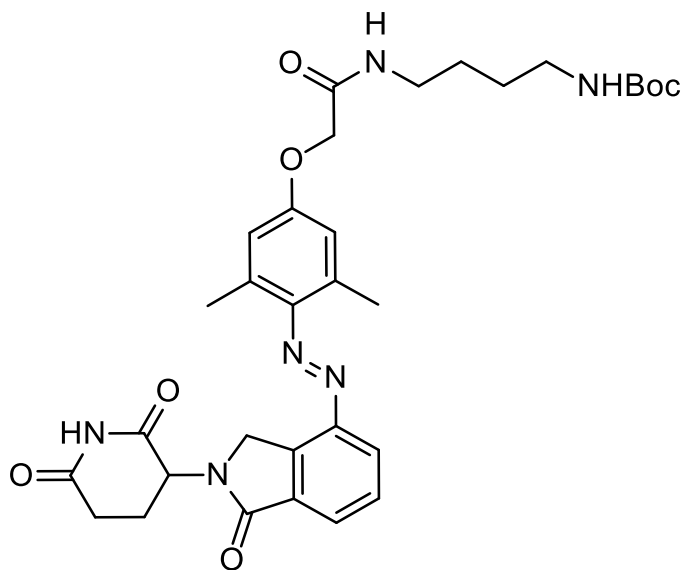
$^1\text{H NMR}$ (400 MHz, DMSO) $\delta = 10.99$ (s, 1H), 8.13 (d, $J = 7.8$ Hz, 1H), 7.89 (d, $J = 7.4$ Hz, 1H), 7.77 (t, $J = 7.7$ Hz, 1H), 6.81 (s, 2H), 5.15 (dd, $J = 13.2, 5.1$ Hz, 1H), 4.80 – 4.72 (m, 3H), 4.63 (d, $J = 18.6$ Hz, 1H), 2.92 (ddd, $J = 18.1, 13.5, 5.4$ Hz, 1H), 2.70 – 2.42 (m, 2H), 2.48 (s, 6H), 2.06 (dd, $J = 13.2, 6.0$ Hz, 1H) ppm.

HRMS (ESI): calcd. for $\text{C}_{23}\text{H}_{23}\text{N}_4\text{O}_6^+$: 451.1618 m/z $[\text{M}+\text{H}]^+$.

Found: 451.1597 m/z $[\text{M}+\text{H}]^+$.

LCMS (ESI): $t_{\text{ret}} = 4.16$ min. 451 m/z $[\text{M}+\text{H}]^+$.

***tert*-Butyl-(4-(2-(4-((2-(2,6-dioxopiperidin-3-yl)-1-oxoisindolin-4-yl)diazenyl)-3,5-dimethylphenoxy)acetamido)butyl)carbamate (3.8)**



3.7 (90.0 mg, 200 μ mol, 1.0 eq.) and HATU (114 mg, 300 μ mol, 1.5 eq.) were dissolved in dry DMF (5 mL) at room temperature. After 5 minutes of stirring *N*-Boc-1,4-diaminobutane (75.2 mg, 400 μ mol, 2.0 eq., 76 μ L) and *i*Pr₂NEt (604 μ mol, 4.0 eq., 105 μ L) were added to the mixture and stirred for an additional 12 h at room temperature. The reaction was diluted with EtOAc (20 mL), separated against 5% LiCl (20 mL), extracted with EtOAc (3x 20 mL) and washed with 10% LiCl (3x 20 mL) and brine (2x 20 mL). The combined organic phase was dried over Na₂SO₄ and concentrated under reduced pressure. Purification of the resulting crude product by flash column chromatography (CH₂Cl₂/MeOH gradient, 0-20% MeOH) gave **3.8** (76.0 mg, 122 μ mol, 61%) as a yellow solid.

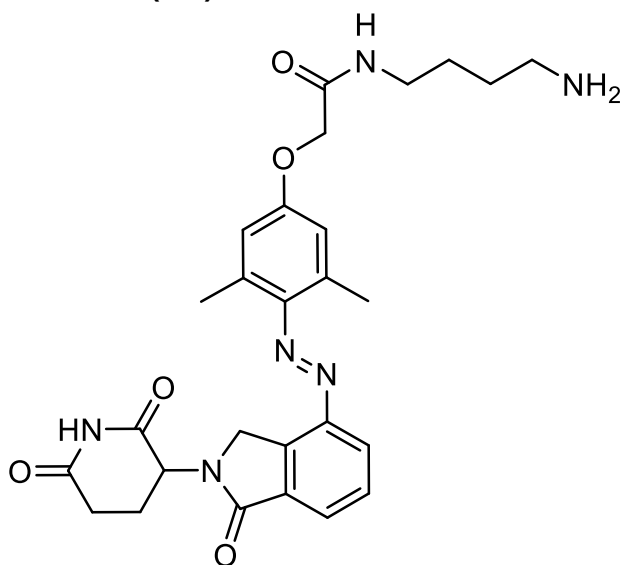
$R_f = 0.33$ [CH₂Cl₂:MeOH, 19:1].

¹H NMR (400 MHz, DMSO) $\delta = 11.00$ (s, 1H), 8.14 – 8.07 (m, 2H), 7.89 (d, *J* = 7.4 Hz, 1H), 7.77 (t, *J* = 7.6 Hz, 1H), 6.84 (s, 2H), 6.77 (t, *J* = 5.8 Hz, 1H), 5.15 (dd, *J* = 13.2, 5.1 Hz, 1H), 4.75 (d, *J* = 18.6 Hz, 1H), 4.63 (d, *J* = 18.6 Hz, 1H), 4.54 (s, 2H), 3.13 (q, *J* = 6.4 Hz, 2H), 2.97 – 2.86 (m, 3H), 2.70 – 2.57 (m, 1H), 2.48 (s, 6H), 2.47 – 2.38 (m, 1H), 2.10 – 2.00 (m, 1H), 1.46 – 1.38 (m, 4H), 1.36 (s, 9H) ppm.

¹³C NMR (100 MHz, CDCl₃) $\delta = 171.22, 169.61, 168.74, 167.98, 157.60, 156.21, 147.43, 145.63, 135.60, 133.99, 133.33, 129.56, 128.50, 125.88, 115.54, 79.49, 67.36, 52.17, 48.44, 40.14, 38.87, 31.72, 28.54, 27.61, 26.91, 23.59, 20.97$ ppm.

HRMS (APCI):	calcd. For C ₃₂ H ₄₁ N ₆ O ₇ ⁺ :	621.3031 m/z [M+H] ⁺ .
	Found:	621.3047 m/z [M+H] ⁺ .
LCMS (ESI):	t _{ret} = 3.80 min.	565 m/z [M+H- <i>t</i> -Butyl] ⁺ .

***N*-(4-Aminobutyl)-2-(4-((2-(2,6-dioxopiperidin-3-yl)isoindolin-4-yl)diazenyl)-3,5-dimethylphenoxy)acetamide (3.9)**



3.8 (50.0 mg, 80.6 μmol, 1.0 eq.) was dissolved in a CH₂Cl₂:TFA mixture (1:1; 4 mL). After 6 h the reaction was concentrated under reduced pressure. The mixture was triturated with MeOH, concentrated, and then dried under high vacuum for 48 h. **3.9** (41.0 mg, 78.8 μmol, 98%) was obtained as red solid with traces of residual TFA.

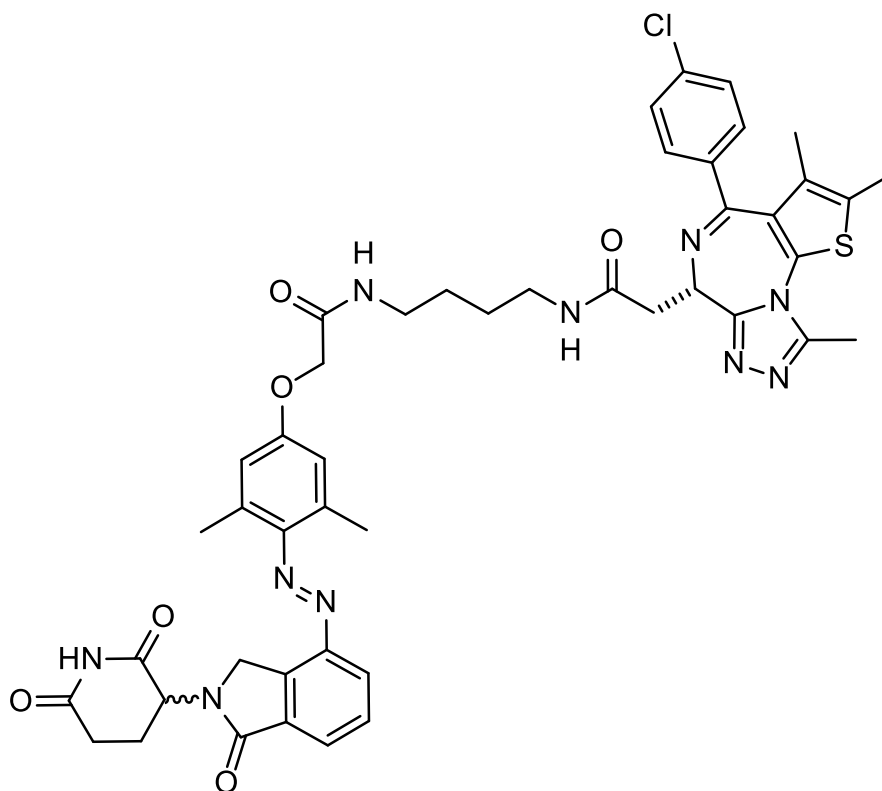
R_f = 0.15 [CH₂Cl₂:MeOH, 2:1].

¹H NMR (400 MHz, DMSO) δ = 11.00 (s, 1H), 8.20 (t, J = 5.9 Hz, 1H), 8.13 (d, J = 7.8 Hz, 1H), 7.90 (d, J = 7.5 Hz, 1H), 7.78 (t, J = 7.7 Hz, 1H), 7.70 (s, 2H), 6.86 (s, 2H), 5.16 (dd, J = 13.3, 4.7 Hz, 1H), 4.75 (d, J = 18.6 Hz, 1H), 4.63 (d, J = 18.7 Hz, 1H), 4.56 (s, 2H), 3.17 (q, J = 8.8, 7.5 Hz, 2H), 2.99 – 2.75 (m, 3H), 2.70 – 2.42 (m, 2H), 2.49 (s, 6H), 2.12 – 2.00 (m, 1H), 1.60 – 1.47 (m, 4H) ppm.

¹³C NMR (100 MHz, DMSO) δ = 172.91, 171.00, 167.30, 167.28, 158.36, 147.02, 144.29, 135.25, 134.35, 133.67, 129.60, 126.99, 124.89, 115.52, 66.94, 51.82, 48.21, 38.59, 37.66, 31.26, 26.10, 24.46, 22.42, 20.64 ppm.

HRMS (APCI):	calcd. For C ₂₇ H ₃₃ N ₆ O ₅ ⁺ :	521.2507 m/z [M+H] ⁺ .
	Found:	521.2503 m/z [M+H] ⁺ .
LCMS (ESI):	t _{ret} = 2.75 min.	507 m/z [M+H] ⁺ .

2-((S)-4-(4-Chlorophenyl)-2,3,9-trimethyl-6H-thieno[3,2-f][1,2,4]triazolo[4,3-a][1,4]diazepin-6-yl)-N-(4-(2-(4-((2-(2,6-dioxopiperidin-3-yl)-1-oxoisindolin-4-yl)diazenyl)-3,5-dimethylphenoxy)acetamido)butyl)acetamide (PHOTAC-I-16)



Into a round bottom flask with dry (+)-JQ1 free acid (9.5 mg, 23.7 μmol , 1 eq.) were added **3.9** (27.3 mg, 47.4 μmol , 2 eq.) and HATU (13.5 mg, 35.5 μmol , 1.5 eq.) under nitrogen atmosphere. The solids were dissolved in dry DMF (1 mL). After addition of *i*-Pr₂NEt (166 μmol , 7.0 eq., 29 μL) the reaction was stirred for 15 h at room temperature. The mixture was then diluted with EtOAc (20 mL), separated against 10% LiCl (30 mL), extracted with EtOAc (3x 20 mL), washed twice with 10% LiCl (2x 20 mL) and brine (2x 20 mL). The reaction was dried over Na₂SO₄ and concentrated under reduced pressure. Purification of the resulting crude product by flash column chromatography (CH₂Cl₂/MeOH gradient, 0 \rightarrow 20% MeOH) gave **PHOTAC-I-16** (14.0 mg, 14.6 μmol , 62%) as an orange solid.

$R_f = 0.13$ [CH₂Cl₂:MeOH, 19:1].

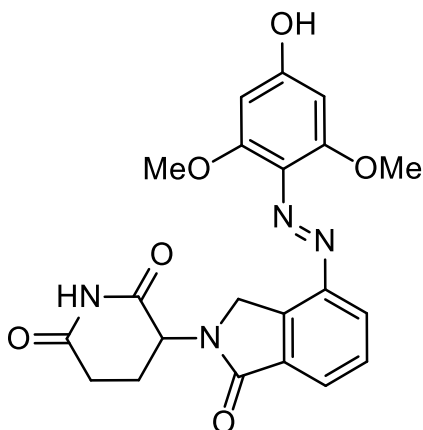
¹H NMR (400 MHz, CDCl₃) δ = 8.33 (d, *J* = 10.2 Hz, 1H), 8.13 (d, *J* = 7.9 Hz, 1H), 7.97 (d, *J* = 7.7 Hz, 1H), 7.68 (t, *J* = 7.7 Hz, 1H), 7.40 (d, *J* = 8.3 Hz, 2H), 7.33 (d, *J* = 8.2 Hz, 2H), 6.85 – 6.79 (m, 2H), 6.72 (s, 2H), 5.21 (dd, *J* = 13.2, 5.0 Hz, 1H), 4.77 (dd, *J* = 17.8, 1.6 Hz, 1H), 4.70 – 4.61 (m, 2H), 4.53 (s, 2H), 3.57 (dd, *J* = 14.2, 8.2 Hz, 1H),

3.40 – 3.24 (m, 5H), 2.95 – 2.74 (m, 2H), 2.67 (s, 3H), 2.47 (s, 6H), 2.46 – 2.36 (m, 1H), 2.39 (s, 3H), 2.24 (dt, J = 9.0, 4.6 Hz, 1H), 1.66 (s, 3H), 1.63 – 1.53 (m, 4H) ppm.

¹³C NMR (100 MHz, CDCl₃) δ = 171.18, 170.53, 169.58, 168.73, 168.05, 164.43, 157.78, 155.56, 150.14, 147.48, 145.56, 137.24, 136.36, 135.66, 133.97, 133.35, 132.16, 131.36, 131.17, 130.62, 130.06, 129.55, 128.93, 128.59, 125.80, 115.64, 67.45, 54.61, 52.18, 48.50, 39.42, 39.21, 38.82, 31.72, 26.94, 26.86, 23.60, 21.06, 14.54, 13.27, 11.93 ppm.

HRMS (ESI):	calcd. For C ₄₆ H ₄₈ CIN ₁₀ O ₆ S ⁺ :	903.3162 m/z [M+H] ⁺ .
	Found:	903.3203 m/z [M+H] ⁺ .

LCMS (ESI):	t _{ret} = 4.44 min.	903 m/z [M+H] ⁺ .
--------------------	------------------------------	------------------------------

3-(4-((4-Hydroxy-2,6-dimethoxyphenyl)diazenyl)-1-oxoisindolin-2-yl)piperidine-2,6-dione (3.10)

Lenalidomide (519 mg, 2.00 mmol, 1.0 eq.) was dissolved in 1 M HCl (40 mL) and concentrated aq. HBF_4 (2 mL) was added to the mixture. After completely dissolving of the starting material, 2 M NaNO_2 solution (1.1 mL) was added to the mixture at 0 °C. After stirring for 1 h the solution was added dropwise into a mixture of 3,5-Dimethoxyphenol (308 mg, 2.00 mmol, 1.0 eq.) in H_2O (50 mL), MeOH (20 mL), NaHCO_3 (4.15 g, 49.4 mmol, 24.7 eq.) and Na_2CO_3 (5.18 g, 49.4 mmol, 24.7 eq.) and stirred for an additional 1 h at 0 °C. Filtration and subsequent washing of the solid residue with EtOAc (3x 20 mL) gave **3.10** (823 mg, 1.94 mmol, 97%) as an orange solid.

R_f = 0.23 [CH_2Cl_2 :MeOH, 19:1].

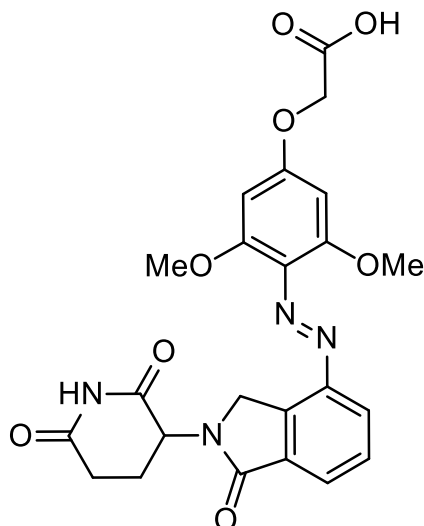
$^1\text{H NMR}$ (400 MHz, DMSO) δ = 14.21 (s, 1H), 11.05 (s, 1H), 8.10 (d, J = 7.8 Hz, 1H), 7.78 (d, J = 7.6 Hz, 1H), 7.71 (t, J = 7.6 Hz, 1H), 6.25 (d, J = 2.4 Hz, 1H), 6.13 (d, J = 2.4 Hz, 1H), 5.16 (dd, J = 13.2, 5.1 Hz, 1H), 4.69 (d, J = 19.2 Hz, 1H), 4.56 (d, J = 19.2 Hz, 1H), 3.93 (s, 3H), 3.87 (s, 3H), 2.94 (ddd, J = 18.0, 13.5, 5.4 Hz, 1H), 2.66 (dt, J = 16.7, 3.4 Hz, 1H), 2.36 (qd, J = 13.1, 4.5 Hz, 1H), 2.15 – 2.06 (m, 1H) ppm.

$^{13}\text{C NMR}$ (100 MHz, DMSO) δ = 172.91, 171.03, 167.23, 166.65, 160.24, 158.09, 144.85, 133.89, 132.61, 129.58, 127.05, 124.15, 123.41, 93.79, 92.02, 56.56, 56.11, 51.77, 48.71, 31.24, 22.71 ppm.

HRMS (ESI): calcd. For $\text{C}_{21}\text{H}_{21}\text{N}_4\text{O}_6^+$: 425.1456 m/z $[\text{M}+\text{H}]^+$.
Found: 425.1458 m/z $[\text{M}+\text{H}]^+$.

LCMS (ESI): t_{ret} = 2.638 min. 425 m/z $[\text{M}+\text{H}]^+$.

2-(4-((2-(2,6-dioxopiperidin-3-yl)-1-oxoisindolin-4-yl)diazenyl)-3,5-dimethoxyphenoxy)acetic acid (3.11)



3.10 (150 mg, 353 μmol , 1.0 eq.) was dissolved in DMSO (25 mL) at 100 °C. The mixture was cooled down to room temperature and *tert*-Butyl bromoacetate (82.7 mg, 424 μmol , 1.2 eq., 63 μL) and *i*-Pr₂NEt (707 μmol , 2.0 eq., 123 μL) were added. After stirring for 3 h, the mixture was diluted with EtOAc (50 mL), separated against NaHCO₃ (50 mL), extracted with EtOAc (3x 50 mL), and washed with 10% LiCl (3x 50 mL) and brine (2x 50 mL). The reaction was concentrated under reduced pressure and then dissolved in a CH₂Cl₂:TFA mixture (1:1, 4 mL). After 3 h the reaction was concentrated under reduced pressure. Purification of the resulting crude product by flash column chromatography (CH₂Cl₂/MeOH + AcOH (1%) gradient, 0 → 20% MeOH/CH₂Cl₂) gave **3.11** (83.0 mg, 0.172 mmol, 49%) as a yellow solid.

$R_f = 0.35$ [CH₂Cl₂:MeOH, 9:1].

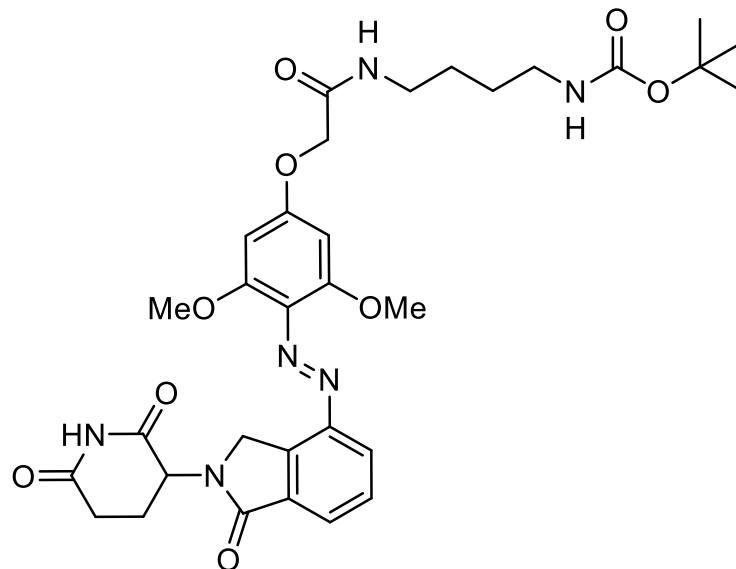
¹H NMR (400 MHz, DMSO) $\delta = 11.06 - 10.99$ (m, 1H), 8.07(E) (d, $J = 7.7$ Hz, 1H)+7.56(Z) (d, $J = 7.5$ Hz, 1H), 7.82(E) (d, $J = 7.5$ Hz, 1H)+6.49(Z) (d, $J = 7.8$ Hz, 1H), 7.74(E) (t, $J = 7.5$ Hz, 1H)+7.28(Z) (t, $J = 7.7$ Hz, 1H), 6.41(E)+6.19(Z) (s, 2H), 5.17 (m, 1H), 4.85 – 4.41 (m, 4H), 3.83 (s, 3H), 3.61 – 3.55 (m, 3H), 2.93 (ddt, $J = 18.6, 12.6, 6.0$ Hz, 1H), 2.71 – 2.56 (m, 1H), 2.43 – 2.28 (m, 1H), 2.05 (ddd, $J = 12.6, 9.6, 4.7$ Hz, 1H) ppm.

HRMS (ESI): calcd. C₂₃H₂₃N₄O₈⁺: 483.1516 m/z [M+H]⁺.

Found: 483.1549 m/z [M+H]⁺.

LCMS (ESI): $t_{\text{ret}} = 2.625$ min. 483 m/z [M+H]⁺.

***N*-(4-Aminobutyl)-2-(4-((2-(2,6-dioxopiperidin-3-yl)-1-oxoisindolin-4-yl)diazenyl)-3,5-dimethoxyphenoxy)acetamide (3.12).**



3.11 (29.0 mg, 60.1 μmol , 1.0 eq.) and HATU (34.3 mg, 120 μmol , 2.0 eq.) were dissolved in dry DMF (5 mL) at room temperature. After 5 min of stirring *N*-Boc-1,4-diaminobutane (22.6 mg, 120 μmol , 2.0 eq., 20 μL) and *i*-Pr₂NEt (240 μmol , 4.0 eq., 40 μL) were added to the mixture and stirred for an additional 12 h at room temperature. The reaction was diluted with EtOAc (20 mL), separated against H₂O/10% LiCl (1:1, 10 mL:10 mL), extracted with EtOAc (2x 20 mL) and washed with 10% LiCl (2x 20 mL) and brine (2x 20 mL). The combined organic phase was dried over Na₂SO₄. The reaction was concentrated under reduced pressure. Purification of the resulting crude product by flash column chromatography (CH₂Cl₂/MeOH 0 \rightarrow 20% MeOH/CH₂Cl₂) gave **3.12** (33.9 mg, 0.052 mmol, 87%) as a yellow solid.

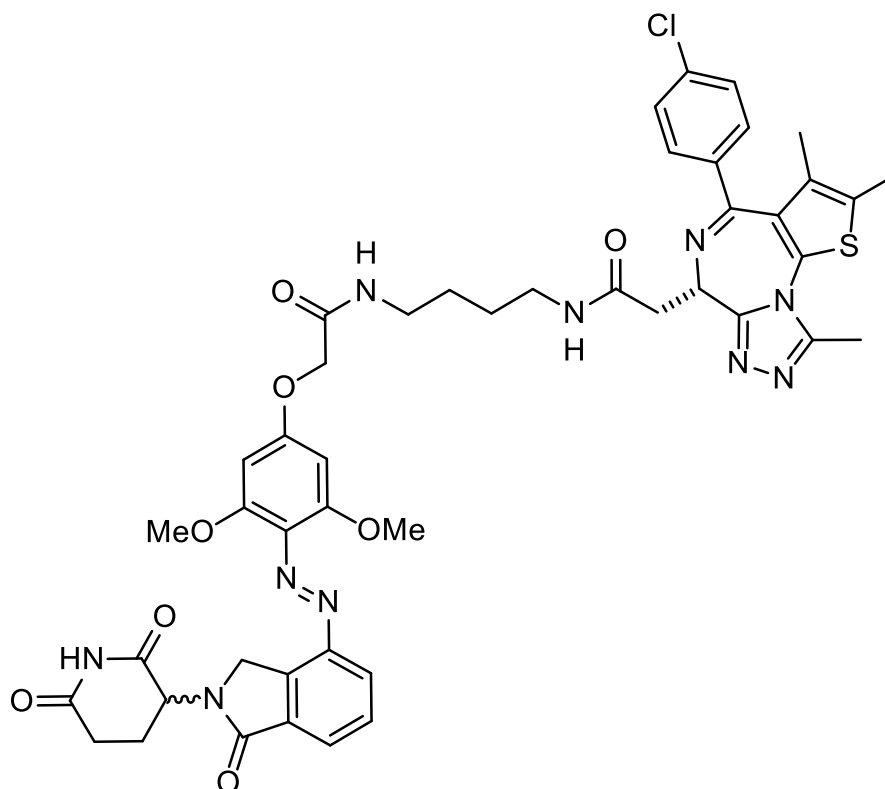
¹H NMR (400 MHz, CDCl₃) δ = 8.33 (s, 2H), 8.20 (d, *J* = 7.9 Hz, 1H), 7.93 (d, *J* = 7.5 Hz, 1H), 7.67 (t, *J* = 7.7, 1H), 6.66 (s, 1H), 6.26 (s, 2H), 6.01 (s, 1H), 5.27 – 5.18 (m, 1H), 4.82 – 4.52 (m, 4H), 3.88 (s, 6H), 3.41 – 3.31 (m, 2H), 3.18 – 3.09 (m, 2H), 2.88 (m, 1H), 2.56 – 2.10 (m, 3H), 1.57 – 1.48 (m, 4H), 1.43 (s, 9H) ppm.

¹³C NMR (100 MHz, CDCl₃) δ = 168.86, 167.54, 160.26, 158.62, 156.22, 155.39, 148.83, 133.24, 132.54, 131.26, 129.31, 128.01, 127.82, 125.12, 123.10, 92.11, 91.54, 79.36, 67.50, 56.58, 55.90, 52.08, 49.21, 40.20, 38.95, 31.75, 28.54, 27.67, 26.92, 23.67 ppm.

HRMS (ESI): calcd. For $C_{27}H_{33}N_6O_9^+$: 553.2405 m/z [M–Boc+2H]⁺.
Found: 553.2384 m/z [M–Boc+2H]⁺.

LCMS (ESI): $t_{ret} = 2.49$ min. 553 m/z [M+H]⁺.

2-((S)-4-(4-Chlorophenyl)-2,3,9-trimethyl-6H-thieno[3,2-f][1,2,4]triazolo[4,3-a][1,4]diazepin-6-yl)-N-(4-(2-(4-((2-(2,6-dioxopiperidin-3-yl)-1-oxoisindolin-4-yl)diazenyl)-3,5-dimethoxyphenoxy)acetamido)butyl)acetamide (PHOTAC-I-17).



3.12 was dissolved in a CH_2Cl_2 :TFA mixture (1:1, 4 mL). After 3 h the reaction was concentrated under reduced pressure and dried in vacuo. The crude deprotected amine (9.3 mg, 16.80 μmol , 2.0 eq.), (+)-JQ1 free acid (8.4 mg, 16.8 μmol , 1.0 eq.) and HATU (9.6 mg, 25.1 μmol , 1.5 eq.) were dissolved in dry DMF (1 mL). After addition of *i*-Pr₂NEt (117 μmol , 7.0 eq., 20 μL) the reaction was stirred for 24 h at room temperature. The mixture was then diluted with EtOAc (20 mL), separated against 5% LiCl (10 mL), extracted with EtOAc (2x 10 mL) and washed twice with 10% LiCl (2x 10 mL) and brine (2x 20 mL). The reaction was dried over Na_2SO_4 and concentrated under reduced pressure. Purification of the resulting crude product by flash column chromatography (CH_2Cl_2 /MeOH gradient, 0→20% MeOH) and HPLC gave **PHOTAC-I-17** (4.6 mg, 4.90 μmol , 29%) as a red solid.

$R_f = 0.13$ [CH_2Cl_2 :MeOH, 19:1].

¹H NMR (600 MHz, CDCl_3) $\delta = 8.55 - 8.41$ (m, 1H), 8.21 (d, $J = 7.7$ Hz, 1H), 7.92 (d, $J = 7.5$ Hz, 1H), 7.67 (t, $J = 7.2$ Hz, 1H), 7.39 (d, $J = 8.2$ Hz, 2H), 7.33 (d, $J = 8.2$ Hz, 2H), 6.87 (t, $J = 6.1$ Hz, 1H), 6.79 (s, 1H), 6.26 (s, 2H), 5.26 – 5.20 (m, 1H), 4.79 – 4.44

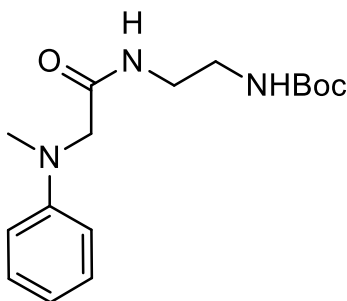
(m, 5H), 3.85 (s, 6H), 3.59 – 3.53 (m, 1H), 3.40 – 3.22 (m, 5H), 2.91 – 2.78 (m, 2H), 2.64 (s, 3H), 2.41 – 2.32 (m, 4H), 2.26 – 2.19 (m, 1H), 1.66 (s, 3H), 1.61 – 1.48 (m, 4H) ppm.

¹³C NMR (150 MHz, CDCl₃) δ = 171.30, 170.56, 169.69, 168.71, 167.50, 164.15, 160.39, 155.36, 148.78, 136.91, 136.51, 133.11, 132.30, 132.09, 131.36, 131.30, 131.01, 130.93, 130.46, 129.83, 129.22, 128.78, 127.49, 124.96, 92.00, 67.38, 56.49, 54.53, 51.91, 49.13, 39.47, 38.98, 38.76, 31.60, 26.80, 26.68, 23.58, 14.42, 13.14, 11.83 ppm.

HRMS (APCI): calcd. for C₄₆H₄₈ClN₁₀O₈S⁺: 935.3060 m/z [M+H]⁺.

Found: 935.3049 m/z [M+H]⁺.

LCMS (ESI): t_{ret} = 3.60 min. 935 m/z [M+H]⁺.

***tert*-Butyl (2-(2-(methyl(phenyl)amino)acetamido)ethyl)carbamate (3.13).**

N-Methyl-*N*-phenylglycine hydrochloride (200 mg, 0.992 mmol, 1.0 eq.) and HATU (566 mg, 1.49 mmol, 1.5 eq.) were dissolved in dry DMF (5 mL) at room temperature. After 5 min of stirring *tert*-butyl (2-aminoethyl)carbamate (318 mg, 1.98 mmol, 2.0 eq.) and *i*Pr₂NEt (3.97 mmol, 4.0 eq., 69 μ L) were added to the mixture and stirred for further 12 h. The reaction was diluted with EtOAc (20 mL), separated against H₂O, and extracted with EtOAc (3 x 20 mL). The combined organic phase was dried over Na₂SO₄ and concentrated under reduced pressure. **3.13** (301 mg, 0.979 mmol, 99%) was obtained as white solid.

$R_f = 0.20$ [Hexane: EtOAc, 4:1].

¹H NMR (400 MHz, CDCl₃) $\delta = 7.31 - 7.22$ (m, 2H), 6.83 (t, $J = 7.3$ Hz, 1H), 6.72 (d, $J = 8.0$ Hz, 2H), 4.77 (s, 1H), 3.85 (s, 2H), 3.37 (q, $J = 5.9$ Hz, 2H), 3.25 – 3.18 (m, 2H), 3.02 (s, 3H), 1.39 (s, 9H) ppm.

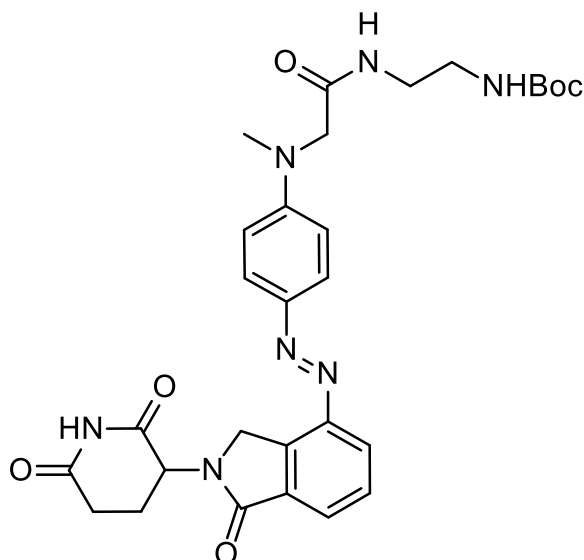
¹³C NMR (100 MHz, CDCl₃) $\delta = 171.34, 156.51, 149.31, 129.51, 118.75, 113.22, 79.65, 58.88, 40.60, 40.01, 31.07, 28.47$ ppm.

HRMS (ESI): calcd. For C₁₆H₂₅N₃O₃Na⁺: 330.1690 m/z [M+Na]⁺.

Found: 330.1751 m/z [M+Na]⁺.

LCMS (ESI): $t_{ret} = 3.49$ min. 252 m/z [M+H-*t*-Butyl]⁺.

***tert*-Butyl-(2-(2-((4-((2-(2,6-dioxopiperidin-3-yl)-1-oxoisoindolin-4-yl)diazenyl)phenyl)(methyl)amino)acetamido)ethyl)carbamate (3.14).**



Lenalidomide (220 mg, 0.849 mmol, 1.0 eq.) was dissolved in 1 M HCl (20 mL). Concentrated aq. HBF₄ (1 mL) was added to the mixture. After completely dissolving the starting material, 2 M NaNO₂ solution (0.47 mL) was added to the mixture at 0 °C. After stirring for 1 h the solution was added dropwise into a mixture of **3.13** (261 mg, 849 mg, 1.0 eq.) in H₂O (20 mL), MeOH (5 mL), NaOAc (1.74 g, 21.2 mmol, 25.0 eq.). The mixture was stirred for 1 h at 0 °C. MeOH was removed under reduced pressure, the aqueous phase extracted with EtOAc (3x 30 mL) and washed with brine (2x 30 mL). The organic phase was dried over Na₂SO₄ and concentrated under reduced pressure. Purification of the resulting crude product by flash column chromatography (CH₂Cl₂/MeOH gradient, 0 → 10% MeOH) gave **3.14** (114 mg, 0.197 mmol, 23%) as an orange solid.

R_f = 0.13 [CH₂Cl₂:MeOH, 19:1].

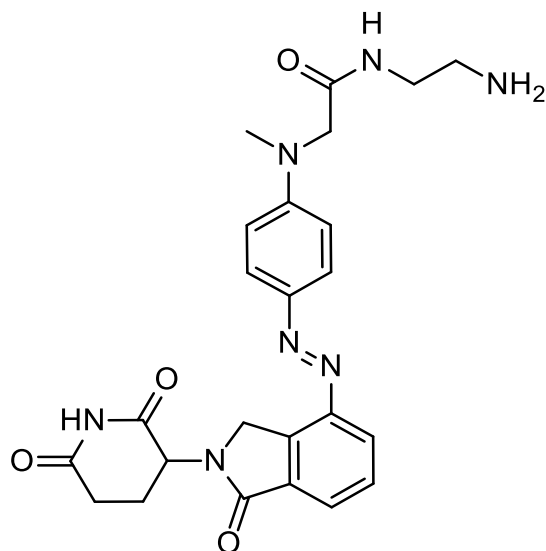
¹H NMR (400 MHz, DMSO) δ = 11.01 (s, 1H), 8.11 – 8.01 (m, 2H), 7.85 (d, J = 8.7 Hz, 2H), 7.79 (d, J = 7.4 Hz, 1H), 7.71 (t, J = 7.6 Hz, 1H), 6.83 – 6.74 (m, 3H), 5.16 (dd, J = 13.1, 5.2 Hz, 1H), 4.77 (d, J = 18.9 Hz, 1H), 4.65 (d, J = 18.9 Hz, 1H), 4.06 (s, 2H), 3.20 – 3.07 (m, 5H), 3.06 – 2.85 (m, 3H), 2.70 – 2.53 (m, 2H), 2.11 – 1.99 (m, 1H), 1.37 (s, 9H) ppm.

¹³C NMR (100 MHz, DMSO) δ = 172.91, 171.05, 168.77, 167.42, 155.65, 152.46, 147.07, 143.18, 133.98, 133.60, 129.39, 127.33, 124.91, 123.62, 111.69, 77.69, 55.35, 51.67, 48.24, 39.62, 38.76, 31.26, 28.22, 22.36 ppm.

HRMS (ESI): calcd. For $C_{29}H_{36}N_7O_6^+$: 578.2649 m/z [M+H]⁺.

Found: 578.2682.

LCMS (ESI): t_{ret} = 3.44 min. 522 m/z [M+H-*t*-butyl]⁺.

***N*-(4-Aminobutyl)-2-((4-((2-(2,6-dioxopiperidin-3-yl)-1-oxoisindolin-4-yl)diazenyl)phenyl)(methyl)amino)acetamide (3.15).**

3.14 (30.0 mg, 0.050 mmol, 1.0 eq.) was dissolved in a CH₂Cl₂:TFA mixture (1:1; 4 mL). After 4 h the reaction was concentrated under reduced pressure, triturated with MeOH, concentrated, and dried under vacuum for 48 h. **3.15** (27.0 mg, 0.049 mmol, 99%) was obtained as red solid with traces of residual TFA.

$R_f = 0.15$ [CH₂Cl₂:MeOH, 1:1].

¹H NMR (400 MHz, DMSO) $\delta = 11.01$ (s, 1H), 8.21 (t, $J = 5.8$ Hz, 1H), 8.07 (d, $J = 7.7$ Hz, 1H), 7.88 – 7.78 (m, 5H), 7.72 (t, $J = 7.6$ Hz, 1H), 6.81 (d, $J = 8.8$ Hz, 2H), 5.16 (dd, $J = 13.1, 5.1$ Hz, 1H), 4.77 (d, $J = 19.0$ Hz, 1H), 4.65 (d, $J = 18.9$ Hz, 1H), 4.10 (s, 2H), 3.33 (q, $J = 6.3$ Hz, 2H), 3.13 (s, 3H), 3.00 – 2.82 (m, 3H), 2.67 – 2.53 (m, 2H), 2.10 – 2.00 (m, 1H) ppm.

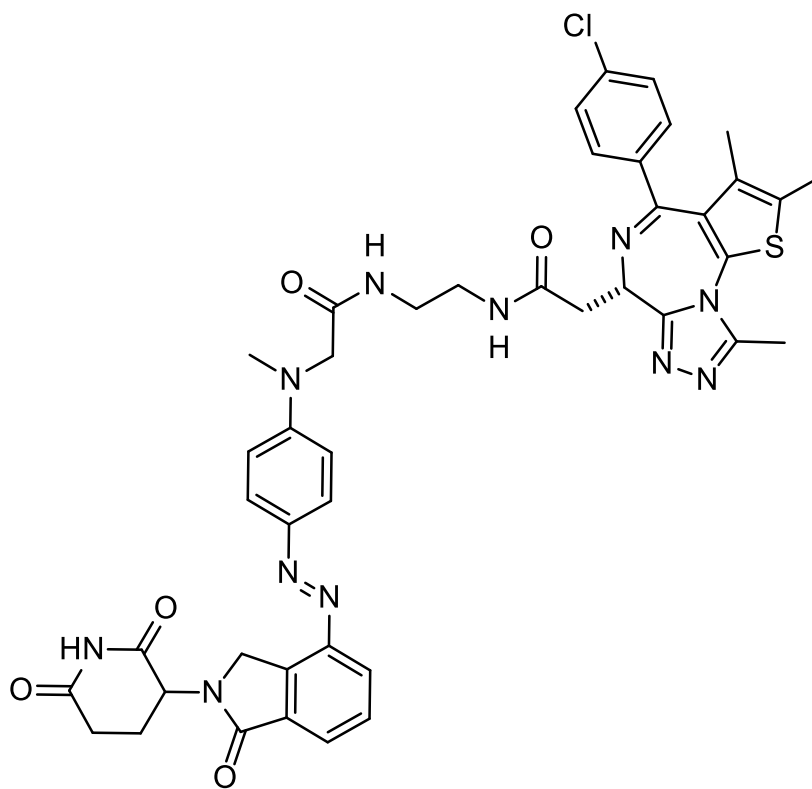
¹³C NMR (100 MHz, DMSO) $\delta = 172.93, 171.07, 169.62, 167.42, 152.47, 147.06, 143.26, 133.99, 133.62, 129.41, 127.38, 124.91, 123.70, 111.76, 55.30, 51.68, 48.25, 39.59, 38.65, 36.40, 31.27, 22.37$ ppm.

HRMS (ESI): calcd. for C₂₄H₂₇N₇O₄⁺: 501.1756 m/z [M+H]⁺.

Found: 501.1762 m/z [M+H]⁺.

LCMS (ESI): $t_{ret} = 2.54$ min. 501 m/z [M+H]⁺.

2-((S)-4-(4-Chlorophenyl)-2,3,9-trimethyl-6H-thieno[3,2-f][1,2,4]triazolo[4,3-a][1,4]diazepin-6-yl)-N-(2-(2-((4-((2-(2,6-dioxopiperidin-3-yl)-1-oxoisindolin-4-yl)diazenyl)phenyl)(methyl)amino)acetamido)ethyl)acetamide (PHOTAC-I-24)



(+)-JQ1 free acid (7.0 mg, 17.5 μmol , 1.0 eq.), **3.15** (16.7 mg, 35.0 μmol , 2.0 eq.) and HATU (10.0 mg, 26.3 μmol , 2 eq.) were dissolved in dry DMF (1 mL). After addition of *i*-Pr₂NEt (123 μmol , 7.0 eq., 21 μL) the reaction was stirred for 24 h at room temperature. The mixture was then diluted with EtOAc (20 mL), separated against 5% LiCl (30 mL), extracted with EtOAc (2x 20 mL) and washed twice with 10% LiCl (2x 20 mL) and brine (2x 20 mL). The reaction was dried over Na₂SO₄ and concentrated under reduced pressure. Purification of the resulting crude product by flash column chromatography (CH₂Cl₂/MeOH gradient, 0→20% MeOH) gave **PHOTAC-I-24** (15.0 mg, 17.1 μmol , 98%) as a red solid.

R_f = 0.07 [CH₂Cl₂:MeOH, 19:1].

¹H NMR (400 MHz, DMSO) δ = 11.00 (s, 1H), 8.24 (d, *J* = 5.1 Hz, 1H), 8.10 – 8.00 (m, 2H), 7.83 (dd, *J* = 9.2, 2.6 Hz, 2H), 7.81 – 7.76 (m, 1H), 7.70 (t, *J* = 7.6 Hz, 1H), 7.46 – 7.38 (m, 4H), 6.84 – 6.71 (m, 2H), 5.19 – 5.10 (m, 1H), 4.76 (d, *J* = 19.9 Hz, 1H), 4.64 (d, *J* = 19.0 Hz, 1H), 4.48 (td, *J* = 7.2, 2.8 Hz, 1H), 4.07 (s, 2H), 3.22 – 3.16 (m, 6H), 3.12 (s, 3H), 2.93 (ddt, *J* = 16.6, 12.6, 4.3 Hz, 1H), 2.69 – 2.50 (m, 5H), 2.39 (s, 3H), 2.06 – 1.95 (m, 1H), 1.60 (d, *J* = 2.5 Hz, 3H) ppm.

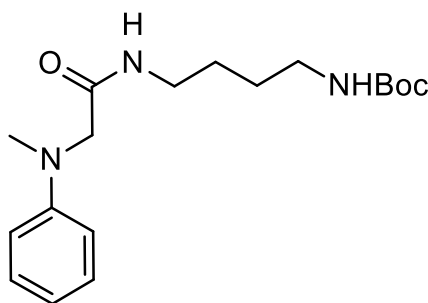
¹³C NMR (100 MHz, DMSO) δ = 172.90, 171.04, 169.84, 168.85, 167.43, 163.02, 155.06, 152.42, 149.81, 147.07, 143.19, 136.70, 135.19, 134.04, 133.60, 132.22, 130.66, 130.12, 129.84, 129.53, 129.35, 128.44, 127.27, 124.89, 123.61, 111.69, 55.40, 53.74, 51.69, 48.27, 39.31, 38.59, 38.22, 37.64, 31.26, 22.35, 14.06, 12.67, 11.27 ppm.

HRMS (APCI): calcd. for C₄₃H₄₃ClN₁₁O₅S⁺: 860.2852 m/z [M+H]⁺.

Found: 860.2845 m/z [M+H]⁺.

LCMS (ESI): t_{ret} = 3.60 min. 860 m/z [M+H]⁺.

***tert*-Butyl (4-(2-(methyl(phenyl)amino)acetamido)butyl)carbamate (3.16)**



N-Methyl-*N*-phenylglycine hydrochloride (202 mg, 1.00 mmol, 1.0 eq.) and HATU (570 mg, 1.50 mmol, 1.5 eq.) were dissolved in dry DMF (5 mL) at room temperature. After 5 min of stirring *tert*-Butyl (4-aminobutyl)carbamate (377 mg, 2.00 mmol, 2.0 eq., 285 μ L) and *i*-Pr₂NEt (4.00 mmol, 4.0 eq., 0.70 mL) were added to the mixture and stirred for further 12 h. The reaction was diluted with EtOAc (20 mL), separated against H₂O, and extracted with EtOAc (3 x 20 mL). The combined organic phase was dried over Na₂SO₄ and concentrated under reduced pressure. **3.16** (306 mg, 0.912 mmol, 91%) was obtained as off-white solid.

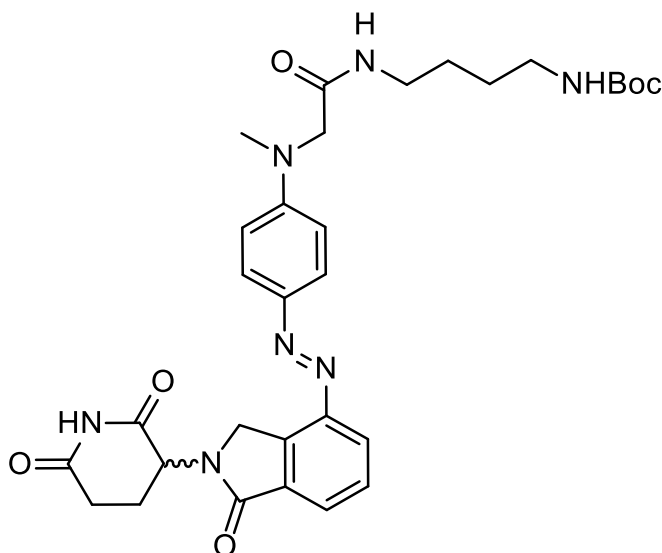
R_f = 0.23 [Hexane: EtOAc, 4:1].

¹H NMR (400 MHz, CDCl₃) δ = 7.27 (t, *J* = 8.0 Hz, 2H), 6.85 (t, *J* = 7.4 Hz, 1H), 6.74 (d, *J* = 8.1 Hz, 2H), 6.66 (s, 1H), 4.52 (s, 1H), 3.85 (s, 2H), 3.28 (q, *J* = 6.6 Hz, 2H), 3.07 (q, *J* = 6.5 Hz, 2H), 3.01 (s, 3H), 1.53 – 1.37 (m, 4H), 1.43 (s, 9H) ppm.

¹³C NMR (100 MHz, CDCl₃) δ = 170.32, 156.07, 149.23, 129.54, 118.99, 113.40, 79.25, 59.05, 40.19, 40.09, 38.91, 28.53, 27.48, 27.00 ppm.

HRMS (ESI):	calcd. for C ₁₈ H ₃₀ N ₃ O ₃ ⁺ :	336.2282 m/z [M+H] ⁺ .
	Found:	336.2242 m/z [M+H] ⁺ .
LCMS (ESI):	t _{ret} = 3.59 min.	336 m/z [M+H] ⁺ .

***tert*-Butyl-(4-(2-((4-((2-(2,6-dioxopiperidin-3-yl)-1-oxoisoindolin-4-yl)diazenyl)phenyl)(methyl)amino)acetamido)butyl)carbamate (3.17)**



Lenalidomide (173 mg, 0.668 mmol, 1.0 eq.) was dissolved in 1 M HCl (20 mL). Concentrated aqueous HBF₄ (1 mL) was added to the mixture. After completely dissolving the starting material, aqueous 2 M NaNO₂ (0.37 mL) was added to the mixture at 0 °C. After stirring for 1 h the solution was added dropwise into a mixture of **3.16** (224.0 mg, 0.668 mmol, 1.0 eq.) in H₂O (20 mL), MeOH (5 mL), NaOAc (1.10 g, 13.4 mmol, 20 eq.). The mixture was stirred for 1 h at 0 °C. MeOH was removed under reduced pressure, the aqueous phase extracted with EtOAc (3x 30 mL) and washed once with brine (1x 30 mL). The organic phase was dried over Na₂SO₄ and concentrated under reduced pressure. Purification of the resulting crude product by flash column chromatography (CH₂Cl₂/MeOH gradient, 0 → 10% MeOH) gave **3.17** (165 mg, 0.272 mmol, 41%) as a yellow solid.

R_f = 0.15 [CH₂Cl₂:MeOH, 19:1].

¹H NMR (400 MHz, CDCl₃) δ = 11.01 (s, 1H), 8.06 (d, J = 7.8 Hz, 1H), 8.00 (t, J = 5.7 Hz, 1H), 7.85 (d, J = 8.9 Hz, 2H), 7.79 (d, J = 7.3 Hz, 1H), 7.71 (t, J = 7.6 Hz, 1H), 6.81 – 6.74 (m, 2H), 5.16 (dd, J = 13.2, 5.0 Hz, 1H), 4.77 (d, J = 19.0 Hz, 1H), 4.65 (d, J =

18.9 Hz, 1H), 4.06 (s, 2H), 3.12 (s, 2H), 3.07 (q, J = 6.3 Hz, 2H), 2.99 – 2.85 (m, 3H), 2.67 – 2.52 (m, 2H), 2.10 – 2.01 (m, 1H), 1.36 (s, 13H) ppm.

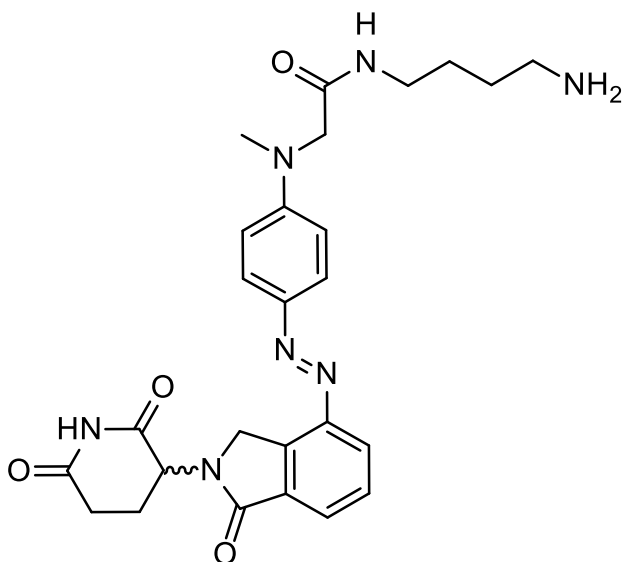
¹³C NMR (100 MHz, DMSO) δ = 172.92, 171.05, 168.43, 167.44, 155.58, 152.49, 147.08, 143.16, 134.04, 133.60, 129.38, 127.25, 124.91, 123.62, 111.63, 77.34, 55.29, 54.92, 51.69, 48.25, 38.29, 31.28, 28.28, 26.96, 26.51, 22.35 ppm.

HRMS (ESI): calcd. for C₃₁H₃₉N₇O₆⁺: 628.2854 m/z [M+Na]⁺.

Found: 628.2883 m/z [M+Na]⁺.

LCMS (ESI): t_{ret} = 3.61 min. 628 m/z [M+Na]⁺.

***N*-(4-aminobutyl)-2-((4-((2-(2,6-dioxopiperidin-3-yl)-1-oxoisindolin-4-yl)diazenyl)phenyl)(methylamino)acetamide (3.18)**



3.17 (30.0 mg, 0.050 mmol, 1 eq.) was dissolved in a CH₂Cl₂:TFA mixture (1:1; 4 mL). After 4 h the reaction was concentrated under reduced pressure. The mixture was triturated with MeOH, concentrated, and then dried under vacuum for 48 h. **3.18** (27.0 mg, 0.049 mmol, 99%) was obtained as a red solid with traces of residual TFA.

R_f = 0.15 [CH₂Cl₂:MeOH, 1:1].

¹H NMR (400 MHz, DMSO) δ = 11.01 (s, 1H), 8.12 – 8.04 (m, 2H), 7.86 (d, J = 8.8 Hz, 2H), 7.80 (d, J = 7.5 Hz, 1H), 7.76 – 7.63 (m, 3H), 6.78 (d, J = 8.8 Hz, 2H), 5.16 (dd, J = 13.2, 5.1 Hz, 1H), 4.77 (d, J = 18.9 Hz, 1H), 4.65 (d, J = 18.9 Hz, 1H), 4.07 (s, 2H),

3.13 (s, 3H), 3.12 – 3.06 (m, 2H), 2.94 (ddd, J = 17.9, 13.4, 5.6 Hz, 1H), 2.79 (q, J = 6.5 Hz, 2H), 2.68 – 2.52 (m, 2H), 2.10 – 1.99 (m, 1H), 1.56 – 1.41 (m, 4H) ppm.

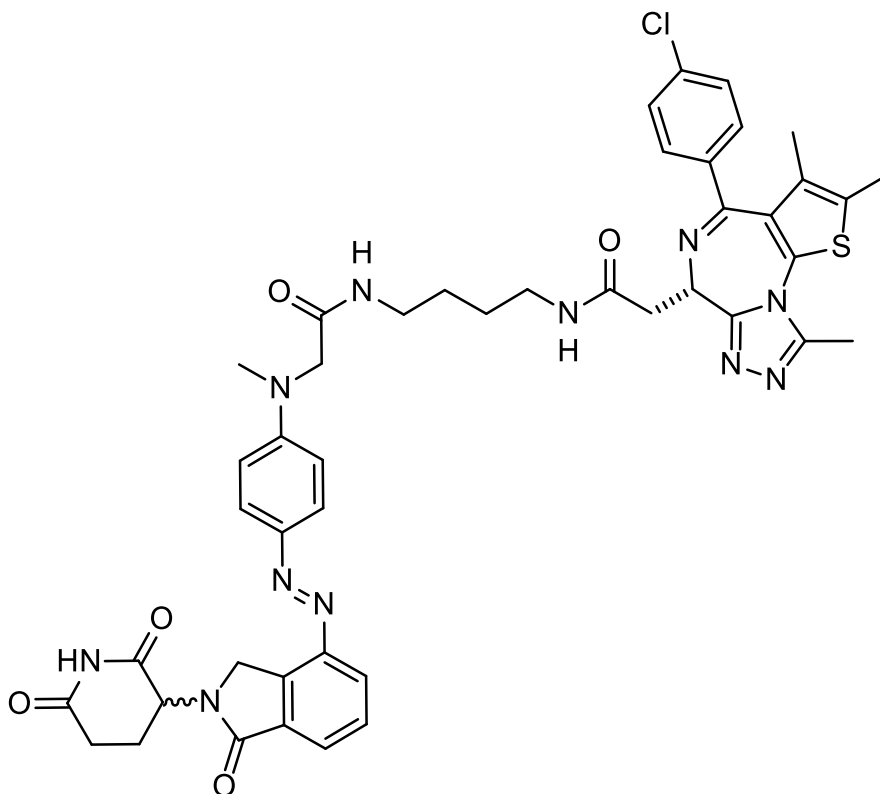
¹³C NMR (100 MHz, DMSO) δ = 13C NMR (101 MHz, DMSO) δ 172.95, 171.08, 168.65, 167.45, 152.48, 147.08, 143.20, 134.02, 133.62, 129.42, 127.32, 124.94, 123.68, 111.67, 55.33, 55.07, 51.69, 48.25, 38.57, 37.89, 31.29, 26.14, 24.49, 22.38 ppm.

HRMS (ESI): calcd. for C₂₆H₃₂N₇O₄⁺: 506.2510 m/z [M+H]⁺.

 Found: 506.2471 m/z [M+H]⁺.

LCMS (ESI): t_{ret} = 2.46 min. 506 m/z [M+H]⁺.

2-((S)-4-(4-Chlorophenyl)-2,3,9-trimethyl-6H-thieno[3,2-f][1,2,4]triazolo[4,3-a][1,4]diazepin-6-yl)-N-(4-(2-((4-((2-(2,6-dioxopiperidin-3-yl)-1-oxoisoindolin-4-yl)diazenyl)phenyl)(methyl)amino)acetamido)butyl)acetamide (PHOTAC-I-23)



Into a round bottom flask with (+)-JQ1 free acid (9.0 mg, 22.5 μmol , 1.0 eq.) were added **3.18** (22.7 mg, 44.9 μmol , 2.0 eq.) and HATU (12.8 mg, 33.7 μmol , 1.5 eq.) under nitrogen atmosphere. The solids were dissolved in dry DMF (1 mL). After addition of *i*-Pr₂NEt (157 μmol , 7.0 eq., 27 μL) the reaction was stirred for 48 h at room temperature. The mixture was then diluted with EtOAc (20 mL), separated against 5% LiCl (30 mL), extracted with EtOAc (2x 20 mL), washed twice with 10% LiCl (2x 20 mL) and brine (2x 20 mL). The organic phase was dried over Na₂SO₄ and concentrated under reduced pressure. Purification of the resulting crude product by flash column chromatography (CH₂Cl₂/MeOH gradient, 0→20% MeOH) gave **PHOTAC-I-23** (7.0 mg, 7.9 μmol , 35%) as a red solid.

R_f = 0.07 [CH₂Cl₂:MeOH, 19:1].

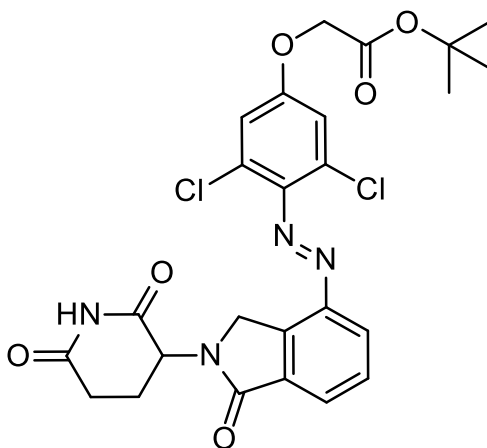
¹H NMR (400 MHz, DMSO-*d*₆) δ = 11.00 (s, 1H), 8.23 – 8.16 (m, 1H), 8.08 – 7.96 (m, 2H), 7.84 (d, *J* = 9.1 Hz, 2H), 7.78 (d, *J* = 7.9 Hz, 1H), 7.69 (t, *J* = 7.5 Hz, 1H), 7.48 (d, *J* = 8.9 Hz, 2H), 7.40 (d, *J* = 8.4 Hz, 2H), 6.77 (d, *J* = 9.3 Hz, 2H), 5.21 – 5.09 (m, 1H), 4.82 – 4.60 (m, 2H), 4.50 (dd, *J* = 8.1, 6.1 Hz, 1H), 4.07 (s, 2H), 3.29 – 3.03 (m, 9H),

2.97 – 2.86 (m, 1H), 2.64 – 2.53 (m, 5H), 2.38 (s, 3H), 2.07 – 1.97 (m, 1H), 1.59 (s, 3H), 1.49 – 1.43 (m, 4H) ppm.

¹³C NMR (100 MHz, DMSO) δ = 172.90, 171.03, 169.33, 168.48, 167.41, 163.03, 155.05, 152.46, 149.81, 147.05, 143.16, 136.72, 135.21, 134.00, 133.58, 132.23, 130.70, 130.11, 129.81, 129.52, 129.34, 128.46, 127.27, 124.90, 123.59, 111.63, 55.31, 53.86, 51.69, 48.24, 39.73, 38.22, 38.15, 37.63, 31.25, 26.69, 26.59, 22.34, 14.04, 12.65, 11.29 ppm.

HRMS (APCI):	calcd. for C ₄₅ H ₄₇ ClN ₁₁ O ₅ S ⁺ :	888.3165 m/z [M+H] ⁺
	found:	888.3139 m/z [M+H] ⁺ .
LCMS (ESI):	t _{ret} = 3.81 min.	888 m/z [M+H] ⁺ .

tert-butyl-2-(3,5-dichloro-4-((2-(2,6-dioxopiperidin-3-yl)-1-oxoisindolin-4-yl)diazenyl)phenoxy)acetate (3.19)



Lenalidomide (519 mg, 2.00 mmol, 1.0 eq.) was dissolved in 1 M HCl (50 mL) and concentrated aqueous HBF₄ (1 mL) was added to the mixture. After completely dissolving the starting material, 2 M NaNO₂ (1.05 mL) was added to the solution at 0 °C. After stirring the solution for 1 h, it was added dropwise into a mixture of 3,5-dichlorophenol (326 mg, 2.00 mmol, 1 eq.) in H₂O (50 mL), MeOH (20 mL), NaHCO₃ (4.15 g, 49.4 mmol, 24.7 eq.) and Na₂CO₃ (5.18 g, 48.9 mmol, 24.5 eq.) at 0°C. Upon addition the solution turned from white to orange/red and was stirred for additional 1 h at 0°C. The reaction was extracted with a CH₂Cl₂:isopropanol mixture (5:1, 2x 100 mL) and washed once with brine (1x 100 mL). The organic phase was dried over Na₂SO₄ and then concentrated under reduced pressure to yield the crude intermediate *p*-hydroxy azobenzene as a yellow solid (330 mg, 38%).

To a solution of the crude *p*-hydroxy azobenzene (300 mg, 0.692 mmol, 1 eq.) dissolved in dry DMF (10 mL) was added K₂CO₃ (294 mg, 2.13 mmol, 3.1 eq.) and tert-butyl bromoacetate (135 mg, 0.692 mmol, 1 eq., 0.102 mL). After addition, the reaction was stirred for 14 h at room temperature. Then, the mixture was diluted with EtOAc (100 mL), separated against saturated NaHCO₃ (50 mL), extracted with EtOAc (3x 50 mL), and washed with aqueous 10% LiCl solution (1x 50 mL) and brine (2x 50 mL). The organic phase was concentrated under reduced pressure. Purification of the resulting crude product by flash column chromatography (Hex/EtOAc gradient, 20 → 100% EtOAc) gave **3.19** (125 mg, 0.227 mmol, 33%) as a yellow solid.

$R_f = 0.58$ [CH_2Cl_2 :MeOH, 19:1].

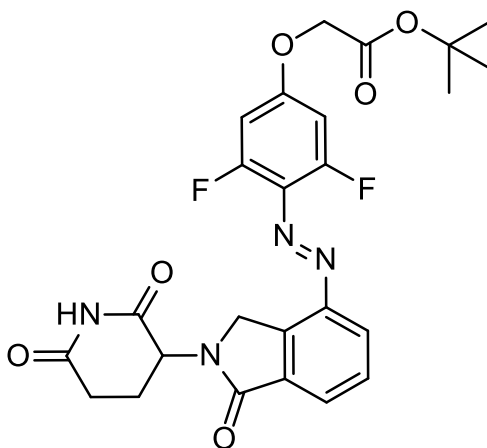
^1H NMR (400 MHz, $\text{DMSO-}d_6$) $\delta = 11.00$ (s, 1H), 8.27 (d, $J = 7.8$ Hz, 1H), 8.02 (d, $J = 7.5$ Hz, 1H), 7.86 (t, $J = 7.7$ Hz, 1H), 7.32 (s, 1H), 5.15 (dd, $J = 13.3, 5.1$ Hz, 1H), 4.89 (s, 2H), 4.79 – 4.61 (m, 2H), 2.90 (td, $J = 13.9, 13.3, 6.7$ Hz, 1H), 2.63 – 2.56 (m, 1H), 2.50 – 2.38 (m, 1H), 2.10 – 2.00 (m, 1H), 1.45 (s, 9H) ppm.

^{13}C NMR (100 MHz, $\text{DMSO-}d_6$) $\delta = 172.82, 170.92, 167.07, 166.86, 157.99, 146.44, 140.51, 134.08, 133.92, 129.93, 129.48, 127.97, 126.72, 116.21, 81.91, 65.61, 51.82, 48.41, 31.21, 27.70, 22.34$ ppm.

HRMS (APCI):	calcd. for $\text{C}_{25}\text{H}_{25}\text{Cl}_2\text{N}_4\text{O}_6^+$:	547.1146 m/z $[\text{M}+\text{H}]^+$
	found:	547.1135 m/z $[\text{M}+\text{H}]^+$.

LCMS (ESI):	$t_{\text{ret}} = 4.43$ min.	547 m/z $[\text{M}+\text{H}]^+$.
--------------------	------------------------------	-----------------------------------

tert-butyl-2-(4-((2-(2,6-dioxopiperidin-3-yl)-1-oxoindolin-4-yl)diazenyl)-3,5-difluorophenoxy)acetate (3.20)



Lenalidomide (259 mg, 1.00 mmol, 1.0 eq.) was dissolved in 1 M HCl (50 mL) and concentrated aqueous HBF₄ (1 mL) was added to the mixture. After completely dissolving the starting material, 2 M NaNO₂ (0.55 mL) was added to the solution at 0 °C. After stirring the solution for 1 h, it was added dropwise into a mixture of 3,5-difluorophenol (156 mg, 1.20 mmol, 1.2 eq.) in H₂O (50 mL), MeOH (20 mL), NaHCO₃ (2.07 g, 24.7 mmol, 24.7 eq.) and Na₂CO₃ (2.59 g, 24.5 mmol, 24.5 eq.) at 0°C. Upon addition the solution turned from white to orange/red and was stirred for additional 1 h at 0°C. The reaction was extracted with a CH₂Cl₂:isopropanol mixture (5:1, 2x 100 mL) and washed once with brine (1x 100 mL). The organic phase was dried over Na₂SO₄ and then concentrated under reduced pressure to yield the crude intermediate *p*-hydroxy azobenzene as a crude yellow solid (430 mg, >99%, still containing some 3,5-difluorophenol).

To a solution of the crude *p*-hydroxy azobenzene (300 mg, 0.749 mmol, 1 eq.) dissolved in dry NMP (6 mL) was added *i*-Pr₂NEt (291 mg, 2.25 mmol, 3 eq., 0.392 ml) and tert-butyl bromoacetate (146 mg, 0.749 mmol, 1 eq., 0.11 mL). After addition, the reaction was stirred for 18 h at room temperature. Then, the mixture was diluted with EtOAc (100 mL), separated against saturated NaHCO₃ (50 mL), extracted with EtOAc (3x 50 mL), and washed with aqueous 10% LiCl solution (1x 50 mL) and brine (2x 50 mL). The organic phase was concentrated under reduced pressure. Purification of the resulting crude product by flash column chromatography (Hx/EA gradient, 20 → 100% EA) gave **3.20** (165 mg, 0.321 mmol, 43%) as a yellow solid.

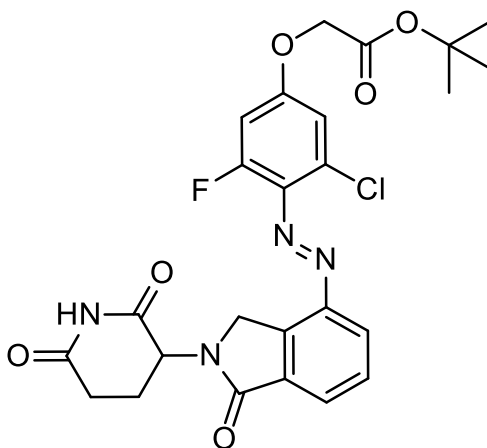
$R_f = 0.47$ [CH_2Cl_2 :MeOH, 19:1].

^1H NMR (400 MHz, $\text{DMSO-}d_6$) $\delta = 11.01$ (s, 1H), 8.19 (d, $J = 7.8$ Hz, 1H), 7.93 (d, $J = 7.5$ Hz, 1H), 7.80 (t, $J = 7.7$ Hz, 1H), 7.04 (d, $J = 11.7$ Hz, 2H), 5.15 (dd, $J = 13.3, 5.1$ Hz, 1H), 4.88 (s, 2H), 4.76 – 4.54 (m, 2H), 2.92 (ddd, $J = 18.2, 13.6, 5.4$ Hz, 1H), 2.66 – 2.57 (m, 1H), 2.41 (qd, $J = 13.2, 4.5$ Hz, 1H), 2.05 (ddd, $J = 12.4, 7.3, 4.9$ Hz, 1H), 1.45 (s, 9H) ppm.

^{13}C NMR (100 MHz, $\text{DMSO-}d_6$) $\delta = 173.29, 171.42, 167.50, 167.28, 161.48$ (t, $J = 14.5$ Hz), 157.06 (dd, $J = 259.1, 7.3$ Hz), 148.03, 134.28, 134.19, 130.23, 129.58, 126.24, 124.97 (t, $J = 9.5$ Hz), 100.65 (dd, $J = 24.3, 2.4$ Hz), 82.45, 66.18, 52.25, 48.78, 31.66, 28.17, 22.95 ppm.

HRMS (APCI):	calcd. for $\text{C}_{25}\text{H}_{25}\text{F}_2\text{N}_4\text{O}_6^+$:	515.1737 m/z $[\text{M}+\text{H}]^+$
	found:	515.1712 m/z $[\text{M}+\text{H}]^+$.
LCMS (ESI):	$t_{\text{ret}} = 4.14$ min.	515 m/z $[\text{M}+\text{H}]^+$.

tert-butyl-2-(3-chloro-4-((2-(2,6-dioxopiperidin-3-yl)-1-oxoisindolin-4-yl)diazenyl)-5-fluorophenoxy)acetate (3.21)



Lenalidomide (519 mg, 2.00 mmol, 1.0 eq.) was dissolved in 1 M HCl (50 mL) and concentrated aqueous HBF_4 (1 mL) was added to the mixture. After completely dissolving the starting material, 2 M NaNO_2 (1.05 mL) was added to the solution at 0 °C. After stirring the solution for 1 h, it was added dropwise into a mixture of 3-chloro-5-fluorophenol (293 mg, 2.00 mmol, 1 eq.) in H_2O (50 mL), MeOH (20 mL), NaHCO_3 (4.15 g, 49.4 mmol, 24.7 eq.) and Na_2CO_3 (5.18 g, 48.9 mmol, 24.5 eq.) at 0°C. Upon addition the solution turned from white to orange/red and was stirred for additional 1 h at 0°C. The reaction was extracted with a CH_2Cl_2 :isopropanol mixture (5:1, 4x 100 mL) and washed once with brine (1x 100 mL). The organic phase was dried over Na_2SO_4 and then concentrated under reduced pressure to yield the crude intermediate *p*-hydroxy azobenzene as an orange solid (750 mg, 90%).

To a solution of the crude *p*-hydroxy azobenzene (750 mg, 1.80 mmol, 1 eq.) dissolved in dry DMF (14 mL) was added K_2CO_3 (764 mg, 5.53 mmol, 3.07 eq.) and tert-butyl bromoacetate (351 mg, 1.8 mmol, 1 eq., 0.266 mL). After addition, the reaction was stirred for 14 h at room temperature. Then, the mixture was diluted with EtOAc (100 mL), separated against saturated NaHCO_3 (50 mL), extracted with EtOAc (3x 50 mL), and washed with aqueous 10% LiCl solution (1x 50 mL) and brine (2x 50 mL). The organic phase was concentrated under reduced pressure. Purification of the resulting crude product by flash column chromatography (Hex/EtOAc gradient, 20 → 100% EtOAc) gave **3.21** (268 mg, 0.505 mmol, 28%) as an orange solid.

$R_f = 0.08$ [Hx:EA,1:1].

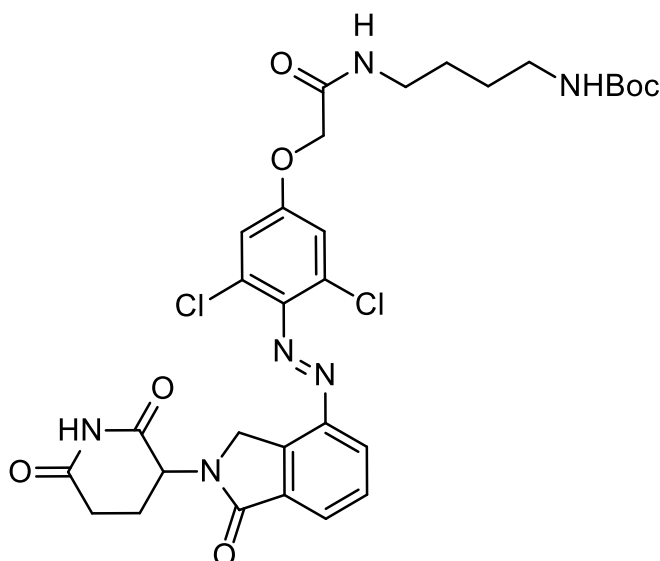
^1H NMR (400 MHz, DMSO- d_6) δ = 11.00 (s, 1H), 8.25 (d, J = 7.8 Hz, 1H), 7.96 (d, J = 7.5 Hz, 1H), 7.83 (t, J = 7.6 Hz, 1H), 7.24 (dd, J = 2.6, 1.3 Hz, 1H), 7.13 (dd, J = 13.4, 2.7 Hz, 1H), 5.15 (dd, J = 13.3, 5.1 Hz, 1H), 4.90 (s, 2H), 4.78 – 4.56 (m, 2H), 2.91 (ddd, J = 18.2, 13.4, 5.3 Hz, 1H), 2.65 – 2.58 (m, 1H), 2.41 (qd, J = 13.2, 4.4 Hz, 1H), 2.11 – 2.01 (m, 1H), 1.45 (s, 9H) ppm.

^{13}C NMR (100 MHz, DMSO- d_6) δ = 172.84, 170.95, 166.96, 166.91, 159.86 (d, J = 13.3 Hz), 153.24 (d, J = 262.7 Hz), 147.29, 134.84 (d, J = 6.3 Hz), 133.85, 133.01, 132.00 (d, J = 8.3 Hz), 130.51, 129.83, 126.09, 112.95 (d, J = 2.6 Hz), 103.58 (d, J = 24.2 Hz), 81.96, 65.68, 51.82, 48.91, 31.24, 27.69, 22.47. ppm.

HRMS (APCI): calcd. for $\text{C}_{25}\text{H}_{25}\text{ClFN}_4\text{O}_6^+$: 531.1441 m/z $[\text{M}+\text{H}]^+$
 found: 531.1443 m/z $[\text{M}+\text{H}]^+$.

LCMS (ESI): $t_{\text{ret}} = 4.27$ min. 531 m/z $[\text{M}+\text{H}]^+$.

***tert*-butyl (4-(2-(3,5-dichloro-4-((2-(2,6-dioxopiperidin-3-yl)-1-oxoisindolin-4-yl)diazenyl)phenoxy)acetamido)butyl)carbamate (3.22)**



3.19 (100 mg, 0.183 mmol) was dissolved in a mixture of TFA and CH₂Cl₂ (1:1; 2 mL) and stirred for 2 h at room temperature. The reaction was diluted with CH₂Cl₂ (5 mL) and concentrated under reduced pressure. The reaction was triturated with Et₂O (5 mL) and concentrated twice, before being dried under vacuum for 48 h. The free acid was obtained as an orange solid and used without further purification.

The free acid (75.0 mg, 0.156 mmol, 1.0 eq.) and HATU (77.4 mg, 0.204 mmol, 1.5 eq.) were dissolved in dry DMF (2 mL) at room temperature. After 5 minutes of stirring *N*-Boc-1,4-diaminobutane (102 mg, 0.543 mmol, 4 eq.) and *i*-Pr₂NEt (70.2 mg, 0.543 mmol, 4 eq., 0.095 mL) were added to the mixture and stirred for additional 14 h at room temperature. The reaction was diluted with EtOAc (40 mL), separated against saturated NH₄Cl (30 mL), and washed with saturated NaHCO₃ (40 mL), 10% LiCl (2x 20 mL) and brine (2x 20 mL). The organic phase was dried over Na₂SO₄ and concentrated under reduced pressure. Purification of the resulting crude product by flash column chromatography (CH₂Cl₂/MeOH gradient, 0-20% MeOH) gave **3.22** (40.4 mg, 0.061 mmol, 45%) as an orange solid.

$R_f = 0.30$ [CH₂Cl₂:MeOH, 19:1].

¹H NMR (400 MHz, DMSO-*d*₆) δ = 10.99 (s, 1H), 8.26 (d, *J* = 7.8 Hz, 1H), 8.17 (t, *J* = 5.8 Hz, 1H), 8.01 (d, *J* = 7.5 Hz, 1H), 7.85 (t, *J* = 7.6 Hz, 1H), 7.32 (s, 2H), 6.78 (t, *J* = 5.7 Hz, 1H), 5.15 (dd, *J* = 13.3, 5.2 Hz, 1H), 4.78 – 4.51 (m, 4H), 3.13 (q, *J* = 6.4 Hz,

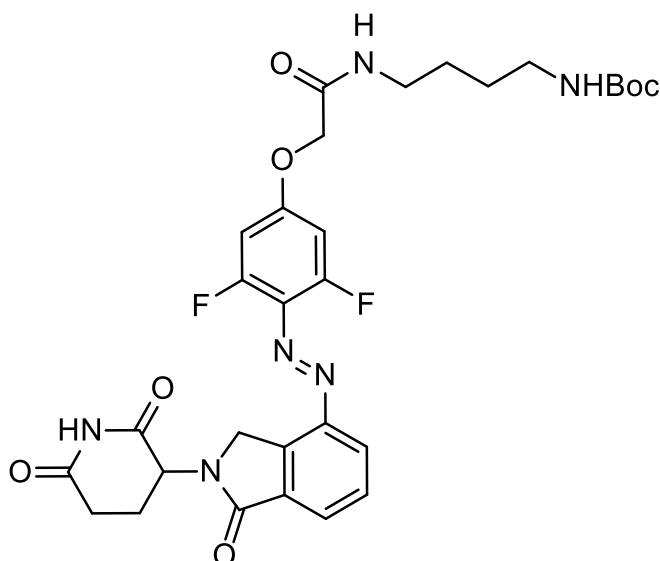
2H), 2.95 – 2.84 (m, 3H), 2.62 – 2.55 (m, 1H), 2.47 – 2.37 (m, 1H), 2.09 – 2.02 (m, 1H), 1.42 – 1.33 (m, 13H) ppm.

¹³C NMR (100 MHz, DMSO-*d*₆) δ = 172.82, 170.92, 166.87, 166.46, 158.02, 155.57, 146.44, 140.44, 134.11, 133.92, 129.93, 129.38, 127.99, 126.70, 116.38, 77.33, 67.49, 51.83, 48.41, 39.31, 38.11, 31.21, 28.26, 26.95, 26.46, 22.35 ppm.

HRMS (APCI): calcd. for $C_{30}H_{34}Cl_2N_6NaO_7^+$: 683.1758 m/z [M+Na]⁺.
found: 683.1778 m/z [M+Na]⁺.

LCMS (ESI): t_{ret} = 3.64 min (*Z*). 659 m/z [M-H]⁻.
 t_{ret} = 3.85 min (*E*). 659 m/z [M-H]⁻.

***tert*-butyl (4-(2-(4-((2-(2,6-dioxopiperidin-3-yl)-1-oxoisoindolin-4-yl)diazenyl)-3,5-difluorophenoxy)acetamido)butyl)carbamate (3.23)**



3.20 (165 mg, 0.321 mmol) was dissolved in a mixture of TFA and CH₂Cl₂ (1:1; 2 mL) and stirred for 2 h at room temperature. The reaction was diluted with CH₂Cl₂ (5 mL) and concentrated under reduced pressure. The reaction was triturated with Et₂O (5 mL) and concentrated twice, before being dried under vacuum for 48 h. The free acid (148 mg, 0.321 mmol, >99%) was obtained as an orange solid and used without further purification.

The free acid (71.5 mg, 0.156 mmol, 1.0 eq.) and HATU (88.9 mg, 0.234 mmol, 1.5 eq.) were dissolved in dry DMF (2 mL) at room temperature. After 5 minutes of stirring *N*-Boc-1,4-diaminobutane (29.4 mg, 0.156 mmol, 1 eq., 0.030 mL) and *i*-Pr₂NEt (80.6 mg, 0.624 mmol, 4 eq., 0.109 mL) were added to the mixture and stirred for additional 14 h at room temperature. The reaction was diluted with EtOAc (40 mL), separated against saturated NH₄Cl (30 mL), and washed with saturated NaHCO₃ (40 mL), 10% LiCl (2x 20 mL) and brine (2x 20 mL). The organic phase was dried over Na₂SO₄ and concentrated under reduced pressure. Purification of the resulting crude product by flash column chromatography (CH₂Cl₂/MeOH gradient, 0-20% MeOH) gave **3.23** (45 mg, 0.072 mmol, 46%) as an orange solid.

$R_f = 0.32$ [CH₂Cl₂:MeOH, 19:1].

¹H NMR (400 MHz, DMSO-*d*₆) $\delta = 11.01$ (s, 1H), 8.21 – 8.14 (m, 2H), 7.93 (d, *J* = 7.5 Hz, 1H), 7.80 (t, *J* = 7.7 Hz, 1H), 7.02 (d, *J* = 11.7 Hz, 2H), 6.78 (t, *J* = 5.7 Hz, 1H), 5.15 (dd, *J* = 13.3, 5.1 Hz, 1H), 4.75 – 4.53 (m, 4H), 3.13 (q, *J* = 6.4 Hz, 2H), 2.97 –

2.85 (m, 3H), 2.66 – 2.56 (m, 1H), 2.40 (qd, $J = 13.2, 4.5$ Hz, 1H), 2.10 – 1.99 (m, 1H), 1.42 – 1.34 (m, 4H), 1.36 (s, 9H) ppm.

^{13}C NMR (100 MHz, DMSO- d_6) $\delta = 172.82, 170.95, 167.03, 166.22, 161.01$ (t, $J = 14.5$ Hz), 156.57 (dd, $J = 259.1, 7.2$ Hz), 155.57, 147.55, 133.81, 133.74, 129.76, 129.03, 125.77, 124.50 (t, $J = 9.7$ Hz), 100.30 (dd, $J = 24.2, 2.5$ Hz), 77.33, 67.64, 51.78, 48.30, 39.31, 38.15, 31.19, 28.26, 26.95, 26.45, 22.48 ppm.

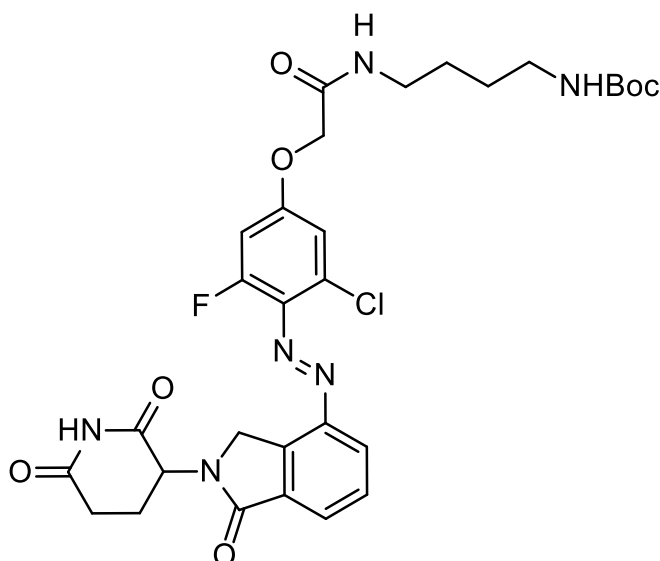
HRMS (APCI): calcd. for $\text{C}_{30}\text{H}_{35}\text{F}_2\text{N}_6\text{O}_7^+$: 629.2530 m/z $[\text{M}+\text{H}]^+$.

 found: 629.2529 m/z $[\text{M}+\text{H}]^+$.

LCMS (ESI): $t_{\text{ret}} = 3.48$ min (*Z*). 627 m/z $[\text{M}-\text{H}]^-$.

$t_{\text{ret}} = 3.66$ min (*E*). 627 m/z $[\text{M}-\text{H}]^-$.

***tert*-butyl (4-(2-(3-chloro-4-((2-(2,6-dioxopiperidin-3-yl)-1-oxoisoindolin-4-yl)diazenyl)-5-fluorophenoxy)acetamido)butyl)carbamate (3.24)**



3.21 (252 mg, 0.475 mmol) was dissolved in a mixture of TFA and CH₂Cl₂ (1:1; 2 mL) and stirred for 2 h at room temperature. The reaction was diluted with CH₂Cl₂ (5 mL) and concentrated under reduced pressure. The reaction was triturated with Et₂O (5 mL) and concentrated twice, before being dried under vacuum for 48 h. The free acid (224 mg, 0.472 mmol, >99%) was obtained as an orange solid and used without further purification.

The free acid (76.4 mg, 0.161 mmol, 1.0 eq.) and HATU (91.6 mg, 0.241 mmol, 1.5 eq.) were dissolved in dry DMF (2 mL) at room temperature. After 5 minutes of stirring *N*-Boc-1,4-diaminobutane (30.2 mg, 0.161 mmol, 1 eq., 0.031 mL) and *i*-Pr₂NEt (83.0 mg, 0.642 mmol, 4 eq., 0.112 mL) were added to the mixture and stirred for additional 16 h at room temperature. The reaction was diluted with EtOAc (40 mL), separated against saturated NH₄Cl (30 mL), and washed with saturated NaHCO₃ (40 mL), 10% LiCl (2x 20 mL) and brine (2x 20 mL). The organic phase was dried over Na₂SO₄ and concentrated under reduced pressure. Purification of the resulting crude product by flash column chromatography (CH₂Cl₂/MeOH gradient, 0-20% MeOH) gave **3.24** (61.5 mg, 0.095 mmol, 59%) as an orange solid.

$R_f = 0.22$ [CH₂Cl₂:MeOH, 19:1].

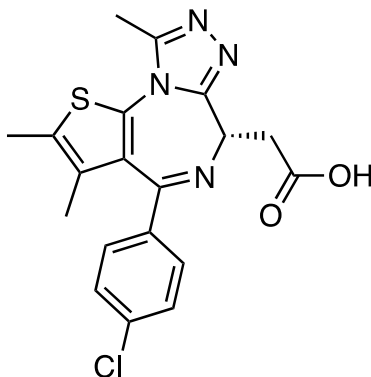
¹H NMR (400 MHz, DMSO-*d*₆) $\delta = 11.01$ (s, 1H), 8.25 (d, *J* = 7.8 Hz, 1H), 8.18 (t, *J* = 5.9 Hz, 1H), 7.96 (d, *J* = 7.5 Hz, 1H), 7.83 (t, *J* = 7.7 Hz, 1H), 7.26 (s, 1H), 7.12 (dd, *J* = 13.4, 2.6 Hz, 1H), 6.78 (t, *J* = 5.8 Hz, 1H), 5.15 (dd, *J* = 13.2, 5.1 Hz, 1H), 4.78 –

4.57 (m, 4H), 3.13 (q, J = 6.3 Hz, 2H), 2.97 – 2.84 (m, 3H), 2.65 – 2.57 (m, 1H), 2.41 (qd, J = 13.0, 3.9 Hz, 1H), 2.09 – 2.03 (m, 1H), 1.51 – 1.32 (m, 13H) ppm.

¹³C NMR (100 MHz, DMSO-*d*₆) δ = 172.84, 170.95, 166.96, 166.31, 159.88 (d, J = 13.3 Hz), 155.57, 153.23 (d, J = 262.9 Hz), 147.29, 134.84 (d, J = 6.3 Hz), 133.84, 133.02, 131.96 (d, J = 8.1 Hz), 130.47, 129.83, 126.08, 113.20 (d, J = 2.4 Hz), 103.63 (d, J = 24.2 Hz), 77.33, 67.57, 51.82, 48.91, 39.43, 38.13, 31.24, 28.26, 26.94, 26.45, 22.48 ppm.

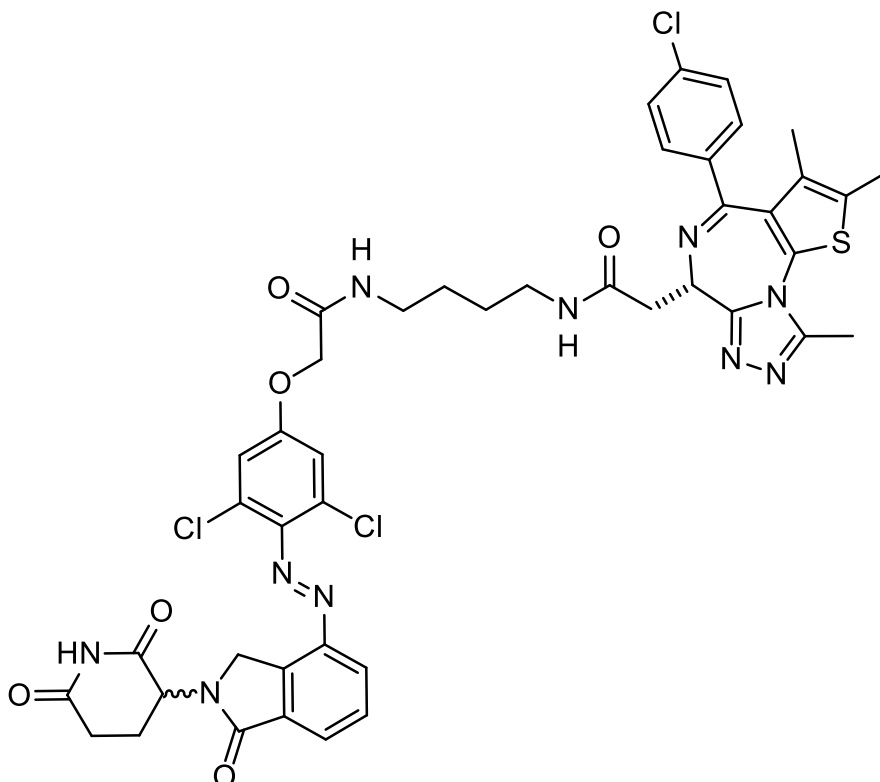
HRMS (APCI):	calcd. for C ₂₅ H ₂₇ ClFN ₆ O ₅ ⁺ :	545.1710 m/z [M–Boc+2H] ⁺ .
	found:	545.1710 m/z [M–Boc+2H] ⁺ .
LCMS (ESI):	t _{ret} = 3.61 min (<i>Z</i>).	643 m/z [M–H] [–] .
	t _{ret} = 3.77 min (<i>E</i>).	643 m/z [M–H] [–] .

(S)-2-(4-(4-chlorophenyl)-2,3,9-trimethyl-6H-thieno[3,2-f][1,2,4]triazolo[4,3-a][1,4]diazepin-6-yl)acetic acid ((+)-JQ1 free acid)



As previously described,^[13] (+)-JQ1 (9 mg, 0.02 mmol, 1 eq.) was dissolved in formic acid (0.5 mL) and stirred for 3 days at room temperature. The reaction was concentrated under reduced pressure and was dried on high vacuum overnight. **(+)-JQ1 free acid** (8.0 mg, 0.02 mmol, >99%) was obtained as yellow solid and used without further purification.

2-((S)-4-(4-chlorophenyl)-2,3,9-trimethyl-6H-thieno[3,2-f][1,2,4]triazolo[4,3-a][1,4]diazepin-6-yl)-N-(4-(2-(3,5-dichloro-4-((2-(2,6-dioxopiperidin-3-yl)-1-oxoisindolin-4-yl)diazenyl)phenoxy)acetamido)butyl)acetamide (PHOTAC-I-18)



3.22 (31.0 mg, 0.047 mmol) was dissolved in TFA/CH₂Cl₂ (1:1; 2mL:2mL) and stirred for 2 h at room temperature. The reaction was diluted with CH₂Cl₂ and concentrated under reduced pressure. The reaction was triturated with Et₂O and dried *in vacuo* for 48 h. The crude product was obtained in quantitative yield as TFA salt (>99%) as an orange solid and used without further purification.

Into a round bottom flask with dry (+)-JQ1 free acid (7.8 mg, 0.019 mmol, 1 eq.) were added the crude amine (32.4 mg, 0.039 mmol, 2 eq.) and HATU (13.3 mg, 0.035 mmol, 1.8 eq.) under nitrogen atmosphere. The solids were dissolved in dry DMF (1 mL). After addition of *i*-Pr₂NEt (18.1 mg, 0.140 mmol, 7.2 eq., 0.024 mL) the reaction was stirred for 16 h at room temperature. The mixture was then diluted with EtOAc (25 mL) separated against saturated NH₄Cl (30 mL) and washed with saturated NaHCO₃ (40 mL), 10% LiCl (2x 20 mL) and brine (2x 20 mL). The organic phase was dried over Na₂SO₄ and concentrated under reduced pressure. Purification of the

resulting crude product by flash column chromatography (CH₂Cl₂/MeOH gradient, 0-20% MeOH) gave **PHOTAC-I-18** (13.4 mg, 0.014 mmol, 73%) as an orange solid.

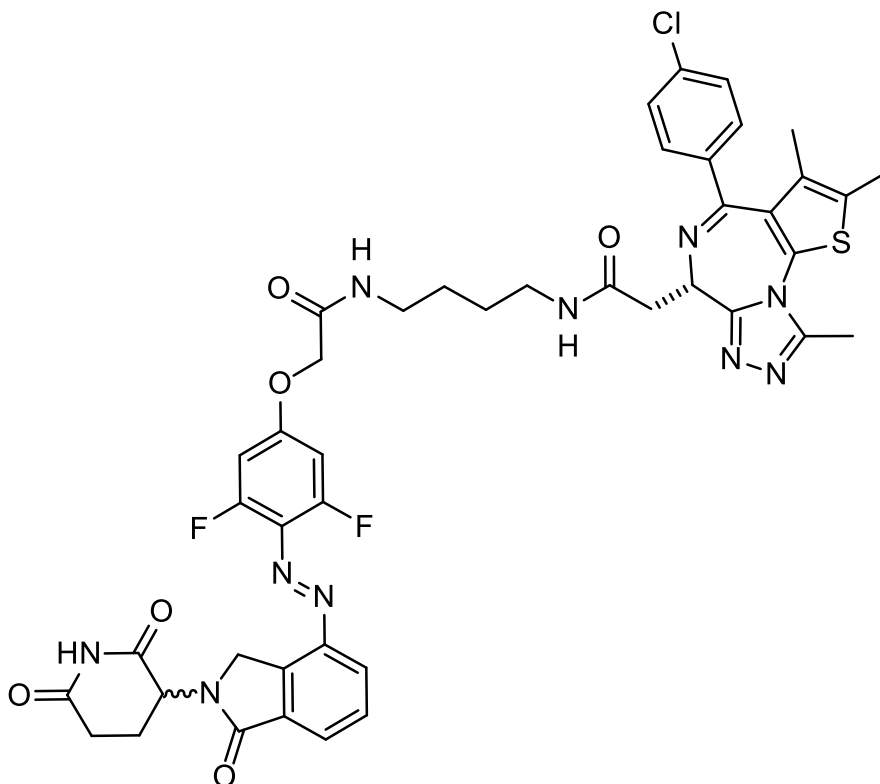
$R_f = 0.08$ [CH₂Cl₂:MeOH, 19:1].

¹H NMR (600 MHz, DMSO-*d*₆) $\delta = 11.00$ (s, 1H), 8.25 (d, *J* = 7.7 Hz, 1H), 8.23 – 8.19 (m, 2H), 8.00 (d, *J* = 7.5 Hz, 1H), 7.84 (t, *J* = 7.7 Hz, 1H), 7.47 (d, *J* = 8.2 Hz, 2H), 7.40 (d, *J* = 8.1 Hz, 2H), 7.31 (s, 2H), 5.13 (dd, *J* = 13.3, 5.1 Hz, 1H), 4.76 – 4.59 (m, 4H), 4.49 (dd, *J* = 8.2, 6.1 Hz, 1H), 3.25 (dd, *J* = 15.1, 8.4 Hz, 1H), 3.21 – 3.05 (m, 5H), 2.88 (ddd, *J* = 18.2, 13.5, 5.4 Hz, 1H), 2.63 – 2.58 (m, 1H), 2.58 (s, 3H), 2.47 – 2.38 (m, 1H), 2.39 (s, 3H), 2.06 – 2.00 (m, 1H), 1.60 (s, 3H), 1.47 (ddd, *J* = 21.3, 11.5, 5.6 Hz, 4H) ppm.

¹³C NMR (150 MHz, DMSO-*d*₆) $\delta = 172.99, 171.04, 169.58, 167.05, 166.68, 163.17, 158.08, 155.19, 149.96, 146.54, 140.55, 136.83, 135.33, 134.13, 133.98, 132.31, 130.84, 130.20, 130.07, 129.93, 129.66, 129.61, 128.56, 128.12, 126.82, 116.47, 67.57, 53.96, 51.98, 48.59, 38.28, 38.16, 37.73, 31.29, 26.70, 26.57, 22.45, 14.13, 12.76, 11.38$ ppm.

HRMS (APCI):	calcd. for C ₄₄ H ₄₂ Cl ₃ N ₁₀ O ₆ S ⁺ :	945.2040 m/z [M+H] ⁺ .
	found:	945.2006 m/z [M+H] ⁺ .
LCMS (ESI):	$t_{\text{ret}} = 3.80$ min (<i>Z</i>).	943 m/z [M+H] ⁺ .
	$t_{\text{ret}} = 3.96$ min (<i>E</i>).	943 m/z [M+H] ⁺ .

2-((S)-4-(4-chlorophenyl)-2,3,9-trimethyl-6H-thieno[3,2-f][1,2,4]triazolo[4,3-a][1,4]diazepin-6-yl)-N-(4-(2-(4-((2-(2,6-dioxopiperidin-3-yl)-1-oxoisindolin-4-yl)diazenyl)-3,5-difluorophenoxy)acetamido)butyl)acetamide (PHOTAC-I-21)



3.23 (35.6 mg, 0.057 mmol) was dissolved in TFA/CH₂Cl₂ (1:1; 2mL:2mL) and stirred for 2 h at room temperature. The reaction was diluted with CH₂Cl₂ and concentrated under reduced pressure. The reaction was triturated with Et₂O and dried *in vacuo* for 48 h. The crude product was obtained in quantitative yield as TFA salt (>99%) as an orange solid and used without further purification.

Into a round bottom flask with dry (+)-JQ1 free acid (7.9 mg, 0.020 mmol, 1 eq.) were added the crude amine (20.6 mg, 0.030 mmol, 1.5 eq.) and HATU (13.5 mg, 0.035 mmol, 1.8 eq.) under nitrogen atmosphere. The solids were dissolved in dry DMF (1 mL). After addition of *i*-Pr₂NEt (18.3 mg, 0.142 mmol, 7.2 eq., 0.025 mL) the reaction was stirred for 16 h at room temperature. The mixture was then diluted with EtOAc (25 mL) separated against saturated NH₄Cl (30 mL) and washed with saturated NaHCO₃ (40 mL), 10% LiCl (2x 20 mL) and brine (2x 20 mL). The organic phase was dried over Na₂SO₄ and concentrated under reduced pressure. Purification of the

resulting crude product by flash column chromatography (CH₂Cl₂/MeOH gradient, 0-20% MeOH) gave **PHOTAC-I-21** (16.9mg, 0.019 mmol, 94%) as an orange solid.

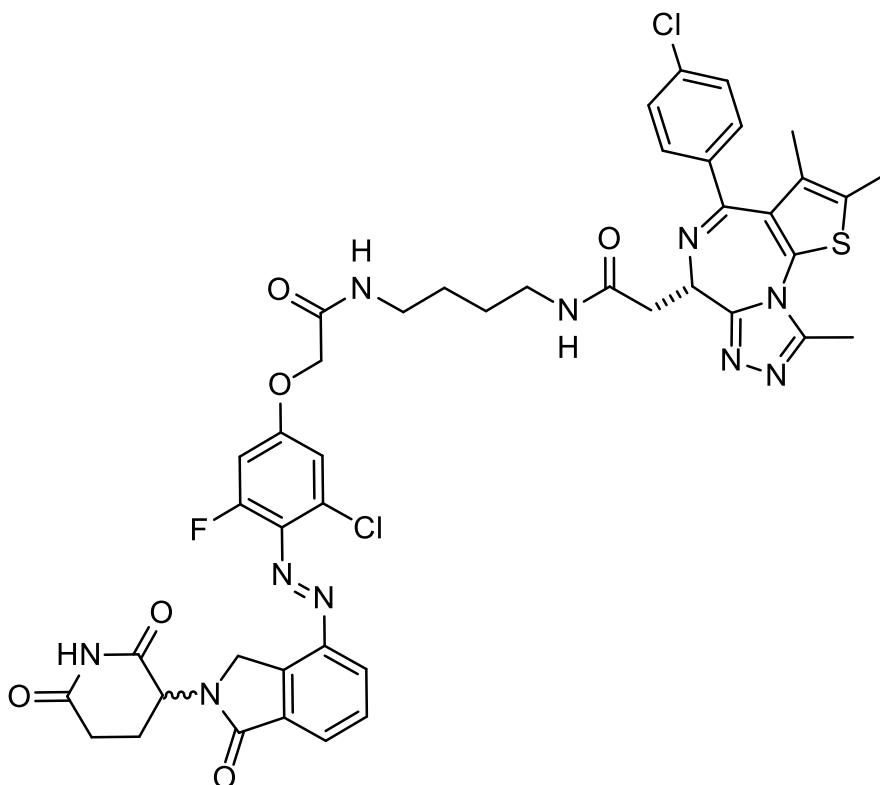
$R_f = 0.09$ [CH₂Cl₂:MeOH, 19:1].

¹H NMR (600 MHz, DMSO-*d*₆) $\delta = 11.02$ (s, 1H), 8.22 (q, *J* = 6.0 Hz, 2H), 8.17 (d, *J* = 7.8 Hz, 1H), 7.93 (d, *J* = 7.5 Hz, 1H), 7.80 (t, *J* = 7.6 Hz, 1H), 7.47 (d, *J* = 8.2 Hz, 2H), 7.40 (d, *J* = 7.7 Hz, 2H), 7.01 (d, *J* = 12.1 Hz, 2H), 5.13 (dd, *J* = 13.2, 5.4 Hz, 1H), 4.71 – 4.55 (m, 4H), 4.51 – 4.47 (m, 1H), 3.27 – 3.21 (m, 1H), 3.20 – 3.05 (m, 5H), 2.90 (ddd, *J* = 18.4, 13.6, 5.4 Hz, 1H), 2.60 – 2.59 (m, 1H), 2.58 (s, 3H), 2.41 – 2.37 (m, 4H), 2.05 (h, *J* = 5.4, 4.1 Hz, 1H), 1.60 (s, 3H), 1.53 – 1.41 (m, 4H) ppm.

¹³C NMR (150 MHz, DMSO-*d*₆) $\delta = 173.00, 171.07, 169.58, 167.22, 166.46, 163.18, 161.07$ (t, *J* = 14.5 Hz), 156.69 (dd, *J* = 259.2, 7.3 Hz), 155.19, 149.97, 147.65, 136.84, 135.33, 133.86, 133.77, 132.31, 130.84, 130.20, 129.94, 129.90, 129.67, 129.27, 128.57, 125.90, 124.61 (t, *J* = 9.5 Hz), 100.40 (dd, *J* = 24.0, 2.2 Hz), 67.72, 53.95, 51.92, 48.48, 38.29, 38.21, 37.72, 31.28, 26.71, 26.58, 22.59, 14.13, 12.77, 11.38 ppm.

HRMS (APCI):	calcd. for C ₄₄ H ₄₁ ClF ₂ N ₁₀ NaO ₆ S ⁺ :	933.2480 m/z [M+Na] ⁺ .
	found:	933.2453 m/z [M+Na] ⁺ .
LCMS (ESI):	$t_{ret} = 3.38$ min (<i>Z</i>).	911 m/z [M+H] ⁺ .
	$t_{ret} = 3.48$ min (<i>E</i>).	911 m/z [M+H] ⁺ .

2-(3-chloro-4-((2-(2,6-dioxopiperidin-3-yl)-1-oxoisindolin-4-yl)diazenyl)-5-fluorophenoxy)-N-(4-(2-((S)-4-(4-chlorophenyl)-2,3,9-trimethyl-6H-thieno[3,2-f][1,2,4]triazolo[4,3-a][1,4]diazepin-6-yl)acetamido)butyl)acetamide (PHOTAC-I-20)



3.24 (50.5 mg, 0.078 mmol) was dissolved in TFA/CH₂Cl₂ (1:1; 2mL:2mL) and stirred for 2 h at room temperature. The reaction was diluted with CH₂Cl₂ and concentrated under reduced pressure. The reaction was triturated with Et₂O and dried *in vacuo* for 48 h. The crude product was obtained in quantitative yield as TFA salt (>99%) as an orange solid and used without further purification.

Into a round bottom flask with dry (+)-JQ1 free acid (7.8 mg, 0.019 mmol, 1 eq.) were added the crude amine (27.9 mg, 0.039 mmol, 2 eq.) and HATU (13.3 mg, 0.035 mmol, 1.8 eq.) under nitrogen atmosphere. The solids were dissolved in dry DMF (1 mL). After addition of *i*-Pr₂NEt (18.1 mg, 0.140 mmol, 7.2 eq., 0.024 mL) the reaction was stirred for 16 h at room temperature. The mixture was then diluted with EtOAc (25 mL) separated against saturated NH₄Cl (30 mL) and washed with saturated NaHCO₃ (40 mL), 10% LiCl (2x 20 mL) and brine (2x 20 mL). The organic phase was dried over Na₂SO₄ and concentrated under reduced pressure. Purification of the

resulting crude product by flash column chromatography (CH₂Cl₂/MeOH gradient, 0-20% MeOH) gave **PHOTAC-I-20** (17.3 mg, 0.019 mmol, 96%) as an orange solid.

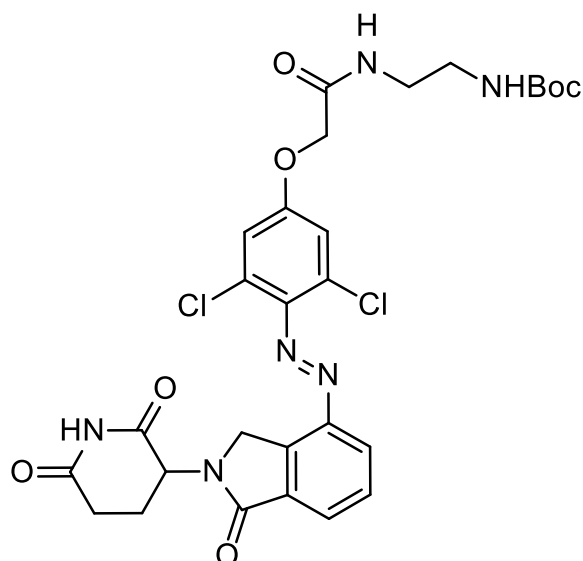
$R_f = 0.07$ [CH₂Cl₂:MeOH, 19:1].

¹H NMR (600 MHz, DMSO-*d*₆) $\delta = 11.01$ (s, 1H), 8.27 – 8.18 (m, 3H), 7.95 (d, *J* = 7.5 Hz, 1H), 7.82 (t, *J* = 7.6 Hz, 1H), 7.47 (d, *J* = 8.2 Hz, 2H), 7.40 (d, *J* = 8.2 Hz, 2H), 7.25 (d, *J* = 2.5 Hz, 1H), 7.10 (dd, *J* = 13.3, 2.7 Hz, 1H), 5.13 (dd, *J* = 13.3, 5.1 Hz, 1H), 4.74 – 4.58 (m, 4H), 4.52 – 4.46 (m, 1H), 3.29 – 3.04 (m, 6H), 2.89 (ddd, *J* = 18.1, 13.4, 5.4 Hz, 1H), 2.65 – 2.59 (m, 1H), 2.58 (s, 3H), 2.44 – 2.34 (m, 4H), 2.10 – 2.01 (m, 1H), 1.60 (s, 3H), 1.47 (ddt, *J* = 16.5, 10.3, 5.7 Hz, 4H) ppm.

¹³C NMR (150 MHz, DMSO-*d*₆) $\delta = 173.00, 171.06, 169.57, 167.13, 166.53, 163.16, 159.94$ (d, *J* = 13.4 Hz), 155.18, 153.32 (d, *J* = 263.0 Hz), 149.95, 147.38, 136.83, 135.32, 135.01 (d, *J* = 6.2 Hz), 133.89, 133.03, 132.31, 132.06 (d, *J* = 8.2 Hz), 130.83, 130.70, 130.19, 129.97, 129.92, 129.65, 128.56, 126.19, 113.29 (d, *J* = 1.8 Hz), 103.71 (d, *J* = 24.2 Hz), 67.65, 53.95, 51.96, 49.09, 38.28, 38.18, 37.72, 31.32, 26.70, 26.56, 22.58, 14.12, 12.76, 11.37 ppm.

HRMS (APCI):	calcd. for C ₄₄ H ₄₂ Cl ₂ FN ₁₀ O ₆ S ⁺ :	927.2365 m/z [M+H] ⁺ .
	found:	927.2319 m/z [M+H] ⁺ .
LCMS (ESI):	<i>t</i> _{ret} = 3.76 min (<i>Z</i>).	927 m/z [M+H] ⁺ .
	<i>t</i> _{ret} = 3.87 min (<i>E</i>).	927 m/z [M+H] ⁺ .

tert-butyl (2-(2-(3,5-dichloro-4-((2-(2,6-dioxopiperidin-3-yl)-1-oxoisindolin-4-yl)diazenyl)phenoxy)acetamido)ethyl)carbamate (3.25)



3.19 (100 mg, 0.183 mmol) was dissolved in a mixture of TFA and CH₂Cl₂ (1:1; 2 mL) and stirred for 2 h at room temperature. The reaction was diluted with CH₂Cl₂ (5 mL) and concentrated under reduced pressure. The reaction was triturated with Et₂O (5 mL) and concentrated twice, before being dried under vacuum for 48 h. The free acid was obtained as an orange solid and used without further purification.

The free acid (24.0 mg, 0.049 mmol, 1.0 eq.) and HATU (27.9 mg, 0.073 mmol, 1.5 eq.) were dissolved in dry DMF (2 mL) at room temperature. After 5 minutes of stirring *N*-Boc-1,4-diaminoethane (31.3 mg, 0.195 mmol, 4 eq.) and *i*-Pr₂NEt (25.3 mg, 0.195 mmol, 4 eq., 0.034 mL) were added to the mixture and stirred for additional 16 h at room temperature. The reaction was diluted with EtOAc (40 mL), separated against saturated NH₄Cl (30 mL), and washed with saturated NaHCO₃ (40 mL), 10% LiCl (2x 20 mL) and brine (2x 20 mL). The organic phase was dried over Na₂SO₄ and concentrated under reduced pressure. Purification of the resulting crude product by flash column chromatography (CH₂Cl₂/MeOH gradient, 0-20% MeOH) gave **3.25** (14.1 mg, 0.022 mmol, 46%) as an orange solid.

$R_f = 0.36$ [CH₂Cl₂:MeOH, 19:1].

¹H NMR (400 MHz, DMSO-*d*₆) δ = 11.00 (s, 1H), 8.26 (dd, *J* = 7.9, 1.0 Hz, 1H), 8.21 (t, *J* = 5.8 Hz, 1H), 8.01 (d, *J* = 7.2 Hz, 1H), 7.85 (t, *J* = 7.7 Hz, 1H), 6.88 (t, *J* = 5.7 Hz, 1H), 5.15 (dd, *J* = 13.3, 5.2 Hz, 1H), 4.78 – 4.60 (m, 4H), 3.17 (q, *J* = 6.4 Hz, 2H), 3.04

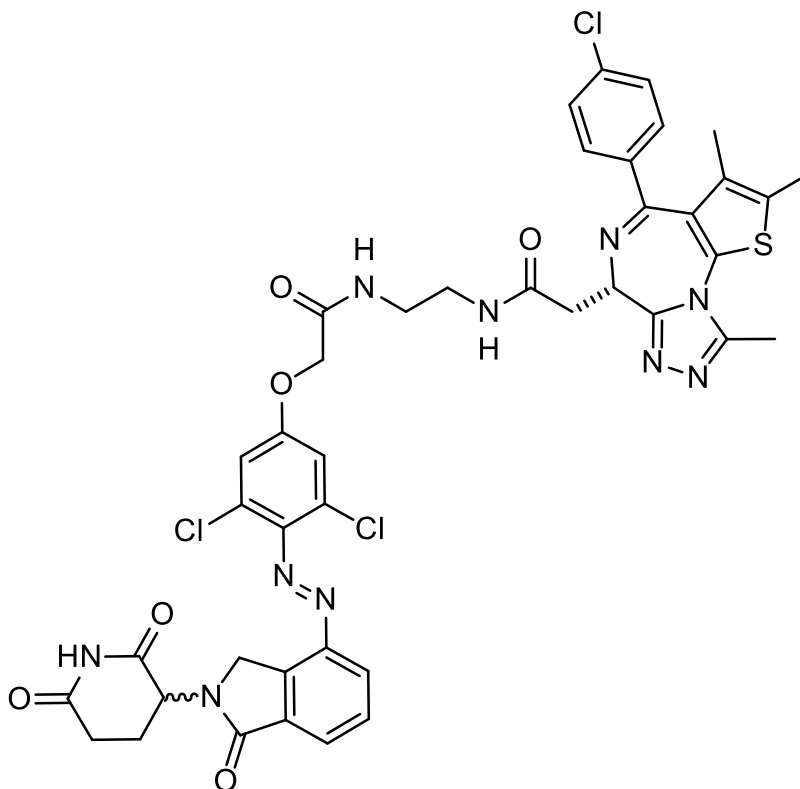
(q, $J = 6.3$ Hz, 2H), 2.90 (ddd, $J = 17.2, 13.5, 5.4$ Hz, 1H), 2.59 (dt, $J = 16.9, 3.2$ Hz, 1H), 2.48 – 2.37 (m, 1H), 2.05 (dtt, $J = 7.8, 5.6, 2.2$ Hz, 1H) 1.38 (s, 9H) ppm.

¹³C NMR (100 MHz, DMSO) $\delta = 172.83, 170.93, 166.87, 161.23, 157.95, 155.77, 146.45, 140.47, 134.09, 133.92, 129.93, 129.42, 128.01, 126.71, 116.39, 77.76, 67.43, 51.83, 48.42, 39.39, 38.80, 31.21, 28.22, 22.37$ ppm.

HRMS (APCI): calcd. for $C_{28}H_{34}Cl_2N_7O_7^+$: 650.1891 m/z $[M]^+$.
 found: 650.1881 m/z $[M+NH_4]^+$.

LCMS (ESI): $t_{ret} = 3.53$ min (*Z*). 655 m/z $[M+Na]^+$.
 $t_{ret} = 3.76$ min (*E*). 655 m/z $[M+Na]^+$.

2-((S)-4-(4-chlorophenyl)-2,3,9-trimethyl-6H-thieno[3,2-f][1,2,4]triazolo[4,3-a][1,4]diazepin-6-yl)-N-(2-(2-(3,5-dichloro-4-((2-(2,6-dioxopiperidin-3-yl)-1-oxoisindolin-4-yl)diazenyl)phenoxy)acetamido)ethyl)acetamide (PHOTAC-I-19)



3.25 (10.9 mg, 0.017 mmol) was dissolved in TFA/CH₂Cl₂ (1:1; 2mL:2mL) and stirred for 2 h at room temperature. The reaction was diluted with CH₂Cl₂ and concentrated under reduced pressure. The reaction was triturated with Et₂O and dried *in vacuo* for 48 h. The crude product was obtained in quantitative yield as TFA salt (>99%) as an orange solid and used without further purification.

Into a round bottom flask with dry (+)-JQ1 free acid (7.0 mg, 0.017 mmol, 1 eq.) were added the crude amine (0.017 mmol, 1 eq.) and HATU (12.0 mg, 0.031 mmol, 1.8 eq.) under nitrogen atmosphere. The solids were dissolved in dry DMF (1 mL). After addition of *i*-Pr₂NEt (16.2 mg, 0.126 mmol, 7.2 eq., 0.022 mL) the reaction was stirred for 16 h at room temperature. The mixture was then diluted with EtOAc (25 mL) separated against saturated NH₄Cl (30 mL) and washed with saturated NaHCO₃ (40 mL), 10% LiCl (2x 20 mL) and brine (2x 20 mL). The organic phase was dried over Na₂SO₄ and concentrated under reduced pressure. Purification of the resulting crude

product by flash column chromatography (CH₂Cl₂/MeOH gradient, 0-20% MeOH) gave **PHOTAC-I-19** (6.8 mg, 0.007 mmol, 43%) as an orange solid.

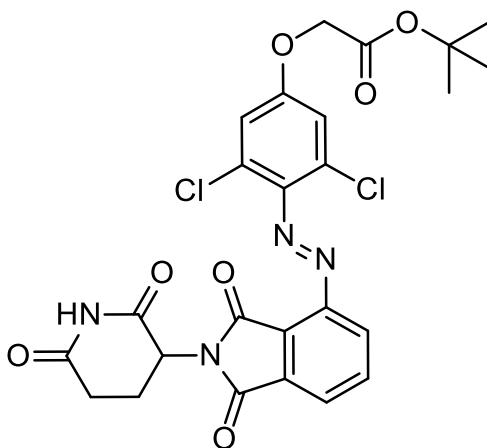
$R_f = 0.13$ [CH₂Cl₂:MeOH, 19:1].

¹H NMR (400 MHz, DMSO-*d*₆) $\delta = 11.00$ (s, 1H), 8.40 (t, $J = 5.3$ Hz, 1H), 8.25 (d, $J = 7.7$ Hz, 2H), 8.01 (dd, $J = 7.6, 1.0$ Hz, 1H), 7.86 (t, $J = 7.7$ Hz, 1H), 7.46 (d, $J = 8.2$ Hz, 2H), 7.41 (d, $J = 8.6$ Hz, 2H), 7.33 (s, 2H), 5.15 (ddd, $J = 13.3, 5.1, 1.4$ Hz, 1H), 4.78 – 4.60 (m, 4H), 4.53 (td, $J = 7.6, 7.2, 1.8$ Hz, 1H), 3.30 – 3.21 (m, 6H), 2.91 (ddd, $J = 17.8, 13.5, 5.4$ Hz, 1H), 2.61 (dd, $J = 6.4, 3.4$ Hz, 1H), 2.58 (d, $J = 1.9$ Hz, 3H), 2.48 – 2.39 (m, 1H), 2.37 (s, 3H), 2.05 (ddtd, $J = 10.2, 7.7, 5.0, 2.6$ Hz, 1H), 1.56 (d, $J = 2.8$ Hz, 3H) ppm.

¹³C NMR (100 MHz, DMSO) $\delta = 172.83, 170.92, 170.27, 170.25, 166.87, 163.11, 157.89, 155.00, 149.86, 146.44, 140.47, 136.73, 135.21, 134.07, 133.92, 132.25, 130.67, 130.13, 129.93, 129.82, 129.46, 129.42, 128.44, 128.03, 126.71, 116.40, 67.43, 53.80, 51.83, 48.42, 40.19, 38.05, 37.67, 31.21, 22.38, 14.00, 12.64, 11.30$ ppm.

HRMS (APCI):	calcd. for C ₄₂ H ₃₇ Cl ₃ N ₁₀ O ₆ S ⁺ :	917.1688 m/z [M] ⁺ .
	found:	917.1648 m/z [M] ⁺ .
LCMS (ESI):	$t_{ret} = 3.56$ min (<i>E</i>).	917 m/z [M+H] ⁺ .

tert-butyl 2-(3,5-dichloro-4-((2-(2,6-dioxopiperidin-3-yl)-1,3-dioxoisindolin-4-yl)diazenyl)phenoxy)acetate (3.26)



Pomalidomide (273 mg, 1.00 mmol, 1.0 eq.) was dissolved in 1 M HCl (50 mL) and concentrated aqueous HBF₄ (1 mL) was added to the mixture. After completely dissolving the starting material, 2 M NaNO₂ (1.05 mL) was added to the solution at 0 °C. After stirring the solution for 1 h, it was added dropwise into a mixture of 3,5-dichlorophenol (171 mg, 1.05 mmol, 1.05 eq.) in H₂O (30 mL), MeOH (10 mL), NaHCO₃ (4.15 g, 49.4 mmol, 24.7 eq.) and Na₂CO₃ (5.18 g, 48.9 mmol, 24.5 eq.) at 0°C. Upon addition the solution turned from white to orange/red and was stirred for additional 1 h at 0°C. The reaction was extracted with a CH₂Cl₂:isopropanol mixture (5:1, 4x 200 mL) and washed once with brine (1x 100 mL). The organic phase was dried over Na₂SO₄ and then concentrated under reduced pressure. The solid was washed with diethyl ether (100 mL) and dried to yield the crude intermediate *p*-hydroxy azobenzene as a red solid (358 mg, 80%).

To a solution of the crude *p*-hydroxy azobenzene (358 mg, 0.80 mmol, 1 eq.) dissolved in dry DMF (14 mL) was added K₂CO₃ (340 mg, 2.46 mmol, 3.1 eq.) and tert-butyl bromoacetate (156 mg, 0.80 mmol, 1 eq., 0.118 mL). After addition, the reaction was stirred for 14 h at room temperature. Then, the mixture was diluted with EtOAc (100 mL), separated against saturated NaHCO₃ (50 mL), extracted with EtOAc (3x 50 mL), and washed with aqueous 10% LiCl solution (1x 50 mL) and brine (2x 50 mL). The organic phase was concentrated under reduced pressure. Purification of the resulting crude product by flash column chromatography (Hx/EA gradient, 20 → 100% EA) gave **3.26** (140 mg, 0.249 mmol, 31%) as a red solid.

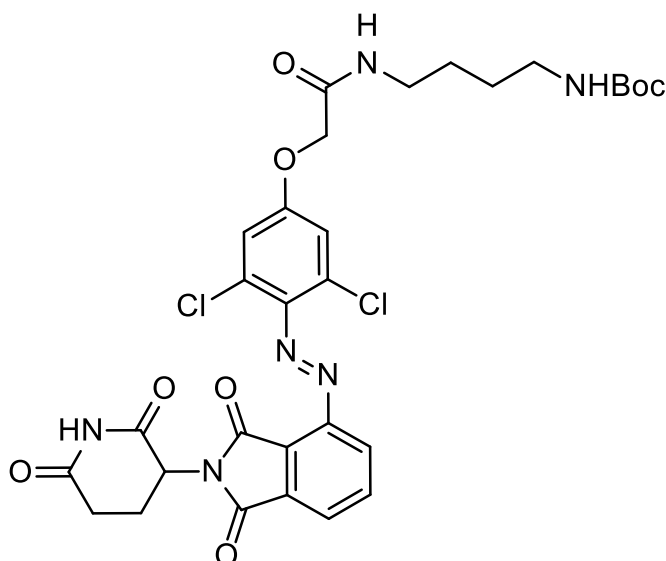
$R_f = 0.51$ [CH_2Cl_2 :MeOH,19:1].

^1H NMR (400 MHz, DMSO- d_6) $\delta = 11.15$ (s, 1H), 8.13 (dd, $J = 7.4, 1.0$ Hz, 1H), 8.04 (t, $J = 7.7$ Hz, 1H), 7.84 (dd, $J = 8.0, 1.0$ Hz, 1H), 7.32 (s, 2H), 5.19 (dd, $J = 12.9, 5.4$ Hz, 1H), 4.89 (s, 2H), 2.89 (ddd, $J = 17.4, 14.1, 5.4$ Hz, 1H), 2.68 – 2.51 (m, 2H), 2.10 (ddd, $J = 12.2, 6.2, 3.8$ Hz, 1H), 1.44 (s, 9H) ppm.

^{13}C NMR (100 MHz, DMSO) $\delta = 172.93, 169.94, 167.17, 166.55, 165.03, 158.72, 147.67, 140.43, 136.37, 133.09, 128.67, 126.07, 125.70, 122.06, 116.39, 82.15, 65.78, 49.25, 31.03, 27.80, 21.99$ ppm.

HRMS (APCI):	calcd. for $\text{C}_{25}\text{H}_{23}\text{Cl}_2\text{N}_4\text{O}_7^+$:	561.0938 m/z $[\text{M}+\text{H}]^+$
	found:	561.0922 m/z $[\text{M}+\text{H}]^+$.
LCMS (ESI):	$t_{\text{ret}} = 3.99$ min (<i>Z</i>).	561 m/z $[\text{M}+\text{H}]^+$.
	$t_{\text{ret}} = 4.35$ min (<i>E</i>).	561 m/z $[\text{M}+\text{H}]^+$.

***tert*-butyl (4-(2-(3,5-dichloro-4-((2-(2,6-dioxopiperidin-3-yl)-1,3-dioxoisindolin-4-yl)diazenyl)phenoxy)acetamido)butyl)carbamate (3.27)**



3.26 (77 mg, 0.137 mmol, 1 eq.) was dissolved in a mixture of TFA and CH₂Cl₂ (1:1; 2 mL) and stirred for 2 h at room temperature. The reaction was diluted with CH₂Cl₂ (5 mL) and concentrated under reduced pressure. The reaction was triturated with Et₂O (5 mL) and concentrated twice, before being dried under vacuum for 48 h. The free acid (69 mg, 0.137 mmol, >99%) was obtained as an orange solid and used without further purification.

The free acid (69.0 mg, 0.137 mmol, 1.0 eq.) and HATU (74.2 mg, 0.195 mmol, 1.43 eq.) were dissolved in dry DMF (2 mL) at room temperature. After 5 minutes of stirring *N*-Boc-1,4-diaminobutane (98 mg, 0.521 mmol, 3.8 eq.) and *i*-Pr₂NEt (67 mg, 0.518 mmol, 3.8 eq., 0.090 mL) were added to the mixture and stirred for additional 14 h at room temperature. The reaction was diluted with EtOAc (40 mL), separated against saturated NH₄Cl (30 mL), and washed with saturated NaHCO₃ (40 mL), 10% LiCl (2x 20 mL) and brine (2x 20 mL). The organic phase was dried over Na₂SO₄ and concentrated under reduced pressure. Purification of the resulting crude product by flash column chromatography (CH₂Cl₂/MeOH gradient, 0-20% MeOH) gave **3.27** (40.4 mg, 0.060 mmol, 44%) as an orange solid and a mixture of *E*- and *Z*-isomers.

$R_f = 0.42$ [CH₂Cl₂:MeOH, 19:1].

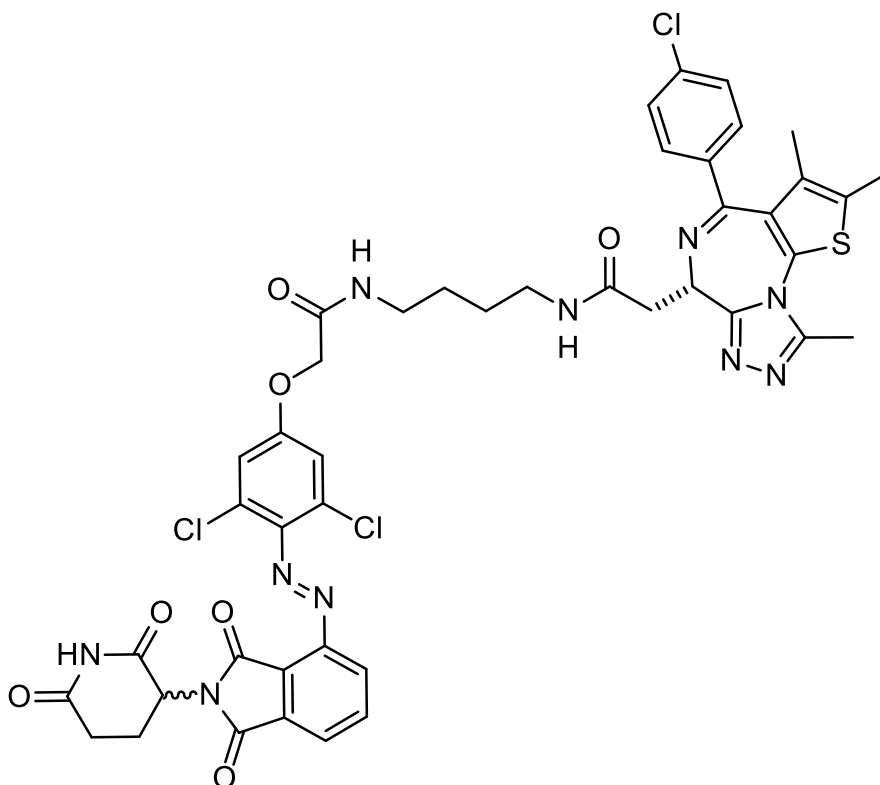
¹H NMR (400 MHz, CDCl₃) δ = 8.30(*E*) (s, 0.5H), 8.04(*E*) (dd, *J* = 7.2, 1.1 Hz, 0.5H), 7.95(*E*) (dd, *J* = 8.1, 1.1 Hz, 0.5H), 7.87(*E*) (dd, *J* = 8.2, 7.2 Hz, 0.5H), 7.43(*Z*) (dd, *J* =

8.4, 7.1 Hz, 0.5H), 7.15(Z) (d, $J = 7.1$ Hz, 0.5H), 7.05 (s, 2H), 6.88(Z) (d, $J = 8.3$ Hz, 0.5H), 6.66(E) 6.28(Z) (s, 1H), 5.04 (m, 1H), 4.53(E) 4.48(S) (s(E), d(Z), $J = 1.9$ Hz, 2H), 3.44 – 3.07 (m, 4H), 3.02 – 2.62 (m, 3H), 2.18 (dtd, $J = 9.6, 5.1, 2.0$ Hz, 1H), 1.65 – 1.44 (m, 4H), 1.43 (s, 9H) ppm.

^{13}C NMR (100 MHz, CDCl_3) $\delta = 170.94, 170.84, 169.24, (Z) 169.05(Z), 167.96(E), 167.72(Z), 166.74(E), 166.72/166.67(E/Z), 165.28(E), 157.53, 156.32/156.26(E/Z), 148.31(E), 145.95(Z), 141.86, 135.86(Z), 135.51(E), 133.29(E), 132.34(Z), 130.14 126.82(E), 126.15(E), 122.20(E), 121.77(Z), 116.18, 113.40(Z), 110.62(Z), 79.43, 67.81(E), 49.64/49.33(E/Z), 43.47(Z), 40.16, 39.54/39.04(E/Z), 31.54/31.38(E/Z), 28.56, 27.76/27.60(E/Z), 26.70/26.47(E/Z), 22.70/22.48(E/Z) ppm.$

HRMS (APCI):	calcd. for $\text{C}_{30}\text{H}_{33}\text{Cl}_2\text{N}_6\text{O}_8^+$:	675.1731 m/z $[\text{M}+\text{H}]^+$
	found:	675.1746 m/z $[\text{M}+\text{H}]^+$.
LCMS (ESI):	$t_{\text{ret}} = 3.17$ min (Z).	697 m/z $[\text{M}+\text{Na}]^+$.
	$t_{\text{ret}} = 3.74$ min (E).	697 m/z $[\text{M}+\text{Na}]^+$.

2-((S)-4-(4-chlorophenyl)-2,3,9-trimethyl-6H-thieno[3,2-f][1,2,4]triazolo[4,3-a][1,4]diazepin-6-yl)-N-(4-(2-(3,5-dichloro-4-((2-(2,6-dioxopiperidin-3-yl)-1,3-dioxoisindolin-4-yl)diazenyl)phenoxy)acetamido)butyl)acetamide (PHOTAC-I-22)



3.27 (16 mg, 0.024 mmol) was dissolved in TFA/CH₂Cl₂ (1:1; 2mL:2mL) and stirred for 2 h at room temperature. The reaction was diluted with CH₂Cl₂ and concentrated under reduced pressure. The reaction was triturated with Et₂O and dried *in vacuo* for 48 h. The crude product was obtained in quantitative yield as TFA salt (>99%) as an orange solid and used without further purification.

Into a round bottom flask with dry (+)-JQ1 free acid (7.0 mg, 0.017 mmol, 1 eq.) were added the crude amine (16.5 mg, 0.024 mmol, 1.3 eq.) and HATU (12.0 mg, 0.031 mmol, 1.8 eq.) under nitrogen atmosphere. The solids were dissolved in dry DMF (1 mL). After addition of *i*-Pr₂NEt (16.2 mg, 0.126 mmol, 7.2 eq., 0.022 mL) the reaction was stirred for 18 h at room temperature. The mixture was then diluted with EtOAc (25 mL) separated against saturated NH₄Cl (30 mL) and washed with saturated NaHCO₃ (40 mL), 10% LiCl (2x 20 mL) and brine (2x 20 mL). The organic phase was dried over Na₂SO₄ and concentrated under reduced pressure. Purification of the

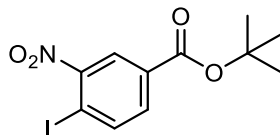
resulting crude product by flash column chromatography (CH₂Cl₂/MeOH gradient, 0-20% MeOH) gave a crude red solid which was further Purified by HPLC ((H₂O/MeCN + 0.1% FA gradient, 5-100% MeCN) to yield **PHOTAC-I-22** (4.1 mg, 0.004 mmol, 25%) as a red solid.

$R_f = 0.08$ [CH₂Cl₂:MeOH, 19:1].

¹H NMR (600 MHz, DMSO-*d*₆) δ = 11.16 (s, 1H), 8.21 (td, *J* = 5.8, 2.3 Hz, 2H), 8.14 (d, *J* = 7.0 Hz, 1H), 8.05 (t, *J* = 7.7 Hz, 1H), 7.85 (dd, *J* = 8.1, 0.9 Hz, 1H), 7.49 (d, *J* = 8.6 Hz, 2H), 7.42 (d, *J* = 8.4 Hz, 2H), 7.35 (s, 2H), 5.21 (dd, *J* = 12.8, 5.5 Hz, 1H), 4.69 (s, 2H), 4.51 (dd, *J* = 8.3, 5.9 Hz, 1H), 3.26 (dd, *J* = 15.0, 8.3 Hz, 1H), 3.22 – 3.07 (m, 5H), 2.90 (ddd, *J* = 17.0, 13.8, 5.5 Hz, 1H), 2.65 – 2.53 (m, 5H), 2.41 (s, 3H), 2.10 (dtd, *J* = 13.0, 5.3, 2.3 Hz, 1H), 1.62 (s, 3H), 1.54 – 1.44 (m, 4H) ppm.

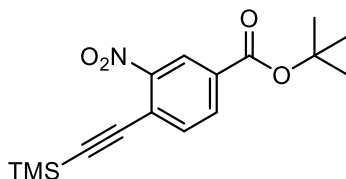
¹³C NMR (150 MHz, DMSO) δ = 173.23, 170.28, 169.84, 166.93, 166.89, 165.38, 163.47, 159.11, 155.57, 150.28, 148.02, 140.71, 137.20, 136.69, 135.68, 133.48, 132.72, 131.16, 130.58, 130.28, 130.02, 129.06, 128.94, 126.39, 126.11, 122.36, 116.93, 68.00, 54.34, 49.61, 38.64, 38.53, 38.10, 31.41, 27.10, 26.97, 22.35, 14.52, 13.15, 11.77 ppm.

HRMS (APCI):	calcd. for C ₄₄ H ₄₀ Cl ₃ N ₁₀ O ₇ S ⁺ :	957.1862 m/z [M+H] ⁺
	found:	957.1821 m/z [M+H] ⁺ .
LCMS (ESI):	$t_{ret} = 3.81$ min (<i>E</i>).	959 m/z [M+H] ⁺ .

***tert*-Butyl 4-iodo-3-nitrobenzoate (3.28)**

3.28 was prepared similar to the previously described method^[42]: Conc. H₂SO₄ (0.5 mL, 10 mmol, 1.0 eq.) was added to a stirred suspension of MgSO₄ (4.9 g, 40.00 mmol, 4.0 eq.) in dry CH₂Cl₂ (30 mL). After 20 min of stirring, 4-iodo-3-nitrobenzoic acid (2.93 g, 10.00 mmol, 1.0 eq.) was added to the mixture and *tert*-butanol (3.67 g, 50.00 mmol, 5.0 eq., 4.7 mL) was added last. After 20 h of stirring the reaction was quenched with sat. NaHCO₃ solution (75 mL). The organic phase was separated, washed with brine (2x 50 mL), dried over Na₂SO₄, and concentrated under reduced pressure. **3.28** (2.31 g, 6.611 mmol, 66%) was obtained as an orange solid. R_f = 0.47 [CH₂Cl₂:MeOH, 9:1].

LCMS (ESI): t_{ret} = 4.71 min. 373 m/z [M+H]⁺.

***tert*-Butyl 3-nitro-4-((trimethylsilyl)ethynyl)benzoate (3.29)**

3.28 (3.81 g, 10.92 mmol, 1.0 eq.), CuI (104 mg, 0.546 mmol, 0.05 eq.) and Pd(PPh₃)₂Cl₂ (383.4 mg, 0.546 mmol, 0.05 eq.) were suspended in dry THF (25 mL). After addition of NEt₃ (3.34 g, 32.77 mmol, 3.0 eq., 4.6 mL) and TMS acetylene (1.50 g, 13.11 mmol, 1.2 eq., 1.9 mL) the reaction mixture was stirred for 3 h. The reaction was diluted with Et₂O (30 mL), filtered through Celite, and concentrated under reduced pressure. Purification of the resulting crude product by flash column chromatography (Hexane/EtOAc gradient, 0→100% EtOAc) gave **3.29** (3.07 g, 9.601 mmol, 88%) as a yellow solid.

$R_f = 0.60$ [Hexane:EtOAc, 10:1].

$^1\text{H NMR}$ (400 MHz, Chloroform-*d*) $\delta = 8.41$ (s, 1H), 8.01 – 7.97 (m, 1H), 7.55 (d, $J = 8.1$ Hz, 1H), 1.47 (s, 9H), 0.15 (s, 9H) ppm.

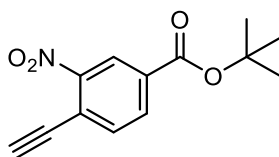
$^{13}\text{C NMR}$ (100 MHz, CDCl₃) $\delta = 163.21, 150.23, 135.18, 133.02, 132.66, 125.49, 121.91, 107.27, 98.96, 82.96, 28.23, -0.32$ ppm.

HRMS (ESI): calcd. for C₁₄H₁₅Br₂N₂⁺: 368.9602 m/z [M+H]⁺

found: 368.9606 m/z [M+H]⁺.

LCMS (ESI, 50 to 100): $t_{\text{ret}} = 4.13$ min. no ions observed.

***tert*-Butyl 4-ethynyl-3-nitrobenzoate (3.30)**



3.29 (1.50 mg, 4.696 mmol, 1.0 eq.) was dissolved in dry THF. After addition of Et₃N·HF (378.8 mg, 2.348 mmol, 0.5 eq., 383 μL) the mixture was stirred for 15 min. The reaction was then diluted with Et₂O (20 mL) and washed with sat. aq. NaHCO₃ (20 mL). The layers were separated, and the aqueous phase was extracted twice with Et₂O (2x 20 mL). The combined organic layers were dried over Na₂SO₄ and concentrated under reduced pressure. Purification of the resulting crude product by flash column chromatography (Hexane/EtOAc gradient, 0→100% EtOAc) gave **3.30** (968.0 mg, 3.915 mmol, 83%) as a yellow solid.

$R_f = 0.38$ [Hexane:EtOAc, 9:1].

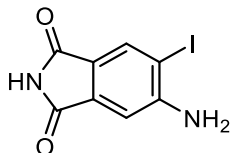
$^1\text{H NMR}$ (400 MHz, CDCl₃) $\delta = 8.60 - 8.57$ (m, 1H), 8.19 – 8.14 (m, 1H), 7.74 (d, $J = 8.1$ Hz, 1H), 3.66 (s, 1H), 1.61 (s, 9H) ppm.

$^{13}\text{C NMR}$ (100 MHz, CDCl₃) $\delta = 163.05, 150.40, 135.63, 133.33, 133.21, 125.57, 120.96, 87.89, 83.12, 78.28, 28.24$ ppm.

HRMS (ESI): calcd. for C₁₃H₁₃NNaO₄⁺: 270.0737 m/z [M+Na]⁺

found: 270.0748 m/z [M+Na]⁺.

LCMS (ESI, 50 to 100): $t_{\text{ret}} = 2.04$ min. no ions observed.

5-Amino-6-iodoisindoline-1,3-dione (3.31)

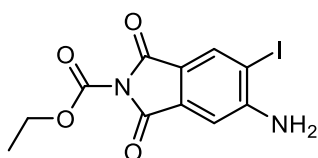
Following the procedure of Merkel et al.,^[16] 4-Aminophtalimide (3.00 g, 18.50 mmol, 1.0 eq.) and NIS (8.33 g, 37.00 mmol, 2.0 eq.) were dissolved in dry DMF (40 mL) and stirred at 45°C for 24 h. H₂O (60 mL) was added and the precipitate was filtered and washed with H₂O (80 mL), a solution of Na₂SO₄ in H₂O (6 g in 60 mL) and again with water (80 mL). **3.31** (4.31 g, 14.95 mmol, 81%) was obtained as a light brown solid.

$R_f = 0.10$ [Hexane:EtOAc, 8:2].

¹H NMR (400 MHz, DMSO-*d*₆) $\delta = 10.89$ (s, 1H), 7.92 (s, 1H), 7.03 (s, 1H), 6.45 (s, 2H) ppm.

¹³C NMR (100 MHz, DMSO) $\delta = 169.11, 167.98, 153.96, 134.91, 133.89, 119.88, 106.64, 86.48$ ppm.

LCMS (ESI): $t_{ret} = 2.59$ min. 289 m/z [M+H]⁺.

Ethyl 5-amino-6-iodo-1,3-dioxoisindoline-2-carboxylate (3.32)

3.31 (1.14 g, 3.968 mmol, 1.0 eq.) was dissolved in MeCN (12 mL) and NEt₃ (1.4 mL) was added at 0°C. A solution of ethyl chloroformate (466 μ L) in MeCN (4 mL) was added dropwise over 1 h at 0°C. The mixture was stirred for further 2 h at 0°C and then warmed up to room temperature and stirred for 1 h. The reaction was concentrated under reduced pressure. A solution of 1 M HCl solution (0.95 mL) in H₂O (23 mL) was added and the mixture is again cooled to 0°C and stirred for 1 h. The solid was filtered and washed twice with a solvent mixture (MeCN/H₂O; 1:4; 2x 10 mL) and dried for 48 h on high vacuum. **3.32** (1.31 g, 3.649 mmol, 92%) was obtained as a light brown solid.

$R_f = 0.08$ [Hexane:EtOAc, 8:2].

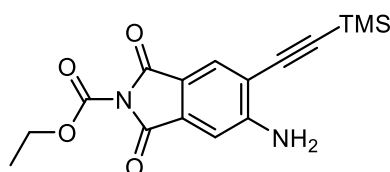
$^1\text{H NMR}$ (400 MHz, DMSO-*d*₆) $\delta = 8.08$ (s, 1H), 7.10 (s, 1H), 6.72 (s, 2H), 4.32 (q, $J = 7.2$ Hz, 2H), 1.29 (t, $J = 7.2$ Hz, 3H) ppm.

$^{13}\text{C NMR}$ (100 MHz, DMSO-*d*₆): $\delta = 163.83, 162.03, 155.06, 148.20, 135.23, 133.07, 117.59, 106.64, 88.63, 63.02, 13.96$ ppm.

HRMS (APCI): calcd. for $\text{C}_{11}\text{H}_{10}\text{IN}_2\text{O}_4^+$: 360.9678 m/z [M+H]⁺.
 found: 360.9680 m/z [M+H]⁺.

LCMS (ESI): $t_{\text{ret}} = 2.76$ min. 393 m/z [M+H+MeOH]⁺.

Ethyl 5-amino-1,3-dioxo-6-((trimethylsilyl)ethynyl)isoindoline-2-carboxylate (3.33)



3.32 (1.03 g, 2.866 mmol, 1.0 eq.), CuI (27.3 mg, 0.143 mmol, 0.05 eq.) and Pd(PPh₃)₂Cl₂ (100.6 mg, 0.143 mmol, 0.05 eq.) were dissolved in dry THF (18 mL) at room temperature. Trimethylsilyl acetylene (844.4 mg, 8.597 mmol, 3.0 eq., 1.2 mL) was added to the mixture and NEt₃ (870.0 mg, 8.597 mmol, 3.0 eq., 1.2 mL) was added last. After 7 h of stirring the reaction was diluted with EtOAc (25 mL), filtered through Celite, and washed with EtOAc (50 mL). The reaction was concentrated under reduced pressure. Purification of the resulting crude product by flash column chromatography (Hexane/EtOAc gradient, 0→100% EtOAc) gave **3.33** (523.0 mg, 1.583 mmol, 55%) as yellow crystals.

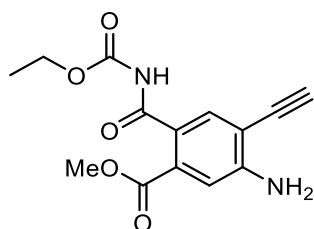
$R_f = 0.33$ [Hexane:EtOAc, 2:1].

$^1\text{H NMR}$ (400 MHz, DMSO) $\delta = 7.64$ (s, 1H), 7.15 (s, 1H), 6.76 (s, 2H), 4.32 (q, $J = 7.1$ Hz, 2H), 1.29 (t, $J = 7.1$ Hz, 3H), 0.27 (s, 9H) ppm.

$^{13}\text{C NMR}$ (100 MHz, CDCl₃) $\delta = 163.99, 163.20, 153.95, 148.88, 132.94, 129.25, 119.04, 113.32, 107.95, 99.23, 77.36, 63.98, 14.28, 0.00$ ppm.

HRMS (APCI): calcd. for $\text{C}_{16}\text{H}_{19}\text{N}_2\text{O}_4\text{SiNa}^+$: 353.0928 m/z [M+Na]⁺.
 found: 353.1201 m/z [M+Na]⁺.

LCMS (ESI): $t_{\text{ret}} = 4.43$ min. 353 m/z [M+Na]⁺.

Ethyl 5-amino-6-ethynyl-1,3-dioxoisindoline-2-carboxylate (3.34)

3.33 (200.0 mg, 605.3 μmol , 1.0 eq.) was dissolved in dry MeOH (5 mL) and K_2CO_3 (167.3 mg, 1.211 mmol, 2.0 eq) was added. After 10 min of stirring the reaction was diluted with H_2O (25 mL), extracted with CH_2Cl_2 (3x 25 mL) and EtOAc (3x 25 mL) and washed twice with brine (2x 30 mL). The organic phase was dried over Na_2SO_4 and concentrated under reduced pressure. **3.34** (95.0 mg, 367.9 μmol , 61%) was obtained as a light orange crystalline solid.

$R_f = 0.50$ [EtOAc:Hexane, 2:1].

$^1\text{H NMR}$ (400 MHz, DMSO) $\delta = 10.89$ (s, 1H), 7.71 (s, 1H), 6.54 (s, 1H), 6.34 (s, 2H), 4.46 (s, 1H), 4.04 (q, $J = 7.1$ Hz, 2H), 3.69 (s, 3H), 1.15 (t, $J = 7.1$ Hz, 3H) ppm.

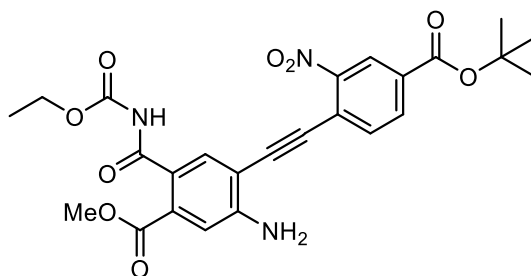
$^{13}\text{C NMR}$ (100 MHz, DMSO) $\delta = 169.34, 164.62, 153.38, 151.54, 140.64, 134.41, 113.20, 111.35, 104.31, 86.34, 79.17, 60.97, 51.63, 14.11$ ppm.

HRMS (APCI): calcd. for $\text{C}_{14}\text{H}_{14}\text{N}_2\text{NaO}_5^+$: 313.0807 m/z $[\text{M}+\text{Na}]^+$.

found: 313.0851 m/z $[\text{M}+\text{Na}]^+$

LCMS (ESI): $t_{\text{ret}} = 2.64$ min. 313 m/z $[\text{M}+\text{Na}]^+$.

Methyl 5-amino-4-(3-(4-(tert-butoxycarbonyl)-2-nitrophenyl)prop-1-yn-1-yl)-2-((ethoxycarbonyl)carbamoyl)benzoate (3.35)



3.30 (140.0 mg, 482.3 μmol , 1.0 eq.), **3.34** (84.2 mg, 241.2 μmol , 1.0 eq.) and NEt_3 (73.2 mg, 723.5 μmol , 1.5 eq., 0.1 mL) were suspended in dry THF (5 mL) under nitrogen. CuI (2.3 mg, 12.10 μmol , 0.025 eq.) and $\text{PdCl}_2(\text{PPh}_3)_2$ (8.5 mg, 12.10 μmol , 0.025 eq.) was added last. After 24 h of stirring the reaction was extracted with CH_2Cl_2 (3x 25 mL) and EtOAc (3x 25 mL) and washed twice with brine (2x 30 mL). Purification of the resulting crude product by flash column chromatography ($\text{CH}_2\text{Cl}_2/\text{MeOH}$ gradient, 0 \rightarrow 2% MeOH) gave **3.35** (127.0 mg, 248.3 μmol , 52%) as orange solid.

$R_f = 0.17$ [$\text{CH}_2\text{Cl}_2:\text{MeOH}$, 19:1].

$^1\text{H NMR}$ (400 MHz, DMSO) $\delta = 10.97$ (s, 1H), 8.55 (d, $J = 1.7$ Hz, 1H), 8.23 (dd, $J = 8.2, 1.7$ Hz, 1H), 8.15 (d, $J = 8.1$ Hz, 1H), 7.87 (s, 1H), 6.68 (s, 2H), 6.62 (s, 1H), 4.05 (q, $J = 7.1$ Hz, 2H), 3.73 (s, 3H), 1.59 (s, 9H), 1.16 (t, $J = 7.1$ Hz, 3H) ppm.

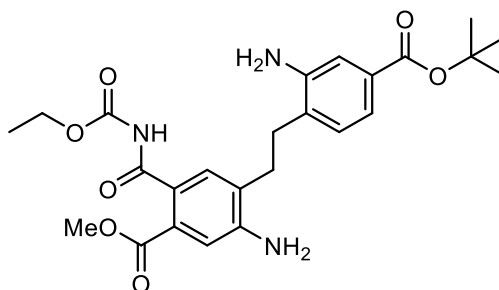
$^{13}\text{C NMR}$ (100 MHz, DMSO) $\delta = 169.21, 164.49, 162.73, 153.69, 151.58, 148.28, 141.76, 135.10, 134.92, 133.30, 131.37, 125.23, 121.39, 113.78, 111.79, 103.46, 95.75, 90.59, 82.45, 61.05, 51.75, 27.67, 14.11$ ppm.

HRMS (APCI): calcd. for $\text{C}_{25}\text{H}_{25}\text{N}_3\text{NaO}_9^+$: 534.1483 m/z [$\text{M}+\text{Na}$] $^+$

found: 534.1423 m/z [$\text{M}+\text{Na}$] $^+$

LCMS (ESI): $t_{\text{ret}} = 4.60$ min. 534 m/z [$\text{M}+\text{Na}$] $^+$.

Methyl 5-amino-4-(2-amino-4-(tert-butoxycarbonyl)phenethyl)-2-((ethoxycarbonyl)carbamoyl)benzoate (3.36)



3.35 (120.0 mg, 250.3 μmol , 1.0 eq.) and 10% Pd/C (26.60 mg, 25.00 μmol , 0.1 eq.) were dissolved in dry MeOH (5 ml) and CH_2Cl_2 (3 mL) under nitrogen. The flask was then charged with H_2 and the reaction mixture was stirred for 24 h. The reaction was filtered over Celite, extracted in EtOAc (3x 25 mL), washed twice with brine (2x 30 mL), and concentrated under reduced pressure. **3.36** (93.0 mg, 205.1 μmol , 82%) was obtained as a yellow oil.

$R_f = 0.17$ [CH_2Cl_2 :MeOH, 9:1].

$^1\text{H NMR}$ (400 MHz, CDCl_3) $\delta = 7.98$ (s, 1H), 7.71 (s, 1H), 7.36 (dd, $J = 7.8, 1.7$ Hz, 1H), 7.32 (d, $J = 1.6$ Hz, 1H), 7.05 (d, $J = 7.8$ Hz, 1H), 6.53 (s, 1H), 4.13 (q, $J = 7.1$ Hz, 2H), 3.80 (s, 3H), 2.80 (ddd, $J = 13.5, 8.2, 4.4$ Hz, 4H), 1.57 (s, 9H), 1.22 (t, $J = 7.2$ Hz, 3H) ppm.

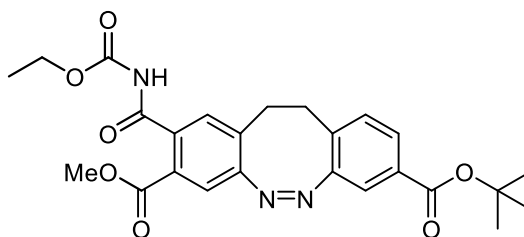
$^{13}\text{C NMR}$ (100 MHz, CDCl_3) $\delta = 170.38, 166.23, 165.95, 151.23, 148.95, 143.63, 137.79, 131.98, 131.38, 130.97, 129.66, 125.55, 120.90, 117.34, 116.48, 113.22, 80.96, 62.39, 52.09, 30.87, 30.30, 28.32, 14.26$ ppm.

HRMS (APCI): calcd. for $\text{C}_{21}\text{H}_{24}\text{N}_3\text{O}_7^+$: 486.2235 m/z $[\text{M}+\text{H}]^+$

found: 486.2232 m/z $[\text{M}+\text{H}]^+$

LCMS (ESI): $t_{\text{ret}} = 3.77$ min. 430 m/z $[\text{M}+\text{H}-t\text{Bu}]^+$.

8-(tert-Butyl) 3-methyl-2-((ethoxycarbonyl)carbamoyl)-11,12-dihydrodibenzo[*c,g*][1,2]diazocine-3,8-dicarboxylate (3.37)



3.36 (53.0 mg, 0.109 mmol, 1 eq.) was dissolved in a mixture of CH₂Cl₂ (6 mL) and AcOH (6 mL). 3-Chloroperoxybenzoic acid (75%, 50.2 mg, 0.218 mmol) was diluted in AcOH (2 mL) and added dropwise over 14 h at room temperature. The reaction was stirred for additional 12 h at 55 °C and the volatiles were removed under reduced pressure. The residue was dissolved in CH₂Cl₂ (10 mL), separated against NaHCO₃ (10 mL), and extracted with CH₂Cl₂ (3x 10 mL). The combined organic phase was washed with brine (2x 30 mL), dried over Na₂SO₄ and the solvent was removed under reduced pressure. Purification of the resulting crude product by flash column chromatography (CH₂Cl₂/MeOH gradient, 0 → 20%) gave **3.37** (38.7 mg, 0.080 mmol, 74%) as a yellow sticky solid.

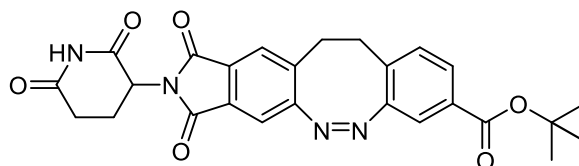
$R_f = 0.35$ [CH₂Cl₂:MeOH, 19:1].

¹H NMR (400 MHz, CDCl₃) $\delta = 7.76 - 7.73$ (m, 1H), 7.70 – 7.66 (m, 2H), 7.48 (d, $J = 1.7$ Hz, 1H), 7.06 (d, $J = 8.0$ Hz, 1H), 6.88 (s, 1H), 4.12 - 4.00 (m, 2H), 3.82 (s, 3H), 3.10 – 2.80 (m, 4H), 1.55 (s, 9H), 1.16 (t, $J = 7.1$ Hz, 3H) ppm.

¹³C NMR (100 MHz, CDCl₃) $\delta = 168.89, 165.35, 164.56, 157.87, 154.92, 150.98, 136.40, 131.95, 131.78, 131.40, 129.93, 129.72, 128.85, 126.60, 120.38, 118.09, 81.69, 62.63, 52.70, 31.69, 31.46, 28.25, 14.17$ ppm.

LCMS (ESI): $t_{ret} = 4.31$ min. 504 m/z [M+Na]⁺.

***tert*-Butyl-2-(2,6-dioxopiperidin-3-yl)-1,3-dioxo-2,3,11,12-tetrahydro-1H-benzo[7,8][1,2]diazocino[3,4-f]isoindole-8-carboxylate (3.38)**



3.37 (13.9 mg, 28.80 μmol , 1.0 eq.), NaOAc (7.10 mg, 86.50 μmol , 3.0 eq.) and 3-aminopiperidine-2,6-dione (7.1 mg, 43.30 μmol , 1.5 eq.) were dissolved in dry MeCN (3 mL) and stirred for 24 h at 82 °C. The mixture was diluted with EtOAc (5 mL), separated against NaHCO_3 (10 mL), and extracted with EtOAc (3x 10 mL). The combined organic phase was washed with brine (2x 10 mL), dried over Na_2SO_4 and the solvent was under reduced pressure. Purification of the resulting crude product by flash column chromatography ($\text{CH}_2\text{Cl}_2/\text{MeOH}$ gradient, 0 \rightarrow 20% MeOH) gave **3.38** (7.1 mg, 14.3 μmol , 50%) as a yellow solid.

$R_f = 0.16$ [$\text{CH}_2\text{Cl}_2:\text{MeOH}$, 19:1].

$^1\text{H NMR}$ (400 MHz, CDCl_3) $\delta = 8.05$ (s, 1H), 7.68 (dd, $J = 8.0, 1.7$ Hz, 1H), 7.54 (d, $J = 2.3$ Hz, 1H), 7.49 – 7.46 (m, 1H), 7.33 (d, $J = 1.8$ Hz, 1H), 7.02 (d, $J = 8.0$ Hz, 1H), 4.91 (dd, $J = 12.1, 5.4$ Hz, 1H), 3.22 – 2.66 (m, 7H), 2.15 – 2.07 (m, 1H), 1.56 (s, 9H) ppm.

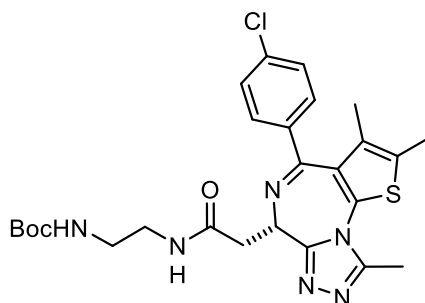
$^{13}\text{C NMR}$ (100 MHz, CDCl_3) $\delta = 170.71, 167.84, 166.43, 166.26, 164.44, 160.30, 154.77, 135.64, 131.70, 131.31, 130.98, 130.43, 130.36, 129.03, 125.17, 120.26, 114.49, 81.93, 49.52, 32.21, 31.47, 31.41, 28.25, 22.69$ ppm.

HRMS (APCI): calcd. for $\text{C}_{26}\text{H}_{25}\text{N}_4\text{O}_6^+$: 488.1880 m/z [$\text{M}+\text{H}$] $^+$.

found: 488.1696 m/z [$\text{M}+\text{H}$] $^+$

LCMS (ESI): $t_{\text{ret}} = 4.17$ min. 511 m/z [$\text{M}+\text{Na}$] $^+$.

***tert*-Butyl (S)-2-(2-(4-(4-chlorophenyl)-2,3,9-trimethyl-6H-thieno[3,2-*f*][1,2,4]triazolo[4,3-*a*][1,4]diazepin-6-yl)acetamido)ethyl)carbamate (3.39)**



(+)-JQ1 (13.2 mg, 32.9 μmol , 1.0 eq.) and HATU (18.8 mg, 49.4 μmol , 1.5 eq.) were dissolved in dry DMF (1 mL) at room temperature. After 5 min of stirring *N*-Boc-1,4-diaminoethane (9.84 mg, 65.9 μmol , 2.0 eq., 10 μL) and *i*-Pr₂NEt (132 μmol , 4.0 eq., 23 μL) were added to the mixture and it was stirred for additional 12 h at room temperature. The reaction was diluted with EtOAc (5 mL), separated against H₂O/10% LiCl (1:1, 5 mL:5 mL), extracted with EtOAc (2x 5 mL) and washed with 10% LiCl (2x 5 mL) and brine (2x 5 mL). The combined organic phase was dried over Na₂SO₄ and concentrated under reduced pressure. Purification of the resulting crude product by flash column chromatography (CH₂Cl₂/MeOH gradient, 0-10% MeOH) gave **3.39** (13.4 mg, 24.7 μmol , 75%) as a yellow solid.

R_f = 0.17 [CH₂Cl₂, MeOH 19:1].

¹H NMR (400 MHz, CDCl₃) δ = 7.39 (d, *J* = 8.5 Hz, 2H), 7.35 (s, 1 H), 7.31 (d, *J* = 8.7 Hz, 2H), 5.43 (s, 1H), 4.66 (t, *J* = 7.0 Hz, 1H), 3.55 (dd, *J* = 14.6, 7.5 Hz, 1H), 3.49 – 3.19 (m, 5H), 2.67 (s, 3H), 2.40 (s, 3H), 1.67 (s, 3H), 1.41 (s, *J* = 13.5 Hz, 9H) ppm.

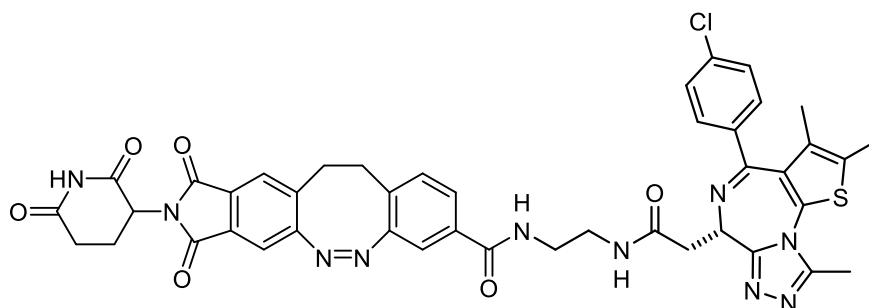
¹³C NMR (100 MHz, CDCl₃) δ = 171.27, 164.12, 156.54, 155.90, 150.10, 136.95, 136.70, 132.19, 131.11, 131.06, 130.71, 130.01, 128.87, 77.16, 54.48, 40.82, 40.20, 39.19, 28.59, 14.56, 13.26, 11.99 ppm.

LCMS (ESI): t_{ret} = 3.84 min.

543 m/z [M+H]⁺.

Analytical data matched previous literature reports.^[30]

***N*-(2-(2-((*S*)-4-(4-chlorophenyl)-2,3,9-trimethyl-6*H*-thieno[3,2-*f*][1,2,4]triazolo[4,3-*a*][1,4]diazepin-6-yl)acetamido)ethyl)-2-(2,6-dioxopiperidin-3-yl)-1,3-dioxo-2,3,11,12-tetrahydro-1*H*-benzo[7,8][1,2]diazocino[3,4-*f*]isoindole-8-carboxamide (PHOTAC-I-15)**



3.39 (8.4 mg, 19.00 μmol , 2.0 eq.) was dissolved in a CH_2Cl_2 :TFA mixture (1:1; 2 mL). After 4 h the reaction was concentrated under reduced pressure. The mixture was triturated with MeOH and then dried under high vacuum for 48 h. **3.38** (4.1 mg, 9.50 μmol , 1.0 eq.) was dissolved in CH_2Cl_2 :TFA (1:1; 1 mL each). After 4 h the reaction was concentrated under reduced pressure. The intermediate was purified by flash column chromatography (CH_2Cl_2 /MeOH gradient, 0 \rightarrow 50% MeOH). Both solids were dissolved in dry DMF (2 mL) and HATU (5.4 mg, 14.2 μmol , 1.5 eq.) was added. Next, *i*-Pr₂NEt (37.9 μmol , 4.0 eq., 7 μL) was added to the mixture and it was stirred for 12 h at room temperature. The reaction was diluted with EtOAc (5 mL), separated against H_2O /10% LiCl (1:1, 5 mL:5 mL), extracted with EtOAc (2x 5 mL) and washed with 10% LiCl (2x 5 mL) and brine (2x 5 mL). The combined organic phase was dried over Na_2SO_4 and concentrated under reduced pressure. Purification of the resulting crude product by flash column chromatography (CH_2Cl_2 /MeOH gradient, 0-20% MeOH) gave **PHOTAC-I-15** (3.9 mg, 4.50 μmol , 48%) as a yellow solid.

$R_f = 0.20$ [CH_2Cl_2 :MeOH, 19:1].

¹H NMR (600 MHz, DMSO) $\delta = 11.09$ (s, 1H), 8.52 – 8.47 (m, 1H), 8.37 – 8.32 (m, 1H), 7.80 (s, 1H), 7.54 (d, $J = 8.0$ Hz, 1H), 7.50 (d, $J = 6.1$ Hz, 1H), 7.47 – 7.43 (m, 2H), 7.42 – 7.38 (m, 3H), 7.16 (d, $J = 8.0$ Hz, 1H), 5.11 – 5.06 (m, 1H), 4.50 (t, $J = 7.1$ Hz, 1H), 3.31 – 3.18 (m, 6H), 3.17 – 3.10 (m, 1H), 3.09 – 3.02 (m, 1H), 3.00 – 2.93 (m, 1H), 2.90 – 2.80 (m, 2H), 2.58 (s, 3H), 2.58 – 2.52 (m, 1H), 2.47 – 2.42 (m, 1H), 2.41 (s, 3H), 2.04 – 1.97 (m, 1H), 1.60 (s, 3H) ppm.

¹³C NMR (150 MHz, DMSO) δ = 172.68, 169.89, 169.78, 166.29, 166.09, 165.09, 163.03, 159.60, 155.09, 154.29, 149.84, 136.72, 135.69, 135.17, 133.38, 132.25, 130.67, 130.50, 130.30, 130.28, 130.13, 129.83, 129.80, 129.55, 128.44, 126.45, 124.97, 117.86, 113.65, 53.79, 49.03, 40.06, 38.13, 37.66, 31.35, 30.87, 30.12, 21.84, 14.05, 12.69, 11.30 ppm.

HRMS (APCI): calcd. for C₄₃H₃₈ClN₁₀O₆S⁺: 857.2380 m/z [M+H]⁺.

found: 857.2394 m/z [M+H]⁺

LCMS (ESI): t_{ret} = 3.76 min. 857 m/z [M+H]⁺.

References

- [1] C. Ash, M. Dubec, K. Donne, T. Bashford, *Lasers Med. Sci.* **2017**, *32*, 1909–1918.
- [2] S. Samanta, A. A. Beharry, O. Sadovski, T. M. McCormick, A. Babalhavaeji, V. Tropepe, G. A. Woolley, *J. Am. Chem. Soc.* **2013**, *135*, 9777–9784.
- [3] M. Dong, A. Babalhavaeji, S. Samanta, A. A. Beharry, G. A. Woolley, *Acc. Chem. Res.* **2015**, *48*, 2662–2670.
- [4] M. Dong, A. Babalhavaeji, C. V. Collins, K. Jarrah, O. Sadovski, Q. Dai, G. A. Woolley, *J. Am. Chem. Soc.* **2017**, *139*, 13483–13486.
- [5] A. Rullo, A. Reiner, A. Reiter, D. Trauner, E. Y. Isacoff, G. A. Woolley, *Chem. Commun.* **2014**, *50*, 14613–14615.
- [6] D. Bléger, J. Schwarz, A. M. Brouwer, S. Hecht, *J. Am. Chem. Soc.* **2012**, *134*, 20597–20600.
- [7] D. B. Konrad, G. Savasci, L. Allmendinger, D. Trauner, C. Ochsenfeld, A. M. Ali, *J. Am. Chem. Soc.* **2020**, *142*, 6538–6547.
- [8] C.-Y. Yang, C. Qin, L. Bai, S. Wang, *Drug Discov. Today Technol.* **2019**, *31*, 43–51.
- [9] K. M. Ricking, S. Mahan, C. R. Corona, M. McDougall, J. D. Vasta, M. B. Robers, M. Urh, D. L. Daniels, *ACS Chem. Biol.* **2018**, *13*, 2758–2770.
- [10] J. Lu, Y. Qian, M. Altieri, H. Dong, J. Wang, K. Raina, J. Hines, J. D. Winkler, A. P. Crew, K. Coleman, C. M. Crews, *Chem. Biol.* **2015**, *22*, 755–763.
- [11] M. Zengerle, K.-H. Chan, A. Ciulli, *ACS Chem. Biol.* **2015**, *10*, 1770–1777.
- [12] G. E. Winter, D. L. Buckley, J. Paulk, J. M. Roberts, A. Souza, S. Dhe-Paganon, J. E. Bradner, *Science* **2015**, *348*, 1376–1381.
- [13] M. Reynders, B. S. Matsuura, M. Bérouti, D. Simoneschi, A. Marzio, M. Pagano, D. Trauner, *Sci. Adv.* **2020**, *6*, eaay5064.
- [14] R. Siewertsen, H. Neumann, B. Buchheim-Stehn, R. Herges, C. Näther, F. Renth, F. Temps, *J. Am. Chem. Soc.* **2009**, *131*, 15594–15595.
- [15] H. Sell, C. Näther, R. Herges, *Beilstein J. Org. Chem.* **2013**, *9*, 1–7.
- [16] M. Merkel, L. Dehmel, N. P. Ernsting, H.-A. Wagenknecht, *Angew. Chem. Int. Ed.* **2017**, *56*, 384–388.
- [17] M. S. Maier, K. Hüll, M. Reynders, B. S. Matsuura, P. Leippe, T. Ko, L. Schäffer, D. Trauner, *J. Am. Chem. Soc.* **2019**, *141*, 17295–17304.
- [18] B. VOLK, K. K. FADGYAS, G. LUKÁCS, M. T. LAURITZ, A. DANCSÓ, I. KIRÁLY, L. PALOTAI, R. KORMÁNY, *Method for the Production of Pomalidomide*, **2017**, WO2017134476A1.
- [19] A. A. Beharry, O. Sadovski, G. A. Woolley, *J. Am. Chem. Soc.* **2011**, *133*, 19684–19687.
- [20] S. Samanta, T. M. McCormick, S. K. Schmidt, D. S. Seferos, G. A. Woolley, *Chem. Commun.* **2013**, *49*, 10314–10316.

- [21] D. B. Konrad, J. A. Frank, D. Trauner, *Chem. – Eur. J.* **2016**, *22*, 4364–4368.
- [22] L. Agnetta, M. Bermudez, F. Riefolo, C. Matera, E. Claro, R. Messerer, T. Littmann, G. Wolber, U. Holzgrabe, M. Decker, *J. Med. Chem.* **2019**, *62*, 3009–3020.
- [23] M. Wegener, M. J. Hansen, A. J. M. Driessen, W. Szymanski, B. L. Feringa, *J. Am. Chem. Soc.* **2017**, *139*, 17979–17986.
- [24] M. Pettersson, C. M. Crews, *Drug Discov. Today Technol.* **2019**, *31*, 15–27.
- [25] G. M. Burslem, C. M. Crews, *Cell* **2020**, *181*, 102–114.
- [26] A. Mourot, M. A. Kienzler, M. R. Banghart, T. Fehrentz, F. M. E. Huber, M. Stein, R. H. Kramer, D. Trauner, *ACS Chem. Neurosci.* **2011**, *2*, 536–543.
- [27] E. S. Fischer, K. Böhm, J. R. Lydeard, H. Yang, M. B. Stadler, S. Cavadini, J. Nagel, F. Serluca, V. Acker, G. M. Lingaraju, R. B. Tichkule, M. Schebesta, W. C. Forrester, M. Schirle, U. Hassiepen, J. Ottl, M. Hild, R. E. J. Beckwith, J. W. Harper, J. L. Jenkins, N. H. Thomä, *Nature* **2014**, *512*, 49–53.
- [28] M. Borowiak, W. Nahaboo, M. Reynders, K. Nekolla, P. Jalinot, J. Hasserodt, M. Rehberg, M. Delattre, S. Zahler, A. Vollmar, D. Trauner, O. Thorn-Seshold, *Cell* **2015**, *162*, 403–411.
- [29] A. Marzio, J. Puccini, Y. Kwon, N. K. Maverakis, A. Arbin, P. Sung, D. Bar-Sagi, M. Pagano, *Mol. Cell* **2019**, *73*, 224-237.e6.
- [30] G. Zhang, R. Liu, Y. Zhong, A. N. Plotnikov, W. Zhang, L. Zeng, E. Rusinova, G. Gerona-Nevarro, N. Moshkina, J. Joshua, P. Y. Chuang, M. Ohlmeyer, J. C. He, M.-M. Zhou, *J. Biol. Chem.* **2012**, *287*, 28840–28851.

4 – Bioluminescence-Controlled Photopharmacology

Martin Reynders^{1,2}, Zi Yao³, Anna C. Love³, Michele Pagano^{4,5,6}, Jennifer A. Prescher^{3,7,8}, and Dirk Trauner^{1,5,9}

¹Department of Chemistry, New York University, New York, NY 10003, USA.

²Department of Chemistry, Ludwig Maximilians University of Munich
81377 Munich, Germany.

³Department of Chemistry, University of California, Irvine, Irvine, CA 92697, USA.

⁴Department of Biochemistry and Molecular Pharmacology, New York University
School of Medicine, New York, NY 10016, USA.

⁵Perlmutter Cancer Center, New York University School of Medicine, New York, NY
10016, USA.

⁶Howard Hughes Medical Institute, New York University School of Medicine, New
York, NY 10016, USA.

⁷Department of Molecular Biology & Biochemistry, University of California, Irvine,
Irvine, CA 92697, USA.

⁸Department of Pharmaceutical Sciences, University of California, Irvine, Irvine, CA
92697, USA.

⁹NYU Neuroscience Institute, New York University School of Medicine, New York, NY
10016, USA.

Introduction

Light delivery into tissue remains a major challenge in photopharmacology and photomedicine. The limited penetration depth of short-wavelength visible light restricts the application of light-activatable drugs to surface exposed tissues that can be targeted by an external light source.^[1,2] Attempts to improve tissue penetration include the generation of red-shifted chromophores that operate within the near-infrared biooptical window.^[3-5] The tissue absorption of light is lower in the red and near infrared spectrum, however scattering of light is high.^[3] An alternative approach to apply light in deep tissue is the use of implantable light-emitting diodes (LEDs) and optical fibers as an internal light source, but these methods require surgery.^[6-10]

A different method to locally generate light in biological tissues is bioluminescence. Bioluminescence originates from the chemical conversion of a substrate catalyzed by the corresponding luciferase and several luciferase-substrate pairs have been identified.^[11] Bioluminescence has found wide application as a readout in biological assays and in bioimaging because of its biocompatibility and low toxicity.^[12] More recently, bioluminescence has also been used to control biological processes and photochemical reactions. Light-sensitive proteins used in optogenetics such as light-oxygen-voltage-sensing (LOV) domains or channelrhodopsins have been used together with luciferases to create optogenetic tools responsive to bioluminescence.^[13,14] In parallel, bioluminescence has been used to control photocatalytic reactions and to induce the cleavage of photolabile protecting groups.^[15-18]

Complementing optogenetic approaches and photolabile protecting groups, small molecule photoswitches have been used to control biological function with light. In photopharmacology, a photoswitch, such as azobenzene, is incorporated into a drug and can reversibly isomerize between an active and inactive isomer in response to irradiation.^[19] We have previously described photochemically targeting chimeras (PHOTACs) that induce the degradation of target proteins in a light dependent fashion.^[20] PHOTACs combine a ligand for the E3 ligase cereblon, an azobenzene photoswitch and a second ligand targeting a protein of interest (POI). Irradiation with violet or blue light results in *E*-to-*Z* isomerization of the PHOTAC, which then forms a productive ternary complex that catalyzes the ubiquitylation of the POI.

Here we want to demonstrate that photoswitchable drugs can be controlled with bioluminescence to induce their biological function. We use PHOTAC-I-3 targeting the

Bromodomain and extraterminal domain (BET) proteins BRD2, BRD3 and BRD4 to demonstrate proof-of-concept (Figure 4.1B).^[20,21] By harnessing the irradiation generated through bioluminescence, we aim to activate photopharmaceuticals locally and provide a strategy to overcome the limited tissue penetration of light.

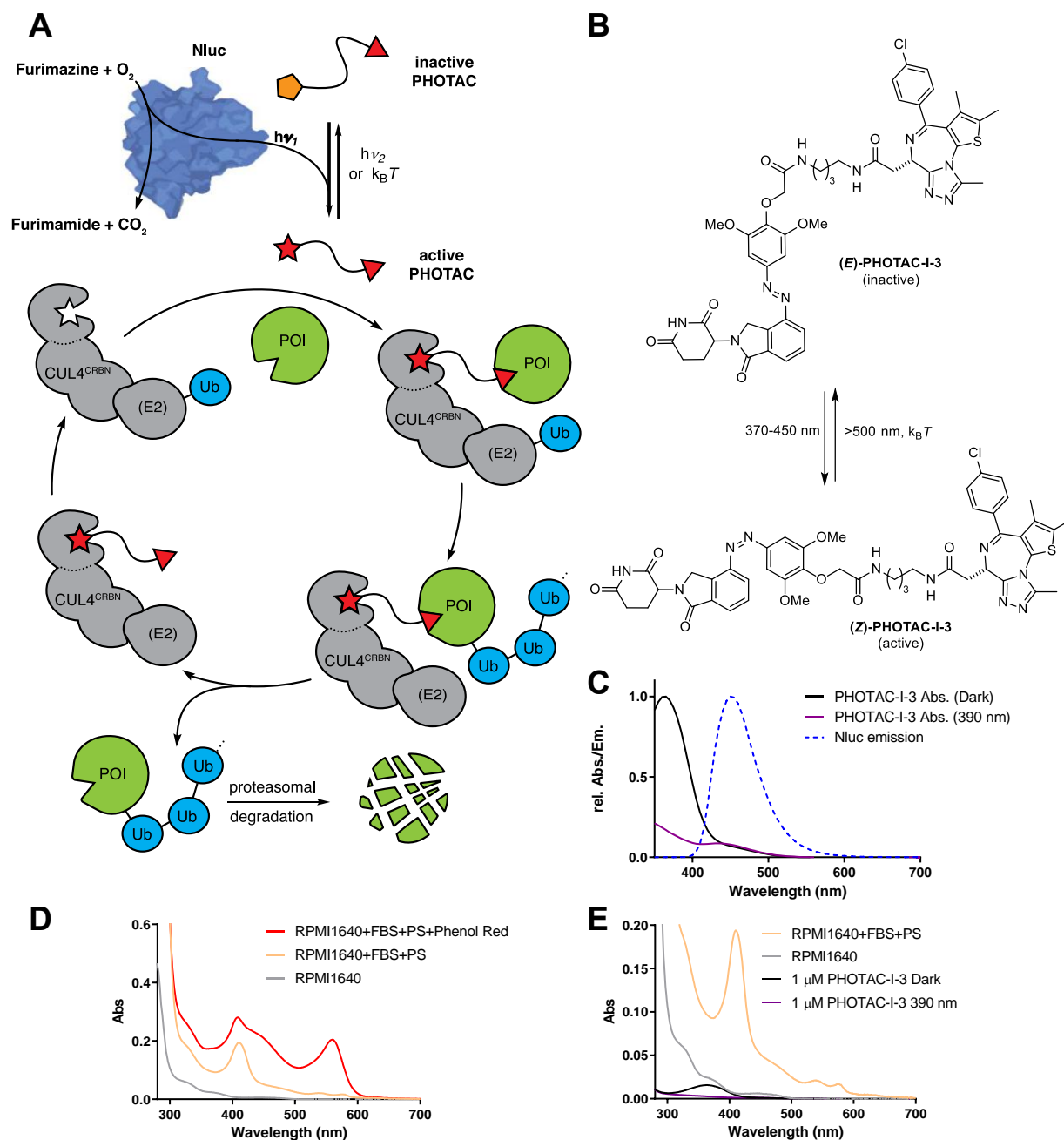


Figure 4.1: Controlling PHOTAC activity with bioluminescence. A) Schematic representation how bioluminescence could drive degradation of a protein of interest (POI) using PHOTACs. B) Structure and photoisomerization of PHOTAC-I-3. C) Relative Absorbance spectra of PHOTAC-I-3 isomers compared to the emission spectrum of Nluc. D) Absorption spectra of RPMI1640 cell culture medium with and without additives. E) Absorption of cell culture media compared to 1 μ M PHOTAC-I-3.

Results

We chose PHOTACs because of their mechanism of action that is based on binding events and not on target occupancy.^[22] Their catalytic mechanism of action only requires partial activation in the form of *E*-to-*Z*-irradiation to achieve efficient BET protein degradation. Further, PHOTAC-I-3 is inactive as a degrader in the dark and thus protein degradation provides a direct readout of bioluminescence induced photoswitching (Figure 4.1A).

The intensity of bioluminescence is low compared to compared to the LEDs commonly used in photopharmacology. In contrast to photocleavable protecting groups which are irreversibly photolyzed upon light exposure, formation of the azobenzene *Z*- isomer is reversible as these photoswitches undergo thermal *Z*-to-*E*-isomerization. In the case of PHOTAC-I-3 the inactivating thermal relaxation proceeds with a half-life of 6.7 h at 37 °C in DMSO.^[20] This rate of inactivation is crucial to maintain reasonable amounts of active PHOTAC after irradiation.

The highest amount of active *Z*-PHOTAC-I-3 can be obtained by 390 nm irradiation.^[20] However mixtures containing moderate amounts *Z*-isomer can be installed by blue light irradiation using wavelengths up to 465 nm. Blue light emitting luciferases such as NanoLuciferase (NLuc) or Gaussia luciferase (GLuc) should be most suited even though the bioluminescence emission spectrum only shows partial overlap with the absorption spectra of PHOTAC-I-3 (Figure 4.1C).^[11,23]

Another factor to be considered is the absorption of tissue culture media and the resulting competition for photons. Phenol red, a common additive in cell culture media, strongly absorbs in the visible spectrum (Figure 4.1D). Even medium containing 10% fetal bovine serum (FBS) commonly used in mammalian cell culture significantly exceeds the absorption of 1 μM PHOTAC-I-3 due to the presence of chromophores like heme (Figure 4.1E). Lastly, active *Z*-PHOTAC-I-3 can also compete for photons and undergo light-induced *Z*-to-*E* isomerization.

To confirm that 450 nm or 465 nm irradiation can still induce BET-protein degradation, we incubated RS4;11 cells with PHOTAC-I-3 and subjected them to pulsed LED-irradiation. Very strong BRD3 and BRD4 degradation was observed, demonstrating that blue light is sufficient to activate PHOTAC-I-3 at high nanomolar concentrations (Figure 4.2).

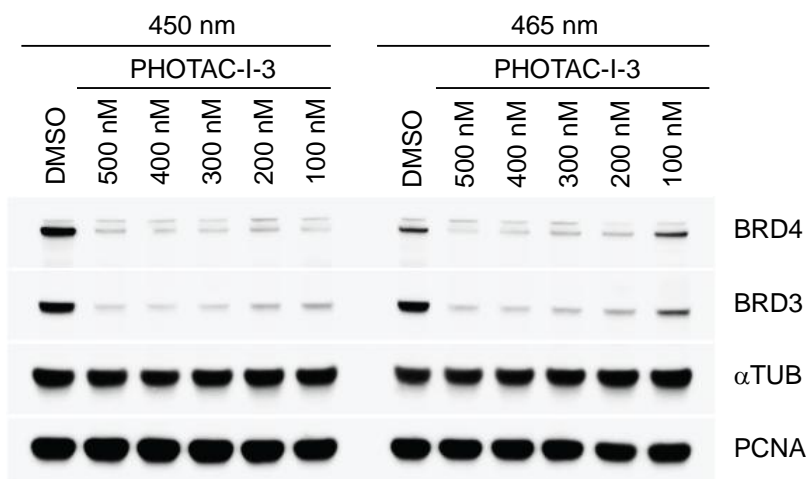


Figure 4.2: Immunoblot analysis of BRD3 and BRD4 degradation in RS4;11 cells cultured in RPMI1640 medium containing FBS and PS, treated with **PHOTAC-I-3** for 12 h and pulsed 450 or 465 nm irradiation (100 ms every 10 s).

Studies on bioluminescence-controlled photolysis employed fusion proteins to colocalize the luciferase and the molecule to be activated.^[15–18] This strategy facilitates direct energy transfer between emitter and chromophore. In contrast, we decided to start our investigation on native systems and external supply of the luciferase to mimic a therapeutic setting.

First, we treated cells with PHOTAC-I-3 and either NLuc or Gluc plus their corresponding substrates for 4 h. We did not observe degradation of BRD4 on this short time frame and proceeded to increase treatment duration (Figure 4.3A). Due to the visibly strong emission of NLuc at short wavelengths and the prolonged emission we continued using NLuc. After 16 h of treatment, we did observe the first evidence of bioluminescence-induced degradation of BRD3 and BRD4 by PHOTAC-I-3 (Figure 4.3B). We also performed the same experiment with PHOTAC-II-5, which targets FKBP12 for degradation, however immunoblotting did not show strong degradation of FKBP12 (Figure S4.1A).

As an alternative to the external supply of luciferase enzyme, we also attempted to induce protein degradation through expression of NLuc in MDA-MB-231 cells. We did observe a small decrease in BRD4 levels that was not as prominent as the degradation induced in RS4;11 cells, likely due to the lower susceptibility of MDA-MB-231 cells to PHOTAC-I-3-mediated protein degradation (Figure S4.1B).^[20]

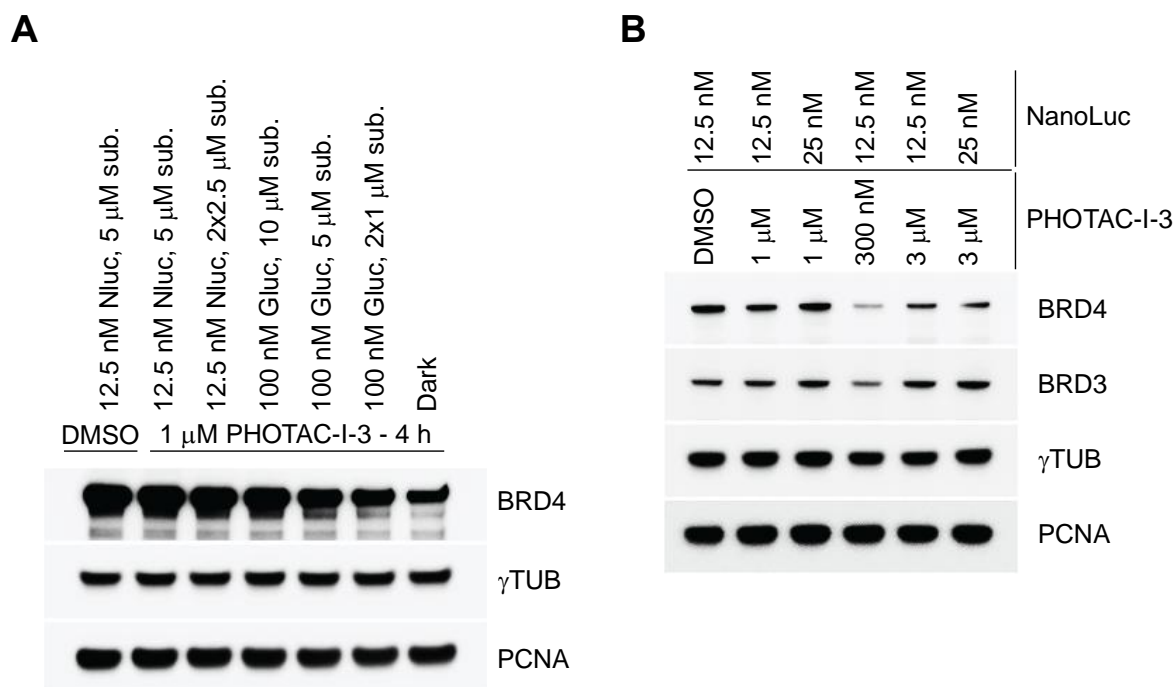


Figure 4.3: Western blot analysis of PHOTAC-I-3 induced BET protein degradation. A) BRD4 levels in RS4;11 cells cultured in RPMI1640 medium containing FBS and PS, following PHOTAC-I-3 treatment for 4 h and bioluminescence from NanoLuc or Gaussia luciferase using the indicated amount of luciferase. Substrate was supplied at the start of the assay or at the start and after 2 h. B) Immunoblot of BRD3 and BRD4 levels after 16 h in RS4;11 cells cultured in RPMI1640 medium containing FBS and PS, treated with PHOTAC-I-3 and NLuc at the indicated concentrations and supplemented with 1 μ L furimazine substrate at the start of the assay and after 4 h.

Subsequently, we tried to shorten the duration of the experiment while increasing the addition frequency and amount of substrate. Initial results were indicated partial degradation of BRD3 and BRD4 when using 1 μ M or 300 nM PHOTAC-I-3 (Figure 4.4A). Next, we probed the ideal timing of substrate addition. Addition of the Furimazine substrate after one third of the total assay duration of 9 h appeared best to induce partial BRD3 and BRD4 degradation, albeit differences between samples were small (Figure 4.4B).

Next, we performed control experiments to confirm that protein degradation is a direct result of the bioluminescence-induced isomerization of PHOTAC-I-3. When treating RS4;11 cells with 300 nM PHOTAC-I-3 for 16 h (Figure 4.5A) or with 1 μ M for 8 h (Figure 4.5B) we observed the strongest effect on BRD3 degradation. Removal of either NLuc or the furimazine substrate or addition of MLN4924, an inhibitor of cullin-RING E3 ligase activity prevented the degradation of BRD3.^[24] Additionally, using the

inactive Me-PHOTAC-I-3 which is unable to bind the E3 ligase did not induce protein degradation either (Figure 4.5A).^[20] This confirms that the observed protein degradation required NLuc and its substrate as well as PHOTAC-I-3-mediated recruitment of BET proteins to the functional cereblon-cullin-RING E3 ligase complex.

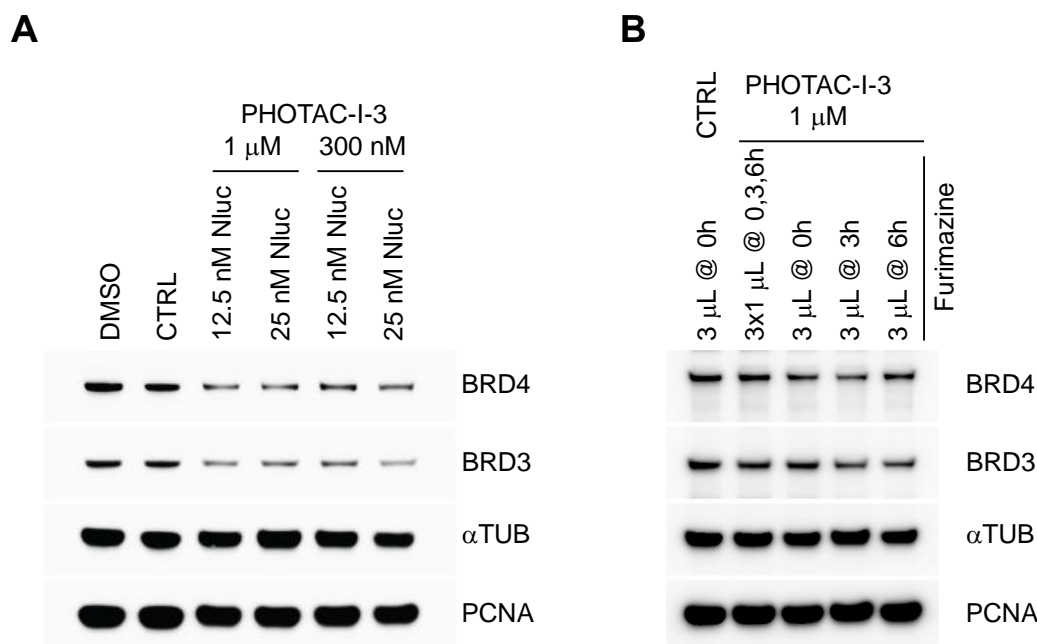


Figure 4.4: Timing of substrate addition to activate PHOTAC-I-3 A) Immunoblot analysis of BRD3 and BRD4 degradation in RS4;11 cells cultured in RPMI1640 medium after treatment with PHOTAC-I-3 and different concentrations of NLuc for a total of 7.5 h and addition of 1 μL of furimazine at the beginning of the assay and after 2.5, 4.5 and 6.5 h. B) Western blot of protein levels after 9 h of PHOTAC-I-3 and NLuc (12.5 nM) treatment and furimazine added at the indicated timepoints.

Discussion and Outlook

Harnessing bioluminescence to drive photopharmacology is a promising approach to overcome the limited tissue penetration of visible light. To demonstrate this concept, we combined PHOTACs with bioluminescence generated by NLuc to drive the degradation of BET proteins BRD3 and BRD4.

The catalytic mechanism of PHOTACs is ideal, since the moderate amounts of the active isomer generated through low-intensity bioluminescence are sufficient to promote protein degradation. The only limitation of PHOTACs is that the active form may compete with the inactive form for protein binding, but this should not limit activity at low concentrations. While we were able to demonstrate proof-of-concept, further optimization could improve the potency and consistency of this approach.

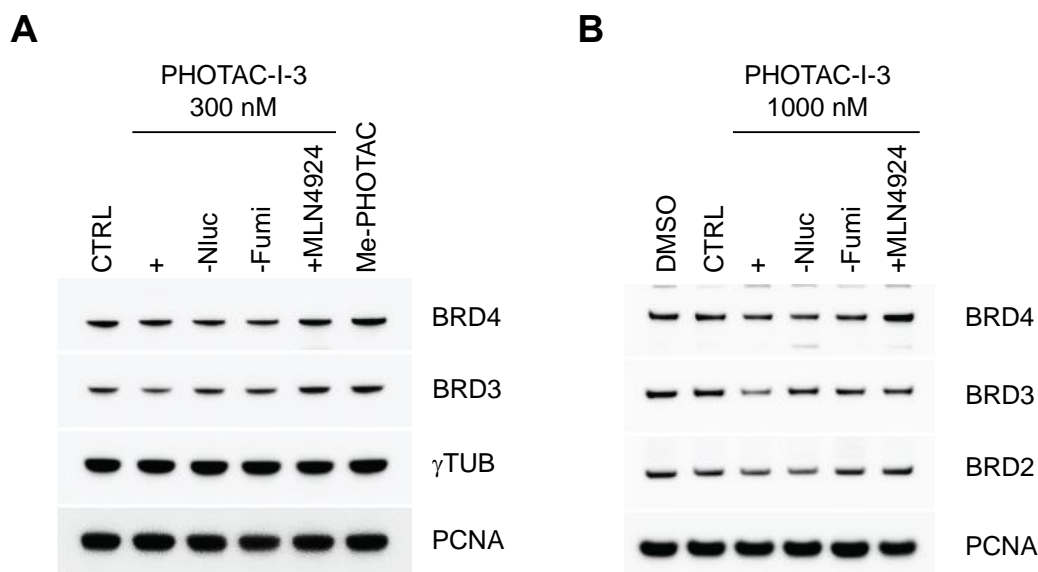


Figure 4.5: Control experiments for bioluminescence induced BET-protein degradation. A) Western blot analysis of BRD3 and BRD4 levels in RS4;11 cells cultured in RPMI1640 medium containing FBS and PS, treated for 16 h and supplemented with 1 μ L furimazine substrate at the start of the assay and after 4 h. B) Western blot analysis of BET protein levels in RS4;11 cells cultured in RPMI1640 and treated for 8 h, adding 1 μ L furimazine every hour (at $t=0, 1, 2, 3, 4, 5, 6, 7$ h). *DMSO* = 1% DMSO co-solvent; *CTRL* = 1% DMSO co-solvent + NLuc (12.5 nM) + furimazine; *+* = *CTRL* + PHOTAC-I-3; *-Nluc* = *CTRL* – NLuc; *-Fumi* = *CTRL* – furimazine; *+MLN4924* = *+* + MLN4924 (1.25 μ M); *Me-PHOTAC* = *+* + Me-PHOTAC-I-3 (same concentration as used for PHOTAC-I-3).

For example, the partial spectral overlap between the azobenzene photoswitch and the luciferase emission could be improved by using azobenzenes featuring a bathochromic shift in absorption.^[4] Further, the emission spectra of luciferase substrate pairs can also be modified through mutation of the luciferase or chemical modification of the substrate.^[11,25,26] Another option to improve the efficiency of bioluminescence-induced photoswitching could be the use of NLuc-POI fusion proteins to enable direct energy transfer from the luciferase to the photoswitch.

A current limitation of most approaches in photopharmacology is a dependence on knowing the boundaries and locations of a disease. However, some diseases such as cancer are localized to several regions, do not have clearly defined boundaries, or can spread to different tissues. Systemic application of an inactive photopharmaceutical could be combined with a luciferase conjugated to an antibody or a specific disease marker. Thereby, light-activation could internally localize to the disease and activate the drug only where it is needed. In contrast to other activation strategies, the activated

drug could return to an inactive state by thermal relaxation when leaving the disease site and thus side effects arising in other tissues could be mitigated.

Supporting Information

Supporting Figure

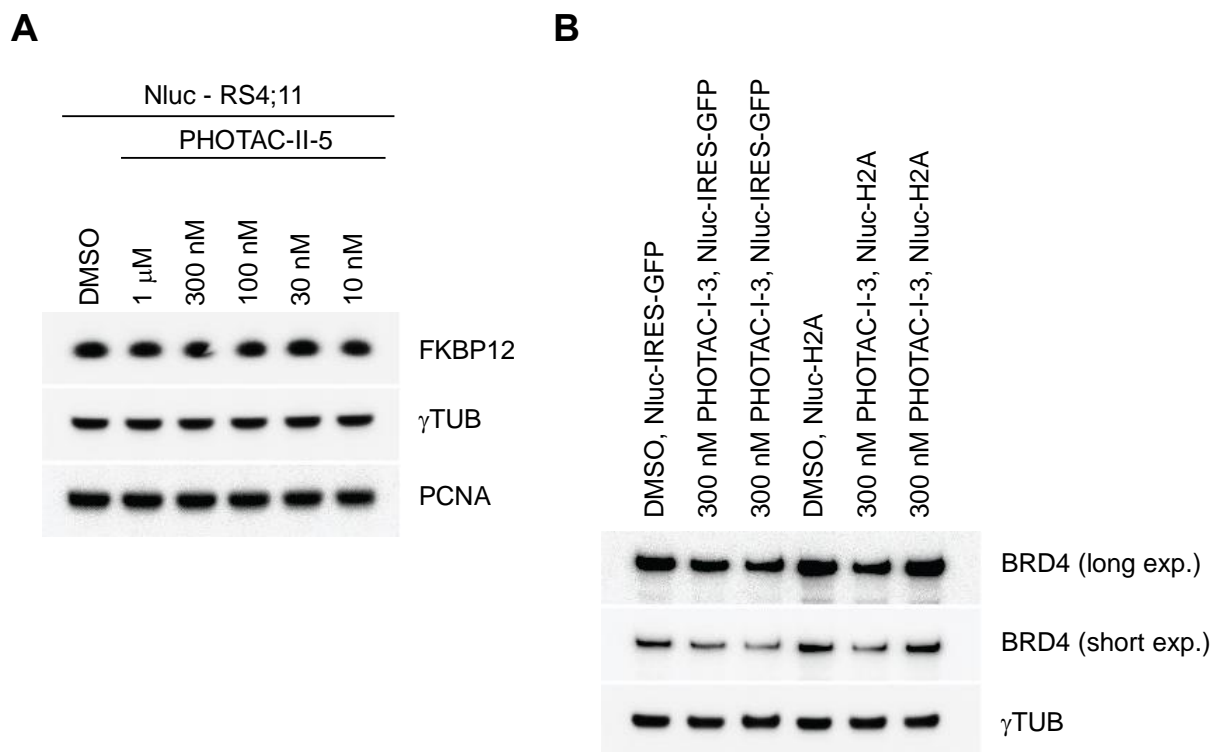


Figure S4.1: A) Immunoblot analysis of FKBP12 levels after treatment of RS4;11 cells with NLuc (12.5 nM) and **PHOTAC-II-5** at different concentrations for 16 h. Furimazine was added at t=0, 4 h. B) Immunoblot analysis of transfected MB-MDA-231 after treatment with **PHOTAC-I-3** for 16 h. Furimazine was added at t=0, 3 h.

Methods

UV-Vis spectroscopy

UV-Vis spectroscopy was performed on a Varian Cary 60 UV-Visible Spectrophotometer using BRAND UV-Cuvette Disposable Spectrophotometer/Photometer Ultra-Micro Cuvettes, BrandTech (10 mm light path) and an Agilent Technologies PCB 1500 Water Peltier system was used for temperature control.

LCMS

LCMS were measured on an Agilent Technologies 1260 II Infinity connected to an Agilent Technologies 6120 Quadrupole mass spectrometer with ESI ionization source. Elution was performed using a gradient from 5:95% to 100:0% MeCN:H₂O with 0.1% formic acid over 5 min, if not indicated otherwise. Separated spectra of the (*Z*)- and (*E*)-isomers could be obtained from the internal UV-VIS detector of the LCMS, by irradiating the sample before injection, and were normalized at the isosbestic point.

LED illumination

For illumination of the cells we used the cell disco system as previously described in the literature.^[27] 5 mm LEDs 450 nm (ELD-450-525) and 465 nm (RLS-B465)) were purchased from Roithner Lasertechnik. Pulsed irradiation was performed using 100 ms pulses every 10 s in 96- or 6-well plates, controlled by an Arduino system.

Cell culture and PHOTAC treatment

The human acute lymphoblastic leukemia RS4;11 (ATCC[®] CRL1873[™]) cell line was purchased from the American Type Culture Collection and cultured in RPMI1640 medium (Gibco) with 10% fetal bovine serum (FBS) and 1% penicillin/ streptomycin (PS) in a humidified incubator at 37 °C with 5% CO₂ in air. For the experiments compounds were serially diluted in RPMI1640 without the dye phenol red (Gibco). MDA-MB-231 cells were cultured in DMEM medium (Gibco) containing 10% fetal bovine serum (FBS) and 1% penicillin/ streptomycin (PS).

Azobenzene stocks and dilutions were strictly kept in the dark and prepared under dim red-light conditions. Furimazine substrate solution was used as purchased (Promega Nano-Glo[®] Luciferase Assay System, N1110). Recombinant enzymes were obtained

from the Prescher lab as the following stock solutions: NLuc 100 μ M, GLuc 1.8 mM. For immunoblotting analysis, cells (2×10^6 for RS4:11) were incubated for the indicated times with PHOTACs and always handled under dim red light. To avoid any light contamination, well plates were placed inside a reflective cardboard box which was placed inside a light-proof box. After incubation, cells were collected in the dark by centrifugation (150 g, 5 min) at 4 °C and the pellets were washed twice with ice cold PBS (1 mL) under dim red light.

Immunoblotting Analysis

Cells were lysed in RIPA buffer containing protease and phosphatase inhibitor and protein concentration was determined using BCA (Thermo Fisher). Immunoblotting was performed as previously described.^[20,28] Briefly, samples were resolved under denaturing and reducing conditions using 4%–12% Bis-Tris gels (NuPAGE) and transferred to a PDVF membrane (Immobilon-P, Millipore). Membranes were blocked with 5% nonfat dried milk, incubated with primary antibodies overnight at 4°C. After washing the membranes, secondary antibodies coupled with horseradish peroxidase were applied. Immunoreactive bands were visualized by enhanced chemiluminescence reagent (Thermo Fisher Scientific) and signal was acquired using ImageQuant LAS 400 (GE).

The following antibodies were used:

Antibodies	Source	Identifier
BRD2	Bethyl	A302-583A
BRD3	Bethyl	A302-368A-1
BRD4	Cell Signaling Technology	#13440
PCNA	dako	cat. No. M0879
α TUBULIN	Sigma Aldrich	T6557
γ TUBULIN	Sigma Aldrich	T6074
FKBP12	Santa Cruz Biotechnology	cat. No. sc-133067
anti-Rabbit IgG, peroxidase-linked antibody	Thermo Fisher	NA934
anti-Mouse IgG, peroxidase-linked antibody	Thermo Fisher	NA931
anti-goat IgG-HRP	Santa Cruz Biotechnology	cat. No. sc-2354

Transfection with NLuc

MB-MDA-231 cells were seeded 24 h before transfection. NLuc-IRES-GFP and NLuc-H2A plasmids were obtained from the Prescher lab and transfected using jetPRIME® according to the manufacturer's instructions. The medium was replaced after 22 h and cells were treated with PHOTAC-I-3 or vehicle and furimazine for 16 hours upon which the cells were collected and subjected to immunoblotting analysis as described above.

References

- [1] T. Lister, P. A. Wright, P. H. Chappell, *J. Biomed. Opt.* **2012**, *17*, 090901.
- [2] C. Ash, M. Dubec, K. Donne, T. Bashford, *Lasers Med. Sci.* **2017**, *32*, 1909–1918.
- [3] M. D. Wheelock, J. P. Culver, A. T. Eggebrecht, *Rev. Sci. Instrum.* **2019**, *90*, 051101.
- [4] M. Dong, A. Babalhavaeji, S. Samanta, A. A. Beharry, G. A. Woolley, *Acc. Chem. Res.* **2015**, *48*, 2662–2670.
- [5] D. B. Konrad, G. Savasci, L. Allmendinger, D. Trauner, C. Ochsenfeld, A. M. Ali, *J. Am. Chem. Soc.* **2020**, *142*, 6538–6547.
- [6] G. Shin, A. M. Gomez, R. Al-Hasani, Y. R. Jeong, J. Kim, Z. Xie, A. Banks, S. M. Lee, S. Y. Han, C. J. Yoo, J.-L. Lee, S. H. Lee, J. Kurniawan, J. Tureb, Z. Guo, J. Yoon, S.-I. Park, S. Y. Bang, Y. Nam, M. C. Walicki, V. K. Samineni, A. D. Mickle, K. Lee, S. Y. Heo, J. G. McCall, T. Pan, L. Wang, X. Feng, T. Kim, J. K. Kim, Y. Li, Y. Huang, R. W. Gereau, J. S. Ha, M. R. Bruchas, J. A. Rogers, *Neuron* **2017**, *93*, 509-521.e3.
- [7] K. Nakajima, T. Kimura, H. Takakura, Y. Yoshikawa, A. Kameda, T. Shindo, K. Sato, H. Kobayashi, M. Ogawa, *Oncotarget* **2018**, *9*, 20048–20057.
- [8] Y. Zhang, A. D. Mickle, P. Gutruf, L. A. McIlvried, H. Guo, Y. Wu, J. P. Golden, Y. Xue, J. G. Grajales-Reyes, X. Wang, S. Krishnan, Y. Xie, D. Peng, C.-J. Su, F. Zhang, J. T. Reeder, S. K. Vogt, Y. Huang, J. A. Rogers, R. W. Gereau, *Sci. Adv.* **2019**, *5*, eaaw5296.
- [9] I. Kirino, K. Fujita, K. Sakanoue, R. Sugita, K. Yamagishi, S. Takeoka, T. Fujie, S. Uemoto, Y. Morimoto, *Sci. Rep.* **2020**, *10*, 22017.
- [10] J. A. Frank, M.-J. Antonini, P.-H. Chiang, A. Canales, D. B. Konrad, I. C. Garwood, G. Rajic, F. Koehler, Y. Fink, P. Anikeeva, *ACS Chem. Neurosci.* **2020**, *11*, 3802–3813.
- [11] Z. M. Kaskova, A. S. Tsarkova, I. V. Yampolsky, *Chem. Soc. Rev.* **2016**, *45*, 6048–6077.
- [12] A. C. Love, J. A. Prescher, *Cell Chem. Biol.* **2020**, *27*, 904–920.
- [13] K. Berglund, K. Clissold, H. E. Li, L. Wen, S. Y. Park, J. Gleixner, M. E. Klein, D. Lu, J. W. Barter, M. A. Rossi, G. J. Augustine, H. H. Yin, U. Hochgeschwender, *Proc. Natl. Acad. Sci.* **2016**, *113*, E358–E367.
- [14] C. K. Kim, K. F. Cho, M. W. Kim, A. Y. Ting, *eLife* **2019**, *8*, e43826.
- [15] E. Lindberg, S. Angerani, M. Anzola, N. Winssinger, *Nat. Commun.* **2018**, *9*, 3539.
- [16] D. Chang, E. Lindberg, S. Feng, S. Angerani, H. Riezman, N. Winssinger, *Angew. Chem. Int. Ed.* **2019**, *58*, 16033–16037.
- [17] D. Chang, S. Feng, V. Girik, H. Riezman, N. Winssinger, *J. Am. Chem. Soc.* **2021**, *143*, 3665–3670.
- [18] R. Weinstain, T. Slanina, D. Kand, P. Klán, *Chem. Rev.* **2020**, DOI 10.1021/acs.chemrev.0c00663.
- [19] J. Broichhagen, J. A. Frank, D. Trauner, *Acc. Chem. Res.* **2015**, *48*, 1947–1960.
- [20] M. Reynders, B. S. Matsuura, M. Bérouti, D. Simoneschi, A. Marzio, M. Pagano, D. Trauner, *Sci. Adv.* **2020**, *6*, eaay5064.
- [21] A. Stathis, F. Bertoni, *Cancer Discov.* **2018**, *8*, 24–36.
- [22] G. M. Burslem, C. M. Crews, *Cell* **2020**, *181*, 102–114.

- [23] M. P. Hall, J. Unch, B. F. Binkowski, M. P. Valley, B. L. Butler, M. G. Wood, P. Otto, K. Zimmerman, G. Vidugiris, T. Machleidt, M. B. Robers, H. A. Benink, C. T. Eggers, M. R. Slater, P. L. Meisenheimer, D. H. Klaubert, F. Fan, L. P. Encell, K. V. Wood, *ACS Chem. Biol.* **2012**, *7*, 1848–1857.
- [24] S. T. Nawrocki, P. Griffin, K. R. Kelly, J. S. Carew, *Expert Opin. Investig. Drugs* **2012**, *21*, 1563–1573.
- [25] C. M. Rathbun, A. A. Ionkina, Z. Yao, K. A. Jones, W. B. Porterfield, J. A. Prescher, *ACS Chem. Biol.* **2021**, *16*, 682–690.
- [26] Z. Yao, B. S. Zhang, R. C. Steinhardt, J. H. Mills, J. A. Prescher, *J. Am. Chem. Soc.* **2020**, *142*, 14080–14089.
- [27] M. Borowiak, W. Nahaboo, M. Reynders, K. Nekolla, P. Jalinot, J. Hasserodt, M. Rehberg, M. Delattre, S. Zahler, A. Vollmar, D. Trauner, O. Thorn-Seshold, *Cell* **2015**, *162*, 403–411.
- [28] A. Marzio, J. Puccini, Y. Kwon, N. K. Maverakis, A. Arbini, P. Sung, D. Bar-Sagi, M. Pagano, *Mol. Cell* **2019**, *73*, 224-237.e6.

5 – PHOTACs Controlling the MDM2-p53 Axis

Martin Reynders^{1,2}, Michele Pagano^{3,4,5}, and Dirk Trauner^{1,4,6}

¹Department of Chemistry, New York University, New York, NY 10003, USA.

²Department of Chemistry, Ludwig Maximilians University of Munich
81377 Munich, Germany.

³Department of Biochemistry and Molecular Pharmacology, New York University
School of Medicine, New York, NY 10016, USA.

⁴Perlmutter Cancer Center, New York University School of Medicine, New York, NY
10016, USA.

⁵Howard Hughes Medical Institute, New York University School of Medicine, New
York, NY 10016, USA.

⁶NYU Neuroscience Institute, New York University School of Medicine, New York, NY
10016, USA.

Abstract

PHOTOchemically TArgeting Chimeras (PHOTACs) are catalytically active drugs that can control protein abundance with light by inducing protein degradation. PHOTACs combine an E3 ligase ligand, a photoswitch and ligand for the target of interest in one molecule. Here we present the development of PHOTACs to control MDM2 and consequently p53 levels. The lead MDM2-PHOTAC is inactive as degrader in the dark but undergoes reversible isomerization upon light irradiation to become active. Light-controlled MDM2 degradation leads to sustained p53 accumulation, which in turn induces apoptosis. This manifests as a 34-fold toxicity increase between light and dark and creates a wide phototherapeutic window. MDM2-PHOTACs could be useful as tools to study the MDM2-p53 axis and as potential drugs in photomedicine.

Introduction

The tumor suppressor protein p53 is a transcription factor that can control numerous biological processes.^[1] A major role of p53 is the induction of cell cycle arrest or apoptosis in response to DNA damage or other cellular stress signals.^[1,2] The abundance of p53 is controlled by MDMX and MDM2. MDM2 is an E3 ligase that promotes the ubiquitylation and subsequent degradation of p53 (**Figure 5.1A**).^[3] As a feedback loop, p53 also controls MDM2 expression. p53 maintains the background expression of several tumor suppressor genes. Mutations of p53 or other mechanisms of wild-type p53 suppression, such as upregulation of MDM2, are commonly found in cancers.^[3–5]

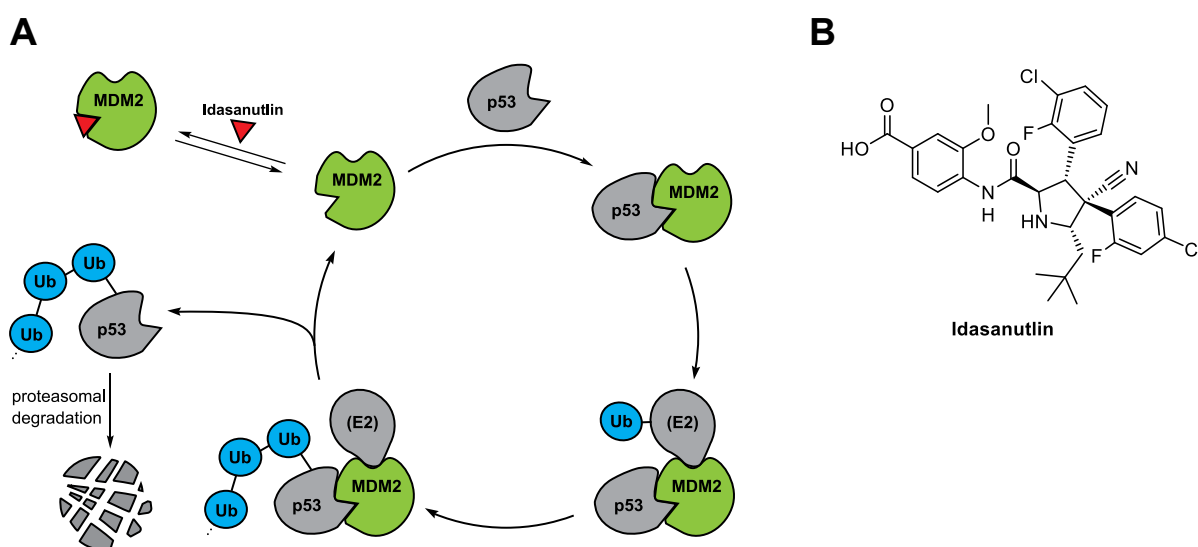


Figure 5.1: A) Schematic representation of p53 degradation by MDM2. B) Structure of the MDM2 inhibitor idasanutlin.

Pharmacological disruption of the MDM2-p53 interaction has been an active area of research. Several small molecules, like idasanutlin (**Figure 5.1B**), that bind MDM2 and stabilize wild-type p53 have entered clinical trials as cancer therapeutics.^[6–9] Despite promising anticancer activity, dose-limiting hematopoietic and gastrointestinal toxicities have been observed. These limit the applicability of MDM2 inhibitors and require adjusted dosing schedules.^[6,10]

An emerging approach to restrict the activity of a molecule to a specific area is photopharmacology.^[11] Through incorporation of a light-responsive chemical moiety, a drug's activity can be precisely controlled by irradiation. This can either be achieved with photoswitches that undergo reversible, light-induced isomerization or with

photolabile protecting groups.^[12–14] Examples for photoswitchable anticancer drugs include microtubule inhibitors,^[15,16] proteasome inhibitors,^[17,18] and membranolytic peptides.^[19,20] Feringa and co-workers have described an idasanutlin derivative with a photolabile protecting group that can be photolyzed with light to yield idasanutlin.^[21] They were able to induce elevated p53 levels and arrest cell growth with 405 nm irradiation, however this approach irreversibly released idasanutlin and diffusion led to partial activity of the drug in non-irradiated cells.^[21]

We set out to develop a photoswitchable probe to reversibly control MDM2 and thereby p53 levels. An emerging addition to the pharmacological toolbox are proteolysis targeting chimeras (PROTACs) that catalyze the ubiquitylation and degradation of target proteins by recruiting them to an E3 ligase, using a bifunctional molecule.^[22] PROTACs degrading MDM2 to rescue wild-type p53 levels have also been described.^[23–26] Further, MDM2 has been employed as a E3 ligase for PROTACs degrading BRD4.^[27]

Recently, we described photochemically targeting chimeras (PHOTACs) as a strategy to control PROTACs with light and thereby adding an extra level of control.^[28] Here we apply this strategy to develop PHOTACs targeting MDM2.

Results

The formation of a productive ternary complex that induces ubiquitylation of the target is the basis for a working PROTAC or PHOTAC. In the case of a bifunctional molecule inducing complex formation between cereblon and MDM2 as a target, the ternary complex could not only induce MDM2 degradation, but also lead to cereblon degradation by the E3 ligase MDM2. Therefore, an ideal PHOTAC must be designed to neither induce cereblon, nor MDM2 degradation in its inactive form (**Figure 5.2**). We based our MDM2-PHOTACs on our modular approach, using azobenzene photoswitches prepared from lenalidomide to recruit cereblon.^[28] Idasanutlin was used as ligand for MDM2, since attachment of a linker on the benzoic acid is tolerated and does not interfere with the interaction between the hydrophobic groups and MDM2.^[9,27] Composition of the linker is a crucial element in PROTAC design to regulate formation of the ternary complex.^[29–31] Therefore, we synthesized PHOTACs with varying linker length to obtain a PHOTAC showing the desired degradation profile after irradiation, while remaining an inactive in the dark (**Figure 5.3A**).

The photophysical properties of **PHOTAC-MDM2-1–4** largely resembled those of previously described PHOTACs (**Figure 5.3B,C, S5.1**).^[28] Upon irradiation, **PHOTAC-MDM2-1–4** underwent reversible *E*-to-*Z* isomerization, with 390 nm irradiation yielding 87% of **Z-PHOTAC-MDM2-3**. Mixtures containing a majority of the *E*-isomer could be obtained by green light irradiation (**Figure 5.3D**). Complete reversion to the *E*-isomer was achieved by thermal relaxation with a half-life of approximately 15 h (**Figure 5.3E**).

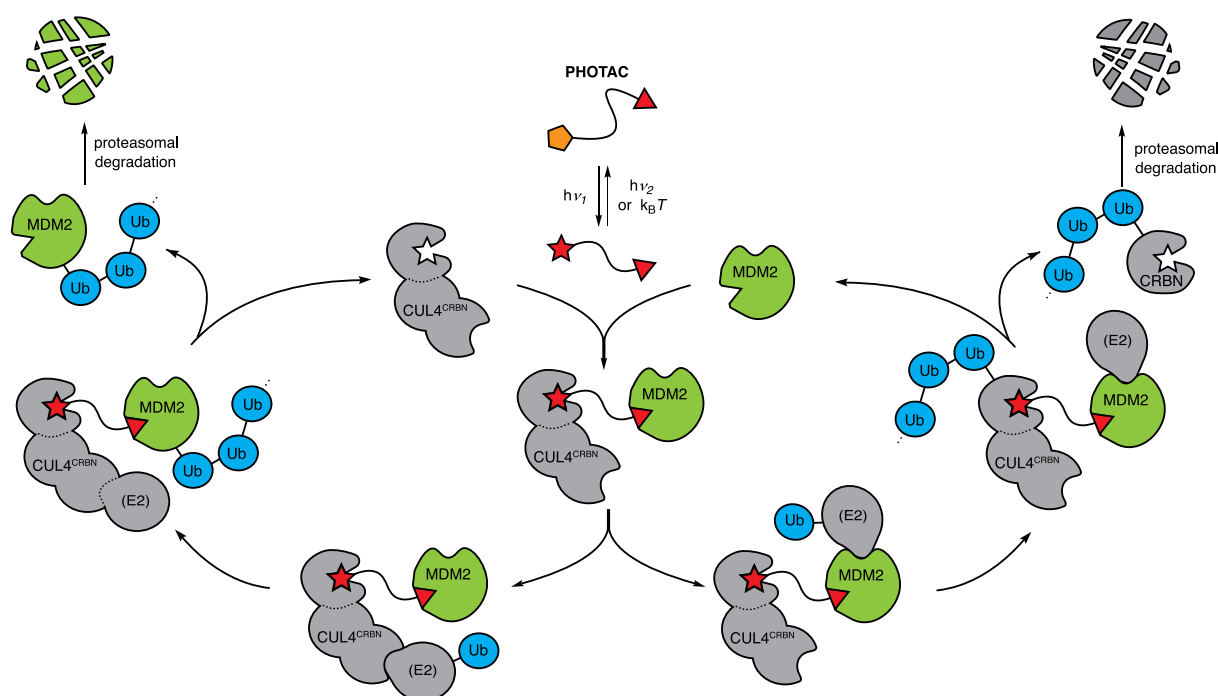


Figure 5.2: Schematic depiction of an ideal **PHOTAC** for MDM2 and cereblon. PHOTACs can be isomerized between an inactive form (yellow pentagon) and an active form (red star) upon irradiation. The active form can catalyze the ubiquitylation of its targets.

Next, we evaluated the effect of **PHOTAC-MDM2-1–4** on RS4;11 acute lymphoblastic leukemia cell viability and proliferation after 72 h in the dark or under pulsed 390 nm irradiation (100 ms pulses every 10 s). **PHOTAC-MDM2-1** bearing the shortest linker only showed a 3-fold lower EC_{50} upon 390 nm irradiation (**Figure 5.4A**). Increasing the linker length with **PHOTAC-MDM2-2** improved the activity upon irradiation showing a 5-fold difference (**Figure 5.4B**). For **PHOTAC-MDM2-3** we observed the largest photopharmacological window (**Figure 5.4C**). Upon activation with 390 nm light pulses, its potency increases more than 30-fold compared to the non-irradiated compound in the dark. Further, the toxicity of **PHOTAC-MDM2-3** is wavelength dependent. Longer

activation wavelengths generate a smaller fraction of the active Z-isomer and correspondingly the effect on viability is lowered (**Figure S5.2A**). A longer linker as used in **PHOTAC-MDM2-4** exhibits a much smaller viability difference upon photoisomerization (**Figure 5.4D**).

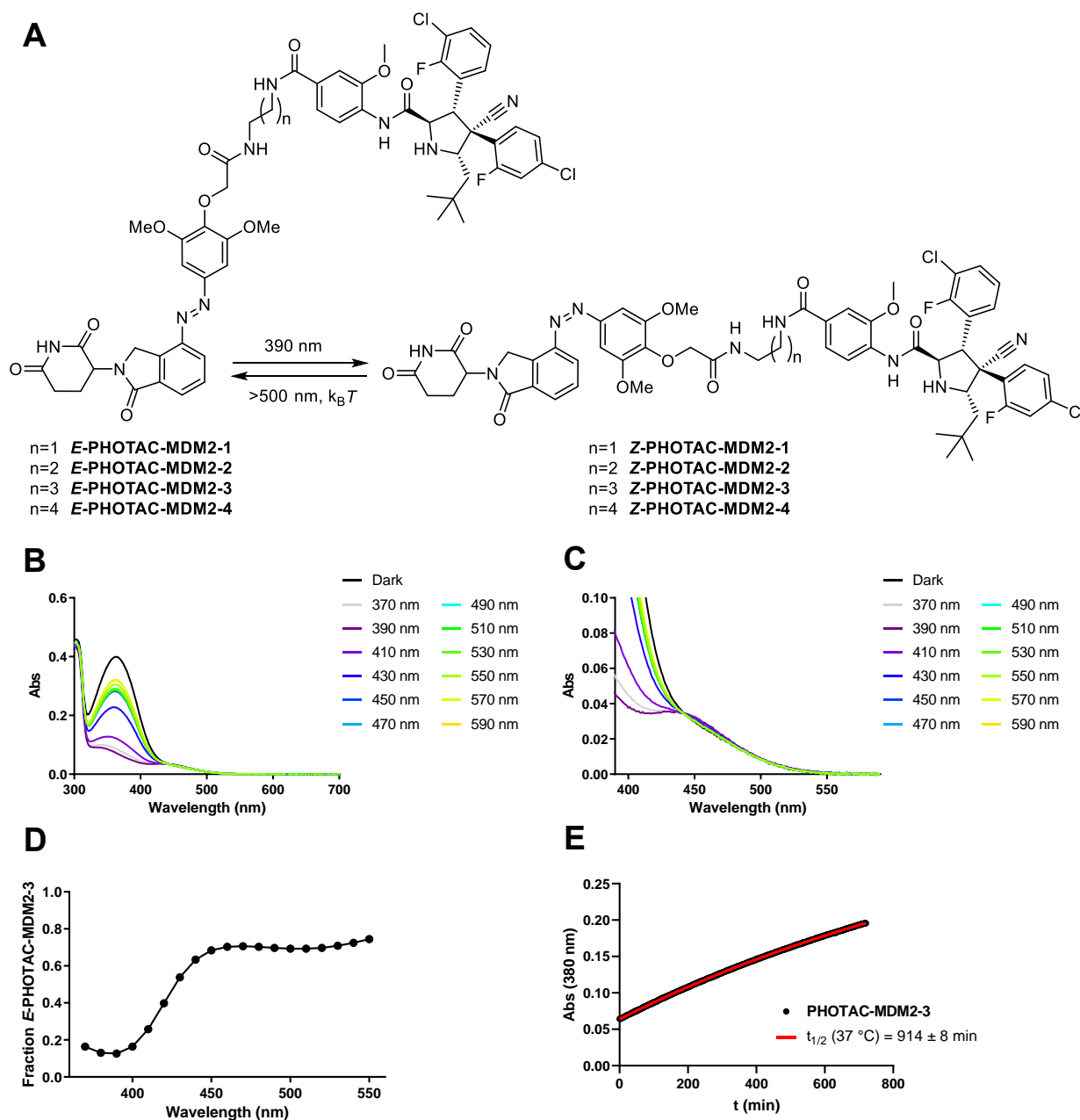


Figure 5.3: Characterization of **PHOTACs** recruiting MDM2. A) Structure and isomerization of **PHOTAC-MDM2-1–4**. B), C) Absorption spectra of **PHOTAC-MDM2-3** after irradiation for 5 min with the indicated wavelength. D) Calculated fraction of *E*-**PHOTAC-MDM2-3** after 5 min irradiation with the indicated wavelength. E) Thermal *Z*-to-*E* isomerization of **PHOTAC-MDM2-3** at 37 °C in DMSO.

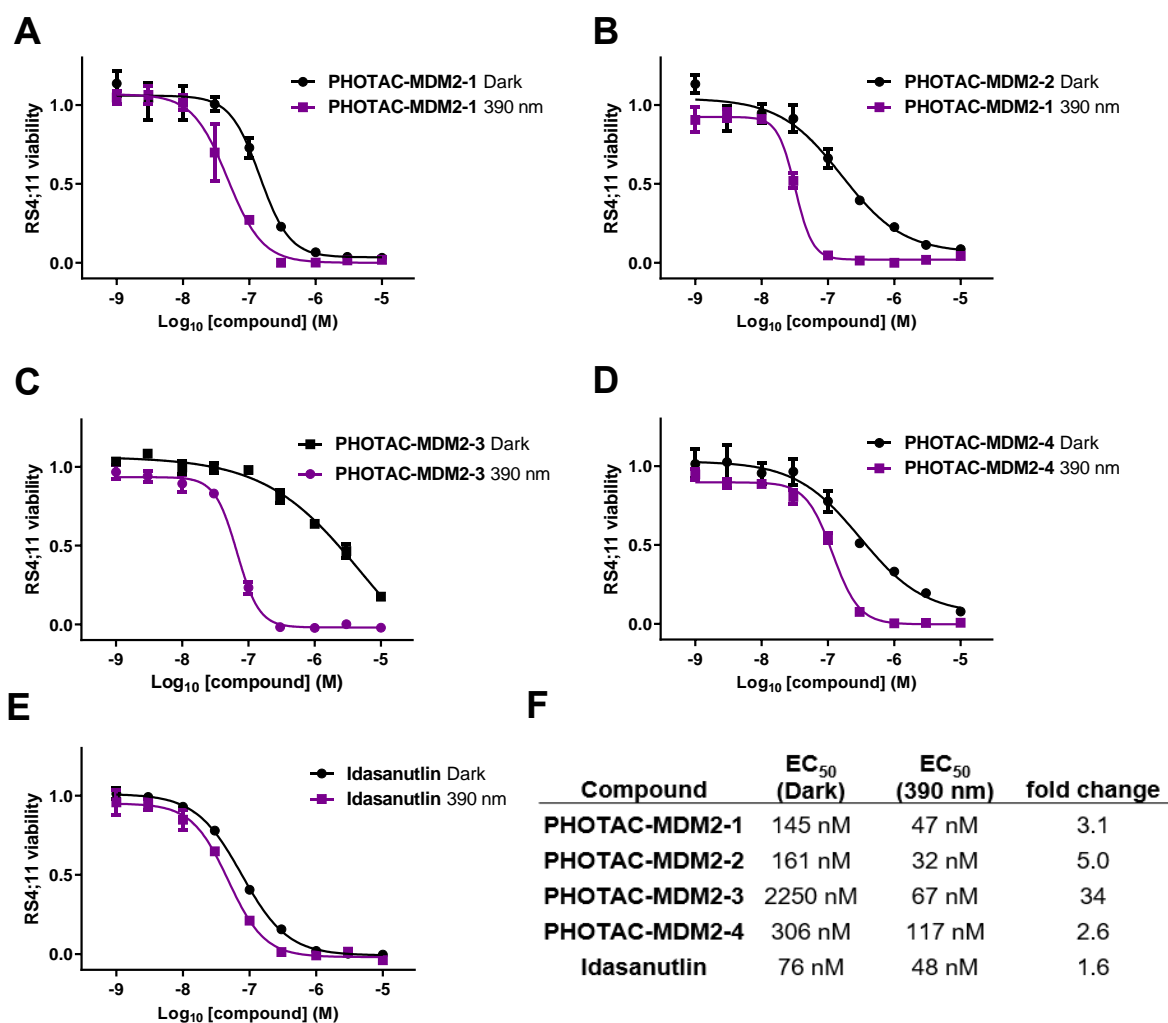


Figure 5.4: Viability effects of PHOTAC-MDM2-1–4. Viability of RS4;11 cells after treatment with A) PHOTAC-MDM2-1, B) PHOTAC-MDM2-2, C) PHOTAC-MDM2-3, D) PHOTAC-MDM2-4, and E) idasanutlin for 72 h in the dark or under pulsed 390 nm irradiation (100 ms every 10 s). F) EC₅₀ values of MDM2 targeting PHOTACs.

Interestingly, we also observed a small but significant effect of 390 nm irradiation for idasanutlin treatment (**Figure 5.4E**). When using 100 ms pulses every 10 s, 390 nm light did not affect the viability of untreated RS4;11 cells (**Figure S5.2D**), however a 1.6-fold lower EC₅₀ could be observed for idasanutlin. Cutting the light-dose in half (75 ms pulses every 15 s) gave a 1.3-fold lower EC₅₀ for idasanutlin combined with 390 nm irradiation compared to incubation in the dark (**Figure S5.2A**). p53 is involved in the cellular response to DNA damage, cellular stress and control of reactive oxygen species (ROS).^[2] At a dose tolerated by untreated cells, 390 nm irradiation could contribute to the generation of ROS and thymine dimers explaining the observed synergy in idasanutlin-treated cells in which p53 levels are upregulated.^[32] In contrast, the EC₅₀ of PHOTAC-MDM2-3 remained unchanged when reducing the light dose by

50%, in accordance with the slow thermal relaxation and a different mechanism of action (**Figure S5.1B**). When activated by 390 nm irradiation, all PHOTACs show a similar degree of cytotoxicity with EC₅₀ values between 32 and 117 nM. The major difference in size of their photopharmacological window stems from their activity in the dark, which is lowest for **PHOTAC-MDM2-3** with an EC₅₀ of 2.25 μM.

Next, we analyzed the ability of **PHOTAC-MDM2-1–4** to degrade MDM2 by Western blot. Degradation of MDM2 should lead to an increase in p53 levels which in turn would promote the induction of apoptosis in RS4;11 cells. Additionally, MDM2 inhibition and the subsequently increased p53 levels could promote MDM2 expression. Increased MDM2 levels have been observed for MDM2 inhibitors and could partially hide MDM2 degradation on the Western blot.^[9] It should be noted that our **PHOTACs** could still act as inhibitors of MDM2 and show a slight increase in p53 levels at high concentrations.

The immunoblot of RS4;11 cells treated with **PHOTAC-MDM2-1** for 12 h showed MDM2 and cereblon degradation upon pulsed 390 nm irradiation at 10 and 1 μM (**Figure 5.5A**). Consequently, p53 levels were strongly increased and cleavage of PARP1 could be observed, indicating the induction of apoptosis.^[33] Degradation of CRBN at 10 μM, an increase in p53 levels and cleaved PARP1 at 10 and 1 μM were observed in the dark, albeit to a lesser extent compared with the irradiated cells. This explains the observed effects on viability and limited phototherapeutic window.

PHOTAC-MDM2-2 with a linker length increased by one methylene unit also induced the degradation of MDM2 and CRBN at 10 μM and lead to higher levels of p53 and cleaved PARP1 at 10 and 1 μM upon 390 nm irradiation (**Figure 5.5B**). In the dark, no pronounced degradation of cereblon or MDM2 was observed, but p53 levels were elevated at 10 μM, 1 μM and 100 nM. A low level of PARP1 cleavage could also be observed in the dark. The not strictly concentration-dependent p53 accumulation indicates a remaining activity as of **PHOTAC-MDM2-2** as MDM2 degrader in the dark.

The lead compound from viability assays, **PHOTAC-MDM2-3**, strongly induced degradation of cereblon and MDM2 at 10 μM and partially reduced MDM2 levels at 1 μM when irradiated with 390 nm (**Figure 5.6A**). As a result of MDM2 degradation, p53 levels soar and cells undergo apoptosis as visualized by caspase 3 and PARP1

cleavage. No degradation of either cereblon or MDM2 was observed in the dark. A small, dose-dependent increase in p53 levels was noticeable in the absence of light, which could be an effect of MDM2 inhibition by the ligand. However, caspase 3 cleavage cannot be observed in the dark and only a slight increase in cleaved PARP1 could be seen with 10 μM of the inactive PHOTAC.

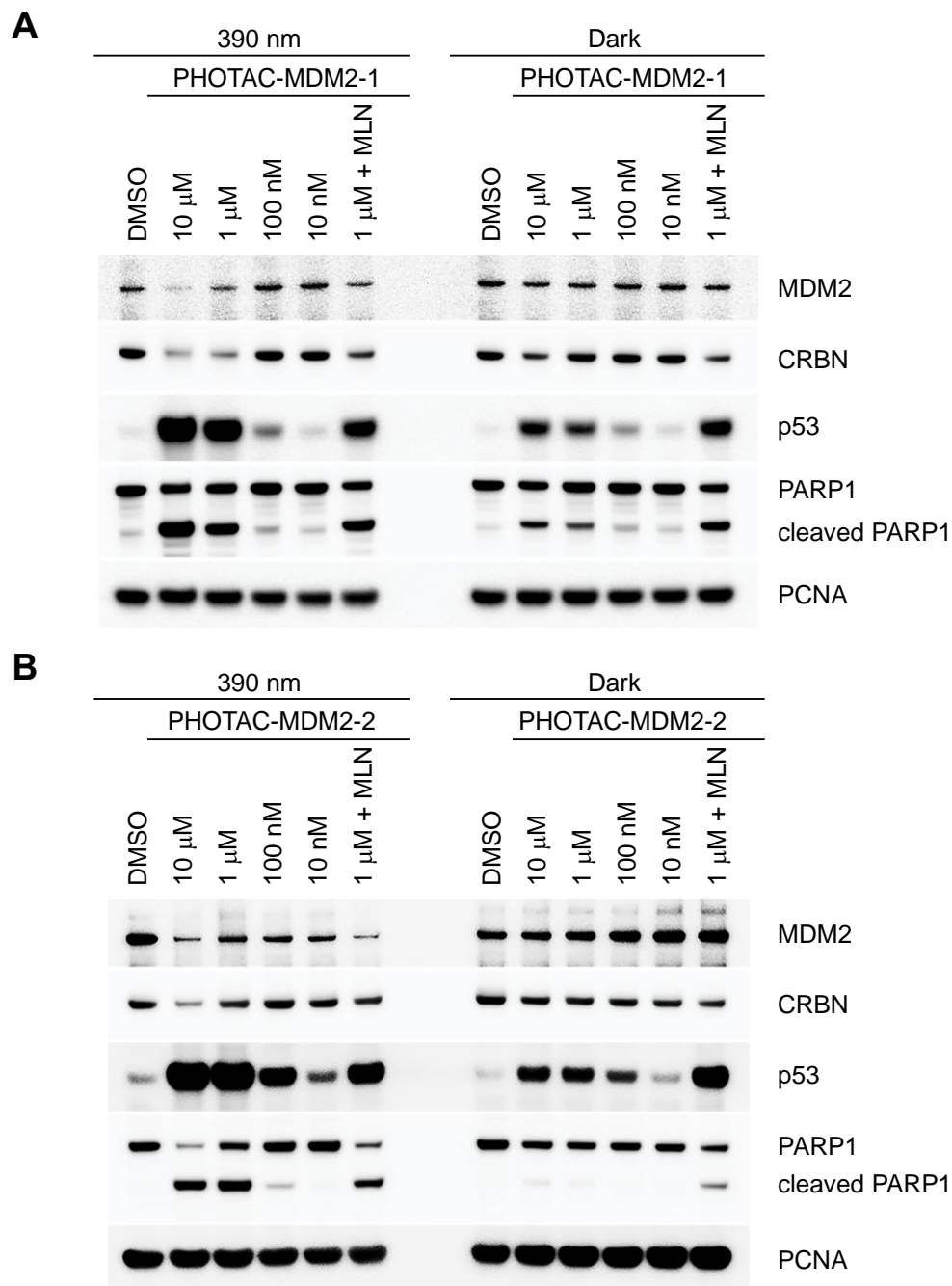


Figure 5.5: *In cellulo* analysis of **PHOTAC-MDM2-1+2**. Immunoblot of RS4;11 cells treated with A) **PHOTAC-MDM2-1** or B) **PHOTAC-MDM2-2** for 12 h in the dark or under pulsed 390 nm irradiation (100 ms every 10 s). MLN = 1.25 μM MLN4924.

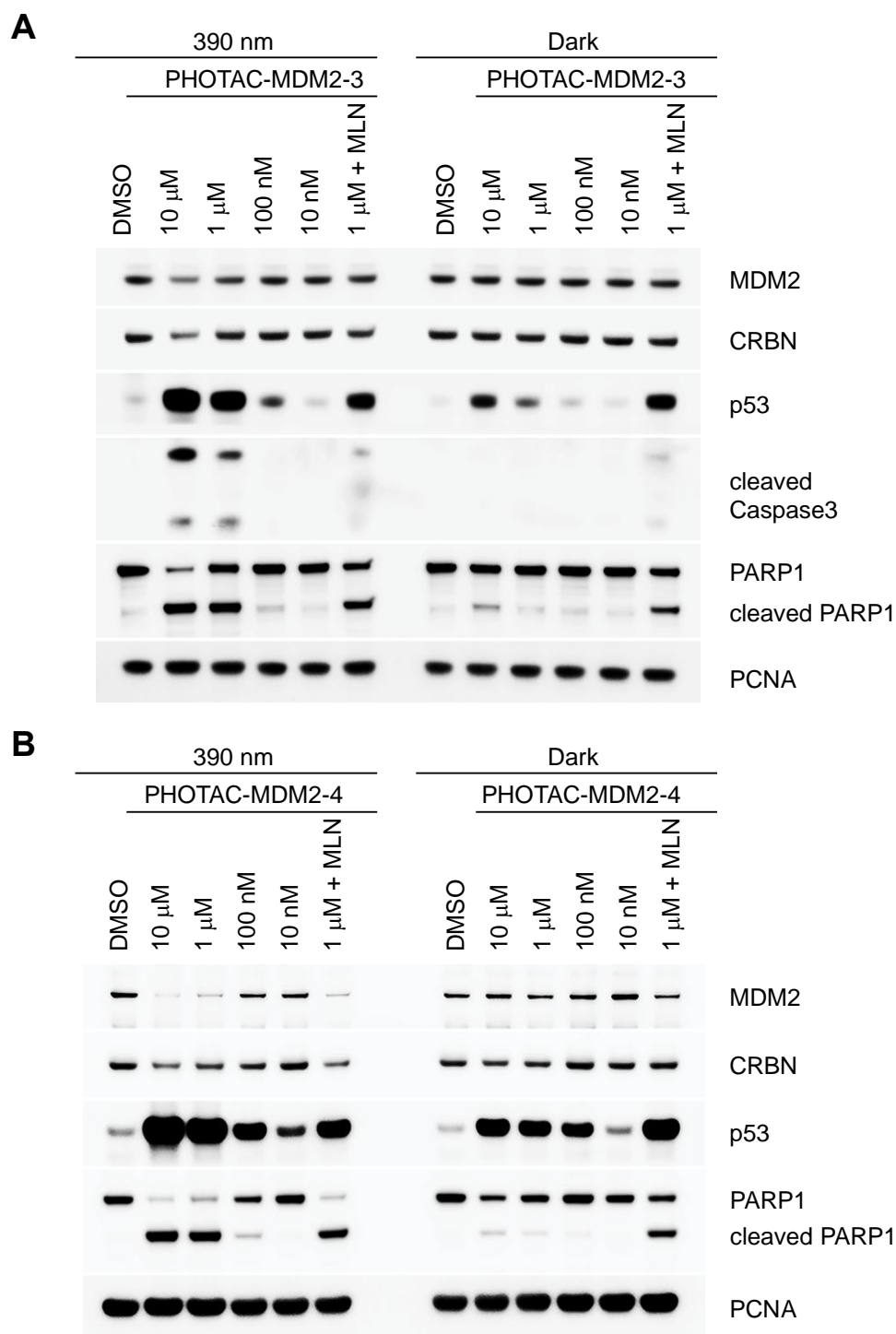


Figure 5.6: *In cellulo* analysis of **PHOTAC-MDM2-3+4**. Immunoblot of RS4;11 cells treated with A) **PHOTAC-MDM2-3** or B) **PHOTAC-MDM2-4** for 12 h in the dark or under pulsed 390 nm irradiation (100 ms every 10 s). MLN = 1.25 μ M MLN4924.

Lastly, **PHOTAC-MDM2-4**, showed partial cereblon degradation at 10 μ M, and the strongest degradation of MDM2 at 10 and 1 μ M. Correspondingly, an increase in levels of p53 and cleaved PARP1 under 390 nm irradiation was observed (**Figure 5.6B**). In the dark, no strong degradation of cereblon or MDM2 could be observed, however the

substantial increase in p53 levels between 10 μM and 100 nM indicates activity of **PHOTAC-MDM2-4** as a degrader of MDM2.

In general, increasing linker length corresponded with lower cereblon degradation and increased MDM2 degradation. appears to be in the sweet spot where no degradation of either cereblon or MDM2 was detected in the dark. This observation could explain the large photopharmacological window observed for **PHOTAC-MDM2-3**.

Culling RING E3 ligases are modified with NEDD8, termed neddylation, to enhance their activity.^[34,35] The neddylation inhibitor MLN4924 should in turn inhibit Cullin RING E3 ligase function.^[36] MLN4924 was not able to rescue CRBN or MDM2 levels under the experimental conditions when used in combination with **MDM2-PHOTACs** (Figure 5.5, 5.6). This could be a result of the long treatment or the strong induction of apoptosis observed for the combination treatment in the light and dark. To further characterize the degradation induced by **PHOTAC-MDM2-3**, we investigated the effect of idasanutlin and lenalidomide addition on protein levels and apoptosis.

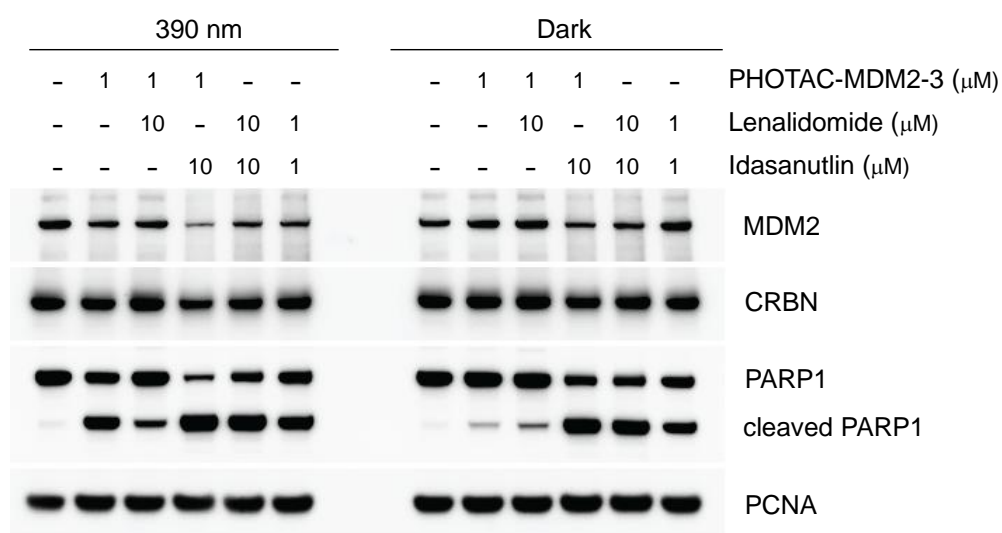


Figure 5.7: Competition experiment for **PHOTAC-MDM2-3**. Western blot analysis of RS4;11 cells treated with the indicated compounds and concentrations for 12 h in the dark or under pulsed 390 nm irradiation (100 ms every 10 s).

Co-treatment of RS4;11 cells with 1 μM **PHOTAC-MDM2-3** and 10 μM lenalidomide under 390 nm irradiation lowered the amount of cleaved PARP1 observed with 1 μM **PHOTAC-MDM2-3** alone (Figure 5.7). This demonstrates that the activity of **PHOTAC-MDM2-3** depends on cereblon binding. Interestingly, combination with 10 μM idasanutlin did not rescue MDM2 levels but led to further MDM2 depletion under

390 nm irradiation. Combined treatment with idasanutlin and lenalidomide did not show such a strong MDM2 reduction and no light-dependence. Another indication that **PHOTAC-MDM2-3** operates under a different mechanism is the higher amount of cleaved PARP1 that was observed for lenalidomide plus idasanutlin in comparison with PHOTAC treatment in the dark. The reduced activity of the *E*-isomer of **PHOTAC-MDM2-3** compared to the parent inhibitors and the possibility to regain full activity when converting **PHOTAC-MDM2-3** to the *Z*-isomer with light highlights the potential of PHOTACs and photopharmacology.

Conclusion

By adapting PHOTACs to target MDM2, we have successfully prepared a series of light- controlled dual cereblon and MDM2 degraders. Depletion of MDM2 would be sufficient for a strong cytotoxic response, but the observed degradation of cereblon by MDM2 does not appear to restrict the MDM2-PHOTACs. This is in line with the hetero- and homo-dimerizing E3 ligase PROTACs previously reported.^[37–39] Considering cereblon as the target of MDM2, the results present the first example of a photoswitchable targeting ligand employed for PHOTACs. Our results further demonstrate that the modular PHOTAC approach can easily be adapted to new targets and facilitate the development of photopharmaceuticals.

The photopharmacological window of **PHOTAC-MDM2-3** toxicity in RS4;11 cells is much larger than achieved with the first generation of PHOTACs for BRD4. The composition of the linker connecting the ligands was crucial to tune protein degradation. Key to the success is the reduced activity of the *E*-isomer in the dark compared to the parent inhibitors and the ability of the *Z*-isomer to regain potent cytotoxicity by inducing protein degradation.

The light-control of MDM2 and p53 levels could be beneficial in a therapeutic setting and PHOTACs could improve the safety profile of MDM2 targeting drugs. **PHOTAC-MDM2-3** provides a promising starting point to develop these drugs for photomedicine and treatment of cancers with wild-type p53. In this context, the observed synergy between idasanutlin and irradiation could further improve efficacy of MDM2 targeting drugs.

Additionally, PHOTACs targeting MDM2 could be employed in cyclotherapy to treat p53 mutant cancers.^[2,40–42] PHOTACs could induce temporary cell cycle arrest in

healthy p53 wild-type cells to protect them from chemotherapeutics targeting proliferating cells. The most affected tissues could be irradiated to mitigate dose-limiting side effects and improve therapeutic outcomes.

Recent work has shown that p53 dynamics control the cell fate after induction, with periodic oscillations leading to cell-cycle arrest, whereas a strong, sustained elevation of p53 levels leads to apoptosis.^[43] Specific variations in p53 dynamics have been observed in different cell lines. These p53 oscillations are regulated through the MDM2 feedback loop.^[43,44] MDM2-PHOTACs can be reversibly activated and thus are ideally suited to modulate p53 levels with spatiotemporal precision. Beyond therapeutic use, we expect that MDM2-PHOTACs will be applied as tools to study p53 dynamics.

Supplementary Figures

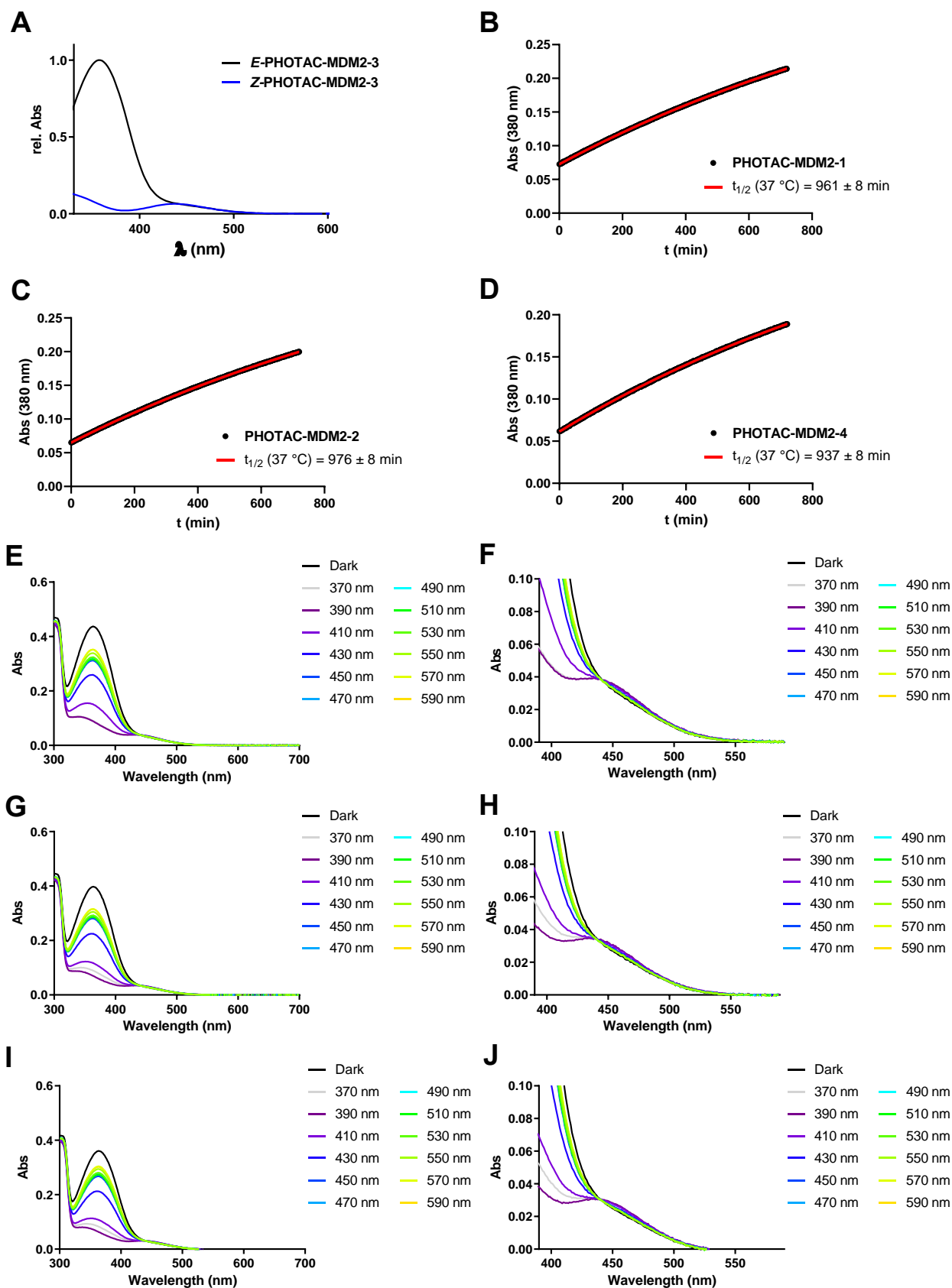


Figure S5.1: Photophysical characterization of MDM2-PHOTACs. A) Absorption spectra of **PHOTAC-I-18** isomers as obtained by LCMS. B)–D) Thermal *Z*-to-*E* isomerization of B) **PHOTAC-MDM2-1**, C) **PHOTAC-MDM2-2**, D) **PHOTAC-MDM2-4**

at 37 °C in DMSO. E)–J) Absorption spectra of E)+F) **PHOTAC-MDM2-1**, G)+H) **PHOTAC-MDM2-2**, I)+J) **PHOTAC-MDM2-4** after irradiation for 5 min with the indicated wavelength.

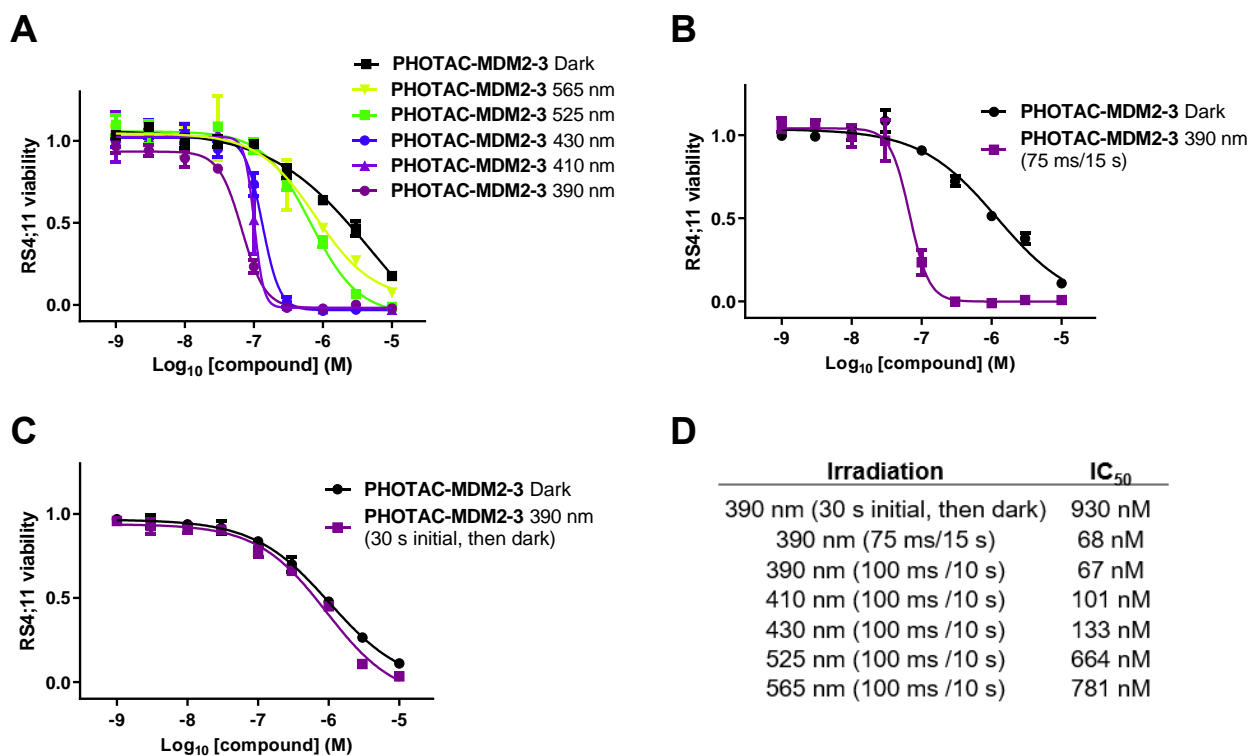


Figure S5.2: Light dependence of **PHOTAC-MDM2-3** toxicity. A) Viability of RS4;11 cells after treatment with **PHOTAC-MDM2-3** for 72 h in the dark or under pulsed irradiation (100 ms every 10 s) with the indicated wavelength. B)+C) Viability of RS4;11 cells after treatment with **PHOTAC-MDM2-3** for 72 h in the dark and B) under pulsed 390 nm irradiation (75 ms every 15 s) or C) with initial 390 nm irradiation (30 s) followed by incubation in the dark. D) Irradiation-dependence of **PHOTAC-MDM2-3** IC₅₀ values in RS4;11 cells after 72 h.

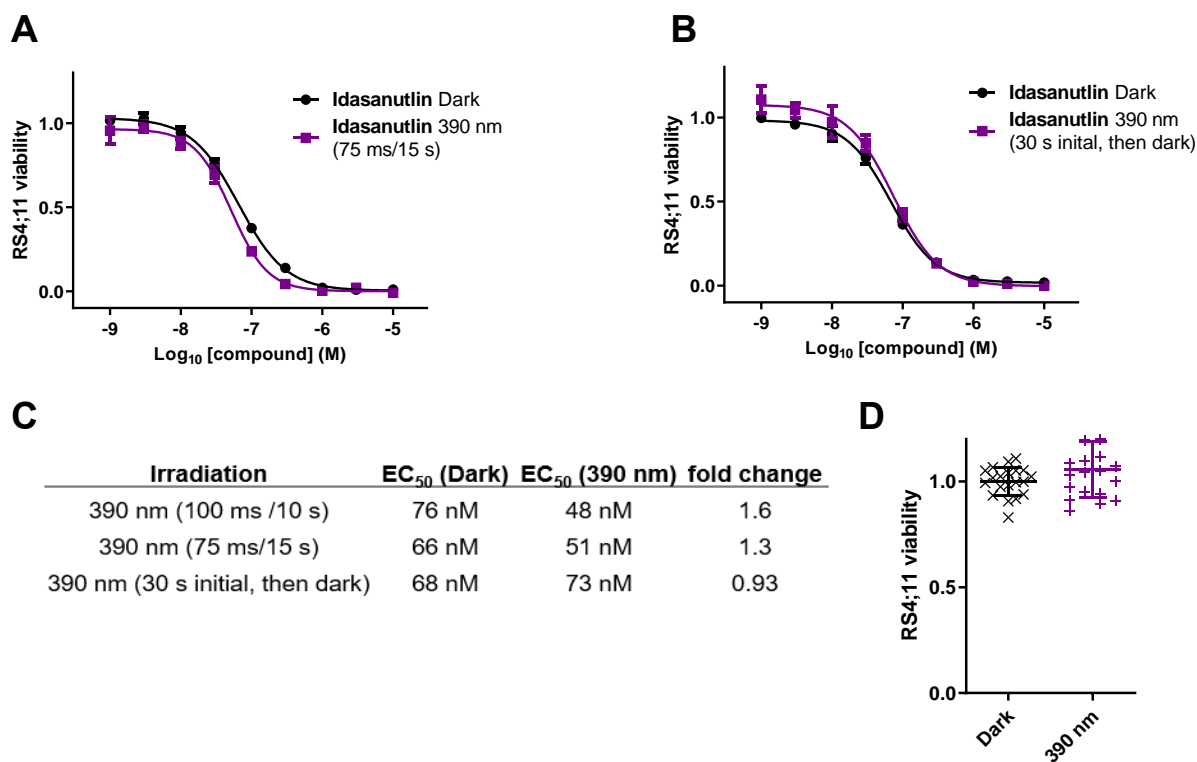


Figure S5.3: Light dependence of idasanutlin toxicity. A)+B) Viability of RS4;11 cells after treatment with Idasanutlin for 72 h in the dark and A) under pulsed 390 nm irradiation (75 ms every 15 s) or B) with initial 390 nm irradiation (30 s) followed by incubation in the dark. C) Light-dependence of idasanutlin IC₅₀ values in RS4;11 cells after 72 h. D) Light-dependence of RS4;11 viability under pulsed 390 nm irradiation (100 ms every 10 s).

Methods

Determination of Photophysical properties

UV-Vis spectrometry was performed on a Varian Cary 60 UV-Visible Spectrophotometer using disposable BRAND UV-Cuvette Disposable Spectrophotometer/Photometer Ultra-Micro Cuvettes, BrandTech (10 mm light path). An Agilent Technologies PCB 1500 Water Peltier system was used for temperature control and samples were irradiated with a Cairn Research Optoscan Monochromator with Optosource High Intensity Arc Lamp equipped with a 75 W UXL-S50A lamp from USHIO Inc. Japan and set to 15 nm full width at half maximum. Samples were stored and prepared under red light to avoid formation of the *Z*-isomers. 10 mM stock solutions were prepared in the dark and diluted to a final concentration of 25 μ M to measure the UV-VIS spectra of **PHOTACs** following irradiation with different wavelengths for 5 min using a monochromator. Measurement was started from the dark-adapted state, followed by 370 nm and further stepwise wavelength increase up to 600 nm. By increasing the wavelength from low to high *Z*- to *E*-isomerization can be observed, whereas going the reverse direction from high to low wavelength, the PSS might not be reached due to low absorptivity above 500 nm. Spectra were recorded in DMSO to avoid any artifacts of aggregation or precipitation.

Thermal relaxation was measured by preirradiating **PHOTACs** with 390 nm light and observing the absorption at 380 nm over 12 h at 37 °C in DMSO in tightly sealed cuvettes. Half-lives were determined by nonlinear regression using GraphPad Prism Version 9.02.

Separated spectra of the *Z*- and *E*-isomers were obtained from the internal UV-VIS detector of the LCMS by irradiating the sample before injection and were normalized at the isosbestic point. Isomer ratios were calculated in the region of largest absorption difference between 330 and 390 nm from the separated spectra obtained by LCMS and the spectra obtained following irradiation with different wavelengths for 5 min, normalized at the isosbestic point.

LED illumination

For illumination of the cells we used the cell disco system as previously described in the literature.^[45] 5 mm LEDs 390 nm (VL390-5-15), 410 nm (VL410-5-15), 430 nm (VL430-5-15), 525 nm (B5-433-B525) and 565 nm (LED565-03U) were purchased from Roithner Lasertechnik. For viability experiments using 390 nm, cells were

preirradiated for 30 s at 390 nm to quickly switch the photoswitches in the active state. Pulsed irradiation was performed using 100 ms pulses every 10 s (unless indicated otherwise) in 96- or 6-well plates, controlled by an Arduino system.

Cell culture

The human acute lymphoblastic leukemia RS4;11 (ATCC[®] CRL1873[™]) cell line was purchased from the American Type Culture Collection and cultured in phenol red-free RPMI1640 medium (Gibco) with 10% fetal bovine serum (FBS) and 1% penicillin/streptomycin (PS) in a humidified incubator at 37 °C with 5% CO₂ in air. For the experiments compounds were serially diluted in phenol red-free RPMI1640 (Gibco) as 2x stock solutions resulting in a final concentration of 1% DMSO during the assay. Azobenzene stocks and dilutions were strictly kept in the dark and prepared under red light conditions.

For immunoblotting analysis, cells (2×10^6 cells for RS4:11) were incubated for the indicated times with PHOTACs, placed in a light-proof box, and preirradiated for 30 s at 390 nm followed by 100 ms pulses every 10 s or were kept in the dark for 4 h. After incubation, cells were collected in the dark by centrifugation (200 g, 5 min) at 4 °C and the pellets were washed twice with ice cold PBS (1 mL).

Colorimetric MTS Assays

The activity of dehydrogenase enzymes in metabolically active cells, as a quantitative measurement for cytotoxicity and proliferation, was determined by colorimetric measurement of the reduction of [3-(4,5-dimethylthiazol-2-yl)-5-(3-carboxymethoxyphenyl)-2-(4-sulfophenyl)-2H-tetrazolium (MTS) to the formazan product. The absorbance of formazan was measured at 500 nm on a FLUOstar Omega microplate reader (BMG Labtech). Cells were treated with different concentrations of PHOTACs (10 μ M to 1 nM) in triplicates using 1% DMSO as cosolvent, and incubated in a 96-well plate for 72 h. The cells were placed in light-proof boxes and exposed to the lighting conditions specified in the experiment for 72 h. Next, 10 μ L of Promega CellTiter 96[®] AQueous One Solution Reagent was added to each well and incubated for further 4-7 hours at 37 °C. The absorbance at 500 nm was measured on a FLUOstar Omega 96-well plate reader (BMG Labtech).

Data was analyzed using GraphPad Prism Version 9.02 (GraphPad Software Inc) and fitted using the [Inhibitor] vs. response -- Variable slope (four parameters) fit. Results represent the mean viability \pm SEM relative to the 1% DMSO treated control. Light dependence of RS4;11 viability was analyzed from all experiments and normalized to cells in the dark. Results are shown as individual data points and mean viability \pm SEM.

Immunoblotting Analysis

Cells were lysed in RIPA buffer containing protease and phosphatase inhibitors (cOmplete™, Mini Protease Inhibitor Cocktail, SigmaAldrich, 4693124001 and Phosphatase Inhibitor Cocktail 3, SigmaAldrich, P0044-1ML) and protein concentration was determined using the BCA method (Thermo Fisher, 23225). Immunoblotting was performed as previously described.^[28,46] Briefly, samples were resolved under denaturing and reducing conditions using 4%–12% Bis-Tris gels (NuPAGE) and transferred to a PDVF membrane (Immobilon-P, Millipore). Membranes were blocked with 5% nonfat dried milk, incubated with primary antibodies overnight at 4°C. After washing the membranes, secondary antibodies coupled with horseradish peroxidase were applied. Immunoreactive bands were visualized using SuperSignal™ Western Blot Enhancer or SuperSignal™ West Femto Maximum Sensitivity Substrate (Thermo Fisher Scientific) and the signal was acquired using an ImageQuant LAS 400 (GE). The following antibodies were used:

Antibodies	Source	Identifier
cl. Caspase 3	Cell Signaling Technology	9661S
CRBN	Novus Biologicals	NBP1-91810
MDM2	Santa Cruz Biotechnology	sc-813
p53	Santa Cruz Biotechnology	sc-6243
PARP1	Cell Signaling Technology	9542S
PCNA	dako	M0879
anti-Rabbit IgG, peroxidase-linked antibody	Thermo Fisher	NA934
anti-Mouse IgG, peroxidase-linked antibody	Thermo Fisher	NA931
anti-goat IgG-HRP	Santa Cruz Biotechnology	sc-2354

Synthetic Procedures and Characterization

General information

The reagents and solvents used in this study were bought from the following chemical suppliers: Acros Organics, Alfa Aesar, Combi-Blocks, Oakwood, OxChem, Sigma-Aldrich and Medkoo Biosciences and were used as purchased.

Dry solvents used in reactions performed under inert atmosphere were obtained by passing the degassed solvents through activated alumina columns. Additionally, dry solvents were stored over molecular sieves under an inert atmosphere.

Column chromatography was carried out on silica gel (60 Å pore size, 40–63 µm, Merck KGaA) using a Teledyne Isco Combiflash EZprep flash purification system.

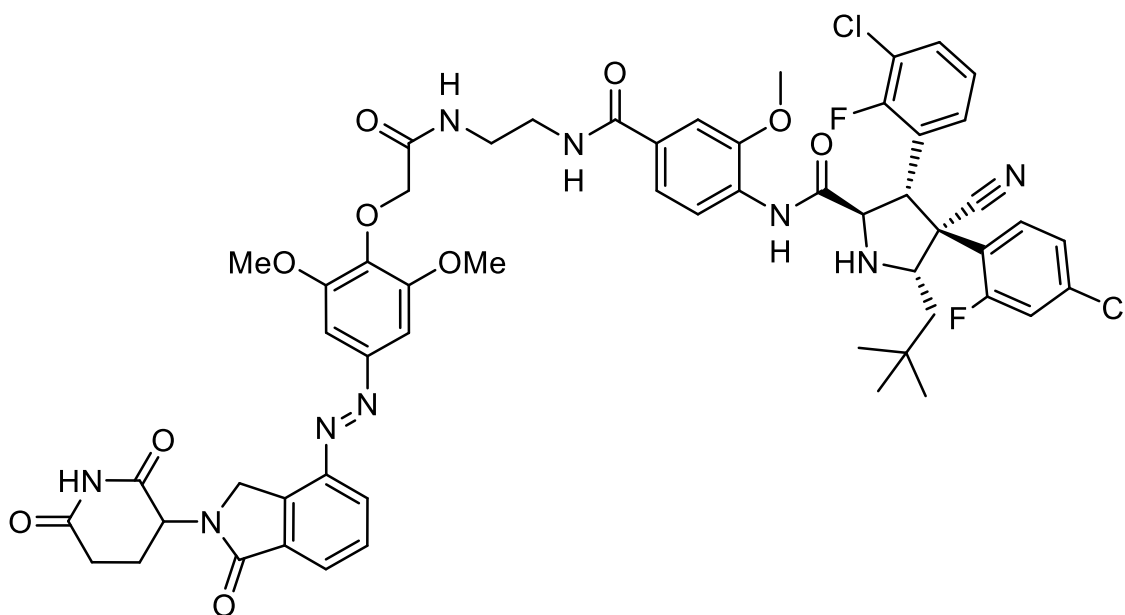
Thin-layer chromatography (TLC) was performed on glass plates precoated with silica gel (0.25 mm, 60-Å pore size, Merck). TLC plates were visualized by exposure to UV light (254 and 366 nm).

NMR spectra were obtained on a Bruker AVIII-600 High Performance Digital NMR Spectrometer (600 MHz for ^1H and 150 MHz for ^{13}C spectra) with CPTCI-cryoprobehead. Integration results and multiplets are reported as observed and denoted as follows: s (singlet), d (doublet), t (triplet), q (quartet), p (pentet), h (hextet), and m (multiplet) and as combinations thereof.

High-resolution mass spectra (HRMS) were recorded on an Agilent Technologies 6224 Accurate-Mass time-of-flight spectrometer with either atmospheric pressure chemical ionization (APCI) or electrospray ionization (ESI) ionization sources.

LCMS were measured on an Agilent Technologies 1260 II Infinity connected to an Agilent Technologies 6120 Quadrupole mass spectrometer with APCI ionization source. Elution was performed using a gradient from 5:95% to 100:0% MeCN:H₂O with 0.1% formic acid over 5 min, if not indicated otherwise. Separated isomer spectra of azobenzenes were obtained by irradiation of the LCMS sample prior to injection.

(2R,3S,4R,5S)-3-(3-(3-chloro-2-fluorophenyl)-4-(4-chloro-2-fluorophenyl)-4-cyano-N-(4-((2-(2-(4-((E)-2-(2,6-dioxopiperidin-3-yl)-1-oxoisoindolin-4-yl)diazenyl)-2,6-dimethoxyphenoxy)acetamido)ethyl)carbamoyl)-2-methoxyphenyl)-5-neopentylpyrrolidine-2-carboxamide (PHOTAC-MDM2-1)



(E)-2-(2-(4-((2-(2,6-dioxopiperidin-3-yl)-1-oxoisoindolin-4-yl)diazenyl)-2,6-dimethoxyphenoxy)acetamido)ethan-1-aminium 2,2,2-trifluoroacetate (15.3 mg, 0.024 mmol, 2.1 eq.) was prepared as previously described^[28] and added to a dried round bottom flask together with Idasanutlin (7.0 mg, 0.011 mmol, 1 eq.) and HATU (9.1 mg, 0.024 mmol, 2.1 eq.) under nitrogen atmosphere. The solids were dissolved in dry DMF (1 mL), *i*-Pr₂NEt (11.2 mg, 0.087 mmol, 7.6 eq., 0.015 mL) was added and the reaction was stirred for 16 h at room temperature. The mixture was then diluted with EtOAc (20 mL) separated against saturated NH₄Cl (25 mL). The organic phase was washed with saturated NaHCO₃ (40 mL), 10% LiCl (2x 20 mL) and brine (2x 20 mL). The organic phase was dried over Na₂SO₄ and concentrated under reduced pressure. Purification of the resulting crude product by flash column chromatography (CH₂Cl₂/MeOH gradient, 0 to 15% MeOH) gave **PHOTAC-MDM2-1** (10.8 mg, 0.010 mmol, 85%) as a yellow solid.

$R_f = 0.54$ [CH₂Cl₂:MeOH, 9:1].

¹H NMR (600 MHz, DMSO-*d*₆) $\delta = 11.03$ (s, 1H), 10.39 (s, 1H), 8.53 (s, 1H), 8.34 – 8.29 (m, 1H), 8.24 – 8.14 (m, 2H), 7.93 (s, 1H), 7.82 – 7.69 (m, 2H), 7.60 – 7.31 (m, 9H), 5.19 – 5.12 (m, 1H), 4.80 (d, *J* = 17.4 Hz, 1H), 4.68 (d, *J* = 18.7 Hz, 1H), 4.60 –

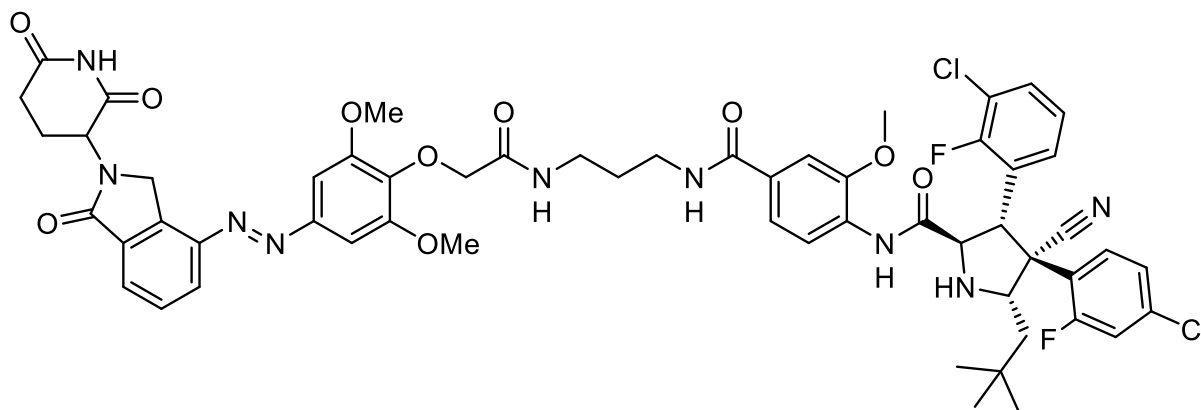
4.54 (m, 2H), 4.46 – 4.41 (m, 2H), 4.37 – 4.29 (m, 1H), 3.98 – 3.86 (m, 10H), 3.44 – 3.38 (m, 4H), 2.92 (d, $J = 17.5$ Hz, 1H), 2.67 – 2.53 (m, 2H), 2.05 (s, 1H), 1.63 (q, $J = 10.8$ Hz, 1H), 1.27 (s, 1H), 0.96 (s, 9H) ppm.

^{13}C NMR (150 MHz, $\text{DMSO-}d_6$) $\delta = 172.93, 171.01$ (2x), 168.57, 167.17, 165.75, 159.51 (d, $J = 251.0$ Hz), 155.56 (d, $J = 246.9$ Hz), 152.65, 148.27, 147.48, 146.36, 139.24, 134.75 (d, $J = 11.3$ Hz), 134.52, 133.83, 130.96 (d, $J = 4.5$ Hz), 130.03, 129.64, 129.59, 129.31, 128.65 (d, $J = 14.4$ Hz), 128.60, 126.00 (d, $J = 13.5$ Hz), 125.64 (d, $J = 2.6$ Hz), 125.50, 125.31 (d, $J = 4.5$ Hz), 120.03, 119.46 (d, $J = 18.7$ Hz), 119.15 (d, $J = 9.3$ Hz), 117.57 (d, $J = 27.2$ Hz), 117.32, 117.00, 109.58, 100.61, 71.78, 64.60, 63.40 (d, $J = 5.9$ Hz), 63.22 (d, $J = 6.4$ Hz), 56.34, 55.77, 51.84, 50.16, 48.31, 43.89, 39.10, 38.19, 31.29, 30.09, 29.50, 22.31 ppm.

HRMS (APCI): calcd. for $\text{C}_{56}\text{H}_{56}\text{Cl}_2\text{F}_2\text{N}_9\text{O}_{10}^+$: 1122.3490 m/z $[\text{M}+\text{H}]^+$.
found: 1122.3459 m/z $[\text{M}+\text{H}]^+$.

LCMS (ESI): $t_{\text{ret}} = 5.07$ min (*E*). 562 m/z $[\text{M}+2\text{H}]^{2+}$.

(2R,3S,4R,5S)-3-(3-chloro-2-fluorophenyl)-4-(4-chloro-2-fluorophenyl)-4-cyano-N-(4-((3-(2-(4-((E)-(2-(2,6-dioxopiperidin-3-yl)-1-oxoisindolin-4-yl)diazenyl)-2,6-dimethoxyphenoxy)acetamido)propyl)carbamoyl)-2-methoxyphenyl)-5-neopentylpyrrolidine-2-carboxamide (PHOTAC-MDM2-2)



(E)-3-(2-(4-((2-(2,6-dioxopiperidin-3-yl)-1-oxoisindolin-4-yl)diazenyl)-2,6-dimethoxyphenoxy)acetamido)propan-1-aminium 2,2,2-trifluoroacetate (15.7 mg, 0.024 mmol, 2.1 eq.) was prepared as previously described^[28] and added to a dried round bottom flask together with Idasanutlin (7.0 mg, 0.011 mmol, 1 eq.) and HATU (9.1 mg, 0.024 mmol, 2.1 eq.) under nitrogen atmosphere. The solids were dissolved in dry DMF (1 mL), *i*-Pr₂NEt (11.2 mg, 0.087 mmol, 7.6 eq., 0.015 mL) was added and the reaction was stirred for 16 h at room temperature. The mixture was then diluted with EtOAc (20 mL) separated against saturated NH₄Cl (25 mL). The organic phase was washed with saturated NaHCO₃ (40 mL), 10% LiCl (2x 20 mL) and brine (2x 20 mL). The organic phase was dried over Na₂SO₄ and concentrated under reduced pressure. Purification of the resulting crude product by flash column chromatography (CH₂Cl₂/MeOH gradient, 0 to 15% MeOH) gave **PHOTAC-MDM2-2** (10.9 mg, 0.010 mmol, 84%) as a yellow solid.

$R_f = 0.54$ [CH₂Cl₂:MeOH, 9:1].

¹H NMR (600 MHz, DMSO-*d*₆) δ = 11.03 (s, 1H), 10.40 (s, 1H), 8.45 (s, 1H), 8.32 (d, *J* = 9.2 Hz, 1H), 8.24 – 8.19 (m, 1H), 8.07 (s, 1H), 7.95 – 7.88 (m, 1H), 7.83 – 7.70 (m, 2H), 7.62 – 7.51 (m, 3H), 7.48 (d, *J* = 8.9 Hz, 1H), 7.42 – 7.31 (m, 5H), 5.18 – 5.12 (m, 1H), 4.81 (d, *J* = 18.7 Hz, 1H), 4.69 (d, *J* = 17.6 Hz, 1H), 4.61 – 4.56 (m, 2H), 4.43 (s, 2H), 4.39 – 4.33 (m, 1H), 3.97 – 3.88 (m, 10H), 3.29 – 3.22 (m, 4H), 2.98 – 2.91 (m, 1H), 2.66 – 2.52 (m, 2H), 2.09 – 2.02 (m, 1H), 1.74 (p, *J* = 6.4 Hz, 2H), 1.68 – 1.59 (m, 1H), 1.30 – 1.24 (m, 1H), 0.97 (s, 9H) ppm.

¹³C NMR (150 MHz, DMSO-*d*₆) δ = 172.93, 171.02 (2x), 168.15, 167.16, 165.53, 159.51 (d, J = 251.3 Hz), 155.56 (d, J = 246.6 Hz), 152.68, 148.31, 147.51, 146.36, 139.26, 134.75 (d, J = 11.6 Hz), 134.51, 133.84, 130.97 (d, J = 4.0 Hz), 130.02, 129.75, 129.66, 129.24, 128.64 (d, J = 12.4 Hz), 128.61, 126.02 (d, J = 13.4 Hz), 125.64 (d, J = 2.7 Hz), 125.50, 125.31 (d, J = 3.7 Hz), 119.90, 119.46 (d, J = 18.8 Hz), 119.17 (d, J = 9.4 Hz), 117.58 (d, J = 27.0 Hz), 117.32, 117.00, 109.56, 100.59, 71.87, 64.63, 63.43 (d, J = 6.1 Hz), 63.23 (d, J = 6.2 Hz), 56.37, 55.79, 51.85, 50.16, 48.32, 43.89, 36.87, 36.13, 31.29, 30.10, 29.51, 29.33, 22.32 ppm.

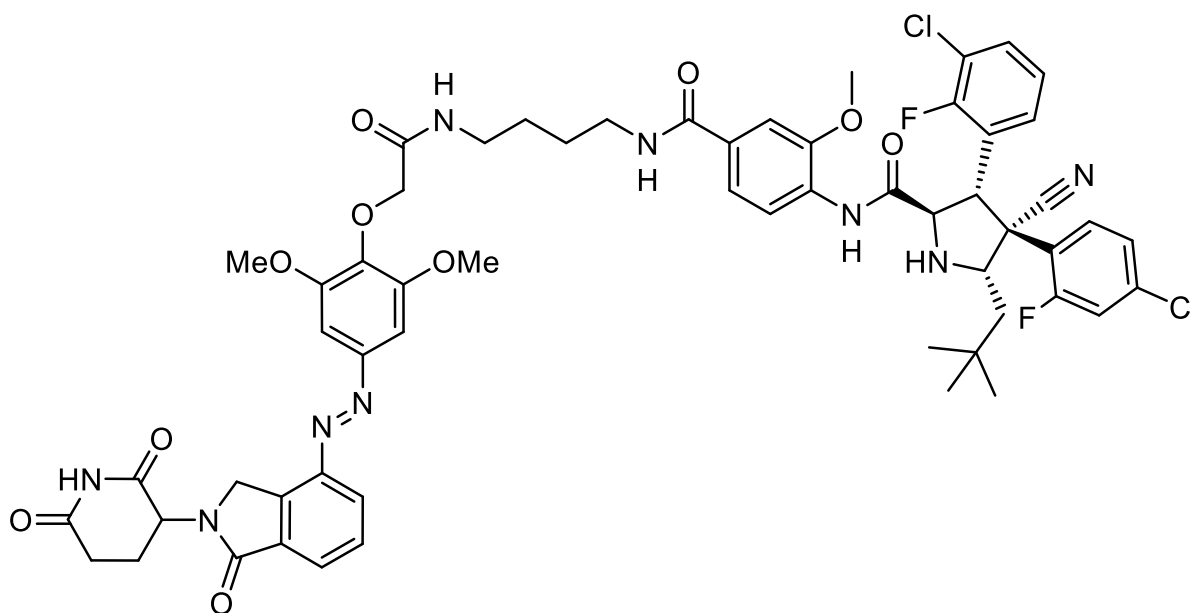
HRMS (APCI): calcd. for C₅₇H₅₈Cl₂F₂N₉O₁₀⁺: 1136.3646 m/z [M+H]⁺.

found: 1136.3591 m/z [M+H]⁺.

LCMS (ESI): t_{ret} = 4.96 min (*Z*). 569 m/z [M+2H]²⁺.

t_{ret} = 5.09 min (*E*). 569 m/z [M+2H]²⁺.

(2R,3S,4R,5S)-3-(3-(3-chloro-2-fluorophenyl)-4-(4-chloro-2-fluorophenyl)-4-cyano-N-(4-(((4-(2-(4-((E)-(2-(2,6-dioxopiperidin-3-yl)-1-oxoisoindolin-4-yl)diazenyl)-2,6-dimethoxyphenoxy)acetamido)butyl)carbamoyl)-2-methoxyphenyl)-5-neopentylpyrrolidine-2-carboxamide (PHOTAC-MDM2-3)



(E)-4-(2-(4-((2-(2,6-dioxopiperidin-3-yl)-1-oxoisoindolin-4-yl)diazenyl)-2,6-dimethoxyphenoxy)acetamido)butan-1-aminium 2,2,2-trifluoroacetate (16.0 mg, 0.024 mmol, 2.1 eq.) was prepared as previously described^[28] and added to a dried round bottom flask together with Idasanutlin (7.0 mg, 0.011 mmol, 1 eq.) and HATU (9.1 mg, 0.024 mmol, 2.1 eq.) under nitrogen atmosphere. The solids were dissolved in dry DMF (1 mL), *i*-Pr₂NEt (11.2 mg, 0.087 mmol, 7.6 eq., 0.015 mL) was added and the reaction was stirred for 16 h at room temperature. The mixture was then diluted with EtOAc (20 mL) separated against saturated NH₄Cl (25 mL). The organic phase was washed with saturated NaHCO₃ (40 mL), 10% LiCl (2x 20 mL) and brine (2x 20 mL). The organic phase was dried over Na₂SO₄ and concentrated under reduced pressure. Purification of the resulting crude product by flash column chromatography (CH₂Cl₂/MeOH gradient, 0 to 15% MeOH) gave **PHOTAC-MDM2-3** (11.5 mg, 0.010 mmol, 88%) as a yellow solid.

$R_f = 0.38$ [CH₂Cl₂:MeOH, 19:1].

¹H NMR (400 MHz, DMSO-*d*₆) δ = 11.03 (s, 1H), 10.38 (s, 1H), 8.44 (t, *J* = 5.6 Hz, 1H), 8.30 (d, *J* = 8.6 Hz, 1H), 8.20 (d, *J* = 7.8 Hz, 1H), 7.96 (t, *J* = 5.8 Hz, 1H), 7.92 (d, *J* = 7.4 Hz, 1H), 7.78 (t, *J* = 7.7 Hz, 1H), 7.74 (t, *J* = 7.3 Hz, 1H), 7.61 – 7.51 (m, 3H), 7.47

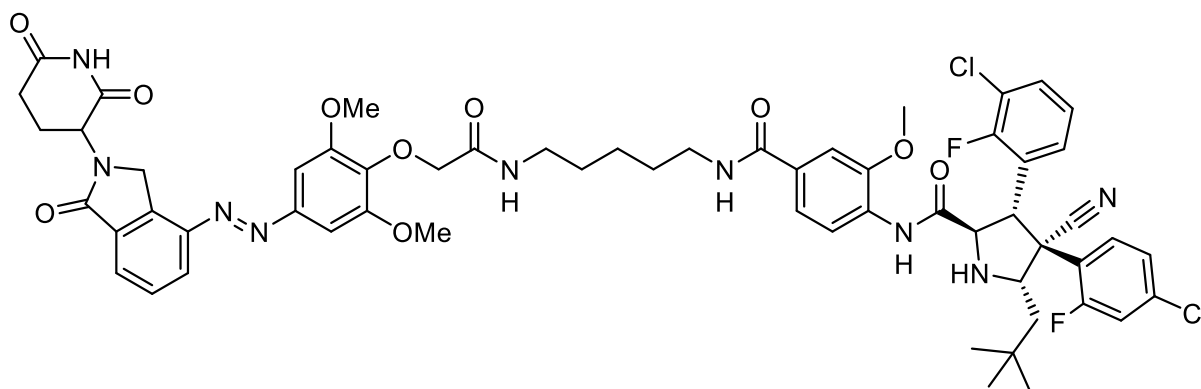
(dd, $J = 8.4, 1.7$ Hz, 1H), 7.42 – 7.33 (m, 5H), 5.15 (dd, $J = 13.3, 5.0$ Hz, 1H), 4.80 (d, $J = 19.1$ Hz, 1H), 4.68 (d, $J = 19.2$ Hz, 1H), 4.61 – 4.57 (m, 2H), 4.43 (s, 2H), 4.42 – 4.29 (m, 1H), 4.00 – 3.87 (m, 10H), 3.32 – 3.19 (m, 4H), 3.01 – 2.90 (m, 1H), 2.68 – 2.52 (m, 2H), 2.10 – 2.02 (m, 1H), 1.65 (dd, $J = 14.2, 9.9$ Hz, 1H), 1.54 (p, $J = 3.5$ Hz, 4H), 1.31 – 1.24 (m, 1H), 1.00 – 0.94 (m, 9H) ppm.

¹³C NMR (150 MHz, DMSO-*d*₆) δ = 173.38, 171.47 (2x), 168.47, 167.63, 165.82, 159.96 (d, $J = 251.1$ Hz), 156.02 (d, $J = 247.0$ Hz), 153.05, 148.75, 147.94, 146.80, 139.71, 135.22 (d, $J = 11.4$ Hz), 134.95, 134.28, 131.43 (d, $J = 3.3$ Hz), 130.49, 130.30, 130.09, 129.61, 129.11 (d, $J = 11.9$ Hz), 129.07, 126.44 (d, $J = 8.9$ Hz), 126.10 (d, $J = 2.8$ Hz), 125.95, 125.77 (d, $J = 3.6$ Hz), 120.38, 119.92 (d, $J = 18.7$ Hz), 119.60 (d, $J = 8.9$ Hz), 118.03 (d, $J = 27.3$ Hz), 117.77, 117.46, 110.00, 101.05, 72.32, 65.06, 63.87 (d, $J = 4.7$ Hz), 63.67 (d, $J = 5.9$ Hz), 56.81, 56.24, 52.31, 50.59, 48.78, 44.34, 39.41, 38.48, 31.74, 30.56, 29.96, 27.19, 27.13, 22.77 ppm.

HRMS (APCI): calcd. for C₅₈H₆₀Cl₂F₂N₉O₁₀⁺: 1150.3803 m/z [M+H]⁺.
 found: 1150.3777 m/z [M+H]⁺.

LCMS (ESI): t_{ret} = 5.09 min (*Z*). 576 m/z [M+2H]²⁺.
 t_{ret} = 5.23 min (*E*). 576 m/z [M+2H]²⁺.

(2R,3S,4R,5S)-3-(3-chloro-2-fluorophenyl)-4-(4-chloro-2-fluorophenyl)-4-cyano-N-(4-((5-(2-(4-((E)-(2-(2,6-dioxopiperidin-3-yl)-1-oxoisoindolin-4-yl)diazenyl)-2,6-dimethoxyphenoxy)acetamido)pentyl)carbamoyl)-2-methoxyphenyl)-5-neopentylpyrrolidine-2-carboxamide (PHOTAC-MDM2-4)



(E)-5-(2-(4-((2-(2,6-dioxopiperidin-3-yl)-1-oxoisoindolin-4-yl)diazenyl)-2,6-dimethoxyphenoxy)acetamido)pentan-1-aminium 2,2,2-trifluoroacetate (16.4 mg, 0.024 mmol, 2.1 eq.) was prepared as previously described^[28] and added to a dried round bottom flask together with Idasanutlin (7.0 mg, 0.011 mmol, 1 eq.) and HATU (9.1 mg, 0.024 mmol, 2.1 eq.) under nitrogen atmosphere. The solids were dissolved in dry DMF (1 mL), *i*-Pr₂NEt (11.2 mg, 0.087 mmol, 7.6 eq., 0.015 mL) was added and the reaction was stirred for 16 h at room temperature. The mixture was then diluted with EtOAc (20 mL) separated against saturated NH₄Cl (25 mL). The organic phase was washed with saturated NaHCO₃ (40 mL), 10% LiCl (2x 20 mL) and brine (2x 20 mL). The organic phase was dried over Na₂SO₄ and concentrated under reduced pressure. Purification of the resulting crude product by flash column chromatography (CH₂Cl₂/MeOH gradient, 0 to 15% MeOH) gave **PHOTAC-MDM2-4** (11.8 mg, 0.010 mmol, 91%) as a yellow solid.

$R_f = 0.35$ [CH₂Cl₂:MeOH, 19:1].

¹H NMR (600 MHz, DMSO-*d*₆) δ = 11.03 (s, 1H), 10.38 (s, 1H), 8.39 (s, 1H), 8.33 – 8.27 (m, 1H), 8.24 – 8.17 (m, 1H), 7.96 – 7.88 (m, 2H), 7.79 (t, *J* = 5.9 Hz, 1H), 7.76 – 7.68 (m, 1H), 7.62 – 7.50 (m, 3H), 7.47 (d, *J* = 8.6 Hz, 1H), 7.41 – 7.29 (m, 5H), 5.20 – 5.12 (m, 1H), 4.81 (d, *J* = 17.6 Hz, 1H), 4.69 (d, *J* = 16.6 Hz, 1H), 4.61 – 4.54 (m, 2H), 4.43 (s, 2H), 4.40 – 4.33 (m, 1H), 4.00 – 3.86 (m, 10H), 3.25 (q, *J* = 6.2 Hz, 2H), 3.20 (q, *J* = 6.2 Hz, 2H), 2.98 – 2.90 (m, 1H), 2.66 – 2.53 (m, 2H), 2.10 – 2.02 (m, 1H),

References

- [1] O. Laptenko, C. Prives, *Cell Death Differ.* **2006**, *13*, 951–961.
- [2] E. R. Kasthuber, S. W. Lowe, *Cell* **2017**, *170*, 1062–1078.
- [3] O. Karni-Schmidt, M. Lokshin, C. Prives, *Annu. Rev. Pathol. Mech. Dis.* **2016**, *11*, 617–644.
- [4] K. Pappas, J. Xu, S. Zairis, L. Resnick-Silverman, F. Abate, N. Steinbach, S. Ozturk, L. H. Saal, T. Su, P. Cheung, H. Schmidt, S. Aaronson, H. Hibshoosh, J. Manfredi, R. Rabadan, R. Parsons, *Mol. Cancer Res.* **2017**, *15*, 1051–1062.
- [5] W. A. Freed-Pastor, C. Prives, *Genes Dev.* **2012**, *26*, 1268–1286.
- [6] M. Konopleva, G. Martinelli, N. Daver, C. Papayannidis, A. Wei, B. Higgins, M. Ott, J. Mascarenhas, M. Andreeff, *Leukemia* **2020**, *34*, 2858–2874.
- [7] Y. Zhao, A. Aguilar, D. Bernard, S. Wang, *J. Med. Chem.* **2015**, *58*, 1038–1052.
- [8] A. Burgess, K. M. Chia, S. Haupt, D. Thomas, Y. Haupt, E. Lim, *Front. Oncol.* **2016**, *6*, DOI 10.3389/fonc.2016.00007.
- [9] Q. Ding, Z. Zhang, J.-J. Liu, N. Jiang, J. Zhang, T. M. Ross, X.-J. Chu, D. Bartkovitz, F. Podlaski, C. Janson, C. Tovar, Z. M. Filipovic, B. Higgins, K. Glenn, K. Packman, L. T. Vassilev, B. Graves, *J. Med. Chem.* **2013**, *56*, 5979–5983.
- [10] L. L. Siu, A. Italiano, W. H. Miller, J.-Y. Blay, J. A. Gietema, Y.-J. Bang, L. R. Mileskin, H. W. Hirte, M. Reckner, B. Higgins, L. Jukofsky, S. Blotner, J. Zhi, S. Middleton, G. L. Nichols, L. C. Chen, *J. Clin. Oncol.* **2014**, *32*, 2535–2535.
- [11] J. Broichhagen, J. A. Frank, D. Trauner, *Acc. Chem. Res.* **2015**, *48*, 1947–1960.
- [12] K. Hüll, J. Morstein, D. Trauner, *Chem. Rev.* **2018**, *118*, 10710–10747.
- [13] R. Weinstain, T. Slanina, D. Kand, P. Klán, *Chem. Rev.* **2020**, DOI 10.1021/acs.chemrev.0c00663.
- [14] I. M. Welleman, M. W. H. Hoorens, B. L. Feringa, H. H. Boersma, W. Szymański, *Chem. Sci.* **2020**, *11*, 11672–11691.
- [15] M. Borowiak, W. Nahaboo, M. Reynders, K. Nekolla, P. Jalinot, J. Hasserodt, M. Rehberg, M. Delattre, S. Zahler, A. Vollmar, D. Trauner, O. Thorn-Seshold, *Cell* **2015**, *162*, 403–411.
- [16] L. Gao, J. C. M. Meiring, A. Varady, I. E. Ruider, C. Heise, M. Wranik, C. D. Velasco, J. A. Taylor, B. Terni, J. Standfuss, C. C. Cabernard, A. Llobet, M. O. Steinmetz, A. R. Bausch, M. Distel, J. Thorn-Seshold, A. Akhmanova, O. Thorn-Seshold, *bioRxiv* **2021**, 2021.03.26.437160.
- [17] M. J. Hansen, W. A. Velema, G. de Bruin, H. S. Overkleeft, W. Szymanski, B. L. Feringa, *ChemBioChem* **2014**, *15*, 2053–2057.

- [18] B. Blanco, K. A. Palasis, A. Adwal, D. F. Callen, A. D. Abell, *Bioorg. Med. Chem.* **2017**, *25*, 5050–5054.
- [19] O. Babii, S. Afonin, A. Yu. Ishchenko, T. Schober, A. O. Negelia, G. M. Tolstanova, L. V. Garmanchuk, L. I. Ostapchenko, I. V. Komarov, A. S. Ulrich, *J. Med. Chem.* **2018**, *61*, 10793–10813.
- [20] O. Babii, S. Afonin, T. Schober, L. V. Garmanchuk, L. I. Ostapchenko, V. Yurchenko, S. Zozulya, O. Tarasov, I. Pishel, A. S. Ulrich, I. V. Komarov, *Future Drug Discov.* **2020**, *2*, FDD28.
- [21] M. J. Hansen, F. M. Feringa, P. Kobauri, W. Szymanski, R. H. Medema, B. L. Feringa, *J. Am. Chem. Soc.* **2018**, *140*, 13136–13141.
- [22] G. M. Burslem, C. M. Crews, *Cell* **2020**, *181*, 102–114.
- [23] Y. Li, J. Yang, A. Aguilar, D. McEachern, S. Przybranowski, L. Liu, C.-Y. Yang, M. Wang, X. Han, S. Wang, *J. Med. Chem.* **2019**, *62*, 448–466.
- [24] B. Wang, S. Wu, J. Liu, K. Yang, H. Xie, W. Tang, *Eur. J. Med. Chem.* **2019**, *176*, 476–491.
- [25] J. Yang, Y. Li, A. Aguilar, Z. Liu, C.-Y. Yang, S. Wang, *J. Med. Chem.* **2019**, *62*, 9471–9487.
- [26] B. Wang, J. Liu, I. Tandon, S. Wu, P. Teng, J. Liao, W. Tang, *Eur. J. Med. Chem.* **2021**, 113425.
- [27] J. Hines, S. Lartigue, H. Dong, Y. Qian, C. M. Crews, *Cancer Res.* **2019**, *79*, 251–262.
- [28] M. Reynders, B. S. Matsuura, M. Bérouti, D. Simoneschi, A. Marzio, M. Pagano, D. Trauner, *Sci. Adv.* **2020**, *6*, eaay5064.
- [29] A. Zorba, C. Nguyen, Y. Xu, J. Starr, K. Borzilleri, J. Smith, H. Zhu, K. A. Farley, W. Ding, J. Schiemer, X. Feng, J. S. Chang, D. P. Uccello, J. A. Young, C. N. Garcia-Irrizary, L. Czabaniuk, B. Schuff, R. Oliver, J. Montgomery, M. M. Hayward, J. Coe, J. Chen, M. Niosi, S. Luthra, J. C. Shah, A. El-Kattan, X. Qiu, G. M. West, M. C. Noe, V. Shanmugasundaram, A. M. Gilbert, M. F. Brown, M. F. Calabrese, *Proc. Natl. Acad. Sci.* **2018**, *115*, E7285–E7292.
- [30] B. E. Smith, S. L. Wang, S. Jaime-Figueroa, A. Harbin, J. Wang, B. D. Hamman, C. M. Crews, *Nat. Commun.* **2019**, *10*, 131.
- [31] R. I. Troup, C. Fallan, M. G. J. Baud, *Explor. Target. Anti-Tumor Ther.* **2020**, *1*, 273–312.
- [32] K. P. Lawrence, T. Douki, R. P. E. Sarkany, S. Acker, B. Herzog, A. R. Young, *Sci. Rep.* **2018**, *8*, 12722.
- [33] S. H. Kaufmann, S. Desnoyers, Y. Ottaviano, N. E. Davidson, G. G. Poirier, *Cancer Res.* **1993**, *53*, 3976–3985.

- [34] K. Wu, A. Chen, Z.-Q. Pan, *J. Biol. Chem.* **2000**, *275*, 32317–32324.
- [35] K. Baek, D. C. Scott, B. A. Schulman, *Curr. Opin. Struct. Biol.* **2021**, *67*, 101–109.
- [36] S. T. Nawrocki, P. Griffin, K. R. Kelly, J. S. Carew, *Expert Opin. Investig. Drugs* **2012**, *21*, 1563–1573.
- [37] C. Maniaci, S. J. Hughes, A. Testa, W. Chen, D. J. Lamont, S. Rocha, D. R. Alessi, R. Romeo, A. Ciulli, *Nat. Commun.* **2017**, *8*, 830.
- [38] C. Steinebach, S. Lindner, N. D. Udeshi, D. C. Mani, H. Kehm, S. Köpff, S. A. Carr, M. Gütschow, J. Krönke, *ACS Chem. Biol.* **2018**, *13*, 2771–2782.
- [39] M. Girardini, C. Maniaci, S. J. Hughes, A. Testa, A. Ciulli, *Bioorg. Med. Chem.* **2019**, *27*, 2466–2479.
- [40] D. Carvajal, C. Tovar, H. Yang, B. T. Vu, D. C. Heimbrook, L. T. Vassilev, *Cancer Res.* **2005**, *65*, 1918–1924.
- [41] D. Kranz, M. Dobbstein, *Cancer Res.* **2006**, *66*, 10274–10280.
- [42] B. Rao, S. Lain, A. M. Thompson, *Br. J. Cancer* **2013**, *109*, 2954–2958.
- [43] X. Chen, J. Chen, S. Gan, H. Guan, Y. Zhou, Q. Ouyang, J. Shi, *BMC Biol.* **2013**, *11*, 73.
- [44] J. Stewart-Ornstein, G. Lahav, *Sci. Signal.* **2017**, *10*, DOI 10.1126/scisignal.aah6671.
- [45] M. Borowiak, W. Nahaboo, M. Reynders, K. Nekolla, P. Jalinot, J. Hasserodt, M. Rehberg, M. Delattre, S. Zahler, A. Vollmar, D. Trauner, O. Thorn-Seshold, *Cell* **2015**, *162*, 403–411.
- [46] A. Marzio, J. Puccini, Y. Kwon, N. K. Maverakis, A. Arbini, P. Sung, D. Bar-Sagi, M. Pagano, *Mol. Cell* **2019**, *73*, 224-237.e6.

6 – PHOTACs Targeting Cell Cycle Kinases

Martin Reynders^{1,2}, Christopher J. Arp¹, Daniele Simoneschi³, Michele Pagano^{3,4,5},
and Dirk Trauner^{1,4,6}

¹Department of Chemistry, New York University, New York, NY 10003, USA.

²Department of Chemistry, Ludwig Maximilians University of Munich
81377 Munich, Germany.

³Department of Biochemistry and Molecular Pharmacology, New York University
School of Medicine, New York, NY 10016, USA.

⁴Perlmutter Cancer Center, New York University School of Medicine, New York, NY
10016, USA.

⁵Howard Hughes Medical Institute, New York University School of Medicine, New
York, NY 10016, USA.

⁶NYU Neuroscience Institute, New York University School of Medicine, New York, NY
10016, USA.

Introduction

Kinases regulate cellular signaling, play a key role in controlling cell cycle progression and deregulation of kinase activity contributes to many diseases. Therefore, kinases are popular drug targets and researchers have focused on the development of selective kinase inhibitors.^[1] Oncology is a major area of interest for kinase inhibitor development leading to numerous approved drugs and many more in clinical trials.^[2] Dysregulation of kinases controlling the cell cycle leads to uncontrolled proliferation and is commonly observed in cancer.^[3]

Cell cycle kinases include the aurora kinases as crucial players in mitosis and the cyclin-dependent kinases (CDK), a family of kinases controlling the cell-cycle and transcription. Aurora kinase A, B and C are a small family of proteins required for normal cell division. Aurora kinase A (AURKA) is required for centrosome and mitotic spindle assembly, whereas aurora kinase B (AURKB) locates to centromeres and is needed for the orientation of chromosomes.^[4,5] AURKA has been classified as an oncogene and inhibitors targeting all aurora kinases as well as selective inhibitors for AURKA have been developed.^[5,6] The inhibition of rapid proliferation is a general therapeutic mechanism of several classes of chemotherapeutics and aurora kinase inhibitors. However, other functions for AURKA with relevance in oncogenic diseases have been uncovered. AURKA has been found to bind and thereby stabilize the oncogene c-Myc in liver and thyroid cancer.^[7,8] Further, AURKA promotes resistance to third-generation EGFR and KRAS(G12C) inhibitors.^[9,10] Additionally, AURKA can phosphorylate the tumor-suppressor protein p53 to modulate its activity and this phosphorylation can lead to degradation of p53 by MDM2.^[11,12] However, not all functions of AURKA are fully understood and no AURKA inhibitor has been clinically approved so far.^[13]

In contrast, three inhibitors of CDKs have gotten clinical approval, namely Palbociclib, Ribociclib and Abemaciclib.^[14] All three are designed as selective CDK4/6 inhibitors with low affinity for other CDKs.^[15,16] CDK4 and CDK6 are activated by D-type cyclins and control G1 to S phase progression in the cell cycle by phosphorylating the retinoblastoma protein (Rb).^[14,17] This pathway is often mutated in caners resulting in aberrant proliferation.^[18] CDK4/6 inhibitors not only induce cell cycle arrest, but also modulate the tumor microenvironment.^[14,19] CDK1, CDK2, CDK7 and CDK9 have also

been targeted with pan-CDK inhibitors, but the first generation of inhibitors was unsuccessful due to low efficacy and dose-limiting toxicities.^[18]

An emerging strategy for pharmacological targeting of kinases are bifunctional molecules termed proteolysis targeting chimeras (PROTACs). PROTACs catalyze the degradation of proteins of interest (POI) by binding to both the POI and an E3 ligase complex, leading to ubiquitylation and proteasomal degradation of the target.^[20,21] Compared to conventional inhibition of the kinase activity, this approach removes the kinase with all its functions. This could provide a mechanistic advantage when targeting kinases like AURKA, which binds and stabilizes c-Myc independent of kinase function. An additional advantage is that PROTACs can be more selective than their parent kinase inhibitors.^[22–24]

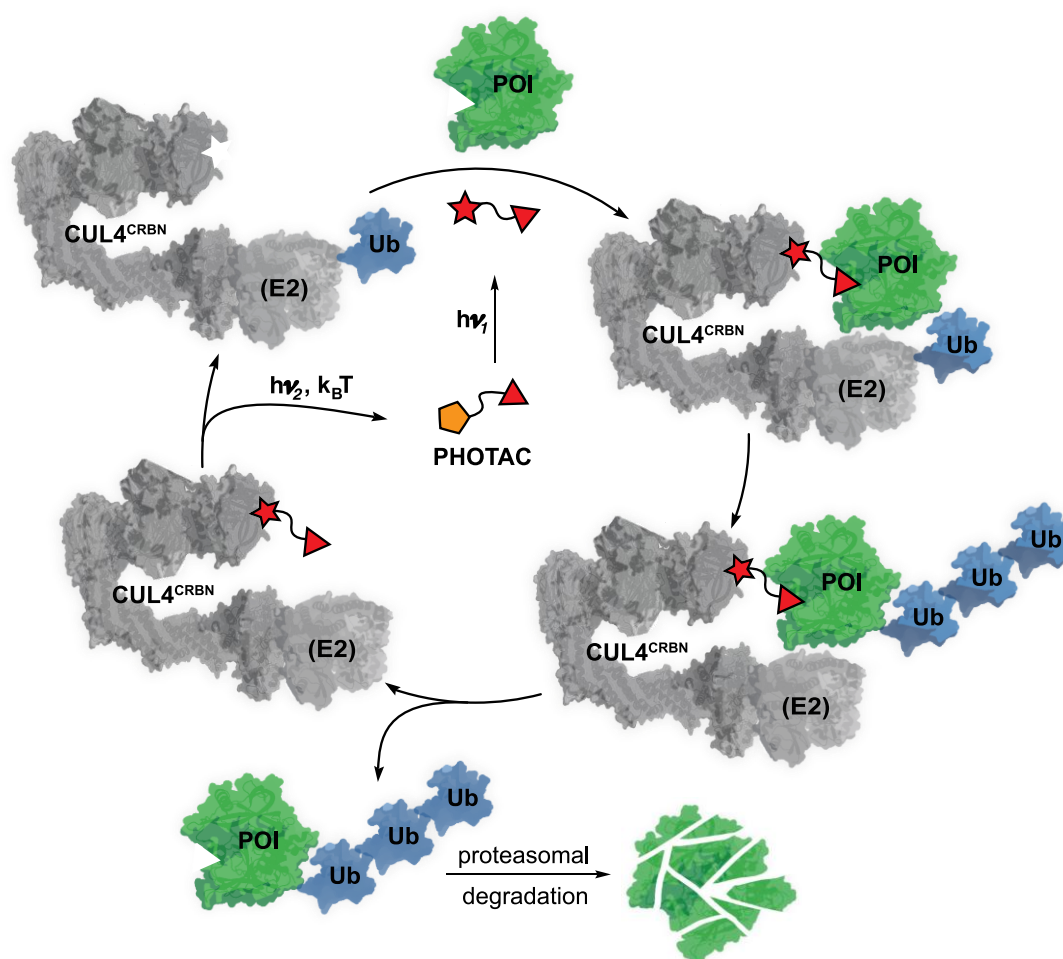


Figure 6.1: PHOTAC mode of action. PHOTACs undergo light-induced isomerization between an inactive form (yellow pentagon) and an active form (red star). The active form can catalyze the ubiquitylation of a protein of interest leading to its proteasomal degradation.

However, degrading the target can also bring additional risk and cause undesired side-effects, especially when targeting CDK and aurora kinases which are important for the survival and proliferation of healthy tissues.^[25,26] We have developed PROTACs whose activity can be regulated with light, termed photochemically targeting chimeras (PHOTACs) (Figure 6.1).^[27] PHOTACs allow spatial and temporal control of target degradation and could be used as research tools to study the effects of protein loss and in precision medicine to improve the safety profile of PROTACs.

Here, we expand the PHOTAC approach to aurora and cyclin-dependent kinases to control their abundance with light and thereby obtain optical control of cytotoxicity and the cell cycle.

Results

Several AURKA inhibitors such as MK-5108 or Alisertib underwent clinical trials and provide a suitable starting point to generate PHOTACs (Figure 6.2A).^[6] Crystal structure of inhibitors bound to AURKA show that the carboxylate group is solvent exposed, providing an ideal attachment point for the generation of PHOTACs (Figure 6.2B,C).^[6,28] PROTACs based on Alisertib targeting AURKA were disclosed recently.^[29] In addition, it was demonstrated that AURKA is prone to PROTAC mediated degradation by using promiscuous kinase inhibitors.^[22,24] We synthesized **PHOTAC-AURKA-1–3** based on our existing PHOTAC platform employing MK-5108 as targeting ligand (Figure 6.3A).^[27] **PHOTAC-AURKA-1–3** recapitulated the photophysical properties of PHOTACs, generating up to 90% of the *Z*-isomer when irradiated with 390 nm light and thermally relaxing back to the *Z*-isomer with a half-life above 20 h in mixtures of DMSO and PBS (Figure 6.3B–E, S6.1). Further, we prepared **PHOTAC-AURKA-4** based on Alisertib, which exhibits similar photophysical properties (Figure 6.4).

Next, we probed the effect of our AURKA-PHOTACs on RS4;11 growth and viability. Incubation with **PHOTAC-AURKA-1–4** for 72 h led to a dose-dependent decrease in viability as expected (Figure 6.5). All PHOTACs became more potent when irradiated with 390 nm light inducing *E*-to-*Z*-isomerization. Interestingly, we did not only observe a shift in potency, but also a mechanistic difference. **PHOTAC-AURKA-1+2** showed strong toxicity upon irradiation with viability dropping to zero, whereas incubation in the

dark led to a constant viability level at high concentrations (Figure 6.5A, B). This viability level between 25 and 30% indicates growth arrest during the 72-h incubation period.

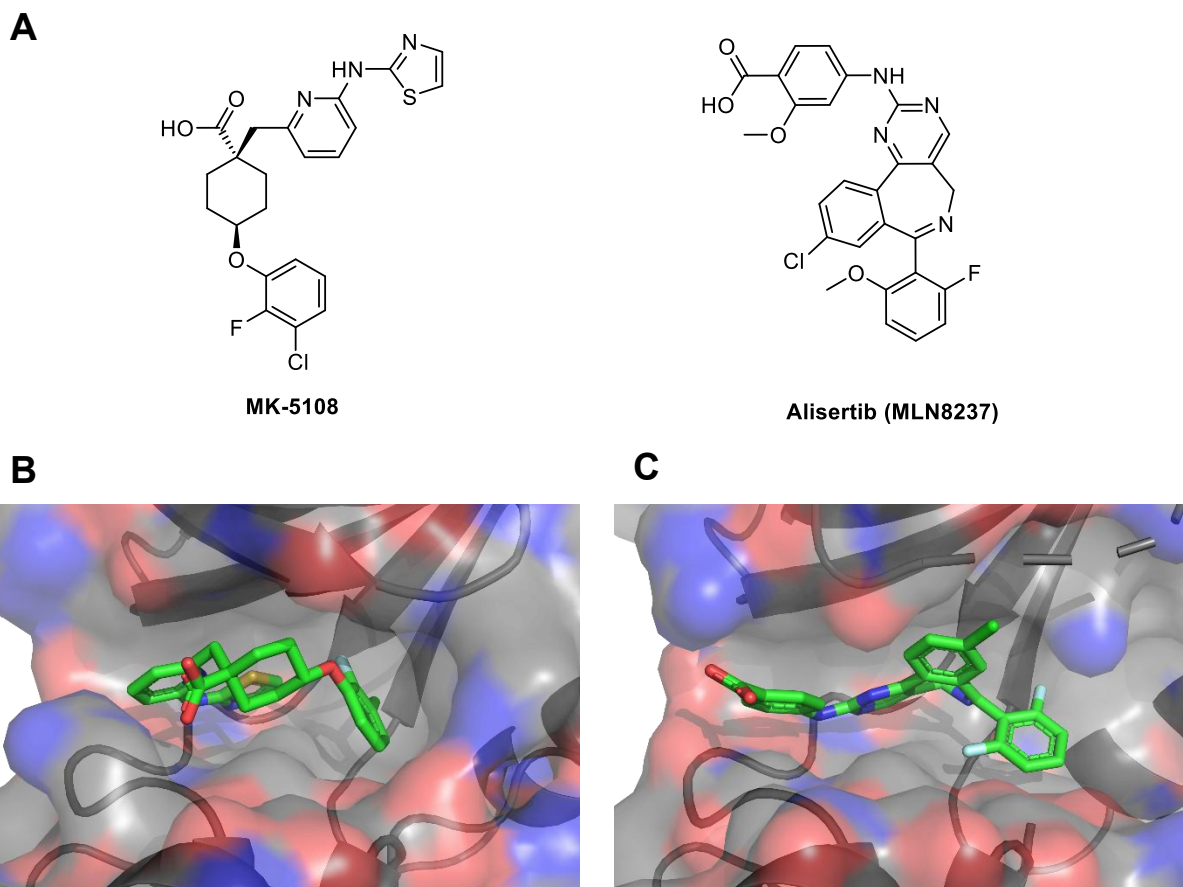


Figure 6.2: AURKA inhibitors. A) Structure of the AURKA inhibitors MK-5108 and Alisertib. B) Crystal structure of MK-5108 bound to the ATP-pocket of AURKA (PDB 5EW9).^[6] C) Crystal structure of MLN8054 an analog of Alisertib bound to the ATP-pocket of AURKA (PDB 2X81).^[28]

Notably, MK-5108 also showed a small response to irradiation, albeit less pronounced than PHOTACs and missing the reduced activity at high concentrations in the dark (Figure 6.5E). While varying the linker length of MK-5108-based PHOTACs did influence overall potency, it did not significantly alter the phototherapeutic window.

Subsequently, we investigated AURKA degradation by immunoblotting of RS4;11 cells treated with **PHOTAC-AURKA-1–4** to further investigate their activity (Figure 6.6). **PHOTAC-AURKA-1** induces strong AURKA degradation both in the dark and with pulsed 390 nm irradiation. However, degradation appeared to be more effective in its irradiated Z-form (Figure 6.6A). **PHOTAC-AURKA-2** recapitulated the strong AURKA degradation but failed to show a pronounced difference between light and dark (Figure

6.6B). Western blots of **PHOTAC-AURKA-3+4** again showed target degradation in both forms of the isomer (Figure 6.6C, D). Reduced potency at 10 μM due to the so called hook-effect indicates that **PHOTAC-AURKA-3+4** function through inducing a ternary complex.^[20,30]

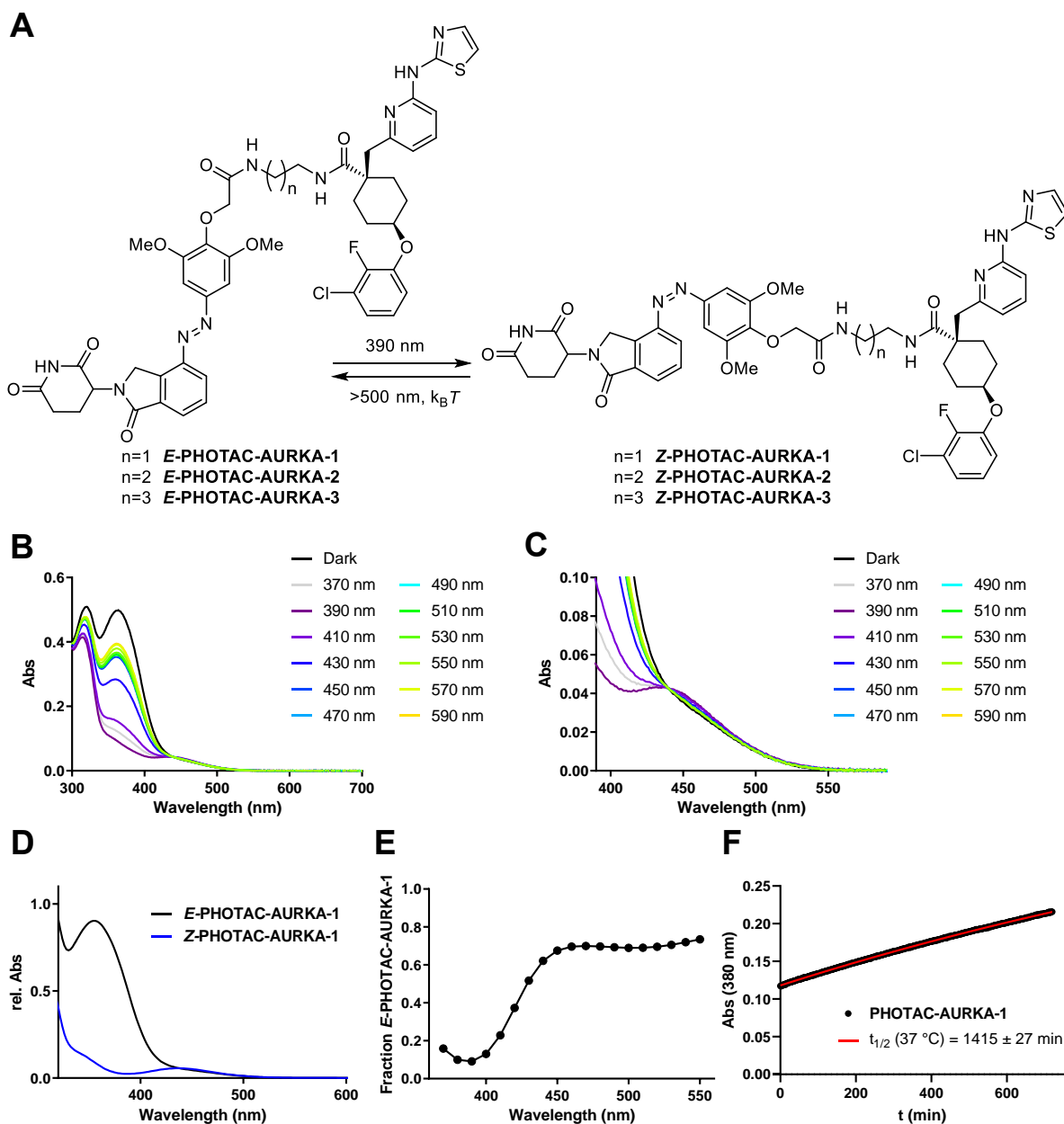


Figure 6.3: Photophysical characterization of **PHOTAC-AURKA-1–3**. A) Structure and isomerization of **PHOTAC-AURKA-1–3**. B), C) Absorption spectra of **PHOTAC-AURKA-1** after irradiation with the indicated wavelength for 5 min. D) Absorption spectra of **PHOTAC-AURKA-1** isomers as obtained by LCMS. E) Calculated fraction of *E*-**PHOTAC-AURKA-1** after 5 min irradiation with the indicated wavelength. F) Thermal *Z*-to-*E* isomerization of **PHOTAC-AURKA-1** at 37 °C in a 1:1 DMSO:PBS (pH 7.4) mixture.

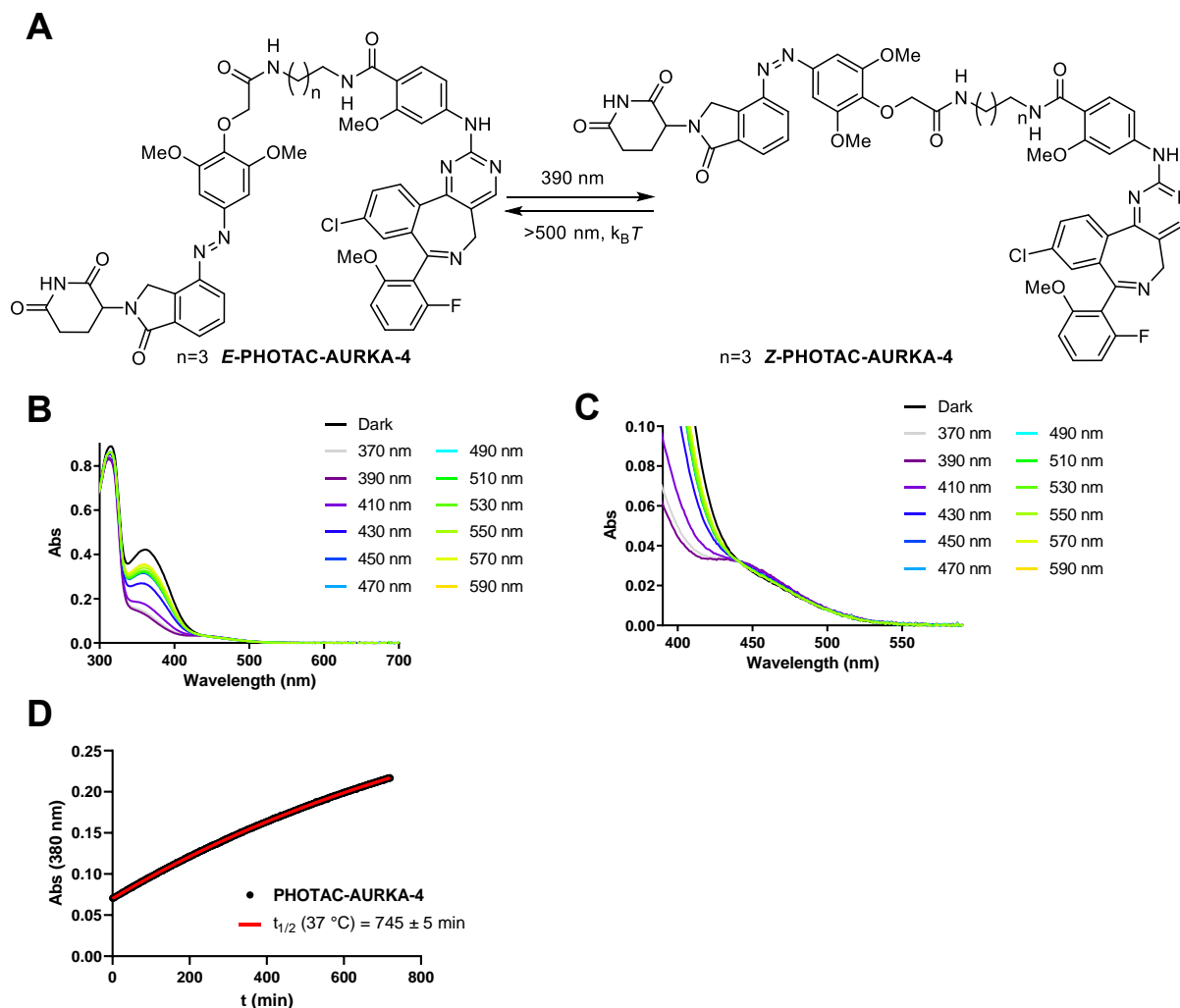


Figure 6.4: Characterization of **PHOTAC-AURKA-4**. A) Structure and isomerization of **PHOTAC-AURKA-4**. B), C) Absorption spectra of **PHOTAC-AURKA-4** after irradiation with the indicated wavelength for 5 min. D) Thermal *Z*-to-*E* isomerization of **PHOTAC-AURKA-4** at 37 °C in DMSO.

Next, we investigated panCDK inhibitors SNS-032 and AT7519. SNS-032 targets CDK2, 7 and 9 and has previously been used to generate a CDK9 selective PROTAC.^[31,32] AT7519 is an inhibitor of CDK1, 2, 4, 5, 6 and 9.^[33,34] Given that these unselective inhibitors can yield a very selective PROTAC, we set out to prepare the corresponding PHOTACs to obtain light control of CDKs. Both inhibitors feature a piperidine ring that is ideally positioned for attachment of our cereblon targeting photoswitch.

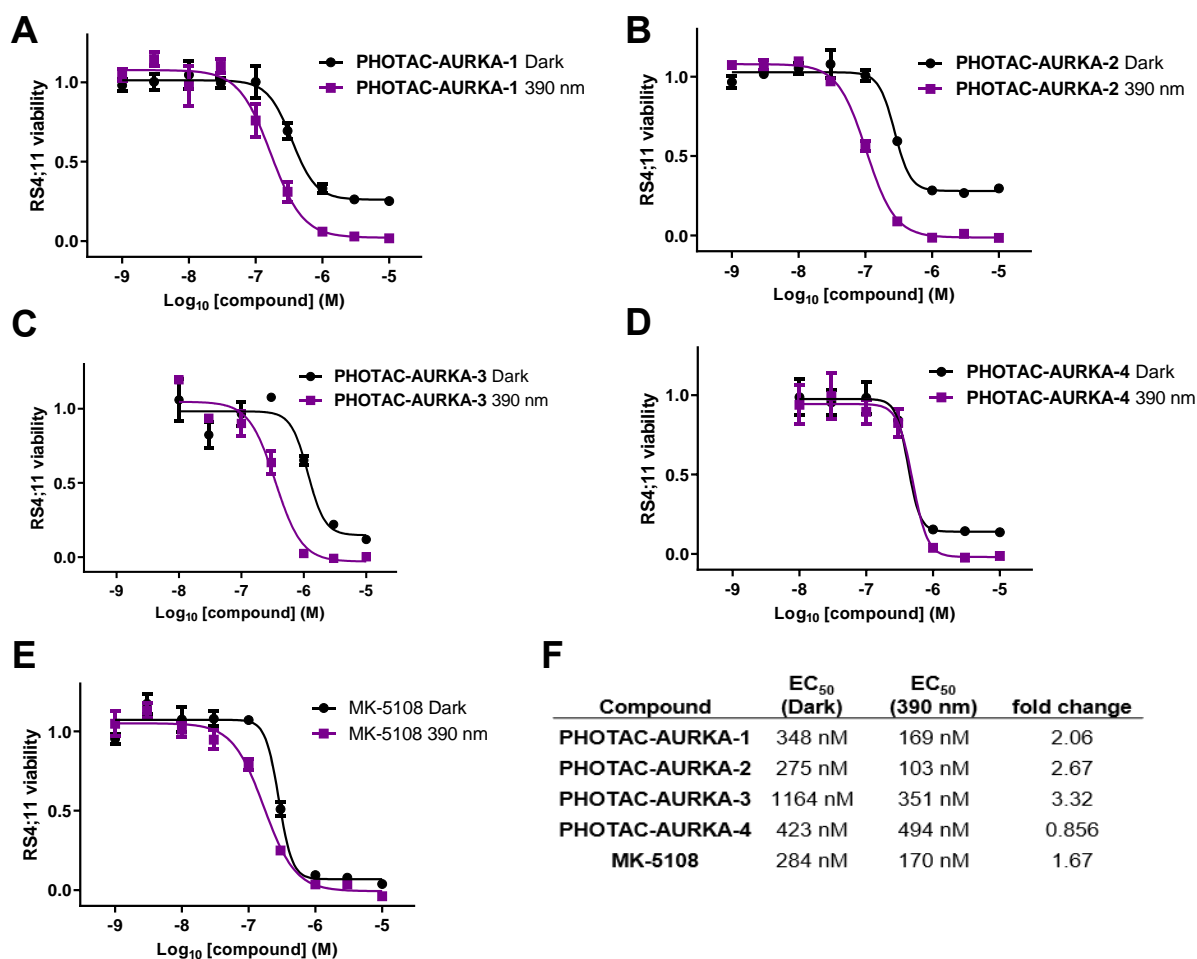


Figure 6.5: Light-dependent viability effects of **PHOTAC-AURKA-1–4**. Viability of RS4;11 cells after treatment with A) **PHOTAC-AURKA-1**, B) **PHOTAC-AURKA-2**, C) **PHOTAC-AURKA-3**, D) **PHOTAC-AURKA-4**, and E) alisertib for 72 h in the dark or under pulsed 390 nm irradiation (100 ms every 10 s). F) EC₅₀ values of AURKA targeting PHOTACs.

PHOTAC-panCDK-1 and **PHOTAC-panCDK-2** kept the photophysical properties of other PHOTACs and isomerize well under 390 nm irradiation (Figure 6.7A–D, 6.8A–D). To get an overview of their utility as light controlled PROTACs, we probed the effect of panCDK PHOTACs on RS4;11 viability. Both **PHOTAC-panCDK-1** and **PHOTAC-panCDK-2** exhibited a potent cytotoxic effect with an EC₅₀ in the nanomolar range, but surprisingly failed to induce a strong activity difference between the dark and irradiated forms (Figure 6.7E, 6.8E). Only a slightly stronger cytotoxic effect for the dark-adapted *E*-isomer could be observed for both PHOTACs. Due to the absence of a phototherapeutic window, we did not investigate these compounds further and decided to pursue PHOTACs based on more selective targeting ligands for CDKs.

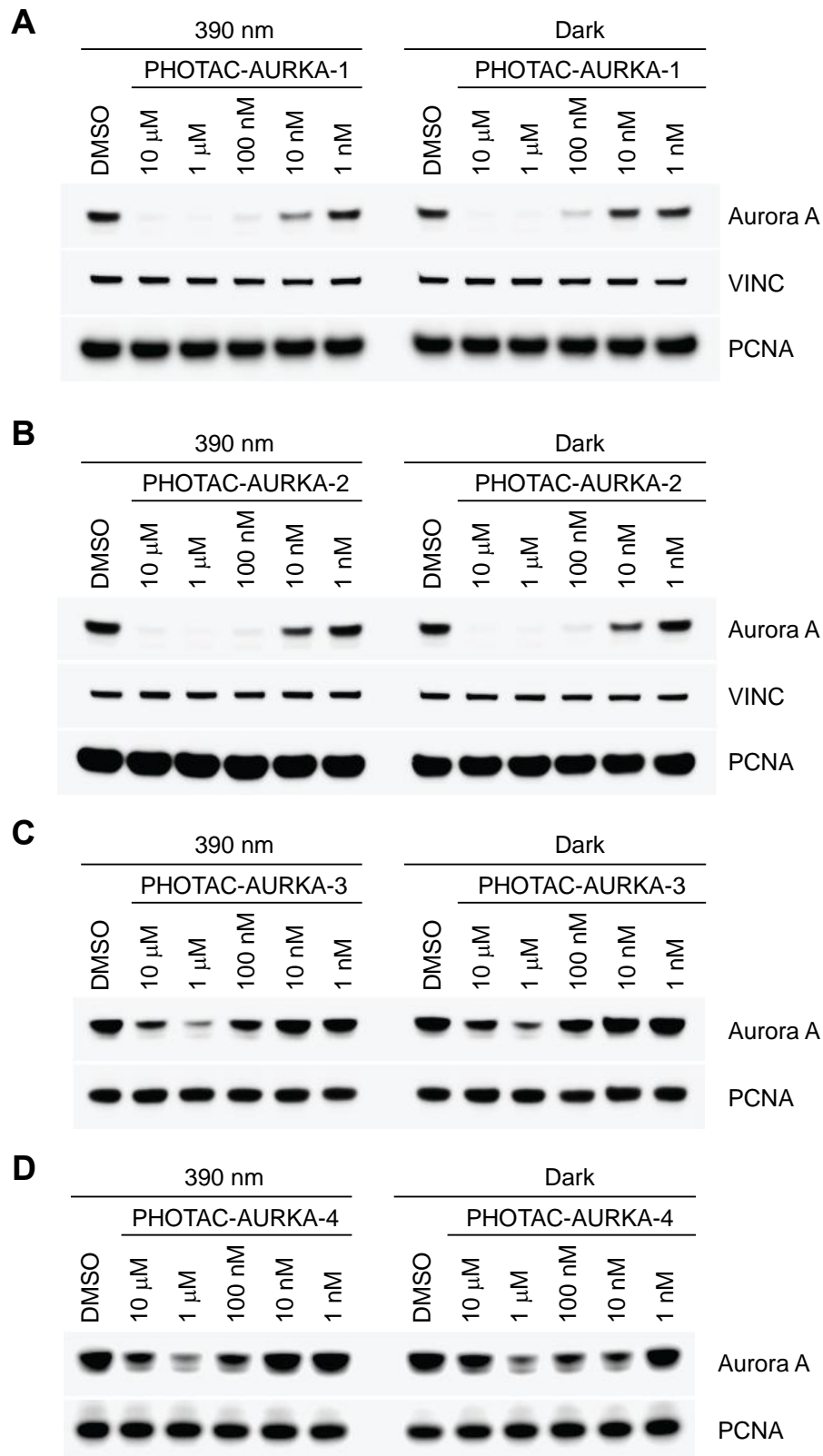


Figure 6.6: *In cellulo* analysis of **PHOTAC**-induced AURKA degradation. Immunoblot of RS4;11 cells treated with A) **PHOTAC-AURKA-1**, B) **PHOTAC-AURKA-2**, C) **PHOTAC-AURKA-3** or D) **PHOTAC-AURKA-4** for 4 h in the dark or under pulsed 390 nm irradiation (100 ms every 10 s).

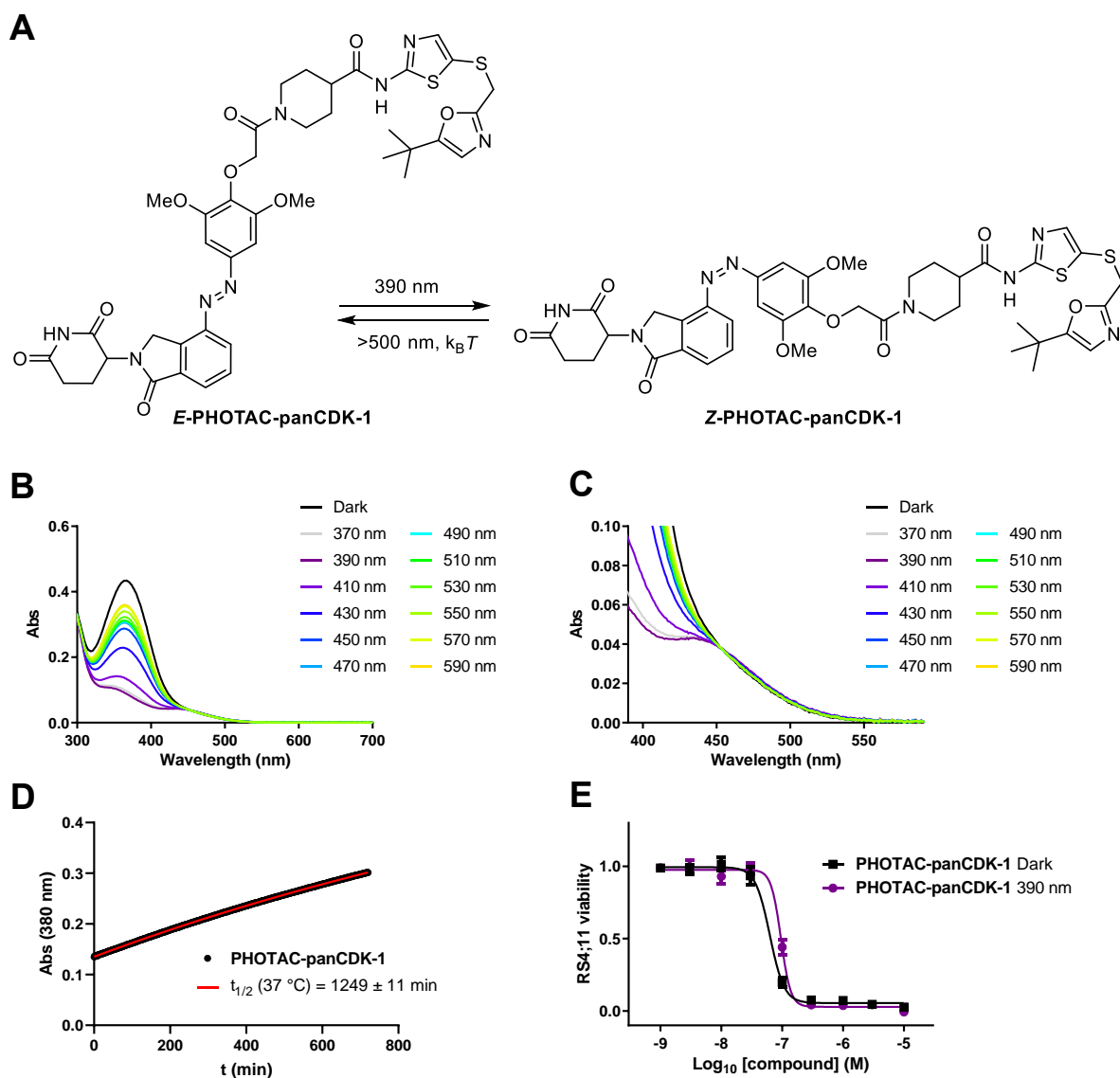


Figure 6.7: Characterization of **PHOTAC-panCDK-1**. A) Structure and isomerization of **PHOTAC-panCDK-1**. B), C) Absorption spectra of **PHOTAC-panCDK-1** after irradiation with the indicated wavelength for 5 min. D) Thermal *Z*-to-*E* isomerization of **PHOTAC-panCDK-1** at 37 °C in a 1:1 DMSO:PBS (pH 7.4) mixture. E) Viability of RS4;11 cells treated with **PHOTAC-panCDK-1** for 72 h in the dark or under pulsed 390 nm irradiation (100 ms every 10 s).

Dual, selective inhibitors of CDK4 and CDK6, such as Palbociclib or Ribociclib are approved for the treatment of breast cancer and have shown great promise in combination with other therapies (Figure 6.9A).^[14,35] Degradation could provide an advantage over inhibition and several PROTACs targeting CDK4 and CDK6 such as BSJ-03-123 have been developed (Figure 6.9C).^[23,36–41]

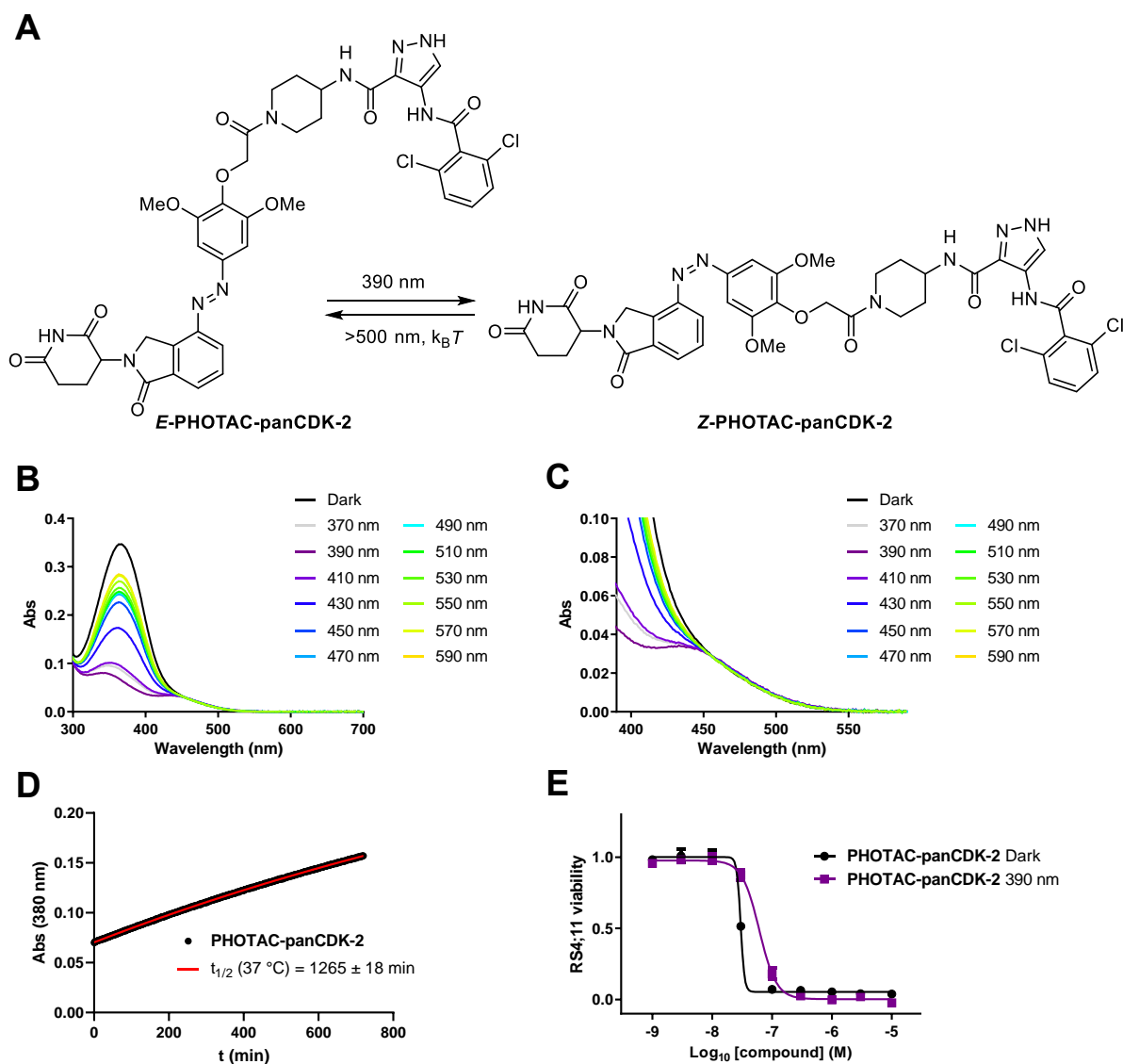


Figure 6.8: Characterization of **PHOTAC-panCDK-2**. A) Structure and isomerization of **PHOTAC-panCDK-2**. B), C) Absorption spectra of **PHOTAC-panCDK-2** after irradiation with the indicated wavelength for 5 min. D) Thermal *Z*-to-*E* isomerization of **PHOTAC-panCDK-2** at 37 °C in a 1:1 DMSO:PBS (pH 7.4) mixture. E) Viability of RS4;11 cells treated with **PHOTAC-panCDK-2** for 72 h in the dark or under pulsed 390 nm irradiation (100 ms every 10 s).

The structure of Palbociclib bound to CDK6 and the reported PROTACs indicate that the piperazine is the perfect attachment point for a linker and ligand to recruit an E3 ligase (Figure 6.9B).^[42]

Starting from Palbociclib we synthesized **PHOTAC-CDK4/6-1–3** with varying length of the linkers (Figure 6.10A, 6.11A). The absorption spectra of **PHOTAC-CDK4/6-1–3** are dominated by the underlying absorption of Palbociclib, but the azobenzene can still

undergo *E*-to-*Z*-isomerization (Figure 6.10B, C, 6.11B, C). Thermal half-lives are above 12 h and appear to increase with increasing linker length (Figure 6.10D, 6.11D).

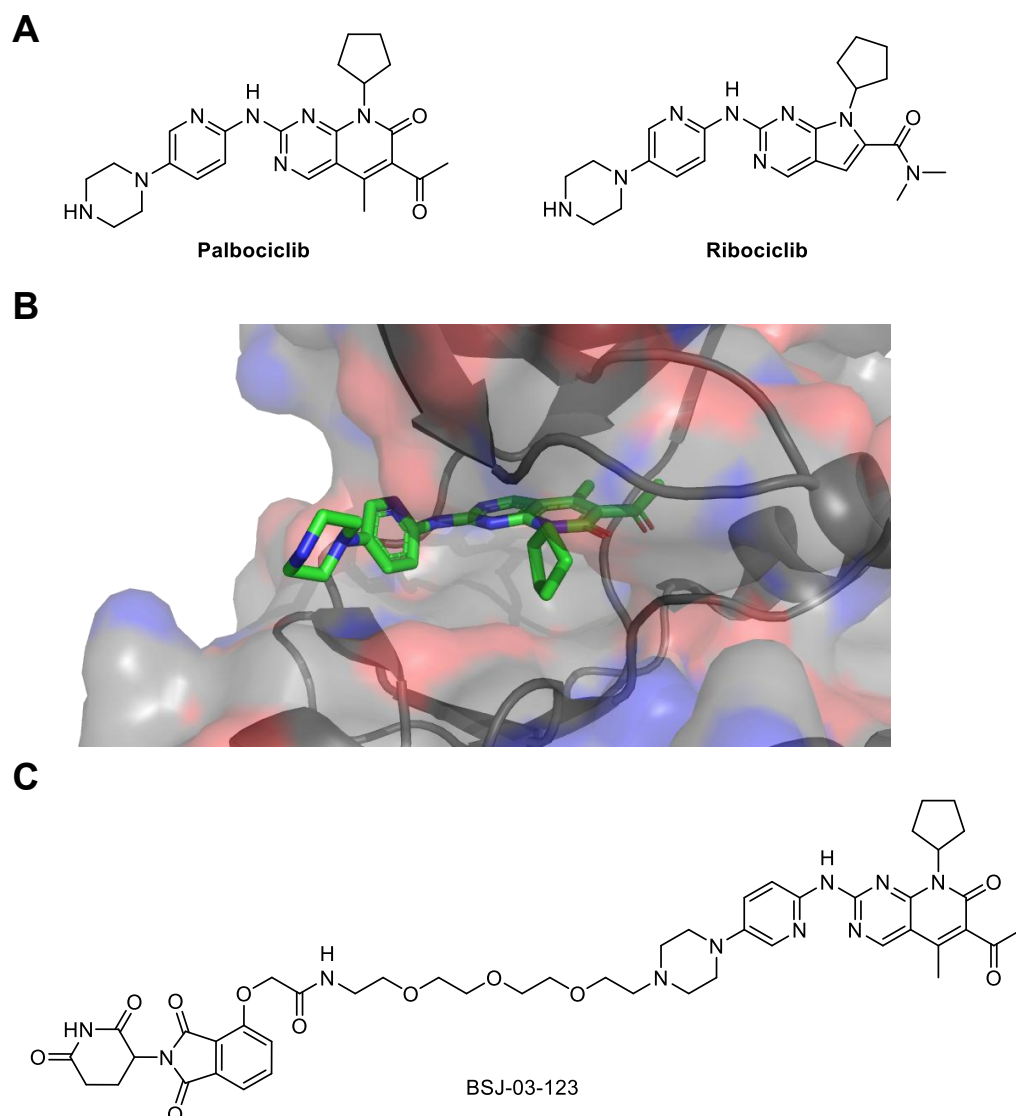


Figure 6.9: CDK4/6 targeting drugs. A) Structure of CDK4/6 inhibitors Palbociclib and Ribociclib. B) Structure of Palbociclib bound to CDK6 (PDB 5L2I).^[42] C) Structure of the CDK4/6 targeting PROTAC BSJ-03-123.^[23]

Viability of RS4;11 cells did not show a significant difference between treatment with irradiated and non-irradiated cells for **PHOTAC-CDK4/6-1** and **PHOTAC-CDK4/6-2** (Figure 6.12A, B). When irradiated, **PHOTAC-CDK4/6-3** led to a more pronounced viability reduction and showed a slightly different profile as visualized by different curve shapes and slopes (Figure 6.12C). Immunoblot analysis of **PHOTAC-CDK4/6-3** revealed reduced levels of both CDK4 and CDK6 in both the irradiated and non-

irradiated cells. Because of CDK4/6 degradation, lower phosphorylation levels of the CDK4/6 substrate Retinoblastoma protein (Rb) could be observed (Figure 6.12D).

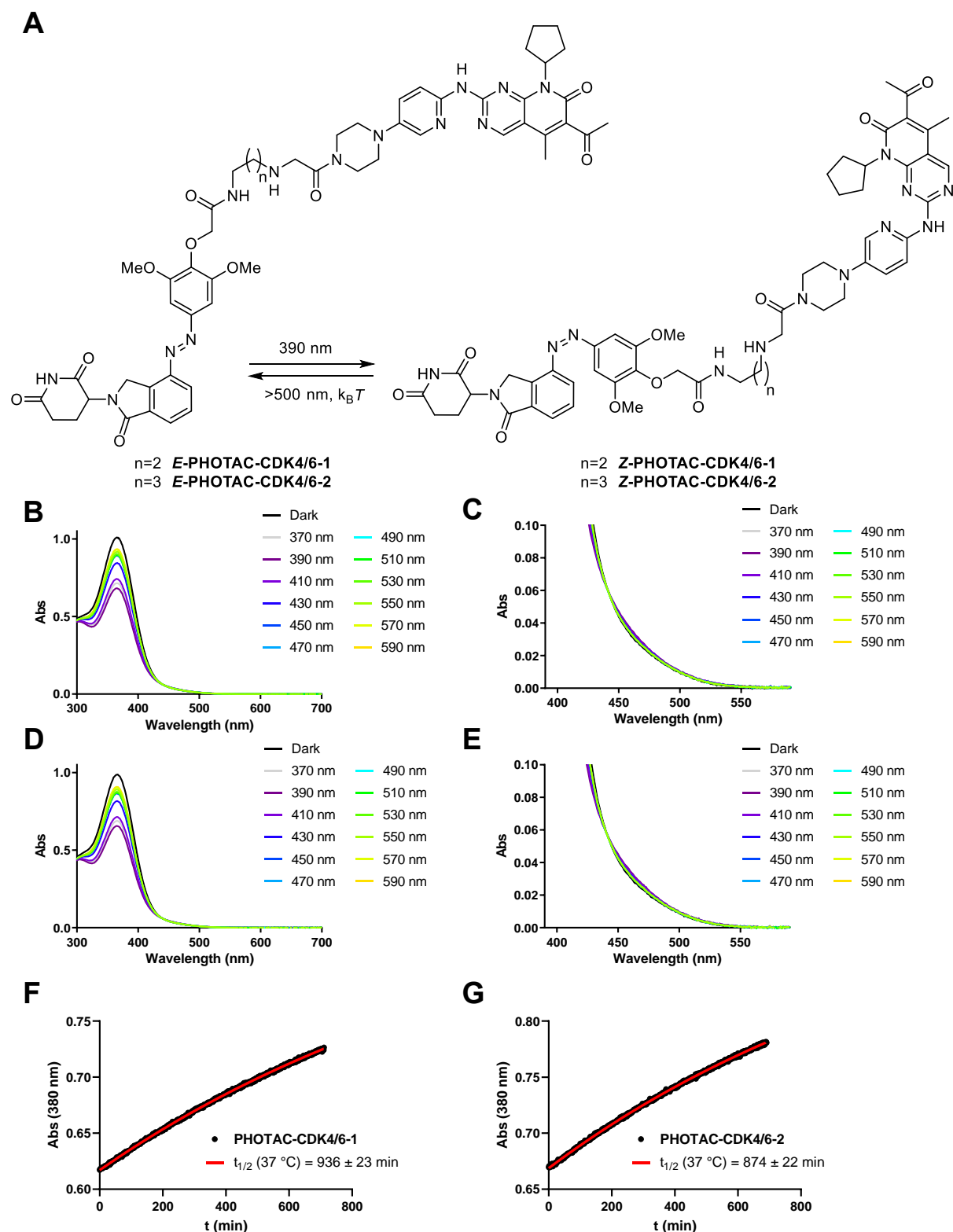


Figure 6.10: Characterization of **PHOTACs** for CDK4/6. A) Structure and isomerization of **PHOTAC-CDK4/6-1+2**. B), C) Absorption spectra of **PHOTAC-CDK4/6-1** after

irradiation with the indicated wavelength for 5 min. D), E) Absorption spectra of **PHOTAC-CDK4/6-2** after irradiation with the indicated wavelength for 5 min. Thermal Z-to-E isomerization of F) **PHOTAC-CDK4/6-1** and G) **PHOTAC-CDK4/6-2** at 37 °C in DMSO.

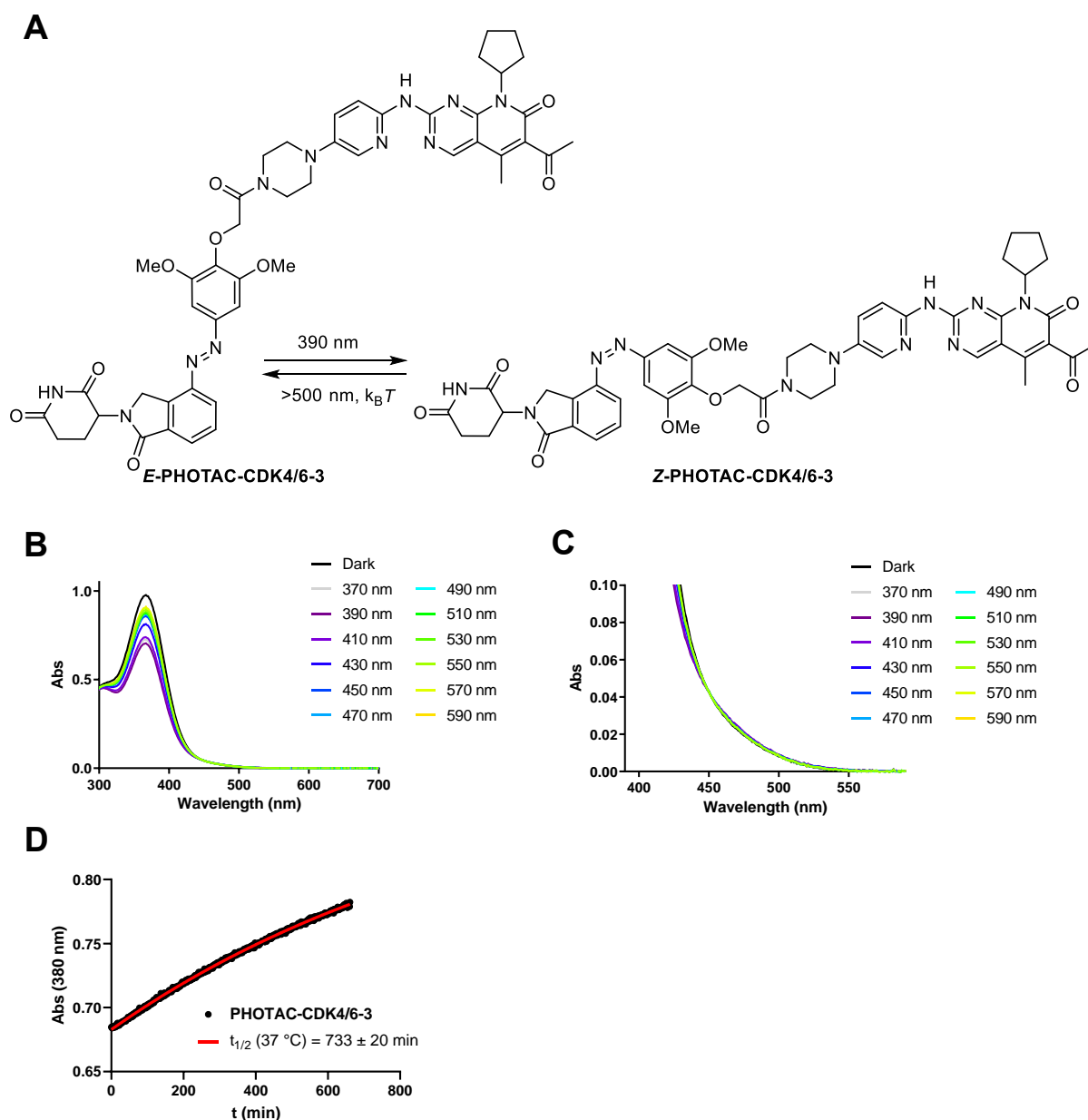


Figure 6.11: Characterization of **PHOTAC-CDK4/6-3**. A) Structure and isomerization of **PHOTAC-CDK4/6-3**. B), C) Absorption spectra of **PHOTAC-CDK4/6-3** after irradiation with the indicated wavelength for 5 min. D) Thermal Z-to-E isomerization of **PHOTAC-CDK4/6-3** at 37 °C in DMSO.

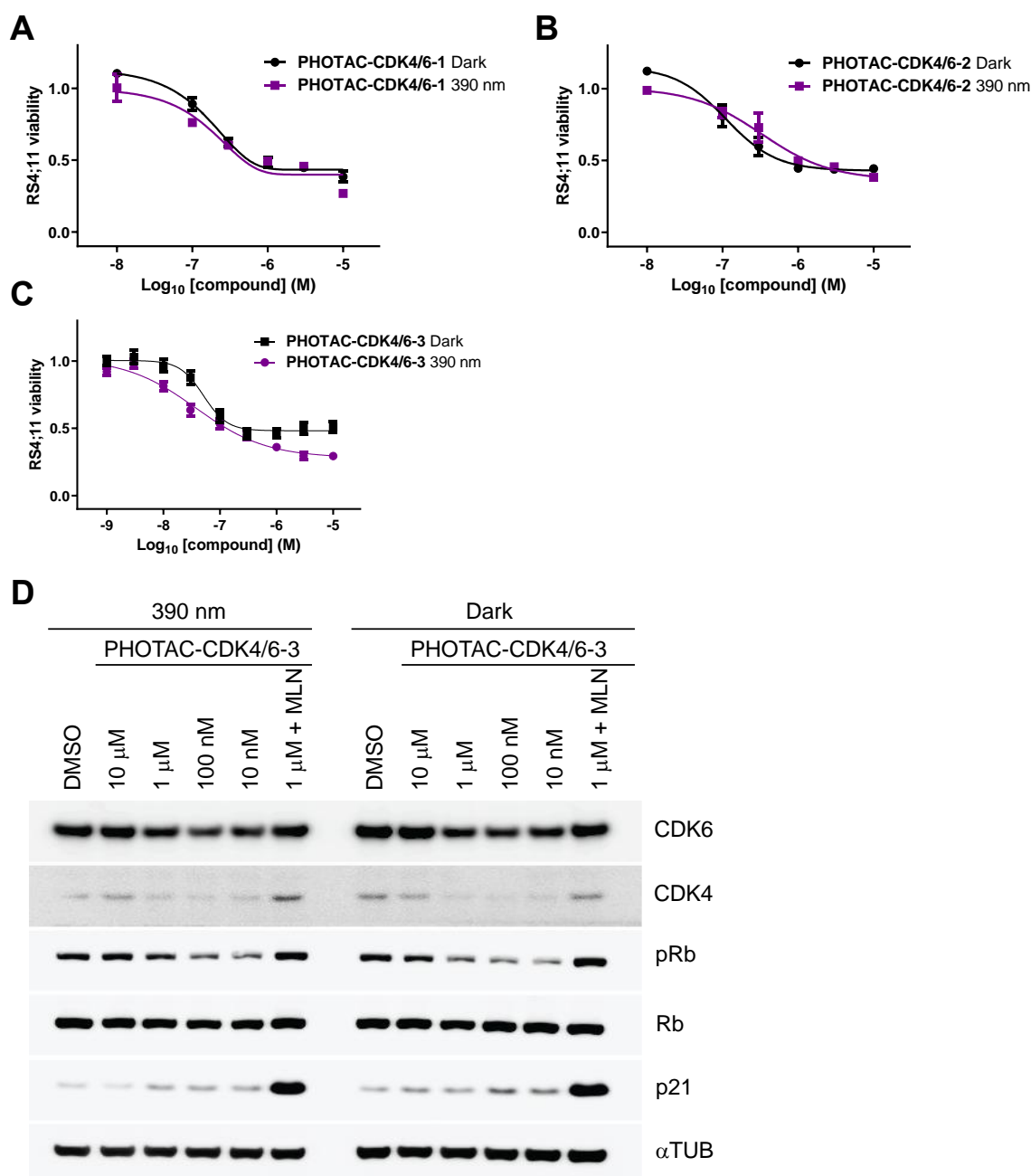


Figure 6.12: Analysis of **PHOTAC-CDK4/6-1–3** in RS4;11 cells. Viability of RS4;11 cells after treatment with A) **PHOTAC-CDK4/6-1**, B) **PHOTAC-CDK4/6-2**, C) **PHOTAC-CDK4/6-3** for 72 h in the dark or under pulsed 390 nm irradiation (100 ms every 10 s). D) Western blot of RS4;11 cells treated with **PHOTAC-CDK4/6-3** for 4 h under pulsed 390 nm irradiation (100 ms every 10 s) or in the dark.

In an attempt to further improve the photophysical properties and phototherapeutic window of this degrader, we switched the Palbociclib targeting ligand with the structurally very similar Ribociclib to create **PHOTAC-CDK4/6-4** (Figure 6.13A). Ribociclib still influences the absorption spectra of **PHOTAC-CDK4/6-4**, but to a lesser extent than Palbociclib due to lower absorption of the ligand (Figure 6.13B, C). In line

with other PHOTACs, *E*-to-*Z*-isomerization was most efficiently induced by 390 nm irradiation, generating up to 60% of the *Z*-isomer (Figure 6.13D+E). Thermal relaxation was as slow as other PHOTACs with a half-life of approximately 20 h in a DMSO-PBS mixture (Figure 6.13F).

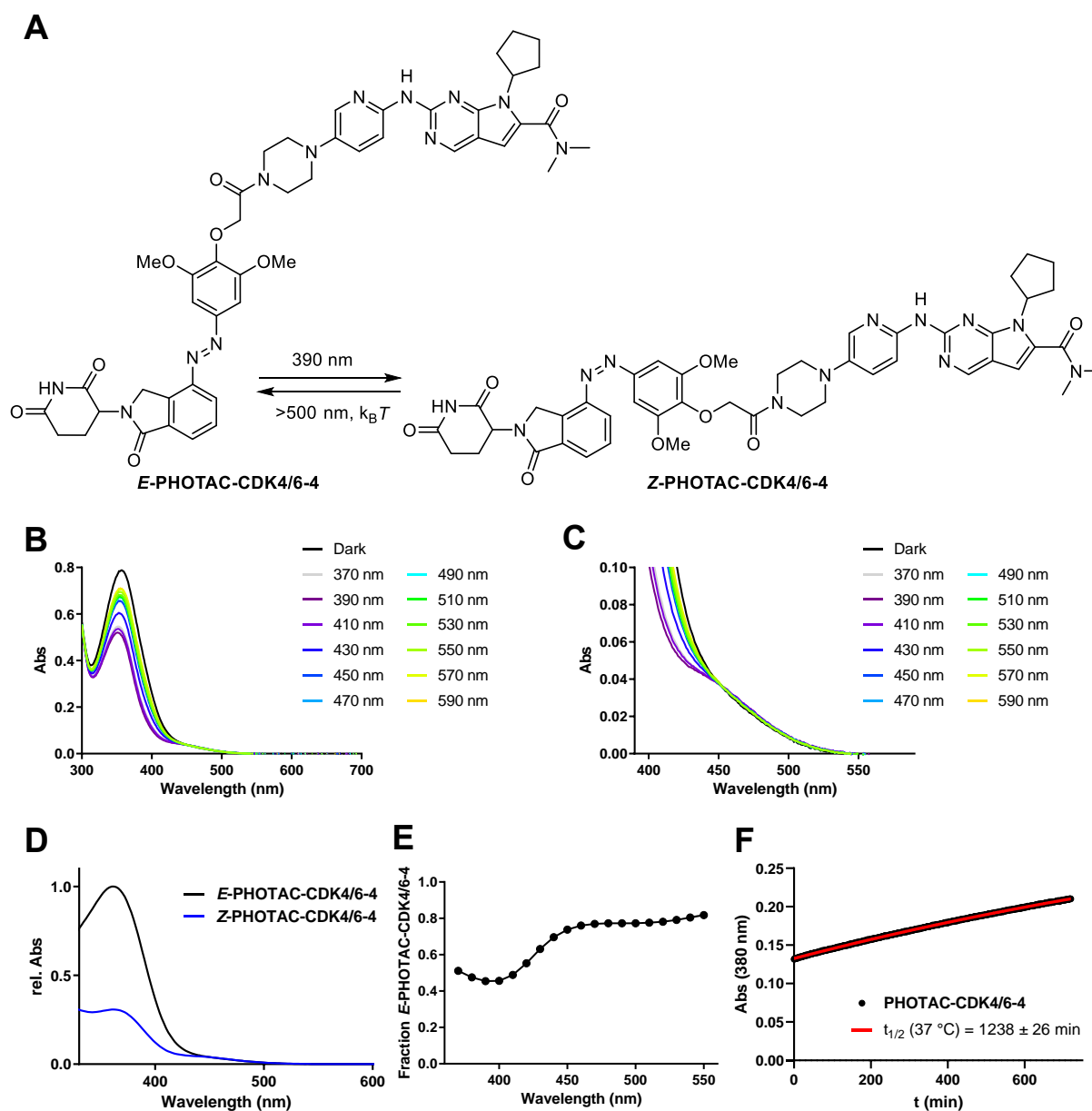


Figure 6.13: Photoswitching of **PHOTAC-CDK4/6-4**. A) Structure and isomerization of **PHOTAC-CDK4/6-4**. B), C) Absorption spectra of **PHOTAC-CDK4/6-4** after irradiation with the indicated wavelength for 5 min. D) Absorption spectra of **PHOTAC-CDK4/6-4** isomers as obtained by LCMS. E) Calculated fraction of *E*- **PHOTAC-CDK4/6-4** after 5 min irradiation with the indicated wavelength. F) Thermal *Z*-to-*E* isomerization of **PHOTAC-CDK4/6-4** at 37 °C in a 1:1 DMSO:PBS (pH 7.4) mixture.

Next, we investigated the effect of **PHOTAC-CDK4/6-4** on RS4;11 viability and observed a remarkable difference between the irradiated and non-irradiated forms. Upon 390 nm pulse irradiation **PHOTAC-CDK4/6-4** showed a strong cytotoxic effect and strongly reduced cell viability while being nearly inactive in the dark (Figure 6.14A). The potency of irradiated **PHOTAC-CDK4/6-4** also surpassed the effect of Ribociclib on RS4;11 cells (Figure 6.14B). An equally strong response and large phototherapeutic windows were also observed in the MOLM13 and MV4-11 acute myeloid leukemia (AML) cell lines (Figure 6.14C, E). Again, Ribociclib did not show any light-dependency (Figure 6.14D). All three cell lines share a general high degree of susceptibility to cereblon-mediated protein degradation.^[43–45] In other cell lines where cereblon mediated protein degradation can be less efficient, such as THP-1, HCT116, U2-OS and MDA-MB-231,^[46] we did not observe a light-dependent viability decrease after **PHOTAC-CDK4/6-4** treatment, which mimicked the inhibitory effect of Ribociclib more closely (Figure S6.2).

To further investigate the phototherapeutic window of **PHOTAC-CDK4/6-4**, we performed the viability assays in leukemia cell lines at concentrations up to 100 μM using 1% DMSO and an additional 1% MeCN to ensure solubility of this large molecule. In the dark up to 100 μM **PHOTAC-CDK4/6-4** did not induce a strong viability decrease in either RS4;11, MV4-11 or MOLM13 cells (Figure 6.15A, C, E). In stark contrast, Ribociclib reduced the amount of viable RS4;11 and MV4-11 cells to zero at 100 μM (Figure 6.15B, D). **PHOTAC-CDK4/6-4** remained potent at high concentrations when activated by pulsed 390 nm irradiation. However, **PHOTAC-CDK4/6-4** led to a partial decrease in viability at lower concentrations ranging from 300 nM to 1 μM in the dark in cells treated with additional MeCN co-solvent. This non-classical effect can be explained by the mechanism of PROTACs which depends on ternary complex formation and thus can be suppressed at high concentrations through saturation of both proteins. Analogous, this effect can also partially be observed in pulse-irradiated cells where concentrations around 1 μM **PHOTAC-CDK4/6-4** appear to be slightly more potent than higher concentrations.

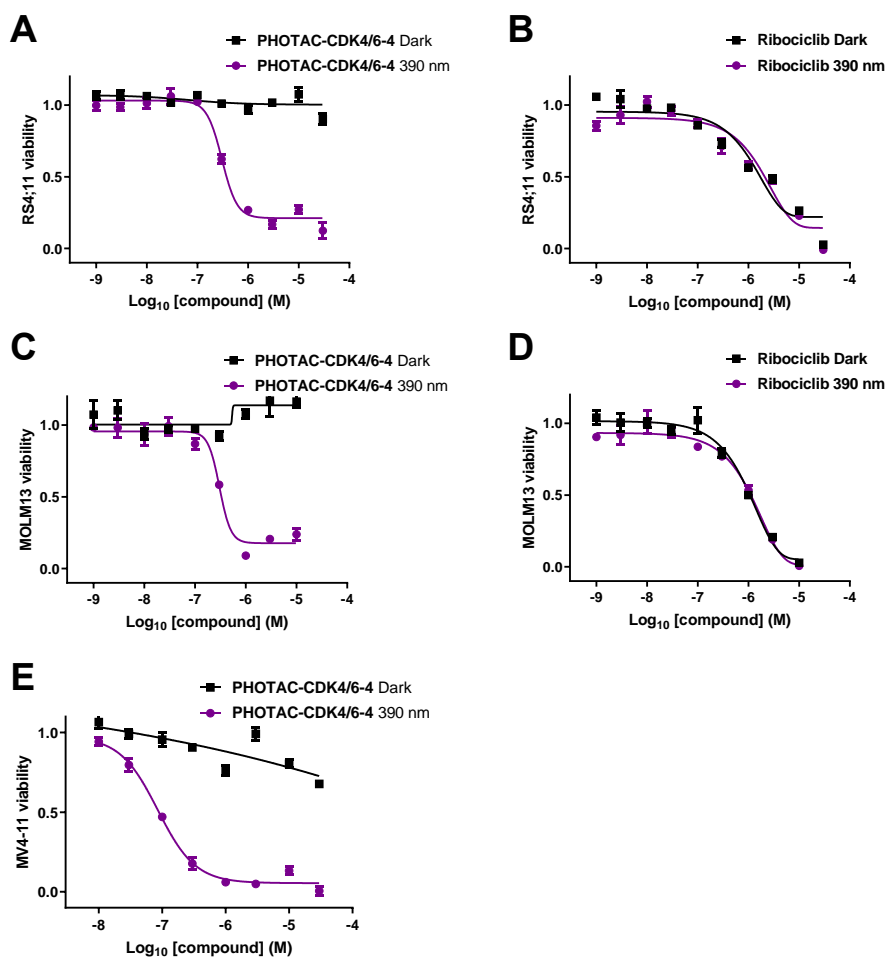


Figure 6.14: Effects of **PHOTAC-CDK4/6-4** on leukemia cell viability. A), B) Viability of RS4;11 cells after treatment with A) **PHOTAC-CDK4/6-4** or B) Ribociclib for 72 h in the dark or with pulsed 390 nm irradiation (100 ms every 10 s). C), D) Viability of MOLM13 cells after treatment with C) **PHOTAC-CDK4/6-4** or D) Ribociclib for 72 h in the dark or with pulsed 390 nm irradiation (100 ms every 10 s). E) Viability of MV4-11 cells after treatment with **PHOTAC-CDK4/6-4** for 72 h in the dark or with pulsed 390 nm irradiation (100 ms every 10 s). Viability normalized to vehicle control containing 1% DMSO in the medium.

The observation of a hook-effect on cell viability already provided an indication that **PHOTAC-CDK4/6-4** mechanistically works like a PROTAC. As an additional control, we also prepared **Me-PHOTAC-CDK4/6-4** bearing a methyl group on the glutarimide to abrogate cereblon binding (Figure 6.16A). The photophysical properties of **Me-PHOTAC-CDK4/6-4** remained largely unchanged (Figure 6.16B–D). As expected, **Me-PHOTAC-CDK4/6-4** did not affect RS4;11 viability in the light or dark showing that the glutarimide is crucial for the activity of **PHOTAC-CDK4/6-4** (Figure 6.16E). We also prepared **PHOTAC-CDK4/6-5** bearing a substituted azobenzene that can undergo *E*-to-*Z* isomerization with yellow light (Figure 6.17A–D). However, **PHOTAC-CDK4/6-5**

did not significantly affect viability and serves to demonstrate how small changes to the molecule lead to diminished potency even if they do not affect the glutarimide or Ribociclib ligand (Figure 6.17E).

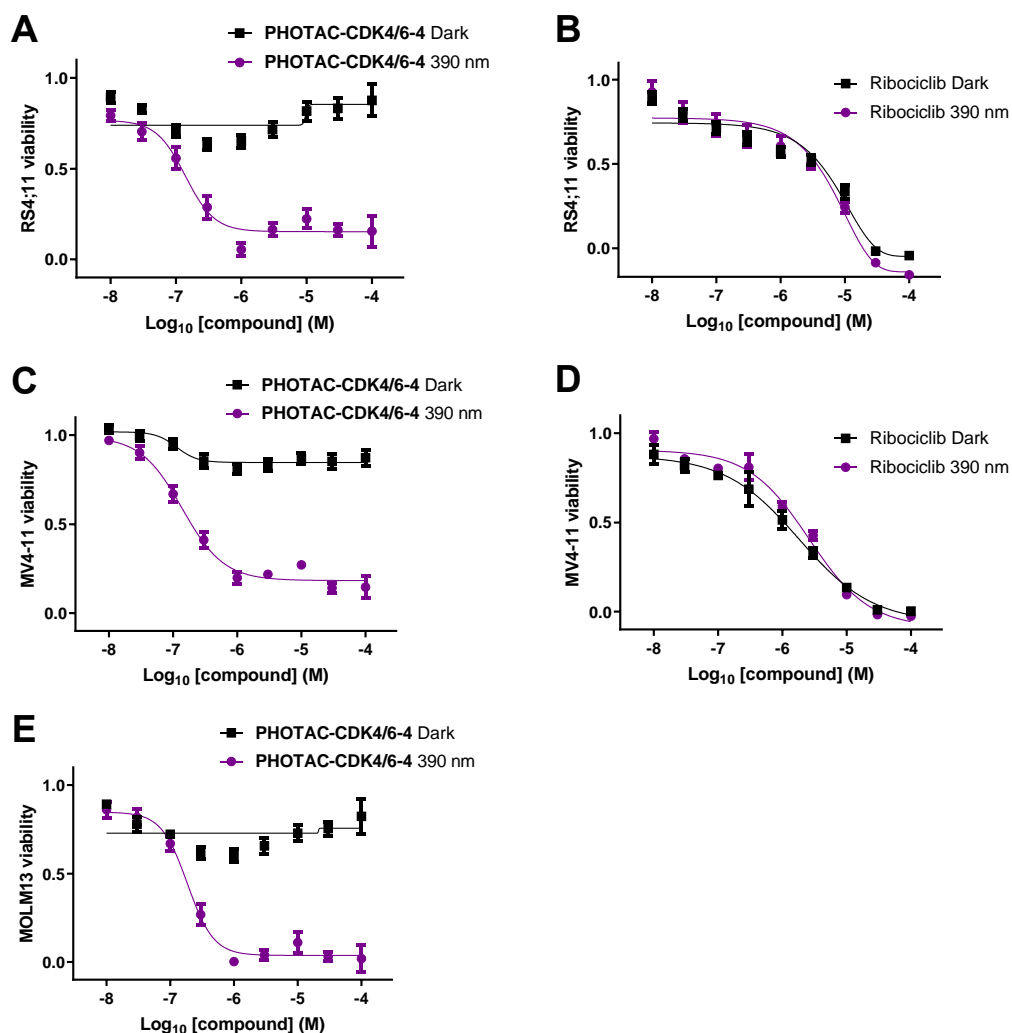


Figure 6.15: Effects of **PHOTAC-CDK4/6-4** on leukemia cell viability using additional co-solvent (1% MeCN) to improve solubility. A), B) Viability of RS4;11 cells after treatment with A) **PHOTAC-CDK4/6-4** or B) Ribociclib for 72 h in the dark or with pulsed 390 nm irradiation (100 ms every 10 s). C), D) Viability of MV4-11 cells after treatment with C) **PHOTAC-CDK4/6-4** or D) Ribociclib for 72 h in the dark or with pulsed 390 nm irradiation (100 ms every 10 s). E) Viability of MOLM13 cells after treatment with **PHOTAC-CDK4/6-4** for 72 h in the dark or with pulsed 390 nm irradiation (100 ms every 10 s). Viability normalized to vehicle control containing 1% DMSO and 1% MeCN in the medium.

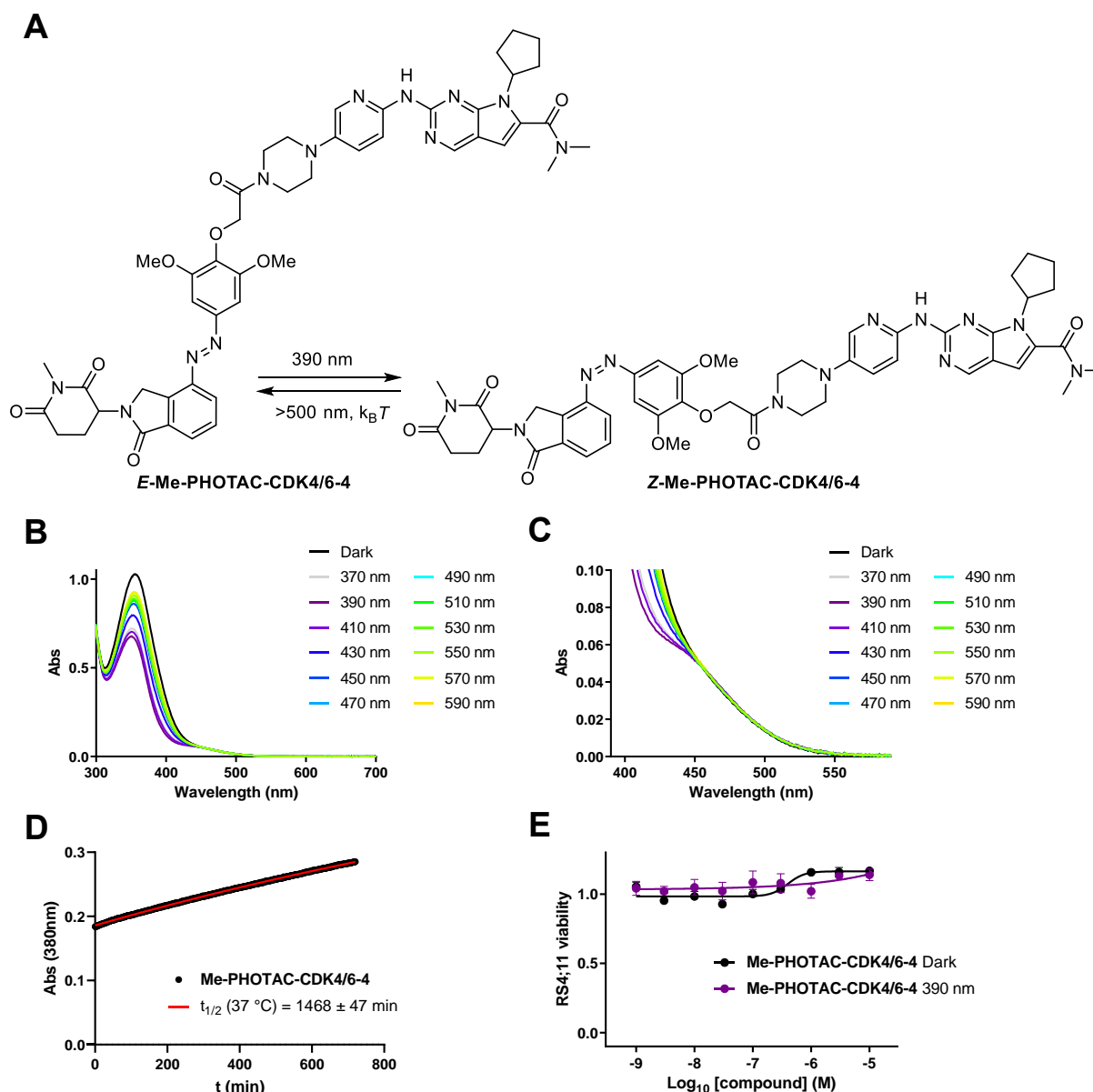


Figure 6.16: Characterization of the inactive control compound **Me-PHOTAC-CDK4/6-4**. A) Structure and isomerization of **Me-PHOTAC-CDK4/6-4**. B), C) Absorption spectra of **Me-PHOTAC-CDK4/6-4** after irradiation with the indicated wavelength for 5 min. D) Thermal Z-to-E isomerization of **Me-PHOTAC-CDK4/6-4** at 37 °C in a 1:1 DMSO:PBS (pH 7.4) mixture. E) Viability of RS4;11 cells treated with **Me-PHOTAC-CDK4/6-4** for 72 h under pulsed 390 nm irradiation (100 ms every 10 s) or in the dark.

Next, we analyzed the effect of **PHOTAC-CDK4/6-4** on CDK4 and CDK6 levels by Western blot analysis. The RS4;11 and MV4-11 cell lines possess a t(4;11) translocation, MOLM13 and THP1 cell lines possess a t(9;11) translocation. These translocations lead to fusion of the mixed lineage leukemia gene (MLL) with either AF4 (4;11) or AF9 (9;11). These fusion proteins induce high CDK6 expression and cell lines become dependent on CDK6 but not CDK4.^[47] Correspondingly, Western Blot analysis

of RS4;11 cells (Figure 6.18A) or MV4-11 cells (Figure 6.18B) show high levels of CDK6 but extremely low levels of CDK4. **PHOTAC-CDK4/6-4** did not induce noticeable CDK6 degradation and no clear light-dependence of CDK4 levels could be observed after a 4 h treatment.

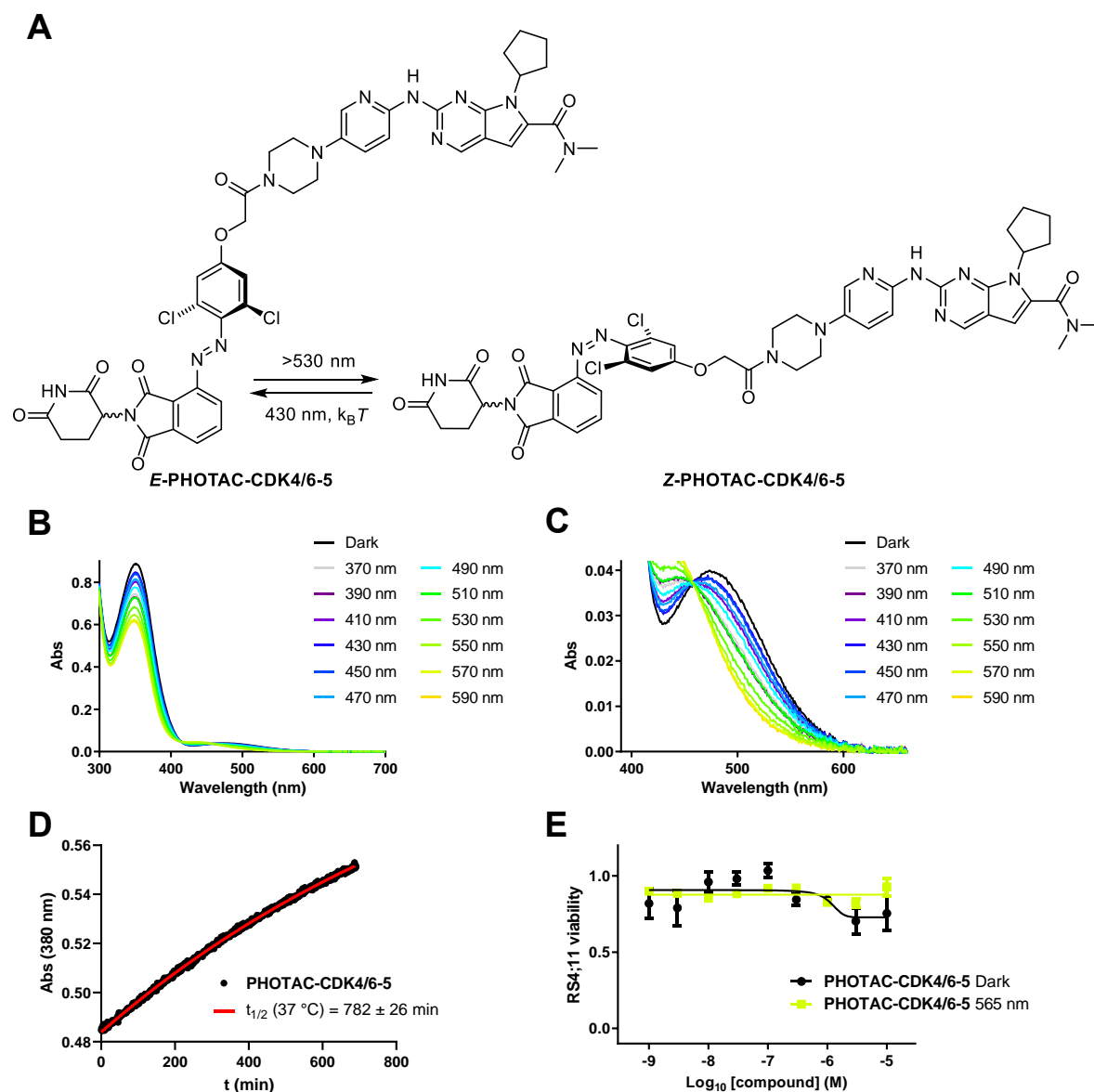


Figure 6.17: Characterization of **PHOTAC-CDK4/6-5**. A) Structure and isomerization of **PHOTAC-CDK4/6-5**. B), C) Absorption spectra of **PHOTAC-CDK4/6-5** after irradiation with the indicated wavelength for 5 min. D) Thermal Z-to-E isomerization of **PHOTAC-CDK4/6-5** at 37 °C in DMSO. E) Viability of RS4;11 cells treated with **PHOTAC-CDK4/6-5** for 72 h under pulsed 565 nm irradiation (100 ms every 10 s) or in the dark.

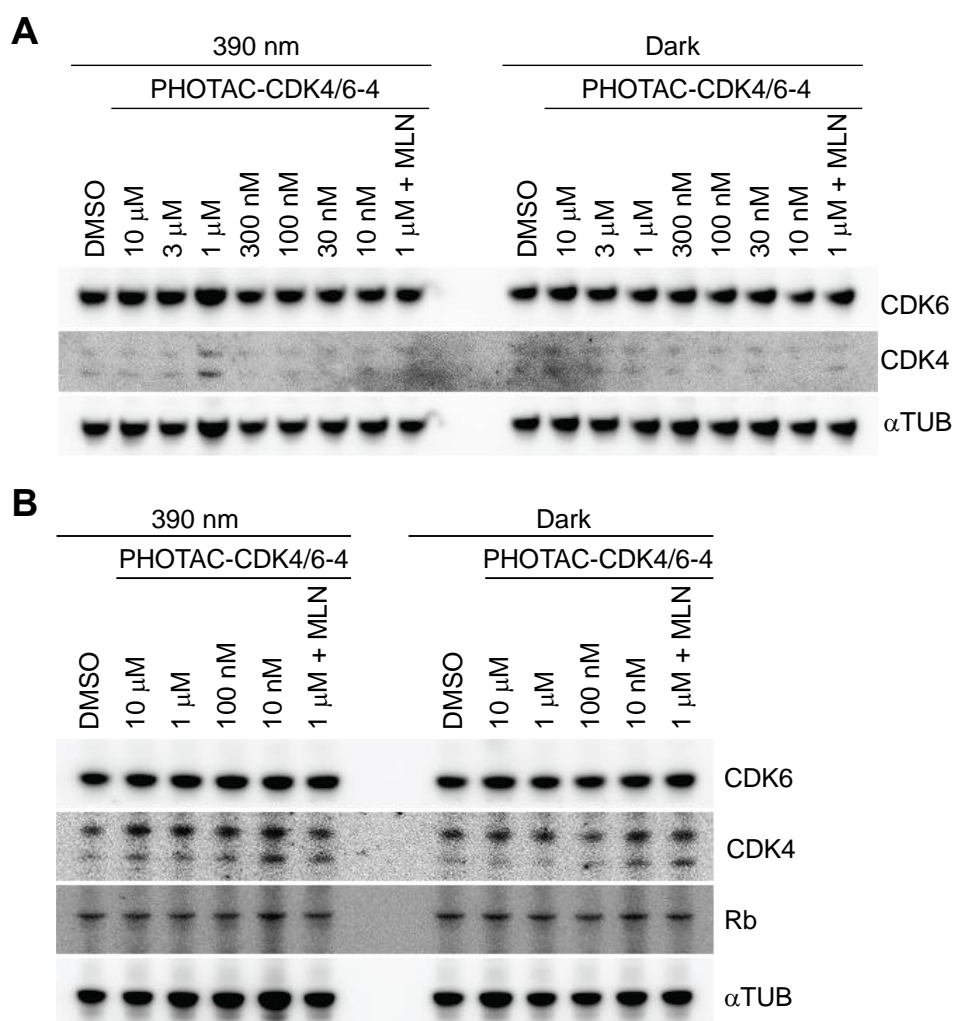


Figure 6.18: Immunoblot analysis of CDK4 and CDK6 levels. A) Western blot of RS4;11 cells treated with **PHOTAC-CDK4/6-4** for 4 h and either pulse irradiated with 390 nm light (left, 100 ms per 10 s) or kept in the dark (right). B) Western blot of MV4-11 cells treated with **PHOTAC-CDK4/6-4** for 4 h and either pulse irradiated with 390 nm light (left, 100 ms per 10 s) or kept in the dark (right).

To further investigate the activity of **PHOTAC-CDK4/6-4**, we monitored protein levels over 24 h (Figure 6.19A). Over the course of the experiment, we could not observe CDK6 degradation. CDK4 levels appeared to be slightly reduced over time both in the dark and upon pulsed 390 nm irradiation. We did however observe a decrease in Cyclin D3 levels for the first 12 h that was more pronounced upon irradiation with 390 nm. While Cyclin D3 as the binding partner of CDK4 and CDK6 could be recruited to the cereblon E3 ligase complex as well, we were unable to consistently observe Cyclin D3 degradation across all cell lines tested (Figure S6.3). We also performed a competition experiment by co-treatment of RS4;11 with 1 μ M **PHOTAC-CDK4/6-4** and a 10-fold excess of the parent ligands Lenalidomide and Ribociclib (Figure 6.19B).

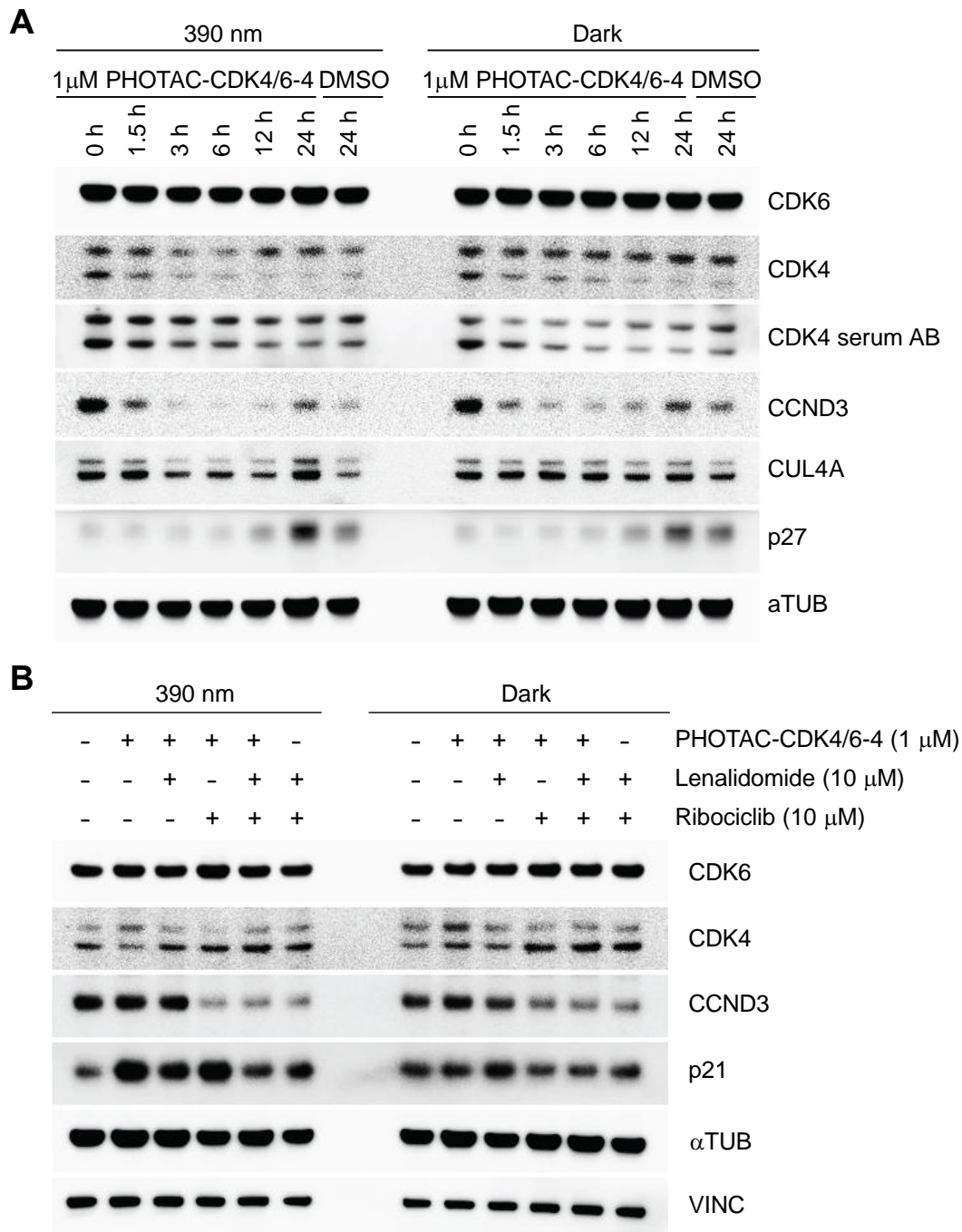


Figure 6.19: Immunoblot analysis of RS4;11 cells treated with **PHOTAC-CDK4/6-4**. A) Western blot of RS4;11 cells treated with **PHOTAC-CDK4/6-4** for the indicated times and either pulse irradiated with 390 nm light (left, 100 ms per 10 s) or kept in the dark (right). B) Competitive displacement of **PHOTAC-CDK4/6-4** analyzed by Western blot of RS4;11 cells treated for 6 h and either pulse irradiated with 390 nm light (left, 100 ms per 10 s) or kept in the dark (right).

Again, CDK6 levels were unaffected and CDK4 levels only slightly decreased upon PHOTAC treatment with 390 nm irradiation. Interestingly, treatments containing Ribociclib led to a very strong decrease of Cyclin D3 levels, linking inhibitory activity to

this reduction. When irradiated with 390 nm light, **PHOTAC-CDK4/6-4** led to increased p21 levels which remained elevated upon co-treatment with either Lenalidomide or Ribociclib but not with both.

Given the reliance of cells on CDK6, but not CDK4, the reduction in CDK4 levels is unlikely to explain the remarkable viability difference observed with **PHOTAC-CDK4/6-4**. Since the results of the viability assays clearly indicate a mechanism based on target protein degradation, but not inhibition, we continued our search for targets of **PHOTAC-CDK4/6-4**.

Ribociclib is described to be a very selective CDK4/6 inhibitor, however it still inhibits other kinases. Ribociclib has been reported to have low affinity for CDK9, CaMK2 $\beta/\gamma/\delta$ (calmodulin-dependent protein kinase II), QIK (Qin-induced kinase) and TNK1 (tyrosine kinase non receptor 1) *in vitro*.^[42] A second study reports AURKA, CaMK2 γ/δ , CDK9, FAK (focal adhesion kinase), FER (FER tyrosine kinase), GAK (cyclin-G-associated kinase) and TNK1 as off-targets of Ribociclib in lung cancer cells.^[16] CaMK2 γ/δ , CDK9, FAK, FER and TNK1 among many others were also observed as major off targets of Palbociclib.^[16] Even though kinases like AURKA were only weakly inhibited by Ribociclib, PROTACs can degrade targets even at low occupancy levels.^[24] In fact, from the set of Ribociclib off-targets, AURKA, CDK9, FER and GAK have been identified as highly degradable kinases when targeted by promiscuous kinase inhibitors.^[24]

Subsequently, we compared the off-targets with the results of two CRISPR-based screens of gene essentiality in AML cell lines to further narrow the number of potential targets of **PHOTAC-CDK4/6-4** that could result in the strong effect on cell viability we have observed.^[48,49] Apart from CDK6 and its binding partner Cyclin D3, AURKA, CDK9 and GAK were found to be essential in MV4-11 and MOLM13 cell lines.

Western blot analysis of RS4;11 and MV4-11 cells treated with **PHOTAC-CDK4/6-4** for 6 h did not show significant degradation of AURKA or CDK9 (Figure 6.20A, B). However, a strong increase of the CDK inhibitor p21 and a decrease in Cyclin D3 levels was observed in both cell lines when treated with **PHOTAC-CDK4/6-4** and light. Further, GAK levels appeared to be reduced in MV4-11 cells when treated with the

active PHOTAC (Figure 6.20B). GAK is needed for progression through mitosis and knockdown of GAK using siRNA causes cell-cycle arrest which could explain the observed effects of **PHOTAC-CDK4/6-4** on the cell cycle and on cell viability.^[50]

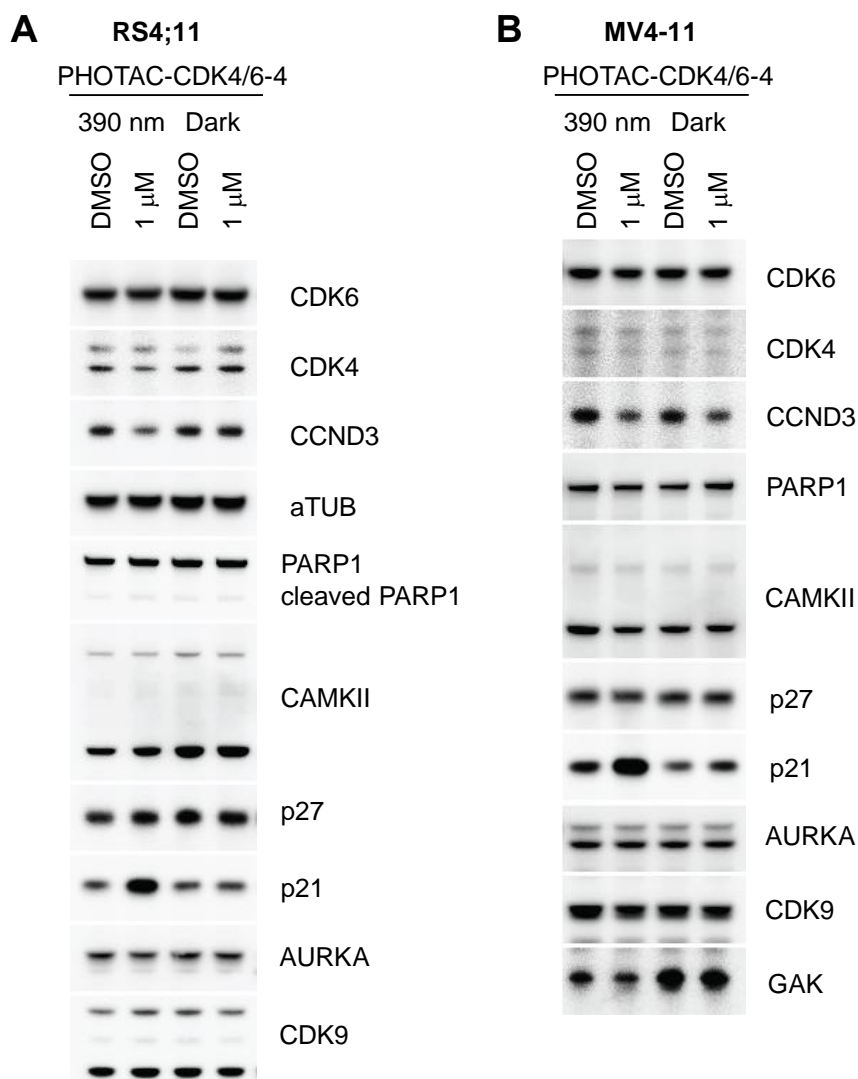


Figure 6.20: Immunoblot analysis of **PHOTAC-CDK4/6-4** targets. A), B) Western blot of A) RS4;11 or B) MV4-11 cells treated with **PHOTAC-CDK4/6-4** for 6 h and either pulse irradiated with 390 nm light (100 ms per 10 s) or kept in the dark.

Discussion and Outlook

Here we have demonstrated the optical control of cell cycle kinase abundance by extending our PHOTAC strategy to kinase inhibitors. This work further highlights the opportunities for PHOTACs targeting kinases and challenges involved in their design. Our PHOTACs targeting AURKA show a mechanistic difference in their effect on cell viability. In the dark **PHOTAC-AURKA-1** and **PHOTAC-AURKA-2** arrest cell viability and growth at 25% to 30% of the control. However, upon pulsed irradiation these PHOTACs induce cell death. This difference to the parent kinase inhibitor could be explained by an improved selectivity for AURKA, which can often be observed for PROTACs.^[26] Degradation of AURKA was still observed in the dark and further shortening of the linker connecting kinase inhibitor and photoswitch could hinder the formation of a productive ternary complex in the dark, thereby improving the phototherapeutic window.

The panCDK PHOTACs based on promiscuous CDK inhibitors outline the challenges and limitations of the PHOTAC approach as they show potent cytotoxicity in both the *E*- and *Z*-isomers. It is possible that different targets are degraded by the two isomers which both lead to potent cytotoxicity, resulting in a similar effect on viability. The generation of PHOTACs requires optimization of the *E*-isomer to be unable to induce a ternary complex and at the same time optimization of the *Z*-isomer for improved potency. This balancing act on the same molecule can succeed on a single target or on a highly homologous family of target proteins but is increasingly difficult to manage with an increasing number of targets.

A similar observation was made for **PHOTAC-CDK4/6-1–3** based on Palbociclib, which lead to decreased cell viability in both in the presence or absence of light. However, changing the targeting ligand to the more selective kinase inhibitor Ribociclib greatly improve the light-response of this system.^[16,42] **PHOTAC-CDK4/6-4** showed an unprecedented phototherapeutic window spanning over three orders of magnitude without strongly affecting viability at the highest concentration tested in the dark. When activated with light, the effect of **PHOTAC-CDK4/6-4** on RS4;11, MV4-11 and MOLM13 leukemia cell viability surpassed that of the parent inhibitor, highlighting the potency of PROTACs and PHOTACs. In contrast, a much lower effect on cell viability was observed in the dark when compared to the parent inhibitor which emphasizes the

improved safety profile **PHOTAC-CDK4/6-4** can offer. In part, the lack of activity in the dark can be explained by the hook-effect. By saturating both binding partners of the ternary complex at high concentrations, **PHOTAC-CDK4/6-4** is unable to form a ternary complex to induce protein degradation. This mechanistic difference presents an advantage over classical photoswitchable inhibitors that may overcome low target affinity and occupy a binding site at very high concentrations.

Surprisingly, **PHOTAC-CDK4/6-4** did not significantly degrade CDK6 and the observed reduction in CDK4 levels could not explain the potency of this PHOTACs. CDK4 knockdown in the used MLL cell lines has no or only marginal effect on their viability. To uncover the target of light-controlled **PHOTAC-CDK4/6-4**-mediated protein degradation, we analyzed the off-targets of Ribociclib. Out of those, AURKA, CDK9 and GAK are prone to degradation and would be able to explain the efficacy of **PHOTAC-CDK4/6-4**.^[24] While both AURKA or CDK9 degradation could explain the lowered cyclin D3 levels, we did not observed their degradation.^[51–53] This leaves GAK a likely target of **PHOTAC-CDK4/6-4**.

Systemic or tissue specific knockouts of GAK are lethal and GAK knockdown induces cell cycle arrest.^[50,54,55] Immunoblot analysis of MV4;11 cells showed a reduction in GAK levels after treatment with activated **PHOTAC-CDK4/6-4**. Off-target activity of kinase inhibitors such as gefitinib on GAK has been proposed as the cause of undesired side-effects.^[55–57] Spatiotemporal control of GAK degradation enabled by PHOTACs could circumvent the limitations of GAK inhibitors and degraders and enable therapeutic targeting of GAK.

Normally, drugs can be turned into photopharmaceuticals by identifying isosteres of azobenzene.^[58] Given the selectivity of **PHOTAC-CDK4/6-4** for leukemia cell lines susceptible to cereblon-based PROTACs, the inverse conversion of an azobenzene into a *Z*-stilbene may be of interest as therapeutic strategy in AML.

In summary, we believe that PHOTACs present a versatile platform to control kinase abundance on demand in native systems by using light as an orthogonal stimulus. Additionally, PHOTACs targeting cell cycle kinases hold promise as light-controlled drugs in photomedicine to treat diseases characterized by unregulated proliferation.

Supporting Information

Supporting Figures

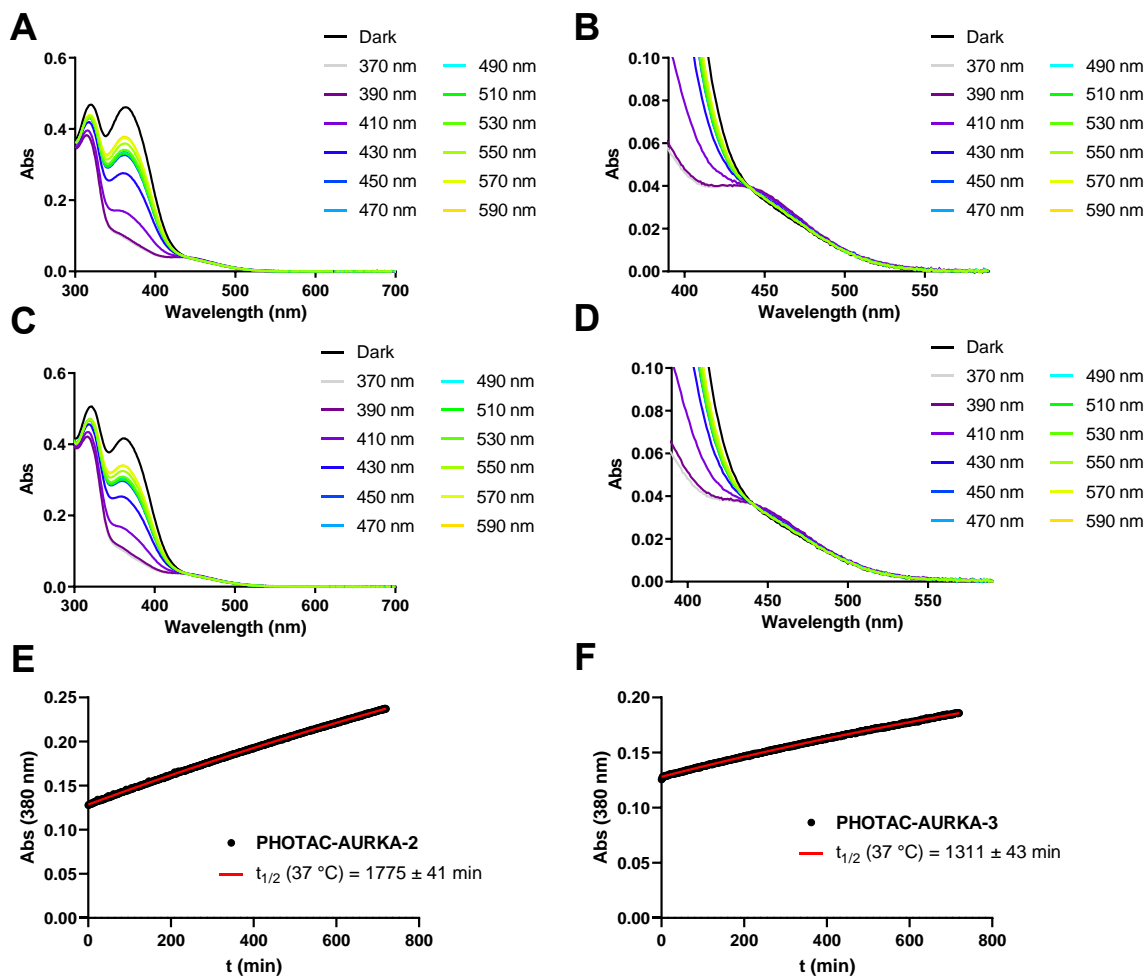


Figure S6.1: Photophysical characterization of **PHOTAC-AURKA-2+3**. Absorption spectra of A), B) **PHOTAC-AURKA-2** or C), D) **PHOTAC-AURKA-3** after irradiation with the indicated wavelength for 5 min. Thermal Z-to-E isomerization of E) **PHOTAC-AURKA-2** or F) **PHOTAC-AURKA-3** at 37 °C in a 1:1 DMSO:PBS (pH 7.4) mixture.

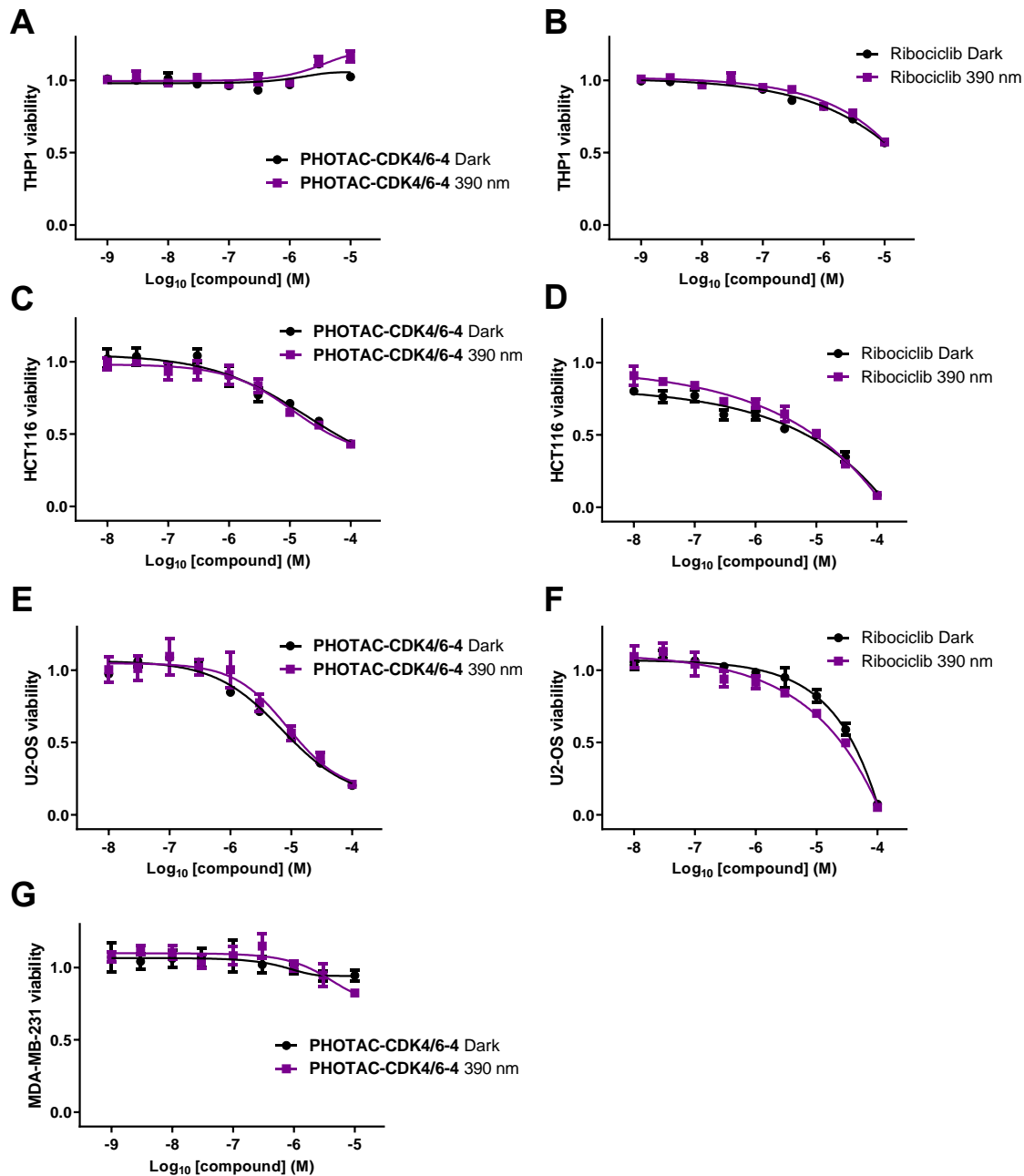


Figure S6.2: Effects of **PHOTAC-CDK4/6-4** on cell viability. Viability of A), B) THP1 cells after treatment with A) **PHOTAC-CDK4/6-4** or B) Ribociclib for 72 h in the dark or with pulsed 390 nm irradiation (100 ms every 10 s). C), D) Viability of HCT116 cells after treatment with C) **PHOTAC-CDK4/6-4** or D) Ribociclib for 72 h in the dark or with pulsed 390 nm irradiation (100 ms every 10 s). E), F) Viability of U2-OS cells after treatment with E) **PHOTAC-CDK4/6-4** or F) Ribociclib for 72 h in the dark or with pulsed 390 nm irradiation (100 ms every 10 s). G) Viability of MDA-MB-231 cells after treatment with **PHOTAC-CDK4/6-4** for 72 h in the dark or with pulsed 390 nm irradiation (100 ms every 10 s). Viability normalized to vehicle control containing 1% DMSO in the medium.

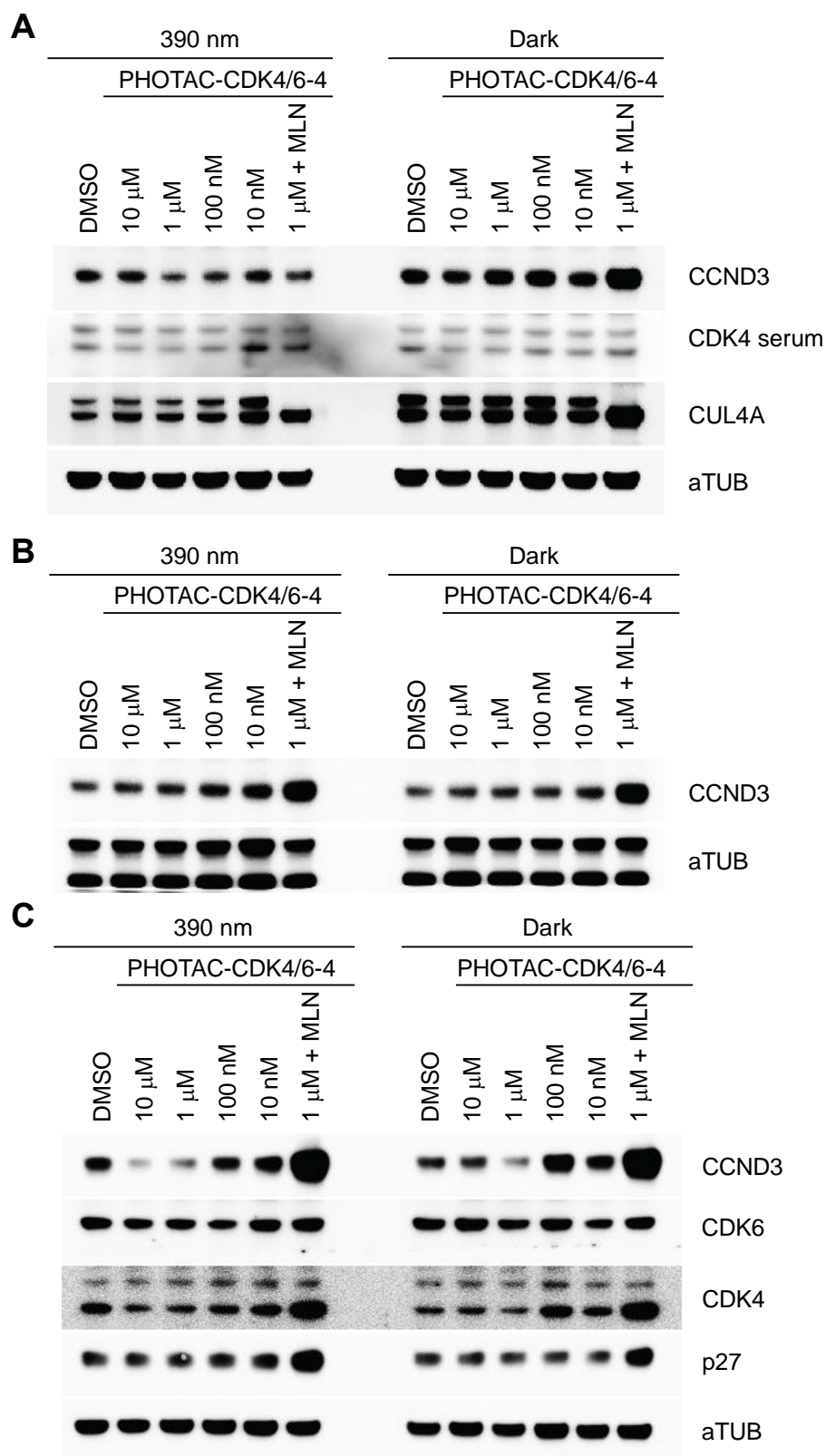


Figure S6.3: Immunoblot analysis of CCND3 levels after **PHOTAC-CDK4/6-4** treatment. Western blot of A) RS4;11, B) MV4-11 or C) MCF7 cells treated with **PHOTAC-CDK4/6-4** for 24 h and either pulse irradiated with 390 nm light (left, 100 ms per 10 s) or kept in the dark (right).

Methods

Determination of Photophysical properties

UV-Vis spectrometry was performed on a Varian Cary 60 UV-Visible Spectrophotometer using BRAND UV-Cuvette Disposable Spectrophotometer/Photometer Ultra-Micro Cuvettes, BrandTech (10 mm light path). Temperature was controlled using an Agilent Technologies PCB 1500 Water Peltier system and samples were irradiated with a Cairn Research Optoscan Monochromator with Optosource High Intensity Arc Lamp equipped with a 75 W UXL-S50A lamp from USHIO Inc. Japan and set to 15 nm full width at half maximum. Samples were stored and prepared under red light to avoid formation of the *Z*-isomers. Special attention was given to **PHOTAC-CDK4/6-4** to avoid light exposure and *Z*-isomer generation. 10 mM stock solutions were prepared in the dark and diluted to a final concentration of 25 μ M to measure the UV-VIS spectra of **PHOTACs** following irradiation with different wavelengths for 5 min using the monochromator. Measurement was started from the dark-adapted state, followed by 370 nm and further stepwise wavelength increase up to 600 nm. By increasing the wavelength from low to high *Z*- to *E*-isomerization can be observed, whereas going the reverse direction from high to low wavelength, the PSS might not be reached due to low absorptivity above 500 nm. Generally, due to the limited intensity and spectral width of the monochromator, slightly different PSSs could be generated with a true monochromatic, high-intensity light source. Spectra were recorded in DMSO to avoid any artifacts of aggregation or precipitation.

Thermal relaxation was measured by preirradiating **PHOTACs** with 390 nm light and recording the absorption at 380 nm wavelength over 12 h at 37 °C in DMSO or DMSO-PBS (pH 7.4) mixtures in tightly sealed cuvettes. Half-lives were determined by nonlinear regression using GraphPad Prism Version 9.02.

Separated spectra of the *Z*- and *E*-isomers were obtained from the internal UV-VIS detector of the LCMS by irradiating the sample before injection and were normalized at the isosbestic point. Isomer ratios were calculated in the region of largest absorption difference between 330 and 390 nm from the separated spectra obtained by LCMS and the spectra obtained following irradiation with different wavelengths for 5 min, normalized at the isosbestic point.

LED illumination

For illumination of the cells we used the cell disco system as previously described in the literature.^[28] 5 mm LEDs 390 nm (VL390-5-15) and 565 nm (LED565-03U) were purchased from Roithner Lasertechnik. Pulsed irradiation was performed using 100 ms pulses every 10 s (unless indicated otherwise) in 96- or 6-well plates on top of a plate with 24 5 mm LEDs, controlled by an Arduino system.

Cell culture

The human acute lymphoblastic leukemia RS4;11 (ATCC[®] CRL1873[™]) cell line was purchased from the American Type Culture Collection (ATCC). MV-4-11 (ATCC[®] CRL-9591[™]) cells were obtained from the ATCC. MOLM13-Cas9 and THP-1 cells were a generous donation from the Aifantis lab. Leukemia cells were incubated in phenol red-free RPMI1640 medium (Gibco) with 10% fetal bovine serum (FBS) and 1% penicillin/ streptomycin (PS) in a humidified incubator at 37 °C with 5% CO₂ in air. HCT-116, U2-OS, MDA-MB-231 and MCF-7 cells were gifted by the Pagano lab and originally purchased from the ATCC. Cells were cultured in a humidified incubator at 37 °C with 5% CO₂ in air in their recommended media (phenol red free) supplemented with 10% fetal bovine serum (FBS) and 1% penicillin/ streptomycin (PS).

For the experiments compounds were serially diluted in phenol red-free medium (Gibco) as 2x stock solutions resulting in a final concentration of 1% DMSO during the assay. Azobenzene stocks and dilutions were strictly kept in the dark and prepared under red light conditions.

Colorimetric MTS Assays

The activity of dehydrogenase enzymes in metabolically active cells, as a quantitative measurement for cytotoxicity and proliferation, was determined by colorimetric measurement of the reduction of [3-(4,5-dimethylthiazol-2-yl)-5-(3-carboxymethoxyphenyl)-2-(4-sulfophenyl)-2H-tetrazolium (MTS) to the formazan product. Cells were treated with different concentrations of PHOTACs prepared by serial dilution in triplicates using 1% DMSO as cosolvent, and incubated in a 96-well plate for 72 h. The cells were placed in light-proof boxes and exposed to the lighting conditions specified in the experiment for 72 h. Next, 10 μ L of Promega CellTiter 96[®] AQueous One Solution Reagent was added to each well and incubated for further 4-

7 hours at 37 °C. The absorbance at 500 nm was measured on a FLUOstar Omega 96-well plate reader (BMG Labtech).

Data was analyzed using GraphPad Prism Version 9.02 (GraphPad Software Inc) and fitted using the [Inhibitor] vs. response -- Variable slope (four parameters) fit. Results represent the mean viability \pm SEM relative to the 1% DMSO treated control.

Immunoblotting Analysis

For immunoblotting analysis, cells (2×10^6 cells for RS4;11, MV4-11, MOLM13, THP1; or adherent cells at 30-35% confluency seeded 24 h prior to the experiment) were incubated for the indicated times with PHOTACs. After incubation, cells were collected in the dark by centrifugation (200 g, 5 min) at 4 °C and the pellets were washed twice with ice cold PBS (1 mL).

Cells were lysed in RIPA buffer containing protease and phosphatase inhibitors (cOmplete™, Mini Protease Inhibitor Cocktail, SigmaAldrich, 4693124001 and Phosphatase Inhibitor Cocktail 3, SigmaAldrich, P0044-1ML) and protein concentration was determined using the BCA method (Thermo Fisher, 23225). Immunoblotting was performed as previously described.^[13,29] Briefly, samples were resolved under denaturing and reducing conditions using 4%–12% Bis-Tris gels (NuPAGE) and transferred to a PDVF membrane (Immobilon-P, Millipore). Membranes were blocked with 5% nonfat dried milk, incubated with primary antibodies overnight at 4°C. After washing the membranes, secondary antibodies coupled with horseradish peroxidase were applied. Immunoreactive bands were visualized using SuperSignal™ Western Blot Enhancer or SuperSignal™ West Femto Maximum Sensitivity Substrate (Thermo Fisher Scientific) and the signal was acquired using an ImageQuant LAS 400 (GE).

The following antibodies were used:

Antibodies	Source	Identifier
AURKA	Cell Signaling Technology	3092
CaMKII	Cell Signaling Technology	3362
CCND3	Thermo Fisher Scientific	MA5-12717
CDK4	Santa Cruz Biotechnology	sc-56277
CDK4 serum	Pagano laboratory	N/A
CDK6	Santa Cruz Biotechnology	sc-53638
CDK9	Cell Signaling Technology	2316
CUL4A	Bethyl Laboratories	A300-739A
GAK	Biotechnne	MAB6918-SP
p21	Cell Signaling Technology	2947
p27	BD Biosciences	610241
PARP1	Cell Signaling Technology	9542S
PCNA	dako	M0879
α TUBULIN	Sigma Aldrich	T6074
Rb	Cell Signaling Technology	9313S
pRb	Cell Signaling Technology	8180S
VINC	Bethyl Laboratories	A302-535A
anti-Rabbit IgG, peroxidase-linked antibody	Thermo Fisher	NA934
anti-Mouse IgG, peroxidase-linked antibody	Thermo Fisher	NA931
anti-goat IgG-HRP	Santa Cruz Biotechnology	sc-2354

Synthetic procedures

General information

The reagents and solvents used in this study were bought from the following chemical suppliers: Acros Organics, Alfa Aesar, Combi-Blocks, Oakwood, OxChem, Sigma-Aldrich, Toronto Research Chemicals and Medkoo Biosciences and were used as purchased.

Dry solvents used in reactions performed under inert atmosphere were obtained by passing the degassed solvents through activated alumina columns. Additionally, dry solvents were stored over molecular sieves under an inert atmosphere.

Column chromatography was carried out on silica gel (60 Å pore size, 40–63 µm, Merck KGaA) using a Teledyne Isco Combiflash EZprep flash purification system.

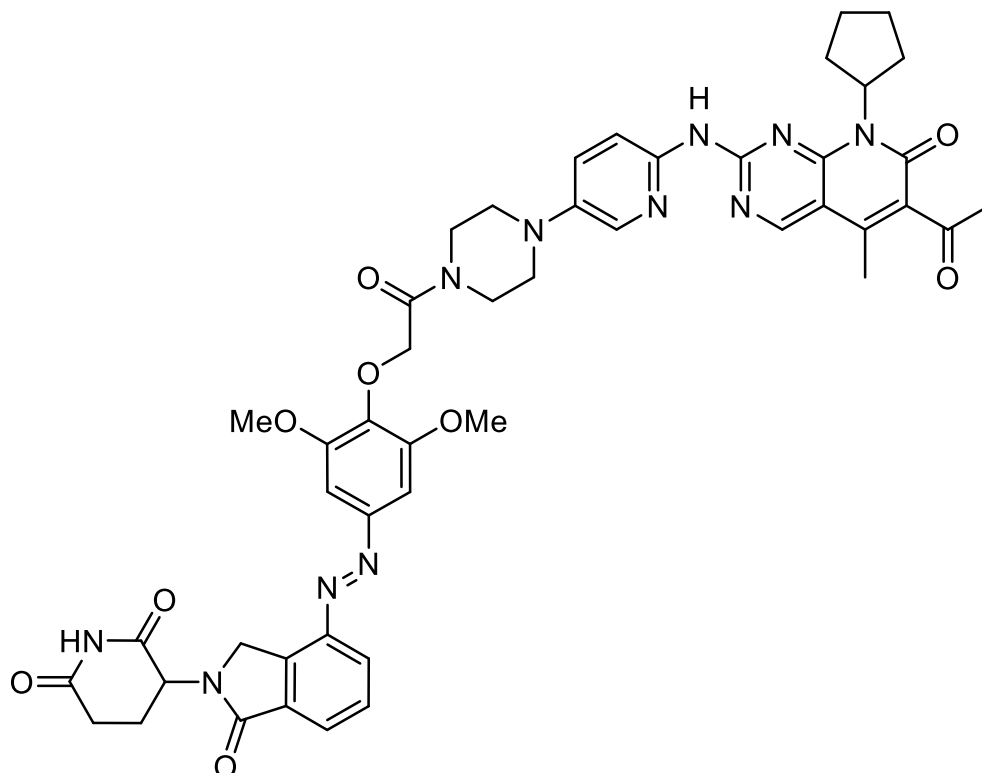
Thin-layer chromatography (TLC) was performed on glass plates precoated with silica gel (0.25 mm, 60-Å pore size, Merck). TLC plates were visualized by exposure to UV light (254 and 366 nm).

NMR spectra were obtained on a Bruker Avance III HD 400 MHz spectrometer equipped with a CryoProbe™ operating at 400 MHz for ¹H and 100 MHz for ¹³C spectra or on a Bruker AVIII-600 High Performance Digital NMR Spectrometer (600 MHz for ¹H and 150 MHz for ¹³C spectra) with CPTCI-cryoprobehead. Integration results and multiplets are reported as observed and denoted as follows: s (singlet), d (doublet), t (triplet), q (quartet), p (pentet), h (hextet), sept (septet), and m (multiplet) and as combinations thereof.

High-resolution mass spectra (HRMS) were recorded on an Agilent Technologies 6224 Accurate-Mass time-of-flight spectrometer with atmospheric pressure chemical ionization (APCI) source.

LCMS were measured on an Agilent Technologies 1260 II Infinity connected to an Agilent Technologies 6120 Quadrupole mass spectrometer with APCI ionization source. Elution was performed using a gradient from 5:95% to 100:0% MeCN:H₂O with 0.1% formic acid over 5 min, if not indicated otherwise. Separated isomer spectra of azobenzenes were obtained by irradiation of the LCMS sample prior to injection.

(E)-3-(4-((4-(2-(4-(6-((6-acetyl-8-cyclopentyl-5-methyl-7-oxo-7,8-dihydropyrido[2,3-d]pyrimidin-2-yl)amino)pyridin-3-yl)piperazin-1-yl)-2-oxoethoxy)-3,5-dimethoxyphenyl)diazenyl)-1-oxoisoindolin-2-yl)piperidine-2,6-dione (PHOTAC-CDK4/6-3)



(E)-2-(4-((2-(2,6-dioxopiperidin-3-yl)-1-oxoisoindolin-4-yl)diazenyl)-2,6-dimethoxyphenoxy)acetic acid (20.0 mg, 0.039 mmol, 1.0 eq.) was prepared as previously described^[27] and combined with Palbociclib (35.3 mg, 0.079 mmol, 2 eq.) and HATU (27.0 mg, 0.071 mmol, 1.8 eq.) under nitrogen atmosphere in a dried round bottom flask. The solids were dissolved in dry DMF (1.5 mL), followed by addition of *i*-Pr₂NEt (25.4 mg, 0.197 mmol, 5 eq., 0.034 mL) and the reaction was stirred for 16 h at room temperature. The reaction mixture was diluted with a 5:1 CH₂Cl₂:*i*PrOH mixture (25 mL) and separated against 10% LiCl (aq., 30 mL). The organic phase was washed with saturated NaHCO₃ (30 mL), 10% LiCl (25 mL) and brine (2x 25 mL), dried over Na₂SO₄ and concentrated under reduced pressure. Purification of the resulting crude product by flash column chromatography (CH₂Cl₂/MeOH gradient, 0 to 20% MeOH) gave **PHOTAC-CDK4/6-3** (33.0 mg, 0.036 mmol, 92%) as a yellow solid.

$R_f = 0.42$ [CH₂Cl₂:MeOH, 19:1].

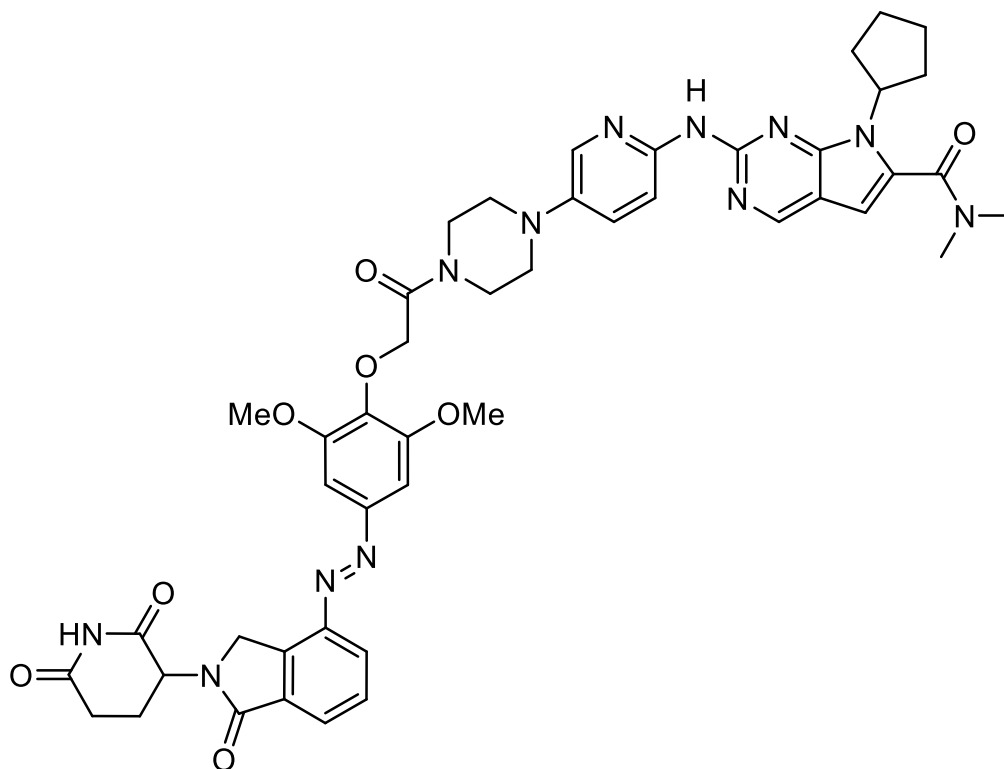
¹H NMR (600 MHz, DMSO-*d*₆) $\delta = 11.04$ (s, 1H), 8.98 (s, 1H), 8.23 (d, *J* = 7.8 Hz, 1H), 8.12 (dd, *J* = 13.7, 3.0 Hz, 1H), 7.95 – 7.86 (m, 2H), 7.81 (t, *J* = 7.7 Hz, 1H), 7.67 –

7.59 (m, 1H), 7.35 (s, 2H), 5.84 (p, J = 8.9 Hz, 1H), 5.17 (dd, J = 13.3, 5.1 Hz, 1H), 4.83 (d, J = 19.0 Hz, 1H), 4.72 (s, 2H), 4.71 (d, J = 17.6 Hz, 1H), 3.93 (s, 6H), 3.82 (t, J = 4.8 Hz, 2H), 3.67 (t, J = 5.2 Hz, 2H), 3.29 (t, J = 5.2 Hz, 2H), 3.21 (t, J = 5.3 Hz, 2H), 2.97 – 2.92 (m, 1H), 2.68 – 2.61 (m, 1H), 2.59 – 2.52 (m, 1H), 2.43 (s, 3H), 2.33 (s, 3H), 2.29 – 2.22 (m, 2H), 2.11 – 2.04 (m, 1H), 1.94 – 1.88 (m, 2H), 1.82 – 1.77 (m, 2H), 1.63 – 1.56 (m, 2H) ppm.

¹³C NMR (150 MHz, DMSO) δ = 202.40, 172.92, 171.01, 167.16, 165.77, 160.69, 158.28, 158.03, 154.78, 153.15, 148.27, 146.38, 144.38, 143.14, 141.97, 139.02, 135.06, 134.52, 133.83, 129.64, 129.59, 128.58, 126.32, 125.44, 115.35, 106.95, 100.60, 70.98, 56.32, 52.93, 51.85, 48.30, 48.30, 47.92, 44.43, 40.92, 31.31, 31.28, 27.59, 27.57, 25.17, 25.15, 22.31, 13.67 ppm.

HRMS (APCI):	calcd. for C ₄₇ H ₅₀ N ₁₁ O ₉ ⁺ :	912.3787 m/z [M+H] ⁺
	found:	912.3788 m/z [M+H] ⁺ .
LCMS (ESI):	t _{ret} = 3.64 min (<i>E</i>).	912 m/z [M+H] ⁺ .

(E)-7-cyclopentyl-2-((5-(4-(2-(4-((2-(2,6-dioxopiperidin-3-yl)-1-oxoisoindolin-4-yl)diazenyl)-2,6-dimethoxyphenoxy)acetyl)piperazin-1-yl)pyridin-2-yl)amino)-N,N-dimethyl-7H-pyrrolo[2,3-d]pyrimidine-6-carboxamide (PHOTAC-CDK4/6-4)



(E)-2-(4-((2-(2,6-dioxopiperidin-3-yl)-1-oxoisoindolin-4-yl)diazenyl)-2,6-dimethoxyphenoxy)acetic acid (16.0 mg, 0.032 mmol, 1.0 eq.) was prepared as previously described^[27] and combined with Ribociclib (13.7 mg, 0.032 mmol, 1 eq.) and HATU (14.4 mg, 0.038 mmol, 1.2 eq.) under nitrogen atmosphere in a dried round bottom flask. The solids were dissolved in dry DMF (1.1 mL), followed by addition of *i*-Pr₂NEt (20.4 mg, 0.158 mmol, 5 eq., 0.027 mL) and the reaction was stirred for 18 h at room temperature and protected from ambient light. The following work-up and purification was also performed under dim light to prevent formation of the *Z*-isomer. The reaction mixture was diluted with a 5:1 CH₂Cl₂:*i*PrOH mixture (20 mL) and separated against 10% LiCl (aq., 20 mL). The organic phase was washed with saturated NaHCO₃ (40 mL), 10% LiCl (20 mL) and brine (2x 20 mL), dried over Na₂SO₄ and concentrated under reduced pressure. Purification of the resulting crude product by flash column chromatography (CH₂Cl₂/MeOH gradient, 0 to 20% MeOH) gave **PHOTAC-CDK4/6-3** (23.3 mg, 0.026 mmol, 82%) as a yellow solid.

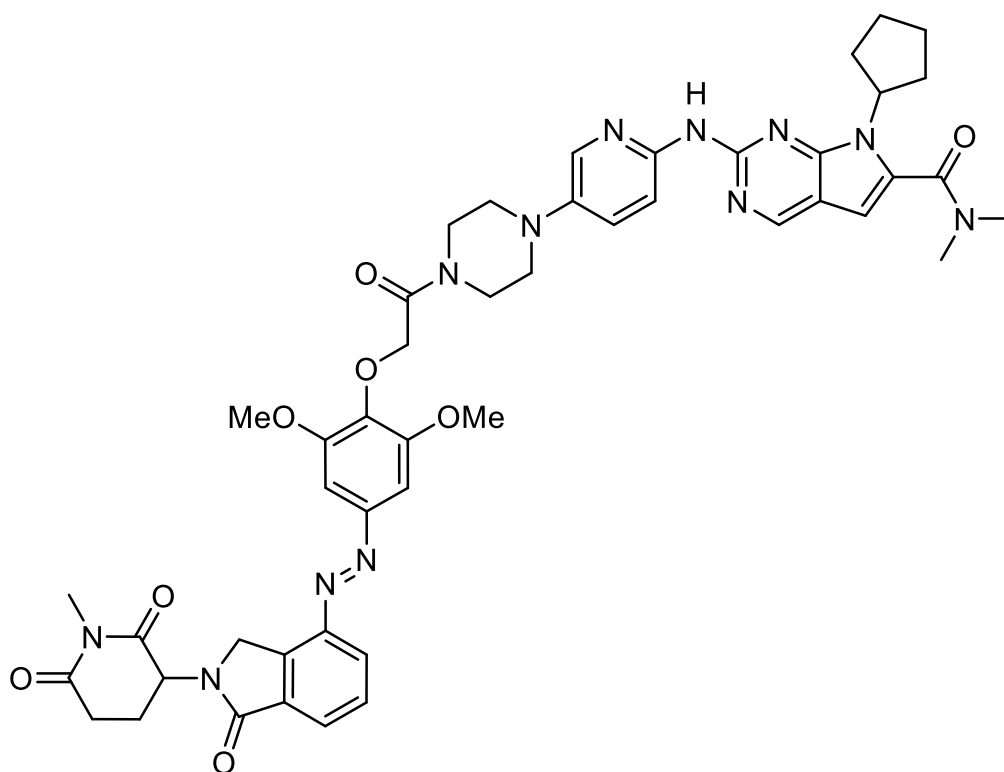
$R_f = 0.24$ [$\text{CH}_2\text{Cl}_2:\text{MeOH}, 20:1$].

^1H NMR (400 MHz, $\text{DMSO}-d_6$) $\delta = 11.03$ (s, 1H), 8.80 (s, 1H), 8.22 (dd, $J = 7.8, 1.1$ Hz, 1H), 8.07 (s, 1H), 8.03 (d, $J = 2.9$ Hz, 1H), 7.92 (dd, $J = 7.5, 1.0$ Hz, 1H), 7.80 (t, $J = 7.7$ Hz, 1H), 7.65 – 7.57 (m, 1H), 7.34 (s, 2H), 6.64 (s, 1H), 5.16 (dd, $J = 13.2, 5.1$ Hz, 1H), 4.86 – 4.66 (m, 5H), 3.93 (s, 6H), 3.80 (t, $J = 5.1$ Hz, 2H), 3.66 (t, $J = 5.0$ Hz, 2H), 3.23 (t, $J = 4.7$ Hz, 2H), 3.16 (t, $J = 4.9$ Hz, 2H), 3.05 (s, 6H), 2.94 (ddd, $J = 17.1, 13.5, 5.4$ Hz, 1H), 2.63 (dt, $J = 18.6, 3.2$ Hz, 1H), 2.58 – 2.52 (m, 1H), 2.46 – 2.37 (m, 2H), 2.12 – 1.93 (m, 5H), 1.66 (ddd, $J = 12.5, 9.6, 5.6$ Hz, 2H) ppm.

^{13}C NMR (100 MHz, DMSO) $\delta = 172.91, 171.01, 167.16, 165.75, 162.76, 154.24, 153.15, 151.30, 151.25, 148.27, 146.38, 146.06, 142.03, 139.04, 136.56, 134.52, 133.83, 132.29, 129.64, 128.57, 126.57, 125.44, 113.05, 112.22, 100.66, 100.61, 70.98, 56.94, 56.33, 51.85, 49.21, 48.78, 48.30, 44.53, 41.02, 38.66, 34.62, 31.28, 29.80, 24.21, 22.31$ ppm.

HRMS (APCI):	calcd. for $\text{C}_{46}\text{H}_{50}\text{N}_{12}\text{O}_8^+$:	898.3875 m/z $[\text{M}]^+$
	found:	898.3844 m/z $[\text{M}]^+$.
LCMS (ESI):	$t_{\text{ret}} = 3.13$ min (<i>Z</i>).	899 m/z $[\text{M}+\text{H}]^+$.
	$t_{\text{ret}} = 3.36$ min (<i>E</i>).	899 m/z $[\text{M}+\text{H}]^+$.

(E)-7-cyclopentyl-2-((5-(4-(2-(2,6-dimethoxy-4-((2-(1-methyl-2,6-dioxopiperidin-3-yl)-1-oxoisoindolin-4-yl)diazenyl)phenoxy)acetyl)piperazin-1-yl)pyridin-2-yl)amino)-N,N-dimethyl-7H-pyrrolo[2,3-d]pyrimidine-6-carboxamide (Me-PHOTAC-CDK4/6-4)



PHOTAC-CDK4/6-4 (18.0 mg, 0.020 mmol, 1.0 eq.) and Cs_2CO_3 (13.0 mg, 0.040 mmol, 2.0 eq.) were added to a dry glass vial under nitrogen atmosphere and suspended in dry DMF (1 mL). 0.05 mL (1.2 eq.) of a methyl iodide solution in dry DMF (341 mg, 2.40 mmol, 0.150 mL methyl iodide in 5 mL DMF) was added. The reaction was stirred for 4 h and protected from ambient light. Next, the mixture was diluted with a 5:1 CH_2Cl_2 :iPrOH mixture (20 mL) and separated against 10% LiCl (aq., 20 mL). The organic phase was washed with saturated NaHCO_3 (30 mL), 10% LiCl (20 mL) and brine (2x 20 mL), dried over Na_2SO_4 and concentrated under reduced pressure. Purification of the resulting crude product by flash column chromatography (CH_2Cl_2 /MeOH gradient, 0 to 20% MeOH) gave **Me-PHOTAC-CDK4/6-4** (14.3 mg, 0.016 mmol, 78%) as a yellow solid.

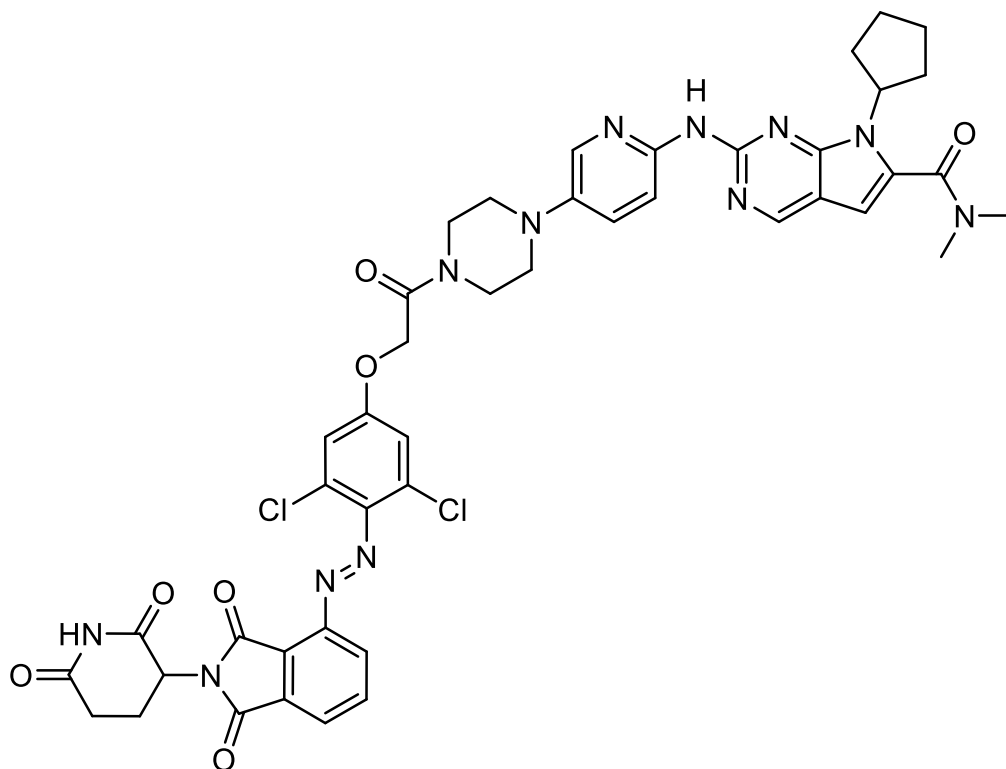
$R_f = 0.30$ [$\text{CH}_2\text{Cl}_2:\text{MeOH}, 19:1$].

$^1\text{H NMR}$ (600 MHz, $\text{DMSO}-d_6$) $\delta = 8.80$ (s, 1H), 8.21 (dd, $J = 6.8$ Hz, 1H), 8.14 – 8.00 (m, 2H), 7.93 (q, $J = 6.6$ Hz, 1H), 7.81 (t, $J = 11.5$ Hz, 1H), 7.59 (s, 1H), 7.34 (s, 2H), 6.63 (s, 1H), 5.22 (dd, $J = 13.1, 6.6$ Hz, 1H), 4.88 – 4.66 (m, 5H), 3.92 (s, 6H), 3.80 (s, 2H), 3.66 (s, 2H), 3.23 (s, 2H), 3.15 (s, 2H), 3.09 – 2.98 (m, 10H), 2.83 – 2.75 (m, 1H), 2.54 (m, 1H), 2.46 – 2.37 (m, 2H), 2.12 – 2.05 (m, 1H), 2.03 – 1.93 (m, 4H), 1.69 – 1.60 (m, 2H) ppm.

$^{13}\text{C NMR}$ (150 MHz, DMSO) $\delta = 171.94, 170.65, 167.21, 165.74, 162.78, 154.17, 153.14, 151.53, 151.24, 148.26, 146.42, 146.15, 142.03, 139.06, 136.48, 134.68, 133.82, 132.34, 129.66, 128.34, 126.31, 125.47, 112.98, 112.16, 100.73, 100.64, 70.97, 56.94, 56.34, 52.37, 49.24, 48.82, 48.25, 44.54, 41.02, 38.81, 34.59, 31.42, 29.79, 26.64, 24.22, 21.59$ ppm.

HRMS (APCI):	calcd. for $\text{C}_{47}\text{H}_{53}\text{N}_{12}\text{O}_8^+$:	913.4104 m/z $[\text{M}+\text{H}]^+$
	found:	913.4073 m/z $[\text{M}+\text{H}]^+$.
LCMS (ESI):	$t_{\text{ret}} = 3.08$ min (<i>Z</i>).	913 m/z $[\text{M}+\text{H}]^+$.
	$t_{\text{ret}} = 3.23$ min (<i>E</i>).	913 m/z $[\text{M}+\text{H}]^+$.

(E)-7-cyclopentyl-2-((5-(4-(2-(3,5-dichloro-4-((2-(2,6-dioxopiperidin-3-yl)-1,3-dioxoisoindolin-4-yl)diazenyl)phenoxy)acetyl)piperazin-1-yl)pyridin-2-yl)amino)-N,N-dimethyl-7H-pyrrolo[2,3-d]pyrimidine-6-carboxamide (PHOTAC-CDK4/6-5)



(E)-2-(3,5-dichloro-4-((2-(2,6-dioxopiperidin-3-yl)-1,3-dioxoisoindolin-4-yl)diazenyl)-phenoxy)acetic acid (20.0 mg, 0.034 mmol, 1.0 eq.) was prepared as previously described (Chapter 3) and combined with Ribociclib (14.7 mg, 0.034 mmol, 1 eq.) and HATU (15.4 mg, 0.041 mmol, 1.2 eq.) under nitrogen atmosphere in a dried round bottom flask. The solids were dissolved in dry DMF (1.1 mL), followed by addition of *i*-Pr₂NEt (21.9 mg, 0.169 mmol, 5 eq., 0.029 mL) and the reaction was stirred for 18 h at room temperature and protected from ambient light. The following work-up and purification was also performed under dim light to prevent formation of the *Z*-isomer. The reaction mixture was diluted with a 5:1 CH₂Cl₂:*i*PrOH mixture (20 mL) and separated against 10% LiCl (aq., 30 mL). The organic phase was washed with saturated NaHCO₃ (40 mL) and brine (2x 20 mL), dried over Na₂SO₄ and concentrated under reduced pressure. Purification of the resulting crude product by flash column chromatography (CH₂Cl₂/MeOH gradient, 0 to 20% MeOH) gave **PHOTAC-CDK4/6-5** (24.3 mg, 0.026 mmol, 78%) as a yellow solid.

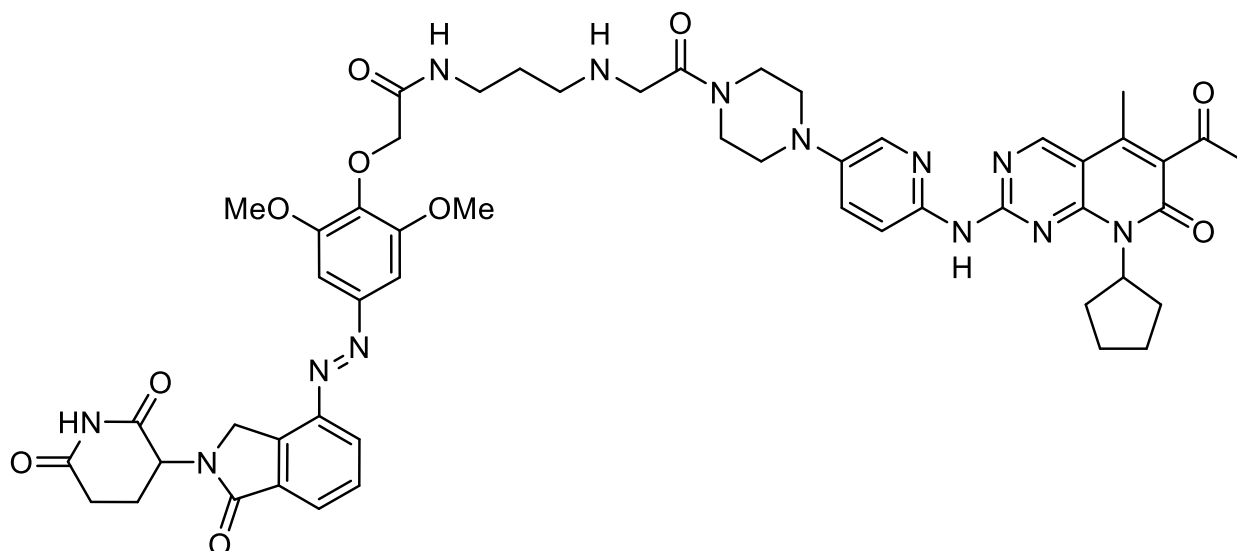
$R_f = 0.13$ [$\text{CH}_2\text{Cl}_2:\text{MeOH}, 19:1$].

^1H NMR (600 MHz, $\text{DMSO-}d_6$) $\delta = 11.15$ (s, 1H), 8.78 (s, 1H), 8.17 – 8.10 (m, 2H), 8.07 – 8.02 (m, 2H), 7.85 (d, $J = 8.0$ Hz, 1H), 7.55 (s, 1H), 7.37 (s, 2H), 6.62 (s, 1H), 5.21 (dd, $J = 12.8, 5.5$ Hz, 1H), 5.16 (s, 2H), 4.74 (p, $J = 8.9$ Hz, 1H), 3.69 – 3.60 (m, 4H), 3.23 (t, $J = 5.1$ Hz, 2H), 3.14 (t, $J = 5.1$ Hz, 2H), 3.09 – 3.02 (m, 6H), 2.90 (ddd, $J = 17.1, 13.8, 5.5$ Hz, 1H), 2.65 – 2.53 (m, 2H), 2.48 – 2.37 (m, 2H), 2.13 – 2.07 (m, 1H), 2.02 – 1.94 (m, 4H), 1.69 – 1.60 (m, 2H) ppm.

^{13}C NMR (150 MHz, DMSO) $\delta = 172.77, 169.82, 166.44, 164.93, 162.82, 159.32, 154.48, 151.79, 151.21, 147.61, 146.33, 141.98, 139.98, 136.26, 136.22, 133.00, 132.14, 128.65, 126.59, 125.86, 125.61, 121.92, 116.37, 112.86, 112.03, 100.62, 66.31, 56.94, 49.14$ (2C), 48.84, 43.78, 41.07, 38.83, 34.57, 30.94, 29.76 (2C), 24.21 (2C), 21.89 ppm.

HRMS (APCI):	calcd. for $\text{C}_{44}\text{H}_{42}\text{Cl}_2\text{KN}_{12}\text{O}_7^+$:	959.2308 m/z $[\text{M}+\text{K}]^+$
	found:	959.2330 m/z $[\text{M}+\text{K}]^+$.
LCMS (ESI):	$t_{\text{ret}} = 3.38$ min (<i>E</i>).	921 m/z $[\text{M}+\text{H}]^+$.

(E)-N-(3-((2-(4-(6-((6-acetyl-8-cyclopentyl-5-methyl-7-oxo-7,8-dihydropyrido[2,3-d]pyrimidin-2-yl)amino)pyridin-3-yl)piperazin-1-yl)-2-oxoethyl)amino)propyl)-2-(4-((2-(2,6-dioxopiperidin-3-yl)-1-oxoisoindolin-4-yl)diazenyl)-2,6-dimethoxyphenoxy)acetamide (PHOTAC-CDK4/6-1)



6-acetyl-2-((5-(4-(2-chloroacetyl)piperazin-1-yl)pyridin-2-yl)amino)-8-cyclopentyl-5-methylpyrido[2,3-d]pyrimidin-7(8H)-one (14.6 mg, 0.028 mmol, 1.0 eq.), prepared as reported^[59], was mixed with (E)-3-(2-(4-((2-(2,6-dioxopiperidin-3-yl)-1-oxoisoindolin-4-yl)diazenyl)-2,6-dimethoxyphenoxy)acetamido)propan-1-aminium 2,2,2-trifluoroacetate (27.3 mg, 0.042 mmol, 1.5 eq.) prepared as previously described.^[27] To this mixture was added sodium carbonate (5.9 mg, 0.056 mmol 2.0 eq.) and dry DMF (6 mL). The mixture was stirred at 80 °C for 24 h and diluted with a 5:1 CH₂Cl₂:iPrOH mixture (20 mL) and separated against water (30 mL). The organic phase was washed with 10% LiCl (aq., 2x 30 mL) and brine (2x 20 mL), dried over Na₂SO₄ and concentrated under reduced pressure. Purification of the resulting crude product by preparative thin layer chromatography (CH₂Cl₂:MeOH:iPrOH 18:2:1) gave **PHOTAC-CDK4/6-1** (8.1 mg, 0.008 mmol, 28%) as a yellow solid.

$R_f = 0.19$ [CH₂Cl₂:MeOH 9:1].

¹H NMR (600 MHz, DMSO-*d*₆) δ = 11.03 (s, 1H), 10.11 (s, 1H), 8.93 (s, 1H), 8.19 (d, *J* = 7.8 Hz, 1H), 8.04 (d, *J* = 3.0 Hz, 1H), 8.00 (t, *J* = 5.8 Hz, 1H), 7.89 (d, *J* = 7.4 Hz, 1H), 7.85 (d, *J* = 8.9 Hz, 1H), 7.77 (t, *J* = 7.7 Hz, 1H), 7.45 (dd, *J* = 9.1, 3.0 Hz, 1H), 7.34 (s, 2H), 5.81 (p, *J* = 9.0 Hz, 1H), 5.15 (dd, *J* = 13.3, 5.1 Hz, 1H), 4.80 (d, *J* = 19.0 Hz, 1H), 4.69 (d, *J* = 18.9 Hz, 1H), 4.42 (s, 2H), 3.94 (s, 6H), 3.60 (m, 2H), 3.57 (t, *J* =

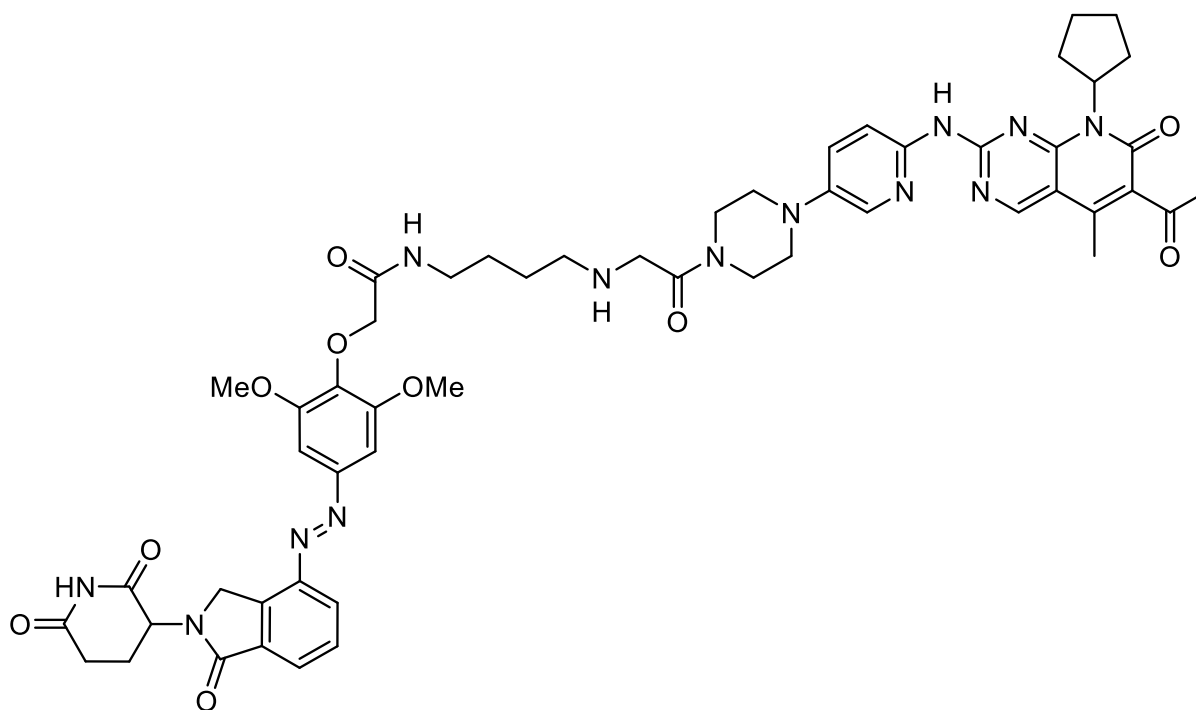
5.0 Hz, 2H), 3.41 (s, 2H), 3.26 (q, J = 6.6 Hz, 2H), 3.13 (m, 2H), 3.09 (t, J = 5.2 Hz, 2H), 2.94 (ddd, J = 17.2, 13.6, 5.5 Hz, 1H), 2.67 – 2.59 (m, 1H), 2.56 (t, J = 6.9 Hz, 2H), 2.54 – 2.50 (m, 1H), 2.42 (s, 3H), 2.30 (s, 3H), 2.27 – 2.20 (m, 2H), 2.10 – 2.04 (m, 1H), 1.90 – 1.85 (m, 2H), 1.81 – 1.72 (m, 2H), 1.64 (p, J = 7.0 Hz, 2H), 1.60 – 1.53 (m, 2H) ppm.

¹³C NMR (150 MHz, DMSO) δ = 202.44, 172.91, 171.01, 169.44, 167.94, 167.12, 160.71, 158.45, 158.26, 158.20, 154.70, 152.60, 148.25, 146.31, 144.74, 143.10, 142.05, 139.27, 135.87, 134.48, 133.81, 129.59, 129.26, 128.60, 125.44, 125.27, 114.94, 106.58, 100.58, 71.87, 56.36, 52.90, 51.84, 50.11, 48.77, 48.42, 48.29, 46.75, 43.79, 40.89, 36.53, 31.31, 31.28, 29.36, 27.55 (2C), 25.12 (2C), 22.30, 13.62 ppm.

HRMS (APCI): calcd. for C₅₂H₆₀N₁₃O₁₀⁺: 1026.4581 m/z [M+H]⁺.
 found: 1026.4545 m/z [M+H]⁺.

LCMS (ESI): t_{ret} = 2.90 min (E). 514 m/z [M+2H]²⁺.

(E)-N-(4-((2-(4-(6-((6-acetyl-8-cyclopentyl-5-methyl-7-oxo-7,8-dihydropyrido[2,3-d]pyrimidin-2-yl)amino)pyridin-3-yl)piperazin-1-yl)-2-oxoethyl)amino)butyl)-2-(4-((2-(2,6-dioxopiperidin-3-yl)-1-oxoisoindolin-4-yl)diazenyl)-2,6-dimethoxyphenoxy)acetamide (PHOTAC-CDK4/6-2)



6-acetyl-2-((5-(4-(2-chloroacetyl)piperazin-1-yl)pyridin-2-yl)amino)-8-cyclopentyl-5-methylpyrido[2,3-d]pyrimidin-7(8H)-one (18.8 mg, 0.036 mmol, 1.0 eq.), prepared as reported^[59], was mixed with (E)-4-(2-(4-((2-(2,6-dioxopiperidin-3-yl)-1-oxoisoindolin-4-yl)diazenyl)-2,6-dimethoxyphenoxy)acetamido)butan-1-aminium 2,2,2-trifluoroacetate (35.9 mg, 0.054 mmol, 1.5 eq.) prepared as previously described.^[27] To this mixture was added sodium carbonate (7.6 mg, 0.072 mmol 2.0 eq.) and dry DMF (3 mL). The mixture was stirred at 50 °C for 18 h followed by stirring for 16 h at room temperature. Next it was diluted with a 5:1 CH₂Cl₂:iPrOH mixture (20 mL) and separated against water (30 mL). The organic phase was washed with 10% LiCl (aq., 2x 30 mL) and brine (2x 20 mL), dried over Na₂SO₄ and concentrated under reduced pressure. Purification of the resulting crude product by preparative thin layer chromatography (CH₂Cl₂:MeOH:iPrOH 18:2:1) gave **PHOTAC-CDK4/6-2** (12.0 mg, 0.012 mmol, 32%) as a yellow solid.

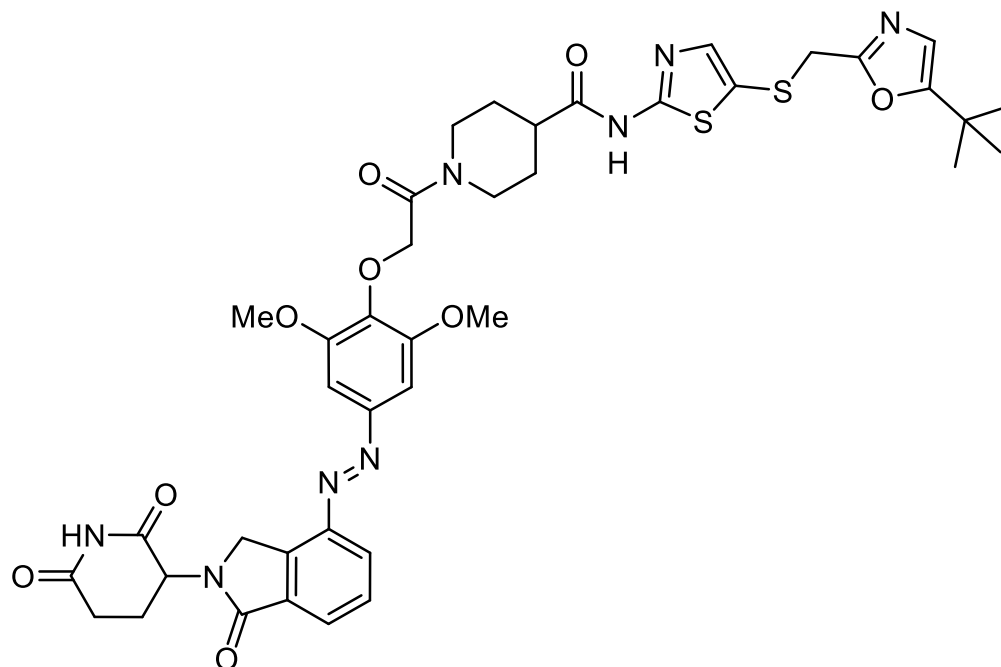
$R_f = 0.19$ [CH_2Cl_2 :MeOH 9:1].

^1H NMR (600 MHz, $\text{DMSO}-d_6$) $\delta = 11.05$ (s, 1H), 10.14 (s, 1H), 8.93 (s, 1H), 8.19 (dd, $J = 7.8, 1.0$ Hz, 1H), 8.05 (d, $J = 3.0$ Hz, 1H), 7.99 (t, $J = 5.8$ Hz, 1H), 7.90 (dd, $J = 7.5, 1.0$ Hz, 1H), 7.85 (d, $J = 9.0$ Hz, 1H), 7.77 (t, $J = 7.6$ Hz, 1H), 7.46 (dd, $J = 9.1, 3.1$ Hz, 1H), 7.34 (s, 2H), 5.81 (p, $J = 9.0$ Hz, 1H), 5.16 (dd, $J = 13.3, 5.1$ Hz, 1H), 4.80 (d, $J = 19.0$ Hz, 1H), 4.68 (d, $J = 19.0$ Hz, 1H), 4.42 (s, 2H), 3.94 (s, 6H), 3.61 (t, $J = 5.4$ Hz, 2H), 3.55 (t, $J = 5.2$ Hz, 2H), 3.43 (s, 2H), 3.20 (q, $J = 6.5$ Hz, 2H), 3.16 – 3.08 (m, 4H), 2.94 (ddd, $J = 17.4, 13.6, 5.5$ Hz, 1H), 2.66 – 2.59 (m, 1H), 2.55 (t, $J = 6.8$ Hz, 2H), 2.54 – 2.50 (m, 1H), 2.42 (s, 3H), 2.29 (s, 3H), 2.27 – 2.20 (m, 2H), 2.08 – 2.04 (m, 1H), 1.91 – 1.85 (m, 2H), 1.81 – 1.72 (m, 2H), 1.59 – 1.42 (m, 6H) ppm.

^{13}C NMR (150 MHz, DMSO) $\delta = 202.52, 172.99, 171.08, 169.25, 167.95, 167.17, 160.74, 158.47, 158.28, 158.26, 154.72, 152.61, 148.27, 146.32, 144.79, 143.12, 142.10, 139.26, 135.91, 134.47, 133.83, 129.64, 129.27, 128.75, 125.50, 125.33, 114.97, 106.60, 100.58, 71.91, 56.38, 52.90, 51.84, 49.98, 48.78$ (2C), 48.44, 48.34, 43.77, 40.93, 38.13, 31.37, 31.31, 27.59 (2C), 26.92, 26.68, 25.18 (2C), 22.33, 13.67 ppm.

HRMS (APCI):	calcd. for $\text{C}_{53}\text{H}_{62}\text{N}_{13}\text{O}_{10}^+$:	1040.4737 m/z $[\text{M}+\text{H}]^+$.
	found:	1040.4733 m/z $[\text{M}+\text{H}]^+$.
LCMS (ESI):	$t_{\text{ret}} = 2.87$ min.	521 m/z $[\text{M}+2\text{H}]^{2+}$.

(E)-N-(5-(((5-(tert-butyl)oxazol-2-yl)methyl)thio)thiazol-2-yl)-1-(2-(4-((2-(2,6-dioxopiperidin-3-yl)-1-oxoisoindolin-4-yl)diazenyl)-2,6-dimethoxyphenoxy)acetyl)piperidine-4-carboxamide (PHOTAC-panCDK-1)



(E)-2-(4-((2-(2,6-dioxopiperidin-3-yl)-1-oxoisoindolin-4-yl)diazenyl)-2,6-dimethoxyphenoxy)acetic acid (15.0 mg, 0.030 mmol, 1.0 eq.) was prepared as previously described^[27] and combined with N-(5-(((5-(tert-butyl)oxazol-2-yl)methyl)thio)thiazol-2-yl)piperidine-4-carboxamide (BMS-387032, 11.2 mg, 0.030 mmol, 1 eq.) and HATU (13.5 mg, 0.035 mmol, 1.2 eq.) under nitrogen atmosphere in a dried round bottom flask. The solids were dissolved in dry DMF (1.0 mL), followed by addition of *i*-Pr₂NEt (19.1 mg, 0.148 mmol, 5 eq., 0.026 mL) and the reaction was stirred for 14 h at room temperature. The reaction mixture was diluted with ethyl acetate (20 mL) and separated against 10% LiCl (aq., 20 mL). The organic phase was washed with saturated NaHCO₃ (40 mL) and brine (2x 20 mL), dried over Na₂SO₄ and concentrated under reduced pressure. Purification of the resulting crude product by flash column chromatography (CH₂Cl₂/MeOH gradient, 0 to 20% MeOH) gave **PHOTAC-panCDK-1** (18.3 mg, 0.022 mmol, 73%) as an orange solid.

$R_f = 0.26$ [CH₂Cl₂:MeOH 20:1].

¹H NMR (400 MHz, DMSO-*d*₆) δ = 12.33 (s, 1H), 11.03 (s, 1H), 8.21 (dd, *J* = 7.8, 1.1 Hz, 1H), 7.92 (dd, *J* = 7.5, 1.1 Hz, 1H), 7.79 (t, *J* = 7.7 Hz, 1H), 7.40 (s, 1H), 7.33 (s, 2H), 6.71 (s, 1H), 5.16 (dd, *J* = 13.2, 5.1 Hz, 1H), 4.86 – 4.61 (m, 4H), 4.35 (d, *J* = 13.0

Hz, 1H), 4.14 (d, $J = 13.5$ Hz, 1H), 4.05 (s, 2H), 3.92 (s, 6H), 3.13 (t, $J = 13.6$ Hz, 1H), 2.94 (ddd, $J = 17.7, 13.4, 5.4$ Hz, 1H), 2.79 (tt, $J = 11.3, 3.8$ Hz, 1H), 2.73 – 2.53 (m, 3H), 2.10 – 2.02 (m, 1H), 1.91 – 1.83 (m, 2H), 1.79 – 1.66 (m, 1H), 1.57 – 1.42 (m, 1H), 1.17 (s, 9H) ppm.

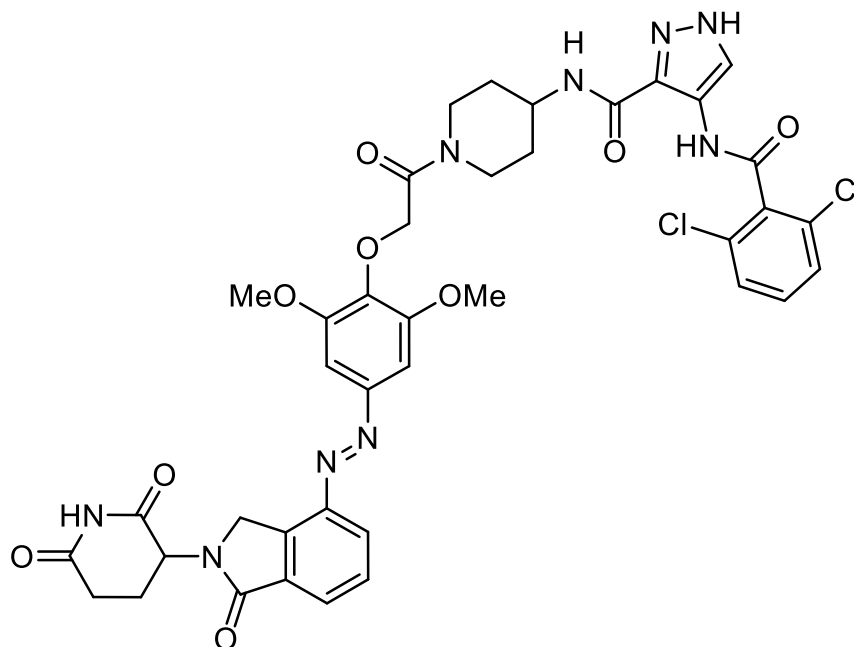
^{13}C NMR (100 MHz, DMSO) $\delta = 173.20, 172.90, 171.01, 167.17, 165.56, 161.17, 160.81, 158.72, 153.10, 148.18, 146.38, 145.13, 139.16, 134.54, 133.82, 129.62, 128.50, 125.40, 120.12, 118.71, 100.60, 71.07, 56.27, 51.86, 48.30, 44.10, 41.15, 40.60, 33.98, 31.28, 30.92, 28.29, 28.16, 27.69, 22.31$ ppm.

HRMS (APCI): calcd. for $\text{C}_{40}\text{H}_{45}\text{N}_8\text{O}_9\text{S}_2^+$: 845.2745 m/z $[\text{M}+\text{H}]^+$.

 found: 845.2745 m/z $[\text{M}+\text{H}]^+$.

LCMS (ESI): $t_{\text{ret}} = 3.98$ min (*E*). 845 m/z $[\text{M}+\text{H}]^+$.

(E)-4-(2,6-dichlorobenzamido)-N-(1-(2-(4-((2-(2,6-dioxopiperidin-3-yl)-1-oxoisoindolin-4-yl)diazenyl)-2,6-dimethoxyphenoxy)acetyl)piperidin-4-yl)-1H-pyrazole-3-carboxamide (PHOTAC-panCDK-2)



(E)-2-(4-((2-(2,6-dioxopiperidin-3-yl)-1-oxoisoindolin-4-yl)diazenyl)-2,6-dimethoxyphenoxy)acetic acid (18.3 mg, 0.036 mmol, 1.0 eq.) was prepared as previously described^[27], combined with the hydrochloride of 4-(2,6-dichlorobenzamido)-N-(piperidin-4-yl)-1H-pyrazole-3-carboxamide (AT-7519, 16.0 mg, 0.038 mmol, 1.06 eq.) and HATU (16.4 mg, 0.043 mmol, 1.2 eq.) under nitrogen atmosphere in a dried round bottom flask. The solids were dissolved in dry DMF (1.2 mL), followed by addition of *i*-Pr₂NEt (27.9 mg, 0.216 mmol, 6 eq., 0.038 mL) and the reaction was stirred for 16 h at room temperature. The reaction mixture was diluted with ethyl acetate (20 mL) and separated against 10% LiCl (aq., 20 mL). The organic phase was washed with saturated NH₄Cl (30 mL), saturated NaHCO₃ (30 mL) and brine (2x 20 mL), dried over Na₂SO₄ and concentrated under reduced pressure. Purification of the resulting crude product by flash column chromatography (CH₂Cl₂/MeOH gradient, 0 to 20% MeOH) gave **PHOTAC-panCDK-2** (29.3 mg, 0.035 mmol, 96%) as a yellow solid.

R_f = 0.59 [CH₂Cl₂:MeOH 9:1].

¹H NMR (400 MHz, DMSO-*d*₆) δ = 13.42 (s, 1H), 11.03 (s, 1H), 10.18 (s, 1H), 8.48 (d, J = 8.1 Hz, 1H), 8.36 (s, 1H), 8.22 (dd, J = 7.8, 1.1 Hz, 1H), 7.92 (dd, J = 7.5, 1.1 Hz, 1H), 7.80 (t, J = 7.7 Hz, 1H), 7.61 – 7.49 (m, 3H), 7.33 (s, 2H), 5.16 (dd, J = 13.2, 5.1

Hz, 1H), 4.86 – 4.63 (m, 4H), 4.34 (d, $J = 13.1$ Hz, 1H), 4.11 (d, $J = 13.8$ Hz, 1H), 4.07 – 3.96 (m, 1H), 3.91 (s, 6H), 3.12 (t, $J = 12.8$ Hz, 1H), 2.94 (ddd, $J = 17.5, 13.5, 5.4$ Hz, 1H), 2.73 – 2.52 (m, 3H), 2.06 (ddd, $J = 11.5, 6.2, 3.9$ Hz, 1H), 1.81 (t, $J = 15.3$ Hz, 2H), 1.70 – 1.45 (m, 2H) ppm.

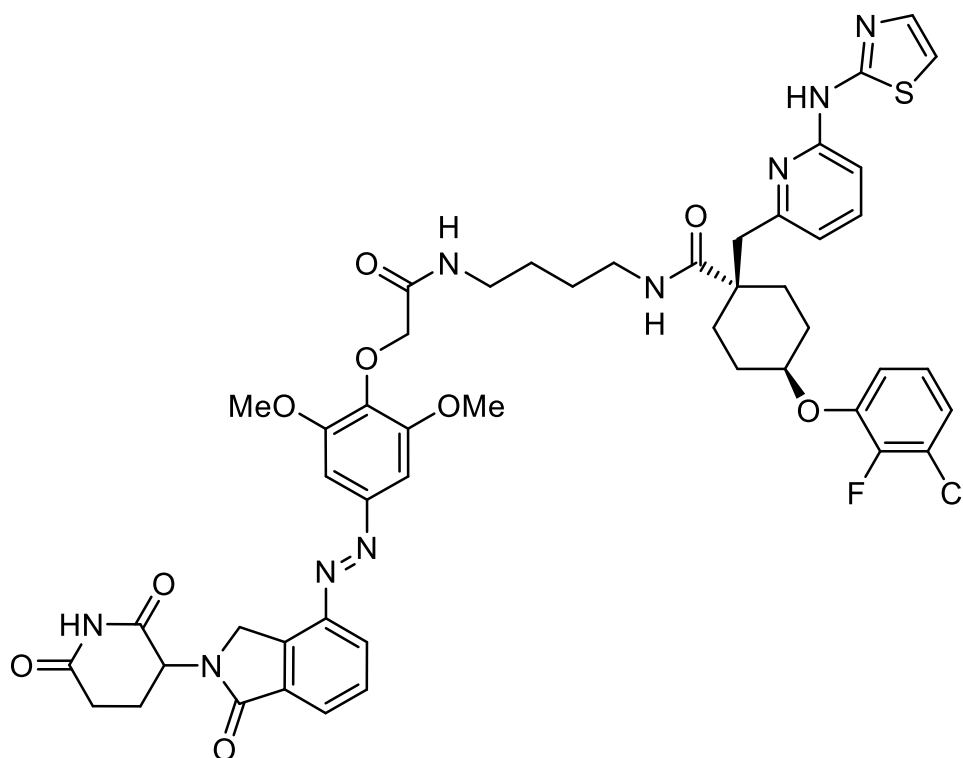
^{13}C NMR (100 MHz, DMSO) $\delta = 172.91, 171.01, 167.16, 165.48, 162.69, 160.28, 153.12, 148.18, 146.39, 139.10, 135.35, 134.52, 133.82, 132.90, 131.90, 131.25, 129.64, 128.54, 128.43, 125.40, 121.51, 120.70, 100.63, 70.91, 56.32, 51.85, 48.30, 45.98, 43.77, 40.52, 31.76, 31.28, 30.82, 22.30$ ppm.

HRMS (APCI): calcd. for $\text{C}_{39}\text{H}_{38}\text{Cl}_2\text{N}_9\text{O}_9^+$: 846.2164 m/z $[\text{M}+\text{H}]^+$.

found: 846.2150 m/z $[\text{M}+\text{H}]^+$.

LCMS (ESI): $t_{\text{ret}} = 3.78$ min (*E*). 846 m/z $[\text{M}+\text{H}]^+$.

(1R,4R)-4-(3-chloro-2-fluorophenoxy)-N-(4-(2-(4-((E)-(2-(2,6-dioxopiperidin-3-yl)-1-oxoisoindolin-4-yl)diazenyl)-2,6-dimethoxyphenoxy)acetamido)butyl)-1-((6-(thiazol-2-ylamino)pyridin-2-yl)methyl)cyclohexane-1-carboxamide (PHOTAC-AURKA-3)



(E)-4-(2-(4-((2-(2,6-dioxopiperidin-3-yl)-1-oxoisoindolin-4-yl)diazenyl)-2,6-dimethoxyphenoxy)acetamido)butan-1-aminium 2,2,2-trifluoroacetate (20.0 mg, 0.030 mmol, 2 eq.) prepared as previously described^[27], (1R,4R)-4-(3-chloro-2-fluorophenoxy)-1-((6-(thiazol-2-ylamino)pyridin-2-yl)methyl)cyclohexane-1-carboxylic acid (MK-5108, 6.9 mg, 0.015 mmol, 1.0 eq.) and HATU (11.4 mg, 0.030 mmol, 2.0 eq.) were combined under nitrogen atmosphere in a dry glass vial. The solids were dissolved in dry DMF (0.7 mL), followed by addition of *i*-Pr₂NEt (20.2 mg, 0.156 mmol, 10.4 eq., 0.027 mL) and the reaction was stirred for 16 h at room temperature. The reaction mixture was diluted with ethyl acetate (20 mL) and separated against 10% LiCl (aq., 20 mL). The organic phase was washed with saturated NaHCO₃ (30 mL) and brine (2x 20 mL), dried over Na₂SO₄ and concentrated under reduced pressure. Purification of the resulting crude product by flash column chromatography (CH₂Cl₂/MeOH gradient, 0 to 20% MeOH) gave **PHOTAC-AURKA-3** (12.6 mg, 0.013 mmol, 84%) as a yellow solid.

$R_f = 0.36$ [CH_2Cl_2 :MeOH 15:1].

$^1\text{H NMR}$ (600 MHz, CDCl_3) $\delta = 11.03$ (s, 1H), 8.20 (d, $J = 7.8$ Hz, 1H), 7.94 (t, $J = 6.0$ Hz, 1H), 7.91 (d, $J = 7.5$ Hz, 1H), 7.79 (t, $J = 7.6$ Hz, 1H), 7.71 – 7.62 (m, 2H), 7.47 (d, $J = 3.9$ Hz, 1H), 7.35 (s, 2H), 7.13 – 7.06 (m, 4H), 6.98 (d, $J = 8.2$ Hz, 1H), 6.73 (d, $J = 7.2$ Hz, 1H), 5.16 (dd, $J = 13.3, 5.2$ Hz, 1H), 4.80 (d, $J = 19.0$ Hz, 1H), 4.69 (d, $J = 19.0$ Hz, 1H), 4.55 – 4.49 (m, 1H), 4.43 (s, 2H), 3.94 (s, 6H), 3.21 – 3.15 (m, 2H), 3.06 – 3.02 (m, 2H), 2.97 – 2.89 (m, 6H), 2.63 (d, $J = 16.7$ Hz, 1H), 2.57 – 2.50 (m, 1H), 2.10 – 2.03 (m, 1H), 1.93 – 1.71 (m, 6H), 1.67 – 1.59 (m, 2H), 1.46 – 1.37 (m, 4H) ppm.

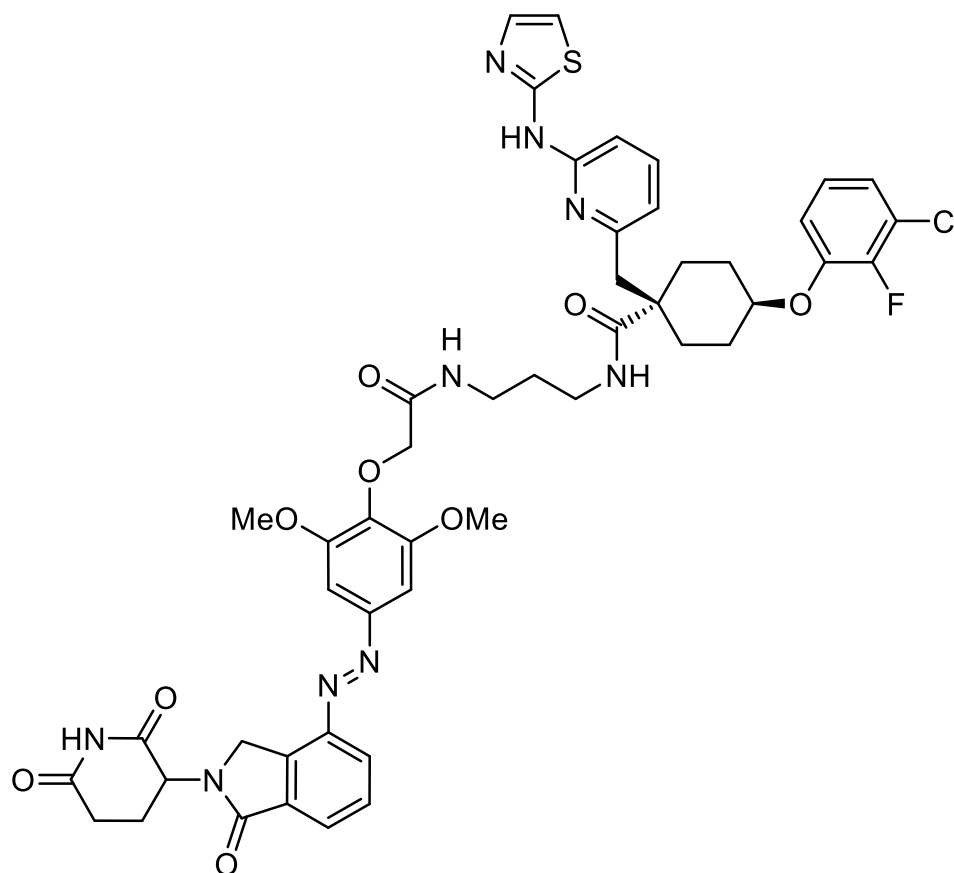
$^{13}\text{C NMR}$ (150 MHz, CDCl_3) $\delta = 173.86, 172.91, 171.01, 167.97, 167.14, 160.31, 155.16, 152.57, 149.68, 148.83$ (d, $J = 245.2$ Hz), 148.28, 146.33, 146.17 (d, $J = 10.1$ Hz), 139.26, 138.27, 138.23, 134.49, 133.82, 129.58, 128.70, 125.49, 124.88 (d, $J = 5.1$ Hz), 121.74, 120.40 (d, $J = 14.9$ Hz), 116.64, 116.48, 111.33, 108.18, 100.67, 74.23, 71.89, 56.37, 51.84, 48.30, 46.53, 46.49, 38.63, 37.99, 31.28, 28.28 (2C), 26.76, 26.68, 26.64, 26.58, 22.32 ppm.

HRMS (APCI): calcd. for $\text{C}_{49}\text{H}_{51}\text{ClFN}_9\text{O}_9\text{S}^+$: 995.3203 m/z $[\text{M}]^+$.

found: 995.3198 m/z $[\text{M}]^+$.

LCMS (ESI): $t_{\text{ret}} = 3.62$ min. 996 m/z $[\text{M}+\text{H}]^+$.

(1R,4R)-4-(3-chloro-2-fluorophenoxy)-N-(3-(2-(4-((E)-2-(2,6-dioxopiperidin-3-yl)-1-oxoisoindolin-4-yl)diazenyl)-2,6-dimethoxyphenoxy)acetamido)propyl)-1-((6-(thiazol-2-ylamino)pyridin-2-yl)methyl)cyclohexane-1-carboxamide (PHOTAC-AURKA-2)



(E)-4-(2-(4-((2-(2,6-dioxopiperidin-3-yl)-1-oxoisoindolin-4-yl)diazenyl)-2,6-dimethoxyphenoxy)acetamido)propan-1-aminium 2,2,2-trifluoroacetate (19.8 mg, 0.030 mmol, 2 eq.) prepared as previously described^[27], (1R,4R)-4-(3-chloro-2-fluorophenoxy)-1-((6-(thiazol-2-ylamino)pyridin-2-yl)methyl)cyclohexane-1-carboxylic acid (MK-5108, 7.0 mg, 0.015 mmol, 1.0 eq.) and HATU (11.5 mg, 0.030 mmol, 2.0 eq.) were combined under nitrogen atmosphere in a dry glass vial. The solids were dissolved in dry DMF (0.7 mL), followed by addition of *i*-Pr₂NEt (20.4 mg, 0.158 mmol, 10.4 eq., 0.024 mL) and the reaction was stirred for 16 h at room temperature. The reaction mixture was diluted with ethyl acetate (20 mL) and separated against 10% LiCl (aq., 20 mL). The organic phase was washed with saturated NH₄Cl (30 mL), saturated NaHCO₃ (30 mL) and brine (2x 20 mL), dried over Na₂SO₄ and concentrated under reduced pressure. Purification of the resulting crude product by flash column

chromatography (CH₂Cl₂/MeOH gradient, 0 to 20% MeOH) gave **PHOTAC-AURKA-2** (9.3 mg, 0.009 mmol, 63%) as a yellow solid.

R_f = 0.47 [CH₂Cl₂:MeOH 9:1].

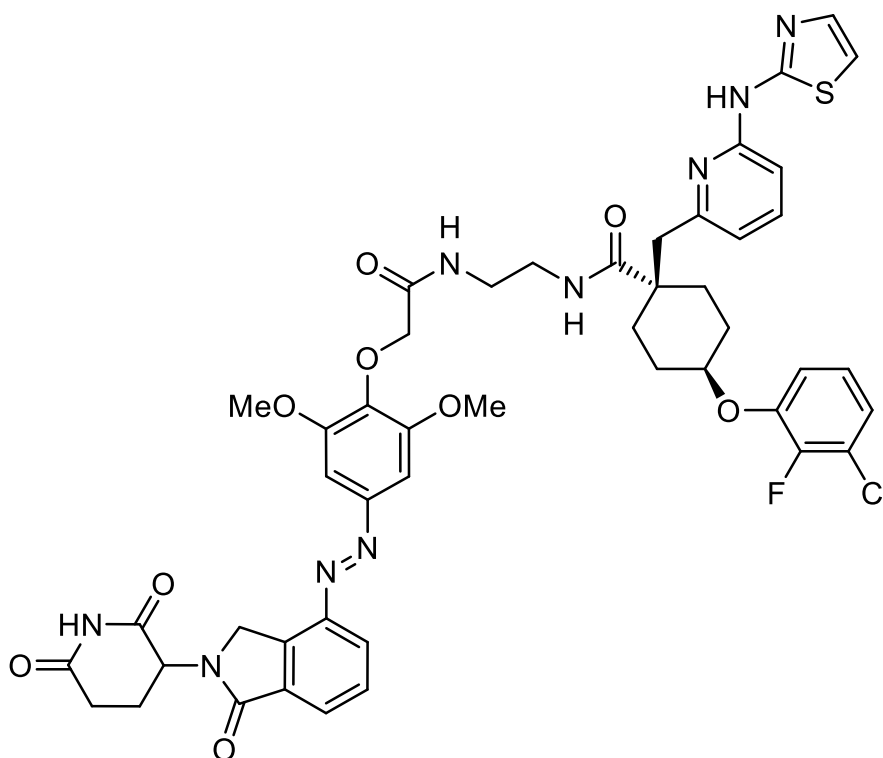
¹H NMR (600 MHz, DMSO-*d*₆) δ = 11.11 (s, 1H), 11.02 (s, 1H), 8.21 (d, J = 7.9 Hz, 1H), 7.99 (t, J = 6.1 Hz, 1H), 7.93 – 7.89 (m, 1H), 7.82 – 7.77 (m, 1H), 7.61 (t, J = 5.9 Hz, 1H), 7.56 – 7.49 (m, 1H), 7.35 (m, 3H), 7.15 – 7.06 (m, 3H), 6.97 – 6.91 (m, 1H), 6.85 (d, J = 8.1 Hz, 1H), 6.59 (d, J = 6.6 Hz, 1H), 5.15 (dd, J = 13.1, 6.9 Hz, 1H), 4.80 (d, J = 18.9 Hz, 1H), 4.68 (d, J = 21.6 Hz, 1H), 4.55 – 4.52 (m, 1H), 4.40 (s, 2H), 3.92 (s, 6H), 3.13 – 3.04 (m, 4H), 2.97 – 2.87 (m, 3H), 2.62 (d, J = 17.7 Hz, 1H), 2.56 – 2.51 (m, 1H), 2.09 – 2.01 (m, 1H), 1.92 – 1.86 (m, 2H), 1.84 – 1.75 (m, 4H), 1.69 – 1.60 (m, 2H), 1.59 – 1.51 (m, 2H) ppm.

¹³C NMR (150 MHz, DMSO) δ = 174.02, 172.93, 171.02, 168.15, 167.17, 159.81, 155.18, 152.69, 150.78, 148.86 (d, J = 246.2 Hz), 148.33, 146.36, 146.20 (d, J = 10.1 Hz), 139.21, 137.52, 137.40, 134.49, 133.84, 129.67, 128.71, 125.51, 124.94 (d, J = 4.8 Hz), 121.85, 120.43 (d, J = 15.1 Hz), 116.64, 116.17, 110.69, 108.10, 100.59, 74.35, 71.82, 56.36, 51.85, 48.32, 46.85, 46.62, 36.21, 35.91, 31.29, 29.31, 28.39 (2C), 26.70 (2C), 22.33 ppm.

HRMS (APCI): calcd. for C₄₈H₄₉ClFN₉NaO₉S⁺: 1004.2939 m/z [M+Na]⁺.
 found: 1004.2986 m/z [M+Na]⁺.

LCMS (ESI): t_{ret} = 4.04 min (*Z*). 982 m/z [M+H]⁺.
 t_{ret} = 4.20 min (*E*). 982 m/z [M+H]⁺.

(1R,4R)-4-(3-chloro-2-fluorophenoxy)-N-(2-(2-(4-((E)-2-(2,6-dioxopiperidin-3-yl)-1-oxoisoindolin-4-yl)diazenyl)-2,6-dimethoxyphenoxy)acetamido)ethyl)-1-((6-(thiazol-2-ylamino)pyridin-2-yl)methyl)cyclohexane-1-carboxamide (PHOTAC-AURKA-1)



(E)-4-(2-(4-((2-(2,6-dioxopiperidin-3-yl)-1-oxoisoindolin-4-yl)diazenyl)-2,6-dimethoxyphenoxy)acetamido)ethan-1-aminium 2,2,2-trifluoroacetate (19.4 mg, 0.030 mmol, 2 eq.) prepared as previously described^[27], (1R,4R)-4-(3-chloro-2-fluorophenoxy)-1-((6-(thiazol-2-ylamino)pyridin-2-yl)methyl)cyclohexane-1-carboxylic acid (MK-5108, 7.0 mg, 0.015 mmol, 1.0 eq.) and HATU (11.5 mg, 0.030 mmol, 2.0 eq.) were combined under nitrogen atmosphere in a dry glass vial. The solids were dissolved in dry DMF (0.7 mL), followed by addition of *i*-Pr₂NEt (20.4 mg, 0.158 mmol, 10.4 eq., 0.024 mL) and the reaction was stirred for 16 h at room temperature. The reaction mixture was diluted with ethyl acetate (20 mL) and separated against 10% LiCl (aq., 20 mL). The organic phase was washed with saturated NH₄Cl (30 mL), saturated NaHCO₃ (30 mL) and brine (2x 20 mL), dried over Na₂SO₄ and concentrated under reduced pressure. Purification of the resulting crude product by flash column chromatography (CH₂Cl₂/MeOH gradient, 0 to 20% MeOH) gave **PHOTAC-AURKA-1** (11.5 mg, 0.012 mmol, 78%) as a yellow solid.

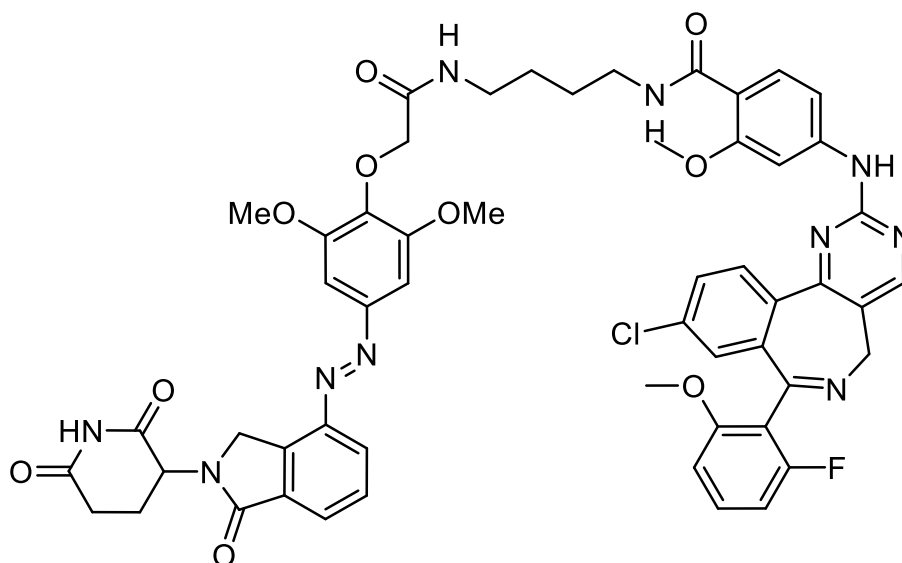
$R_f = 0.44$ [CH_2Cl_2 :MeOH 9:1].

^1H NMR (600 MHz, DMSO- d_6) $\delta = 11.12$ (s, 1H), 11.03 (s, 1H), 8.21 (d, $J = 7.5$ Hz, 1H), 8.00 (t, $J = 5.4$ Hz, 1H), 7.94 – 7.89 (m, 1H), 7.82 – 7.76 (m, 1H), 7.69 (t, $J = 5.4$ Hz, 1H), 7.56 – 7.51 (m, 1H), 7.37 – 7.33 (m, 3H), 7.09 – 7.04 (m, 3H), 6.97 – 6.93 (m, 1H), 6.85 (d, $J = 6.7$ Hz, 1H), 6.59 (d, $J = 7.1$ Hz, 1H), 5.15 (dd, $J = 12.8, 6.1$ Hz, 1H), 4.80 (d, $J = 19.2$ Hz, 1H), 4.69 (d, $J = 19.1$ Hz, 1H), 4.46 – 4.43 (m, 1H), 4.40 (s, 2H), 3.92 (s, 6H), 3.28 – 3.23 (m, 2H), 3.20 (t, $J = 5.6$ Hz, 2H), 2.99 – 2.86 (m, 3H), 2.63 (d, $J = 17.9$ Hz, 1H), 2.58 – 2.52 (m, 1H), 2.09 – 2.03 (m, 1H), 1.92 – 1.85 (m, 2H), 1.80 – 1.72 (m, 4H), 1.65 – 1.58 (m, 2H) ppm.

^{13}C NMR (150 MHz, DMSO) $\delta = 174.39, 172.93, 171.02, 168.47, 167.16, 159.81, 155.10, 152.69, 150.75, 148.91$ (d, $J = 245.8$ Hz), 148.33, 146.35, 146.16 (d, $J = 10.1$ Hz), 139.13, 137.50, 137.39, 134.49, 133.83, 129.66, 128.70, 125.51, 124.89 (d, $J = 4.8$ Hz), 121.88, 120.44 (d, $J = 15.1$ Hz), 116.65, 116.13, 110.69, 108.09, 100.59, 74.32, 71.72, 56.36, 51.85, 48.32, 47.02, 46.72, 38.83, 38.10, 31.29, 28.22 (2C), 26.57 (2C), 22.32 ppm.

HRMS (APCI):	calcd. for $\text{C}_{47}\text{H}_{48}\text{ClFN}_9\text{O}_9\text{S}^+$:	968.2963 m/z $[\text{M}+\text{H}]^+$.
	found:	968.2958 m/z $[\text{M}+\text{H}]^+$.
LCMS (ESI):	$t_{\text{ret}} = 3.93$ min (<i>Z</i>).	968 m/z $[\text{M}+\text{H}]^+$.
	$t_{\text{ret}} = 4.02$ min (<i>E</i>).	968 m/z $[\text{M}+\text{H}]^+$.

(E)-4-((9-chloro-7-(2-fluoro-6-methoxyphenyl)-5H-benzo[c]pyrimido[4,5-e]azepin-2-yl)amino)-N-(4-(2-(4-((2-(2,6-dioxopiperidin-3-yl)-1-oxoisoindolin-4-yl)diazenyl)-2,6-dimethoxyphenoxy)acetamido)butyl)-2-methoxybenzamide (PHOTAC-AURKA-4)



(E)-4-(2-(4-((2-(2,6-dioxopiperidin-3-yl)-1-oxoisoindolin-4-yl)diazenyl)-2,6-dimethoxyphenoxy)acetamido)butan-1-aminium 2,2,2-trifluoroacetate (20.0 mg, 0.030 mmol, 2 eq.) prepared as previously described^[27], 4-((9-chloro-7-(2-fluoro-6-methoxyphenyl)-5H-benzo[c]pyrimido[4,5-e]azepin-2-yl)amino)-2-methoxybenzoic acid (Alisertib/MLN8237, 7.8 mg, 0.015 mmol, 1.0 eq.) and HATU (11.4 mg, 0.030 mmol, 2.0 eq.) were combined under nitrogen atmosphere in a dry glass vial. The solids were dissolved in dry DMF (0.7 mL), followed by addition of *i*-Pr₂NEt (17.9 mg, 0.139 mmol, 9.2 eq., 0.024 mL) and the reaction was stirred for 16 h at room temperature. The reaction mixture was diluted with ethyl acetate (20 mL) and separated against 10% LiCl (aq., 20 mL). The organic phase was washed with saturated NaHCO₃ (30 mL) and brine (2x 20 mL), dried over Na₂SO₄ and concentrated under reduced pressure. Purification of the resulting crude product by flash column chromatography (CH₂Cl₂/MeOH gradient, 0 to 20% MeOH) gave **PHOTAC-AURKA-4** (10.3 mg, 0.010 mmol, 65%) as a yellow solid.

$R_f = 0.35$ [CH₂Cl₂:MeOH 15:1].

¹H NMR (600 MHz, DMSO-*d*₆) δ = 11.03 (s, 1H), 10.16 (s, 1H), 8.70 (s, 1H), 8.30 (d, *J* = 8.5 Hz, 1H), 8.19 (d, *J* = 7.7 Hz, 1H), 8.06 (t, *J* = 5.8 Hz, 1H), 7.98 (t, *J* = 5.9 Hz, 1H), 7.95 – 7.91 (m, 1H), 7.90 (d, *J* = 7.5 Hz, 1H), 7.85 – 7.75 (m, 3H), 7.47 – 7.36 (m, 2H),

7.35 (s, 2H), 7.24 (s, 1H), 7.13 – 6.72 (m, 2H), 5.15 (dd, $J = 13.2, 5.2$ Hz, 1H), 4.80 (d, $J = 19.0$ Hz, 1H), 4.68 (d, $J = 19.0$ Hz, 1H), 4.44 (s, 2H), 3.94 (s, 6H), 3.90 (s, 3H), 3.34 – 3.29 (m, 2H), 3.26 – 3.12 (m, 4H), 2.98 – 2.85 (m, 4H), 2.65 – 2.59 (m, 1H), 2.58 – 2.50 (m, 1H), 2.10 – 2.02 (m, 1H), 1.57 – 1.52 (m, 4H) ppm.

^{13}C NMR (150 MHz, DMSO) $\delta = 172.91, 171.01, 167.98, 167.14, 164.39, 160.88, 160.77, 159.54$ (d, $J = 243.6$ Hz), $159.42, 157.78$ (d, $J = 6.4$ Hz), $157.69, 157.21, 152.59, 148.27, 146.33, 144.30, 139.28, 137.41, 135.27, 134.65, 134.48, 133.81, 131.53$ (d, $J = 8.2$ Hz), $131.34, 130.93, 130.51, 129.61, 128.65, 127.48, 125.45, 123.19, 117.32, 115.10, 110.38, 108.09, 101.45, 100.60, 71.88, 56.34, 55.63, 51.85, 49.16, 48.31, 44.15, 39.18, 38.64, 38.04, 31.27, 26.83, 26.73, 22.31$ ppm.

HRMS (APCI): calcd. for $\text{C}_{54}\text{H}_{50}\text{ClFKN}_{10}\text{O}_{10}^{+}$: 1091.3016 m/z $[\text{M}+\text{K}]^{+}$.
 found: 1091.3021 m/z $[\text{M}+\text{K}]^{+}$.

LCMS (ESI): $t_{\text{ret}} = 4.26$ min. 1053 m/z $[\text{M}+\text{H}]^{+}$.

References

- [1] S. Müller, A. Chaikuad, N. S. Gray, S. Knapp, *Nat. Chem. Biol.* **2015**, *11*, 818–821.
- [2] F. M. Ferguson, N. S. Gray, *Nat. Rev. Drug Discov.* **2018**, *17*, 353–377.
- [3] S. Lapenna, A. Giordano, *Nat. Rev. Drug Discov.* **2009**, *8*, 547–566.
- [4] S. M. A. Lens, E. E. Voest, R. H. Medema, *Nat. Rev. Cancer* **2010**, *10*, 825–841.
- [5] A. C. Borisa, H. G. Bhatt, *Eur. J. Med. Chem.* **2017**, *140*, 1–19.
- [6] C. O. de Groot, J. E. Hsia, J. V. Anzola, A. Motamedi, M. Yoon, Y. L. Wong, D. Jenkins, H. J. Lee, M. B. Martinez, R. L. Davis, T. C. Gahman, A. Desai, A. K. Shiau, *Front. Oncol.* **2015**, *5*, DOI 10.3389/fonc.2015.00285.
- [7] D. Dauch, R. Rudalska, G. Cossa, J.-C. Nault, T.-W. Kang, T. Wuestefeld, A. Hohmeyer, S. Imbeaud, T. Yevsa, L. Hoenicke, T. Pantsar, P. Bozko, N. P. Malek, T. Longerich, S. Laufer, A. Poso, J. Zucman-Rossi, M. Eilers, L. Zender, *Nat. Med.* **2016**, *22*, 744–753.
- [8] Y. Li, X. Li, J. Pu, Q. Yang, H. Guan, M. Ji, B. Shi, M. Chen, P. Hou, *Thyroid* **2018**, *28*, 1642–1654.
- [9] K. N. Shah, R. Bhatt, J. Rotow, J. Rohrberg, V. Olivas, V. E. Wang, G. Hemmati, M. M. Martins, A. Maynard, J. Kuhn, J. Galeas, H. J. Donnella, S. Kaushik, A. Ku, S. Dumont, G. Krings, H. J. Haringsma, L. Robillard, A. D. Simmons, T. C. Harding, F. McCormick, A. Goga, C. M. Blakely, T. G. Bivona, S. Bandyopadhyay, *Nat. Med.* **2019**, *25*, 111–118.
- [10] J. Y. Xue, Y. Zhao, J. Aronowitz, T. T. Mai, A. Vides, B. Qeriqi, D. Kim, C. Li, E. de Stanchina, L. Mazutis, D. Risso, P. Lito, *Nature* **2020**, *577*, 421–425.
- [11] H. Katayama, K. Sasai, H. Kawai, Z.-M. Yuan, J. Bondaruk, F. Suzuki, S. Fujii, R. B. Arlinghaus, B. A. Czerniak, S. Sen, *Nat. Genet.* **2004**, *36*, 55–62.
- [12] K. Sasai, W. Treekitkarnmongkol, K. Kai, H. Katayama, S. Sen, *Front. Oncol.* **2016**, *6*, DOI 10.3389/fonc.2016.00247.
- [13] A. P. Damodaran, L. Vaufrey, O. Gavard, C. Prigent, *Trends Pharmacol. Sci.* **2017**, *38*, 687–700.
- [14] M. E. Klein, M. Kovatcheva, L. E. Davis, W. D. Tap, A. Koff, *Cancer Cell* **2018**, *34*, 9–20.
- [15] C. I. Wells, J. D. Vasta, C. R. Corona, J. Wilkinson, C. A. Zimprich, M. R. Ingold, J. E. Pickett, D. H. Drewry, K. M. Pugh, M. K. Schwinn, B. (Brian) Hwang, H. Zegzouti,

- K. V. M. Huber, M. Cong, P. L. Meisenheimer, T. M. Willson, M. B. Robers, *Nat. Commun.* **2020**, *11*, 2743.
- [16] N. J. Sumi, B. M. Kuenzi, C. E. Knezevic, L. L. Remsing Rix, U. Rix, *ACS Chem. Biol.* **2015**, *10*, 2680–2686.
- [17] D. Simoneschi, G. Rona, N. Zhou, Y.-T. Jeong, S. Jiang, G. Milletti, A. A. Arbin, A. O’Sullivan, A. A. Wang, S. Nithikasem, S. Keegan, Y. Siu, V. Cianfanelli, E. Maiani, F. Nazio, F. Cecconi, F. Boccalatte, D. Fenyö, D. R. Jones, L. Busino, M. Pagano, *Nature* **2021**, *592*, 789–793.
- [18] C. Sánchez-Martínez, M. J. Lallena, S. G. Sanfeliciano, A. de Dios, *Bioorg. Med. Chem. Lett.* **2019**, *29*, 126637.
- [19] J. Deng, E. S. Wang, R. W. Jenkins, S. Li, R. Dries, K. Yates, S. Chhabra, W. Huang, H. Liu, A. R. Aref, E. Ivanova, C. P. Paweletz, M. Bowden, C. W. Zhou, G. S. Herter-Sprie, J. A. Sorrentino, J. E. Bisi, P. H. Lizotte, A. A. Merlino, M. M. Quinn, L. E. Bufe, A. Yang, Y. Zhang, H. Zhang, P. Gao, T. Chen, M. E. Cavanaugh, A. J. Rode, E. Haines, P. J. Roberts, J. C. Strum, W. G. Richards, J. H. Lorch, S. Parangi, V. Gunda, G. M. Boland, R. Bueno, S. Palakurthi, G. J. Freeman, J. Ritz, W. N. Haining, N. E. Sharpless, H. Arthanari, G. I. Shapiro, D. A. Barbie, N. S. Gray, K.-K. Wong, *Cancer Discov.* **2018**, *8*, 216–233.
- [20] D. P. Bondeson, A. Mares, I. E. D. Smith, E. Ko, S. Campos, A. H. Miah, K. E. Mulholland, N. Routly, D. L. Buckley, J. L. Gustafson, N. Zinn, P. Grandi, S. Shimamura, G. Bergamini, M. Faelth-Savitski, M. Bantscheff, C. Cox, D. A. Gordon, R. R. Willard, J. J. Flanagan, L. N. Casillas, B. J. Votta, W. den Besten, K. Famm, L. Kruidenier, P. S. Carter, J. D. Harling, I. Churcher, C. M. Crews, *Nat. Chem. Biol.* **2015**, *11*, 611–617.
- [21] G. M. Burslem, C. M. Crews, *Cell* **2020**, *181*, 102–114.
- [22] D. P. Bondeson, B. E. Smith, G. M. Burslem, A. D. Buhimschi, J. Hines, S. Jaime-Figueroa, J. Wang, B. D. Hamman, A. Ishchenko, C. M. Crews, *Cell Chem. Biol.* **2018**, *25*, 78-87.e5.
- [23] M. Brand, B. Jiang, S. Bauer, K. A. Donovan, Y. Liang, E. S. Wang, R. P. Nowak, J. C. Yuan, T. Zhang, N. Kwiatkowski, A. C. Müller, E. S. Fischer, N. S. Gray, G. E. Winter, *Cell Chem. Biol.* **2018**, DOI 10.1016/j.chembiol.2018.11.006.
- [24] K. A. Donovan, F. M. Ferguson, J. W. Bushman, N. A. Eleuteri, D. Bhunia, S. Ryu, L. Tan, K. Shi, H. Yue, X. Liu, D. Dobrovolsky, B. Jiang, J. Wang, M. Hao, I. You, M. Teng, Y. Liang, J. Hatcher, Z. Li, T. D. Manz, B. Groendyke, W. Hu, Y. Nam, S. Sengupta, H. Cho, I. Shin, M. P. Agius, I. M. Ghobrial, M. W. Ma, J. Che, S. J. Buhrlage, T. Sim, N. S. Gray, E. S. Fischer, *Cell* **2020**, *183*, 1714-1731.e10.

- [25] K. Moreau, M. Coen, A. X. Zhang, F. Pachi, M. P. Castaldi, G. Dahl, H. Boyd, C. Scott, P. Newham, *Br. J. Pharmacol.* **n.d.**, *n/a*, DOI 10.1111/bph.15014.
- [26] X. Sun, H. Gao, Y. Yang, M. He, Y. Wu, Y. Song, Y. Tong, Y. Rao, *Signal Transduct. Target. Ther.* **2019**, *4*, 1–33.
- [27] M. Reynders, B. S. Matsuura, M. Bérouti, D. Simoneschi, A. Marzio, M. Pagano, D. Trauner, *Sci. Adv.* **2020**, *6*, eaay5064.
- [28] D. A. Sloane, M. Z. Trikic, M. L. H. Chu, M. B. A. C. Lamers, C. S. Mason, I. Mueller, W. J. Savory, D. H. Williams, P. A. Evers, *ACS Chem. Biol.* **2010**, *5*, 563–576.
- [29] B. Adhikari, J. Bozilovic, M. Diebold, J. D. Schwarz, J. Hofstetter, M. Schröder, M. Wanior, A. Narain, M. Vogt, N. Dudvarski Stankovic, A. Baluapuri, L. Schönemann, L. Eing, P. Bhandare, B. Kuster, A. Schlosser, S. Heinzlmeir, C. Sottriffer, S. Knapp, E. Wolf, *Nat. Chem. Biol.* **2020**, 1–10.
- [30] A. Zorba, C. Nguyen, Y. Xu, J. Starr, K. Borzilleri, J. Smith, H. Zhu, K. A. Farley, W. Ding, J. Schiemer, X. Feng, J. S. Chang, D. P. Uccello, J. A. Young, C. N. Garcia-Irrizary, L. Czabaniuk, B. Schuff, R. Oliver, J. Montgomery, M. M. Hayward, J. Coe, J. Chen, M. Niosi, S. Luthra, J. C. Shah, A. El-Kattan, X. Qiu, G. M. West, M. C. Noe, V. Shanmugasundaram, A. M. Gilbert, M. F. Brown, M. F. Calabrese, *Proc. Natl. Acad. Sci.* **2018**, *115*, E7285–E7292.
- [31] R. Chen, W. G. Wierda, S. Chubb, R. E. Hawtin, J. A. Fox, M. J. Keating, V. Gandhi, W. Plunkett, *Blood* **2009**, *113*, 4637–4645.
- [32] C. M. Olson, B. Jiang, M. A. Erb, Y. Liang, Z. M. Doctor, Z. Zhang, T. Zhang, N. Kwiatkowski, M. Boukhali, J. L. Green, W. Haas, T. Nomanbhoy, E. S. Fischer, R. A. Young, J. E. Bradner, G. E. Winter, N. S. Gray, *Nat. Chem. Biol.* **2018**, *14*, 163–170.
- [33] P. G. Wyatt, A. J. Woodhead, V. Berdini, J. A. Boulstridge, M. G. Carr, D. M. Cross, D. J. Davis, L. A. Devine, T. R. Early, R. E. Feltell, E. J. Lewis, R. L. McMenamin, E. F. Navarro, M. A. O'Brien, M. O'Reilly, M. Reule, G. Saxty, L. C. A. Seavers, D.-M. Smith, M. S. Squires, G. Trewartha, M. T. Walker, A. J.-A. Woolford, *J. Med. Chem.* **2008**, *51*, 4986–4999.
- [34] M. S. Squires, R. E. Feltell, N. G. Wallis, E. J. Lewis, D.-M. Smith, D. M. Cross, J. F. Lyons, N. T. Thompson, *Mol. Cancer Ther.* **2009**, *8*, 324–332.
- [35] B. O'Leary, R. S. Finn, N. C. Turner, *Nat. Rev. Clin. Oncol.* **2016**, *13*, 417–430.
- [36] B. Jiang, E. S. Wang, K. A. Donovan, Y. Liang, E. S. Fischer, T. Zhang, N. S. Gray, *Angew. Chem. Int. Ed.* **2019**, *58*, 6321–6326.
- [37] S. Rana, M. Bendjennat, S. Kour, H. M. King, S. Kizhake, M. Zahid, A. Natarajan, *Bioorg. Med. Chem. Lett.* **2019**, *29*, 1375–1379.

- [38] B. Zhao, K. Burgess, *Chem. Commun.* **2019**, *55*, 2704–2707.
- [39] S. Su, Z. Yang, H. Gao, H. Yang, S. Zhu, Z. An, J. Wang, Q. Li, S. Chandarlapaty, H. Deng, W. Wu, Y. Rao, *J. Med. Chem.* **2019**, DOI 10.1021/acs.jmedchem.9b00871.
- [40] C. Steinebach, Y. L. D. Ng, I. Sosič, C.-S. Lee, S. Chen, S. Lindner, L. P. Vu, A. Bricelj, R. Haschemi, M. Monschke, E. Steinwarz, K. G. Wagner, G. Bendas, J. Luo, M. Gütschow, J. Krönke, *Chem. Sci.* **2020**, *11*, 3474–3486.
- [41] X. Wu, X. Yang, Y. Xiong, R. Li, T. Ito, T. A. Ahmed, Z. Karoulia, C. Adamopoulos, H. Wang, L. Wang, L. Xie, J. Liu, B. Ueberheide, S. A. Aaronson, X. Chen, S. G. Buchanan, W. R. Sellers, J. Jin, P. I. Poulikakos, *Nat. Cancer* **2021**, *2*, 429–443.
- [42] P. Chen, N. V. Lee, W. Hu, M. Xu, R. A. Ferre, H. Lam, S. Bergqvist, J. Solowiej, W. Diehl, Y.-A. He, X. Yu, A. Nagata, T. VanArsdale, B. W. Murray, *Mol. Cancer Ther.* **2016**, *15*, 2273–2281.
- [43] G. E. Winter, D. L. Buckley, J. Paulk, J. M. Roberts, A. Souza, S. Dhe-Paganon, J. E. Bradner, *Science* **2015**, *348*, 1376–1381.
- [44] D. Remillard, D. L. Buckley, J. Paulk, G. L. Brien, M. Sonnett, H.-S. Seo, S. Dastjerdi, M. Wühr, S. Dhe-Paganon, S. A. Armstrong, J. E. Bradner, *Angew. Chem. Int. Ed.* **2017**, *56*, 5738–5743.
- [45] Y. Li, J. Yang, A. Aguilar, D. McEachern, S. Przybranowski, L. Liu, C.-Y. Yang, M. Wang, X. Han, S. Wang, *J. Med. Chem.* **2019**, *62*, 448–466.
- [46] P. Ottis, C. Palladino, P. Thienger, A. Britschgi, C. Heichinger, M. Berrera, A. Julien-Laferriere, F. Roudnicky, T. Kam-Thong, J. R. Bischoff, B. Martoglio, P. Pettazzoni, *ACS Chem. Biol.* **2019**, *14*, 2215–2223.
- [47] M. Van der Linden, M. Willekes, E. van Roon, L. Seslija, P. Schneider, R. Pieters, R. Stam, *Cell Cycle* **2014**, *13*, 834–844.
- [48] T. Wang, H. Yu, N. W. Hughes, B. Liu, A. Kendirli, K. Klein, W. W. Chen, E. S. Lander, D. M. Sabatini, *Cell* **2017**, *168*, 890-903.e15.
- [49] R. M. Meyers, J. G. Bryan, J. M. McFarland, B. A. Weir, A. E. Sizemore, H. Xu, N. V. Dharia, P. G. Montgomery, G. S. Cowley, S. Pantel, A. Goodale, Y. Lee, L. D. Ali, G. Jiang, R. Lubonja, W. F. Harrington, M. Strickland, T. Wu, D. C. Hawes, V. A. Zhivich, M. R. Wyatt, Z. Kalani, J. J. Chang, M. Okamoto, K. Stegmaier, T. R. Golub, J. S. Boehm, F. Vazquez, D. E. Root, W. C. Hahn, A. Tsherniak, *Nat. Genet.* **2017**, *49*, 1779–1784.
- [50] H. Shimizu, I. Nagamori, N. Yabuta, H. Nojima, *J. Cell Sci.* **2009**, *122*, 3145–3152.
- [51] S. Boffo, A. Damato, L. Alfano, A. Giordano, *J. Exp. Clin. Cancer Res.* **2018**, *37*, 36.

- [52] H. McCalmont, K. L. Li, L. Jones, J. Toubia, S. C. Bray, D. A. Casolari, C. Mayoh, S. E. Samaraweera, I. D. Lewis, R. K. Prinjha, N. Smithers, S. Wang, R. B. Lock, R. J. D'Andrea, *Blood Adv.* **2020**, *4*, 296–300.
- [53] N. Zhong, S. Shi, H. Wang, G. Wu, Y. Wang, Q. Ma, H. Wang, Y. Liu, J. Wang, *Int. J. Oncol.* **2016**, *49*, 1028–1038.
- [54] D. Lee, X. Zhao, Y.-I. Yim, E. Eisenberg, L. E. Greene, *Mol. Biol. Cell* **2008**, *19*, 2766–2776.
- [55] H. Tabara, Y. Naito, A. Ito, A. Katsuma, M. A. Sakurai, S. Ohno, H. Shimizu, N. Yabuta, H. Nojima, *PLOS ONE* **2011**, *6*, e26034.
- [56] A. Chaikuad, T. Keates, C. Vincke, M. Kaufholz, M. Zenn, B. Zimmermann, C. Gutiérrez, R. Zhang, C. Hatzos-Skintges, A. Joachimiak, S. Muyldermans, F. W. Herberg, S. Knapp, S. Müller, *Biochem. J.* **2014**, *459*, 59–69.
- [57] C. R. M. Asquith, B.-T. Berger, J. Wan, J. M. Bennett, S. J. Capuzzi, D. J. Crona, D. H. Drewry, M. P. East, J. M. Elkins, O. Fedorov, P. H. Godoi, D. M. Hunter, S. Knapp, S. Müller, C. D. Torrice, C. I. Wells, H. S. Earp, T. M. Willson, W. J. Zuercher, *J. Med. Chem.* **2019**, *62*, 2830–2836.
- [58] J. Broichhagen, J. A. Frank, D. Trauner, *Acc. Chem. Res.* **2015**, *48*, 1947–1960.
- [59] P. Wang, J. Huang, K. Wang, Y. Gu, *Eur. J. Med. Chem.* **2016**, *122*, 546–556.

7 – Towards Photoswitchable Molecular Glue Degraders

Martin Reynders^{1,2}, Michele Pagano^{3,4,5}, and Dirk Trauner^{1,4,6}

¹Department of Chemistry, New York University, New York, NY 10003, USA.

²Department of Chemistry, Ludwig Maximilians University of Munich
81377 Munich, Germany.

³Department of Biochemistry and Molecular Pharmacology, New York University
School of Medicine, New York, NY 10016, USA.

⁴Perlmutter Cancer Center, New York University School of Medicine, New York, NY
10016, USA.

⁵Howard Hughes Medical Institute, New York University School of Medicine, New
York, NY 10016, USA.

⁶NYU Neuroscience Institute, New York University School of Medicine, New York, NY
10016, USA.

Introduction

Molecular glues are small molecules that induce and stabilize interactions between two proteins. Unlike bifunctional molecules, molecular glues do not possess high affinity for both targets individually. In recent years, thalidomide and analogs thereof, termed immunomodulatory drugs (IMiDs), have been identified as molecular glue degraders.^[1–3] IMiDs function by recruiting zinc finger transcription factors to the E3 ligase cereblon inducing their ubiquitylation and subsequent degradation by the proteasome. The first identified substrates of this mechanism were the IKZF1 (Ikaros) and IKZF3 (Aiolos) transcription factors.^[1–3] Since then, additional substrates of IMiD-induced degradation have been discovered, such as casein kinase 1 α (CK1 α),^[4] GSPT1,^[5] SALL4,^[6,7] p63^[8] and several others.^[9] The proteins bind the same surface of IMiD-bound cereblon through a common β -hairpin fold, even though they differ in sequence. Neo-substrate selectivity is determined by the difference in IMiD structure and possibly by expression levels.^[9]

The degradation of most of these neo-substrates contributes to the anti-cancer effect of IMiDs, but targets such as p63 and SALL4 are responsible for their teratogenic activity.^[6–8] Analogous to PROTACs, IMiDs operate under a catalytic mechanism based on ubiquitylation, which sets them apart from classical inhibitors based on target occupancy. In addition to their antitumor effect, IMiDs are also used in inflammatory diseases and thalidomide was notoriously used as a sedative.^[10] However, with systemic exposure to the drug, adverse events such as hematologic side effects or neurotoxicity can occur.^[11,12] Thus, the ability to restrict the activity of these drugs to specific tissues could mitigate side effects and solve this problem. One approach in that direction is photopharmacology, a field which aims to regulate the activity of drugs in both time and space.^[13] Photopharmaceuticals can be prepared either through attachment of a photolabile protecting group to the drug or by incorporation of a photoswitch into the pharmacophore that undergoes reversible transformation upon light exposure.^[14]

We and others have previously developed strategies to control the activity of cereblon-based bifunctional degraders with light.^[15–18] Here we attempt to expand this method to generate photoswitchable molecular glue degraders (**Figure 7.1**). In addition to the cereblon-binding molecular glues mentioned above, two other classes of molecular

glue degraders have emerged recently. Indisulam and analogs recruit RBM39 for degradation by the DCAF15 E3-Ligase complex^[19–21] and another class of glues induced an interaction between the CUL4-DDB1 E3 ligase complex and CDK12, which leads to the degradation of CDK12-bound cyclin K.^[22–24]

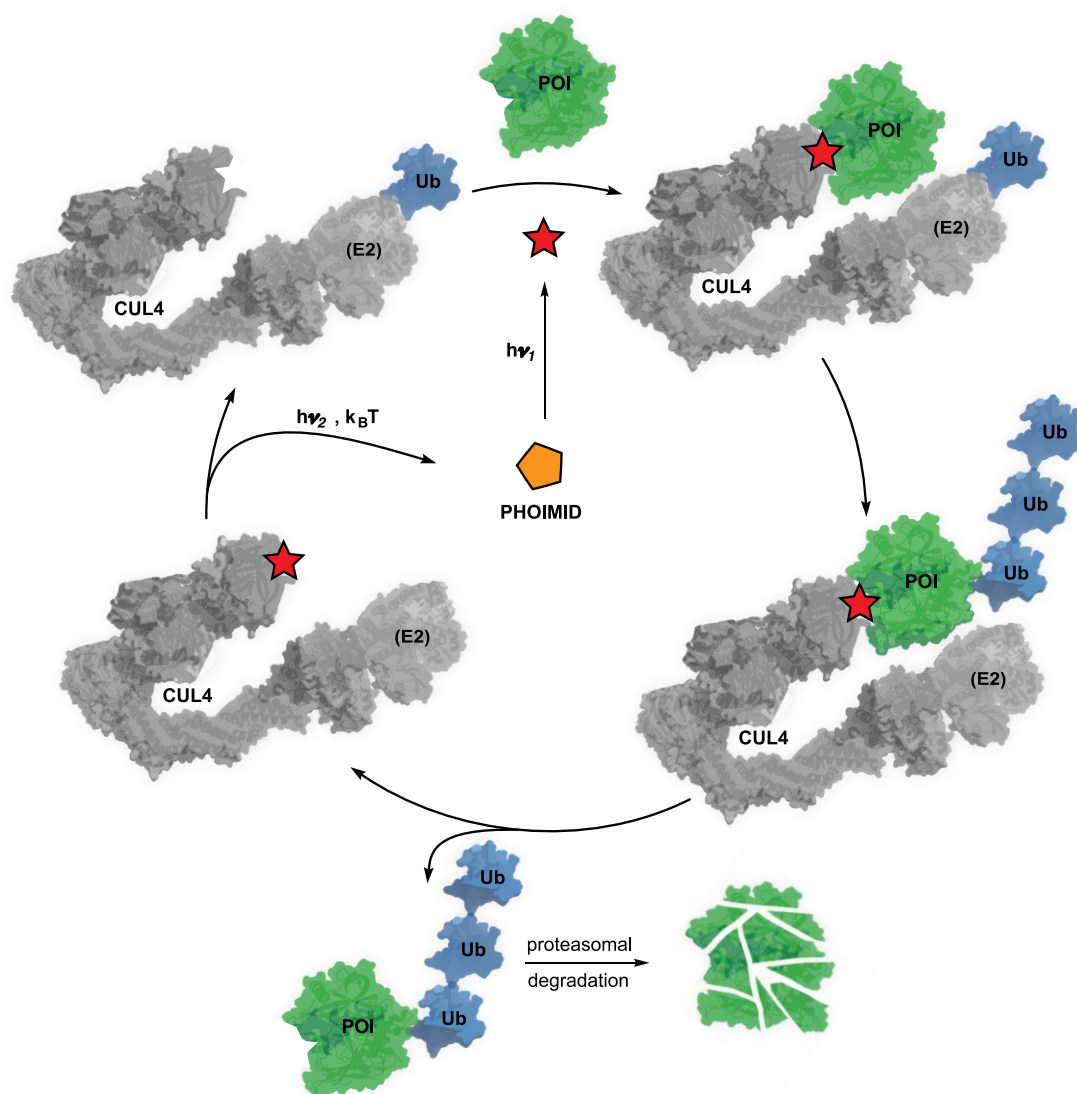


Figure 7.1: A) Schematic representation of a photoswitchable molecular glue (PHOIMID) inducing the catalytic ubiquitylation of a protein of interest (POI).

Results

Molecular glues modulate the surface of one protein which enables binding of another protein. Therefore, their design is challenging and their discovery was mostly serendipitous, in contrast to bifunctional degraders.^[23] IMiDs constitute the largest class of molecular glues that induce neo-substrate degradation with several approved drugs and many more in clinical trials (**Figure 7.2**). In addition to structure activity relationship studies, several crystal structures cereblon-binding IMiDs were reported that guide our design.^[5,9,25,26]

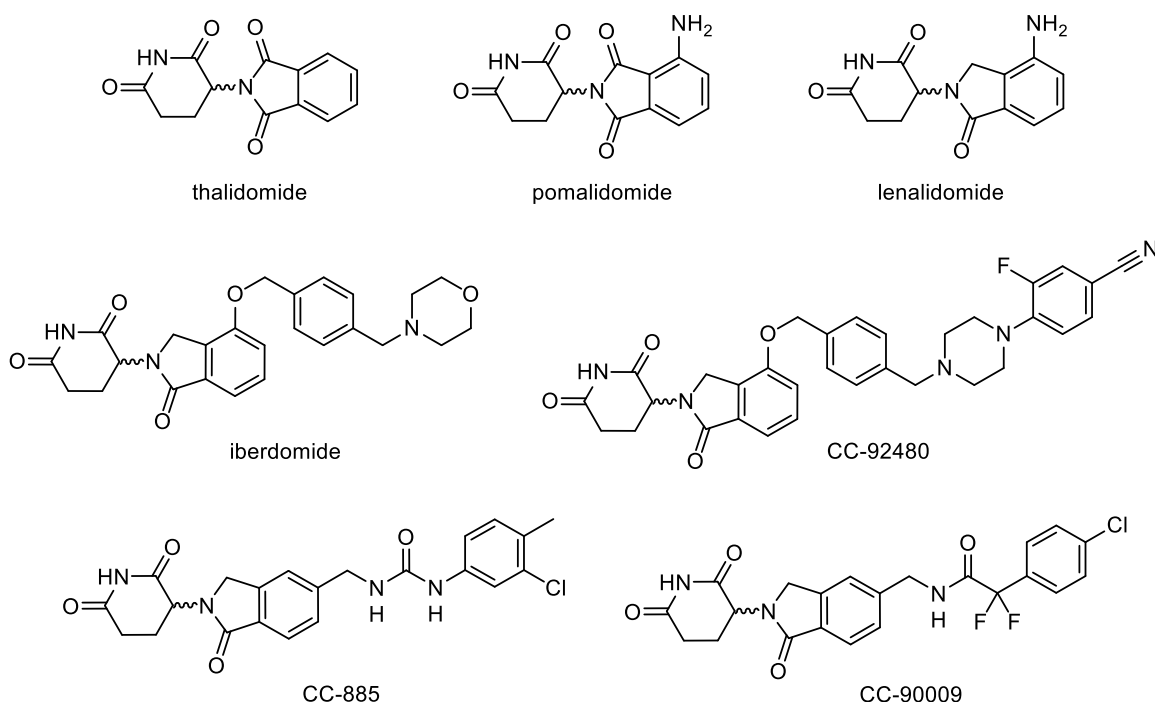


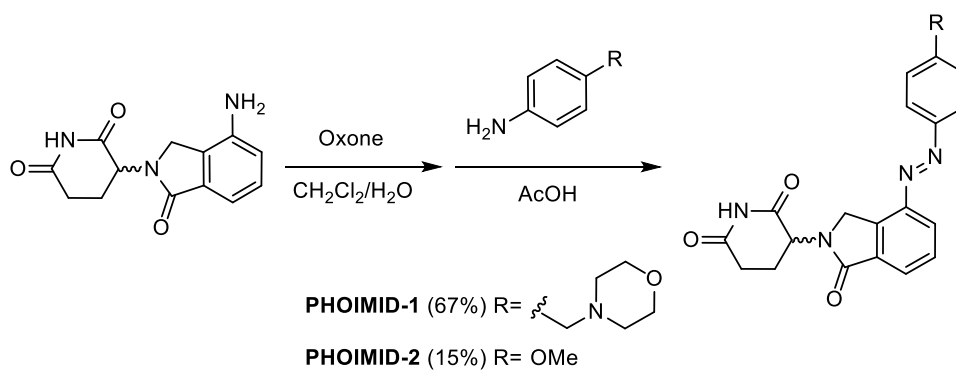
Figure 7.2: Cereblon binding molecular glues that induce degradation of neo-substrates.

An easy way to incorporate a photoswitch is the replacement of azobenzene isosteres^[13] such as the benzyl phenyl ether found in iberdomide.^[26] Alternatively, an existing aromatic ring can be extended to an azobenzene. Existing molecular glues (**Figure 7.2**) or PROTACs that still retain the ability to act as a molecular glue degrader show that substituents in the 3'- or 4'-position of the aryl ring can be tolerated.^[27–30]

Synthesis of PHOIMiDs was possible by oxidizing the amine on the glutarimide building block to the nitroso, followed by Baeyer-Mills coupling with the corresponding anilines (**Figure 7.3**). The oxidation step was performed with a minimal amount of water to dissolve the Oxone and a large volume of dichloromethane to solubilize the

starting material in the organic phase and prevent overoxidation. Due to the modular nature of this synthesis, larger libraries of PHOIMIDs could be prepared this way.

A



B

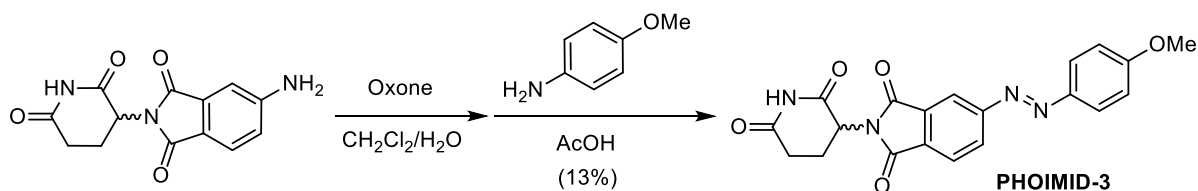


Figure 7.3: A) Synthesis of PHOIMID-1 and PHOIMID-2. B) Synthesis of PHOIMID-3.

Next, we investigated the photophysical properties of these photoswitches. The azolog of iberdomide, PHOIMID-1, most efficiently underwent *E*-to-*Z* isomerization upon 370 nm irradiation and an absorbance maximum at 337 nm (**Figure 7.4B,C**). In contrast, PHOIMID-2 showed a bathochromic shift in absorption with an absorbance maximum at 359 nm and the highest amount of *Z*-isomer was generated using 390 nm irradiation (**Figure 7.4E,F**). Half-lives of the thermal *Z*-to-*E* isomerization varied between 3.5 h for PHOIMID-1 and 17 h for PHOIMID-2 (**Figure 7.4G,H**). The absorption maximum of PHOIMID-3 showed a further bathochromic shift to 377 nm (**Figure 7.5B,C**). The highest amount of *Z*-isomer could still be generated with 390 nm irradiation, corresponding to a local minimum in *Z*-isomer absorption at that wavelength (**Figure 7.5D,E**). Thermal *Z*-to-*E* isomerization proceeded with a half-life of 14.7 h (**Figure 7.5F**).

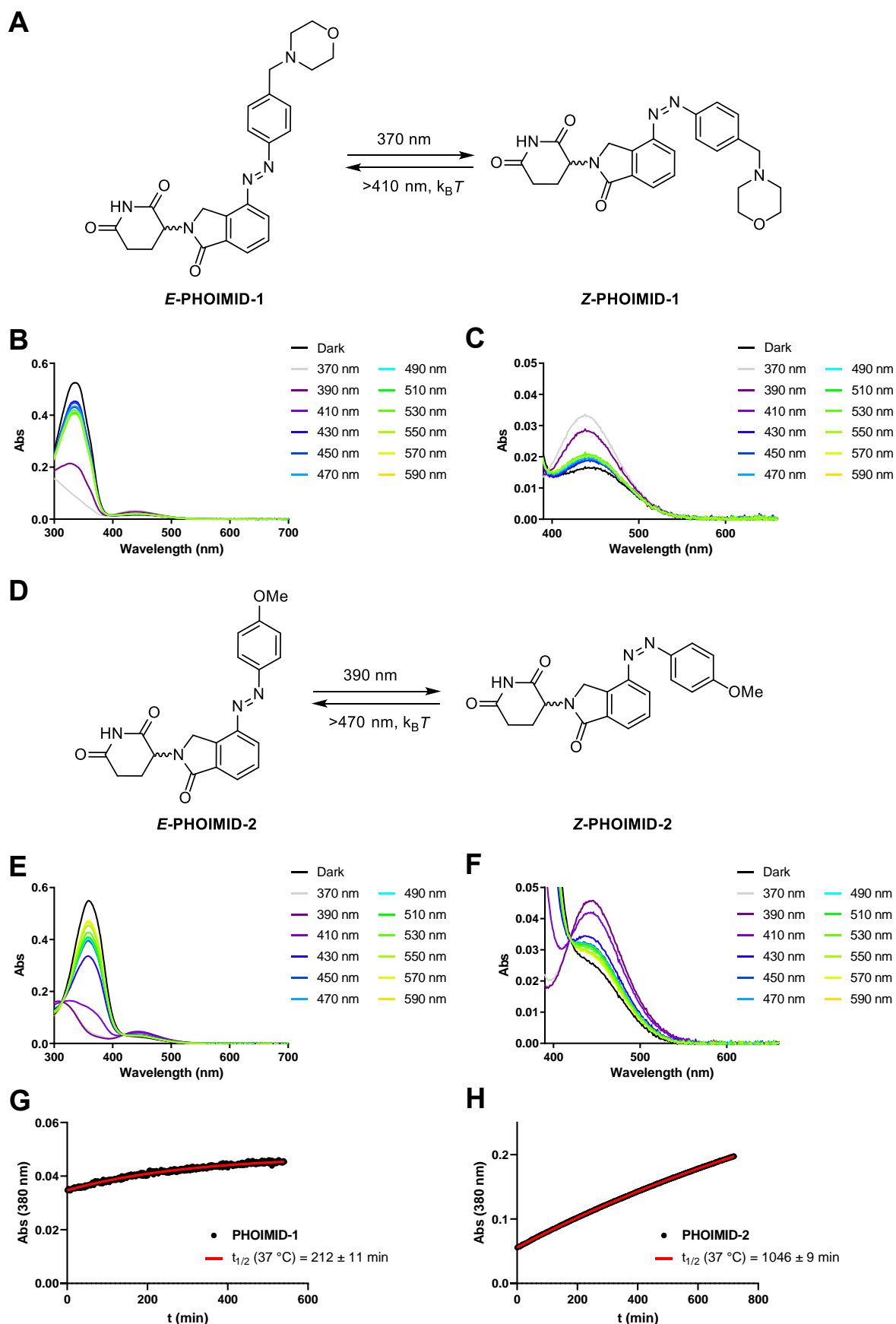


Figure 7.4: Characterization of **PHOIMID-1**. A) Structure and isomerization of **PHOIMID-1**. B), C) Absorption spectra of **PHOIMID-1** after 5 min of irradiation with the indicated wavelength. D) Structure and isomerization of **PHOIMID-2**. E), F) Absorption

spectra of **PHOIMID-2** after 5 min of irradiation with the indicated wavelength. G) Thermal *Z*-to-*E* isomerization of **PHOIMID-1** at 37 °C in a 1:1 mixture of DMSO and PBS (pH 7.4). G) Thermal *Z*-to-*E* isomerization of **PHOIMID-2** at 37 °C in a 1:1 mixture of DMSO and PBS (pH 7.4).

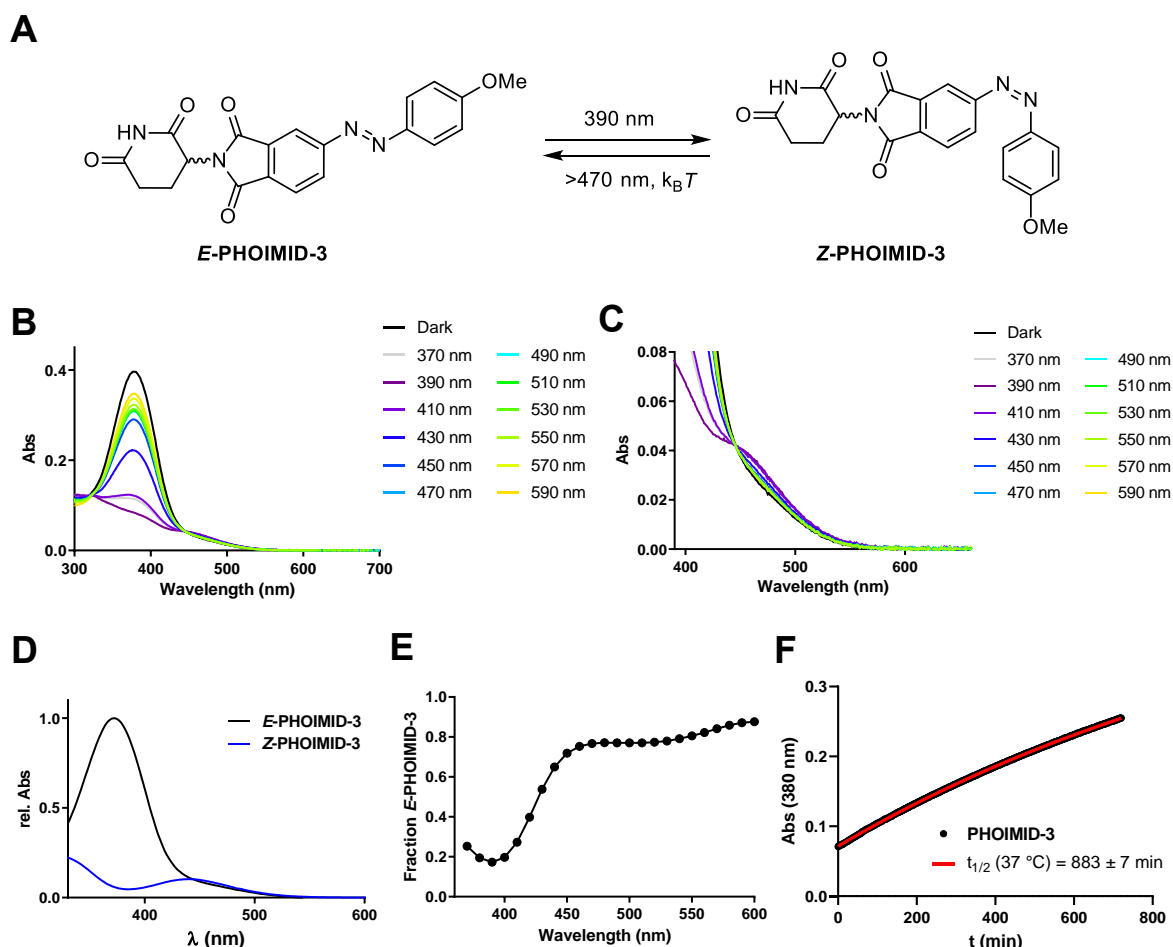


Figure 7.5: Characterization of **PHOIMID-3**. A) Structure and isomerization of **PHOIMID-3**. B), C) Absorption spectra of **PHOIMID-3** after 5 min of irradiation with the indicated wavelength. D) Absorption spectra of separated **PHOIMID-3** isomers as obtained by LCMS. E) Calculated fraction of **E-PHOIMID-3** after 5 min irradiation with the indicated wavelength. F) Thermal *Z*-to-*E* isomerization of **PHOIMID-1** at 37 °C in a 1:1 mixture of DMSO and PBS (pH 7.4).

Next, we investigated the ability of PHOIMIDs to degrade neo-substrates. PHOIMID-1 and PHOIMID-2 did not show any degradation of typical neo-substrates such as CK1 α , GSPT1 or Ikaros (**Figure 7.7A, S7.4A**). PHOIMID-3 did not lead to protein degradation after 4 h (Figure S7.4B). After 15 h we could observe partial degradation of Aiolos upon 390 nm irradiation, but not in the dark (**Figure 7.7B**). However, lenalidomide is much

more potent than PHOIMID-3 in inducing neo-substrate degradation (**Figure 7.7B**). A general concern when using azobenzenes in biological systems is the possibility of reducing the diazene.^[31,32] The absence of degradation for PHOIMID-1 and PHOIMID-2 shows that the azobenzene is stable towards reduction to lenalidomide, which would result in significant degradation.

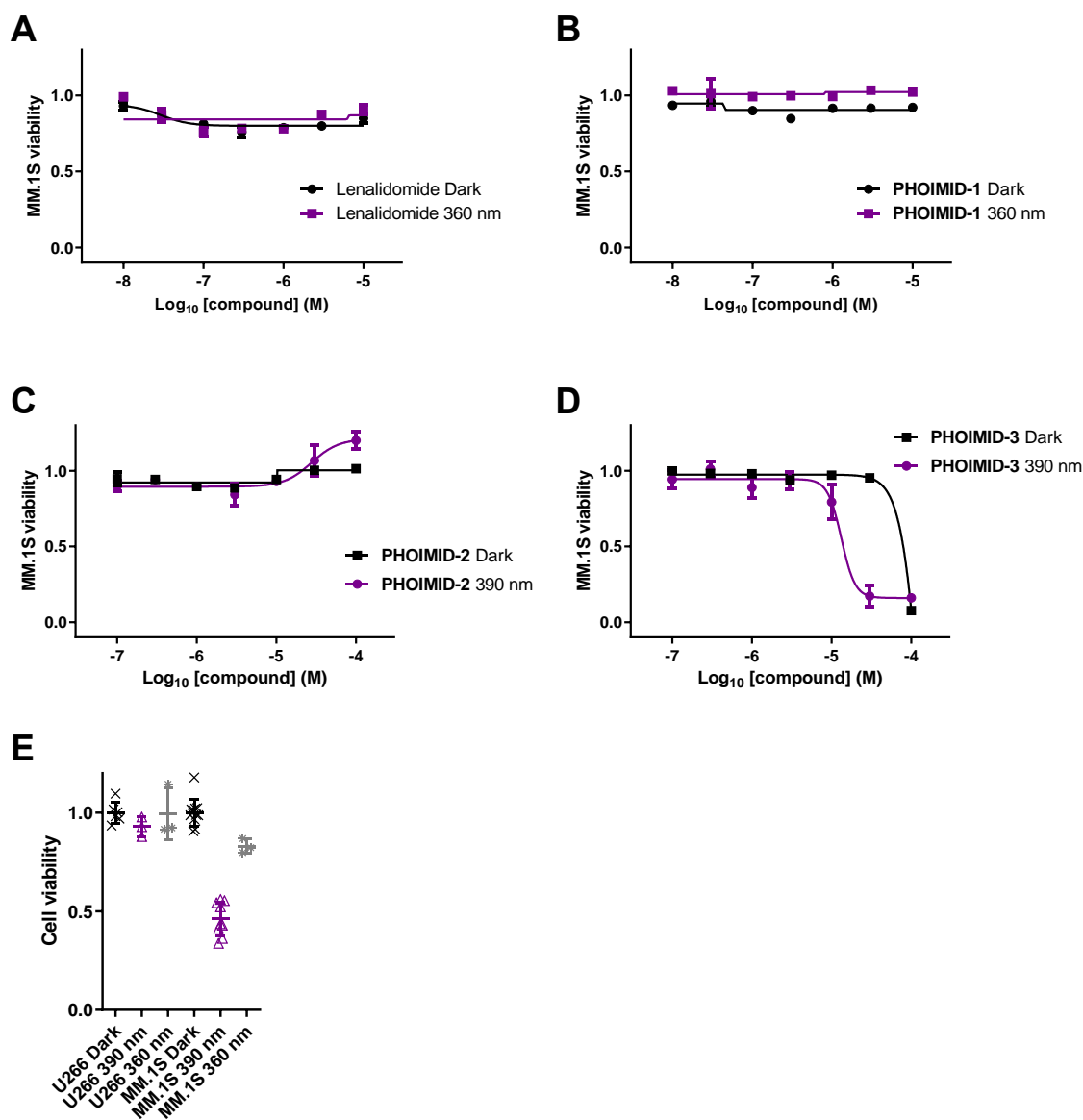


Figure 7.6: Cytotoxic activity of **PHOIMIDs**. A), B) Normalized viability of MM.1S cells after treatment with lenalidomide (A) or **PHOIMID-1** (B) for 72 h in the dark or under pulsed 360 nm irradiation (100 ms every 10 s). C), D) Normalized viability of MM.1S cells after treatment with **PHOIMID-2** (C) or **PHOIMID-3** (D) for 72 h in the dark or under pulsed 390 nm irradiation (100 ms every 10 s). E) Effect of irradiation (100 ms pulses every 10 s) on U266 and MM.1S viability.

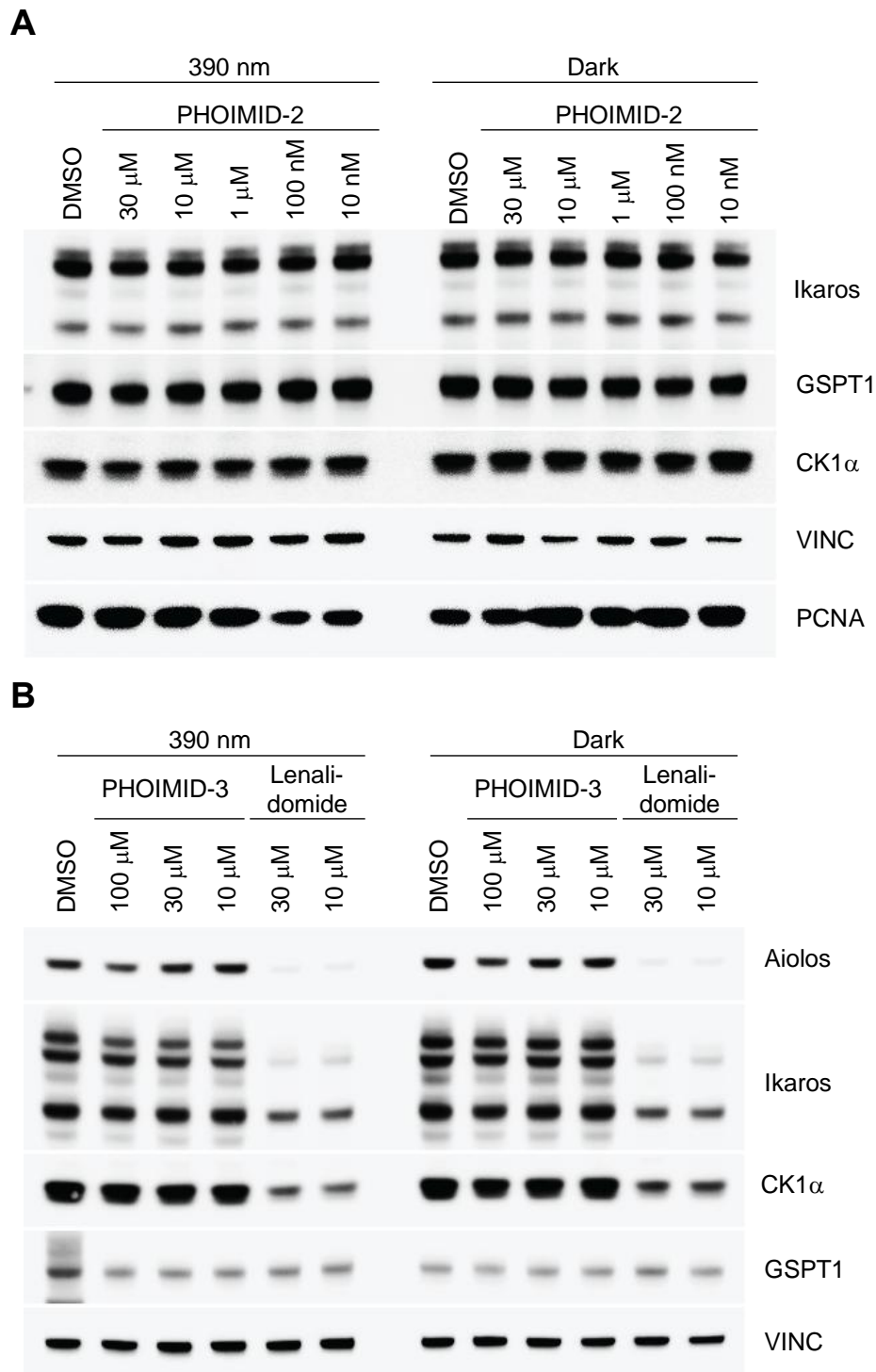


Figure 7.7: A) Immunoblot analysis after treatment of RS4;11 cells with **PHOIMID-2** for 12 h at the indicated concentrations. Cells were either irradiated with 100 ms pulses of 390 nm light every 10 s (left) or kept the dark (right). B) Western Blot of RS4;11 cells treated with **PHOIMID-3** or lenalidomide for 15 h at the indicated concentrations under pulsed 390 nm irradiation (left, 100 ms per 10 s) or in the dark (right).

A different scaffold of molecular glue degraders is found in CR8. It functions by forming a protein-protein-interaction (PPI) between DDB1 (bound to the CUL4 E3 ligase) and CDK12. CDK12 then recruits cyclin K, which is ubiquitylated and degraded. Structurally similar CDK12 inhibitors like roscovitine do not induce cyclin K degradation. We designed AzoCR8 by replacing the biaryl motif, which is essential for the DDB1 interaction, with a *Z*-azobenzene (**Figure 7.8A**). Although a biaryl is not a classical structural motif for replacement by an azobenzene, azologisation can be successful.^[33] Modeling of Azo-CR8 into the crystal structure of CR8 bound to DDB1 and CDK12,^[22] indicated that the *Z*-isomer may mimic CR8 binding, whereas the *E*-isomer could not (**Figure S7.5**). Azo-CR8 could be synthesized from 2,6-dichloropurine in 3 steps (**Figure 7.8B**).

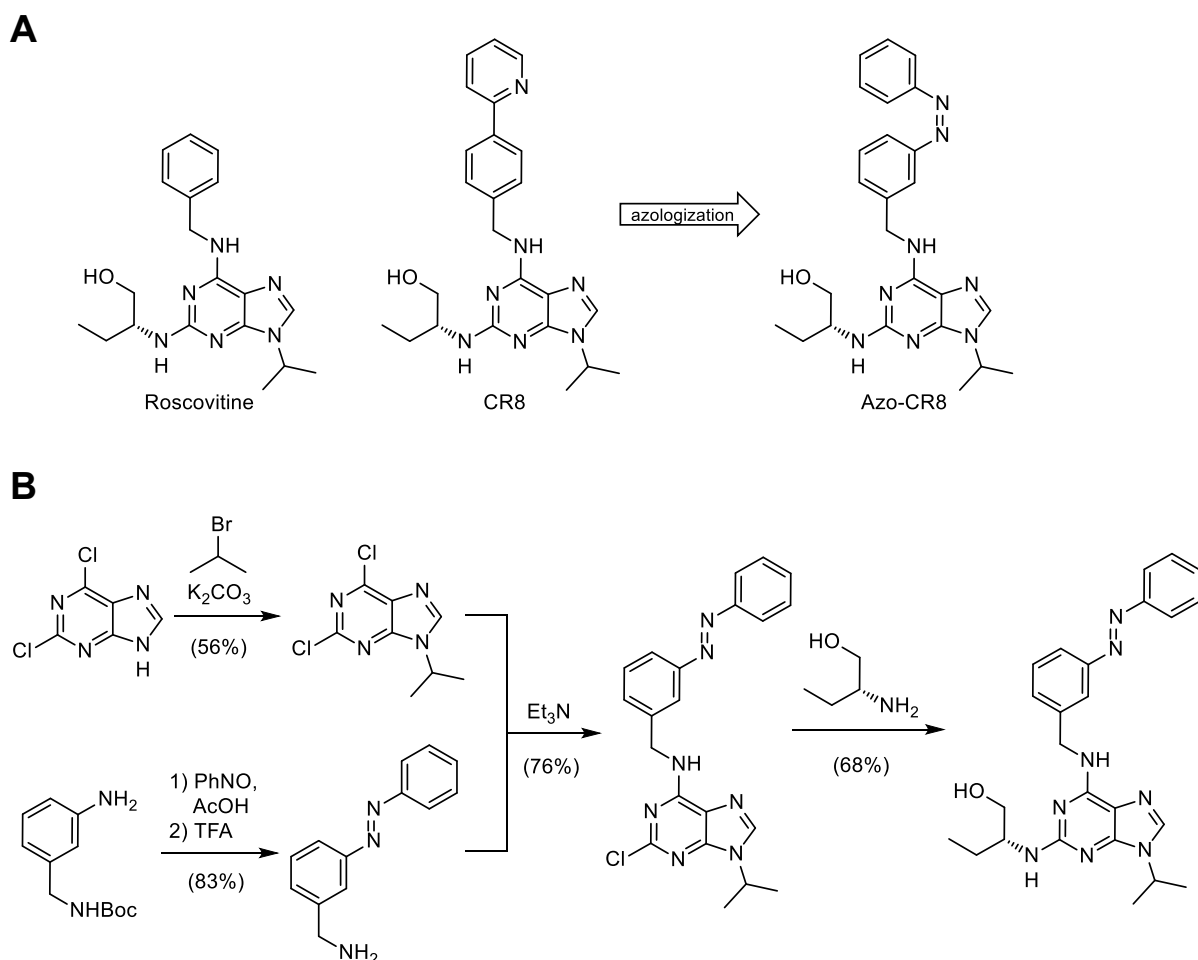


Figure 7.8: A) Structures of CDK inhibitors roscovitine and CR8 and design of **Azo-CR8**. B) Synthesis of **Azo-CR8**.

AzoCR8 underwent efficient *E*-to-*Z* isomerization upon 360 or 370 nm and the *Z*-isomer had a thermal half-life of 5 h (**Figure 7.9B–D**). Azo-CR8 did not show any difference on the viability of RS4;11 cells between incubation in the dark or under pulsed 360 nm irradiation (**Figure 7.9E**). We also did not observe degradation of cyclin K or changes in CDK12 levels after incubation of RS4;11 or HEK293T cells with AzoCR8 either in the dark or under pulsed 360 nm irradiation (**Figure 7.10A,B**). The results indicate that the *Z*-AzoCR8 is unable to form the productive ternary complex observed for CR8 based on the difference in 3D-structure between biaryl and *Z*-azobenzene.

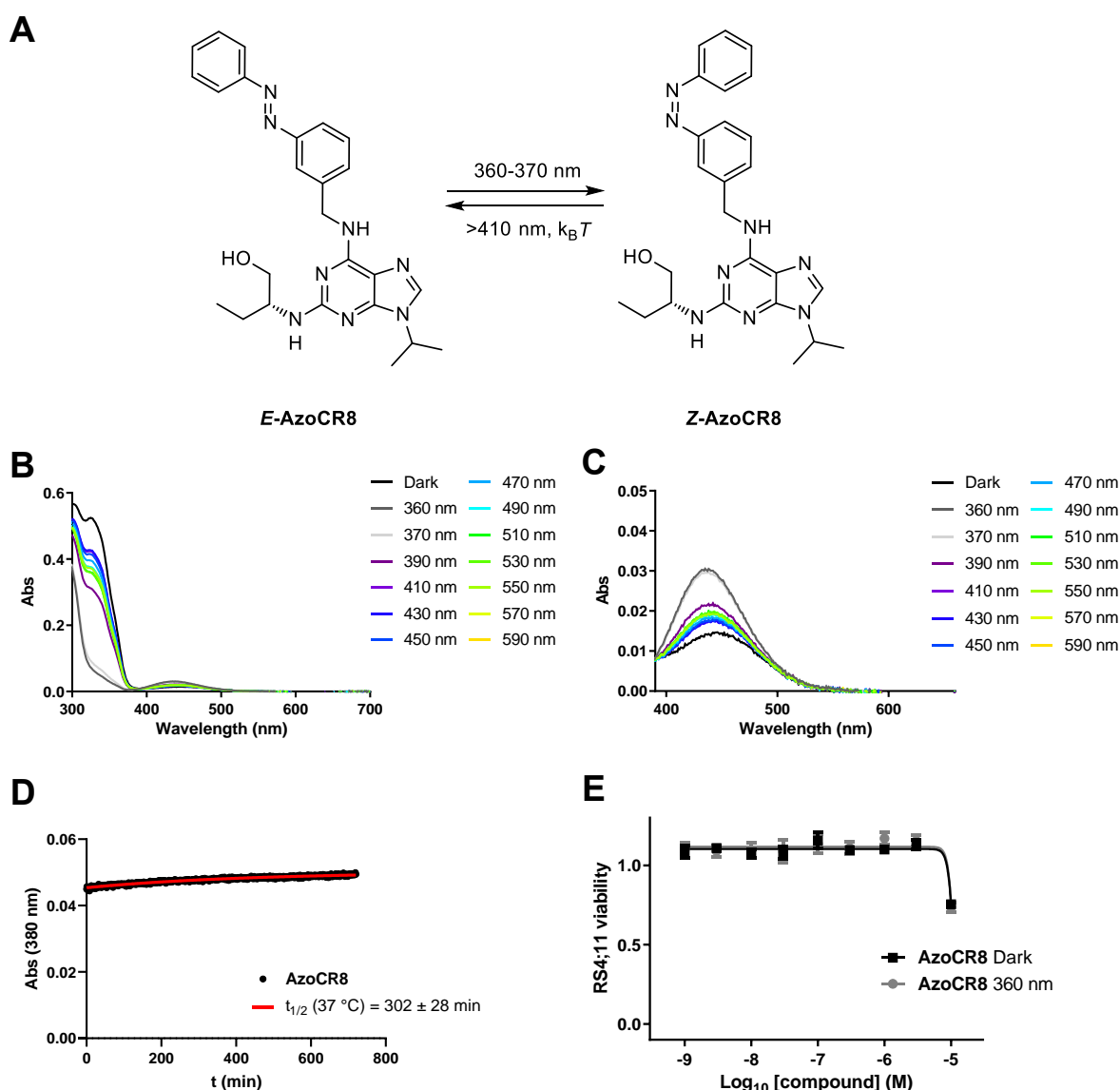


Figure 7.9: Characterization of **Azo-CR8** A) Structure and isomerization of **Azo-CR8**. B), C) Absorption spectra of **Azo-CR8** after 5 min of irradiation with the indicated wavelength. D) Thermal *Z*-to-*E* isomerization of **PHOTAC-I-15** at 37 °C in a 1:1 mixture of DMSO and PBS (pH 7.4). E) Viability of RS4;11 cells after treatment

with **Azo-CR8** for 72 h in the dark or under pulsed 360 nm irradiation (100 ms every 10 s).

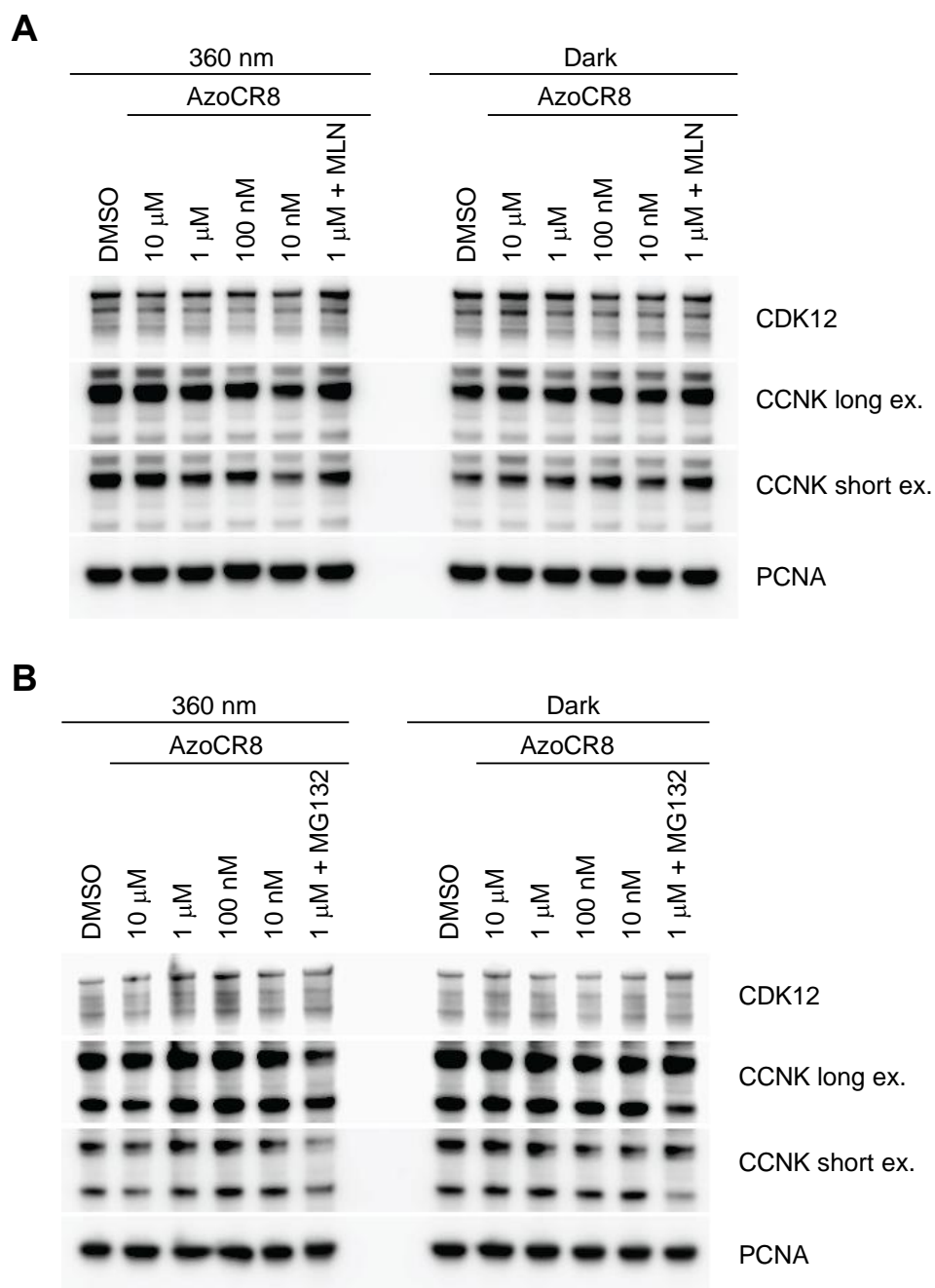


Figure 7.10: A) Immunoblot analysis of RS4;11 cells treated with **Azo-CR8** for 4 h. Cells were either irradiated with pulses of 360 nm light (left, 100 ms every 10 s) or kept in the dark (right). B) Immunoblot analysis of HEK293T cells treated with **Azo-CR8** for 16 h at the indicated concentrations under pulsed 360 nm irradiation (left, 100 ms per 10 s) or in the dark (right). MLN = 1.25 μ M MLN4924, MG132 = 1.25 μ M MG132.

Summary and Outlook

We have described the design and synthesis of several photoswitchable molecular glues based on azobenzenes. Both substitution patterns explored with PHOIMIDs showed good photoswitching, but only PHOIMID-3 exhibited a light-dependent viability effect in MM.1S cells. Further, PHOIMID-3 showed moderate degradation of Aiolos at high concentrations. Therefore, PHOIMID-3 is an ideal candidate for further development into a more potent photoswitchable molecular glue. The modular synthesis developed herein will allow the rapid generation of a library of PHOIMIDs using commercial anilines to optimize their ability to degrade neo-substrates of cereblon.

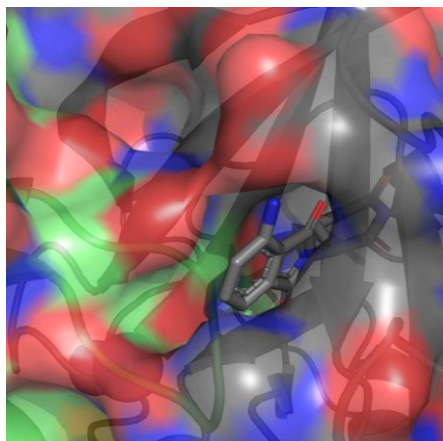
The strong effect of 390 nm irradiation on MM.1S viability could be mitigated by preparing PHOIMIDs with red-shifted absorption spectra.^[34–39] However, the synergy between irradiation and activation of a photopharmacological agent using the same wavelength could also be exploited for therapeutic applications, since the susceptibility towards light was not observed in other cell lines.

Further, this work generates important structure activity relationship data on photoswitchable cereblon ligands, which will aid the development of PHOTACs. Several PROTACs are reported that function as a molecular glue to induce the degradation of neo-substrates.^[27–30,40] Depending on the therapeutic target it can either be beneficial or undesirable to promote the degradation of cereblon neo-substrates and therefore it is critical to understand the underlying design principles to incorporate the photoswitch.

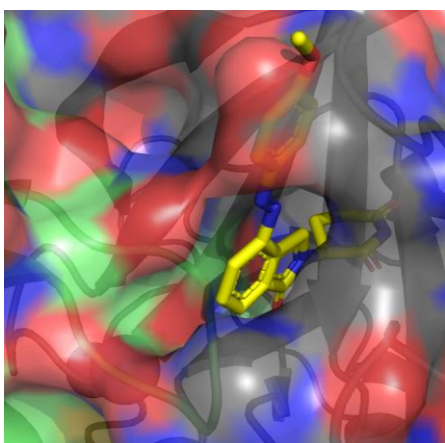
Optimized PHOIMIDs could be applied in photomedicine to treat cancers and inflammatory diseases analogous to the application of IMiDs. Further they could find use as tool compounds in chemical optogenetics to enable the optical control of fusion proteins using the IMiD-inducible degron system.^[41–43]

Supplementary Figures

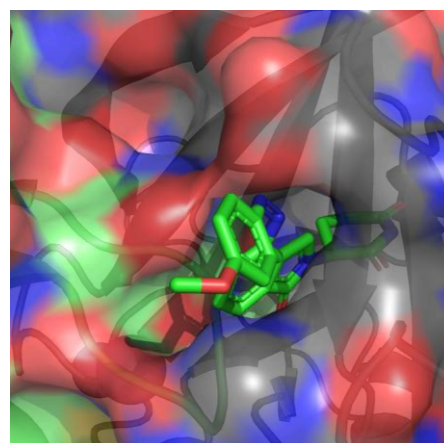
A



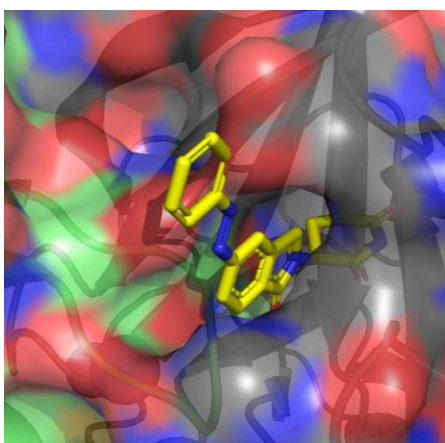
B



C



D



E

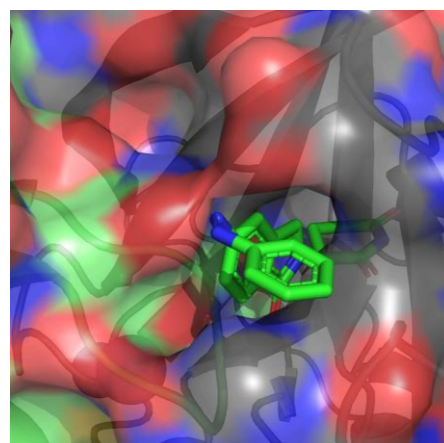


Figure S7.1: Model of pomalidomide and PHOIMIDs binding the complex between cereblon (gray) and Ikaros (green) (PDB 6H0F).^[9] A) Pomalidomide (gray) bound to the cereblon-Ikaros complex. B) **E-PHOIMID-2** (yellow) clashing with the complex. C) **Z-PHOIMID-2** (green) modeled into to the complex. D) **E-isomer** model of 4-substituted lenalidomide (yellow) in the complex. E) **Z-isomer** model of 4-substituted lenalidomide (green) bound to the complex. Models were created using Schrödinger Maestro 11.9.

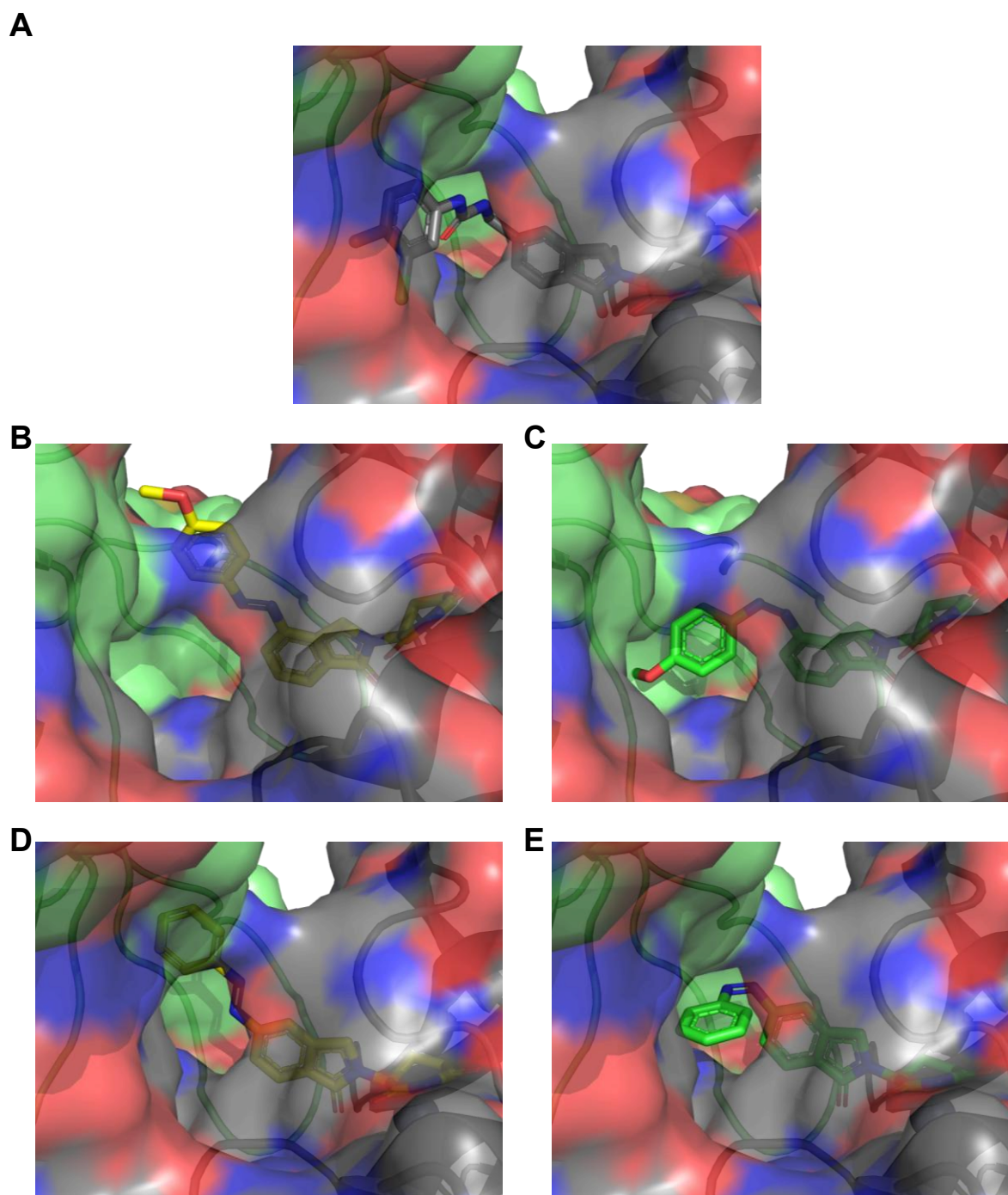


Figure S7.2: Model of CC-885 and photoswitchable IMiDs binding the complex between cereblon (gray) and GSPT1 (green) (PDB 5HXB).^[5] A) CC-885 (gray) bound to the cereblon-GSPT1 complex. B) *E*-PHOIMID-2 (yellow) clashing with the complex. C) *Z*-PHOIMID-2 (green) interacting and clashing with the complex. D) *E*-isomer model of 4-substituted lenalidomide (yellow) extending into GSPT1. E) *Z*-isomer model of 4-substituted lenalidomide (green) bound to the complex without steric constraints. Models were created using Schrödinger Maestro 11.9.

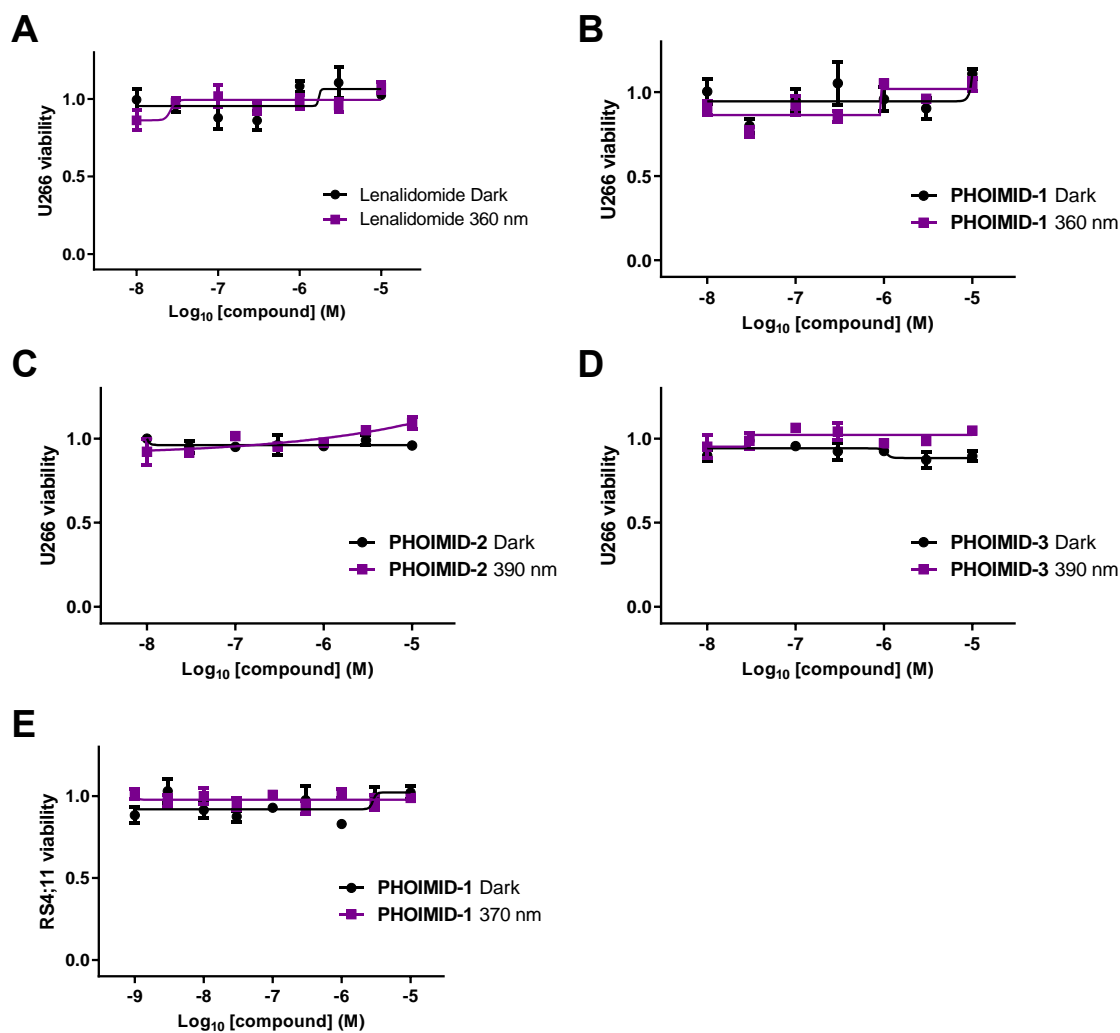


Figure S7.3: *In cellulo* activity of **PHOIMIDs**. A)–D) Viability of U266 cells after treatment with lenalidomide (A), **PHOIMID-1** (B), **PHOIMID-2** (C) or **PHOIMID-3** (D) for 72 h in the dark or under pulsed irradiation (A, B) 360 nm / C), D) 390 nm, 100 ms every 10 s). E) Viability of RS4;11 cells after treatment with **PHOIMID-1** for 72 h in the dark or under pulsed 370 nm irradiation (100 ms every 10 s).

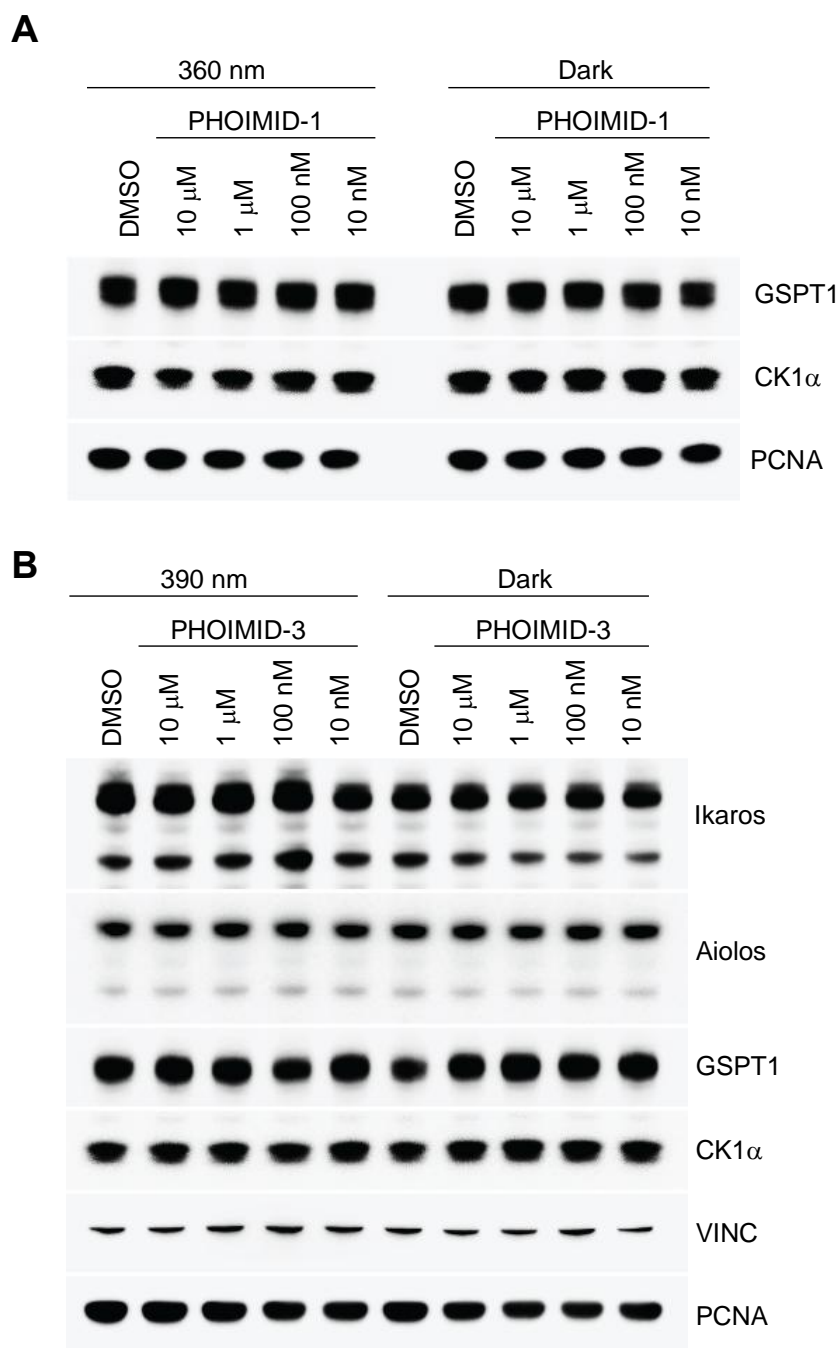


Figure S7.4: A) Immunoblot analysis of RS4;11 cells treated with **PHOIMID-1** for 4 h. Cells were either irradiated with pulses of 360 nm light (left, 100 ms every 10 s) or kept in the dark (right). B) Immunoblot analysis of RS4;11 cells treated with **PHOIMID-3** for 4 h at the indicated concentrations under pulsed 360 nm irradiation (left, 100 ms per 10 s) or in the dark (right).

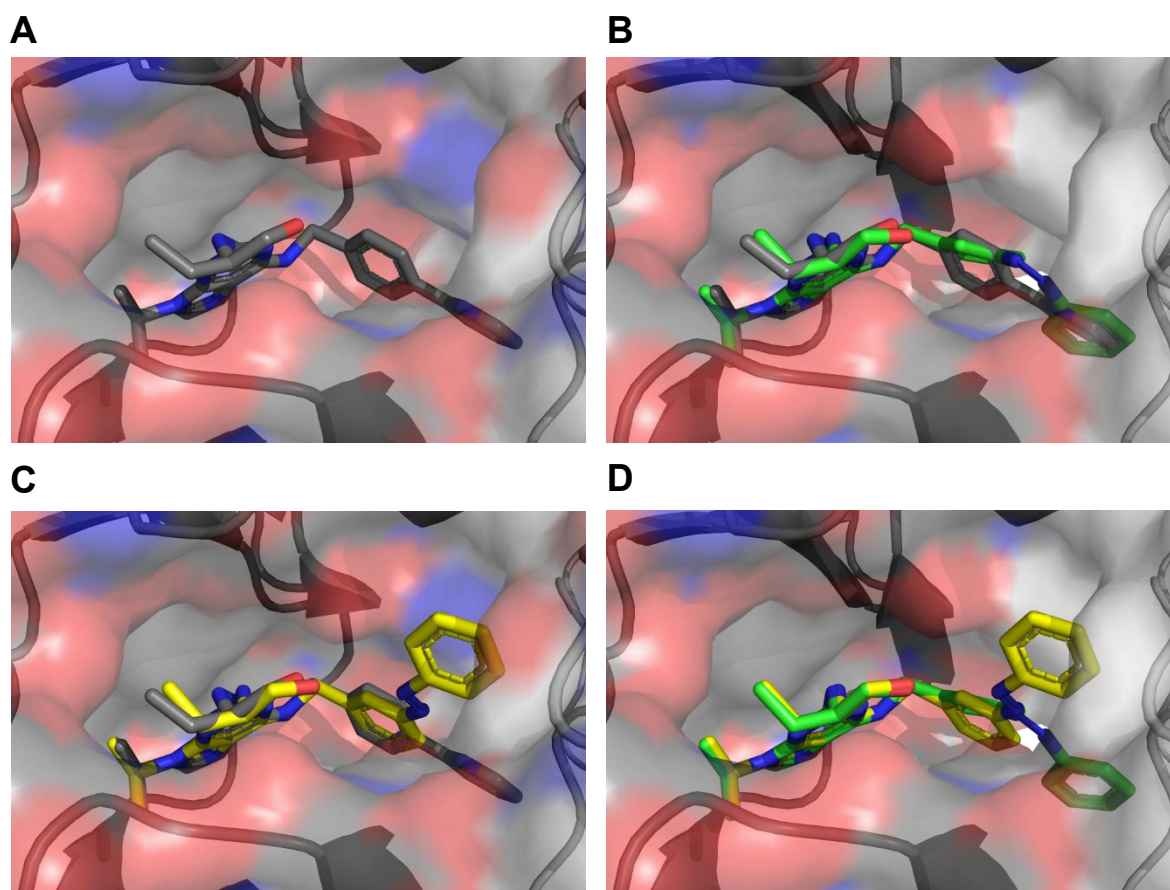


Figure S7.5: Model of a CR8 and **AzoCR8** binding in the CDK12 (gray)-Cyclin K (white) complex (PDB 6TD3).^[22] A) CR8 (gray) bound to the CDK12-Cyclin K complex. B) Overlay of **Z-AzoCR8** (green) and CR8. C) Overlay of **E-AzoCR8** (yellow) and CR8. D) Overlay of both isomers. Models were created using Schrödinger Maestro 11.9.

Methods

Determination of Photophysical properties

UVVis spectrometry was performed on a Varian Cary 60 UV-Visible Spectrophotometer using BRAND UV-Cuvette Disposable Spectrophotometer/Photometer Ultra-Micro Cuvettes, BrandTech (10 mm light path). An Agilent Technologies PCB 1500 Water Peltier system was used for temperature control and samples were irradiated with a Cairn Research Optoscan Monochromator with Optosource High Intensity Arc Lamp equipped with a 75 W UXL-S50A lamp (USHIO Inc. Japan) and set to 15 nm full width at half maximum. Samples were stored and prepared under red light to avoid formation of the *Z*-isomers. 10 mM stock solutions were prepared in the dark and diluted to a final concentration of 25 μ M to measure the UV-VIS spectra of **PHOTACs** following irradiation with different wavelengths for 5 min using a monochromator. Measurement was started from the dark-adapted state, followed by 370 nm and further stepwise wavelength increase in 10 nm increments up to 600 nm. By increasing the wavelength from low to high, a realistic estimate *Z*- to *E*-isomerization can be obtained, whereas going the reverse direction from high to low wavelength, the PSSs might not be reached due to low absorptivity above 500 nm. Spectra were recorded in DMSO to avoid any artifacts of aggregation or precipitation. Thermal relaxation was measured by preirradiating **PHOTACs** with 390 nm light and observing the absorption at 380 nm over 12 h at 37 °C in DMSO in tightly sealed cuvettes. Half-lives were determined by nonlinear regression using GraphPad Prism Version 9.02.

Separated spectra of the *Z*- and *E*-isomers were obtained from the internal UV-VIS detector of the LCMS by irradiating the sample before injection and were normalized at the isosbestic point. Isomer ratios were calculated in the region of largest absorption difference between 330 and 390 nm from the separated spectra obtained by LCMS and the spectra obtained following irradiation with different wavelengths for 5 min, normalized at the isosbestic point.

LED illumination

For illumination of the cells we used the cell disco system as previously described in the literature.^[44] 5 mm LEDs 360 nm (XSL-360-5E), 370 nm (XSL-370-5E), 390 nm (VL390-5-15) were purchased from Roithner Lasertechnik. For viability experiments using 390 nm, cells were preirradiated for 30 s at 390 nm to quickly switch the

photoswitches in the active state. Pulsed irradiation was performed using 100 ms pulses every 10 s (unless indicated otherwise) in 96- or 6-well plates, controlled by an Arduino system.

Cell culture

The human acute lymphoblastic leukemia RS4;11 (ATCC[®] CRL1873[™]) cell line was purchased from the American Type Culture Collection and cultured in phenol red-free RPMI1640 medium (Gibco) with 10% fetal bovine serum (FBS) and 1% penicillin/streptomycin (PS) in a humidified incubator at 37 °C with 5% CO₂ in air. For the experiments compounds were serially diluted in phenol red-free RPMI1640 (Gibco) as 2x stock solutions resulting in a final concentration of 1% DMSO during the assay. Azobenzene stocks and dilutions were strictly kept in the dark and prepared under red light conditions.

For immunoblotting analysis, cells (2×10^6 cells for RS4:11) were incubated for the indicated times with PHOTACs, placed in a light-proof box, and preirradiated for 30 s at 390 nm followed by 100 ms pulses every 10 s or were kept in the dark for 4 h. After incubation, cells were collected in the dark by centrifugation (200 g, 5 min) at 4 °C and the pellets were washed twice with ice cold PBS (1 mL).

Colorimetric MTS Assays

The activity of dehydrogenase enzymes in metabolically active cells, as a quantitative measurement for cytotoxicity and proliferation, was determined by colorimetric measurement of the reduction of [3-(4,5-dimethylthiazol-2-yl)-5-(3-carboxymethoxyphenyl)-2-(4-sulfophenyl)-2H-tetrazolium (MTS) to the formazan product. The absorbance of formazan was measured at 500 nm on a FLUOstar Omega microplate reader (BMG Labtech). Cells were treated with different concentrations of PHOTACs (10 μ M to 1 nM) in triplicates using 1% DMSO as cosolvent, and incubated in a 96-well plate for 72 h. The cells were placed in light-proof boxes and exposed to the lighting conditions specified in the experiment for 72 h. Well plates were placed on top of the LED plates, however when using 360 nm LEDs, the LED plate was placed on top of the 96-well plate at a 10 cm distance. After 72 h, 10 μ L of Promega CellTiter 96[®] AQueous One Solution Reagent was added to each well and incubated for further 4-

7 hours at 37 °C. The absorbance at 500 nm was measured on a FLUOstar Omega 96-well plate reader (BMG Labtech).

Data was analyzed using GraphPad Prism Version 9.02 (GraphPad Software Inc) and fitted using the [Inhibitor] vs. response -- Variable slope (four parameters) fit. Results represent the mean viability \pm SEM relative to the 1% DMSO treated control. Light dependence of cell viability (Figure 7.6E) was analyzed from all experiments and normalized to cells in the dark. Results are shown as individual data points and mean viability \pm SD.

Immunoblotting Analysis

Cells were lysed in RIPA buffer containing protease and phosphatase inhibitors (cOmplete™, Mini Protease Inhibitor Cocktail, SigmaAldrich, 4693124001 and Phosphatase Inhibitor Cocktail 3, SigmaAldrich, P0044-1ML) and protein concentration was determined using the BCA method (Thermo Fisher, 23225). Immunoblotting was performed as previously described.^[16] Briefly, samples were resolved under denaturing and reducing conditions using 4%–12% Bis-Tris gels (NuPAGE) and transferred to a PDVF membrane (Immobilon-P, Millipore). Membranes were blocked with 5% nonfat dried milk, incubated with primary antibodies overnight at 4°C. After washing the membranes, secondary antibodies coupled with horseradish peroxidase were applied. Immunoreactive bands were visualized using SuperSignal™ Western Blot Enhancer or SuperSignal™ West Femto Maximum Sensitivity Substrate (Thermo Fisher Scientific) and the signal was acquired using an ImageQuant LAS 400 (GE). The following antibodies were used:

Antibodies	Source	Identifier
Aiolos	Cell Signaling Technology	15103S
CDK12	Cell Signaling Technology	11973S
CyclinK (CCNK)	Bethyl Laboratories	A301-939A
CK1 α	Santa Cruz Biotechnology	sc-74582
GSPT1	proteintech	10763-I-AP
Ikaros	Cell Signaling Technology	14859S
PCNA	dako	M0879
VINC	Bethyl Laboratories	A302-535A
anti-Rabbit IgG, peroxidase-linked antibody	Thermo Fisher	NA934
anti-Mouse IgG, peroxidase-linked antibody	Thermo Fisher	NA931
anti-goat IgG-HRP	Santa Cruz Biotechnology	sc-2354

Synthetic Procedures and Characterization

General information

The reagents and solvents used in this study were bought from the following chemical suppliers: Acros Organics, Alfa Aesar, Combi-Blocks, Oakwood, OxChem, Sigma-Aldrich and Medkoo Biosciences and were used as purchased.

Dry solvents used in reactions performed under inert atmosphere were obtained by passing the degassed solvents through activated alumina columns. Additionally, dry solvents were stored over molecular sieves under an inert atmosphere.

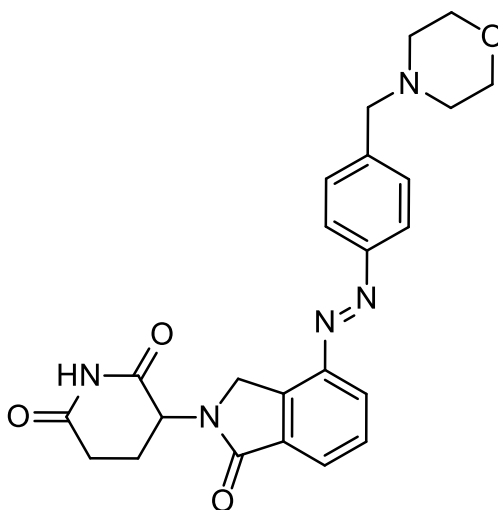
Column chromatography was carried out on silica gel (60 Å pore size, 40–63 µm, Merck KGaA) using a Teledyne Isco Combiflash EZprep flash purification system.

Thin-layer chromatography (TLC) was performed on glass plates precoated with silica gel (0.25 mm, 60-Å pore size, Merck). TLC plates were visualized by exposure to UV light (254 and 366 nm).

NMR spectra were obtained on a Bruker Avance III HD 400 MHz spectrometer equipped with a CryoProbe™ operating at 400 MHz for ¹H and 100 MHz for ¹³C spectra. Integration results and multiplets are reported as observed and denoted as follows: s (singlet), d (doublet), t (triplet), q (quartet), p (pentet), h (hextet), sept (septet), and m (multiplet) and as combinations thereof.

High-resolution mass spectra (HRMS) were recorded on an Agilent Technologies 6224 Accurate-Mass time-of-flight spectrometer with either atmospheric pressure chemical ionization (APCI) or electrospray ionization (ESI) ionization sources.

LCMS were measured on an Agilent Technologies 1260 II Infinity connected to an Agilent Technologies 6120 Quadrupole mass spectrometer with APCI ionization source. Elution was performed using a gradient from 5:95% to 100:0% MeCN:H₂O with 0.1% formic acid over 5 min, if not indicated otherwise. Separated isomer spectra of azobenzenes were obtained by irradiation of the LCMS sample prior to injection.

(E)-3-(4-((4-(morpholinomethyl)phenyl)diazenyl)-1-oxoisindolin-2-yl)piperidine-2,6-dione (PHOIMID-1)

Powdered lenalidomide (30.0 mg, 0.116 mmol, 1.0 eq.) was suspended in CH₂Cl₂ (30 mL) and ultrasonicated for 3 min. Oxone (142.3 mg, 0.231 mmol, 2.0 eq.) was dissolved in water (1 mL) and added to the vigorously stirred lenalidomide solution. The reaction was stirred for 18 h, water (5 mL) was added, and the layers were separated. Acetic acid (10 mL) and 4-Morpholin-4-ylmethyl-phenylamine (30.0 mg, 0.116 mmol, 1.0 eq.) were added to the organic layer and the mixture was concentrated to remove most of the CH₂Cl₂. The acetic acid mixture was stirred for 24 h at room temperature and concentrated in vacuo. The crude residue was dissolved with a 5:1 CHCl₃:iPrOH mixture (15 mL), separated against saturated NaHCO₃ (20 mL), washed with 10% LiCl (15 mL) and brine (15 mL), dried over Na₂SO₄ and concentrated under reduced pressure. Purification of the resulting crude product by flash column chromatography (CH₂Cl₂/MeOH gradient, 0 to 20% MeOH) gave **PHOIMID-1** (7.9 mg, 0.018 mmol, 15%) as a yellow solid.

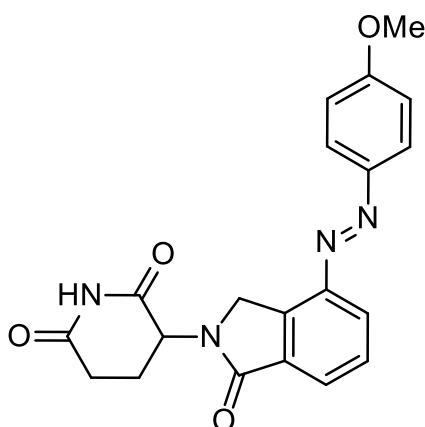
$R_f = 0.31$ [CH₂Cl₂:MeOH 19:1].

¹H NMR (400 MHz, DMSO-*d*₆) $\delta = 11.02$ (s, 1H), 8.24 (dd, *J* = 7.8, 1.1 Hz, 1H), 8.00 – 7.91 (m, 3H), 7.81 (t, *J* = 7.6 Hz, 1H), 7.57 (s, 2H), 5.18 (dd, *J* = 13.2, 5.1 Hz, 1H), 4.81 (d, *J* = 19.1 Hz, 1H), 4.68 (d, *J* = 19.2 Hz, 1H), 3.69 – 3.53 (m, 6H), 2.94 (ddd, *J* = 17.8, 13.3, 5.2 Hz, 1H), 2.66 – 2.53 (m, 2H), 2.40 (s, 4H), 2.04 (m, 1H) ppm.

¹³C NMR (100 MHz, DMSO) $\delta = 172.91, 170.98, 167.12, 151.20, 146.55, 134.37, 133.80, 131.50, 129.82, 129.68, 129.06, 125.57, 122.71, 66.12, 61.83, 53.15, 51.68, 48.26, 31.24, 22.33$ ppm.

HRMS (APCI):	calcd. for C ₂₄ H ₂₆ N ₅ O ₄ ⁺ :	448.1979 m/z [M+H] ⁺ .
	found:	448.1973 m/z [M+H] ⁺ .
LCMS (ESI):	t _{ret} = 2.26 min.	448 m/z [M+H] ⁺ .

**(E)-3-(4-((4-methoxyphenyl)diazenyl)-1-oxoisindolin-2-yl)piperidine-2,6-dione
(PHOIMID-2)**



Powdered lenalidomide (50.0 mg, 0.193 mmol, 1.0 eq.) was suspended in CH₂Cl₂ (50 mL) and ultrasonicated for 3 min. Oxone (237.1 mg, 0.386 mmol, 2.0 eq.) was dissolved in water (1.5 mL) and added to the vigorously stirred lenalidomide solution. The reaction was stirred for 18 h, water (5 mL) was added, and the layers were separated. Acetic acid (15 mL) and *p*-Anisidine (23.8 mg, 0.193 mmol, 1.0 eq.) were added to the organic layer and the mixture was concentrated to remove most of the CH₂Cl₂. The acetic acid mixture was stirred for 24 h at room temperature and concentrated in vacuo. The crude residue was dissolved with ethyl acetate (25 mL), separated against saturated NaHCO₃ (25 mL), washed with 10% LiCl (20 mL) and brine (20 mL), dried over Na₂SO₄ and concentrated under reduced pressure. Purification of the resulting crude product by flash column chromatography (CH₂Cl₂/MeOH gradient, 0 to 20% MeOH) gave **PHOIMID-2** (49 mg, 0.129 mmol, 67%) as a yellow solid.

R_f = 0.44 [CH₂Cl₂:MeOH 19:1].

¹H NMR (400 MHz, DMSO-*d*₆) δ = 11.01 (s, 1H), 8.17 (dd, J = 7.8, 1.1 Hz, 1H), 7.99 (d, J = 9.0 Hz, 2H), 7.88 (dd, J = 7.5, 1.1 Hz, 1H), 7.78 (t, J = 7.7 Hz, 1H), 7.15 (d, J =

9.0 Hz, 2H), 5.17 (dd, $J = 13.3, 5.0$ Hz, 1H), 4.80 (d, $J = 19.1$ Hz, 1H), 4.67 (d, $J = 19.1$ Hz, 1H), 3.88 (s, 3H), 3.00 – 2.87 (m, 1H), 2.68 – 2.52 (m, 2H), 2.03 (qt, $J = 7.4, 5.6, 2.4$ Hz, 1H) ppm.

^{13}C NMR (100 MHz, DMSO) $\delta = 172.92, 171.01, 167.23, 162.58, 146.62, 146.34, 134.26, 133.73, 129.56, 128.40, 124.87$ (2x), 114.65, 55.77, 51.69, 48.26, 31.25, 22.33 ppm.

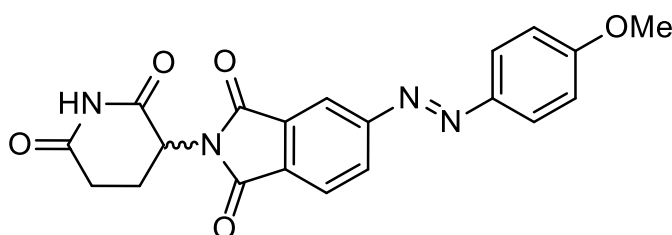
HRMS (APCI): calcd. for $\text{C}_{20}\text{H}_{19}\text{N}_4\text{O}_4^+$: 379.1401 m/z $[\text{M}+\text{H}]^+$.

found: 379.1387 m/z $[\text{M}+\text{H}]^+$.

LCMS (ESI): $t_{\text{ret}} = 2.84$ min (*Z*). 379 m/z $[\text{M}+\text{H}]^+$.

$t_{\text{ret}} = 3.59$ min (*E*). 379 m/z $[\text{M}+\text{H}]^+$.

(*E*)-2-(2,6-dioxopiperidin-3-yl)-5-((4-methoxyphenyl)diazenyl)isoindoline-1,3-dione (PHOIMID-3)



5-amino-2-(2,6-dioxopiperidin-3-yl)isoindoline-1,3-dione (50.0 mg, 0.183 mmol, 1.0 eq.) was suspended in CH_2Cl_2 (50 mL) and ultrasonicated for 3 min. Oxone (225 mg, 0.366 mmol, 2.0 eq.) was dissolved in water (1.5 mL) and added to the vigorously stirred lenalidomide solution. The reaction was stirred for 18 h, water (5 mL) was added, and the layers were separated. Acetic acid (15 mL) and *p*-Anisidine (23.8 mg, 0.193 mmol, 1.0 eq.) were added to the organic layer and the mixture was concentrated to remove most of the CH_2Cl_2 . The acetic acid mixture was stirred for 24 h at room temperature and concentrated in vacuo. The crude residue was dissolved with ethyl acetate (25 mL), separated against saturated NaHCO_3 (25 mL), washed with 10% LiCl (20 mL) and brine (20 mL), dried over Na_2SO_4 and concentrated under reduced pressure. Purification of the resulting crude product by flash column chromatography ($\text{CH}_2\text{Cl}_2/\text{MeOH}$ gradient, 0 to 20% MeOH) gave **PHOIMID-3** (9.4 mg, 0.024 mmol, 26%) as a yellow solid.

$R_f = 0.39$ [$\text{CH}_2\text{Cl}_2:\text{MeOH}$ 19:1].

$^1\text{H NMR}$ (400 MHz, $\text{DMSO-}d_6$) $\delta = 11.16$ (s, 1H), 8.30 (dd, $J = 8.0, 1.7$ Hz, 1H), 8.20 (d, $J = 1.6$ Hz, 1H), 8.13 (d, $J = 7.9$ Hz, 1H), 8.02 (d, $J = 8.9$ Hz, 2H), 7.20 (d, $J = 9.0$ Hz, 2H), 5.21 (dd, $J = 12.9, 5.4$ Hz, 1H), 3.90 (s, 3H), 2.91 (ddd, $J = 17.4, 14.0, 5.4$ Hz, 1H), 2.69 – 2.53 (m, 2H), 2.10 (m, 1H) ppm.

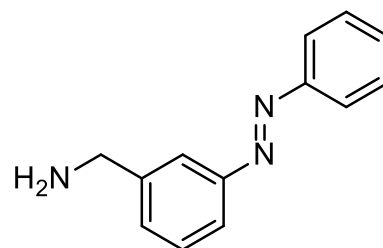
$^{13}\text{C NMR}$ (100 MHz, DMSO) $\delta = 172.75, 169.76, 166.53, 166.43, 163.17, 156.13, 146.10, 132.84, 131.86, 129.68, 125.53, 124.95, 115.27, 114.91, 55.85, 49.23, 30.93, 21.96$ ppm.

HRMS (APCI): calcd. for $\text{C}_{20}\text{H}_{17}\text{N}_4\text{O}_5^+$: 393.1193 m/z $[\text{M}+\text{H}]^+$.

 found: 393.1182 m/z $[\text{M}+\text{H}]^+$.

LCMS (ESI): $t_{\text{ret}} = 3.26$ min (*Z*). 393 m/z $[\text{M}+\text{H}]^+$.

$t_{\text{ret}} = 3.93$ min (*E*). 393 m/z $[\text{M}+\text{H}]^+$.

(E)-(3-(phenyldiazenyl)phenyl)methanamine (7.1)

tert-butyl (3-aminobenzyl)carbamate (222.3 mg, 1.00 mmol, 1.0 eq.) and nitrosobenzene (107 mg, 1.10 mmol, 1.1 eq.) were dissolved in CH₂Cl₂ (30 mL) and acetic acid (10 mL). The mixture was stirred for 36 h at room temperature and concentrated *in vacuo*. The crude residue was dissolved with CH₂Cl₂ (40 mL), separated against saturated NaHCO₃ (40 mL), washed with brine (2x30 mL), dried over Na₂SO₄, and concentrated under reduced pressure. Purification of the resulting crude product by flash column chromatography (CH₂Cl₂/MeOH gradient, 0 to 20% MeOH) gave a crude red oil (273 mg) that was dissolved in TFA:CH₂Cl₂ (1:1; 2 mL) and stirred for 1 h at room temperature. The reaction was diluted with CH₂Cl₂ (10 mL) and concentrated under reduced pressure. The reaction was triturated with Et₂O (3x5 mL) and dried *in vacuo* for 48 h. The product was obtained as TFA salt (269 mg, 0.827 mmol, 83%) as an orange solid and used without further purification.

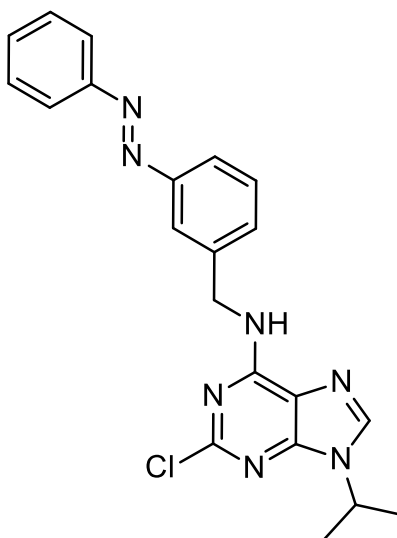
R_f = 0.33 [Boc-protected, Hx:EA 5:1].

¹H NMR (400 MHz, DMSO-*d*₆) δ = 1H NMR (400 MHz, DMSO-*d*₆) δ 8.35 (s, 3H), 8.02 (d, J = 2.0 Hz, 1H), 7.95 – 7.88 (m, 3H), 7.70 – 7.57 (m, 5H), 4.18 (s, 2H) ppm.

¹³C NMR (100 MHz, DMSO) δ = 152.09, 151.96, 135.67, 132.17, 132.07, 130.06, 129.81, 123.44, 122.75, 122.65, 42.14 ppm.

HRMS (APCI): calcd. for C₁₃H₁₄N₃⁺: 212.1182 m/z [M+H]⁺.
 found: 212.1185 m/z [M+H]⁺.

LCMS (ESI): t_{ret} = 2.57 min. 212 m/z [M+H]⁺.

(E)-2-chloro-9-isopropyl-N-(3-(phenyldiazenyl)benzyl)-9H-purin-6-amine (7.2)

7.1 (120.0 mg, 0.369 mmol, 1.42 eq.) and 2,6-dichloro-9-isopropyl-9H-purine (60.0 mg, 0.260 mmol, 1.0 eq.) were dissolved in *n*-butanol (2 mL). Triethylamine (65.7 mg, 0.649 mmol, 0.090 mL, 2.5 eq.) was added and reaction mixture was sealed in a vial and heated in a microwave at 105 °C for 3 h. The mixture was then diluted with ethyl acetate (25 mL) separated against 10% LiCl aq. (25 mL) and washed with saturated NH₄Cl (30 mL), saturated NaHCO₃ (30 mL), 10% LiCl aq. (25 mL) and brine (2x 25 mL). The organic phase was dried over Na₂SO₄ and concentrated under reduced pressure. Purification of the resulting crude product by flash column chromatography (CH₂Cl₂/MeOH gradient, 0-20% MeOH) gave **7.2** (79.7 mg, 0.196 mmol, 76%) as an orange solid.

$R_f = 0.39$ [CH₂Cl₂:MeOH 19:1].

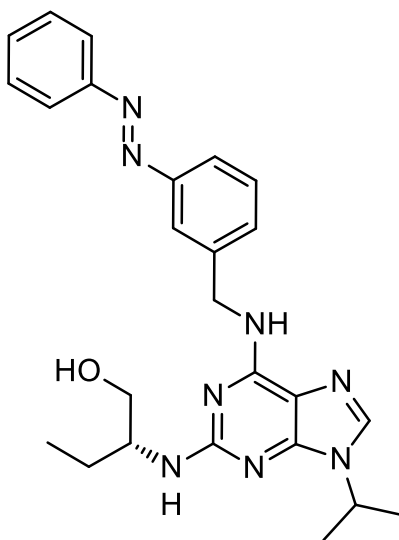
¹H NMR (400 MHz, DMSO-*d*₆) $\delta = 8.91$ (t, *J* = 5.4 Hz, 1H), 8.29 (s, 1H), 7.92 – 7.82 (m, 3H), 7.77 (td, *J* = 4.5, 1.9 Hz, 1H), 7.57 (m, 5H), 4.75 (d, *J* = 5.7 Hz, 2H), 4.67 (hept, *J* = 7.3, 6.7 Hz, 1H), 1.49 (d, *J* = 6.8 Hz, 6H) ppm.

¹³C NMR (100 MHz, DMSO) $\delta = 154.94, 152.79, 152.06, 151.98, 149.54, 141.05, 139.66, 131.68, 130.64, 129.60, 129.55, 122.60, 121.52, 121.24, 118.55, 46.89, 43.04, 22.19$ ppm.

HRMS (APCI): calcd. for C₂₁H₂₁ClN₇⁺: 406.1541 m/z [M+H]⁺.
 found: 406.1551 m/z [M+H]⁺.

LCMS (ESI): *t*_{ret} = 4.86 min. 406 m/z [M+H]⁺.

(*R,E*)-2-((9-isopropyl-6-((3-(phenyldiazenyl)benzyl)amino)-9H-purin-2-yl)amino)butan-1-ol (Azo-CR8)



7.2 (30.0 mg, 0.074 mmol, 1.0 eq.) and (*R*)-(-)-2-Amino-1-butanol (1886 mg, 21.16 mmol, 2 mL, 286 eq.) sealed in a vial under argon atmosphere and heated in a microwave at 140 °C for 4 h. The mixture was then diluted with ethyl acetate (20 mL) separated against water (50 mL) and the organic phase was washed with saturated NH₄Cl (35 mL), saturated NaHCO₃ (35 mL), 10% LiCl aq. (25 mL) and brine (2x 25 mL). The organic phase was dried over Na₂SO₄ and concentrated under reduced pressure. Purification of the resulting crude product by flash column chromatography (CH₂Cl₂/MeOH gradient, 0-20% MeOH) gave **Azo-CR8** (22.9 mg, 0.050 mmol, 68%) as an orange solid.

R_f = 0.48 [CH₂Cl₂:MeOH 19:1].

¹H NMR (400 MHz, DMSO-*d*₆) δ = 8.04 (s, 1H), 7.90 (d, *J* = 1.8 Hz, 1H), 7.87 (dd, *J* = 7.9, 1.8 Hz, 2H), 7.83 (s, 1H), 7.75 (dt, *J* = 7.6, 1.7 Hz, 1H), 7.63 – 7.49 (m, 5H), 5.93 (s, 1H), 4.86 – 4.61 (m, 2H), 4.53 (hept, *J* = 6.7 Hz, 1H), 3.87 – 3.74 (m, 1H), 3.52 – 3.36 (m, 2H), 1.65 – 1.35 (m, 8H), 0.80 (t, *J* = 7.5 Hz, 3H) ppm.

¹³C NMR (100 MHz, DMSO) δ = 158.74, 154.19, 151.93, 151.91, 150.51, 142.33, 135.27, 131.47, 130.62, 129.45, 129.18, 122.47, 121.27, 121.08, 113.46, 62.95, 54.09, 45.74, 42.61, 23.86, 22.00, 10.64 ppm.

HRMS (APCI): calcd. for C₂₅H₃₁N₈O⁺: 459.2615 m/z [M+H]⁺.
 found: 459.2623 m/z [M+H]⁺.

LCMS (ESI): *t*_{ret} = 3.74 min. 459 m/z [M+H]⁺.

References

- [1] A. K. Gandhi, J. Kang, C. G. Havens, T. Conklin, Y. Ning, L. Wu, T. Ito, H. Ando, M. F. Waldman, A. Thakurta, A. Klippel, H. Handa, T. O. Daniel, P. H. Schafer, R. Chopra, *Br. J. Haematol.* **2014**, *164*, 811–821.
- [2] J. Krönke, N. D. Udeshi, A. Narla, P. Grauman, S. N. Hurst, M. McConkey, T. Svinkina, D. Heckl, E. Comer, X. Li, C. Ciarlo, E. Hartman, N. Munshi, M. Schenone, S. L. Schreiber, S. A. Carr, B. L. Ebert, *Science* **2014**, *343*, 301–305.
- [3] G. Lu, R. E. Middleton, H. Sun, M. Naniong, C. J. Ott, C. S. Mitsiades, K.-K. Wong, J. E. Bradner, W. G. Kaelin, *Science* **2014**, *343*, 305–309.
- [4] J. Krönke, E. C. Fink, P. W. Hollenbach, K. J. MacBeth, S. N. Hurst, N. D. Udeshi, P. P. Chamberlain, D. R. Mani, H. W. Man, A. K. Gandhi, T. Svinkina, R. K. Schneider, M. McConkey, M. Järås, E. Griffiths, M. Wetzler, L. Bullinger, B. E. Cathers, S. A. Carr, R. Chopra, B. L. Ebert, *Nature* **2015**, *523*, 183–188.
- [5] M. E. Matyskiela, G. Lu, T. Ito, B. Pagarigan, C.-C. Lu, K. Miller, W. Fang, N.-Y. Wang, D. Nguyen, J. Houston, G. Carmel, T. Tran, M. Riley, L. Nosaka, G. C. Lander, S. Gaidarova, S. Xu, A. L. Ruchelman, H. Handa, J. Carmichael, T. O. Daniel, B. E. Cathers, A. Lopez-Girona, P. P. Chamberlain, *Nature* **2016**, *535*, 252–257.
- [6] K. A. Donovan, J. An, R. P. Nowak, J. C. Yuan, E. C. Fink, B. C. Berry, B. L. Ebert, E. S. Fischer, *eLife* **2018**, *7*, e38430.
- [7] M. E. Matyskiela, S. Couto, X. Zheng, G. Lu, J. Hui, K. Stamp, C. Drew, Y. Ren, M. Wang, A. Carpenter, C.-W. Lee, T. Clayton, W. Fang, C.-C. Lu, M. Riley, P. Abdubek, K. Blease, J. Hartke, G. Kumar, R. Vessey, M. Rolfe, L. G. Hamann, P. P. Chamberlain, *Nat. Chem. Biol.* **2018**, *14*, 981–987.
- [8] T. Asatsuma-Okumura, H. Ando, M. D. Simone, J. Yamamoto, T. Sato, N. Shimizu, K. Asakawa, Y. Yamaguchi, T. Ito, L. Guerrini, H. Handa, *Nat. Chem. Biol.* **2019**, 1–8.
- [9] Q. L. Sievers, G. Petzold, R. D. Bunker, A. Renneville, M. Stabicki, B. J. Liddicoat, W. Abdulrahman, T. Mikkelsen, B. L. Ebert, N. H. Thomä, *Science* **2018**, *362*, DOI 10.1126/science.aat0572.
- [10] D. Millrine, T. Kishimoto, *Trends Mol. Med.* **2017**, *23*, 348–361.
- [11] H. Ludwig, M. Delforge, T. Facon, H. Einsele, F. Gay, P. Moreau, H. Avet-Loiseau, M. Boccadoro, R. Hajek, M. Mohty, M. Cavo, M. A. Dimopoulos, J. F. San-Miguel, E. Terpos, S. Zweegman, L. Garderet, M.-V. Mateos, G. Cook, X. Leleu, H. Goldschmidt, G. Jackson, M. Kaiser, K. Weisel, N. W. C. J. van de Donk, A. Waage, M. Beksac, U. H. Mellqvist, M. Engelhardt, J. Caers, C. Driessen, J. Bladé, P. Sonneveld, *Leukemia* **2018**, *32*, 1542–1560.
- [12] U. H. Patel, M. A. Mir, J. K. Sivik, D. Raheja, M. K. Pandey, G. Talamo, *Hematol. Rep.* **2015**, *7*, DOI 10.4081/hr.2015.5704.
- [13] J. Broichhagen, J. A. Frank, D. Trauner, *Acc. Chem. Res.* **2015**, *48*, 1947–1960.
- [14] I. M. Welleman, M. W. H. Hoorens, B. L. Feringa, H. H. Boersma, W. Szymański, *Chem. Sci.* **2020**, *11*, 11672–11691.
- [15] G. Xue, K. Wang, D. Zhou, H. Zhong, Z. Pan, *J. Am. Chem. Soc.* **2019**, DOI 10.1021/jacs.9b06422.
- [16] M. Reynders, B. S. Matsuura, M. Bérouti, D. Simoneschi, A. Marzio, M. Pagano, D. Trauner, *Sci. Adv.* **2020**, *6*, eaay5064.

- [17] Y. Naro, K. Darrah, A. Deiters, *J. Am. Chem. Soc.* **2020**, DOI 10.1021/jacs.9b12718.
- [18] J. Liu, H. Chen, L. Ma, Z. He, D. Wang, Y. Liu, Q. Lin, T. Zhang, N. Gray, H. Ü. Kaniskan, J. Jin, W. Wei, *Sci. Adv.* **2020**, *6*, eaay5154.
- [19] X. Du, O. A. Volkov, R. M. Czerwinski, H. Tan, C. Huerta, E. R. Morton, J. P. Rizzi, P. M. Wehn, R. Xu, D. Nijhawan, E. M. Wallace, *Structure* **2019**, *27*, 1625-1633.e3.
- [20] D. E. Bussiere, L. Xie, H. Srinivas, W. Shu, A. Burke, C. Be, J. Zhao, A. Godbole, D. King, R. G. Karki, V. Hornak, F. Xu, J. Cobb, N. Carte, A. O. Frank, A. Frommlet, P. Graff, M. Knapp, A. Fazal, B. Okram, S. Jiang, P.-Y. Michellys, R. Beckwith, H. Voshol, C. Wiesmann, J. M. Solomon, J. Paulk, *Nat. Chem. Biol.* **2020**, *16*, 15–23.
- [21] T. B. Faust, H. Yoon, R. P. Nowak, K. A. Donovan, Z. Li, Q. Cai, N. A. Eleuteri, T. Zhang, N. S. Gray, E. S. Fischer, *Nat. Chem. Biol.* **2020**, *16*, 7–14.
- [22] M. Słabicki, Z. Kozicka, G. Petzold, Y.-D. Li, M. Manojkumar, R. D. Bunker, K. A. Donovan, Q. L. Sievers, J. Koepfel, D. Suchyta, A. S. Sperling, E. C. Fink, J. A. Gasser, L. R. Wang, S. M. Corsello, R. S. Sellar, M. Jan, D. Gillingham, C. Scholl, S. Fröhling, T. R. Golub, E. S. Fischer, N. H. Thomä, B. L. Ebert, *Nature* **2020**, *585*, 293–297.
- [23] C. Mayor-Ruiz, S. Bauer, M. Brand, Z. Kozicka, M. Siklos, H. Imrichova, I. H. Kalthener, E. Hahn, K. Seiler, A. Koren, G. Petzold, M. Fellner, C. Bock, A. C. Müller, J. Zuber, M. Geyer, N. H. Thomä, S. Kubicek, G. E. Winter, *Nat. Chem. Biol.* **2020**, *16*, 1199–1207.
- [24] L. Lv, P. Chen, L. Cao, Y. Li, Z. Zeng, Y. Cui, Q. Wu, J. Li, J.-H. Wang, M.-Q. Dong, X. Qi, T. Han, *eLife* **2020**, *9*, e59994.
- [25] G. Petzold, E. S. Fischer, N. H. Thomä, *Nature* **2016**, *532*, 127–130.
- [26] M. E. Matyskiela, W. Zhang, H.-W. Man, G. Muller, G. Khambatta, F. Baculi, M. Hickman, L. LeBrun, B. Pagarigan, G. Carmel, C.-C. Lu, G. Lu, M. Riley, Y. Satoh, P. Schafer, T. O. Daniel, J. Carmichael, B. E. Cathers, P. P. Chamberlain, *J. Med. Chem.* **2018**, *61*, 535–542.
- [27] M. Ishoey, S. Chorn, N. Singh, M. G. Jaeger, M. Brand, J. Paulk, S. Bauer, M. A. Erb, K. Parapatics, A. C. Müller, K. L. Bennett, G. F. Ecker, J. E. Bradner, G. E. Winter, *ACS Chem. Biol.* **2018**, *13*, 553–560.
- [28] B. Jiang, E. S. Wang, K. A. Donovan, Y. Liang, E. S. Fischer, T. Zhang, N. S. Gray, *Angew. Chem. Int. Ed.* **2019**, *58*, 6321–6326.
- [29] J. Yang, Y. Li, A. Aguilar, Z. Liu, C.-Y. Yang, S. Wang, *J. Med. Chem.* **2019**, *62*, 9471–9487.
- [30] M. Hanafi, X. Chen, N. Neamati, *J. Med. Chem.* **2021**, *64*, 1626–1648.
- [31] A. A. Beharry, O. Sadoyski, G. A. Woolley, *J. Am. Chem. Soc.* **2011**, *133*, 19684–19687.
- [32] L. Gao, J. C. M. Meiring, Y. Kraus, M. Wranik, T. Weinert, S. D. Pritzl, R. Bingham, E. Ntoulou, K. I. Jansen, N. Olieric, J. Standfuss, L. C. Kapitein, T. Lohmüller, J. Ahlfeld, A. Akhmanova, M. O. Steinmetz, O. Thorn-Seshold, *Cell Chem. Biol.* **2021**, *28*, 228-241.e6.
- [33] X. Gómez-Santacana, S. M. de Munnik, P. Vijayachandran, D. Da Costa Pereira, J. P. M. Bebelman, I. J. P. de Esch, H. F. Vischer, M. Wijtmans, R. Leurs, *Angew. Chem. Int. Ed.* **2018**, *57*, 11608–11612.

- [34] S. Samanta, A. A. Beharry, O. Sadovski, T. M. McCormick, A. Babalhavaeji, V. Tropepe, G. A. Woolley, *J. Am. Chem. Soc.* **2013**, *135*, 9777–9784.
- [35] M. Dong, A. Babalhavaeji, S. Samanta, A. A. Beharry, G. A. Woolley, *Acc. Chem. Res.* **2015**, *48*, 2662–2670.
- [36] M. Dong, A. Babalhavaeji, C. V. Collins, K. Jarrah, O. Sadovski, Q. Dai, G. A. Woolley, *J. Am. Chem. Soc.* **2017**, *139*, 13483–13486.
- [37] A. Rullo, A. Reiner, A. Reiter, D. Trauner, E. Y. Isacoff, G. A. Woolley, *Chem. Commun.* **2014**, *50*, 14613–14615.
- [38] D. Bléger, J. Schwarz, A. M. Brouwer, S. Hecht, *J. Am. Chem. Soc.* **2012**, *134*, 20597–20600.
- [39] D. B. Konrad, G. Savasci, L. Allmendinger, D. Trauner, C. Ochsenfeld, A. M. Ali, *J. Am. Chem. Soc.* **2020**, *142*, 6538–6547.
- [40] K. A. Donovan, F. M. Ferguson, J. W. Bushman, N. A. Eleuteri, D. Bhunia, S. Ryu, L. Tan, K. Shi, H. Yue, X. Liu, D. Dobrovolsky, B. Jiang, J. Wang, M. Hao, I. You, M. Teng, Y. Liang, J. Hatcher, Z. Li, T. D. Manz, B. Groendyke, W. Hu, Y. Nam, S. Sengupta, H. Cho, I. Shin, M. P. Agius, I. M. Ghobrial, M. W. Ma, J. Che, S. J. Buhrlage, T. Sim, N. S. Gray, E. S. Fischer, *Cell* **2020**, *183*, 1714-1731.e10.
- [41] V. Koduri, S. K. McBrayer, E. Liberzon, A. C. Wang, K. J. Briggs, H. Cho, W. G. Kaelin, *Proc. Natl. Acad. Sci.* **2019**, *116*, 2539–2544.
- [42] S. Yamanaka, Y. Shoya, S. Matsuoka, H. Nishida-Fukuda, N. Shibata, T. Sawasaki, *Commun. Biol.* **2020**, *3*, 1–14.
- [43] S. Carbonneau, S. Sharma, L. Peng, V. Rajan, D. Hainzl, M. Henault, C. Yang, J. Hale, J. Shulok, J. Tallarico, J. Porter, J. L. Brogdon, G. Dranoff, J. E. Bradner, M. Hild, C. P. Guimaraes, *Cell Chem. Biol.* **2020**, *0*, DOI 10.1016/j.chembiol.2020.11.012.
- [44] M. Borowiak, W. Nahaboo, M. Reynders, K. Nekolla, P. Jalinot, J. Hasserodt, M. Rehberg, M. Delattre, S. Zahler, A. Vollmar, D. Trauner, O. Thorn-Seshold, *Cell* **2015**, *162*, 403–411.

8 – Tag-based PHOTACs Towards Controlling Fusion Proteins with Light

Martin Reynders^{1,2}, Michele Pagano^{3,4,5}, and Dirk Trauner^{1,4,6}

¹Department of Chemistry, New York University, New York, NY 10003, USA.

²Department of Chemistry, Ludwig Maximilians University of Munich
81377 Munich, Germany.

³Department of Biochemistry and Molecular Pharmacology, New York University
School of Medicine, New York, NY 10016, USA.

⁴Perlmutter Cancer Center, New York University School of Medicine, New York, NY
10016, USA.

⁵Howard Hughes Medical Institute, New York University School of Medicine, New
York, NY 10016, USA.

⁶NYU Neuroscience Institute, New York University School of Medicine, New York, NY
10016, USA.

Introduction

Knockdown or knockout of proteins are widely used to investigate protein function. Common techniques such as genome editing using CRISPR-Cas9 to knockout genes or conditional methods like RNA interference modulate the expression of the target protein.^[1] However RNAi is limited by the natural degradation speed of the existing protein. Alternatively, proteins can be destabilized by attaching a small peptide degron that induces degradation by the proteasome.^[2] Approaches to modulate protein degradation using a combination of degrons and small-molecules include the auxin-inducible degron (AID) system to deplete proteins and FKBP12-fusion based strategies to either stabilize or destabilize a protein of interest (POI) using the Shield-1 ligand.^[3-5] These methods can change protein abundance on demand through a chemical stimulus. Complementary optogenetic approaches have also been developed to control the abundance of fusion proteins with light.^[6-11] These approaches are however limited by background activity in the absence of light and the size of the photoresponsive domain.^[2,12]

The emergence of proteolysis targeting chimeras (PROTACs) added another versatile tool to rapidly degrade POIs.^[13,14] PROTACs were equipped with specific ligands to promote the ubiquitylation and degradation of either HaloTag or FKBP12^{F36V} fusion proteins.^[15-18] HaloPROTACs covalently bind to HaloTag fusion proteins with a chloroalkane ligand, whereas FKBP12^{F36V}-targeting PROTACs, called dTAGs, utilize a non-covalent ligand modified to selectively target the mutant FKBP in a bump-hole approach.^[15,19]

We have developed photochemically targeting chimeras (PHOTACs) to control PROTAC-mediated protein degradation with light.^[20] Our PHOTACs are inactive in the dark but can be reversibly activated with light to induce the catalytic ubiquitylation of POIs. Here we aim to utilize our PHOTAC approach to render dTAGs and HaloPROTACs light-responsive. Thereby, we want to generate tools to precisely modulate fusion protein abundance with the precision that light offers.

Results

Our initial proof-of-concept for PHOTACs included PHOTAC-II-5 recruiting wild-type FKBP12 to the cereblon cullin-RING E3 ligase complex in a light-dependent fashion to promote its ubiquitylation and degradation (Figure 8.1A). dTAG13 analogously harnesses cereblon for induced protein degradation, but features a modified ligand targeting FKBP12^{F36V} (Figure 8.1B). We designed **dTAG-PHOTACs** based on PHOTAC-II-5 by employing the ligand for mutant FKBP12. Thus, **dTAG-PHOTACs** could catalytically induce the degradation of FKBP12^{F36V}-fusion proteins instead of wildtype FKBP12 in a light-dependent fashion (Figure 8.2).

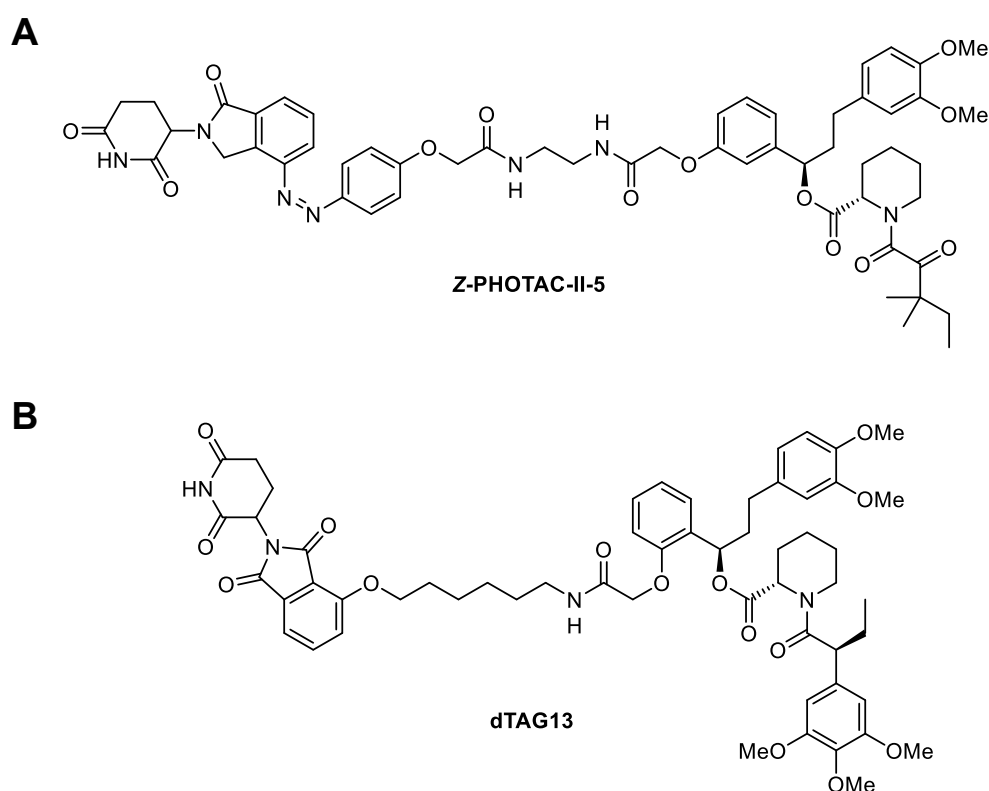


Figure 8.1: Chemical structure of FKBP12 degraders. A) Structure of PHOTAC-II-5, which can induce wildtype FKBP12 degradation. B) Structure of dTAG13 that induces the degradation of FKBP12^{F36V} fusion proteins.

The synthesis of the specific ligand targeting mutant FKBP12 as used in dTAG-13 was not yet reported. We began our synthesis by preparing **8-1** from the corresponding benzaldehyde and acetophenone as previously described.^[21] Similar to the procedure by Jørgensen and Bols,^[22] **8-1** was reduced to **8-2** and subsequently alkylated using *tert*-butyl bromoacetate to yield **8-3** (Figure 8.3). Next, we performed a Corey-Bakshi-Shibata (CBS) reduction of **8-3** using the (S)-(-)-2-Methyl-CBS-oxazaborolidine to

obtain **8-4**, which was directly coupled with (S)-N-Fmoc-piperidine-2-carboxylic acid and converted to **8-5**. Deprotecting of the Fmoc protecting group using piperidine yielded **8-6** which was coupled to (S)-2-(3,4,5-Trimethoxyphenyl)butanoic acid to give **8-7**. Deprotection of **8-7** had to be carefully monitored as **8-8** decomposed under acidic conditions before the deprotection was complete. The best yields were obtained by deprotection in formic acid, but it was necessary to separate **8-8** from its decomposition products by flash column chromatography and directly use it in the next step. Coupling of **8-8** to the corresponding primary amine azobenzenes yielded **dTAG-PHOTAC-1** and **dTAG-PHOTAC-2** (Figure 8.3).

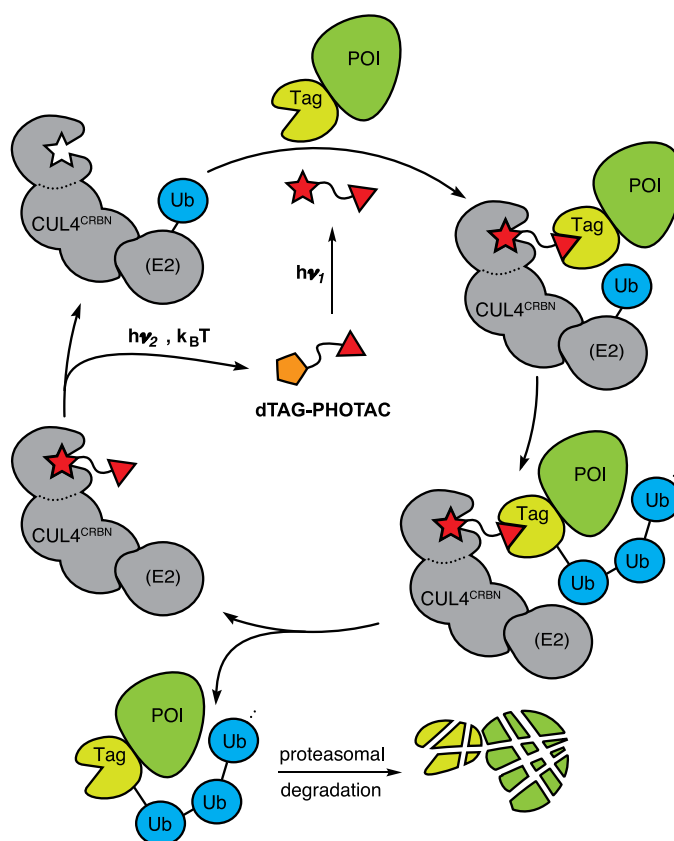


Figure 8.2: Schematic mechanism of a **dTAG-PHOTAC**. **dTAG-PHOTACs** can be isomerized between an inactive form (yellow pentagon) and an active form (red star) upon irradiation. The active form can catalyze the ubiquitylation of tagged fusion proteins.

Next, we characterized the photophysical properties of **dTAG-PHOTACs**. Both **dTAG-PHOTAC-1** and **dTAG-PHOTAC-2** showed efficient photoswitching as observed for other PHOTACs and the highest amount of the *Z*-isomer could be generated using 380 or 390 nm (Figure 8.4). Up to 89 % **Z-dTAG-PHOTAC-1** and even up to 98% **Z-dTAG-PHOTAC-2** could be obtained, whereas *Z*-to-*E* isomerization with green light

generated more than 80% of the *E*-isomer (Figure 8.5B, E). Thermal relaxation proceeded slow with half-lives above 20 h in a 1:1 DMSO:PBS mixture for both **dTAG-PHOTACs** (Figure 8.5C, F).

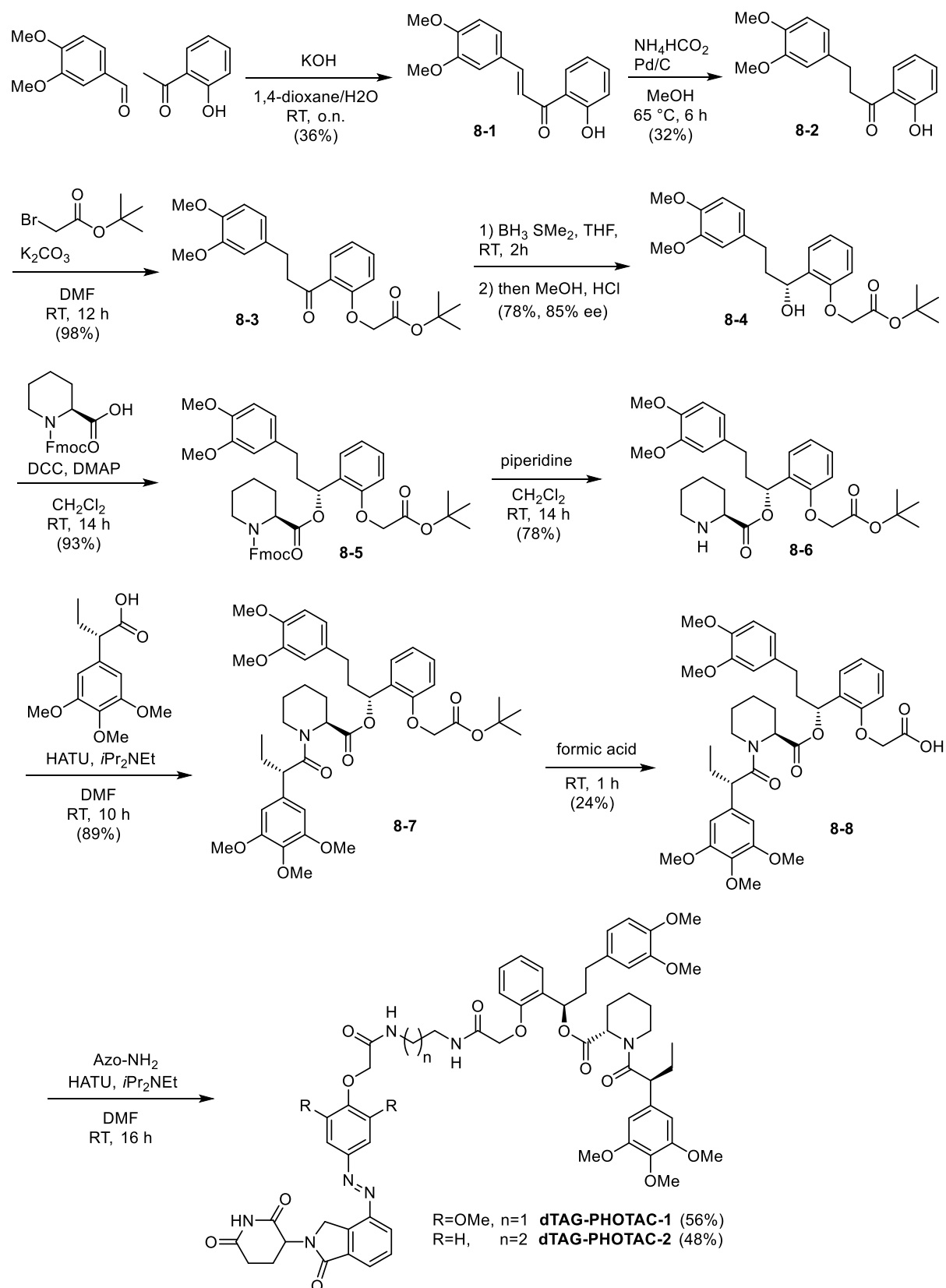


Figure 8.3: Synthesis of **dTAG-PHOTACs**.

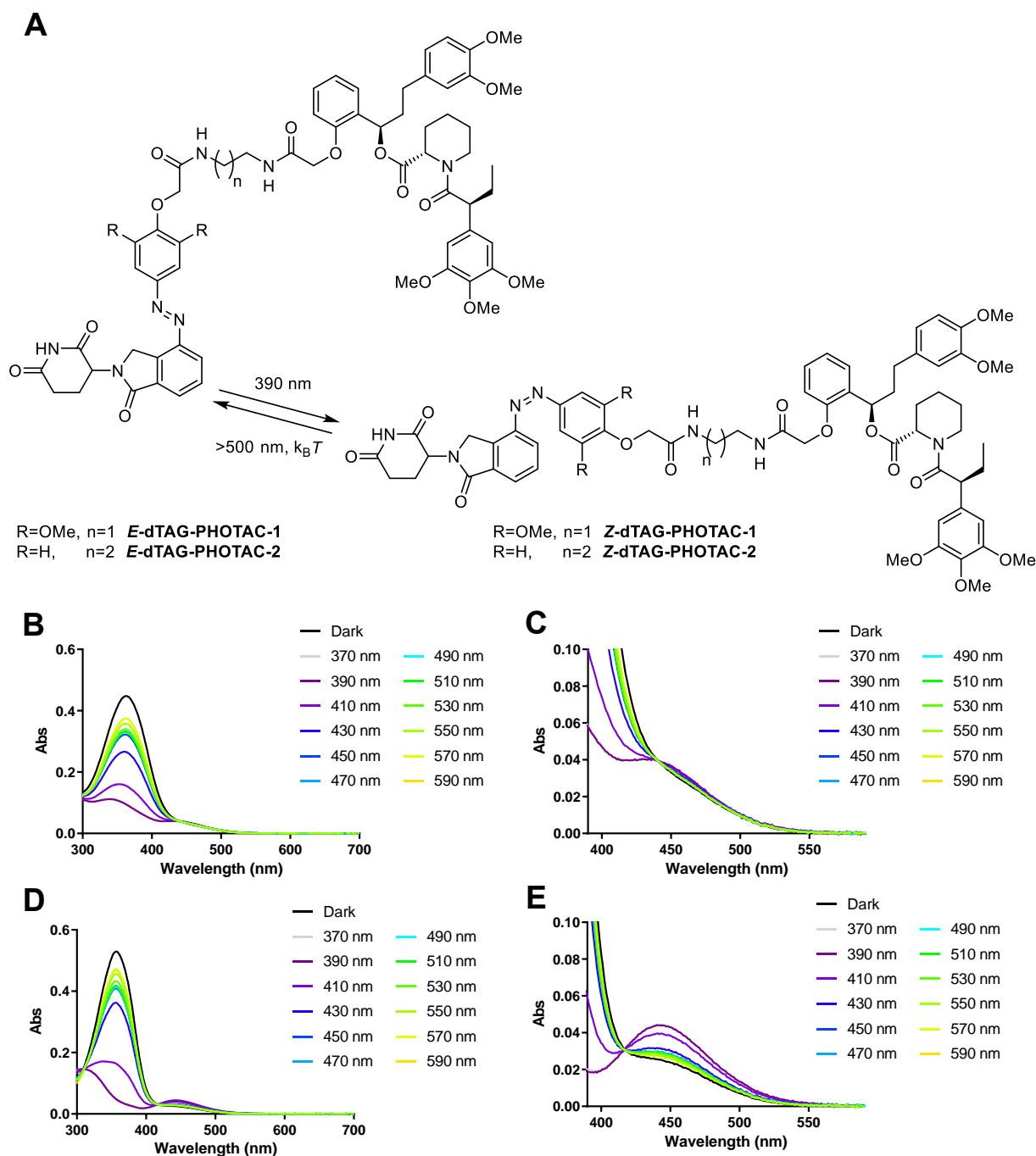


Figure 8.4: Characterization of **dTAG-PHOTACs**. A) Structure and isomerization of **dTAG-PHOTAC-1+2**. B), C) Absorption spectra of **dTAG-PHOTAC-1** after irradiation with the indicated wavelength for 5 min. D), E) Absorption spectra of **dTAG-PHOTAC-2** after irradiation with the indicated wavelength for 5 min.

As a secondary approach we also designed **HaloPHOTACs**. In contrast to FKBP12 binders, HaloPROTACs and **HaloPHOTACs** covalently bind to the HaloTag. Consequently, protein degradation induced by **HaloPHOTACs** would not be catalytic (Figure 8.6). Only HaloPROTACs recruiting the VHL E3 ligase complex have been reported so far.

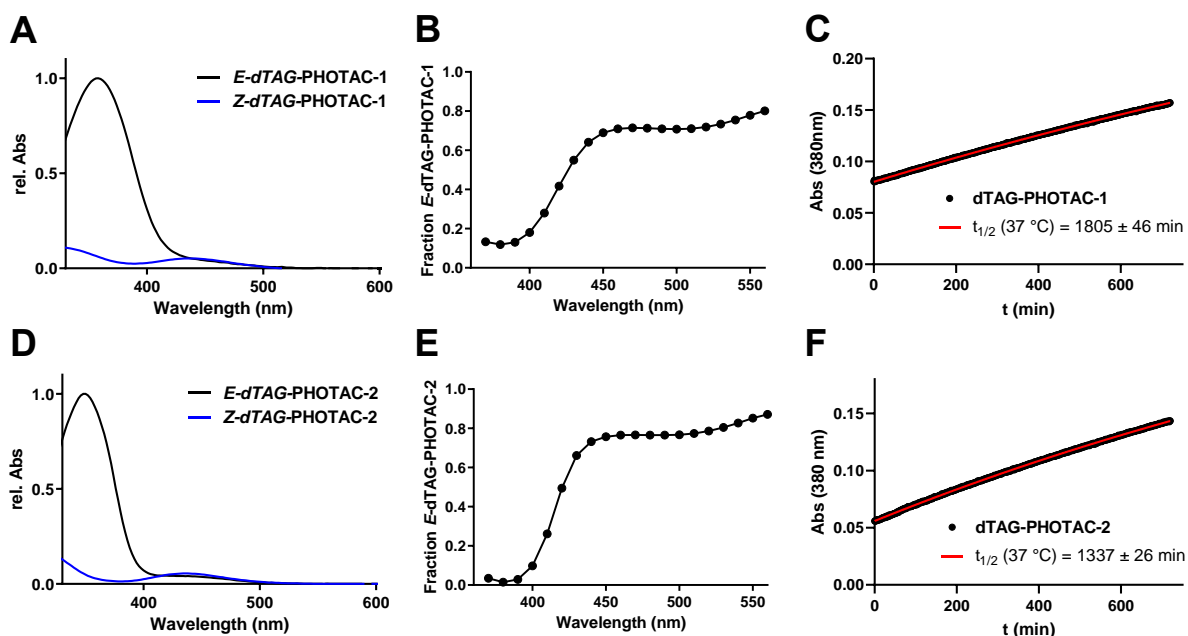


Figure 8.5: Photophysical characterization of **dTAG-PHOTACs**. A) Absorption spectra of **dTAG-PHOTAC-1** isomers as obtained by LCMS. B) Calculated fraction of **E-dTAG-PHOTAC-1** after 5 min irradiation with the indicated wavelength. C) Thermal Z-to-E isomerization of **dTAG-PHOTAC-1** at 37 °C in a 1:1 DMSO:PBS (pH 7.4) mixture. D) Absorption spectra of **dTAG-PHOTAC-2** isomers as obtained by LCMS. E) Calculated fraction of **E-dTAG-PHOTAC-2** after 5 min irradiation with the indicated wavelength. F) Thermal Z-to-E isomerization of **dTAG-PHOTAC-2** at 37 °C in a 1:1 DMSO:PBS (pH 7.4) mixture.

In the absence of existing PROTACs as a design basis for **HaloPHOTACs**, we based our design on fluorophore HaloTag ligand conjugates to estimate the minimal linker length required for binding.^[23,24] Based on this we designed **HaloPHOTAC-1** and created a model of **HaloPHOTAC-1** bound to both cereblon and the HaloTag protein based on existing crystal structures.^[24,25] Our model indicates that the Z-isomer is sufficiently large to bind both proteins simultaneously and thus could potentially induce a ternary complex to induce ubiquitylation of the HaloTag (Figure 8.7).

We synthesized **HaloPHOTAC-1** and **HaloPHOTAC-2** (Figure 8.8A) and investigated their photoswitching. Photophysical properties largely mimicked those of the **dTAG-PHOTACs** with 380-390 nm irradiation mostly generating the Z-isomer (Figure 8.8B–E). Higher amounts of the Z-isomer were generated for **HaloPHOTAC-2** lacking the two methoxy groups on the azobenzene (Figure 8.8G, J), but overall, both PHOTACs are suitable for further investigation.

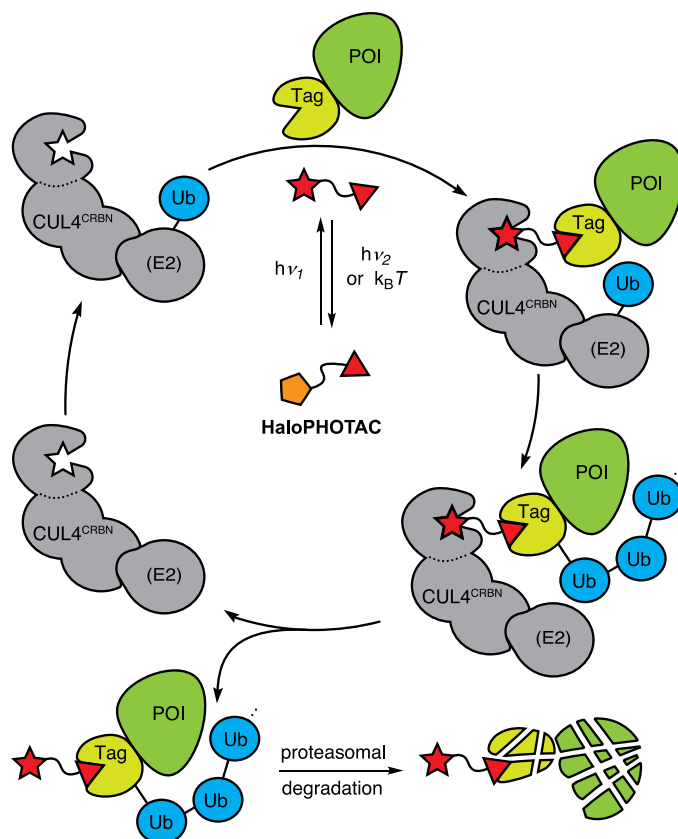


Figure 8.6: Schematic mechanism of a **HaloPHOTAC**. HaloPHOTACs can be isomerized between an inactive form (yellow pentagon) and an active form (red star) upon irradiation and covalently bind to the HaloTag. The active form induces the degradation of fusion proteins.

Discussion and Outlook

Here we developed PHOTACs for the purpose of controlling the abundance of fusion proteins with light. We generated a synthetic route towards **dTAG-PHOTACs** and successfully prepared two photoswitchable degraders for further characterization *in cellulo*. For this, a cell line stably expressing FKBP12^{F36V} with two hemagglutinin (HA) tags could be used. The added molecular weight of the tags (2.2 kDa) will allow the detection of both wildtype and mutant FKBP12 simultaneously to confirm selectivity of **dTAG-PHOTACs**.

In parallel, we also created **HaloPHOTACs** as a complementary strategy for the degradation of fusion proteins. In contrast to **dTAG-PHOTACs**, **HaloPHOTACs** bind the HaloTag covalently and consequently operate non-catalytic. However, their relatively low molecular weight could improve bioavailability.^[26] Their robust photoswitching makes them ideal candidates for further applications *in cellulo*.

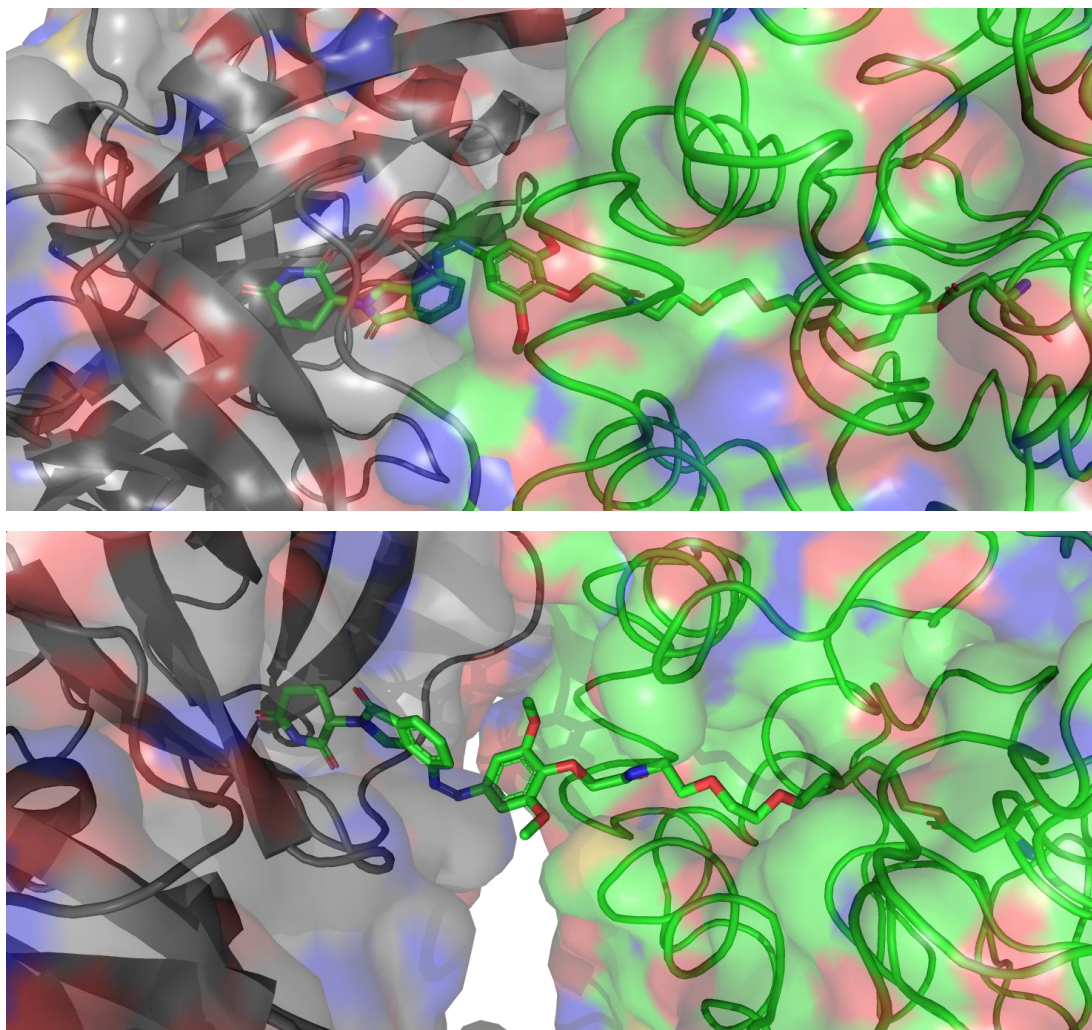


Figure 8.7: Model of ternary complex formation between cereblon (gray, PDB 4CI2)^[25] and HaloTag (green, PDB 5VNP)^[24] and **HaloPHOTAC-1**. The model was created using Schrödinger Maestro 11.9 and PyMOL version 2.2.3.

The tag based PHOTACs developed herein combine small molecule and optogenetic approaches towards protein degradation. Since degradation requires tagged proteins, the expression could be limited to cell types or tissues of interest to further enhance the selectivity beyond the localization that light affords. An advantage of PHOTACs is their reversibility and wavelength-dependence of the incident light. This enables setting defined protein levels and could be used to mimic naturally occurring protein oscillations. Further, **dTAG-PHOTACs** and **HaloPHOTACs** could benefit from improved photoswitches with different photophysical properties such as short thermal half-lives or red-shifted absorption spectra (Chapter 3).

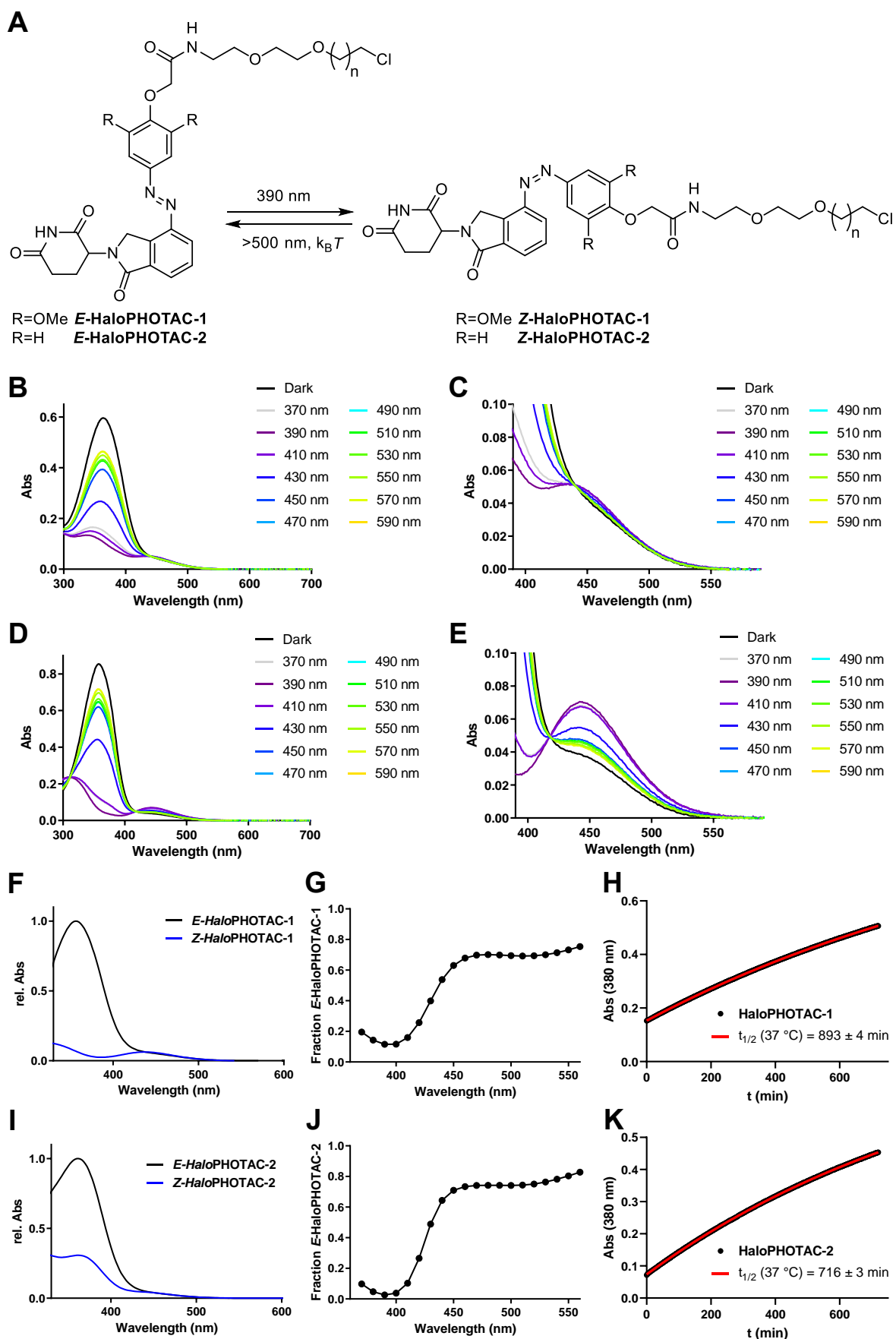


Figure 8.8: Photophysical characterization of HaloPHOTACs A) Structure and isomerization of HaloPHOTAC-1+2. B), C) Absorption spectra of HaloPHOTAC-1

after irradiation with the indicated wavelength for 5 min. D), E) Absorption spectra of **HaloPHOTAC-2** after irradiation with the indicated wavelength for 5 min. F) Absorption spectra of **HaloPHOTAC-1** isomers as obtained by LCMS. G) Calculated fraction of *E*-**HaloPHOTAC-1** after 5 min irradiation with the indicated wavelength. H) Thermal *Z*-to-*E* isomerization of **HaloPHOTAC-1** at 37 °C in DMSO. I) Absorption spectra of **HaloPHOTAC-2** isomers as obtained by LCMS. J) Calculated fraction of *E*-**HaloPHOTAC-2** after 5 min irradiation with the indicated wavelength. K) Thermal *Z*-to-*E* isomerization of **HaloPHOTAC-2** at 37 °C in DMSO.

Supporting Information

Determination of Photophysical properties

UV-Vis spectrometry was performed on a Varian Cary 60 UV-Visible Spectrophotometer using BRAND UV-Cuvette Disposable Spectrophotometer/Photometer Ultra-Micro Cuvettes, BrandTech (10 mm light path). Temperature was controlled using an Agilent Technologies PCB 1500 Water Peltier system and samples were irradiated with a Cairn Research Optoscan Monochromator with Optosource High Intensity Arc Lamp equipped with a 75 W UXL-S50A lamp from USHIO Inc. Japan and set to 15 nm full width at half maximum. Samples were stored and prepared under red light to avoid formation of the *Z*-isomers. 10 mM stock solutions were prepared in the dark and diluted to a final concentration of 25 μ M to measure the UV-VIS spectra of **PHOTACs** following irradiation with different wavelengths for 5 min using the monochromator. Measurement was started from the dark-adapted state, followed by 370 nm and further stepwise wavelength increase up to 600 nm. By increasing the wavelength from low to high *Z*- to *E*-isomerization can be observed, whereas going the reverse direction from high to low wavelength, the PSS might not be reached due to low absorptivity above 500 nm. Generally, due to the limited intensity and spectral width of the monochromator, slightly different PSSs could be generated with a true monochromatic, high-intensity light source. Spectra were recorded in DMSO to avoid any artifacts of aggregation or precipitation.

Thermal relaxation was measured by preirradiating **PHOTACs** with 390 nm light and recording the absorption at 380 nm wavelength over 12 h at 37 °C in DMSO or DMSO-PBS (pH 7.4) mixtures in tightly sealed cuvettes. Half-lives were determined by nonlinear regression using GraphPad Prism Version 9.02.

Separated spectra of the *Z*- and *E*-isomers were obtained from the internal UV-VIS detector of the LCMS by irradiating the sample before injection and were normalized at the isosbestic point. Isomer ratios were calculated in the region of largest absorption difference between 330 and 390 nm from the separated spectra obtained by LCMS and the spectra obtained following irradiation with different wavelengths for 5 min, normalized at the isosbestic point.

Synthetic procedures

General information

The reagents and solvents used in this study were bought from the following chemical suppliers: Acros Organics, Alfa Aesar, Combi-Blocks, Oakwood, OxChem, Sigma-

Aldrich, Toronto Research Chemicals and Medkoo Biosciences and were used as purchased.

Dry solvents used in reactions performed under inert atmosphere were obtained by passing the degassed solvents through activated alumina columns. Additionally, dry solvents were stored over molecular sieves under an inert atmosphere.

Column chromatography was carried out on silica gel (60 Å pore size, 40–63 µm, Merck KGaA) using a Teledyne Isco Combiflash EZprep flash purification system.

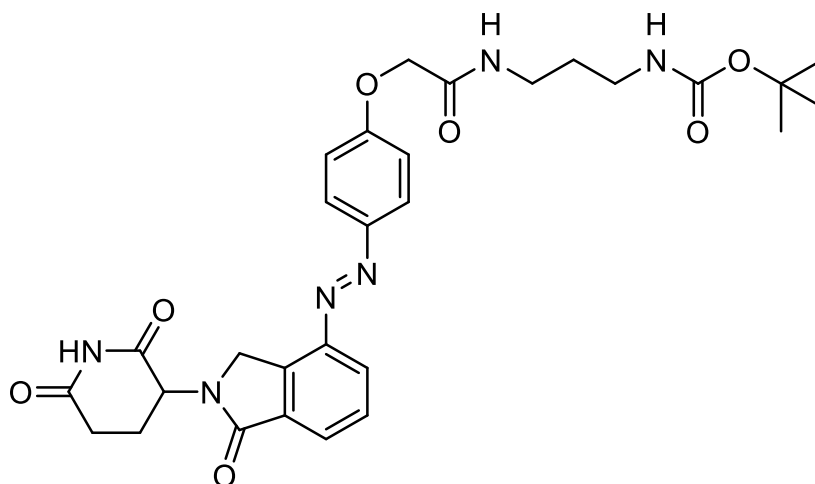
Thin-layer chromatography (TLC) was performed on glass plates precoated with silica gel (0.25 mm, 60-Å pore size, Merck). TLC plates were visualized by exposure to UV light (254 and 366 nm).

NMR spectra were obtained on a Bruker Avance III HD 400 MHz spectrometer equipped with a CryoProbe™ operating at 400 MHz for ¹H and 100 MHz for ¹³C spectra or on a Bruker AVIII-600 High Performance Digital NMR Spectrometer (600 MHz for ¹H and 150 MHz for ¹³C spectra) with CPTCI-cryoprobehead. Integration results and multiplets are reported as observed and denoted as follows: s (singlet), d (doublet), t (triplet), q (quartet), p (pentet), h (hextet), sept (septet), and m (multiplet) and as combinations thereof.

High-resolution mass spectra (HRMS) were recorded on an Agilent Technologies 6224 Accurate-Mass time-of-flight spectrometer with atmospheric pressure chemical ionization (APCI) source.

LCMS were measured on an Agilent Technologies 1260 II Infinity connected to an Agilent Technologies 6120 Quadrupole mass spectrometer with APCI ionization source. Elution was performed using a gradient from 5:95% to 100:0% MeCN:H₂O with 0.1% formic acid over 5 min, if not indicated otherwise. Separated isomer spectra of azobenzenes were obtained by irradiation of the LCMS sample prior to injection.

***tert*-butyl (3-(2-(4-((2-(2,6-dioxopiperidin-3-yl)-1-oxoisindolin-4-yl)diazenyl)phenoxy)acetamido)propyl)carbamate (8-9)**



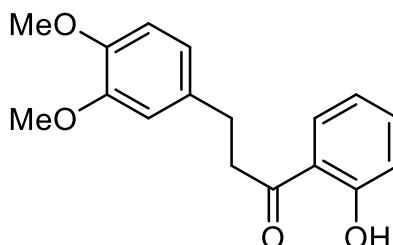
2-(4-((2-(2,6-dioxopiperidin-3-yl)-1-oxoisindolin-4-yl)diazenyl)phenoxy)acetic acid^[20] (40.0 mg, 0.095 mmol, 1.0 eq.), *N*-Boc-1,3-diaminopropane (49.5 mg, 0.284 mmol, 3.0 eq.) and HATU (43.2 mg, 0.114 mmol, 1.2 eq.) were combined under nitrogen atmosphere. The solids were dissolved in dry DMF (1 mL). After addition of *i*-Pr₂NEt (49.0 mg, 0.379 mmol, 4 eq., 0.066 mL) the reaction was stirred for 16 h at room temperature. The mixture was then diluted with EtOAc (20 mL) separated against water (10 mL) and washed with saturated NaHCO₃ (30 mL), 10% LiCl (20 mL) and brine (2x 20 mL). The organic phase was dried over Na₂SO₄ and concentrated under reduced pressure. Purification of the resulting crude product by flash column chromatography (CH₂Cl₂/MeOH gradient, 0-20% MeOH) yielded **8-9** (34 mg, 0.059 mmol, 62%) as an orange solid.

$R_f = 0.59$ [CH₂Cl₂:MeOH,9:1].

¹H NMR (400 MHz, CDCl₃) $\delta = 8.18$ (dd, $J = 7.8, 1.2$ Hz, 1H), 8.02 – 7.96 (m, 2H), 7.93 (d, $J = 9.0$ Hz, 2H), 7.70 (t, $J = 7.7$ Hz, 1H), 7.09 (d, $J = 8.9$ Hz, 2H), 5.26 (dd, $J = 13.3, 5.1$ Hz, 1H), 4.86 (d, $J = 18.0$ Hz, 1H), 4.74 (d, $J = 18.0$ Hz, 1H), 4.60 (s, 2H), 3.42 (q, $J = 6.3$ Hz, 2H), 3.18 (q, $J = 6.4$ Hz, 2H), 2.99 – 2.81 (m, 2H), 2.46 (qd, $J = 13.1, 5.0$ Hz, 1H), 2.32 – 2.21 (m, 1H), 1.68 (p, $J = 6.5$ Hz, 2H), 1.44 (s, 9H) ppm.

¹³C NMR (100 MHz, CDCl₃) $\delta = 170.99, 169.48, 168.68, 167.91, 160.26, 156.82, 147.90, 147.13, 134.17, 133.36, 129.67, 129.57, 125.96, 125.10, 115.30, 79.68, 67.58, 52.11, 48.34, 37.22, 35.61, 31.75, 30.34, 28.53, 23.62$ ppm.

LCMS (ESI): $t_{ret} = 3.27$ min (*Z*). 601m/z [M+Na]⁺, 577 m/z [M-H]⁻.
 $t_{ret} = 3.65$ min (*E*). 601m/z [M+Na]⁺, 577 m/z [M-H]⁻.

3-(3,4-dimethoxyphenyl)-1-(2-hydroxyphenyl)propan-1-one (8-2)

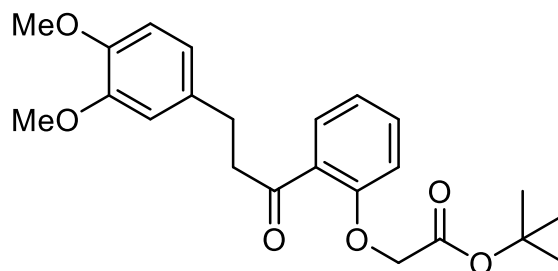
Similar to the procedure by Jørgensen and Bols^[22], (*E*)-3-(3,4-dimethoxyphenyl)-1-(2-hydroxyphenyl)prop-2-en-1-one (**8-1**, 2.80 g, 9.85 mmol, 1.0 eq.), Pd/C (10%, 314 mg, 0.295 mmol, 0.03 eq.) and ammonium formate (1.86 g, 29.5 mmol, 3 eq.) were dissolved in methanol (30 mL) and heated under reflux for 4 h. The hot mixture was filtered over celite and concentrated. The crude solid was purified by flash column chromatography (Hex/EA gradient, 0-100% EA) and yielded **8-2** (906 mg, 3.16 mmol, 32%) as a colorless solid.

¹H NMR (400 MHz, CDCl₃) δ = 12.31 (s, 1H), 7.75 (dd, J = 8.0, 1.6 Hz, 1H), 7.46 (ddd, J = 8.6, 7.2, 1.6 Hz, 1H), 6.99 (dd, J = 8.4, 1.1 Hz, 1H), 6.88 (ddd, J = 8.2, 7.2, 1.1 Hz, 1H), 6.83 – 6.75 (m, 3H), 3.87 (s, 3H), 3.86 (s, 3H), 3.31 (dd, J = 8.3, 6.9 Hz, 2H), 3.02 (dd, J = 8.2, 7.1 Hz, 2H) ppm.

¹³C NMR (100 MHz, CDCl₃) δ = 205.67, 162.59, 149.09, 147.67, 136.49, 133.42, 129.98, 120.30, 119.44, 119.05, 118.69, 111.93, 111.51, 56.08, 55.99, 40.44, 29.89 ppm.

LCMS (ESI): $t_{\text{ret}} = 4.16$ min. 287 m/z [M+H]⁺.

The analytical data matched those described in the literature.^[27]

***tert*-butyl 2-(2-(3-(3,4-dimethoxyphenyl)propanoyl)phenoxy)acetate (**8-3**)**

8-2 (443.0 mg, 1.55 mmol, 1.0 eq.) and K_2CO_3 (885.0 mg, 6.19 mmol, 4.0 eq.) were suspended in DMF (5 mL). *tert*-butyl bromoacetate (317.0 mg, 1.63 mmol, 1.05 eq., 0.240 mL) was added and the mixture stirred for 12 h. Next, the reaction mixture was diluted with EtOAc (40 mL) separated against water (50 mL) and washed with saturated $NaHCO_3$ (30 mL), 10% LiCl (30 mL) and brine (50 mL). The organic phase was dried over Na_2SO_4 and concentrated under reduced pressure. Purification of the resulting crude product by flash column chromatography (Hex/EA gradient, 0-100% EA) yielded **8-3** (608 mg, 1.52 mmol, 98%) as a colorless solid.

$R_f = 0.37$ [Hx:EA, 1:1].

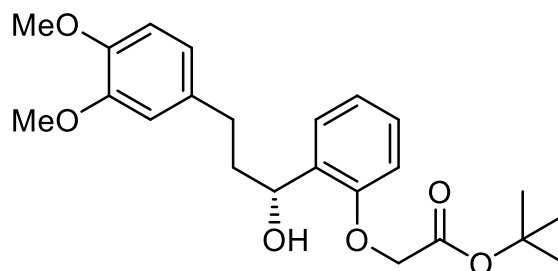
1H NMR (400 MHz, $CDCl_3$) $\delta = 7.68$ (dd, $J = 7.7, 1.8$ Hz, 1H), 7.41 (ddd, $J = 8.3, 7.3, 1.8$ Hz, 1H), 7.03 (td, $J = 7.5, 0.9$ Hz, 1H), 6.82 – 6.75 (m, 4H), 4.58 (s, 2H), 3.86 (s, 3H), 3.84 (s, 3H), 3.42 (t, $J = 7.7$ Hz, 2H), 2.99 (t, $J = 7.7$ Hz, 2H), 1.45 (s, 9H) ppm.

^{13}C NMR (100 MHz, $CDCl_3$) $\delta = 201.96, 167.26, 156.74, 148.88, 147.27, 134.46, 133.27, 130.73, 128.98, 121.68, 120.37, 112.12, 112.03, 111.30, 82.77, 66.01, 56.03, 55.89, 45.73, 30.15, 28.12$ ppm.

HRMS (APCI): calcd. for $C_{23}H_{28}NaO_6^+$: 423.1778 m/z $[M+Na]^+$
 found: 423.1771 m/z $[M+Na]^+$.

LCMS (ESI): $t_{ret} = 4.56$ min. 423 m/z $[M+Na]^+$.

tert-butyl (R)-2-(2-(3-(3,4-dimethoxyphenyl)-1-hydroxypropyl)phenoxy)acetate
(8-4)

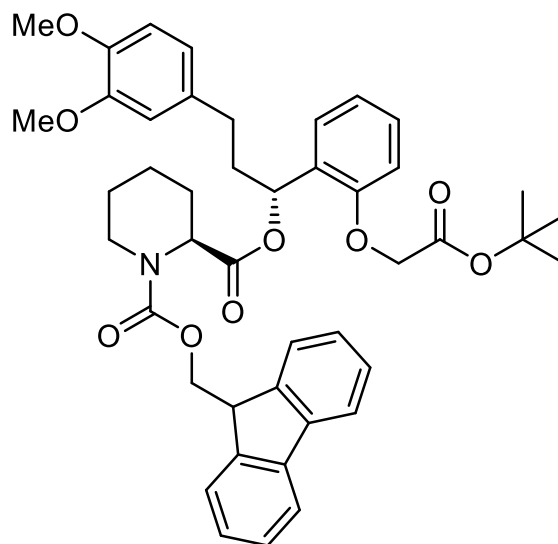


Adapted from the procedure by Jørgensen and Bols^[22], **8-3** (580.0 mg, 1.45 mmol, 1.0 eq.) was dissolved in THF (5 mL) under nitrogen atmosphere. A mixture of borane dimethylsulfide (165 mg, 2.172 mmol, 0.206 mL, 1.5 eq.) was prepared in 6 mL THF. (S)-(-)-2-Methyl-CBS-oxazaborolidine (1 M stock in toluene, 0.157 mL, 0.145 mmol, 0.1 eq.) was added to 2 mL of the borane dimethylsulfide solution and combined with the solution of **8-3** in THF. The residual 4 mL of the borane dimethylsulfide solution were added dropwise over 1 h at 0 °C. The resulting mixture was stirred for 1 h at room temperature before adding a saturated NH₄Cl solution (20 mL). The mixture was extracted with ethyl acetate (50 mL), was twice with water (50 mL) and brine (50 mL). The organic phase was dried over Na₂SO₄ and concentrated under reduced pressure. Purification of the resulting crude product by flash column chromatography (Hex/EA gradient, 0-100% EA) yielded **8-4** (457 mg, 1.14 mmol, 78%, 85% e.e.) as a colorless oil. The product was directly used in the following synthetic step.

$R_f = 0.09$ [Hx:EA,5:1].

HRMS (APCI):	calcd. for C ₂₃ H ₃₀ NaO ₆ ⁺ :	425.1935 m/z [M+Na] ⁺
	found:	425.1939 m/z [M+Na] ⁺ .
LCMS (ESI):	$t_{ret} = 4.28$ min.	425 m/z [M+Na] ⁺ .

1-((9H-fluoren-9-yl)methyl) 2-((R)-1-(2-(2-(tert-butoxy)-2-oxoethoxy)phenyl)-3-(3,4-dimethoxyphenyl)propyl) (S)-piperidine-1,2-dicarboxylate (8-5)



Adapted from the procedure by Yang et al.^[28], **8-4** (450 mg, 1.12 mmol, 1.0 eq.) and (S)-*N*-Fmoc-piperidine-2-carboxylic acid (432 mg, 1.23 mmol, 1.1 eq.), *N,N*-dicyclohexylcarbodiimide (277 mg, 1.34 mmol, 1.2 eq.) and 4-dimethylaminopyridine (82 mg, 0.67 mmol, 0.6 eq.) were suspended in dry CH₂Cl₂ under nitrogen atmosphere. The mixture was stirred for 16 h, filtered, washed twice with a 1:1 mixture of sat. aq. NH₄Cl and 0.2 M HCl (2x50 mL), followed by washing with sat. aq. NaHCO₃ (30 mL) and brine (30 mL). The organic phase was dried over Na₂SO₄ and concentrated under reduced pressure. Purification of the resulting crude product by flash column chromatography (Hex/EA gradient, 0-100% EA) yielded **8-5** (766 mg, 1.04 mmol, 93%) as a colorless oil.

$R_f = 0.08$ [Hx:EA,5:1].

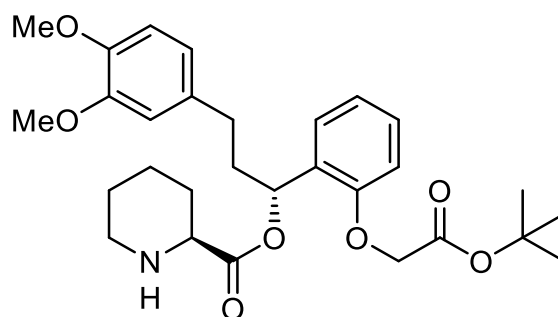
¹H NMR (400 MHz, CDCl₃) $\delta = 7.80 - 7.69$ (m, 2H), 7.59 (dd, $J = 10.6, 7.5$ Hz, 1H), 7.48 (dd, $J = 25.9, 7.6$ Hz, 1H), 7.42 – 7.26 (m, 4H), 7.20 (tt, $J = 11.8, 5.4$ Hz, 2H), 6.93 (dt, $J = 22.7, 7.5$ Hz, 1H), 6.75 – 6.61 (m, 4H), 6.31 (dt, $J = 12.0, 6.2$ Hz, 1H), 5.09 – 4.89 (m, 1H), 4.52 (s, 2H), 4.47 – 4.05 (m, 4H), 3.85 – 3.76 (m, 6H), 3.27 – 2.99 (m, 1H), 2.71 – 2.45 (m, 2H), 2.41 – 2.29 (m, 1H), 2.24 – 2.12 (m, 2H), 1.81 – 1.48 (m, 4H), 1.45 (s, 9H), 1.39 – 1.25 (m, 1H) ppm.

¹³C NMR (100 MHz, CDCl₃, minor rotamer in parenthesis) $\delta = 170.87(170.85), 167.94(167.85), 156.49(156.05), (154.66)154.59, 148.87, (147.26)147.23, 144.26(144.18), 144.04, 143.96, 141.41(141.36, 141.32), 134.33(134.21),$

129.44(129.29), (128.82)128.71, 127.78, 127.19, (126.84)126.70, 125.23(125.12),
121.66, 120.26(120.20), 120.07, 111.86(111.79), 111.52, 111.27, 82.32, (71.90)71.67,
67.92(67.87), 66.07, 56.03, 55.89, (55.06)54.67, 47.39, 42.11(41.99), (37.30)37.25,
31.34, 28.17, (27.24)27.02, 25.01(24.76), 20.96(20.86) ppm.

HRMS (APCI): calcd. for $C_{44}H_{50}NO_9^+$: 736.3480 m/z $[M+H]^+$
 found: 736.3455 m/z $[M+H]^+$.

LCMS (ESI, 50to100% MeCN): t_{ret} = 4.20 min. 755 m/z $[M+H_3O]^+$.

**(R)-1-(2-(2-(tert-butoxy)-2-oxoethoxy)phenyl)-3-(3,4-dimethoxyphenyl)propyl
(S)-piperidine-2-carboxylate (8-6)**

8-5 (700 mg, 0.951 mmol, 1.0 eq.) was dissolved in CH₂Cl₂ (10 mL) and piperidine (810 mg, 9.51 mmol, 0.94 mL, 10 eq.) was added. The resulting solution was stirred for 14 h at room temperature. The crude product was concentrated under reduced pressure and purified by flash column chromatography (CH₂Cl₂/MeOH gradient, 0-20% MeOH) yielding **8-6** (379 mg, 0.738 mmol, 78%) as a colorless oil.

R_f = 0.10 [Hx:EA, 1:3].

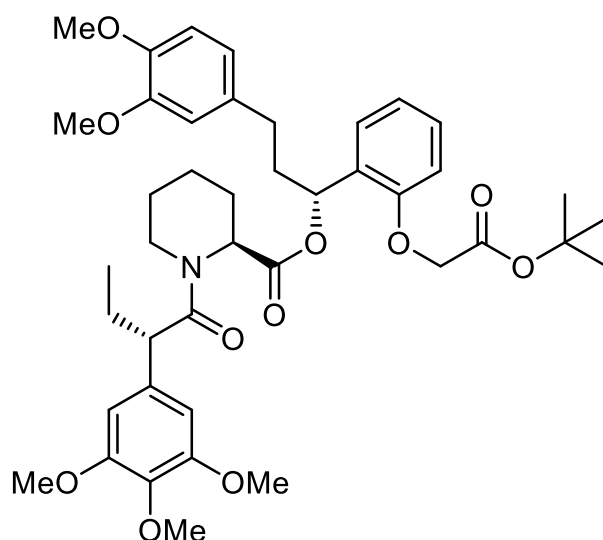
¹H NMR (400 MHz, CDCl₃) δ = 7.32 (dd, J = 7.6, 1.7 Hz, 1H), 7.20 (ddd, J = 8.2, 7.4, 1.7 Hz, 1H), 6.97 (td, J = 7.5, 1.0 Hz, 1H), 6.78 – 6.67 (m, 4H), 6.28 (dd, J = 7.0, 5.7 Hz, 1H), 4.52 (s, 2H), 3.85 (s, 3H), 3.83 (s, 3H), 3.39 (dd, J = 9.8, 3.3 Hz, 1H), 3.07 (dt, J = 11.7, 3.6 Hz, 1H), 2.72 – 2.53 (m, 3H), 2.24 – 2.14 (m, 2H), 2.10 – 2.01 (m, 1H), 1.86 – 1.75 (m, 2H), 1.68 – 1.47 (m, 1H), 1.45 (s, 9H) ppm.

¹³C NMR (100 MHz, CDCl₃) δ = 172.79, 167.91, 154.64, 148.86, 147.22, 134.41, 129.61, 128.63, 126.61, 121.57, 120.25, 111.83, 111.52, 111.23, 82.28, 71.03, 66.06, 58.87, 56.01, 55.91, 45.78, 36.97, 31.54, 29.39, 28.14, 25.97, 24.27 ppm.

HRMS (APCI): calcd. for C₂₉H₄₀NO₇⁺: 514.2799 m/z [M+H]⁺
 found: 514.2803 m/z [M+H]⁺.

LCMS (ESI): t_{ret} = 3.72 min. 514 m/z [M+H]⁺.

**(R)-1-(2-(2-(tert-butoxy)-2-oxoethoxy)phenyl)-3-(3,4-dimethoxyphenyl)propyl
(S)-1-((S)-2-(3,4,5-trimethoxyphenyl)butanoyl)piperidine-2-carboxylate (8-7)**



(S)-2-(3,4,5-Trimethoxyphenyl)butanoic acid (65.2 mg, 0.257 mmol, 1.05 eq.) and HATU (107 mg, 0.281 mmol, 1.15 eq.) were dissolved in dry DMF (2 mL). After 3 min *i*-Pr₂NEt (94.7 mg, 0.733 mmol, 3.0 eq., 0.128 mL) was added and the mixture was stirred for 2 min, before being added into a solution of **8-6** (700 mg, 0.951 mmol, 1.0 eq.) in DMF (1 mL). The reaction mixture was stirred for 10 h, diluted with CH₂Cl₂ (40 mL) and separated against saturated NH₄Cl (25 mL) and washed with saturated NaHCO₃ (30 mL), 10% LiCl (30 mL) and brine (30 mL). The organic phase was dried over Na₂SO₄ and concentrated under reduced pressure. Purification of the resulting crude product by flash column chromatography (Hex/EA gradient, 0-100% EA) yielded **8-7** (163 mg, 0.271 mmol, 89%) as a colorless oil.

$R_f = 0.76$ [CH₂Cl₂:MeOH, 19:1].

¹H NMR (400 MHz, CDCl₃) $\delta = 7.17 - 7.12$ (m, 1H), 6.96 (dd, $J = 7.7, 1.7$ Hz, 1H), 6.85 (td, $J = 7.5, 1.0$ Hz, 1H), 6.75 (d, $J = 7.9$ Hz, 1H), 6.75 – 6.64 (m, 2H), 6.65 (d, $J = 7.9$ Hz, 1H), 6.41 (s, 2H), 6.19 (dd, $J = 7.7, 5.0$ Hz, 1H), 5.52 (d, $J = 4.2$ Hz, 1H), 4.47 (s, 2H), 3.86 – 3.82 (m, 7H), 3.76 (s, 3H), 3.64 (s, 6H), 3.58 (t, $J = 7.2$ Hz, 1H), 2.90 – 2.83 (m, 1H), 2.67 – 2.51 (m, 2H), 2.36 – 2.27 (m, 1H), 2.25 – 2.17 (m, 1H), 2.13 – 2.03 (m, 2H), 1.78 – 1.65 (m, 3H), 1.62 – 1.57 (m, 1H), 1.48 – 1.43 (m, 10H), 1.39 – 1.29 (m, 1H), 0.90 (t, $J = 7.4$ Hz, 3H) ppm.

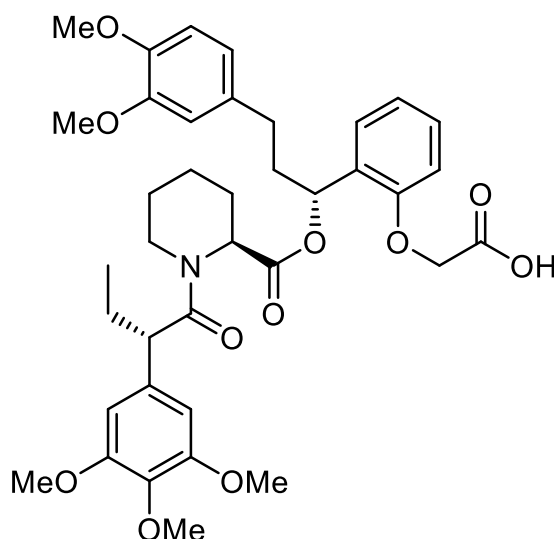
¹³C NMR (100 MHz, CDCl₃) $\delta = 172.62, 170.59, 167.85, 154.29, 153.31, 148.88, 147.25, 136.72, 135.52, 134.34, 129.61, 128.44, 126.50, 121.70, 120.34, 111.92,$

111.26, 111.14, 105.03, 82.30, 71.12, 65.98, 60.87, 56.41, 56.05, 55.94, 52.14, 50.94, 43.57, 37.37, 31.39, 28.61, 28.17, 27.05, 25.59, 21.06, 12.75 ppm.

HRMS (APCI): calcd. for $C_{42}H_{56}NO_{11}^+$: 750.3848 m/z $[M+H]^+$
found: 750.3850 m/z $[M+H]^+$.

LCMS (ESI): t_{ret} = 5.30 min. 772 m/z $[M+Na]^+$.

2-(2-((R)-3-(3,4-dimethoxyphenyl)-1-(((S)-1-((S)-2-(3,4,5-trimethoxyphenyl)butanoyl)piperidine-2-carbonyloxy)propyl)phenoxy)acetic acid (8-8)

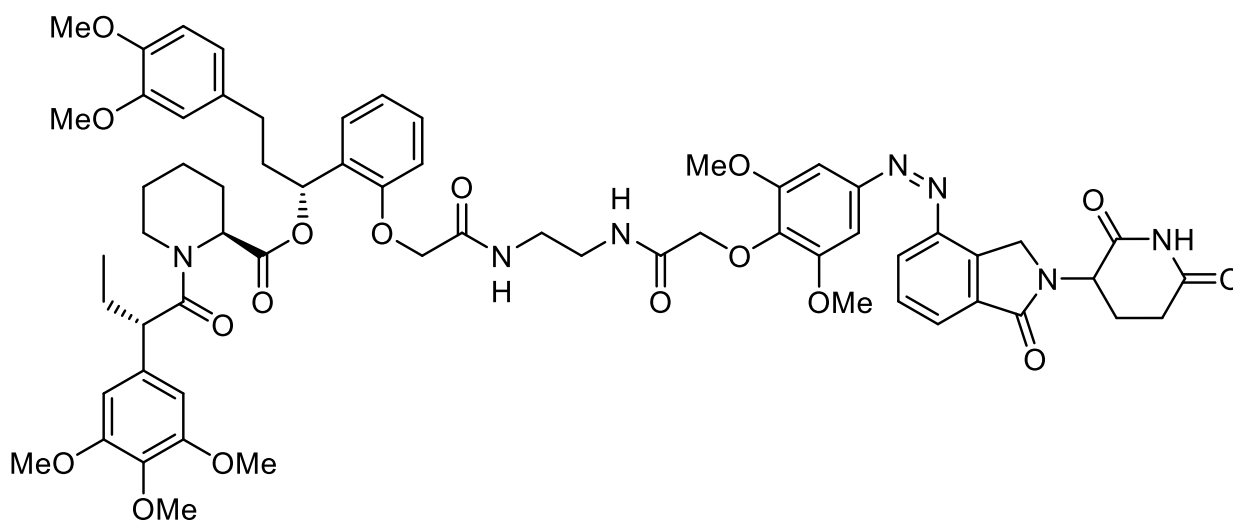


8-7 (60.0 mg, 0.080 mmol) was dissolved in formic acid (1 mL) and stirred for 90 min at room temperature while monitoring conversion by TLC and LCMS. The mixture was concentrated under reduced pressure at 30 °C and the crude residue co-evaporated twice with CH_2Cl_2 (5 mL) at 30 °C, followed by co-evaporation twice with Et_2O (5 mL) at 30 °C. To the residue was added Et_2O (10 mL), the suspension was filtered and the residue was with Et_2O (10 mL). The combined Et_2O extracts were concentrated and the resulting crude product was purified by flash column chromatography (Hx:EA 1:1+0.1% formic acid) yielding **8-8** (13.2 mg, 0.019 mmol, 24%) as a colorless, sticky oil. The sensitive product was directly used in the next step.

R_f = 0.07 [Hx:EA 1:1+0.1% formic acid].

LCMS (ESI): t_{ret} = 4.01 min. 695 m/z $[M+H]^+$.

(1R)-3-(3,4-dimethoxyphenyl)-1-(2-(2-((2-(2-(4-((2-(2,6-dioxopiperidin-3-yl)-1-oxoisoindolin-4-yl)diazenyl)-2,6-dimethoxyphenoxy)acetamido)ethyl)amino)-2-oxoethoxy)phenyl)propyl (2S)-1-((S)-2-(3,4,5-trimethoxyphenyl)butanoyl)piperidine-2-carboxylate (dTAG-PHOTAC-1)



Into a round bottom flask with dry **8-8** (6.7 mg, 0.010 mmol, 1.0 eq.) were added (*E*)-4-(2-(4-((2-(2,6-dioxopiperidin-3-yl)-1-oxoisoindolin-4-yl)diazenyl)-2,6-dimethoxyphenoxy)acetamido)ethan-1-aminium 2,2,2-trifluoroacetate^[20] (11.2 mg, 0.019 mmol, 2.0 eq.) and HATU (6.6 mg, 0.017 mmol, 1.8 eq.) under nitrogen atmosphere. The solids were dissolved in dry DMF (1 mL). After addition of *i*-Pr₂NEt (8.7 mg, 0.068 mmol, 7.0 eq., 0.012 mL) the reaction was stirred for 16 h at room temperature. The mixture was then diluted with EtOAc (25 mL) separated against saturated NH₄Cl (30 mL) and washed with saturated NaHCO₃ (30 mL), 10% LiCl (2x 20 mL) and brine (2x 20 mL). The organic phase was dried over Na₂SO₄ and concentrated under reduced pressure. Purification of the resulting crude product by flash column chromatography (CH₂Cl₂/MeOH gradient, 0-20% MeOH) gave **dTAG-PHOTAC-1** (6.2 mg, 0.005 mmol, 56%) as a yellow solid.

$R_f = 0.42$ [CH₂Cl₂:MeOH, 19:1].

¹H NMR (600 MHz, DMSO-*d*₆) δ 11.03 (s, 1H), 8.21 (d, *J* = 7.8 Hz, 1H), 8.13 – 8.04 (m, 1H), 8.02 – 7.98 (m, 1H), 7.92 (d, *J* = 7.4 Hz, 1H), 7.80 (t, *J* = 7.6 Hz, 1H), 7.37 – 7.31 (m, 2H), 7.17 (ddd, *J* = 8.8, 6.9, 2.2 Hz, 1H), 6.89 – 6.72 (m, 5H), 6.65 – 6.60 (m, 1H), 6.55 (s, 2H), 6.06 (dd, *J* = 8.2, 4.8 Hz, 1H), 5.32 (dd, *J* = 6.0, 2.3 Hz, 1H), 5.16 (dd, *J* = 13.3, 5.1 Hz, 1H), 4.81 (d, *J* = 19.0 Hz, 1H), 4.69 (d, *J* = 19.0 Hz, 1H), 4.53 –

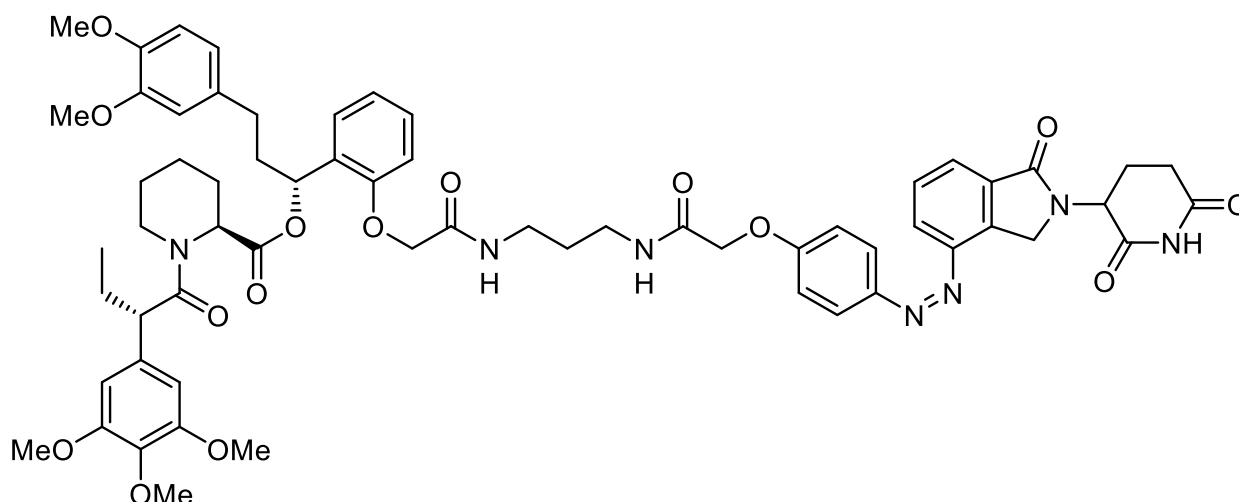
4.46 (m, 2H), 4.39 (s, 2H), 4.07 – 4.00 (m, 1H), 3.95 – 3.90 (m, 6H), 3.88 – 3.83 (m, 1H), 3.75 – 3.62 (m, 9H), 3.57 – 3.52 (m, 6H), 3.30 – 3.22 (m, 4H), 2.94 (ddd, J = 18.0, 13.5, 5.5 Hz, 1H), 2.67 – 2.46 (m, 4H), 2.43 – 2.34 (m, 1H), 2.19 – 2.13 (m, 1H), 2.06 (dp, J = 11.2, 3.9 Hz, 1H), 1.98 (dq, J = 10.2, 5.8, 4.4 Hz, 1H), 1.95 – 1.82 (m, 2H), 1.65 – 1.50 (m, 4H), 1.43 – 1.32 (m, 1H), 1.16 – 1.09 (m, 1H), 0.80 (t, J = 7.3 Hz, 3H). ppm.

¹³C NMR (150 MHz, DMSO-*d*₆) δ = 172.91, 171.95, 171.00, 170.41, 168.50, 167.80, 167.15, 154.15, 152.68, 152.64, 148.56, 148.31, 146.95, 146.35, 139.22, 135.96, 135.56, 134.50, 133.83, 133.39, 129.65, 128.86, 128.67, 125.95, 125.49, 121.14, 119.91, 112.13, 112.07, 111.77, 105.06, 104.80, 100.58, 71.74, 69.82, 67.29, 59.76, 56.32, 55.49, 55.45, 55.27, 51.85, 51.41, 48.66, 48.30, 42.89, 38.42, 37.96, 36.38, 31.27, 30.52, 28.06, 26.27, 24.96, 22.31, 20.49, 12.27 ppm.

HRMS (APCI): calcd. for C₆₃H₇₄N₇O₁₇⁺: 1200.5136 m/z [M+H]⁺
 found: 1200.5077 m/z [M+H]⁺.

LCMS (ESI): t_{ret} = 4.06 min. (E) 1219 m/z [M+H+H₂O]⁺.
 t_{ret} = 3.98 min. (Z) 1219 m/z [M+H+H₂O]⁺.

(1R)-3-(3,4-dimethoxyphenyl)-1-(2-(2-((3-(2-(4-((2-(2,6-dioxopiperidin-3-yl)-1-oxoisoindolin-4-yl)diazenyl)phenoxy)acetamido)propyl)amino)-2-oxoethoxy)phenyl)propyl (2S)-1-((S)-2-(3,4,5-trimethoxyphenyl)butanoyl)piperidine-2-carboxylate (dTAG-PHOTAC-2)



8-9 (31 mg, 0.050 mmol) was dissolved in TFA/CH₂Cl₂ (1:1; 2mL:2mL) and stirred for 2 h at room temperature. The reaction was diluted with CH₂Cl₂ and concentrated under reduced pressure. The reaction was triturated with Et₂O and dried *in vacuo* for 48 h. The crude product was obtained in quantitative yield as TFA salt (>99%) as an orange solid and used without further purification.

Into a round bottom flask with dry **8-8** (6.7 mg, 0.010 mmol, 1.0 eq.) were added the crude deprotected amine (11.4 mg, 0.019 mmol, 2.0 eq.) and HATU (6.6 mg, 0.017 mmol, 1.8 eq.) under nitrogen atmosphere. The solids were dissolved in dry DMF (1 mL). After addition of *i*-Pr₂NEt (16.2 mg, 0.126 mmol, 7.2 eq., 0.022 mL) the reaction was stirred for 16 h at room temperature. The mixture was then diluted with EtOAc (25 mL) separated against saturated NH₄Cl (30 mL) and washed with saturated NaHCO₃ (30 mL), 10% LiCl (2x 20 mL) and brine (2x 20 mL). The organic phase was dried over Na₂SO₄ and concentrated under reduced pressure. Purification of the resulting crude product by flash column chromatography (CH₂Cl₂/MeOH gradient, 0-20% MeOH) gave **dTAG-PHOTAC-2** (5.4 mg, 0.005 mmol, 48%) as a yellow solid.

$R_f = 0.34$ [CH₂Cl₂:MeOH,19:1].

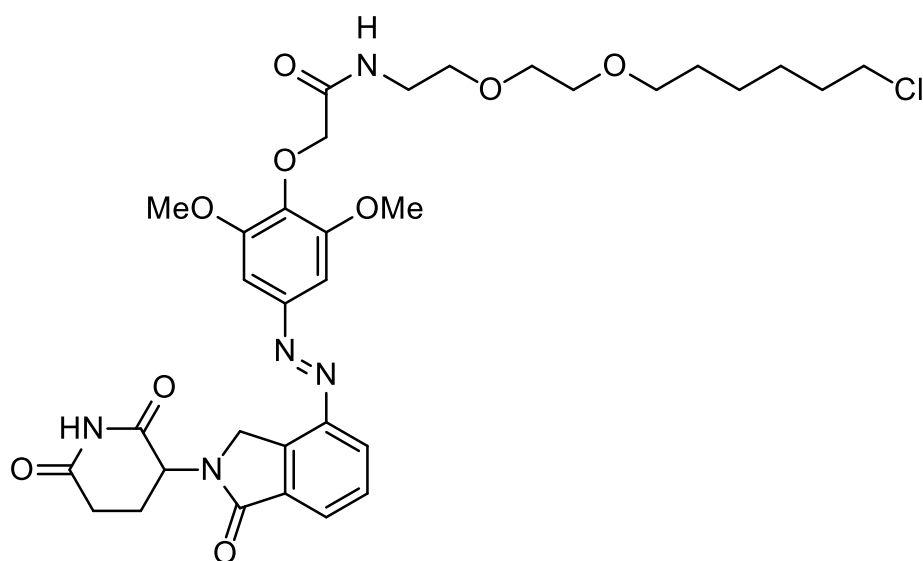
¹H NMR (600 MHz, DMSO-*d*₆) $\delta = 11.02$ (s, 1H), 8.23 – 8.15 (m, 2H), 7.97 (d, *J* = 8.9 Hz, 2H), 7.91 – 7.87 (m, 2H), 7.78 (t, *J* = 7.6 Hz, 1H), 7.20 (ddd, *J* = 8.6, 7.0, 2.2 Hz, 1H), 7.17 – 7.14 (m, 2H), 6.88 (t, *J* = 8.8 Hz, 1H), 6.83 – 6.76 (m, 3H), 6.73 (d, *J* = 1.9

Hz, 1H), 6.63 (dd, J = 8.2, 1.9 Hz, 1H), 6.55 (s, 2H), 6.06 (dd, J = 8.4, 4.8 Hz, 1H), 5.32 (d, J = 4.1 Hz, 1H), 5.17 (dd, J = 13.3, 5.2 Hz, 1H), 4.79 (d, J = 19.0 Hz, 1H), 4.67 (d, J = 19.0 Hz, 1H), 4.60 (s, 2H), 4.52 – 4.47 (m, 2H), 4.07 – 4.01 (m, 1H), 3.86 (t, J = 7.2 Hz, 1H), 3.75 – 3.66 (m, 9H), 3.55 (d, J = 10.4 Hz, 6H), 3.20 – 3.08 (m, 4H), 2.94 (ddd, J = 17.2, 13.5, 5.5 Hz, 1H), 2.65 – 2.51 (m, 4H), 2.43 – 2.33 (m, 1H), 2.15 (d, J = 13.0 Hz, 1H), 2.07 – 1.96 (m, 2H), 1.96 – 1.84 (m, 2H), 1.64 – 1.50 (m, 6H), 1.41 – 1.31 (m, 1H), 1.17 – 1.09 (m, 1H), 0.80 (t, J = 7.3 Hz, 3H) ppm.

¹³C NMR (150 MHz, DMSO-*d*₆) δ = 172.91, 171.95, 170.99, 170.42, 167.51, 167.21, 167.10, 160.86, 154.08, 152.64, 148.56, 146.96, 146.69, 146.58, 135.96, 135.56, 134.29, 133.74, 133.36, 129.57, 128.84, 128.67, 128.48, 126.03, 124.99, 124.74, 121.15, 119.93, 115.38, 112.13, 112.08, 111.77, 105.05, 69.79, 67.28, 67.17, 59.77, 55.90, 55.49, 55.28, 51.66, 51.41, 48.66, 48.24, 42.88, 36.37, 35.94, 35.85, 31.25, 30.53, 29.25, 28.06, 26.29, 24.95, 22.33, 20.50, 12.27 ppm.

HRMS (APCI): calcd. for C₆₂H₇₂N₇O₁₅⁺: 1154.5081 m/z [M+H]⁺
 found: 1154.5024 m/z [M+H]⁺.

LCMS (ESI): t_{ret} = 4.12 min. (E) 597 m/z [M+H+H₂O+Na]²⁺.
 t_{ret} = 3.92 min. (Z) 597 m/z [M+H+H₂O+Na]²⁺.

(E)-N-(2-(2-((6-chlorohexyl)oxy)ethoxy)ethyl)-2-(4-((2-(2,6-dioxopiperidin-3-yl)-1-oxoisindolin-4-yl)diazenyl)-2,6-dimethoxyphenoxy)acetamide (HaloPHOTAC-1)

tert-Butyl (2-(2-((6-chlorohexyl)oxy)ethoxy)ethyl)carbamate (365 mg, 1.127 mmol) prepared as previously reported^[29] was dissolved in a CH₂Cl₂:TFA mixture (5:1; 6 mL) and stirred for 1.5 h at room temperature. The reaction was concentrated under a nitrogen stream and the crude product was triturated with Et₂O (3x 10 mL) and concentrated under reduced pressure at 30 °C. Next, the product was dried in vacuo at -50 °C for 2 h. After warming to room temperature, the crude sticky solid was directly used in the next step without further purification.

The crude 2-(2-((6-chlorohexyl)oxy)ethoxy)ethan-1-aminium 2,2,2-trifluoroacetate (65.4 mg, 0.292 mmol, 3.0 eq.) was combined with (*E*)-2-(4-((2-(2,6-dioxopiperidin-3-yl)-1-oxoisindolin-4-yl)diazenyl)-2,6-dimethoxy-phenoxy)acetic acid (50 mg, 0.097 mmol, 1.0 eq.) prepared as previously described^[20] and HATU (74.1 mg, 0.195 mmol, 2.0 eq.) under nitrogen atmosphere in a dried round bottom flask. The mixture was dissolved in dry DMF (1 mL), followed by addition of *i*-Pr₂NEt (50.4 mg, 0.390 mmol, 4 eq., 0.068 mL) and stirred for 16 h at room temperature. The reaction mixture was diluted with ethyl acetate (25 mL) and separated against 10% LiCl (aq., 30 mL). The organic phase was washed with saturated NaHCO₃ (25 mL), 10% LiCl (25 mL) and brine (2x 25 mL), dried over Na₂SO₄ and concentrated under reduced pressure. Purification of the resulting crude product by flash column chromatography (CH₂Cl₂/MeOH gradient, 0 to 20% MeOH) gave **HaloPHOTAC-1** (54.6 mg, 0.079 mmol, 81%) as a yellow solid.

$R_f = 0.22$ [CH_2Cl_2 :MeOH 19:1].

^1H NMR (400 MHz, DMSO- d_6) $\delta = 11.03$ (s, 1H), 8.22 (dd, $J = 7.8, 1.1$ Hz, 1H), 8.03 (t, $J = 5.7$ Hz, 1H), 7.92 (dd, $J = 7.6, 1.1$ Hz, 1H), 7.80 (t, $J = 7.7$ Hz, 1H), 7.36 (s, 2H), 5.16 (dd, $J = 13.2, 5.1$ Hz, 1H), 4.82 (d, $J = 19.1$ Hz, 1H), 4.69 (d, $J = 19.1$ Hz, 1H), 4.45 (s, 2H), 3.95 (s, 6H), 3.57 (t, $J = 6.6$ Hz, 2H), 3.55 – 3.46 (m, 6H), 3.41 – 3.32 (m, 4H), 3.00 – 2.89 (m, 1H), 2.68 – 2.52 (m, 2H), 2.11 – 2.02 (m, 1H), 1.70 – 1.61 (m, 2H), 1.45 (p, $J = 6.8$ Hz, 2H), 1.37 – 1.19 (m, 4H) ppm.

^{13}C NMR (100 MHz, DMSO) $\delta = 172.90, 171.00, 168.19, 167.15, 152.56, 148.31, 146.34, 139.26, 134.49, 133.83, 129.64, 128.66, 125.49, 100.53, 71.91, 70.21, 69.66, 69.45, 68.99, 56.35, 51.84, 48.30, 45.33, 38.28, 31.99, 31.28, 29.06, 26.11, 24.90, 22.33$ ppm.

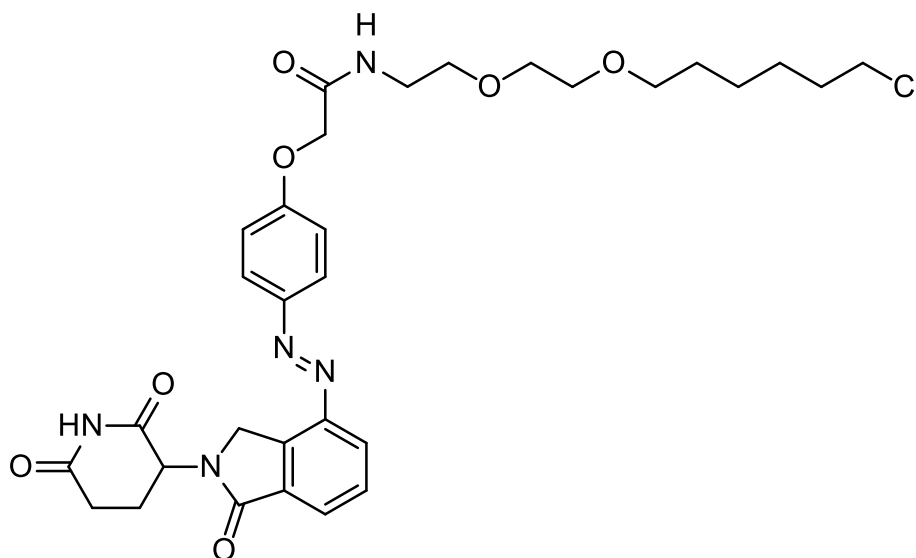
HRMS (APCI): calcd. for $\text{C}_{33}\text{H}_{43}\text{ClN}_5\text{O}_9^+$: 688.2744 m/z $[\text{M}+\text{H}]^+$.

found: 688.2718 m/z $[\text{M}+\text{H}]^+$.

LCMS (ESI): $t_{\text{ret}} = 4.16$ min. (E) 688 m/z $[\text{M}+\text{H}]^+$.

$t_{\text{ret}} = 3.91$ min. (Z) 688 m/z $[\text{M}+\text{H}]^+$.

(E)-N-(2-(2-((6-chlorohexyl)oxy)ethoxy)ethyl)-2-(4-((2-(2,6-dioxopiperidin-3-yl)-1-oxoisoindolin-4-yl)diazenyl)phenoxy)acetamide (HaloPHOTAC-2)



tert-Butyl (2-(2-((6-chlorohexyl)oxy)ethoxy)ethyl)carbamate (365 mg, 1.127 mmol) prepared as previously reported^[29] was dissolved in a CH₂Cl₂:TFA mixture (5:1; 6 mL) and stirred for 1.5 h at room temperature. The reaction was concentrated under a nitrogen stream and the crude product was triturated with Et₂O (3x 10 mL) and concentrated under reduced pressure at 30 °C. Next, the product was dried in vacuo at -50 °C for 2 h. After warming to room temperature, the crude sticky solid was directly used in the next step without further purification.

The crude 2-(2-((6-chlorohexyl)oxy)ethoxy)ethan-1-aminium 2,2,2-trifluoroacetate (37.3 mg, 0.167 mmol, 3.0 eq.) was combined with (E)-2-(4-((2-(2,6-dioxopiperidin-3-yl)-1-oxoisoindolin-4-yl)diazenyl)phenoxy)acetic acid (25 mg, 0.056 mmol, 1.0 eq.) prepared as previously described^[20] and HATU (42.3 mg, 0.111 mmol, 2.0 eq.) under nitrogen atmosphere in a dried round bottom flask. The mixture was dissolved in dry DMF (1 mL), followed by addition of *i*-Pr₂NEt (28.8 mg, 0.223 mmol, 4 eq., 0.039 mL) and stirred for 16 h at room temperature. The reaction mixture was diluted with ethyl acetate (25 mL) and separated against 10% LiCl (aq., 30 mL). The organic phase was washed with saturated NaHCO₃ (25 mL), 10% LiCl (25 mL) and brine (2x 25 mL), dried over Na₂SO₄ and concentrated under reduced pressure. Purification of the resulting crude product by flash column chromatography (CH₂Cl₂/MeOH gradient, 0 to 20% MeOH) gave **HaloPHOTAC-2** (28.7 mg, 0.046 mmol, 82%) as a yellow solid.

$R_f = 0.20$ [CH_2Cl_2 :MeOH 19:1].

^1H NMR (400 MHz, DMSO- d_6) $\delta = 11.02$ (s, 1H), 8.23 – 8.14 (m, 2H), 7.99 (d, $J = 9.0$ Hz, 2H), 7.89 (dd, $J = 7.6, 1.1$ Hz, 1H), 7.78 (t, $J = 7.7$ Hz, 1H), 7.21 – 7.13 (m, 2H), 5.17 (dd, $J = 13.2, 5.1$ Hz, 1H), 4.79 (d, $J = 19.1$ Hz, 1H), 4.67 (d, $J = 19.2$ Hz, 1H), 4.63 (s, 2H), 3.58 (t, $J = 6.6$ Hz, 2H), 3.54 – 3.43 (m, 6H), 3.39 – 3.27 (m, 4H), 3.00 – 2.90 (m, 1H), 2.67 – 2.51 (m, 2H), 2.10 – 1.98 (m, 1H), 1.71 – 1.61 (m, 2H), 1.46 (p, $J = 6.7$ Hz, 2H), 1.38 – 1.18 (m, 4H) ppm.

^{13}C NMR (100 MHz, DMSO) $\delta = 172.91, 170.99, 167.21, 167.15, 160.88, 146.69, 146.58, 134.28, 133.74, 129.57, 128.47, 124.99, 124.74, 115.38, 70.20, 69.56, 69.41, 68.80, 67.12, 51.66, 48.24, 45.34, 38.32, 31.99, 31.25, 29.06, 26.11, 24.91, 22.34$ ppm.

HRMS (APCI): calcd. for $\text{C}_{31}\text{H}_{38}\text{ClN}_5\text{O}_7^+$: 627.2460 m/z $[\text{M}]^+$.

found: 627.2467 m/z $[\text{M}]^+$.

LCMS (ESI): $t_{\text{ret}} = 4.03$ min. (E) 628 m/z $[\text{M}+\text{H}]^+$.

$t_{\text{ret}} = 3.72$ min. (Z) 628 m/z $[\text{M}+\text{H}]^+$.

References

- [1] R. C. Wilson, J. A. Doudna, *Annu. Rev. Biophys.* **2013**, *42*, 217–239.
- [2] F. Faden, S. Mielke, D. Lange, N. Dissmeyer, *Biol. Chem.* **2014**, *395*, 737–762.
- [3] K. Nishimura, T. Fukagawa, H. Takisawa, T. Kakimoto, M. Kanemaki, *Nat. Methods* **2009**, *6*, 917–922.
- [4] L. A. Banaszynski, L. Chen, L. A. Maynard-Smith, A. G. Lisa Ooi, T. J. Wandless, *Cell* **2006**, *126*, 995–1004.
- [5] K. M. Bonger, L. Chen, C. W. Liu, T. J. Wandless, *Nat. Chem. Biol.* **2011**, *7*, 531–537.
- [6] C. Renicke, D. Schuster, S. Usherenko, L.-O. Essen, C. Taxis, *Chem. Biol.* **2013**, *20*, 619–626.
- [7] K. M. Bonger, R. Rakhit, A. Y. Payumo, J. K. Chen, T. J. Wandless, *ACS Chem. Biol.* **2014**, *9*, 111–115.
- [8] S. Usherenko, H. Stibbe, M. Musc , L.-O. Essen, E. A. Kostina, C. Taxis, *BMC Syst. Biol.* **2014**, *8*, DOI 10.1186/s12918-014-0128-9.
- [9] A. Hermann, J. F. Liewald, A. Gottschalk, *Curr. Biol.* **2015**, *25*, R749–R750.
- [10] J. Baaske, P. Gonschorek, R. Engesser, A. Dominguez-Monedero, K. Raute, P. Fischbach, K. M ller, E. Cachat, W. W. A. Schamel, S. Minguet, J. A. Davies, J. Timmer, W. Weber, M. D. Zurbriggen, *Sci. Rep.* **2018**, *8*, 15024.
- [11] S. Hasenj ger, J. Trauth, S. Hepp, J. Goenrich, L.-O. Essen, C. Taxis, *ACS Synth. Biol.* **2019**, *8*, 1026–1036.
- [12] J. Trauth, J. Scheffer, S. Hasenj ger, C. Taxis, *ACS Omega* **2019**, *4*, 2766–2778.
- [13] K. M. Sakamoto, K. B. Kim, A. Kumagai, F. Mercurio, C. M. Crews, R. J. Deshaies, *Proc. Natl. Acad. Sci.* **2001**, *98*, 8554–8559.
- [14] G. M. Burslem, C. M. Crews, *Cell* **2020**, *181*, 102–114.
- [15] D. L. Buckley, K. Raina, N. Darricarrere, J. Hines, J. L. Gustafson, I. E. Smith, A. H. Miah, J. D. Harling, C. M. Crews, *ACS Chem. Biol.* **2015**, *10*, 1831–1837.
- [16] B. Nabet, J. M. Roberts, D. L. Buckley, J. Paulk, S. Dastjerdi, A. Yang, A. L. Leggett, M. A. Erb, M. A. Lawlor, A. Souza, T. G. Scott, S. Vittori, J. A. Perry, J. Qi, G. E. Winter, K.-K. Wong, N. S. Gray, J. E. Bradner, *Nat. Chem. Biol.* **2018**, *14*, 431.
- [17] H. Tovell, A. Testa, C. Maniaci, H. Zhou, A. R. Prescott, T. Macartney, A. Ciulli, D. R. Alessi, *ACS Chem. Biol.* **2019**, *14*, 882–892.
- [18] B. Nabet, F. M. Ferguson, B. K. A. Seong, M. Kuljanin, A. L. Leggett, M. L. Mohardt, A. Robichaud, A. S. Conway, D. L. Buckley, J. D. Mancias, J. E. Bradner, K. Stegmaier, N. S. Gray, *Nat. Commun.* **2020**, *11*, 4687.
- [19] T. Clackson, W. Yang, L. W. Rozamus, M. Hatada, J. F. Amara, C. T. Rollins, L. F. Stevenson, S. R. Magari, S. A. Wood, N. L. Courage, X. Lu, F. Cerasoli, M. Gilman, D. A. Holt, *Proc. Natl. Acad. Sci.* **1998**, *95*, 10437–10442.
- [20] M. Reynders, B. S. Matsuura, M. B routi, D. Simoneschi, A. Marzio, M. Pagano, D. Trauner, *Sci. Adv.* **2020**, *6*, eaay5064.
- [21] V. Zwick, A.-O. Chatzivasileiou, N. Deschamps, M. Roussaki, C. A. Sim es-Pires, A. Nurisso, I. Denis, C. Blanquart, N. Martinet, P.-A. Carrupt, A. Detsi, M. Cuendet, *Bioorg. Med. Chem. Lett.* **2014**, *24*, 5497–5501.
- [22] F. P. J rgensen, M. Bols, *J. Org. Chem.* **2018**, *83*, 6050–6055.

- [23]J. B. Grimm, B. P. English, J. Chen, J. P. Slaughter, Z. Zhang, A. Revyakin, R. Patel, J. J. Macklin, D. Normanno, R. H. Singer, T. Lionnet, L. D. Lavis, *Nat. Methods* **2015**, *12*, 244–250.
- [24]Y. Liu, M. Fares, N. P. Dunham, Z. Gao, K. Miao, X. Jiang, S. S. Bollinger, A. K. Boal, X. Zhang, *Angew. Chem. Int. Ed.* **2017**, *56*, 8672–8676.
- [25]E. S. Fischer, K. Böhm, J. R. Lydeard, H. Yang, M. B. Stadler, S. Cavadini, J. Nagel, F. Serluca, V. Acker, G. M. Lingaraju, R. B. Tichkule, M. Schebesta, W. C. Forrester, M. Schirle, U. Hassiepen, J. Ottl, M. Hild, R. E. J. Beckwith, J. W. Harper, J. L. Jenkins, N. H. Thomä, *Nature* **2014**, *512*, 49–53.
- [26]S. D. Edmondson, B. Yang, C. Fallan, *Bioorg. Med. Chem. Lett.* **2019**, *29*, 1555–1564.
- [27]J. Hunter, S. Rice, R. Lowe, C. M. Pask, S. Warriner, V. Sridharan, *Tetrahedron Lett.* **2017**, *58*, 4400–4402.
- [28]“Investigating Protein–Ligand Interactions with a Mutant FKBP Possessing a Designed Specificity Pocket | Journal of Medicinal Chemistry,” can be found under <https://pubs.acs.org/doi/10.1021/jm9904396>, **n.d.**
- [29]S. Rubner, A. Scharow, S. Schubert, T. Berg, *Angew. Chem. Int. Ed.* **2018**, *57*, 17043–17047.

9 – Controlling the Covalent Reactivity of a Kinase Inhibitor with Light

Martin Reynders^{1,2}, Apirat Chaikuad^{3,4}, Benedict-Tilman Berger^{3,4}, Katharina Bauer⁵, Pierre Koch⁵, Stefan Laufer⁵, Stefan Knapp^{3,4,6} and Dirk Trauner^{1,*}

¹Department of Chemistry, New York University, New York, NY 10003, USA.

²Department of Chemistry, Ludwig Maximilians University of Munich
81377 Munich, Germany.

³Buchmann Institute for Molecular Life Sciences and Institute for Pharmaceutical Chemistry, Johann Wolfgang Goethe-University, 60438 Frankfurt am Main, Germany.

⁴Structural Genomics Consortium Frankfurt, 60438 Frankfurt am Main, Germany.

⁵Department of Pharmaceutical / Medicinal Chemistry, Eberhard-Karls-University Tübingen, 72076 Tübingen, Germany.

⁶German Cancer Network (DKTK), Frankfurt/Mainz site, 60438 Frankfurt am Main, Germany.

Abstract

Covalent kinase inhibitors account for some of the most successful drugs that have recently entered the clinic and many others are in preclinical development. A common strategy is to target cysteines in the vicinity of the ATP binding site using an acrylamide electrophile. To increase the tissue selectivity of kinase inhibitors, it could be advantageous to control the reactivity of these electrophiles with light. Here, we introduce covalent inhibitors of the kinase JNK3 that function as photoswitchable affinity labels (PALs). Our lead compounds contain a diazocine photoswitch, are poor non-covalent inhibitors in the dark, and becomes effective covalent inhibitors after irradiation with visible light. Our proposed mode of action is supported by X-ray structures that explain why these compounds are unreactive in the dark and undergo proximity-based covalent attachment following exposure to light.

Introduction

The development of protein kinase inhibitors is one of the most active areas of medicinal chemistry. Early on, selectivity amongst the more than 500 members of the human kinome was considered a major challenge since the ATP binding site of protein kinases is highly conserved. In recent years, however, a wide range of selective inhibitors have emerged that have put such concerns largely to rest. One strategy that has proven to be particularly successful is the covalent engagement of native cysteines that are present in the vicinity of the ATP binding site with suitable electrophiles. Several covalent kinase inhibitors that target the “cysteinome”, such as afatinib, ibrutinib, osimertinib, and neratinib, are now clinically approved (Figure 9.1A).^[1] Most of them feature an acrylamide “warhead” that is poorly reactive towards water and other weak nucleophiles but undergoes rapid bioconjugation following non-covalent binding and placement into the trajectory of a suitable cysteinate anion.^[2,3]

To target covalent inhibitors to kinases expressed in specific cells and tissues, one could take advantage of the temporal and spatial precision that light affords. This could be done, for instance, with a caging group that masks the part of the molecule that binds noncovalently (Figure 9.1B).^[4,5] Alternatively, the covalent reactivity could be concealed with a photoreactive group that delivers a suitable electrophile upon irradiation. Although caging groups for electrophiles, such as α -haloketones,^[6] have been reported, they have not been applied, to the best of our knowledge, to covalent kinase inhibitors. A third alternative for the design of light activatable covalent inhibitors is shown in Figure 9.1C. It involves a photoswitch that keeps the electrophile away from the nucleophile in the dark form but allows for proximity-based rate enhancement and efficient bioconjugation after photoisomerization. Photoswitchable tethered ligands (PTLs) and photoswitchable affinity labels (PALs) have been reported for the optical control of a wide variety of enzymes and receptors that feature engineered cysteines or native electrophiles, respectively.^[7]

Non-covalently binding photoswitchable kinase inhibitors have been explored, but their development has proven to be challenging.^[4,8–13] This prompted us to focus on covalent inhibitors, which have advantages in terms of residency time and selectivity. Amongst these, compounds that target the cysteinome have proven to be most effective, due to the nucleophilicity of this residue and its occurrence close to the ATP binding site in a variety of important kinases.^[3]

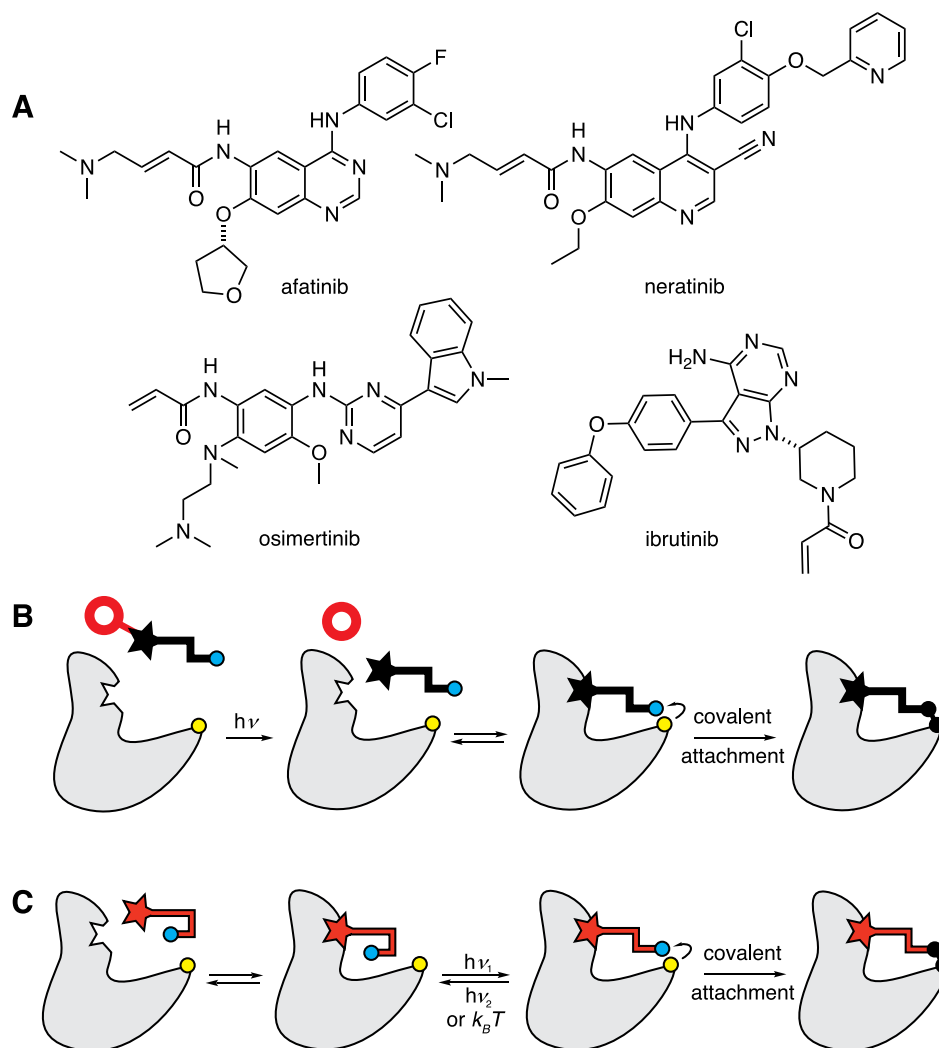


Figure 9.1. A) Representative FDA-approved covalent kinase inhibitors binding irreversibly to specific cysteine residues. B) Photoactivation through caging. C) Photoactivation through photoswitching.

We report here the development of covalent inhibitors for the MAP kinase JNK3 that function as PALs targeting a native cysteine close to the ATP binding site (Cys154). Our lead compound contains a diazocine photoswitch, is a comparatively weak noncovalent inhibitor in the dark, and becomes an effective covalent inhibitor of JNK3 upon irradiation with 400 nm light.

The MAP kinase c-Jun N-terminal kinase 3, abbreviated as JNK3, is mainly expressed in the central nervous system, testes, and pancreatic β -cells, in contrast to its ubiquitously expressed isoforms JNK1 and JNK2.^[14] JNK1-3 are key signaling enzymes in the cellular stress response and JNK3 has been targeted for the treatment of neurodegenerative diseases, including Alzheimer's, Huntington's and Parkinson's disease, and type 2 diabetes.^[14,15]

The development of reversible and selective JNK inhibitors that bind non-covalently has proved to be difficult.^[16] However, JNK3 features Cys154 in the vicinity of the ATP binding site that has been exploited for the covalent attachment of inhibitors with improved kinome selectivity.^[17,18] So far, no JNK inhibitor has progressed to clinical testing. Pharmacological intervention is further complicated by the nature of JNK signaling, where the time course of either kinase activity or inhibition is crucial in controlling the cellular outcome, which can range from cell survival to apoptosis.^[19,20,15] Given the importance of spatiotemporal control of the JNK pathway,^[21,22] implementation of light-sensitivity into our JNK inhibitors represents a compelling strategy to further improve their utility.

Results

Our photoswitchable inhibitors are based on the known ligand **1**, which combines a pyridinylimidazole hinge-binding motif with a diarylamide spacer that connects to a cysteine-reactive acrylamide (Figure 9.2A). It is important to preserve the pyridinylimidazole moiety binding the ATP-pocket, since incorporation of a photoswitch into this crucial motif would negatively influence potency and selectivity of our inhibitor.^[23] Therefore, we replaced the central diarylamide of **1**, which does not engage in hydrogen bonding, as shown by a recent structure, with an isosteric azobenzene.^[17] This afforded the photoswitchable JNK inhibitor **2**, which was designed to be reactive in the dark adapted *trans* state and remain a non-covalent inhibitor when irradiated to preferentially adopt the *cis* form. To ensure that the photoswitchable inhibitor would be unreactive in the dark and would become active only after irradiation, we next implemented a sign-inversion approach,^[24] replacing the azobenzene moiety with a diazocine photoswitch. Diazocines are known to be more stable in the bent *cis* form and isomerize to the thermodynamically less stable elongated *trans* form upon isomerization with violet-blue light.^[25] This strategy led to the light-activated JNK3 inhibitor **3**, which is shown both in its *cis* form and its *trans* form in Figure 9.2A. Molecular docking confirmed that both isomers should be able to bind to the ATP-pocket of JNK3 but only the metastable *trans* form would be able to reach and covalently bind to Cys154. In addition to this, we designed a version with an (*E*)-dimethylaminocrotyl amide electrophile, which is known to improve solubility and reactivity, yielding inhibitor **4**. The half-life, absorption spectra and photostationary state (PSS) are strongly dependent on azobenzene substituents, which are in part

dictated by the requisite pharmacophore and the appended electrophile. Therefore, we also explored a version with a meta-meta substitution pattern in the diazocine, i.e. compound **5**. Finally, we designed a control compound **6**, which bears a propionamide and is therefore not cysteine-reactive.

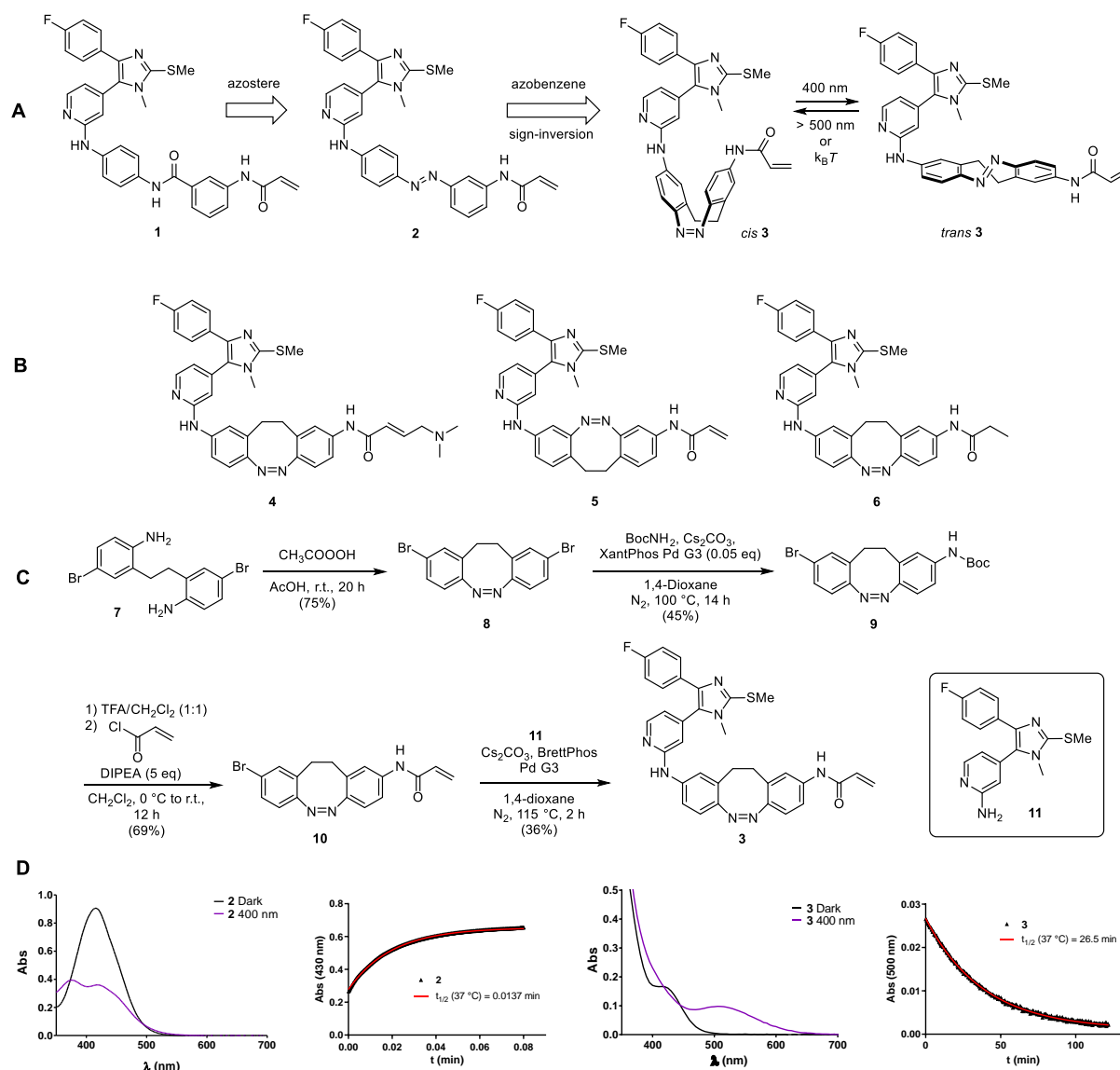


Figure 9.2. Design and synthesis of the covalent photoswitchable inhibitors. A) Azologization of the known covalent inhibitor **1** and sign inversion to yield diazocine **3**. B) Additional photoswitchable JNK3 inhibitors prepared. C) Synthesis of diazocine **3**. D) Absorption spectra of inhibitors **2** and **3** in the dark or after 400 nm irradiation for 3 minutes in DMSO and thermal characterization of **2** and **3** in a 1:1 mixture of DMSO and PBS (pH 7.4).

The representative synthesis of inhibitor **3** is shown in Figure 9.1C. It started with ethylene dianiline **7**, which underwent oxidative cyclization to afford diazocine **8**.^[26] Slow addition of the oxidant favors the desired intramolecular Baeyer-Mills reaction

and avoids overoxidation (see Supporting Scheme 1).^[26] Desymmetrization through Buchwald coupling with *tert*-butyl carbamate yielded **9**, which underwent deprotection and acylation to afford acrylamide **10**. Another Buchwald coupling with the known pyridinylimidazole ligand **11**^[18,23] yielded the desired photoswitchable inhibitor **3**. Covalent inhibitors **4** and **5**, as well as the propionamide control compound **6** were prepared in a similar fashion (see Supporting Information).

With compound **2-6** in hand, we turned to their photophysical characterization (Figure 9.2D, S9.1). In keeping with the general photophysical behavior of substituted diazocines, the absorption bands are not well separated and in particular, amino substituted diazocines show only partial *cis*-to-*trans* isomerization at the 400 nm PSS.^[26] However, this is not a functional flaw for a PAL since the PSS is a dynamic equilibrium and continued pulse irradiation will therefore enrich the covalently bound inhibitor over time. The meta-meta-substituted diazocine **5** showed lower extinction coefficients than the corresponding para-para substituted diazocines **3** and **4** (Figure S9.1).

Relaxation to the thermodynamically favored *cis* state could be achieved via irradiation with longer wavelengths (500- 600 nm) or thermally. The latter occurs on a timescale of minutes to hours in DMSO or mixtures of DMSO and PBS (Figure 9.2D, S9.1). In aqueous environments, amino substituted azobenzenes such as **2** relax within seconds whereas the corresponding diazocines are substantially more stable in their *trans* states.^[24,27]

Following their photophysical characterization, the inhibitors were tested for their ability to inhibit JNK3 *in vitro* (Figure 9.3, Supporting Table 1). This was determined through measuring the phosphorylation of the immobilized kinase substrate ATF-2 at different inhibitor concentrations after incubation for 50 minutes. Kinase activity was determined with an ELISA assay, following a previously published method.^[28] Photoswitches were either pulse-irradiated every 5 s for 100 ms or kept in the dark during the 50 min reaction time. As expected, the parent inhibitor **1** did not respond to 400 nm irradiation. No light-dependency was observed for its azostere **2**, which had reduced potency compared to **1**. The lack of response to irradiation was in line with the fast relaxation of a red-shifted *p*-amino substituted azobenzene and the reactivity of the acrylamide in the thermodynamically stable *trans* form of the azobenzene.

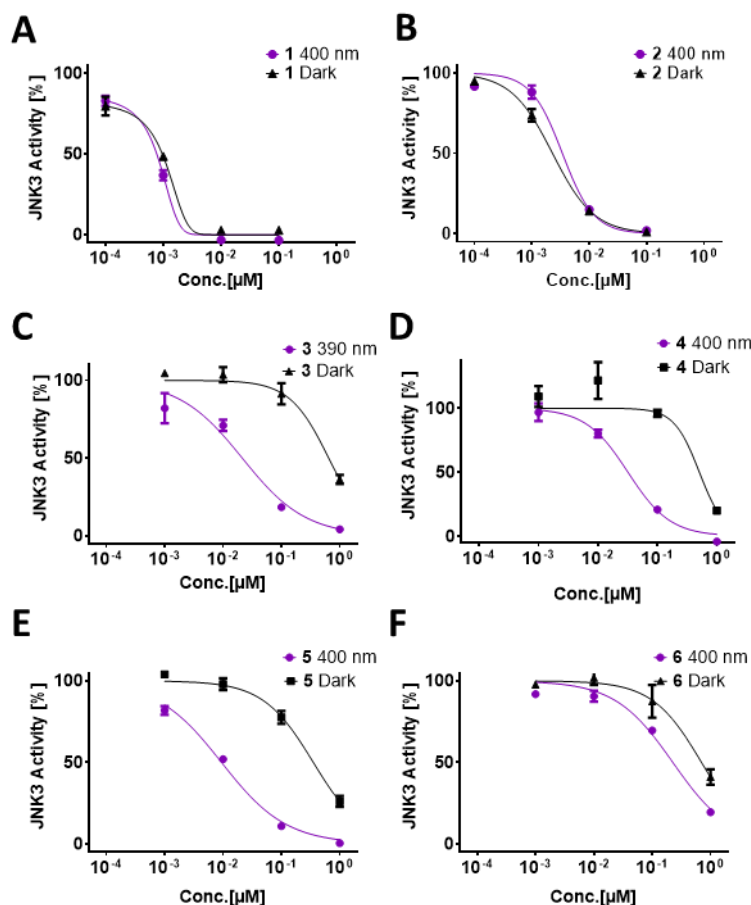


Figure 9.3. *In vitro* characterization. Quantitative ELISA assay of differential ATF-2 phosphorylation by JNK3 for 50 min at 37 C in the dark or with pulsed irradiation (100 ms every 5 s) and inhibitors: A) 1 B) 2 C) 3 D) 4 E) 5 F) 6.

Photoswitchable inhibitor **3**, which incorporates a para, para-substituted diazocine, was a weak inhibitor of JNK3 in the dark ($IC_{50} = 646$ nM) but showed much stronger inhibition at all tested concentrations after pulse-irradiation with 390 nm light ($IC_{50} = 21.4$ nM). Compound **4**, which bears a dimethylaminocrotyl amide as electrophilic warhead, showed improved solubility but showed JNK3 inhibition with similar potency in the dark ($IC_{50} = 507$ nM) and after irradiation ($IC_{50} = 31.9$ nM). The meta, meta-substitution pattern on the diazocine in **5** gave similar results compared to **3**, with a pronounced increase in JNK3 inhibition upon isomerization to its more potent *trans* form after 400 nm irradiation. Interestingly, once isomerization and potential covalent attachment took place, inhibition by compounds **3** and **5** was found to be irreversible. Use of an inactivating 565 nm pulse after the activating light pulse did not restore kinase activity (Figure S9.2).

Thus, it appears that binding to the ATP binding site was too tight to pull the pyridinylimidazole from the active site. Indeed, non-covalent inhibitors that contained this motif did bind to JNK3 and p38 α in the low nanomolar concentration range.^[23] Alternatively, covalent attachment of the inhibitor could inhibit kinase function even if the ligand does not occupy the ATP-pocket. The non-covalent, propionamide control compound **6** only showed a small increase in JNK3 inhibitory activity upon 400 nm irradiation. This small activity difference was probably due to an increased steric clash of the *cis* isomer with the glycine-rich loop which was in agreement with a non-covalent mechanism of inhibition where isomerization only changes positioning of the propionamide.

We demonstrated cellular target engagement of the inhibitors using the NanoBRET tracer displacement assay^[29] and determined the IC₅₀s to be in the high nanomolar to low micromolar range (Figure S9.3). The observed improvement in potency after 400 nm irradiation was not as prominent as in the *in vitro* assay. However, the potent cellular activity of the inhibitors harboring the diazocine moiety demonstrated target engagement, suggesting that these inhibitors represent lead structures for further development, including *in vivo* studies.

To confirm covalent labelling, we performed mass spectrometry of JNK3 and inhibitor **4** incubated under pulsed 400 nm irradiation (Figure S9.4). A mass shift corresponding to the molecular weight of **4** was observed, demonstrating covalent adduct formation in a 1:1 ratio.

To gain further insight into the mode of action of our compounds, we carried out structural studies using X-ray crystallography. To this end, we soaked crystals of JNK3 with inhibitor **4**, which showed improved solubility, whilst pulse-irradiating with 400 nm light. We collected several datasets after different irradiation schedules and observed clear electron density that supported a non-covalent as well as covalent binding mode of **4** (Figure 9.4A, B and C).

Both isomers have the ATP-mimetic pyridinylimidazole moiety in the same position which was interacting with the hinge region, the adenine pocket, and the hydrophobic pocket in a similar manner to the same moiety of the starting compound **1** (Figure 9.4A). However, the electrophilic warhead reached Cys154 only in the elongated *trans* isomer but not in the bent *cis* form present in the dark (Figure 9.4 and Supporting Figure S9.5). This enabled covalent adduct formation, which was not feasible with the *cis* isomer. As such, inhibitor **4** operated in the manner indicated in Figure 9.1C.

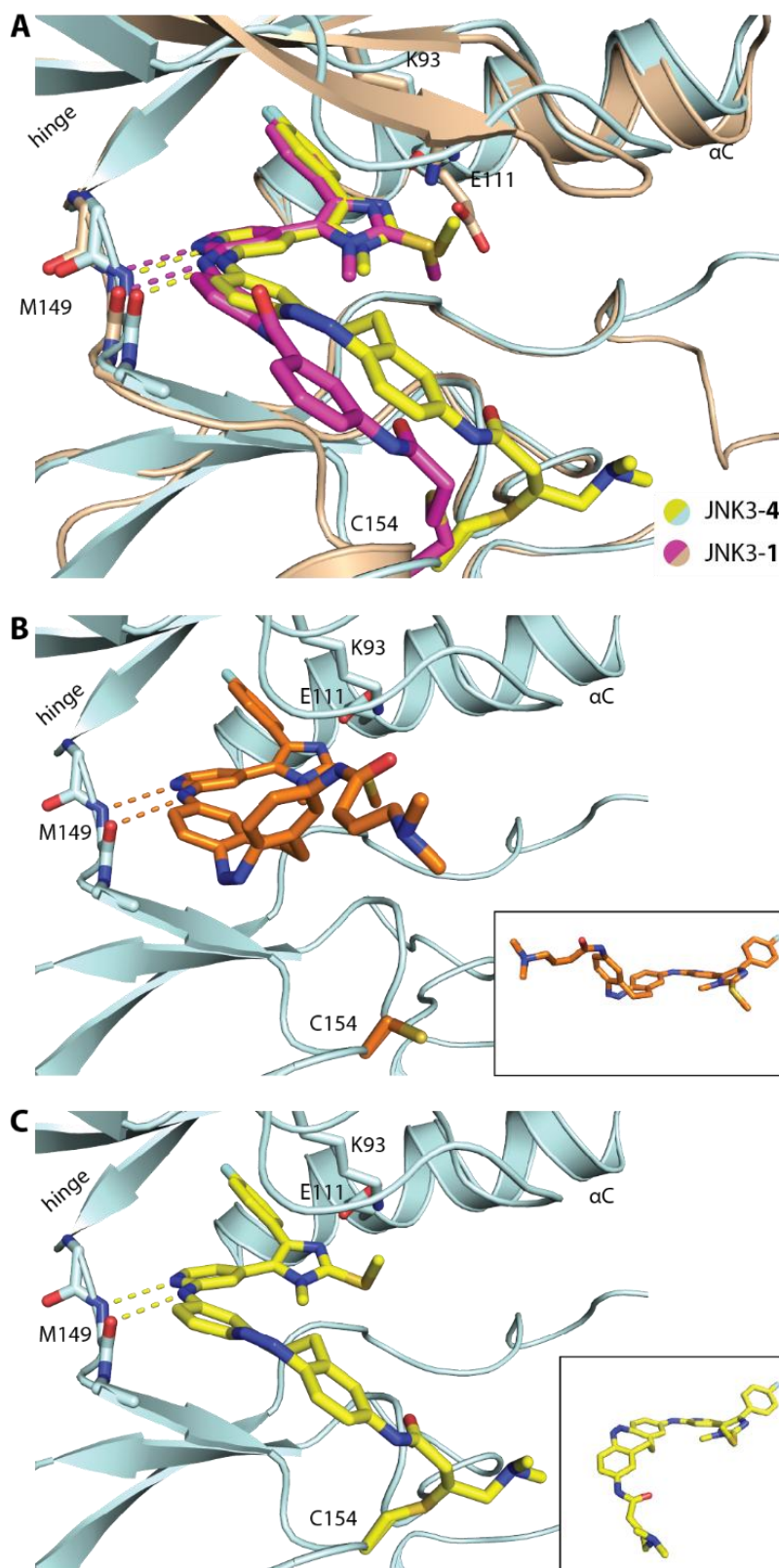


Figure 9.4. X-ray analysis of **4** bound to JNK3. A) Structural overlay of **1** and **4** covalently bound to JNK3. B) The bent cis isomer cannot reach Cys154 and only binds non-covalently. C) The extended isomer binds covalently to Cys154. The crystal structures have been deposited to the wwPDB with accession codes 7ORE and 7ORF.

Summary

In summary, we developed covalent kinase inhibitors that can be activated by irradiation and function as photoactivated affinity labels. Notably, our approach has advantages over caged inhibitors, since it largely retains the properties of the parent drug, whereas a caging group adds significant molecular weight and can negatively impact cellular uptake and distribution. Additionally, the uncaging reaction generates byproducts, whereas our inhibitors just undergo a reversible isomerization. While we were unable to show reversibility on target, an unbound inhibitor can still revert to its inactive form, whereas an uncaged inhibitor will always remain active.

Our most successful inhibitor incorporates a new class of photoswitch, viz. diazocines, a moiety that is increasingly used to convert compounds that are constitutively inactive in the dark into light-activated ones. X-ray crystallography provides further insight into the mode of action of a photoswitchable inhibitor bound to its target.^[30,31] Our strategy could be easily transferred to other kinase targets that harbor a cysteine in positions close to the ATP binding site once suitable inhibitors and linkers have been developed and may therefore serve as a prototype for future photoswitchable covalent kinase inhibitors.

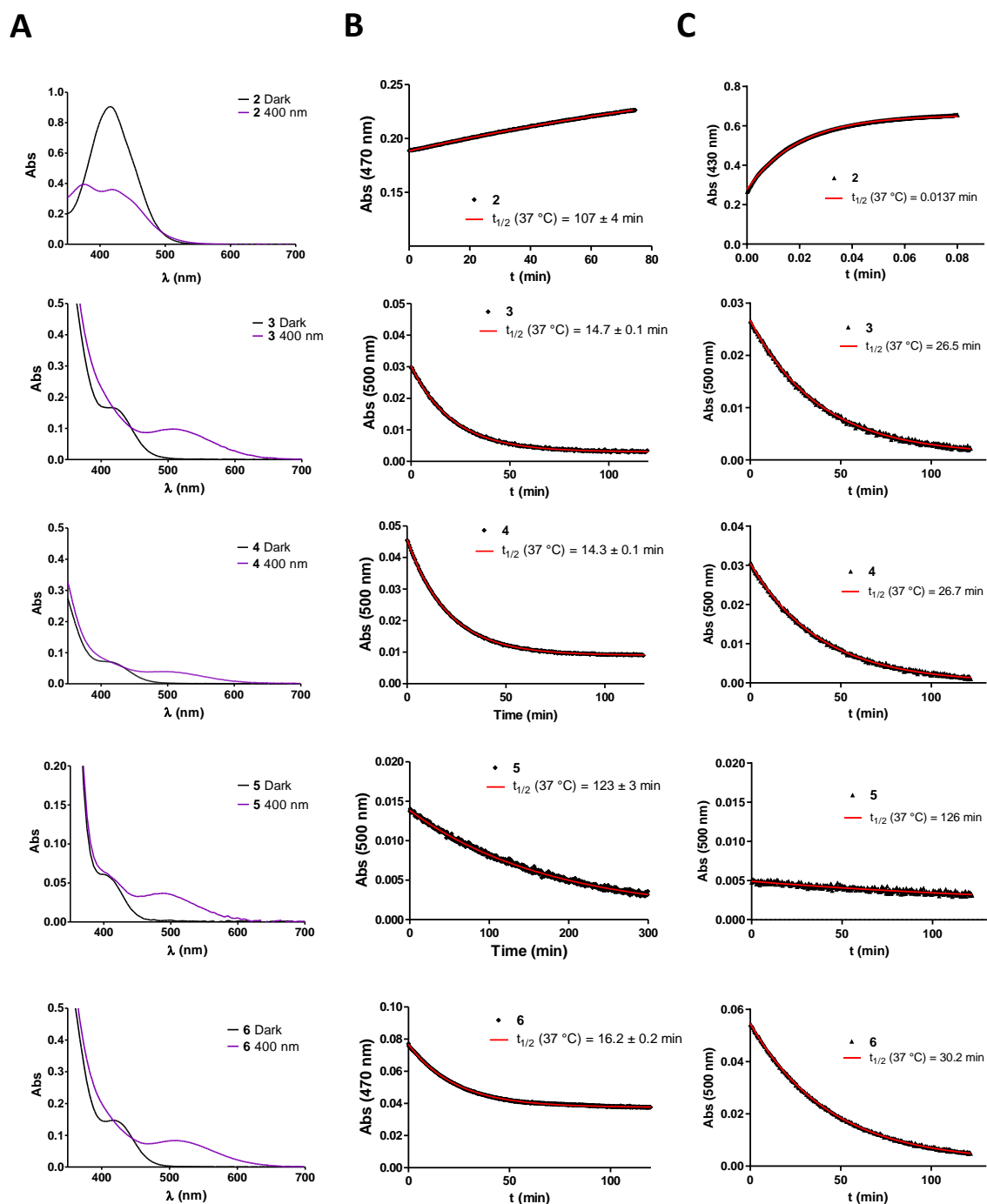
Acknowledgements

M.R. and D.T. thank the German Research Foundation (DFG) for financial support (SFB749). Nuclear magnetic resonance spectra were acquired using the TCI cryoprobe supported by the NIH (OD016343). We thank Silke Bauer and Jens Strobach for assistance in the *in vitro* assays. SK, AC and B-TB are grateful for support by the German cancer network DKTK as well as the SGC, a charity a registered charity (number 1097737) that receives funds from AbbVie, Bayer Pharma AG, Boehringer Ingelheim, Canada Foundation for Innovation, Eshelman Institute for Innovation, Genome Canada, Innovative Medicines Initiative (EU/EFPIA), Janssen, Merck KGaA Darmstadt Germany, MSD, Novartis Pharma AG, Ontario Ministry of Economic Development and Innovation, Pfizer, São Paulo Research Foundation-FAPESP, Takeda, and Wellcome. The authors thank staffs at BESSY and Diamond synchrotron for their assistance during data collection.

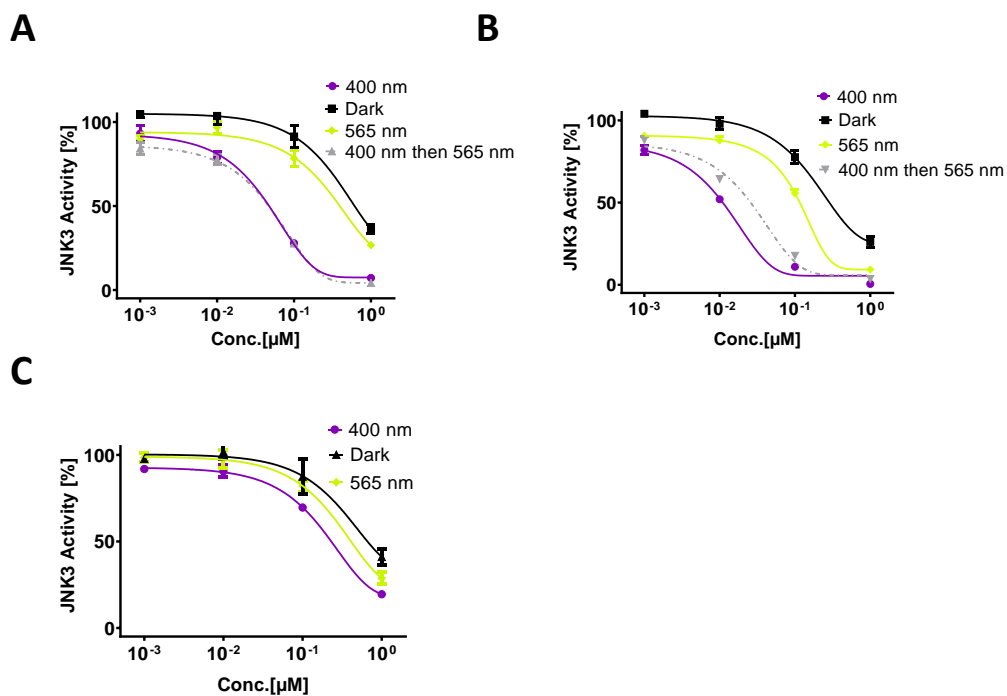
Author Contributions

S.L. and D.T. conceived the study. M.R. designed, synthesized, and characterized compounds. K.B. and M.R. performed in vitro assays. A.C. collected and analyzed X-ray data. B.-T.B. performed NanoBRET assays. S.K., P.K., S.L. and D.T. supervised experiments. M.R. and D.T. wrote the manuscript with contributions of all authors.

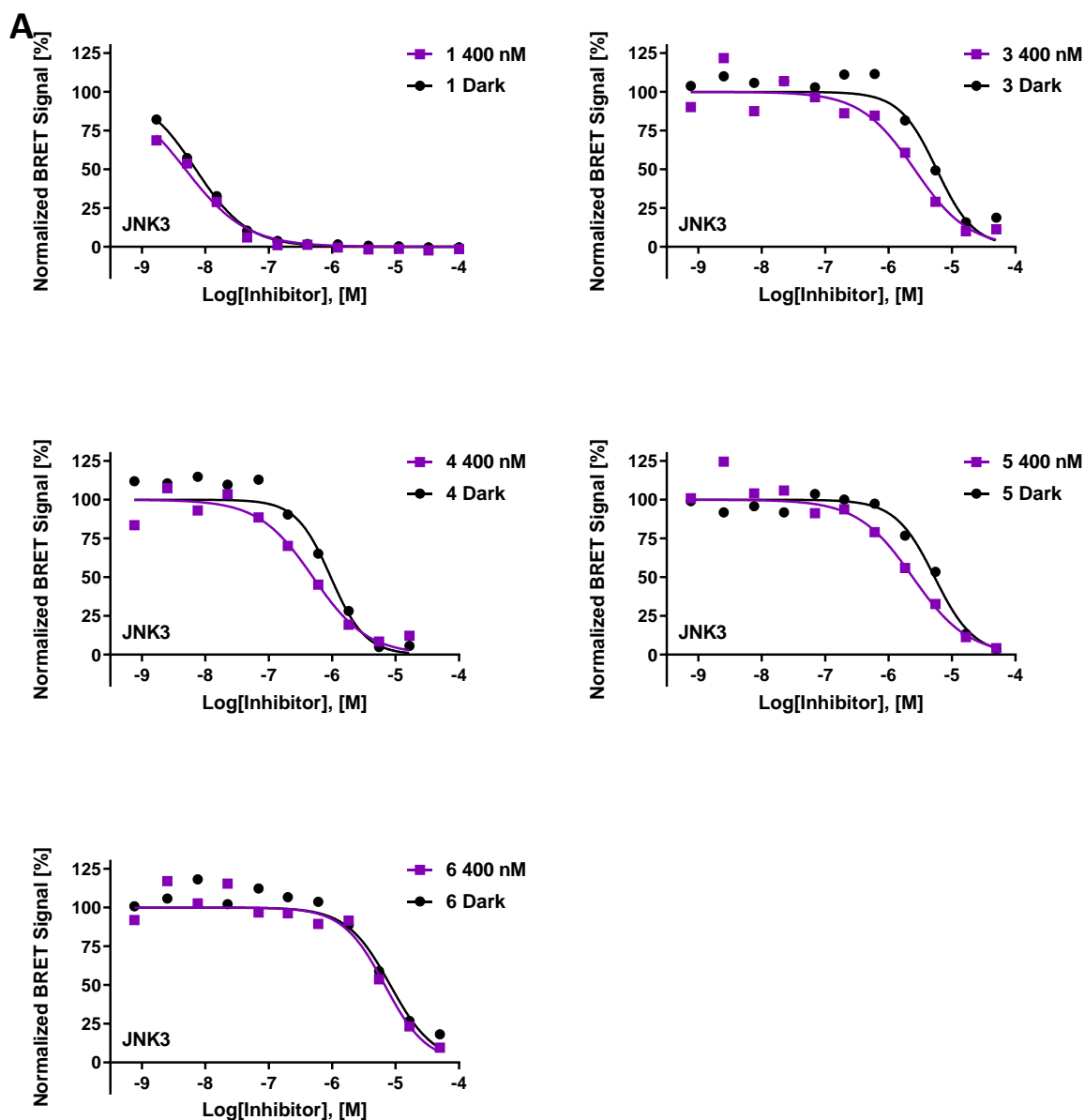
Supplementary Figures



Supporting Figure S9.1. Photophysical properties. **A)** Absorption spectra of the photoswitchable inhibitors in DMSO, in the dark or after 400 nm irradiation for 3 minutes. **B)** Thermal relaxation of **2**, **3**, **4**, **5** and **6** in DMSO. **C)** Thermal relaxation of **2**, **3**, **4**, **5** and **6** in a 1:1 (vol%) mixture of DMSO and PBS (pH 7.4).



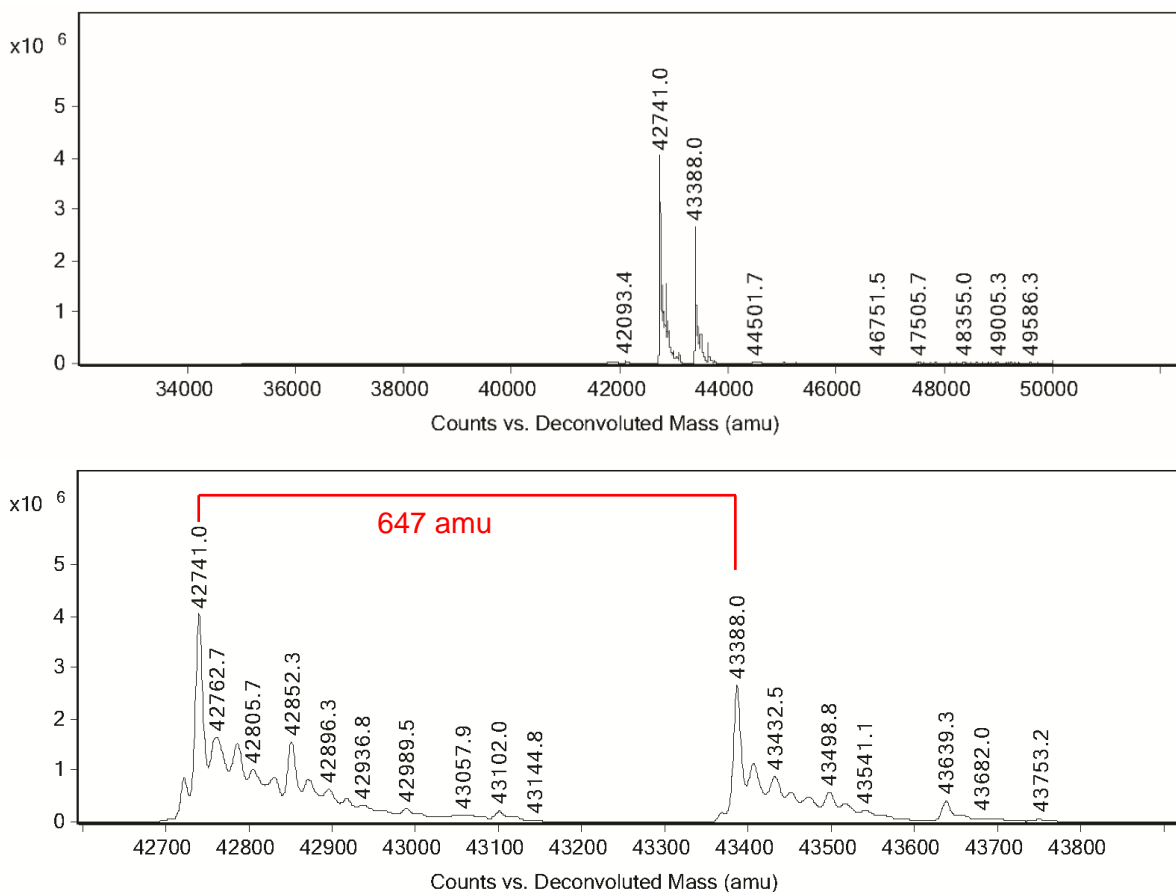
Supporting Figure S9.2. Reversibility. Quantitative ELISA assay of differential ATF-2 phosphorylation by JNK3 for 50 min at 37 °C in the dark or using pulsed irradiation with 390/400 nm, 565 nm (100 ms every 5 s) or 400 nm (100 ms every 10 s) directly followed by a 565 nm pulse (400 ms every 10 s) and inhibitors: A) **3** B) **5** C) **6**.



B

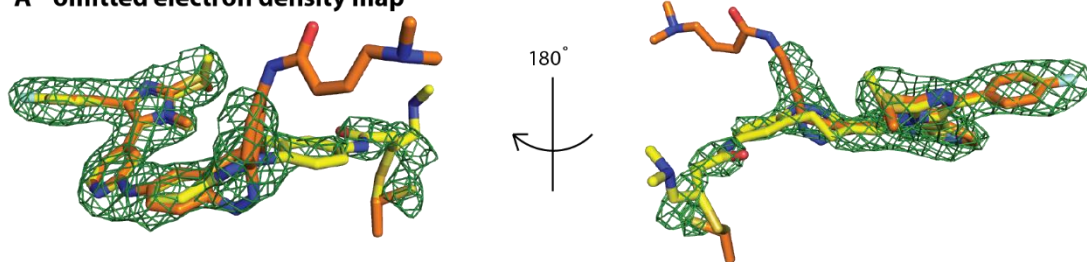
Inhibitor	Dark		400 nm	
	Average	SEM	Average	SEM
1	7,12E-09	2,32E-10	1,07E-08	2,90E-09
3	5,83E-06	8,26E-08	2,46E-06	5,45E-08
4	9,51E-07	n=1	4,98E-07	n=1
5	9,06E-06	1,19E-06	2,45E-06	3,40E-08
6	1,28E-05	1,61E-06	1,51E-05	2,89E-06

Supporting Figure S9.3. *In cellulo* NanoBRET tracer displacement assay for JNK3. A) JNK3 tracer displacement in the dark or with pulsed 400 nm irradiation (100 ms every 10 s). Error bars are smaller than the symbol size and not shown. B) IC₅₀ values of the JNK inhibitors.

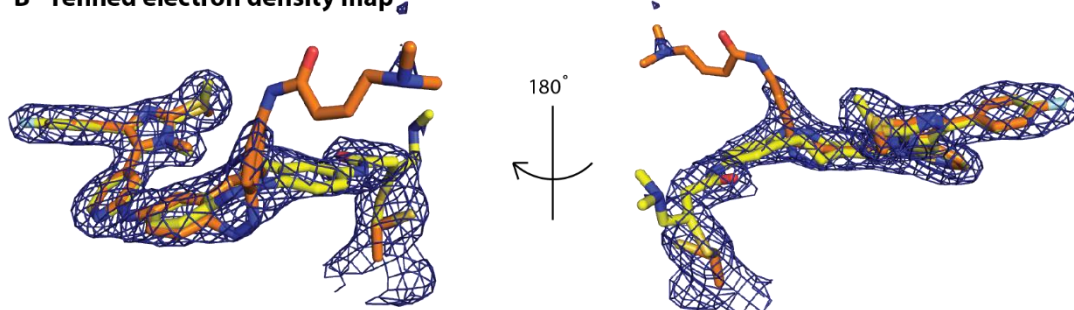


Supporting Figure S9.4. Mass spectrometry of covalent adduct formation between JNK3 and inhibitor **4** (647 g/mol) at 3-fold excess, after 2 h of incubation under pulsed 400 nm irradiation.

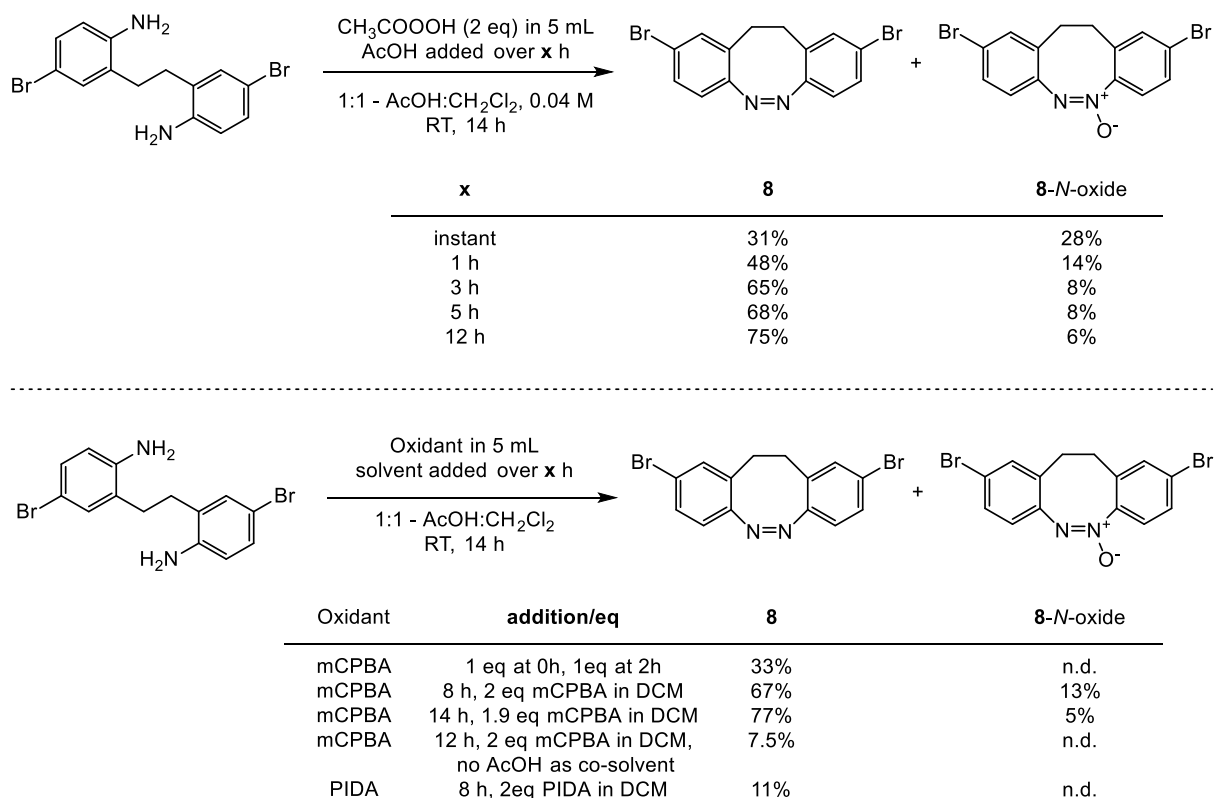
A omitted electron density map



B refined electron density map



Supporting Figure S9.5. Electron density map for **4**. A) $|F_o|-|F_c|$ omitted map contoured at 3σ . B) $|2F_o|-|F_c|$ refined map contoured at 1σ .



Supporting Scheme 1. Initial screen and optimization of the oxidative cyclization.

	IC ₅₀ (Irradiation) nM	IC ₅₀ (Dark) nM	fold change
1	0.772	0.9627	1.25
2	3.41	2.3	0.67
3	21.4	646	30.3
4	31.9	507	15.9
5	9.43	352	37.4
6	226	700	3.10

Supporting Table T1. IC₅₀ values of 1-6 in the *in vitro* ATF-2 phosphorylation assay corresponding to Figure 9.3.

Supporting Information

JNK3 inhibition *in vitro*

Inhibition of JNK3 *in vitro* was determined by measuring the phosphorylation of the immobilized kinase substrate ATF-2 at different inhibitor concentrations in triplicates after incubation for 50 minutes. Kinase activity was determined with an ELISA assay, following the previously published method.^[1] Photoswitches were serially diluted under reduced light conditions and applied to the 96-well plate containing ATF-2. After addition of all assay components, the plates were either pulse-irradiated every 5 s for 100 ms or kept in the dark during the 50 min kinase reaction time using a cell DISCO^[2]. Normalized data was plotted GraphPad Prism 9 software using the “[Inhibitor] vs. normalized response -- Variable slope” fit with the following equation $Y=100/(1+(IC50/X)^{HillSlope})$. Data is presented as mean \pm SD. Error bars smaller than the symbol size are not shown.

Crystal structure determination of Inhibitor bound JNK3

The kinase domain of JNK3 (aa 39-402) was recombinantly co-expressed with lambda phosphatase in *E. coli* Rosetta. The histidine-tagged protein was purified by Ni²⁺-affinity chromatography. The tag was removed using TEV protease, and the cleaved protein was further purified by size exclusion chromatography. The protein in 50mM HEPES, pH 7.5, 100mM NaCl and 0.5mM TCEP at 12 mg/ml was mixed with AMP-PCP and MgCl₂, and the complexed was crystallized using sitting drop vapor diffusion method at 4 °C and the condition containing either i) 34% PEG400 and 0.1 M MES, pH 6.0 (crystals used for **1**) or ii) 16% medium-molecular weight PEG smears^[3] and 0.1 M HEPES, pH 7.8 (crystals used for **4**). Soaking was performed with 10 mM compounds, and for **4** during soaking the crystals were pulse-irradiated with 400 nm light (100 ms every 10 s) for 2.5 days. The crystals were cryo-protected using ethylene glycol, and the diffraction data were collected at BESSY beamline 14.2 or Diamond beamline i04. Data were processed using iMosflm^[4] or XDS^[5], and subsequently scaled with aimless.^[6] Molecular replacement was performed using Phaser^[7] and the published JNK3 coordinates (PDB ID: 4x21).^[8] Model rebuilding alternated with refinement was performed in COOT^[9] and Refmac,^[10] respectively. Data collection and refinement statistics are summarized in Supporting Table T2. The crystal structures have been deposited to the wwPDB with accession codes 7ORE and 7ORF.

Complex	JNK3-1	JNK3-4
PDB accession code	7ORF	7ORE
Data Collection		
Resolution ^a (Å)	30.11-1.70 (1.79-1.70)	29.65-2.18 (2.30-2.18)
Spacegroup	<i>P2₁2₁2</i>	<i>P2₁2₁2</i>
Cell dimensions	<i>a</i> = 58.9, <i>b</i> = 71.2, <i>c</i> = 108.1 Å	<i>a</i> = 52.9, <i>b</i> = 71.1, <i>c</i> = 107.5 Å
	$\alpha, \beta, \gamma = 90.0^\circ$	$\alpha, \beta, \gamma = 90.0^\circ$
No. unique reflections ^a	47,324 (6,810)	21,811 (3,134)
Completeness ^a (%)	99.0 (100.0)	99.9 (99.9)
<i>I</i> / σ ^a	12.0 (2.0)	10.6 (2.1)
<i>R</i> _{merge} ^a	0.097 (0.817)	0.101 (0.903)
CC (1/2)	0.998 (0.669)	0.997 (0.876)
Redundancy ^a	6.5 (6.1)	7.1 (7.1)
Refinement		
No. atoms in refinement (P/L/O) ^b	2,871/ 42/ 439	2,843/ 141/ 92
B factor (P/L/O) ^b (Å ²)	24/ 19/ 36	54/ 49/ 55
<i>R</i> _{fact} (%)	16.7	21.6
<i>R</i> _{free} (%)	20.5	27.6
rms deviation bond ^c (Å)	0.016	0.007
rms deviation angle ^c (°)	1.6	1.3

^a Values in brackets show the statistics for the highest resolution shells.

^b P/L/O indicate protein, ligand molecules presented in the active sites, and other (water and solvent molecules), respectively.

^c rms indicates root-mean-square.

Supporting Table T2. Data collection and refinement statistics.

JNK3 inhibition *in cellulo*

Inhibition The assay was performed as described previously.^[29,32,33] In brief: Full-length JNK3 ORF (Promega, NV1481) cloned in frame with a C-terminal NanoLuc-fusion were transfected into HEK293T cells using FuGENE HD (Promega, E2312) and proteins were allowed to express for 20h. Serially diluted inhibitor and NanoBRET Kinase Tracer K5 (Promega, N2500) at 300 nM were pipetted into white 96-well plates (Corning 3600) using an Echo acoustic dispenser (Labcyte). The corresponding JNK3-transfected cells were added and reseeded at a density of 2×10^5 cells/mL after trypsinization and resuspending in Opti-MEM without phenol red (Life Technologies). The system was allowed to equilibrate for 2 hours at 37°C/5% CO₂ prior to BRET measurements either in the dark or while pulsed-irradiating at 400 nm (100 ms every 10 s) using a 24-LED cell DISCO^[34]. To measure BRET, NanoBRET NanoGlo Substrate + Extracellular NanoLuc Inhibitor (Promega, N2161) was added as per the manufacturer's protocol, and filtered luminescence was measured on a PHERAstar FSX plate reader (BMG Labtech) equipped with 450 nm BP filter (donor) and 610 nm LP filter (acceptor). Competitive displacement data were then graphed using GraphPad Prism 8 software using a normalized 4-parameter curve fit with the following equation: $Y=100/(1+10^{((\text{LogIC50}-X)*\text{HillSlope}))})$.

Note that irradiation at 400 nm caused partial bleaching of the tracer molecule and that the photoswitch could also interfere with the resonance energy transfer.

JNK3 mass spectrometry

The kinase domain of JNK3 (0.3 mM) was mixed with photoswitchable inhibitor **4** (0.9 mM, 3-fold excess), and the mixture was pulse-irradiated (every 5 s for 100 ms) for 2 h. Mass spectrometry was performed on an Agilent 6230 TOF LC/MS.

Determination of Photophysical properties

UVVis spectra were recorded on a Varian Cary 60 UV-Visible Spectrophotometer using disposable BRAND UV-Cuvette Disposable Spectrophotometer/Photometer Ultra-Micro Cuvettes, BrandTech (10 mm light path), connected to an Agilent Technologies PCB 1500 Water Peltier system for temperature control and samples were irradiated with different monochromatic wavelengths using a Cairn Research Optoscan Monochromator with Optosource High Intensity Arc Lamp equipped with a 75 W UXL-S50A lamp from USHIO Inc. Japan and set to 15 nm full width at half

maximum. Samples were stored and prepared under red light to avoid formation of the (*Z*)-isomers. 10 mM stock solutions were prepared in the dark and diluted to a final concentration of 25 μ M for measurement. UV-VIS spectra in the dark and following irradiation for 5 min using the monochromator.

Thermal relaxation was measured by preirradiating inhibitors with 400 nm irradiation and observing the absorption at the indicated wavelength at 37 °C in DMSO in tightly sealed cuvettes.

Synthetic and Analytical Methods and Materials

All reagents and solvents used in this study were purchased from the following chemical suppliers: ABCR, Acros Organics, Alfa Aesar, Ark Pharm, Combi-Blocks, Oakwood, OxChem, Sigma-Aldrich, Strem and were used as purchased. Dry solvents used in reactions performed under inert atmosphere were either purchased from Acros organics and stored over mol sieves or obtained by passing the degassed solvents through activated alumina columns.

Chromatographic separation was carried out on silica gel (60 Å pore size, 40–63 μ m, Merck KGaA) using a Teledyne Isco Combiflash EZprep flash purification system. Thin-layer chromatography (TLC) was performed on glass plates precoated with silica gel (0.25 mm, 60-Å pore size, Merck). TLC plates were visualized by exposure to UV light (254 and 366 nm).

NMR spectra were obtained on a Bruker Avance III HD 400 MHz spectrometer equipped with a CryoProbeTM operating at 400 MHz for ¹H and 100 MHz for ¹³C spectra.

Integration results and multiplets are reported as observed and denoted as follows: s (singlet), d (doublet), t (triplet), q (quartet), p (pentet), h (hextet), and m (multiplet) and as combinations thereof.

Purity of final compounds was determined from NMR spectra.

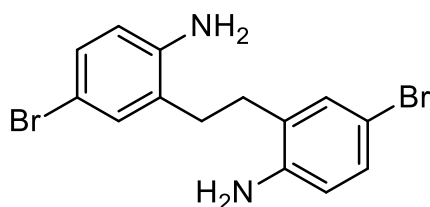
High-resolution mass spectra (HRMS) were acquired using an Agilent Technologies 6224 Accurate-Mass time-of-flight spectrometer with either atmospheric pressure chemical ionization (APCI) or electrospray ionization (ESI) ionization sources.

LCMS was performed on an Agilent Technologies 1260 II Infinity connected to an Agilent Technologies 6120 Quadrupole mass spectrometer with ESI ionization source. Elution was performed using a gradient from 5:95% to 100:0% MeCN:H₂O with 0.1%

formic acid over 5 min, if not indicated otherwise. Separated isomer spectra of azobenzenes were obtained by irradiation of the LCMS sample prior to injection.

Synthetic Procedures

2,2'-(ethane-1,2-diyl)bis(4-bromoaniline) (**7**)



2,2'-Ethylenedianiline (4.25 g, 20.0 mmol) was dissolved in MeCN (50 mL) and *N*-Bromosuccinimide (7.12 g, 40.0 mmol, 2.0 eq.) in MeCN (100 mL) was added dropwise over 7 h at room temperature. The reaction was concentrated under reduced pressure and the resulting residue was redissolved in EtOAc (50 mL) and washed with aqueous NaOH solution (1 M, 3 x 30 mL), saturated aqueous NaHCO₃ solution (30 mL) and brine (50 mL). The organic phase was dried over Na₂SO₄ and concentrated under reduced pressure. Purification of the resulting crude product by flash column chromatography (Hx/EA gradient, 0→100% EA) gave **7** (6.39 g, 17.3 mmol, 86%) as a light brown solid.

$R_f = 0.38$ [Hx:EA, 1:1].

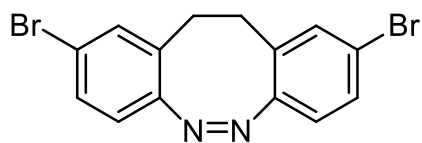
¹H NMR (400 MHz, DMSO-d₆): $\delta = 7.14$ (d, $J = 2.4$ Hz, 2H), 6.99 (dd, $J = 8.5, 2.4$ Hz, 2H), 6.55 (d, $J = 8.5$ Hz, 2H), 5.07 (s, 4H), 2.58 (s, *br*, 4H) ppm.

¹³C NMR (100 MHz, DMSO-d₆): $\delta = 146.1, 131.5, 129.4, 127.9, 116.7, 107.2, 29.5$ ppm.

HRMS (ESI): calcd. for C₁₄H₁₅Br₂N₂⁺: 368.9602 m/z [M+H]⁺

found: 368.9606 m/z [M+H]⁺.

LCMS (ESI): $t_{ret} = 3.31$ min. 369, 371 m/z [M+H]⁺.

2,9-dibromo-11,12-dihydrodibenzo[c,g][1,2]diazocine (8)

7 (740 mg, 2 mmol) was dissolved in a mixture of CH₂Cl₂ (50 mL) and AcOH (50 mL). Peracetic acid (0.68 mL, 4 mmol, 39%wt in AcOH) was diluted in 10 mL AcOH and added dropwise over 12 h at room temperature in the dark using a syringe pump. The reaction was stirred for additional 4 h and the volatiles were removed in vacuo. The residue was taken up in CH₂Cl₂ (60 mL) and extracted with 30 mL of 0.5 M NaOH. The organic phase was washed with saturated aqueous NaHCO₃ solution (30 mL) and brine (50 mL). The organic phase was dried over Na₂SO₄ and concentrated under reduced pressure. Purification of the resulting crude product by flash column chromatography (Hx/EA gradient, 0→10% EA) gave **8** (549 mg, 1.5 mmol, 75%) as a yellow solid.

$R_f = 0.43$ [Hx:EA, 9:1].

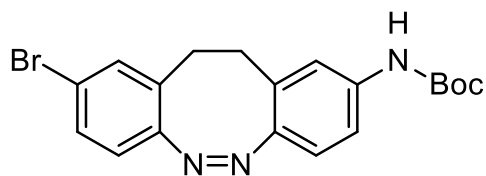
¹H NMR (400 MHz, Chloroform-d): $\delta = 7.28$ (dd, $J = 8.4, 1.9$ Hz, 2H), 7.16 (d, $J = 1.9$ Hz, 2H), 6.72 (d, $J = 8.4$ Hz, 2H), 2.98 – 2.65 (m, 4H) ppm.

¹³C NMR (100 MHz, Chloroform-d): $\delta = 154.16, 132.60, 130.16, 129.97, 120.78, 120.74, 31.42$ ppm.

HRMS (APCI): calcd. for C₁₄H₁₁Br₂N₂⁺: 366.92630 m/z [M+H]⁺

found: 366.9264 m/z [M+H]⁺.

LCMS (ESI): $t_{ret} = 5.38$ min. 365, 367 m/z [M+H]⁺.

tert-butyl-(9-bromo-11,12-dihydrodibenzo[c,g][1,2]diazocin-2-yl)carbamate (9)

8 (732 mg, 2.00 mmol), tert-butyl carbamate (352 mg, 3.00 mmol), caesium carbonate (978 mg, 2 mmol) and XantPhos Pd G3 (95 mg, 0.1 mmol) were added to a Schlenk tube under nitrogen atmosphere and suspended in degassed 1,4-dioxane (20 mL). The reaction mixture was stirred at 100 °C for 4 h and separated between EtOAc (40 mL) and water. The aqueous phase was extracted with EtOAc (40 mL), and the combined organic extracts were washed with saturated aqueous NaHCO₃ solution (2x25 mL) and brine (50 mL). The organic phase was dried over Na₂SO₄ and concentrated under reduced pressure. Purification of the resulting crude product by flash column chromatography (Hx/EA gradient, 0→100% EA) gave **9** (498 mg, 1.24 mmol, 38%; 49% **8** recovered) as a yellow solid.

$R_f = 0.25$ [Hx:EA, 5:1].

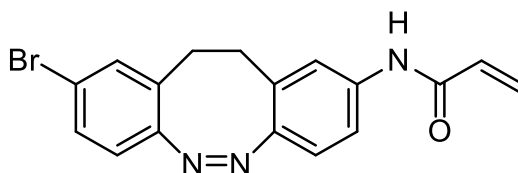
¹H NMR (400 MHz, Chloroform-*d*): $\delta = 7.24$ (dd, $J = 8.5$ Hz, 1.3 Hz, 1H), 7.18 (s, 1H), 7.15 (d, $J = 1.4$ Hz, 1H), 7.04 (dd, $J = 8.5$, 2.1 Hz, 1H), 6.79 (d, $J = 8.5$ Hz, 1H), 6.70 (d, $J = 8.4$ Hz, 1H), 6.42 (s, 1H), 2.82 (s, 4H), 1.48 (s, 9H). ppm.

¹³C NMR (100 MHz, Chloroform-*d*): $\delta = 154.38$, 152.62, 150.72, 137.63, 132.44, 130.64, 129.88, 128.71, 120.83, 120.42, 120.30, 118.97, 116.74, 80.99, 31.97, 31.50, 28.44 ppm.

HRMS (ESI): calcd. for C₁₉H₂₁BrN₃O₂⁺: 402.0812 m/z [M+H]⁺

found: 402.0838 m/z [M+H]⁺.

LCMS (ESI, 25to100): $t_{ret} = 4.07$ min. 402/404 m/z [M+H]⁺.

***N*-(9-bromo-11,12-dihydrodibenzo[*c,g*][1,2]diazocin-2-yl)acrylamide (**10**)**

9 (90.1 mg, 0.224 mmol) was dissolved in a mixture of CH₂Cl₂ (1 mL) and TFA (1 mL) and stirred for 2 h. The volatiles were removed under reduced pressure and the resulting residue was resuspended in CH₂Cl₂ (2 mL) and DIPEA (0.195 mL, 1.12 mmol) was added. After cooling the solution to 0 °C, acryloyl chloride (41 mg, 0.447 mmol, 0.036 mL) was added dropwise and the reaction was allowed to warm up to RT over 14 h. The reaction mixture was diluted with CH₂Cl₂ (20 mL) and washed with saturated aqueous NaHCO₃ solution (20 mL) and brine (20 mL). The organic phase was dried over Na₂SO₄ and concentrated under reduced pressure. Purification of the resulting crude product by flash column chromatography (Hx/EA gradient, 0→100% EA) gave **10** (55 mg, 0.15 mmol, 69%) as a yellow solid.

$R_f = 0.38$ [Hx:EA, 1:1].

¹H NMR (400 MHz, DMSO-*d*₆): $\delta = 7.95$ (s, 1H), 7.43 (s, 1H), 7.31 (dd, $J = 8.5, 2.2$ Hz, 1H), 7.23 (dd, $J = 8.3, 2.0$ Hz, 1H), 7.11 (d, $J = 2.0$ Hz, 1H), 6.79 (d, $J = 8.4$ Hz, 1H), 6.69 (d, $J = 8.4$ Hz, 1H), 6.36 (dd, $J = 16.9, 1.4$ Hz, 1H), 6.22 (dd, $J = 16.8, 10.1$ Hz, 1H), 5.68 (dd, $J = 10.1, 1.4$ Hz, 1H), 2.77 (s, *br*, 4H) ppm.

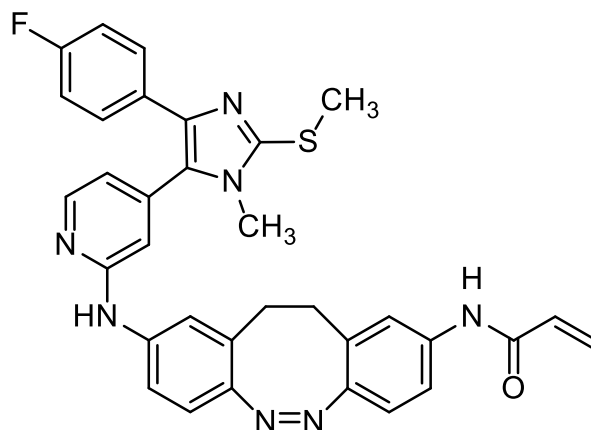
¹³C NMR (100 MHz, DMSO-*d*₆): $\delta = 163.89, 154.19, 151.68, 137.16, 132.44, 130.99, 130.47, 129.88, 128.74, 128.24, 120.74, 120.74, 120.52, 120.01, 118.38, 31.73, 31.43$ ppm.

HRMS (APCI): calcd. for C₁₇H₁₅BrN₃O⁺: 356.0393 m/z [M+H]⁺

found: 356.0393 m/z [M+H]⁺.

LCMS (ESI, 25to100): $t_{ret} = 2.94$ min. 356/358 m/z [M+H]⁺.

***N*-(9-((4-(4-fluorophenyl)-1-methyl-2-(methylthio)-1H-imidazol-5-yl)pyridin-2-yl)amino)-11,12-dihydrodibenzo[*c,g*][1,2]diazocin-2-yl)acrylamide (**3**)**



10 (54 mg, 0.15 mmol), **11** (52 mg, 0.17 mmol), caesium carbonate (130 mg, 0.400 mmol) and BrettPhos Pd G3 (3.6 mg, 0.004 mmol) were added to a Schlenk tube under nitrogen atmosphere and suspended in degassed 1,4-dioxane (20 mL). The reaction mixture was stirred at 115 °C for 2 h cooled to RT and separated between EtOAc (20 mL) and water (20 mL). The aqueous phase was extracted with EtOAc (20 mL), and the combined organic extracts were washed with saturated aqueous NaHCO₃ solution (10 mL) and brine (20 mL). The organic phase was dried over Na₂SO₄ and concentrated under reduced pressure. Purification of the resulting crude product by flash column chromatography (Hex/EtOAc gradient, 0→100% EtOAc) gave **3** (17 mg, 0.029 mmol, 19%, purity >98%) as a yellow solid.

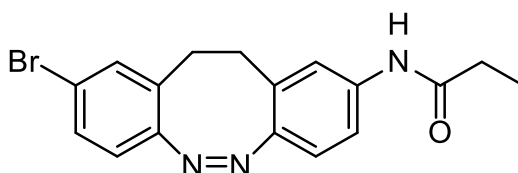
$R_f = 0.40$ [CH₂Cl₂:MeOH, 19:1].

¹H NMR (400 MHz, Chloroform-*d*): $\delta = 8.20$ (d, $J = 5.2$ Hz, 1H), 7.78 (s, 1H), 7.43 (dd, $J = 8.4, 5.4$ Hz, 2H), 7.29 (d, $J = 17.6$ Hz, 2H), 7.09 – 7.01 (m, 2H), 6.93 (t, $J = 8.5$ Hz, 2H), 6.84 (d, $J = 2.2$ Hz, 1H), 6.75 (dd, $J = 14.9, 8.4$ Hz, 2H), 6.64 (d, $J = 5.3$ Hz, 1H), 6.60 (s, 1H), 6.35 (d, $J = 16.8$ Hz, 1H), 6.20 (dd, $J = 16.8, 10.1$ Hz, 1H), 5.68 (d, $J = 10.0$ Hz, 1H), 3.43 (s, 3H), 2.82 (s, br, 2H), 2.67 (s, 3H), 2.56 (s, br, 2H), 1.25 (s, 3H). ppm.

¹³C NMR (100 MHz, Chloroform-*d*): $\delta = 163.78, 162.06$ (d, $J = 246.3$ Hz), 156.14, 151.97, 150.76, 148.75, 144.99, 140.40, 139.00, 138.88, 136.84, 131.04, 130.20 (d, $J = 3.1$ Hz), 129.43, 129.35, 129.08 (d, $J = 7.9$ Hz), 128.11, 128.11, 120.73, 120.64, 120.46, 120.18, 118.29, 118.14, 116.04, 115.38 (d, $J = 21.4$ Hz), 110.20, 31.98, 31.77, 29.83, 16.16 ppm.

HRMS (APCI):	calcd. for C ₃₃ H ₂₉ FN ₇ OS ⁺ :	590.21328 m/z [M+H] ⁺
found:		590.2127 m/z [M+H] ⁺ .
LCMS (ESI):	t _{ret} = 3.59 min.	590 m/z [M+H] ⁺ .

***N*-(9-bromo-11,12-dihydrodibenzo[*c,g*][1,2]diazocin-2-yl)propionamide (12)**



9 (106 mg, 0.263 mmol) was dissolved in a mixture of CH₂Cl₂ (1 mL) and TFA (1 mL) and stirred for 2 h. The volatiles were removed under reduced pressure and the resulting residue was resuspended in CH₂Cl₂ (2 mL) and DIPEA (0.275 mL, 1.58 mmol) was added. After cooling the solution to 0 °C, propionyl chloride (48.7 mg, 0.526 mmol, 0.046 mL) was added dropwise and the reaction was allowed to warm up to RT over 14 h. The reaction mixture was diluted with CH₂Cl₂ (20 mL) and washed with saturated aqueous NaHCO₃ solution (20 mL) and brine (20 mL). The organic phase was dried over Na₂SO₄ and concentrated under reduced pressure. Purification of the resulting crude product by flash column chromatography (Hx/EA gradient, 0→100% EA) gave **12** (24 mg, 0.079 mmol, 30%) as a yellow solid.

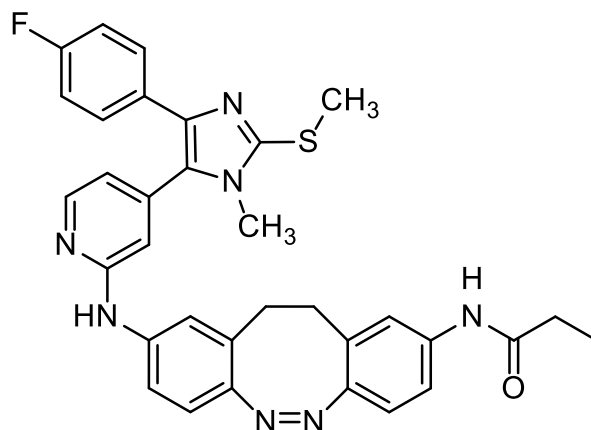
R_f = 0.35 [Hx:EA, 1:1].

¹H NMR (400 MHz, Chloroform-*d*): δ = 7.35 (s, 1H), 7.27 – 7.20 (m, 2H), 7.14 (s, 2H), 6.81 (d, J = 8.5 Hz, 1H), 6.70 (d, J = 8.3 Hz, 1H), 2.82 (d, br, J = 78.5 Hz, 4H), 2.34 (q, J = 7.5 Hz, 2H), 1.20 (t, J = 7.5 Hz, 3H) ppm.

¹³C NMR (100 MHz, Chloroform-*d*): δ = 172.11, 154.34, 151.53, 137.24, 132.47, 130.55, 129.90, 128.74, 120.78, 120.48, 120.43, 120.07, 117.96, 31.84, 31.50, 30.87, 9.69 ppm.

HRMS (APCI):	calcd. for C ₁₇ H ₁₇ BrN ₃ O ⁺ :	358.0550 m/z [M+H] ⁺
found:		358.0540 m/z [M+H] ⁺ .
LCMS (ESI):	t _{ret} = 3.81 min.	358 m/z [M+H] ⁺ .

***N*-9-((4-(4-(4-fluorophenyl)-1-methyl-2-(methylthio)-1H-imidazol-5-yl)pyridin-2-yl)amino)-11,12-dihydrodibenzo[*c,g*][1,2]diazocin-2-yl)propionamide (**6**)**



12 (24 mg, 0.067 mmol), **11** (25.3 mg, 0.080 mmol), caesium carbonate (58 mg, 0.18 mmol) and BrettPhos Pd G3 (2 mg, 0.002 mmol) were added to a Schlenk tube under nitrogen atmosphere and suspended in degassed 1,4-dioxane (5 mL). The reaction mixture was stirred at 120 °C for 1.5 h cooled to RT and separated between EtOAc (20 mL) and water (20 mL). The aqueous phase was extracted with EtOAc (20 mL), and the combined organic extracts were washed with saturated aqueous NaHCO₃ solution (10 mL) and brine (20 mL). The organic phase was dried over Na₂SO₄ and concentrated under reduced pressure. Purification of the resulting crude product by flash column chromatography (CH₂Cl₂/MeOH gradient, 0→10% MeOH) gave **6** (16 mg, 0.027 mmol, 40%, purity >98%) as a yellow solid.

$R_f = 0.40$ [CH₂Cl₂:MeOH, 19:1].

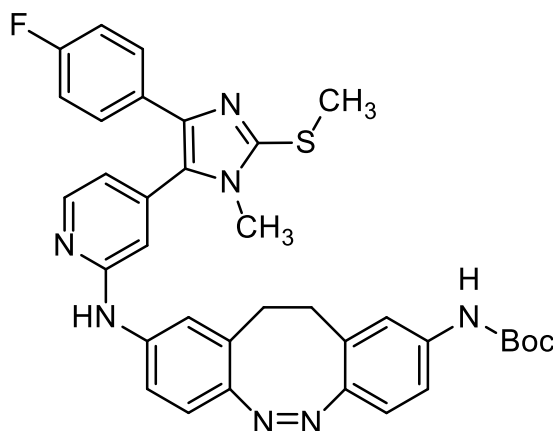
¹H NMR (400 MHz, Chloroform-*d*): $\delta = 8.22$ (d, $J = 5.2$ Hz, 1H), 7.47 – 7.38 (m, 3H), 7.28 (s, 1H), 7.19 (dd, $J = 8.4, 1.6$ Hz, 1H), 7.06 (dd, $J = 8.5, 2.1$ Hz, 1H), 6.96 (s, 1H), 6.93 (t, $J = 8.8$ Hz, 2H), 6.84 (d, $J = 2.0$ Hz, 1H), 6.75 (dd, $J = 15.5, 8.5$ Hz, 2H), 6.65 (dd, $J = 5.2, 1.2$ Hz, 1H), 6.59 (s, 1H), 3.43 (s, 3H), 2.81 (s, br, 2H), 2.68 (s, 3H), 2.64 (s, br, 2H), 2.28 (q, $J = 7.5$ Hz, 2H), 1.14 (t, $J = 7.5$ Hz, 3H) ppm.

¹³C NMR (100 MHz, Chloroform-*d*): $\delta = 172.33, 162.05$ (d, $J = 246.2$ Hz), 156.17, 151.68, 150.72, 148.91, 144.93, 140.36, 139.01, 138.83, 137.01, 130.23 (d, $J = 3.2$ Hz), 129.44, 129.28, 129.05 (d, $J = 7.9$ Hz), 128.11, 120.74, 120.34, 120.34, 120.19, 118.06, 117.93, 116.06, 115.36 (d, $J = 21.4$ Hz), 110.16, 31.98, 31.96, 31.81, 30.74, 16.14, 9.68 ppm.

HRMS (APCI): calcd. for C₃₃H₃₀FN₇NaOS⁺: 614.2109 m/z [M+Na]⁺
found: 614.2086 m/z [M+Na]⁺.

LCMS (ESI): $t_{\text{ret}} = 3.62$ min. 592 m/z [M+H]⁺.

tert-butyl-(9-((4-(4-(4-fluorophenyl)-1-methyl-2-(methylthio)-1H-imidazol-5-yl)pyridin-2-yl)amino)-11,12-dihydrodibenzo[c,g][1,2]diazocin-2-yl)carbamate (13)



9 (94 mg, 0.30 mmol) **11** (121 mg, 0.300 mmol), caesium carbonate (257 mg, 0.790 mmol) and BrettPhos Pd G3 (6.8 mg, 0.008 mmol) were added to a Schlenk tube under nitrogen atmosphere and suspended in degassed 1,4-dioxane (10 mL). After stirring at 90 °C for 16 h, the reaction was diluted with EtOAc (50 mL) and washed with saturated aqueous NaHCO₃ solution (25 mL), water (50 mL) and brine (50 mL). The organic phase was dried over Na₂SO₄ and concentrated under reduced pressure. Purification of the resulting crude product by flash column chromatography (Hx/EA gradient, 0→100% EA) gave **13** (150 mg, 0.236 mmol, 79%) as a yellow solid.

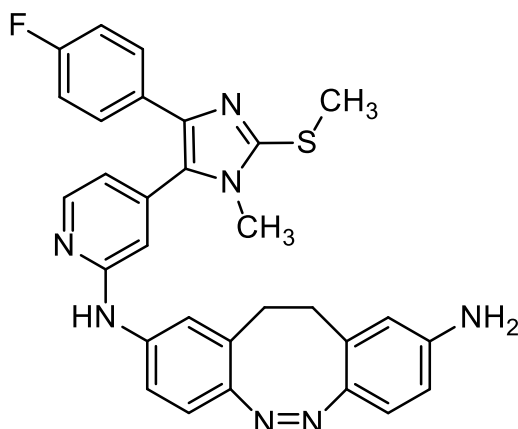
$R_f = 0.54$ [Hx:EA, 1:2].

¹H NMR (400 MHz, DMSO-d₆): $\delta = 8.22$ (dd, $J = 5.2, 0.8$ Hz, 1H), 7.48 – 7.42 (m, 2H), 7.14 (s, 1H), 7.02 (ddd, $J = 10.4, 8.5, 2.3$ Hz, 2H), 6.96 (t, $J = 8.7$ Hz, 2H), 6.88 – 6.83 (m, 2H), 6.77 (dd, $J = 17.7, 8.5$ Hz, 2H), 6.66 (dd, $J = 5.2, 1.4$ Hz, 1H), 6.63 (t, $J = 1.1$ Hz, 1H), 6.47 (s, 1H), 3.44 (s, 3H), 2.81 (s, br, 4H), 2.69 (s, 3H), 1.47 (s, 9H) ppm.

¹³C NMR (100 MHz, DMSO-d₆): $\delta = 162.10$ (d, $J = 246.2$ Hz), 156.11, 152.70, 150.93, 150.86, 148.77, 145.07, 140.54, 139.00, 138.72, 137.37, 130.25 (d, $J = 3.2$ Hz), 129.58, 129.18, 129.12 (d, $J = 7.9$ Hz), 128.04, 120.87, 120.54, 120.51, 118.86, 118.22, 116.67, 116.04, 115.40 (d, $J = 21.4$ Hz), 109.88, 80.89, 32.00, 31.96, 29.84, 28.43, 16.09 ppm.

HRMS (ESI): calcd. for $C_{35}H_{34}FN_7O_2S^+$: 636.2552 m/z $[M+H]^+$
 found: 636.2566 m/z $[M+H]^+$.
LCMS (ESI): $t_{ret} = 4.34$ min. 636 m/z $[M+H]^+$.

***N*²-(4-(4-(4-fluorophenyl)-1-methyl-2-(methylthio)-1H-imidazol-5-yl)pyridin-2-yl)-11,12-dihydrodibenzo[c,g][1,2]diazocine-2,9-diamine (14)**



13 (110 mg, 0.173 mmol) was dissolved in a mixture of CH_2Cl_2 (1 mL) and TFA (1 mL) and stirred at RT for 2 h. The reaction was quenched with saturated aqueous $NaHCO_3$ solution (20 mL), extracted with CH_2Cl_2 (20 mL), and washed with brine (50 mL). The organic phase was dried over Na_2SO_4 and concentrated under reduced pressure. Purification of the resulting crude product by flash column chromatography ($CH_2Cl_2/MeOH$ gradient, 0→20% MeOH) gave **14** (91.7 mg, 0.171 mmol, 99%) as a yellow solid.

$R_f = 0.43$ [$CH_2Cl_2:MeOH$, 19:1].

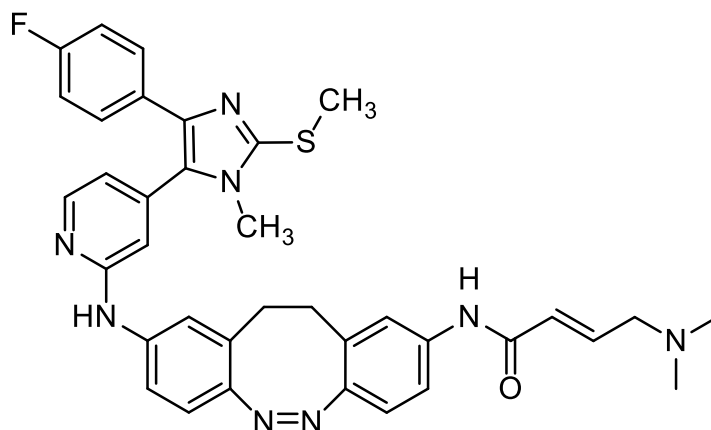
¹H NMR (400 MHz, Chloroform-*d*): $\delta = 8.24$ (d, $J = 5.1$ Hz, 1H), 7.47 (ddd, $J = 8.4, 5.3, 2.5$ Hz, 2H), 7.03 – 6.90 (m, 3H), 6.84 (d, $J = 2.2$ Hz, 1H), 6.73 (dd, $J = 13.0, 8.4$ Hz, 2H), 6.67 (dd, $J = 5.2, 1.0$ Hz, 2H), 6.61 (s, 1H), 6.44 (dd, $J = 8.3, 2.4$ Hz, 1H), 6.23 (d, $J = 2.3$ Hz, 1H), 3.44 (s, 3H), 2.70 (s, 3H), 2.67 (s, br, 4H) ppm.

¹³C NMR (100 MHz, DMSO-*d*₆): $\delta = 162.13$ (d, $J = 246.3$ Hz), 156.39, 151.32, 149.14, 147.79, 145.49, 144.98, 140.48, 138.84, 138.41, 130.28 (d, $J = 3.2$ Hz), 130.09, 129.35, 129.06 (d, $J = 7.9$ Hz), 128.21, 121.58, 120.89, 120.74, 118.62, 116.04, 115.41 (d, $J = 21.3$ Hz), 115.32, 113.36, 109.54, 32.14, 31.95, 31.85, 29.85 ppm.

HRMS (ESI): calcd. for $C_{30}H_{27}FN_7S^+$: 536.2027 m/z $[M+H]^+$
 found: 536.2049 m/z $[M+H]^+$.

LCMS (ESI): $t_{\text{ret}} = 3.28 \text{ min.}$ 536 m/z [M+H]⁺.

(E)-4-(dimethylamino)-N-(9-((4-(4-fluorophenyl)-1-methyl-2-(methylthio)-1H-imidazol-5-yl)pyridin-2-yl)amino)-11,12-dihydrodibenzo[c,g][1,2]diazocin-2-yl)but-2-enamide (4)



(E)-4-(dimethylamino)but-2-enoic acid hydrochloride (6.8 mg, 0.041 mmol) was suspended in dry THF (1 mL) under a nitrogen atmosphere. Oxalyl chloride (5.2 mg, 0.041 mmol, 0.004 mL) and DMF (0.013 mmol, 0.001 mL) were added at 0 °C and the suspension was allowed to warm to RT over 2 h. After removal of the volatiles under reduced pressure, **14** (17 mg, 0.032 mmol) was added under a nitrogen atmosphere and dissolved in THF (2 mL) at 0 °C. DIPEA (0.127 mmol, 0.022 mL) was added, and the reaction was allowed to warm to RT over 2 h and stirred for another 14 h.

The reaction was separated between EtOAc (50 mL) and aqueous Na₂CO₃ solution (1 M, 25 mL). The organic phase was dried over Na₂SO₄ and concentrated under reduced pressure. Purification of the resulting crude product by flash column chromatography (CH₂Cl₂/MeOH gradient with 0.1% NEt₃, 0→20% MeOH) gave **4** (9.0 mg, 0.014 mmol, 44%, purity >95%) as a yellow solid.

$R_f = 0.40$ [CH₂Cl₂:MeOH, 19:1].

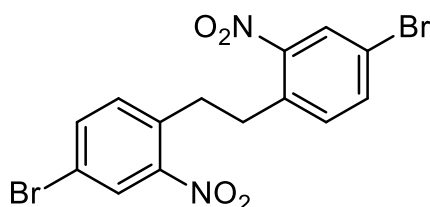
¹H NMR (400 MHz, DMSO-d₆): $\delta = 10.02$ (s, 1H), 9.16 (s, 1H), 8.25 (d, J = 5.2 Hz, 1H), 7.51 – 7.37 (m, 6H), 7.11 (tt, J = 9.1, 2.0 Hz, 2H), 6.79 (t, J = 8.5 Hz, 2H), 6.76 (dd, J = 5.3, 1.3 Hz, 1H), 6.72-6.64 (m, 2H), 6.19 (d, J = 15.4 Hz, 1H), 3.39 (s, 3H), 3.02 (d, J = 5.0 Hz, 2H), 2.76 (s, br, 4H), 2.64 (s, 3H), 2.15 (s, 6H) ppm.

¹³C NMR (100 MHz, DMSO-d₆): $\delta = 163.17$, 161.00 (d, J = 243.5 Hz), 156.05, 150.91, 148.80, 148.22, 143.63, 141.50, 140.29, 138.95, 137.89, 136.76, 130.47 (d, J = 3.0 Hz), 128.86, 128.42, 128.22 (d, J = 8.0 Hz), 128.07, 125.69, 119.80, 119.53, 119.44,

117.91, 117.41, 116.10, 115.37, 115.19 (d, $J = 21.4$ Hz), 111.71, 59.65, 45.12, 31.57, 31.54, 31.20, 15.28 ppm.

HRMS (APCI): calcd. for $C_{36}H_{36}FN_8OS^+$: 647.2711 m/z $[M+H]^+$
 found: 647.2708 m/z $[M+H]^+$.
LCMS (ESI): $t_{ret} = 2.91$ min. 647 m/z $[M+H]^+$.

1,2-bis(4-bromo-2-nitrophenyl)ethane (**15**)



4-bromo-2-nitrophenyl (1.08 g, 5.00 mmol) was dissolved in dry THF (30 mL) and *t*BuOK (617 mg, 5.5 mmol) was added at 0 °C. After 2 minutes bromine (0.33 mL, 6.5 mmol) was added, and the reaction was stirred for another 5 min until it was quenched into ice water (175 mL).

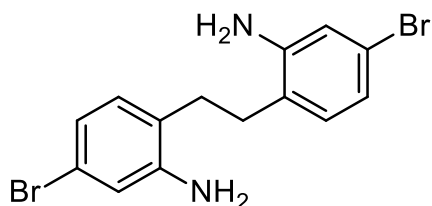
The aqueous phase was extracted with CH_2Cl_2 (3x100 mL) and washed with saturated aqueous $Na_2S_2O_3$ solution (50 mL), saturated aqueous $NaHCO_3$ solution (50 mL) and brine (50 mL). The organic phase was dried over Na_2SO_4 and concentrated under reduced pressure. Purification of the resulting crude product by flash column chromatography (Hx/EA gradient, 0→50% EA) gave **15** (681 mg, 1.58 mmol, 63%) as a gray-brown solid.

$R_f = 0.46$ [Hx:EA, 5:1].

1H NMR (400 MHz, Chloroform-*d*) $\delta = 8.12$ (d, $J = 2.0$ Hz, 2H), 7.68 (dd, $J = 8.2, 2.1$ Hz, 2H), 7.29 (d, $J = 8.3$ Hz, 2H), 3.18 (s, 4H) ppm.

^{13}C NMR (100 MHz, Chloroform-*d*): $\delta = 147.97, 137.86, 135.43, 131.19, 128.48, 126.70, 34.37$ ppm.

HRMS (APCI): calcd. for $C_{14}H_{11}Br_2N_2O_4^+$: 412.8954 m/z $[M+H-H_2O]^+$
 found: 412.8959 m/z $[M+H-H_2O]^+$.
LCMS (ESI): $t_{ret} = 5.10$ min. 453 m/z $[M+Na]^+$.

6,6'-(ethane-1,2-diyl)bis(3-bromoaniline) (16)

15 (600 mg, 1.40 mmol) was dissolved in 1,4-dioxane (60 mL) and a solution of sodium sulfide nonahydrate (1.68 g, 6.98 mmol) in water (6 mL) was added. The mixture was heated to 100 °C for 16 h. The volatiles were removed under reduced pressure and the resulting residue was resuspended in EtOAc (50 mL) and saturated aqueous NaHCO₃ solution (50 mL), extracted once more with EtOAc (50 mL) and the combined organic extracts were washed with saturated aqueous NaHCO₃ solution (50 mL) and brine (50 mL). The organic phase was dried over Na₂SO₄ and concentrated under reduced pressure. Purification of the resulting crude product by flash column chromatography (Hx/EA gradient, 0→100% EA) gave **16** (266 mg, 0.719 mmol, 52%) as a light brown solid.

$R_f = 0.35$ [Hx:EA, 1:1].

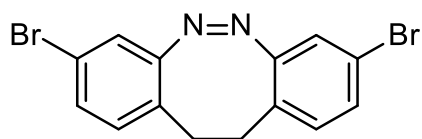
¹H NMR (400 MHz, Chloroform-d): $\delta = 6.86 - 6.83$ (m, 4H), 6.81 (dd, $J = 1.7, 0.9$ Hz, 2H), 3.63 (s, 4H), 2.71 (s, 4H). ppm.

¹³C NMR (100 MHz, DMSO-d₆): $\delta = 145.80, 131.12, 124.71, 121.92, 120.73, 118.50, 30.40$. ppm.

HRMS (APCI): calcd. for C₁₄H₁₅Br₂N₂⁺: 370.9576 m/z [M+H]⁺

found: 370.9574 m/z [M+H]⁺.

LCMS (ESI): $t_{ret} = 4.43$ min. 371 m/z [M+H]⁺.

3,8-dibromo-11,12-dihydrodibenzo[c,g][1,2]diazocine (17)

16 (15 mg, 0.041 mmol) was dissolved in a mixture of CH₂Cl₂ (1 mL) and AcOH (1 mL). Peracetic acid (0.014 mL, 0.082 mmol, 39%wt in AcOH) was diluted in 2 mL AcOH and added dropwise over 12 h at room temperature in the dark using a syringe pump. The reaction was stirred for additional 4 h and the volatiles were removed in vacuo. The residue was taken up in CH₂Cl₂ (20 mL) and extracted with 20 mL of 0.5 M NaOH. The organic phase was washed with saturated aqueous NaHCO₃ solution (25 mL) and brine (25 mL). The organic phase was dried over Na₂SO₄ and concentrated under reduced pressure. Purification of the resulting crude product by flash column chromatography (Hx/EA gradient, 0→100% EA) gave **17** (11.8 mg, 0.032 mmol, 78%) as a yellow, crystalline solid.

$R_f = 0.32$ [Hx:EA, 5:1].

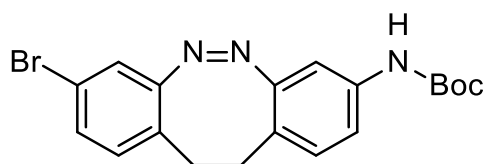
¹H NMR (400 MHz, Chloroform-d): $\delta = 7.17$ (dd, $J = 8.2, 2.0$ Hz, 2H), 7.01 (d, $J = 2.0$ Hz, 2H), 6.86 (d, $J = 8.2$ Hz, 2H), 2.97 – 2.66 (m, 4H). ppm.

¹³C NMR (100 MHz, Chloroform-d): $\delta = 156.07, 131.38, 130.55, 126.96, 121.94, 120.42, 31.19$ ppm.

HRMS (APCI): calcd. for C₁₄H₁₁Br₂N₂⁺: 364.9284 m/z [M+H]⁺

found: 364.9278 m/z [M+H]⁺.

LCMS (ESI): $t_{ret} = 4.89$ min. 367 m/z [M+H]⁺.

tert-butyl-(8-bromo-11,12-dihydrodibenzo[c,g][1,2]diazocin-3-yl)carbamate (18)

17 (126 mg, 0.344 mmol), tert-butyl carbamate (32.3 mg, 0.275 mmol), caesium carbonate (337 mg, 1.03 mmol) and XantPhos Pd G3 (16 mg, 0.017 mmol) were added to a Schlenk tube under nitrogen atmosphere and suspended in degassed 1,4-dioxane (3.4 mL). The reaction mixture was stirred at 90 °C for 12 h. After cooling to RT, the reaction was diluted with EtOAc (30 mL) and filtered through a silica plug (2x1 cm). The organic phase was concentrated under reduced pressure. Purification of the resulting crude product by flash column chromatography (Hx/EA gradient, 0→100% EA) gave **18** (52.0 mg, 0.129 mmol, 47%) as a yellow solid.

$R_f = 0.24$ [Hx:EA, 5:1].

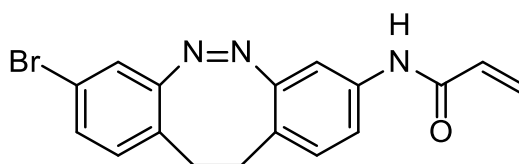
$^1\text{H NMR}$ (400 MHz, Chloroform-d): $\delta = 7.12$ (dd, $J = 8.1, 2.1$ Hz, 1H), 7.09 – 7.02 (m, 1H), 6.96 (d, $J = 2.0$ Hz, 1H), 6.92 – 6.80 (m, 3H), 6.56 (s, 1H), 2.94 – 2.58 (m, 4H), 1.47 (s, 9H) ppm.

$^{13}\text{C NMR}$ (100 MHz, Chloroform-d): $\delta = 156.22, 155.53, 152.53, 137.43, 131.28, 130.41, 130.14, 127.50, 122.00, 121.78, 120.04, 117.25, 108.59, 80.88, 31.40, 30.92, 28.39$ ppm.

HRMS (APCI): calcd. for $\text{C}_{19}\text{H}_{21}\text{BrN}_3\text{O}_2^+$: 402.0812 m/z $[\text{M}+\text{H}]^+$

found: 402.0792 m/z $[\text{M}+\text{H}]^+$.

LCMS (ESI, 25to100): $t_{\text{ret}} = 4.07$ min. 402, 404 m/z $[\text{M}+\text{H}]^+$.

***N*-(8-bromo-11,12-dihydrodibenzo[*c,g*][1,2]diazocin-3-yl)acrylamide (19)**

18 (26 mg, 0.065 mmol) was dissolved in a mixture of CH₂Cl₂ (1 mL) and TFA (1 mL) and stirred for 2 h. The volatiles were removed under reduced pressure and the resulting residue was resuspended in CH₂Cl₂ (10 mL), washed with saturated aqueous NaHCO₃ solution (20 mL), and concentrated under reduced pressure. CH₂Cl₂ (10 mL) and DIPEA (0.027 mL, 0.20 mmol) was added to the yellow solid. After cooling the solution to -5 °C, acryloyl chloride (7.6 mg, 0.085 mmol, 0.007 mL) was added and the reaction was allowed to warm up to RT over 2 h and stirred for an additional 2 h. The reaction mixture was diluted with EtOAc (20 mL) and washed with saturated aqueous NaHCO₃ solution (2x20 mL) and brine (20 mL). The organic phase was dried over Na₂SO₄ and concentrated under reduced pressure. Purification of the resulting crude product by flash column chromatography (Hx/EA gradient, 0→100% EA) gave **19** (13.4 mg, 0.038 mmol, 59%) as a yellow, crystalline solid.

$R_f = 0.40$ [Hx:EA, 4:1].

¹H NMR (400 MHz, Chloroform-*d*): $\delta = 7.34$ (d, $J = 5.7$ Hz, 2H), 7.13 (dd, $J = 8.2, 2.0$ Hz, 1H), 7.10 (s, 1H), 6.98 – 6.92 (m, 2H), 6.85 (d, $J = 8.2$ Hz, 1H), 6.40 (dd, $J = 16.8, 1.0$ Hz, 1H), 6.19 (dd, $J = 16.8, 10.2$ Hz, 1H), 5.75 (dd, $J = 10.2, 1.0$ Hz, 1H), 2.98 – 2.65 (m, 4H) ppm.

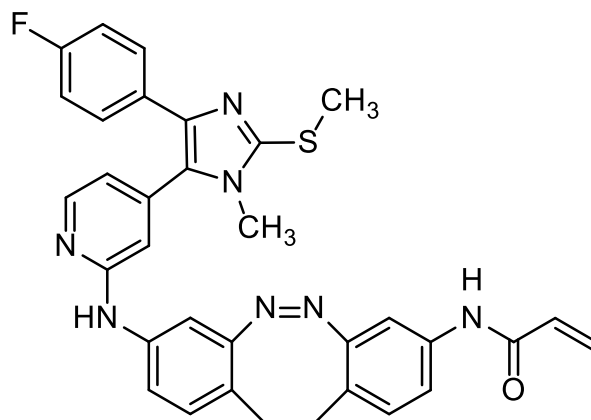
¹³C NMR (100 MHz, Chloroform-*d*): $\delta = 163.54, 156.24, 155.54, 136.77, 131.35, 130.97, 130.57, 130.29, 128.38, 127.41, 123.87, 121.80, 120.19, 118.82, 110.05, 31.37, 31.10$ ppm.

HRMS (ESI): calcd. for C₁₇H₁₅BrN₃O⁺: 356.0393 m/z [M+H]⁺

found: 356.0384 m/z [M+H]⁺.

LCMS (ESI): $t_{ret} = 3.90$ min. 356 m/z [M+H]⁺.

***N*-(8-((4-(4-fluorophenyl)-1-methyl-2-(methylthio)-1H-imidazol-5-yl)pyridin-2-yl)amino)-11,12-dihydrodibenzo[*c,g*][1,2]diazocin-3-yl)acrylamide (**5**)**



19 (13.4 mg, 0.038 mmol), **11** (16.7 mg, 0.053 mmol), caesium carbonate (33 mg, 0.10 mmol) and BrettPhos Pd G3 (1 mg, 0.001 mmol) were added to a Schlenk tube under nitrogen atmosphere and suspended in degassed 1,4-dioxane (1.5 mL). The reaction mixture was stirred at 110 °C for 10 h cooled to RT. After diluting with EtOAc (10 mL) the suspension was filtered through a silica plug (2x1 cm), further washed with EtOAc (20 mL). The organic phase was concentrated under reduced pressure. Purification of the resulting crude product by flash column chromatography (CH₂Cl₂/MeOH gradient, 0→20% MeOH) gave **5** (8.1 mg, 0.014 mmol, 36%, purity >95%) as a yellow solid.

$R_f = 0.43$ [CH₂Cl₂:MeOH, 19:1].

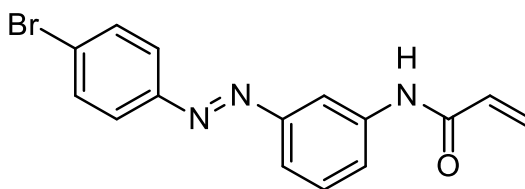
¹H NMR (400 MHz, DMSO-*d*₆): $\delta = 10.15$ (s, 1H), 9.21 (s, 1H), 8.27 (d, *J* = 5.2 Hz, 1H), 7.47 – 7.39 (m, 3H), 7.31 (d, *J* = 2.0 Hz, 1H), 7.25 – 7.20 (m, 2H), 7.10 (t, *J* = 9.0 Hz, 2H), 7.04 (d, *J* = 8.3 Hz, 1H), 6.95 (d, *J* = 8.4 Hz, 1H), 6.76 (dd, *J* = 5.2, 1.3 Hz, 1H), 6.69 (s, 1H), 6.35 (dd, *J* = 17.0, 10.0 Hz, 1H), 6.21 (dd, *J* = 17.0, 2.1 Hz, 1H), 5.72 (dd, *J* = 10.0, 2.1 Hz, 1H), 3.39 (s, 3H), 2.74 (d, *J* = 5.9 Hz, 4H), 2.64 (s, 3H) ppm.

¹³C NMR (100 MHz, DMSO-*d*₆): $\delta = 163.15, 161.01$ (d, *J* = 243.5 Hz), 156.02, 155.22, 155.15, 148.20, 143.64, 140.00, 138.97, 137.46, 136.77, 131.58, 130.46 (d, *J* = 3.0 Hz), 130.22, 130.04, 128.22 (d, *J* = 8.1 Hz), 128.05, 127.11, 123.28, 119.67, 117.69, 116.55, 115.38, 115.20 (d, *J* = 21.5 Hz), 111.79, 108.70, 106.84, 31.55, 30.58, 30.34, 15.28 ppm.

HRMS (APCI): calcd. for C₃₃H₂₉FN₇OS⁺: 590.21328 m/z [M+H]⁺

found: 590.2111 m/z [M+H]⁺.

LCMS (ESI): $t_{ret} = 3.74$ min. 590 m/z [M+H]⁺.

(E)-N-(3-((4-bromophenyl)diazenyl)phenyl)acrylamide (20)

4-Bromoaniline (354 mg, 2.06 mmol) was dissolved in CH₂Cl₂ (7 mL), and Oxone (2.52 g, 4.12 mmol) dissolved in water (7 mL) was added. The biphasic mixture was vigorously stirred for 16 h at RT. After addition of CH₂Cl₂ (30 mL) and extraction with brine (2x25 mL) the organic phase was dried over Na₂SO₄ and concentrated under reduced pressure. To give a faint yellow solid (335 mg, 1.80 mmol, 87%) which was directly dissolved in acetic acid (15 mL). After adding N-(3-aminophenyl)acrylamide (243 mg, 1.5 mmol, prepared as described^[35]) the reaction was stirred for 14 h at RT. The volatiles were removed under reduced pressure and the crude mixture separated between in CHCl₃ (75 mL) and a 1:1 mixture of water and saturated aqueous NaHCO₃ solution (50 mL). The aqueous phase was extracted with CHCl₃ (75 mL), and the combined organic phases were washed with saturated aqueous NaHCO₃ solution (50 mL) and brine (50 mL). The organic phase was dried over Na₂SO₄ and concentrated under reduced pressure. Purification of the resulting crude product by flash column chromatography (Hx/EA gradient, 15→30% EA) gave **20** (201 mg, 0.609 mmol, 41%) as an orange solid.

$R_f = 0.12$ [Hx:EA, 5:1].

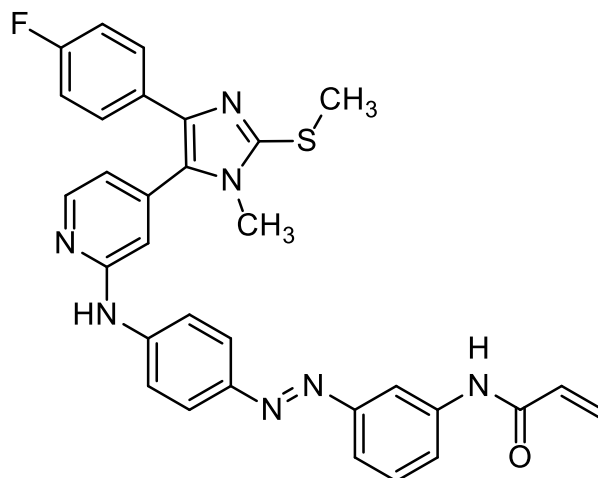
¹H NMR (400 MHz, DMSO-d₆): $\delta = 10.49$ (s, 1H), 8.34 (t, $J = 2.0$ Hz, 1H), 7.91-7.83 (m, 5H), 7.70 (ddd, $J = 7.9, 2.0, 1.1$ Hz, 1H), 7.61 (t, $J = 7.9$ Hz, 1H), 6.52 (dd, $J = 17.0, 10.1$ Hz, 1H), 6.36 (dd, $J = 17.0, 2.0$ Hz, 1H), 5.86 (dd, $J = 10.0, 2$ Hz, 1H) ppm.

¹³C NMR (100 MHz, DMSO-d₆): $\delta = 163.9, 152.6, 151.17, 140.5, 133.1, 132.1, 130.3, 127.9, 125.5, 124.9, 122.9, 119.8, 112.4$ ppm.

HRMS (APCI): calcd. for C₁₅H₁₃BrN₃O⁺: 330.0237 m/z [M+H]⁺

found: 330.0231 m/z [M+H]⁺.

LCMS (ESI): $t_{ret} = 4.61$ min. 330 m/z [M+H]⁺.

(E)-N-(3-((4-((4-(4-(4-fluorophenyl)-1-methyl-2-(methylthio)-1H-imidazol-5-yl)pyridin-2-yl)amino)phenyl)diazenyl)phenyl)acrylamide (2)

20 (36 mg, 0.11 mmol) **11** (31 mg, 0.10 mmol), caesium carbonate (130 mg, 0.790 mmol) and BrettPhos Pd G3 (2.0 mg, 0.0025 mmol) were added to a Schlenk tube under argon atmosphere and suspended in degassed 1,4-dioxane (1.5 mL). After stirring at 110 °C for 2 h, the reaction was filtered through a silica pad (1x2 cm) and washed with EtOAc (20 mL) and methanol (10 mL). The organic phase was concentrated under reduced pressure. Purification of the resulting crude product by flash column chromatography (Hx/EA gradient, 25→75% EA) gave **2** (16 mg, 0.027 mmol, 29%, purity >90%) as an orange solid.

$R_f = 0.20$ [Hx:EA, 1:1].

¹H NMR (400 MHz, DMSO-*d*₆): $\delta = 10.41$ (s, 1H), 9.74 (s, 1H), 8.39 (dd, $J = 5.2, 0.7$ Hz, 1H), 8.22 (t, $J = 2.0$ Hz, 1H), 7.95 (d, $J = 9.1$ Hz, 2H), 7.90 – 7.86 (m, 2H), 7.79 (ddd, $J = 7.9, 2.1, 1.2$ Hz, 1H), 7.61 – 7.57 (m, 1H), 7.54 (d, $J = 7.9$ Hz, 1H), 7.51 – 7.44 (m, 2H), 7.19 – 7.13 (m, 2H), 6.93 – 6.87 (m, 2H), 6.48 (dd, $J = 17.0, 10.1$ Hz, 1H), 6.31 (dd, $J = 16.9, 2.0$ Hz, 1H), 5.81 (dd, $J = 10.1, 2.0$ Hz, 1H), 3.46 (s, 3H), 2.67 (s, 3H) ppm.

¹³C NMR (100 MHz, DMSO-*d*₆): $\delta = 163.84, 161.55$ (d, $J = 243.6$ Hz), 156.11, 153.07, 148.83, 146.11, 145.42, 144.34, 140.42, 139.72, 137.49, 132.17, 130.95 (d, $J = 3.1$ Hz), , 130.13, 128.85 (d, $J = 8.1$ Hz), 128.41, 127.77, 124.59, 121.56, 119.14, 118.09, 116.87, 115.73 (d, $J = 21.4$ Hz), 113.06, 112.05, 32.10, 15.74 ppm.

¹⁹F NMR (377 MHz, DMSO-*d*₆): $\delta = -115.57$ (tt, $J = 8.9, 5.6$ Hz) ppm.

HRMS (ESI): calcd. for C₃₁H₂₇FN₇OS⁺: 564.1976 m/z [M+H]⁺

found: 564.1975 m/z [M+H]⁺.

LCMS (ESI, 5to100 over 10min): $t_{\text{ret}} = 8.32$ min. 564 m/z [M+H]⁺.

References

- [1] R. Roskoski, *Pharmacol. Res.* 2019, *144*, 19–50.
- [2] Q. Liu, Y. Sabnis, Z. Zhao, T. Zhang, S. J. Buhrlage, L. H. Jones, N. S. Gray, *Chem. Biol.* 2013, *20*, 146–159.
- [3] A. Chaikuad, P. Koch, S. A. Laufer, S. Knapp, *Angew. Chem. Int. Ed.* 2018, *57*, 4372–4385.
- [4] C. L. Fleming, M. Grøtli, J. Andréasson, *ChemPhotoChem* 2019, *3*, 318–326.
- [5] D. Kolarski, A. Sugiyama, G. Breton, C. Rakers, D. Ono, A. Schulte, F. Tama, K. Itami, W. Szymanski, T. Hirota, B. L. Feringa, *J. Am. Chem. Soc.* 2019, *141*, 15784–15791.
- [6] A. Kobori, T. Yamauchi, Y. Nagae, A. Yamayoshi, A. Murakami, *Bioorg. Med. Chem.* 2012, *20*, 5071–5076.
- [7] P. Leippe, J. Koehler Leman, D. Trauner, *Biochemistry* 2017, *56*, 5214–5220.
- [8] R. Ferreira, J. R. Nilsson, C. Solano, J. Andréasson, M. Grøtli, *Sci. Rep.* 2015, *5*, 9769.
- [9] D. Wilson, J. W. Li, N. R. Branda, *ChemMedChem* 2017, *12*, 284–287.
- [10] M. W. H. Hoorens, M. E. Ourailidou, T. Rodat, P. E. van der Wouden, P. Kobauri, M. Kriegs, C. Peifer, B. L. Feringa, F. J. Dekker, W. Szymanski, *Eur. J. Med. Chem.* 2019, *179*, 133–146.
- [11] M. Schehr, C. Ianes, J. Weisner, L. Heintze, M. P. Müller, C. Pichlo, J. Charl, E. Brunstein, J. Ewert, M. Lehr, U. Baumann, D. Rauh, U. Knippschild, C. Peifer, R. Herges, *Photochem. Photobiol. Sci.* 2019, *18*, 1398–1407.
- [12] L. Heintze, D. Schmidt, T. Rodat, L. Witt, J. Ewert, M. Kriegs, R. Herges, C. Peifer, *Int. J. Mol. Sci.* 2020, *21*, 8961.
- [13] D. Schmidt, T. Rodat, L. Heintze, J. Weber, R. Horbert, U. Girreser, T. Raeker, L. Bußmann, M. Kriegs, B. Hartke, C. Peifer, *ChemMedChem* 2018, *13*, 2415–2426.
- [14] E. T. Coffey, *Nat. Rev. Neurosci.* 2014, *15*, 285–299.
- [15] G. Solinas, B. Becattini, *Mol. Metab.* 2017, *6*, 174–184.
- [16] P. Koch, M. Gehringer, S. A. Laufer, *J. Med. Chem.* 2015, *58*, 72–95.
- [17] T. Zhang, F. Inesta-Vaquera, M. Niepel, J. Zhang, S. B. Ficarro, T. Machleidt, T. Xie, J. A. Marto, N. Kim, T. Sim, J. D. Laughlin, H. Park, P. V. LoGrasso, M. Patricelli, T. K. Nomanbhoy, P. K. Sorger, D. R. Alessi, N. S. Gray, *Chem. Biol.* 2012, *19*, 140–154.

- [18] F. Muth, A. El-Gokha, F. Ansideri, M. Eitel, E. Döring, A. Sievers-Engler, A. Lange, F. M. Boeckler, M. Lämmerhofer, P. Koch, S. A. Laufer, *J. Med. Chem.* 2017, *60*, 594–607.
- [19] J.-J. Ventura, A. Hübner, C. Zhang, R. A. Flavell, K. M. Shokat, R. J. Davis, *Mol. Cell* 2006, *21*, 701–710.
- [20] C. H. Nijboer, H. J. C. Bonestroo, J. Zijlstra, A. Kavelaars, C. J. Heijnen, *Neurobiol. Dis.* 2013, *54*, 432–444.
- [21] A. Zeke, M. Misheva, A. Reményi, M. A. Bogoyevitch, *Microbiol. Mol. Biol. Rev.* 2016, *80*, 793–835.
- [22] R. M. M.-F. de Mera, L.-L. Li, A. Popinigis, K. Cisek, M. Tuittila, L. Yadav, A. Serva, M. J. Courtney, *Nat. Commun.* 2017, *8*, 1–18.
- [23] F. Muth, M. Günther, S. M. Bauer, E. Döring, S. Fischer, J. Maier, P. Drückes, J. Köppler, J. Trappe, U. Rothbauer, P. Koch, S. A. Laufer, *J. Med. Chem.* 2015, *58*, 443–456.
- [24] J. B. Trads, K. Hüll, B. S. Matsuura, L. Laprell, T. Fehrentz, N. Görldt, K. A. Kozek, C. D. Weaver, N. Klöcker, D. M. Barber, D. Trauner, *Angew. Chem. Int. Ed.* 2019, *58*, 15421–15428.
- [25] R. Siewertsen, H. Neumann, B. Buchheim-Stehn, R. Herges, C. Näther, F. Renth, F. Temps, *J. Am. Chem. Soc.* 2009, *131*, 15594–15595.
- [26] M. S. Maier, K. Hüll, M. Reynders, B. S. Matsuura, P. Leippe, T. Ko, L. Schäffer, D. Trauner, *J. Am. Chem. Soc.* 2019, *141*, 17295–17304.
- [27] K. Hüll, J. Morstein, D. Trauner, *Chem. Rev.* 2018, *118*, 10710–10747.
- [28] M. Goettert, S. Luik, R. Graeser, S. A. Laufer, *J. Pharm. Biomed. Anal.* 2011, *55*, 236–240.
- [29] J. D. Vasta, C. R. Corona, J. Wilkinson, C. A. Zimprich, J. R. Hartnett, M. R. Ingold, K. Zimmerman, T. Machleidt, T. A. Kirkland, K. G. Huwiler, R. F. Ohana, M. Slater, P. Otto, M. Cong, C. I. Wells, B.-T. Berger, T. Hanke, C. Glas, K. Ding, D. H. Drewry, K. V. M. Huber, T. M. Willson, S. Knapp, S. Müller, P. L. Meisenheimer, F. Fan, K. V. Wood, M. B. Robers, *Cell Chem. Biol.* 2018, *25*, 206-214.e11.
- [30] V. Arkhipova, H. Fu, M. W. H. Hoorens, G. Trinco, L. N. Lameijer, E. Marin, B. L. Feringa, G. J. Poelarends, W. Szymanski, D. J. Slotboom, A. Guskov, *J. Am. Chem. Soc.* 2021, *143*, 1513–1520.
- [31] S. Pospich, F. Küllmer, V. Nasufović, J. Funk, A. Belyy, P. Bieling, H.-D. Arndt, S. Raunser, *Angew. Chem. Int. Ed.* 2021, *60*, 8678–8682.

- [32] M. Forster, A. Chaikuad, T. Dimitrov, E. Döring, J. Holstein, B.-T. Berger, M. Gehringer, K. Ghoreschi, S. Müller, S. Knapp, S. A. Laufer, *J. Med. Chem.* 2018, *61*, 5350–5366.
- [33] S. Röhm, B.-T. Berger, M. Schröder, A. Chaikuad, R. Winkel, K. F. W. Hekking, J. J. C. Benningshof, G. Müller, R. Tesch, M. Kudolo, M. Forster, S. Laufer, S. Knapp, *J. Med. Chem.* 2019, *62*, 10757–10782.
- [34] M. Borowiak, W. Nahaboo, M. Reynders, K. Nekolla, P. Jalinot, J. Hasserodt, M. Rehberg, M. Delattre, S. Zahler, A. Vollmar, D. Trauner, O. Thorn-Seshold, *Cell* 2015, *162*, 403–411.
- [35] Z. Song, Y. Jin, Y. Ge, C. Wang, J. Zhang, Z. Tang, J. Peng, K. Liu, Y. Li, X. Ma, *Bioorg. Med. Chem.* 2016, *24*, 5505–5512.

10 – Expanding Photoswitchable Covalent Inhibitors

Martin Reynders^{1,2} and Dirk Trauner^{1,3,4},

¹Department of Chemistry, New York University, New York, NY 10003, USA.

²Department of Chemistry, Ludwig Maximilians University of Munich
81377 Munich, Germany.

³Perlmutter Cancer Center, New York University School of Medicine, New York, NY
10016, USA.

⁴NYU Neuroscience Institute, New York University School of Medicine, New York, NY
10016, USA.

Introduction

Kinases catalyze the phosphorylation of proteins and thereby control many cellular signaling pathways through this key posttranslational modification. The kinase family includes more than 500 members that phosphorylate a specific set of substrates to regulate activity, localization, or structure of these proteins.^[1] Small molecule probes to regulate kinase activity have seen great progress as tools and therapeutics and the development of selective inhibitors for understudied kinases is ongoing.^[2,3] A general method to improve kinase selectivity and on-target potency is the generation of covalent kinase inhibitors.^[4,5] Most covalent kinase inhibitors consist of a ligand for the ATP binding site connected to an electrophilic warhead. The electrophile can react with a specific amino acid side chain in close proximity to the binding site, such as a cysteine.^[5,6]

In parallel, the interest in strategies to control kinase activity and target phosphorylation with light has grown, but design of small molecule tools proved to be challenging.^[7,8] Incorporation of a photoswitch into the pharmacophore of an optimized pharmacophore can often require significant changes that reduce activity or specificity of the inhibitor.

We have previously developed photoswitchable, covalent inhibitors for the c-Jun N-terminal kinase 3 (JNK3) based on diazocine photoswitches (Chapter 9).^[9,10] These diazocine based molecules exist in a bent form in the dark which is thermodynamically stable and they can be switched to an elongated isomer with visible light. The covalent warhead can reach and react with a cysteine in vicinity of the ATP binding site only after irradiation to generate the elongated isomer. Consequently, the formation of a covalent bond can be controlled by light. This design could be adapted to other covalent kinase inhibitors where incorporation of a diazocine is tolerable.

A biaryl amide in-between the hinge-binding motif and the covalent warhead exists not only in the JNK3 inhibitors, where we replaced it with a diazocine photoswitch, but also in JNK1–3, CDK7 and PI5P4K inhibitors.^[11–14] JNK-IN-7 has been developed as a probe for JNK1–3.^[11] While the expression of JNK3 is restricted to specific tissues, JNK1 and JNK2 are ubiquitously expressed.^[15] These kinases are part of the mitogen-activated protein kinase (MAPK) family and regulate the cellular stress response.

Development of JNK inhibitors has progressed slowly even though JNK1–3 are implicated in several diseases.^[16,17] It has further been shown that the timing of JNK activity is crucial in determining the cellular fate.^[17,18] Photoswitchable inhibitors are ideal tools for the dynamic manipulation of kinase activity since they can be controlled with the spatiotemporal precision light offers.^[19]

A second example for a covalent kinase inhibitor is THZ1 which targets CDK7.^[12] CDK7 forms the Cdk-activating kinase (CAK) together with cyclin H and MAT1.^[20] CAK itself is a part of the transcription factor II human (TFIIH) multiprotein complex which functions in transcription initiation and DNA repair.^[21,22] THZ1 has been studied as cancer treatment and as a tool compound.^[12,23–27] Due to the essentiality of CDK7, being able to control the activity of CDK7 inhibitors with light appears beneficial.

Here we aim to adapt our existing design strategy to generate photoswitchable, covalent kinase inhibitors for JNK1–3 and CDK7. The generated photopharmaceuticals could serve as versatile biological tools to further understand the signaling dynamics of these kinases, but also as therapeutics with reduced side-effects in photomedicine.

Results

Previously we have replaced a biaryl amide with a diazocine photoswitch to obtain a light-responsive JNK3 inhibitor (Chapter 9). JNK-IN-7, a covalent JNK1–3 inhibitor, features the same biaryl amide linker connecting the ATP pocket binding moiety and acrylic warhead (Figure 10.1A). The difference in selectivity is a consequence of JNK-IN-7 not binding a second hydrophobic pocket present in JNK3.^[11,28]

The preparation of our photoswitchable JNK1–3 inhibitor followed the synthetic route of our previous covalent inhibitors and employed the Baeyer-Mills coupling for the oxidative diazocine formation (Figure 10.1B).^[29] Subsequent Buchwald-Hartwig aminations followed by deprotection and acylation with the covalent warhead gave **MR-II-265** in 6 steps from commercial starting materials.

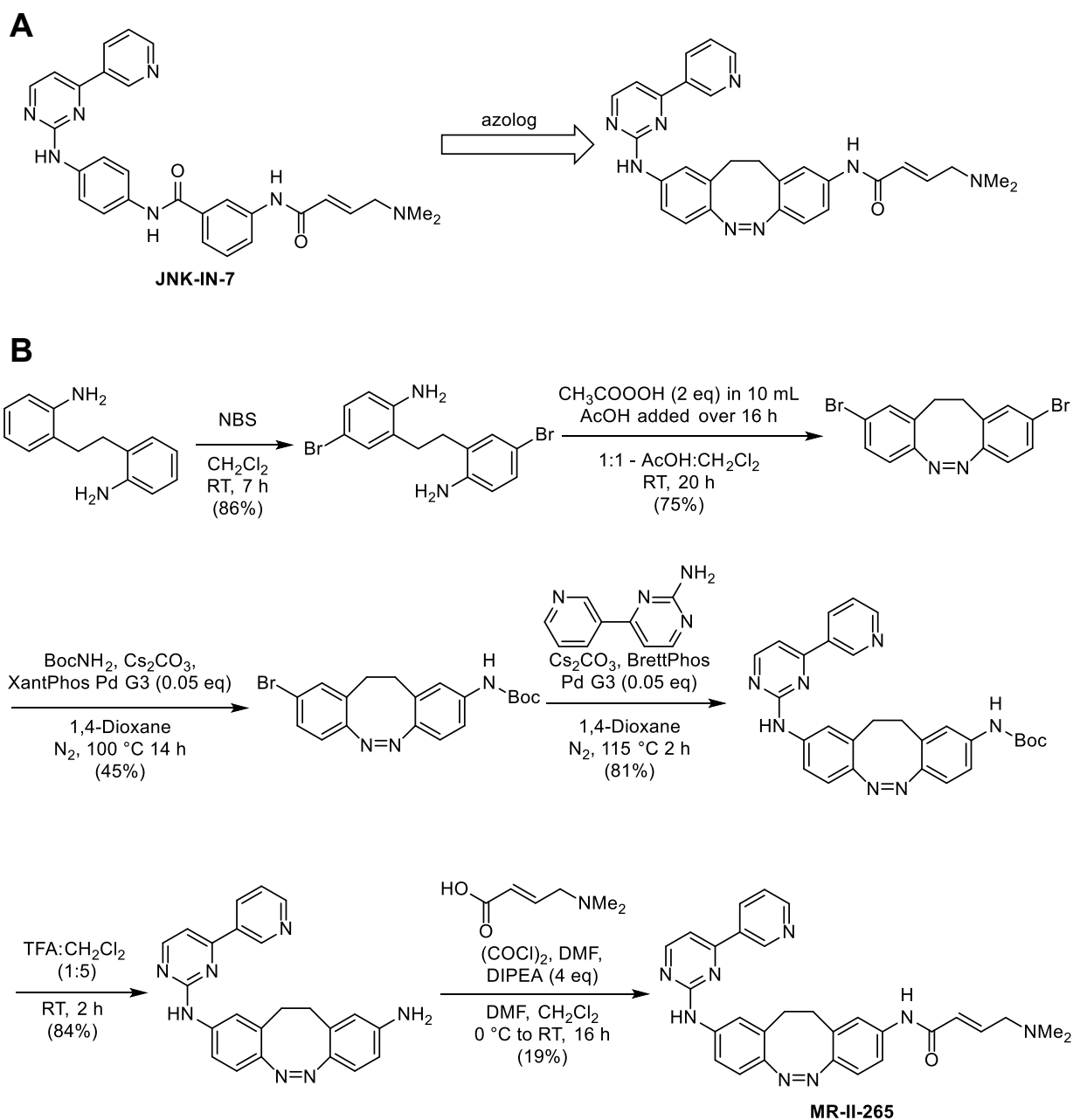


Figure 10.1: A) Design of **MR-II-265** as azolog of JNK-IN-7. B) Synthesis of **MR-II-265**.

MR-II-265 shows the characteristic absorption bands of diazocines and efficiently underwent isomerization to the *trans* isomer when irradiated with blue light between 400 and 430 nm (Figure 10.2B).^[9,29] The *cis* isomer was efficiently generated with green light irradiation (>500 nm). Alternatively, **MR-MB-265** underwent thermal relaxation to the *cis* isomer with a half-life of 42 min in DMSO or 27 min in a more aqueous environment (Figure 10.2D, E).

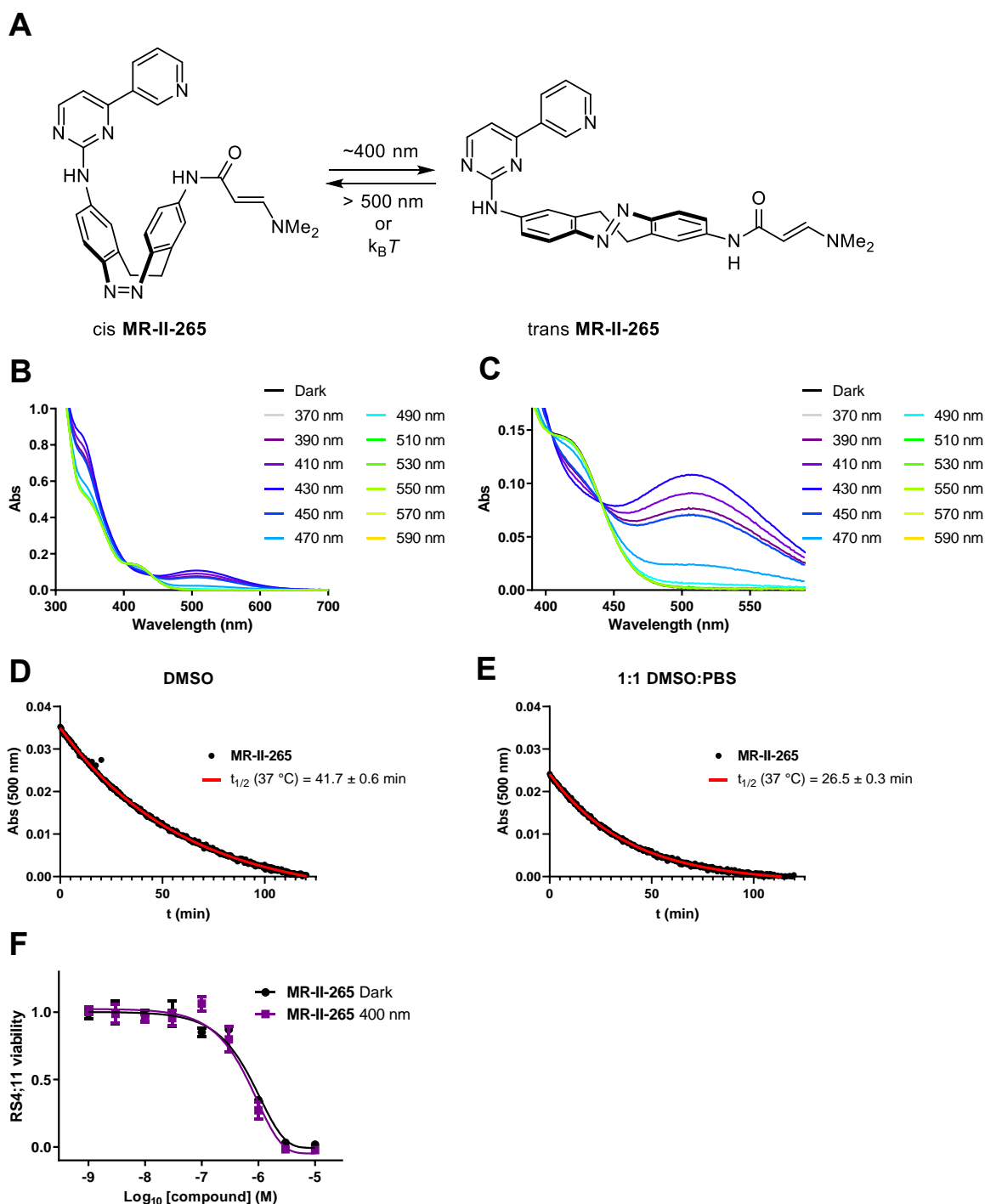


Figure 10.2: Characterization of **MR-II-265**. A) Structure and isomerization of **MR-II-265**. B), C) Absorption spectra of **MR-II-265** (50 μ M in DMSO) after irradiation with the indicated wavelength for 5 min. D), E) Thermal *Z*-to-*E* isomerization of **MR-II-265** at 37 °C in the indicated solvents. F) Viability of RS4;11 cells treated with **MR-II-265** for 72 h in the dark or with pulsed 400 nm irradiation (100 ms per 10 s).

MR-II-265 decreased the viability of RS4;11 cells in a dose dependent fashion, but no effect of photoswitching on cell viability could be observed (Figure 10.2F). However, this inhibitor is not designed as a cytotoxic agent. Additionally, the ATP binding pocket

scaffold shows structural similarity to other kinase inhibitors such as imatinib, which may explain the effect on viability. Further on-target characterization will be required to determine the activity of **MR-II-265**.

Next, we applied our diazocine design of covalent inhibitors to convert THZ1 into a photoswitch (Figure 10.3A). The synthesis started by Buchwald-Hartwig amination of a THZ1 building block, followed by deprotection of the aniline and a second Buchwald-Hartwig amination using the same diazocine intermediate as before (Figure 10.3B). Deprotection of the aniline followed by acylation with the covalent warhead and a final deprotection of the indole successfully yielded **MR-II-309** (Figure 10.3B).

Upon exposure to blue light **MR-II-309** efficiently isomerized to the elongated *trans* form (Figure 10.4A–C). Again, formation of the *cis* isomer could be induced with either green light (>500 nm) irradiation or by thermal relaxation with a half-life of 42 minutes in DMSO (Figure 10.4D). Notably, for this covalent application high isomer ratios in favor of the *trans* isomer are not strictly necessary, as diazocine photoswitches are in a dynamic equilibrium when irradiated. On average, all molecules will be converted to the *trans* isomer temporarily and thus be able to bind covalently when sufficient light intensity is provided (see Chapter 9). Another advantage of diazocines is the quantitative reversion to the *cis* isomer with green light.^[9] This enables precise control of these switches at all times when alternating between blue and green light.

Based on the therapeutic potential of THZ1, we investigated the effect of **MR-II-309** on cell viability. **MR-II-309** showed a strong effect on RS4;11 viability (Figure 10.4E). The cytotoxic effect was more pronounced when cells were irradiated with pulsed 400 nm light and even appeared to persist at lower concentrations. A small difference in MDA-MB-231 cell viability could also be observed between light and dark for treatment with **MR-II-309** (Figure 10.4F). The overall reduced potency and small phototherapeutic window observed is in line with the low potency of THZ1 in this cell line.^[12]

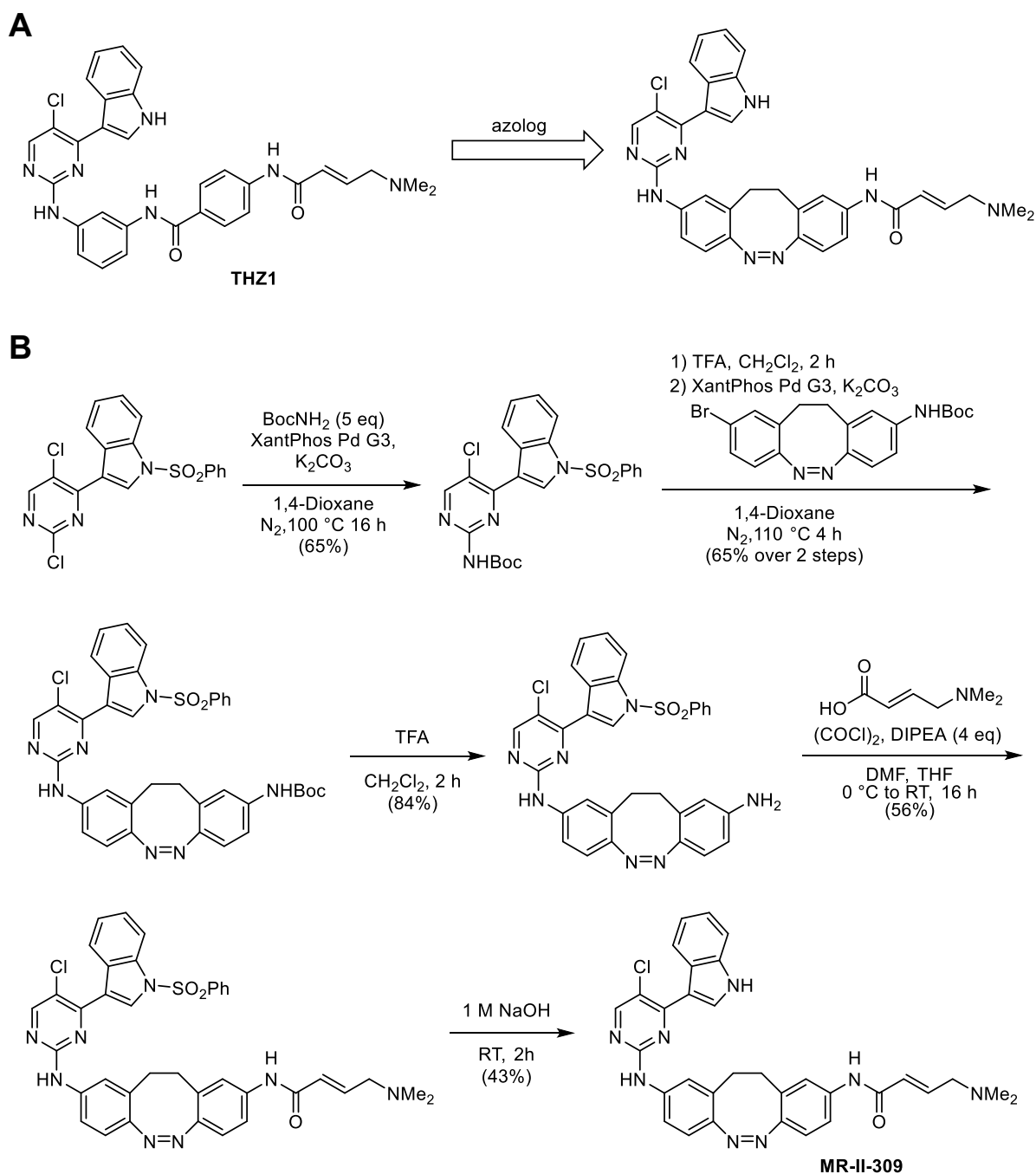


Figure 10.3: A) Design of **MR-II-309** as azolog of JNK-IN-7. B) Synthesis of **MR-II-309**.

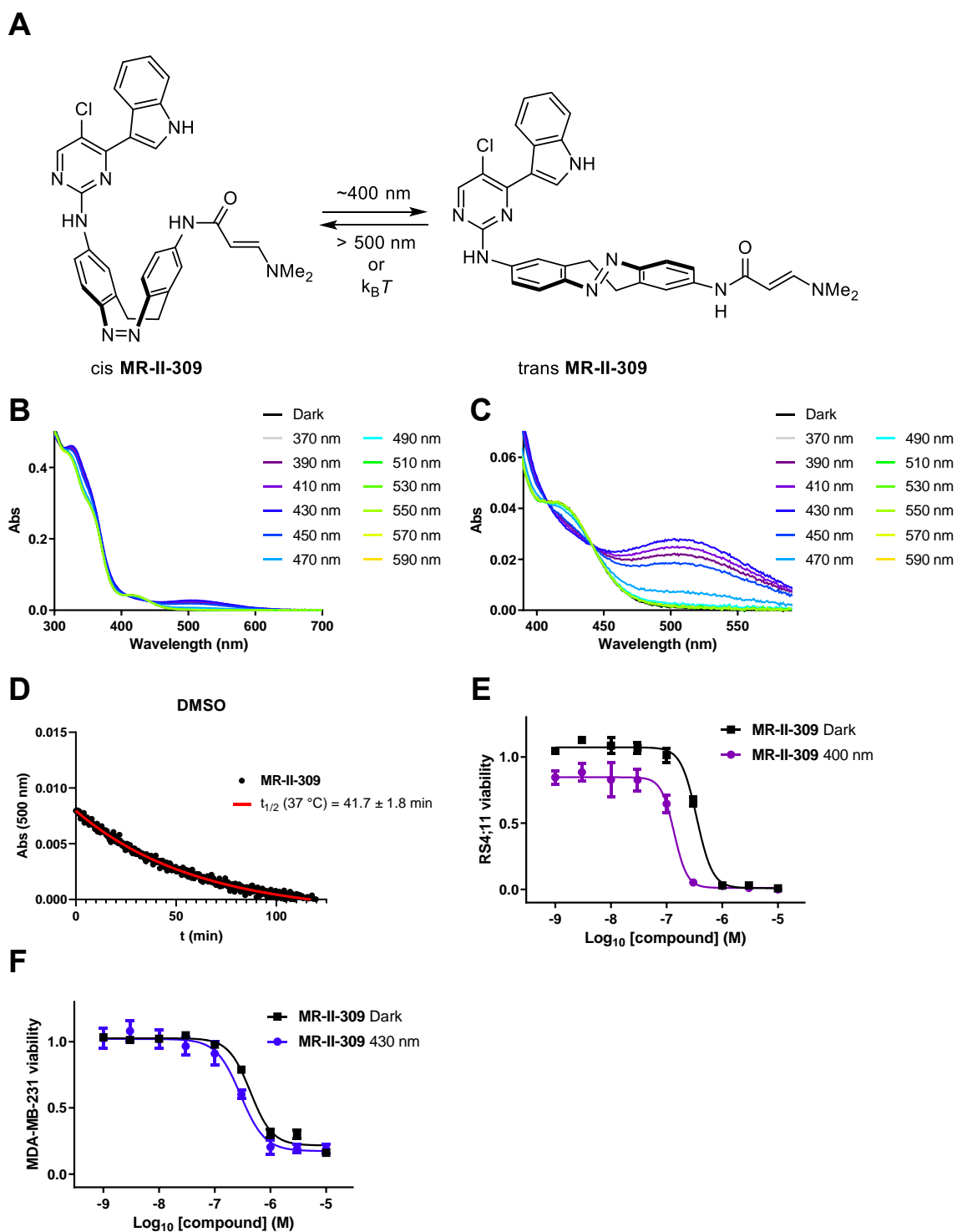


Figure 10.4: Characterization of **MR-II-309**. A) Structure and isomerization of **MR-II-309**. B), C) Absorption spectra of **MR-II-309** (25 μM in DMSO) after irradiation with the indicated wavelength for 5 min. D) Thermal *Z*-to-*E* isomerization of **MR-II-309** at 37 $^\circ\text{C}$ in DMSO. E) Viability of RS4;11 cells treated with **MR-II-309** for 72 h in the dark or with pulsed 400 nm irradiation (100 ms per 10 s). F) Viability of MDA-MB-231 cells treated with **MR-II-309** for 72 h in the dark or with pulsed 430 nm irradiation (100 ms per 10 s).

Discussion and Outlook

Here we applied our covalent inhibitor design based on diazocines to JNK1-3 and CDK7 as targets. Both compounds possess favorable photophysical properties and can be used *in cellulo*. The JNK inhibitor **MR-II-265** did not affect RS4;11 cell viability in a light-dependent fashion. However, a strong effect on JNK inhibition in the absence of stress stimuli is not expected. Further characterization of the ability of **MR-II-265** to inhibit JNK1–3 *in vitro* and *in cellulo* will be needed.

Initial data for the photoswitchable, covalent CDK7 inhibitor **MR-II-309** is promising. The light-dependent cytotoxicity could be further evaluated in different cell lines, such as T-cell acute lymphoblastic lymphoma cells that have shown to be highly sensitive to THZ1.^[12] Further optimizing the position of the covalent warhead on the diazocine could facilitate covalent bond formation and phototherapeutic window of **MR-II-309**. It will be necessary to validate activity on CDK7 by direct readouts since cell viability integrates many cellular effects of the drug.

Photoswitchable CDK7 inhibitors such as **MR-II-309** could also be used in the treatment of small cell lung cancer (SCLC). SCLC has shown promising sensitivity to CDK7 inhibitors.^[27] The lung is accessible by bronchoscopy, which could be performed to locally activate the inhibitor in the tumor. Thereby, the activated inhibitor could covalently bind and inhibit CDK7 in the tumor, while remaining a non-covalent inhibitor with lower residence time in other tissues. We believe the different mechanism of action could reduce potential side-effect of CDK7 inhibitor treatment and improve the therapeutic outcome.

Supporting Information

Methods

Determination of Photophysical properties

UV-Vis spectrometry was performed on a Varian Cary 60 UV-Visible Spectrophotometer using BRAND UV-Cuvette Disposable Spectrophotometer/Photometer Ultra-Micro Cuvettes, BrandTech (10 mm light path). An Agilent Technologies PCB 1500 Water Peltier system was used for temperature control and samples were irradiated with a Cairn Research Optoscan Monochromator with Optosource High Intensity Arc Lamp equipped with a 75 W UXL-S50A lamp from USHIO Inc. Japan and set to 15 nm full width at half maximum. Samples were stored and prepared under red light to avoid formation of the *Z*-isomers. 10 mM stock solutions were prepared in the dark and diluted to a final concentration of 50 or 25 μ M to measure the UV-VIS spectra following irradiation with different wavelengths for 5 min using a monochromator. Measurement was started from the dark-adapted state, followed by 370 nm and further stepwise wavelength increase up to 600 nm. By increasing the wavelength from low to high *Z*- to *E*-isomerization can be observed, whereas going the reverse direction from high to low wavelength, the PSS might not be reached due to low absorptivity above 500 nm. Spectra were recorded in DMSO to avoid any artifacts of aggregation or precipitation.

Thermal relaxation was measured by preirradiating the switches with 390 nm light and observing the absorption at 500 nm over 12 h at 37 °C in DMSO in tightly sealed cuvettes. Half-lives were determined by nonlinear regression using GraphPad Prism Version 9.02.

LED illumination

For illumination of the cells we used the cell disco system as previously described in the literature.^[30] 5 mm LEDs 390 nm (VL390-5-15), 400 nm (RLS-UV400), 430 nm (VL430-5-15) were purchased from Roithner Lasertechnik. Pulsed irradiation of 96- or 6-well plates was performed using 100 ms pulses every 10 s (unless indicated otherwise) controlled by an Arduino system.

Cell culture

The human acute lymphoblastic leukemia RS4;11 (ATCC[®] CRL1873[™]) cell line was

purchased from the American Type Culture Collection and cultured in phenol red-free RPMI1640 medium (Gibco) with 10% fetal bovine serum (FBS) and 1% penicillin/streptomycin (PS) in a humidified incubator at 37 °C with 5% CO₂ in air. For the experiments compounds were serially diluted in phenol red-free RPMI1640 (Gibco) as 2x stock solutions resulting in a final concentration of 1% DMSO during the assay. Azobenzene stocks and dilutions were strictly kept in the dark and prepared under red light conditions. MDA-MB-231 cells were cultured in DMEM without phenol red containing 10% fetal bovine serum (FBS) and 1% penicillin/ streptomycin (PS) and seeded 24 h before treatment.

Colorimetric MTS Assays

The activity of dehydrogenase enzymes in metabolically active cells, as a quantitative measurement for cytotoxicity and proliferation, was determined by colorimetric measurement of the reduction of [3-(4,5-dimethylthiazol-2-yl)-5-(3-carboxymethoxyphenyl)-2-(4-sulfophenyl)-2H-tetrazolium (MTS) to the formazan product. The absorbance of formazan was measured at 500 nm on a FLUOstar Omega microplate reader (BMG Labtech). Cells were treated with different concentrations of PHOTACs (10 μ M to 1 nM) in triplicates using 1% DMSO as cosolvent, and incubated in a 96-well plate for 72 h. The cells were placed in light-proof boxes and exposed to the lighting conditions specified in the experiment for 72 h. Next, 10 μ L of Promega CellTiter 96[®] AQueous One Solution Reagent was added to each well and incubated for further 4-7 hours at 37 °C. The absorbance at 500 nm was measured on a FLUOstar Omega 96-well plate reader (BMG Labtech).

Data was analyzed using GraphPad Prism Version 9.02 (GraphPad Software Inc) and fitted using the [Inhibitor] vs. response -- Variable slope (four parameters) fit. Results represent the mean viability \pm SEM relative to the 1% DMSO treated control. Light dependence of RS4;11 viability was analyzed from all experiments and normalized to cells in the dark. Results are shown as individual data points and mean viability \pm SEM.

Synthetic Procedures and Characterization

General information

The reagents and solvents used in this study were bought from the following chemical suppliers: Acros Organics, Alfa Aesar, Combi-Blocks, Oakwood, OxChem, Sigma-

Aldrich, Toronto Research Chemicals and Medkoo Biosciences and were used as purchased.

Dry solvents used in reactions performed under inert atmosphere were obtained by passing the degassed solvents through activated alumina columns. Additionally, dry solvents were stored over molecular sieves under an inert atmosphere.

Column chromatography was carried out on silica gel (60 Å pore size, 40–63 µm, Merck KGaA) using a Teledyne Isco Combiflash EZprep flash purification system.

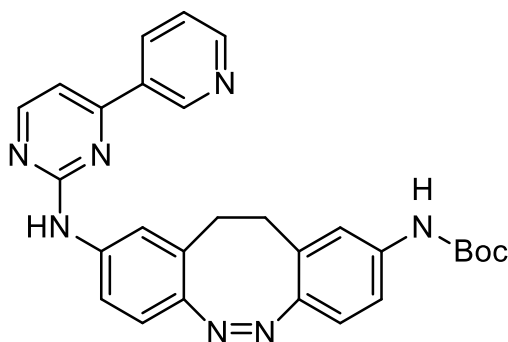
Thin-layer chromatography (TLC) was performed on glass plates precoated with silica gel (0.25 mm, 60-Å pore size, Merck). TLC plates were visualized by exposure to UV light (254 and 366 nm).

NMR spectra were obtained on a Bruker Avance III HD 400 MHz spectrometer equipped with a CryoProbe™ operating at 400 MHz for ¹H and 100 MHz for ¹³C spectra or on a Bruker AVIII-600 High Performance Digital NMR Spectrometer (600 MHz for ¹H and 150 MHz for ¹³C spectra) with CPTCI-cryoprobehead. Integration results and multiplets are reported as observed and denoted as follows: s (singlet), d (doublet), t (triplet), q (quartet), p (pentet), h (hextet), sept (septet), and m (multiplet) and as combinations thereof.

High-resolution mass spectra (HRMS) were recorded on an Agilent Technologies 6224 Accurate-Mass time-of-flight spectrometer with either atmospheric pressure chemical ionization (APCI) or electrospray ionization (ESI) ionization sources.

LCMS were measured on an Agilent Technologies 1260 II Infinity connected to an Agilent Technologies 6120 Quadrupole mass spectrometer with APCI ionization source. Elution was performed using a gradient from 5:95% to 100:0% MeCN:H₂O with 0.1% formic acid over 5 min, if not indicated otherwise. Separated isomer spectra of azobenzenes were obtained by irradiation of the LCMS sample prior to injection.

***tert*-butyl (Z)-(9-((4-(pyridin-3-yl)pyrimidin-2-yl)amino)-11,12-dihydrodibenzo[*c,g*][1,2]diazocin-2-yl)carbamate (MR-II-259)**



tert-butyl-(9-bromo-11,12-dihydrodibenzo[*c,g*][1,2]diazocin-2-yl)carbamate (201.1 mg, 0.500 mmol, 1.0 eq.) prepared as previously described (Chapter 9), 4-(Pyridin-3-yl)pyrimidin-2-amine (215.2 mg, 1.250 mmol, 2.5 eq.), BrettPhos PdG3 (11.3 mg, 0.013 mmol, 0.025 eq.) and cesium carbonate (325.8 mg, 1.00 mmol, 2.0 eq.) were added to a flame dried Schlenk tube under nitrogen atmosphere. Dry 1,4-dioxane (3 mL) was added and the mixture was heated to 110 °C for 6 h. The mixture was then diluted with CH₂Cl₂ (40 mL) and separated against water (40 mL). The layers were separated and the aqueous phase was extracted with CH₂Cl₂ (40 mL). The combined organic phase was washed with saturated NaHCO₃ (2x30 mL) and brine (2x 30 mL). The organic phase was dried over Na₂SO₄ and concentrated under reduced pressure. Purification of the resulting crude product by flash column chromatography (CH₂Cl₂/MeOH gradient, 0-20% MeOH) yielded **MR-II-259** (200 mg, 0.405 mmol, 81%) as a yellow solid.

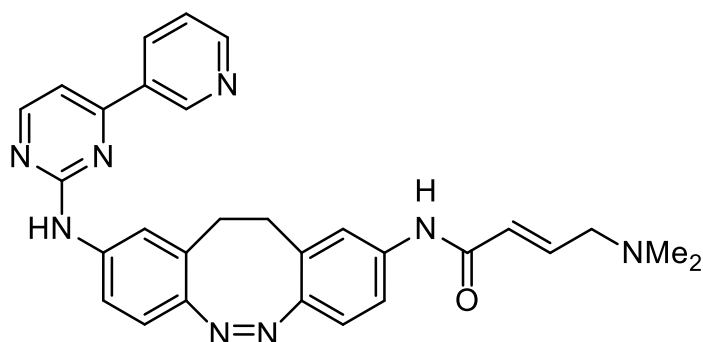
$R_f = 0.32$ [CH₂Cl₂:MeOH 19:1].

¹H NMR (400 MHz, CDCl₃) δ = 9.20 (s, 1H), 8.74 (d, *J* = 4.7 Hz, 1H), 8.47 (d, *J* = 4.8 Hz, 1H), 8.28 (dt, *J* = 8.0, 1.7 Hz, 1H), 7.47 – 7.43 (m, 1H), 7.40 (dd, *J* = 8.5, 2.0 Hz, 1H), 7.33 (d, *J* = 2.0 Hz, 1H), 7.21 – 7.13 (m, 4H), 7.04 (s, 1H), 6.87 (d, *J* = 8.4 Hz, 1H), 6.81 (d, *J* = 8.6 Hz, 1H), 3.09 – 2.65 (m, 4H), 1.44 (s, 9H) ppm.

¹³C NMR (100 MHz, CDCl₃) δ = 162.48, 160.37, 159.24, 152.82, 151.59, 151.12, 151.01, 148.68, 138.07, 137.67, 134.49, 132.65, 129.47, 129.31, 123.76, 121.07, 120.32, 120.27, 118.94, 118.11, 116.69, 108.47, 80.56, 32.15, 31.98, 28.43 ppm.

HRMS (APCI):	calcd. for C ₂₈ H ₂₈ N ₇ O ₂ ⁺ :	494.2299 m/z [M+H] ⁺ .
	found:	494.2299 m/z [M+H] ⁺ .
LCMS (ESI):	t _{ret} = 3.82 min.	494 m/z [M+H] ⁺ .

***(E)*-4-(dimethylamino)-N-((*Z*)-9-((4-(pyridin-3-yl)pyrimidin-2-yl)amino)-11,12-dihydrodibenzo[*c,g*][1,2]diazocin-2-yl)but-2-enamide (MR-II-265)**



MR-II-259 (180 mg, 0.365 mmol) was dissolved in a 1:2 TFA:CH₂Cl₂ mixture (6 mL) and stirred for 2 h at room temperature. The reaction mixture was diluted with CH₂Cl₂ (10 mL) and poured into saturated NaHCO₃ (30 mL). The aqueous layer was extracted with a 5:1 CH₂Cl₂:MeOH mixture (30 mL) and the organic phases were washed with saturated NaHCO₃ (2x30 mL) and brine (2x 30 mL), concentrated under reduced pressure and subjected to flash column chromatography (CH₂Cl₂/MeOH gradient, 0-20% MeOH) yielding the deprotected aniline (120 mg, 0.305 mmol, 84%) as a yellow solid that was directly used in the next step.

(E)-4-(dimethylamino)but-2-enoic acid hydrochloride (21.9 mg, 0.132 mmol 1.3 eq.) was suspended in dry THF (1 mL) under a nitrogen atmosphere. Oxalyl chloride (16.8 mg, 0.132 mmol, 0.011 mL, 1.3 eq.) and DMF (0.010 mmol, 0.001 mL, 0.1 eq.) were added at 0 °C and the suspension was allowed to warm to RT over 2 h. After removal of the volatiles under reduced pressure, the deprotected intermediate (40 mg, 0.102 mmol, 1 eq.) was added under a nitrogen atmosphere and the solids were dissolved in THF (2 mL) at 0 °C. DIPEA (52.6 mg, 0.407 mmol, 0.071 mL, 4.0 eq.) was added and the reaction was allowed to warm to room temperature over 2 h and stirred for another 14 h.

The reaction was diluted with a 1:4 *i*PrOH:CHCl₃ mixture (25 mL) and separated against an aqueous Na₂CO₃ solution (1 M, 25 mL). The organic phase was washed with brine (15 mL), dried over Na₂SO₄, and concentrated under reduced pressure. Purification of the resulting crude product by high-performance liquid chromatography (H₂O/MeCN + 0.1% formic acid, 10 – 100% MeCN) gave **MR-II-265** (9.5 mg, 0.019 mmol, 19%) as a yellow solid.

$R_f = 0.06$ [CH₂Cl₂:MeOH 19:1].

¹H NMR (400 MHz, DMSO-*d*₆) δ = 10.03 (s, 1H), 9.77 (s, 1H), 9.31 (d, *J* = 1.8 Hz, 1H), 8.73 (dd, *J* = 4.8, 1.5 Hz, 1H), 8.58 (d, *J* = 5.2 Hz, 1H), 8.46 (dt, *J* = 8.0, 1.9 Hz, 1H), 8.18 (s, 1H), 7.65 (dd, *J* = 8.6, 2.1 Hz, 1H), 7.62 – 7.55 (m, 2H), 7.49 (d, *J* = 5.2 Hz, 1H), 7.41 (dd, *J* = 8.5, 2.0 Hz, 1H), 6.85 (dd, *J* = 11.7, 8.5 Hz, 2H), 6.67 (dt, *J* = 15.4, 5.9 Hz, 1H), 6.18 (d, *J* = 15.4 Hz, 1H), 3.05 (d, *J* = 5.1 Hz, 2H), 2.88 – 2.72 (m, 4H), 2.16 (s, 6H) ppm.

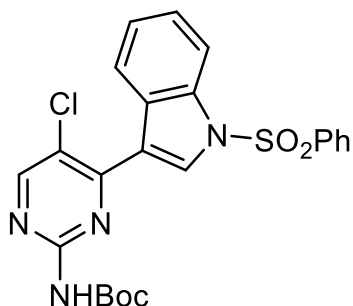
¹³C NMR (100 MHz, DMSO) δ = 163.10, 161.55, 159.95, 159.38, 151.53, 150.88, 149.47, 148.15, 141.01, 139.28, 137.94, 134.34, 132.11, 128.77, 128.24, 126.00, 123.94, 119.70, 119.59, 119.55, 119.28, 117.51, 117.17, 108.41, 59.47, 44.93, 31.69, 31.26 ppm.

HRMS (APCI): calcd. for C₂₉H₂₉N₈O⁺: 505.2459 m/z [M+H]⁺.

found: 505.2459 m/z [M+H]⁺.

LCMS (ESI): *t*_{ret} = 3.67 min. 505 m/z [M+H]⁺.

***tert*-butyl (5-chloro-4-(1-(phenylsulfonyl)-1H-indol-3-yl)pyrimidin-2-yl)carbamate (MR-II-263)**



3-(2,5-dichloropyrimidin-4-yl)-1-(phenylsulfonyl)-1H-indole (100.0 mg, 0.247 mmol, 1.0 eq.), *tert*-butyl carbamate (72.3 mg, 0.618 mmol, 2.5 eq.), potassium carbonate (51.1 mg, 0.370 mmol, 1.5 eq.) and XantPhos Pd G3 (11.4 mg, 0.012 mmol, 0.05 eq.) were added to a flame dried Schlenk tube under nitrogen atmosphere and suspended in degassed 1,4-dioxane (1.5 mL). The mixture was heated to 110 °C for 6 h and allowed to cool to room temperature. The reaction mixture was then diluted with CH₂Cl₂ (25 mL) and separated against water (25 mL). The layers were separated and the aqueous phase was extracted with CH₂Cl₂ (25 mL). The organic phase was washed with saturated NaHCO₃ (30 mL) and brine (30 mL), dried over Na₂SO₄ and concentrated under reduced pressure. Purification of the resulting crude product by flash column chromatography (Hexanes/EtOAc gradient, 0-100% EtOAc) yielded **MR-II-263** (48 mg, 0.099 mmol, 40%) as a colorless solid.

$R_f = 0.77$ [CH₂Cl₂:MeOH 19:1].

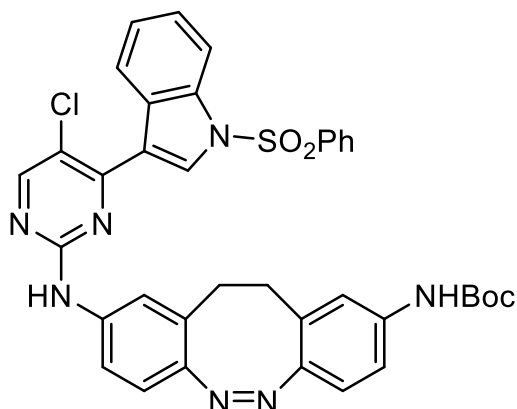
¹H NMR (400 MHz, CDCl₃) $\delta = 8.71 - 8.66$ (m, 2H), 8.60 (s, 1H), 8.06 – 8.01 (m, 1H), 7.95 (d, J = 7.8 Hz, 2H), 7.61 – 7.53 (m, 2H), 7.47 (t, J = 7.8 Hz, 2H), 7.43 – 7.36 (m, 2H), 1.55 (s, 9H) ppm.

¹³C NMR (100 MHz, CDCl₃) $\delta = 158.65, 157.56, 155.61, 150.25, 137.85, 134.70, 134.50, 130.68, 129.65, 129.02, 127.15, 125.81, 124.67, 123.84, 121.53, 117.15, 113.28, 81.93, 28.35$ ppm.

HRMS (APCI):	calcd. for C ₂₃ H ₂₂ ClN ₄ O ₄ S ⁺ :	485.1045 m/z [M+H] ⁺ .
	found:	485.1030 m/z [M+H] ⁺ .

LCMS (ESI):	$t_{ret} = 4.99$ min.	485 m/z [M+H] ⁺ .
--------------------	-----------------------	------------------------------

***tert*-butyl (Z)-(9-((5-chloro-4-(1-(phenylsulfonyl)-1H-indol-3-yl)pyrimidin-2-yl)amino)-11,12-dihydrodibenzo[c,g][1,2]diazocin-2-yl)carbamate (MR-II-266)**



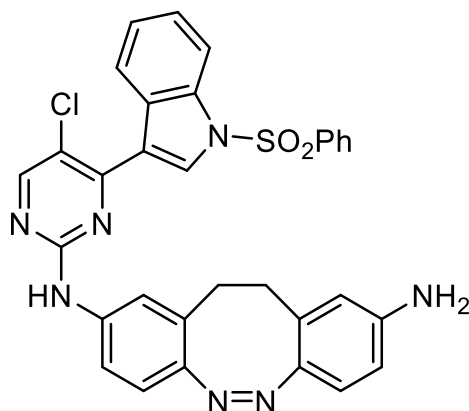
MR-II-263 (50.0 mg, 0.103 mmol, 1.0 eq.) was dissolved in a 1:1 TFA:CH₂Cl₂ mixture (0.5 mL) and stirred for 1 h at room temperature. After removal of the volatiles *in vacuo*, *tert*-butyl-(9-bromo-11,12-dihydrodibenzo[c,g][1,2]diazocin-2-yl)carbamate (49.8 mg, 0.124 mmol, 1.2 eq.) prepared as previously described (Chapter 9), potassium carbonate (50.0 mg, 0.362 mmol, 3.5 eq.) and XantPhos Pd G3 (9.8 mg, 0.010 mmol, 0.10 eq.) were added to a flame dried Schlenk tube under nitrogen atmosphere and suspended in degassed 1,4-dioxane (5 mL). The mixture was heated to 110 °C for 4 h and allowed to cool to room temperature. The reaction mixture was then diluted with ethyl acetate (20 mL), filtered through celite and the organic phase was concentrated under reduced pressure. Purification of the resulting crude product by flash column chromatography (Hexanes/EtOAc gradient, 0-100% EtOAc) yielded **MR-II-266** (47 mg, 0.067 mmol, 65%) as a yellow solid that was directly used in the next step.

¹H NMR (400 MHz, CDCl₃) δ = 8.57 (s, 1H), 8.44 (s, 1H), 8.25 (d, J = 8.1 Hz, 1H), 8.04 (d, J = 8.3 Hz, 1H), 7.97 (d, J = 8.0 Hz, 2H), 7.59 (t, J = 7.4 Hz, 1H), 7.49 (t, J = 7.8 Hz, 2H), 7.45 – 7.34 (m, 3H), 7.31 – 7.11 (m, 3H), 7.01 (dd, J = 8.6, 2.3 Hz, 1H), 6.83 (t, J = 9.4 Hz, 2H), 6.38 (s, 1H), 3.06 – 2.57 (m, 4H), 1.46 (s, 9H) ppm.

¹³C NMR (100 MHz, DMSO) δ = 158.33, 157.82, 157.07, 152.64, 150.93, 150.82, 138.05, 137.94, 137.34, 134.75, 134.47, 130.21, 129.68, 129.30, 129.25, 128.91, 127.20, 125.68, 124.25, 123.25, 120.63, 120.46, 119.79, 118.85, 118.39, 117.72, 117.39, 116.61, 113.45, 80.88, 32.16, 31.99, 28.43 ppm.

LCMS (ESI): $t_{\text{ret}} = 5.49$ min. 706 m/z [M+H]⁺.

(Z)-N2-(5-chloro-4-(1-(phenylsulfonyl)-1H-indol-3-yl)pyrimidin-2-yl)-11,12-dihydrodibenzo[c,g][1,2]diazocine-2,9-diamine (MR-II-278)



MR-II-266 (40.0 mg, 0.057 mmol) was dissolved in a 1:1 TFA:CH₂Cl₂ mixture (2 mL) and stirred for 2 h at room temperature. The reaction mixture was diluted with CH₂Cl₂ (10 mL) and poured into saturated NaHCO₃ (20 mL). The aqueous layer was extracted with a 5:1 CH₂Cl₂:MeOH mixture (20 mL) and the organic phases were washed with saturated NaHCO₃ (2x15 mL) and brine (2x 15 mL), concentrated under reduced pressure and subjected to flash column chromatography (CH₂Cl₂/MeOH gradient, 0-20% MeOH) yielding **MR-II-278** (29 mg, 0.048 mmol, 84%) as a yellow solid.

$R_f = 0.45$ [CH₂Cl₂:MeOH 19:1].

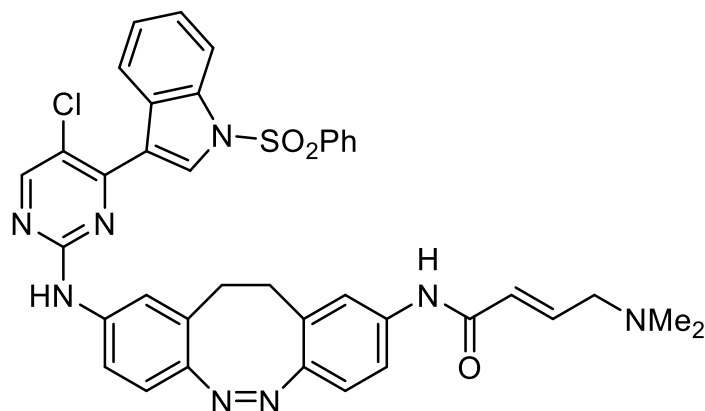
¹H NMR (400 MHz, DMSO-*d*₆) δ = 9.85 (s, 1H), 8.63 (d, *J* = 6.8 Hz, 2H), 8.29 (d, *J* = 7.9 Hz, 1H), 8.12 (d, *J* = 7.7 Hz, 2H), 8.03 (d, *J* = 8.4 Hz, 1H), 7.74 (t, *J* = 7.4 Hz, 1H), 7.64 (t, *J* = 7.8 Hz, 2H), 7.54 (d, *J* = 2.0 Hz, 1H), 7.52 – 7.43 (m, 2H), 7.33 (t, *J* = 7.6 Hz, 1H), 6.74 (d, *J* = 8.5 Hz, 1H), 6.61 (d, *J* = 8.4 Hz, 1H), 6.36 (dd, *J* = 8.4, 2.2 Hz, 1H), 6.21 (d, *J* = 2.1 Hz, 1H), 5.14 (s, 2H), 2.70 – 2.55 (m, 4H) ppm.

¹³C NMR (100 MHz, DMSO) δ = 158.25, 157.89, 155.76, 149.99, 147.82, 145.40, 138.42, 136.43, 135.20, 133.70, 130.10, 129.71, 128.99, 128.55, 128.24, 127.09, 125.73, 124.13, 123.16, 121.10, 119.80, 119.23, 117.49, 116.91, 116.88, 113.46, 112.97, 111.89, 31.62, 31.41 ppm.

HRMS (APCI): calcd. for C₃₂H₂₅ClN₇O₂S⁺: 607.1507 m/z [M+H]⁺.
found: 607.1502 m/z [M+H]⁺.

LCMS (ESI): $t_{ret} = 4.75$ min. 606 m/z [M+H]⁺.

(E)-N-((Z)-9-((5-chloro-4-(1-(phenylsulfonyl)-1H-indol-3-yl)pyrimidin-2-yl)amino)-11,12-dihydrodibenzo[c,g][1,2]diazocin-2-yl)-4-(dimethylamino)but-2-enamide
(MR-II-296)



(E)-4-(dimethylamino)but-2-enoic acid hydrochloride (7.1 mg, 0.043 mmol 1.3 eq.) was suspended in dry THF (1 mL) under a nitrogen atmosphere. Oxalyl chloride (5.4 mg, 0.043 mmol, 0.004 mL, 1.3 eq.) and DMF (0.007 mmol, 0.001 mL, 0.2 eq.) were added at 0 °C, the suspension was ultrasonicated for 30 s and then allowed to warm to room temperature over 2 h. After removal of the volatiles under reduced pressure, **MR-II-278** (20 mg, 0.033 mmol, 1 eq.) was added under a nitrogen atmosphere and the solids were dissolved in THF (2 mL) at 0 °C. DIPEA (17.1 mg, 0.132 mmol, 0.023 mL, 4.0 eq.) was added and the reaction was allowed to warm to room temperature and stirred for a total of 16 h.

The reaction was diluted with a 1:4 *i*PrOH:CHCl₃ mixture (25 mL) and separated against an aqueous Na₂CO₃ solution (1 M, 25 mL). The organic phase was washed with brine (10 mL), dried over Na₂SO₄, and concentrated under reduced pressure. Purification of the resulting crude product by flash column chromatography (CH₂Cl₂/MeOH gradient, 0-20% MeOH) yielded **MR-II-296** (13.2 mg, 0.018 mmol, 56%) as a yellow solid.

$R_f = 0.39$ [CH₂Cl₂:MeOH 19:1].

¹H NMR (400 MHz, CDCl₃) δ = 8.55 (s, 1H), 8.41 (s, 1H), 8.24 (d, J = 8.0 Hz, 1H), 8.02 (d, J = 8.4 Hz, 1H), 7.96 (d, J = 7.9 Hz, 2H), 7.58 (t, J = 7.4 Hz, 1H), 7.48 (t, J = 7.7 Hz, 2H), 7.45 – 7.35 (m, 4H), 7.32 – 7.18 (m, 4H), 6.88 (dt, J = 14.9, 6.0 Hz, 1H), 6.82 (d, J = 8.4 Hz, 2H), 6.06 (d, J = 15.2 Hz, 1H), 3.08 (d, J = 5.6 Hz, 2H), 3.00 – 2.55 (m, 4H), 2.24 (s, 6H) ppm.

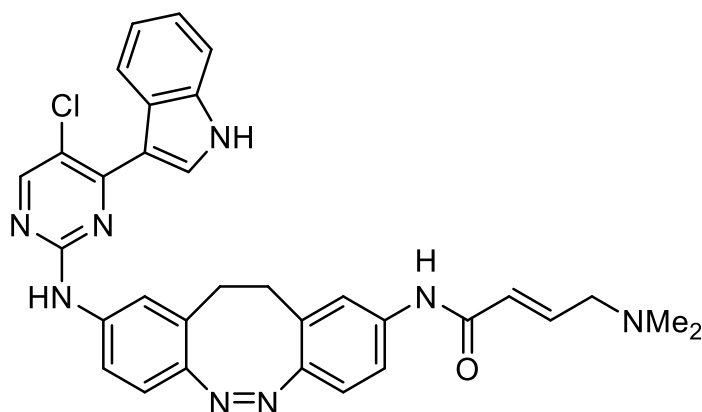
¹³C NMR (100 MHz, CDCl₃) δ = 163.48, 158.28, 157.82, 157.00, 151.97, 150.77, 142.05, 138.15, 137.88, 136.94, 134.71, 134.48, 130.15, 129.67, 129.41, 129.13, 128.88, 127.17, 126.20, 125.68, 124.23, 123.27, 120.51, 120.48, 120.20, 119.85, 118.39, 118.01, 117.71, 117.42, 113.42, 60.21, 45.41, 32.13, 31.81 ppm.

HRMS (APCI): calcd. for C₃₈H₃₄ClN₈O₃S⁺: 717.2158 m/z [M+H]⁺.

found: 717.2155 m/z [M+H]⁺.

LCMS (ESI): t_{ret} = 3.92 min. 717 m/z [M+H]⁺.

(E)-N-((Z)-9-((5-chloro-4-(1H-indol-3-yl)pyrimidin-2-yl)amino)-11,12-dihydro-dibenzo[c,g][1,2]diazocin-2-yl)-4-(dimethylamino)but-2-enamide (MR-II-309)



MR-II-296 (13.0 mg, 0.018 mmol, 1.0 eq.) was dissolved in aqueous NaOH (1 M, 1 mL) and stirred for 2 h at room temperature. The reaction was quenched with aqueous HCl (1 M, 1 mL) and diluted with saturated NaHCO₃ (5 mL). The aqueous phase was extracted with a 5:1 CH₂Cl₂:iPrOH mixture (2x20 mL) and the organic phase was washed with brine (10 mL), dried over Na₂SO₄, and concentrated under reduced pressure. Purification of the resulting crude product by preparative thin layer chromatography (CH₂Cl₂:MeOH, 6:1) gave **MR-II-309** (4.5 mg, 0.008 mmol, 43%) as a yellow solid.

R_f = 0.12 [CH₂Cl₂:MeOH 6:1].

¹H NMR (600 MHz, DMSO-*d*₆) δ = 11.94 (s, 1H), 10.20 (s, 1H), 9.65 (s, 1H), 8.53 – 8.43 (m, 3H), 7.63 (s, 1H), 7.54 (d, *J* = 8.6 Hz, 1H), 7.51 (d, *J* = 8.1 Hz, 1H), 7.49 – 7.47 (m, 1H), 7.46 – 7.43 (m, 1H), 7.24 (t, *J* = 7.5 Hz, 1H), 7.13 (t, *J* = 7.6 Hz, 1H), 6.83

(dd, $J = 21.9, 8.5$ Hz, 2H), 6.68 (dt, $J = 14.5, 6.6$ Hz, 1H), 6.29 (d, $J = 15.3$ Hz, 1H), 3.52 – 3.43 (m, 2H), 2.90 – 2.61 (m, 4H), 2.45 (s, 6H) ppm.

^{13}C NMR (150 MHz, DMSO) $\delta = 162.98, 158.47, 158.24, 157.61, 151.52, 149.91, 139.79, 138.22, 136.54, 131.62, 129.28, 128.69, 126.49, 123.21, 123.01, 121.19, 120.15, 120.02, 119.58, 118.08, 117.91, 115.98, 112.39, 111.16, 58.48, 43.88, 32.10, 31.60$ ppm.

HRMS (APCI): calcd. for $\text{C}_{64}\text{H}_{57}\text{Cl}_2\text{N}_{16}\text{O}^+$: 1135.4273 m/z $[\text{2M}+\text{H}-\text{H}_2\text{O}]^+$.

 found: 1135.4317 m/z $[\text{2M}+\text{H}-\text{H}_2\text{O}]^+$.

LCMS (ESI): $t_{\text{ret}} = 3.70$ min. 577 m/z $[\text{M}+\text{H}]^+$.

References

- [1] G. Manning, D. B. Whyte, R. Martinez, T. Hunter, S. Sudarsanam, *Science* **2002**, *298*, 1912–1934.
- [2] F. M. Ferguson, N. S. Gray, *Nat. Rev. Drug Discov.* **2018**, *17*, 353–377.
- [3] D. Essegian, R. Khurana, V. Stathias, S. C. Schürer, *Cell Rep. Med.* **2020**, *1*, 100128.
- [4] Q. Liu, Y. Sabnis, Z. Zhao, T. Zhang, S. J. Buhrlage, L. H. Jones, N. S. Gray, *Chem. Biol.* **2013**, *20*, 146–159.
- [5] A. Chaikuad, P. Koch, S. A. Laufer, S. Knapp, *Angew. Chem. Int. Ed.* **2018**, *57*, 4372–4385.
- [6] T. Zhang, J. M. Hatcher, M. Teng, N. S. Gray, M. Kostic, *Cell Chem. Biol.* **2019**, *26*, 1486–1500.
- [7] C. L. Fleming, M. Grøtli, J. Andréasson, *ChemPhotoChem* **2019**, *3*, 318–326.
- [8] M. Schehr, C. Ianes, J. Weisner, L. Heintze, M. P. Müller, C. Pichlo, J. Charl, E. Brunstein, J. Ewert, M. Lehr, U. Baumann, D. Rauh, U. Knippschild, C. Peifer, R. Herges, *Photochem. Photobiol. Sci.* **2019**, *18*, 1398–1407.
- [9] R. Siewertsen, H. Neumann, B. Buchheim-Stehn, R. Herges, C. Näther, F. Renth, F. Temps, *J. Am. Chem. Soc.* **2009**, *131*, 15594–15595.
- [10] R. Siewertsen, J. B. Schönborn, B. Hartke, F. Renth, F. Temps, *Phys. Chem. Chem. Phys.* **2010**, *13*, 1054–1063.
- [11] T. Zhang, F. Inesta-Vaquera, M. Niepel, J. Zhang, S. B. Ficarro, T. Machleidt, T. Xie, J. A. Marto, N. Kim, T. Sim, J. D. Laughlin, H. Park, P. V. LoGrasso, M. Patricelli, T. K. Nomanbhoy, P. K. Sorger, D. R. Alessi, N. S. Gray, *Chem. Biol.* **2012**, *19*, 140–154.
- [12] N. Kwiatkowski, T. Zhang, P. B. Rahl, B. J. Abraham, J. Reddy, S. B. Ficarro, A. Dastur, A. Amzallag, S. Ramaswamy, B. Tesar, C. E. Jenkins, N. M. Hannett, D. McMillin, T. Sanda, T. Sim, N. D. Kim, T. Look, C. S. Mitsiades, A. P. Weng, J. R. Brown, C. H. Benes, J. A. Marto, R. A. Young, N. S. Gray, *Nature* **2014**, *511*, 616–620.
- [13] S. Kalan, R. Amat, M. M. Schachter, N. Kwiatkowski, B. J. Abraham, Y. Liang, T. Zhang, C. M. Olson, S. Larochelle, R. A. Young, N. S. Gray, R. P. Fisher, *Cell Rep.* **2017**, *21*, 467–481.
- [14] S. C. Sivakumaren, H. Shim, T. Zhang, F. M. Ferguson, M. R. Lundquist, C. M. Browne, H.-S. Seo, M. N. Paddock, T. D. Manz, B. Jiang, M.-F. Hao, P. Krishnan, D. G. Wang, T. J. Yang, N. P. Kwiatkowski, S. B. Ficarro, J. M. Cunningham, J. A. Marto, S. Dhe-Paganon, L. C. Cantley, N. S. Gray, *Cell Chem. Biol.* **2020**, *27*, 525-537.e6.
- [15] E. T. Coffey, *Nat. Rev. Neurosci.* **2014**, *15*, 285–299.
- [16] P. Koch, M. Gehringer, S. A. Laufer, *J. Med. Chem.* **2015**, *58*, 72–95.
- [17] G. Solinas, B. Becattini, *Mol. Metab.* **2017**, *6*, 174–184.
- [18] J.-J. Ventura, A. Hübner, C. Zhang, R. A. Flavell, K. M. Shokat, R. J. Davis, *Mol. Cell* **2006**, *21*, 701–710.
- [19] W. A. Velema, W. Szymanski, B. L. Feringa, *J. Am. Chem. Soc.* **2014**, *136*, 2178–2191.

- [20] P. Kaldis, *Cell. Mol. Life Sci. CMLS* **1999**, *55*, 284–296.
- [21] R. Shiekhattar, F. Mermelstein, R. P. Fisher, R. Drapkin, B. Dynlacht, H. C. Wessling, D. O. Morgan, D. Reinberg, *Nature* **1995**, *374*, 283–287.
- [22] J.-M. Egly, F. Coin, *DNA Repair* **2011**, *10*, 714–721.
- [23] B.-B. Li, B. Wang, C.-M. Zhu, D. Tang, J. Pang, J. Zhao, C.-H. Sun, M.-J. Qiu, Z.-R. Qian, *Chronic Dis. Transl. Med.* **2019**, *5*, 155–169.
- [24] S. Diab, M. Yu, S. Wang, *J. Med. Chem.* **2020**, DOI 10.1021/acs.jmedchem.9b01985.
- [25] K. A. Nilson, J. Guo, M. E. Turek, J. E. Brogie, E. Delaney, D. S. Luse, D. H. Price, *Mol. Cell* **2015**, *59*, 576–587.
- [26] G. He, X. Yang, G. Wang, J. Qi, R. Mao, Z. Wu, Z. Zhou, *Front. Mol. Neurosci.* **2017**, *10*, DOI 10.3389/fnmol.2017.00365.
- [27] C. L. Christensen, N. Kwiatkowski, B. J. Abraham, J. Carretero, F. Al-Shahrour, T. Zhang, E. Chipumuro, G. S. Herter-Sprie, E. A. Akbay, A. Altabef, J. Zhang, T. Shimamura, M. Capelletti, J. B. Reibel, J. D. Cavanaugh, P. Gao, Y. Liu, S. R. Michaelsen, H. S. Poulsen, A. R. Aref, D. A. Barbie, J. E. Bradner, R. E. George, N. S. Gray, R. A. Young, K.-K. Wong, *Cancer Cell* **2014**, *26*, 909–922.
- [28] F. Muth, A. El-Gokha, F. Ansideri, M. Eitel, E. Döring, A. Sievers-Engler, A. Lange, F. M. Boeckler, M. Lämmerhofer, P. Koch, S. A. Laufer, *J. Med. Chem.* **2017**, *60*, 594–607.
- [29] M. S. Maier, K. Hüll, M. Reynders, B. S. Matsuura, P. Leippe, T. Ko, L. Schäffer, D. Trauner, *J. Am. Chem. Soc.* **2019**, *141*, 17295–17304.
- [30] M. Borowiak, W. Nahaboo, M. Reynders, K. Nekolla, P. Jalinot, J. Hasserodt, M. Rehberg, M. Delattre, S. Zahler, A. Vollmar, D. Trauner, O. Thorn-Seshold, *Cell* **2015**, *162*, 403–411.

11 – An Oxidative Approach Enables Efficient Access to Cyclic Azobenzenes

Martin S. Maier^{1,2}, Katharina Hüll^{1,2,‡}, Martin Reynders^{1,2,‡}, Bryan S. Matsuura^{1,2,‡}, Philipp Leippe², Tongil A. Ko¹, Lukas Schäffer² and Dirk Trauner^{1,2,*}

¹Department of Chemistry, New York University, New York, NY 10003, USA.

²Department of Chemistry, Ludwig Maximilians University of Munich 81377 Munich, Germany.

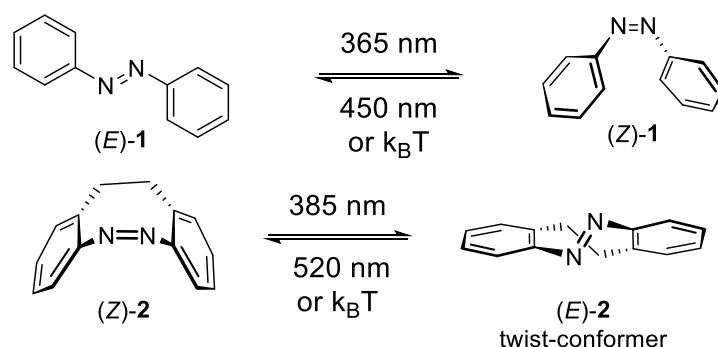
[‡]These authors contributed equally.

Abstract

Azobenzenes are versatile photoswitches that have found widespread use in a variety of fields, ranging from photo-pharmacology to the material sciences. In addition to regular azobenzenes the cyclic diazocines have recently emerged. Although diazocines have fascinating conformational and photophysical properties, their use has been limited by their synthetic accessibility. Herein, we present a general, high-yielding protocol that relies on the oxidative cyclization of dianilines. In combination with a modular substrate synthesis, it allows for rapid access to diversely functionalized diazocines on gram scales. Our work systematically explores substituent effects on the photoisomerization and thermal relaxation of diazocines. It will enable their incorporation into a wide variety of functional molecules, unlocking the full potential of these emerging photoswitches. The method can be applied to the synthesis of a new cyclic azobenzene with a nine-membered central ring and distinct properties.

Introduction

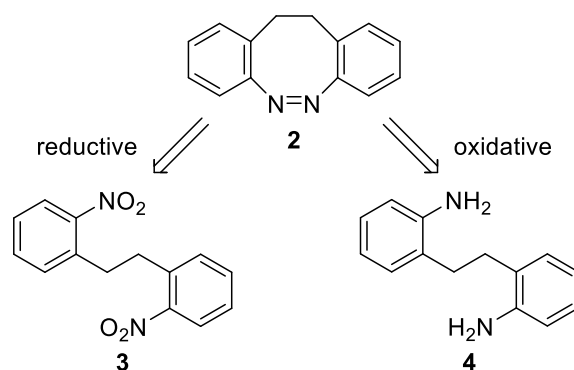
Azobenzene photoswitches contain a diaryl diazene moiety that can exist either in an (*E*) or in a (*Z*) configuration. In general, the elongated (*E*) or *trans* form is thermodynamically preferred and the bent (*Z*) or *cis* form is subject to gradual thermal isomerization (Scheme 11.1). The half-lives for this thermal relaxation range from picoseconds to days,^[1] and photoswitches whose thermal relaxation is comparatively slow are often designated as “bistable”. Irradiation of azobenzenes with monochromatic light establishes a photostationary state (PSS) that depends on both the extinction coefficients of the two isomers at a particular wavelength and their respective isomerization quantum yields. Photostationary states as high as (*Z*)/(*E*) \approx 90/10 can be achieved but are generally lower.^[2–4] Due to their photostability, facile synthesis and relatively low molecular weight, azobenzenes have become the photoswitch of choice in many applications. They have been successfully incorporated in photopharmaceuticals, in photoresponsive functional materials, such as polymers and hydrogels, or in catalysts that can be controlled with light.^[5–11]



Scheme 11.1. Photoswitching of azobenzene (**1**)^[1] compared to diazocine (**2**)^[22]

Despite their long history and popularity, there is still a need to tailor the properties of azobenzenes. One important direction is red shifting the action spectra whilst maintaining thermal bistability.^[12–20] Significant progress towards this goal has been made by developing tetra-*ortho*-substituted azobenzenes, but these are marked by increased steric bulk and changes in dipole moment, which can interfere with their function. Another desirable feature are highly biased PSS, both for wavelengths that favor the (*Z*) isomer and those that give preference to the (*E*) isomer. Although thermal relaxation can revert azobenzenes fully to their (*E*) form, this process can be slow with bistable variants and the faster photochemical conversion to the (*E*) isomer is generally

incomplete. Lastly, it can be useful to employ photoswitches that are bent in their default form, i.e. in the absence of light, and become elongated upon irradiation. This is especially true in photopharmacology where tonic “dark-activity” is often undesirable. Cyclic azobenzenes, wherein the diazene unit is embedded in an eight-membered ring, meet many of these challenges. The parent compound of this class is 5,6-dihydrodibenzo[*c,g*][1,2]diazocine (“diazocine”), which had already been discovered at the beginning of the last century.^[21] It found little attention until recently, when its remarkable photophysical properties were recognized by Herges and Temps.^[22,23] Contrary to regular azobenzenes, the thermodynamically preferred form of diazocines is the (*Z*) isomer due to the increased strain that the ring-system imposes on the (*E*) isomer (Scheme 11.1). In addition, diazocines can be switched to more than 90% of the (*E*) isomer and quantitatively back to the (*Z*) isomer by irradiation with visible wavelengths around 400 nm and 520 nm, respectively.^[22]



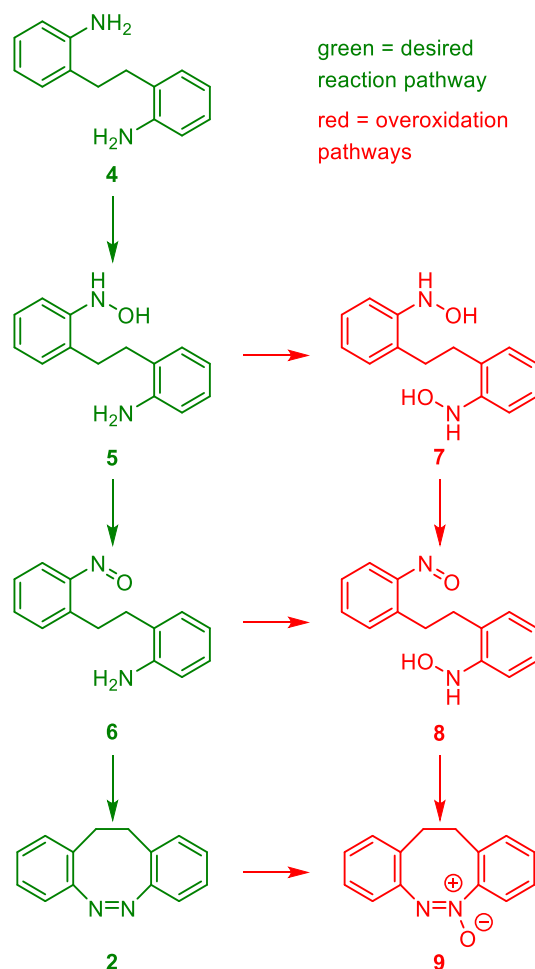
Scheme 11.2. Synthetic approaches towards the diazocine core.

Despite these remarkable photophysical properties, diazocines have found relatively few applications to date. The reason for this has been their limited availability due to lack of effective synthetic methods.^[21,22,24–44] Most reported diazocines have been synthesized by a reductive cyclization of 2,2'-dinitrodibenzyls (Scheme 11.2).^[21,22,24–38,41–43] Apart from low yields, a major limitation of the reductive cyclization is that it does not give straightforward access to unsymmetrical diazocines.^[32–38,41–43] In addition to the reductive cyclization approach, conditions based on oxidation of 2,2'-ethylenedianilines or hydroxylamine-aniline analogs have been reported, albeit with low to mediocre yields.^[39,40,42] Very recently, an oxidative strategy has been applied in a synthesis of a photoswitchable glutamate derivative.^[40] However, the potential of the oxidative cyclization of 2,2'-ethylenedianilines has not been

investigated systematically and a practical, generally applicable and high-yielding protocol for the synthesis diazocines has been lacking.

Results

1. Mechanistic considerations. Our investigation commenced with the optimization of reaction conditions for the oxidative cyclization of the commercially available 2,2'-ethylenedianiline **4** to the corresponding diazocine **2**. We considered four key requirements which needed to be fulfilled to make this an effective process (Scheme 11.3). First, it would be necessary to selectively oxidize 2,2'-ethylenedianiline **4** to 2-amino-2'-nitrosodibenzyl **6**, without formation of the dihydroxylamine **7** from intermediate **5**. Second, the cyclization of the nitroso-aniline **6** to diazocine **2** via a Baeyer-Mills reaction has to be faster than the oxidation to nitroso-hydroxylamine **8**.



Scheme 11.3. Mechanistic considerations for an oxidative cyclization approach towards diazocines.

Third, the product diazocine **2** must not be oxidized further to form the azoxy compound **9**. Fourth, intermolecular reactions leading to oligomeric or polymeric structures need to be suppressed. While temperature, concentration, and rate of addition of the oxidant are important considerations for optimization with respect to the second and fourth conditions, the other two conditions are more dependent on the inherent reactivity of the substrates. Based on our mechanistic scheme, we expected slow addition of the oxidant to be the most important parameter.

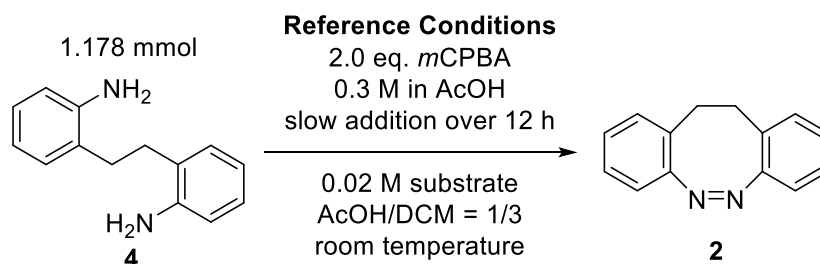
2. Development of reaction conditions. Most commonly, the oxidation of anilines to nitrosobenzenes is performed in a biphasic system of DCM/water using Oxone[®] as an oxidant. The ensuing Baeyer-Mills reaction is typically performed in acetic acid and mixtures of acetic acid with DCM or toluene. As these two sets of conditions are not compatible, we decided to use typical solvent-systems of the Baeyer-Mills reaction, such as pure acetic acid or acetic acid/DCM, as the solvent and peroxyacetic acids as the oxidant. To simplify the workup, we initially focused on peracetic acid.

After optimization of oxidant addition rate, stoichiometry and substrate concentrations, we were able to obtain diazocine **2** by the slow addition of two equivalents of peracetic acid in acetic acid to a dilute solution of 2,2'-ethylenedianiline **4** within a twelve hour period in a yield of more than 70%, which was already substantially superior to any previously reported value.^[21,22,24–44] However, we noticed several inconsistencies during the course of this initial optimization. The most important observations were a noticeably fluctuating yield, a highly detrimental effect of copper salts as well as an unexpected relation between the obtained yields and the equivalents of peracetic acid that were employed.

We suspected the underlying issue to be the presence of considerable amounts of hydrogen peroxide in the commercial peracetic acid solutions. This “dormant oxidant” may either directly participate in the oxidation or slowly be transformed to peracetic acid, thus resulting in an incorrect stoichiometry. The effect can be expected to be more prominent under conditions that should activate the hydrogen peroxide (e.g. the presence of transition metal ions), which agrees with the observed results. Additionally, we confirmed the reactivity of hydrogen peroxide in acetic acid by treatment of 2,2'-ethylenedianiline with urea hydrogen peroxide as a source of “dry” hydrogen peroxide. This led to the slow formation of diazocine, but could unfortunately not be developed into a synthetically practical procedure.

Building on the knowledge gained from our initial optimization with peracetic acid, we continued our search for optimal reaction conditions (Table 11.1). We did not perform an additional screening on the rate of addition as well as equivalents of oxidant and continued with the theoretically ideal stoichiometry of two equivalents of oxidant and the addition of oxidant within twelve hours. To identify a more reliable oxidant we compared the most commonly employed commercially available percarboxylic acids. Among peracetic acid, *m*CPBA and MMPP, we found that *m*CPBA performed best. The use of *m*CPBA to prepare nitrosobenzenes from anilines is well precedented.^[45–47] A screen of solvent mixtures revealed that diluting acetic acid with DCM or toluene resulted in a further increased yield, although a sizeable fraction of acetic acid was necessary for optimal results. Increasing the temperature proved to be slightly detrimental to the reaction outcome, while higher concentrations of the *m*CPBA solution (0.6 M) and substrate (0.04 M) were tolerated without a negative effect on the yield.

Copper salts were reported to be beneficial to the formation of azobenzenes by oxidative dimerization of anilines with peroxy acids.^[48] However, we observed that addition of copper acetate reduced the yield and an increased amount of unreacted starting material remained. This supports that our reaction does not depend on trace amounts of metal salts. Finally, we confirmed that the undesired overoxidation of diazocine **2** to azoxy compound **9** does not occur in the presence of unreacted dianiline **4** (see Supporting Information). This finding supports our initial reasoning about the importance of slow addition. Azoxy compound **9** does not primarily result from oxidation of desired product **2**, but forms through nitroso-hydroxylamine **8** (see Scheme 11.3).



Entry	Variation from Reference Conditions	Yield ^a
1	none	86%
2	Solvent AcOH	75%
3	Solvent AcOH/DCM = 1/1	86%
4	Solvent AcOH/PhMe = 1/1	84%
5	Solvent AcOH/DCM = 1/9	81%
6	Entry 4 + 40 °C	82%
7	Entry 4 + 60 °C	76%
8	0.01 M substrate	85%
9	0.04 M substrate	85%
10	Entry 9 + 0.6 M <i>m</i> CPBA	86%
11	Entry 10 + 0.06 M substrate	79%
12	Entry 10 + catalytic Cu(II)	59%

Table 11.1. Optimization of the oxidative cyclization of 2,2'-ethylenedianiline – selected examples. ^aDetermined by ¹H-NMR spectroscopy with dimethyl terephthalate as internal standard.

3. Investigation of reaction scope. After optimizing reaction conditions for the parent system, we applied our best protocol to various monosubstituted 2,2'-ethylenedianilines (compounds **10–30**, Table 11.2). For a majority of these compounds, we obtained the cyclization products in yields similar to or only slightly lower than observed for the parent system. Substituents that only weakly affect the electronic nature of the arenes, such as most halogens and alkyl groups, had virtually no effect on the yield of the cyclization. The yields observed for the fluorinated compounds followed a trend, decreasing from *para*- to *meta*- to *ortho*-fluoro substitution.

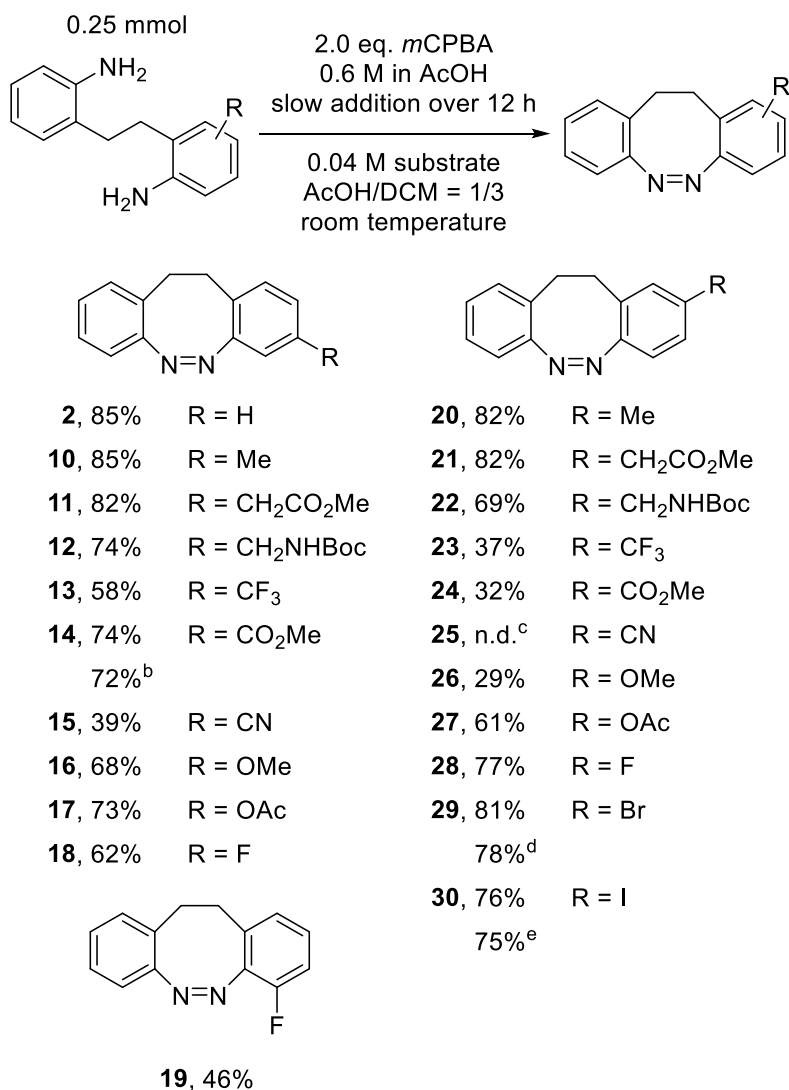
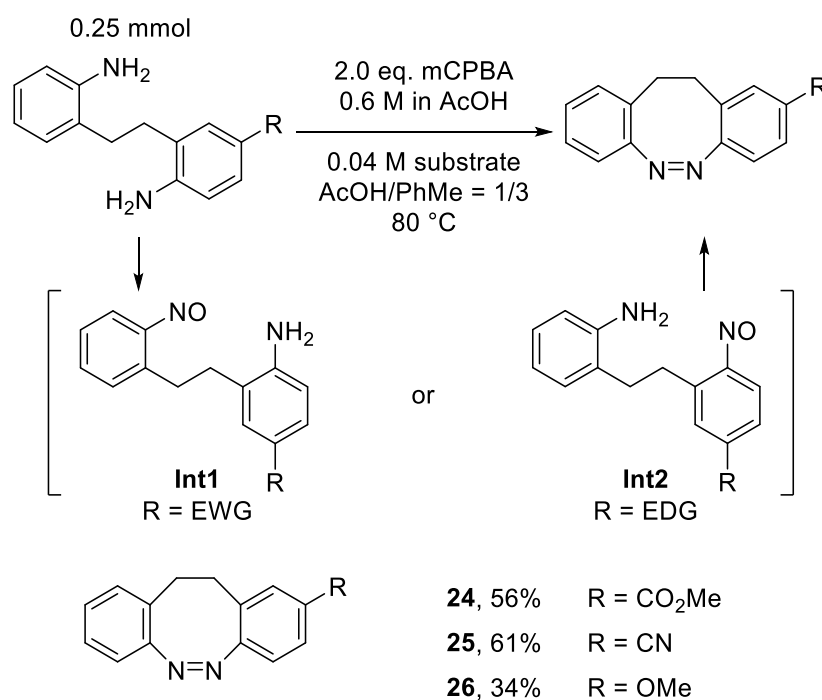


Table 11.2. Oxidative cyclization yields^a of monosubstituted 2,2'-ethylenedianilines. ^aIsolated yields are reported. ^b4.28 mmol scale. ^cNot determined. ^d7.90 mmol scale. ^e7.69 mmol scale.

Notably, the presence of both strongly electron-withdrawing and electron-donating substituents resulted in a significant reduction in yield. *Para*-substituted substrates gave generally lower yields than the corresponding *meta*-substituted ones, both for electron-withdrawing and electron-donating substituents. We reasoned that low-yielding substrates would undergo a highly selective oxidation of one of the two amino groups (see Scheme 11.4). In the corresponding intermediates **Int1** and **Int2** the more nucleophilic aniline moiety is now oxidized, which leaves a deactivated aniline moiety in **Int1** and a deactivated nitrosobenzene moiety in **Int2**. This would make the subsequent Baeyer-Mills cyclization comparatively slow in both cases.

Additionally, the tendency for intermolecular, instead of intramolecular, reactions would be increased, as the unreacted substrates (not shown) carry a more reactive amino group than the corresponding intermediates **Int1** and **Int2**. These considerations led us to explore whether, instead of the slow addition protocol, one-batch addition and increased temperatures might be beneficial in these cases.

We tested this alternative protocol for the three compounds that were the most problematic for our slow addition method (Scheme 11.4). Gratifyingly, we now obtained the known^[32] *para*-cyano diazocine **25** in a respectable yield of 61%. The yield of the *para*-methyl ester diazocine **24** also was improved substantially to 56%. However, the *para*-methoxy product **26** was only obtained with slightly increased yield. A different factor seems to affect the yield in this case. The most probable explanation is the reactivity of *para*-alkoxy-nitrosobenzenes towards nucleophilic aromatic substitution.^[49]



Scheme 4. Synthesis of diazocines using a one-batch addition protocol and presumed intermediates due to oxidation selectivity.

Next, we turned our attention towards disubstituted diazocines (compounds **31–41**, Table 11.3). Considering the large number of combinatorial possibilities, we selected only a small number of examples. Our main goals were to obtain an appropriate set of disubstituted diazocines to investigate the photophysical properties of substituted

diazocines, to determine the limitations of our approach and to explore how substituent effects of the monosubstituted substrates extend to disubstituted substrates.

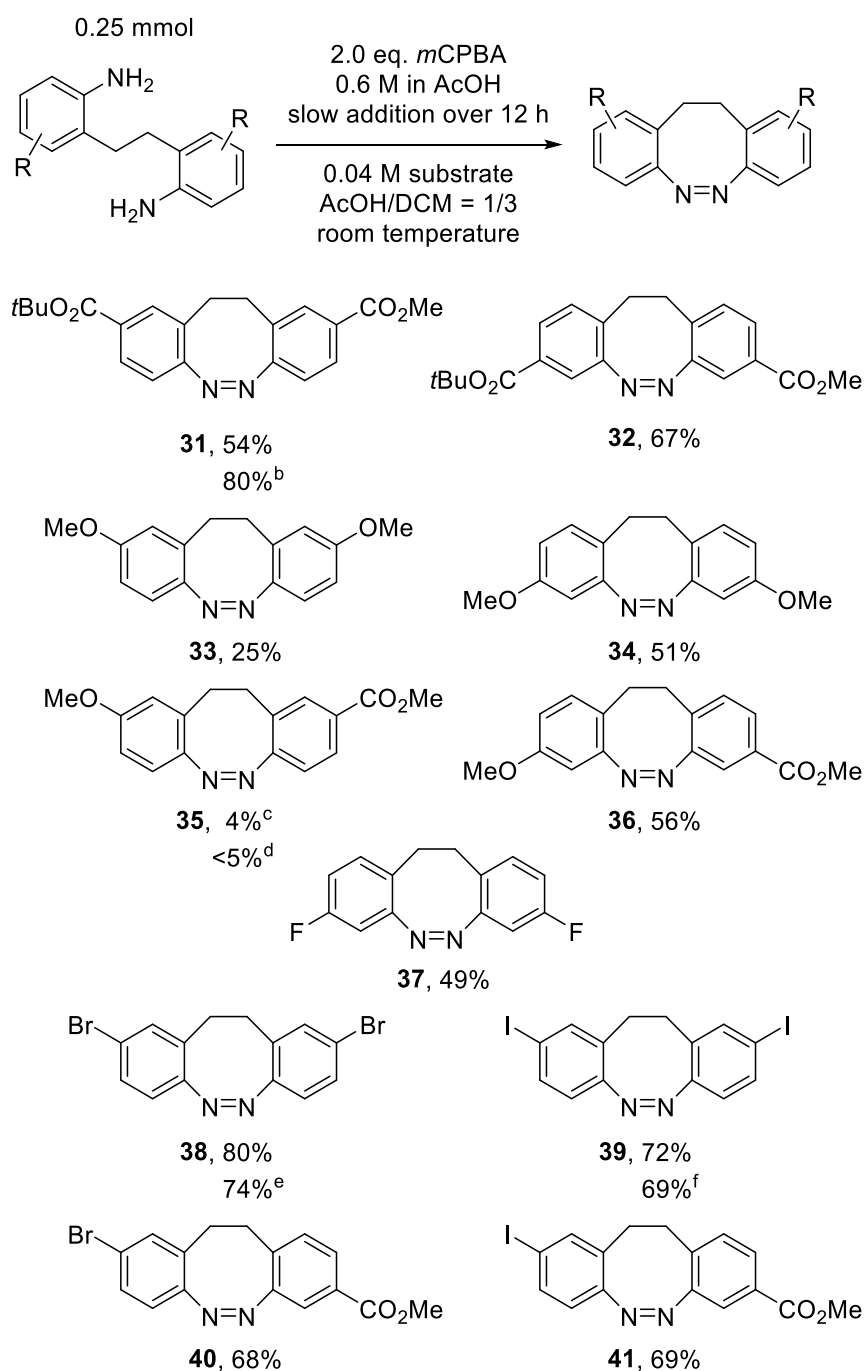
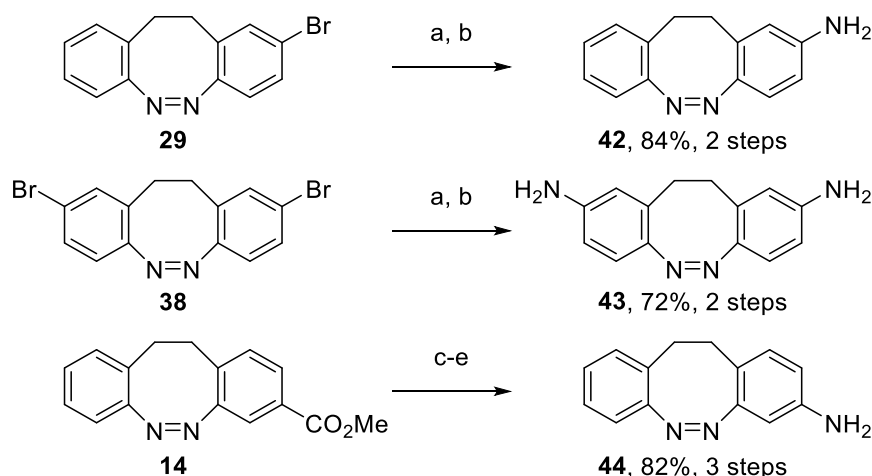


Table 11.3. Oxidative cyclization yields^a of disubstituted 2,2'-ethylenedianilines. ^aIsolated yields are reported. ^b80 °C. ^c0.832 mmol scale, 0.03 M substrate. ^d0.156 mmol scale, batch addition protocol. ^e7.16 mmol scale. ^f7.87 mmol scale.

Employing our standard slow addition protocol, we observed that for most compounds the substituent effects were additive. The yields decreased compared to the

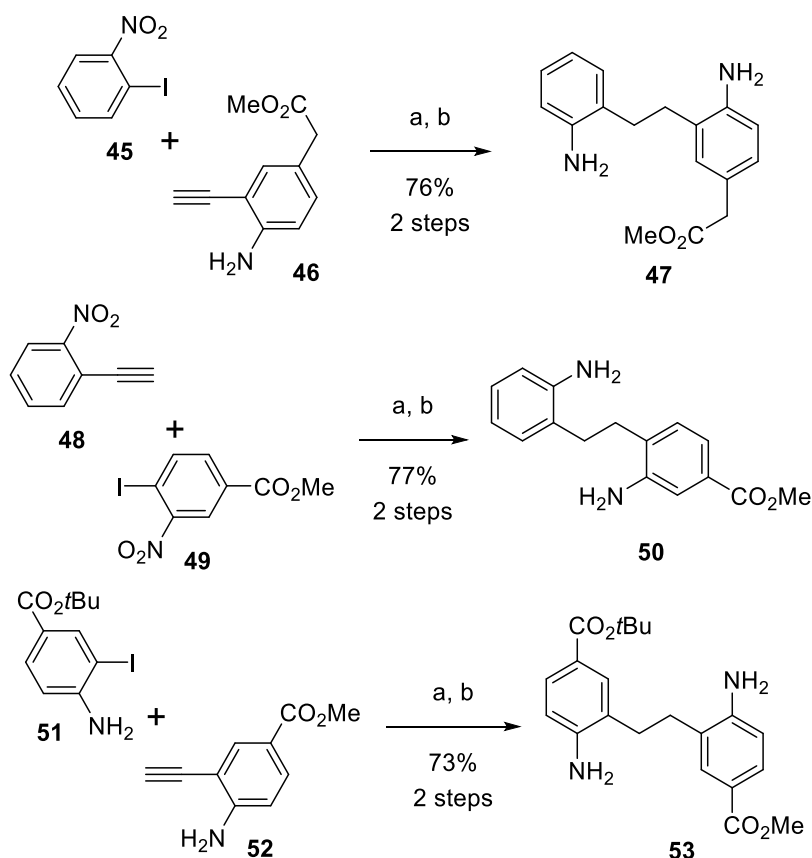
corresponding monosubstituted analogs but remained in a synthetically useful range. A clear exception was found in the *para*-diester compound **31**, where the yield was significantly increased compared to the *para*-ester **24**. Performing the reaction at higher temperature further increased the yield to 80%, a level similar to the parent compound **5**. An example that shows a limitation of our approach, for both the slow and batch addition protocols, is the push-pull diazocine **35**. Still, we were able to obtain a sufficient quantity for photophysical characterization of this diazocine.

4. Late-stage derivatization. Despite the large number of mono- and disubstituted diazocines accessible with our oxidative method, it could not readily deliver amino substituted diazocines. Therefore, we developed a practical late-stage derivatization (Scheme 11.5). The known *para*-amino-diazocine **42**^[34] was synthesized in 84% yield from the *para*-bromo diazocine **29**^[32] by Buchwald-Hartwig coupling with *tert*-butyl carbamate, followed by deprotection of the Boc group by treatment with TBAF.^[50] Although the TFA protocol could be used, TBAF afforded a cleaner product and avoided side reactions resulting from the presence of *tert*-butyl cations. The known *para*-diamino diazocine **43**^[26] was prepared in 72% yield in an identical fashion to the monoamino compound **42**. To access the *meta*-amino diazocine **44**, we started from *meta*-ester **14**. Ester hydrolysis followed by Curtius rearrangement in the presence of allyl alcohol, followed by removal of the Alloc group gave the desired product **44** in 82% yield.



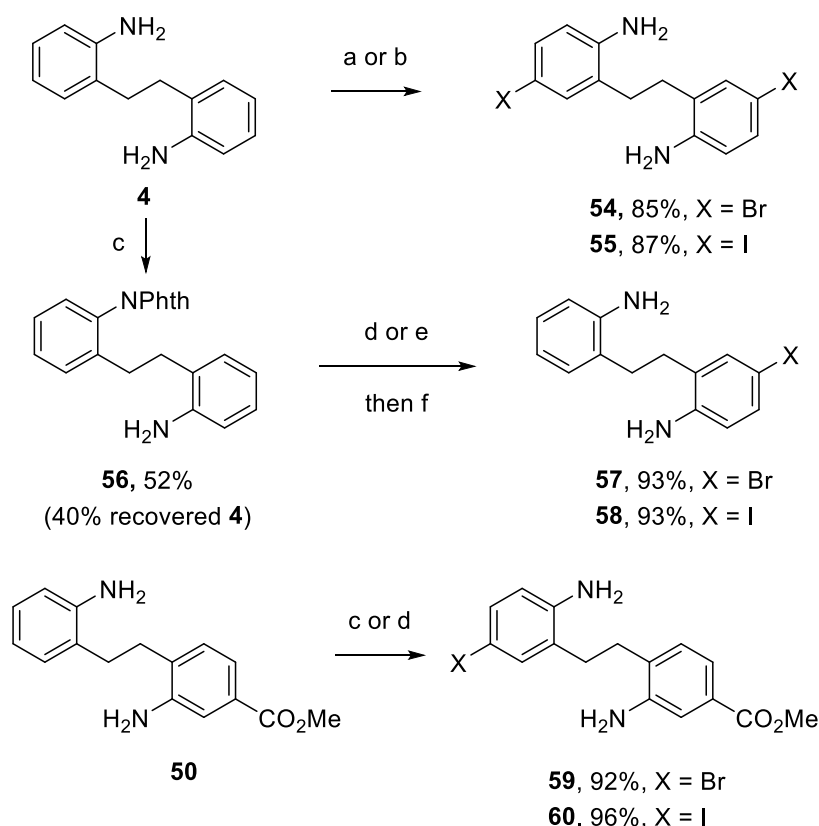
Scheme 11.5. Late-stage diversification. a) BocNH₂, Cs₂CO₃, XantPhos Pd G3, 1,4-dioxane, 100 °C; b) TBAF·3H₂O, Me-THF, 70 °C; c) LiOH, THF/MeOH/H₂O; d) Allyl alcohol, DPPA, Et₃N, PhMe, RT to 80 °C; e) pyrrolidine, Pd(PPh₃)₄, DCM.

5. Cyclization substrate synthesis. A major advantage of the oxidative cyclization approach is the relative ease with which the requisite 2,2'-ethylenedianilines can be accessed. To this end, we developed a Sonogashira coupling strategy, which is exemplified in Scheme 11.6. Several combinations of alkynes and aryl halides are possible, pending on the nature of the coupling partners and their oxidation states. The first and most useful variant is based on the coupling of a 2-aminophenylacetylene with 2-iodonitro-benzene, as depicted for dianiline **47**. The second route proceeds through the coupling of a 2-nitrophenylacetylene with a 2-iodonitrobenzene, which is exemplified for compound **50**. In some cases, however, considerable decomposition of the 2-nitrophenylacetylenes was observed under the conditions of the Sonogashira coupling.^[51–57] The third route involved the coupling of a 2-amino-phenylacetylene with a 2-iodoaniline as shown for dianiline **53**. This route is less general, as 2,2'-diamino-diphenylacetylenes tend to undergo cyclization to indoles.^[58–62] Regarding the hydrogenation of the diarylacetylenes, we found that substrates must not contain any contaminants remaining from the Sonogashira reaction. Otherwise, we observed significant catalyst poisoning resulting in unreasonably high catalyst loading. Since our cross-coupling approach involves a hydrogenation step that is not compatible with aryl halides, we prepared several halo-substituted dianilines via electrophilic aromatic substitution (Scheme 11.7).



Scheme 11.6. Example 2,2'-ethylenedianiline syntheses by Sonogashira coupling/hydrogenation. a) $\text{PdCl}_2(\text{PPh}_3)_2$, CuI , Et_3N , THF, RT; then TMS-acetylene; b) H_2 , Pd/C, MeOH/DCM.

While the synthesis of the precursors leading to the symmetrical *para*-dihalogenated compounds **54** and **55** was straightforward, access to precursors of monohalo diazocines was more difficult. We initially used an unselective, statistical halogenation followed by purification via chromatography and precipitation. However, to avoid the tedious separation of mono- and dihalogenation products, as well as unreacted substrate, we developed a more scalable and practical sequence. Desymmetrization of the commercially available dianiline **4** by protection of one amino group as the phthalimide, followed by highly selective halogenation of phthalimide **56** and deprotection allowed to access the desired products **57** and **58** without any chromatographic purification. Selective halogenation could also be achieved by exploiting electronic differences in substituted dianilines. We tested this on ester **50**, which afforded the halogenation products **59** and **60** in high yield and without any undesired isomers.



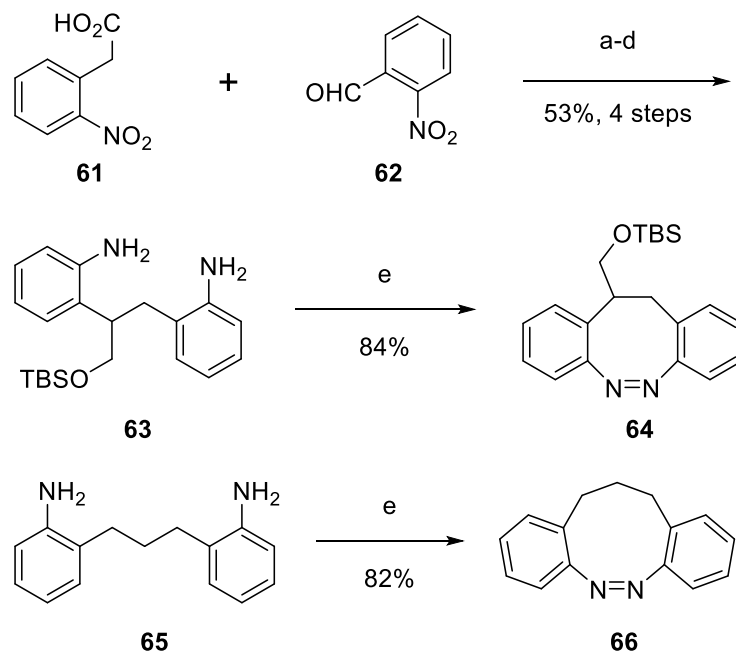
Scheme 11.7. Halogenation of 2,2'-ethylenedianilines. a) NBS (2 eq.), DMSO; b) NIS (2 eq.), DMSO; c) phthalic anhydride, BSA, PhMe, reflux; d) NBS (1 eq.), DMSO; e) NIS (1 eq.), DMSO; f) $\text{N}_2\text{H}_4 \cdot \text{H}_2\text{O}$, THF, reflux.

6. New Cyclic Azobenzenes. Cyclic azobenzenes may not only be substituted on their arene moieties but also on their central ring.^[38,40] Indeed, several hetero-diazocines have recently emerged.^[41–44] Confident in our new methodology, we have begun to explore cyclic azobenzenes with substitutions on the central bridge and with an increased ring size (Scheme 11.8).

Condensation^[63] of aldehyde **62** with acid **61**, followed by carboxylic acid reduction, TBS-protection and hydrogenation afforded cyclization precursor **63** in 53% yield over four steps. The oxidative cyclization of the dianiline **63** to diazocine **64** proceeded in 84% yield, which is virtually the same efficiency as for the unsubstituted parent system. The dianiline **65**^[64] could be cyclized equally well to diazonine **66**, affording the first cyclic azobenzene that features a propylene bridge in the central ring.

Both syntheses of dianilines **63** and **65** can in principle be adapted to allow access to symmetric and non-symmetric substitution on the aromatic rings as well as to the halogenation strategy that we described in the previous section. Thus, the syntheses

of diazocine **64** and diazonine **66** may be used as blueprints for new types of azobenzenes with interesting photophysical and pharmacological features.



Scheme 11.8. Synthesis of new cyclic azobenzenes. a) Ac_2O , Et_3N , neat, $50\text{ }^\circ\text{C}$; b) EtOCOCI , Et_3N , THF then NaHB_4 , H_2O ; c) TBSOTf , 2,6-lutidine, DCM; d) H_2 , Pd/C, MeOH/DCM; e) *m*CPBA in AcOH (2 eq, slow addition), AcOH/DCM = 1/3.

7. UV-Vis Spectroscopic Characterization. With more than forty cyclic azobenzenes in hand, we turned towards their photophysical characterization in order to gain insight into the effects of substituents and backbone-modifications on UV-Vis spectra and photoswitching behavior. To determine the optimal wavelength (λ_{opt}) for a high (*Z*)/(*E*) ratio, we illuminated a $50\text{ }\mu\text{M}$ DMSO solution of each compound for 10 minutes in 20 nm increments from 540 nm to 360 nm and measured the resulting absorption spectra (Figures S11.4 to S11.8).

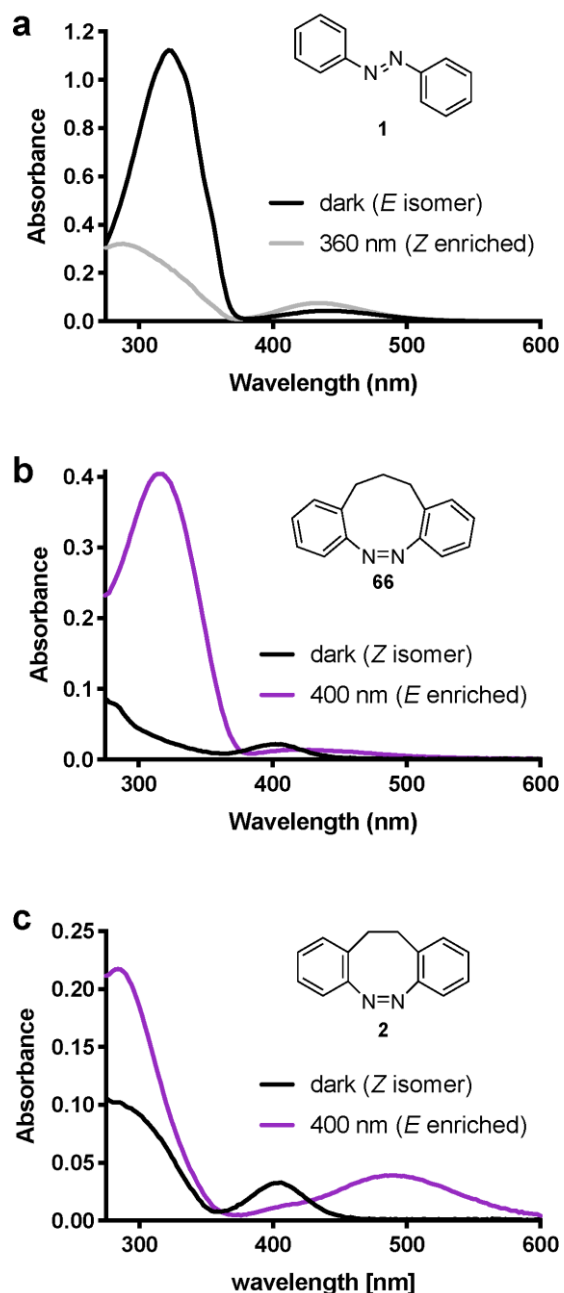


Figure 11.1. Comparison of UV-Vis spectra of a) azobenzene **1** b) diazocine **66** and c) diazocine **2** in the dark and under illumination. All spectra in DMSO, 50 μM .

For all diazocines, the lowest energy absorption was not significantly affected by substitution and typically centered around 400 nm for the (*Z*) isomer and around 490 nm for the (*E*) isomer. Like the parent compound **2**, the majority of the diazocines can be isomerized most efficiently to their thermodynamically less stable (*E*) form with 400 nm light (Tables 11.4 and S11.1). A slightly longer wavelength of 420 nm or even 440 nm was required in the case of several electron-rich diazocines. The backbone-

substituted compound **64** also did not show special features compared to the parent system **2**.

Finally, we also investigated the spectra and switching of the nine-membered diazonine **66**. Analogously to the eight-membered system, it could be isomerized to the (*E*) isomer with 400 nm irradiation and back to the (*Z*) isomer using 520 nm light. Interestingly, compared to the (*E*) isomer of diazocine **2** the spectrum of the (*E*) isomer of diazonine **66** exhibits a notably higher absorbance for the band corresponding to the $\pi\pi^*$ -transition, which also is found at a longer wavelength of 316 nm. Therefore, the spectrum of (*E*) diazonine resembles that of a regular (*E*) azobenzene, while the (*Z*) diazonine spectrum is similar to (*Z*) diazocine (Figure 11.1 and Table S11.3).

The comparatively small effect of substituents on the lowest energy absorption band of diazocines are not surprising since it results from a $\pi\pi^*$ -excitation.^[23] A stronger effect was observed for the next absorption band at shorter wavelengths, which corresponds to a $\pi\pi^*$ -transition. This band was notably red-shifted for diazocines carrying electron-donating substituents (e.g. compounds **16** and **26**) or with a push-pull substitution. Increased overlap of the bands corresponding to $\pi\pi^*$ -transitions of the (*E*) forms with the $\pi\pi^*$ -transitions of the (*Z*) forms might be contributing to the poorer switching behavior observed for these diazocines (see PSS investigation by NMR spectroscopy below).

8. Thermal Relaxation. In respect to thermal relaxation, we observed broad variability (Tables 11.4 and S11.1) with trends similar to regular azobenzenes. Thermal relaxation was monitored in 50 μM DMSO solution at 25 °C over a period of 24 hours. Reduced half-lives for the (*E*) isomer were observed with electron-withdrawing groups in *meta*-position as well as both electron-withdrawing and electron donating groups in *para*-position. Strong electron withdrawing groups and push-pull substitution in *para*-position resulted in rapidly relaxing photoswitches. When comparing the effect of a substituent in *meta*-position to the same substituent in *para*-position, we found that *para*-substituted compounds were generally more affected than their *meta*-substituted counterparts. To determine the effect of water on the relaxation rates, we also investigated solutions in PBS/DMSO mixtures for three selected compounds (see Table S11.2). Surprisingly, we observed up to two or three times longer half-lives upon increasing the fraction of the aqueous component in the solvent mixture.

None of the aromatic substitutions resulted in a major increase in relaxation times compared to the parent system **2**. However, improved bistability could be achieved by changes in the central ring system. An increased thermal stability of the (*E*) form was observed for the ethylene-bridge substituted diazocine **64**. For diazocine **66** no relaxation could be observed at room temperature after enrichment of the (*E*) isomer by both UV-Vis (40 hours) as well as NMR measurements (two weeks). Still, diazocine **66** did fully relax to the (*Z*) isomer upon prolonged storage in the solid state in the dark. The high bistability of diazocine **66** is expected to be connected to the low energy difference between (*E*) and (*Z*) isomer, which is a consequence of the longer three carbon bridge ($\Delta G_{Z \rightarrow E} = 10.6$ kJ/mol in the gas phase and 17.4 kJ/mol in DMSO, see Tables S14 and S15).

9. PSS investigation by NMR spectroscopy. Having determined the best switching wavelengths and relaxation times, we turned towards determination of the PSS compositions (Tables 11.4 and S11.1, Figure S11.3). We chose to determine the PSS as (*Z*)/(*E*) ratio observed with one pulse ¹H-NMR spectroscopy measurements of 10 mM solutions in DMSO-*d*₆. The samples were first measured before illumination, then after 30 seconds of illumination with a 390 nm high-power LED and after successive 30 seconds of illumination with a 520 nm high-power LED (Prizmatix). We additionally tested the (*Z*) to (*E*) isomerization with a 460 nm high-power LED and a 415 nm Mic-LED (Prizmatix) for the compounds where we had either determined an optimal switching wavelength higher than 400 nm in our UV-Vis experiments or where we observed poor (*Z*)/(*E*) ratios (>20/80) after 390 nm illumination.

Despite handling the samples without precautions to avoid exposure to ambient light, most samples contained no detectable (*E*) isomer and all diazocines showed an initial (*Z*)/(*E*) ratio of at least 97/3. For the (*Z*) to (*E*) isomerization upon irradiation with violet/blue light, we observed distinct differences between individual groups of diazocines. With the majority of the compounds, we were able to establish a PSS between 12/88 and 19/81. This included compounds with electron-withdrawing substituents, backbone-substitution, some electron-donating substituents and weakly interacting substituents, such as alkyl or halogen, which all showed excellent PSS. However, methoxy and most amino substituents lowered the (*E*) isomer fraction and more of the (*Z*) isomer remained. Furthermore, the push-pull combination of methoxy

and methyl ester led to a drastic PSS deterioration, regardless of their position on the ring.

The photoisomerization from the (*E*) to the (*Z*) form was found to be highly effective for all diazocines. In all cases illumination with 520 nm led to quantitative isomerization to the thermodynamically favored (*Z*) form. This is an important distinction from regular azobenzenes. In summary, all tested diazocines can be reversibly isomerized with visible light.

For diazonine **66** we observed no (*E*) isomer before illumination and a PSS of 14/86 after illumination with 390 nm light. While this result for the (*Z*) to (*E*) isomerization was virtually identical to the unsubstituted diazocine **2**, a non-quantitative conversion was observed for the (*E*) to (*Z*) photoisomerization of diazonine **66** and only a (*Z*)/(*E*) ratio of 89/11 could be achieved with 520 nm light. Still, the value for the photoisomerization to the thermodynamically preferred form is better for diazonine **66** than for azobenzene **1**, which exhibited at best a PSS of 83/17 for (*Z*) to (*E*) isomerization in DMSO (Table S11.4).

Finally, it is important to mention that we had to reduce the concentration of azobenzene **1** for our NMR experiments from 10 mM to 1 mM, as we had observed a very low (*E*) to (*Z*) conversion at 10 mM. Probably this issue results from incomplete sample penetration during irradiation due to complete absorption of light. This issue is alleviated by the lower extinction coefficients of diazocine and diazonine. Thus, at least at the present concentrations, both diazocines and the diazonine allow for a more rapid and efficient establishment of the PSS than regular azobenzenes.

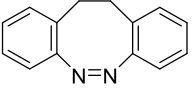
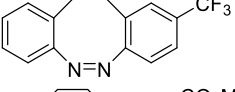
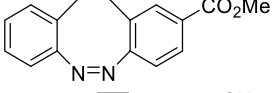
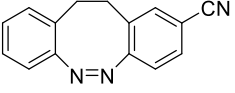
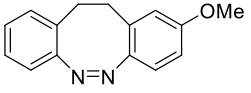
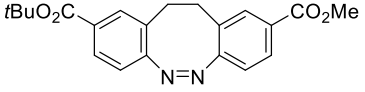
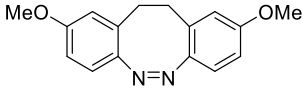
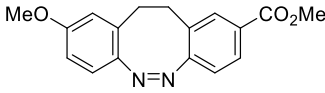
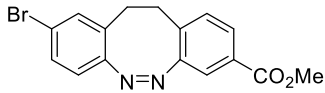
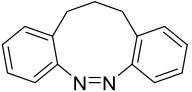
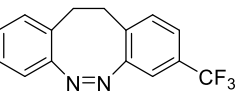
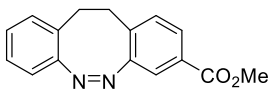
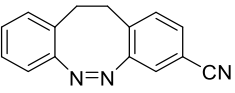
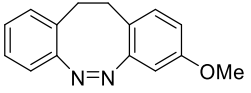
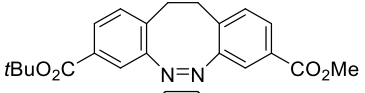
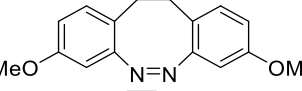
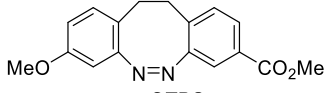
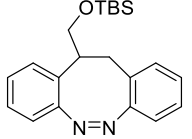
Compound	$\lambda_{\text{opt}}^{\text{a}}$	$T_{1/2}$	PSS (<i>Z/E</i>) ^b	
	2	400 nm	9.4 h	12/88 ^c
	23	400 nm	51 min	12/88 ^c
	24	400 nm	14 min	14/86 ^c
	25	400 nm	6 min	15/85 ^c
	26	420 nm	3.0 h	33/67 ^c
	31	400 nm	24 min	14/86 ^c
	33	420 nm	3.5 h	32/68 ^c
	35	420 nm	2.2 min	55/45 ^c
	40	400 nm	4.7 h	14/86 ^c
	66	400 nm	n.d. ^e	14/86 ^c
	13	400 nm	4.3 h	14/86 ^c
	14	380 nm	6.7 h	14/86 ^c
	15	400 nm	3.3 h	14/86 ^c
	16	420 nm	10.4 h	45/55 ^d
	32	400 nm	6.0 h	15/85 ^c
	34	420 nm	11.2 h	55/45 ^d
	36	420 nm	7.5 h	52/48 ^d
	64	400 nm	14.2h	19/81 ^c

Table 11.4. Photophysical properties of selected cyclic azobenzenes. ^aFor (*Z*) to (*E*) switching, determined by UV-Vis spectroscopy. ^bFor (*Z*) to (*E*) switching, determined by ¹H-NMR spectroscopy in DMSO-*d*₆. ^c390 nm. ^d415 nm. ^eNot determined, no measurable isomerization within two weeks.

Conclusion

The broad implementation of diazocines as photoswitches with useful new functional properties has been limited by their poor synthetic accessibility. With this work, we have shown that the oxidative cyclization of dianilines can largely overcome this limitation. In combination with a modular cross coupling approach to furnish the cyclization substrates, as well as late-stage functionalization, the oxidative protocol gives access to a wide variety of diazocines that are substituted on one or both aromatic rings. Additionally, we were able to prepare a diazonine with a nine-membered ring and a diazocine substituted on the ethylene bridge, which we consider the vanguard of new types of photoswitches.

Furthermore, we have compared the photophysical properties and thermal relaxation data of diazocines. This allowed us to identify substitution patterns that are tolerated without affecting the useful photoswitch characteristics of the parent system as well as the patterns that should be avoided due to their detrimental effects. Based on our results, it is also possible to tune the thermal relaxation of diazocines over a broad range. This knowledge will facilitate the choice of diazocines in a variety of applications.

Acknowledgments

K.H. thanks the Studienstiftung des deutschen Volkes for a PhD scholarship. B.S.M. thanks the Alexander von Humboldt Foundation for a postdoctoral research fellowship. D.T. was supported by the European Research Council (Advanced Grant 268795) and thanks the Centre for Integrated Protein Science Munich (CIPSM). M.R. and D.T. thank the German Research Foundation (DFG) for financial support (SFB749). We further acknowledge National Institutes of Health (NIH) support (OD016343). T.K. thanks New York University for a MacCracken fellowship. The Shared Instrumentation Facility at the New York University Department of Chemistry was supported by a NIH Research Facilities Improvement Award (C06 RR-16572-01) and a NIH S10 grant (OD016343). The authors thank Dr. Chin Lin for his assistance with NMR spectroscopy and mass

spectrometry and Christopher Arp for programming the MATLAB interface to control the monochromator.

Abbreviations

DCM, dichloromethane; THF, tetrahydrofuran; DMSO, dimethyl sulfoxide; *m*CPBA, *meta*-chloroperoxybenzoic acid; MMPP, magnesium monoperoxyphthalate; TBAF, tetra-*N*-butylammonium fluoride; NIS, *N*-iodosuccinimide; NBS, *N*-bromosuccinimide; TFA, trifluoroacetic acid; BSA, Bis(trimethylsilyl)acetamide; Boc, *tert*-butyloxycarbonyl; TBS, *tert*-butyldimethylsilyl; Alloc, allyloxycarbonyl; EWG, electron-donating group; EDG, electron-withdrawing group; PSS, photostationary state; UV, ultraviolet; Vis, visible; NMR, nuclear magnetic resonance; LED, light-emitting diode.

Supporting Figures

wavelength	time
600 nm	10 s (dummy time at resting wavelength)
540 nm	600 s
520 nm	600 s
500 nm	600 s
480 nm	600 s
460 nm	600 s
440 nm	600 s
420 nm	600 s
400 nm	600 s
380 nm	600 s
360 nm	600 s

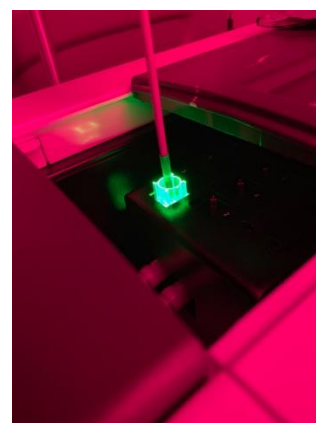


Figure S11.1: Left: Protocol for the determination of the optimal switching wavelength. Right: Picture of a sample being illuminated in the UV-Vis spectrometer.

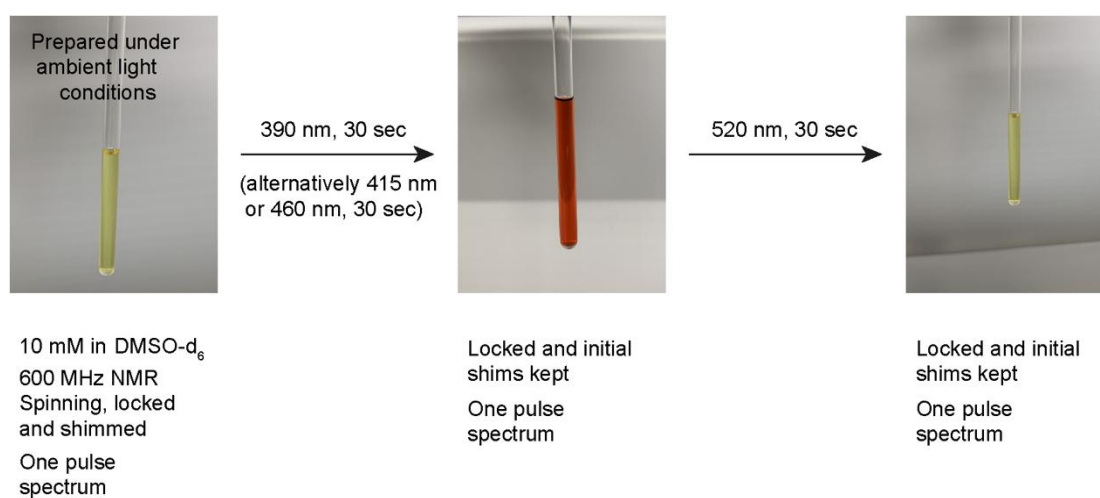


Figure S11.2: Workflow for the investigation of the photostationary states by ¹H-NMR spectroscopy.

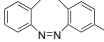
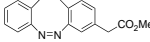
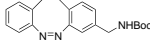
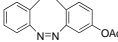
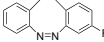
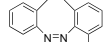
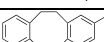
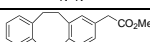
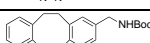
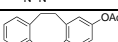
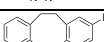
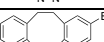
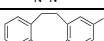
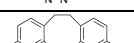
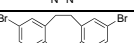
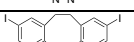
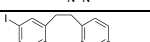
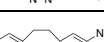
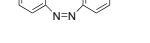
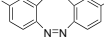
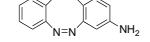
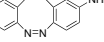
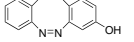
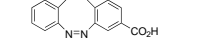
Compound	$\lambda_{\text{opt}}^{\text{a}}$	$T_{1/2}$	PSS (Z/E) ^b
 10	400 nm	9.3 h	17/83 ^c
 11	400 nm	8.9 h	14/86 ^c
 12	400 nm	8.9 h	17/83 ^c
 17	400 nm	8.0 h	15/85 ^c
 18	400 nm	5.7 h	13/87 ^c
 19	400 nm	11.0 h	15/85 ^c
 20	400 nm	6.8 h	15/85 ^c
 21	400 nm	7.9 h	14/86 ^c
 22	400 nm	7.9 h	14/86 ^c
 27	400 nm	8.7 h	17/83 ^c
 28	400 nm	9.5 h	13/87 ^c
 29	400 nm	5.6 h	14/86 ^c
 30	400 nm	4.9 h	15/85 ^c
 37	400 nm	5.9 h	15/85 ^c
 38	400 nm	4.0 h	15/85 ^c
 39	400 nm	3.2 h	19/81 ^c
 41	400 nm	4.3 h	17/83 ^c
 42	400 and 360 nm	16 min	85/15 ^c
 43	440 nm	14 min	73/27 ^c
 44	360 – 420 nm	13.2 h	61/39 ^c
 SI-95	420 nm	2.1 h	44/56 ^d
 SI-96	420 nm	11.3 h	61/39 ^c
 SI-97	400 nm	8.6 h	12/88 ^c
 SI-98	420 nm	3.0 h	15/85 ^e

Table S11.1: Photophysical properties of diazocines. ^aFor (Z) to (E) switching, determined by UV-Vis spectroscopy. ^bFor (Z) to (E) switching, determined by ¹H-NMR spectroscopy in DMSO-*d*₆. ^c390 nm. ^d415 nm. ^e460 nm.


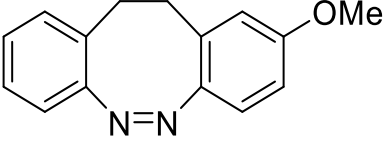
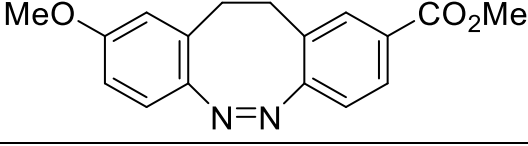
Compound	$T_{1/2}$ DMSO	$T_{1/2}$ 50% PBS/ DMSO	$T_{1/2}$ 90% PBS/ DMSO
 25	6.4 min	6.9 min	13.4 min
 26	181.1 min	283.1 min	532.0 min
 35	1.9 min	2.3 min	4.6 min

Table S11.2: Effect of water on thermal relaxation: Comparison of half-lives^a for thermal (*E*) to (*Z*) isomerization of selected diazocines in DMSO and PBS/DMSO mixtures. ^aDetermined according to the general protocol, but each sample was measured only once and the samples were prepared by diluting the DMSO stock solution with the specified solvent mixture instead of DMSO.

Transition	(<i>E</i>)- 1 ^a	(<i>Z</i>)- 1 ^b	(<i>E</i>)- 66 ^c	(<i>Z</i>)- 66 ^a	(<i>E</i>)- 2 ^c	(<i>Z</i>)- 2 ^a
$\pi\pi^*$	322 nm	280 nm	316 nm	280 nm	284 nm	286 nm
$n\pi^*$	444 nm	430 nm	426 nm	406 nm	494 nm	405 nm

Table S11.3: $\pi\pi^*$ - and $n\pi^*$ -absorption maxima of azobenzene **1**, diazocine **66** and diazocine **2** in DMSO (50 μ M). ^aNon-irradiated sample. ^bAfter 360 nm illumination. ^cAfter 400 nm illumination.

Entry ^a	λ	PSS (<i>Z</i> / <i>E</i>)
1 ^{b,c}	365 nm	17/83
2	non-irradiated sample	3/97
3 ^c	365 nm	60/40
4 ^d	415 nm	17/83 ^c
5	390 nm	18/82
6	460 nm	23/77
7	520 nm	35/65

Table S11.4: (*Z*)/(*E*) ratios of 1 mM azobenzene **1** in DMSO-*d*₆ determined by ¹H-NMR spectroscopy after 30 seconds of irradiation at different wavelengths. ^aThe entries in

this table refer to the same sample and are ordered from top to bottom according to the sequence of irradiation, except for the entry 1, which refers to a more concentrated sample that was measured separately. ^b10 mM. ^cThe determination of the optimal wavelength for switching to (*Z*)-1 by UV-Vis spectroscopy (see Figure S11.5) did not include wavelengths below 360 nm. Thus, at shorter wavelengths a higher conversion from (*E*)/(*Z*) may be possible. ^dThe optimal wavelength for switching to (*E*)-1 determined by UV-Vis spectroscopy (see Figure S11.5) was 420 nm.

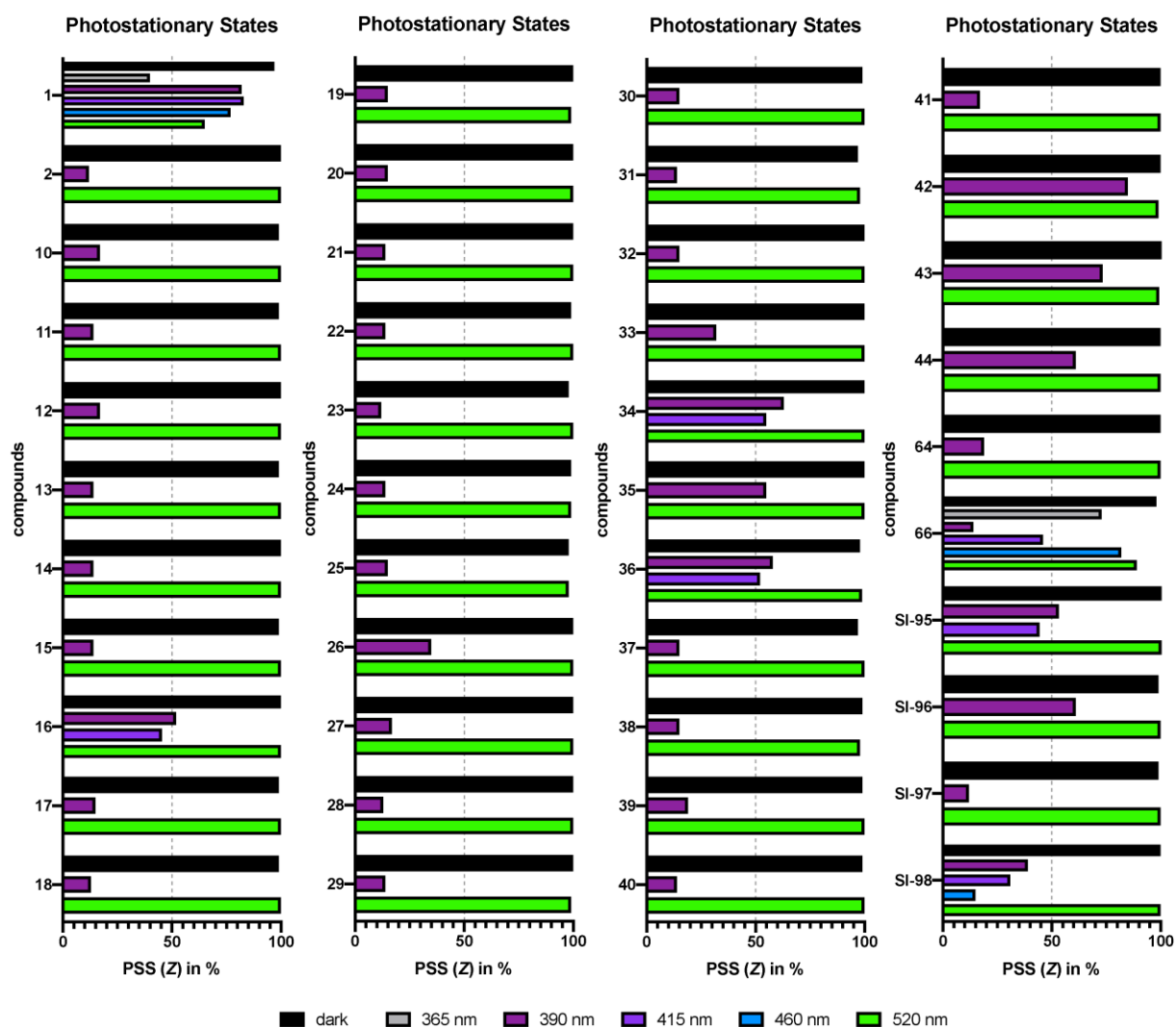


Figure S11.3: Overview of the fraction of (*Z*)-isomer determined by ¹H-NMR spectroscopy for the non-irradiated sample (prepared under ambient light conditions, labeled as “dark”) and the PSS at different wavelengths. Values for 390 and 520 nm irradiation are depicted for all compounds and values for 365, 415 and 460 nm irradiation are shown for selected compounds or if a better PSS composition was obtained.

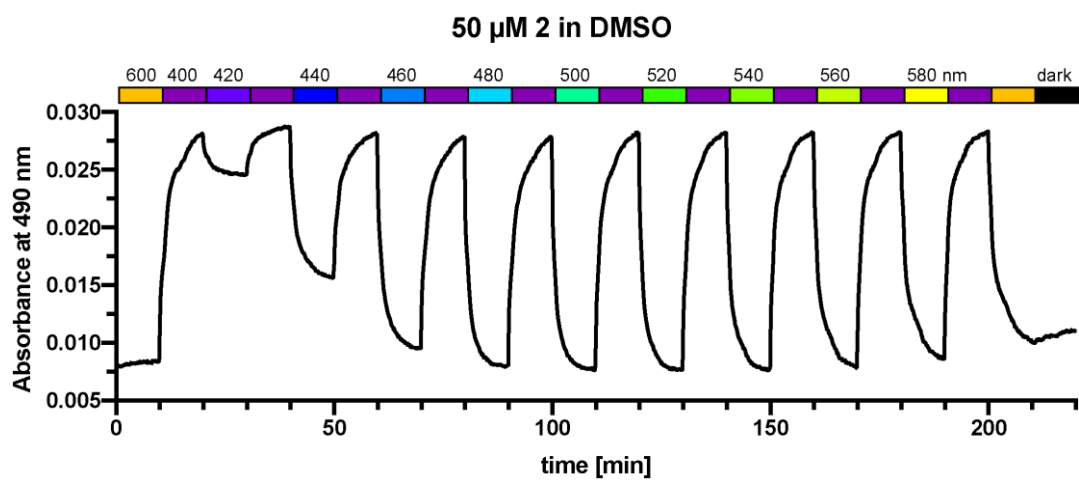


Figure S11.4: Determination of the ideal wavelength to switch diazocine **2** from (*E*) to (*Z*).

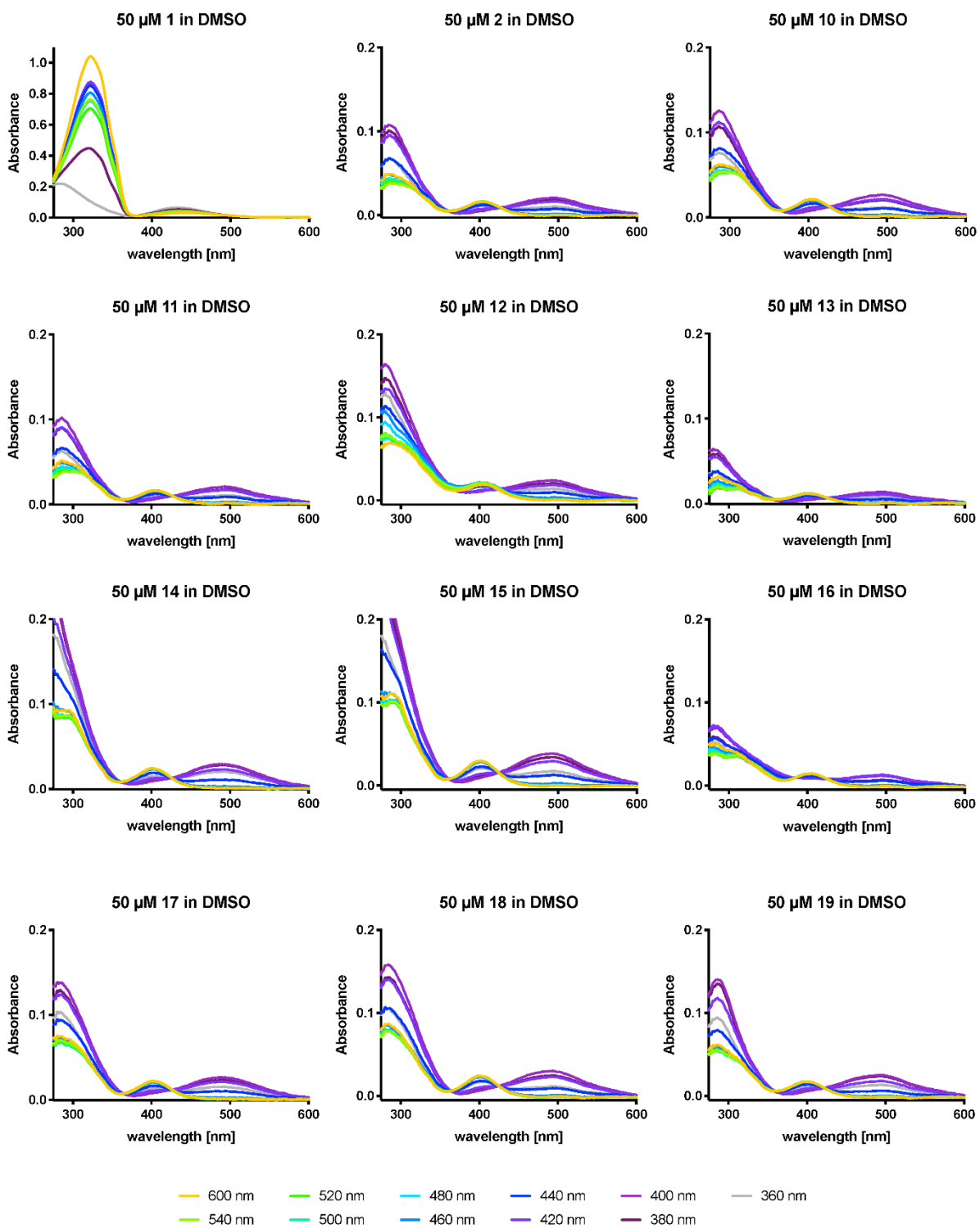


Figure S11.5: UV-Vis spectra of compounds 1, 2, 10-19.

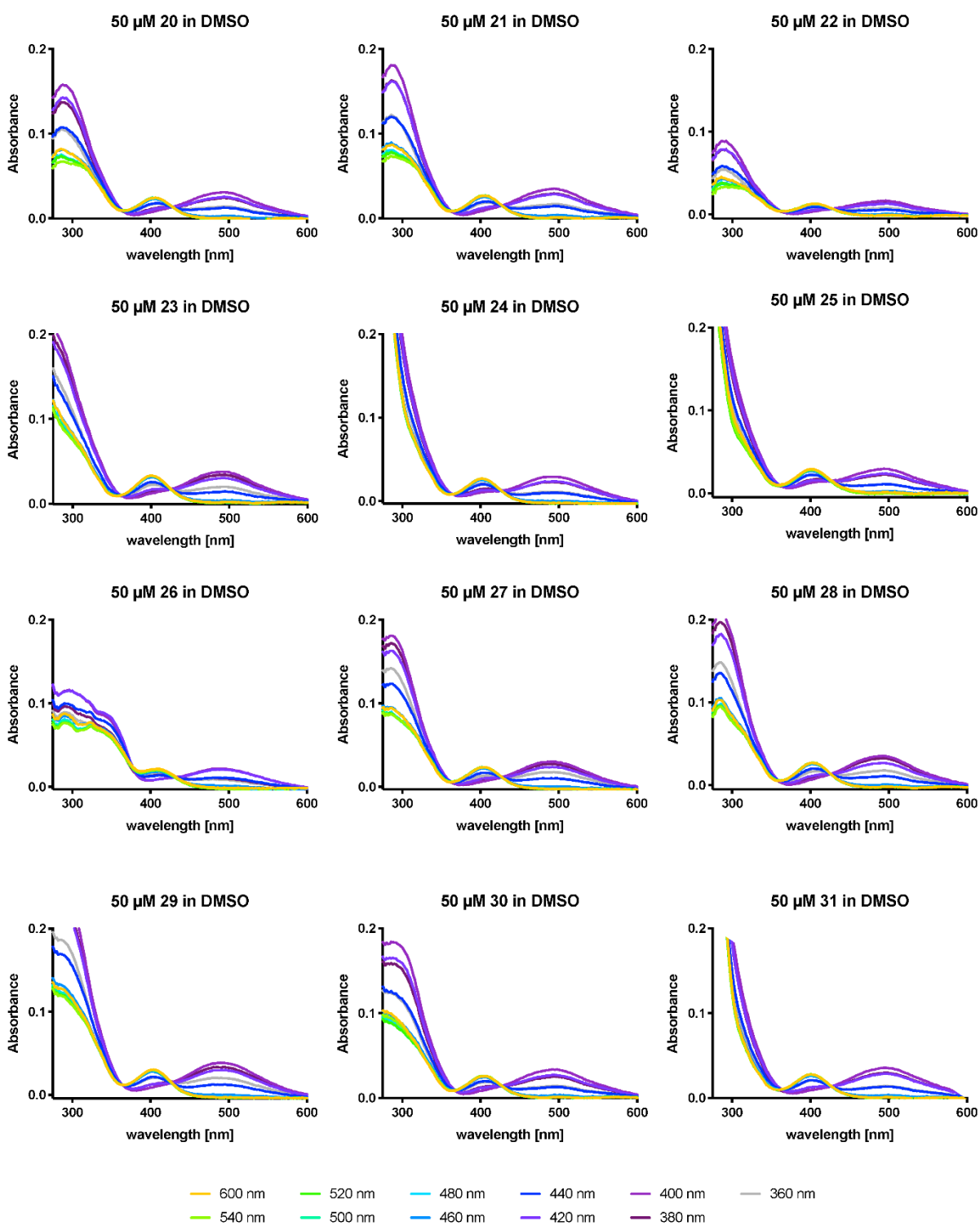


Figure S11.6: UV-Vis spectra of compounds 20-31.

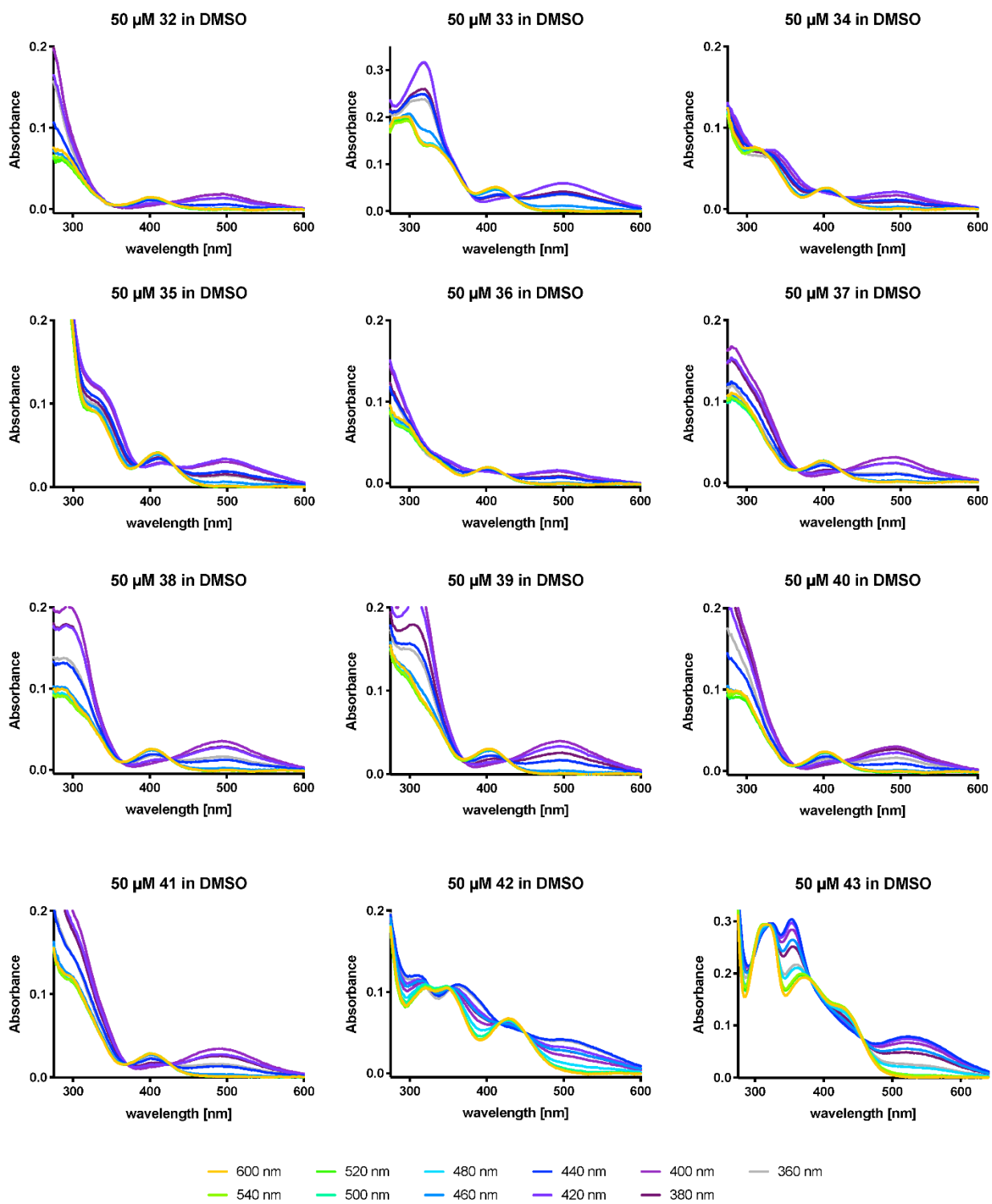


Figure S11.7: UV-Vis spectra of compounds **32-43**.

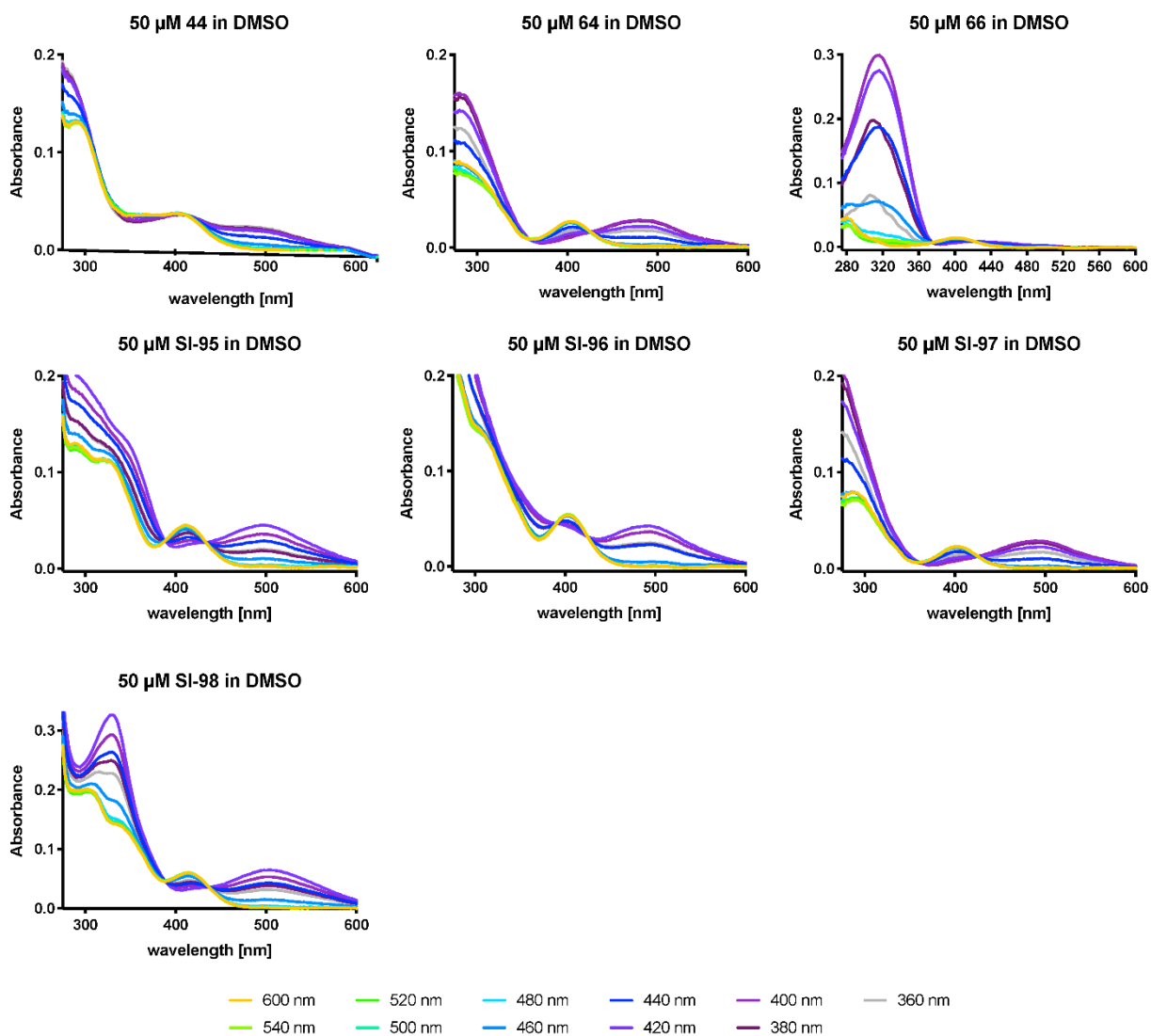


Figure S11.8: UV-Vis spectra of compounds **44**, **64**, **66**, **SI-95-SI-98**.

Supporting Information

Detailed supporting information, synthetic procedures and methods are not part of this thesis and available free of charge via the Internet at <https://doi.org/10.1021/jacs.9b08794>.

References

- [1] J. Broichhagen, J. A. Frank, D. Trauner, *Acc. Chem. Res.* **2015**, *48*, 1947–1960.
- [2] Pietro. Bortolus, Sandra. Monti, *J. Phys. Chem.* **1979**, *83*, 648–652.
- [3] Y. Ito, H. Ito, T. Matsuura, *Tetrahedron Lett.* **1988**, *29*, 563–566.
- [4] E. Fischer, *J. Am. Chem. Soc.* **1960**, *82*, 3249–3252.
- [5] A. A. Beharry, G. A. Woolley, *Chem. Soc. Rev.* **2011**, *40*, 4422–4437.
- [6] W. Szymański, J. M. Beierle, H. A. V. Kistemaker, W. A. Velema, B. L. Feringa, *Chem. Rev.* **2013**, *113*, 6114–6178.
- [7] K. Hüll, J. Morstein, D. Trauner, *Chem. Rev.* **2018**, *118*, 10710–10747.
- [8] A. Natansohn, P. Rochon, *Chem. Rev.* **2002**, *102*, 4139–4176.
- [9] I. Tomatsu, K. Peng, A. Kros, *Adv. Drug Deliv. Rev.* **2011**, *63*, 1257–1266.
- [10] V. Blanco, D. A. Leigh, V. Marcos, *Chem. Soc. Rev.* **2015**, *44*, 5341–5370.
- [11] R. Göstl, A. Senf, S. Hecht, *Chem. Soc. Rev.* **2014**, *43*, 1982–1996.
- [12] D. Bléger, J. Schwarz, A. M. Brouwer, S. Hecht, *J. Am. Chem. Soc.* **2012**, *134*, 20597–20600.
- [13] T. Wendler, C. Schütt, C. Näther, R. Herges, *J. Org. Chem.* **2012**, *77*, 3284–3287.
- [14] S. Samanta, A. Babalhavaeji, M. Dong, G. A. Woolley, *Angew. Chem. Int. Ed.* **2013**, *52*, 14127–14130.
- [15] S. Samanta, A. A. Beharry, O. Sadovski, T. M. McCormick, A. Babalhavaeji, V. Tropepe, G. A. Woolley, *J. Am. Chem. Soc.* **2013**, *135*, 9777–9784.
- [16] C. E. Weston, R. D. Richardson, P. R. Haycock, A. J. P. White, M. J. Fuchter, *J. Am. Chem. Soc.* **2014**, *136*, 11878–11881.
- [17] M. Dong, A. Babalhavaeji, S. Samanta, A. A. Beharry, G. A. Woolley, *Acc. Chem. Res.* **2015**, *48*, 2662–2670.
- [18] D. B. Konrad, J. A. Frank, D. Trauner, *Chem. – Eur. J.* **2016**, *22*, 4364–4368.
- [19] J. Calbo, C. E. Weston, A. J. P. White, H. S. Rzepa, J. Contreras-García, M. J. Fuchter, *J. Am. Chem. Soc.* **2017**, *139*, 1261–1274.
- [20] M. Dong, A. Babalhavaeji, C. V. Collins, K. Jarrah, O. Sadovski, Q. Dai, G. A. Woolley, *J. Am. Chem. Soc.* **2017**, *139*, 13483–13486.
- [21] H. Duval, *Bull. Soc. Chim. Fr.* **1910**, *7*, 727–732.
- [22] R. Siewertsen, H. Neumann, B. Buchheim-Stehn, R. Herges, C. Näther, F. Renth, F. Temps, *J. Am. Chem. Soc.* **2009**, *131*, 15594–15595.
- [23] R. Siewertsen, J. B. Schönborn, B. Hartke, F. Renth, F. Temps, *Phys. Chem. Chem. Phys.* **2010**, *13*, 1054–1063.
- [24] W. W. Paudler, A. G. Zeiler, *J. Org. Chem.* **1969**, *34*, 3237–3239.
- [25] H. Sell, C. Näther, R. Herges, *Beilstein J. Org. Chem.* **2013**, *9*, 1–7.

- [26] S. Samanta, C. Qin, A. J. Lough, G. A. Woolley, *Angew. Chem. Int. Ed.* **2012**, *51*, 6452–6455.
- [27] C. Deo, N. Bogliotti, R. Métivier, P. Retailleau, J. Xie, *Chem. – Eur. J.* **2016**, *22*, 9092–9096.
- [28] W. Moormann, D. Langbehn, R. Herges, *Synthesis* **2017**, *49*, 3471–3475.
- [29] S. Li, G. Han, W. Zhang, *Macromolecules* **2018**, *51*, 4290–4297.
- [30] Q. Zhu, S. Wang, P. Chen, *Org. Lett.* **2019**, *21*, 4025–4029.
- [31] W. Moormann, D. Langbehn, R. Herges, *Beilstein J. Org. Chem.* **2019**, *15*, 727–732.
- [32] D. K. Joshi, M. J. Mitchell, D. Bruce, A. J. Lough, H. Yan, *Tetrahedron* **2012**, *68*, 8670–8676.
- [33] T. Tellkamp, J. Shen, Y. Okamoto, R. Herges, *Eur. J. Org. Chem.* **2014**, *2014*, 5456–5461.
- [34] F. Eljabu, J. Dhruval, H. Yan, *Bioorg. Med. Chem. Lett.* **2015**, *25*, 5594–5596.
- [35] M. Jun, D. K. Joshi, R. S. Yalagala, J. Vanloon, R. Simionescu, A. J. Lough, H. L. Gordon, H. Yan, *ChemistrySelect* **2018**, *3*, 2697–2701.
- [36] L. Albert, A. Peñalver, N. Djokovic, L. Werel, M. Hoffarth, D. Ruzic, J. Xu, L.-O. Essen, K. Nikolic, Y. Dou, O. Vázquez, *ChemBioChem* **2019**, *20*, 1417–1429.
- [37] E. R. Thapaliya, J. Zhao, G. C. R. Ellis-Davies, *ACS Chem. Neurosci.* **2019**, *10*, 2481–2488.
- [38] R. Löw, T. Rusch, F. Röhricht, O. Magnussen, R. Herges, *Beilstein J. Org. Chem.* **2019**, *15*, 1485–1490.
- [39] J. Wang, J. He, C. Zhi, B. Luo, X. Li, Y. Pan, X. Cao, H. Gu, *RSC Adv.* **2014**, *4*, 16607–16611.
- [40] G. Cabré, A. Garrido-Charles, À. González-Lafont, W. Moormann, D. Langbehn, D. Egea, J. M. Lluch, R. Herges, R. Alibés, F. Busqué, P. Gorostiza, J. Hernando, *Org. Lett.* **2019**, *21*, 3780–3784.
- [41] M. Hammerich, C. Schütt, C. Stähler, P. Lentès, F. Röhricht, R. Höppner, R. Herges, *J. Am. Chem. Soc.* **2016**, *138*, 13111–13114.
- [42] M. Schehr, C. Ianes, J. Weisner, L. Heintze, M. P. Müller, C. Pichlo, J. Charl, E. Brunstein, J. Ewert, M. Lehr, U. Baumann, D. Rauh, U. Knippschild, C. Peifer, R. Herges, *Photochem. Photobiol. Sci.* **2019**, *18*, 1398–1407.
- [43] P. Lentès, E. Stadler, F. Roehricht, A. Brahms, J. Groebner, F. D. Sonnichsen, G. Gescheidt, R. Herges, *J. Am. Chem. Soc.* **2019**, DOI 10.1021/jacs.9b06104.
- [44] M. Schehr, D. Hugenbusch, T. Moje, C. Näther, R. Herges, *Beilstein J. Org. Chem.* **2018**, *14*, 2799–2804.
- [45] T. Kajimoto, K. Yahiro, T. Nohara, *Chem. Lett.* **1988**, *17*, 1113–1114.

- [46] C. Bleasdale, M. K. Ellis, P. B. Farmer, B. T. Golding, K. F. Handley, P. Jones, W. McFarlane, *J. Label. Compd. Radiopharm.* **1993**, *33*, 739–746.
- [47] R. Reuter, H. A. Wegner, *Beilstein J. Org. Chem.* **2012**, *8*, 877–883.
- [48] E. Pfeil, K. H. Schmidt, *Justus Liebigs Ann. Chem.* **1964**, *675*, 36–42.
- [49] J. T. Hays, H. L. Young, H. H. Espy, *J. Org. Chem.* **1967**, *32*, 158–162.
- [50] S. Routier, L. Saugé, N. Ayerbe, G. Coudert, J.-Y. Mérour, *Tetrahedron Lett.* **2002**, *43*, 589–591.
- [51] M. Hooper, S. H. Imam, *J. Chem. Soc. Perkin 1* **1985**, 1583–1587.
- [52] B. C. G. Söderberg, S. P. Gorugantula, C. R. Howerton, J. L. Petersen, S. W. Dantale, *Tetrahedron* **2009**, *65*, 7357–7363.
- [53] R.-R. Liu, S.-C. Ye, C.-J. Lu, G.-L. Zhuang, J.-R. Gao, Y.-X. Jia, *Angew. Chem. Int. Ed.* **2015**, *54*, 11205–11208.
- [54] N. Marien, B. Brigou, B. Pinter, F. De Proft, G. Verniest, *Org. Lett.* **2015**, *17*, 270–273.
- [55] E. J. M. Maduli, S. J. Edeson, S. Swanson, P. A. Procopiou, J. P. A. Harrity, *Org. Lett.* **2015**, *17*, 390–392.
- [56] H. Peng, J. Ma, L. Duan, G. Zhang, B. Yin, *Org. Lett.* **2019**, DOI 10.1021/acs.orglett.9b01849.
- [57] P. S. Dhote, C. V. Ramana, *Org. Lett.* **2019**, DOI 10.1021/acs.orglett.9b02035.
- [58] A. Arcadi, S. Cacchi, G. Fabrizi, F. Ghirga, A. Goggiamani, A. Iazzetti, F. Marinelli, *Beilstein J. Org. Chem.* **2018**, *14*, 2411–2417.
- [59] A. L. Rodriguez, C. Koradin, W. Dohle, P. Knochel, *Angew. Chem. Int. Ed.* **2000**, *39*, 2488–2490.
- [60] J. E. Perea-Buceta, T. Wirtanen, O.-V. Laukkanen, M. K. Mäkelä, M. Nieger, M. Melchionna, N. Huittinen, J. A. Lopez-Sanchez, J. Helaja, *Angew. Chem. Int. Ed.* **2013**, *52*, 11835–11839.
- [61] G. Abbiati, A. Arcadi, M. Chiarini, F. Marinelli, E. Pietropaolo, E. Rossi, *Org. Biomol. Chem.* **2012**, *10*, 7801–7808.
- [62] C. Koradin, W. Dohle, A. L. Rodriguez, B. Schmid, P. Knochel, *Tetrahedron* **2003**, *59*, 1571–1587.
- [63] M. Pailer, A. Schleppek, A. Meller, *Monatshefte Für Chem. Verwandte Teile Anderer Wiss.* **1958**, *89*, 211–219.
- [64] P. Molina, M. Alajarín, P. Sánchez-Andrada, J. S. Carrió, M. Martínez-Ripoll, J. E. Anderson, M. L. Jimeno, J. Elguero, *J. Org. Chem.* **1996**, *61*, 4289–4299.

Appendix

List of abbreviations

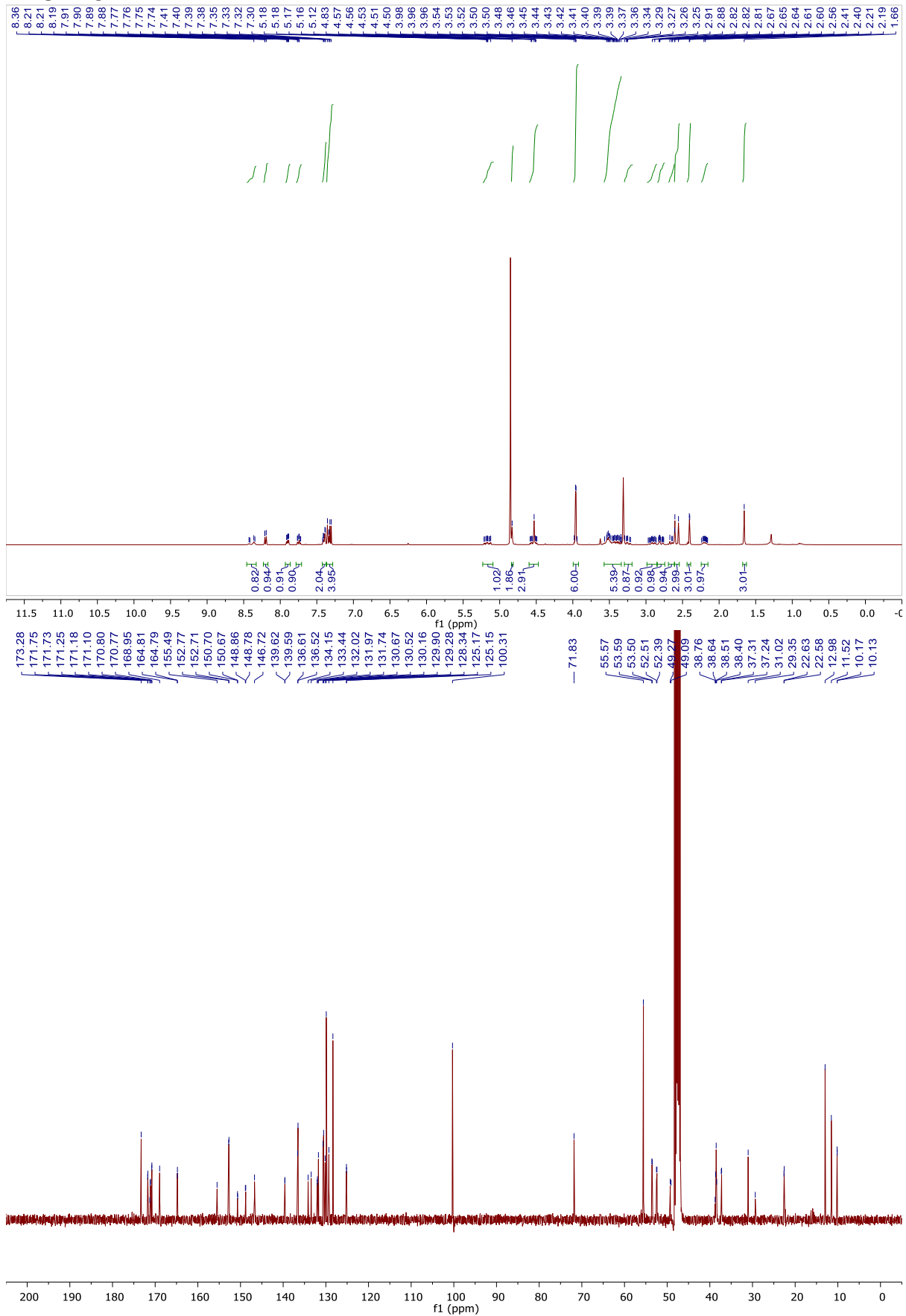
Ac	Acetyl
APCI	Atmospheric pressure chemical ionization
aq.	aqueous
AURKA	aurora kinase A
BCA	bicinchoninic acid
BET	bromodomain and extra terminal domain
Boc	tert-butoxycarbonyl
br	broad
BRD	Bromodomain-containing protein
BSA	bovine serum albumin
Bu	butyl
calcd	calculated
CCND3	cyclin D3
CDK	cycin-dependent kinase
CRBN	cereblon
DCM	dichlormethane
DIPEA	ethyldiisopropylamine
DMEM	Dulbecco's Modified Eagle's Medium
DMF	N,N-dimethylformamide
DMSO	Dimethylsulfoxide
DNA	desoxyribonucleic acid
EA	ethyl acetate
EC50	Half maximal effective concentration
EGFR	Epidermal Growth Factor Receptor
eq	equivalent(s)
ESI	Electrospray ionization
Et	ethyl
FA	formic acid
FBS	fetal bovine serum
FKBP	FK506 binding protein
Fmoc	fluorenylmethoxycarbonyl
GAK	Cyclin-G-associated kinase
GLuc	Gaussia luciferase
HPLC	High-performance liquid chromatography
HRMS	high-resolution mass spectrometry
HRP	Horseradish peroxidase
IC50	half maximal inhibitory concentration
IR	infrared
J	coupling constant
JNK	c-Jun N-terminal kinase
LCMS	Liquid chromatography–mass spectrometry

LED	Light-emitting diode
LOV	Light-oxygen-voltage-sensing
mCPBA	meta-chloroperoxybenzoic
MDM2	Mouse double minute 2 homolog
Me	methyl
min	minute(s)
MTS	[3-(4,5-dimethylthiazol-2-yl)-5-(3-carboxymethoxyphenyl)-2-(4-sulfophenyl)-2H-tetrazolium
MW	molecular
MWM	molecular weight marker
NBS	N-bromosuccinimide
nBu	n-butyl
NIS	N-iodosuccinimide
Nluc	NanoLuciferase
NMR	nuclear magnetic resonance
PARP1	Poly [ADP-ribose] polymerase 1
PBS	phosphate-buffered saline
PCNA	Proliferating cell nuclear antigen
PCR	polymerase chain reaction
PDT	Photodynamic Therapy
PDVF	Polyvinylidenfluorid
Ph	phenyl
PHOTAC	photochemically targeting chimera
POI	protein of interest
ppm	parts per million
PROTAC	proteolysis targeting chimera
PSS	photostationary state
Rb	retinoblastoma protein
Rf	retardation factor
RNA	ribonucleic acid
RPMI	Roswell Park Memorial Institute
RT	room temperature
SAR	structure-activity relationship
sat.	saturated
SD	Standard deviation
SEM	standard error of mean
T	temperature
TBAF	tetrabutylammonium fluoride
TBS	tert-butyldimethylsilyl
tBu	tert-butyl
TEA	triethylamine
TFA	trifluoroacetic acid
THF	tetrahydrofuran
TLC	thin-layer chromatography
TMS	trimethylsilyl
TMSCl	trimethylsilyl chloride
TOF	time-of-flight

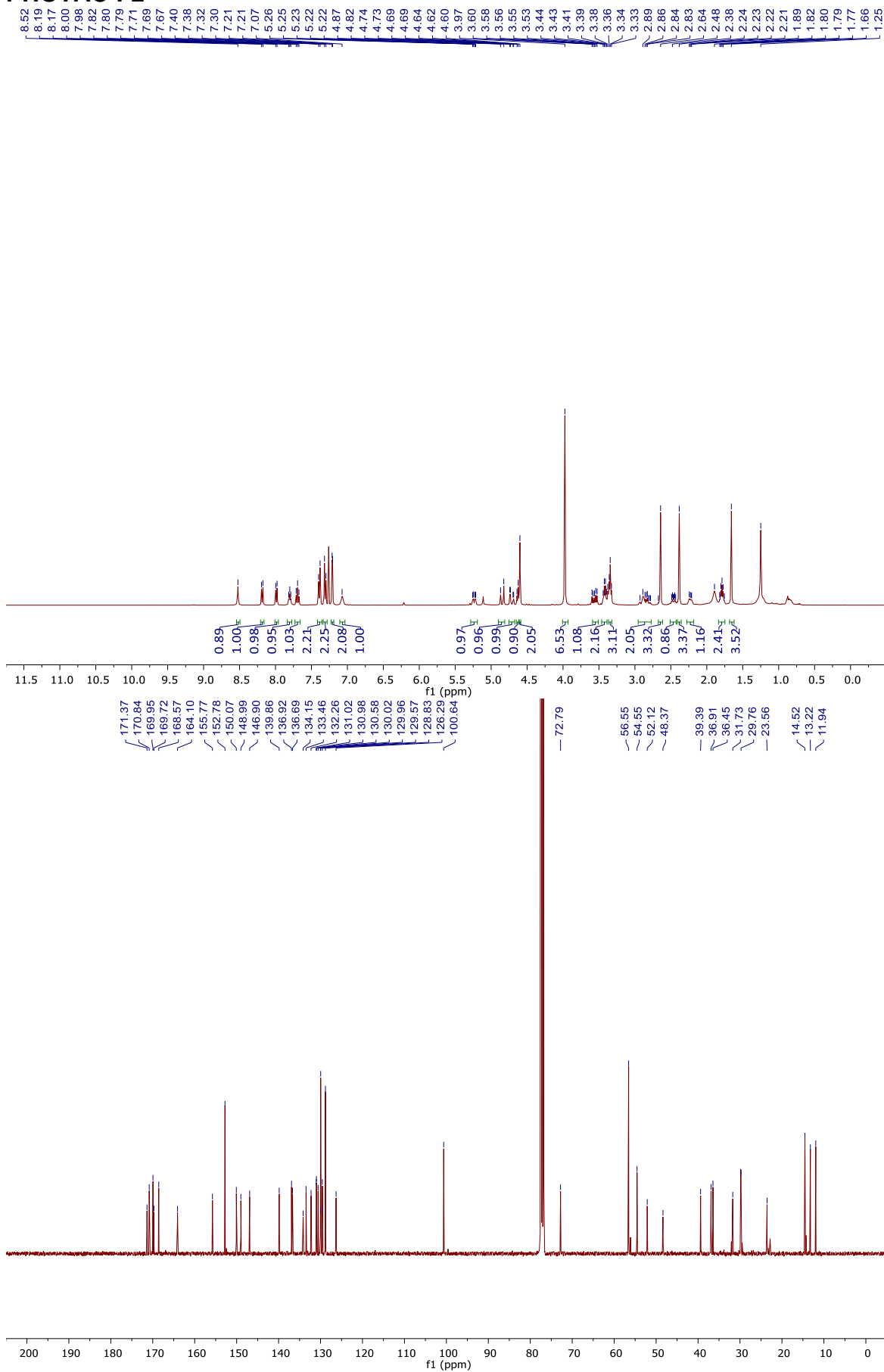
TUB	tubulin
UV	ultraviolet
VHL	Von Hippel–Lindau tumor suppressor
VINC	vinculin
Vis	visible
Xantphos	4,5-bis(diphenylphosphino)-9,9-dimethylxanthene

NMR spectra

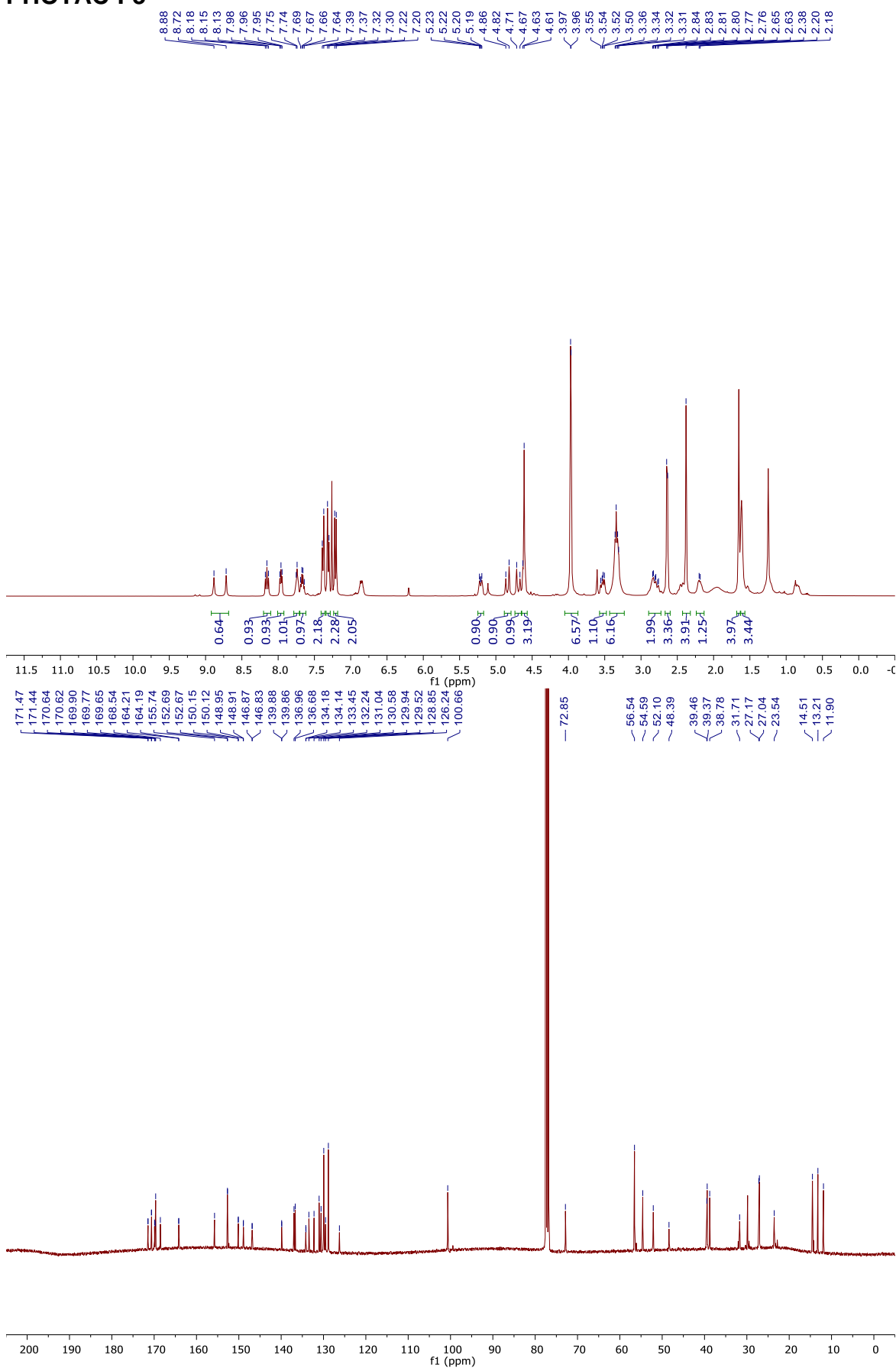
PHOTAC-I-1



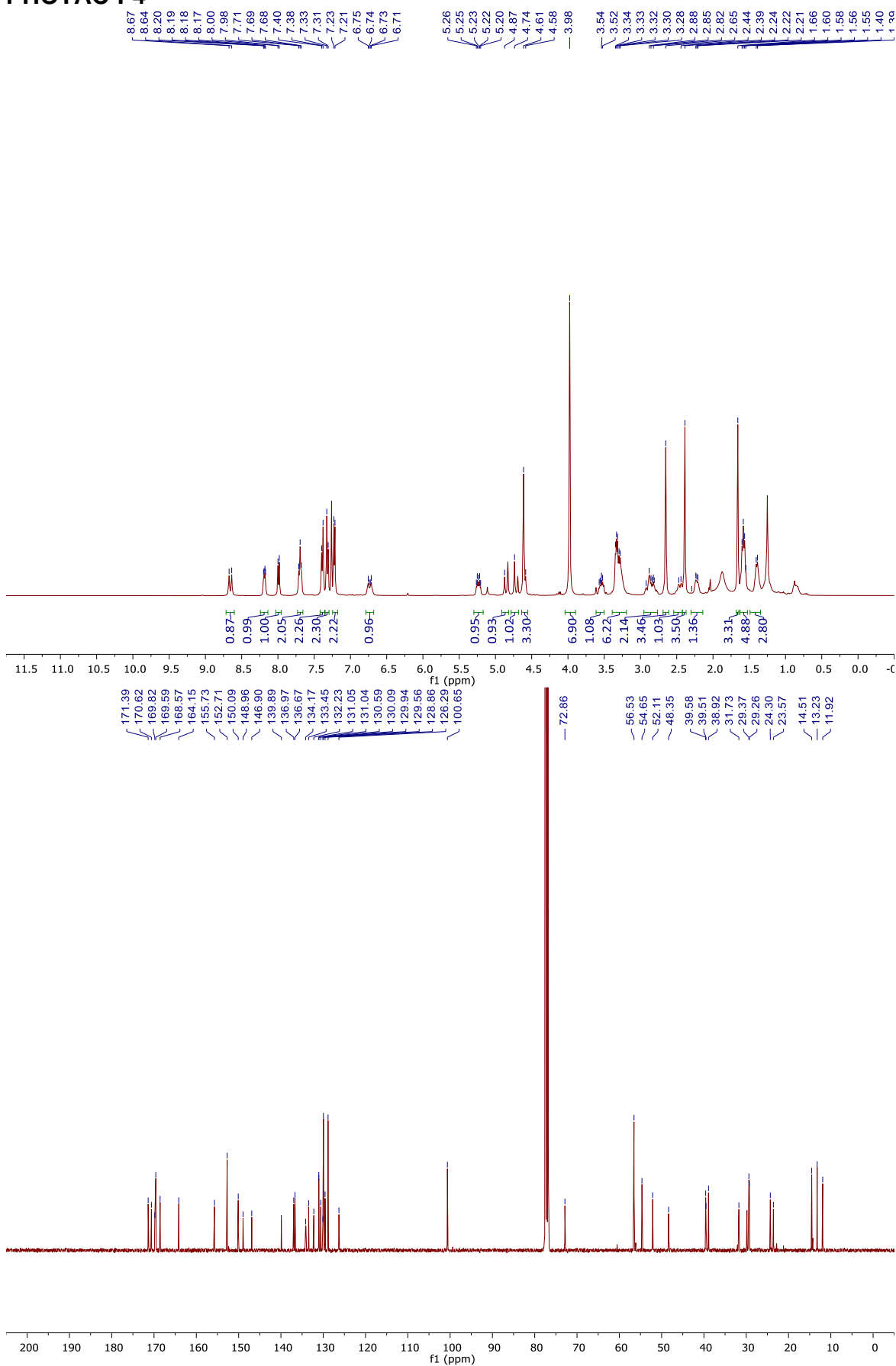
PHOTAC-I-2



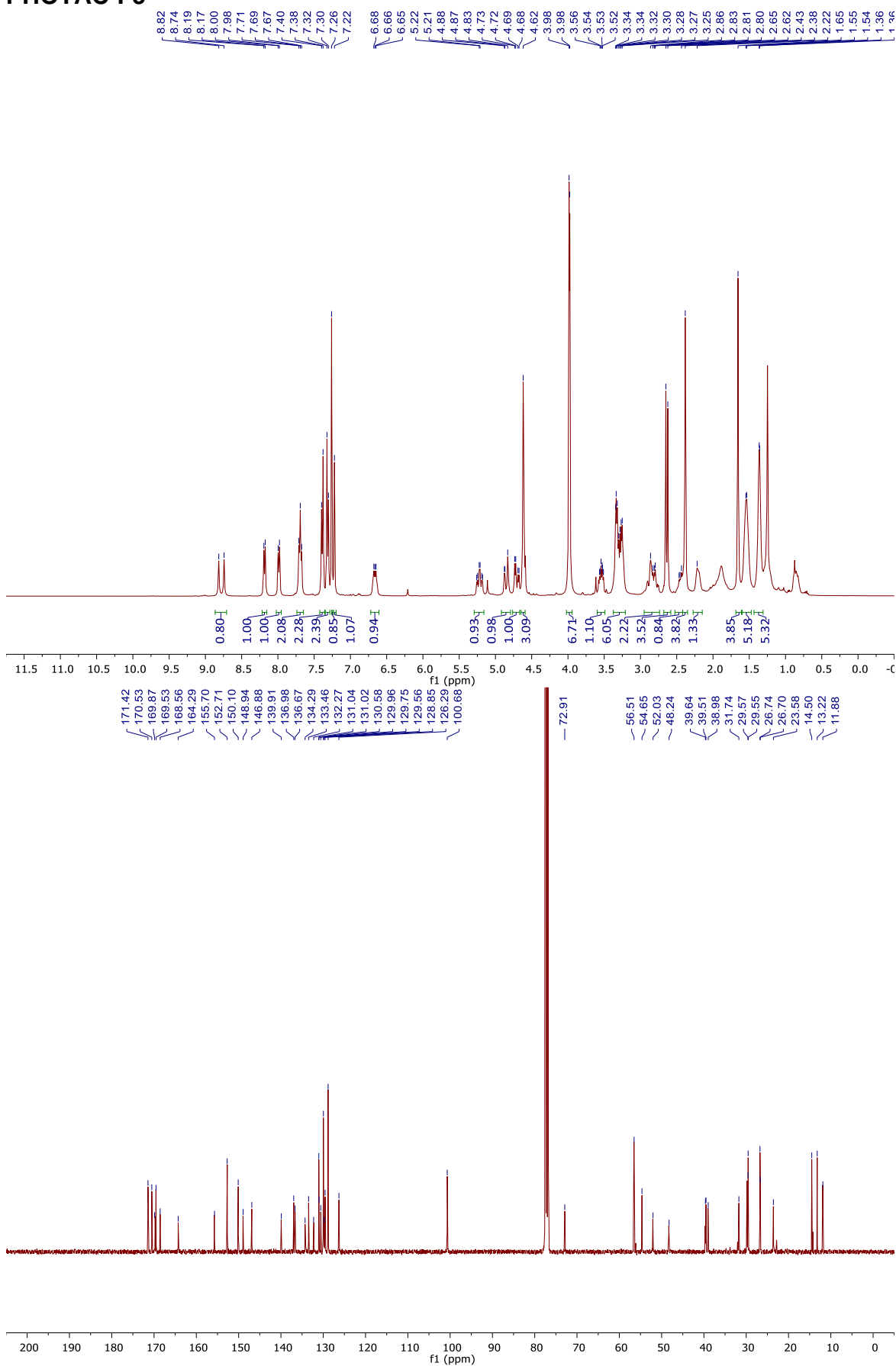
PHOTAC-I-3



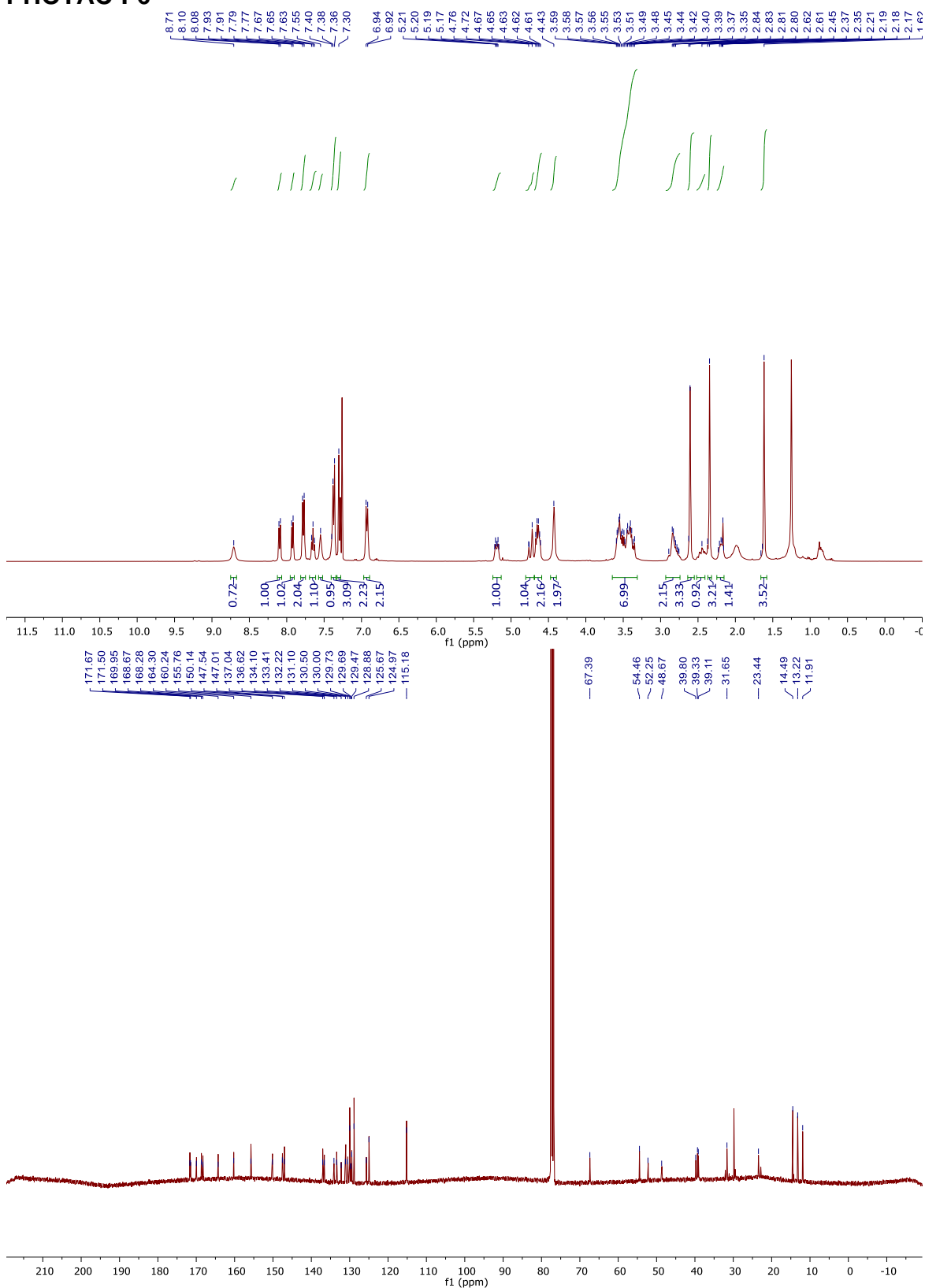
PHOTAC-I-4



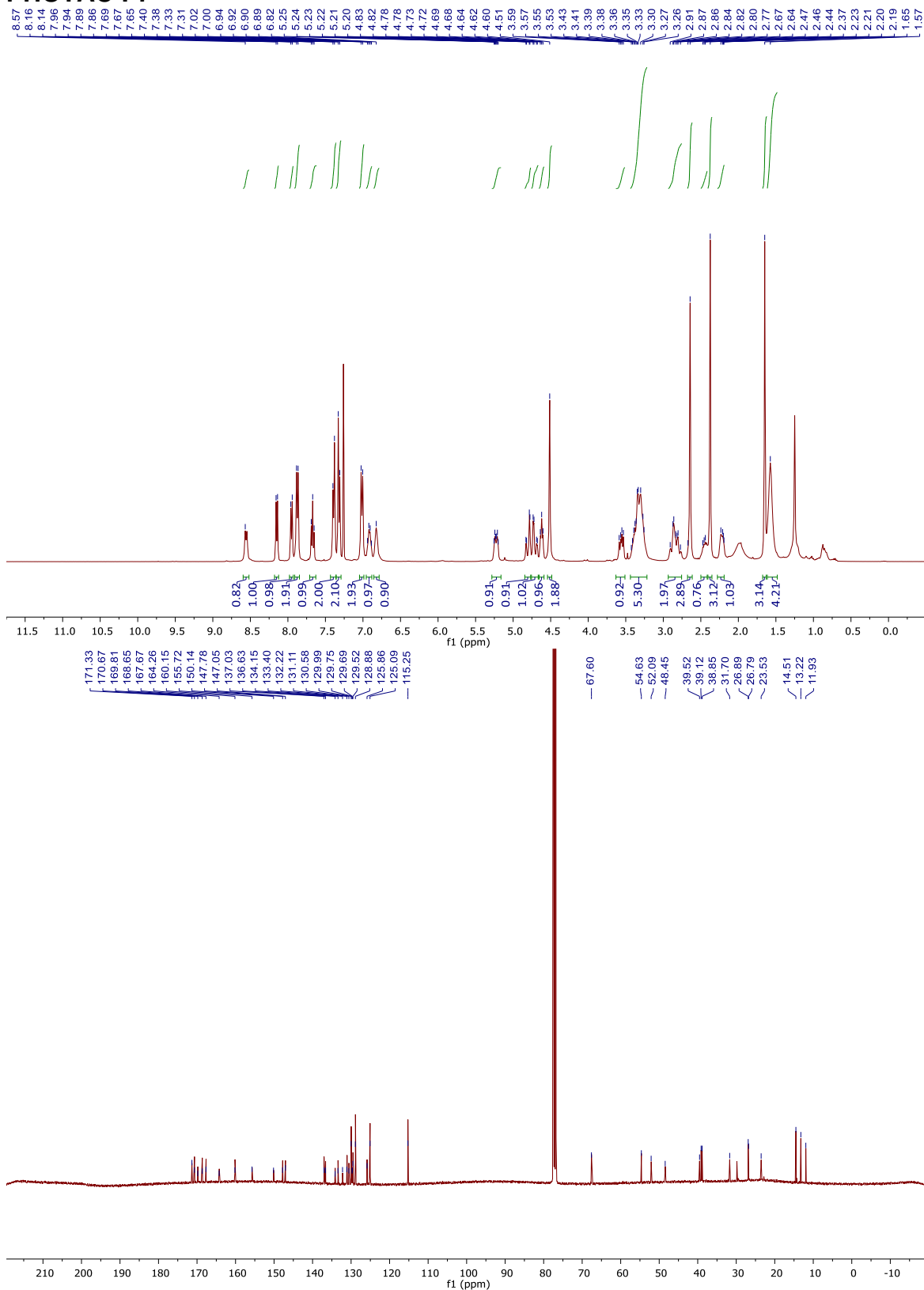
PHOTAC-I-5



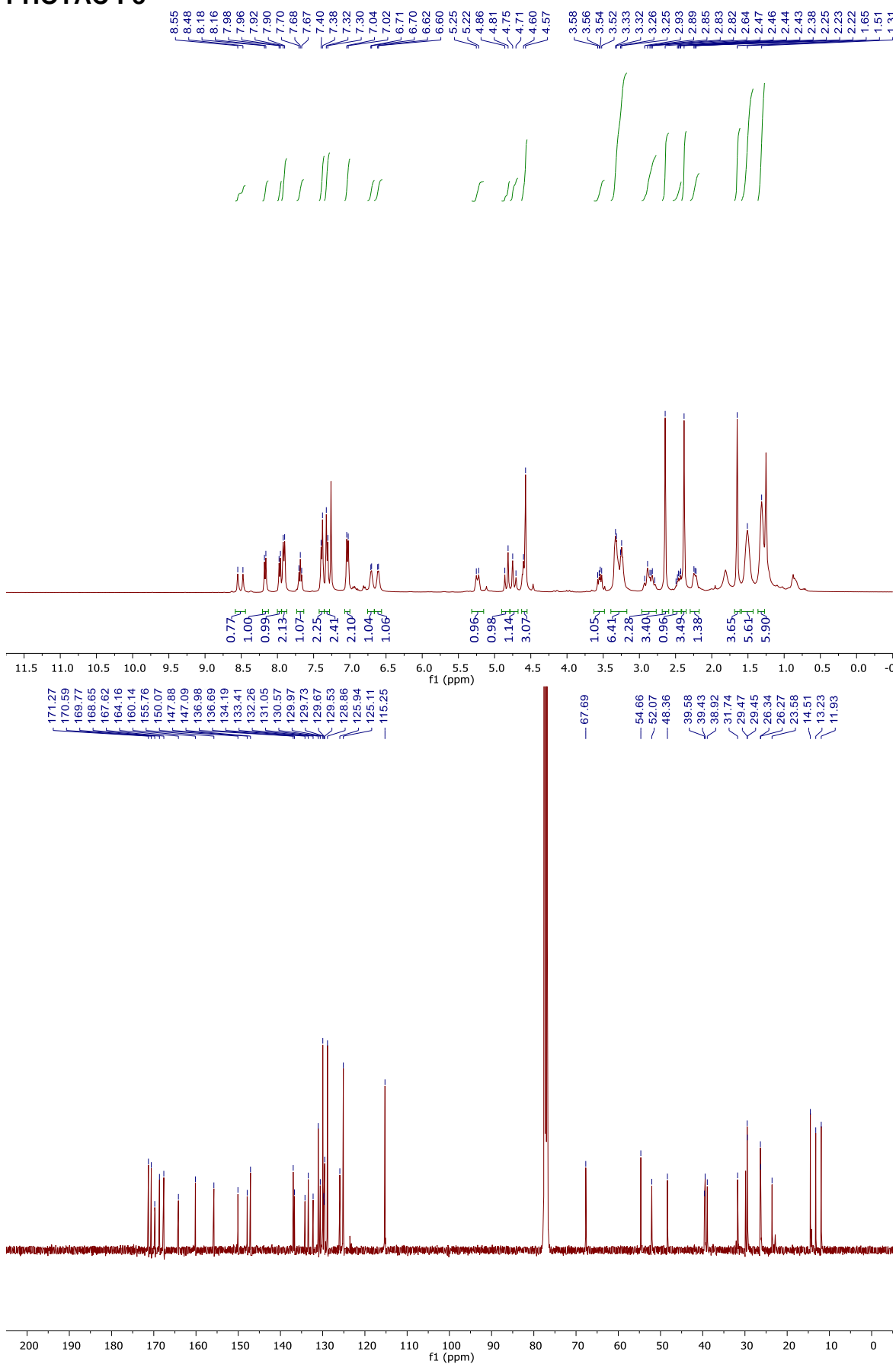
PHOTAC-I-6



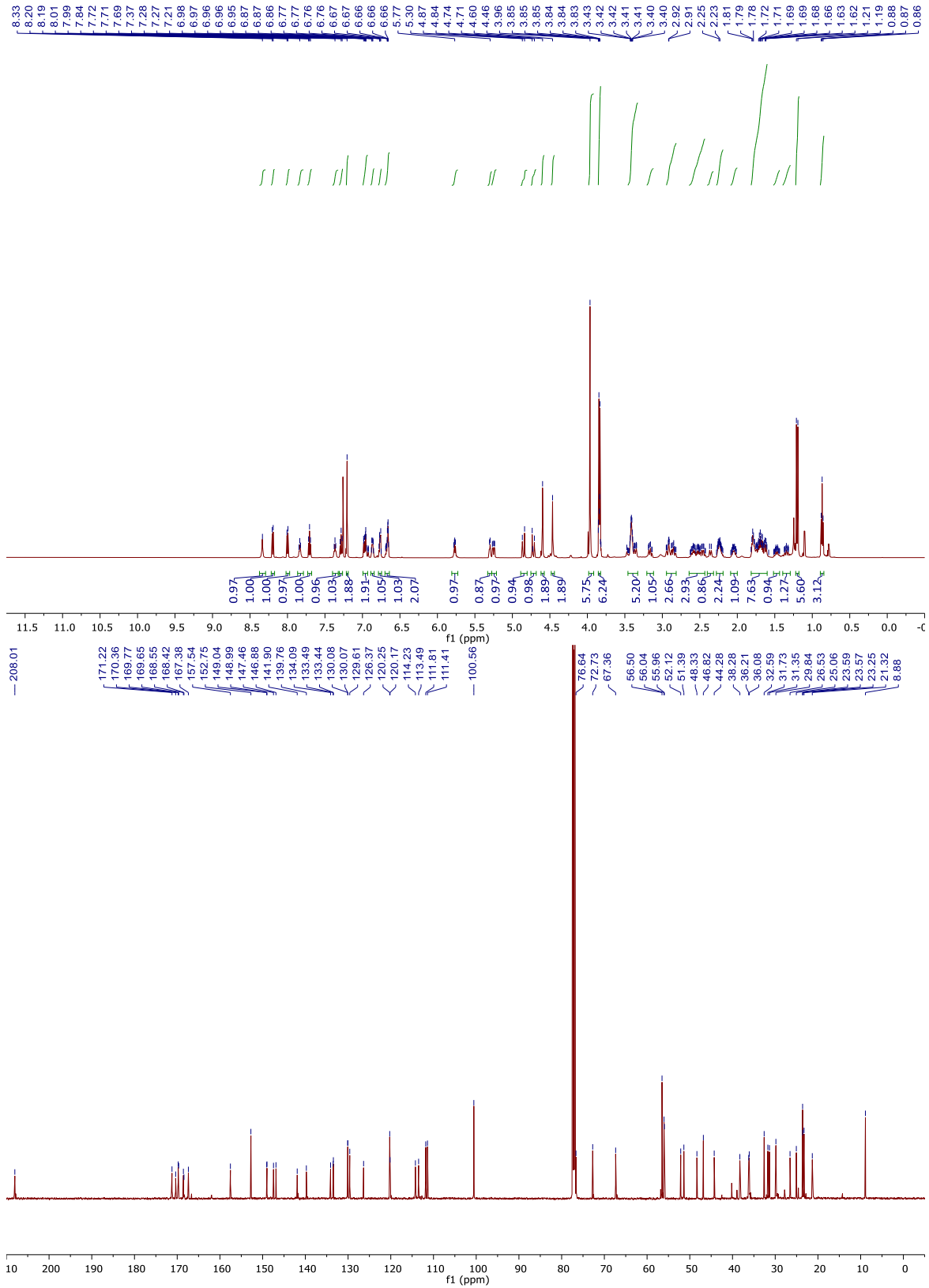
PHOTAC-I-7



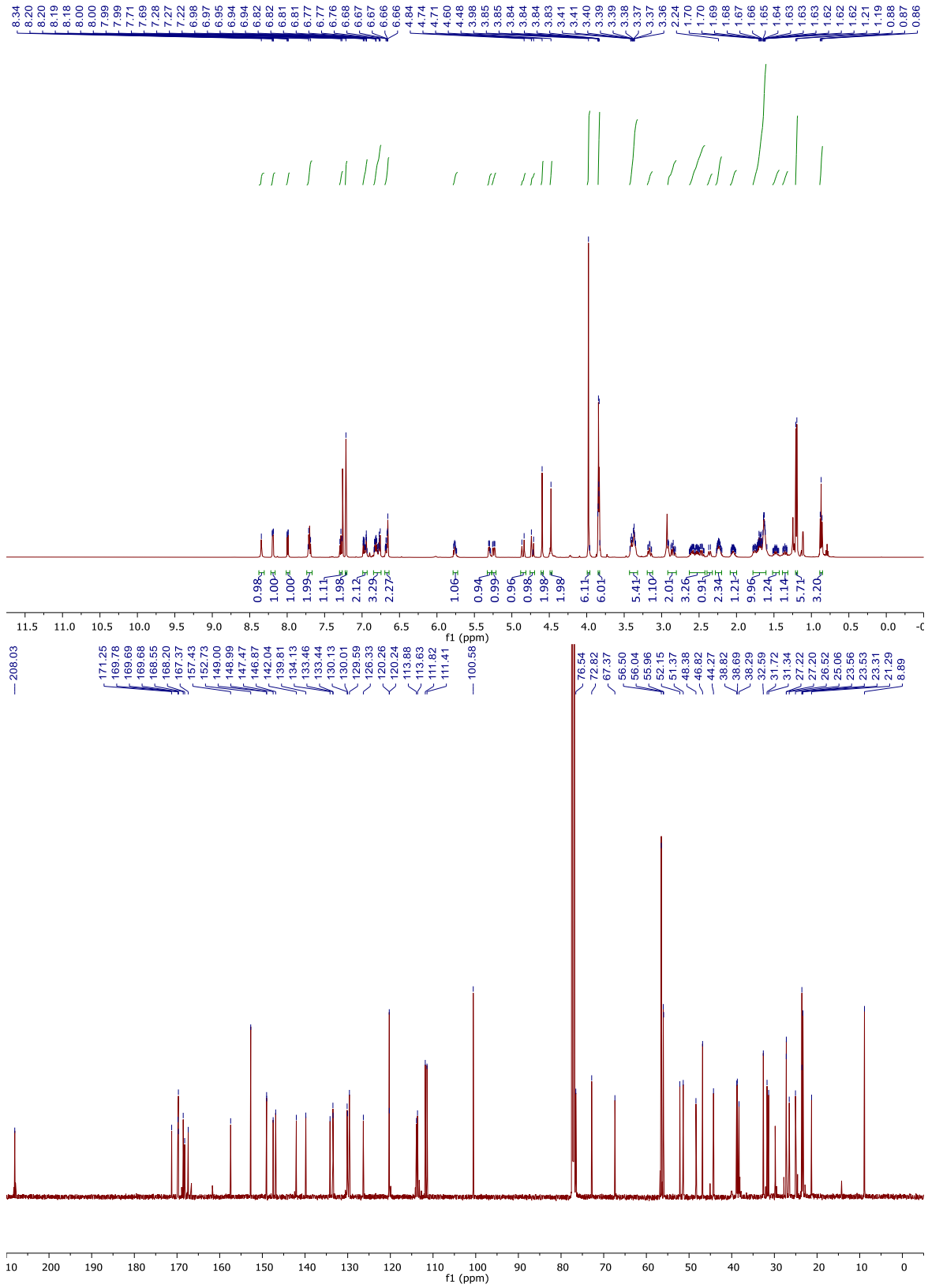
PHOTAC-I-8



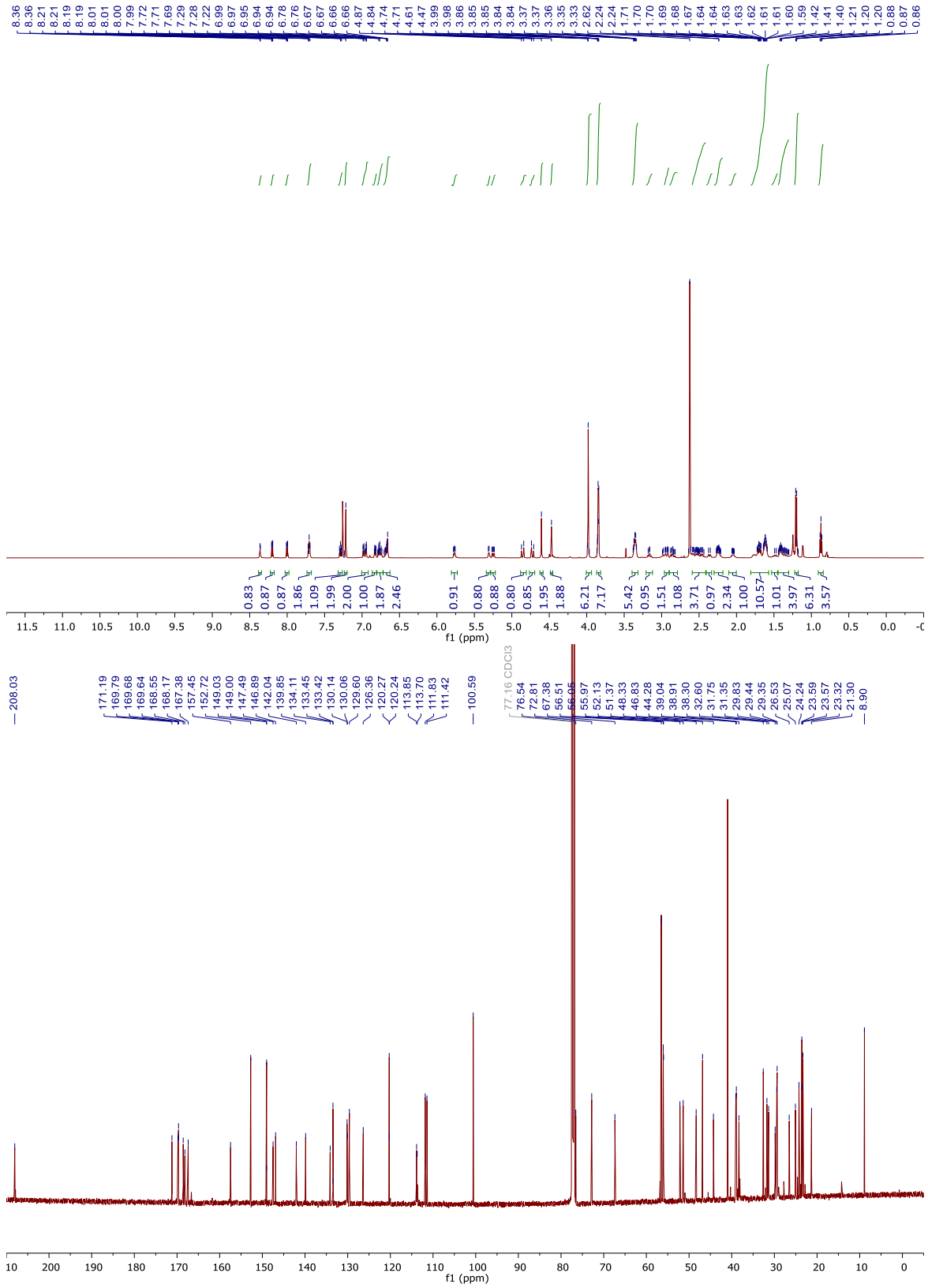
PHOTAC-II-1



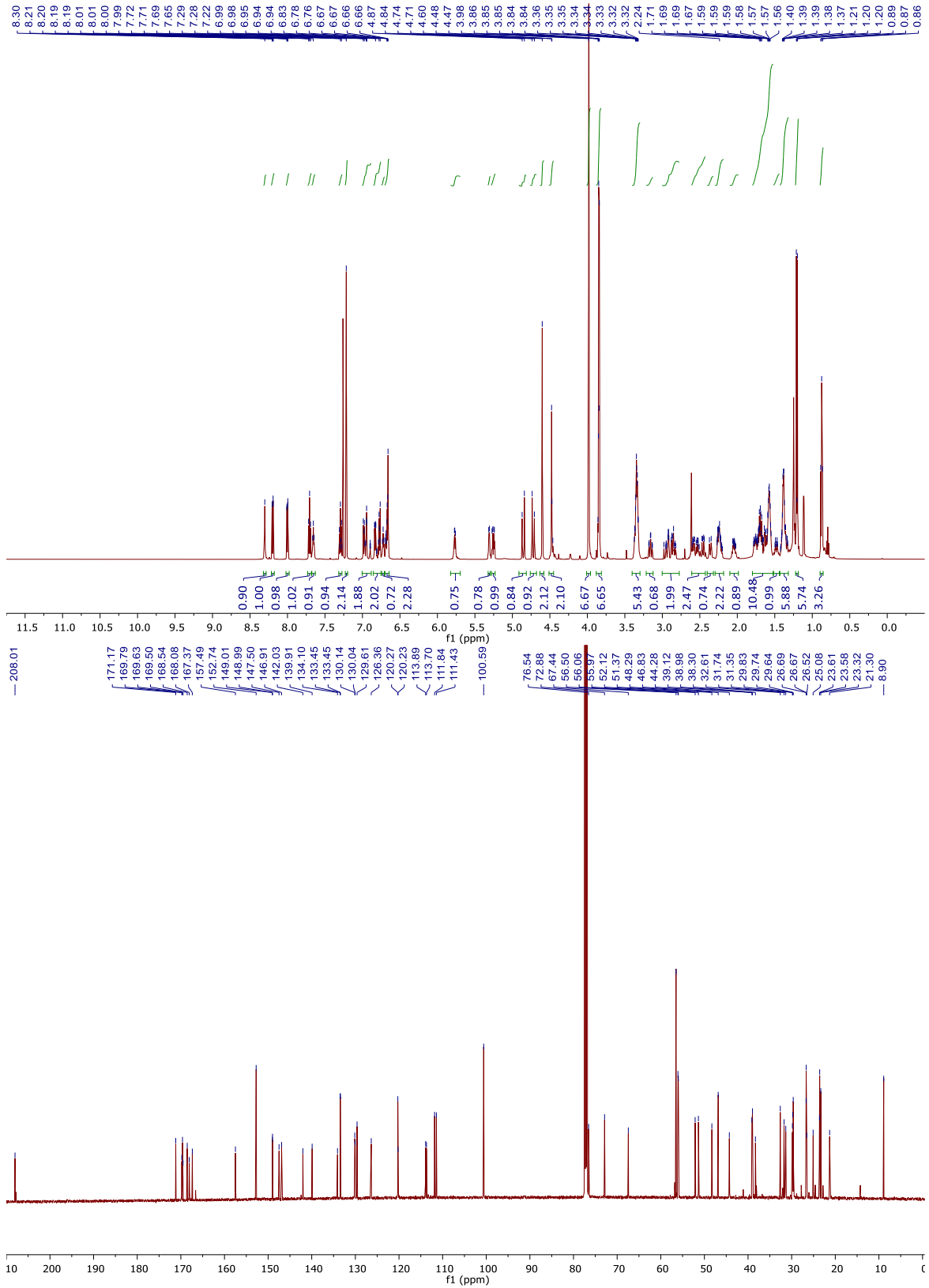
PHOTAC-II-2



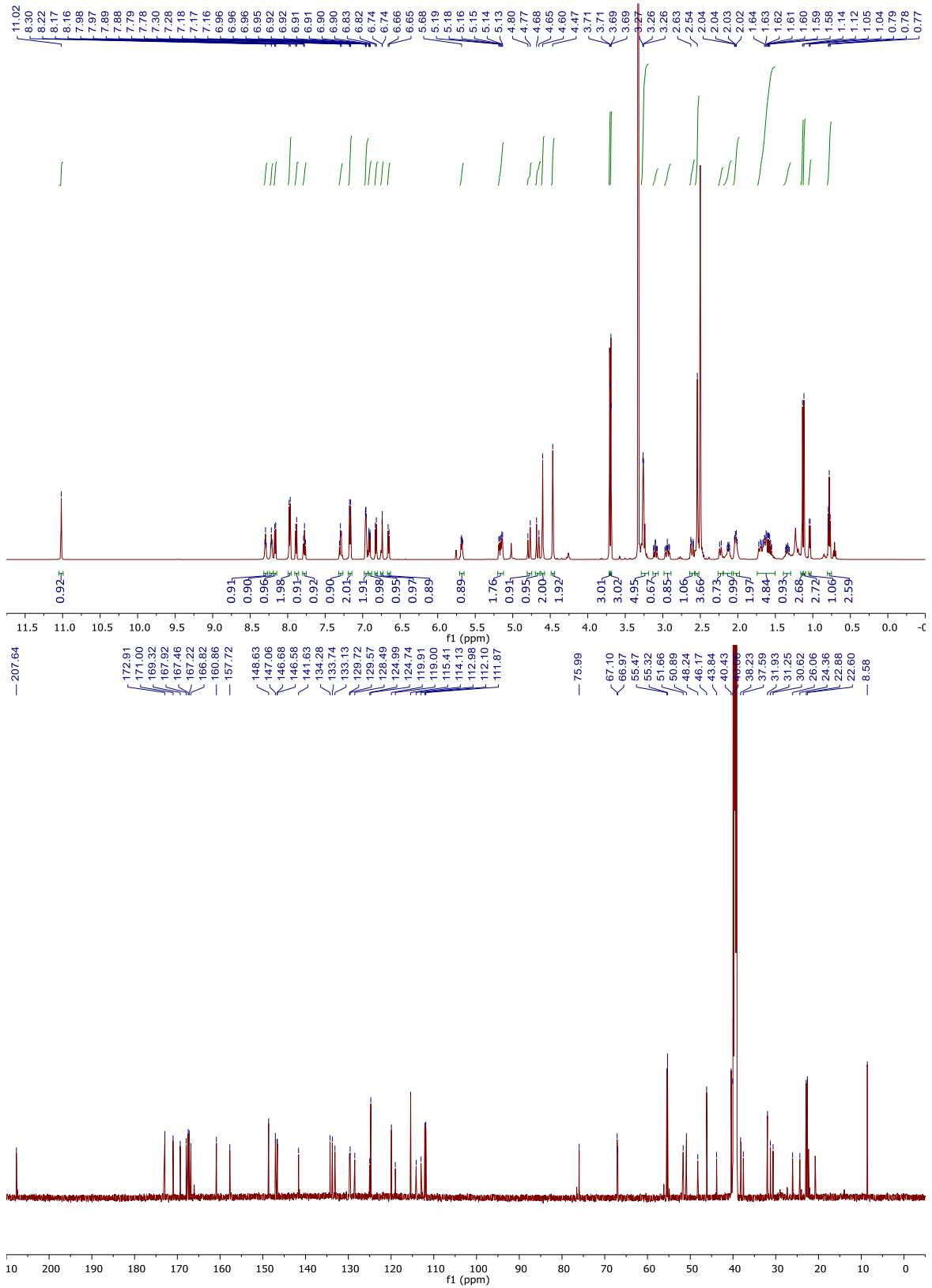
PHOTAC-II-3



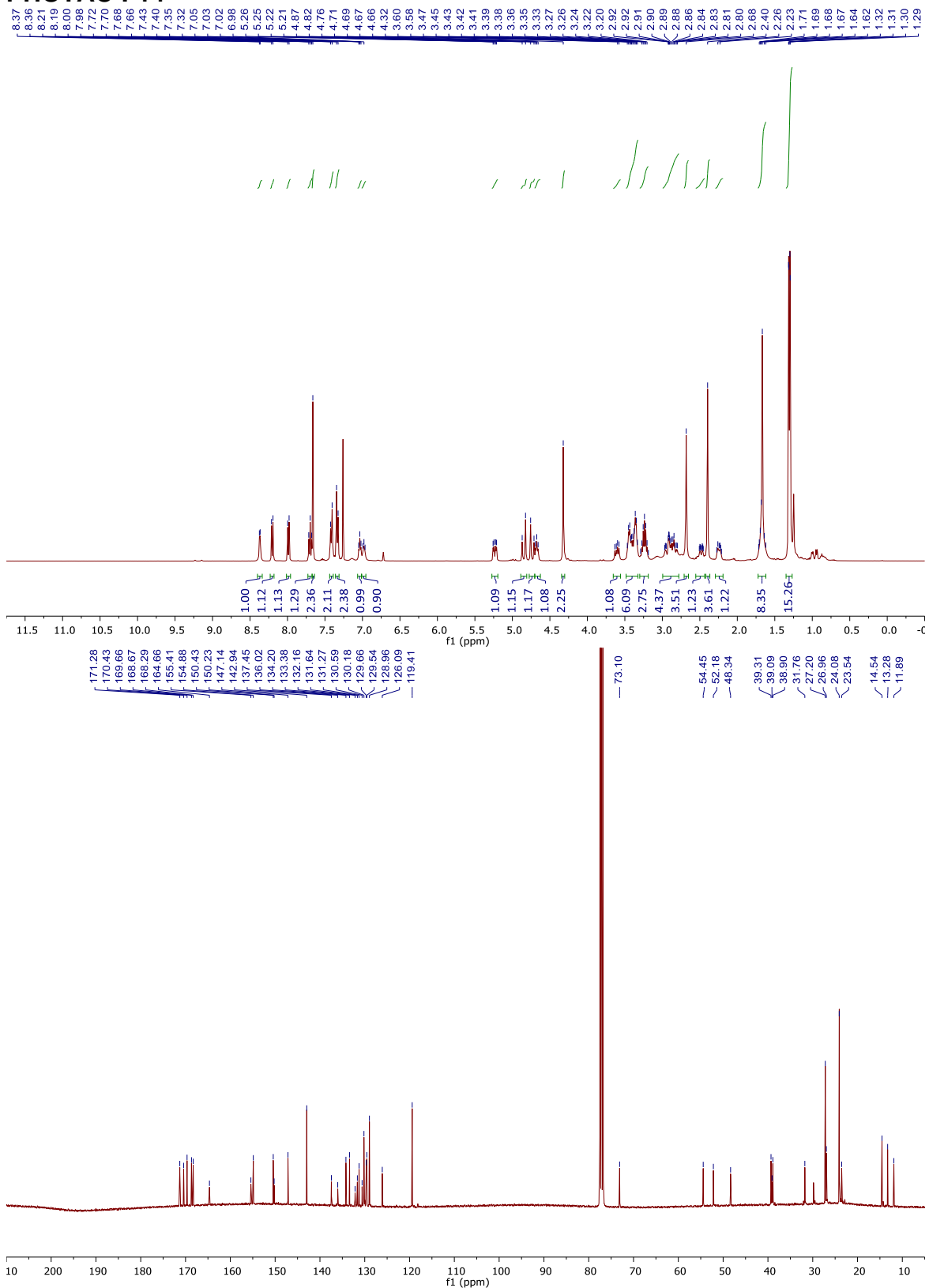
PHOTAC-II-4



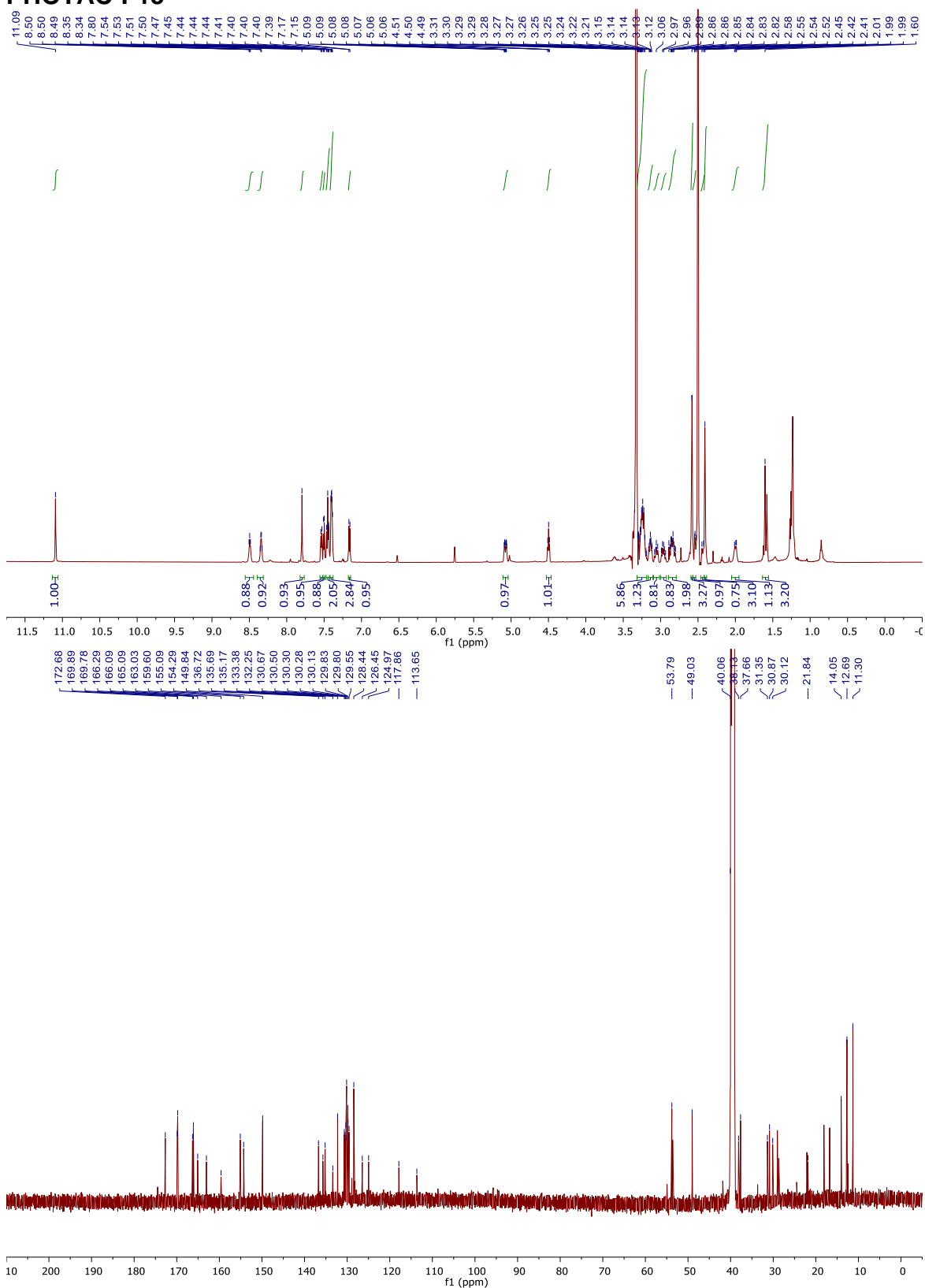
PHOTAC-II-5



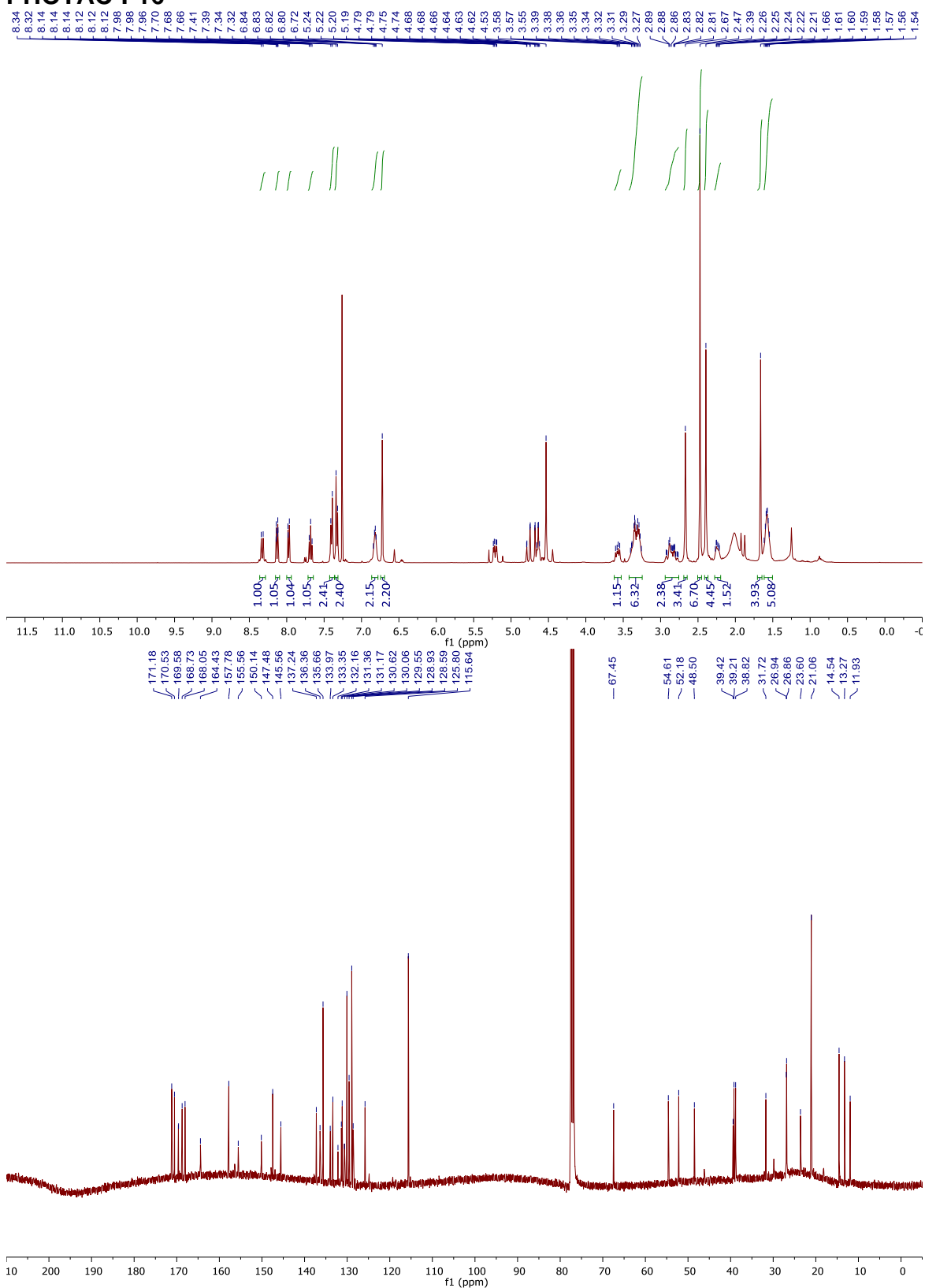
PHOTAC-I-14



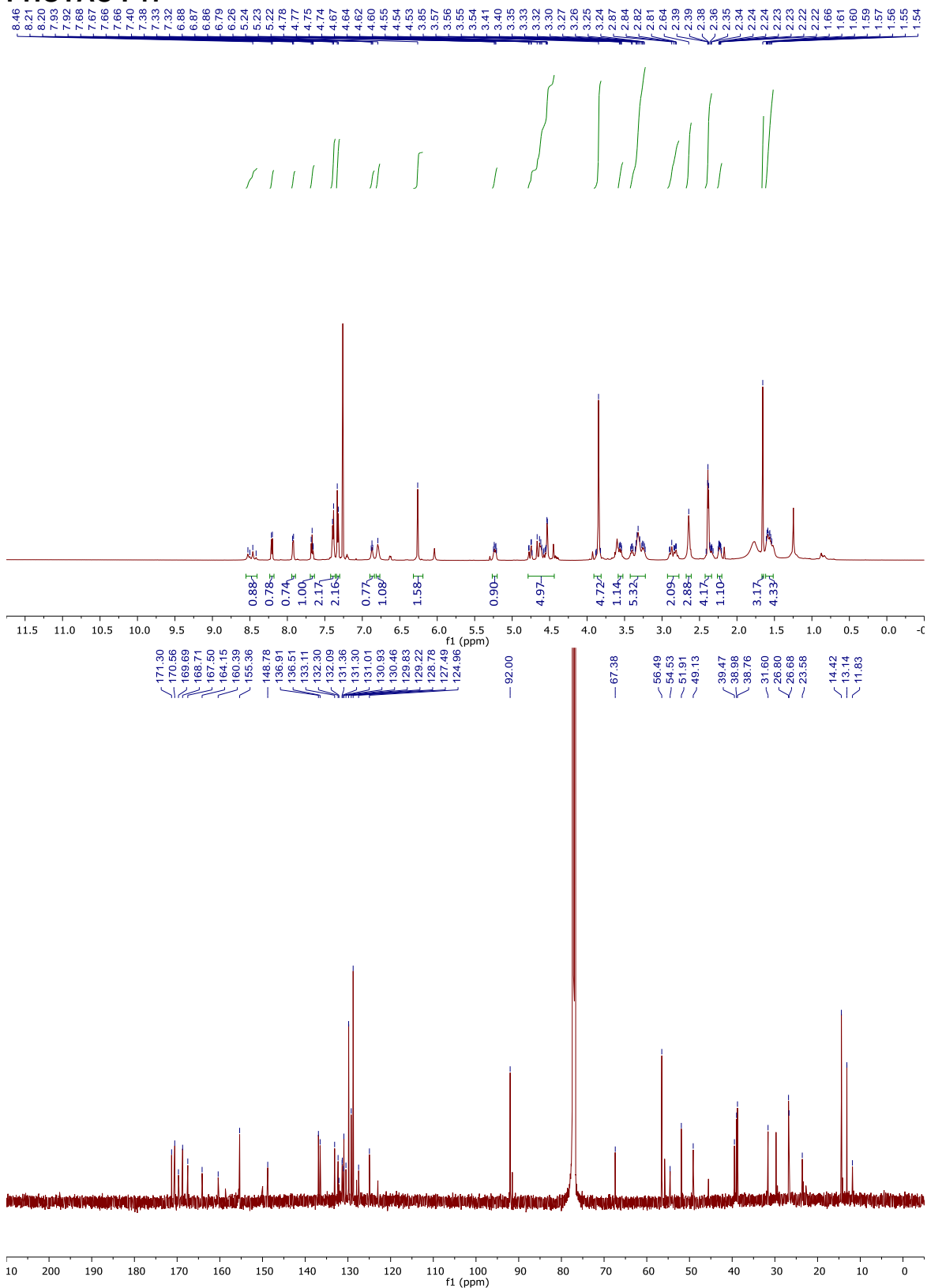
PHOTAC-I-15



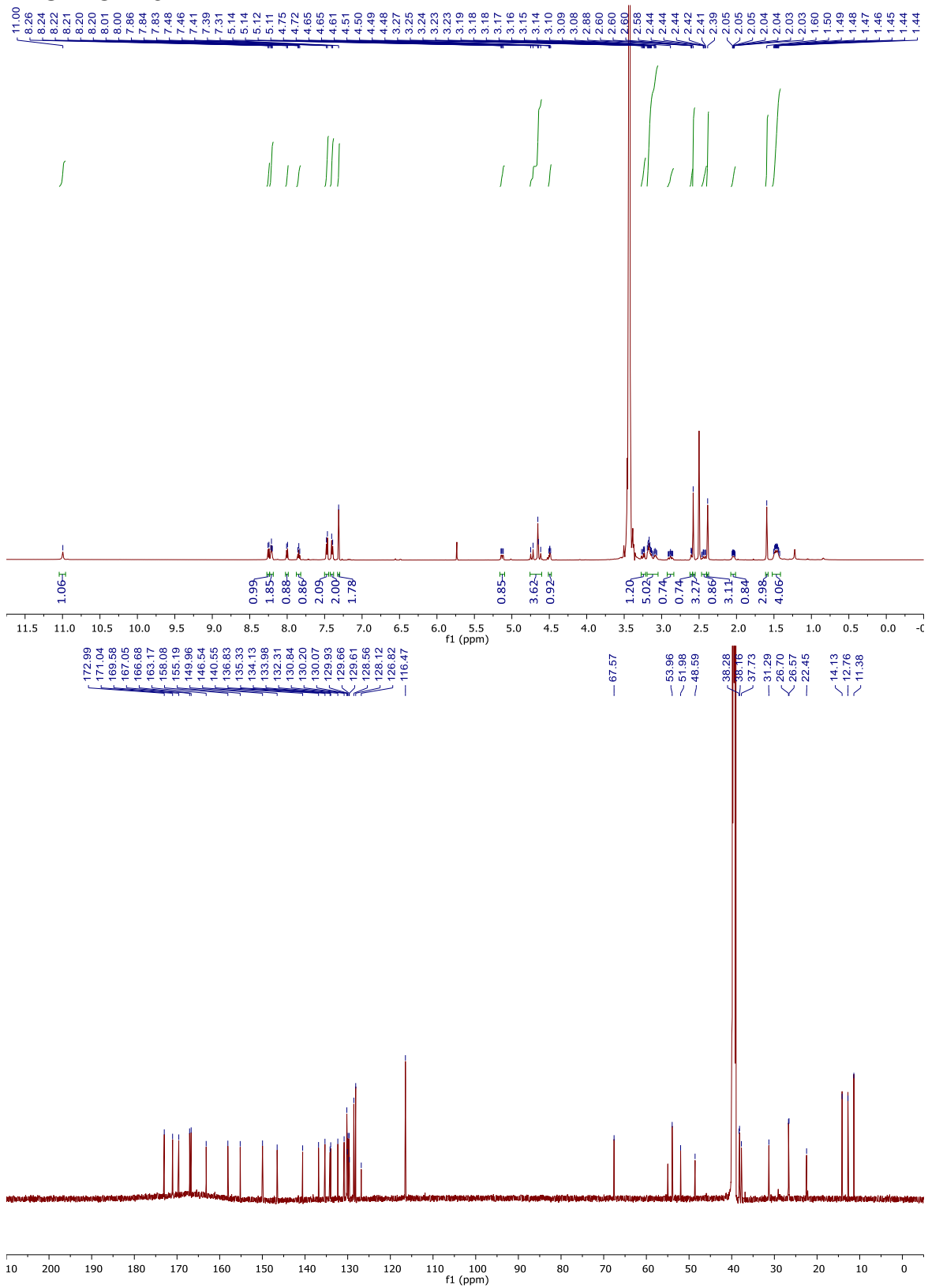
PHOTAC-I-16



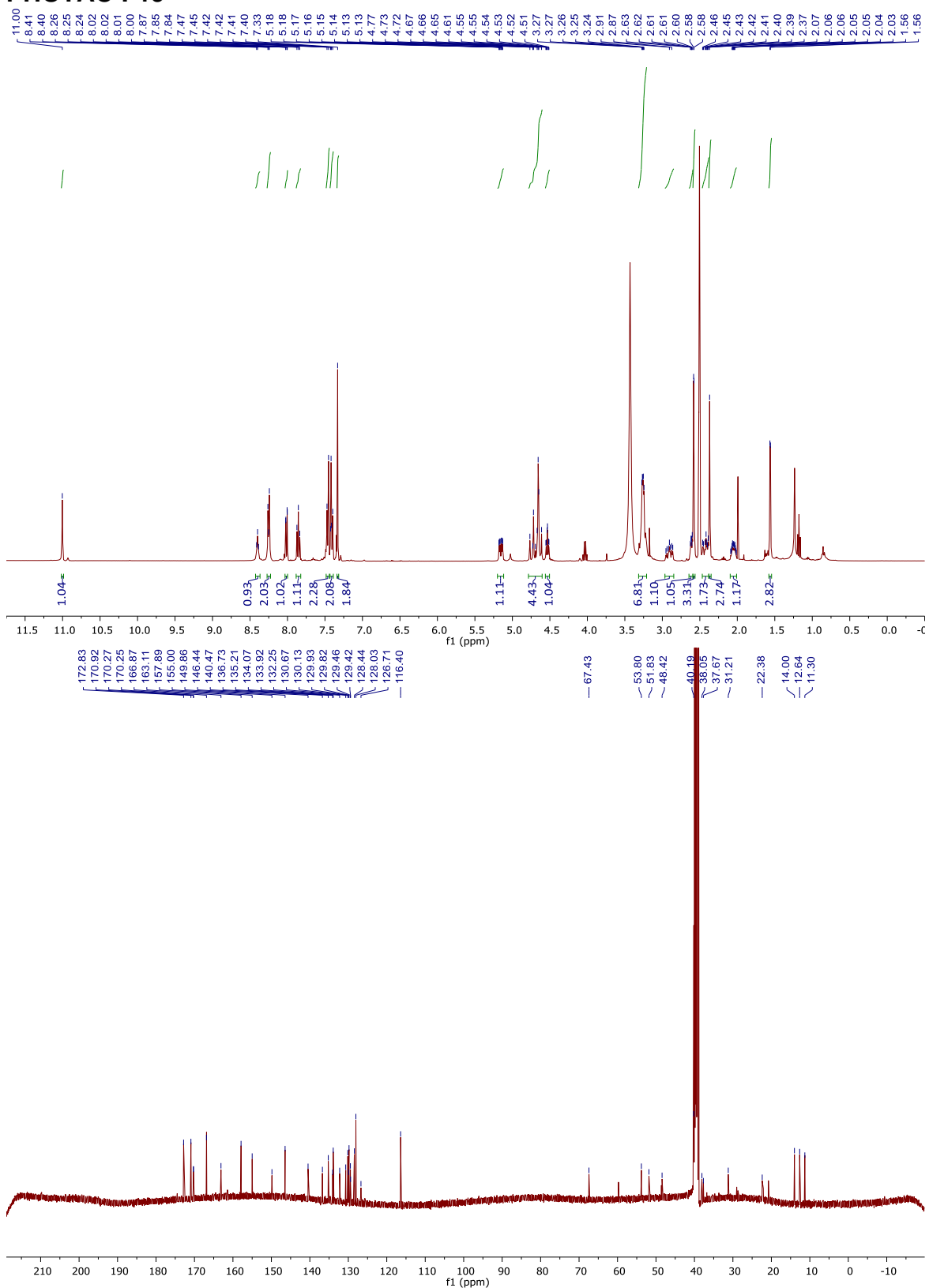
PHOTAC-I-17



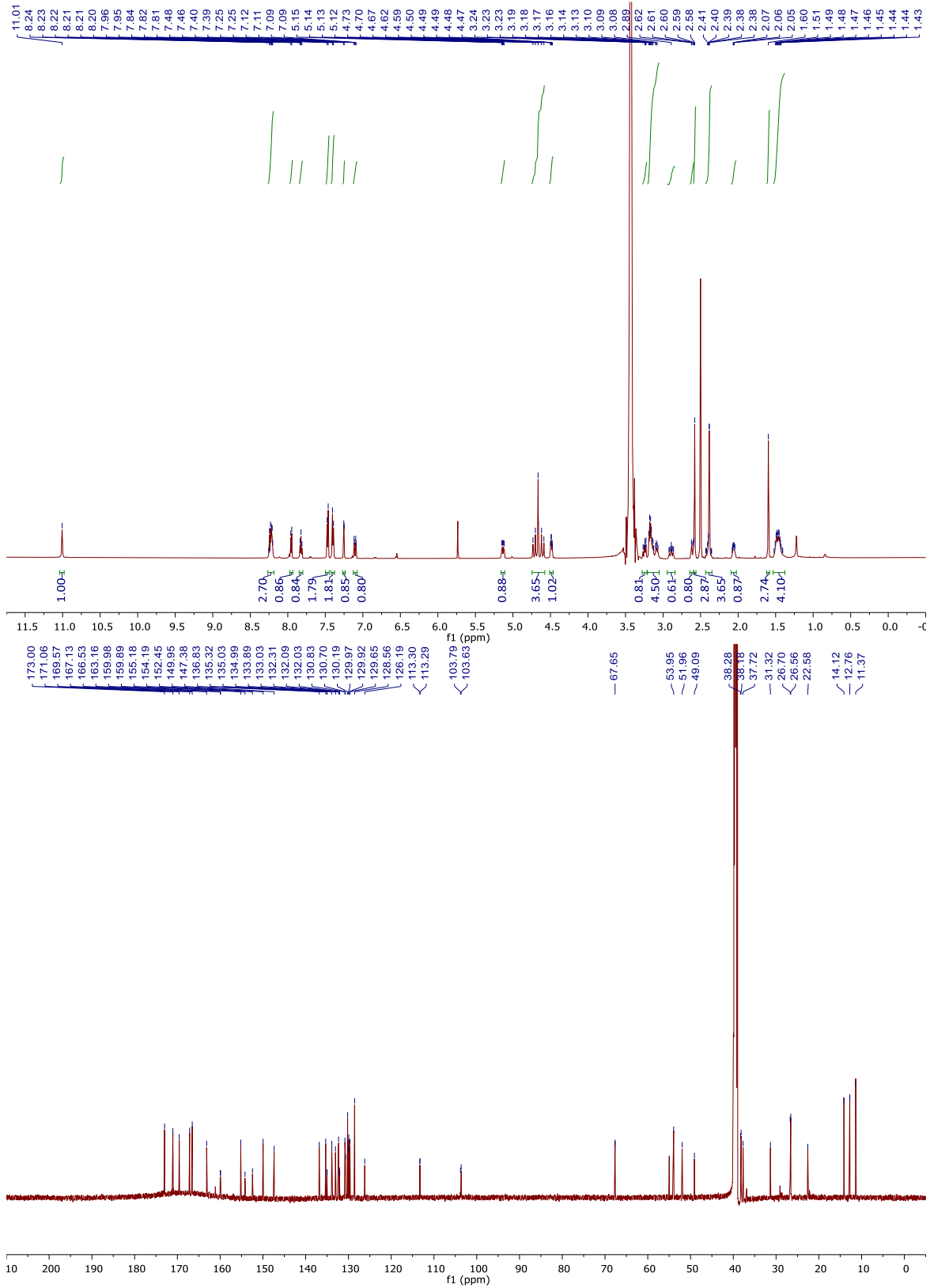
PHOTAC-I-18



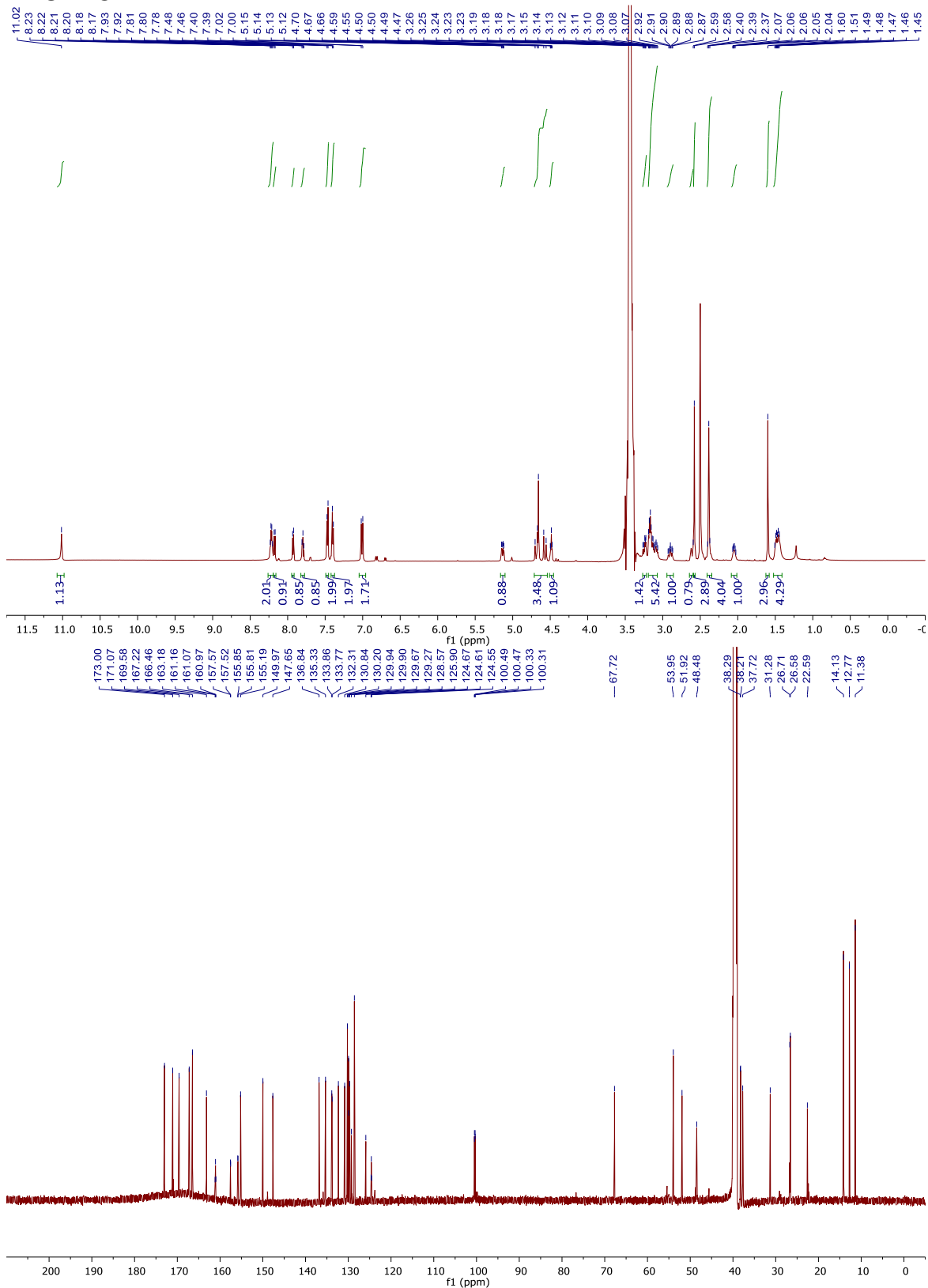
PHOTAC-I-19



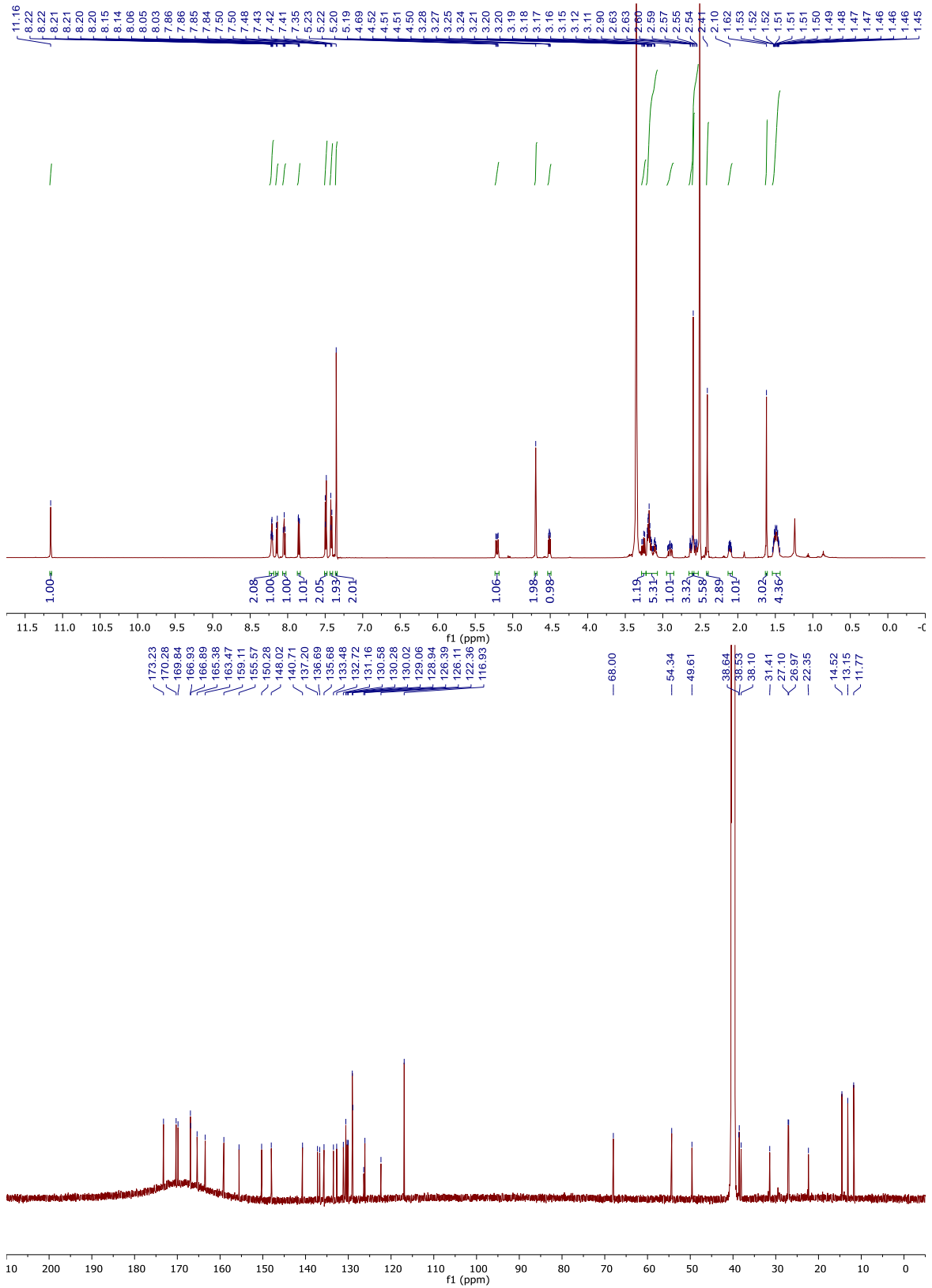
PHOTAC-I-20



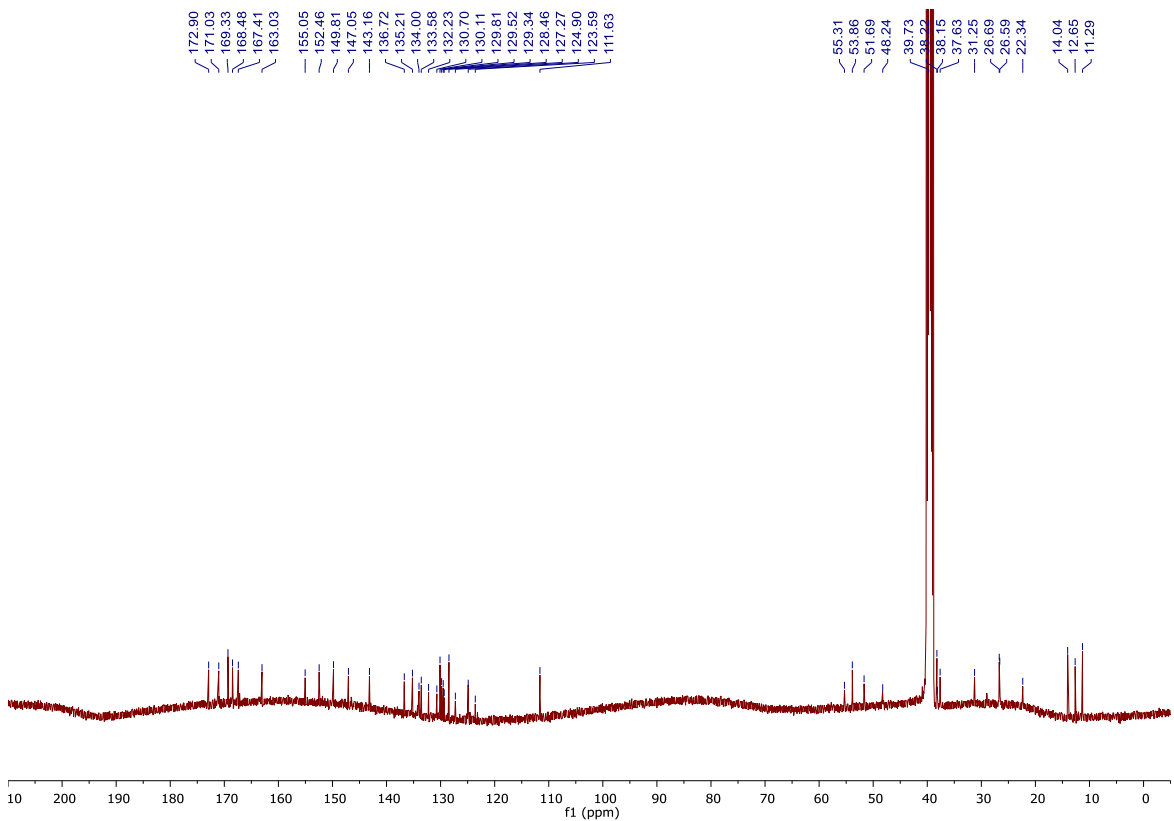
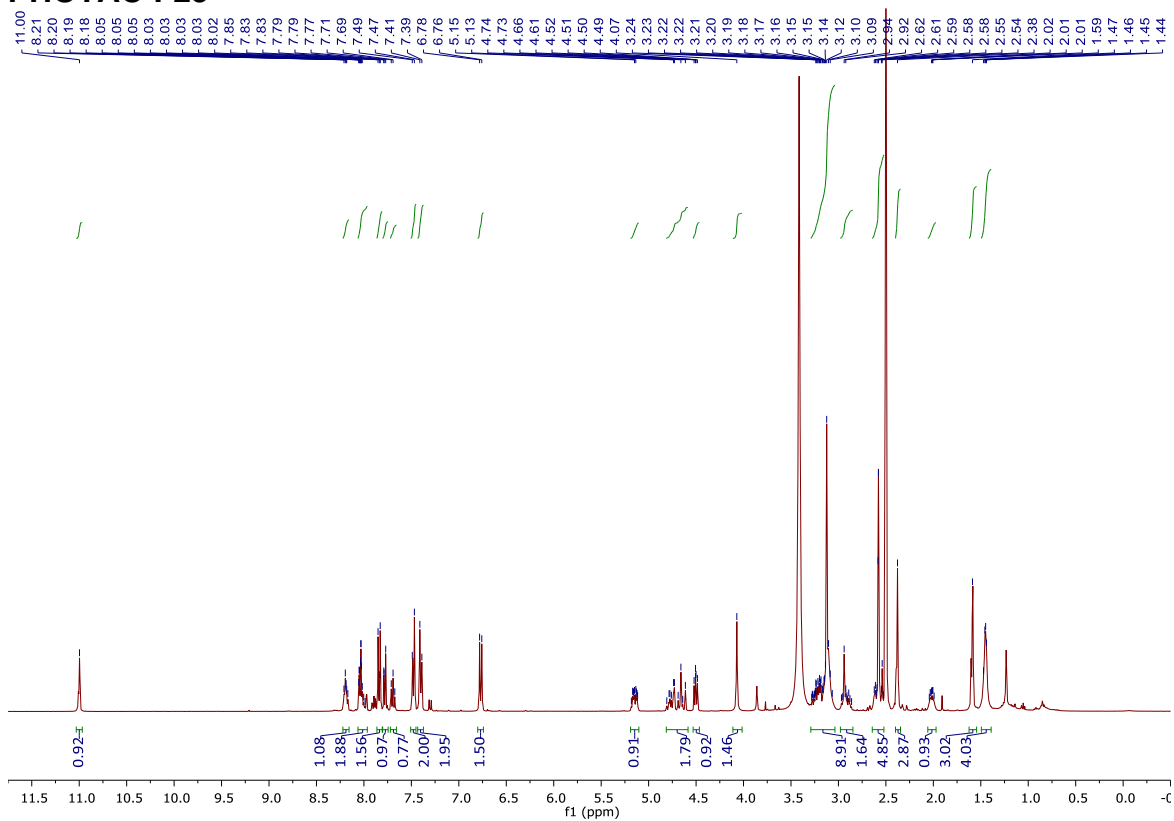
PHOTAC-I-21



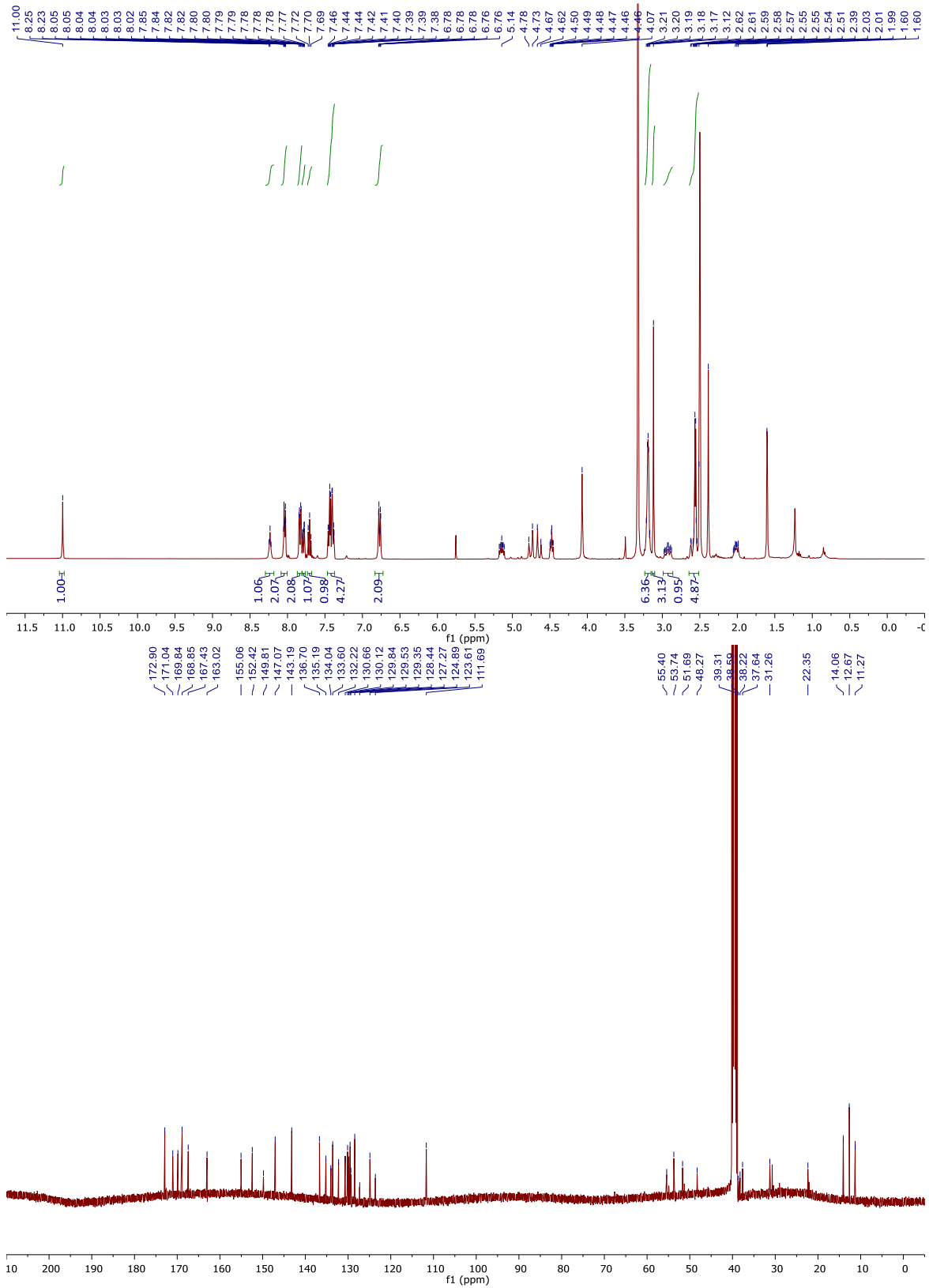
PHOTAC-I-22



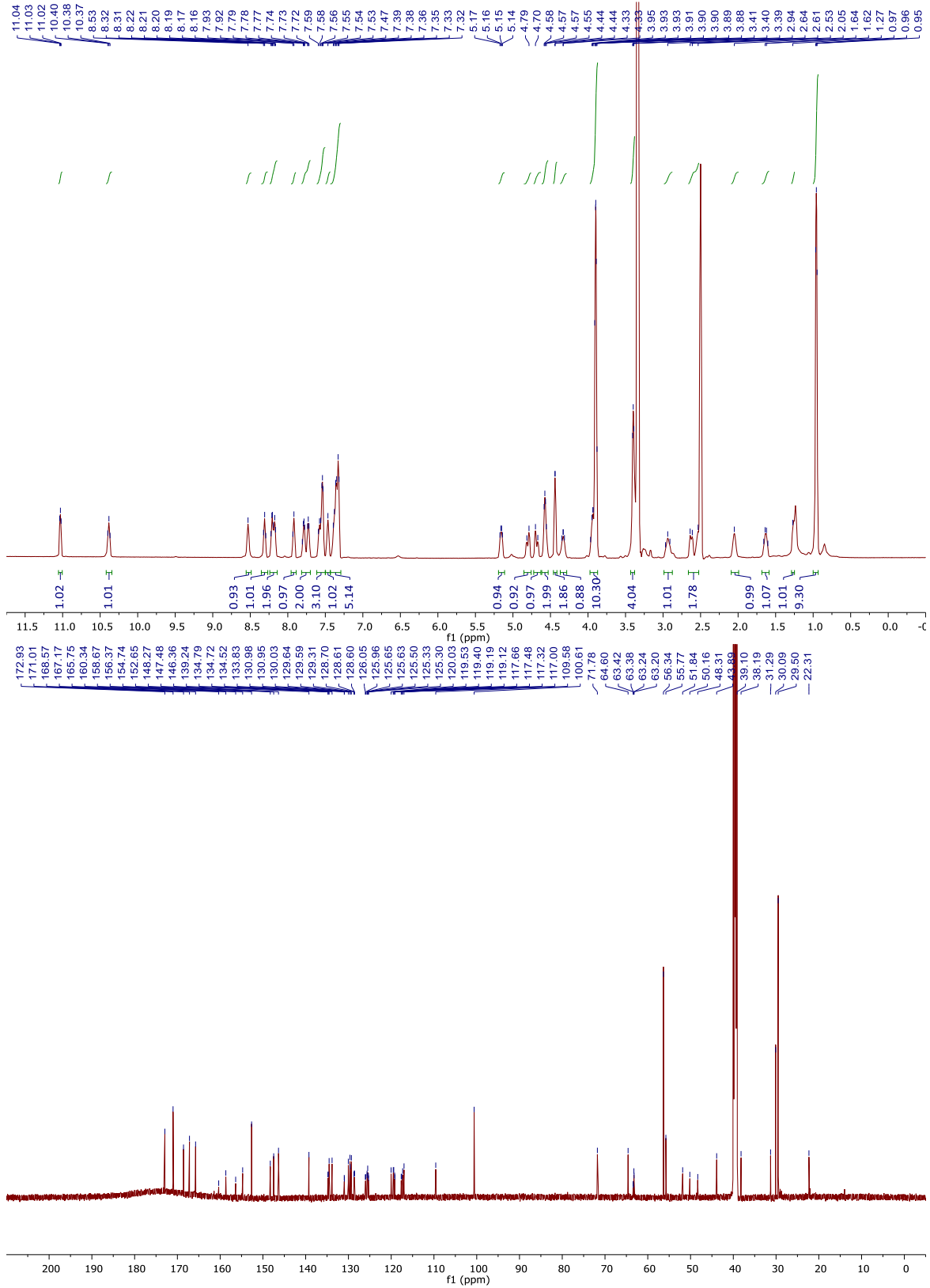
PHOTAC-I-23



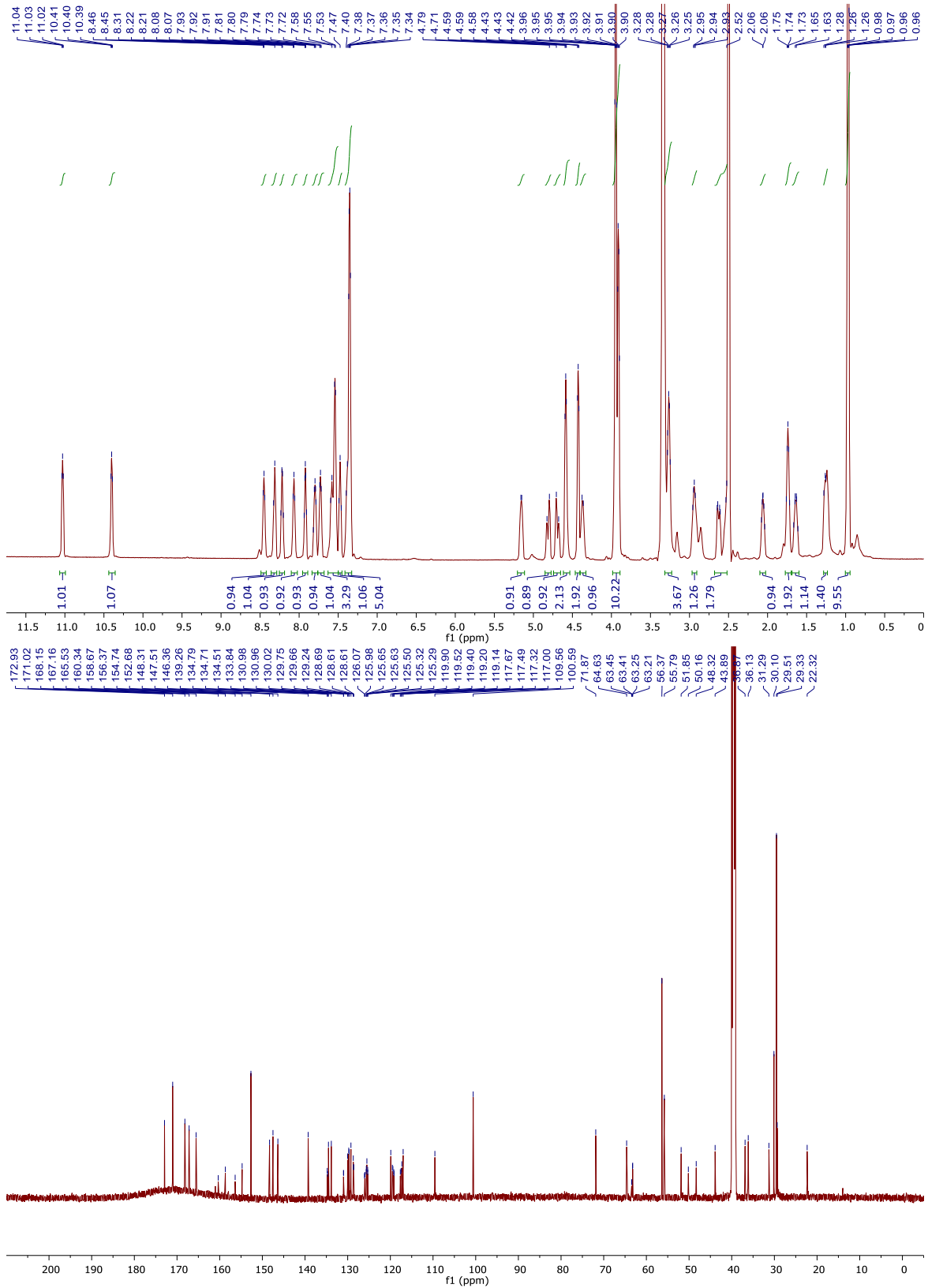
PHOTAC-I-24



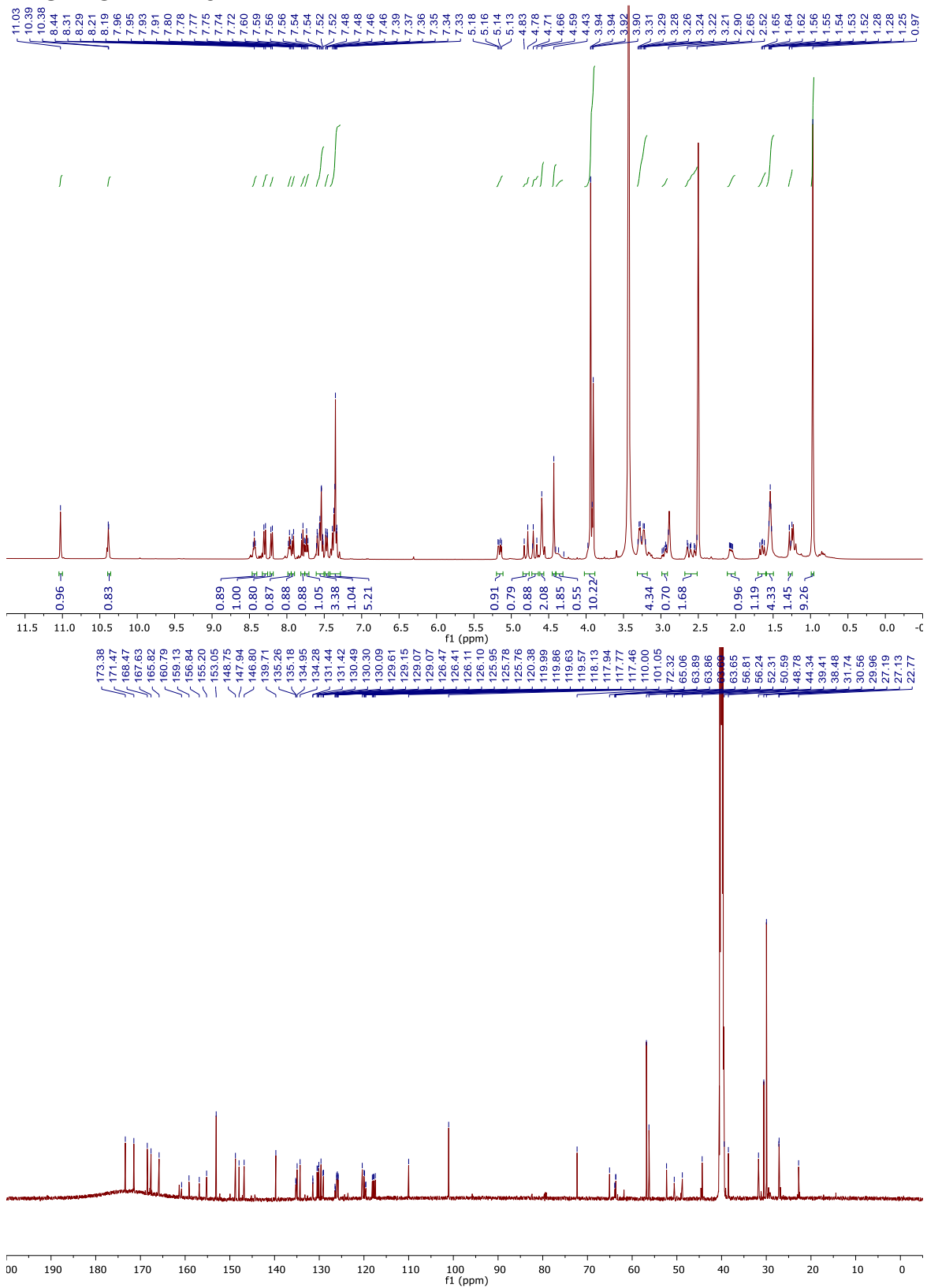
PHOTAC-MDM2-1



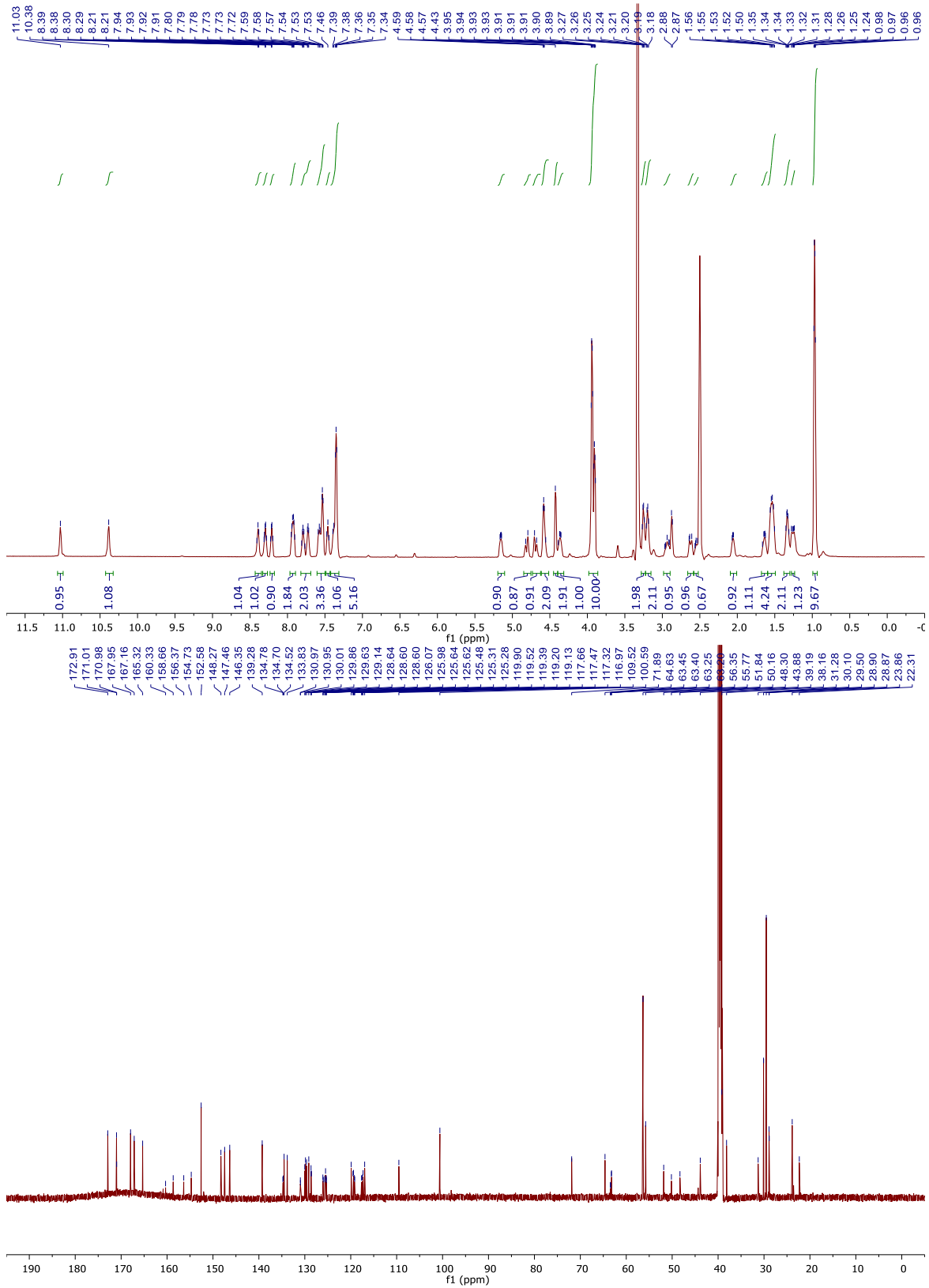
PHOTAC-MDM2-2



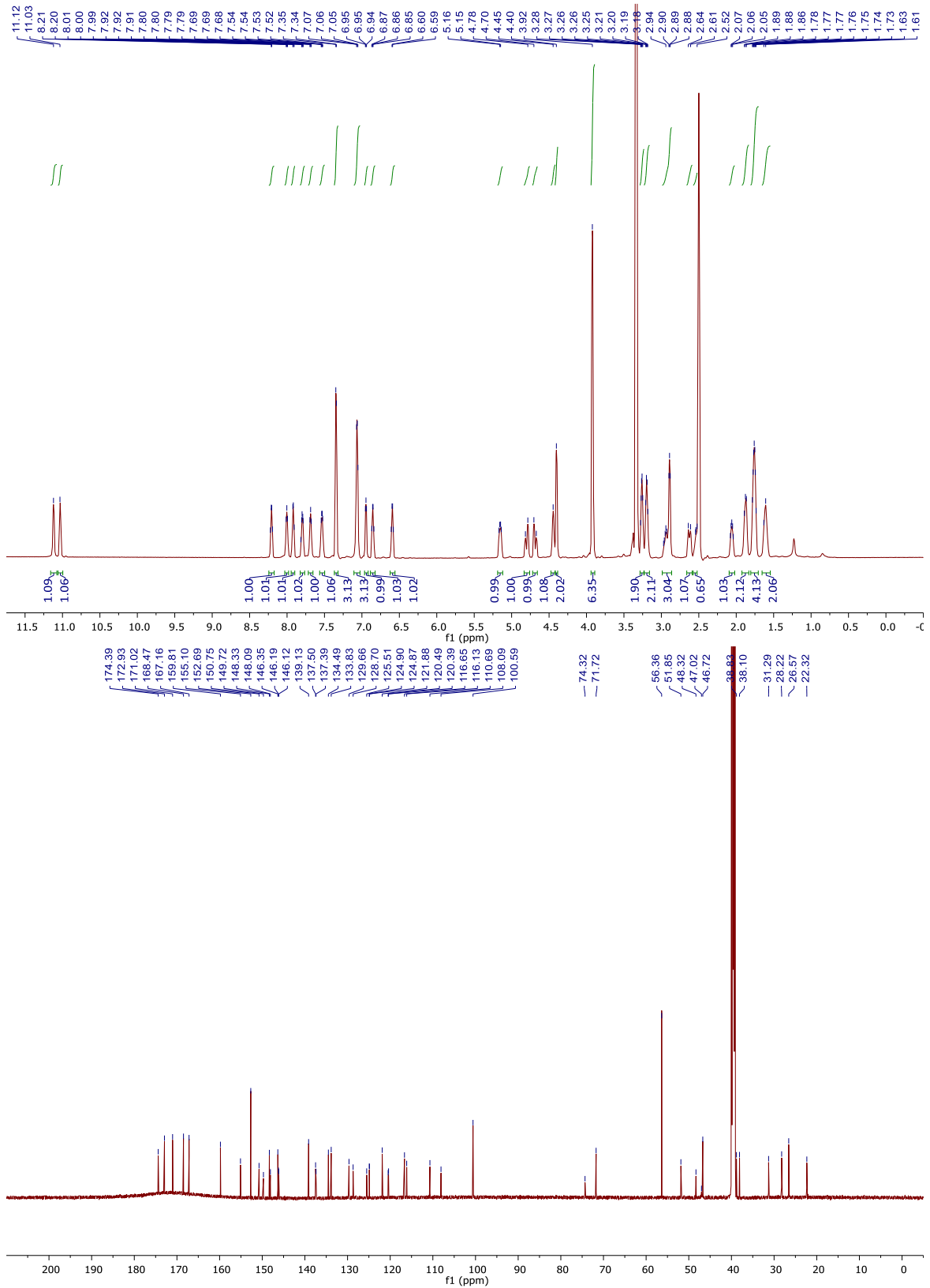
PHOTAC-MDM2-3



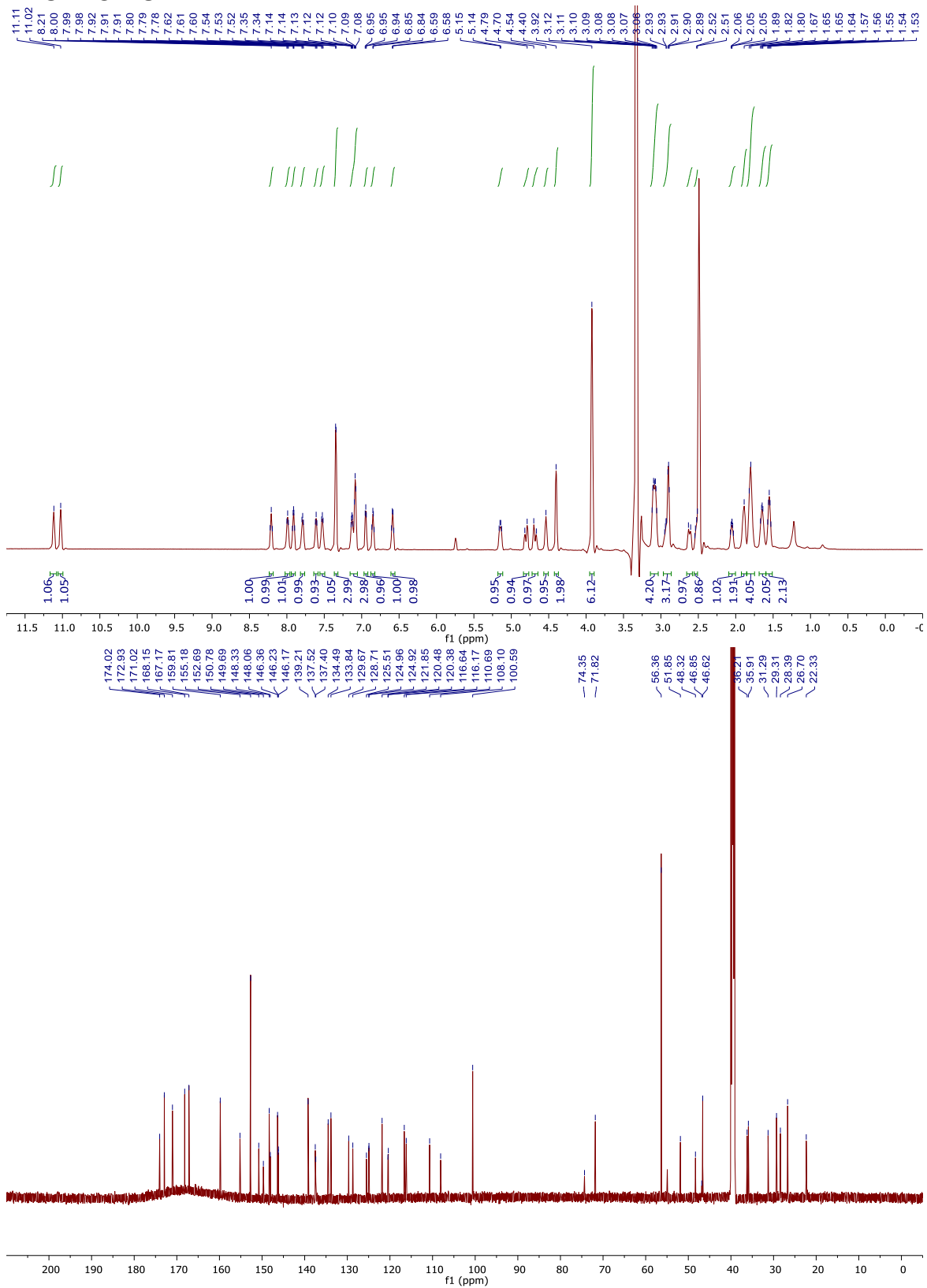
PHOTAC-MDM2-4



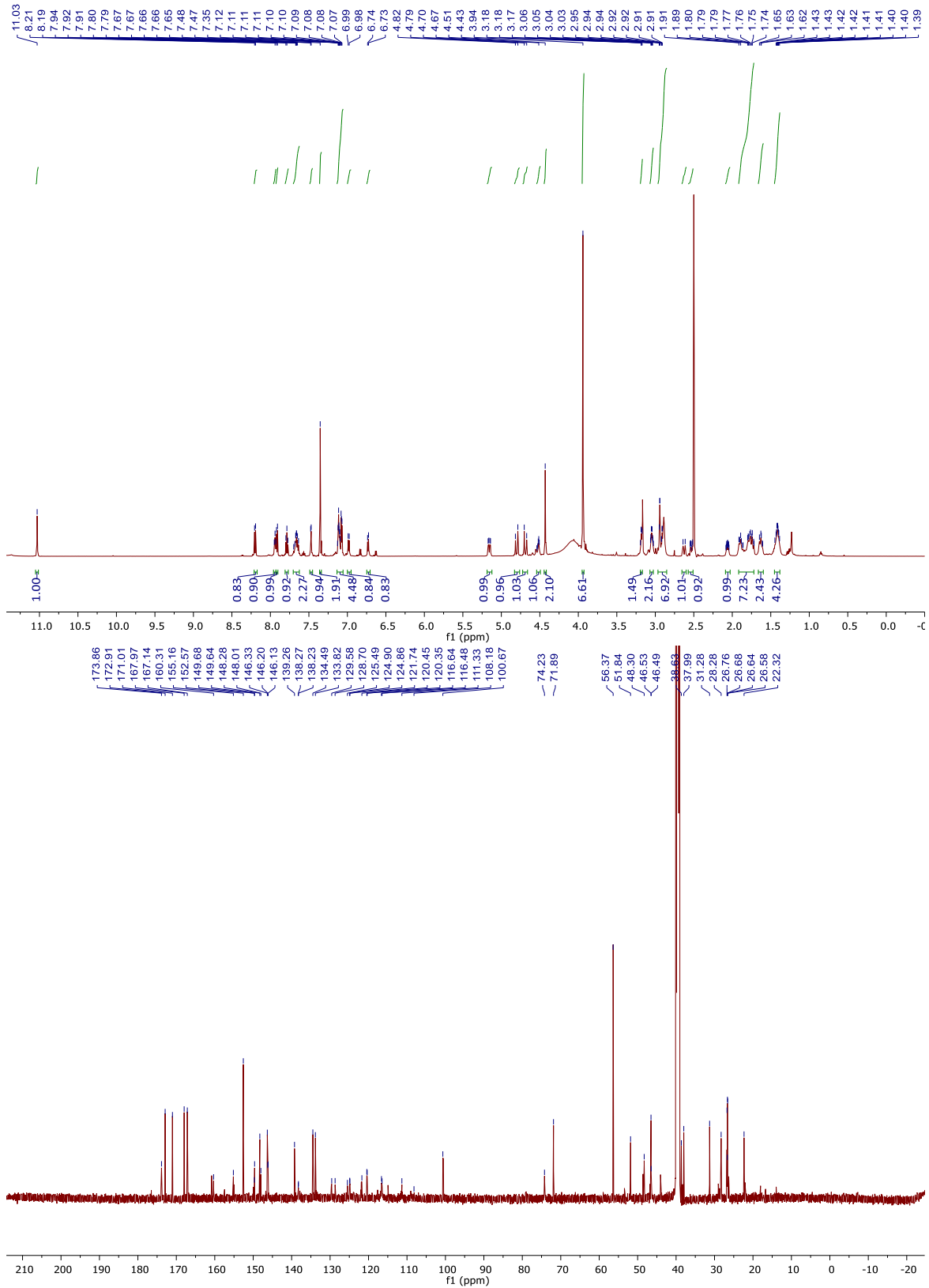
PHOTAC-AURKA-1



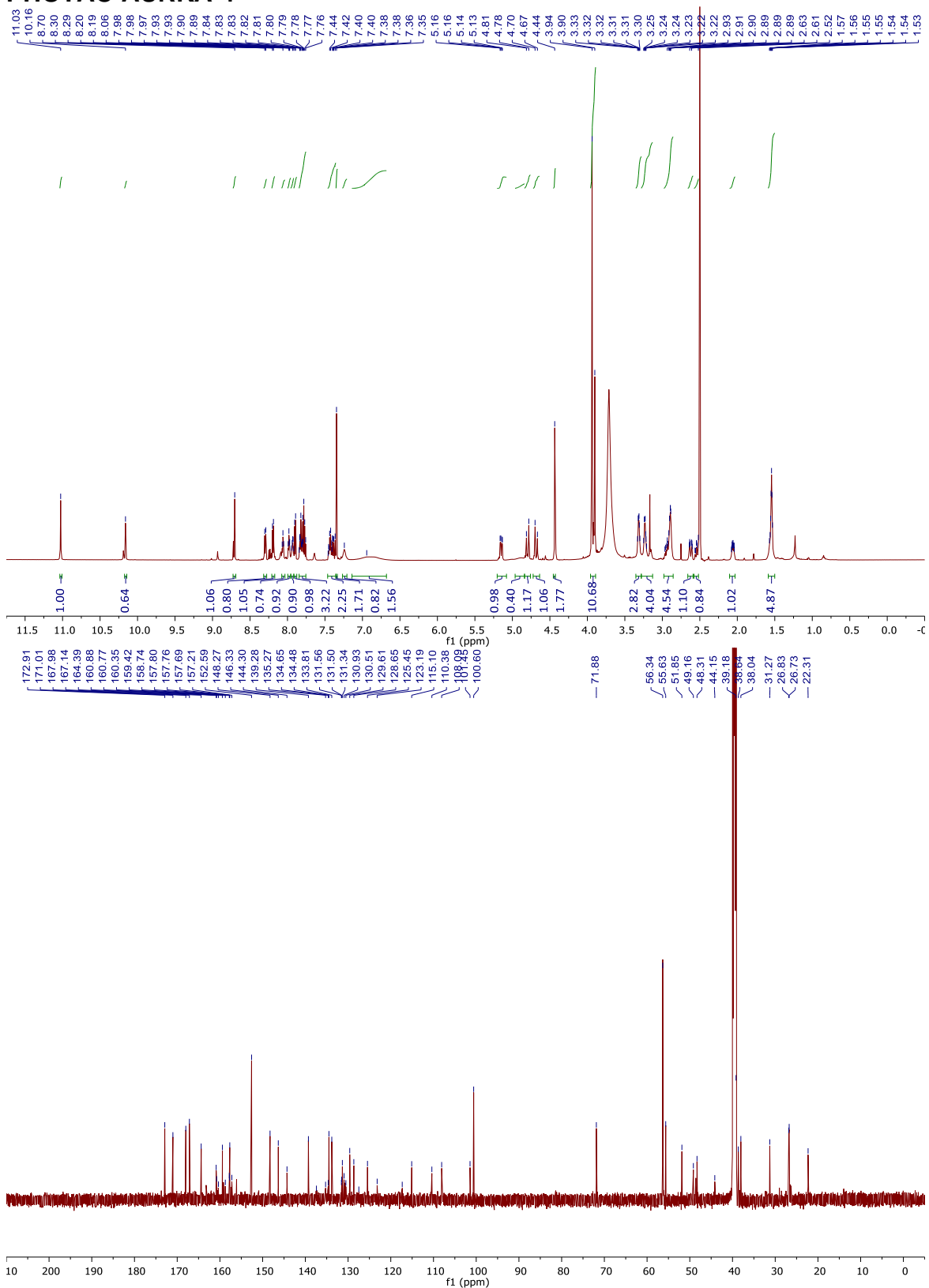
PHOTAC-AURKA-2



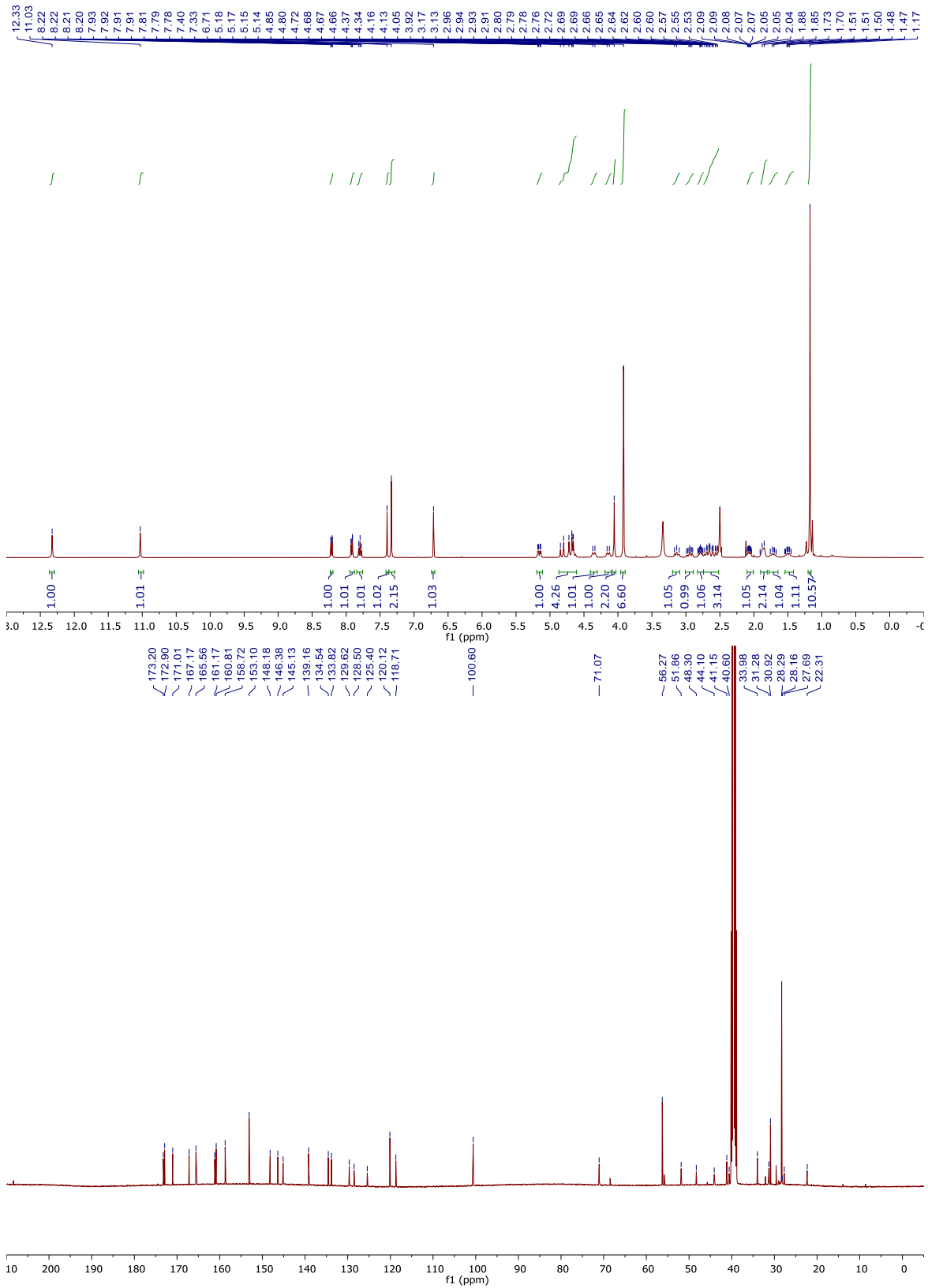
PHOTAC-AURKA-3



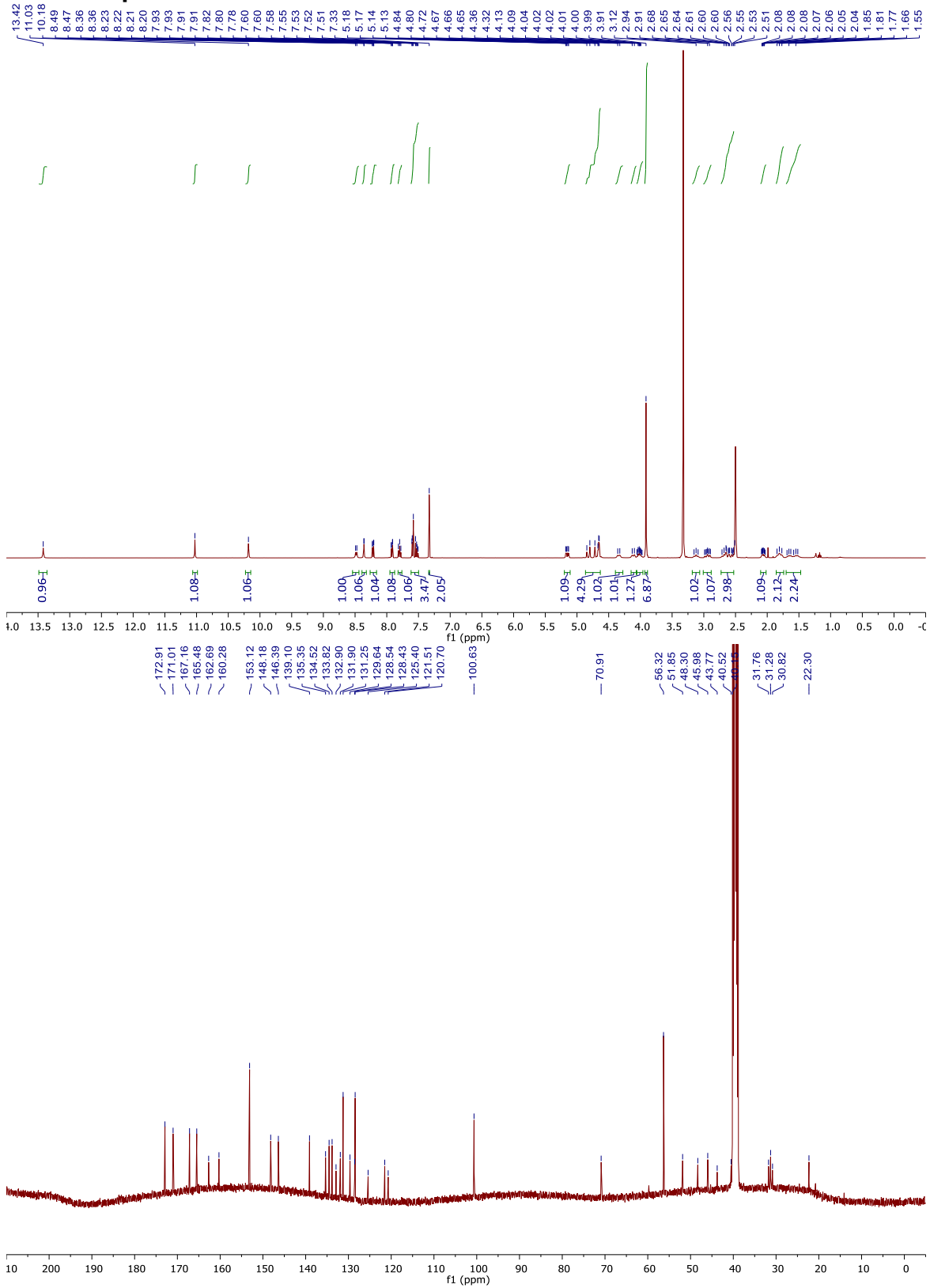
PHOTAC-AURKA-4



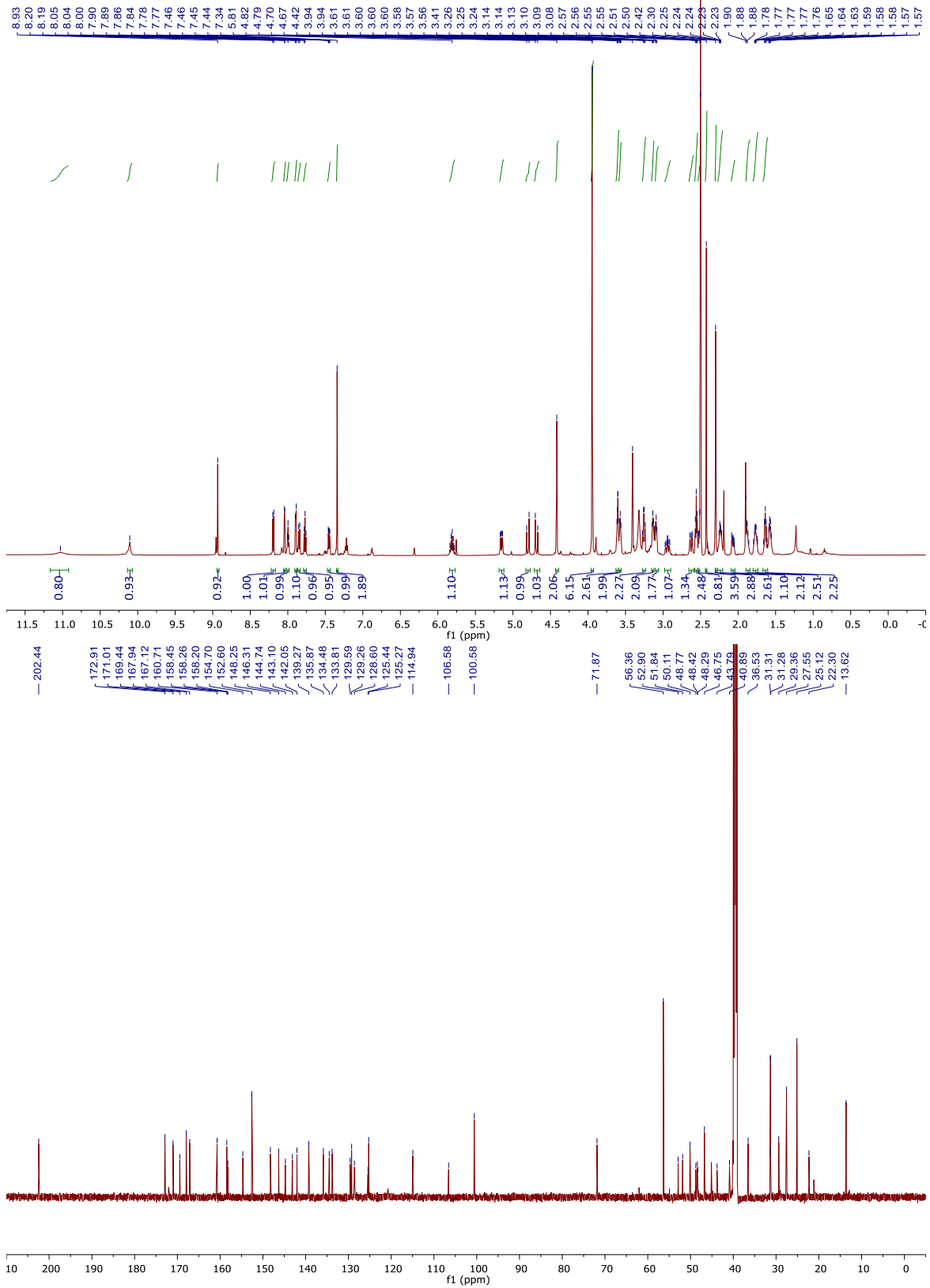
PHOTAC-panCDK-1



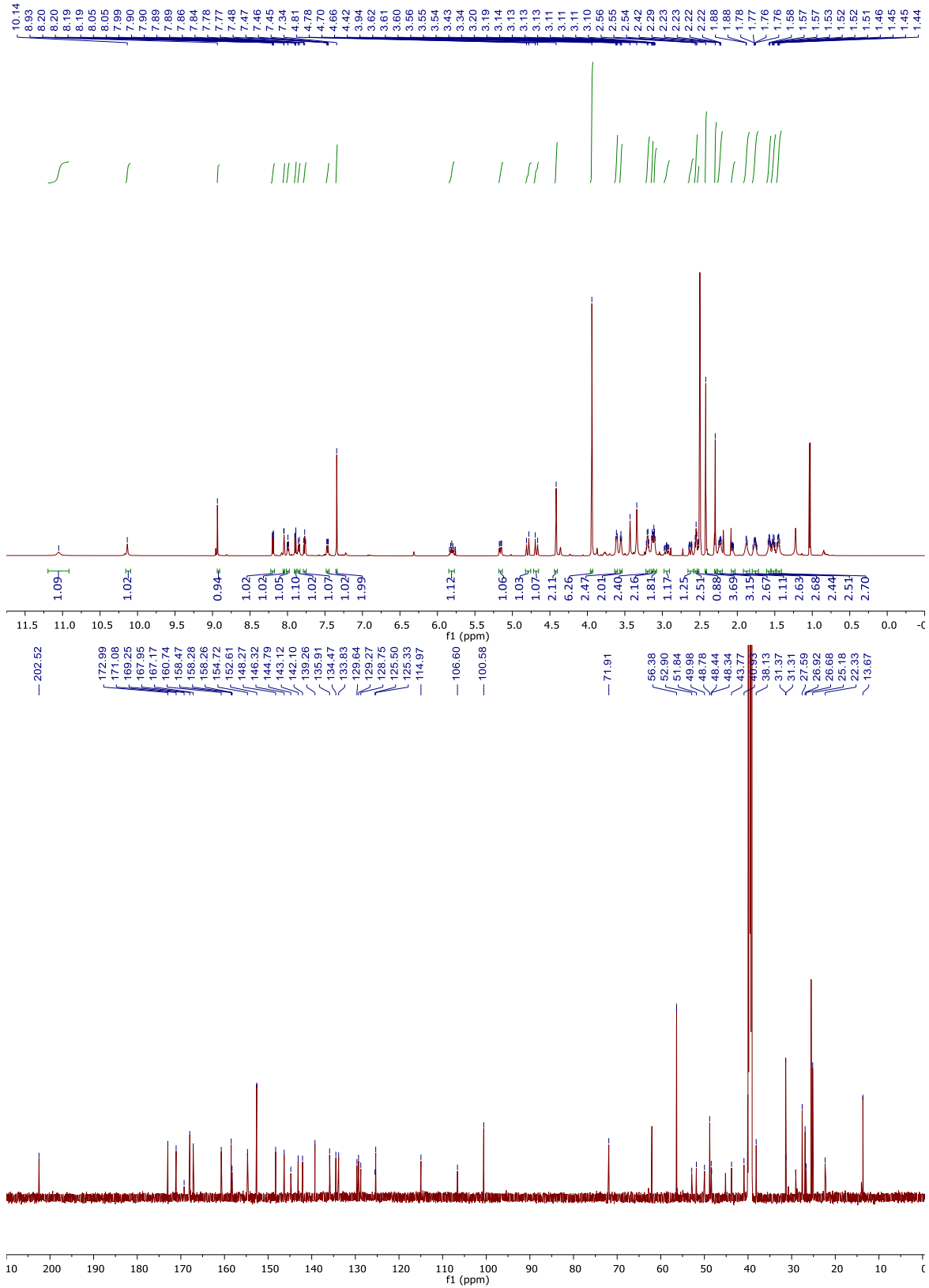
PHOTAC-panCDK-2



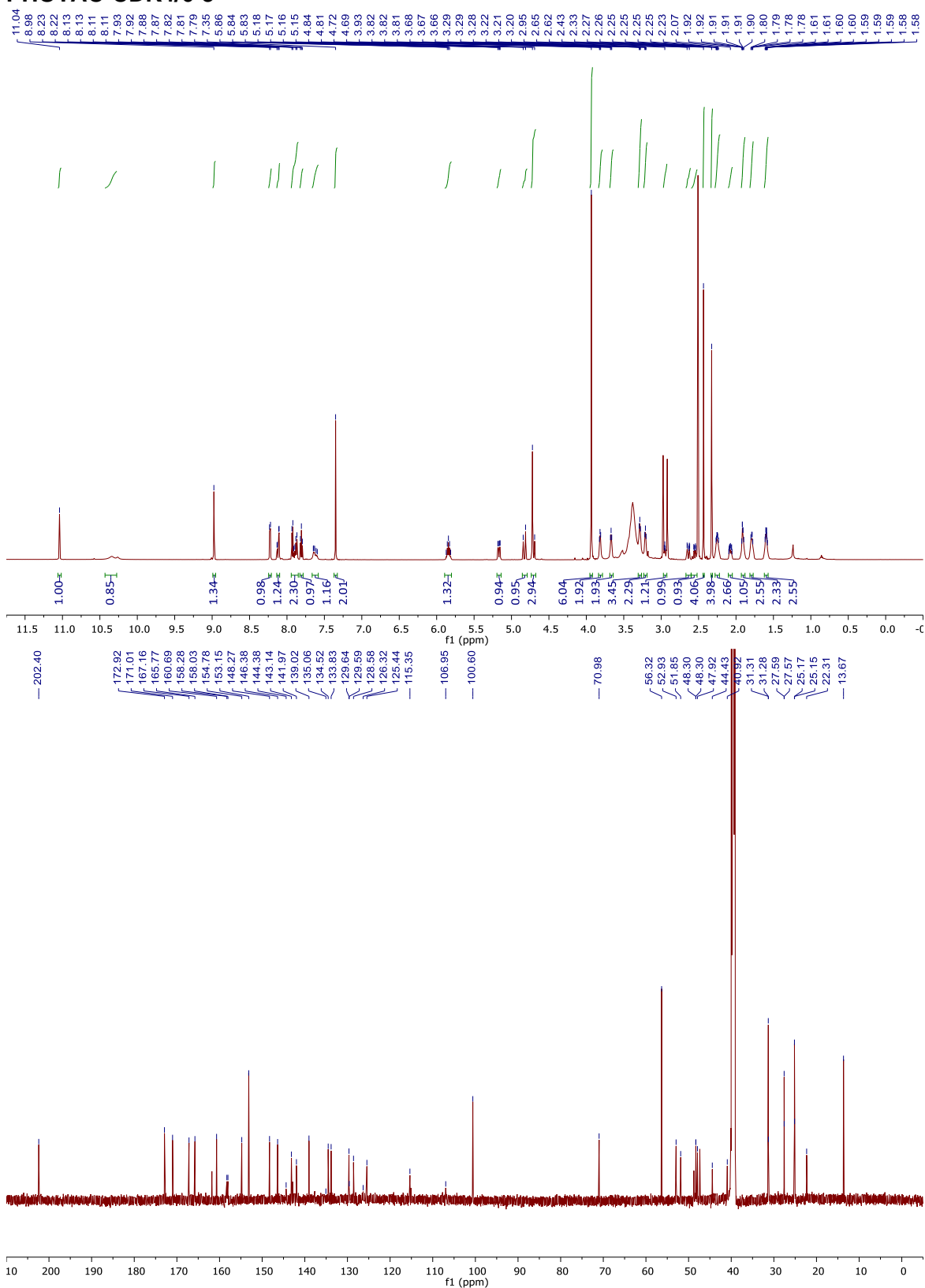
PHOTAC-CDK4/6-1



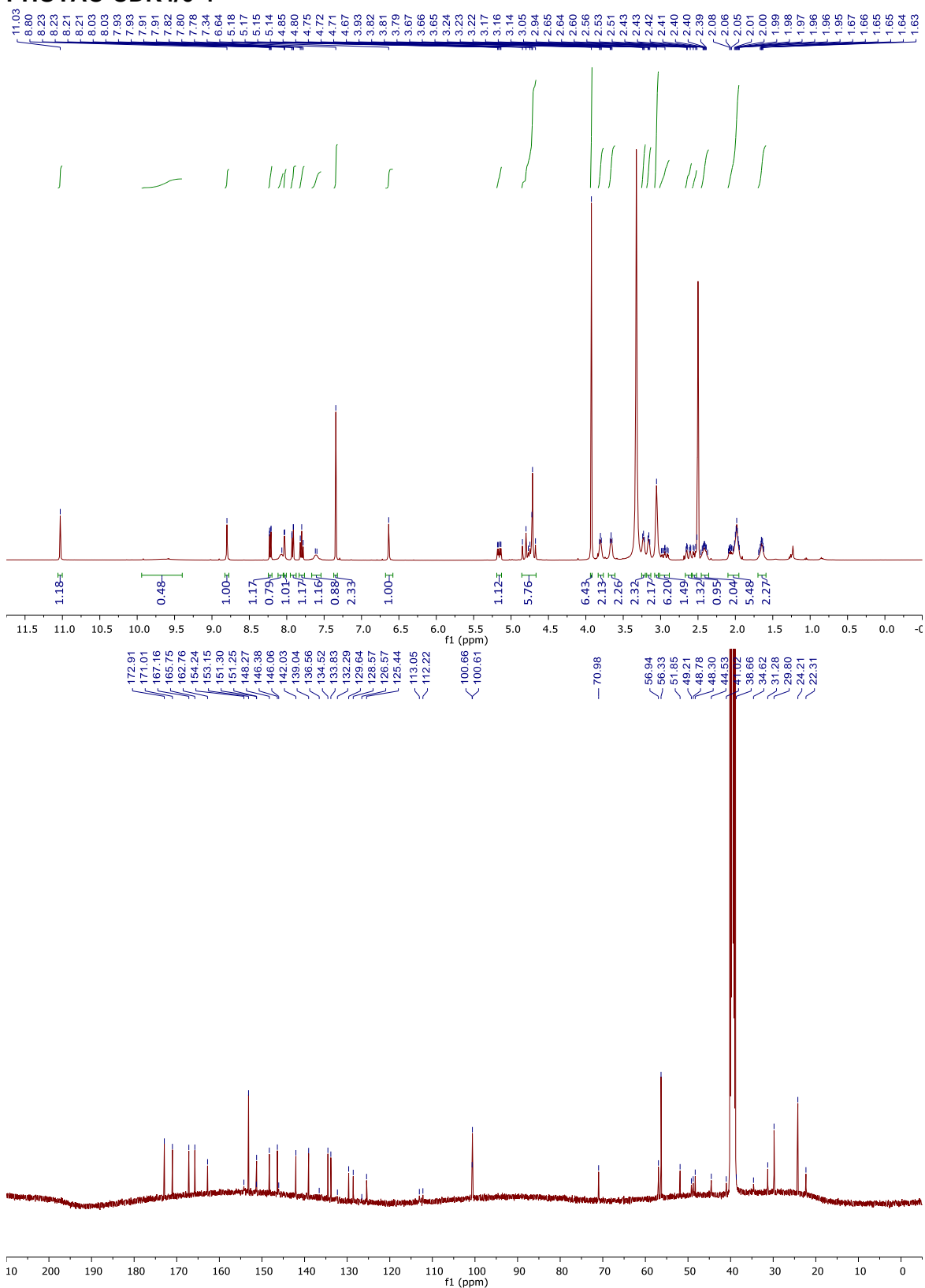
PHOTAC-CDK4/6-2



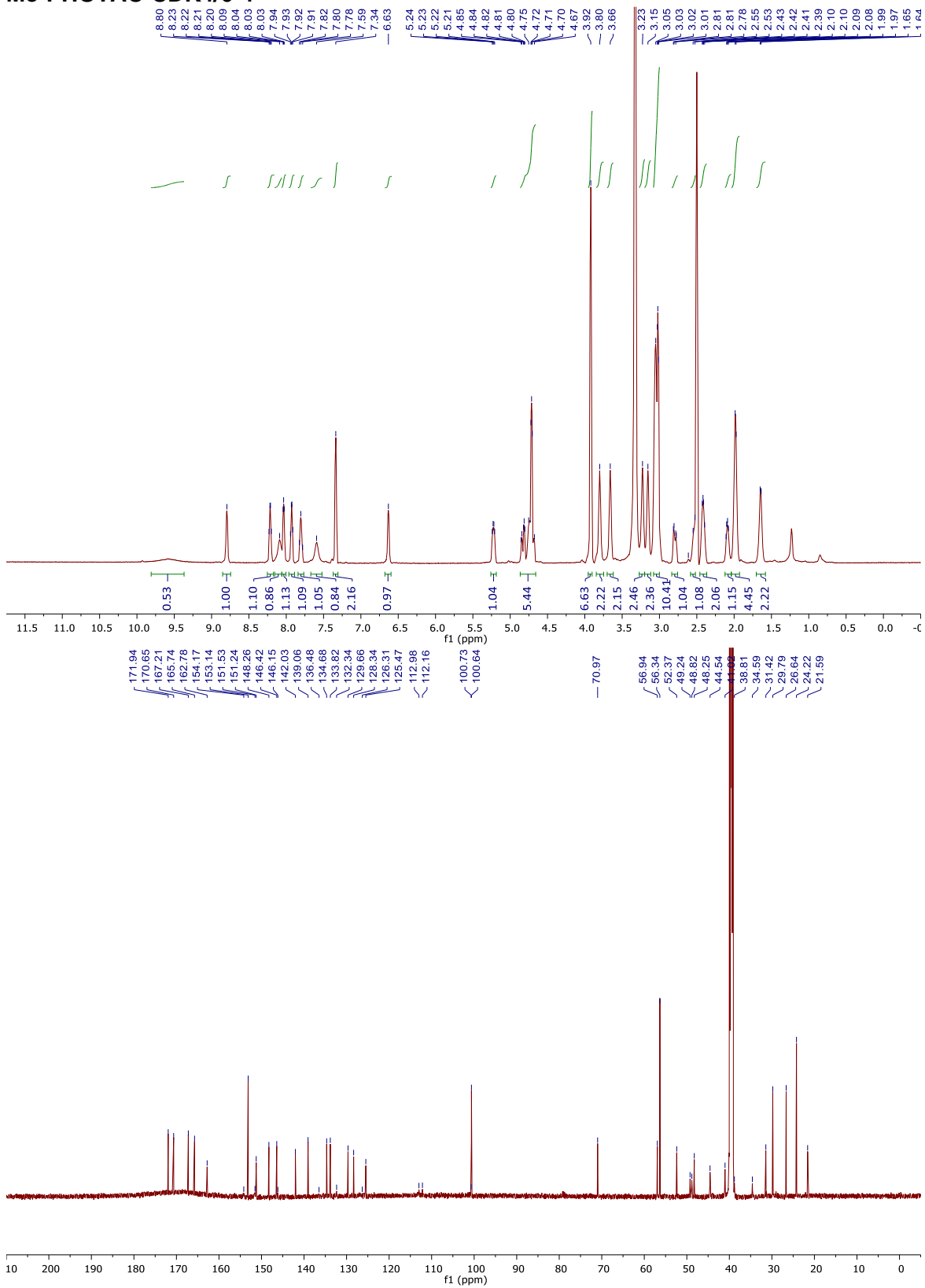
PHOTAC-CDK4/6-3



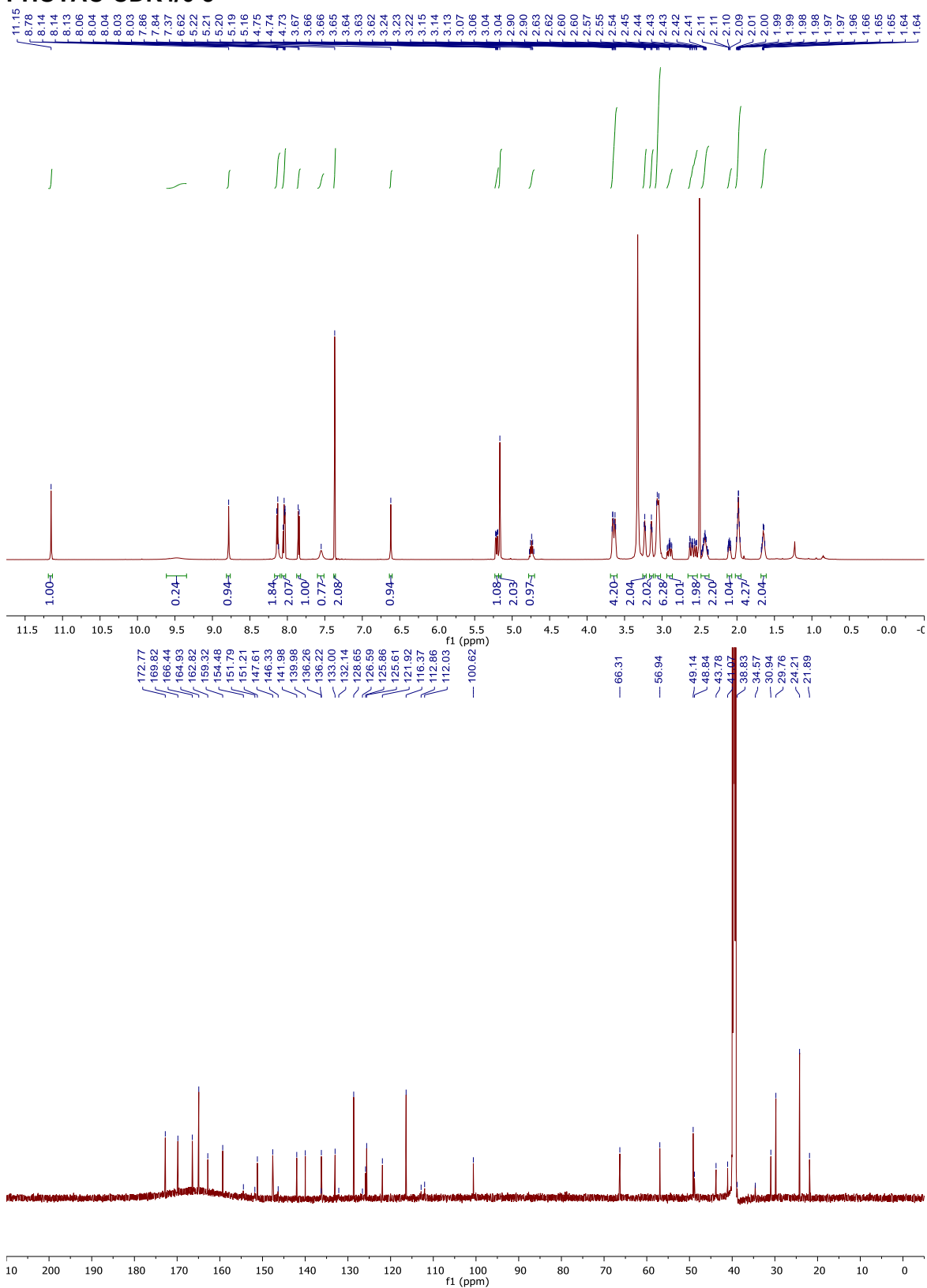
PHOTAC-CDK4/6-4



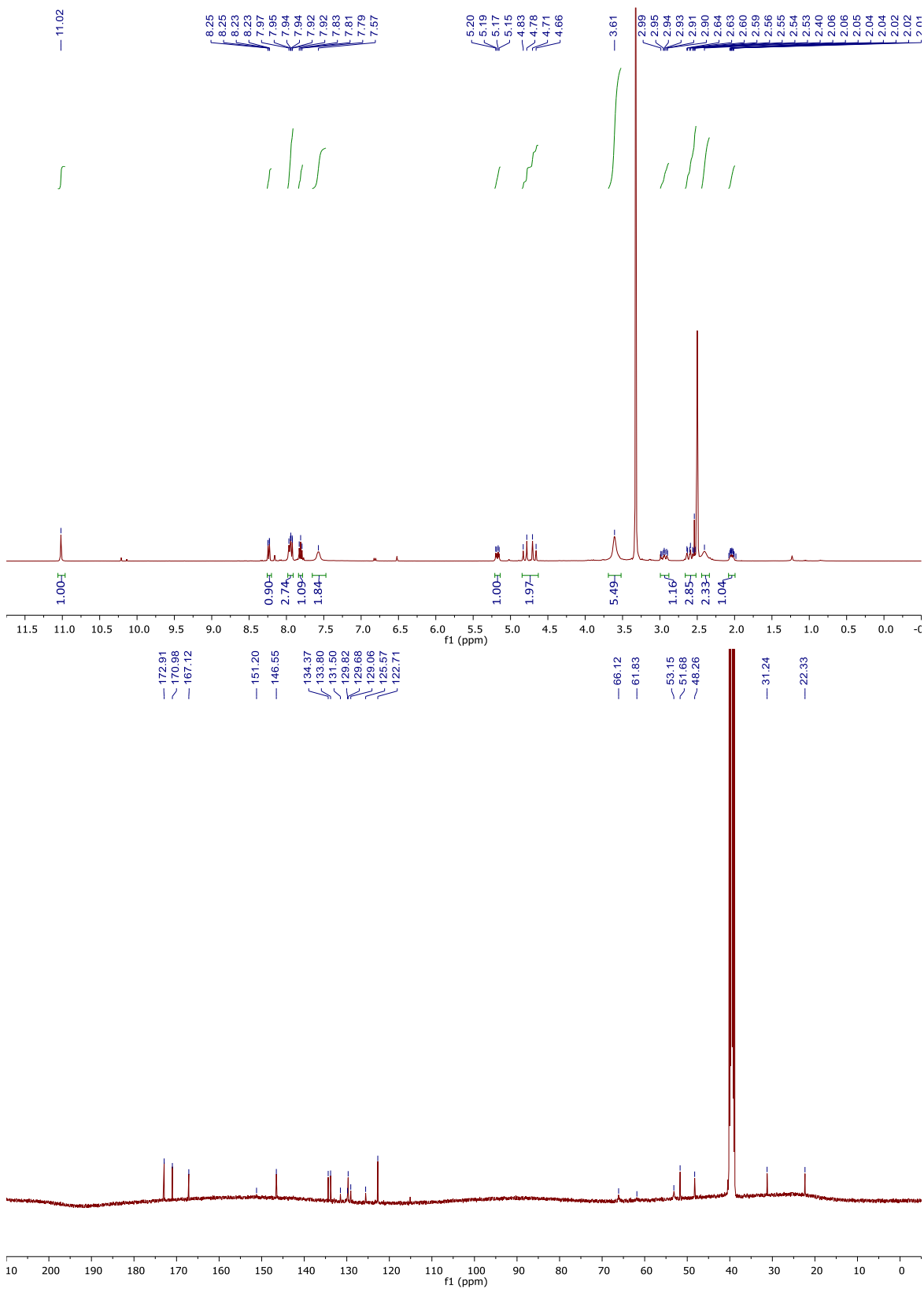
Me-PHOTAC-CDK4/6-4



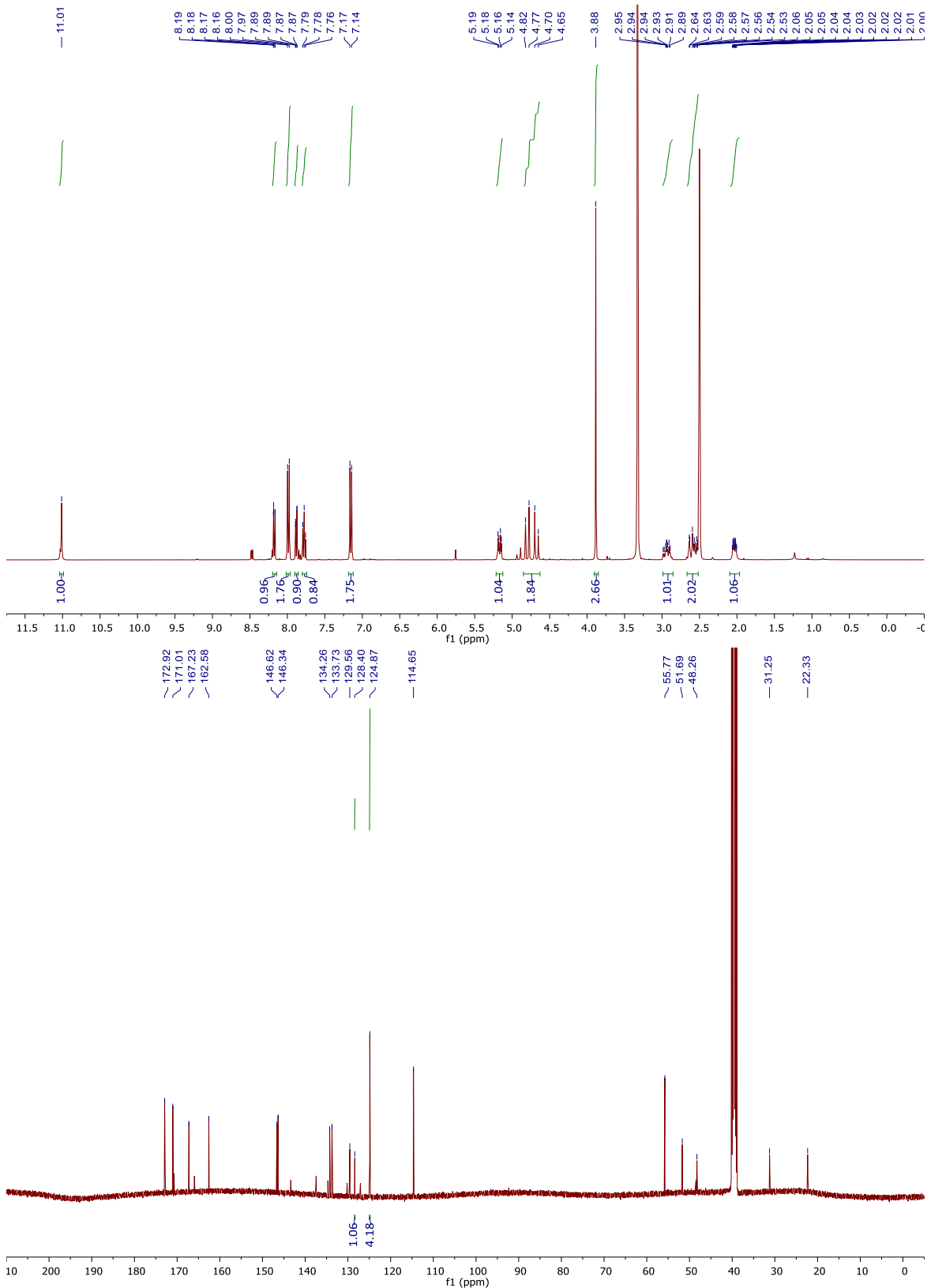
PHOTAC-CDK4/6-5



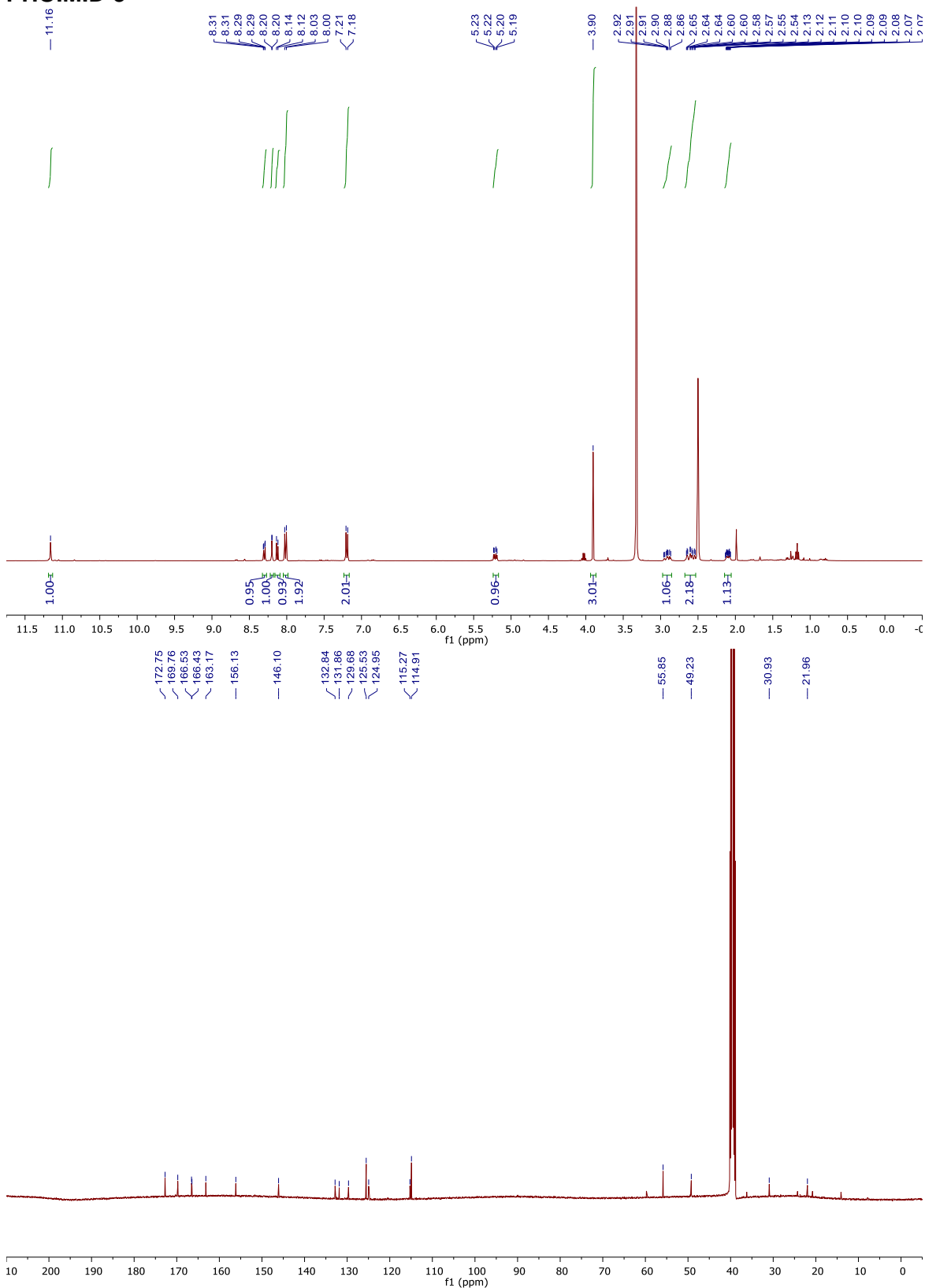
PHOIMID-1



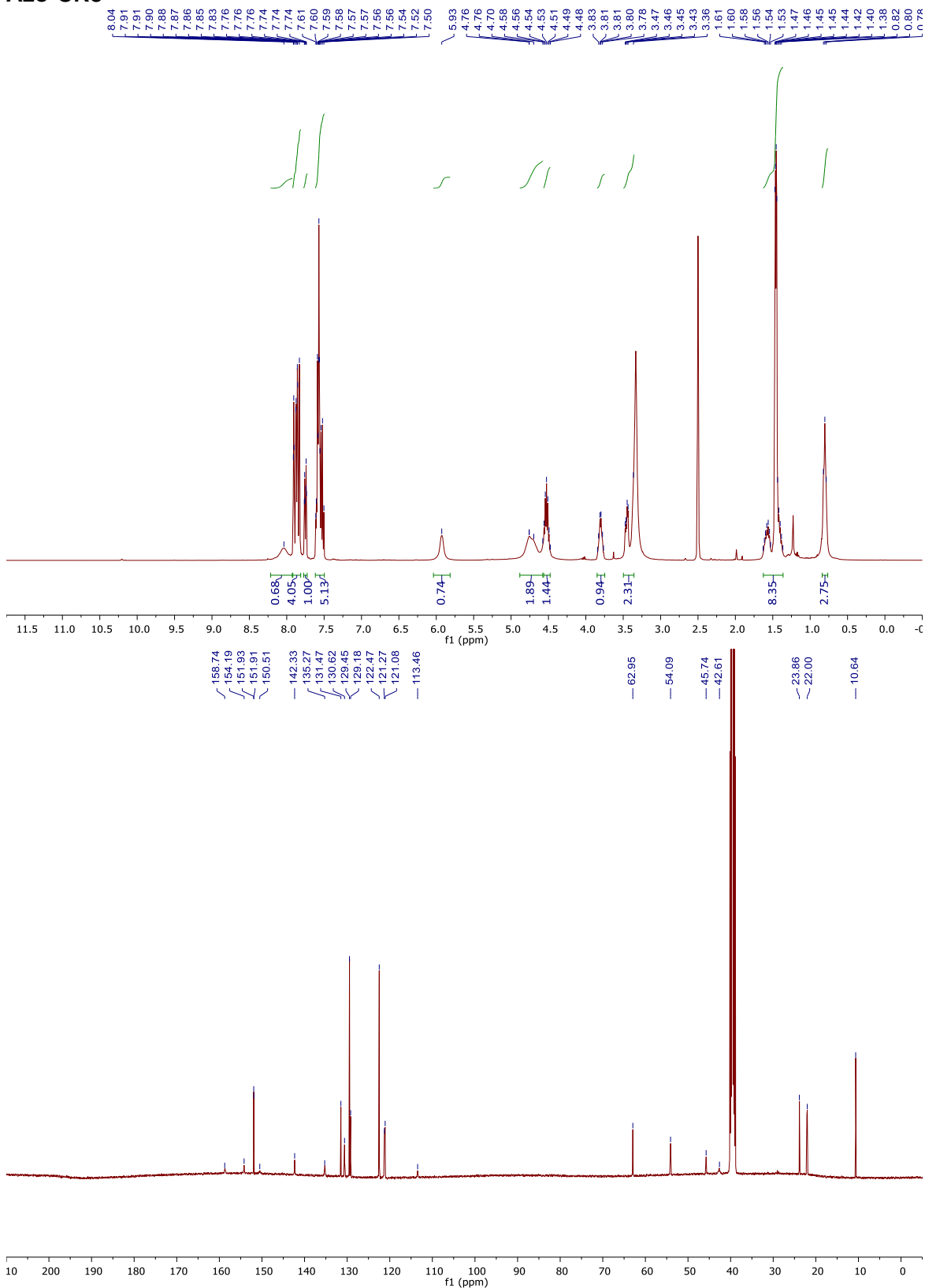
PHOIMID-2



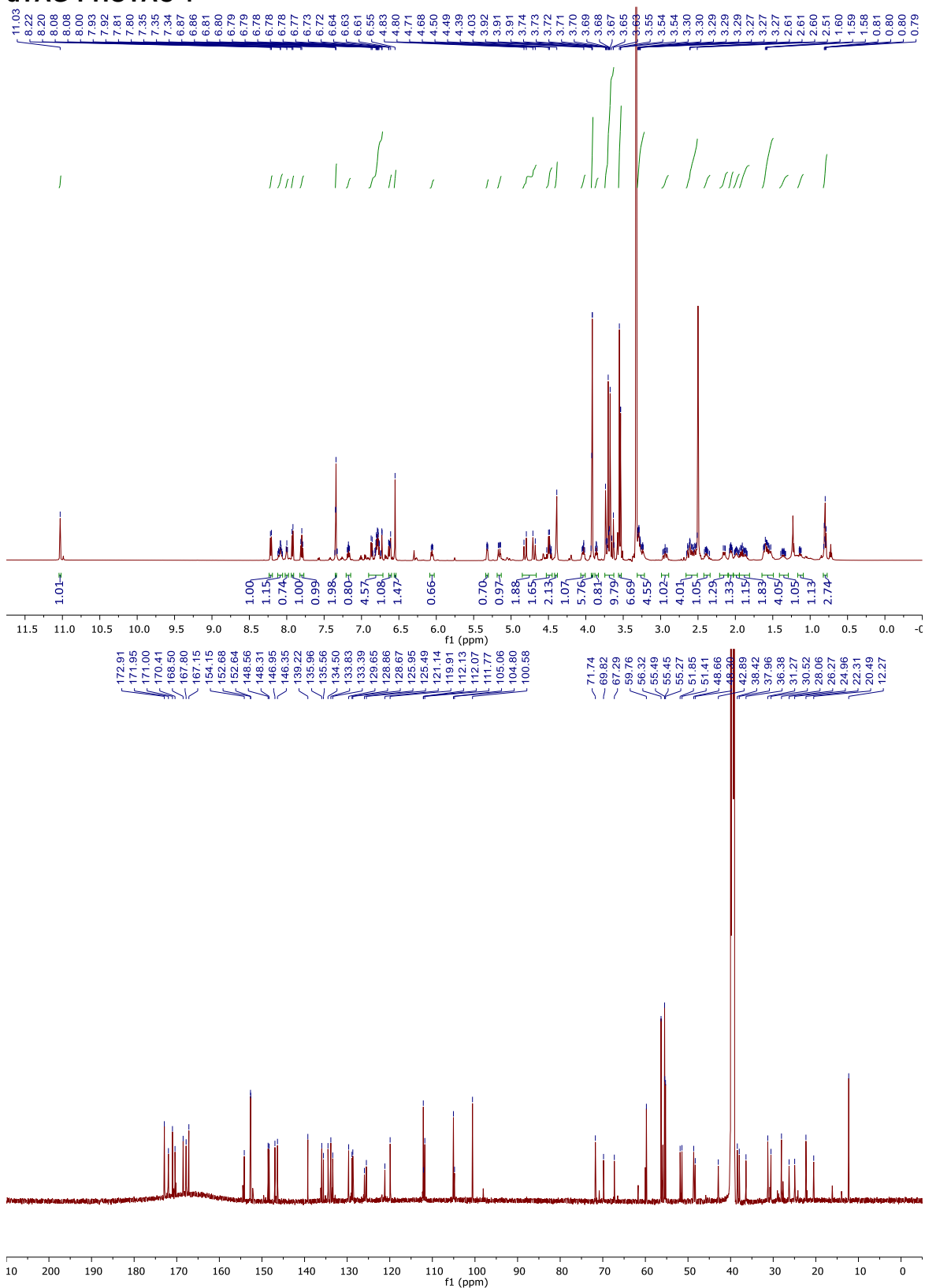
PHOIMID-3



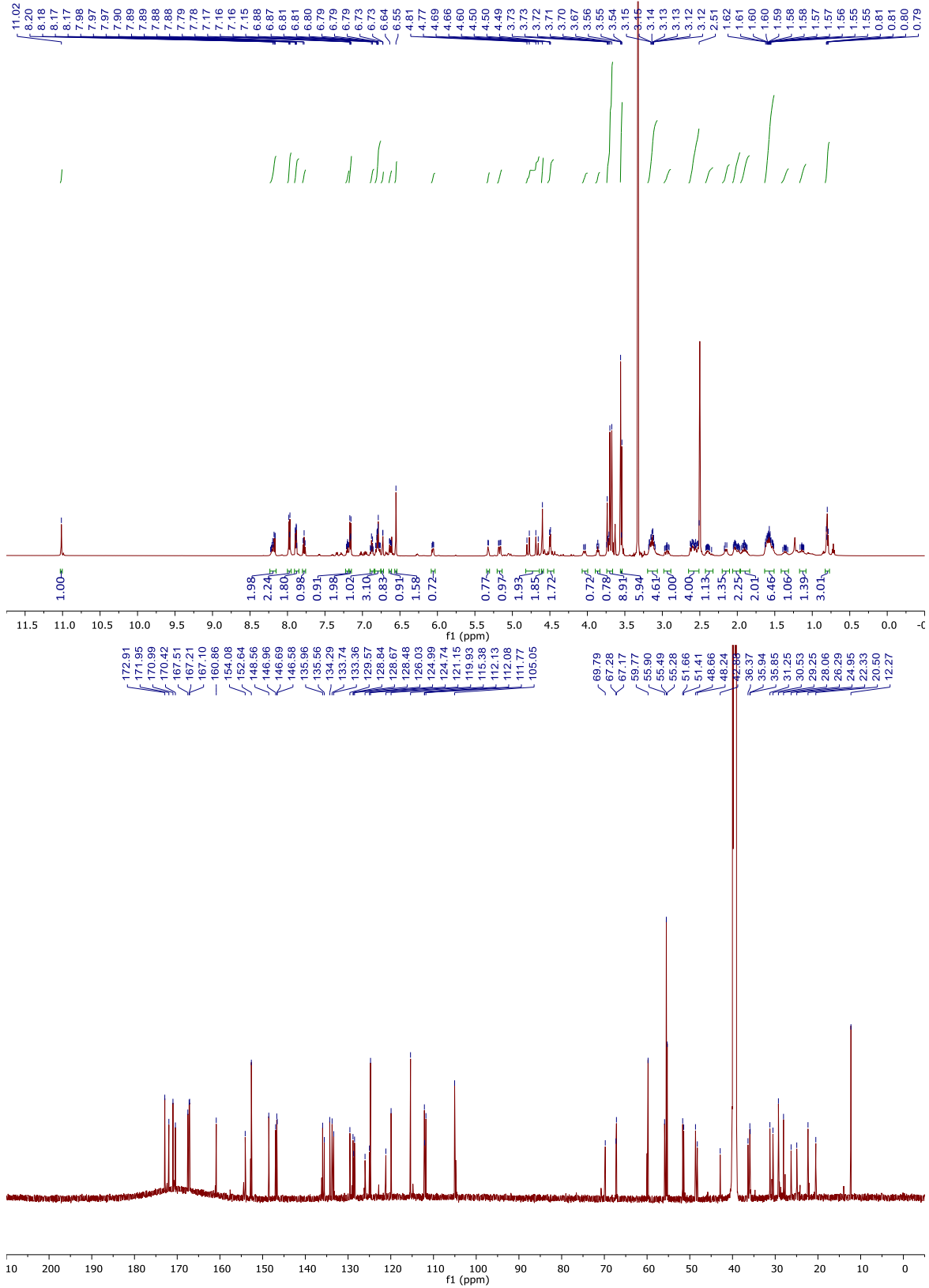
Azo-CR8



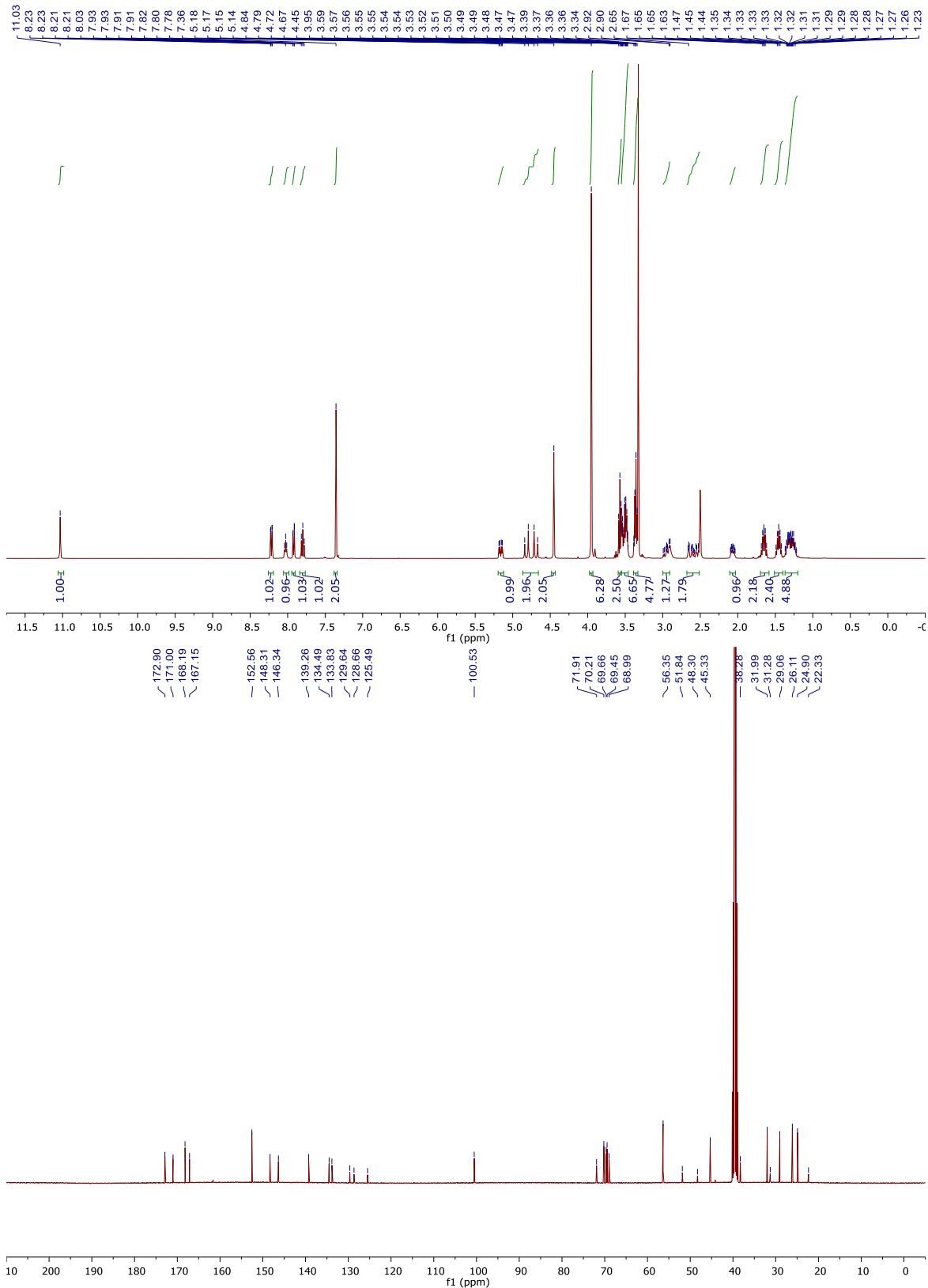
dTAG-PHOTAC-1



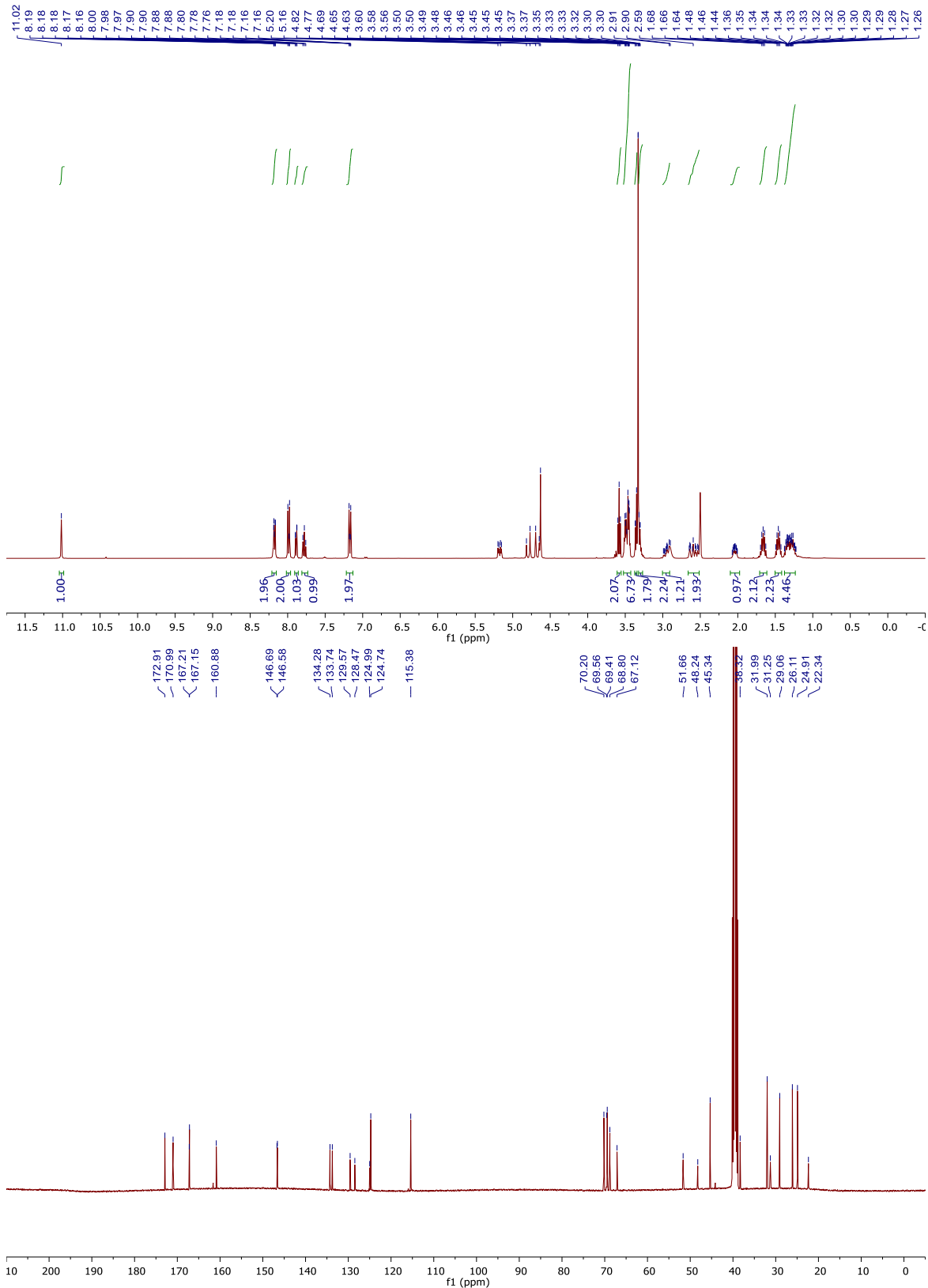
dTAG-PHOTAC-2



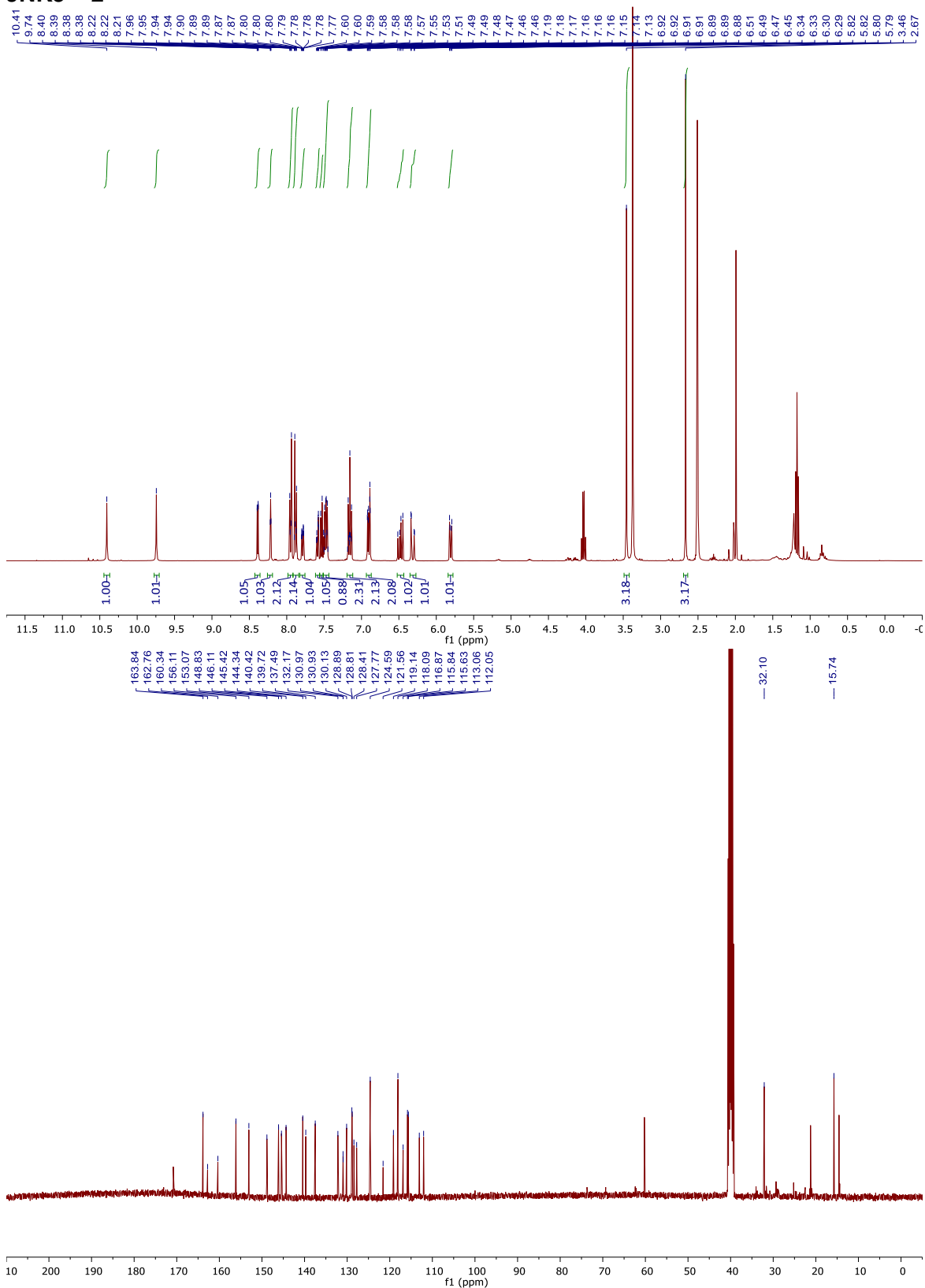
HalophOTAC-1



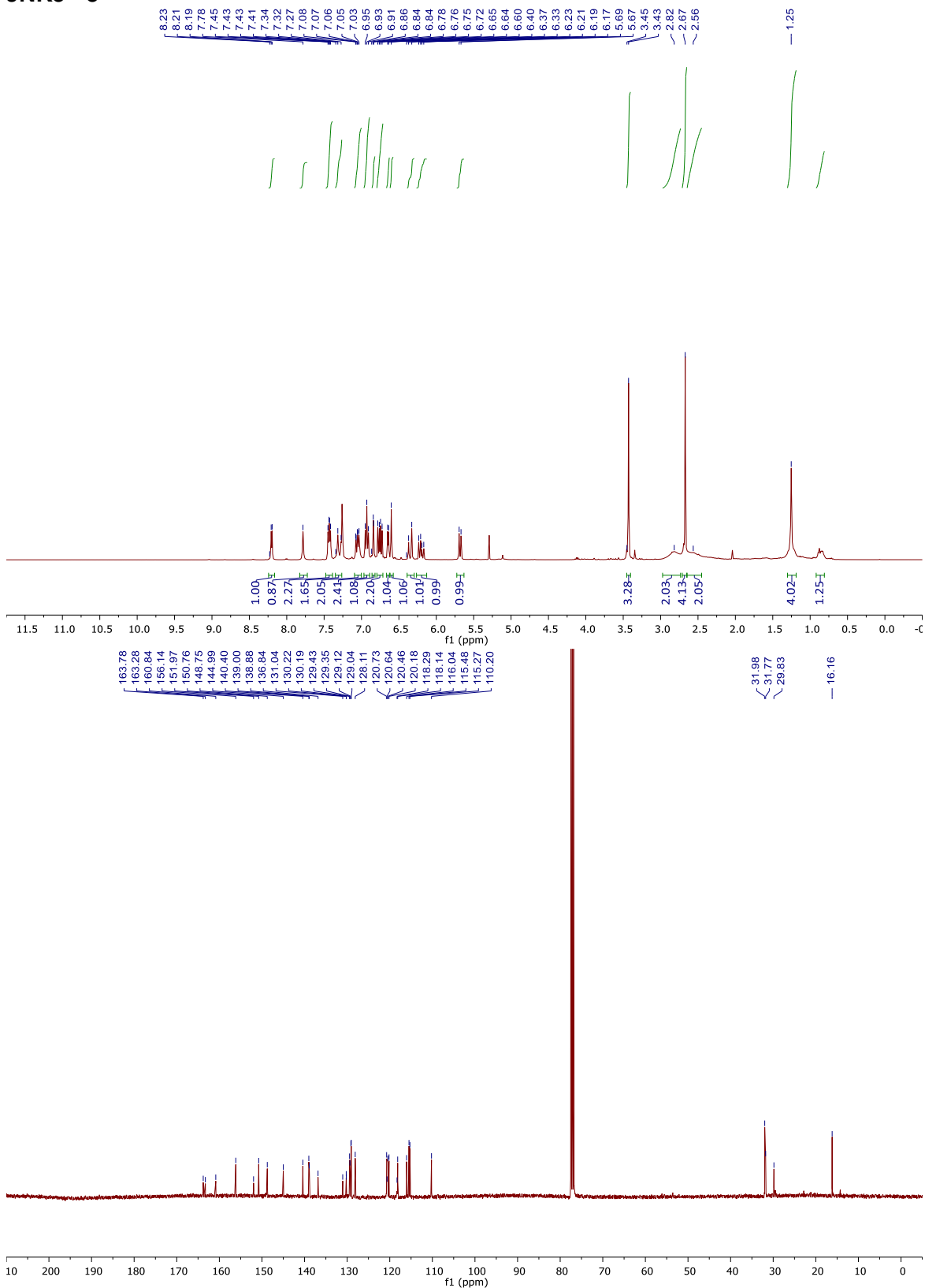
HalophOTAC-2



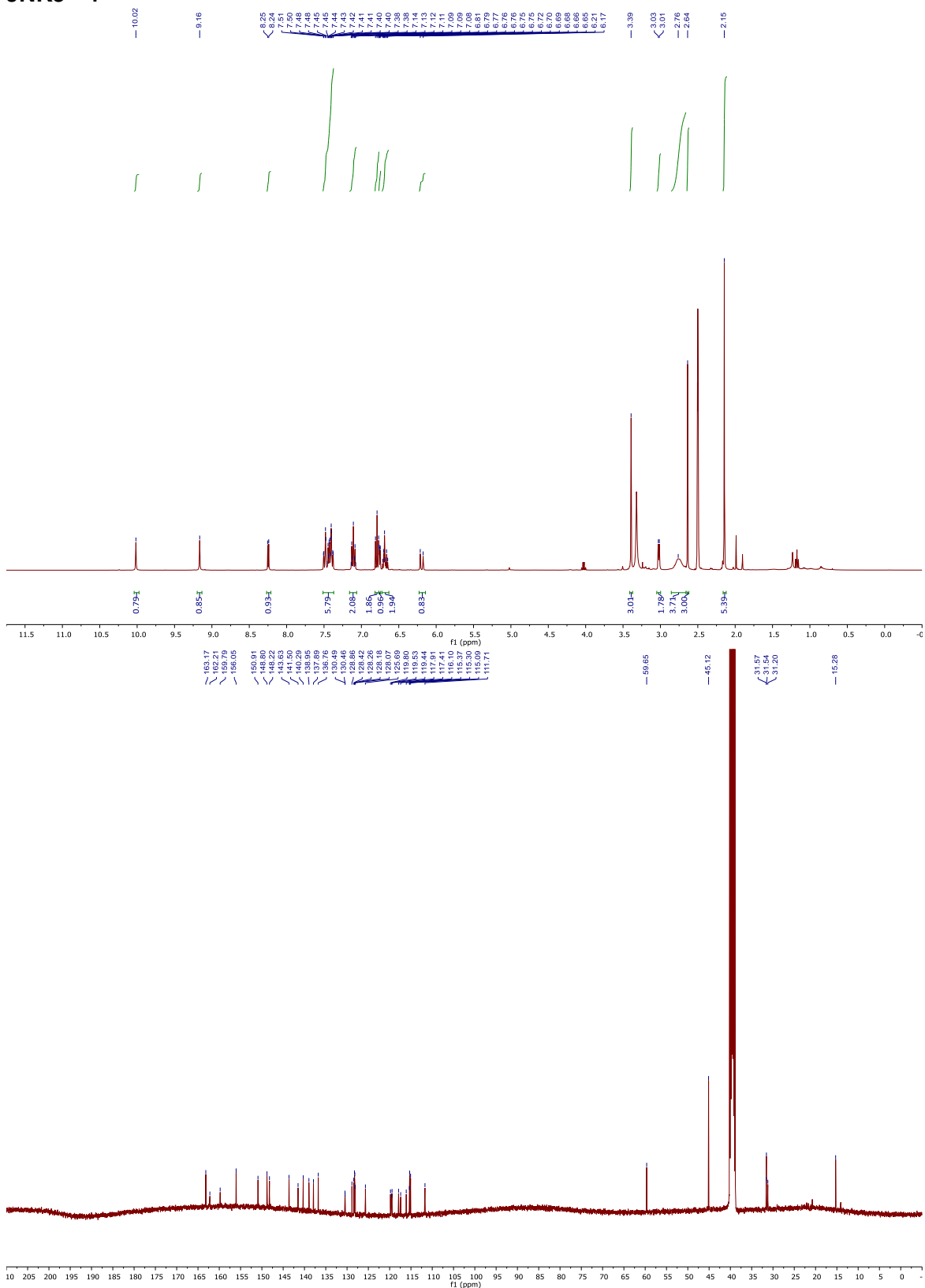
JNK3 - 2



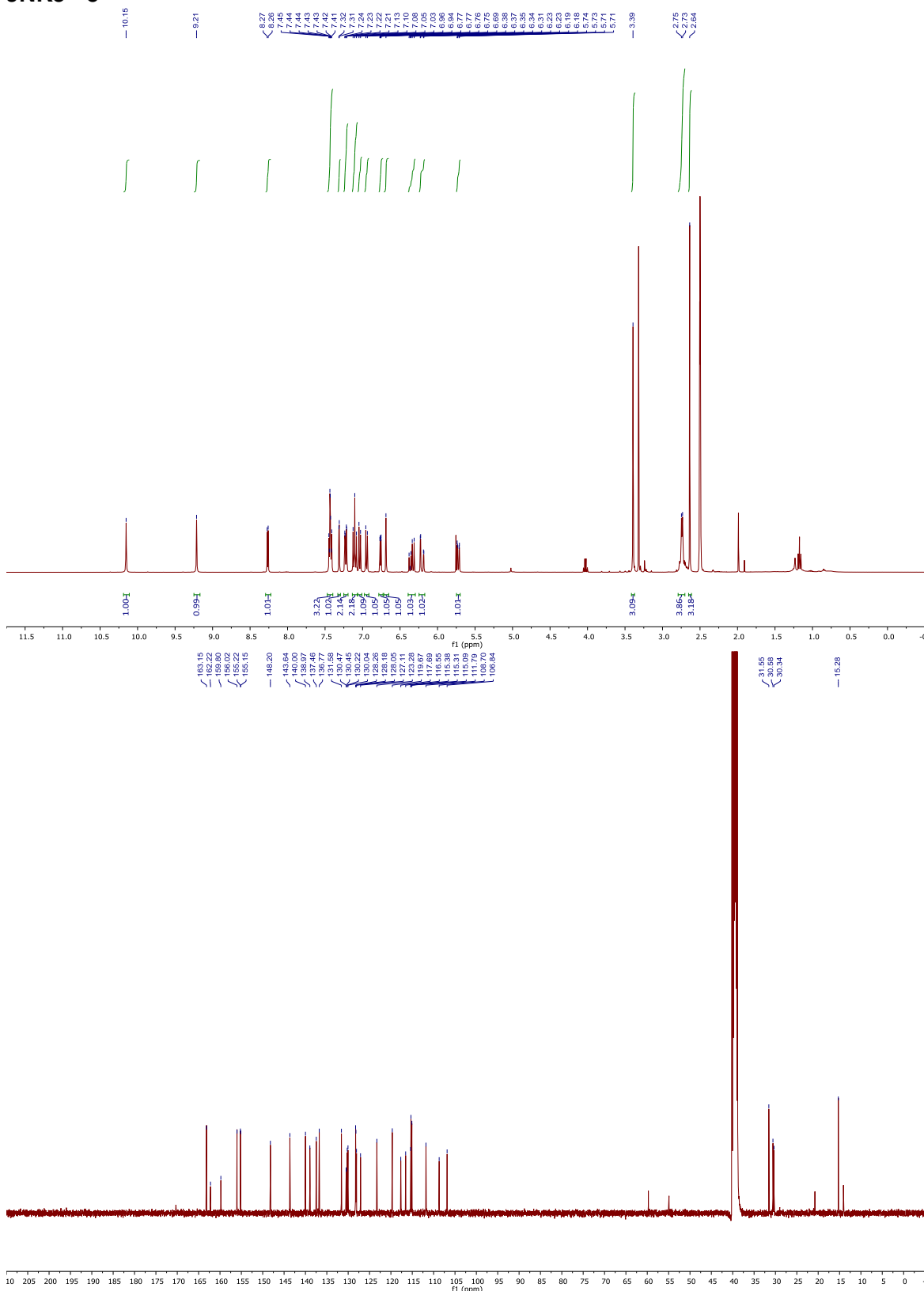
JNK3 - 3



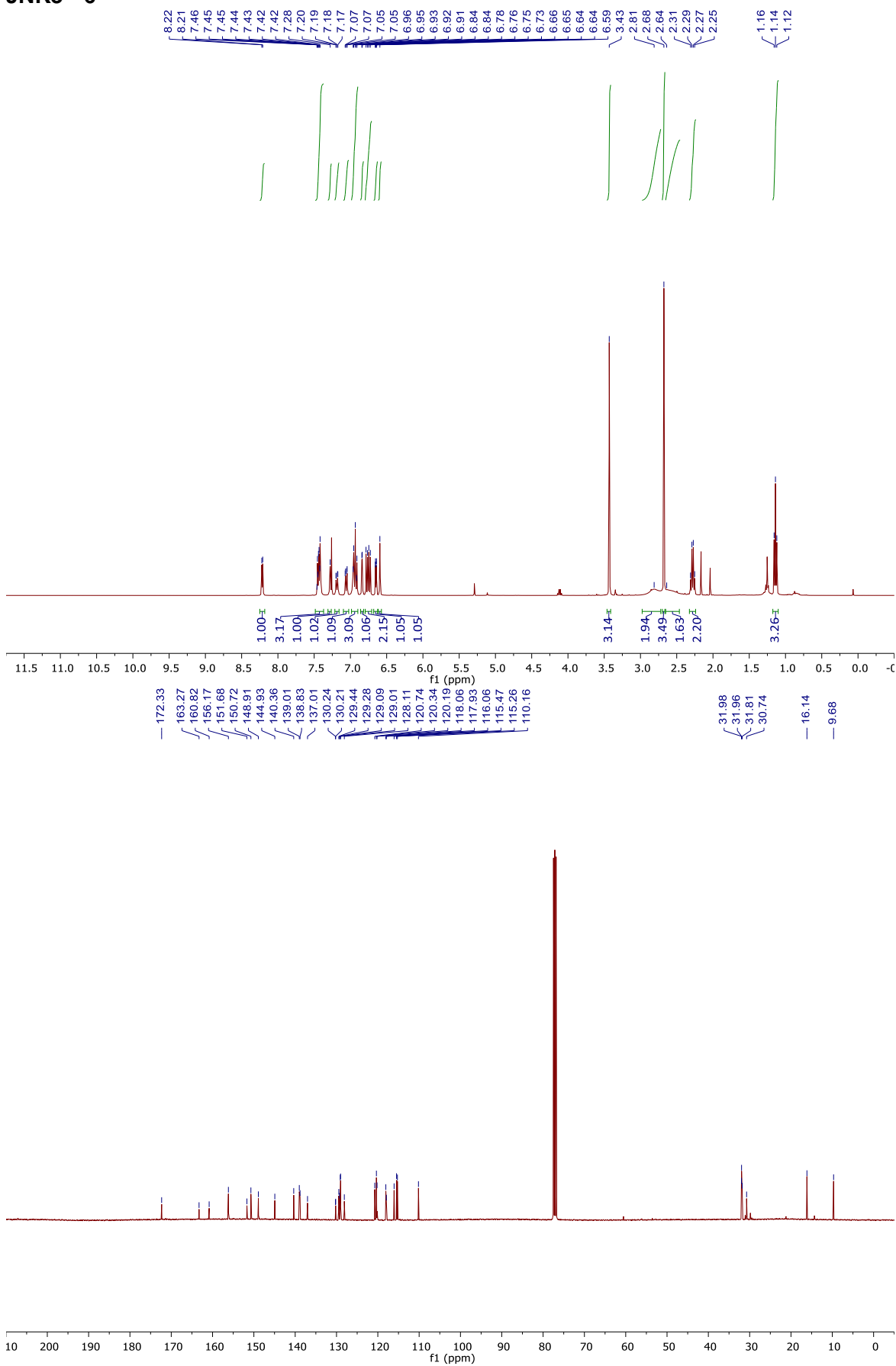
JNK3 - 4



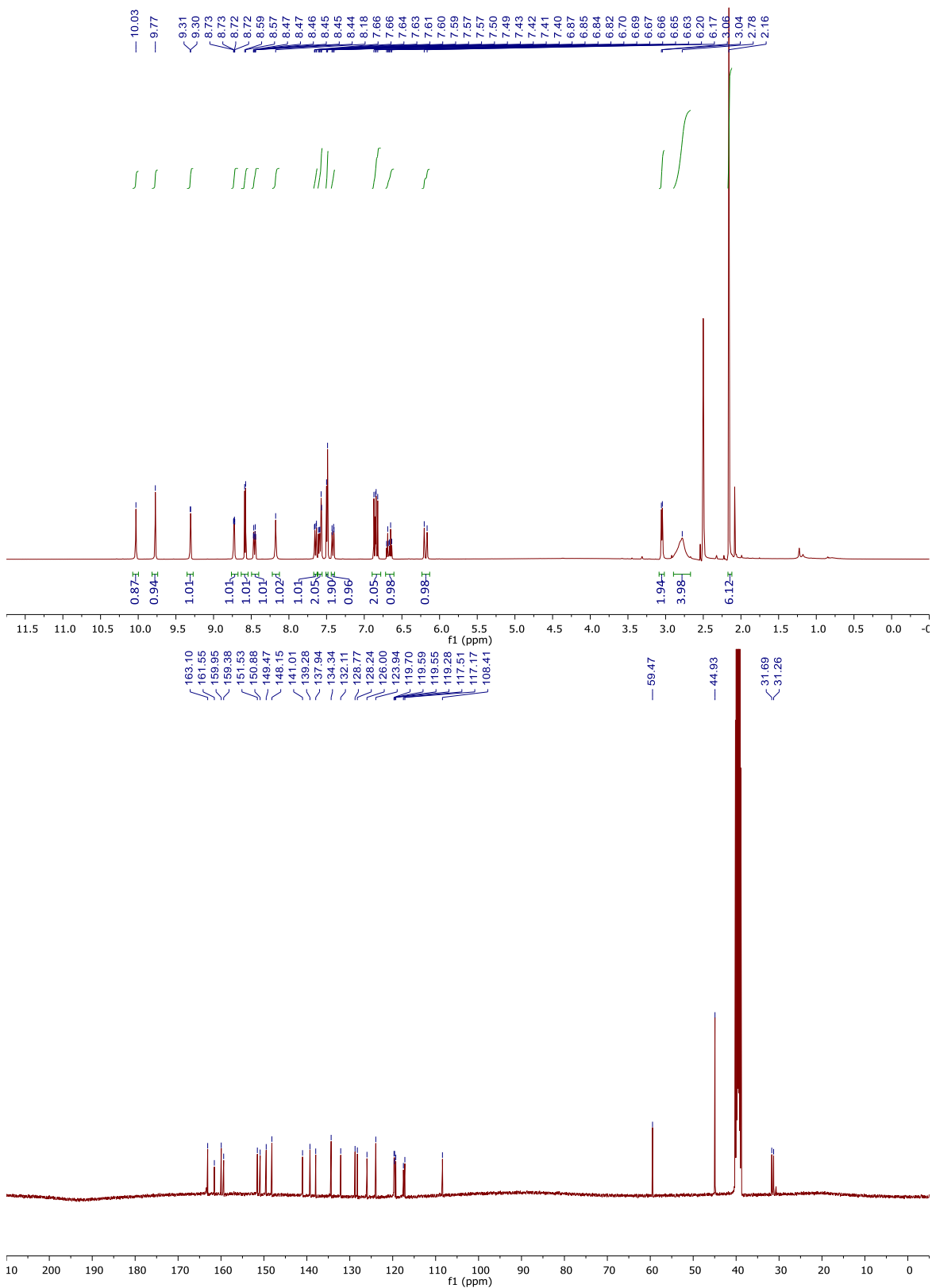
JNK3 - 5



JNK3 - 6



MR-II-265



MR-II-309

